Computational and Mathematical Methods in Medicine

Social Network-Based Medical Informatics with a Deep Learning Perspective

Lead Guest Editor: Muhammad Zubair Asghar
Guest Editors: Ibrahim Hameed and Shakeel Ahmad

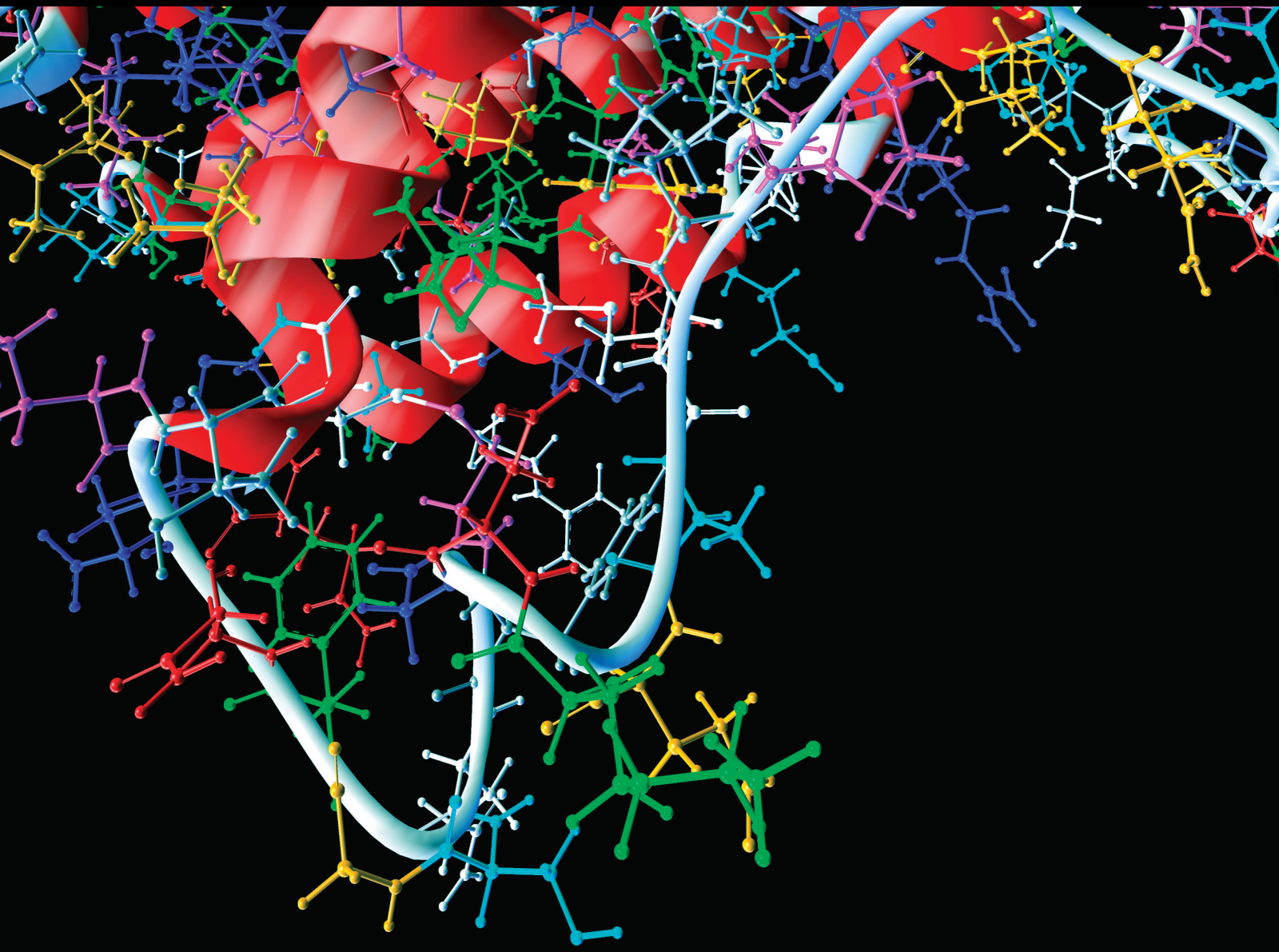

Social Network-Based Medical Informatics with a Deep Learning Perspective

Computational and Mathematical Methods in Medicine

Social Network-Based Medical Informatics with a Deep Learning Perspective

Lead Guest Editor: Muhammad Zubair Asghar
Guest Editors: Ibrahim Hameed and Shakeel Ahmad

Contents

Retracted: A Systematic Literature Review on Particle Swarm Optimization Techniques for Medical Diseases Detection
Computational and Mathematical Methods in Medicine
Retraction (1 page), Article ID 9825640, Volume 2023 (2023)

Retracted: Efficient Prediction of Missed Clinical Appointment Using Machine Learning
Computational and Mathematical Methods in Medicine
Retraction (1 page), Article ID 9795312, Volume 2023 (2023)

Retracted: Brain Decoding Using fMRI Images for Multiple Subjects through Deep Learning
Computational and Mathematical Methods in Medicine
Retraction (1 page), Article ID 9785636, Volume 2023 (2023)

Retracted: Influence of Health Education Based on IMB on Prognosis and Self-Management Behavior of Patients with Chronic Heart Failure
Computational and Mathematical Methods in Medicine
Retraction (1 page), Article ID 9828324, Volume 2023 (2023)

Retracted: Left Atrial Appendage Depth and Tachycardia Bradycardia Syndrome as Important Predictors of Left Atrial Appendage Thrombus in Patients with Nonvalvular Atrial Fibrillation
Computational and Mathematical Methods in Medicine
Retraction (1 page), Article ID 9827568, Volume 2023 (2023)

Retracted: Self-Adaptation Resource Allocation for Continuous Offloading Tasks in Pervasive Computing
Computational and Mathematical Methods in Medicine
Retraction (1 page), Article ID 9826547, Volume 2023 (2023)

Retracted: GEO Database Screening Combined with In Vitro Experiments to Study the Mechanism of hsa_circ_0003570 in Infantile Hemangiomas
Computational and Mathematical Methods in Medicine
Retraction (1 page), Article ID 9826474, Volume 2023 (2023)

Retracted: Controversy on Positive Peritoneal Cytology of Endometrial Carcinoma
Computational and Mathematical Methods in Medicine
Retraction (1 page), Article ID 9814020, Volume 2023 (2023)

Retracted: Corydalis decumbens Can Exert Analgesic Effects in a Mouse Neuropathic Pain Model by Modulating MAPK Signaling
Computational and Mathematical Methods in Medicine
Retraction (1 page), Article ID 9808106, Volume 2023 (2023)

Retracted: Timosaponin AIII Suppresses RAP1 Signaling Pathway to Enhance the Inhibitory Effect of Paclitaxel on Nasopharyngeal Carcinoma
Computational and Mathematical Methods in Medicine
Retraction (1 page), Article ID 9804984, Volume 2023 (2023)

Contents

Retracted: Recognition of Human Body Feature Changes in Sports Health Based on Deep Learning
Computational and Mathematical Methods in Medicine
Retraction (1 page), Article ID 9865029, Volume 2023 (2023)

Retracted: An Improved Brain MRI Classification Methodology Based on Statistical Features and Machine Learning Algorithms
Computational and Mathematical Methods in Medicine
Retraction (1 page), Article ID 9845962, Volume 2023 (2023)

Retracted: An Inhibitor of Nuclear Factor-Kappa B Pathway Attenuates the Release of TGF-β1 and Inhibits the Fibrogenic Progress in a Model of Airway Remodeling Induced by Acrolein
Computational and Mathematical Methods in Medicine
Retraction (1 page), Article ID 9843487, Volume 2023 (2023)

Retracted: Status Quo Analysis of Physical Fitness Test Data Based on Health Monitoring
Computational and Mathematical Methods in Medicine
Retraction (1 page), Article ID 9842627, Volume 2023 (2023)

Retracted: Breast Tumor Detection and Classification in Mammogram Images Using Modified YOLOv5 Network
Computational and Mathematical Methods in Medicine
Retraction (1 page), Article ID 9837528, Volume 2023 (2023)

Retracted: Paeoniflorin Can Improve Acute Lung Injury Caused by Severe Acute Pancreatitis through Nrf2/ARE Pathway
Computational and Mathematical Methods in Medicine
Retraction (1 page), Article ID 9837218, Volume 2023 (2023)

Retracted: Predicting Characteristics Associated with Breast Cancer Survival Using Multiple Machine Learning Approaches
Computational and Mathematical Methods in Medicine
Retraction (1 page), Article ID 9832573, Volume 2023 (2023)

Retracted: A Diagnostic Model of Volleyball Techniques and Tactics Based on Wireless Communication Network
Computational and Mathematical Methods in Medicine
Retraction (1 page), Article ID 9872404, Volume 2022 (2022)

Retracted: Prevention Methods of Fitness and Bodybuilding Exercise Injury Based on Data Mining
Computational and Mathematical Methods in Medicine
Retraction (1 page), Article ID 9869812, Volume 2022 (2022)

Contents

[Retracted] Predicting Characteristics Associated with Breast Cancer Survival Using Multiple Machine Learning Approaches
Mohammad Nazmul Haque, Tahia Tazin, Mohammad Monirujjaman Khan, Shahla Faisal, Sobhee Md. Ibraheem, Haneen Algethami, and Faris A. Almalki
Research Article (12 pages), Article ID 1249692, Volume 2022 (2022)

[Retracted] lncRNA GHET1 Promotes the Progression of Triple-Negative Breast Cancer *via* Regulation of miR-377-3p/GRSF1 Signaling Axis
Yu Wang and Chen Li
Research Article (15 pages), Article ID 8366569, Volume 2022 (2022)

[Retracted] Prevention Methods of Fitness and Bodybuilding Exercise Injury Based on Data Mining
Jun Xie
Research Article (13 pages), Article ID 7083991, Volume 2022 (2022)

[Retracted] Effect of Dexmedetomidine on Cardiac Output among Parturient with Severe Preeclampsia after Cesarean Section
Yanxiang Lv, Ying Zhou, Yuan Qiao, Rui Hu, Yan Liang, Yanan Lian, and Tongqiang He
Research Article (7 pages), Article ID 4742350, Volume 2022 (2022)

[Retracted] Factors That Affect Maternal Mortality in Rwanda: A Comparative Study with India and Bangladesh
Mugenzi Patrick, Muhammad Sami uz Zaman, Ghazala Afzal, Minhas Mahsud, and Mumuni Napari Hanifatu
Research Article (9 pages), Article ID 1940188, Volume 2022 (2022)

[Retracted] The Effect of Endoscopy on Patients with Malignant Esophageal Cancer after Medical Treatment and Chemotherapy
Yu Liu, Lingqiong Zhao, Xingping Tan, Nana Liu, and Teng Long
Research Article (12 pages), Article ID 7906302, Volume 2022 (2022)

[Retracted] Influence of Health Education Based on IMB on Prognosis and Self-Management Behavior of Patients with Chronic Heart Failure
Wei Liu, Yan Zhang, Hai-jing Liu, Tian Song, and Song Wang
Research Article (13 pages), Article ID 8517802, Volume 2022 (2022)

[Retracted] An Inhibitor of Nuclear Factor-Kappa B Pathway Attenuates the Release of TGF-β1 and Inhibits the Fibrogenic Progress in a Model of Airway Remodeling Induced by Acrolein
Peng Chen, Xiaoxia Wang, Yanping Li, and Hong Liu
Research Article (7 pages), Article ID 4984634, Volume 2022 (2022)

[Retracted] Controversy on Positive Peritoneal Cytology of Endometrial Carcinoma
Yi-Si Liu, Hui-Min Wang, and Yan Gao
Review Article (5 pages), Article ID 1906769, Volume 2022 (2022)

Contents

[Retracted] Machine Learning-Based Automated Diagnostic Systems Developed for Heart Failure Prediction Using Different Types of Data Modalities: A Systematic Review and Future Directions
Ashir Javeed, Shafqat Ullah Khan, Liaqat Ali, Sardar Ali, Yakubu Imrana, and Atiqur Rahman
Review Article (30 pages), Article ID 9288452, Volume 2022 (2022)

[Retracted] COVID-19 Detection Based on Lung Ct Scan Using Deep Learning Techniques
S. V. Kogilavani, J. Prabhu, R. Sandhiya, M. Sandeep Kumar, UmaShankar Subramaniam, Alagar Karthick, M. Muhibbullah, and Sharmila Banu Sheik Imam
Research Article (13 pages), Article ID 7672196, Volume 2022 (2022)

[Retracted] An Improved Strategy for Task Scheduling in the Parallel Computational Alignment of Multiple Sequences
Muhammad Ishaq, Asfandyar Khan, Mazliham Mohd Su'ud, Muhammad Mansoor Alam, Javed Iqbal Bangash, and Abdullah Khan
Research Article (11 pages), Article ID 8691646, Volume 2022 (2022)

[Retracted] Energy Efficiency and Reliability Considerations in Wireless Body Area Networks: A Survey
Farman Ullah, M. Zahid Khan, Gulzar Mehmood, Muhammad Shuaib Qureshi, and Muhammad Fayaz
Review Article (15 pages), Article ID 1090131, Volume 2022 (2022)

[Retracted] Social Media Analytics for Pharmacovigilance of Antiepileptic Drugs
Anwar Ali Yahya, Yousef Asiri, and Ibrahim Alyami
Research Article (24 pages), Article ID 8965280, Volume 2022 (2022)

[Retracted] Breast Tumor Detection and Classification in Mammogram Images Using Modified YOLOv5 Network
Aqsa Mohiyuddin, Asma Basharat, Usman Ghani, Veselý Peter, Sidra Abbas, Osama Bin Naeem, and Muhammad Rizwan
Research Article (16 pages), Article ID 1359019, Volume 2022 (2022)

[Retracted] MKA: A Scalable Medical Knowledge-Assisted Mechanism for Generative Models on Medical Conversation Tasks
Ke Liang, Sifan Wu, and Jiayi Gu
Research Article (10 pages), Article ID 5294627, Volume 2021 (2021)

[Retracted] An Improved Brain MRI Classification Methodology Based on Statistical Features and Machine Learning Algorithms
Muhammad Fayaz, Muhammad Shuaib Qureshi, Karlygash Kussainova, Bermet Burkanova, Ayman Aljarbouh, and Muhammad Bilal Qureshi
Research Article (14 pages), Article ID 8608305, Volume 2021 (2021)

Contents

Hindawi
Computational and Mathematical Methods in Medicine
Volume 2023, Article ID 9854236, 1 page
https://doi.org/10.1155/2023/9854236

Retraction

Retracted: Influential Usage of Big Data and Artificial Intelligence in Healthcare

Computational and Mathematical Methods in Medicine

Received 10 October 2023; Accepted 10 October 2023; Published 11 October 2023

This article has been retracted by Hindawi following an investigation undertaken by the publisher [1]. This investigation has uncovered evidence of one or more of the following indicators of systematic manipulation of the publication process:

(1) Discrepancies in scope

(2) Discrepancies in the description of the research reported

(3) Discrepancies between the availability of data and the research described

(4) Inappropriate citations

(5) Incoherent, meaningless and/or irrelevant content included in the article

(6) Peer-review manipulation

The presence of these indicators undermines our confidence in the integrity of the article's content and we cannot, therefore, vouch for its reliability. Please note that this notice is intended solely to alert readers that the content of this article is unreliable. We have not investigated whether authors were aware of or involved in the systematic manipulation of the publication process.

Wiley and Hindawi regrets that the usual quality checks did not identify these issues before publication and have since put additional measures in place to safeguard research integrity.

We wish to credit our own Research Integrity and Research Publishing teams and anonymous and named external researchers and research integrity experts for contributing to this investigation.

The corresponding author, as the representative of all authors, has been given the opportunity to register their agreement or disagreement to this retraction. We have kept a record of any response received.

References

[1] Y. C. Yang, S. U. Islam, A. Noor, S. Khan, W. Afsar, and S. Nazir, "Influential Usage of Big Data and Artificial Intelligence in Healthcare," *Computational and Mathematical Methods in Medicine*, vol. 2021, Article ID 5812499, 13 pages, 2021.

Hindawi
Computational and Mathematical Methods in Medicine
Volume 2023, Article ID 9846497, 1 page
https://doi.org/10.1155/2023/9846497

Retraction

Retracted: Social Media Analytics for Pharmacovigilance of Antiepileptic Drugs

Computational and Mathematical Methods in Medicine

Received 10 October 2023; Accepted 10 October 2023; Published 11 October 2023

This article has been retracted by Hindawi following an investigation undertaken by the publisher [1]. This investigation has uncovered evidence of one or more of the following indicators of systematic manipulation of the publication process:

(1) Discrepancies in scope

(2) Discrepancies in the description of the research reported

(3) Discrepancies between the availability of data and the research described

(4) Inappropriate citations

(5) Incoherent, meaningless and/or irrelevant content included in the article

(6) Peer-review manipulation

The presence of these indicators undermines our confidence in the integrity of the article's content and we cannot, therefore, vouch for its reliability. Please note that this notice is intended solely to alert readers that the content of this article is unreliable. We have not investigated whether authors were aware of or involved in the systematic manipulation of the publication process.

Wiley and Hindawi regrets that the usual quality checks did not identify these issues before publication and have since put additional measures in place to safeguard research integrity.

We wish to credit our own Research Integrity and Research Publishing teams and anonymous and named external researchers and research integrity experts for contributing to this investigation.

The corresponding author, as the representative of all authors, has been given the opportunity to register their agreement or disagreement to this retraction. We have kept a record of any response received.

References

[1] A. A. Yahya, Y. Asiri, and I. Alyami, "Social Media Analytics for Pharmacovigilance of Antiepileptic Drugs," *Computational and Mathematical Methods in Medicine*, vol. 2022, Article ID 8965280, 24 pages, 2022.

Hindawi
Computational and Mathematical Methods in Medicine
Volume 2023, Article ID 9840132, 1 page
https://doi.org/10.1155/2023/9840132

Retraction

Retracted: COVID-19 Detection Based on Lung Ct Scan Using Deep Learning Techniques

Computational and Mathematical Methods in Medicine

Received 10 October 2023; Accepted 10 October 2023; Published 11 October 2023

This article has been retracted by Hindawi following an investigation undertaken by the publisher [1]. This investigation has uncovered evidence of one or more of the following indicators of systematic manipulation of the publication process:

(1) Discrepancies in scope

(2) Discrepancies in the description of the research reported

(3) Discrepancies between the availability of data and the research described

(4) Inappropriate citations

(5) Incoherent, meaningless and/or irrelevant content included in the article

(6) Peer-review manipulation

The presence of these indicators undermines our confidence in the integrity of the article's content and we cannot, therefore, vouch for its reliability. Please note that this notice is intended solely to alert readers that the content of this article is unreliable. We have not investigated whether authors were aware of or involved in the systematic manipulation of the publication process.

Wiley and Hindawi regrets that the usual quality checks did not identify these issues before publication and have since put additional measures in place to safeguard research integrity.

We wish to credit our own Research Integrity and Research Publishing teams and anonymous and named external researchers and research integrity experts for contributing to this investigation.

The corresponding author, as the representative of all authors, has been given the opportunity to register their agreement or disagreement to this retraction. We have kept a record of any response received.

References

[1] S. V. Kogilavani, J. Prabhu, R. Sandhiya et al., "COVID-19 Detection Based on Lung Ct Scan Using Deep Learning Techniques," *Computational and Mathematical Methods in Medicine*, vol. 2022, Article ID 7672196, 13 pages, 2022.

Hindawi
Computational and Mathematical Methods in Medicine
Volume 2023, Article ID 9823571, 1 page
https://doi.org/10.1155/2023/9823571

Retraction

Retracted: MKA: A Scalable Medical Knowledge-Assisted Mechanism for Generative Models on Medical Conversation Tasks

Computational and Mathematical Methods in Medicine

Received 10 October 2023; Accepted 10 October 2023; Published 11 October 2023

This article has been retracted by Hindawi following an investigation undertaken by the publisher [1]. This investigation has uncovered evidence of one or more of the following indicators of systematic manipulation of the publication process:

(1) Discrepancies in scope

(2) Discrepancies in the description of the research reported

(3) Discrepancies between the availability of data and the research described

(4) Inappropriate citations

(5) Incoherent, meaningless and/or irrelevant content included in the article

(6) Peer-review manipulation

The presence of these indicators undermines our confidence in the integrity of the article's content and we cannot, therefore, vouch for its reliability. Please note that this notice is intended solely to alert readers that the content of this article is unreliable. We have not investigated whether authors were aware of or involved in the systematic manipulation of the publication process.

Wiley and Hindawi regrets that the usual quality checks did not identify these issues before publication and have since put additional measures in place to safeguard research integrity.

We wish to credit our own Research Integrity and Research Publishing teams and anonymous and named external researchers and research integrity experts for contributing to this investigation.

The corresponding author, as the representative of all authors, has been given the opportunity to register their agreement or disagreement to this retraction. We have kept a record of any response received.

References

[1] K. Liang, S. Wu, and J. Gu, "MKA: A Scalable Medical Knowledge-Assisted Mechanism for Generative Models on Medical Conversation Tasks," *Computational and Mathematical Methods in Medicine*, vol. 2021, Article ID 5294627, 10 pages, 2021.

Hindawi
Computational and Mathematical Methods in Medicine
Volume 2023, Article ID 9757086, 1 page
https://doi.org/10.1155/2023/9757086

Retraction

Retracted: Internet of Things with Deep Learning-Based Face Recognition Approach for Authentication in Control Medical Systems

Computational and Mathematical Methods in Medicine

Received 10 October 2023; Accepted 10 October 2023; Published 11 October 2023

This article has been retracted by Hindawi following an investigation undertaken by the publisher [1]. This investigation has uncovered evidence of one or more of the following indicators of systematic manipulation of the publication process:

(1) Discrepancies in scope

(2) Discrepancies in the description of the research reported

(3) Discrepancies between the availability of data and the research described

(4) Inappropriate citations

(5) Incoherent, meaningless and/or irrelevant content included in the article

(6) Peer-review manipulation

The presence of these indicators undermines our confidence in the integrity of the article's content and we cannot, therefore, vouch for its reliability. Please note that this notice is intended solely to alert readers that the content of this article is unreliable. We have not investigated whether authors were aware of or involved in the systematic manipulation of the publication process.

Wiley and Hindawi regrets that the usual quality checks did not identify these issues before publication and have since put additional measures in place to safeguard research integrity.

We wish to credit our own Research Integrity and Research Publishing teams and anonymous and named external researchers and research integrity experts for contributing to this investigation.

The corresponding author, as the representative of all authors, has been given the opportunity to register their agreement or disagreement to this retraction. We have kept a record of any response received.

References

[1] T. Hussain, D. Hussain, I. Hussain et al., "Internet of Things with Deep Learning-Based Face Recognition Approach for Authentication in Control Medical Systems," *Computational and Mathematical Methods in Medicine*, vol. 2022, Article ID 5137513, 17 pages, 2022.

Hindawi
Computational and Mathematical Methods in Medicine
Volume 2023, Article ID 9846079, 1 page
https://doi.org/10.1155/2023/9846079

Retraction

Retracted: Factors That Affect Maternal Mortality in Rwanda: A Comparative Study with India and Bangladesh

Computational and Mathematical Methods in Medicine

Received 3 October 2023; Accepted 3 October 2023; Published 4 October 2023

This article has been retracted by Hindawi following an investigation undertaken by the publisher [1]. This investigation has uncovered evidence of one or more of the following indicators of systematic manipulation of the publication process:

(1) Discrepancies in scope

(2) Discrepancies in the description of the research reported

(3) Discrepancies between the availability of data and the research described

(4) Inappropriate citations

(5) Incoherent, meaningless and/or irrelevant content included in the article

(6) Peer-review manipulation

The presence of these indicators undermines our confidence in the integrity of the article's content and we cannot, therefore, vouch for its reliability. Please note that this notice is intended solely to alert readers that the content of this article is unreliable. We have not investigated whether authors were aware of or involved in the systematic manipulation of the publication process.

In addition, our investigation has also shown that one or more of the following human-subject reporting requirements has not been met in this article: ethical approval by an Institutional Review Board (IRB) committee or equivalent, patient/participant consent to participate, and/or agreement to publish patient/participant details (where relevant).

Wiley and Hindawi regrets that the usual quality checks did not identify these issues before publication and have since put additional measures in place to safeguard research integrity.

We wish to credit our own Research Integrity and Research Publishing teams and anonymous and named external researchers and research integrity experts for contributing to this investigation.

The corresponding author, as the representative of all authors, has been given the opportunity to register their agreement or disagreement to this retraction. We have kept a record of any response received.

References

[1] M. Patrick, M. S. u. Zaman, G. Afzal, M. Mahsud, and M. N. Hanifatu, "Factors That Affect Maternal Mortality in Rwanda: A Comparative Study with India and Bangladesh," *Computational and Mathematical Methods in Medicine*, vol. 2022, Article ID 1940188, 9 pages, 2022.

Hindawi
Computational and Mathematical Methods in Medicine
Volume 2023, Article ID 9796860, 1 page
https://doi.org/10.1155/2023/9796860

Retraction

Retracted: Rehabilitation Treatment of Muscle Strain in Athlete Training under Intelligent Intervention

Computational and Mathematical Methods in Medicine

Received 3 October 2023; Accepted 3 October 2023; Published 4 October 2023

This article has been retracted by Hindawi following an investigation undertaken by the publisher [1]. This investigation has uncovered evidence of one or more of the following indicators of systematic manipulation of the publication process:

(1) Discrepancies in scope

(2) Discrepancies in the description of the research reported

(3) Discrepancies between the availability of data and the research described

(4) Inappropriate citations

(5) Incoherent, meaningless and/or irrelevant content included in the article

(6) Peer-review manipulation

The presence of these indicators undermines our confidence in the integrity of the article's content and we cannot, therefore, vouch for its reliability. Please note that this notice is intended solely to alert readers that the content of this article is unreliable. We have not investigated whether authors were aware of or involved in the systematic manipulation of the publication process.

In addition, our investigation has also shown that one or more of the following human-subject reporting requirements has not been met in this article: ethical approval by an Institutional Review Board (IRB) committee or equivalent, patient/participant consent to participate, and/or agreement to publish patient/participant details (where relevant).

Wiley and Hindawi regrets that the usual quality checks did not identify these issues before publication and have since put additional measures in place to safeguard research integrity.

We wish to credit our own Research Integrity and Research Publishing teams and anonymous and named external researchers and research integrity experts for contributing to this investigation.

The corresponding author, as the representative of all authors, has been given the opportunity to register their agreement or disagreement to this retraction. We have kept a record of any response received.

References

[1] Y. Qiao, L. Zhang, and B. Zhang, "Rehabilitation Treatment of Muscle Strain in Athlete Training under Intelligent Intervention," *Computational and Mathematical Methods in Medicine*, vol. 2022, Article ID 5403681, 11 pages, 2022.

Hindawi
Computational and Mathematical Methods in Medicine
Volume 2023, Article ID 9858237, 1 page
https://doi.org/10.1155/2023/9858237

Retraction

Retracted: Evaluating Deep Neural Network Architectures with Transfer Learning for Pneumonitis Diagnosis

Computational and Mathematical Methods in Medicine

Received 8 August 2023; Accepted 8 August 2023; Published 9 August 2023

This article has been retracted by Hindawi following an investigation undertaken by the publisher [1]. This investigation has uncovered evidence of one or more of the following indicators of systematic manipulation of the publication process:

(1) Discrepancies in scope

(2) Discrepancies in the description of the research reported

(3) Discrepancies between the availability of data and the research described

(4) Inappropriate citations

(5) Incoherent, meaningless and/or irrelevant content included in the article

(6) Peer-review manipulation

The presence of these indicators undermines our confidence in the integrity of the article's content and we cannot, therefore, vouch for its reliability. Please note that this notice is intended solely to alert readers that the content of this article is unreliable. We have not investigated whether authors were aware of or involved in the systematic manipulation of the publication process.

Wiley and Hindawi regrets that the usual quality checks did not identify these issues before publication and have since put additional measures in place to safeguard research integrity.

We wish to credit our own Research Integrity and Research Publishing teams and anonymous and named external researchers and research integrity experts for contributing to this investigation.

The corresponding author, as the representative of all authors, has been given the opportunity to register their agreement or disagreement to this retraction. We have kept a record of any response received.

References

[1] S. Krishnamurthy, K. Srinivasan, S. M. Qaisar, P. M. D. R. Vincent, and C. Chang, "Evaluating Deep Neural Network Architectures with Transfer Learning for Pneumonitis Diagnosis," *Computational and Mathematical Methods in Medicine*, vol. 2021, Article ID 8036304, 12 pages, 2021.

Hindawi
Computational and Mathematical Methods in Medicine
Volume 2023, Article ID 9849173, 1 page
https://doi.org/10.1155/2023/9849173

Retraction

Retracted: Machine Learning-Based Automated Diagnostic Systems Developed for Heart Failure Prediction Using Different Types of Data Modalities: A Systematic Review and Future Directions

Computational and Mathematical Methods in Medicine

Received 8 August 2023; Accepted 8 August 2023; Published 9 August 2023

This article has been retracted by Hindawi following an investigation undertaken by the publisher [1]. This investigation has uncovered evidence of one or more of the following indicators of systematic manipulation of the publication process:

(1) Discrepancies in scope

(2) Discrepancies in the description of the research reported

(3) Discrepancies between the availability of data and the research described

(4) Inappropriate citations

(5) Incoherent, meaningless and/or irrelevant content included in the article

(6) Peer-review manipulation

The presence of these indicators undermines our confidence in the integrity of the article's content and we cannot, therefore, vouch for its reliability. Please note that this notice is intended solely to alert readers that the content of this article is unreliable. We have not investigated whether authors were aware of or involved in the systematic manipulation of the publication process.

Wiley and Hindawi regrets that the usual quality checks did not identify these issues before publication and have since put additional measures in place to safeguard research integrity.

We wish to credit our own Research Integrity and Research Publishing teams and anonymous and named external researchers and research integrity experts for contributing to this investigation.

The corresponding author, as the representative of all authors, has been given the opportunity to register their agreement or disagreement to this retraction. We have kept a record of any response received.

References

[1] A. Javeed, S. U. Khan, L. Ali, S. Ali, Y. Imrana, and A. Rahman, "Machine Learning-Based Automated Diagnostic Systems Developed for Heart Failure Prediction Using Different Types of Data Modalities: A Systematic Review and Future Directions," *Computational and Mathematical Methods in Medicine*, vol. 2022, Article ID 9288452, 30 pages, 2022.

Hindawi
Computational and Mathematical Methods in Medicine
Volume 2023, Article ID 9897817, 1 page
https://doi.org/10.1155/2023/9897817

Retraction

Retracted: Energy Efficiency and Reliability Considerations in Wireless Body Area Networks: A Survey

Computational and Mathematical Methods in Medicine

Received 1 August 2023; Accepted 1 August 2023; Published 2 August 2023

This article has been retracted by Hindawi following an investigation undertaken by the publisher [1]. This investigation has uncovered evidence of one or more of the following indicators of systematic manipulation of the publication process:

(1) Discrepancies in scope

(2) Discrepancies in the description of the research reported

(3) Discrepancies between the availability of data and the research described

(4) Inappropriate citations

(5) Incoherent, meaningless and/or irrelevant content included in the article

(6) Peer-review manipulation

The presence of these indicators undermines our confidence in the integrity of the article's content and we cannot, therefore, vouch for its reliability. Please note that this notice is intended solely to alert readers that the content of this article is unreliable. We have not investigated whether authors were aware of or involved in the systematic manipulation of the publication process.

Wiley and Hindawi regrets that the usual quality checks did not identify these issues before publication and have since put additional measures in place to safeguard research integrity.

We wish to credit our own Research Integrity and Research Publishing teams and anonymous and named external researchers and research integrity experts for contributing to this investigation.

The corresponding author, as the representative of all authors, has been given the opportunity to register their agreement or disagreement to this retraction. We have kept a record of any response received.

References

[1] F. Ullah, M. Z. Khan, G. Mehmood, M. S. Qureshi, and M. Fayaz, "Energy Efficiency and Reliability Considerations in Wireless Body Area Networks: A Survey," *Computational and Mathematical Methods in Medicine*, vol. 2022, Article ID 1090131, 15 pages, 2022.

Hindawi
Computational and Mathematical Methods in Medicine
Volume 2023, Article ID 9825640, 1 page
https://doi.org/10.1155/2023/9825640

Retraction

Retracted: A Systematic Literature Review on Particle Swarm Optimization Techniques for Medical Diseases Detection

Computational and Mathematical Methods in Medicine

Received 1 August 2023; Accepted 1 August 2023; Published 2 August 2023

This article has been retracted by Hindawi following an investigation undertaken by the publisher [1]. This investigation has uncovered evidence of one or more of the following indicators of systematic manipulation of the publication process:

(1) Discrepancies in scope

(2) Discrepancies in the description of the research reported

(3) Discrepancies between the availability of data and the research described

(4) Inappropriate citations

(5) Incoherent, meaningless and/or irrelevant content included in the article

(6) Peer-review manipulation

The presence of these indicators undermines our confidence in the integrity of the article's content and we cannot, therefore, vouch for its reliability. Please note that this notice is intended solely to alert readers that the content of this article is unreliable. We have not investigated whether authors were aware of or involved in the systematic manipulation of the publication process.

Wiley and Hindawi regrets that the usual quality checks did not identify these issues before publication and have since put additional measures in place to safeguard research integrity.

We wish to credit our own Research Integrity and Research Publishing teams and anonymous and named external researchers and research integrity experts for contributing to this investigation.

The corresponding author, as the representative of all authors, has been given the opportunity to register their agreement or disagreement to this retraction. We have kept a record of any response received.

References

[1] S. Pervaiz, Z. Ul-Qayyum, W. H. Bangyal, L. Gao, and J. Ahmad, "A Systematic Literature Review on Particle Swarm Optimization Techniques for Medical Diseases Detection," *Computational and Mathematical Methods in Medicine*, vol. 2021, Article ID 5990999, 10 pages, 2021.

Hindawi
Computational and Mathematical Methods in Medicine
Volume 2023, Article ID 9795312, 1 page
https://doi.org/10.1155/2023/9795312

Retraction

Retracted: Efficient Prediction of Missed Clinical Appointment Using Machine Learning

Computational and Mathematical Methods in Medicine

Received 1 August 2023; Accepted 1 August 2023; Published 2 August 2023

This article has been retracted by Hindawi following an investigation undertaken by the publisher [1]. This investigation has uncovered evidence of one or more of the following indicators of systematic manipulation of the publication process:

(1) Discrepancies in scope

(2) Discrepancies in the description of the research reported

(3) Discrepancies between the availability of data and the research described

(4) Inappropriate citations

(5) Incoherent, meaningless and/or irrelevant content included in the article

(6) Peer-review manipulation

The presence of these indicators undermines our confidence in the integrity of the article's content and we cannot, therefore, vouch for its reliability. Please note that this notice is intended solely to alert readers that the content of this article is unreliable. We have not investigated whether authors were aware of or involved in the systematic manipulation of the publication process.

Wiley and Hindawi regrets that the usual quality checks did not identify these issues before publication and have since put additional measures in place to safeguard research integrity.

We wish to credit our own Research Integrity and Research Publishing teams and anonymous and named external researchers and research integrity experts for contributing to this investigation.

The corresponding author, as the representative of all authors, has been given the opportunity to register their agreement or disagreement to this retraction. We have kept a record of any response received.

References

[1] Z. Qureshi, A. Maqbool, A. Mirza et al., "Efficient Prediction of Missed Clinical Appointment Using Machine Learning," *Computational and Mathematical Methods in Medicine*, vol. 2021, Article ID 2376391, 10 pages, 2021.

Hindawi
Computational and Mathematical Methods in Medicine
Volume 2023, Article ID 9785636, 1 page
https://doi.org/10.1155/2023/9785636

Retraction

Retracted: Brain Decoding Using fMRI Images for Multiple Subjects through Deep Learning

Computational and Mathematical Methods in Medicine

Received 1 August 2023; Accepted 1 August 2023; Published 2 August 2023

This article has been retracted by Hindawi following an investigation undertaken by the publisher [1]. This investigation has uncovered evidence of one or more of the following indicators of systematic manipulation of the publication process:

(1) Discrepancies in scope

(2) Discrepancies in the description of the research reported

(3) Discrepancies between the availability of data and the research described

(4) Inappropriate citations

(5) Incoherent, meaningless and/or irrelevant content included in the article

(6) Peer-review manipulation

The presence of these indicators undermines our confidence in the integrity of the article's content and we cannot, therefore, vouch for its reliability. Please note that this notice is intended solely to alert readers that the content of this article is unreliable. We have not investigated whether authors were aware of or involved in the systematic manipulation of the publication process.

Wiley and Hindawi regrets that the usual quality checks did not identify these issues before publication and have since put additional measures in place to safeguard research integrity.

We wish to credit our own Research Integrity and Research Publishing teams and anonymous and named external researchers and research integrity experts for contributing to this investigation.

The corresponding author, as the representative of all authors, has been given the opportunity to register their agreement or disagreement to this retraction. We have kept a record of any response received.

References

[1] M. B. Qureshi, L. Azad, M. S. Qureshi, S. Aslam, A. Aljarbouh, and M. Fayaz, "Brain Decoding Using fMRI Images for Multiple Subjects through Deep Learning," *Computational and Mathematical Methods in Medicine*, vol. 2022, Article ID 1124927, 10 pages, 2022.

Hindawi
Computational and Mathematical Methods in Medicine
Volume 2023, Article ID 9828324, 1 page
https://doi.org/10.1155/2023/9828324

Retraction

Retracted: Influence of Health Education Based on IMB on Prognosis and Self-Management Behavior of Patients with Chronic Heart Failure

Computational and Mathematical Methods in Medicine

Received 27 June 2023; Accepted 27 June 2023; Published 28 June 2023

This article has been retracted by Hindawi following an investigation undertaken by the publisher [1]. This investigation has uncovered evidence of one or more of the following indicators of systematic manipulation of the publication process:

(1) Discrepancies in scope

(2) Discrepancies in the description of the research reported

(3) Discrepancies between the availability of data and the research described

(4) Inappropriate citations

(5) Incoherent, meaningless and/or irrelevant content included in the article

(6) Peer-review manipulation

The presence of these indicators undermines our confidence in the integrity of the article's content and we cannot, therefore, vouch for its reliability. Please note that this notice is intended solely to alert readers that the content of this article is unreliable. We have not investigated whether authors were aware of or involved in the systematic manipulation of the publication process.

In addition, our investigation has also shown that one or more of the following human-subject reporting requirements has not been met in this article: ethical approval by an Institutional Review Board (IRB) committee or equivalent, patient/participant consent to participate, and/or agreement to publish patient/participant details (where relevant).

Wiley and Hindawi regrets that the usual quality checks did not identify these issues before publication and have since put additional measures in place to safeguard research integrity.

We wish to credit our own Research Integrity and Research Publishing teams and anonymous and named external researchers and research integrity experts for contributing to this investigation.

The corresponding author, as the representative of all authors, has been given the opportunity to register their agreement or disagreement to this retraction. We have kept a record of any response received.

References

[1] W. Liu, Y. Zhang, H. Liu, T. Song, and S. Wang, "Influence of Health Education Based on IMB on Prognosis and Self-Management Behavior of Patients with Chronic Heart Failure," *Computational and Mathematical Methods in Medicine*, vol. 2022, Article ID 8517802, 13 pages, 2022.

Hindawi
Computational and Mathematical Methods in Medicine
Volume 2023, Article ID 9827568, 1 page
https://doi.org/10.1155/2023/9827568

Retraction

Retracted: Left Atrial Appendage Depth and Tachycardia Bradycardia Syndrome as Important Predictors of Left Atrial Appendage Thrombus in Patients with Nonvalvular Atrial Fibrillation

Computational and Mathematical Methods in Medicine

Received 27 June 2023; Accepted 27 June 2023; Published 28 June 2023

This article has been retracted by Hindawi following an investigation undertaken by the publisher [1] This investigation has uncovered evidence of one or more of the following indicators of systematic manipulation of the publication process:

(1) Discrepancies in scope

(2) Discrepancies in the description of the research reported

(3) Discrepancies between the availability of data and the research described

(4) Inappropriate citations

(5) Incoherent, meaningless and/or irrelevant content included in the article

(6) Peer-review manipulation

The presence of these indicators undermines our confidence in the integrity of the article's content and we cannot, therefore, vouch for its reliability. Please note that this notice is intended solely to alert readers that the content of this article is unreliable. We have not investigated whether authors were aware of or nvolved in the systematic manipulation of the publication process.

In addition, our investigation has also shown that one or more of the following human-subject reporting requirements has not been met in this article: ethical approval by an Institutional Review Board (IRB) committee or equivalent, patient/participant consent to participate, and/or agreement to publish patient/participant details (where relevant).

Wiley and Hindawi regrets that the usual quality checks did not identify these issues before publication and have since put additional measures in place to safeguard research integrity.

We wish to credit our own Research Integrity and Research Publishing teams and anonymous and named external researchers and research integrity experts for contributing to this investigation.

The corresponding author, as the representative of all authors, has been given the opportunity to register their agreement or disagreement to this retraction. We have kept a record of any response received.

References

[1] Y. He, P. Chen, Z. Zhu, J. Sun, and Y. Zhao, "Left Atrial Appendage Depth and Tachycardia Bradycardia Syndrome as Important Predictors of Left Atrial Appendage Thrombus in Patients with Nonvalvular Atrial Fibrillation," *Computational and Mathematical Methods in Medicine*, vol. 2022, Article ID 4632823, 5 pages, 2022.

Hindawi
Computational and Mathematical Methods in Medicine
Volume 2023, Article ID 9826547, 1 page
https://doi.org/10.1155/2023/9826547

Retraction

Retracted: Self-Adaptation Resource Allocation for Continuous Offloading Tasks in Pervasive Computing

Computational and Mathematical Methods in Medicine

Received 27 June 2023; Accepted 27 June 2023; Published 28 June 2023

This article has been retracted by Hindawi following an investigation undertaken by the publisher [1]. This investigation has uncovered evidence of one or more of the following indicators of systematic manipulation of the publication process:

(1) Discrepancies in scope

(2) Discrepancies in the description of the research reported

(3) Discrepancies between the availability of data and the research described

(4) Inappropriate citations

(5) Incoherent, meaningless and/or irrelevant content included in the article

(6) Peer-review manipulation

The presence of these indicators undermines our confidence in the integrity of the article's content and we cannot, therefore, vouch for its reliability. Please note that this notice is intended solely to alert readers that the content of this article is unreliable. We have not investigated whether authors were aware of or involved in the systematic manipulation of the publication process.

Wiley and Hindawi regrets that the usual quality checks did not identify these issues before publication and have since put additional measures in place to safeguard research integrity.

We wish to credit our own Research Integrity and Research Publishing teams and anonymous and named external researchers and research integrity experts for contributing to this investigation.

The corresponding author, as the representative of all authors, has been given the opportunity to register their agreement or disagreement to this retraction. We have kept a record of any response received.

References

[1] A. Ehsan, K. Z. Haider, S. Faisal, F. M. Zahid, and I. M. Wangari, "Self-Adaptation Resource Allocation for Continuous Offloading Tasks in Pervasive Computing," *Computational and Mathematical Methods in Medicine*, vol. 2022, Article ID 8040487, 13 pages, 2022.

Hindawi
Computational and Mathematical Methods in Medicine
Volume 2023, Article ID 9826474, 1 page
https://doi.org/10.1155/2023/9826474

Retraction

Retracted: GEO Database Screening Combined with In Vitro Experiments to Study the Mechanism of hsa_circ_0003570 in Infantile Hemangiomas

Computational and Mathematical Methods in Medicine

Received 27 June 2023; Accepted 27 June 2023; Published 28 June 2023

This article has been retracted by Hindawi following an investigation undertaken by the publisher [1]. This investigation has uncovered evidence of one or more of the following indicators of systematic manipulation of the publication process:

(1) Discrepancies in scope

(2) Discrepancies in the description of the research reported

(3) Discrepancies between the availability of data and the research described

(4) Inappropriate citations

(5) Incoherent, meaningless and/or irrelevant content included in the article

(6) Peer-review manipulation

The presence of these indicators undermines our confidence in the integrity of the article's content and we cannot, therefore, vouch for its reliability. Please note that this notice is intended solely to alert readers that the content of this article is unreliable. We have not investigated whether authors were aware of or involved in the systematic manipulation of the publication process.

Wiley and Hindawi regrets that the usual quality checks did not identify these issues before publication and have since put additional measures in place to safeguard research integrity.

We wish to credit our own Research Integrity and Research Publishing teams and anonymous and named external researchers and research integrity experts for contributing to this investigation.

The corresponding author, as the representative of all authors, has been given the opportunity to register their agreement or disagreement to this retraction. We have kept a record of any response received.

References

[1] Y. Tian, S. Zhuang, J. Zhang et al., "GEO Database Screening Combined with In Vitro Experiments to Study the Mechanism of hsa_circ_0003570 in Infantile Hemangiomas," *Computational and Mathematical Methods in Medicine*, vol. 2022, Article ID 5643742, 13 pages, 2022.

Hindawi
Computational and Mathematical Methods in Medicine
Volume 2023, Article ID 9814020, 1 page
https://doi.org/10.1155/2023/9814020

Retraction

Retracted: Controversy on Positive Peritoneal Cytology of Endometrial Carcinoma

Computational and Mathematical Methods in Medicine

Received 27 June 2023; Accepted 27 June 2023; Published 28 June 2023

This article has been retracted by Hindawi following an investigation undertaken by the publisher [1]. This investigation has uncovered evidence of one or more of the following indicators of systematic manipulation of the publication process:

(1) Discrepancies in scope

(2) Discrepancies in the description of the research reported

(3) Discrepancies between the availability of data and the research described

(4) Inappropriate citations

(5) Incoherent, meaningless and/or irrelevant content included in the article

(6) Peer-review manipulation

The presence of these indicators undermines our confidence in the integrity of the article's content and we cannot, therefore, vouch for its reliability. Please note that this notice is intended solely to alert readers that the content of this article is unreliable. We have not investigated whether authors were aware of or involved in the systematic manipulation of the publication process.

Wiley and Hindawi regrets that the usual quality checks did not identify these issues before publication and have since put additional measures in place to safeguard research integrity.

We wish to credit our own Research Integrity and Research Publishing teams and anonymous and named external researchers and research integrity experts for contributing to this investigation.

The corresponding author, as the representative of all authors, has been given the opportunity to register their agreement or disagreement to this retraction. We have kept a record of any response received.

References

[1] Y. Liu, H. Wang, and Y. Gao, "Controversy on Positive Peritoneal Cytology of Endometrial Carcinoma," *Computational and Mathematical Methods in Medicine*, vol. 2022, Article ID 1906769, 5 pages, 2022.

Hindawi
Computational and Mathematical Methods in Medicine
Volume 2023, Article ID 9808106, 1 page
https://doi.org/10.1155/2023/9808106

Retraction

Retracted: Corydalis decumbens Can Exert Analgesic Effects in a Mouse Neuropathic Pain Model by Modulating MAPK Signaling

Computational and Mathematical Methods in Medicine

Received 27 June 2023; Accepted 27 June 2023; Published 28 June 2023

This article has been retracted by Hindawi following an investigation undertaken by the publisher [1]. This investigation has uncovered evidence of one or more of the following indicators of systematic manipulation of the publication process:

(1) Discrepancies in scope

(2) Discrepancies in the description of the research reported

(3) Discrepancies between the availability of data and the research described

(4) Inappropriate citations

(5) Incoherent, meaningless and/or irrelevant content included in the article

(6) Peer-review manipulation

The presence of these indicators undermines our confidence in the integrity of the article's content and we cannot, therefore, vouch for its reliability. Please note that this notice is intended solely to alert readers that the content of this article is unreliable. We have not investigated whether authors were aware of or involved in the systematic manipulation of the publication process.

Wiley and Hindawi regrets that the usual quality checks did not identify these issues before publication and have since put additional measures in place to safeguard research integrity.

We wish to credit our own Research Integrity and Research Publishing teams and anonymous and named external researchers and research integrity experts for contributing to this investigation.

The corresponding author, as the representative of all authors, has been given the opportunity to register their agreement or disagreement to this retraction. We have kept a record of any response received.

References

[1] Y. Chen, Z. Jiang, A. Zhang, R. He, Z. Zhou, and S. Xu, "Corydalis decumbens Can Exert Analgesic Effects in a Mouse Neuropathic Pain Model by Modulating MAPK Signaling," *Computational and Mathematical Methods in Medicine*, vol. 2022, Article ID 7722951, 8 pages, 2022.

Hindawi
Computational and Mathematical Methods in Medicine
Volume 2023, Article ID 9804984, 1 page
https://doi.org/10.1155/2023/9804984

Retraction

Retracted: Timosaponin AIII Suppresses RAP1 Signaling Pathway to Enhance the Inhibitory Effect of Paclitaxel on Nasopharyngeal Carcinoma

Computational and Mathematical Methods in Medicine

Received 27 June 2023; Accepted 27 June 2023; Published 28 June 2023

This article has been retracted by Hindawi following an investigation undertaken by the publisher [1]. This investigation has uncovered evidence of one or more of the following indicators of systematic manipulation of the publication process:

(1) Discrepancies in scope

(2) Discrepancies in the description of the research reported

(3) Discrepancies between the availability of data and the research described

(4) Inappropriate citations

(5) Incoherent, meaningless and/or irrelevant content included in the article

(6) Peer-review manipulation

The presence of these indicators undermines our confidence in the integrity of the article's content and we cannot, therefore, vouch for its reliability. Please note that this notice is intended solely to alert readers that the content of this article is unreliable. We have not investigated whether authors were aware of or involved in the systematic manipulation of the publication process.

Wiley and Hindawi regrets that the usual quality checks did not identify these issues before publication and have since put additional measures in place to safeguard research integrity.

We wish to credit our own Research Integrity and Research Publishing teams and anonymous and named external researchers and research integrity experts for contributing to this investigation.

The corresponding author, as the representative of all authors, has been given the opportunity to register their agreement or disagreement to this retraction. We have kept a record of any response received.

References

[1] X. Li, W. Lu, T. Zhou, F. Zhao, and L. Yang, "Timosaponin AIII Suppresses RAP1 Signaling Pathway to Enhance the Inhibitory Effect of Paclitaxel on Nasopharyngeal Carcinoma," *Computational and Mathematical Methods in Medicine*, vol. 2022, Article ID 6756676, 8 pages, 2022.

Hindawi
Computational and Mathematical Methods in Medicine
Volume 2023, Article ID 9791271, 1 page
https://doi.org/10.1155/2023/9791271

Retraction

Retracted: The Effect of Endoscopy on Patients with Malignant Esophageal Cancer after Medical Treatment and Chemotherapy

Computational and Mathematical Methods in Medicine

Received 27 June 2023; Accepted 27 June 2023; Published 28 June 2023

This article has been retracted by Hindawi following an investigation undertaken by the publisher [1]. This investigation has uncovered evidence of one or more of the following indicators of systematic manipulation of the publication process:

(1) Discrepancies in scope

(2) Discrepancies in the description of the research reported

(3) Discrepancies between the availability of data and the research described

(4) Inappropriate citations

(5) Incoherent, meaningless and/or irrelevant content included in the article

(6) Peer-review manipulation

The presence of these indicators undermines our confidence in the integrity of the article's content and we cannot, therefore, vouch for its reliability. Please note that this notice is intended solely to alert readers that the content of this article is unreliable. We have not investigated whether authors were aware of or involved in the systematic manipulation of the publication process.

Wiley and Hindawi regrets that the usual quality checks did not identify these issues before publication and have since put additional measures in place to safeguard research integrity.

We wish to credit our own Research Integrity and Research Publishing teams and anonymous and named external researchers and research integrity experts for contributing to this investigation.

The corresponding author, as the representative of all authors, has been given the opportunity to register their agreement or disagreement to this retraction. We have kept a record of any response received.

References

[1] Y. Liu, L. Zhao, X. Tan, N. Liu, and T. Long, "The Effect of Endoscopy on Patients with Malignant Esophageal Cancer after Medical Treatment and Chemotherapy," *Computational and Mathematical Methods in Medicine*, vol. 2022, Article ID 7906302, 12 pages, 2022.

Hindawi
Computational and Mathematical Methods in Medicine
Volume 2023, Article ID 9785034, 1 page
https://doi.org/10.1155/2023/9785034

Retraction

Retracted: lncRNA GHET1 Promotes the Progression of Triple-Negative Breast Cancer via Regulation of miR-377-3p/GRSF1 Signaling Axis

Computational and Mathematical Methods in Medicine

Received 27 June 2023; Accepted 27 June 2023; Published 28 June 2023

This article has been retracted by Hindawi following an investigation undertaken by the publisher [1]. This investigation has uncovered evidence of one or more of the following indicators of systematic manipulation of the publication process:

(1) Discrepancies in scope

(2) Discrepancies in the description of the research reported

(3) Discrepancies between the availability of data and the research described

(4) Inappropriate citations

(5) Incoherent, meaningless and/or irrelevant content included in the article

(6) Peer-review manipulation

The presence of these indicators undermines our confidence in the integrity of the article's content and we cannot, therefore, vouch for its reliability. Please note that this notice is intended solely to alert readers that the content of this article is unreliable. We have not investigated whether authors were aware of or involved in the systematic manipulation of the publication process.

Wiley and Hindawi regrets that the usual quality checks did not identify these issues before publication and have since put additional measures in place to safeguard research integrity.

We wish to credit our own Research Integrity and Research Publishing teams and anonymous and named external researchers and research integrity experts for contributing to this investigation.

The corresponding author, as the representative of all authors, has been given the opportunity to register their agreement or disagreement to this retraction. We have kept a record of any response received.

References

[1] Y. Wang and C. Li, "lncRNA GHET1 Promotes the Progression of Triple-Negative Breast Cancer via Regulation of miR-377-3p/GRSF1 Signaling Axis," *Computational and Mathematical Methods in Medicine*, vol. 2022, Article ID 8366569, 15 pages, 2022.

Hindawi
Computational and Mathematical Methods in Medicine
Volume 2023, Article ID 9767846, 1 page
https://doi.org/10.1155/2023/9767846

Retraction

Retracted: Information Monitoring of Animal Husbandry Industry Based on the Internet of Things and Wireless Communication System

Computational and Mathematical Methods in Medicine

Received 27 June 2023; Accepted 27 June 2023; Published 28 June 2023

This article has been retracted by Hindawi following an investigation undertaken by the publisher [1]. This investigation has uncovered evidence of one or more of the following indicators of systematic manipulation of the publication process:

(1) Discrepancies in scope

(2) Discrepancies in the description of the research reported

(3) Discrepancies between the availability of data and the research described

(4) Inappropriate citations

(5) Incoherent, meaningless and/or irrelevant content included in the article

(6) Peer-review manipulation

The presence of these indicators undermines our confidence in the integrity of the article's content and we cannot, therefore, vouch for its reliability. Please note that this notice is intended solely to alert readers that the content of this article is unreliable. We have not investigated whether authors were aware of or involved in the systematic manipulation of the publication process.

Wiley and Hindawi regrets that the usual quality checks did not identify these issues before publication and have since put additional measures in place to safeguard research integrity.

We wish to credit our own Research Integrity and Research Publishing teams and anonymous and named external researchers and research integrity experts for contributing to this investigation.

The corresponding author, as the representative of all authors, has been given the opportunity to register their agreement or disagreement to this retraction. We have kept a record of any response received.

References

[1] Y. Shen, "Information Monitoring of Animal Husbandry Industry Based on the Internet of Things and Wireless Communication System," *Computational and Mathematical Methods in Medicine*, vol. 2022, Article ID 8794044, 12 pages, 2022.

Hindawi
Computational and Mathematical Methods in Medicine
Volume 2023, Article ID 9765359, 1 page
https://doi.org/10.1155/2023/9765359

Retraction

Retracted: miR-141-3p Regulates EZH2 to Attenuate Porphyromonas gingivalis Lipopolysaccharide-Caused Inflammation and Inhibition of Osteogenic Differentiation in Human Periodontal Ligament Stem Cells

Computational and Mathematical Methods in Medicine

Received 27 June 2023; Accepted 27 June 2023; Published 28 June 2023

This article has been retracted by Hindawi following an investigation undertaken by the publisher [1]. This investigation has uncovered evidence of one or more of the following indicators of systematic manipulation of the publication process:

(1) Discrepancies in scope

(2) Discrepancies in the description of the research reported

(3) Discrepancies between the availability of data and the research described

(4) Inappropriate citations

(5) Incoherent, meaningless and/or irrelevant content included in the article

(6) Peer-review manipulation

The presence of these indicators undermines our confidence in the integrity of the article's content and we cannot, therefore, vouch for its reliability. Please note that this notice is intended solely to alert readers that the content of this article is unreliable. We have not investigated whether authors were aware of or involved in the systematic manipulation of the publication process.

Wiley and Hindawi regrets that the usual quality checks did not identify these issues before publication and have since put additional measures in place to safeguard research integrity.

We wish to credit our own Research Integrity and Research Publishing teams and anonymous and named external researchers and research integrity experts for contributing to this investigation.

The corresponding author, as the representative of all authors, has been given the opportunity to register their agreement or disagreement to this retraction. We have kept a record of any response received.

References

[1] Z. Zhu and J. Xiong, "miR-141-3p Regulates EZH2 to Attenuate Porphyromonas gingivalis Lipopolysaccharide-Caused Inflammation and Inhibition of Osteogenic Differentiation in Human Periodontal Ligament Stem Cells," *Computational and Mathematical Methods in Medicine*, vol. 2022, Article ID 4634925, 11 pages, 2022.

Hindawi
Computational and Mathematical Methods in Medicine
Volume 2023, Article ID 9756383, 1 page
https://doi.org/10.1155/2023/9756383

Retraction

Retracted: Network Information Security Platform Based on Artificial Intelligence for the Elderly's Health "Integration of Physical, Medical, and Nursing Care"

Computational and Mathematical Methods in Medicine

Received 27 June 2023; Accepted 27 June 2023; Published 28 June 2023

This article has been retracted by Hindawi following an investigation undertaken by the publisher [1]. This investigation has uncovered evidence of one or more of the following indicators of systematic manipulation of the publication process:

(1) Discrepancies in scope

(2) Discrepancies in the description of the research reported

(3) Discrepancies between the availability of data and the research described

(4) Inappropriate citations

(5) Incoherent, meaningless and/or irrelevant content included in the article

(6) Peer-review manipulation

The presence of these indicators undermines our confidence in the integrity of the article's content and we cannot, therefore, vouch for its reliability. Please note that this notice is intended solely to alert readers that the content of this article is unreliable. We have not investigated whether authors were aware of or involved in the systematic manipulation of the publication process.

Wiley and Hindawi regrets that the usual quality checks did not identify these issues before publication and have since put additional measures in place to safeguard research integrity.

We wish to credit our own Research Integrity and Research Publishing teams and anonymous and named external researchers and research integrity experts for contributing to this investigation.

The corresponding author, as the representative of all authors, has been given the opportunity to register their agreement or disagreement to this retraction. We have kept a record of any response received.

References

[1] Z. Yang, S. Xia, and S. Feng, "Network Information Security Platform Based on Artificial Intelligence for the Elderly's Health "Integration of Physical, Medical, and Nursing Care"," *Computational and Mathematical Methods in Medicine*, vol. 2022, Article ID 5975054, 11 pages, 2022.

Hindawi
Computational and Mathematical Methods in Medicine
Volume 2023, Article ID 9753817, 1 page
https://doi.org/10.1155/2023/9753817

Retraction

Retracted: Effect of Dexmedetomidine on Cardiac Output among Parturient with Severe Preeclampsia after Cesarean Section

Computational and Mathematical Methods in Medicine

Received 27 June 2023; Accepted 27 June 2023; Published 28 June 2023

This article has been retracted by Hindawi following an investigation undertaken by the publisher [1]. This investigation has uncovered evidence of one or more of the following indicators of systematic manipulation of the publication process:

(1) Discrepancies in scope

(2) Discrepancies in the description of the research reported

(3) Discrepancies between the availability of data and the research described

(4) Inappropriate citations

(5) Incoherent, meaningless and/or irrelevant content included in the article

(6) Peer-review manipulation

The presence of these indicators undermines our confidence in the integrity of the article's content and we cannot, therefore, vouch for its reliability. Please note that this notice is intended solely to alert readers that the content of this article is unreliable. We have not investigated whether authors were aware of or involved in the systematic manipulation of the publication process.

Wiley and Hindawi regrets that the usual quality checks did not identify these issues before publication and have since put additional measures in place to safeguard research integrity.

We wish to credit our own Research Integrity and Research Publishing teams and anonymous and named external researchers and research integrity experts for contributing to this investigation.

The corresponding author, as the representative of all authors, has been given the opportunity to register their agreement or disagreement to this retraction. We have kept a record of any response received.

References

[1] Y. Lv, Y. Zhou, Y. Qiao et al., "Effect of Dexmedetomidine on Cardiac Output among Parturient with Severe Preeclampsia after Cesarean Section," *Computational and Mathematical Methods in Medicine*, vol. 2022, Article ID 4742350, 7 pages, 2022.

Hindawi
Computational and Mathematical Methods in Medicine
Volume 2023, Article ID 9895751, 1 page
https://doi.org/10.1155/2023/9895751

Retraction

Retracted: Analysis of Influencing Factors for Chronic Diseases: A Large Sample Epidemiological Survey from Liaoyang

Computational and Mathematical Methods in Medicine

Received 27 June 2023; Accepted 27 June 2023; Published 28 June 2023

This article has been retracted by Hindawi following an investigation undertaken by the publisher [1]. This investigation has uncovered evidence of one or more of the following indicators of systematic manipulation of the publication process:

(1) Discrepancies in scope

(2) Discrepancies in the description of the research reported

(3) Discrepancies between the availability of data and the research described

(4) Inappropriate citations

(5) Incoherent, meaningless and/or irrelevant content included in the article

(6) Peer-review manipulation

The presence of these indicators undermines our confidence in the integrity of the article's content and we cannot, therefore, vouch for its reliability. Please note that this notice is intended solely to alert readers that the content of this article is unreliable. We have not investigated whether authors were aware of or involved in the systematic manipulation of the publication process.

Wiley and Hindawi regrets that the usual quality checks did not identify these issues before publication and have since put additional measures in place to safeguard research integrity.

We wish to credit our own Research Integrity and Research Publishing teams and anonymous and named external researchers and research integrity experts for contributing to this investigation.

The corresponding author, as the representative of all authors, has been given the opportunity to register their agreement or disagreement to this retraction. We have kept a record of any response received.

References

[1] C. Jiang and Q. Wang, "Analysis of Influencing Factors for Chronic Diseases: A Large Sample Epidemiological Survey from Liaoyang," *Computational and Mathematical Methods in Medicine*, vol. 2022, Article ID 1537906, 6 pages, 2022.

Hindawi
Computational and Mathematical Methods in Medicine
Volume 2023, Article ID 9875676, 1 page
https://doi.org/10.1155/2023/9875676

Retraction

Retracted: An Improved Strategy for Task Scheduling in the Parallel Computational Alignment of Multiple Sequences

Computational and Mathematical Methods in Medicine

Received 27 June 2023; Accepted 27 June 2023; Published 28 June 2023

This article has been retracted by Hindawi following an investigation undertaken by the publisher [1]. This investigation has uncovered evidence of one or more of the following indicators of systematic manipulation of the publication process:

(1) Discrepancies in scope

(2) Discrepancies in the description of the research reported

(3) Discrepancies between the availability of data and the research described

(4) Inappropriate citations

(5) Incoherent, meaningless and/or irrelevant content included in the article

(6) Peer-review manipulation

The presence of these indicators undermines our confidence in the integrity of the article's content and we cannot, therefore, vouch for its reliability. Please note that this notice is intended solely to alert readers that the content of this article is unreliable. We have not investigated whether authors were aware of or involved in the systematic manipulation of the publication process.

Wiley and Hindawi regrets that the usual quality checks did not identify these issues before publication and have since put additional measures in place to safeguard research integrity.

We wish to credit our own Research Integrity and Research Publishing teams and anonymous and named external researchers and research integrity experts for contributing to this investigation.

The corresponding author, as the representative of all authors, has been given the opportunity to register their agreement or disagreement to this retraction. We have kept a record of any response received.

References

[1] M. Ishaq, A. Khan, M. M. Su'ud, M. M. Alam, J. I. Bangash, and A. Khan, "An Improved Strategy for Task Scheduling in the Parallel Computational Alignment of Multiple Sequences," *Computational and Mathematical Methods in Medicine*, vol. 2022, Article ID 8691646, 11 pages, 2022.

Hindawi
Computational and Mathematical Methods in Medicine
Volume 2023, Article ID 9865158, 1 page
https://doi.org/10.1155/2023/9865158

Retraction

Retracted: Exploration of the Effect of Icariin on Nude Mice with Lung Cancer Bone Metastasis via the OPG/RANKL/RANK System

Computational and Mathematical Methods in Medicine

Received 27 June 2023; Accepted 27 June 2023; Published 28 June 2023

This article has been retracted by Hindawi following an investigation undertaken by the publisher [1]. This investigation has uncovered evidence of one or more of the following indicators of systematic manipulation of the publication process:

(1) Discrepancies in scope

(2) Discrepancies in the description of the research reported

(3) Discrepancies between the availability of data and the research described

(4) Inappropriate citations

(5) Incoherent, meaningless and/or irrelevant content included in the article

(6) Peer-review manipulation

The presence of these indicators undermines our confidence in the integrity of the article's content and we cannot, therefore, vouch for its reliability. Please note that this notice is intended solely to alert readers that the content of this article is unreliable. We have not investigated whether authors were aware of or involved in the systematic manipulation of the publication process.

Wiley and Hindawi regrets that the usual quality checks did not identify these issues before publication and have since put additional measures in place to safeguard research integrity.

We wish to credit our own Research Integrity and Research Publishing teams and anonymous and named external researchers and research integrity experts for contributing to this investigation.

The corresponding author, as the representative of all authors, has been given the opportunity to register their agreement or disagreement to this retraction. We have kept a record of any response received.

References

[1] Z. Ruilian, G. Ying, S. Hongmei, and G. Lihua, "Exploration of the Effect of Icariin on Nude Mice with Lung Cancer Bone Metastasis via the OPG/RANKL/RANK System," *Computational and Mathematical Methods in Medicine*, vol. 2022, Article ID 2011625, 9 pages, 2022.

Hindawi
Computational and Mathematical Methods in Medicine
Volume 2023, Article ID 9865029, 1 page
https://doi.org/10.1155/2023/9865029

Retraction

Retracted: Recognition of Human Body Feature Changes in Sports Health Based on Deep Learning

Computational and Mathematical Methods in Medicine

Received 27 June 2023; Accepted 27 June 2023; Published 28 June 2023

This article has been retracted by Hindawi following an investigation undertaken by the publisher [1]. This investigation has uncovered evidence of one or more of the following indicators of systematic manipulation of the publication process:

(1) Discrepancies in scope

(2) Discrepancies in the description of the research reported

(3) Discrepancies between the availability of data and the research described

(4) Inappropriate citations

(5) Incoherent, meaningless and/or irrelevant content included in the article

(6) Peer-review manipulation

The presence of these indicators undermines our confidence in the integrity of the article's content and we cannot, therefore, vouch for its reliability. Please note that this notice is intended solely to alert readers that the content of this article is unreliable. We have not investigated whether authors were aware of or involved in the systematic manipulation of the publication process.

Wiley and Hindawi regrets that the usual quality checks did not identify these issues before publication and have since put additional measures in place to safeguard research integrity.

We wish to credit our own Research Integrity and Research Publishing teams and anonymous and named external researchers and research integrity experts for contributing to this investigation.

The corresponding author, as the representative of all authors, has been given the opportunity to register their agreement or disagreement to this retraction. We have kept a record of any response received.

References

[1] C. Jiao, "Recognition of Human Body Feature Changes in Sports Health Based on Deep Learning," *Computational and Mathematical Methods in Medicine*, vol. 2022, Article ID 1736350, 14 pages, 2022.

Hindawi
Computational and Mathematical Methods in Medicine
Volume 2023, Article ID 9845962, 1 page
https://doi.org/10.1155/2023/9845962

Retraction

Retracted: An Improved Brain MRI Classification Methodology Based on Statistical Features and Machine Learning Algorithms

Computational and Mathematical Methods in Medicine

Received 27 June 2023; Accepted 27 June 2023; Published 28 June 2023

This article has been retracted by Hindawi following an investigation undertaken by the publisher [1]. This investigation has uncovered evidence of one or more of the following indicators of systematic manipulation of the publication process:

(1) Discrepancies in scope

(2) Discrepancies in the description of the research reported

(3) Discrepancies between the availability of data and the research described

(4) Inappropriate citations

(5) Incoherent, meaningless and/or irrelevant content included in the article

(6) Peer-review manipulation

The presence of these indicators undermines our confidence in the integrity of the article's content and we cannot, therefore, vouch for its reliability. Please note that this notice is intended solely to alert readers that the content of this article is unreliable. We have not investigated whether authors were aware of or involved in the systematic manipulation of the publication process.

Wiley and Hindawi regrets that the usual quality checks did not identify these issues before publication and have since put additional measures in place to safeguard research integrity.

We wish to credit our own Research Integrity and Research Publishing teams and anonymous and named external researchers and research integrity experts for contributing to this investigation.

The corresponding author, as the representative of all authors, has been given the opportunity to register their agreement or disagreement to this retraction. We have kept a record of any response received.

References

[1] M. Fayaz, M. S. Qureshi, K. Kussainova, B. Burkanova, A. Aljarbouh, and M. B. Qureshi, "An Improved Brain MRI Classification Methodology Based on Statistical Features and Machine Learning Algorithms," *Computational and Mathematical Methods in Medicine*, vol. 2021, Article ID 8608305, 14 pages, 2021.

Hindawi
Computational and Mathematical Methods in Medicine
Volume 2023, Article ID 9843487, 1 page
https://doi.org/10.1155/2023/9843487

Retraction

Retracted: An Inhibitor of Nuclear Factor-Kappa B Pathway Attenuates the Release of TGF-β1 and Inhibits the Fibrogenic Progress in a Model of Airway Remodeling Induced by Acrolein

Computational and Mathematical Methods in Medicine

Received 27 June 2023; Accepted 27 June 2023; Published 28 June 2023

This article has been retracted by Hindawi following an investigation undertaken by the publisher [1]. This investigation has uncovered evidence of one or more of the following indicators of systematic manipulation of the publication process:

(1) Discrepancies in scope

(2) Discrepancies in the description of the research reported

(3) Discrepancies between the availability of data and the research described

(4) Inappropriate citations

(5) Incoherent, meaningless and/or irrelevant content included in the article

(6) Peer-review manipulation

The presence of these indicators undermines our confidence in the integrity of the article's content and we cannot, therefore, vouch for its reliability. Please note that this notice is intended solely to alert readers that the content of this article is unreliable. We have not investigated whether authors were aware of or involved in the systematic manipulation of the publication process.

Wiley and Hindawi regrets that the usual quality checks did not identify these issues before publication and have since put additional measures in place to safeguard research integrity.

We wish to credit our own Research Integrity and Research Publishing teams and anonymous and named external researchers and research integrity experts for contributing to this investigation.

The corresponding author, as the representative of all authors, has been given the opportunity to register their agreement or disagreement to this retraction. We have kept a record of any response received.

References

[1] P. Chen, X. Wang, Y. Li, and H. Liu, "An Inhibitor of Nuclear Factor-Kappa B Pathway Attenuates the Release of TGF-β1 and Inhibits the Fibrogenic Progress in a Model of Airway Remodeling Induced by Acrolein," *Computational and Mathematical Methods in Medicine*, vol. 2022, Article ID 4984634, 7 pages, 2022.

Hindawi
Computational and Mathematical Methods in Medicine
Volume 2023, Article ID 9842627, 1 page
https://doi.org/10.1155/2023/9842627

Retraction

Retracted: Status Quo Analysis of Physical Fitness Test Data Based on Health Monitoring

Computational and Mathematical Methods in Medicine

Received 27 June 2023; Accepted 27 June 2023; Published 28 June 2023

This article has been retracted by Hindawi following an investigation undertaken by the publisher [1]. This investigation has uncovered evidence of one or more of the following indicators of systematic manipulation of the publication process:

(1) Discrepancies in scope

(2) Discrepancies in the description of the research reported

(3) Discrepancies between the availability of data and the research described

(4) Inappropriate citations

(5) Incoherent, meaningless and/or irrelevant content included in the article

(6) Peer-review manipulation

The presence of these indicators undermines our confidence in the integrity of the article's content and we cannot, therefore, vouch for its reliability. Please note that this notice is intended solely to alert readers that the content of this article is unreliable. We have not investigated whether authors were aware of or involved in the systematic manipulation of the publication process.

In addition, our investigation has also shown that one or more of the following human-subject reporting requirements has not been met in this article: ethical approval by an Institutional Review Board (IRB) committee or equivalent, patient/participant consent to participate, and/or agreement to publish patient/participant details (where relevant).

Wiley and Hindawi regrets that the usual quality checks did not identify these issues before publication and have since put additional measures in place to safeguard research integrity.

We wish to credit our own Research Integrity and Research Publishing teams and anonymous and named external researchers and research integrity experts for contributing to this investigation.

The corresponding author, as the representative of all authors, has been given the opportunity to register their agreement or disagreement to this retraction. We have kept a record of any response received.

References

[1] W. Ye and X. Shao, "Status Quo Analysis of Physical Fitness Test Data Based on Health Monitoring," *Computational and Mathematical Methods in Medicine*, vol. 2022, Article ID 3931404, 13 pages, 2022.

Hindawi
Computational and Mathematical Methods in Medicine
Volume 2023, Article ID 9837528, 1 page
https://doi.org/10.1155/2023/9837528

Retraction

Retracted: Breast Tumor Detection and Classification in Mammogram Images Using Modified YOLOv5 Network

Computational and Mathematical Methods in Medicine

Received 27 June 2023; Accepted 27 June 2023; Published 28 June 2023

This article has been retracted by Hindawi following an investigation undertaken by the publisher [1]. This investigation has uncovered evidence of one or more of the following indicators of systematic manipulation of the publication process:

(1) Discrepancies in scope

(2) Discrepancies in the description of the research reported

(3) Discrepancies between the availability of data and the research described

(4) Inappropriate citations

(5) Incoherent, meaningless and/or irrelevant content included in the article

(6) Peer-review manipulation

The presence of these indicators undermines our confidence in the integrity of the article's content and we cannot, therefore, vouch for its reliability. Please note that this notice is intended solely to alert readers that the content of this article is unreliable. We have not investigated whether authors were aware of or involved in the systematic manipulation of the publication process.

Wiley and Hindawi regrets that the usual quality checks did not identify these issues before publication and have since put additional measures in place to safeguard research integrity.

We wish to credit our own Research Integrity and Research Publishing teams and anonymous and named external researchers and research integrity experts for contributing to this investigation.

The corresponding author, as the representative of all authors, has been given the opportunity to register their agreement or disagreement to this retraction. We have kept a record of any response received.

References

[1] A. Mohiyuddin, A. Basharat, U. Ghani et al., "Breast Tumor Detection and Classification in Mammogram Images Using Modified YOLOv5 Network," *Computational and Mathematical Methods in Medicine*, vol. 2022, Article ID 1359019, 16 pages, 2022.

Hindawi
Computational and Mathematical Methods in Medicine
Volume 2023, Article ID 9837218, 1 page
https://doi.org/10.1155/2023/9837218

Retraction

Retracted: Paeoniflorin Can Improve Acute Lung Injury Caused by Severe Acute Pancreatitis through Nrf2/ARE Pathway

Computational and Mathematical Methods in Medicine

Received 27 June 2023; Accepted 27 June 2023; Published 28 June 2023

This article has been retracted by Hindawi following an investigation undertaken by the publisher [1]. This investigation has uncovered evidence of one or more of the following indicators of systematic manipulation of the publication process:

(1) Discrepancies in scope

(2) Discrepancies in the description of the research reported

(3) Discrepancies between the availability of data and the research described

(4) Inappropriate citations

(5) Incoherent, meaningless and/or irrelevant content included in the article

(6) Peer-review manipulation

The presence of these indicators undermines our confidence in the integrity of the article's content and we cannot, therefore, vouch for its reliability. Please note that this notice is intended solely to alert readers that the content of this article is unreliable. We have not investigated whether authors were aware of or involved in the systematic manipulation of the publication process.

Wiley and Hindawi regrets that the usual quality checks did not identify these issues before publication and have since put additional measures in place to safeguard research integrity.

We wish to credit our own Research Integrity and Research Publishing teams and anonymous and named external researchers and research integrity experts for contributing to this investigation.

The corresponding author, as the representative of all authors, has been given the opportunity to register their agreement or disagreement to this retraction. We have kept a record of any response received.

References

[1] Y. Hu and W. Yang, "Paeoniflorin Can Improve Acute Lung Injury Caused by Severe Acute Pancreatitis through Nrf2/ARE Pathway," *Computational and Mathematical Methods in Medicine*, vol. 2022, Article ID 5712219, 7 pages, 2022.

Hindawi
Computational and Mathematical Methods in Medicine
Volume 2023, Article ID 9832573, 1 page
https://doi.org/10.1155/2023/9832573

Retraction

Retracted: Predicting Characteristics Associated with Breast Cancer Survival Using Multiple Machine Learning Approaches

Computational and Mathematical Methods in Medicine

Received 27 June 2023; Accepted 27 June 2023; Published 28 June 2023

This article has been retracted by Hindawi following an investigation undertaken by the publisher [1]. This investigation has uncovered evidence of one or more of the following indicators of systematic manipulation of the publication process:

(1) Discrepancies in scope

(2) Discrepancies in the description of the research reported

(3) Discrepancies between the availability of data and the research described

(4) Inappropriate citations

(5) Incoherent, meaningless and/or irrelevant content included in the article

(6) Peer-review manipulation

The presence of these indicators undermines our confidence in the integrity of the article's content and we cannot, therefore, vouch for its reliability. Please note that this notice is intended solely to alert readers that the content of this article is unreliable. We have not investigated whether authors were aware of or involved in the systematic manipulation of the publication process.

Wiley and Hindawi regrets that the usual quality checks did not identify these issues before publication and have since put additional measures in place to safeguard research integrity.

We wish to credit our own Research Integrity and Research Publishing teams and anonymous and named external researchers and research integrity experts for contributing to this investigation.

The corresponding author, as the representative of all authors, has been given the opportunity to register their agreement or disagreement to this retraction. We have kept a record of any response received.

References

[1] M. N. Haque, T. Tazin, M. M. Khan et al., "Predicting Characteristics Associated with Breast Cancer Survival Using Multiple Machine Learning Approaches," *Computational and Mathematical Methods in Medicine*, vol. 2022, Article ID 1249692, 12 pages, 2022.

Hindawi
Computational and Mathematical Methods in Medicine
Volume 2022, Article ID 9872404, 1 page
https://doi.org/10.1155/2022/9872404

Retraction

Retracted: A Diagnostic Model of Volleyball Techniques and Tactics Based on Wireless Communication Network

Computational and Mathematical Methods in Medicine

Received 4 November 2022; Accepted 4 November 2022; Published 22 November 2022

Computational and Mathematical Methods in Medicine has retracted the article titled "A Diagnostic Model of Volleyball Techniques and Tactics Based on Wireless Communication Network" [1] due to concerns that the peer review process has been compromised.

Following an investigation conducted by the Hindawi Research Integrity team [2], significant concerns were identified with the peer reviewers assigned to this article; the investigation has concluded that the peer review process was compromised. We therefore can no longer trust the peer review process and the article is being retracted with the agreement of the Chief Editor.

The authors do not agree to the retraction.

References

[1] Z. Yuan, Y. Zhang, B. Li, and X. Jin, "A Diagnostic Model of Volleyball Techniques and Tactics Based on Wireless Communication Network," *Computational and Mathematical Methods in Medicine*, vol. 2022, Article ID 2185908, 12 pages, 2022.

[2] L. Ferguson, "Advancing Research Integrity Collaboratively and with Vigour," 2022, https://www.hindawi.com/post/advancing-research-integrity-collaboratively-and-vigour/.

Hindawi
Computational and Mathematical Methods in Medicine
Volume 2022, Article ID 9869812, 1 page
https://doi.org/10.1155/2022/9869812

Retraction

Retracted: Prevention Methods of Fitness and Bodybuilding Exercise Injury Based on Data Mining

Computational and Mathematical Methods in Medicine

Received 4 November 2022; Accepted 4 November 2022; Published 16 November 2022

Computational and Mathematical Methods in Medicine has retracted the article titled "Prevention Methods of Fitness and Bodybuilding Exercise Injury Based on Data Mining" [1] due to concerns that the peer review process has been compromised.

Following an investigation conducted by the Hindawi Research Integrity team [2], significant concerns were identified with the peer reviewers assigned to this article; the investigation has concluded that the peer review process was compromised. We therefore can no longer trust the peer review process and the article is being retracted with the agreement of the Chief Editor.

References

[1] J. Xie, "Prevention Methods of Fitness and Bodybuilding Exercise Injury Based on Data Mining," *Computational and Mathematical Methods in Medicine*, vol. 2022, Article ID 7083991, 13 pages, 2022.

[2] L. Ferguson, "Advancing Research Integrity Collaboratively and with Vigour," 2022, https://www.hindawi.com/post/advancing-research-integrity-collaboratively-and-vigour/.

Hindawi
Computational and Mathematical Methods in Medicine
Volume 2023, Article ID 9826547, 1 page
https://doi.org/10.1155/2023/9826547

Retraction

Retracted: Self-Adaptation Resource Allocation for Continuous Offloading Tasks in Pervasive Computing

Computational and Mathematical Methods in Medicine

Received 27 June 2023; Accepted 27 June 2023; Published 28 June 2023

This article has been retracted by Hindawi following an investigation undertaken by the publisher [1]. This investigation has uncovered evidence of one or more of the following indicators of systematic manipulation of the publication process:

(1) Discrepancies in scope

(2) Discrepancies in the description of the research reported

(3) Discrepancies between the availability of data and the research described

(4) Inappropriate citations

(5) Incoherent, meaningless and/or irrelevant content included in the article

(6) Peer-review manipulation

The presence of these indicators undermines our confidence in the integrity of the article's content and we cannot, therefore, vouch for its reliability. Please note that this notice is intended solely to alert readers that the content of this article is unreliable. We have not investigated whether authors were aware of or involved in the systematic manipulation of the publication process.

Wiley and Hindawi regrets that the usual quality checks did not identify these issues before publication and have since put additional measures in place to safeguard research integrity.

We wish to credit our own Research Integrity and Research Publishing teams and anonymous and named external researchers and research integrity experts for contributing to this investigation.

The corresponding author, as the representative of all authors, has been given the opportunity to register their agreement or disagreement to this retraction. We have kept a record of any response received.

References

[1] A. Ehsan, K. Z. Haider, S. Faisal, F. M. Zahid, and I. M. Wangari, "Self-Adaptation Resource Allocation for Continuous Offloading Tasks in Pervasive Computing," *Computational and Mathematical Methods in Medicine*, vol. 2022, Article ID 8040487, 13 pages, 2022.

Hindawi
Computational and Mathematical Methods in Medicine
Volume 2022, Article ID 8040487, 13 pages
https://doi.org/10.1155/2022/8040487

Research Article

Self-Adaptation Resource Allocation for Continuous Offloading Tasks in Pervasive Computing

Aiman Ehsan,[1] Khurram Zeeshan Haider,[1,2] Shahla Faisal,[2,3] Faisal Maqbool Zahid,[2,3] and Isaac Mwangi Wangari[4]

[1]*Department of Software Engineering, Government College University, Faisalabad, Pakistan*
[2]*Center of Data Science, Government College University, Faisalabad, Pakistan*
[3]*Department of Statistics, Government College University, Faisalabad, Pakistan*
[4]*Department of Mathematics and Computer Science, Bomet University College, Bomet, Kenya*

Correspondence should be addressed to Isaac Mwangi Wangari; mwangiisaac@aims.ac.za

Received 19 January 2022; Revised 18 March 2022; Accepted 31 May 2022; Published 28 June 2022

Academic Editor: Muhammad Zubair Asghar

Advancement in technology has led to an increase in data. Consequently, techniques such as deep learning and artificial intelligence which are used in deciphering data are increasingly becoming popular. Further, advancement in technology does increase user expectations on devices, including consumer interfaces such as mobile apps, virtual environments, or popular software systems. As a result, power from the battery is consumed fast as it is used in providing high definition display as well as in charging the sensors of the devices. Low latency requires more power consumption in certain conditions. Cloud computing improves the computational difficulties of smart devices with offloading. By optimizing the device's parameters to make it easier to find optimal decisions for offloading tasks, using a metaheuristic algorithm to transfer the data or offload the task, cloud computing makes it easier. In cloud servers, we offload the tasks and limit their resources by simulating them in a virtual environment. Then we check resource parameters and compare them using metaheuristic algorithms. When comparing the default algorithm FCFS to ACO or PSO, we find that PSO has less battery or makespan time compared to FCFS or ACO. The energy consumption of devices is reduced if their resources are offloaded, so we compare the results of metaheuristic algorithms to find less battery usage or makespan time, resulting in the PSO increasing battery life or making the system more efficient.

1. Introduction

Fast technology increases data and further increases user expectations on devices, including consumer interfaces such as mobile apps, virtual environments, or popular software systems. The power of the battery, therefore, charges to the advanced display, sensor, or screens that quickly consume the battery [1, 2]. The processor or devices generate large amounts of data, resulting in long delays or excessive power consumption. After all, a low latency requires increased power consumption in certain conditions. To improve the computational difficulties of smart devices with offloading, cloud computing is considered to play a significant role [3–5]. By optimizing the device's parameters so that it becomes easier to find optimal decisions for offloading tasks, a metaheuristic algorithm is used to migrate the data or to offload the task [6]. When comparing the default algorithm FCFS to ACO or PSO, we find that PSO has a lower battery or makespan time than FCFS or ACO [7]. The energy consumption of devices is reduced if their resources are offloaded, so we compare the results of the algorithms to find less battery usage or makespan time, resulting in the PSO increasing battery life or making the system more efficient [8].

We have to utilize the resources or offload the task to consume time, energy cost, power consumption, and computational power, to minimize the energy usage of the smart devices we offload tasks in the cloud network and check resource parameters by using some methods [3, 9–11]. Our future job, according to the computational findings, is to offload the task using some metaheuristic algorithm combo,

and the imitations conclude that the current task offloading method achieved a well-traded-off presentation between power usage ability and task execution. By applying a combo of metaheuristic algorithms using a simulator, we can check the parameters of the power usage or the job completion time [4]. To achieve energy or power consumption goals, we use cloud computing to offload the job or spread its resources. For efficiency measurements, we use metaheuristic algorithms [12, 13].

The goal of this paper is to optimize the resources for computational tasks and offload the task to the cloud server through a virtual environment. In particular, we use metaheuristic algorithms for measuring the battery time or makespan and then compare the results to investigate which strategy reduces the makespan time or uses more energy. Our main contribution is that we decreased the energy consumption/battery usage and saved the execution time of the tasks by optimally offloading them on the other resources available. For this purpose, we proposed an efficient fitness function in the metaheuristic algorithms, i.e., ACO and PSO, which guaranteed an extensive increase in the efficiency of the cloud network in lesser iterations as compared to the work done in the literature. Metaheuristic algorithms were also chosen in an optimal fashion using CloudSim to resolve energy consumption. It was done by comparing algorithms in a rigorously precise manner which yielded promising numerical results in the simulation to reduce energy, battery usage, and resource allocation. To achieve energy or power consumption goals, we have used a cloud computing advantage to offload the task as well as allocate its resources. We set the resource limit to allow for certain big computational tasks that can be performed using cloud or edge computing. The use of a metaheuristic algorithm for task offloading and the simulated results reveal the strategy of reducing the makespan time as well as energy usage at the most.

2. Related Work

In the digital world, task offloading from smart devices to cloud servers has been considered to be a successful technique for increasing smartphone functionality and battery life [14]. Power costs and energy usage, both of which are big issues, have been used to determine the effectiveness of task offloading. These two characteristics allow smartphone devices to make informed decisions about whether or not to execute task offloading [1, 2, 15–18]. Traditional Online Code Offloading, as well as Adaptive Partitioning and Dynamic Selective Offloading, is less efficient than the metaheuristic algorithm task offloading framework [19, 20]. In this paper, we point out that, the offloading task can also be used to model one of the D2D interactions. In many research fields such as sensor communications, IoT, and device (M2M) systems, offloading can be utilized as a modern communication tool [21, 22]. Pervasive computing enables consumers to connect to an app quickly and reliably (MCC) using stratified computers. Although it is difficult to deliver complex services on low-power devices such as smartphones and tablet computers, it is possible. To resolve the problem, numerous approaches have been proposed, including implementation or structure modifications (for details, please see Table 1). They assume that just by actively splitting the request and offloading most of the execution time to either an efficient nearby proxy, this issue can be solved [12, 20, 23, 24].

2.1. Offloading. An automated task offloading engine cannot make its choice correctly by ignoring the operating conditions and network environment. Cloud servers used multiple methods to offload the task using servers that are the most basic or general among the computations fields [24, 25]. For the storage volume and computation size, the cloud is the most appropriate or efficient, and the latency can restrict its operation and provide the computational goal from resource-restricted to high-resource technology; a technique used to send edge servers to the cloud will improve the efficiency of the requests. It is too difficult to pick the cloud platform for the offloading algorithm [25, 26]. Single servers or several servers are used to offload the task. The advantages of offloading are shown in Figure 1. The system is the design to offload the task in a server through a wireless network for offloading [4, 23, 27–29].

2.2. Edge with Cloud. Edge is a server for tiny device datacenters that are used. The computational power for an edge cloud is distributed by the edge servers [11, 25]. Edge computing improves the network, where the data hubs are another form of storage, for the location of the access point. The edge server is often used for the smart devices' offloading endpoint to decrease the users' power or expense. The edge computing architecture illustrates the connection between the beneficial elements of the mobile cloud computing [4, 9, 25].

2.3. Computational Offloading. Current findings of computational offloading typically operate on smart technologies. Energy usage or power cost is the top point of interest over the issues with the short battery time of the larger smart devices [12, 30]. The highest priority is the processing time for optimization using smart devices. We use technology for offloading the task from smart devices for available resources to consume energy or resources [31, 32]. Essentially, the offloading approach allows the developers to manually describe the intent needed for further system success. Increasing the delay or contact with static code analysis and dynamic code analysis, which makes the performance good, we use improved adaptively [4, 20]. We used some techniques such as ThinkAir or cloudlet to improve performance, which manages the virtual machine (VM) with the cloud that offloads the task of improving scalability and variance similarly [5]. A perfect environment for allocating, synchronizing, or completing the code in shifting phases may be sorted by a virtual computer or handheld cloud computing. There are two approaches to complete or comparatively code the program on the server to offload based on the customer's requirement [25]. The fine-grained approach has two methods, the coarse-grained and fine-grained.

2.4. Performance Metrics. The algorithms are compared on the basis of the following performance metrics.

Table 1: Evaluation table.

Author Year	Method	Purpose	Description
Erana Veerappa Dinesh Subramaniam	Gray wolf optimization	In the current time, task offloading from smartphones to cloud servers has proven to be a promising technique for increasing smartphone functionality and battery life. The cost of communication and energy usage are used to determine the effectiveness of task offloading [17]	Strength We offer a new framework that uses a task scheduler to reduce energy usage during HMCC task offloading [10]. The suggested system uses a multiobjective function to model the scheduler, which takes into account network metrics, cloud parameters, and other system data Weakness The outcome in tangling also not accurate result in global optimization. Low precision or poor local optimization
Kaiyang Liu (2016) [18]	An iterative decoupling algorithm	Internet of things offers a new concept to improve the abilities through offloading the computational resources to consume less energy from smart phones; we offload resources to cloud server.	Strength To use less energy, the users of smart devices offload work with an appropriate data connection and contact efficiency, and offloading decision strategy is studied Weakness It takes large computation period
Kai Lin (2018) [23]	Fruit fly algorithm	An offloading algorithm fruit fly is suggested to enhance the distribution by offloading and utilizes its resources to achieve less energy usage under responsibilities assigned. Energy consumption, time, and cost efficiency, relative to cooperative multitask, allocated total on an ant colony optimization algorithm and algorithm based on the heuristic server. The findings further suggest the efficiency of the algorithm suggested by contrasting that with current algorithms	Strength The simulation outcomes show that the average FOTO algorithm promises better energy efficiency, reduced processing times, and also reduced datacenter costs which are used for edge computing in advanced applications. For further study into mobile offloading across numerous mobile devices, a cooperative device-to-device communication system will be established, allowing mobile devices to assist each other in offloading duties. This method can increase channel capacity while maintaining high bandwidth efficiency, allowing task offloading to be better utilized Weakness Less accuracy or bad optimal solution
Jing Zhang, Weiwei Xia (2018) [3]	Subalgorithms	Low power consumption and low computing capacities restrict the installation of high computational programs on smart devices	Strength The appropriate approach that impedes efficiency that analyzes the characteristics will transfer the intensive apps as on a cloud Weakness Problem not solving independently
Men his chin, Ben Liang, Min dong (2016)	Heuristic algorithm	Each smartphone user requires several independent tasks that share the resource while offloads workload to the cloud network for less computational power through other methods [33]	Strength Currently, we work on improving the offloading and allocating contact tools for all projects, to eliminate electricity expenses, computing costs, and delays for all consumers. Our approach can be applied to several users and activities where even the machine sophistication of thorough search becomes costly Weakness This method is not providing optimal solution
Rahul Yadav (2020) [34]	Heuristic approach	To solve the energy consumption and resource allocation problem in this paper used an energy efficient computation.	Strength It is better for the energy saving, latency, and energy latency cost than overall schemes [34]
Muhammad Shafiq (2021) [35]	RL based	Computation Offloading using Reinforcement Learning (CORL) For more energy, less battery time, and delay in portable machines, there are not enough resources for allocate these, so in this research, we proposed some work to handle this situation	Strength Better offloading decisions in a quick time [35]

2.4.1. Makespan. It is the completion time of the last job to leave the system. Let $p(i, j)$ be the execution time of the offloading task on ith VM of jth cloudlet task, and the processing time of the offloading task for ith VM is characterized as $l(i) = \sum p(i, j)$. The independent planning job is measured as $L_{\max} = \max(L_I)$. This is the cloudlet VM's component. $n >$

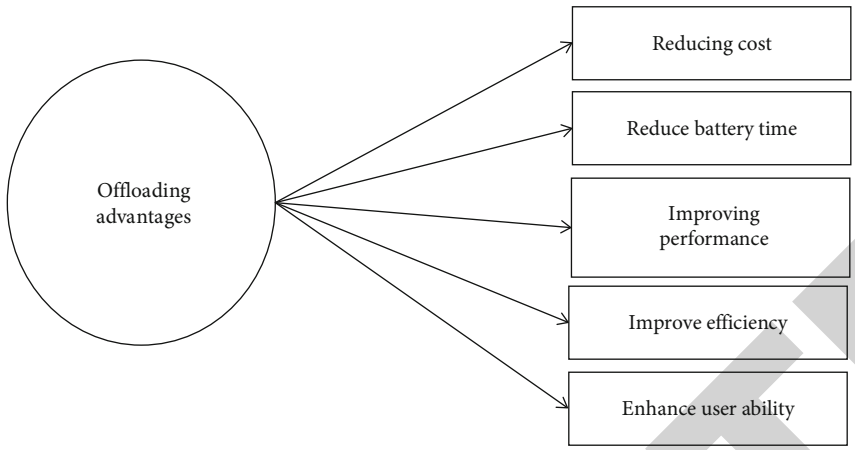

Figure 1: Offloading advantages.

m means some task greater than the makespan, so we have to reduce the time of makespan. We use multiobjective optimization for makespan output that requires maximization or minimization or helps VM makespan. The number of tasks associated with N that offloads the number of tasks on VM such as several tasks on makespan M cloudlets and the problem of makespan minimization is considered as hard. The maximum level for feature optimization is defined in the formula. Offloading makespan is defined as G, where makespan time is measured with the maximum limit in the equation where the task's processing time takes the maximum limit to offload the task on VM to the cloudlet. So the link between measured makespan limit tasks and offloading is valid for all makespan offloading tasks; the optimal makespan identified with O is formulated by changing the relationship with task offloading based on the optimal makespan [36]. Here is the equation of makespan.

$$\begin{aligned} &m \times L_{\max}, \\ &m \times L_{\max} > \mathrm{G}, \\ &m \times O > G, \end{aligned} \tag{1}$$

where the number of task = makespan is m, $L_{\max}$ is the maximum limit = offloading of task, and$O$ is the optimum.

The execution time offloading task ($t \in Tt \in T$) is a term used to describe the time it takes to receive input data that is expressed (T_w), and if t is the processing time, the T_w is defined by

$$T_w = \frac{\max_i(t)}{\overrightarrow{B}}, \tag{2}$$

where $\max_i(t)$ shows the largest data that was received for time t and $\overrightarrow{B}$ is the mean bandwidth of cloudlet VMs. The time duration of the offloading task is the sum of $(T_w + T_e T_w + T_e)$.

The completion time of cloudlet virtual machine is defined by

$$T_t = \sum_{t \in T} [T_w + T_e], \tag{3}$$

assumed VM_i, $i = 1 \cdots m$ with the overall obtainability of cloudlet on VM denoted by m.

$$T_e = \frac{MI(t)}{MIPS(VM(i))}, \tag{4}$$

then the quantity of the success period of the offloading task. The extreme achievement period is termed the makespan, which is given as $makespan = \max(T_{t-1t}, T_{t-2t}, , T_{t-mt})$ for a cloudlet VM task offloading [10].

2.4.2. Battery Consumption. Task offloading also reduce the battery time by using an algorithm to offload the task on the cloud. Performance metrics improve the battery power. We assign the resources of the task with these performance metrics. Task offloading also reduce the battery time by using an algorithm to offload the task on the cloud. We decrease the task resources with makespan or execution time using a cloud network. To decrease makespan, or execution time, we allocate task resources to task requests. Consider EC_{jk} is the energy that the task operating on the VM absorbs. EC_r denotes the VM's power-consuming amount or T_e execution completion time [17]. The consumption of energy (EC) is measured as

$$EC_{jk=} EC_r . T_e, \tag{5}$$

The total energy consumed is computed as

$$f_2(x) = \sum_{i=1}^{j} \sum_{n=1}^{k} EC_{jk}, \tag{6}$$

where j represents the numeral jobs used and k represents the number of VMs used, and $f_2(x)$ represents the total

energy used in offloading tasks by using several tasks and virtual machines.

3. Methodology

Our motive is to reduce the resources of the devices by using the best algorithm that takes fewer resources to allocate the task. There are two approaches for allocating resources: task offloading or task scheduling using performance metrics [18]. Task offloading is the best method to offload the resources or to attain the performance metrics using the task offloading technique. We use cloud computing to provide the services of offloading the task resources with makespan, energy usage, or battery time reduction. To offload the task resources by makespan or battery processing time, we use two efficiency metrics in the cloud network. In comparison to such algorithms, cloud computing platforms use CloudSim to consume energy [24, 37]. First, we simulate the task offloading using the OMNet simulator where the task is offloading on different devices using a wireless network with cloud servers. A basic simulation is done to offload the task using the wireless network from devices to the cloud server, but we cannot distribute the resources here because there is no broker class, so later we have done our simulation in the cloud network for offloading the task resources [17, 21]. Task management in cloud computing is a core challenge that limits the system's performance. The Network CloudSim Switch, Network Datacenter, and Network Datacenter Broker include three key objects [38]. We create a datacenter in clouds, we generate a host in the datacenter, or VM is generated in the host. VMs are the virtual machines representing the cloud's smart devices. Through the cloudlets, it requests to offload the task requests [37]. If a VM cannot attain, so it sends it to another VM to accomplish the task request; we have to model tasks on a VM. We aim to evaluate the device resources with various algorithms. If a VM or device does not handle the task request, then the task transfers to another VM, so the device requires less energy and resources.

To reduce the task resources, we compare some of the algorithms for high computation. But to reduce the resources of the task for makespan or battery use, the result of the ant colony optimization algorithm or the First Come First Serve algorithm is not enough. So, we searched for the best algorithm where we get the least resource time so that we compare the outcome of these three ant colony optimization (ACO) algorithm, First Come First Serve (FCFS) algorithm, or particle swarm optimization (PSO) algorithm to allocate task resources by offloading tasks. The algorithms were implemented according to the following procedural flow whose detail is presented in Figure 2.

3.1. Implementation through Cladism Network. Here is the first step explaining the function of setting up VM. It is the first step in launching cloudlets and virtual machines. With features such as VM ID, CPU capacity, and memory, Per VM was added. Similarly, cloudlets with a name, volume, and file size are created. Using some technique, we offload the task and utilize its resources in the simulator. In the simulation, we will be using VM, cloudlets, and cloud servers [37].

3.2. Using Algorithms. We will use the first come first serve algorithm as default and check its parameters after this by using ant colony optimization to minimize the makespan or battery time that will result in less time, and then we compare particle swarm optimization to decrease the battery time than ACO or resulting less time. Assign the cloudlets according to their specifications to the virtual computers, such as capacity needs and bandwidth [26].

3.3. Assign the Task to Cloudlets. Begin simulating the implementation of cloudlets. We can use CloudSim to simulate the task offloading, where a datacenter is created to offload the task; VM is created as a user computer hosting the required user's device to offload, where the task request is submitted to the datacenter as the cloudlets. We establish a datacenter to simulate whereby host VM is generated or cloudlets are asked to unload the task to the cloud. Cloudlets are the task requesting the request to the queue to offload the request, and the user's computer is a VM that transfers the task to offload the task resource, and the datacenter is generated to offload the task, using the datacenter as cloud storage [37, 38].

3.4. Selection of Algorithm Parameters. Simulating the job is a resource and now evaluating its parameters such as makespan time and battery time. These parameters are determined by positioning the VM algorithm in the simulation, sending the cloudlets to order the activity to be unloaded in the cloud, and checking its resource allocation parameters. We offload the assignment for allocating the resource in this analysis, so we use metrics of makespan to decrease the makespan period or decrease the battery power time, which increases the device's capability. According to objective characteristics, parameters such as makespan, response time, waiting time, and load are calculated or power [36].

3.5. Analysis. Through analyzing the parameters of different cloudlets, the effect is evaluated. Using the parameters, we analyze the time of makespan or battery time. To evaluate the time that decreases the battery capacity, we can verify the makespan time. We will determine the makespan period after having the outcome of these and will also measure the battery time with less energy.

3.6. Task Offloading Workflow. We assign the task to request using battery usage or makespan performance metrics. It is easier to reserve the funds for allocating mission offloading. The latency requirement, energy and time required for mobile execution, the time required for cloud implementation, the input data size for cloud implementation, and the corresponding data size resulting from cloud implementation are all considered in the task offloading model. Know that there are two tasks on the computer that are the same. The work release is then said to have interruptions because cloud execution requires more energy than mobile execution and has a lower latency requirement when job offloading with cloud execution. Depending on the channel and local

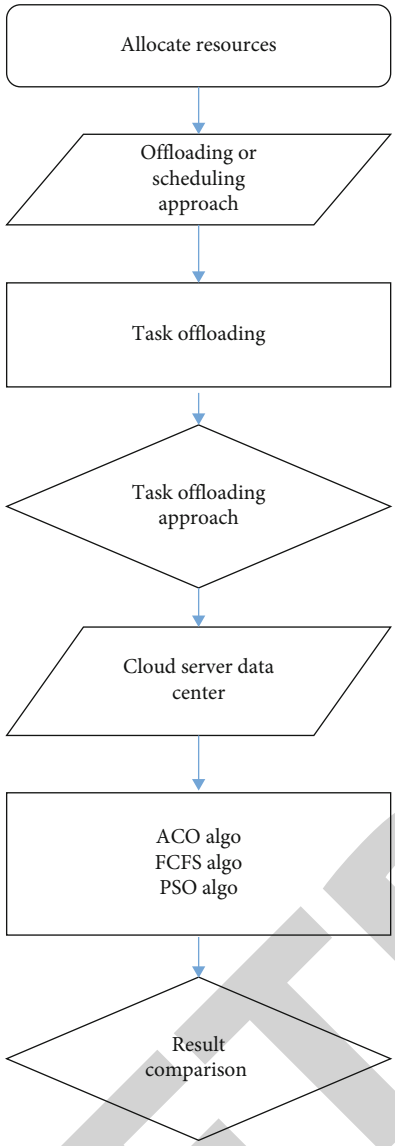

Figure 2: Systematic flow adopted for offloading task.

conditions, the amount of energy required for cloud execution varies. These considerations, however, have little impact on smartphone deployment. So, it is believed that the consumption of energy during mobile execution is steady. Either on cloud computers or a cloud server, cloud execution takes place. The energy required for cloud server execution during uplink and downlink transmission is determined by energy consumption. Based on the completion of specified data rate parameters on both input and output transfers, the latency state is fulfilled by telephone or cloud execution. It might appear like there is a single entry point for each cloudlet, and the system uses one cloudlet to offload work. However, the cloud execution process is limited in computational capacity. During the task offloading procedure, if the smartphone is outside the range of access points, the cloudlet is executed. The given data is transferred through the task offloading using cloudlet, and the output data is composed. The energy used by both the uplink and downlink during cloud

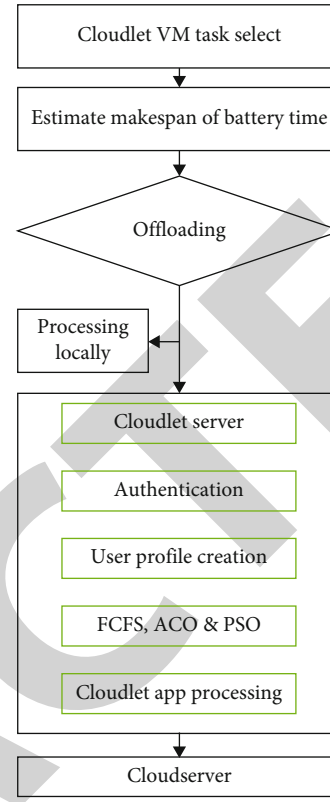

Figure 3: Workflow in the cloud computing task offloading.

execution at cloudlets is included in the total energy used during the transfers.

4. System Design of Offloading

In the task offloading framework with a multiobjective feature, the current task offloading architecture uses a specific optimization technique for task offloading. The new method works with competing priorities like processing time and electricity prices. The workflow in the cloud computing task offloading environment is then planned using a multiobjective task offloading model shown in Figure 3.

4.1. Simulation Design for Offloading. Makespan and energy costs are said to maximize brand awareness by optimizing resource usage based on the minimization feature. Makespan is processed completion time and is characterized also as a combination of time consumed or process average amount in the flow. On a VM, the makespan is controlled by the task's size and computation capability, and it may be expressed using this equation: T = size of task/capability for computing. Energy costs were calculated as the product of the time of execution as well as the VM access rates, where it is assumed that certain every minute, cloud infrastructure is charging. P = VM × process time. The workflow was identified to use a series of the assigned task, and it is known as a workflow during its interconnectivity. The task offloading time needs the maximization or minimization of the resource through makespan.

1. Initialization:
I. Initialize the pheromone value to a positive constant for each path between tasks and resources.
II. Optimal solution = null
III. Place the m ants on random resources
2. Solution construction of each unit:
Repeat for each ant
Put the starting resource in tabs list of this ant (for the first task)
For all the remaining tasks
a. Choose the next resource r_j for the next task t_j by applying the following transition role.
$m_{ij} = (T_{ij})^2 (n_{ij})^x / \sum k\, alloqwed (T_{ij})^x (n_{ij})^v$ *if j allowed, mean not in tab list*
else 0
b. Put the selected resource in previous step into tab list of this ant
End For
Until each ant builds its solution
3. Fitness: *compute the fitness value of the solution of each ant*
4. Replacement: *replace the optimal solution with the ant's solution having best fitness value if its fitness value is better than optimal solution.*
5. Pheromone updating:
6. Empty tab lists of all ants
7. Repeat steps 2 to 6 until the stopping condition is met. Stopping condition may be the maximum number of iterations or no change in fitness value of ants' solutions in consecutive iterations
8. Output: *Print Optimal solution*
End Procedure

Algorithm 1: Ant Colony Optimization (ACO).

4.2. Metaheuristic Algorithm. Metaheuristics, on either side, represent methods that are independent of an issue. As such, they will not benefit from the current problems' complexity. It is not greedy in particular. In particular, a slight regression of a method can also be tolerated the designed to simulate methodology which helps to investigate an optimal solution very systematically and therefore to achieve a better solution that can often correspond with either the best solution [6, 39, 40]. Metaheuristic would be a problem-independent method, but to apply the methodology to the nature of the problem, it will be essential to do great of all its intrinsic parameters.

In this research, we use a metaheuristic algorithm to improve the ability with the combination of hybrid algorithms.

(i) Nature-inspired or problem independent

(ii) Close to the optimal solution

4.3. First Come First Serve (FCFS) Algorithm. First Come First Serve is an algorithm that performs queued requests and procedures immediately to arrive. That is the shortest and fastest algorithm. This algorithm is a method that allows the task to be offloaded. Energy is expended or the mission is discharged. FCFS (First Come First Serve) efficiency and enhanced FCFS discharge algorithms for complex real-time computer systems in which tasks arrive as a random process and each task have a laxity that determines the maximum time a task can wait for the operation. The key objective is to accomplish the mission of offloading to enhance the efficacy of the makespan of First Come First Serve, where makespan S1 is taken into account so that the makespan S2 for the proposed ant colony optimization enhances it and the particle swarm optimization algorithm improves the efficiency of S2 that makespan is less than the makespan of both for offloading's resulting in the offloading.

4.4. Ant Colony Optimization. ACO was the first algorithm based on swarm intelligence. In essence, ACO mimics social ants' harvesting activity in a colony, and pheromone is used to model ants' local encounters and communications. Every ant deposits pheromones, and they eventually evaporate over time. Ant colony optimization is an optimal solution for computational problems; they find the shortest path for the food. Ants release the pheromone which is easy to find the best path [41].

(i) Based on swarm intelligence

(ii) Optimal for local search

The equation of the ant colony optimization is

$$m_{ij} = \frac{(T_{ij})^2 (n_{ij})^x}{\Sigma (T_{ij})^x (n_{ij})^v} \tag{7}$$

where m_{ij} relates to the pheromone value to task t_i and resourcer_j. n_{ij} denotes the heuristic function. x determine the influence of pheromone value. v determines the influence of heuristic function. x is the inspired value for the pheromone, and v is the expected inspired value that shows the importance of heuristic function.

The algorithm of ACO is as follows:

1. for *each particle k* in *K* ***do***
2. *Calculate* the *fitness value*
3. if $Fit(X_k)$ is *better than* $Fit(L_k)$ ***then***
4. *Update* the *best individual Lk*
5. ***end***
6. if $Fit(L_k)$ is *better than* $Fit(G)$ ***then***
7. *Update* the *global best* ***G***
8. ***end***
9. *Update velocity variables via* :
10. $V_k = wV_{k+C_1r_1}(L_k - X_k) + c_2r_2(G - X_k)$
11. $Sig(V_k) = 1/1 + e^{-Vk}$
12. *Generate a series* of *uniform random number* rand in $[0, 1]$.
13. *Update* the *binary position* $X_k : X_k = (Sig(V_k) > \text{rand})$.
14. ***end***
15. ***until*** *Maximum iterations* or *stopping condition* is *satisfied* ;

Algorithm 2: Particle Swarm Optimization PSO.

Table 2: Experimental setup and parameter settings.

Virtual machine parameter	Size = 10000; image size Int ram = 512; VM memory Int MIPS = 1000
Cloudlets constraints	Length = 500 File size = 300 Output size = 300 Pe`s number = 1
Number of datacenters	1
Number of VM	5
No of cloudlets	100-500
Nature of cloudlets	Independent
Performance metrics analysis	Makespan or battery usage
Hardware configuration	Processor: Intel (R) Core ™ i3 -2310 M CPU@ 2.10GHz Hard disk: 1 TB Ram: 2 GB.
Software configuration	Operating system: Windows 10pro Simulation software for offloading: omnetpp Simulation software for resource allocation: CloudSim 3.03 IDE: NetBeans: 8.1 Java version: JDK 1.8-172

4.5. Particle Swarm Optimization. The particle swarm optimization (PSO) algorithm was suggested once it was improved from several perspectives. PSO can be made more efficient by refining its iterative mechanism or by combining the initial parameters and heuristic methods with the original PSO algorithm [42]. It swarms the particle, optimizes iteratively, and tries to improve the particle position [42]. It schedules tasks on virtual machines with the goal of task scheduling tasks on virtual machines and reducing task response time [7, 43].

(i) Optimal for global search

(ii) Update position or velocity

(iii) Shortest path in a graph

(iv) Less numb of iterations

(v) Fast evaluation

(vi) Easy mathematical formulation

(vii) Degree of imbalance close to 1

Equation of particle swarm optimization
i^{th} where t is the iterations.
$(t + 1)i^{th}$ Particle updates position and velocity

$$\overrightarrow{X_t}(\mathrm{t}+1) = \overrightarrow{X_t}(\mathrm{t}) + \overrightarrow{V_1}(\mathrm{t}+1). \tag{8}$$

Velocity updates particles

$$\overrightarrow{V_1}(\mathrm{t}+1) = \omega * \overrightarrow{V_1}(\mathrm{t}) + C_1r_1\left(\overrightarrow{X_1} - \overrightarrow{X_1}(t)\right) + C_2r_2\overrightarrow{Z_1} - \overrightarrow{X_1}(t)\Big) \tag{9}$$

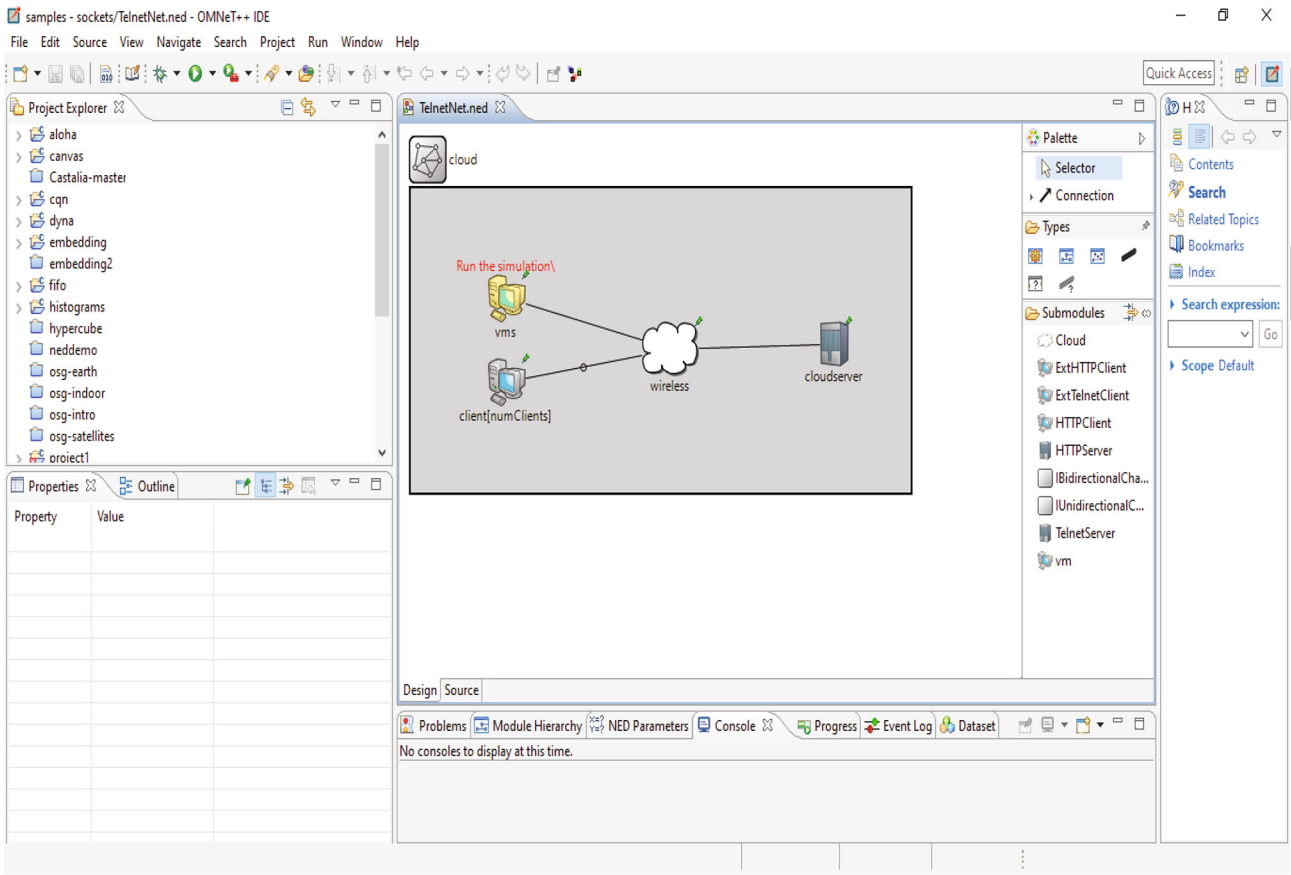

Figure 4: Offloading simulation using OMNet++ IDE.

The algorithm code for offloading using PSO is as follows [43].

5. Results and Discussion

In CloudSim 3.03 and the NetBeans IDE, FCFS, ACO, and PSO algorithms are introduced. By taking "makespan" as a core concern, a performance function is added, and the performance index of each algorithm is measured. A broker class datacenter is used which transmits the cloudlets with the fitness value to the available virtual machine. For various tasks and virtual machines, the start time, completion time, and execution time of cloudlets are noted. CloudSim entities carry out the simulation, and their configuration is described as follows.

5.1. Experimental Setup and Parameter Settings. Parameters of the simulation configuration for the experimentation and the cloudlets that were used are represented in Table 2.

5.2. Simulation Results. In the simulator, the architecture of our simulation is built where tasks are offloaded to a separate VM ID in the datacenter. In the omnetpp simulator, where a cloud server is used as a datacenter, VM is created for hosting devices, or the wireless network that is created for accessing the VM or datacenter, and the task requests that submit the task download request are cloudlets.

For the omnetpp simulations, a system is developed that will unload the operation of computers and will increase the computing ability of machines with high capacity. We design a framework where a data server is used to offload the service; we use the cloud server as a datacenter; the virtual machine of the VM is generated for the computer of the appropriate user by a wireless network that sends tasks (see Figure 4). Cloudlets operate with the job order, and VM requests to unload the task in the datacenter to improve efficiency.

We took 200 cloudlets in the end, which are submitted on VM. The cloudlet, VM, host, and datacenter settings are kept the same. FCFS, ACO, or PSO are compared for energy consumption. This comparison table shows the time gap in makespan or battery capacity. We used metaheuristic-based algorithms to offload the task using cloudlets (0-200). ACO parameters are settled as $\alpha = 2$, $\beta = 3$, $t_j = 200$, $R_j = 5$ (VM), or max iteration = 100, and PSO parameters are set as $c_1 = 2$, $c_2 = 2$, and w (initial weight); it linearly varies among 0.9 to 0.03 encoding schema = matrix representation.

5.3. FCFS Result. The output of the 200 cloudlets is presented in Table 3 which assigns the task request to the VM that is offloading the task into the datacenter. The required files show the time before the execution or after the execution and also the start time or finish time, so the makespan

Table 3: Yielded values for FCFS.

Cloudlet ID	Status	Priority	Datacenter ID	VM ID	Time	Start time	Finish time	Input file size	Output file size	Battery before exec	Battery after exec	Required files
0	Success	4	2	0	0.11	37.15	37.26	30000	30000	99	98.84	7.766917
1	Success	1	2	1	0.11	15.45	15.56	30000	30000	98.84	98.28	28.47368
2	Success	4	2	2	0.11	36.27	36.38	30000	30000	98.28	97.92	17.94737
98	Success	1	4	18	0.11	16.31	16.42	30000	30000	61.13	60.69	22.09774
99	Queued	3	4	19	-1	0	-1	30000	30000	60.69	60.39	14.66917
197	Queued	4	4	17	-1	0	-1	30000	30000	22.91	22.88	1.691729
198	Queued	3	4	18	-1	0	-1	30000	30000	22.88	22.19	34.65414
199	Queued	2	4	19	-1	0	-1	30000	30000	22.19	22.07	5.864662
						Makespan 37.59				Battery usage 99-22.07		76.93

Table 4: Yielded values for ACO.

Cloudlet ID	Status	Priority	Datacenter ID	VM ID	Time	Start time	Finish time	Input file size	Output file size	Battery before exec	Battery after exec	Required files
0	Success	1	2	0	0.11	21.46	21.57	30000	30000	99	98.92	20.55639
1	Success	4	2	1	0.11	12.15	12.26	30000	30000	98.92	98.79	28.30075
2	Queued	3	2	2	-1	0	-1	30000	30000	98.79	98.68	36.5188
	—				—				—		—	
98	Queued	2	4	18	-1	0	-1	30000	30000	68.13	67.69	26.80451
99	Queued	2	4	19	-1	0	-1	30000	30000	67.69	67.39	27.30827
100	Success	5	2	0	26.26	0.2	26.46	30000	30000	67.39	67.18	26.26316
	—				—				—		—	
197	Queued	3	4	17	-1	0	-1	30000	30000	32.96	32.82	4.210526
198	Queued	2	4	18	-1	0	-1	30000	30000	32.66	32.47	17.07519
199	Queued	4	4	19	-1	0	-1	30000	30000	32.47	32.23	17.96241
						Makespan 30.82				Battery usage 99-32.23		66.77

Table 5: Yielded values for PSO.

Cloudlet ID	Status	Priority	Datacenter ID	VM ID	Time	Start time	Finish time	Input file size	Output file size	Battery before exec	Battery after exec	Required files
0	Success	4	2	0	0.11	6.42	6.53	30000	30000	99	98.94	3.165414
1	Success	4	2	1	0.11	16.24	16.35	30000	30000	98.94	98.82	28.2406
2	Success	3	2	2	0.11	9.05	9.16	30000	30000	98.71	98.59	9.458647
	—		—				—		—			
98	Success	3	4	18	0.11	11.23	11.34	30000	30000	79.11	78.88	36.90977
99	Success	5	4	19	0.11	17.55	17.66	30000	30000	78.88	78.62	22.96992
100	Success	4	2	0	0.11	6.64	6.75	30000	30000	78.62	76.28	33.73684
	—		—				—		—			
198	Queued	3	4	18	-1	0	-1	30000	30000	54.87	54.74	10.45113
199	Queued	5	4	19	-1	0	-1	30000	30000	54.74	54.58	12.85714
						Makespan 21.78				Battery usage 44.42		99-54.58

Table 6: Results comparison calculations.

No. of cloudlets	FCFS		ACO		PSO	
	Makespan (in sec.)	Battery usage (in %)	Makespan (in sec.)	Battery usage (in %)	Makespan (in sec.)	Battery usage (in %)
50	9.39	99 – 88.28 = 10.72	7.7	99 – 90.95 = 8.05	5.8	99 – 92.06 = 6.94
100	18.82	99 – 66.21 = 32.79	15.51	99 – 80.01 = 18.99	10.89	99 – 84.89 = 14.11
150	27.8	99 – 45.94 = 53.06	22.72	99 – 60.02 = 38.98	16.33	99 – 70.78 = 28.22
200	37.59	99 – 22.07 = 76.93	30.82	99 – 32.23 = 66.77	21.78	99 – 54.58 = 44.42

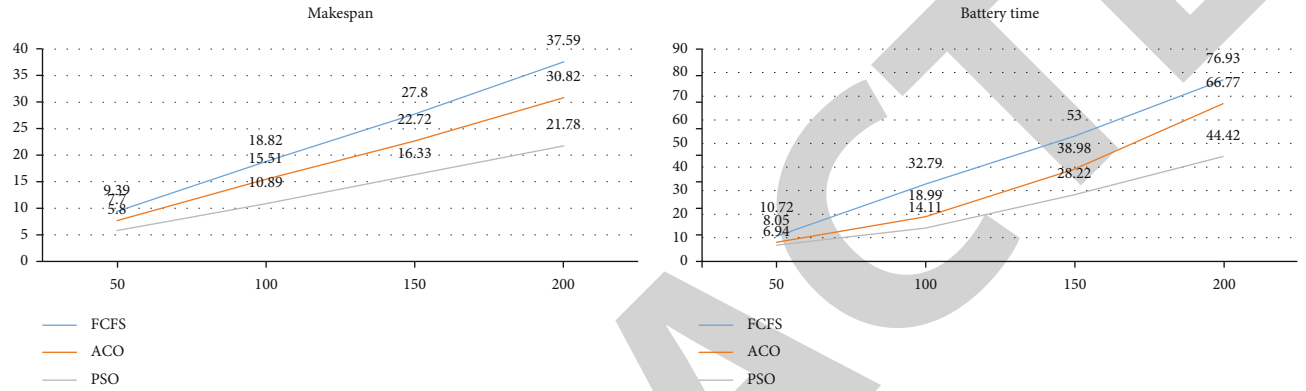

Figure 5: Graphical representation of makespan and battery time.

time shows the less time. Here is the output of the FCFS algorithm with 200 cloudlets.

The FCFS shows the battery life that comes in the order. FCFS resulting makespan time is 37.59, whereas the battery time after execution is 76.93%.

5.4. ACO Result. The ant colony optimization algorithm is based on the behaviors of ants seeking a passage between their colony and a food supply, and it looks for an optimum route in a network. The performance of the 200 cloudlets that assign the work request to the VM that offloads the task to the datacenter is investigated, and the results are presented in Table 4. We delegate VM IDs as a user device in the simulation to order the datacenter to unload the task by cloudlets that request the task to be unloaded in the cloud. The appropriate files often show the start time or completion time before the execution or after the execution so that the makespan time displays less time.

Here is the result generated with 200 cloudlets. ACO provides better results than FCFS; it reduced the makespan time to 30.82 or battery time to 66.77%. We attached the link to 200 cloudlets.

5.5. PSO Result. Now we investigate the performance of 200 cloudlets using 5 VM assigning the assignment to the datacenter so that we use the algorithm of particle swarm optimization which is metaheuristic algorithm. It is created on a shared set of N swarm-sized entities, called a swarm. We take cloudlet IDs which is assigned the request to the virtual machine; the virtual machine assigns the job to be discharged into the datacenter. We allocate VM IDs as a user computer to request in the simulation and the datacenter to unload the task through cloudlets that request the task to be unloaded in the cloud. The performance results in Table 5 indicates the time before or after the execution of the makespan time or battery use time, and the optimization algorithm for particle swarm is better for reducing the makespan time or reducing energy consumption.

PSO performance is better than ACO; it reduces makespan time by 21.78 or battery time by 44.42% (see Table 6); thus, PSO algorithm is better for increasing the efficiency of the device for computational tasks. By using PSO, it reduces the time of execution and makespan. The performance of the particle swarm optimization algorithm is found to be better than these algorithms; it reduces battery usage or enhances the ability of the device; ACO reduces the time of makespan as well as battery time, but particle swarm optimization results in improving the device.

Here, initially, we took battery percentage = 99%, and then each algorithm consumed battery (battery before execution- battery after execution), e.g., in PSO (99 – 54.58 = 44.42), i.e., least in the segment, and shows PSO dominated the results of FCFS and ACO.

Finding reduced time with calculating the PSO to FCFS or PSO to ACO. Overall analysis showed that the evaluation of the time is calculated where PSO is executed time calculated by the FCFS time, so here is the formula we used to calculate the final execution time. Decrease = Original number – new number. Find makespan time and battery usage time result, so we calculate where PSO final execution time is calculated

with FCFS time or ACO. PSO execution time is less than these algorithms; thus, PSO reduces more time.

Makespan time

PSO = 21.78 to FCFS = 37.59 is = 42.06%.

PSO = 21.78 to ACO = 30.82 is = 29.33%.

Battery usage time

PSO = 44.42 to FCFS = 76.93 is = 42.26%.

PSO = 44.42 to ACO = 66.77 is = 33.47%.

Our main purpose is to reduce energy consumption to increase device efficiency. Using metaheuristic algorithms, offload the task and utilize its resources for enhancing the device's capability. Particle swarm optimization reduces the time of execution more than FCFS or ACO or makes the device efficient to handle the task load. Task offloading is better to offload the tasks on the server and make the device more convenient to execute the tasks. Through metaheuristic algorithms comparison, we calculate the execution time of battery usage or makespan time so we find out the PSO is reducing more time than others.

The results in Figure 5 showing makespan time between FCFS, ACO, and PSO confirm the difference between these cloudlets, whereas the graph of battery time usage shows the reduction of battery life between FCFS, ACO, and PSO offloading which is showing the battery life using 50-200 cloudlets.

6. Conclusion and Recommendations

We analyze the performance of the FCFS, ACO, or PSO and find that the ACO performs better than FCFS as well as the PSO. Furthermore, the simulation results showed that the PSO reduces more energy than either of the others. The results of simulations also revealed that the time of execution power is reduced by offloading and the accuracy of job offloading is improved. The ACO makespan is 7% or energy 9.80% less than FCFS, whereas the PSO performs 9% in makespan and 22% in battery time well from ACO.

In our research, we maximize the resource utilization of the machine using heuristic algorithms that reduce the resource availability time that improve the efficiency of the machine. Such measurements help in determining the time complexity and indeed the cloud server during the offloading of the task. In the long term, it is possible to improve the proposed method by taking into consideration the probability of outages associated with real-time network metrics. Offloading is very necessary for effective usage in the cloud world. Different cloud environment offloading algorithms based on this paper are compared with algorithms and evaluated distinguishable offloading parameters such as resource allocation makespan or battery time. In some iterations, PSO and ACO fall into local optima when child tasks exist for better conversion rate and QoS awareness which is a limitation of this research. This can be further enhanced to attain a better response for global optimization in the future. The proposed work can also be implemented in the future as a hybrid of ACO or PSO, or metaheuristic methods, like cost parameters, like cost estimation, or resource usage in the cloud computing environment.

Data Availability

The data can be requested from the corresponding author.

Conflicts of Interest

The authors declare no conflict of interest.

References

[1] C. You and K. Huang, "Multiuser resource allocation for mobile-edge computation offloading," in *2016 IEEE Global Communications Conference (GLOBECOM)*, Washington, DC, USA, 2016.

[2] T. X. Tran and D. Pompili, "Joint task offloading and resource allocation for multi-server mobile-edge computing networks," *IEEE Transactions on Vehicular Technology*, vol. 68, no. 1, pp. 856–868, 2019.

[3] J. Zhang, W. Xia, F. Yan, and L. Shen, "Joint computation offloading and resource allocation optimization in heterogeneous networks with mobile edge computing," *IEEE Access*, vol. 6, pp. 19324–19337, 2018.

[4] J. Zhu, *Computation Offloading and Task Scheduling among Multi-Robot Systems*, resreport, School of Information and Communication Technology Kth Royal Institute Of Technology, Stockholm, Sweden, 2017.

[5] J. Liu, Y. Mao, J. Zhang, and K. B. Letaief, "Delay-optimal computation task scheduling for mobile-edge computing systems," in *2016 IEEE international symposium on information theory (ISIT)*, Barcelona, Spain, 2016.

[6] A. Abbas, A. Raza, F. Aadil, and M. Maqsood, "Meta-heuristic-based offloading task optimization in mobile edge computing," *International Journal of Distributed Sensor Networks*, vol. 17, no. 6, 2021.

[7] S. Guan and A. Boukerche, "A MEC-based distributed offloading model for ubiquitous and time-constraint offloading," in *2019 IEEE/ACM 23rd international symposium on distributed simulation and real time applications (DS-RT)*, Cosenza, Italy, 2019.

[8] A. Mtibaa, K. A. Harras, and A. Fahim, "Towards computational offloading in mobile device clouds," in *2013 IEEE 5th international conference on cloud computing technology and science*, Bristol, UK, 2013.

[9] K. Akherfi, M. Gerndt, and H. Harroud, "Mobile cloud computing for computation offloading: issues and challenges," *Applied Computing and Informatics*, vol. 14, no. 1, pp. 1–16, 2018.

[10] E. V. Dinesh Subramaniam and V. Krishnasamy, "Energy aware smartphone tasks offloading to the cloud using gray wolf optimization," *Journal of Ambient Intelligence and Humanized Computing*, vol. 12, no. 3, pp. 3979–3987, 2021.

[11] Y. Cui, Y. Liang, and R. Wang, "Intelligent task offloading algorithm for mobile edge computing in vehicular networks," in *2020 IEEE 91st vehicular technology conference (VTC2020-spring)*, Antwerp, Belgium, 2020.

[12] A. Mathew, N. E. Deepu, and M. Mohan, "Intelligent edge security with dynamic task offloading in fog environment," in *2019 international conference on communication and electronics systems (ICCES)*, Coimbatore, India, 2019.

[13] D. Rahbari and M. Nickray, "Task offloading in mobile fog computing by classification and regression tree," *Peer-to-Peer Networking and Applications*, vol. 13, no. 1, pp. 104–122, 2020.

Hindawi
Computational and Mathematical Methods in Medicine
Volume 2023, Article ID 9865158, 1 page
https://doi.org/10.1155/2023/9865158

Retraction

Retracted: Exploration of the Effect of Icariin on Nude Mice with Lung Cancer Bone Metastasis via the OPG/RANKL/RANK System

Computational and Mathematical Methods in Medicine

Received 27 June 2023; Accepted 27 June 2023; Published 28 June 2023

This article has been retracted by Hindawi following an investigation undertaken by the publisher [1]. This investigation has uncovered evidence of one or more of the following indicators of systematic manipulation of the publication process:

(1) Discrepancies in scope

(2) Discrepancies in the description of the research reported

(3) Discrepancies between the availability of data and the research described

(4) Inappropriate citations

(5) Incoherent, meaningless and/or irrelevant content included in the article

(6) Peer-review manipulation

The presence of these indicators undermines our confidence in the integrity of the article's content and we cannot, therefore, vouch for its reliability. Please note that this notice is intended solely to alert readers that the content of this article is unreliable. We have not investigated whether authors were aware of or involved in the systematic manipulation of the publication process.

Wiley and Hindawi regrets that the usual quality checks did not identify these issues before publication and have since put additional measures in place to safeguard research integrity.

We wish to credit our own Research Integrity and Research Publishing teams and anonymous and named external researchers and research integrity experts for contributing to this investigation.

The corresponding author, as the representative of all authors, has been given the opportunity to register their agreement or disagreement to this retraction. We have kept a record of any response received.

References

[1] Z. Ruilian, G. Ying, S. Hongmei, and G. Lihua, "Exploration of the Effect of Icariin on Nude Mice with Lung Cancer Bone Metastasis via the OPG/RANKL/RANK System," *Computational and Mathematical Methods in Medicine*, vol. 2022, Article ID 2011625, 9 pages, 2022.

Hindawi
Computational and Mathematical Methods in Medicine
Volume 2022, Article ID 2011625, 9 pages
https://doi.org/10.1155/2022/2011625

Research Article

Exploration of the Effect of Icariin on Nude Mice with Lung Cancer Bone Metastasis via the OPG/RANKL/RANK System

Zhao Ruilian,[1,2] **Gao Ying**,[3] **Shen Hongmei**,[1] **and Guo Lihua**[4]

[1]*Department of Integrated Traditional and Western Medicine, Tumor Hospital of Yunnan Province, The Third Affiliated Hospital of Kunming Medical College, Kunming, Yunnan 650118, China*
[2]*College of Clinical Medicine, Nanjing University of Traditional Chinese Medicine, Nanjing, Jiangsu 210000, China*
[3]*Department of Physiatry, The Second People's Hospital of Kunming, Kunming, Yunnan 650000, China*
[4]*Traditional Chinese Medicine Hospital of Yunnan Province, Kunming, Yunnan 650000, China*

Correspondence should be addressed to Guo Lihua; ynszyyguolihua@163.com

Received 19 January 2022; Revised 18 April 2022; Accepted 26 April 2022; Published 28 May 2022

Academic Editor: Shakeel Ahmad

Epimedium is a traditional Chinese medicine that is most commonly prescribed by practitioners of Chinese medicine for the clinical treatment of malignant tumor bone metastasis. The main component of Epimedium is icariin (ICA). Studies have shown that ICA inhibits bone resorption of osteoclasts through the OPG/RANKL/RANK signaling pathway. Osteoclasts are the only cells in the body that have a bone-destroying capability. The OPG/RANKL/RANK system consists of cytokines that play major roles in osteoclast formation. Therefore, our study selected the OPG/RANKL/RANK system as the research target to investigate the effect of ICA on nude mice with lung cancer bone metastasis. We established the model of bone metastasis in nude mice, intervened the model with icariin and zoledronic acid, and detected the levels of OPG and RANKL by ELISA and western blot. The results showed that ICA had a significant inhibitory effect on bone metastases in nude mice. ICA achieved its antibone metastasis effect in nude mice with lung cancer via inhibiting RANKL expression and simultaneously increasing OPG expression. ICA not only alleviated osteolytic bone destruction caused by bone metastases, but it also reduced weight loss in tumor-bearing nude mice at the late stage of the experiment. The role of ICA in preventing bone metastasis of lung cancer merits further investigation.

1. Introduction

The predilection sites for metastases from lung cancer are the bones [1]. Bone metastasis causes a series of complications such as severe pain, pathological fracture, fatal hypercalcemia, spinal cord compression, and other nerve compression symptoms, which seriously affect the quality of life of the patients [2–4]. Currently, the drugs used in clinical practice to prevent and treat bone metastasis are mainly bisphosphonates [5–7]. These drugs not only display inhibitory effects toward bone destruction but also have antitumor effects. However, long-term use of bisphosphonates may lead to side effects (such as anemia, thrombocytopenia, bone pain, and renal functional impairment), which limits the application of the drugs to a certain extent [8–10].

Epimedium (Yin Yang Huo) is a Chinese herbal medicine that is commonly used in clinical practice for bone injury [11, 12]. Icariin (ICA) is one of the main components of Epimedium extract. In recent years, a number of studies focusing on various bone injuries in animal models of experimental osteoporosis have confirmed the direct effects of Epimedium [13–16] or icariin on the skeletal system and the effects of Epimedium on the expression of bone-related proteins and genes [17–19]. Early in 1985, some Chinese researchers found that Epimedium injection can significantly promote the growth of chicken embryo femur and the synthesis of proteoglycan in vitro, suggesting that Epimedium has a direct effect on the bone system. The results of systematic review and meta-analysis demonstrated that ovariectomized rats treated with icariin had significantly higher bone mineral density (femur

and lumbar spine) and lower bone turnover markers (serum alkaline phosphatase and osteocalcin) compared with the ovariectomized control group [20]. Some studies have showed that icariin can prevent overall progression of chronic high-dose alcohol-induced osteopenia in a rat model, in a dose-dependent manner. Icariin promotes bone formation and inhibits bone loss and effectively restores bone structure and strength in chronic high-dose alcohol-induced osteopenic rats. Bone metabolism reversal is evidenced by increased BV/TV, BMD, MAR, percent trabecular area, and biomechanical properties and elevated [21]. The researchers used New Zealand rabbits as models which were immunized with antigen-induced arthritis (AIA) and treated with icariin. Histological analysis and TEM sections of cartilage in the ICA-treated group showed a low level of chondrocyte destruction. Micro-CT analysis showed that the bone mineral density value and bone structural level in ICA-treated rabbits were significantly higher compared with those in the AIA group. Immunohistochemistry and real-time PCR analysis showed that icariin treatment reduced RANKL expression and enhanced OPG expression levels, as compared to the AIA group. These data indicate that ICA suppresses articular bone loss and prevents joint destruction. This study also determined that ICA regulated articular bone loss in part by regulating RANKL and OPG expression [22].

In addition, the antitumor mechanisms of Epimedium have been explored in many experimental studies. Research demonstrated that ICA has the potential to upregulate LMP/TAP-related molecules and induce the expression of MHC-I, which increases the immune surveillance and keeps cancer in remission. ICA showed an antitumor effect both in vitro and in vivo and may be an effective antigen adjuvant for cancer treatment by enhancing tumor-specific immunity [23]. Some researchers found that icariin can suppress tumor growth and enhance the antitumor activity of 5-FU in CRC by inhibiting NF-κB activity. The antitumor activity of icariin is implicated in the suppression of NF-κB activity and consequent downregulation of the gene products regulated by NF-κB [24].

However, there are few reports on the experimental study of icariin for the antibone metastasis of malignant tumors. Many studies have shown that osteoclasts are the only cells that can destroy bone in vivo. OPG/RANKL/RANK system is a cytokine that plays a major role in the formation of osteoclasts. Therefore, the present study established a nude mice model of lung cancer bone metastasis as the research objective and explored the mechanisms of action of ICA in the nude mice model of lung cancer bone metastasis based on a series of cytokines that play major roles in osteoclast formation (namely, osteoprotegerin (OPG)/receptor activator of nuclear factor kappa-*B* ligand (RANKL)/receptor activator of nuclear factor kappa-*B* (RANK)).

2. Materials and Methods

2.1. Experimental Animals and Cells. Specific pathogen-free (SPF) grade nude mice, 4-6 weeks of age and weighing approximately 19-20 g, were purchased from Beijing Hua Fukang Biotechnology Co., Ltd. and maintained in the Cancer Research Institute of Yunnan Cancer Hospital. SPC-A-1 lung cancer cells were purchased from the cell bank of Chinese Academy of Science, Shanghai, and subcultured in the Cancer Research Institute of Yunnan Cancer Hospital.

2.2. Cell Culture. SPC-A-1 lung cancer cells were cultured in high-glucose Dulbecco's Modified Eagle's Medium (DMEM, Sigma, USA) supplemented with 10% fetal bovine serum (FBS, Sigma) and 1% penicillin/streptomycin (Sigma) under standard conditions (37°C, 5% CO_2, and saturated humidity). The cells were passaged when cell viability exceeded 90%, and the cell adherence rate reached 80%-90%. To passage the cells, the cells were digested with trypsin. Cells in the logarithmic growth phase at a density of 80-90% were collected for future assays.

2.3. Establishment of the Animal Model. A total of 24 nude mice were divided into 4 groups using the random number method (6 mice per group). The care of the animals involved in the experiments and procedures was conducted in conformity with the guidelines on the Administration of Lab Animals and the guidelines on the Humane Treatment of Laboratory Animals (MOST 2006a). This study was approved by the Animal Care and Use Committee of Kunming Medical College (Kunming, China).

The 4 groups included the blank bone metastasis model group (NS), the ICA (CAS: 489-32-7, PLC ≥ 98%; Sichuan Victory Biological Technology Co., Ltd., China) 20 mg/kg + bone metastasis group (ICA20), the ICA 10 mg/kg + bone metastasis group (ICA10), and the zoledronic acid (H20140218, Swiss Novartis Pharmaceutical Co., Ltd.) + bone metastasis group (ZOL). Cells in the logarithmic growth phase at a density of 80-90% were used to construct the animal model. One day before the cells were collected, the culture medium was removed and replaced with fresh medium. Prior to trypsin digestion, 7 large flasks of cells were examined under a microscope (Olympus, Japan) to confirm the absence of contamination. After trypsinization, the cells were collected. The collected cells were washed three times with precooled normal saline to completely remove the serum. Subsequently, the cell pellets were diluted in normal saline to the desired concentration. Each mouse was inoculated with 3×10^6 cells, and the inoculation volume was 30 μL/mouse. After the cells were digested, counted, and diluted, the centrifuge tubes containing the cell suspension were placed on ice, which reduced cell metabolism and ensured cell viability.

Prior to inoculation, the cells in the cell suspension were thoroughly dispersed with a Pasteur pipette, which prevented the reduction of the cell survival rate caused by cell clustering. At the time of cell inoculation, the mice were immobilized using restrainers. The cells were then inoculated using disposable insulin syringes.

The conditions of the mice were observed daily after inoculation of the cells, including food intake, water intake, hair color, mental state, tumor metastasis, and tumor growth. In addition, all groups of nude mice were weighed before establishment of the bone metastasis model, on the 3rd, 10th, and 17th days after establishment of the bone metastasis model

and before sacrifice of the mice. The details of the body weight changes in all groups of mice were recorded.

2.4. Mode of Administration. ICA (20 mg/bottle) was first dissolved in 200 μL of dimethyl sulfoxide (DMSO) and then adjusted to the desired concentrations with normal saline (20 mg/kg and 10 mg/kg group). The prepared ICA solution was stored at 4°C for future assays. The dose administered to the mice was calculated according to the following formula: 9.1 × mg/kg. Since the average body weight of the mice was 20 g, the actual doses administered were 3.64 mg/mouse (ICA20) and 1.82 mg/mouse (ICA10). Both groups of mice received intragastric administration of ICA on the 3rd day after inoculation of tumor cells. Thereafter, ICA was administered once daily (0.1 mL) for a total of 20 doses.

Zoledronic acid (4 mg/bottle) was first dissolved in 5 mL of sterile saline and then diluted to 4 μg/mL with 1000 mL of 0.9% normal saline. The normal dosage for humans is 4 mg/50 kg (i.e., 0.08 mg/kg). Therefore, the dose administered to the mice would be 0.728 mg/kg according to the formula 9.1 × mg/kg. Since the average body weight of the mice was 20 g and the volume of the intraperitoneal injection was 0.2 mL, the content of zoledronic acid would be 0.4 μg. The mice received an intraperitoneal injection of zoledronic acid on the 3rd day after inoculation of tumor cells. Thereafter, zoledronic acid was injected once every other day (0.2 mL) for a total of 10 doses.

2.5. Specimen Collection. All sacrificed mice were dissected. The mouse skull, spine, ribs, limb bones, scapulae, and pelvises were examined by the naked eye for the formation of bone metastases. In addition, the number of bone metastases was recorded.

After the bone metastases and the suspected bone metastases were removed, tumor size was measured. Specifically, the longest and the shortest axes of the tumors were measured using an electronic Vernier caliper.

Mouse blood was extracted from the eyeballs, placed at room temperature (RT) for 30 min, and then centrifuged at 3000 r/min for 5 min. The sera was transferred to 1.5-mL cryotubes and stored at -80°C in an ultra-low temperature freezer.

The collected tumors were photographed with a digital camera. A portion of the tumors was quickly frozen in liquid nitrogen for western blot analysis, while another portion was fixed in formalin for pathological examination.

2.6. Enzyme-Linked Immunosorbent Assay (ELISA). ELISA was used to analyze the levels of RANKL and OPG in serum samples of the nude mice. In the pre-experiments, standard curves were generated based on the standards provided in the kit. In addition, two randomly selected serum samples were diluted to obtain a gradient to determine the optimal dilution ratios for the analysis of the serum samples and standard curves. Standard curves were also plotted in the formal experiment. All serum samples were diluted according to the ratio determined in the pre-experiment. The data were analyzed using a microplate reader (Thermo Scientific, USA). All serum samples were diluted according to the ratio determined in the pre-experiment. Sample analysis was performed in single-wells.

2.7. Western Blot. Total protein was extracted from various groups of tissue specimens. First, radioimmunoprecipitation assay (RIPA) lysis buffer was mixed thoroughly with phenylmethanesulfonyl fluoride (PMSF) at a volume ratio of 100 : 1. The mixture was placed on ice for future use. Subsequently, the weighed tissue specimens were cut into small pieces using disinfected scissors and transferred to the bottom of the homogenizer. The prepared lysis buffer was then added at a ratio of 1 part lysis buffer to 1 gram of tissue. After addition of the lysis buffer, the tissue specimens were homogenized at high speed for several minutes on ice in an attempt to completely break down the tissues. The liquid in the homogenizer was transferred to Eppendorf (EP) tubes, further lysed on ice for 30 min, and then centrifuged at 4°C and 1200 r for 30 min. The resulting supernatants were the total protein solution. The supernatants were collected, aliquoted, and stored at -80°C. The supernatants were subjected to protein quantification by the Bradford method using bovine serum albumin (BSA) as the standard. Glyceraldehyde 3-phosphate dehydrogenase (GAPDH) was used as an internal reference protein. Protein samples (20 μg each) were separated by sodium dodecyl sulfate polyacrylamide gel electrophoresis (SDS-PAGE) on a 10% gel, transferred to nitrocellulose membranes (100 V, 1 h), blocked in blocking solution at 37°C for 1 h, and incubated with primary antibodies at 4°C overnight. Moreover, another membrane was incubated with Tris-buffered saline-Tween-20 (TBS-T) solution containing no primary antibody, which served as the negative control. After repeated washing, the membranes were incubated with alkaline phosphatase (AP)-labeled anti-IgG antibody at RT for 1 h with gentle shaking. After washing, the expressions of RANKL and OPG were examined by western blotting. The absorbance (A) value of each band was determined by image analysis and quantitatively analyzed.

2.8. Pathological Hematoxylin and Eosin (HE) Staining. Paraffin sections were prepared from tissues fixed in 10% neutral formalin solution via the following steps: fixation, dehydration, clearing, infiltration, embedding, and sectioning. After the tissue sections were stained with HE and mounted in neutral resin, the histomorphological characteristics of the mouse bone metastases were examined under a microscope.

2.9. Statistical Analysis. The data in the present study were analyzed using SPSS 21.0 software. The means of multiple samples were subjected to significance testing using one-way analysis of variance (ANOVA). Nonparametric statistical analysis of quantitative survival data was conducted to compare the survival rates of the mice. A p value of less than 0.05 was considered statistically significant.

3. Results

3.1. General Condition of the Animals. The survival of mice in each group was observed after the establishment of the model. During the experimental period, there were 2 deaths in the NS group and 1 death in the ICA10 group. None of

the mice in the ZOL group and ICA20 group died. However, there was no statistically significant difference in the mortality rate among the groups of mice ($p > 0.05$).

Body weight changed in various groups of mice during the experimental period. Before construction of the bone metastasis model, there was no significant difference in the average body weight between the groups of mice ($p > 0.05$). On the 3rd day after the establishment of the model (i.e., at the start of drug administration), none of the mouse groups exhibited a significant change in average body weight. In addition, there was no significant difference in the average body weight among the groups ($p > 0.05$). On the 10th day after establishment of the model (i.e., after 1 week of drug administration), all groups of mice showed varying degrees of average body weight loss. However, there was still no significant difference in average body weight among the groups ($p < 0.05$). On the 17th day after establishment of the model (i.e., after 2 weeks of drug administration), all groups of mice continued to show a decrease in average body weight. The average weight loss in the NS group was not significantly different from that in the ZOL group and ICA10 group ($p > 0.05$). However, a significant difference in the average weight loss was detected between the NS group and ICA20 group ($p < 0.05$). There was no significant difference between all the other groups. Before the mice were sacrificed (i.e., after 3 weeks of drug administration), all groups of mice continued to show a decline in average body weight. In addition, mouse activity, food intake, and water intake also decreased. Two mice in the NS group and one mouse in the ICA10 group died. The average weight loss in the NS group was not significantly different from that in the ZOL group and ICA10 group ($p > 0.05$). However, a significant difference in average weight loss was detected between the NS group and ICA20 group ($p < 0.05$) and between the ZOL group and ICA20 group ($p < 0.05$) (Table 1).

3.2. Tumor Growth Status. Femoral cavity injection resulted in a tumorigenesis rate of 100% in all groups of mice. However, no distant bone metastasis and metastasis to other organs occurred. After the mice were sacrificed, the femur metastases were removed, and the volume and weight of the metastatic tumors were measured (Figure 1(a)). The mean tumor volume and weight were significantly decreased in the ICA20 group in comparison to the NS, ZOL, and the ICA10 groups ($p < 0.05$). In contrast, there was no significant difference in tumor volume and weight among the other groups ($p > 0.05$) (Figures 1(b) and 1(c)).

3.3. Pathological Examination of Mouse Bone Metastases. One specimen of bone metastases was randomly selected from each group for pathological examination. After fixation and decalcification, the specimens were embedded in paraffin and sectioned. HE staining was performed to examine the effect of tumors on bone injury (Figure 2). The results showed that in the NS group, lung cancer cells caused apparent bone destruction. In addition, the infiltration of a large number of irregular tumor cells was observed in the bone cortex and medullary cavity. The tumor cells had enlarged nuclei and displayed apparent atypia. Certain amounts of tumor cells were observed in the medullary cavity of the mice in the ZOL and ICA10 groups. However, the ZOL and ICA10 groups displayed lower degrees of bone destruction and trabecular bone destruction in comparison to the NS group. In the ICA20 group, a certain number of tumor cells were present in the medullary cavity. Bone destruction and trabecular bone destruction were less severe in the ICA20 group than in the NS, ZOL, and ICA10 groups.

3.4. ELISA Analysis of RANKL and OPG Levels in Mouse Serum. The ELISA results are shown in Figure 3. Compared with the NS group, the serum OPG and RANKL levels and OPG/RANKL ratio were significantly increased in all other groups ($p < 0.05$). The serum OPG levels were significantly increased in the ICA10 group in comparison to the ZOL group. However, there was no significant difference in serum RANKL content between the ZOL group and ICA10 group ($p > 0.05$). The serum OPG and RANKL levels and OPG/RANKL ratio were significantly increased in the ICA20 group in comparison to the ZOL group ($p < 0.05$).

3.5. Western Blot Analysis of RANKL and OPG Expression in Bone Metastases. Two specimens were randomly selected from each group and subjected to western blot analysis. The results are shown in Figures 4(a)–4(c). Compared with the NS group, all other groups showed significantly increased expression levels of OPG and RANKL proteins and a significantly elevated OPG/RANKL ratio in the bone metastases ($p < 0.05$). Compared with the ZOL group, the expression of OPG was significantly increased in the ICA10 group ($p < 0.05$). However, there was no significant difference in RANKL expression between the ZOL group and ICA10 group ($p > 0.05$). The serum OPG and RANKL levels and OPG/RANKL ratio were significantly increased in the ICA20 group in comparison to the ZOL group ($p < 0.05$). The results were basically consistent with the expression levels of OPG and RANKL in serum.

4. Discussion

Epimedium is a traditional Chinese medicine that is most commonly prescribed by practitioners of Chinese medicine for the clinical treatment of malignant tumor bone metastasis. The main component of Epimedium is ICA [25]. To date, a large number of studies have described the intervening effect of ICA, the main component of Epimedium, in various animal models of bone injuries (mainly experimental osteoporosis) and various bone-related cells (mainly osteoblasts). Studies have shown that a combination of ICA and stem cells not only improves the osteoporosis-induced bone loss and microstructural destruction of bone tissue in a rat model but also reduces liver and kidney damage in osteoporotic rats [26]. A meta-analysis of the antiosteoporotic effect of ICA showed that ICA has a significant antiosteoporotic effect in ovariectomized rats [27]. In addition, a number of studies have shown that ICA inhibits bone resorption of osteoclasts through the OPG/RANKL/RANK signaling pathway [28].

Osteoclasts are the only cells in the body that have a bone-destroying capability. There is currently no conclusive evidence that tumor cells have the ability to directly destroy bone. The OPG/RANKL/RANK system consists of cytokines that play major roles in osteoclast formation. Osteoclasts originate

Table 1: Body weight changes of mice in various groups (g).

Group	D0	D3	D10	D17	D21
NS	19.78 ± 0.53	19.81 ± 0.85	18.75 ± 0.62	17.03 ± 0.52	16.61 ± 0.42
ZOL	19.89 ± 0.78	19.79 ± 0.95	18.73 ± 0.39	17.61 ± 0.87	16.98 ± 0.55
ICA10	19.88 ± 0.91	19.92 ± 0.49	18.88 ± 0.74	17.78 ± 0.76	16.88 ± 0.76
ICA20	19.65 ± 0.87	19.84 ± 0.79	18.95 ± 0.77	18.11 ± 0.74 *	17.45 ± 0.81 * #

Data was expressed as mean ± SD. $*p < 0.05$ vs. NS group; $\#p < 0.05$ vs. ZOL group. NS: the blank bone metastasis model group; ZOL: the zoledronic acid + bone metastasis group; ICA20: icariin 20 mg/kg + bone metastasis group; ICA10: icariin 10 mg/kg + bone metastasis group.

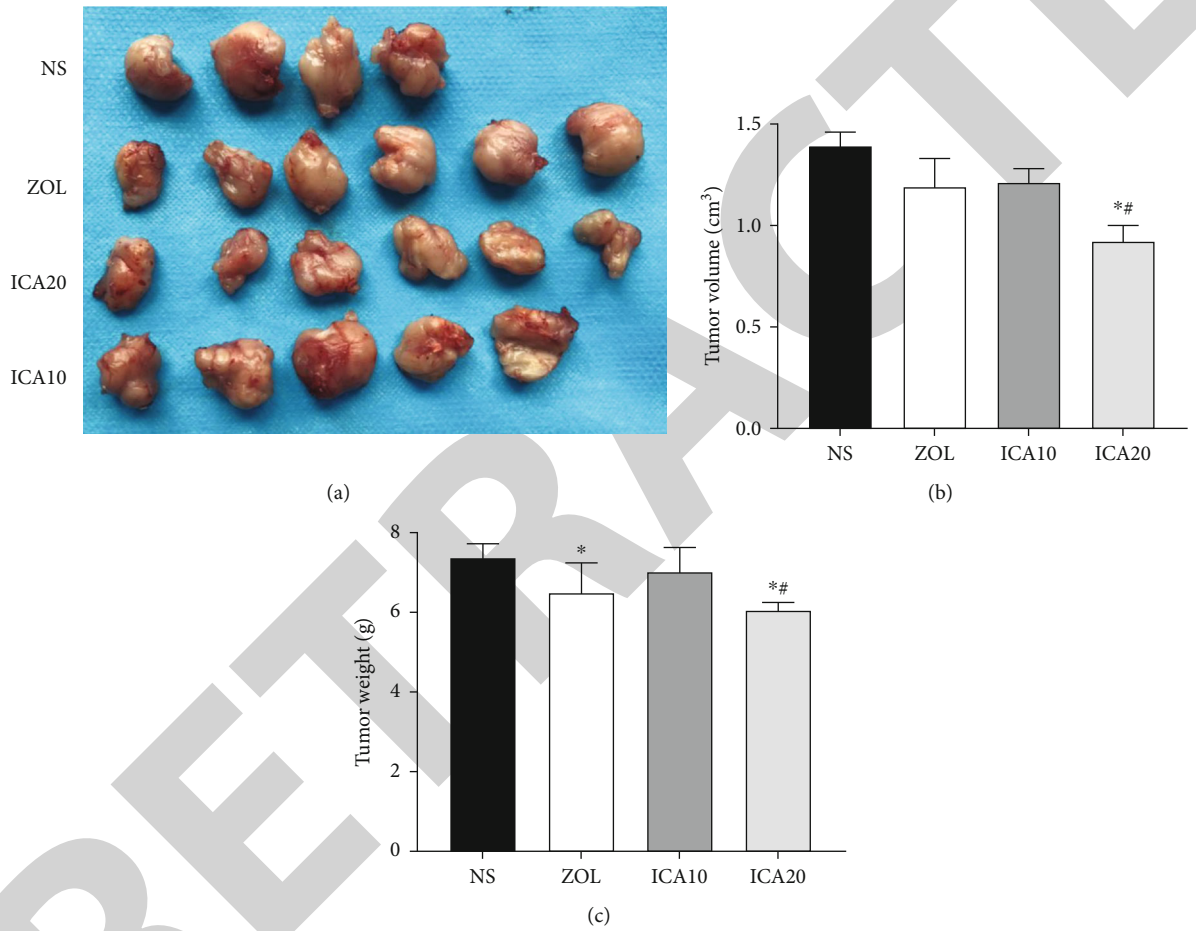

Figure 1: Effect of Icariin on xenograft tumor growth. (a) Images of representative tumors excised from mice in each groups. Tumor volume (b) and weight (c) were measured. $*p < 0.05$ vs. NS group; $\#p < 0.05$ vs. ZOL group. NS: the blank bone metastasis model group; ZOL: the zoledronic acid + bone metastasis group; ICA20: icariin 20 mg/kg + bone metastasis group; ICA10: icariin 10 mg/kg + bone metastasis group.

from the mononuclear macrophage system in hematopoietic tissues. The formation of osteoclasts is regulated by a variety of physicochemical factors. The interaction of RANKL/RANK molecules represents the ultimate common pathway in this process. In the presence of macrophage colony-stimulating factor (M-CSF), osteoclast precursors or osteoclasts contact osteoblasts or bone marrow stromal cells, which allow the binding of RANKL to RANK. Binding of RANKL to RANK stimulates the activation and differentiation of osteoclasts via intracellular signaling pathways. OPG blocks the interaction between RANKL and RANK by binding to RANKL, thereby inhibiting the differentiation of osteoclasts and reducing bone resorption. Therefore, OPG/RANKL/RANK form a trinity system: RANKL on the surface of osteoblasts binds to RANK on the surface of osteoclasts, which promotes the maturation and activation of osteoclasts. In addition, osteoblasts secrete OPG, which binds to RANKL. The binding of OPG/RANKL prevents RANKL from binding to RANK on the surface of osteoclasts and terminates bone resorption, thereby regulating bone resorption and bone formation [29].

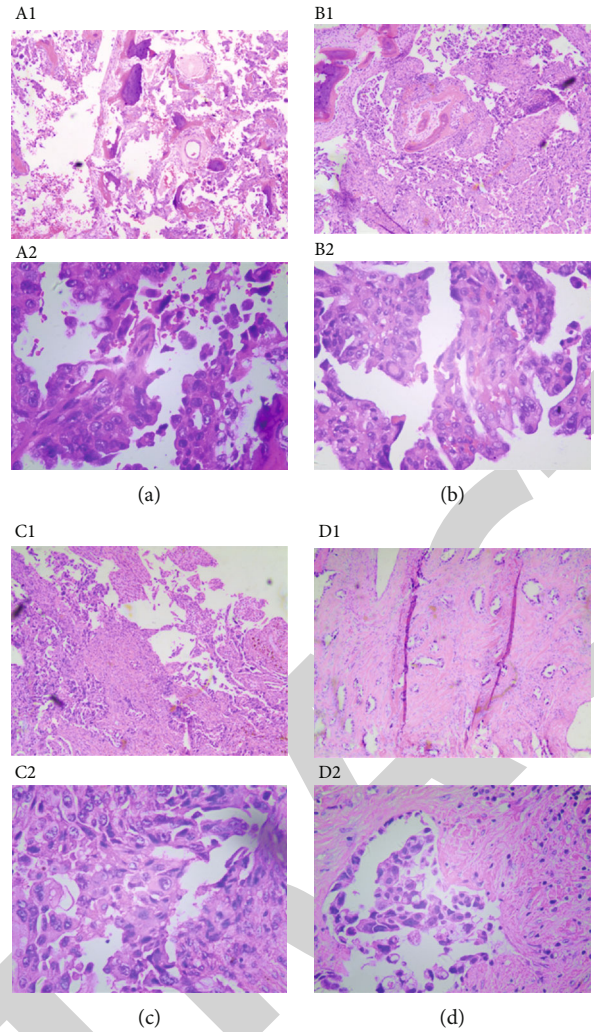

Figure 2: HE staining of tumor in various groups. (a1 and a2) NS group; (b1 and b2) ZOL group; (c1 and c2) ICA10 group; (d1 and d2) ICA20 group. (a1)–(d1) ×4 magnification; (a2)–(d2) ×20 magnification.

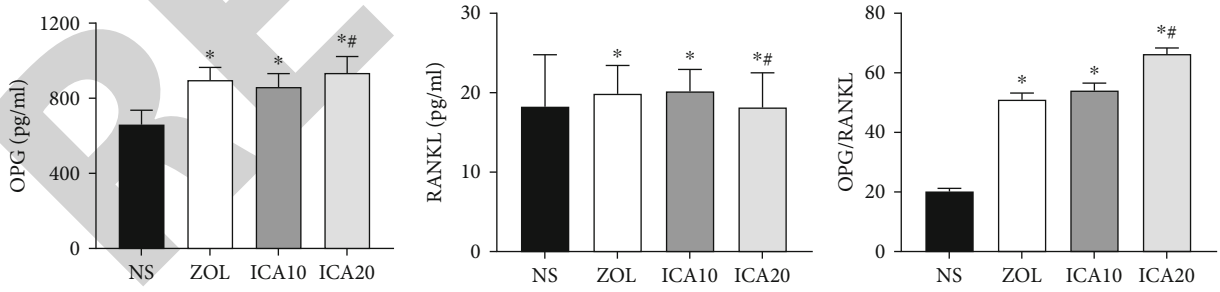

Figure 3: Comparison of ELISA analysis of RANKL and OPG levels in different groups. $*p < 0.05$ vs. NS group; $\#p < 0.05$ vs. ZOL group.

The OPG/RANKL/RANK system is closely related to bone destruction caused by malignant tumors [30]. The mechanisms by which tumor metastasis induces bone destruction have been studied [31]. It is currently believed that metastatic tumor cells directly or indirectly activate the differentiation and maturation of osteoclasts and osteoblasts, resulting in tumor-induced osteoclastic and osteogenic bone destruction [32, 33].

Therefore, the present study selected the OPG/RANKL/RANK system as the research target to investigate the effect of ICA on nude mice with lung cancer bone metastasis. The results showed that ICA had a significant inhibitory effect on bone metastases in nude mice. The tumor volume and weight were reduced in the ICA20 group in comparison to the NS, ZOL, and ICA10 groups. No significant differences were observed in tumors between the ICA10 group and

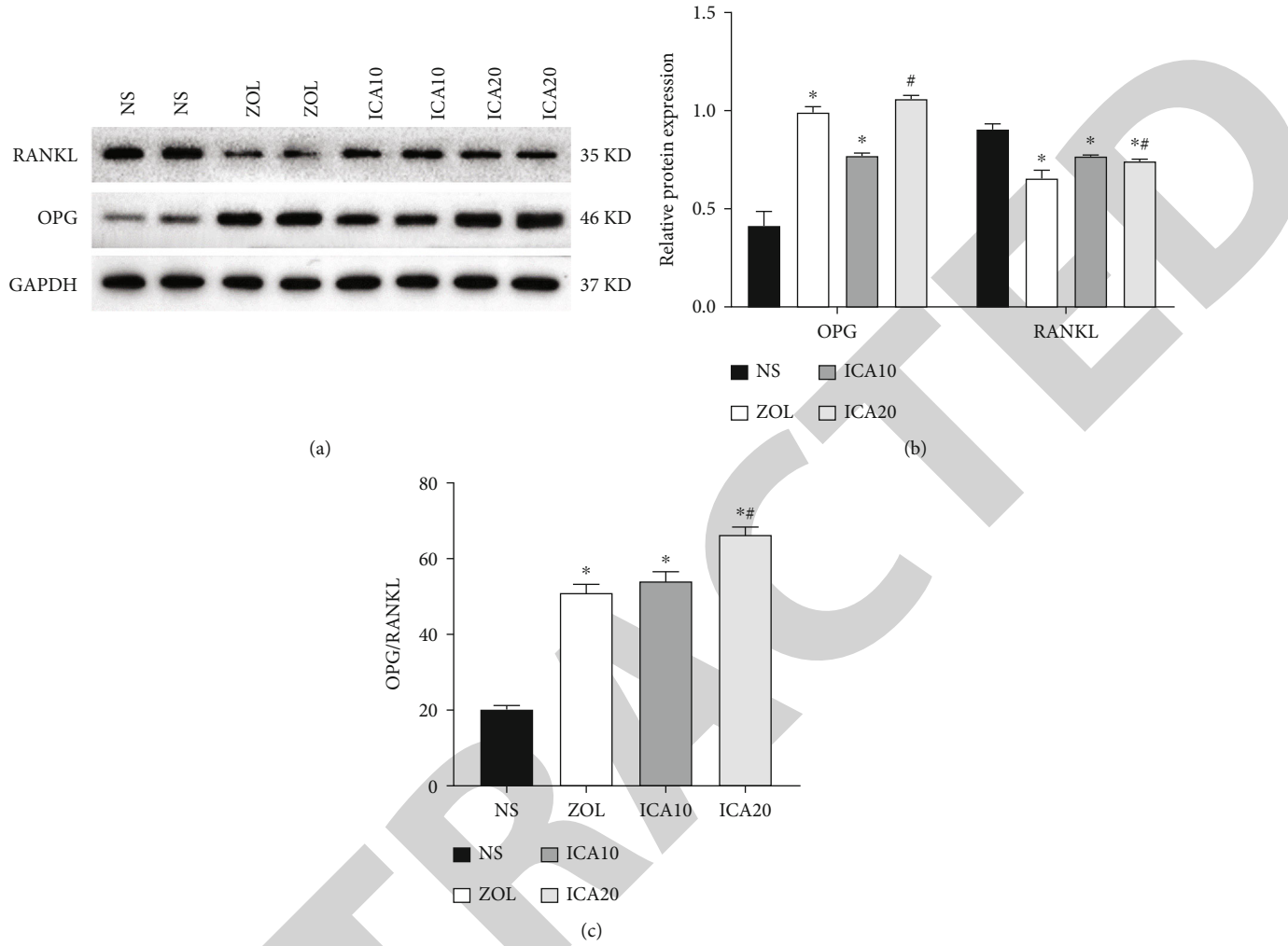

Figure 4: Effect of icariin on the protein expressions of OPG/RANKL. (a) The protein expressions of OPG and RANKL were detected by western blot. (b) Gray value analysis of OPG and RANKL. (c) The ratio of OPG/RANKL. $*p < 0.05$ vs. NS group; $\#p < 0.05$ vs. ZOL group.

blank group. However, the average tumor volume and tumor weight were increased in the ICA10 group compared with the ZOL group. At the end of the experiment, the extent of weight loss was less pronounced in the ICA20 group in comparison to the NS, ZOL, and ICA10 groups. None of the mice in the ICA20 group had died by the end of the experiment. Moreover, food and water intake were more normal in the ICA20 group compared with the other groups. These results demonstrated that, compared with zoledronic acid, a high dose of ICA not only provided a tumor inhibitory effect but also improved the overall life quality of the nude mice. However, the above effects were not apparent in the low-dose ICA group.

To examine the degree of bone destruction, randomized pathological HE staining of bone metastases was performed in the four groups of specimens. Compared with the NS group, a lower degree of bone destruction was observed in the ICA20, ZOL, and ICA10 groups. The ICA20 group showed the lowest degree of bone destruction. Moreover, tumor cell infiltration was reduced in the ICA20 group in comparison to the other groups. The above results demonstrated that ICA improved the tumor-induced osteolytic destruction of femur bone in nude mice.

In the present study, ELISA and western blot analysis of the OPG/RANKL/RANK system yielded consistent results. The serum and tumor tissue expression of OPG were the highest in the ICA20 group among all the groups. Western blot analysis of the tumor tissues showed that the expression level of RANKL was higher in the ICA20 group than in the ZOL group. However, the ICA20 group showed the lowest OPG/RANKL ratio among all the groups, which was consistent with the lowest degree of bone destruction in the ICA20 group. The effect of low-dose ICA (ICA10 group) on OPG/RANKL/RANK was weaker than that of ZOL. However, OPG expression was still significantly higher in the ICA10 group in comparison to the NS group. In contrast, RANKL expression was significantly lower in the ICA10 group in comparison to the NS group. The above results demonstrated that the inhibitory effect of ICA on lung cancer bone metastasis was no weaker than zoledronic acid. Moreover, compared with zoledronic acid, ICA had an overall inhibitory effect on tumors.

Recent research has confirmed ICA can regulate bone formation by upregulating the OPG/RANKL expression ratio in human osteoblast cells [34]. ICA could alleviate or lessen the degree of articular cartilage destruction in CIA rats, and its mechanism might be associated with reducing serum levels of RANKL and elevating levels of OPG, thus further decreasing the ratio of RANKL/OPG [35]. ICA could inhibit bone resorption of osteoclasts through regulating the OPG/RANKL signal pathway [36]. Our results are basically consistent with the results obtained by other researchers in experimental studies of the antitumor effect of ICA. Comparing these studies, this study confirmed that ICA can also regulate bone formation by upregulating the OPG/RANKL expression ratio on bone metastases of mice for the first time.

In summary, the results of the present study showed that ICA achieved its antibone metastasis effect in nude mice with lung cancer via inhibiting RANKL expression and simultaneously increasing OPG expression. ICA not only alleviated osteolytic bone destruction caused by bone metastases, but it also reduced weight loss in tumor-bearing nude mice at the late stage of the experiment. The role of ICA in preventing bone metastasis of lung cancer merits further investigation. There is currently no precedent for the use of ICA alone in clinical practice in the form of a traditional Chinese medicine monomer. However, it is often used clinically as an ingredient in compounds in Chinese medicines. Therefore, the antitumor and antibone metastatic effects of ICA in the nude mouse model of lung cancer bone metastasis necessitate further and in-depth pharmacological, toxicological, and mechanistic investigations.

Data Availability

The data used to support the findings of this study are available from the corresponding author upon request.

Conflicts of Interest

The authors declare that they have no conflicts of interest.

Acknowledgments

This work was supported by the Science Research Fund Project of Yunnan Provincial Health Department Establishment of Research Institutes (No. 2016NS099) and the Science Research Fund Project of Yunnan Provincial Department of Education (No. 2018JS225).

References

[1] J. J. Yin, C. B. Pollock, and K. Kelly, "Mechanisms of cancer metastasis to the bone," *Cell Research*, vol. 15, no. 1, pp. 57–62, 2005.

[2] X. T. Wu, J. W. Zhou, L. C. Pan, and T. Ge, "Clinical features and prognostic factors in patients with bone metastases from non-small cell lung cancer," *Journal of International Medical Research*, vol. 48, no. 5, article 300060520925644, 2020.

[3] R. E. Coleman, "Metastatic bone disease: clinical features, pathophysiology and treatment strategies," *Cancer Treatment Reviews*, vol. 27, no. 3, pp. 165–176, 2001.

[4] G. Selvaggi and G. V. Scagliotti, "Management of bone metastases in cancer: a review," *Critical Reviews in Oncology/Hematology*, vol. 56, no. 3, pp. 365–378, 2005.

[5] M. Aapro, P. A. Abrahamsson, J. J. Body et al., "Guidance on the use of bisphosphonates in solid tumours: recommendations of an international expert panel," *Annals of Oncology*, vol. 19, no. 3, pp. 420–432, 2008.

[6] K. Zarogoulidis, E. Boutsikou, P. Zarogoulidis et al., "The impact of zoledronic acid therapy in survival of lung cancer patients with bone metastasis," *International Journal of Cancer*, vol. 125, no. 7, pp. 1705–1709, 2009.

[7] A. D. Joshi, J. A. Carter, M. F. Botteman, and S. Kaura, "Cost-effectiveness of zoledronic acid in the management of skeletal metastases in patients with lung cancer in France, Germany, Portugal, the Netherlands, and the United kingdom," *Clinical Therapeutics*, vol. 33, no. 3, pp. 291–304.e8, 2011.

[8] L. S. Rosen, D. Gordon, S. Tchekmedyian et al., "Zoledronic acid versus placebo in the treatment of skeletal metastases in patients with lung cancer and other solid tumors: a phase III, double-blind, randomized trial–the zoledronic acid lung cancer and other solid tumors study group," *Journal of Clinical Oncology*, vol. 21, no. 16, pp. 3150–3157, 2003.

[9] L. S. Rosen, D. Gordon, N. S. Tchekmedyian et al., "Long-term efficacy and safety of zoledronic acid in the treatment of skeletal metastases in patients with nonsmall cell lung carcinoma and other solid tumors: a randomized, phase III, double-blind, placebo-controlled trial," *Cancer*, vol. 100, no. 12, pp. 2613–2621, 2004.

[10] N. LeVasseur, M. Clemons, B. Hutton, R. Shorr, and C. Jacobs, "Bone-targeted therapy use in patients with bone metastases from lung cancer: a systematic review of randomized controlled trials," *Cancer Treatment Reviews*, vol. 50, pp. 183–193, 2016.

[11] Y. Chen, J. H. Huang, Y. Ning, and Z. Y. Shen, "Icariin and its pharmaceutical efficacy: research progress of molecular mechanism," *Journal of Chinese Integrative Medicine*, vol. 9, no. 11, pp. 1179–1184, 2011.

[12] J. Zhao, S. Ohba, Y. Komiyama, M. Shinkai, U. I. Chung, and T. Nagamune, "Icariin: a potential osteoinductive compound for bone tissue engineering," *Tissue Engineering. Part A*, vol. 16, no. 1, pp. 233–243, 2010.

[13] I. R. Indran, R. L. Liang, T. E. Min, and E. L. Yong, "Preclinical studies and clinical evaluation of compounds from the genus *Epimedium* for osteoporosis and bone health," *Pharmacology & Therapeutics*, vol. 162, pp. 188–205, 2016.

[14] H. Ma, X. He, Y. Yang, M. Li, D. Hao, and Z. Jia, "The genus Epimedium: an ethnopharmacological and phytochemical review," *Journal of Ethnopharmacology*, vol. 134, no. 3, pp. 519–541, 2011.

[15] J. Lin, J. Zhu, Y. Wang et al., "Chinese single herbs and active ingredients for postmenopausal osteoporosis: from preclinical evidence to action mechanism," *Bioscience Trends*, vol. 11, no. 5, pp. 496–506, 2017.

[16] Z. Wang, D. Wang, D. Yang, W. Zhen, J. Zhang, and S. Peng, "The effect of icariin on bone metabolism and its potential clinical application," *Osteoporosis International*, vol. 29, no. 3, pp. 535–544, 2018.

[17] Y. Tang, Y. Li, D. Xin, L. Chen, Z. Xiong, and X. Yu, "Icariin alleviates osteoarthritis by regulating autophagy of chondrocytes by mediating PI3K/AKT/mTOR signaling," *Bioengineered*, vol. 12, no. 1, pp. 2984–2999, 2021.

Hindawi
Computational and Mathematical Methods in Medicine
Volume 2023, Article ID 9808106, 1 page
https://doi.org/10.1155/2023/9808106

Retraction

Retracted: Corydalis decumbens Can Exert Analgesic Effects in a Mouse Neuropathic Pain Model by Modulating MAPK Signaling

Computational and Mathematical Methods in Medicine

Received 27 June 2023; Accepted 27 June 2023; Published 28 June 2023

This article has been retracted by Hindawi following an investigation undertaken by the publisher [1]. This investigation has uncovered evidence of one or more of the following indicators of systematic manipulation of the publication process:

(1) Discrepancies in scope

(2) Discrepancies in the description of the research reported

(3) Discrepancies between the availability of data and the research described

(4) Inappropriate citations

(5) Incoherent, meaningless and/or irrelevant content included in the article

(6) Peer-review manipulation

The presence of these indicators undermines our confidence in the integrity of the article's content and we cannot, therefore, vouch for its reliability. Please note that this notice is intended solely to alert readers that the content of this article is unreliable. We have not investigated whether authors were aware of or involved in the systematic manipulation of the publication process.

Wiley and Hindawi regrets that the usual quality checks did not identify these issues before publication and have since put additional measures in place to safeguard research integrity.

We wish to credit our own Research Integrity and Research Publishing teams and anonymous and named external researchers and research integrity experts for contributing to this investigation.

The corresponding author, as the representative of all authors, has been given the opportunity to register their agreement or disagreement to this retraction. We have kept a record of any response received.

References

[1] Y. Chen, Z. Jiang, A. Zhang, R. He, Z. Zhou, and S. Xu, "Corydalis decumbens Can Exert Analgesic Effects in a Mouse Neuropathic Pain Model by Modulating MAPK Signaling," *Computational and Mathematical Methods in Medicine*, vol. 2022, Article ID 7722951, 8 pages, 2022.

Hindawi
Computational and Mathematical Methods in Medicine
Volume 2022, Article ID 7722951, 8 pages
https://doi.org/10.1155/2022/7722951

Research Article

Corydalis decumbens Can Exert Analgesic Effects in a Mouse Neuropathic Pain Model by Modulating MAPK Signaling

Yunting Chen,[1] Zongbin Jiang,[2] Aimin Zhang,[2] Ruilin He,[2] Zenghua Zhou,[2] and Shengrong Xu[2]

[1]*Department of Pain Management, The Affiliated Hospital of Guizhou Medical University, Guiyang, 550004 Guizhou, China*
[2]*Department of Pain Management, The Second Affiliated Hospital of Guangxi Medical University, 166 DaXue East Road, Nanning, 530007 Guangxi, China*

Correspondence should be addressed to Zongbin Jiang; gxykdx2018@163.com

Received 21 January 2022; Revised 2 April 2022; Accepted 21 April 2022; Published 27 May 2022

Academic Editor: Muhammad Zubair Asghar

Objectives. This study is aimed at investigating the analgesic effect of the administration of Corydalis decumbens (CD) in a mouse model of postherpetic neuralgia (PHN) and at elucidating its mechanism of analgesic action. *Methods*. Adult Kunming (KM) mice were randomly divided into control, CD, and vehicle-treated groups. Neuropathic pain was induced with a single intraperitoneal injection of resiniferatoxin (RTX). Thermal hyperalgesia was assessed with a hot/cold plate test, and mechanical allodynia was evaluated using von Frey filaments. The activation states of astrocytes, microglia, and the mitogen-activated protein kinase (MAPK) pathway in the spinal cord were determined by immunofluorescence staining and Western blot analysis of Iba-1, GFAP, phospho-p38, and phospho-Jun N-terminal kinase (JNK). *Results*. RTX diminished thermal sensitivity and gradually increased sensitivity to tactile stimulation. The expression of Iba-1, GFAP, phospho-p38 MAPK, and phospho-JNK was upregulated in the RTX-induced postherpetic neuralgia mouse model. Systemic treatment with CD significantly ameliorated thermal sensitivity and mechanical hyperalgesia and was accompanied by a reduction in the expression of Iba-1 and GFAP and reduced phosphorylation of p38 and JNK. *Conclusions*. This study suggests that CD is effective at ameliorating mechanical hyperalgesia in PHN mice and that its mechanism of action may involve modulation of MAPK phosphorylation and glial cell activation. Thus, CD may be a promising alternative therapy for PHN.

1. Introduction

The rhizome of Corydalis decumbens Pers. (CD, named "Xiatianwu" in Chinese, family Papaveraceae) has been used as a Traditional Chinese Medicine (TCM) for the treatment of hemiplegia, hypertension, sciatica, and rheumatic arthritis, and it is officially listed in the Chinese Pharmacopoeia. Prior research has confirmed that alkaloids are the main active ingredients in CD, including protopine, tetrahydropalmatine, palmatine hydrochloride, and bicuculline [1]. Preinjection of protopine has been suggested to restrain the production of proinflammatory cytokines [2, 3] and also alleviate hydrogen peroxide-induced oxidative stress and apoptosis. Pretreatment with protopine can increase cell viability; improve the antioxidant activities of superoxide dismutase, catalase, and glutathione peroxidase; and reduce malondialdehyde levels in PC12 cells that have been injured with H_2O_2 [4]. Furthermore, tetrahydropalmatine possesses antihyperalgesic properties by reinforcing dopamine D1 receptor-mediated dopaminergic transmission [5], and the spatial learning and memory impairment that are induced by repeated administration of methamphetamine could be reversed by tetrahydropalmatine [6, 7]. Although the analgesic effect and anti-inflammatory bioactivity of many alkaloids derived from the rhizome of CD have been investigated, little research has been conducted to describe in detail the mechanism underlying the analgesic effect of CD injections to treat pain.

Postherpetic neuralgia (PHN) is a neuropathic pain syndrome resulting from a severe complication of herpes zoster infection [8]. Patients with PHN often exhibit profound mechanical allodynia and impairment of thermal sensitivity

[9, 10]. While mechanical allodynia and hyperalgesia can be induced by an inoculation with varicella zoster virus or herpes simplex virus type 1 on the hind paw of rats or mice, the viral infection models are often incapable of inducing thermal impairment and have the shortcoming of developing tissue inflammation, skin lesions, and paralysis through spreading of the virus in the central nervous system [11–13]. Previous studies have demonstrated that systemic treatment with resiniferatoxin (RTX), an ultrapotent transient receptor potential vanilloid 1 (TRPV1) agonist, generates long-lasting paradoxical changes in thermal and mechanical sensitivities and can replicate the unique clinical symptoms of patients with PHN [14, 15]. Therefore, intraperitoneal injections of RTX have been used as a nonviral PHN model to explore new treatments that may effectively control this chronic pain condition [16, 17].

Activation of glial cells throughout the central nervous system, which comprise the spinal cord and cortex, and hyperactivation of proinflammatory mediators or neuropeptides are known to be critical in mediating neuropathic pain [18–21]. The mitogen-activated protein kinases (MAPK) are a family of serine/threonine protein kinases that consist of three primary members: extracellular signal-regulated kinase (ERK1/2), p38 mitogen-activated protein kinase (p38), and c-Jun N-terminal kinase (JNK). Many studies suggest that phosphorylation of p38, ERK, and JNK plays a significant role in neuropathic pain [22–25], and therefore, inhibition of the p38 MAPK pathway and/or activation of spinal microglia may be a potential therapeutic target for the treatment of cancer-induced bone pain [22]. Increased ERK, JNK, and p38 activation was demonstrated in a rat model of noncompressive lumbar disk herniation [26]. MAPK phosphorylation in the spinal cord regulates the intracellular responses that drive different downstream signaling events in neuropathic pain [27, 28]. The anti-inflammatory effect of protopine, an alkaloid derived from CD, can inhibit the phosphorylation of MAPK and the activation of NF-κB [3].

This study investigated whether injections of CD could produce antinociceptive effects in a PHN mouse model that was induced by an intraperitoneal injection of RTX. The study further explored the mechanisms underlying CD-mediated antinociception and focused on the involvement of astrocytes and microglia and the activity of the p38 and JNK signaling pathways in the spinal cord. Our findings indicate that injections of CD can regulate the pain threshold by limiting the activation of microglia and astrocytes and by reducing the phosphorylation of JNK and p38 MAPK pathway components in the spinal cord.

2. Materials and Methods

2.1. Animals. Adult male Kunming (KM) mice (body weight, 18~22 g) were housed under a regular light-dark cycle in standard transparent plastic cages with *ad libitum* access to food and water. All handling procedures were approved and reviewed by the Guizhou Medical University (NO.1800959) and conducted in accordance with the guidelines of the International Association for the Study of Pain.

2.2. Experimental Design and PHN Model. Adult KM mice were randomly divided into three groups according to the random number table: control, CD, and vehicle-treated groups (20 per group). The PHN model was utilized in mice for the CD and vehicle-treated groups. Each mouse in the CD and vehicle-treated groups received a single intraperitoneal injection of RTX (50 μg/kg, Sigma, St. Louis, MO), which was dissolved in a mixture of 10% Tween-80 and 10% ethanol in normal saline [29]. The control group received an equal volume of normal saline. According to the dose-to-dose relationship between humans and animals, the CD group was administered daily intraperitoneal injections of 120 μg/kg of CD (Z36020694) in 2 mL of solution that contained protopine (0.4 mg/branch, JiangXi Herbisky Co., Ltd.) beginning 1 week after the RTX injection and lasting for 2 weeks. The vehicle-treated group received an equal volume of vehicle (normal saline containing 10% Tween-80 and 10% ethanol). The experimental design and process are shown in Figure 1(a).

2.3. Nociceptive Behavioral Tests. The behavior tests included mechanical (von Frey filament test) and thermal (hot-plate test) responses. Tests were assessed on the 1st day (T0) before RTX injection and the 1st (T1), 3rd (T2), 5th (T3), and 7th days (T4) after RTX administration and the 1st (T5), 3rd (T6), 5th (T7), 7th (T8), and 14th days (T9) after the initiation of CD injections. All tests were performed blinded to the groups and were conducted during the light phase. All mice were habituated to the testing environment for 30 min before assessment, during which time the exploratory and grooming activities were terminated.

2.3.1. Hot-Plate Test. Thermal hyperalgesia was measured according to the methods described by Li et al. [30]. The hot-plate (IITC, USA) test was implemented at a constant temperature of 55 ± 0.5°C. The mice were enclosed in a plexiglass cage. The paw withdrawal thermal latency to thermal stimulation response (biting or licking hind paws or jumping) was recorded. Each test consisted of three independent trials separated by 30 min intervals. The mean latency for each mouse was calculated. A cutoff of 60 s was used to avoid potential tissue damage.

2.3.2. Von Frey Filament Test. Mechanical allodynia was assessed using von Frey filaments (Stoelting, USA) by placing mice on an elevated wire mesh platform, and the paw withdrawal mechanical threshold (PWMT) was evaluated following application of von Frey filaments to the hind paw [27]. The test was initiated using a 1.0 g filament and ranged from 0.07 to 6 g, depending on the response (decreasing the strength after a positive response and increasing it after a negative response). The stimulation time was less than 5 s, with minimal intervals of 5 min. Biting, rapid pulling back, or shaking of the hind limb during or just after the stimulus was taken as a positive reaction.

2.4. Immunofluorescence. At two time points, one before the T4 CD injection and one after the last (T9), nociceptive behavioral responses were measured (T9). The mice were anesthetized with 2% sodium pentobarbital (20 mg/kg) and

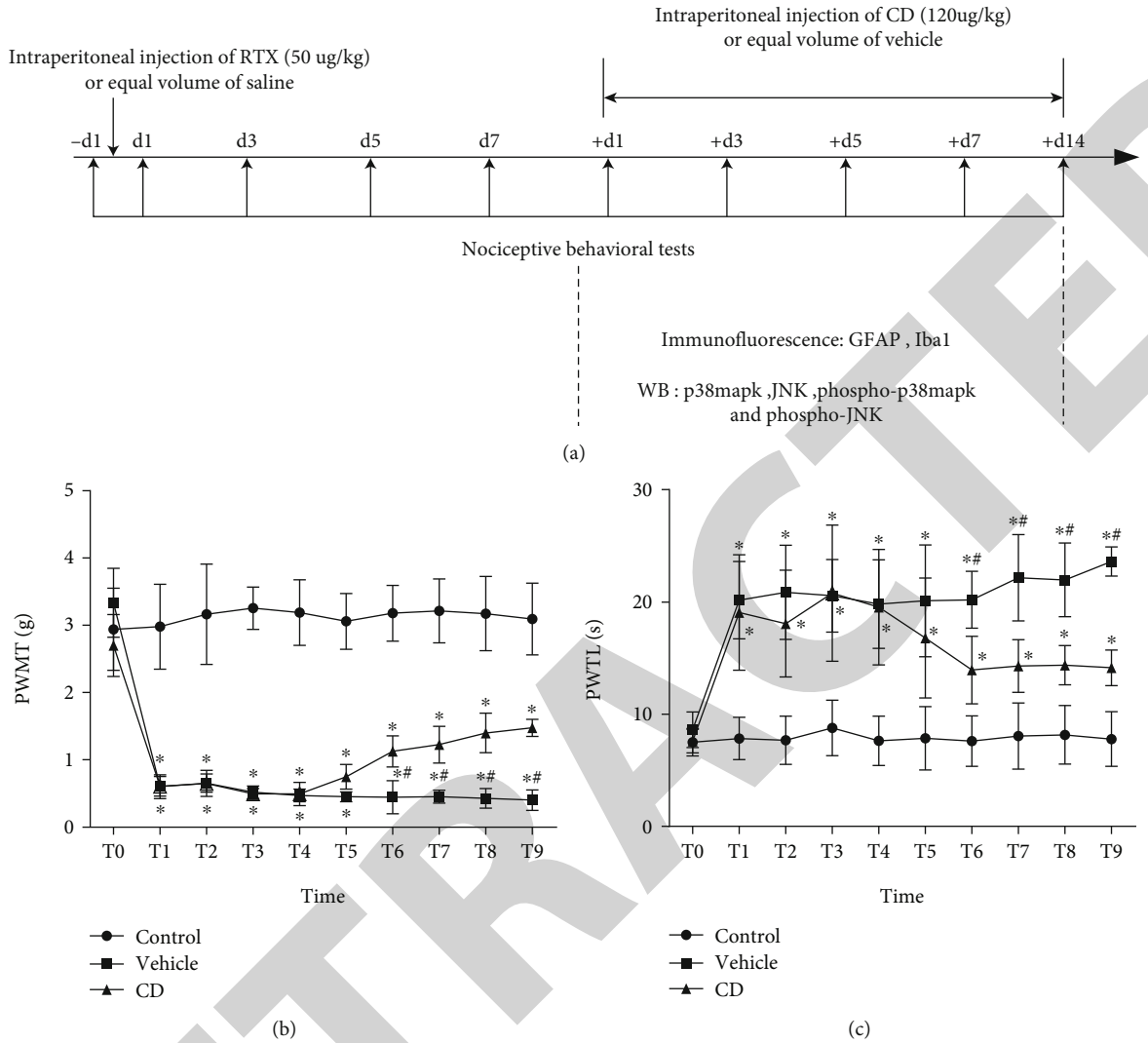

Figure 1: Administration of Corydalis decumbens reverses mechanical allodynia and thermal hyperalgesia. (a) Detailed timeline for the research program. Nociceptive behavioral tests were conducted on the 1st day before RTX injection and on the 1st, 3rd, 5th, and 7th days after RTX injection and on the 1st, 3rd, 5th, 7th, and 14th days after the administration of CD. The immunofluorescence and Western blot experiments were conducted before the CD injection treatment and after the last nociceptive behaviors were measured. (b, c) The administration of Corydalis decumbens attenuates mechanical allodynia and thermal hyperalgesia in a mouse model of neuropathic pain. $^{*}P < 0.05$ compared to the control group; $^{\#}P < 0.05$ compared with T4.

perfused transcardially with 50 mL of sterilized saline, followed by 100 mL of freshly prepared cold 4% paraformaldehyde in 0.1 M phosphate-buffered saline, (pH 7.4). The L4–L6 segments of the spinal cord were removed and post-fixed in 4% paraformaldehyde, and the fixed samples were dehydrated, embedded in paraffin, and sectioned (3 μm thickness, Leica, USA) [27, 31]. The slides were rehydrated, and antigen retrieval was performed prior to immunohistochemical staining. Slides were rinsed with PBS and incubated in a blocking buffer containing 0.3% Triton™ X-100 and 5% normal serum from the same species as the secondary antibody, in 0.1% PBS for 1 h at room temperature. Slides were then incubated with primary mouse anti-GFAP antibody (1 : 300, #3670, Cell Signaling Technology) and rabbit anti-Iba1 antibody (1 : 50, #019-19741, Wako Pure Chemical Industries, Osaka, Japan) for 24 h at 4°C. This incubation was followed by the addition of the corresponding secondary antibodies that were conjugated with Alexa Fluor®: 488-labeled goat anti-rabbit IgG (1 : 250) and 555-labeled Donkey anti-mouse IgG (1 : 250) in a dark chamber for 1 h. Finally, the sections were washed with PBS, a coverslip was applied, and stained sections were examined. Photographs were obtained under a fluorescent microscope (OLYMPUS, Japan), and both the intensities and areas of Iba1 and GFAP staining were measured using the ImageJ software (NIH, Bethesda, USA).

2.5. Western Blotting. Animals were decapitated under anesthesia with 2% sodium pentobarbital (20 mg/kg), and the L4-L6 spinal cord was quickly removed and homogenized in RIPA lysis buffer containing protease and phosphatase inhibitors. Total protein was extracted, and protein concentrations were quantified using a BCA Protein Assay Kit (70-PQ0012, MultiSciences Biotech Co., Ltd., China). A 20 μg of

total protein from each sample was loaded onto each lane, separated by 12% SDS-PAGE, and then transferred to a PVDF membrane in transfer buffer containing methanol. The membranes were blocked with 5% nonfat dry milk for 1 h, washed in Tris-buffered saline containing 0.1% Tween-20 (TBST), and then incubated with the following primary antibodies overnight at 4°C: rabbit anti-p38 MAPK antibody (1 : 1000, #8690T, Cell Signaling Technology), rabbit anti-phospho-p38 MAPK antibody (1 : 1000, #4511, Cell Signaling Technology), rabbit anti-SAPK/JNK antibody (1 : 1000, #9252T, Cell Signaling Technology), mouse anti-phospho-SAPK/JNK antibody (1 : 2000, #9255, Cell Signaling Technology), and anti-GAPDH antibody (1 : 20000, PTG). The membranes were washed with TBST and incubated with anti-rabbit or anti-mouse HRP-conjugated secondary antibodies for 1 h. Subsequently, the immunoreactive bands were detected using an ECL reagent (LK-P1421, MultiSciences Biotech Co., Ltd., China), and the intensities of the protein bands were measured by densitometry using the ImageJ software.

2.6. Statistical Analysis. Results are expressed as the mean ± SEM ($\bar{x} \pm s$). The behavioral data were analyzed by an ANOVA test followed by a Bonferroni test as a multiple comparison analysis. Alteration of the expression of the proteins detected was analyzed using a one-way ANOVA, followed by a Bonferroni test. Differences were considered to be statistically significant based on a criterion of $P < 0.05$.

3. Results

3.1. CD Administration Ameliorated RTX-Induced Neuropathy. PWMT and thermal latency were determined at T0-T9. Prior to RTX injections, there were no significant differences in both PWMT and thermal latency among the three groups at T0 (Figures 1(b) and 1(c), $P > 0.05$). From T1 to T4, RTX induced a significant decrease in PWMT and increase in thermal latency in the CD and vehicle-treated groups, compared with the control group ($P < 0.05$). From T6 to T9, intraperitoneal injections of 120 μg/kg CD significantly ameliorated the mechanical hypersensitivity and decreased the withdrawal thermal latency compared with the vehicle group ($P < 0.05$).

3.2. CD Administration Significantly Reduced the Expression of GFAP and Iba1 in RTX-Induced PHN Mice. Immunofluorescence was utilized to identify changes in GFAP and Iba1 expression in the ipsilateral L4–L6 spinal cord. Previous research has shown that microglia and astrocytes are rapidly activated in the RTX-induced neuropathic pain models [9]. In this investigation, immunofluorescent images substantiated that these intraperitoneal injections of RTX significantly increased GFAP and Iba1 immunoreactivity in the spinal cord compared to the control group ($P < 0.05$). Compared to T4, protein levels of GFAP and Iba1 were significantly decreased in the CD treatment group at T9 ($P < 0.05$), but not in the vehicle group. These data suggest that RTX significantly stimulated microglia and astrocyte activation. Intraperitoneal administration of CD prominently inhibited RTX-induced astrocyte and microglia activation, as treatment with vehicle after RTX injection did not prevent activation (Figure 2).

3.3. Treatment with CD Effectively Attenuated p38 and JNK Phosphorylation in the Spinal Cord of RTX-Induced PHN Mice. Prior studies have confirmed that JNK and p38 MAPK activities promote the initiation and maintenance of neuropathic pain [23, 32]. These kinases are activated by phosphorylation. Western blotting was utilized to investigate if the administration of CD modulated the phosphorylation state of these two proteins. Western blotting demonstrated that RTX injections significantly increased the amount of phospho-JNK and phospho-p38 MAPK in L4-L6 spinal cord at T4 compared to the control group (Figure 3, $P < 0.05$). Following treatment with CD, the phosphorylation of p38 and JNK in the spinal cord was significantly reduced at T9 compared with T4. The expression levels of phospho-JNK and phospho-p38 were not changed in the vehicle group at T9 compared with T4. Therefore, these data suggest that intraperitoneal therapy with CD can attenuate RTX-induced phosphorylation of JNK and p38 MAPK (Figure 3).

4. Discussion

In this study, we investigated the mechanism of action of CD in a mouse model of postherpetic neuralgia and its potential use as a treatment for neuropathic pain. Behavioral testing indicated that CD administration improved thermal perception and alleviated mechanical allodynia in RTX-induced neuropathy. Furthermore, treatment with CD also suppressed the activation of microglia and astrocytes and significantly attenuated the expression of phospho-JNK and phospho-p38. Taken together, this study suggests that the analgesic effect of CD is in part due to the suppression of GFAP and Iba-1 expression, as well as downregulation of p38 and JNK phosphorylation in the spinal cord.

Neuropathic pain is a common form of chronic pain that is associated with peripheral and central nerve injury and is characterized by spontaneous pain, hyperalgesia, allodynia, and paresthesia [33]. PHN is a common category of neuropathic pain that can persist for months to years and negatively affects the quality of life and activities of daily life [34, 35]. Its clinical treatment is challenging due to the limited efficacy and severe side effects of conventional analgesics such as opioids, tricyclic antidepressants, anticonvulsants, and nonsteroidal anti-inflammatory drugs [35]. As a TCM, CD has anti-inflammatory and analgesic effects and is currently used in the treatment of rheumatoid arthritis [36, 37]. The alkaloids in CD, such as protopine and tetrahydropalmatine, can also attenuate hyperalgesia and suppress an inflammatory response [2, 38, 39]. Our current research evaluated the antinociceptive effects of CD in RTX-induced PHN mice.

In recent years, our understanding of PHN has centered on the action of neurotransmitters and ion channels. More recently, the critical importance of glial cells in the initiation and maintenance of neuropathic pain has become apparent [27, 40]. Activated spinal cord glia have been observed in

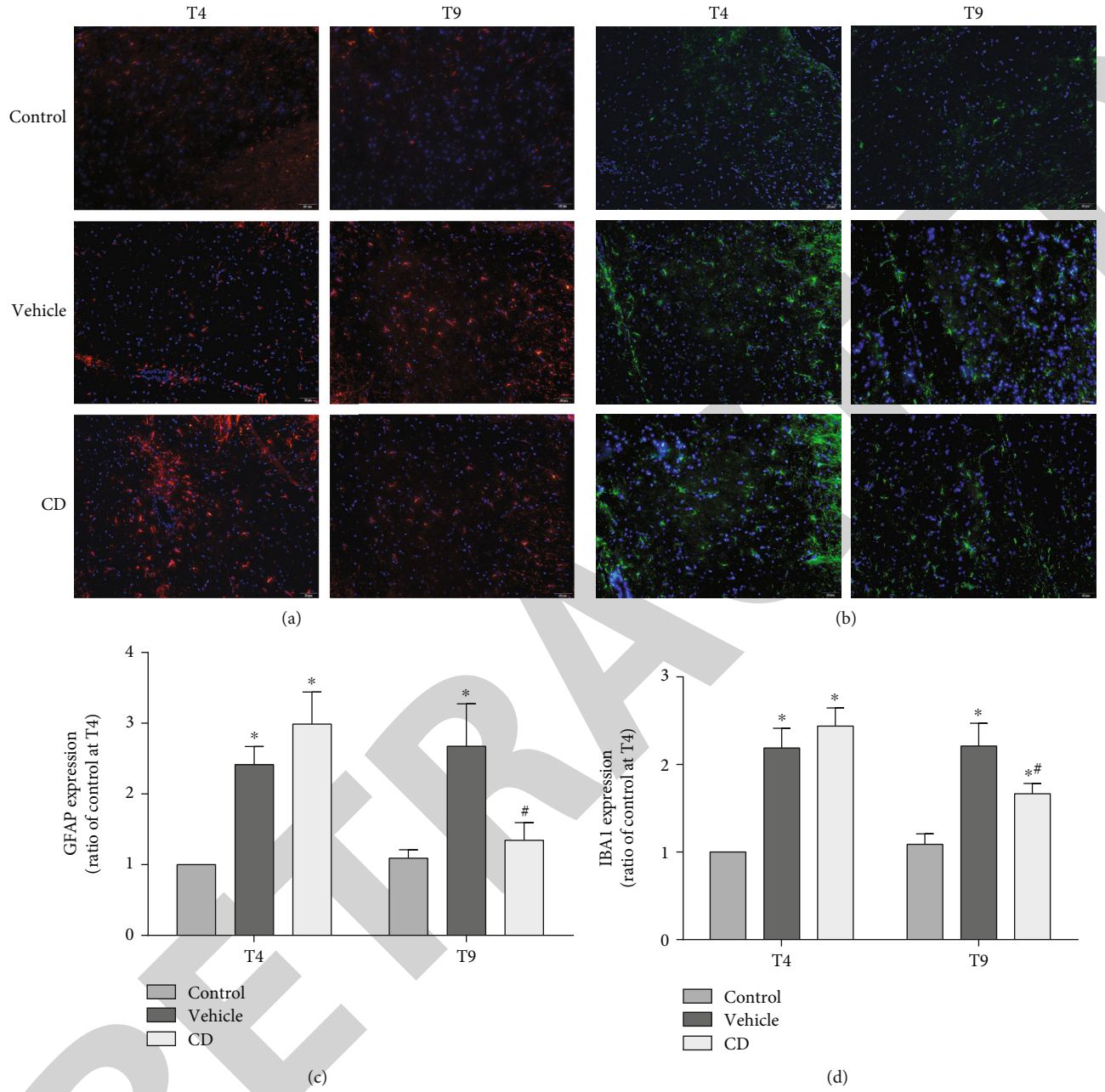

Figure 2: Corydalis decumbens decreases RTX-induced microglial and astrocyte activation in the spinal cord. Immunofluorescence results are expressed as fold changes relative to the control group at T4. (a) GFAP and (c) Iba1, representative photomicrographs of spinal cord sections in the control, vehicle, and CD groups. Image analysis data for GFAP (b) and Iba1 (d). Data are presented as the mean ± SD. $^{*}P < 0.05$ compared with T0; $^{\#}P < 0.05$ compared with T4.

neuropathic pain models, including in the presence of inflammation, nerve injury, and cancer [22, 41, 42]. There is evidence that astrocytes and microglia are activated in the etiopathogenesis of RTX-induced neuropathic pain. Treatment with the glial inhibitors minocycline and fluorocitrate attenuated nociceptive hyperalgesia and the expression of glial cell-related proteins [9]. In addition, in a bone cancer pain model, the natural polyphenol morin attenuated mechanical hyperalgesia and free movement pain by inhibiting the expression of GFAP in the spinal cord [43]. The elevated expression of Iba-1 and OX-42 in diabetic rats significantly declined with intrathecal injections of minocycline, with mechanical allodynia and thermal hyperalgesia also being attenuated [44]. The present investigation demonstrates that the systemic administration of CD could inhibit RTX-induced activation of microglia and astrocytes in the spinal cord and thus attenuate thermal hyperalgesia and mechanical allodynia in mice.

One possible intracellular mechanism that may be correlated with glial cell activation in neuropathic conditions is MAPK pathway activation. Previous studies have demonstrated that JNK phosphorylation in astrocytes and p38

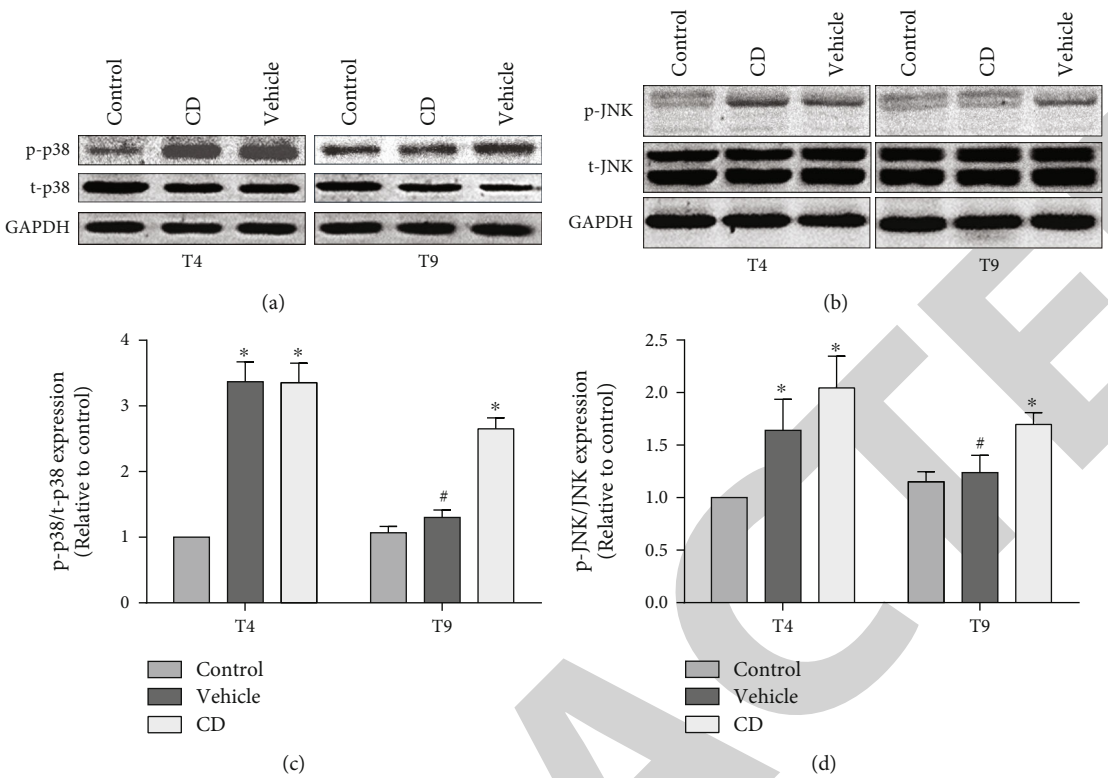

Figure 3: Corydalis decumbens suppresses the phosphorylation of p38 and JNK in the spinal cord. Western blots are expressed as fold changes relative to the control group at T4. (a, c) Western blots indicate that the expression of p-p38/p38 relative to the control was increased in the vehicle and CD groups after injection of RTX at T4, which was significantly inhibited by Corydalis decumbens. (b, d) Western blots indicate that the expression relative to the control was increased in the vehicle and CD groups after injection of RTX. When treated with CD, the expression of p-JNK/JNK was decreased in the CD group. Data are presented as the mean ± SD. $^{*}P < 0.05$ compared with T0; $^{\#}P < 0.05$ compared with T4.

phosphorylation in microglia may be involved in modulating pain conduction in neuropathic states [27]. In chronic constriction injury-induced neuropathic pain models, phosphorylated ERK1/2 and p38 MAPK are elevated [45], and phosphorylation of JNK signaling pathway components participated in pain signal transduction in astrocytes [46]. Furthermore, intraperitoneal injection of RTX leads to the upregulation of p38 MAPK, and treatment with fluorocitrate and minocycline can relieve nociceptive behaviors and reduce p38 expression [9]. Western blotting and immunofluorescence analysis in this study revealed that RTX enhanced the expression of phospho-p38 and phospho-JNK in the spinal cord. The administration of CD dramatically suppressed the expression of phospho-JNK and phopsho-p38.

This study utilized an RTX-induced neuropathic pain model to explore the antinociceptive effects of CD. The study evaluated pain behavior utilizing hot-plate and von Frey tests. The results revealed that significant analgesic effects began on the third day (T6) after treatment with CD. Suppression of glial cell activation and reduced phosphorylation of p38 MAPK and JNK may be strongly related to the potential clinical benefits of CD administration for reducing neuropathic pain.

5. Conclusion

In summary, this study has unveiled a novel direction for the potential treatment of postherpetic pain. The administration of CD significantly alleviated neuropathic pain, attenuated mechanical hypersensitivity, and improved the thermal sensitivity that was induced by RTX. This investigation suggests that the analgesic effect of CD may be associated with glial cells (astrocytes, microglia), p38 MAPK, and JNK. Therefore, CD is a promising candidate for use as a therapeutic analgesic agent.

Data Availability

The data used to support the findings of this study are available from the corresponding author upon request.

Conflicts of Interest

The authors declare that there is no conflict of interest in this investigation.

Authors' Contributions

Zonbin Jiang and Ruilin He conceived and designed the experiments. Yunting Chen, Aimin Zhang, Zenghua Zhou,

and Shengrong Xu performed the experiments. Yunting Chen and Aimin Zhang analyzed the data. Yunting Chen contributed to the preparation of the paper.

Acknowledgments

This study was supported in part by the Natural Science Foundation of Guangxi (2016GXNSFAA380172) and the grants of the Guangxi Zhuang Autonomous Region Health and Family Planning Commission (GZLC16-30).

References

[1] Y. Shen, C. Han, Y. Jiang, X. Zhou, Z. Zhu, and X. Lei, "Rapid quantification of four major bioactive alkaloids in *Corydalis decumbens* (Thunb.) Pers. by pressurised liquid extraction combined with liquid chromatography-triple quadrupole linear ion trap mass spectrometry," *Talanta*, vol. 84, no. 4, pp. 1026–1031, 2011.

[2] D. S. Bae, Y. H. Kim, C. H. Pan et al., "Protopine reduces the inflammatory activity of lipopolysaccharide-stimulated murine macrophages," *BMB Reports*, vol. 45, no. 2, pp. 108–113, 2012.

[3] M. B. Alam, M. K. Ju, Y. G. Kwon, and S. H. Lee, "Protopine attenuates inflammation stimulated by carrageenan and LPS via the MAPK/NF-κB pathway," *Food and Chemical Toxicology*, vol. 131, p. 110583, 2019.

[4] X. H. Xiao, J. Liu, J. Hu et al., "Protective effects of protopine on hydrogen peroxide-induced oxidative injury of PC12 cells via Ca^{2+} antagonism and antioxidant mechanisms," *European Journal of Pharmacology*, vol. 591, no. 1-3, pp. 21–27, 2008.

[5] H. H. Zhou, D. L. Wu, L. Y. Gao, Y. Fang, and W. H. Ge, "L-Tetrahydropalmatine alleviates mechanical hyperalgesia in models of chronic inflammatory and neuropathic pain in mice," *Neuroreport*, vol. 27, no. 7, pp. 476–480, 2016.

[6] G. F. Cao, Y. Zhang, L. Zhu et al., "The inhibitory effect of levo-tetrahydropalmatine on the methamphetamine- induced spatial memory impairment in mice," *Neuroscience Letters*, vol. 672, pp. 34–39, 2018.

[7] Y. J. Chen, Y. L. Liu, Q. Zhong et al., "Tetrahydropalmatine protects against methamphetamine-induced spatial learning and memory impairment in mice," *Neuroscience Bulletin*, vol. 28, no. 3, pp. 222–232, 2012.

[8] H. J. Forbes, K. Bhaskaran, S. L. Thomas et al., "Quantification of risk factors for postherpetic neuralgia in herpes zoster patients: a cohort study," *Neurology*, vol. 87, no. 1, pp. 94–102, 2016.

[9] Y. S. Lei, Y.'. Sun, C.'. Lu, Z. Ma, and X. Gu, "Activated glia increased the level of proinflammatory cytokines in a resiniferatoxin-induced neuropathic pain rat model," *Regional Anesthesia and Pain Medicine*, vol. 41, no. 6, pp. 744–749, 2016.

[10] J. Zou, X. Dong, Y. Li et al., "Deep sequencing identification of differentially expressed miRNAs in the spinal cord of resiniferatoxin-treated rats in response to electroacupuncture," *Neurotoxicity Research*, vol. 36, no. 2, pp. 387–395, 2019.

[11] Y. Kuraishi and A. Sasaki, "Animal models and pharmacology of herpetic and postherpetic pain," *Current Topics in Behavioral Neurosciences*, vol. 20, pp. 57–74, 2014.

[12] R. G. Dalziel, S. Bingham, D. Sutton et al., "Allodynia in rats infected with varicella zoster virus–a small animal model for post-herpetic neuralgia," *Brain Research Reviews*, vol. 46, no. 2, pp. 234–242, 2004.

[13] I. Takasaki, T. Andoh, K. Shiraki, and Y. Kuraishi, "Allodynia and hyperalgesia induced by herpes simplex virus type-1 infection in mice," *Pain*, vol. 86, no. 1, pp. 95–101, 2000.

[14] X. C. Yuan, C. H. Wu, F. Gao et al., "Activation and expression of μ-calpain in dorsal root contributes to RTX-induced mechanical allodynia," *Molecular Pain*, vol. 13, p. 174480691771916, 2017.

[15] H. L. Pan, G. M. Khan, K. D. Alloway, and S. R. Chen, "Resiniferatoxin induces paradoxical changes in thermal and mechanical sensitivities in rats: mechanism of action," *Journal of Neuroscience*, vol. 23, no. 7, pp. 2911–2919, 2003.

[16] H. P. Li, W. Su, Y. Shu et al., "Electroacupuncture decreases netrin-1-induced myelinated afferent fiber sprouting and neuropathic pain through mu-opioid receptors," *Journal of Pain Research*, vol. 12, pp. 1259–1268, 2019.

[17] B. H. Hong, J. Sun, H. Zheng et al., "Effect of tetrodotoxin pellets in a rat model of postherpetic neuralgia," *Marine Drugs*, vol. 16, no. 6, p. 195, 2018.

[18] U. Ali, E. Apryani, H. Y. Wu, X. F. Mao, H. Liu, and Y. X. Wang, "Low frequency electroacupuncture alleviates neuropathic pain by activation of spinal microglial IL-10/β-endorphin pathway," *Biomedicine & Pharmacotherapy*, vol. 125, p. 109898, 2020.

[19] H. Yang, L. Wu, H. Deng et al., "Anti-inflammatory protein TSG-6 secreted by bone marrow mesenchymal stem cells attenuates neuropathic pain by inhibiting the TLR2/MyD88/NF-κB signaling pathway in spinal microglia," *Journal of Neuroinflammation*, vol. 17, no. 1, p. 154, 2020.

[20] Y. Yin, H. Park, S. Y. Lee et al., "Analgesic effect of toll-like receptor 4 antagonistic peptide 2 on mechanical allodynia induced with spinal nerve ligation in rats," *Experimental Neurobiology*, vol. 28, no. 3, pp. 352–361, 2019.

[21] F. Yang, W. J. Luo, W. Sun et al., "SDF1-CXCR4 signaling maintains central post-stroke pain through mediation of glial-neuronal interactions," *Frontiers in Molecular Neuroscience*, vol. 10, 2017.

[22] M. J. Liu, M. Yao, H. Wang et al., "$P2Y_{12}$ receptor-mediated activation of spinal microglia and p38MAPK pathway contribute to cancer-induced bone pain," *Journal of Pain Research*, vol. 10, pp. 417–426, 2017.

[23] Y. J. Qu, L. Jia, X. Zhang, H. Wei, and S. W. Yue, "MAPK pathways are involved in neuropathic pain in rats with chronic compression of the dorsal root ganglion," *Evidence-based Complementary and Alternative Medicine*, vol. 2016, Article ID 6153215, 8 pages, 2016.

[24] J. Zhou, W. Lin, H. Chen, Y. Fan, and C. Yang, "TRESK contributes to pain threshold changes by mediating apoptosis via MAPK pathway in the spinal cord," *Neuroscience*, vol. 339, pp. 622–633, 2016.

[25] C. H. Guo, L. Bai, H. H. Wu et al., "The analgesic effect of rolipram is associated with the inhibition of the activation of the spinal astrocytic JNK/CCL2 pathway in bone cancer pain," *International Journal of Molecular Medicine*, vol. 38, no. 5, pp. 1433–1442, 2016.

[26] G. S. Miao, Z. H. Liu, S. X. Wei, J. G. Luo, Z. J. Fu, and T. Sun, "Lipoxin A_4 attenuates radicular pain possibly by inhibiting spinal ERK, JNK and NF-κB/p65 and cytokine signals, but not p38, in a rat model of non-compressive lumbar disc herniation," *Neuroscience*, vol. 300, pp. 10–18, 2015.

Hindawi
Computational and Mathematical Methods in Medicine
Volume 2023, Article ID 9756383, 1 page
https://doi.org/10.1155/2023/9756383

Retraction

Retracted: Network Information Security Platform Based on Artificial Intelligence for the Elderly's Health "Integration of Physical, Medical, and Nursing Care"

Computational and Mathematical Methods in Medicine

Received 27 June 2023; Accepted 27 June 2023; Published 28 June 2023

This article has been retracted by Hindawi following an investigation undertaken by the publisher [1]. This investigation has uncovered evidence of one or more of the following indicators of systematic manipulation of the publication process:

(1) Discrepancies in scope

(2) Discrepancies in the description of the research reported

(3) Discrepancies between the availability of data and the research described

(4) Inappropriate citations

(5) Incoherent, meaningless and/or irrelevant content included in the article

(6) Peer-review manipulation

The presence of these indicators undermines our confidence in the integrity of the article's content and we cannot, therefore, vouch for its reliability. Please note that this notice is intended solely to alert readers that the content of this article is unreliable. We have not investigated whether authors were aware of or involved in the systematic manipulation of the publication process.

Wiley and Hindawi regrets that the usual quality checks did not identify these issues before publication and have since put additional measures in place to safeguard research integrity.

We wish to credit our own Research Integrity and Research Publishing teams and anonymous and named external researchers and research integrity experts for contributing to this investigation.

The corresponding author, as the representative of all authors, has been given the opportunity to register their agreement or disagreement to this retraction. We have kept a record of any response received.

References

[1] Z. Yang, S. Xia, and S. Feng, "Network Information Security Platform Based on Artificial Intelligence for the Elderly's Health "Integration of Physical, Medical, and Nursing Care"," *Computational and Mathematical Methods in Medicine*, vol. 2022, Article ID 5975054, 11 pages, 2022.

Hindawi
Computational and Mathematical Methods in Medicine
Volume 2022, Article ID 5975054, 11 pages
https://doi.org/10.1155/2022/5975054

Research Article

Network Information Security Platform Based on Artificial Intelligence for the Elderly's Health "Integration of Physical, Medical, and Nursing Care"

Zongyou Yang,[1,2] Siyong Xia,[1] and Sheng Feng[3]

[1]*Department of Physical Education, Chongqing Jiaotong University, Nanan, 400074 Chongqing, China*
[2]*School of Physical Education, Southwest University, Beibei, 400700 Chongqing, China*
[3]*Physical Education Department of Chongqing Medical and Pharmaceutical College, Chongqing 401331, China*

Correspondence should be addressed to Sheng Feng; 10772@cqmpc.edu.cn

Received 18 January 2022; Accepted 16 April 2022; Published 27 May 2022

Academic Editor: Shakeel Ahmad

With the development of my country's economy and society and the improvement of civilization, the silver wave has gradually come. The country has launched a multifaceted pension model, such as institutional pension, home-based pension, and pension real estate. With the increasing aging of the population, traditional elderly care services can no longer meet the growing needs of the elderly. This research mainly discusses the construction of a network information security platform based on artificial intelligence for the elderly's health "integration of physical, medical, and nursing care." The platform consists of five modules: health records, follow-up plans, remote training, health education, and remote consultation. Each module is equipped with a corresponding main interface and/or subinterface. Some modules also have submodules as needed. The structure is reasonable, and the interface is displayed. The combined medical care service model is divided into medical care, care care, and medical care. Among them, the medical care model mainly provides long-term comprehensive care services for the disabled, demented, semidisabled, and other elderly groups. The support-oriented model is mainly for self-care or semi-self-care elderly groups, providing rehabilitation monitoring and life care services. In terms of the overall effect of the platform, 13 users (81.25%) gave a high evaluation of the overall effect of the platform. This research will promote the development of the smart elderly care industry.

1. Introduction

In order to alleviate the problems caused by an aging society, my country has invested in the establishment of a series of elderly apartments, but because it is in its infancy, there are still many areas that need to be improved, especially in terms of demand that are limited to regular meals and housing. And so on, the requirements for the elderly's physical condition monitoring, behavioral status monitoring, and medical recovery have not been well realized.

With the increasing degree of aging in my country, old-age care has become a series of serious problems brought about by the aging process in China. On the premise of ensuring the health of the elderly, it combines intelligent technology to improve the living environment and lifestyle of the elderly, thereby improving living standards of the elderly. The research on the medical and nursing integrated network information security platform can meet the above-mentioned innovative functions and guarantee functions, which has very important research significance.

Information technology, artificial intelligence, and Internet technology were applied to the elderly care service industry, informatization of elderly care services, innovation and integration of elderly care service institutions at all levels, upgrading of traditional elderly care service industries, and improvement of service quality and diversity. Artificial intelligence technology affects all aspects of us. Makridakis believes that industry and the digital (information) revolution have had a significant impact on almost all aspects of society, life, companies, and employment. He will be able

to use the Internet to buy goods and obtain services from anywhere in the world and take advantage of the unlimited additional benefits of the widespread use of artificial intelligence inventions. Although his research avoids the dangers and disadvantages of increased unemployment and increased wealth inequality, it cannot guarantee that it will provide huge opportunities for new products/services and huge increases in productivity [1]. Liu et al. believe that Fuzzy Petri Net (FPN) is a potential modeling technique for knowledge representation and reasoning in rule-based expert systems. In view of this constantly evolving research field, their work provides an overview of improved FPN theories and models from the perspectives of reasoning algorithms, knowledge representation, and FPN models. In addition, they also investigated the application of FPN in solving practical problems in various fields. Although they provided insights and a robust roadmap for further research in this field, the research still lacks innovation [2]. Etminaniesfahani et al. introduce a new metaheuristic algorithm. The Fibonacci indicator algorithm proposed by them has been verified on multiple benchmark functions of up to 100 dimensions, and it can converge and search with algorithms such as DE extension, PSO extension, ABC, ABC-PS, CS, MCS, and GSA. Comparing global optimal capabilities in different research fields, they finally demonstrated the performance of the algorithm through two engineering design problems. Although the application of their proposed Fibonacci indicator algorithm in a wide range of benchmark functions shows its ability to deal with difficult optimization problems, the algorithm is not very smart [3]. Kupcsik et al. believe that in robotics, low-level controllers are usually used to allow robots to solve specific tasks in a fixed environment. In order to adapt the strategy to the new context, they use the hierarchical approach by learning the upper-level strategy that generalizes the low-level controller to the new context. They proposed a new model-based context strategy search algorithm, which can generalize low-level controllers and is data-efficient. Although the learning framework they proposed accelerates the learning process by two orders of magnitude, while learning high-quality strategies, the research process is too complicated [4]. The state has issued a series of documents and policies, pointing out that it is necessary to promote the connection between medical and health care and elderly care service models and to explore new models of elderly care services.

In today's social context, the problem of old-age care is becoming more and more prominent. With the support of pension policies in recent years, pension institutions have emerged, and more and more elderly people have favored and chosen pension institutions. The platform consists of five modules: health records, follow-up plans, remote training, health education, and remote consultation. Each module is equipped with a corresponding main interface and/or subinterface. Some modules also have submodules as needed. The structure is reasonable, and the interface is displayed, which is friendly and has stable operation of the system and convenient and quick operation. The user enters the platform by entering the user name and password granted and uses each module of the platform to realize the creation, editing, query, and viewing of health files; the creation, editing, query, and viewing of follow-up plans; remote training-related videos, courseware, and examination questions uploading, viewing, and downloading online; and uploading, viewing, and downloading health education-related documents, remote consultation application, review, and query functions. It is suggested to innovate the development model of the old-age service industry based on the national conditions, with the government as the leading role, the market to participate, and the development of basic old-age services as the core. At the same time, actively publicize, mobilize all social forces to join, and raise funds.

2. Research Method

2.1. Artificial Intelligence. Driven by smart technology, in the process of continuous development, some regions continue to integrate the latest smart technologies such as big data, artificial intelligence, and deep learning and reasonably add them to the original system, which is in depth with home care, community care, and institutional care, integrating, exploring, and developing a variety of hobbies and convenient services that can satisfy the elderly and even the elderly living alone and gradually form a new elderly care service system under smart elderly care, so that elderly care services can benefit more elderly people and promote the service line combination of online and offline, software and hardware, information and service, and technology and personnel. "Smart elderly care" can monitor the health of the elderly in an all-around way. For example, wrist sphygmomanometers, watch-type GPS locators, etc., can not only monitor the physical condition of the elderly anytime, anywhere, but also know their activity trajectories.

The evaluation of the effect of information interaction in the context of smart medical care is not only a measure to measure the state of user information exchange and interaction but also the direction of the development strategy of smart medical care. It can be an in-depth analysis of the essential needs of their own information interaction in the context of smart medical care and their important impact on the future development of medical care. At the same time, the evaluation of the effect of information interaction in the context of smart medical treatment can guide smart medical platforms and institutions to enhance their core competitiveness, provide high-quality services, and promote the dynamic adaptation and organic integration of smart medical platforms and institutions, users, and the smart medical context. It goes without saying.

By integrating and optimizing medical resources and pension resources, establishing a collaborative and innovative comprehensive service platform, and exploring a sound "integration of medical care and nursing care" service model and effective long-term care methods, we can provide a reference for the public health service topic of smart elderly care. The evaluation system of information interaction in the context of smart medical treatment runs through the entire medical process. It should be a complete scientific system, including the comprehensiveness of the user subject, as well as the integrity and systemicity of information

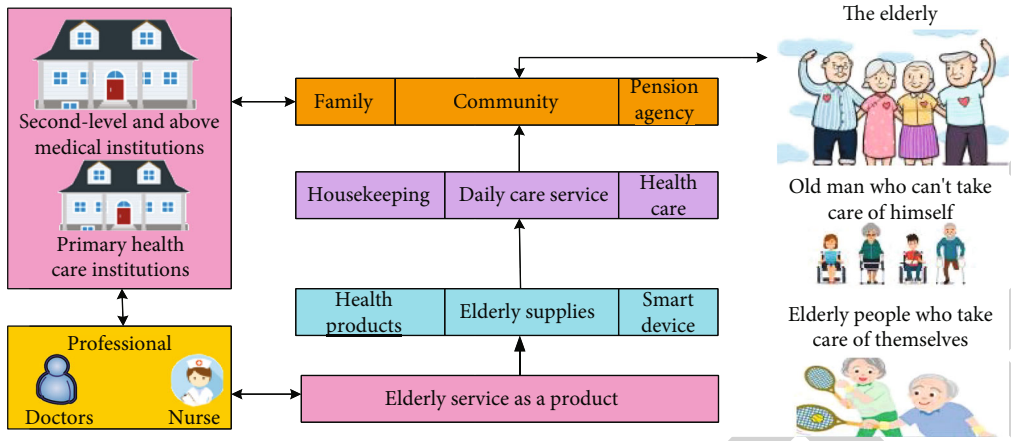

Figure 1: Medical care integration model.

interaction. The results of the effect evaluation should be able to reveal the roles and connections between various levels, various dimensions, and various indicators. These indicators are effective for users, and their internal connections can be fully presented through some form of association. The evaluation process and results also need to maintain integrity and reveal user information interaction through hierarchical and structured result presentation, so that the results can maintain objectivity and authenticity. Normalize each column of the judgment matrix, namely [5],

$$b_{mn} = \frac{a_{mn}}{\sum_{i=1}^{n} a_{mn}} \ (m, n = 1, 2, 3, \cdots, n). \tag{1}$$

After normalization, the sum of the elements in each column is 1. The normalized judgment matrix of each column is added by row, namely [6],

$$V = \sum_{j=1}^{N} B_{mn} \ (m, n = 1, 2, 3, \cdots, n). \tag{2}$$

The intelligent elderly care system is based on the Internet of Things technology, and electronic chip devices are implanted in the home elderly care equipment, so that the daily life of the elderly is in a remote monitoring state. Normalize the vector $V = [v_1, v_2, \cdots, v_n]^T$ [7]:

$$w_i = \frac{v_i}{\sum_{i=1}^{n} v_i} \ (i, j = 1, 2, 3, \cdots, n). \tag{3}$$

Calculate the largest characteristic root $\lambda_{\max}$ of the judgment matrix. Calculate the consistency index CI [8]:

$$\mathrm{CI} = \frac{\lambda - n}{n - 1}. \tag{4}$$

Calculate the consistency ratio CR [9]:

$$\mathrm{CR} = \frac{\mathrm{CI}}{\mathrm{RI}}. \tag{5}$$

To optimize the effect of information interaction from the user's perspective, it is necessary to take the actual needs of users as the starting point and guide users to actively participate in smart medical information interaction activities. On the one hand, it is necessary to clarify the needs and expectations of users to participate in smart medical care, so as to ensure the enthusiasm and initiative of users to participate in smart medical information interaction activities; on the other hand, it is necessary to improve user information literacy to ensure that users can perform in the context of smart medical care. Interactive behavior of high-quality medical information [10]:

$$S(p) = \exp\left(-\frac{\|p - X\|_2^2}{\sigma^2}\right), \tag{6}$$

$$S(p) = \max S^*(P). \tag{7}$$

P is the amount of information, and $S(p)$ is the entropy of information exchange [11].

2.2. Combination of Medical and Nursing Care. Closely combine the basic life care and medical and health services of the elderly, so that they can enjoy convenient and high-quality medical and health care services in the process of providing for the elderly, that is, treatment when they are ill and convalescence when they are free, so as to improve the quality of life of the elderly. The old-age care model of the combination of medical and elderly care can connect elderly care institutions, society, communities, and families together and provide diversified elderly care services for the elderly. The services include life care, entertainment, health care, and long-term care. Its purpose is to provide diversified elderly care services for all types of elderly.

The elderly can enjoy elderly care services in various relevant places. The medical care integration model can better provide the elderly with advanced medical technology, equipment, and professional medical personnel, bring better and richer elderly care services to the elderly, and improve the quality of their elderly life. The old-age service model of the combination of medical and elderly care is aimed

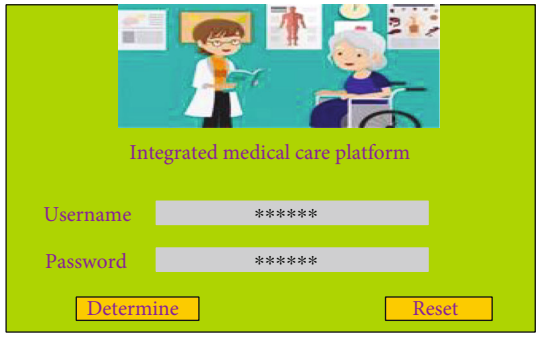

Figure 2: Platform login interface.

not only at the elderly who are suffering from diseases but also for the elderly who can take care of themselves; they can get satisfaction from the old-age services and the prevention and control of diseases. Elderly people suffering from illnesses can get better recovery and control through this old-age care service model that combines medical and elderly care.

There are many different classification standards for the medical and elderly care service model. According to the different positioning of "medicine" and "nourishment," the combined medical care service model can be divided into medical care, care care, and medical care. Among them, the medical care model is mainly for disability and dementia. Elderly groups such as semidisabled need to provide long-term comprehensive care services, which are common in traditional medical institutions; the support-based model is mainly for self-care or semi-self-care elderly groups, which need to provide rehabilitation monitoring and life care services, which are common in nursing homes or community welfare homes, etc.; the mode of equal emphasis on medical care and care is mainly for self-care, just-needed care, and all-stage elderly groups, which need to provide services such as health care and life care, which are commonly found in new independent elderly communities or nursing apartments. The medical care integration model is shown in Figure 1.

Using A as the criterion-level judgment matrix, normalize each column of A to [12]

$$W_{ih} = \frac{a_{ih}}{\sum_{j=1}^{h} a_{ih}}. \tag{8}$$

Sum up W_{ih} according to the line to get [13]

$$W_i = \sum_{j=1}^{n} W_i. \tag{9}$$

Normalize W_i [14]:

$$\lambda = \frac{1}{n}\sum_{i=1}^{n} \frac{(bw)_i}{w}. \tag{10}$$

Here, in order to judge the effectiveness of CI, we define a concept called random consistency RI, which is used to help researchers have a limit on CI [15]:

$$\mathrm{RI} = \frac{\mathrm{CI}_1 + \mathrm{CI}_2 + \cdots + \mathrm{CI}_N}{n}. \tag{11}$$

The realization of artificial intelligence empowered community home care services depends on the development of artificial intelligence technology. The artificial intelligence community needs to strengthen the collection capabilities of elderly care data and improve the storage and computing capabilities of the elderly care information platform. At the same time, the intelligence of the pension algorithm model must be improved. It is necessary to not only improve the instrumental characteristics of AI-enabled community home care services but also reflect the humanized characteristics of artificial intelligence-enabled community home care services. The sample is represented as points distributed on the three-dimensional space S [16]:

$$\left(\phi_{ol}^1, \phi_{om}^1, \phi_{on}^1\right), \left(\phi_{ol}^2, \phi_{om}^2, \phi_{on}^2\right), \cdots, \left(\phi_{ol}^n, \phi_{om}^n, \phi_{on}^n\right). \tag{12}$$

Define the two-dimensional properties of Gaussian kernel local density and distance for the point, which are, respectively, denoted as [17]

$$\vartheta = \sum_{jI\{S\}} e^{-\left(d_{ij}/d\right)2}, \quad d_c > 0. \tag{13}$$

The total number is $N = \tau(\tau - 1)/2$, in ascending order [18]:

$$N = \frac{\tau(\tau - 1)}{2}. \tag{14}$$

2.3. Construction of an Integrated Network Information Security Platform for Medical and Nursing Care. The platform is composed of five modules: health records, follow-up plan, remote training, health education, and remote consultation. Each module has a corresponding main interface and/or subinterface. Some modules also have submodules as needed. The structure is reasonable, and the interface is displayed and has a friendly and stable operation of the system and convenient and quick operation. The user enters the platform by entering the user name and password granted and uses the various modules of the platform to realize the creation, editing, query, and viewing of health files; the creation, editing, query, and viewing of follow-up plans; remote training-related videos, courseware, and examination questions upload, online viewing, and downloading; uploading, online viewing, and downloading of health education-related documents; and remote consultation application, review, and query functions. The platform login interface is shown in Figure 2.

(1) *Health File Module.* The health file module displays the main interface by default and displays the health files of the elderly in the form of a list, which is simple and clear at a glance. Through list reading, you

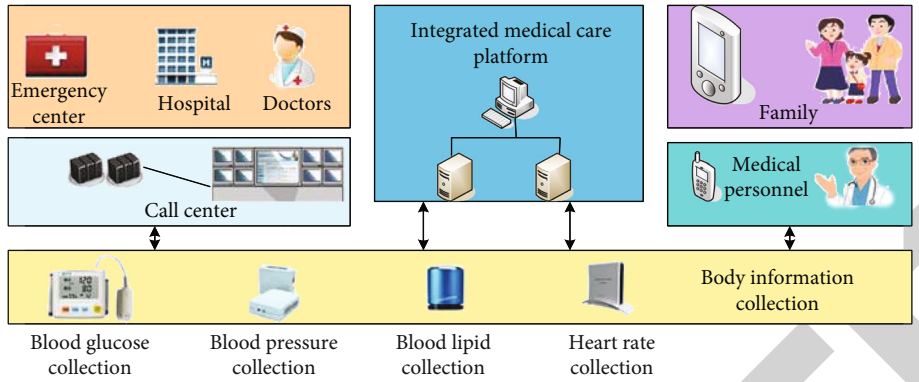

Figure 3: Platform construction architecture.

Table 1: General information on the elderly in the community.

Parameter	Project	Number of cases	Composition ratio (%)
Income and expenditure	Have balance	78	19.02
	Break even	275	67.07
	Make ends meet	57	13.90
	Own expense	37	9.02
Medical insurance type	Rural health insurance	271	66.10
	Urban medical insurance	81	19.76
	Business insurance	133	5.12
Illness	Health	277	32.44
	Sick	78	67.56

can quickly get the key information of a certain health file, such as file number, name, age, file establishment time, and chronic disease status; through the ascending and descending order next to the key information, you can sort the key information, such as sorting by age from big to small, quickly understand the information of the oldest elders, and grasp the age distribution range of the elders in the community. The health file list has a query function, which can be classified and searched according to conditions such as gender, chronic disease, and file establishment time and can also be searched according to file number, name, and ID number and can also be comprehensively searched for multiple conditions. The comprehensive use of functions facilitates community medical staff to quickly obtain key information about the elderly and to understand the health status of the elderly in time. Different color signs of different types of elderly are prominent and clearly displayed, which is convenient for quickly obtaining the classification level of the elderly and also avoids the monotony of the interface and relieves visual fatigue. There are 5 subinterfaces under the main interface, which are basic personal information, health examination, mental state, depression state, and self-care ability. Through the filling and viewing of each subinterface, the establishment and view of the elderly health files are completed. The combined use of drop-down menus and option buttons in the subinterface reduces the frequency of keyboard use, saves information filling time, improves information accuracy and work efficiency, and is particularly important for the insufficient allocation of medical staff in community hospitals. The option setting of the evaluation form entry assigns points. When the entry information is filled in, the system automatically generates the evaluation total score and evaluation level, reducing the process of manual score calculation, improving the efficiency and accuracy of the evaluation, and making the nursing management work more scientific, standardized, and efficient.

(2) *Follow-Up Plan Module*. This module contains 3 submodules, namely, hypertension follow-up plan, diabetes follow-up plan, and special elderly follow-up plan; each submodule contains 1 main interface and 3 subinterfaces, which are follow-up records, follow-up information, and follow-up rules. The researcher adopted a similar design for each submodule, only the display content is different, and the same is true for each interface. This design makes the form of the module and interface more unified, clear, and simple and easy to operate; it also avoids the difficulty and cumbersome nursing management work caused by the module or interface being too

Table 2: The scores of home care needs of the elderly in the community.

Project	Overall demand	Illness care	Prevent disease	Health promotion
Total score	60.24 ± 11.16	25.90 ± 7.00	11.95 ± 1.74	22.39 ± 4.35
Average score	3.54 ± 0.66	3.24 ± 0.88	3.98 ± 0.58	3.73 ± 0.72

Table 3: Ranking of demand for home care services for the elderly in the community.

Parameter	Number of cases in demand	Percentage (%)	Rank
Income and expenditure	366	89.27	1
Medical insurance type	352	85.85	2
Illness	33 1	80.73	4
Own expense	330	80.49	5
Rural health insurance	315	76.83	6
Urban medical insurance	31 2	76.10	7
Business insurance	302	73.66	8
Health	292	71.22	9
Sick	280	68.29	10

complicated, which affects the effect of the platform. The main interface displays follow-up plans in the form of a list. Only the name, age, follow-up type, number of follow-ups, next follow-up time, and other important information of each follow-up plan are displayed in the list, which is simple and clear and easy to read quickly. The paging display of the follow-up plan bar not only improves the loading speed of the page, reduces the opening time of the page, and increases the timeliness of the user's visit but also avoids the bad experience brought to the user by the information listing, makes the important information prominent, and improves the browsing experience convenience. Click on a follow-up plan to view all follow-up records of someone. The follow-up records are also displayed in the form of a list. Click on a follow-up record to view the detailed information of a certain follow-up of someone. Click the "rules" button to enable the follower to quickly understand the corresponding chronic disease follow-up plan, each follow-up subtype, and its corresponding follow-up cycle, provide a reference for the follower, ensure the correct formulation of the follow-up cycle for the elderly, and achieve the health of the elderly real-time observation and dynamic tracking of the situation.

(3) *Remote Training Module*. The remote training module contains a main interface and 3 subinterfaces. The conversion between the main interface and the subinterfaces is realized by clicking on the corresponding fields. The nodes of the main and subinterfaces are distinct, and the conversion is smooth to ensure that the information is clear. The details are appropriate, and it is convenient for users to browse and obtain the best information according to their needs. The training theme of the main interface includes the training sequence, which clearly shows the current training sequence and the total number of remote trainings. By viewing the video subinterface, courseware subinterface, and test question subinterface, you can obtain AVI videos, PPT courseware, and word test questions of related training topics in turn. Not only can you watch online, but also you can "download and print" through the upper right corner of the subinterface button to download and print the corresponding materials, which is convenient for community nurses to study at flexible times and different occasions, reasonable arrangement of study plans, and improvement of the efficiency and enthusiasm of distance training.

(4) *Health Education Module*. The health education module includes the main interface and a subinterface. The main interface displays health education information in the form of a list, including sequence and title, so that community nurses can obtain corresponding health education materials according to their needs. Each health education material contains comprehensive knowledge of definition, etiology, classification, symptoms, treatment, and nursing. Community nurses strengthen their comprehensive understanding of the disease through the study of health education materials, thereby improving their own health education ability and level. Through the "download" and "print" buttons, the corresponding health education materials can also be downloaded and printed, which is convenient for community nurses to store safely and learn flexibly.

(5) *Remote Consultation Module*. The remote consultation module contains 3 submodules, which in turn are consultation application, consultation review, and consultation view. Community nurses use the keyboard or drop-down list to enter the complete information in three parts: basic patient information, patient condition introduction, and consultation purpose, and complete the consultation application initiated at our hospital. The setting of the drop-down list reduces the number of keyboard input and saves the time for filling out the consultation application, which not only improves the work efficiency but also ensures the accuracy of the consultation application information. Consultation experts

Table 4: Single factor analysis of the demand for home care for the elderly in the community.

Project	Number of cases	Mean ± standard deviation
Local	331	60.34 ± 11.17
Out of town	79	59.82 ± 11.20
Elementary school and below	110	57.55 ± 14.08
Junior high school	242	61.15 ± 10.20
High school and above	58	61.53 ± 7.45

Table 5: Multiple linear regression analysis of community elderly care needs at home.

Variable	*B*	Beta	15.126
Constant	56.669	—	7.109
Illness	8.228	0.346	5.202
Age	3.554	0.237	-5.983
Income and expenditure	-4.981	-0.225	3.595
Education	2.712	0.153	-2. 921

can query, view, and fill in the corresponding consultation review results on the consultation review interface, while community nurses cannot operate on the consultation review interface; community nurses can query and view the review status and review of the consultation application that has been initiated through the consultation review interface. For the result, the setting of different user access permissions on the consultation review interface ensures the standardized management and safety of the system, which not only ensures the security and authenticity of the data but also protects the privacy of the hospital and patients [19]. The constructed platform architecture is shown in Figure 3.

3. Results

In this part of the study, a total of 420 questionnaires were distributed, and 410 valid questionnaires were recovered, with an effective recovery rate of 97.62%. Among the 410 community elders, there were 166 males (40.49%) and 244 females (59.51%); 189 cases (46.10%) aged 60-69, 150 cases (36.59%) aged 70-79, and 71 cases (17.32%) aged 80 and older; 133 were healthy cases (32.44%), and 277 were sick cases (67.56%), of which 55.96% of the elderly suffer from two or more diseases at the same time, and the top three chronic diseases are hypertension (35.40%), diabetes (21.50%), and coronary atherosclerotic heart disease (19.00%). The general information about the elderly in the community is shown in Table 1.

The total score of community elderly care needs for home care is 60.24 ± 11.16 points, showing a relatively high level; the total scores of each dimension are disease care 25.90 ± 7.00 points, disease prevention 11.95 ± 1.74 points, and health promotion 22.39 ± 4.35 points. The average score of each dimension shows that disease prevention needs have the highest score, followed by health promotion needs, and disease care needs have the lowest score. Table 2 shows the scores of home care needs for the elderly in the community.

Combine those who selected "not needed," "not much needed," and "indifferent" in the questionnaire and record them as no need for the nursing service item; combine those who selected "need" and "very in need" and record them as correct There is a demand for this nursing service item. Table 3 shows the ranking of demand for home care services for the elderly in the community.

A single factor analysis of the home care needs of the elderly in the community with different demographic characteristics found that the older the age, the higher the demand; the higher the education level, the higher the demand; married elderly people have higher demand than unmarried, divorced, and widowed elderly; for income and expenditure, demand for the surplus is higher; the demand of the sick elderly is higher; the self-care ability is negatively correlated with the demand; the lower the self-care ability, the higher the demand. The single factor analysis of the demand for home care for the elderly in the community is shown in Table 4.

The factors influencing the needs for home care for the elderly in the community are disease, age, income and expenditure, education, marital status, and self-care ability according to the standard regression coefficient. The multiple linear regression analysis of the demand for home care for the elderly in the community is shown in Table 5.

There were 28 males and 60 females in the test group, with an average age of 73.56 ± 6.30 years, and 38 males and 54 females in the control group, with an average age of 73.74 ± 6.04 years. The comparison of the general data of the two groups of community elderly at baseline was not statistically significant ($P > 0.05$), indicating that the general data of the two groups of community elderly at baseline were comparable. The situation of the elderly in the two groups of communities is shown in Figure 4.

Effectiveness evaluation: in terms of operating convenience, 13 (81.25%) users thought that the platform was friendly and easy to operate; in terms of system stability, 4 (25.00%) users encountered network instability, freezes, and lags during use and black screen and other situations; in terms of application value, 14 (87.50%) users believe that through this platform, they can learn advanced nursing technology and experience in general hospitals, provide more high-quality and efficient nursing services for the elderly, and can also deal with problems that the institution cannot solve in a timely manner. In terms of the overall effect of the platform, 13 users (81.25%) have a high evaluation of

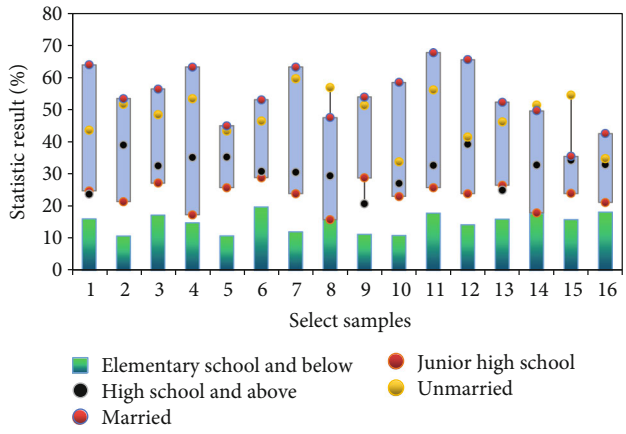

Figure 4: The situation of the two groups of elderly in the community.

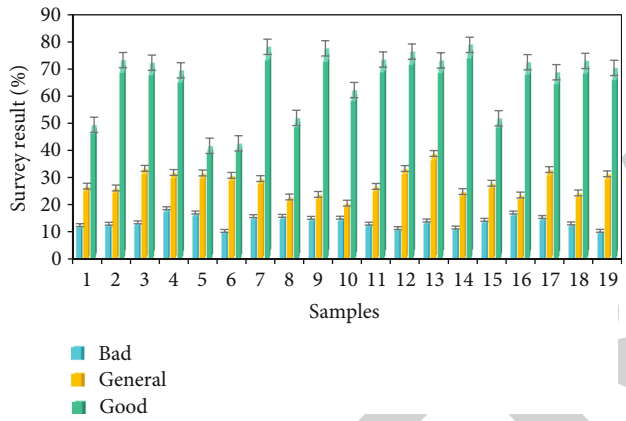

Figure 5: Evaluation results of the platform.

the overall effect of the platform. Another 3 users made suggestions to the platform. The content includes that the follow-up time is more individualized and not easy to remember in time. It is recommended that when the follow-up date is approaching, the system pops up a prompt message; when the health file information is completed and submitted, the system does not display the submission status; it is recommended to add the submission status prompt box; and increase the statistical function of the query results. The evaluation results of the platform are shown in Figure 5.

One month later, the differences in the total scores of the health self-management ability of the two groups of community elders and the scores of each dimension were statistically significant ($P < 0.05$). After one month of intervention, the experimental group had better health self-management ability than the control group. The result after 1 month is shown in Figure 6.

After the intervention for 3 months, the difference in satisfaction of the two groups of community elderly home care services in all aspects was statistically significant ($P < 0.05$). After the intervention for 3 months, the test group's satisfaction with home care services was higher than that of the control group. The intervention satisfaction after 3 months is shown in Figure 7.

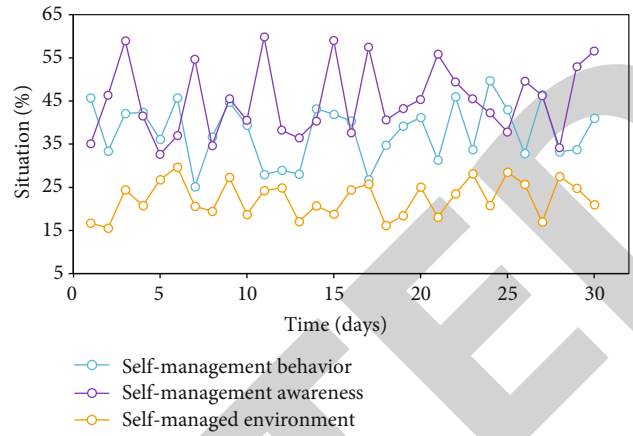

Figure 6: Results after 1 month of intervention.

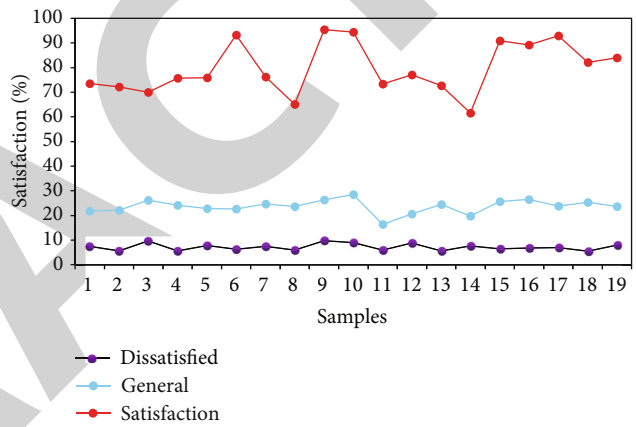

Figure 7: Satisfaction after 3 months of intervention.

After 6 months of intervention, the difference in satisfaction between the two groups of community elderly home care services in all aspects was statistically significant ($P < 0.05$). After 6 months of intervention, the test group's satisfaction with home care services was higher than that of the control group. Intervention 6 results after one month are shown in Table 6.

4. Discussion

In reality, the status quo in most areas is still the separation of medical care and support and their own governance. Even if the medical care integration model is established, the development effect is not very satisfactory. As a result, the elderly cannot truly enjoy their old age, whether it is physical or not physical. Mental health should be actively dealt with, which shows that the medical care integration model can well solve the problem of the health needs of the elderly, which also confirms the necessity of the construction of the medical care integration model. Even if the abovementioned series of problems are solved, the constructed medical care integration service model may still have problems such as resource imbalance, waste of resources, and low utilization efficiency. How to use the concepts and theories of artificial intelligence to be organic with the medical care

Table 6: Results after 6 months of intervention.

Project		Satisfaction	General	Dissatisfied
Instrument appearance	Test group	60	26	2
	Control group	46	34	12
Professional knowledge	Test group	58	28	2
	Control group	42	38	6
Service attitude	Test group	57	25	16
	Control group	43	33	6

integration service model combined and the real realization of artificial intelligence in the elderly care service system is also a question worth pondering [20, 21].

Medical care integration services can be seen as a commodity or a quasipublic product. Therefore, specific to the provider, the provider can be a for-profit organization or a nonprofit organization, or it can be a public sector such as the government. In the process, it is clear that it is not enough to rely solely on a certain aspect of the force. As a service with a more prominent quasipublic product attribute, it must be led by the government, and the effective forces and resources of all aspects must be integrated. It requires the government, profit, and nonprofit organizations to work together to meet the growing demand for services. In terms of service targets, the medical care integration service should not be aimed at all aging people. It should be said that the medical care integration service is essentially an organic system with two levels. The first is "medical." At the level, the medical treatment here involves all aspects, and more is for the aging groups who suffer from chronic diseases and need long-term real-time monitoring; the "nourishing" level is mainly for the daily life of the aging people and should also be taken care of and contains its spiritual needs and psychological needs. Therefore, the target of medical care integration service should be a group with high demand for medical services and certain obstacles to living ability. Only by accurately positioning the service target can we use resources better and more efficiently. The service content should not be based on the traditional daily life care of the aging population. In addition to meeting the physical needs of the aging population, it should pay more attention to the psychological and spiritual needs of the population. In the interpretation of connotation, not only the physical integrity but also the psychological and social adaptability are more important [22]. In addition, medical services should not be separated from the old-age service system but should be integrated into it, and even for specific groups of people, medical services should be the mainstay, and medical services should be regarded as one of the equally important service contents [23, 24].

Based on the analysis of the different levels of the artificial intelligence medical care integration service model, it should also be analyzed in combination with the actual situation in my country. The characteristics of my country's urban and rural areas are very obvious, and the differences are significant. The urban elderly population is relatively better than the rural elderly in all aspects. The population and the educational level of the urban elderly population are generally higher than that of the rural elderly population; these are all factors to be considered [25]. In addition, in the precise segmentation of service targets, we should consider that the current needs of the elderly group are actually multilayered and diverse. Not all elderly groups have "nourishing" service needs, which are completely relevant to life. Or for groups who are basically able to take care of themselves, more needs are the needs for "medicine"; even if it is the need for "medicine," it is only for the elderly who are diagnosed or self-reported with chronic diseases, and there is medical integration. The service needs are often disabled or partially disabled elderly people and elderly people with or without chronic diseases. These should be carefully divided and considered when constructing the artificial intelligence medical care integration service model. The differences are different. The population adopts different service systems and models, which is the integration of artificial intelligence medical care in a complete sense [26–29].

5. Conclusion

This article takes the perspective of artificial intelligence as the starting point, first analyzes the current situation of China's elderly care service demand and supply, and points out that China's current population aging status and future development trends are not optimistic, and it is for the improvement and further development of China's elderly care service system. Put forward an unprecedentedly huge challenge and at the same time analyze in detail several needs of the elderly themselves, mainly including economic needs, health and medical needs, life care needs, and mental and psychological needs; from the number of elderly care service institutions and related elderly care services, the policy is combed to have a more comprehensive understanding of the current status of the supply of elderly care services, and at the same time, it briefly introduces the development history of China's elderly care service system, etc., and discusses the construction of artificial intelligence+medical care based on a series of issues such as the contradiction between demand and supply. The necessity of the integrated service model, starting with the traditional medical care integrated service model case and public perception, analyzes the operating mode of the medical care integrated service organization and on this basis analyzes its advantages, disadvantages, opportunities, and challenges. The traditional medical care integrated service model has many drawbacks,

and it cannot fundamentally meet the diversified needs of the elderly, and it also brings certain pressure to the society. Based on this, it has triggered the exploration of the artificial intelligence+medical care integrated service model.

Data Availability

No data were used to support this study.

Conflicts of Interest

The authors declare that they have no conflicts of interest.

Acknowledgments

This work was supported by the Key Project of Chongqing Education Science "13th Five-Year Plan," No. 2020-GX-116; Project of Chongqing Education Science "13th Five-Year Plan," No. 2019-GX-324; and 2021 Key Project of Teaching Reform Research of Chongqing Jiaotong University (Serial number: 2102004).

References

[1] S. Makridakis, "The forthcoming artificial intelligence (AI) revolution: its impact on society and firms," *Futures*, vol. 90, pp. 46–60, 2017.

[2] H. C. Liu, J. X. You, Z. Li, and G. Tian, "Fuzzy Petri nets for knowledge representation and reasoning: a literature review," *Engineering Applications of Artificial Intelligence*, vol. 60, pp. 45–56, 2017.

[3] A. Etminaniesfahani, A. Ghanbarzadeh, and Z. Marashi, "Fibonacci indicator algorithm: a novel tool for complex optimization problems," *Engineering Applications of Artificial Intelligence*, vol. 74, pp. 1–9, 2018.

[4] A. Kupcsik, M. P. Deisenroth, J. Peters, A. P. Loh, P. Vadakkepat, and G. Neumann, "Model-based contextual policy search for data-efficient generalization of robot skills," *Artificial Intelligence*, vol. 247, pp. 415–439, 2017.

[5] H. Lu, Y. Li, M. Chen, H. Kim, and S. Serikawa, "Brain intelligence: go beyond artificial intelligence," *Mobile Networks and Applications*, vol. 23, no. 2, pp. 368–375, 2018.

[6] D. Hassabis, D. Kumaran, C. Summerfield, and M. Botvinick, "Neuroscience-inspired artificial intelligence," *Neuron*, vol. 95, no. 2, pp. 245–258, 2017.

[7] D. Pomorski and P. B. Perche, "Inductive learning of decision trees: application to fault isolation of an induction motor," *Engineering Applications of Artificial Intelligence*, vol. 14, no. 2, pp. 155–166, 2017.

[8] T. Hester and P. Stone, "Intrinsically motivated model learning for developing curious robots," *Artificial Intelligence*, vol. 247, pp. 170–186, 2017.

[9] V. Yevgeniy and K. Murat, "Adversarial machine learning," *Synthesis Lectures on Artificial Intelligence and Machine Learning*, vol. 12, no. 3, pp. 1–169, 2018.

[10] S. V. Albrecht and P. Stone, "Autonomous agents modelling other agents: a comprehensive survey and open problems," *Artificial Intelligence*, vol. 258, pp. 66–95, 2018.

[11] L. Wei, P. Xing, J. Zeng, J. X. Chen, R. Su, and F. Guo, "Improved prediction of protein-protein interactions using novel negative samples, features, and an ensemble classifier," *Artificial Intelligence in Medicine*, vol. 83, pp. 67–74, 2017.

[12] C. Cath, S. Wachter, B. Mittelstadt, M. Taddeo, and L. Floridi, "Artificial intelligence and the 'good society': the US, EU, and UK approach," *Science and Engineering Ethics*, vol. 24, no. 2, pp. 1–24, 2017.

[13] A. F. Chen, A. C. Zoga, and A. R. Vaccaro, "Point/counterpoint: artificial intelligence in healthcare," *Healthcare Transformation*, vol. 2, no. 2, pp. 84–92, 2017.

[14] M. Hutson, "Artificial intelligence faces reproducibility crisis," *Science*, vol. 359, no. 6377, pp. 725-726, 2018.

[15] E. K. Zavadskas, R. Bausys, B. Juodagalviene, and I. Garnyte-Sapranaviciene, "Model for residential house element and material selection by neutrosophic MULTIMOORA method," *Engineering Applications of Artificial Intelligence*, vol. 64, pp. 315–324, 2017.

[16] D. M. Roijers and S. Whiteson, "Multi-objective decision making," *Synthesis Lectures on Artificial Intelligence and Machine Learning*, vol. 11, no. 1, pp. 1–129, 2017.

[17] E. Burton, J. Goldsmith, S. Koenig, B. Kuipers, N. Mattei, and T. Walsh, "Ethical considerations in artificial intelligence courses," *AI Magazine*, vol. 38, no. 2, pp. 22–34, 2017.

[18] A. Agrawal, J. S. Gans, and A. Goldfarb, "What to expect from artificial intelligence," *MIT Sloan Management Review*, vol. 58, no. 3, pp. 23–26, 2017.

[19] J. Bryson and A. Winfield, "Standardizing ethical design for artificial intelligence and autonomous systems," *Computer*, vol. 50, no. 5, pp. 116–119, 2017.

[20] T. Hirasawa, K. Aoyama, T. Tanimoto et al., "Application of artificial intelligence using a convolutional neural network for detecting gastric cancer in endoscopic images," *Gastric Cancer*, vol. 21, no. 4, pp. 653–660, 2018.

[21] Y. U. Bin and K. Kumbier, "Artificial intelligence and statistics," *Frontiers of Information Technology & Electronic Engineering*, vol. 19, no. 1, pp. 6–9, 2018.

[22] T. J. Huang, "Imitating the brain with neurocomputer a "new" way towards artificial general intelligence," *International Journal of Automation and Computing*, vol. 14, no. 5, pp. 520–531, 2017.

[23] C. Joshi and U. K. Singh, "Information security risks management framework - a step towards mitigating security risks in university network," *Journal of Information Security and Applications*, vol. 35, pp. 128–137, 2017.

[24] X. Qian, X. Liu, J. Pei, P. M. Pardalos, and L. Liu, "A game-theoretic analysis of information security investment for multiple firms in a network," *Journal of the Operational Research Society*, vol. 68, no. 10, pp. 1290–1305, 2017.

[25] A. A. Grusho, P. O. Abaev, S. Y. Shorgin, and E. E. Timonina, "Graphs for information security control in software defined networks," *AIP Conference Proceedings*, vol. 1863, no. 1, pp. 1–4, 2017.

[26] A. Nangue, E. E. F. Ta Gn, and E. Tonye, "Computer network and information security," *International Journal of Computer Network and Information Security*, vol. 12, no. 6, pp. 14–29, 2021.

Hindawi
Computational and Mathematical Methods in Medicine
Volume 2023, Article ID 9804984, 1 page
https://doi.org/10.1155/2023/9804984

Retraction

Retracted: Timosaponin AIII Suppresses RAP1 Signaling Pathway to Enhance the Inhibitory Effect of Paclitaxel on Nasopharyngeal Carcinoma

Computational and Mathematical Methods in Medicine

Received 27 June 2023; Accepted 27 June 2023; Published 28 June 2023

This article has been retracted by Hindawi following an investigation undertaken by the publisher [1]. This investigation has uncovered evidence of one or more of the following indicators of systematic manipulation of the publication process:

(1) Discrepancies in scope

(2) Discrepancies in the description of the research reported

(3) Discrepancies between the availability of data and the research described

(4) Inappropriate citations

(5) Incoherent, meaningless and/or irrelevant content included in the article

(6) Peer-review manipulation

The presence of these indicators undermines our confidence in the integrity of the article's content and we cannot, therefore, vouch for its reliability. Please note that this notice is intended solely to alert readers that the content of this article is unreliable. We have not investigated whether authors were aware of or involved in the systematic manipulation of the publication process.

Wiley and Hindawi regrets that the usual quality checks did not identify these issues before publication and have since put additional measures in place to safeguard research integrity.

We wish to credit our own Research Integrity and Research Publishing teams and anonymous and named external researchers and research integrity experts for contributing to this investigation.

The corresponding author, as the representative of all authors, has been given the opportunity to register their agreement or disagreement to this retraction. We have kept a record of any response received.

References

[1] X. Li, W. Lu, T. Zhou, F. Zhao, and L. Yang, "Timosaponin AIII Suppresses RAP1 Signaling Pathway to Enhance the Inhibitory Effect of Paclitaxel on Nasopharyngeal Carcinoma," *Computational and Mathematical Methods in Medicine*, vol. 2022, Article ID 6756676, 8 pages, 2022.

Hindawi
Computational and Mathematical Methods in Medicine
Volume 2022, Article ID 6756676, 8 pages
https://doi.org/10.1155/2022/6756676

Research Article

Timosaponin AIII Suppresses RAP1 Signaling Pathway to Enhance the Inhibitory Effect of Paclitaxel on Nasopharyngeal Carcinoma

Xiaofeng Li,[1] Wen Lu,[1] Tianjiao Zhou,[1] Feng Zhao,[1] and Li Yang[2]

[1]*Department of Otorhinolarynology, Head and Neck Surgery, Shanghai Jiao Tong University Affiliated Sixth People's Hospital, Shanghai 200233, China*
[2]*Department of Head and Neck Surgery, People's Hospital of Guang'an City, Guang'an 638001, China*

Correspondence should be addressed to Li Yang; yang2323492@163.com

Received 19 January 2022; Revised 14 April 2022; Accepted 22 April 2022; Published 9 May 2022

Academic Editor: Shakeel Ahmad

Although PTX has been identified as an effective drug for nasopharyngeal carcinoma (NPC) therapy, it has serious side effects in the human body. Previous studies have shown that timosaponin AIII (TSAIII) can inhibit the malignant progression of NPC cells. This study investigated the active mechanism of the combination of TSAIII and paclitaxel (PTX) on NPC. Cellular viability, apoptosis, apoptotic factors, and RAP1 signaling regulators were detected in the PNC cells (CNE-1 and HNE-2) and the subcutaneous CNE-1 transplanted nude mice treated with PTX or/and TSAIII. The results showed that TSAIII notably strengthened the inhibitory effect of PTX on the proliferation of NPC cells CNE-1 and HNE-2; upregulated the expression of Bax B-cell lymphoma 2 (Bcl-2)/Bcl-xL-associated death promoter (Bad), and Ras-associated protein1 (RAP1) GTPase activating protein (Rap1GAP); inhibited the level of Bcl-2, RAP1, and Ras guanine nucleotide releasing protein (RasGRP2); and significantly enhanced the promoting effect of PTX on apoptosis in the CNE-1 and HNE-2 cells. Besides, TSAIII strengthened the inhibitory effect of PTX on xenograft tumor in nude mice without adverse reactions. In conclusion, the combination administration of TSAIII and PTX had a significantly therapeutic effect on NPC and avoided the PTX's side effects, which may have acted as a new direction for the study of therapeutic approaches for NPC clinically.

1. Introduction

Nasopharyngeal carcinoma (NPC) is a malignant tumor that occurs in the superior wall (roof) and medial wall of the nasopharyngeal cavity. NPC has an insidious onset and the incidence ranks first among ear, nose, and throat malignancies [1]. Most NPC patients have a more dangerous prognosis due to late diagnosis. So far, radiotherapy is the main treatment manner for NPC. Chemotherapy is regarded as a supplement treatment. However, it is not applicable for patients with advanced NPC because both radiotherapy and chemotherapy can lead to drug tolerance [2]. Despite advanced radiotherapy and chemotherapy techniques now, the 5-year survival rate of the patients with NPC has not been significantly improved yet [3]. Therefore, it is urgent to find a way with high efficacy and less side effects for the treatment of NPC.

Paclitaxel (PTX) belongs to diterpenoid alkaloid compounds, which has been confirmed as the new generation of cancer chemotherapy drug clinically [4]. Clinical studies have confirmed that patients receiving PTX chemotherapy are often prone to various side effects, such as neuropathic pain and myelosuppression [5]. It is reported that drug combination can significantly improve therapeutic efficacy and reduce side effects in the treatment of NPC [6]. Zhou et al. recently showed that some traditional Chinese medicine (TCM) monomers can enhance the antitumor effect of PTX [7]. Hence, the combination of

TCM and PTX may be an effective method and reduce side effects for NPC therapy.

Timosaponin AIII (TSAIII), a steroidal saponin, is the main pharmacologically active component in rhizoma anemarrhenae (A Chinese medical herbs) [8]. Some studies have shown that TSAIII has pharmacological effects including anti-inflammation and anticancer [9]. Besides, it is reported that TSAIII not only can significantly promote the apoptosis of melanoma [10], colorectal cancer [11], breast cancer [12], and osteosarcoma [13] but also inhibit their metastatic activity.

Small GTPase Ras-associated protein 1 (RAP1) is a major member of inside-out signaling cascades to activate integrin [14, 15]. Dysfunction of the RAP1 signal involves tumor metastasis and invasion. Activation of the RAP1 signaling is correlated to the aggressive phenotypes of malignancy [16, 17]. Indeed, in the prostate cancer [18], glioblastoma [19], non-small-cell lung cancer [20], melanoma [21], breast cancer [22], and pancreatic cancer [23], RAP1 revealed a prooncogenic activity to promote invasion and migration of tumor cells. On the other hand, GTPase activating protein RAP1GAP acts as a negative regulator of Rap1 activity, which is always found to be downregulated in many cancers [24].

Consequently, this study investigated the effect and the mechanism of the combination of PTX and TSAIII on the occurrence and development of NPC via RAP1 regulation *in vitro* and *in vivo*.

2. Materials and Methods

2.1. Culture of Cells. Human NPC cell lines CNE-1 and HNE-2 were purchased from Biovector NTCC (Beijing, China). The cells were cultured in RPMI-1640 culture medium with 10% of fetal bovine serum (FBS, Hyclone, Logan, UT, USA) and 1% of penicillin-streptomycin (100 U/mL, Invitrogen; Carlsbad, CA, USA) in an incubator with 5% of CO_2 at 37°C.

2.2. Cellular Viability Assay. The CCK-8 kit (Abcam, Cambridge, United Kingdom) was utilized for the analysis of cellular viability. Firstly, CNE-1 and HNE-2 cells with a density of 5×10^3/mL/well were seeded in a 96-well plate. After adherence of the cells, TSAIII (0, 10, 20, 40, 80, and120 μM) and/or PTX (0, 2, 4, 8, 16, and 32 μM) were/was added in the cells respectively for 72-hour incubation. Subsequently, each well was added 10 μL of CCK-8 reagent for another 4-hour incubation. Then, Synergy HTX Multi-Mode Reader (Agilent Technologies: Richardson, TX) was applied to detect absorbance values of the solutions at 450 nm.

2.3. Apoptosis Assay. The cells were treated by TSAIII (10 μM) and/or PTX (8 μM). After 72 h, the cells were digested using trypsin and then collected, washed with precooled PBS, and suspended with 1x binding buffer. Subsequently, the cells were mixed with 5 μL of annexin V-FITC or/and 5 μL of propidium iodide (PI) under a light avoidance condition at ambient temperature for 15 min. After adding 1x binding buffer for the resuspension of the cells, flow cytometry was conducted for the detection of apoptosis.

2.4. RT-qPCR. TRIzol reagent (Invitrogen, Carlsbad, CA, USA) was adopted to extract total RNA from the detecting cells. Following, according to the instruction of PrimeScript RT kit (TaKaRa, Tokyo, Japan), mRNA was reverse transcribed into cDNA. The expression of mRNA were determined by RT-qPCR with SYBR green I Master Mix kits (Invitrogen) using corresponding primers (Table 1). In 7500 real-time PCR system (Applied Biosystems, America), GAPDH acted as the internal control.

Table 1

Gene	Primer sequence (5′-3′)
Bax	Forward: 5′-CCCGAGAGGTCTTTTTCCGAG-3′
	Reverse: 5′-CCAGCCCATGATGGTTCTGAT-3′
Bad	Forward: 5′-CCCAGAGTTTGAGCCGAGTG-3′
	Reverse: 5′-CCCATCCCTTCGTCGTCCT-3′
Bcl-2	Forward: 5′-CGGTTCAGGTACTCAGTCATCC-3′
	Reverse: 5′-GGTGGGGTCATGTGTGTGG-3′
RAP1	Forward: 5′-GCGAGTAGTTGGCAAAGAGC-3′
	Reverse: 5′-ACTATGGGCCTAGAGCAGCA-3′
RAP1GAP	Forward: 5′-CTACCGGAAGCACTTTCTCG-3′
	Reverse: 5′-CACACACCAACTTTGCCAT-3′
RasGRP2	Forward: 5′-ACAATCCCGGAAGGACAACTC-3′
	Reverse: 5′-GTCTATGTCGATTAGGCTGCTG-3′
GAPDH	Forward: 5′-GCACCGTCAAGGCTGAGAAC-3′
	Reverse: 5′-TGGTGAAGACGCCAGTGGA-3′

2.5. Experimental Animal. Shanghai Animal Center (Shanghai, China) provided 20 chargeable male BALB/nude mice (age: 4-6 weeks). Shanghai Sixth People's Hospital Affiliated to Shanghai Jiao Tong University approved the animal experiments. And the animal experiments were performed according to the National Institutes of Health Guidelines for Animal Care.

Twenty male BALB/nude mice (age: 4-6 weeks) (Shanghai Animal Center, Shanghai, China) were randomly divided into control, PTX (10 mg/kg), TSAIII (40 mg/kg), and PTX +TSAIII groups (five mice/group). All the mice were injected subcutaneously with 100 μL of phosphate buffer saline (PBS) solution containing 5×10^6 CNE-1 cells in the right axillary region. After four weeks raise, the tumor volume was calculated as $1/2 \times (\text{length} \times \text{width}^2)$. Four weeks later, the mice were sacrificed. The mice' bodies and the tumor were weighted and recorded. Partial tumor tissues were fixed in 4% of paraformaldehyde for H&E and immunohistochemical staining analyses.

2.6. Statistical Analysis. All experiments were independently repeated three times. The statistical analysis of the data was conducted with SPSS 24.0 (IBM-SPSS, Chicago, IL, USA). And the data was presented as mean ± standard deviation (SD). Student's *t*-test and one-way analysis of variance were carried out for the comparisons between two groups and among multiple groups, respectively. The differences were

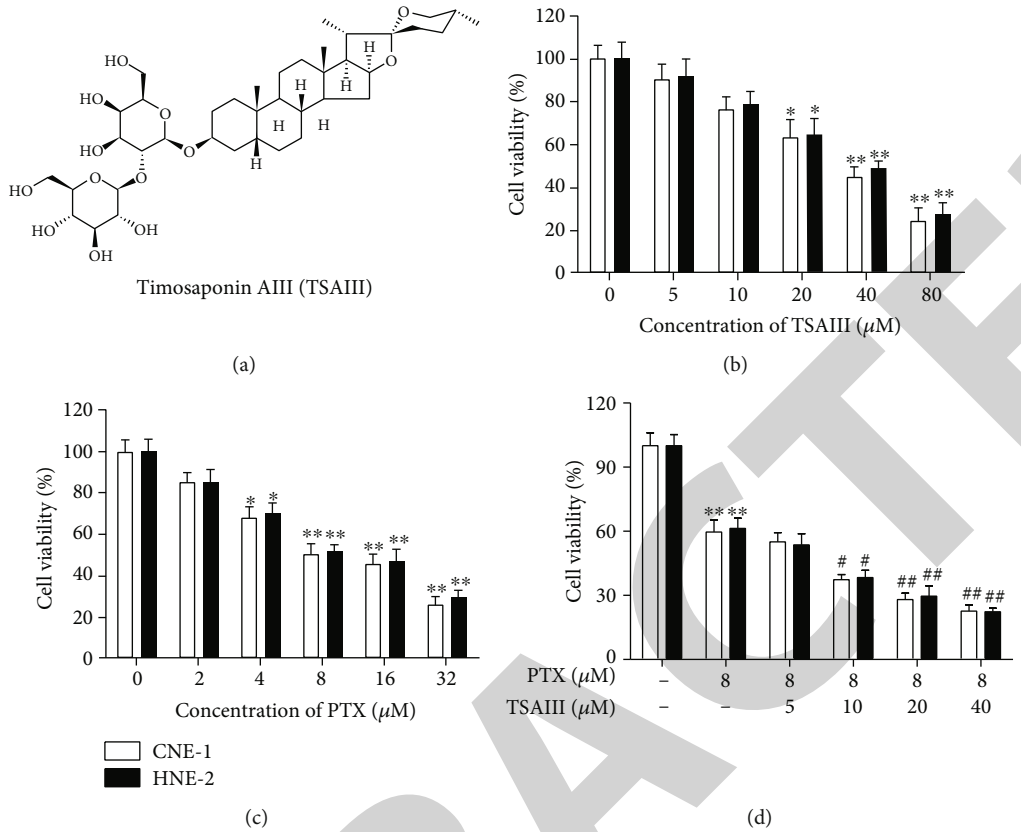

Figure 1: Effect of TSAIII combined with PTX on cellular proliferation of the nasopharyngeal carcinoma cells (PNCs). (a) Chemical structure of TSAIII. (b–d) CCK-8 was applied to test the cell viability of CNE-1 and HNE-2 cells treated by TSAIII (b), PTX (c), and PTX0+TSAIII (d). $^{*}P < 0.05$ and $^{**}P < 0.01$ vs. the 0.0 μM group, $^{\#\#}P < 0.01$ vs. the 8 μM PTX or 5 μM TSAIII.

regarded to be significant if $P < 0.05$. All data presentations were plotted with GraphPad Prism 7.0 software (GraphPad Software, San Diego, CA, USA).

3. Results

3.1. TSAIII Strengthened the Inhibitory Effect of Paclitaxel on the Proliferation of NPC Cells. To examine the effect of TSAIII combined with PTX on NPC development, different concentrations of TSAIII and PTX were utilized to treat CNE-1 and HNE-2 cells *in vitro*. The TSAIII structure was shown in Figure 1(a). Cellular proliferation test revealed that both TSAII and PTX significantly suppressed the cellular proliferation of either HNE-2 or CNE-1 cells in a dose-dependent manner ($P < 0.05$) (Figures 1(b) and 1(c)). Moreover, the inhibitory effect of PTX on the proliferation of CNE-1 and HNE-2 cells was more significant at a concentration of 8 μM ($P < 0.01$) (Figure 1(c)); therefore, the concentration of PTX was determined to be 8 μM in subsequent experiments. Further treatment of the CNE-1 and the HNE-2 cells with both TSAIII and PTX at the same time revealed that the inhibitory effect of the PTX on the cellular proliferation was notably enhanced by TSAIII ($P < 0.05$) (Figure 1(d)) with a dose-dependent manner. These data expressed that TSAII combined with PTX had a synergistic effect on cellular proliferative inhibition in the CNE-1 and the HNE-2 cells.

3.2. TSAIII Strengthened the Promoting Effect of PTX on Apoptosis of CNE-1 and HNE-2 cells. To further testify the synergistic effect of TSAIII on the PTX-caused NPC progression, flow cytometry was conducted to detect the cellular apoptosis. The results of the detection indicated that PTX alone significantly promoted cellular apoptosis of CNE-1 and HNE-2 ($P < 0.05$). And the apoptosis was notably higher in the TSAIII+PTX group than that in the PTX or TSAIII alone group ($P < 0.05$) (Figure 2(a)). Western blot detection of the apoptosis-related proteins showed that PTX alone obviously increased Bax and B-cell lymphoma 2 (Bcl-2)/Bcl-xL-associated death promoter (Bad) expression and significantly decreased Bcl-2 expression ($P < 0.05$). Notably, simultaneous supplement with TSAIII strengthened the regulative effect of PTX on the apoptotic proteins. The protein expression of Bax and Bad was further increased, while Bcl-2 expression was further reduced ($P < 0.05$) (Figure 2(b)). These results indicated that TSAIII had a synergistic role in the proapopotic activity of PTX in the CNE-1 and HNE-2 cells.

3.3. TSAIII Strengthened the Anti-NPC Effect of PTX by Modulating RAP1 Pathway. The mechanism of the synergistic action of TSAIII and PTX was further investigated. Rap1 is reported to potentially regulate oncogenesis, metastasis, immune evasion, and chemoresistance [24]. RT-qPCR analysis revealed that both PTX and TSAIII could significantly

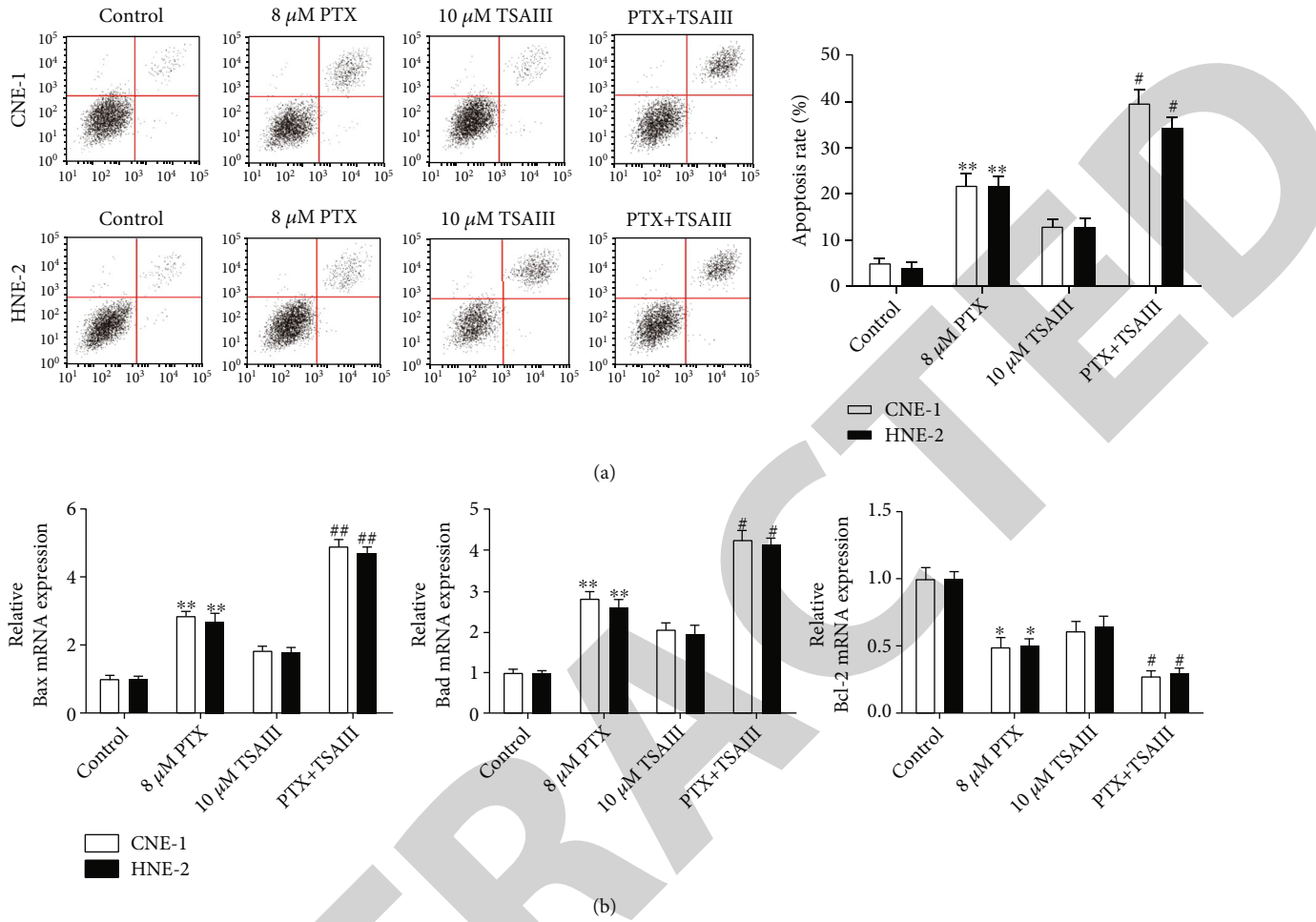

Figure 2: Effect of combination of TSAIII and PTX on apoptosis of the PNCs. (a) Flow cytometry was utilized to determine the cellular apoptosis in the indicated group of CNE-1 and HNE-2 cells. (b) RT-qPCR was applied to test the mRNA expression of Bax, Bad, and Bcl-2 in CNE-1 and HNE-2 cells. $^{*}P < 0.05$ and $^{**}P < 0.01$ vs. the control group; $^{\#}P < 0.05$ and $^{\#\#}P < 0.01$ vs. 8 μM PTX or 10 μM TSAIII.

increase the gene expression of *RAP1GAP* and reduce the expression of *RAP1* and *RasGRP2* ($P < 0.05$). Interestingly, the combination of TSAIII and PTX had an enhanced effect on the above gene expression compared with single use of either TSAIII or PTX ($P < 0.05$) (Figures 3(a) and 3(b)), disclosing that the increased inhibitory effect of the combination of TSAIII and PTX on NPC was related to the inhibition of the RAP1 pathway.

3.4. TSAIII and PTX Exerted a Synergistic Antitumor Activity In Vivo. A xenograft mouse model was utilized to validate the synergistic antitumor effect of TSAIII and PTX *in vivo*. The results showed that either PTX or TSAIII obviously reduce tumor volume and weight ($P < 0.05$). The inhibitory effect of the combination of PTX with TSAIII on tumor growth was significantly increased ($P < 0.05$) (Figures 4(a)–4(c)). Besides, the weight of the mice in the combined treatment group was not significantly different compared with the control group ($P > 0.05$). These data indicated that combination of PTX with TSAIII had less side effects on the mice (Figure 4(d)). All results above suggested that the synergistic antitumor effect of the combination of TSAIII with PTX was verified as well *in vivo*.

3.5. TSAIII Promoted the PTX-Induced Effects on Cellular Apoptosis in Tumor Tissues In Vivo. H&E staining and immunohistochemical assays were processed to determine the cellular apoptosis in the tumor tissues. The H&E staining showed that the apoptotic cells in tumor tissues declined significantly in the TSAIII+PTX group compared with the single administration of either the TSAIII or PTX group (Figure 5(a)). Besides, the immunohistochemical assays also revealed that the combination of TSAIII with PTX further increased the expression of caspase-3 and Bax in tumor tissues compared with the single administration of either TSAIII or PTX (Figures 5(b) and 5(c)). All the *in vivo* experimental results above demonstrated that TSAIII enhanced the induced effects of PTX on cellular apoptosis in tumor tissues.

4. Discussion

It's reported that the most widely applied anticancer drug at present is PTX. However, the resistance of the PTX can cause the failure of the treatment for the cancers [25]. Chen et al. have reported that TCM monomers combined with

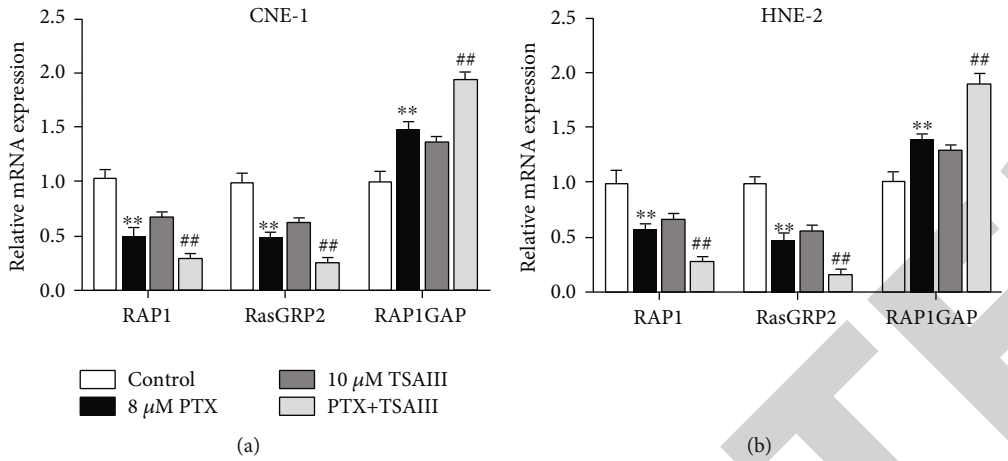

Figure 3: Effect of combination of TSAII and PTX on RAP1 pathway-regulating factors in the NPCs. RT-qPCR was applied to analyze the mRNA levels of RAP1 pathway-regulating factors in the indicated group of CNE-1 (a) and HNE-2 (b) cells. $^{**}P < 0.01$ vs. the control group; $^{\#\#}P < 0.01$ vs. 8 μM PTX or 10 μM TSAIII.

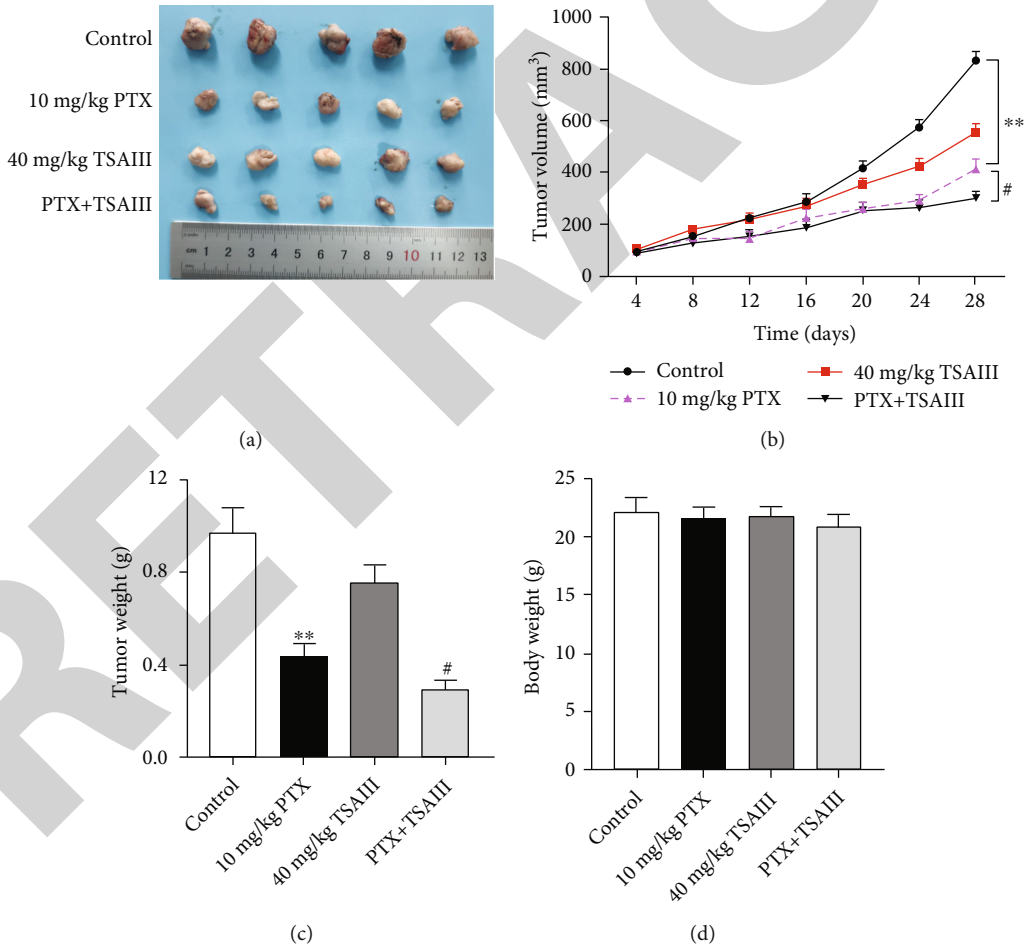

Figure 4: Effect of TSAIII combined with PTX on the growth of transplanted PNC tumor in nude mice. Images showed the tumor size (a), volume (b), weight (c), and nude mice weight ($n = 5$) (d) 4 weeks after inoculation of the xenografts tumor in nude mice at the indicated conditions. $^{**}P < 0.01$ vs. the control group; $^{\#}P < 0.05$ vs. 10 mg/kg PTX or 40 mg/kg TSAIII.

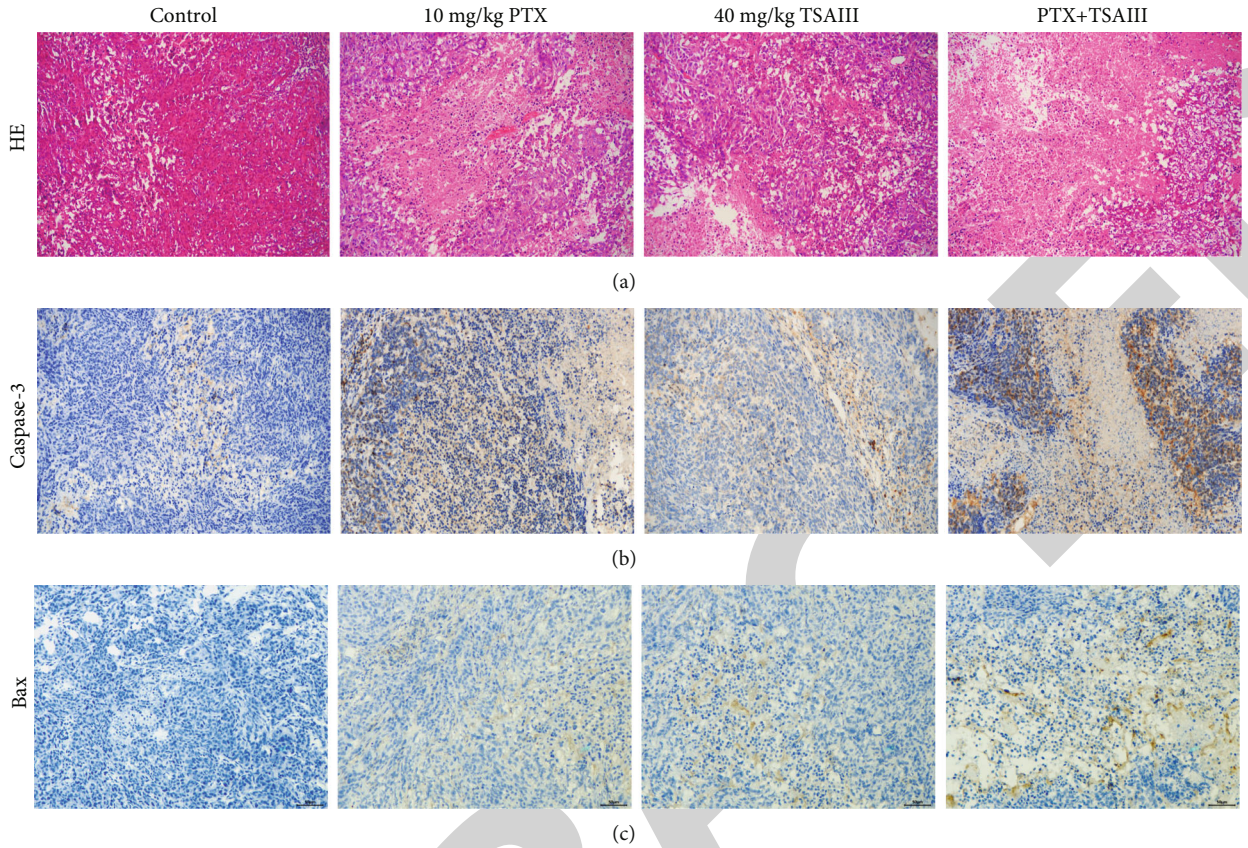

Figure 5: Effect of TSAIII combined with PTX on cell apoptosis in tumor tissue of the nude mice. (a) H&E staining was utilized to check the cell apoptosis in tumor tissues of the indicated group. Immunohistochemical staining was performed to determine caspase-3 (b) and Bax (c) expressions in the PNC tumor tissues of the indicated group.

PTX have been applied as an alternative therapy for the tumors and got good results [26]. In this study, we found that TSAIII significantly strengthened the inhibitory effect of PTX on the NPC growth and metastasis via decreasing the cellular proliferation and increasing the cellular apoptosis *in vitro* and *in vivo*. Detail study of the anti- and proapoptotic regulator balance revealed that TSAIII upregulated the expression level of Bax and Bad but declined the expression level of Bcl-2. Usually, the antiapoptotic and proapoptotic protein regulator balance is a critical important to decide whether the cells go through apoptosis. Deregulation of apoptosis is believed to be one of the cancer's hallmarks [27]. Both Bax and Bad are the crucial proapoptotic regulators, while Bcl-2 is an important antiapoptotic factor. All of them are involved in the regulation of extrinsic apoptotic pathway [28]. Thus, TSAIII strengthened the antioncogenesis of PTX on the NPCs through downregulation of Bax and Bad and upregulation of Bcl-2 to improve the NPC apoptosis. We noticed that either PTX or TSAIII alone exhibited the antitumor activity via Bax and Bad inhibition and Bcl-2 elevation to prohibit PNC proliferation and improve apoptosis. Interestingly, the combination of PTX with TSAIII created more effective antitumor activity than single use of either PTX or TSAIII, mechanically, which revealed more inhibitory effect on Bax and Bad, but more activation power on Bcl-2 to much inhibit proliferation and much improver apoptosis in the PNCs. More importantly, combination administration of PTX with TSAIII did not show obvious side effects in the xenograft mouse model assay, because the body weight between the PTX+TSAIII group and either PTX or TSAIII group did not have any significant difference.

RAP1 is a GTPase protein that can interact with other proteins to regulate physiological and pathological processes such as migration, invasion, and metastasis of tumor cells [29–31]. Lost control of the RAP1 signal is associated with tumor growth and metastasis. RAP1 signaling activation is reported in many types of cancers [18–20, 22]. Inactivation form of RAP1 (RAP1-GDP) is positively regulated by guanine nucleotide exchange factors (GEFs), including cAMP, Epac, C3G, RapGRP2, and PDZ-GEF, to form a Rap1-GTP (activation form). On the other hand, the activated form of Rap1-GTP is negatively regulated by GTPase activation proteins (GAPs), including Rap1GAP and SPA-1 [24]. Our data showed that combination of the PTX with TSAIII improved the inhibitory effect of RAP1 and RasGRP2 induced by either PTX or TSAIII alone, further inhibiting the PNC growth. It has been shown that CD38 can promote RasGRP2/RAP1-mediated adhesion and migration of chronic lymphocytic leukemia cells by increasing intracellular Ca^{2+} levels [32]. However, either PTX or TSAIII also revealed the prohibited activity on Rap1-GAP. A study shows Rap1GAP as a tumor suppressor can inhibit the development and progression of many tumors [33, 34]. Therefore, the balance of RasGRP2 and RAP1 with Rap1-GAP will decide the tumor direction.

Thus, our results verified that TSAIII inhibited PNC growth via the inhibition of the RAP1 pathway in CNE-1 and HNE-2 cells, thereby playing a synergistic role with PTX to prohibit NPC cells. The combined treatment of TSAIII and PTX further emphasized the proapoptotic effect of PTX via RAP1 pathway suppression in NPC cells.

In summary, it is found in this study that, in vitro and *in vivo*, TSAIII has enhanced the anti-tumor effect of PTX on NPC cells. The combination of TSAIII and PTX offers a new research direction for the clinical treatment of NPC. The limitation of this study is the lack of a systemic examination of the side effect of the PTX+TSAIII combination on the hematological, hepatic, renal, and cardiological systems in the xenograft mouse model.

Data Availability

The data used to support the findings of this study are available from the corresponding author upon request.

Conflicts of Interest

The authors declare that they have no competing interests.

References

[1] Y. P. Chen, A. T. Chan, Q. T. Le, P. Blanchard, Y. Sun, and J. Ma, "Nasopharyngeal carcinoma," *Lancet*, vol. 394, no. 10192, pp. 64–80, 2019.

[2] W. K. J. Lam and J. Y. K. Chan, "Recent advances in the management of nasopharyngeal carcinoma," *F1000Research*, vol. 7, 2018.

[3] L. F. Wang, C. Y. Chai, W. R. Kuo, C. F. Tai, K. W. Lee, and K. Y. Ho, "Correlation between proliferating cell nuclear antigen and p 53 protein expression and 5-year survival rate in nasopharyngeal carcinoma," *American Journal of Otolaryngology*, vol. 27, no. 2, pp. 101–105, 2006.

[4] N. I. Marupudi, J. E. Han, K. W. Li, V. M. Renard, B. M. Tyler, and H. Brem, "Paclitaxel: a review of adverse toxicities and novel delivery strategies," *Expert Opinion on Drug Safety*, vol. 6, no. 5, pp. 609–621, 2007.

[5] S. P. Bisch, A. Sugimoto, M. Prefontaine et al., "Treatment tolerance and side effects of intraperitoneal carboplatin and dose-dense intravenous paclitaxel in ovarian cancer," *Journal of Obstetrics and Gynaecology Canada*, vol. 40, no. 10, pp. 1283–1287, 2018.

[6] A. Davenport, M. Frezza, M. Shen et al., "Celastrol and an EGCG pro-drug exhibit potent chemosensitizing activity in human leukemia cells," *International Journal of Molecular Medicine*, vol. 25, no. 3, pp. 465–470, 2010.

[7] L. Zou, X. Liu, J. Li et al., "Tetramethylpyrazine enhances the antitumor effect of paclitaxel by inhibiting angiogenesis and inducing apoptosis," *Front Pharmacology*, vol. 10, article 707, 2019.

[8] F. Y. Han, X. Y. Song, J. J. Chen, G. D. Yao, and S. J. Song, "Timosaponin AIII: a novel potential anti-tumor compound from Anemarrhena asphodeloides," *Steroids*, vol. 140, pp. 125–130, 2018.

[9] Y. Wang, L. Xu, L. L. Lou et al., "Timosaponin AIII induces apoptosis and autophagy in human melanoma A375-S2 cells," *Archives of Pharmacal Research*, vol. 40, no. 1, pp. 69–78, 2017.

[10] K. M. Kim, A. R. Im, S. H. Kim, J. W. Hyun, and S. Chae, "Timosaponin AIII inhibits melanoma cell migration by suppressing COX-2 and in vivo tumor metastasis," *Cancer Science*, vol. 107, no. 2, pp. 181–188, 2016.

[11] Y. J. Kang, H. J. Chung, J. W. Nam et al., "Cytotoxic and antineoplastic activity of timosaponin A-III for human colon cancer cells," *Journal of Natural Products*, vol. 74, no. 4, pp. 701–706, 2011.

[12] C. H. Tsai, C. W. Yang, J. Y. Wang et al., "Timosaponin AIII suppresses hepatocyte growth factor-induced invasive activity through sustained ERK activation in breast cancer MDA-MB-231 cells," *Evidence-Based Complementary and Alternative Medicine*, vol. 2013, Article ID 421051, 10 pages, 2013.

[13] O. Jung and S. Y. Lee, "Synergistic anticancer effects of timosaponin AIII and ginsenosides in MG63 human osteosarcoma cells," *Journal of Ginseng Research*, vol. 43, no. 3, pp. 488–495, 2019.

[14] A. Banno and M. H. Ginsberg, "Integrin activation," *Biochemical Society Transactions*, vol. 36, no. 2, pp. 229–234, 2008.

[15] H. Harjunpää, M. Llort Asens, C. Guenther, and S. C. Fagerholm, "Cell adhesion molecules and their roles and regulation in the immune and tumor microenvironment," *Front Immunology*, vol. 10, p. 1078, 2019.

[16] M. Alemayehu, M. Dragan, C. Pape et al., "β-Arrestin 2 regulates lysophosphatidic acid-induced human breast tumor cell migration and invasion via Rap 1 and IQGAP1," *PLoS One*, vol. 8, no. 2, article e56174, 2013.

[17] Y. Yang, M. Li, Y. Yan et al., "Expression of RAP1B is associated with poor prognosis and promotes an aggressive phenotype in gastric cancer," *Oncol Reports*, vol. 34, no. 5, pp. 2385–2394, 2015.

[18] C. L. Bailey, P. Kelly, and P. J. Casey, "Activation of Rap 1 promotes prostate cancer metastasis," *Cancer Research*, vol. 69, no. 12, pp. 4962–4968, 2009.

[19] J. Sayyah, A. Bartakova, N. Nogal, L. A. Quilliam, D. G. Stupack, and J. H. Brown, "The Ras-related protein, Rap 1A, mediates thrombin-stimulated, integrin-dependent glioblastoma cell proliferation and tumor growth," *Journal of Biological Chemistry*, vol. 289, no. 25, pp. 17689–17698, 2014.

[20] L. Xiao, X. Lan, X. Shi et al., "Cytoplasmic RAP1 mediates cisplatin resistance of non-small cell lung cancer," *Cell Death & Disease*, vol. 8, no. 5, article e2803, 2017.

[21] S. Zhou, Y. Liang, X. Zhang et al., "SHARPIN promotes melanoma progression via Rap 1 signaling pathway," *Journal of Investigative Dermatology*, vol. 140, no. 2, pp. 395–403, 2020.

[22] E. A. McSherry, K. Brennan, L. Hudson, A. D. Hill, and A. M. Hopkins, "Breast cancer cell migration is regulated through junctional adhesion molecule-a-mediated activation of Rap 1 GTPase," *Breast Cancer Research*, vol. 13, no. 2, pp. 1–14, 2011.

[23] M. Huang, S. Anand, E. A. Murphy et al., "EGFR-dependent pancreatic carcinoma cell metastasis through Rap 1 activation," *Oncogene*, vol. 31, no. 22, pp. 2783–2793, 2012.

[24] C. K. Looi, L. W. Hii, S. C. Ngai, C. O. Leong, and C. W. Mai, "The role of Ras-associated protein 1 (Rap 1) in cancer: bad actor or good player?," *Biomedicines*, vol. 8, no. 9, article 334, 2020.

[25] T. M. Abu Samaan, M. Samec, A. Liskova, P. Kubatka, and D. Büsselberg, "Paclitaxel's mechanistic and clinical effects on breast cancer," *Biomolecules*, vol. 9, no. 12, article 789, 2019.

Hindawi
Computational and Mathematical Methods in Medicine
Volume 2023, Article ID 9837218, 1 page
https://doi.org/10.1155/2023/9837218

Retraction

Retracted: Paeoniflorin Can Improve Acute Lung Injury Caused by Severe Acute Pancreatitis through Nrf2/ARE Pathway

Computational and Mathematical Methods in Medicine

Received 27 June 2023; Accepted 27 June 2023; Published 28 June 2023

This article has been retracted by Hindawi following an investigation undertaken by the publisher [1]. This investigation has uncovered evidence of one or more of the following indicators of systematic manipulation of the publication process:

(1) Discrepancies in scope

(2) Discrepancies in the description of the research reported

(3) Discrepancies between the availability of data and the research described

(4) Inappropriate citations

(5) Incoherent, meaningless and/or irrelevant content included in the article

(6) Peer-review manipulation

The presence of these indicators undermines our confidence in the integrity of the article's content and we cannot, therefore, vouch for its reliability. Please note that this notice is intended solely to alert readers that the content of this article is unreliable. We have not investigated whether authors were aware of or involved in the systematic manipulation of the publication process.

Wiley and Hindawi regrets that the usual quality checks did not identify these issues before publication and have since put additional measures in place to safeguard research integrity.

We wish to credit our own Research Integrity and Research Publishing teams and anonymous and named external researchers and research integrity experts for contributing to this investigation.

The corresponding author, as the representative of all authors, has been given the opportunity to register their agreement or disagreement to this retraction. We have kept a record of any response received.

References

[1] Y. Hu and W. Yang, "Paeoniflorin Can Improve Acute Lung Injury Caused by Severe Acute Pancreatitis through Nrf2/ARE Pathway," *Computational and Mathematical Methods in Medicine*, vol. 2022, Article ID 5712219, 7 pages, 2022.

Hindawi
Computational and Mathematical Methods in Medicine
Volume 2022, Article ID 5712219, 7 pages
https://doi.org/10.1155/2022/5712219

Research Article

Paeoniflorin Can Improve Acute Lung Injury Caused by Severe Acute Pancreatitis through Nrf2/ARE Pathway

Yanyan Hu and Wei Yang

Department of Gastroenterology, Xiangyang Central Hospital, Affiliated Hospital of Hubei University of Arts and Science, Xiangyang 441021, China

Correspondence should be addressed to Wei Yang; jxyt1986@126.com

Received 28 January 2022; Revised 22 March 2022; Accepted 6 April 2022; Published 9 May 2022

Academic Editor: Muhammad Zubair Asghar

Objective. To evaluate the potential therapeutic effect of paeoniflorin on acute lung injury induced by severe acute pancreatitis (SAP) and to initially explore the possible protective mechanisms of paeoniflorin. *Method*. The SAP lung injury rat model was established by retrograde injection of 5% sodium taurocholate to the cholangiopancreatic duct. H&E staining was used to detect pathological changes in rat lung tissue. W/D ratio method, serum amylase (AMY), and lipase activity were used to assess the degree of lung injury in rats. Oxidation indicators such as LDH, MDA, and SOD in lung tissue were measured. Levels of inflammatory factors TNF-α, IL-6, and IL-10 were measured in bronchoalveolar lavage fluid (BALF). At the same time, Western blot was used to detect the expression of related proteins in the Nrf2/ARE signaling pathway. *Results*. In SAP rats, paeoniflorin treatment could significantly alleviate lung injury conditions such as pulmonary edema and inflammatory cell infiltration in lung tissue and reduce serum amylase and lipase activities. Paeoniflorin can reduce the content of LDH and MDA in lung tissue and increase the content of SOD. In addition, ELISA results showed that paeoniflorin could inhibit the levels of TNF-α and IL-6 in BALF and upregulate the levels of IL-10. Paeoniflorin could upregulate the expression of Nrf2/ARE signaling pathway proteins Cyt-Nrf2, HO-1, and NQO1 in lung tissue of SAP rats. *Conclusion*. Paeoniflorin may improve acute lung injury in rats with severe pancreatitis by inhibiting inflammation and oxidative stress response. These effects may be related to activating the Nrf2/ARE signaling pathway.

1. Introduction

Acute pancreatitis is one of the common acute abdominal diseases in clinical practice. It is caused by abnormal activation of trypsinogen, which could lead to an inflammatory reaction in the pancreatic tissues and the whole body and cause damage and dysfunction of the pancreas and other organs [1]. Its condition progresses rapidly and has many complications. About a quarter of patients will develop severe acute pancreatitis (SAP) [2]. It is difficult to treat clinically and easily leads to death. Acute lung injury is a common complication in the early stage of SAP and is the primary cause of high mortality in patients [3]. Acute lung injury is a disease characterized by excessive inflammatory response and oxidative stress. It is caused by alveolar injury and forms inflammatory noncardiogenic pulmonary edema. Therefore, improving lung injury is a crucial step in treating SAP and has important clinical significance.

Traditional Chinese medicine has a unique effect on the conditioning of visceral irregularities. Paeoniflorin (PAE) is derived from red peony roots, a water-soluble monoterpenoid glycoside with antioxidant, antitumor, and immunomodulatory effects. Its clinical medicinal value has received increasing attention due to its minimal toxic side effects [4]. In a 2019 review, Xiang et al. systematically summarized the antitumor activity of paeoniflorin [5]. Studies have found that PAE also plays an essential role in treating various non-neoplastic diseases. PAE can inhibit the nerve center and gastrointestinal inflammation responses [6, 7]. P. Wang et al. found that PAE may alleviate acute necrotizing pancreatitis-induced acute kidney injury through the MAPK signaling pathway [7]. However, the effect of PAE on SAP

on lung injury and the molecular mechanism is not fully understood.

Nrf2, as a critical transcription factor regulating antioxidative stress, is expressed in multiple organs of the whole body such as the lung, liver, and kidney and interacts with the antioxidant response element (ARE) to initiate the transcription and expression of downstream antioxidant genes. This promotes the synthesis and secretion of antioxidant enzymes, reducing tissue ROS levels, thereby enhancing the body's antioxidant capacity [8]. The Nrf2/ARE pathway has the functions of detoxification and neutralization. It is also because the antioxidant enzymes and II detoxifying enzymes regulated by the pathway can remove harmful substances such as ROS. Therefore, Nrf2/ARE can be used as a drug target for the prevention and treatment of inflammation, cancer, diabetes, respiratory diseases, and neurodegenerative diseases. Nrf2/ARE signaling is a molecular target for treating lung injury. Upregulating its expression can enhance cell ROS-scavenging ability, reduce acute lung inflammation responses, and repair lung injury [9]. Heme oxygenase-1 (HO-1) is the rate-limiting enzyme of heme metabolism encoded by the hmox-1 gene. It plays a protective role in various organs by regulating production through the transcription factor Nrf2 under the induction of various stimuli. And one of its end products, carbon monoxide, has the same anti-inflammatory, antiapoptotic, and antiproliferative effects as HO-1 [10, 11]. Quinone oxidoreductase (NQO1) is one of the primary downstream target genes of Nrf2 and is considered to be the main antioxidant [12]. Studies have shown that the NQO1 promoter region is involved in lung injury, the expression of NQO1 is upregulated in response to oxidative stress, and the increase of NQO1 expression can prevent hyperoxic lung injury [13]. The Nrf2/HO-1/NQO1 signaling pathway is an essential mechanism for Nrf2 to increase antioxidant enzyme activity and reduce oxidative stress damage [14]. In addition, studies have shown that PAE can play a protective role through the Nrf2-mediated signaling pathway. Chen et al. found that PAE can play a protective role against cholestasis-induced liver injury in rats by activating the Nrf2 signaling pathway [15]. Research by Yang et al. showed that PAE could inhibit the oxidative stress of nerve cells induced by diabetes by promoting the dissociation of Nrf2 from the Keap1 complex [16]. Therefore, PAE may play a protective role through the Nrf2/ARE signaling pathway in the lung injury of SAP rats.

Severe acute pancreatitis (SAP) lung injury model was established in this study. It explored the effects of paeoniflorin in the lungs of SAP rats in terms of histological changes in lung injury, the severity of pulmonary edema, and changes in a series of biochemical indicators after paeoniflorin treatment. The function of the injury and the possible mechanism provide a theoretical basis for the clinical treatment of lung injury in severe acute pancreatitis.

2. Materials and Methods

2.1. Experimental Animals. 48 adult male SD rats were purchased from Shanghai Southern Model Biology Center. One-week adaptive feeding conditions were $24 \pm 1^{\circ}C$, relative humidity 65%, and light/dark cycle 12 h; food and water were freely available. All research protocols involving animals in this study after adaptive feeding were approved by the Institutional Animal Ethics Committee of the Guangdong Provincial Medical Laboratory Animal Center (C202201-1) and carried out according to the approved guidelines.

2.2. Main Testing Reagents, Drugs, and Instruments. Paeoniflorin and dexamethasone were purchased from Aladdin (Shanghai, China). Sodium taurocholate was purchased from Sigma, USA. ELISA kit was purchased from Nanjing Jiancheng Bioengineering Institute Co., Ltd. Saline was purchased from Nanjing Xiaoying Pharmaceutical Group Co., Ltd. Rabbit-derived β-actin (ab8227), Nrf2 (ab92946), HO-1 (ab13248), NQO1 (ab80588), and Lamin B (ab16048) primary antibodies, goat anti-rabbit secondary antibody (ab6721), goat anti-mouse secondary antibodies (ab6789) were purchased from Abcam, USA. Superoxide dismutase (SOD) activity detection kit (BC0170), malondialdehyde (MDA) content detection kit (BC0025), lactate dehydrogenase (LDH) activity detection kit (BC0680), SDS-PAGE gel preparation kit (P1200), and 10xTBST buffer (T1081) were purchased from Beijing Solarbio Co., Ltd. Nuclear protein and cytoplasmic protein extraction kit (P0028), BeyoECL Moon (Extremely sensitive ECL chemiluminescence kit) (P0018FM), BCA kit (P0012), and HE staining reagent (C0105S) were purchased from Shanghai Beyotime Biotechnology.

2.3. Model Establishment and Grouping Administration. The model was prepared by referring to the method in the literature [17]: after depilation, the rats were anesthetized intraperitoneally with2% pentobarbital sodium at a dose of 30 mg/kg and fixed in the operating table. After laparotomy, the rats were selected to grind the needle, and the opening of the duodenal papilla of the 1 mi syringe slowly entered the pancreaticobiliary duct and injected with 5% sodium taurocholate solution was injected into the pancreatic tissue of rats at the injection rate of 0.1 ml/min. Once the tissue swelling and congestion were found, it indicated that the model was established successfully. Then, the microartery clamp was removed, the needle was pulled out, and the abdominal cavity was closed layer by layer. The rats with acute pancreatitis were forbidden to eat and drink freely after operation. When the rats showed symptoms such as drinking a lot of water, reluctance to eat or drink, dull fur, shortness of breath, wheezing, murmur on lung auscultation, significantly increased serum amylase, pancreatic edema, hemorrhage, and necrosis, etc., it indicated that the model was successful.

48 rats were randomly divided into 4 groups, with 12 rats in each group. Sham operation group (Sham): the same amount of normal saline was retrogradely injected into the biliopancreatic duct. SAP group: 5% sodium taurocholate (1 ml/kg) was retrogradely injected into the biliopancreatic duct at a rate of 0.1 ml/min. After 30 minutes, rats were intragastrically administered with normal saline. Paeoniflorin

treatment group (Pae) group: 30 minutes after SAP modeling, the rats were intragastrically administered paeoniflorin (40 mg/kg). Dexamethasone-positive control group (Dex): 30 min after SAP modeling, the rats were intraperitoneally injected with dexamethasone (2 mg/kg). After 24 hours of treatment, the rats were sacrificed, and blood, pancreatic tissue, lung tissue, and bronchoalveolar lavage fluid (BALF) were collected for index detection.

2.4. Determination of Lung Wet-to-Dry Weight (W/D) Ratio. Fresh right lung tissues were weighed to obtain the wet weight of the lung tissue, then placed in a 60°C constant temperature incubator for baking for 2 days, and then weighed to obtain the dry weight of the lung tissue. The W/D value was calculated. The formula is as follows: W/D = wet weight/dry weight, which is an indicator that reflects the degree of pulmonary edema.

2.5. H&E Staining. The lung tissues were fixed in 10% formaldehyde for 48 hours and then embedded in paraffin for sectioning (5 μm). Lung tissue sections were selected and sequentially deparaffinized in xylene and ethanol. After drying at room temperature, the sections were stained with hematoxylin and eosin solution. Finally, the sections were dehydrated with alcohol, treated with xylene, and sealed. The pathological changes of lung tissue were observed under a light microscope, and the experiment was repeated three times.

2.6. Detection of Rat Biochemical Indicators. About 3 ml of rat serum was taken and placed into an automatic blood biochemical analyzer to detect α-amylase and lipase activity indicators. The lung tissues were taken, and the contents of LDH, MDA, and SOD in the lung tissues of rats were detected according to the instructions of the lactate dehydrogenase (LDH), malondialdehyde (MDA), and superoxide dismutase (SOD) kits.

2.7. ELISA. After 24 hours of treatment, BALF was collected by lavage of the lungs three times with 500 μl of sterile PBS (total volume of 1.5 ml). The expression levels of TNF-α, IL-6, and IL-10 in BALF of each group of rats were detected according to the instructions of the ELISA kit.

2.8. Western Blot. Tissue protein was extracted according to the instructions of the Nuclear and Cytoplasmic Protein Extraction Kit. Protein concentration was measured with a BCA kit. Equal amounts of protein samples were subsequently separated by 10% SDS-PAGE and transferred to PVDF membranes. Blocking was performed for 1 h in blocking solution (prepared in TBST) containing 5% skimmed milk powder. The membranes were incubated with primary antibodies overnight at 4°C. After washing 3 times with TBST, the membranes were incubated with secondary antibodies for 2 h. ECL luminescence agent was added, and the FliorchemHD2 imaging system was used for scanning analysis and photography.

2.9. Statistical Analysis. The experimental data was plotted using each group's mean ± standard deviation (SD), and statistical analysis was performed using SPSS 20 software. A one-way analysis of variance was used for multiple group comparisons. $p < 0.05$ as the difference was considered statistically significant.

3. Results

3.1. Paeoniflorin Can Effectively Reduce Lung Injury in SAP Rats. The W/D ratio of the lung is a sensitive indicator of the severity of lung injury. H&E staining and the W/D method were used to evaluate the degree of lung injury in each group of acute pancreatitis rats. H&E staining showed that the lung tissue of rats in the Sham group showed no injury. The interstitial lung tissue of rats of the SAP group had prominent edema, congestion, a large number of inflammatory cell infiltration, and alveolar structure destruction. Pathological changes such as interstitial edema, hemorrhage, and inflammatory cell infiltration in the lung tissues in the Pae group and the Dex group were significantly reduced compared with those in the SAP group (Figure 1(a)). The W/D method showed that the SAP group, Pae group, and Dex group exhibited apparent pulmonary edema injury compared with the Sham group. Still, the damages in the Pae group and Dex group were significantly reduced compared with the SAP group (Figure 1(b)). The severity of SAP-related acute lung injury could be assessed by detecting the activity of amylase and lipase in the serum of each group. As shown in Figures 1(c) and 1(d), the activities of amylase and lipase in the serum of rats in the SAP, Pae, and Dex groups were significantly higher than those in the Sham group ($p < 0.01$). However, after treatment with paeoniflorin and dexamethasone, SAP rats showed significantly reduced amylase and lipase activities. It indicated that paeoniflorin could effectively reduce lung tissue damage in SAP rats.

3.2. Paeoniflorin Inhibits Oxidative Stress in Lung Injury in SAP Rats. The levels of LDH, MDA, and SOD in lung tissue of SAP rats treated with PAE were measured. As shown in Figures 2(a)–2(c), compared with the Sham group, the LDH activity and MDA secretion of the rats in each SAP model group increased significantly, while the activity of the antioxidant enzyme SOD decreased significantly. The oxidative index levels were opposite between the Pae group and SAP group. This suggests that paeoniflorin could substantially inhibit the oxidative stress response in the lung injury of SAP rats.

3.3. Paeoniflorin Alleviates Inflammatory Response in Lung Injury in SAP Rats. Further, ELISA was conducted to detect the levels of inflammatory factors in the BALF of rats in each group (Figures 3(a)–3(c)). Compared with the Sham group, the levels of proinflammatory factors TNF-α and IL-6 in the BALF of rats in the SAP group, Pae group, and Dex groups were significantly increased. In contrast, the level of anti-inflammatory factor IL-10 was reduced considerably. However, the levels of TNF-α and IL-6 in BALF of rats in the Pae group and the Dex group were significantly lower than that of the SAP group, with IL-10 levels considerably higher than in the SAP group. These results indicate that paeoniflorin can dramatically alleviate the inflammatory response in the lung injury of SAP rats.

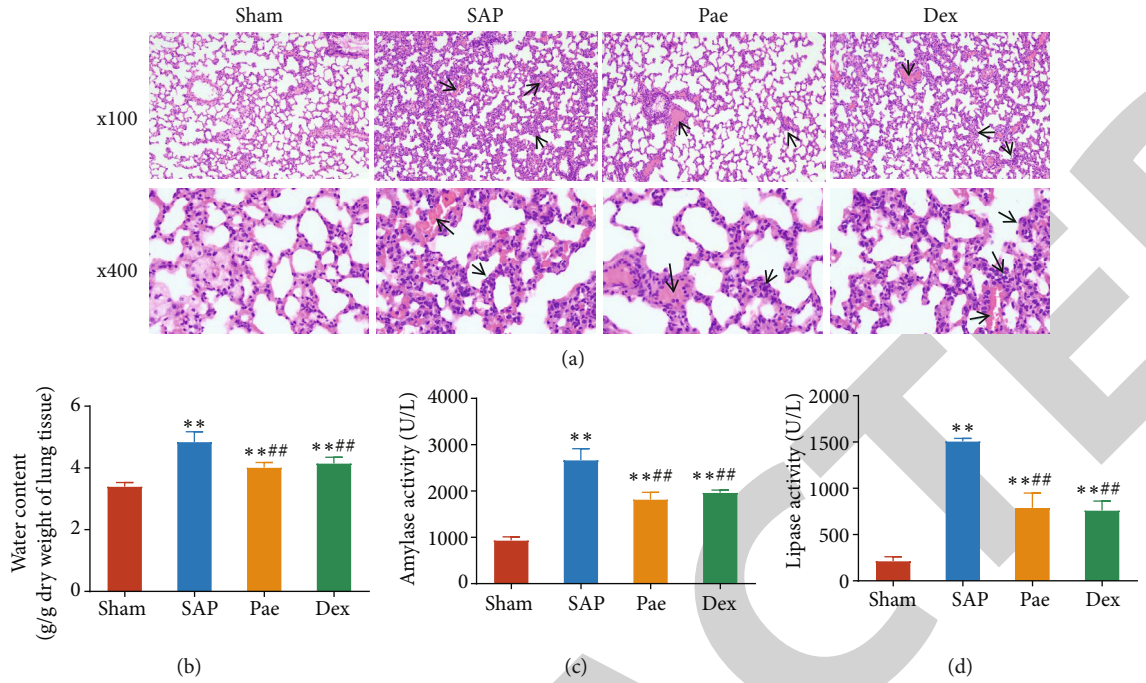

Figure 1: Paeoniflorin can reduce pancreatic and lung injury in rats with severe acute pancreatitis. (a) H&E staining was used to observe the pathological changes in the lung tissue of each group of rats. (b) W/D-specific gravity method was used to detect the water content of the lung tissue of each group. (c) Biochemical detection of amylase activity in the serum of each group of rats. (d) Biochemical detection of lipase activity in the serum of rats in each group. $^{**}p < 0.01$ vs. Sham group; $^{\#\#}p < 0.01$ vs. SAP group.

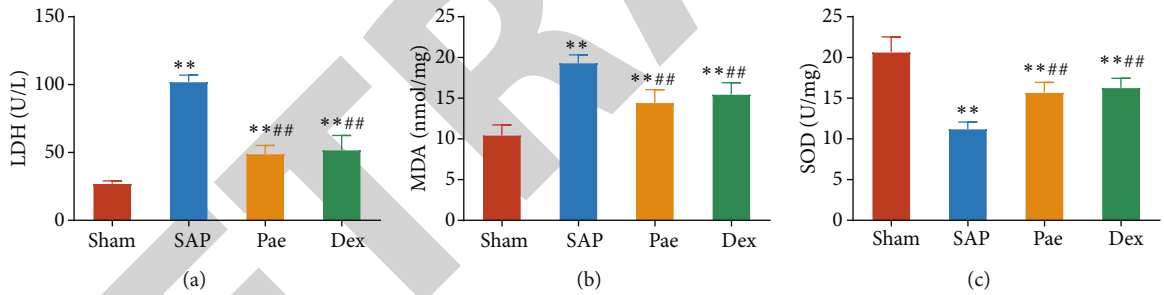

Figure 2: Paeoniflorin reduces oxidative stress levels in the lung tissue of SAP rats. (a–c) The contents of LDH activity (a), MDA (b), and SOD (c) in the lung tissue of rats in each group were detected. $^{**}p < 0.01$ vs. Sham group, $^{\#\#}p < 0.01$ vs. SAP group.

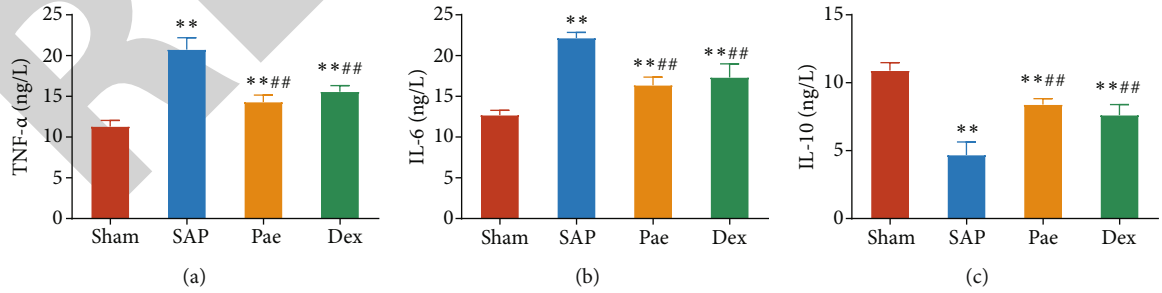

Figure 3: Paeoniflorin alleviated the inflammatory response in lung injury in SAP rats. (a–c) The levels of TNF-α (a), IL-6 (b), and IL-10 (c) in bronchoalveolar lavage fluid (BALF) of rats in each group were detected by ELISA. $^{**}p < 0.01$ vs. Sham group; $^{\#\#}p < 0.01$ vs. SAP group.

3.4. Paeoniflorin Activates the Nrf2/ARE Signaling Pathway in Lung Injury in SAP Rats. To clarify whether paeoniflorin protects the molecular mechanism against lung injury in SAP rats by activating the Nrf2/ARE pathway, the expression of proteins Nrf2 (Cyt-Nrf2), heme oxygenase 1 (HO-1), quinone oxidoreductase 1 (NQO1), and nuclear Nrf2 (Nuc-Nrf2) of the Nrf2/ARE pathway was examined by Western blot. Compared with the Sham group, the expression levels

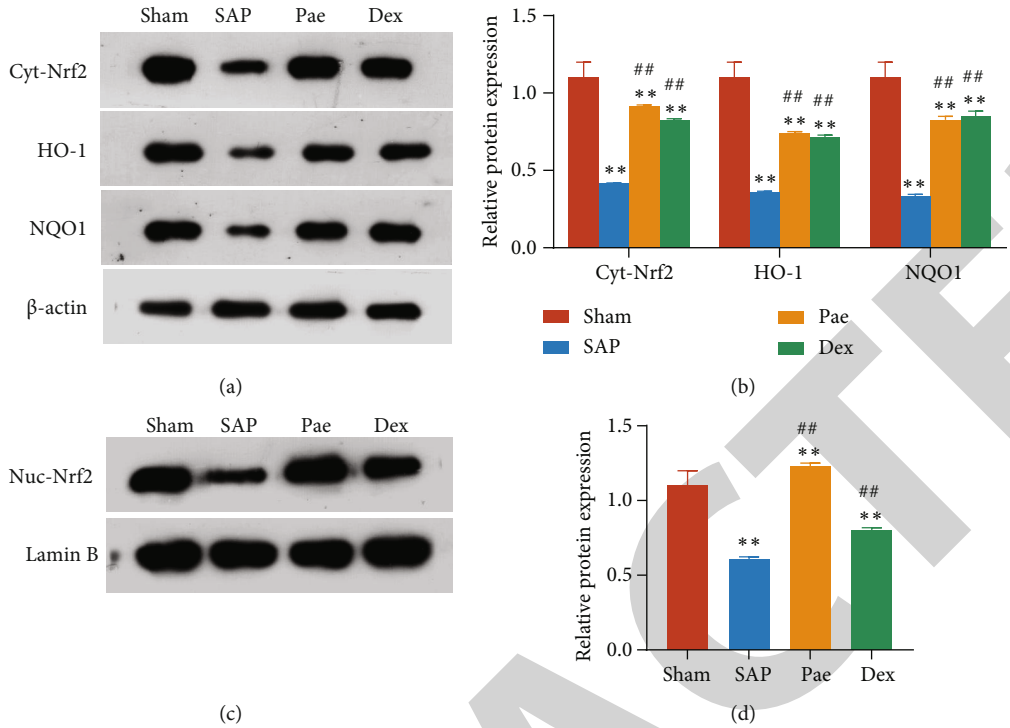

Figure 4: Paeoniflorin activates the Nrf2/ARE signaling pathway in lung injury in SAP rats. (a and b) The expression of total cellular proteins Nrf2, HO-1, and NQO1 in lung tissue of each group of rats. (c and d) The expression of nuclear Nrf2 protein in the lung tissue of each group of rats. $^{**}p < 0.01$ vs. Sham group; $^{\#\#}p < 0.01$ vs. SAP group.

of HO-1, NQO1, and Cyt-Nrf2 in the lung tissues of rats in the SAP group, Pae group, and Dex groups were significantly reduced ($p < 0.01$), and the expression of Nuc-Nrf2 in the nucleus was significantly downregulated ($p < 0.01$). While in the Pae group and Dex group, Cyt-Nrf2, HO-1, NQO1 protein expression was significantly higher than the SAP group with nuclear Nuc-Nrf2 protein expression which was also significantly upregulated ($p < 0.01$) (Figure 4). This result indicates that paeoniflorin can exert a protective effect by activating the Nrf2/ARE signaling pathway in the lung injury of SAP rats.

4. Discussion

Acute pancreatitis is a common emergency department disease with rapid onset, rapid progression, and complex mechanisms. It can rapidly progress to SAP with a mortality rate as high as 31%. SAP patients experience not only pancreatic tissue ischemia and necrosis but also induced systemic acute inflammatory reactions and cause renal and pulmonary multiple organ injury and functional failure in more severe cases. Acute lung injury is a common complication in the initial stage of SAP patients, and it is also the most important cause of death in patients [18]. Paeoniflorin is a commonly used traditional Chinese medicine with pharmacological effects such as antidepressant, anti-inflammatory, analgesic, antitumor, hepatoprotective, neuroprotection, immune regulation, and the prevention and treatment of diabetic complications [19]. Many studies have shown that PAE plays a vital role in lung damage caused by various diseases. Ling et al. found that PAE reduces the inflammatory response and oxidative stress damage in rats with septic acute lung injury by activating the Nrf2/Keap1 signaling pathway and has preventive and protective effects on the lung tissue septic acute lung injury rats [20]. Zhang et al. also found that paeoniflorin can reduce endotoxin-induced lung injury in mice by inhibiting lung tissue neutrophil infiltration, MPO content, and cPLA2 activity [21]. However, whether paeoniflorin can play a protective role in SAP lung injury is still unclear.

A rat model of SAP lung injury was constructed by retrograde injection of sodium taurocholate into the biliopancreatic duct of the rat in this study. The lung tissues of rats in the model group showed obvious lung injury symptoms such as edema and congestion and a large number of inflammatory cell infiltrations. Serum amylase is currently the most commonly used and prevalent detection index in diagnosing SAP in clinical practice [22]. The increase in serum lipase concentration due to the destruction of pancreatic follicles in SAP is one of the significant manifestations of pancreatitis [23]. In this study, amylase and lipase activity in the serum of rats in the SAP group increased significantly. SOD, MDA, and LDH are three substances used to evaluate the body's oxidative stress response and antioxidant capacity. Many studies have shown that when the body undergoes an oxidative stress response, the levels of MDA and LDH increase, while the level of SOD decreases [24, 25]. It was found that the levels of MDA and LDH were significantly increased in the serum of rats of the model group, with SOD levels significantly decreased. These results were consistent with the study on multiple complications secondary to SAP by Chen et al. [26]. In summary, all of the above shows that the rat SAP lung injury model was successfully constructed in this study.

Studies have found that 100 mg/kg paeoniflorin intervention can reduce serum amylase and lipase levels in the SAP rat model [27]. SAP rats were fed with 40 mg/kg paeoniflorin in this study. The levels of serum amylase and lipase after this treatment were significantly downregulated, indicating that lower concentrations of paeoniflorin can inhibit the progression of SAP. However, in this study, the effects of different concentrations of paeoniflorin on various biochemical indicators of SAP rat were not studied, so the optimal concentration of paeoniflorin to exert its effect remains unclear.

Zhao et al. [28] observed that paeoniflorin exerts a protective effect on rat cholestasis induced by ANIT by inhibiting oxidative stress response. It is reported that paeoniflorin also has the function of inhibiting inflammation response by downregulating the secretion of cytokines such as TNF-α, IL-1β, and IL-6 [7, 29]. In this study, it was also found that after feeding paeoniflorin as treatment, the water content in the lung tissue of rats was significantly reduced with the levels of TNF-α and IL-6 in BALF reduced considerably, and the level of IL-10 was increased significantly. The content of LDH and MDA in the tissue was significantly reduced, while the content of SOD increased markedly. It was also found that the effect of paeoniflorin in inhibiting oxidative stress and inflammatory response was not significantly different from the effect of the positive control of intraperitoneal injection of dexamethasone in SAP rats. This shows that paeoniflorin can improve lung injury caused by SAP and relieve oxidative stress and inflammatory response. Its effect is not significantly different from the clinical anti-inflammatory drug dexamethasone in anti-inflammatory and antioxidant properties.

Although we confirmed that the paeoniflorin group significantly increased the protein expression levels of Nrf2, HO-1, and NQO1 in rat lung tissues, paeoniflorin may ameliorate SAP lung injury by activating the Nrf2/ARE signaling pathway. Whether paeoniflorin can also act through other molecular signaling pathways and its role is not known. Therefore, it is necessary to explore further other possible signaling pathways that PAE can protect the lung tissue of SAP lung injury rats to provide a more comprehensive research basis for PAE treatment of SAP lung injury, which is essential for implementing effective treatment.

5. Conclusion

In summary, paeoniflorin can inhibit the inflammatory response and oxidative stress damage in rats with SAP lung injury and has a preventive and protective effect on the lung tissue of rats with SAP lung injury. This protective effect may be related to activating the Nrf2/ARE signal pathway. The foundation is laid for applying new drugs to treat SAP lung injury in clinical practice in this study.

Data Availability

The data used to support the findings of this study are available from the corresponding author upon request.

Conflicts of Interest

The authors declare that they have no competing interests.

References

[1] P. J. Lee and G. I. Papachristou, "New insights into acute pancreatitis," *Nature Reviews. Gastroenterology & Hepatology*, vol. 16, no. 8, pp. 479–496, 2019.

[2] P. G. Lankisch, M. Apte, and P. A. Banks, "Acute pancreatitis," *Lancet*, vol. 386, no. 9988, pp. 85–96, 2015.

[3] L. Huang, Y. Jiang, Z. Sun, Z. Gao, J. Wang, and D. Zhang, "Autophagy strengthens intestinal mucosal barrier by attenuating oxidative stress in severe acute pancreatitis," *Digestive Diseases and Sciences*, vol. 63, no. 4, pp. 910–919, 2018.

[4] S. H. Wu, D. G. Wu, and Y. W. Chen, "Chemical constituents and bioactivities of plants from the genus Paeonia," *Chemistry & Biodiversity*, vol. 7, no. 1, pp. 90–104, 2010.

[5] Y. Xiang, Q. Zhang, S. Wei, C. Huang, Z. Li, and Y. Gao, "Paeoniflorin: a monoterpene glycoside from plants of Paeoniaceae family with diverse anticancer activities," *The Journal of Pharmacy and Pharmacology*, vol. 72, no. 4, pp. 483–495, 2020.

[6] Z. Ma, L. Chu, H. Liu et al., "Paeoniflorin alleviates non-alcoholic steatohepatitis in rats: involvement with the ROCK/NF-κB pathway," *International Immunopharmacology*, vol. 38, pp. 377–384, 2016.

[7] P. Wang, W. Wang, Q. Shi et al., "Paeoniflorin ameliorates acute necrotizing pancreatitis and pancreatitis-induced acute renal injury," *Molecular Medicine Reports*, vol. 14, no. 2, pp. 1123–1131, 2016.

[8] W. Tu, H. Wang, S. Li, Q. Liu, and H. Sha, "The anti-inflammatory and antioxidant mechanisms of the Keap1/Nrf2/ARE signaling pathway in chronic diseases," *Aging and Disease*, vol. 10, no. 3, pp. 637–651, 2019.

[9] R. Joo Choi, M. S. Cheng, and Y. Shik Kim, "Desoxyrhapontigenin up-regulates Nrf2-mediated heme oxygenase-1 expression in macrophages and inflammatory lung injury," *Redox Biology*, vol. 2, pp. 504–512, 2014.

[10] M. L. M. Pereira, C. R. F. Marinho, and S. Epiphanio, "Could heme oxygenase-1 be a new target for therapeutic intervention in malaria-associated acute lung injury/acute respiratory distress syndrome?," *Frontiers in Cellular and Infection Microbiology*, vol. 8, p. 161, 2018.

[11] S. W. Ryter and A. M. Choi, "Targeting heme oxygenase-1 and carbon monoxide for therapeutic modulation of inflammation," *Translational Research*, vol. 167, no. 1, pp. 7–34, 2016.

[12] L. Li, H. Dong, E. Song, X. Xu, L. Liu, and Y. Song, "Nrf2/ARE pathway activation, HO-1 and NQO1 induction by polychlorinated biphenyl quinone is associated with reactive oxygen species and PI3K/AKT signaling," *Chemico-Biological Interactions*, vol. 209, pp. 56–67, 2014.

[13] Y. Ling, Z. Z. Li, J. F. Zhang et al., "MicroRNA-494 inhibition alleviates acute lung injury through Nrf2 signaling pathway via NQO1 in sepsis-associated acute respiratory distress syndrome," *Life Sciences*, vol. 210, pp. 1–8, 2018.

[14] Y. Feng, R. Cui, Z. Li et al., "Methane alleviates acetaminophen-induced liver injury by inhibiting inflammation, oxidative stress, endoplasmic reticulum stress, and apoptosis through the Nrf2/HO-1/NQO1 signaling pathway," *Oxidative Medicine and Cellular Longevity*, vol. 2019, Article ID 7067619, 14 pages, 2019.

Hindawi
Computational and Mathematical Methods in Medicine
Volume 2023, Article ID 9826474, 1 page
https://doi.org/10.1155/2023/9826474

Retraction

Retracted: GEO Database Screening Combined with In Vitro Experiments to Study the Mechanism of hsa_circ_0003570 in Infantile Hemangiomas

Computational and Mathematical Methods in Medicine

Received 27 June 2023; Accepted 27 June 2023; Published 28 June 2023

This article has been retracted by Hindawi following an investigation undertaken by the publisher [1]. This investigation has uncovered evidence of one or more of the following indicators of systematic manipulation of the publication process:

(1) Discrepancies in scope

(2) Discrepancies in the description of the research reported

(3) Discrepancies between the availability of data and the research described

(4) Inappropriate citations

(5) Incoherent, meaningless and/or irrelevant content included in the article

(6) Peer-review manipulation

The presence of these indicators undermines our confidence in the integrity of the article's content and we cannot, therefore, vouch for its reliability. Please note that this notice is intended solely to alert readers that the content of this article is unreliable. We have not investigated whether authors were aware of or involved in the systematic manipulation of the publication process.

Wiley and Hindawi regrets that the usual quality checks did not identify these issues before publication and have since put additional measures in place to safeguard research integrity.

We wish to credit our own Research Integrity and Research Publishing teams and anonymous and named external researchers and research integrity experts for contributing to this investigation.

The corresponding author, as the representative of all authors, has been given the opportunity to register their agreement or disagreement to this retraction. We have kept a record of any response received.

References

[1] Y. Tian, S. Zhuang, J. Zhang et al., "GEO Database Screening Combined with In Vitro Experiments to Study the Mechanism of hsa_circ_0003570 in Infantile Hemangiomas," *Computational and Mathematical Methods in Medicine*, vol. 2022, Article ID 5643742, 13 pages, 2022.

Hindawi
Computational and Mathematical Methods in Medicine
Volume 2022, Article ID 5643742, 13 pages
https://doi.org/10.1155/2022/5643742

Research Article

GEO Database Screening Combined with In Vitro Experiments to Study the Mechanism of hsa_circ_0003570 in Infantile Hemangiomas

Yu Tian,[1] Shihao Zhuang,[2] Jiantao Zhang,[1] Tonghui You,[1] Zihang Xu,[3] Wanli Yang,[3] Bin Hao,[1] Weifeng Wang,[4,5] and Tao Yang[1]

[1]*Shanxi Bethune Hospital, Shanxi Academy of Medical Sciences, Tongji Shanxi Hospital, Third Hospital of Shanxi Medical University, Taiyuan 030032, China*
[2]*Fujian Children's Hospital; Fujian Maternity and Child Health Hospital, Affiliated Hospital of Fujian Medical University, Fuzhou 350000, China*
[3]*Third Hospital of Shanxi Medical University, Shanxi Bethune Hospital, Shanxi Academy of Medical Sciences, Tongji Shanxi Hospital, Taiyuan 030032, China*
[4]*Department of Central Laboratory, Shanghai Tenth People's Hospital, Tongji University School of Medicine, Shanghai 200435, China*
[5]*Department of Clinical Laboratory Medicine, Longhua Hospital Shanghai University of Traditional Chinese Medicine, Shanghai 200030, China*

Correspondence should be addressed to Bin Hao; sxdyyxgwkhb@126.com, Weifeng Wang; weifengdangdao@163.com, and Tao Yang; 646808009@qq.com

Yu Tian, Shihao Zhuang, and Jiantao Zhang contributed equally to this work.

Received 17 January 2022; Accepted 31 March 2022; Published 28 April 2022

Academic Editor: Muhammad Zubair Asghar

Objective. In this study, we screened out a type of differentially expressed circular RNA in infantile hemangioma (IH) cells and analyzed the mechanism in the malignant biological behavior of IH. *Methods.* Based on the GSE98795, GSE100682, and GSE43742 datasets, differential expression analysis of circRNAs, microRNAs, and mRNAs was performed. The relative expression level of RNA was detected by quantitative real-time polymerase chain reaction (qRT-PCR). MTT assay, Transwell, flow cytometry analysis, and western blot were used to study the effects of hsa_circ_0003570, hsa-miR-138-5p, and RGS5 on the proliferation and apoptosis of hemangioma endothelial cells (HEMECs). *Results.* The hsa_circ_0003570 and *RGS5* mRNA were upregulated in HEMECs, but hsa-miR-138-5p was downregulated. Silencing of hsa_circ_0003570 inhibited the proliferation of HEMECs and promoted the apoptosis of HEMECs. The malignant biological behaviors of hsa_circ_0003570 on the proliferation and apoptosis of HEMECs were reversed by hsa-miR-138-5p. Hsa_circ_0003570 acted as the ceRNA of hsa-miR-138-5p and upregulated the expression of RGS5. Silencing of RGS5 inhibited the proliferation, migration, and invasion of HEMECs and promoted apoptosis. *Conclusion.* Hsa_circ_0003570 promotes IH cell proliferation and inhibits IH cell apoptosis through hsa-miR-138-5p/RGS5 axis.

1. Introduction

IH is a kind of soft tissue benign tumor in infants and young children [1]. The incidence was about 3 to 5% and increased in recent years [2–4]. Although most IH are benign and have a self-limiting course, about 10% of IH can grow rapidly and cause serious complications, such as bleeding, ulceration, and impaired appearance, requiring early active intervention [5, 6].

Current research evidence showed that the occurrence and development of IH were jointly regulated by exogenous

factors such as tissue hypoxia, developmental defects, and endogenous genes [6–10]. Noncoding RNA (ncRNA) occupies 98%-99% of the human genome transcript, and it has been confirmed that it can affect the occurrence and development of various diseases by regulating gene expression [11, 12].

Circular RNA is a special type of ncRNAs, which is formed by alternative splicing of precursor mRNA. It is a closed-ring structure with the 3′ and the 5′ ends connected by a covalent bond [13]. circRNA has the characteristics of high abundance, high stability, sequence conservation, tissue and developmental stage specificity, etc., and it is an important regulatory factor in the occurrence and development of diseases [14, 15]. The current findings suggested that circRNAs could act as a molecular sponges for microRNAs, competitive endogenous RNAs (ceRNAs), and binding microRNAs and preventing them from binding to downstream target genes, thereby regulating gene expression [16]. In addition, circRNA can also play a role in transcription and splicing regulation [17], circRNA-protein interaction [18, 19], and translation protein [20].

Both angiogenesis and revascularization are involved in the occurrence of IH, but the specific mechanism needs to be further studied [21]. A feasible approach is to screen differentially expressed genes, microRNAs, and circRNAs in IH and study how they function in the occurrence of IH, which may provide new evidence for understanding the mechanism of IH.

In this study, we selected hsa_circ_0003570, hsa-miR-138-5p, and RGS5 for research by analyzing the differential transcription profiles of GSE98795, GSE100682, and GSE43742 datasets. Through bioinformatics tools, it was found that hsa_circ_0003570 and hsa-miR-138-5p as well as hsa-miR-138-5p and RGS5 had complementary pairing sequences. Therefore, we speculate that the hsa_circ_0003570/hsa-miR-138-5p/RGS5 axis may play a key role in the occurrence of IH. To prove our hypothesis, we studied the role of hsa_circ_0003570, hsa-miR-138-5p, and RGS5 in the malignant biological behavior of IH in the hemangioma endothelial cells (HEMEC) model, and through our research results, we provided a new direction for the treatment of IH. The flow chart was shown in Figure 1.

2. Materials and Methods

2.1. Datasets. The GSE98795 dataset [22] was used for differential expression analysis of circRNAs, the GSE100682 dataset was for microRNAs, and the GSE43742 dataset was for mRNAs, all these datasets were obtained from GEO DataSets (https://www.ncbi.nlm.nih.gov/gds/).

2.2. Cell Culture. Human dermal microvascular endothelial cells (HDMVECs) and HEMECs were cultured in DMEM (Invitrogen, Carlsbad, CA, USA) with 10% FBS (Gibco, Carlsbad, CA, USA) and incubated in a humidified atmosphere containing 5% CO_2 at 37°C.

2.3. Cell Transfection. The hsa_circ_0003570 small interfering RNA (named si-hsa_circ_0003570)-1, 2, 3 and si-no temple control (NC), hsa-miR-138-5p mimic, hsa-miR-138-5p inhibitor, hsa-miR-NC, pGL3-hsa_circ_0003570 wild-type (WT), pGL3-hsa_circ_0003570 mutant (MUT), pGL3-RGS5 wild-type (WT), pGL3-RGS5 mutant (MUT), short hairpin RNA no temple control (sh-NC), and sh-RGS5 were synthetized by GenePharma (Shanghai, China). The recombinant plasmid was transfected into HEMECs with Lipofectamine 2000 (Invitrogen, Carlsbad, CA). QRT-PCR and western blot were used to detect transfection efficiency. In order to screen the stable transfected HEMECs with the highest silencing efficiency, HEMECs were divided into 5 groups: control, si-NC, si-hsa_circ_0003570-1, and si-hsa_circ_0003570-2, si-hsa_circ_0003570-3. In order to analyze the role of hsa-miR-138-5p in hsa_circ_0003570-silenced HEMECs, HEMECs were divided into 5 groups: control, si-NC, si-hsa_circ_0003570, si-hsa_circ_0003570 +hsa-miR-138-5p inhibitor, and hsa-miR-138-5p inhibitor. In dual luciferase assay, HEMECs were divided into 8 group: hsa-miR-NC+pGL3-hsa_circ_0003570 WT, hsa-miR-NC +pGL3-hsa_circ_0003570 MUT, hsa-miR-138-5p mimic +pGL3-hsa_circ_0003570 WT, hsa-miR-138-5p mimic +pGL3-hsa_circ_0003570 MUT, hsa-miR-NC+pGL3-RGS5 WT, hsa-miR-NC+pGL3-RGS5 MUT, hsa-miR-138-5p mimic+ pGL3-RGS5 WT, and hsa-miR-138-5p mimic +pGL3-RGS5 MUT. In order to study the effect of RGS5 silencing on the malignant biological behavior of HEMECs, HEMECs were divided into 3 group: control, sh-NC, and sh-RGS5. All samples were run in triplicate.

2.4. Quantitative Real-Time Polymerase Chain Reaction (qRT-PCR). Total RNA was isolated from HEMECs with Trizol reagent (Life Technologies Corporation, Carlsbad, CA, USA). One-Step SYBR PrimeScript RT-PCR Kit (TakaraBio, Inc., Japan) was used to detect the expression of hsa_circ_0003570, hsa-miR-138-5p, and *RGS5* mRNA. The PCR conditions were 95°C for 5 min, then 95°C for 10s, 58°C for 20s, and 72°C for 30s, and repeated for 45 cycles. The primer sequences of hsa_circ_0003570 were 5′-AACT TGTGTCCAGAAAGTGCTT-3′(forward); 5′-AAGATG GCACAGCACACGC-3′ (reverse). Hsa-miR-138-5p: 5′-GCCGAGCTGGTGTTGTGAAT-3′ (forward); 5′-GTGC AGGGTCCGAGGTATTC-3′ (reverse). *RGS5* mRNA: 5′-AAGATGGCTGAGAAGGCAAA-3′ (forward); 5′-TCAGGGCATGGATTCTTTTC-3′ (reverse). U6: 5′-AACG CTTCACGAATTTGCGT-3′ (forward); 5′-CTCGCTTCG GCAGCACA-3′ (reverse). The relative expression level was calculated by $2^{-\Delta\Delta Ct}$. All samples were run in triplicate.

2.5. MTT Assay. After 24 h of transfection, HEMECs were digested with trypsin. HEMECs were seeded 5×10^3 cells/well in 96-well. After incubated for 0, 24, 48, and 72 h, MTT (Sigma-Aldrich, St. Louis, MO, USA) was added to every well and incubated for 4 h. Then, 150 μl of DMSO was added into each well and mixed for 10 min. The absorbance at 490 nm was detected at 0 h, 24 h, 48 h, and 72 h. All samples were run in triplicate.

2.6. Transwell Assay. HEMECs were harvested after 24 h transfection. Migration and invasion of transfection

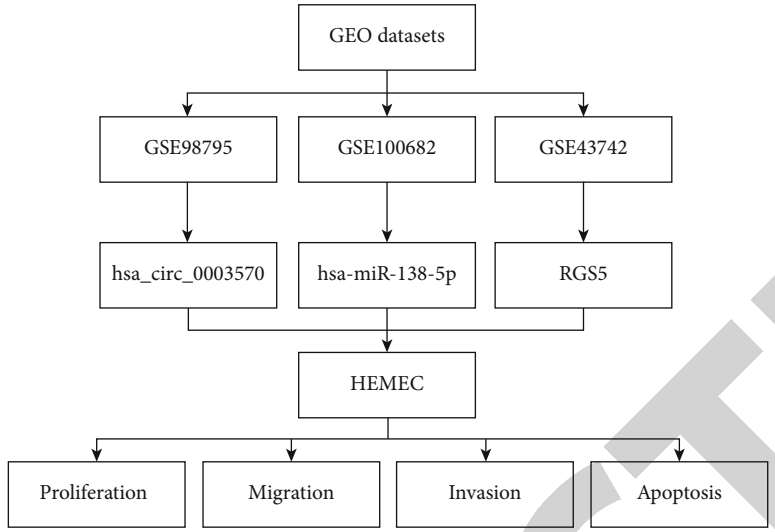

Figure 1: The flow chart of this study.

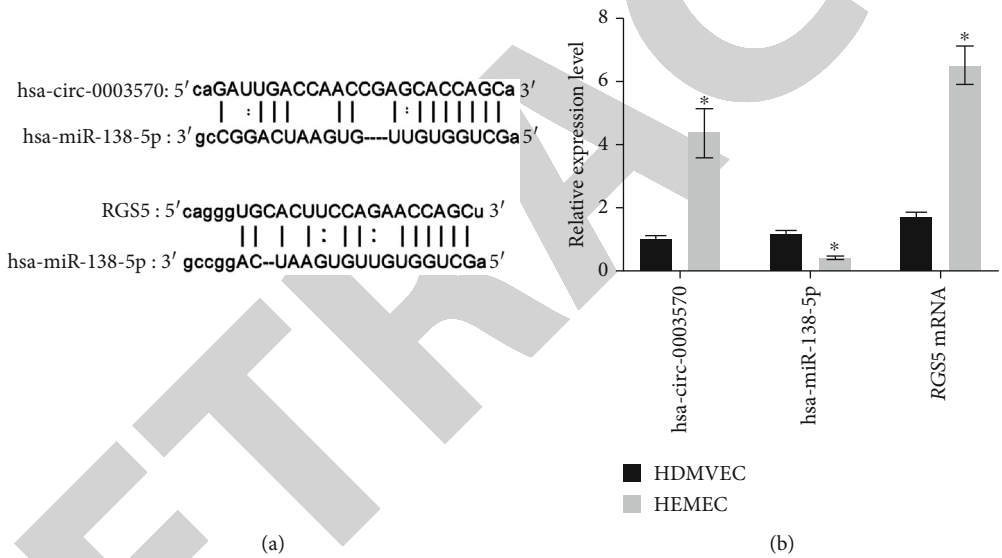

Figure 2: Analysis of hsa_circ_0003570, hsa-miR-138-5p, and *RGS5* mRNA expression levels in human dermal microvascular endothelial cells (HDMVECs) and hemangioma endothelial cells (HEMECs). (a) Binding sites' prediction of hsa_circ_0003570 and *RGS5* mRNA with hsa-miR-138-5p by the Encyclopedia of RNA Interactomes (ENCORI). (b) Quantitative real-time polymerase chain reaction (qRT-PCR) was used to detect the expression levels of hsa_circ_0003570, hsa-miR-138-5p, and *RGS5* mRNA in HDMVEC and HEMEC. $^{*}p < 0.05$, compared with HDMVEC.

HEMECs were detected by Transwell assay. The specific experimental procedures refer to the research of Zhou et al. [23]. All samples were run in triplicate.

2.7. Dual Luciferase Assay. The sequence of hsa_circ_0003570 and RGS5 and their mutant sequence of hsa-miR-138-5p binding sites were synthesized by PCR and cloned into pGL3-Basic (Promega, Madison, WI, USA). The pGL3-hsa_circ_0003570 WT or pGL3-hsa_circ_0003570 MUT and hsa-miR-138-5p mimic (or has-miR-NC) were cotransfected into HEMECs, and pGL3-RGS5 WT, pGL3-RGS5 MUT, and hsa-miR-138-5p mimic (or has-miR-NC) were cotransfected into HEMECs. The luciferase activities were detected by the Dual-Lucifer Reporter Assay System 48 h later, and the relative luciferase activity was calculated by normalizing to Renilla luciferase activity. All samples were run in triplicate.

2.8. Western Blot. Total protein in HEMECs was separated by SDS-PAGE. The proteins were transferred onto polyvinylidene fluoride (PVDF) membranes from SDS-PAGE. Then incubated the PVDF membrane with rabbit anti-RGS5 (ab96799, 1: 1500, Abcam, Cambridge, MA) primary antibodies at 4°C for 12 h-16 h, then incubated at room temperature for 2 hours with secondary antibody. RGS5 protein was visualized using ECL Plus Western blotting Detection Reagents (Millipore, Billerica, MA).

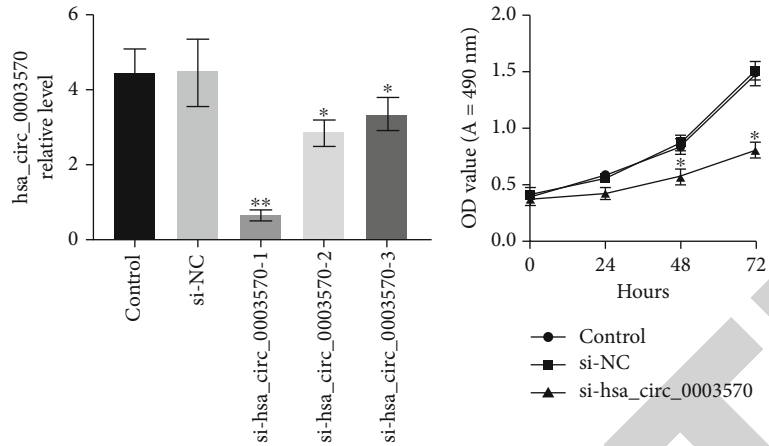

(a)

(b)

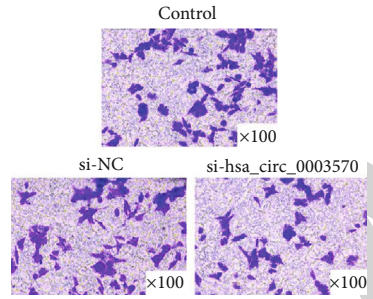

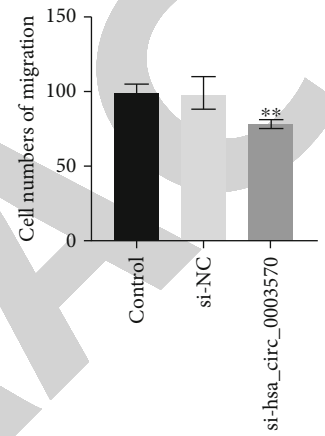

(c)

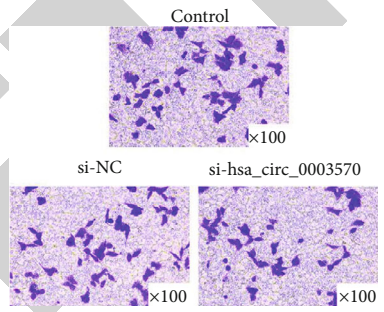

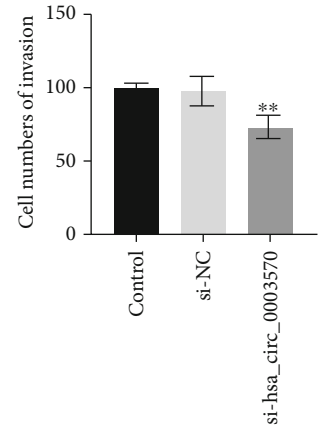

(d)

Figure 3: Continued.

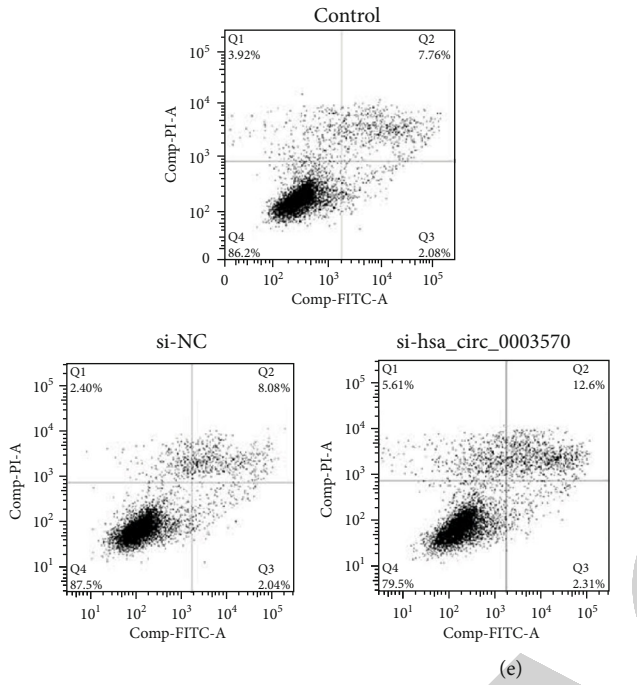

Figure 3: Silencing hsa_circ_0003570 inhibited the proliferation, migration, and invasion of HEMEC and promoted apoptosis. (a) The relative expression level of hsa_circ_0003570 to U6 was detected by quantitative real-time polymerase chain reaction (qRT-PCR) after no transfection group (control), no template control (si-NC), si-hsa_circ_0003570-1, si-hsa_circ_0003570-2, and si-hsa_circ_0003570-3 transfection. (b) The cell proliferation ability of HEMEC transfected with control, si-NC, and si-hsa_circ_0003570 was detected by MTT assay. (c) and (d) The cell migration ability and invasion ability of HEMEC transfected with control, si-NC, and si-hsa_circ_0003570 were detected by Transwell assay. (e) The apoptosis rate of HEMEC transfected with control, si-NC, and si-hsa_circ_0003570 was detected by flow cytometry. $^{*}p < 0.05$, $^{**}p < 0.01$, $^{***}p < 0.001$, compared with control.

2.9. Statistical Analysis. Discontinuous variables should be presented as percentages, while continuous variables in normal distribution should be described as mean ± standard deviation (SD) or else reported as median (range). Variance homogeneous and normal distributed continuous variables could be compared by student *t*-test, otherwise, the Mann–Whitney *U*-test or Kruskal-Wallis *H*-test would be used, $p < 0.05$ indicated that the difference was statistically significant. The statistical analyses were presented by GraphPad Prism 8.0 (GraphPad Software, San Diego, CA).

3. Results

3.1. Human Infantile Hemangioma Endothelial Cells (HEMECs) from Proliferating Tumor Transcriptome Analysis. Based on the GEO database, the GSE98795 dataset was selected for differential expression analysis of circRNAs in this study. A total of 234 circRNAs were upregulated, and 374 circRNAs were downregulated (Supplementary Table 1, FC (abs) cut-off value 1.0). The GSE100682 dataset was selected for differential expression analysis of microRNAs. The results showed that 329 microRNAs were upregulated and 337 microRNAs were downregulated (Supplementary Table 2, logFC cut-off value 1.0). The GSE43742 dataset was selected for differential expression analysis of mRNAs. The results showed that 23 mRNAs were upregulated and 25 mRNAs were downregulated (Supplementary Table 3, logFC cut-off value 2.0).

In this study, we chose hsa_circ_0003570, hsa-miR-138-5p, and RGS5 for research, because according to the Encyclopedia of RNA Interactomes (ENCORI) [24], analysis results showed that both hsa_circ_0003570 and RGS5 had binding sites to hsa-miR-138-5p (Figure 2(a)). We detected the expression levels of hsa_circ_0003570, hsa-miR-138-5p, and *RGS5* mRNA in human dermal microvascular endothelial cells (HDMVECs) and HEMECs, respectively. The results showed that hsa_circ_0003570 and *RGS5* mRNA were upregulated in HEMECs, and hsa-miR-138-5p was downregulated, the differences were significant ($p < 0.05$, Figure 2(b)).

3.2. Silencing of hsa_circ_0003570 Inhibited the Proliferation and Promoted Apoptosis of HEMECs. We found that hsa_circ_0003570 was highly expressed in HEMECs according to the GSE98795 dataset, indicating that hsa_circ_0003570 might have carcinogenic effects. In order to analyze the role of hsa_circ_0003570 in the biological behavior of HEMECs, we constructed three groups of hsa_circ_0003570 small interfering RNAs (siRNAs) to silence hsa_circ_0003570, respectively, named si-hsa_circ_0003570-1, si-hsa_circ_0003570-2, and si-hsa_circ_0003570-3, and the no template control (si-NC) and the nontransfection group (control) were used as controls.

We chose si-hsa_circ_0003570-1 (named si-hsa_circ_0003570) with the highest silencing efficiency for subsequent research (Figure 3(a)). Compared with the control, the cell proliferation ability of si-hsa_circ_0003570 transfected with

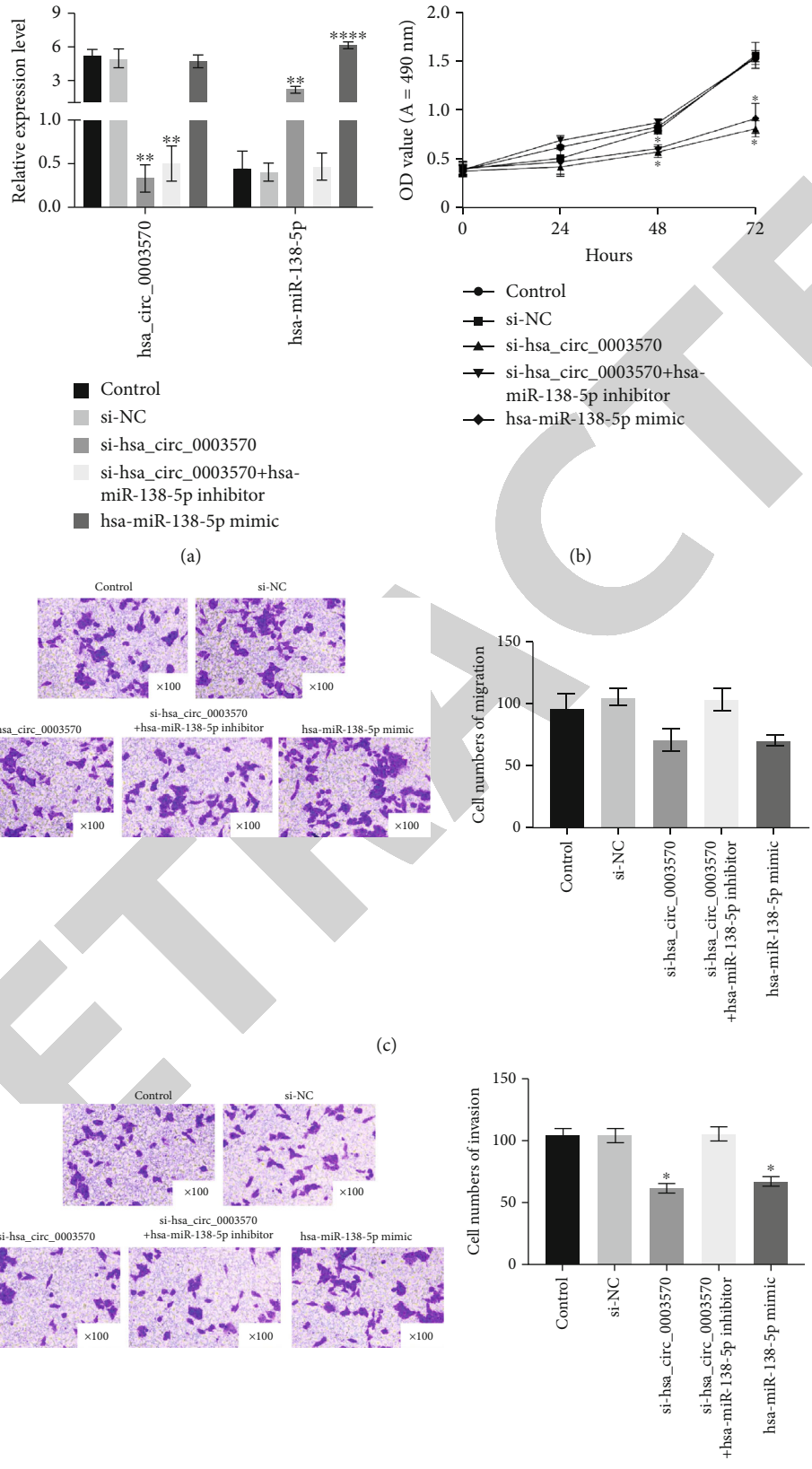

Figure 4: Continued.

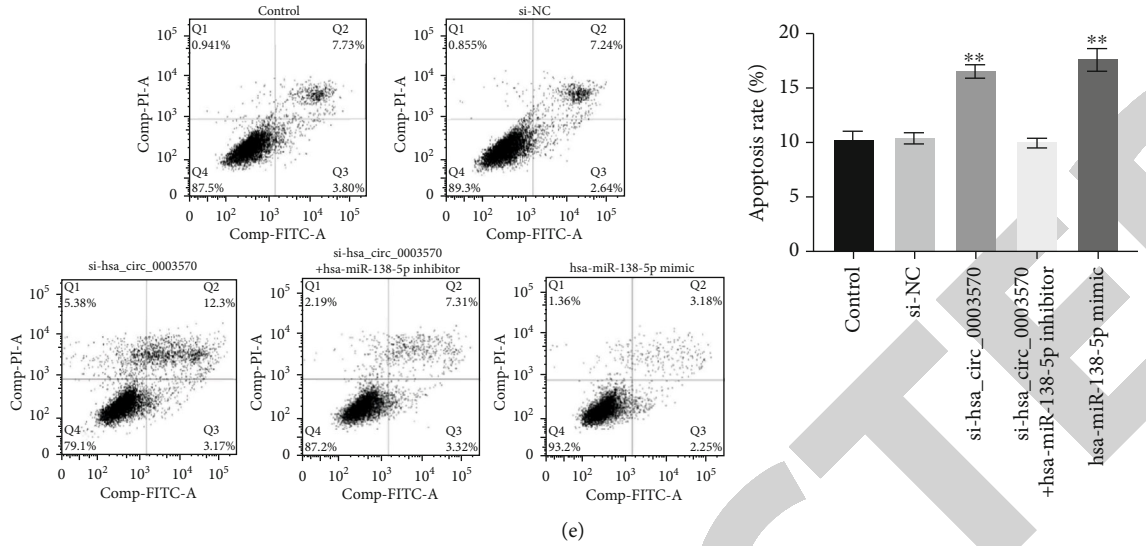

Figure 4: The effect of hsa_circ_0003570 on the malignant biological behavior of HEMEC cells could be reversed by hsa-miR-138-5p. (a) The expression levels of hsa_circ_0003570 and hsa-miR-138-5p in HEMEC transfected with no transfection group (control), no temple control (si-NC), si-hsa_circ_0003570, si-hsa_circ_0003570+hsa-miR-138-5p inhibitor, and hsa-miR-138-5p mimic were detected by quantitative real-time polymerase chain reaction (qRT-PCR). (b) The cell proliferation ability of HEMEC transfected with control, si-NC, si-hsa_circ_0003570, si-hsa_circ_0003570+hsa-miR-138-5p inhibitor, and hsa-miR-138-5p mimic was detected by MTT. (c) and (d) Cell migration and invasion ability of HEMEC transfected with control, si-NC, si-hsa_circ_0003570, si-hsa_circ_0003570+hsa-miR-138-5p inhibitor, and hsa-miR-138-5p mimic was detected by Transwell assay. (e) The apoptosis rate of HEMEC transfected with control, si-NC, si-hsa_circ_0003570, si-hsa_circ_0003570+hsa-miR-138-5p inhibitor, and hsa-miR-138-5p mimic was detected by flow cytometry. $^{*}p < 0.05$, $^{**}p < 0.01$, compared with Control.

HEMECs decreased significantly ($p < 0.05$, Figure 3(b)). The migration and invasion capabilities of HEMECs were significantly reduced after transfection with si-hsa_circ_0003570 ($p < 0.01$, Figures 3(c) and 3(d)). The apoptosis rate of HEMECs after transfection with si-hsa_circ_0003570 was significantly higher than that of the control ($p < 0.001$, Figure 3(e)). The results indicated that silencing of hsa_circ_0003570 inhibited the proliferation and promoted apoptosis of HEMECs.

3.3. The Effect of hsa_circ_0003570 on the Malignant Biological Behavior of HEMECs Could Be Reversed by hsa-miR-138-5p. To further analyze the role of hsa-miR-138-5p in hsa_circ_0003570-silenced HEMECs, the expression level of hsa_circ_0003570 and hsa-miR-138-5p in HEMECs transfected with control, si-NC, si-hsa_circ_0003570, si-hsa_circ_0003570+hsa-miR-138-5p inhibitor, and hsa-miR-138-5p mimic was shown in Figure 4(a). The results showed that compared with the control, the proliferation ability of HEMECs was significantly decreased after transfection with si-hsa_circ_0003570 and hsa-miR-138-5p mimic ($p > 0.05$), no significant change in the proliferation ability after si-hsa_circ_0003570+hsa-miR-138-5p inhibitor transfection significantly ($p > 0.05$, Figure 4(b)). After transfection with si-hsa_circ_0003570 and hsa-miR-138-5p mimic, the migration and invasion capabilities of HEMECs were significantly reduced ($p < 0.05$), but HEMECs transfected with si-hsa_circ_0003570+hsa-miR-138-5p inhibitor were not ($p > 0.05$, Figures 4(c) and 4(d)).

The apoptotic rate of HEMECs after transfection with si-hsa_circ_0003570 and hsa-miR-138-5p mimic was significantly higher than the control ($p < 0.05$), but there was no significant change in the apoptosis rate of HEMECs after cotransfection with si-hsa_circ_0003570+hsa-miR-138-5p inhibitor ($p > 0.05$, Figure 4(e)). The above results indicated that the effect of hsa_circ_0003570 on the malignant biological behavior of HEMECs could be reversed by hsa-miR-138-5p.

3.4. Hsa_circ_0003570 Upregulated the Expression of RGS5 through Sponging hsa-miR-138-5p. According to the prediction results of ENCORI, both hsa_circ_0003570 and *RGS5* had binding sites with hsa-miR-138. The wild-type luciferase vector (pGL3-hsa_circ_0003570 WT, pGL3-RGS5 WT) and mutant luciferase vector (pGL3-hsa_circ_0003570 MUT, pGL3-RGS5 MUT) were constructed, respectively (Figures 5(a) and 5(c)). Next, hsa-miR-138-5p mimic and pGL3-hsa_circ_0003570 WT, pGL3-hsa_circ_0003570 MUT, pGL3-RGS5 WT, and pGL3-RGS5 MUT were transfected into HEMECs, respectively. According to the results, the luciferase activity of hsa-miR-138-5p mimic and pGL3-hsa_circ_0003570 WT, hsa-miR-138-5p mimic, and pGL3-RGS5 WT was significantly reduced after transfection, while hsa-miR-138-5p mimic and pGL3-hsa_circ_0003570 MUT, hsa-miR-138-5p mimic, and pGL3-RGS5 MUT did not change significantly after transfection (Figures 5(b) and 5(d)). Then, the control, NC, si-hsa_circ_0003570, hsa-miR-138-5p mimic, si-hsa_circ_0003570+hsa-miR-138-5p inhibitor, and hsa-miR-138-5p inhibitor were transfected into HEMECs, respectively, and the expression levels of hsa_circ_0003570, hsa-miR-138-5p, and *RGS5* mRNA were detected by qRT-PCR. The results showed that compared

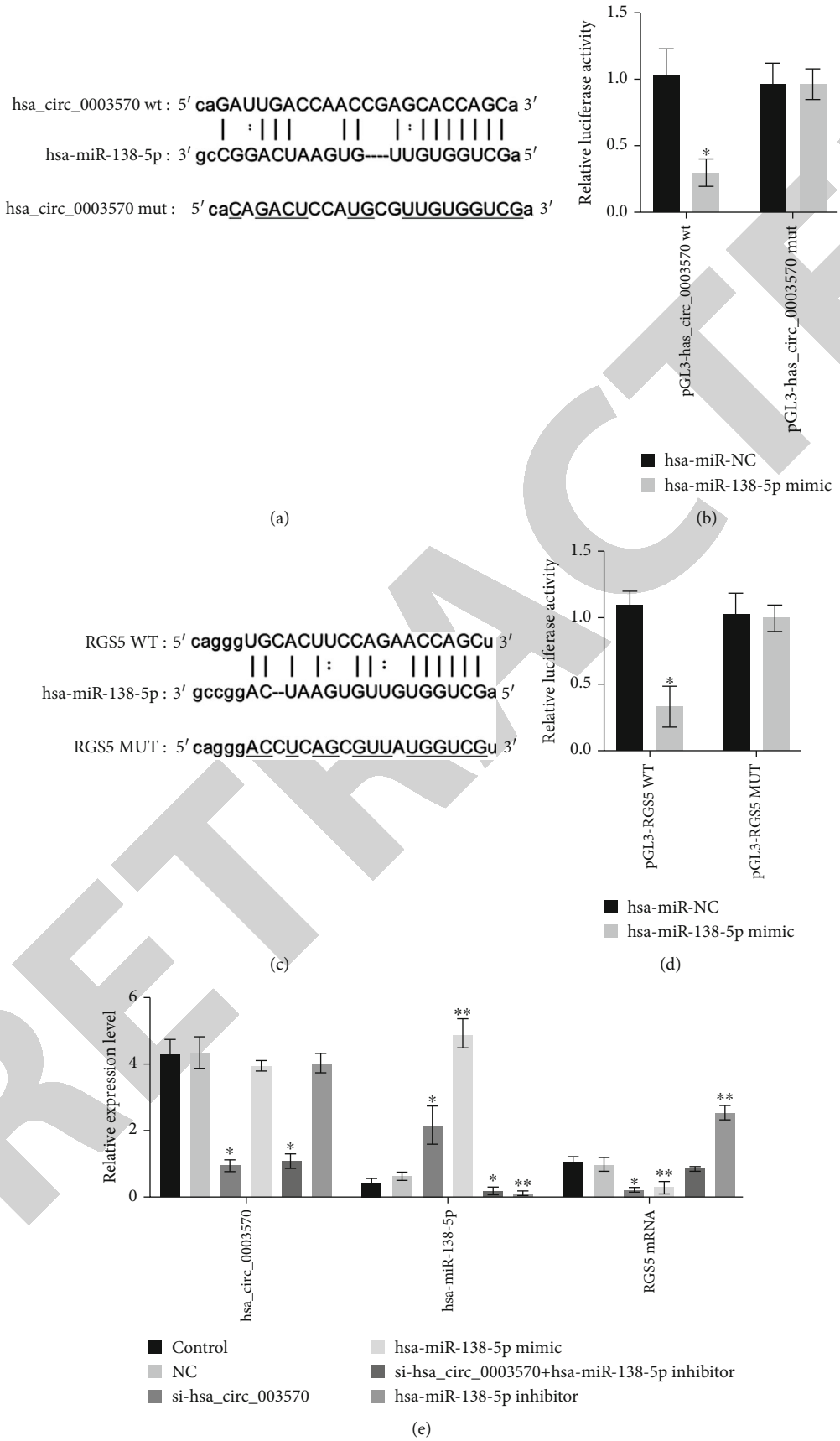

Figure 5: Continued.

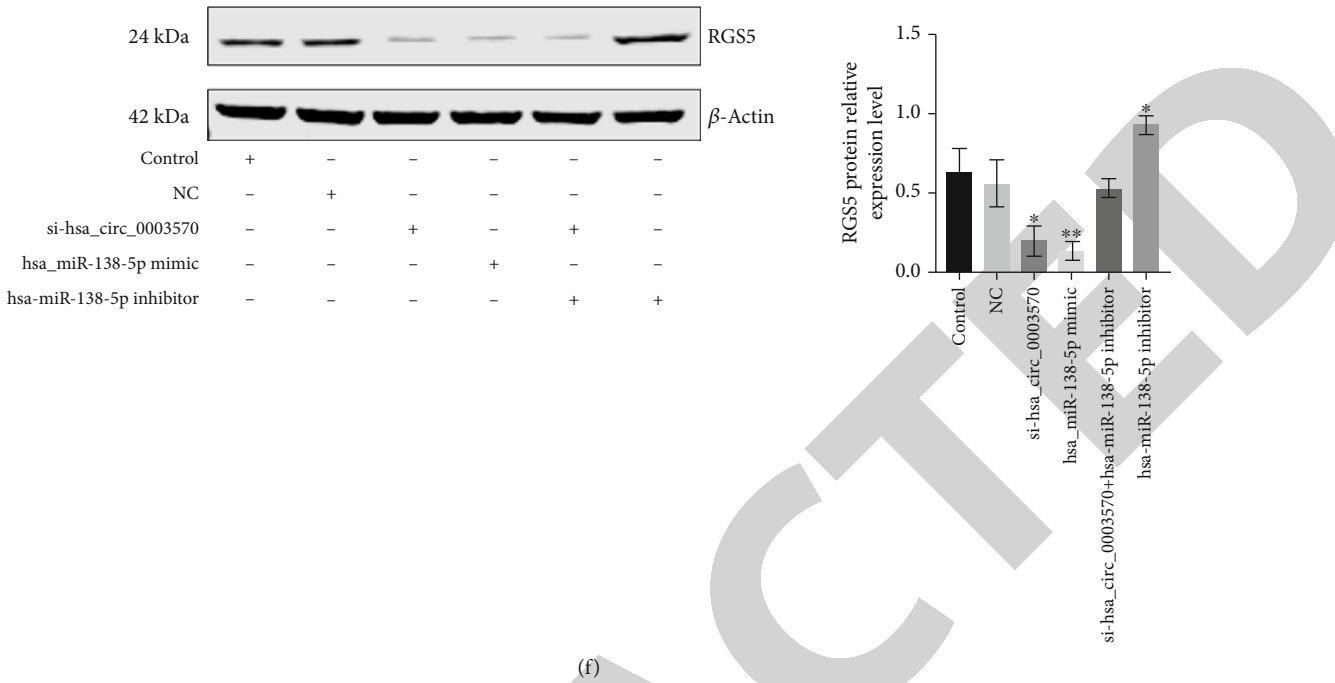

Figure 5: hsa_circ_0003570, as the ceRNA of hsa-miR-138-5p, upregulated the expression of RGS5. (a) Putative miRNA binding sites in hsa_circ_0003570 and RGS5. (b) Putative miRNA binding sites in RGS5. (c) Detection of luciferase activity after hsa-miR-138-5p mimic and pGL3-hsa_circ_0003570 WT or pGL3-hsa_circ_0003570 MUT. (d) Luciferase activity detection after transfection with hsa-miR-138-5p mimic and pGL3-RGS5 WT or pGL3-RGS5 MUT. (e) Relative expression level of hsa_circ_0003570, hsa-miR-138-5p, and *RGS5* mRNA in HEMEC transfected with control, NC, si-hsa_circ_0003570, hsa-miR-138-5p mimic, si-hsa_circ_0003570+hsa-miR-138-5p inhibitor, and hsa-miR-138-5p inhibitor detected by qRT-PCR. (f) The relative expression of RGS5 in HEMEC after transfection with control, NC, si-hsa_circ_0003570, hsa-miR-138-5p mimic, si-hsa_circ_0003570+hsa-miR-138-5p inhibitor, and hsa-miR-138-5p inhibitor. $^*p < 0.05$, compared with control.

with control, the expression level of hsa-miR-138-5p increased after transfection of si-hsa_circ_0003570 or hsa-miR-138-5p mimic, while the expression level of *RGS5* mRNA was inhibited.

After transfection with hsa-miR-138-5p inhibitor, the expression level of hsa-miR-138-5p was significantly reduced, and *RGS5* mRNA was increased. After transfection with si-hsa_circ_0003570+hsa-miR-138-5p inhibitor, the expression level of hsa-miR-138-5p decreased, but the expression level of *RGS5* mRNA did not change significantly (Figure 5(e)). Western blot results showed that compared with control, the expression of RGS5 protein was significantly reduced after transfection with si-hsa_circ_0003570 or hsa-miR-138-5p mimic. After transfection with hsa-miR-138-5p inhibitor, the expression level of RGS5 protein increased. And RGS5 expression level did not change significantly when transfected with si-hsa_circ_0003570+hsa-miR-138-5p inhibitor (Figure 5(f)). These results indicated that hsa_circ_0003570, as the ceRNA of hsa-miR-138-5p, upregulated the expression of RGS5.

3.5. RGS5 Knockdown Inhibited the Proliferation and Promoted Apoptosis of HEMECs. In order to further study the effect of RGS5 on the malignant biological behavior of HEMECs, we constructed a short hairpin RNA (shRNA) (sh-RGS5) targeting RGS5 to silence the expression of *RGS5* gene. The results of qRT-PCR and western blot showed that we successfully constructed RGS5-silenced HEMECs (Figures 6(a) and 6(b)). The results of the MTT assay showed that compared with the control, the cell proliferation ability of HEMECs transfected with sh-RGS5 was significantly reduced ($p < 0.05$, Figure 6(c)). Results showed that the migration and invasion capabilities of HEMECs were significantly reduced after sh-RGS5 transfection ($p < 0.01$, Figures 6(d) and 6(e)). The apoptosis rate of HEMECs after sh-RGS5 transfection was significantly higher than the control ($p < 0.001$, Figure 6(f)). These results indicated that RGS5 knockdown inhibited the proliferation and promoted apoptosis of HEMEC.

4. Discussion

Circular RNA is a kind of ncRNA molecule with a special closed circular structure. It has the characteristics of high stability, conservation, and tissue specificity. In recent years, it has become a hot spot in the field of ncRNA research [15, 25–27]. Studies have found that circRNAs are differentially expressed in tumors [28, 29], cardiovascular diseases [30–32], nervous system, and other diseases [33, 34] and affect the occurrence and development of diseases through various mechanisms.

There are many differentially expressed circRNAs in hemangioma. For example, Yuan et al. [35] found that circAP2A2 can promote the proliferation and invasion of IH

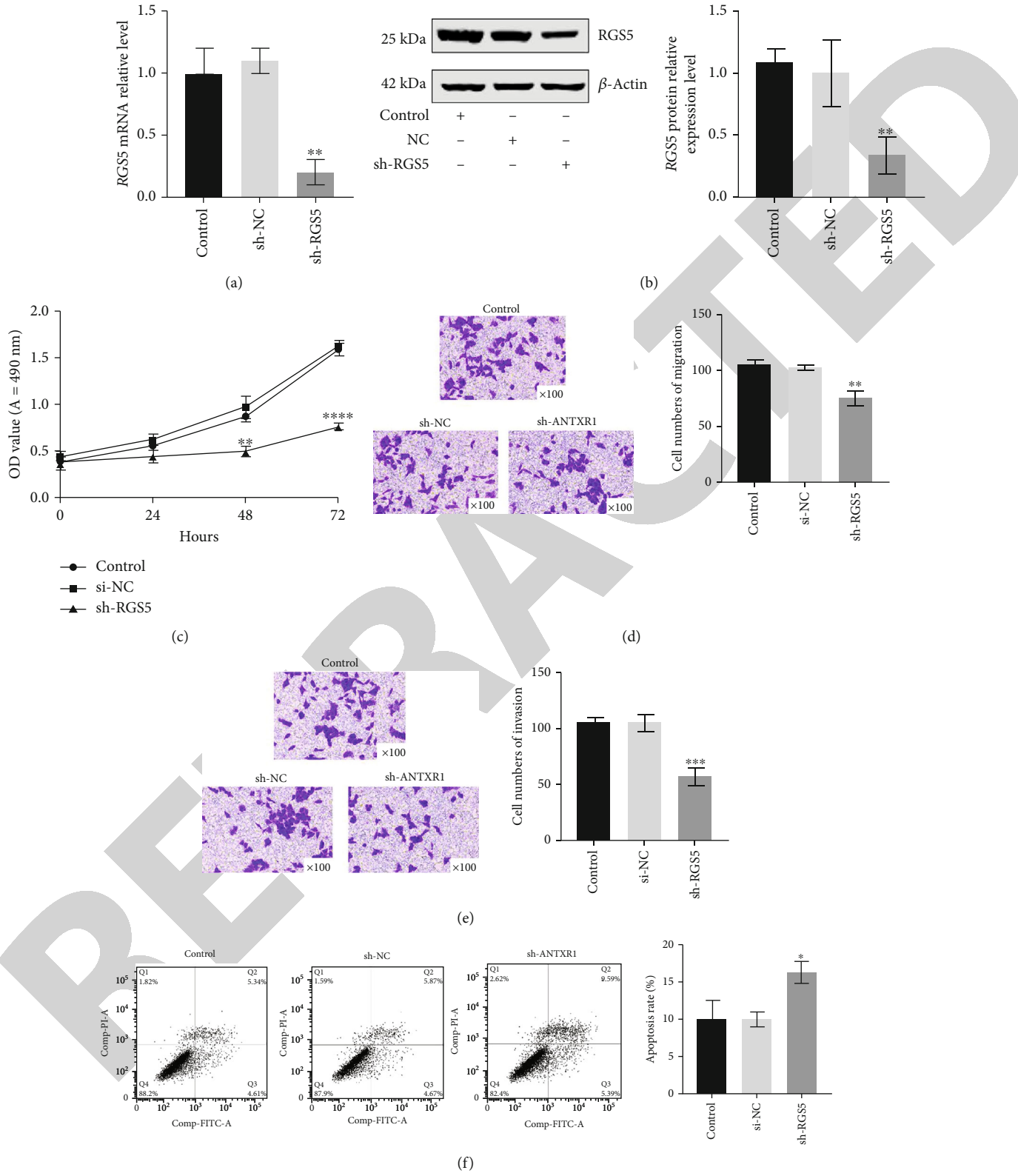

Figure 6: RGS5 knockdown inhibited the proliferation, migration, and invasion of HEMEC cells and promoted apoptosis. (a) *RGS5* mRNA expression level of HEMEC transfected with after control, sh-NC, and sh-RGS5 was detected by qRT-PCR. (b) RGS5 protein expression level in HEMEC transfected with after control, sh-NC, and sh-RGS5 was detected by western blot. (c) The cell proliferation ability of HEMEC transfected with after control, sh-NC, and sh-RGS5 was detected by MTT assay. (d) and (e) The cell migration ability and invasion ability of HEMEC transfected with after control, sh-NC, and sh-RGS5 was detected by Transwell assay. (f) The apoptosis rate of HEMEC transfected with after control, sh-NC, and sh-RGS5 was detected by flow cytometry. $^{*}p < 0.05$, $^{**}p < 0.01$, $^{***}p < 0.001$, $^{****}p < 0.0001$, compare with control.

by regulating the miR-382-5p/VEGFA axis. Through RNA-Seq research, Li et al. [36] found that among 9811 identified circRNAs, 249 candidate genes were differentially expressed, including 124 upregulated and 125 downregulated circRNAs. The study of these circRNAs is of great value for the prevention and treatment of IH and explaining the mechanism of IH occurrence and development.

In this study, we combined with the results of the GSE98795 dataset [22] and found that hsa_circ_0003570 in HEMECs was upregulated. In order to further verify the possible mechanism of hsa_circ_0003570 in the occurrence and development of IH, small interfering RNA were used to knock down the expression level of hsa_circ_0003570 in HEMECs. The results showed that silencing of hsa_circ_0003570 inhibited the proliferation and promoted apoptosis of HEMECs. This result indicated that hsa_circ_0003570 might be the oncogene of IH.

A lot of research evidence showed that circRNAs could be used as ceRNA to regulate gene expression and participated in the occurrence of diseases [16, 37, 38]. Therefore, we analyzed the data in the GSE100682 dataset, combined with target prediction information, and selected hsa-miR-138-5p for research. Studies had shown that hsa-miR-138-5p could promote the angiogenesis of HUVECs infected by human cytomegalovirus (HCMV) through activating SIRT1-p-STAT3 approach [39]. This showed that hsa-miR-138-5p played an important role in angiogenesis. In this study, we found that the expression level of hsa-miR-138-5p in HEMECs was significantly downregulated, and hsa-miR-138-5p could reverse the effect of hsa_circ_0003570 on the proliferation, migration, invasion, and apoptosis of HEMECs. Therefore, we speculated that hsa-miR-138-5p might mediate the regulation of hsa_circ_0003570 on the expression of key downstream genes.

We further studied in the GSE43742 dataset and found that the expression of 23 mRNAs was upregulated and 25 mRNAs downregulated. Combined with the results of target prediction, we found that the *RGS5* gene was upregulated HEMECs, which was consistent with the study by Stiles et al. [40]. In addition, the *RGS5* gene also has a binding site for hsa-miR-138-5p. Further studies had shown that silencing *RGS5* inhibited the proliferation and promoted apoptosis of HEMECs. This showed that RGS5 may be the oncogene of IH. The luciferase assay experiment confirmed that hsa_circ_0003570, as the ceRNA of hsa-miR-138-5p, upregulated the expression of RGS5. Therefore, we speculate that hsa_circ_0003570 participates in the regulation of the malignant biological behavior of IH through hsa-miR-138-5p/RGS5 axis and is expected to become a potential target for IH therapy.

Our research has some shortcomings that need to be improved. First of all, there is a lack of research evidence support for tissue samples, our findings have only been validated in HEMEC cell line, and further study in tissue samples and other cell lines are needed to solve these problems. In fact, the results of in vitro need to be confirmed in in vivo. In addition, the mechanism of IH is relatively complicated, and there may be a large number of other pathways involved to study.

5. Conclusion

In conclusion, our research confirmed that hsa_circ_0003570 regulated the proliferation, migration, and invasion of IH through hsa-miR-138-5p/RGS5 axis and inhibited apoptosis, which could be a potential target for IH therapy.

Data Availability

The data used to support the findings of this study are available from the corresponding author upon request.

Conflicts of Interest

The authors declare that there are no conflicts of interest.

Authors' Contributions

YT, WWF, and HB conceived and designed the experiments; TY, ZSH, ZJT, and YTH performed the experiments; XZH and YWL analyzed the data; and YT and TY wrote the manuscript. All authors read and approved the final manuscript. Yu Tian, Shihao Zhuang, and Jiantao Zhang contributed equally to this work.

Acknowledgments

This work was supported by the National Natural Science Foundation of China (81760900) and Shanxi Health Committee Project (201201043).

Supplementary Materials

The following analysis results were based on the data from the GSE98795 dataset. Infantile hemangioma tumor tissue was obtained from 3 female patients 4-7 months old and 1 male patient 4 months old. The adjacent normal skin tissue was also obtained from 3 female patients 4-7 months old and 1 male patient 4 months old. The results of GEO2R analysis showed that a total of 234 circRNAs were upregulated and 374 circRNAs were downregulated (FC (abs) cut-off value 1.0) in the infantile hemangioma tumor tissue. *(Supplementary Materials)*

References

[1] D. H. Darrow, A. K. Greene, A. J. Mancini, and A. J. Nopper, "Diagnosis and management of infantile hemangioma," *Pediatrics*, vol. 136, no. 4, pp. e1060–e1104, 2015.

[2] A. Munden, R. Butschek, W. L. Tom et al., "Prospective study of infantile haemangiomas: incidence, clinical characteristics and association with placental anomalies," *The British Journal of Dermatology*, vol. 170, no. 4, pp. 907–913, 2014.

[3] K. R. Anderson, J. J. Schoch, C. M. Lohse, J. L. Hand, D. M. Davis, and M. M. Tollefson, "Increasing incidence of infantile hemangiomas (IH) over the past 35 years: correlation with decreasing gestational age at birth and birth weight," *Journal of the American Academy of Dermatology*, vol. 74, no. 1, pp. 120–126, 2016.

[4] C. Leaute-Labreze, J. I. Harper, and P. H. Hoeger, "Infantile haemangioma," *Lancet*, vol. 390, no. 10089, pp. 85–94, 2017.

[5] C. J. F. Smith, S. F. Friedlander, M. Guma, A. Kavanaugh, and C. D. Chambers, "Infantile hemangiomas: an updated review on risk factors, pathogenesis, and treatment," *Birth defects research*, vol. 109, no. 11, pp. 809–815, 2017.

[6] Y. S. Soliman and A. Khachemoune, "Infantile hemangiomas: our current understanding and treatment options," *Dermatology Online Journal*, vol. 24, no. 9, 2018.

[7] E. Castrén, P. Salminen, M. Vikkula, A. Pitkäranta, and T. Klockars, "Inheritance patterns of infantile hemangioma," *Pediatrics*, vol. 138, no. 5, p. 5, 2016.

[8] J. W. Byun, H. Y. An, S. D. Yeom, S. J. Lee, and H. Y. Chung, "NDRG1 and FOXO1 regulate endothelial cell proliferation in infantile haemangioma," *Experimental Dermatology*, vol. 27, no. 6, pp. 690–693, 2018.

[9] S. R. Janmohamed, T. Brinkhuizen, J. C. den Hollander et al., "Support for the hypoxia theory in the pathogenesis of infantile haemangioma," *Clinical and Experimental Dermatology*, vol. 40, no. 4, pp. 431–437, 2015.

[10] M. R. Ritter, R. A. Butschek, M. Friedlander, and S. F. Friedlander, "Pathogenesis of infantile haemangioma: new molecular and cellular insights," *Expert Reviews in Molecular Medicine*, vol. 9, no. 32, pp. 1–19, 2007.

[11] M. JS Mattick IV, "Non-coding RNA," *Human molecular genetics*, vol. 15, supplement 1, pp. R17–R29, 2006.

[12] H. Coker, G. Wei, and N. Brockdorff, "m6A modification of non-coding RNA and the control of mammalian gene expression," *Biochimica et Biophysica Acta (BBA)-Gene Regulatory Mechanisms*, vol. 1862, no. 3, pp. 310–318, 2019.

[13] K. Y. Hsiao, H. S. Sun, and S. J. Tsai, "Circular RNA – new member of noncoding RNA with novel functions," *Experimental Biology and Medicine (Maywood, N.J.)*, vol. 242, no. 11, pp. 1136–1141, 2017.

[14] J. Sun, B. Li, C. Shu, Q. Ma, and J. Wang, "Functions and clinical significance of circular RNAs in glioma," *Molecular Cancer*, vol. 19, no. 1, p. 34, 2020.

[15] L. S. Kristensen, M. S. Andersen, L. V. W. Stagsted, K. K. Ebbesen, T. B. Hansen, and J. Kjems, "The biogenesis, biology and characterization of circular RNAs," *Nature Reviews. Genetics*, vol. 20, no. 11, pp. 675–691, 2019.

[16] X. Gu, M. Li, Y. Jin, D. Liu, and F. Wei, "Identification and integrated analysis of differentially expressed lncRNAs and circRNAs reveal the potential ceRNA networks during PDLSC osteogenic differentiation," *BMC Genetics*, vol. 18, no. 1, p. 100, 2017.

[17] X. Li, L. Yang, and L. L. Chen, "The biogenesis, functions, and challenges of circular RNAs," *Molecular Cell*, vol. 71, no. 3, pp. 428–442, 2018.

[18] X. Huang, M. He, S. Huang et al., "Circular RNA circERBB2 promotes gallbladder cancer progression by regulating PA2G4-dependent rDNA transcription," *Molecular Cancer*, vol. 18, no. 1, p. 166, 2019.

[19] J. Luo, H. Liu, S. Luan, and Z. Li, "Guidance of circular RNAs to proteins' behavior as binding partners," *Cellular and Molecular Life Sciences*, vol. 76, no. 21, pp. 4233–4243, 2019.

[20] Y. Yang, X. Fan, M. Mao et al., "Extensive translation of circular RNAs driven by _N_ ^{6}-methyladenosine," *Cell Research*, vol. 27, no. 5, pp. 626–641, 2017.

[21] Y. Fu, Z. G. Yang, and L. Y. Zhao, "Angiogenesis characteristics of infantile hemangioma and feasibility observation of transplantation model of human hemangioma on mice," *European Review for Medical and Pharmacological Sciences*, vol. 21, no. 6, pp. 1276–1280, 2017.

[22] C. Fu, R. Lv, G. Xu et al., "Circular RNA profile of infantile hemangioma by microarray analysis," *PLoS One*, vol. 12, no. 11, article e0187581, 2017.

[23] L. Zhou, X. Jia, and X. Yang, "LncRNA-TUG1 promotes the progression of infantile hemangioma by regulating miR-137/IGFBP5 axis," *Human Genomics*, vol. 15, no. 1, p. 50, 2021.

[24] J. H. Li, S. Liu, H. Zhou, L. H. Qu, and J. H. Yang, "starBase v2.0: decoding miRNA-ceRNA, miRNA-ncRNA and protein-RNA interaction networks from large-scale CLIP-Seq data," *Nucleic Acids Research*, vol. 42, no. D1, pp. D92–D97, 2014.

[25] L. Szabo and J. Salzman, "Detecting circular RNAs: bioinformatic and experimental challenges," *Nature Reviews. Genetics*, vol. 17, no. 11, pp. 679–692, 2016.

[26] X. Chen, T. Yang, W. Wang et al., "Circular RNAs in immune responses and immune diseases," *Theranostics*, vol. 9, no. 2, pp. 588–607, 2019.

[27] Z. Zhang, T. Yang, and J. Xiao, "Circular RNAs: promising biomarkers for human diseases," *eBioMedicine*, vol. 34, pp. 267–274, 2018.

[28] J. He, Q. Xie, H. Xu, J. Li, and Y. Li, "Circular RNAs and cancer," *Cancer Letters*, vol. 396, pp. 138–144, 2017.

[29] L. Xia, M. Song, M. Sun, F. Wang, and C. Yang, "Circular RNAs as biomarkers for cancer," *Advances in Experimental Medicine and Biology*, vol. 1087, pp. 171–187, 2018.

[30] Y. Devaux, E. E. Creemers, R. A. Boon et al., "Circular RNAs in heart failure," *European Journal of Heart Failure*, vol. 19, no. 6, pp. 701–709, 2017.

[31] M. Carrara, P. Fuschi, C. Ivan, and F. Martelli, "Circular RNAs: methodological challenges and perspectives in cardiovascular diseases," *Journal of Cellular and Molecular Medicine*, vol. 22, no. 11, pp. 5176–5187, 2018.

[32] Q. Zhou, Z. Zhang, Y. Bei, G. Li, and T. Wang, "Circular RNAs as novel biomarkers for cardiovascular diseases," *Advances in Experimental Medicine and Biology*, vol. 1087, pp. 159–170, 2018.

[33] L. Xie, M. Mao, K. Xiong, and B. Jiang, "Circular RNAs: a novel player in development and disease of the central nervous system," *Frontiers in Cellular Neuroscience*, vol. 11, p. 354, 2017.

[34] R. Akhter, "Circular RNA and Alzheimer's disease," *Advances in Experimental Medicine and Biology*, vol. 1087, pp. 239–243, 2018.

[35] X. Yuan, Y. Xu, Z. Wei, and Q. Ding, "CircAP2A2 acts as a ceRNA to participate in infantile hemangiomas progression by sponging miR-382-5p via regulating the expression of VEGFA," *Journal of Clinical Laboratory Analysis*, vol. 34, no. 7, article e23258, 2020.

[36] J. Li, Q. Li, L. Chen, Y. Gao, and J. Li, "Expression profile of circular RNAs in infantile hemangioma detected by RNA-Seq," *Medicine (Baltimore)*, vol. 97, no. 21, article e10882, 2018.

[37] M. Huang, Z. Zhong, M. Lv, J. Shu, Q. Tian, and J. Chen, "Comprehensive analysis of differentially expressed profiles of lncRNAs and circRNAs with associated co-expression and ceRNA networks in bladder carcinoma," *Oncotarget*, vol. 7, no. 30, pp. 47186–47200, 2016.

[38] J. Zhu, X. Zhang, W. Gao, H. Hu, X. Wang, and D. Hao, "lncRNA/circRNA-miRNA-mRNA ceRNA network in lumbar intervertebral disc degeneration," *Molecular Medicine Reports*, vol. 20, no. 4, pp. 3160–3174, 2019.

Hindawi
Computational and Mathematical Methods in Medicine
Volume 2023, Article ID 9765359, 1 page
https://doi.org/10.1155/2023/9765359

Retraction

Retracted: miR-141-3p Regulates EZH2 to Attenuate Porphyromonas gingivalis Lipopolysaccharide-Caused Inflammation and Inhibition of Osteogenic Differentiation in Human Periodontal Ligament Stem Cells

Computational and Mathematical Methods in Medicine

Received 27 June 2023; Accepted 27 June 2023; Published 28 June 2023

This article has been retracted by Hindawi following an investigation undertaken by the publisher [1]. This investigation has uncovered evidence of one or more of the following indicators of systematic manipulation of the publication process:

(1) Discrepancies in scope

(2) Discrepancies in the description of the research reported

(3) Discrepancies between the availability of data and the research described

(4) Inappropriate citations

(5) Incoherent, meaningless and/or irrelevant content included in the article

(6) Peer-review manipulation

The presence of these indicators undermines our confidence in the integrity of the article's content and we cannot, therefore, vouch for its reliability. Please note that this notice is intended solely to alert readers that the content of this article is unreliable. We have not investigated whether authors were aware of or involved in the systematic manipulation of the publication process.

Wiley and Hindawi regrets that the usual quality checks did not identify these issues before publication and have since put additional measures in place to safeguard research integrity.

We wish to credit our own Research Integrity and Research Publishing teams and anonymous and named external researchers and research integrity experts for contributing to this investigation.

The corresponding author, as the representative of all authors, has been given the opportunity to register their agreement or disagreement to this retraction. We have kept a record of any response received.

References

[1] Z. Zhu and J. Xiong, "miR-141-3p Regulates EZH2 to Attenuate Porphyromonas gingivalis Lipopolysaccharide-Caused Inflammation and Inhibition of Osteogenic Differentiation in Human Periodontal Ligament Stem Cells," *Computational and Mathematical Methods in Medicine*, vol. 2022, Article ID 4634925, 11 pages, 2022.

Hindawi
Computational and Mathematical Methods in Medicine
Volume 2022, Article ID 4634925, 11 pages
https://doi.org/10.1155/2022/4634925

Research Article

miR-141-3p Regulates EZH2 to Attenuate Porphyromonas gingivalis Lipopolysaccharide-Caused Inflammation and Inhibition of Osteogenic Differentiation in Human Periodontal Ligament Stem Cells

Zhu Zhu and Jie Xiong

Dongfeng Stomatological Hospital, Hubei University of Medicine, Shiyan, Hubei 442000, China

Correspondence should be addressed to Jie Xiong; jiexiong1005@163.com

Received 17 January 2022; Revised 24 March 2022; Accepted 31 March 2022; Published 25 April 2022

Academic Editor: Shakeel Ahmad

Objective. miR-141-3p has been demonstrated to be both anti-inflammatory and osteoprotective. This study is aimed at investigating the effect of miR-141-3p on osteogenic differentiation of human periodontal ligament stem cells (hPDLSCs) stimulated by Porphyromonas gingivalis lipopolysaccharide (PgLPS) and its mechanism. *Methods*. PgLPS was used to induce an inflammatory environment, and overexpression of miR-141-3p was done to assess its effect on hPDLSCs in an inflammatory environment. The level of miR-141-3p and EZH2 in hPDLSCs from each treatment group was detected via qRT-PCR, and the inflammatory factors IL-6 and IL-8 in the supernatant of each group were detected by ELISA. ALP staining and alizarin red staining were used to assess the effect of miR-141-3p on the osteogenic differentiation ability of hPDLSCs, and also, western blot was used to detect expression of osteogenic differentiation-related proteins. Further, dual-luciferase reporter assay examined whether miR-141-3p targeted EZH2. *Results*. PgLPS led to a significant decrease of miR-141-3p in hPDLSCs. Overexpression of miR-141-3p could enhance ALP activity and alizarin red staining intensity and increase Runx2, OPN and OCN protein expression levels in PgLPS-treated hPDLSCs. Additionally, miR-141-3p could reduce IL-6 and IL-8. miR-141-3p could target and negatively regulate EZH2, and overexpression of EZH2 reversed the promoting effect of miR-141-3p on osteogenic differentiation. *Conclusion*. miR-141-3p can attenuate PgLPS-induced inhibition of osteogenic differentiation and inflammation in hPDLSCs by negatively regulating EZH2.

1. Introduction

Periodontitis is a chronic inflammatory disease caused by subgingival plaque accumulation and specific periodontal pathogens, which can progressively destroy the connective tissue around the teeth and cause stomatitis [1, 2]. If the initial inflammatory response is not adequately resolved, periodontitis will cause destruction of alveolar bone, periodontal ligaments, and cementum, ultimately leading to tooth loss [3, 4]. According to epidemiological surveys, periodontitis is currently one of the six most common diseases in the world, affecting about 734 million people with an overall prevalence of 11.2%, and the global prevalence of periodontal diseases has been growing rapidly in the past two decades [5, 6].

Periodontal ligament stem cells (PDLSCs) are a class of heterogeneous pluripotent stem cells with physiological self-replication capacity and multilineage differentiation potential [7]. PDLSCs can potentially differentiate into multiple cell types, especially osteoblasts or cementoblasts. Studies have shown that PDLSC can be applied to periodontal regeneration in dogs, rats, and sheep [7]. Sano et al. found that cocultured PDLSCs with umbilical vein endothelial cells revealed that cocultured spheroids enhanced periodontal tissue regeneration [8]. Some experimental evidence has also confirmed that

osteogenic differentiation of PDLSCs can improve periodontal tissue regeneration, providing important application value for bone tissue maintenance, bone regeneration, and periodontal tissue repair in dental clinical practice [9–11].

MicroRNAs (miRNAs), a class of conserved endogenous noncoding small RNAs of about 21–25 nt in length, are found in eukaryotes and can regulate gene expression by posttranscriptional control [12]. miRNAs are involved in regulating various physiological and pathological processes such as cell proliferation, differentiation, apoptosis, inflammation, tumorigenesis, and tumor progression [13]. According to researches, a variety of miRNAs are involved in regulating the homeostasis and pathological processes of periodontal tissue and play a coordinating role in periodontal tissue inflammation and bone remodeling through different pathways [14, 15].

miR-141-3p was demonstrated to lower expression in the gingiva of periodontitis patients [16]. However, its expression, function, and molecular regulatory mechanism during osteogenic differentiation of hPDLSCs are unknown. Therefore, in this study, the regulatory function of miR-141-3p on osteogenic differentiation of hPDLSCs in an inflammatory environment was explored with PgLPS-induced hPDLSCs as a model of periodontitis. Our study provides an important theoretical basis for explaining the osteogenic differentiation of hPDLSCs under inflammatory conditions and how to promote oral tissue regeneration. Also, our results contribute to the development of new ideas and treatments of using hPDLSCs for tissue regeneration.

2. Methods

2.1. Cell Culture. hPDLSCs were obtained from the American Type Culture Collection (ATCC) and cultured in α-MEM medium (Gibco, USA) containing 10% fetal bovine serum (FBS; Gibco, USA) at 37°C in a 5% CO_2 incubator. The cell culture medium was changed every 3 days.

2.2. Cell Transfection. miR-141-3p mimic and its negative control (100 nM), miR-141-3p inhibitor and its negative control (100 nM), and pcDNA3.2-EZH2 and no-load pcDNA3.2 (2 μg) were purchased from GenePharma (Shanghai, China). Cells with 70%-80% confluence in 6-well plates were transfected according to the instructions of Lipofectamine 2000 reagent (Invitrogen, Carlsbad, CA, USA). Cells were divided into 6 groups, and PgLPS treatment was carried out 24 h after transfection [1]: control group: no PgLPS, no transfection [2]; PgLPS group: 1 μg/ml PgLPS, no transfection [3]; PgLPS+NC mimic group: 1 μg/ml PgLPS, cells transfected with negative mimics [4]; PgLPS+miR-141-3p mimic group: 1 μg/ml PgLPS, cells transfected with miR-141-3p mimics [5]; PgLPS+miR-141-3p+pcNC group: 1 μg/ml PgLPS, cells transfected with miR-141-3p mimics and negative pcDNA3.2 [6]; and PgLPS +miR-141-3p+EZH2 group: 1 μg/ml PgLPS, cells transfected with miR-141-3p mimics and pcDNA3.2-EZH2.

2.3. ELISA. Cell culture supernatants were collected from each group, and cell debris removed by centrifugation. The levels of IL-6 and IL-8 in the supernatant were measured with ELISA kits (Multisciences Biotech), and all operations were performed in strict accordance with the instructions.

Table 1: Primer sequences.

Primer		Sequence (5′-3′)
miR-141-3p	Forward	CTTCCAGTACAGTGTTGG
	Reverse	GAACATGTCTGCGTATCTC
U6	Forward	UUCUCCGAACGUGUCACGUTT
	Reverse	UGACACGUUCGGAGAATT
EZH2	Forward	GACCTCTGTCTTACTTGTGGAGC
	Reverse	CGTCAGATGGTGCCAGCAATAG
GAPDH	Forward	GGAGCGAGATCCCTCCAAAAT
	Reverse	GGCTGTTGTCATACTTCTCATGG

2.4. qRT-PCR. Cells and tissue samples were collected, and total RNA was extracted by using TRIzol (Invitrogen, Carlsbad, CA, USA). Reverse transcription was performed by using a reverse transcription kit (TaKaRa, Tokyo, Japan), and all operations were performed according to the instruction. The expression of target genes was detected with LightCycler 480 qRT-PCR (Roche, Indianapolis, IN, USA), and reaction conditions were performed according to the instructions of the qRT-PCR kit (SYBR Green Mix, Roche Diagnostics, Indianapolis, IN). Thermal cycling parameters were as follows: 95°C for 10s, 45 cycles of 95°C for 5 s, 60°C for 10s, 72°C for 10 s, and 72°C for 5 min. Three replicates per reaction were set up for qRT-PCR. GAPDH was used for internal reference. Data analysis was performed by the $2^{-\Delta\Delta Ct}$ method, where $\Delta\Delta$Ct = treatment group (Ct target gene − Ct internal reference) − control group (Ct target gene − Ct internal reference). The sequences of the amplimers for each gene and the internal reference are listed in Table 1.

2.5. Osteogenic Induction. Third-passage hPDLSCs were evenly seeded in 24-well culture plates, and when confluence reached 60%-70%, the cell culture medium was replaced with osteogenic induction solution to induce cell differentiation into osteoblasts. The solution was changed every 2-3 two days; the induction was carried out for 1, 3, 7, 14, and 24 days, respectively. Alkaline phosphatase staining (on day 7 of induction) and alizarin red staining (on day 21 of induction) were then completed. The formulation of osteogenic induction solution was as follows: adding vitamin C (100 μM), P-sodium glycerophosphate (10 mM), and dexamethasone (10 nM) into α-MEM complete medium containing 10% FBS.

2.6. Alkaline Phosphatase (ALP) Staining and Activity Detection. First, PBS was used to rinse hPDLSCs on day 7 of osteogenic differentiation and then aspirated. Then, fixing solution was added and incubated with the cells for 30 min. Next, ALP staining solution was added to the plates for incubation at room temperature for 12 min, and the incubation was protected from light. On completion of incubation, the cells were rinsed with ddH_2O, and counterstaining was performed if necessary. After successful staining, the cells were dried to observe the staining of cells. The activity of ALP

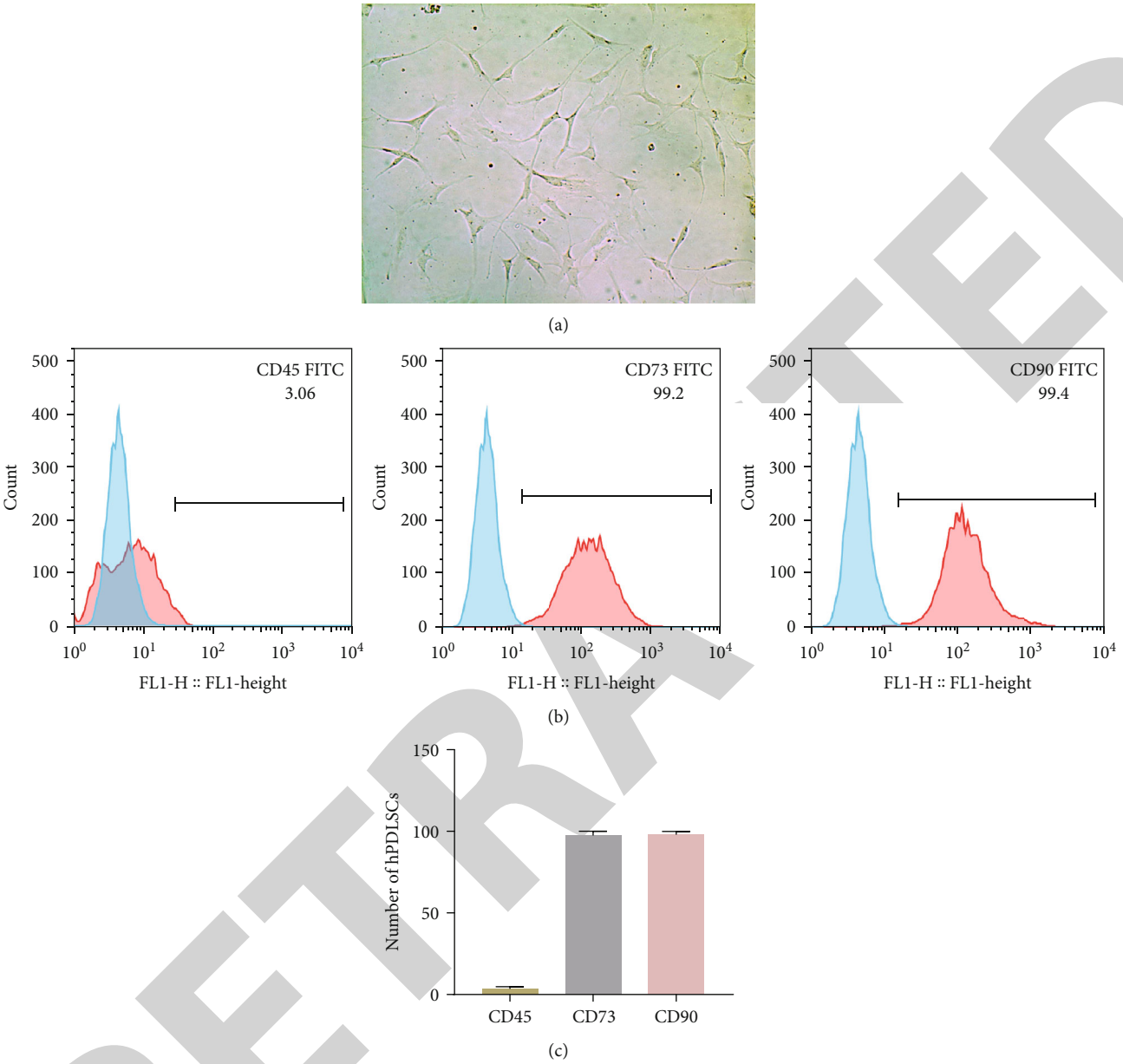

Figure 1: Isolation and identification of hPDLSCs. (a) hPDLSCs isolated from periodontal ligament tissue; (b, c) Flow cytometry-based detection of hPDLSC markers CD45, CD37, and CD90.

was detected with ALP activity kit (Beyotime, Shanghai, China) according to the manufacturer's protocol.

2.7. Alizarin Red Staining. First, PBS was used to rinse hPDLSCs on day 7 of osteogenic differentiation and then aspirated. Then, 4% paraformaldehyde was added and incubated with the cells for 30 min. After rinsing step with ddH_2O, 2% alizarin red staining solution with a pH of 4.24 was then added into the cell culture plate for 8-15 min staining at room temperature. Next, the staining solution was aspirated, followed by rinsing step using ddH_2O; counterstaining was performed if necessary. The cells were dried to observe the formation of the mineralized nodule and quantified calcium level with spectrophotometry at 562 nm.

2.8. Western Blot. Cells were lysed with RIPA lysis solution (Beyotime) to obtain protein samples. After measuring protein concentration with BCA kit (Beyotime), the protein was added into a corresponding volume of loading buffer (Beyotime) and fully mixed. The mixture was heated in boiling water for 5 min to denature proteins. Then, proteins were transferred to PVDF membrane, followed by 1 h blocking using 5% nonfat dry milk. Primary antibodies (GAPDH (5174S, 1 : 1000, Cell Signaling, Boston, USA), RUNX2 (# 12556S, 1 : 1000, Cell Signaling,

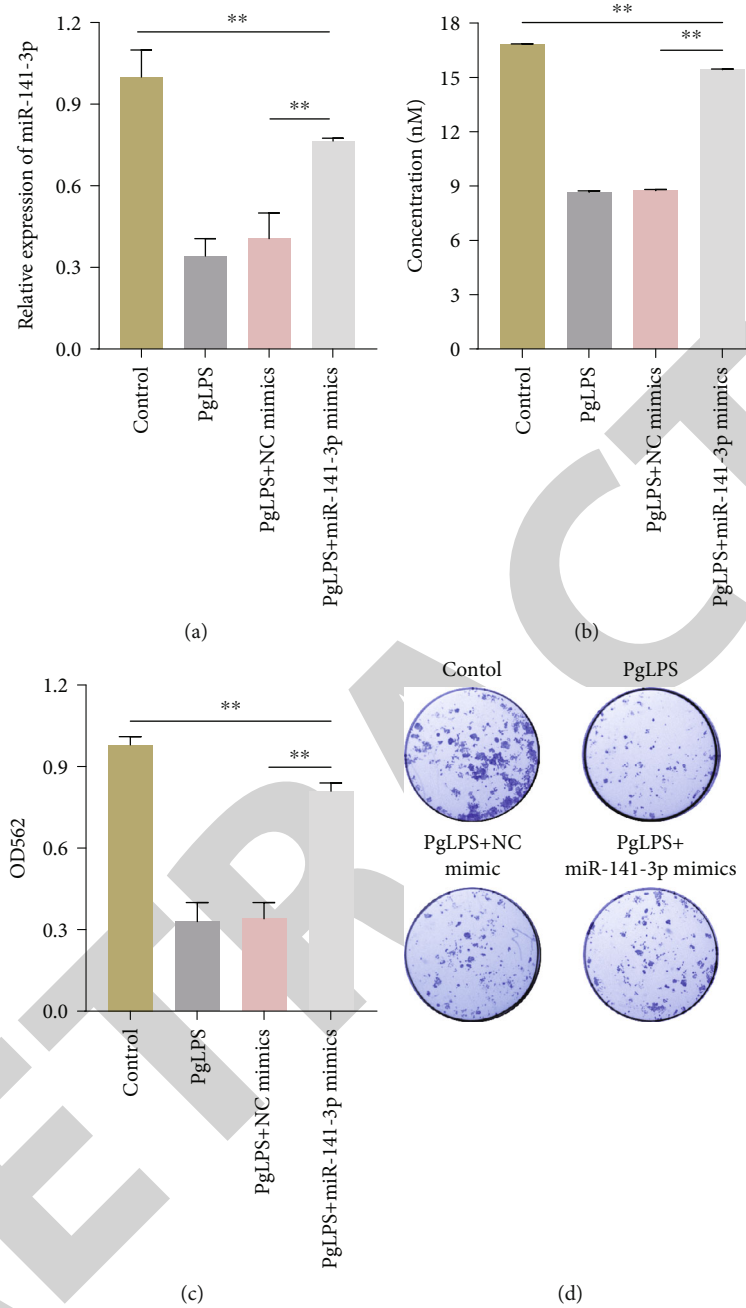

Figure 2: Continued.

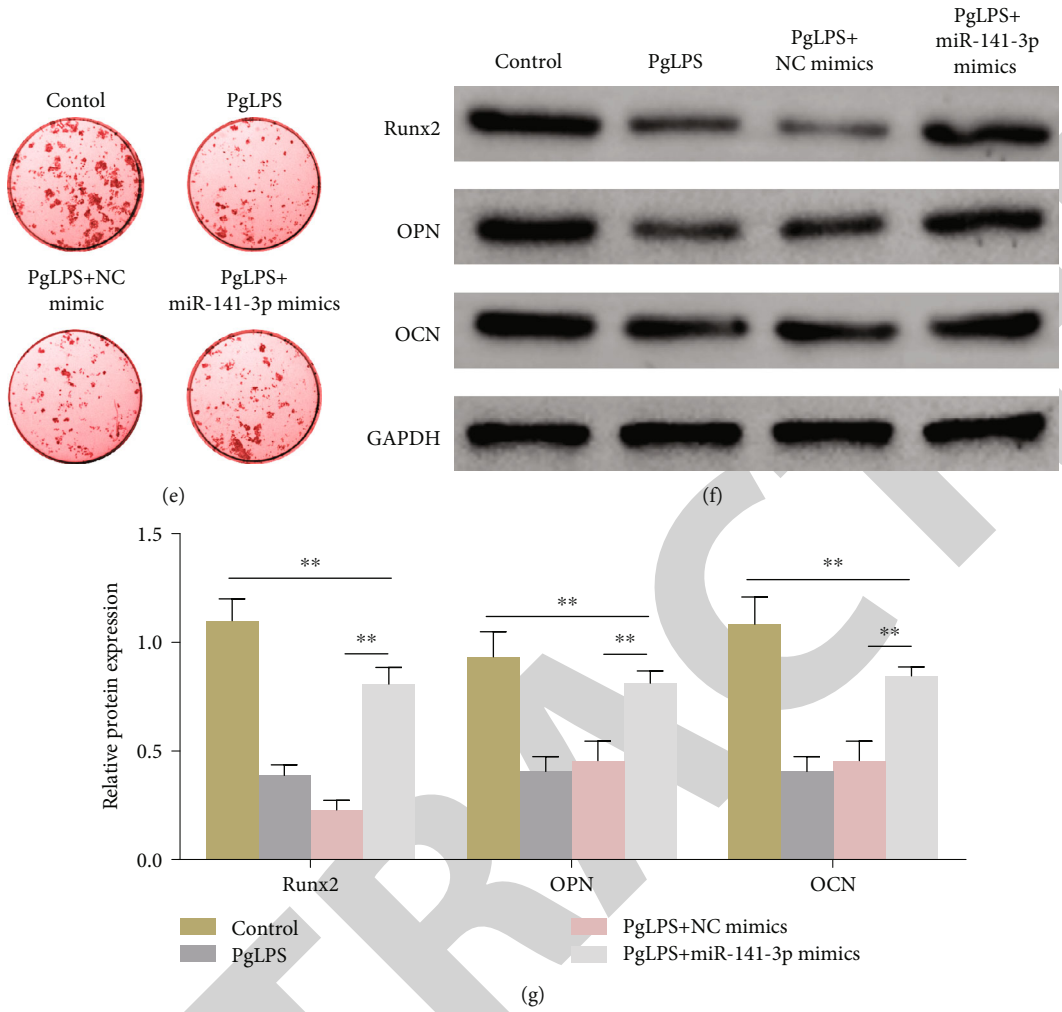

FIGURE 2: miR-141-3p attenuates PgLPS-caused inhibition of osteogenic differentiation in hPDLSCs. (a) qRT-PCR-based measurement of miR-141-3p expression; (b, d) ALP staining and ALP activity levels; (c, e) alizarin red staining and quantification of calcium level; (f, g) western blot-based detection of Runx2, OPN, and OCN protein expression. $^{*}P < 0.05$ and $^{**}P < 0.01$.

Boston, USA), OPN (ab8448, 1 : 1000, Abcam, Boston, USA), OCN (ab133612, 1 : 1000, Abcam, Boston, USA), and EZH2 (# 5246S, 1 : 1000, Cell Signaling, Boston, USA)) were added into the membrane and incubated overnight at 4°C. The next day, the membrane was rinsed 3 times prior to 1 h incubation with secondary antibodies (horseradish peroxidase-labeled IgG, 1 : 5000, Beijing CoWin Biosciences Co., Ltd., China, Beijing) at room temperature. After the developer was dropped on the membrane, the detection was performed by chemiluminescence imaging system (Bio-Rad).

2.9. Dual-Luciferase Reporter Assay. Through the online database TargetScan (http://www.targetscan.org/vert_72/), the binding site of miR-141-3p and EZH2 was predicted. According to the predicted results, the wild sequence and mutant sequence (mut-EZH2, wt-EZH2) of the binding site were designed and synthesized, respectively. These sequences were inserted into the luciferase reporter gene vector (pGL3-Basic), respectively, and then cotransfected HEK293T cells with miR-141-3p mimic (0, 150 nM, 300 nM, GenePharma), respectively. After mixing well, 100 μl of cell lysis solution was added and the cells were allowed to fully lyse on a shaker for 20 min at room temperature. 50 μl of luciferase reaction solution (Promega, Madison WI, USA) was added to 50 μl of lysed cells to measure Firefly luciferase activity, while 50 μl of Stop & Glo reagent (Promega, USA) for detecting Renilla luciferase activity. Renilla luciferase activity was used as an internal reference, and the ratio of Firefly luciferase activity to Renilla luciferase activity was the relative activity of luciferase. Three replicates were set up for the experiment.

2.10. Statistical Analysis. The experimental data were shown in the form of mean ± standard deviation (SD). One-way analysis of variance (one-way ANOVA) was performed by using GraphPad Prism 8.0 software, and multiple comparisons of the mean were carried out with the Tukey method. The result difference was considered to have statistical significance if $P < 0.05$.

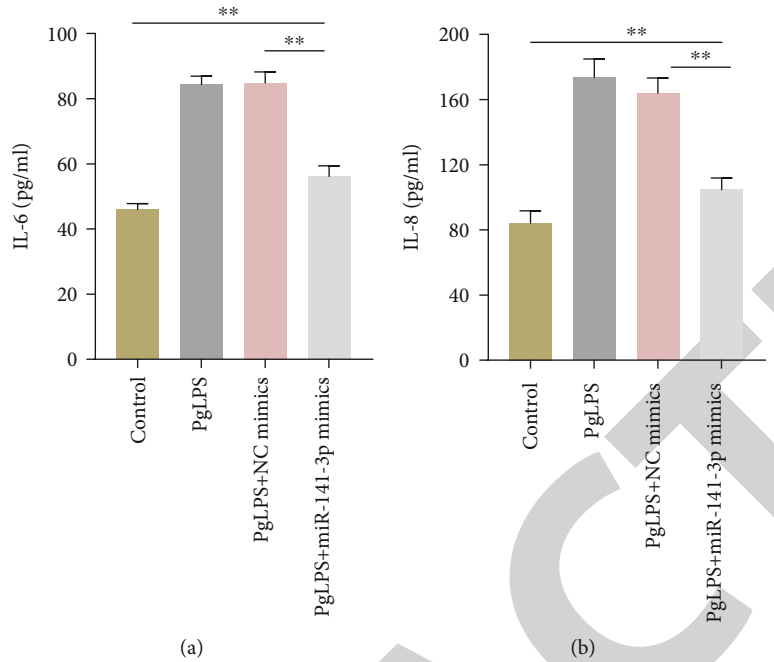

Figure 3: miR-141-3p attenuates the inflammatory response induced by PgLPS. (a, b) ELISA assay for IL-6 (a) and IL-8 (b) expression. $^{*}P < 0.05$ and $^{**}P < 0.01$.

3. Results

3.1. Isolation and Identification of Human Periodontal Ligament Stem Cells (hPDLSCs). Primary cells were scattered somewhere at the bottom of the culture flask or around tissue blocks (Figure 1(a)). Most of the cells were cord-like, long, and spindle-like in shape, with plump cell body, round or oval nuclei, and distinct and visible nucleoli. After about 5-10 days of culture, the adherent cells swirled and grew radially around tissue blocks, with a rapid growth rate. Even some cells fused with each other and showed multilayer growth, and at this time, the ratio of 1 : 1 could be selected for subculture. The flow cytometry showed the positive expression of hPDLSC surface antigens CD73 and CD90 and negative expression of CD45, suggesting that hPDLSCs were successfully isolated (Figures 1 (b)–1(c)).

3.2. miR-141-3p Attenuates PgLPS-Caused Inhibition of Osteogenic Differentiation in hPDLSCs. The expression of miR-141-3p in each treatment group was detected by qRT-PCR. The results showed that miR-141-3p was significantly downregulated in hPDLSCs treated with PgLPS, while it increased significantly after transfection of miR-141-3p mimics (Figure 2(a)). The results of ALP and alizarin red staining showed that PgLPS treatment significantly inhibited the osteogenic differentiation ability of hPDLSCs, and the inhibitory effect was alleviated after miR-141-3p overexpression (Figures 2(b)–2(e)). Then, the protein levels of osteogenic markers were detected with western blot. Protein expression levels of Runx2, OPN, and OCN were significantly decreased after PgLPS treatment, while they increased after miR-141-3p overexpression (Figures 2(f) and 2(g)).

3.3. miR-141-3p Attenuates Inflammation Induced by PgLPS. After PgLPS treatment, the levels of IL-6 and IL-8 were significantly increased. Compared with the PgLPS+NC mimic group, their expression showed a marked reduction in the PgLPS+miR-141-3p mimic group, indicating that miR-141-3p could attenuate the inflammatory response induced by PgLPS (Figures 3(a) and 3(b)).

3.4. miR-141-3p Targets EZH2. The levels of EZH2 in the cells of each treatment group were measured by qRT-PCR (Figure 4(a)). PgLPS treatment significantly increased EZH2 level while transfection of miR-141-3p caused a decrease of its expression level. Figure 4(b) showed the targeted binding site of miR-141-3p and EZH2, and dual-luciferase reporter assay further validated that miR-141-3p targeted EZH2 (Figure 4(c)).

3.5. EZH2 Reverses the Therapeutic Effect of miR-141-3p on PgLPS-Induced hPDLSCs. The results of ALP and alizarin red staining showed that miR-141-3p overexpression increased the osteogenic activity of hPDLSCs, and EZH2 counteracted this promoting effect (Figures 5(a)–5(d)). The effect of EZH2 on the inflammatory response of hPDLSCs was confirmed by using ELISA analysis. The results showed that compared with the PgLPS group, the levels of IL-6 and IL-8 in the PgLPS +miR-141-3p+pcNC group were significantly decreased; compared with the PgLPS+miR-141-3p+pcNC group, their expression was significantly increased in the PgLPS+miR-141-3p +EZH2 group (Figures 5(e) and 5(f)). The result of western blot indicated that the promoting effect of miR-141-3p on Runx2, OPN, and OCN protein expression could be reversed by upregulating EZH2 (Figures 5(g) and 5(h)).

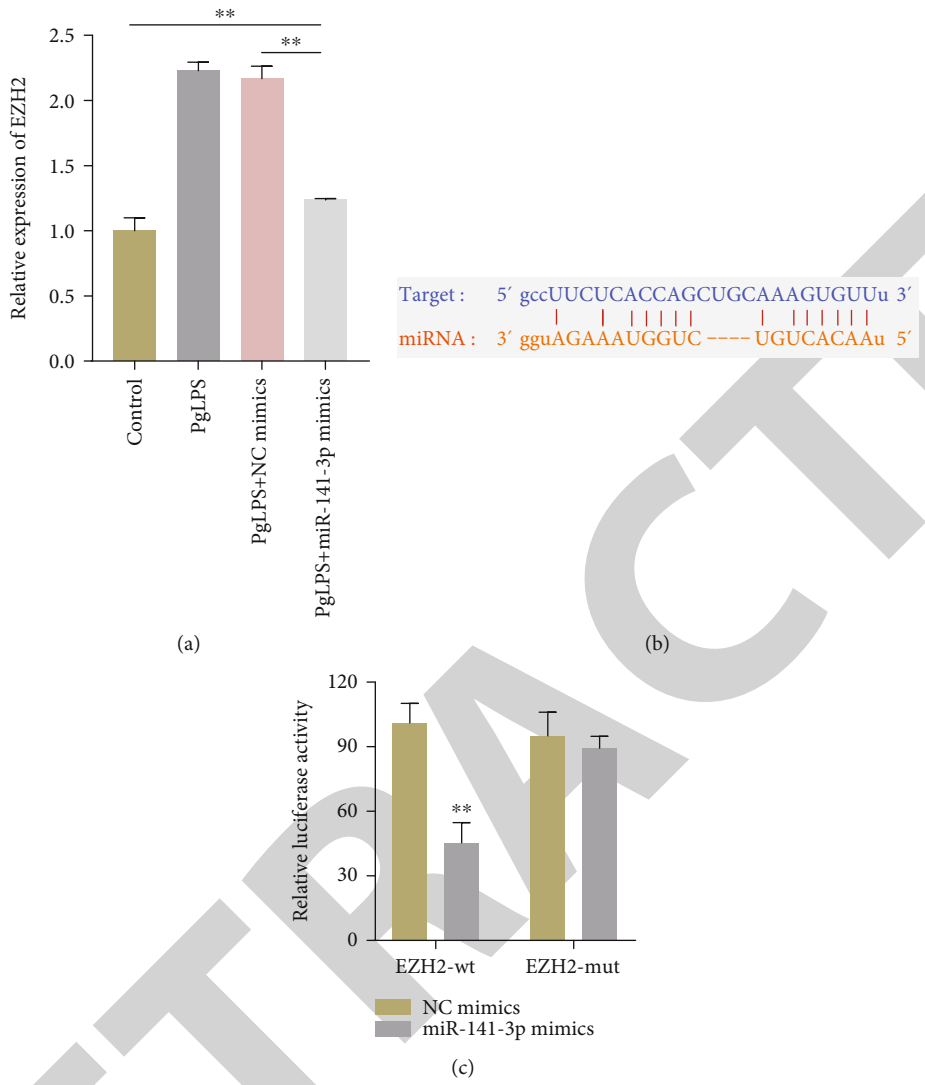

FIGURE 4: miR-141-3p targets EZH2. (a) qRT-PCR-based measurement of mRNA levels of EZH2 in the cells of each group. (b) The predicted binding site of miR-141-3p and EZH2. (c) Dual-luciferase reporter gene assay was performed after hPDLSCs were cotransfected with luciferase reporter genes containing mut-/wt-EZH2 and miR-141-3p mimics. $^{*}P < 0.05$ and $^{**}P < 0.01$.

4. Discussion

Periodontitis is a destructive periodontal inflammatory disease characterized pathologically by periodontal tissue inflammation, periodontal pocket formation, alveolar bone resorption, and progressive attachment loss [17] Plaques contribute to the development of periodontitis, but plaques not fully account for this development. Sufficient evidence has shown that the occurrence of periodontitis is an excessive inflammatory response (immune response) of the host to pathogenic microorganisms and their toxic products, further leading to periodontal tissue destruction. Once periodontal tissues are lost, the primary goal of periodontal therapy is to regenerate diseased tissues into their original form, structure, and function as far as possible [18].

PDLSCs are a kind of undifferentiated mesenchymal stem cells in the periodontal ligament with the potential to differentiate into osteoblasts or cementoblasts. PDLSCs can form cementum-periodontium-alveolar bone-like structures *in vivo*, thus constructing new periodontal tissue structures and rebuilding periodontal attachment [9, 19]. Therefore, PDLSCs become ideal candidates for cell therapy for treating injuries due to trauma or periodontal diseases [20]. The occurrences of many inflammatory diseases and autoimmune diseases are associated with defects in mesenchymal stem cell function *in vivo* [21]. Lipopolysaccharide induces the expression of proinflammatory cytokines during inflammation, which in turn promotes apoptosis to reduce the proliferation rate of mesenchymal stem cells [22]. PDLSCs interact with the inflammatory microenvironment to regulate cell stemness,

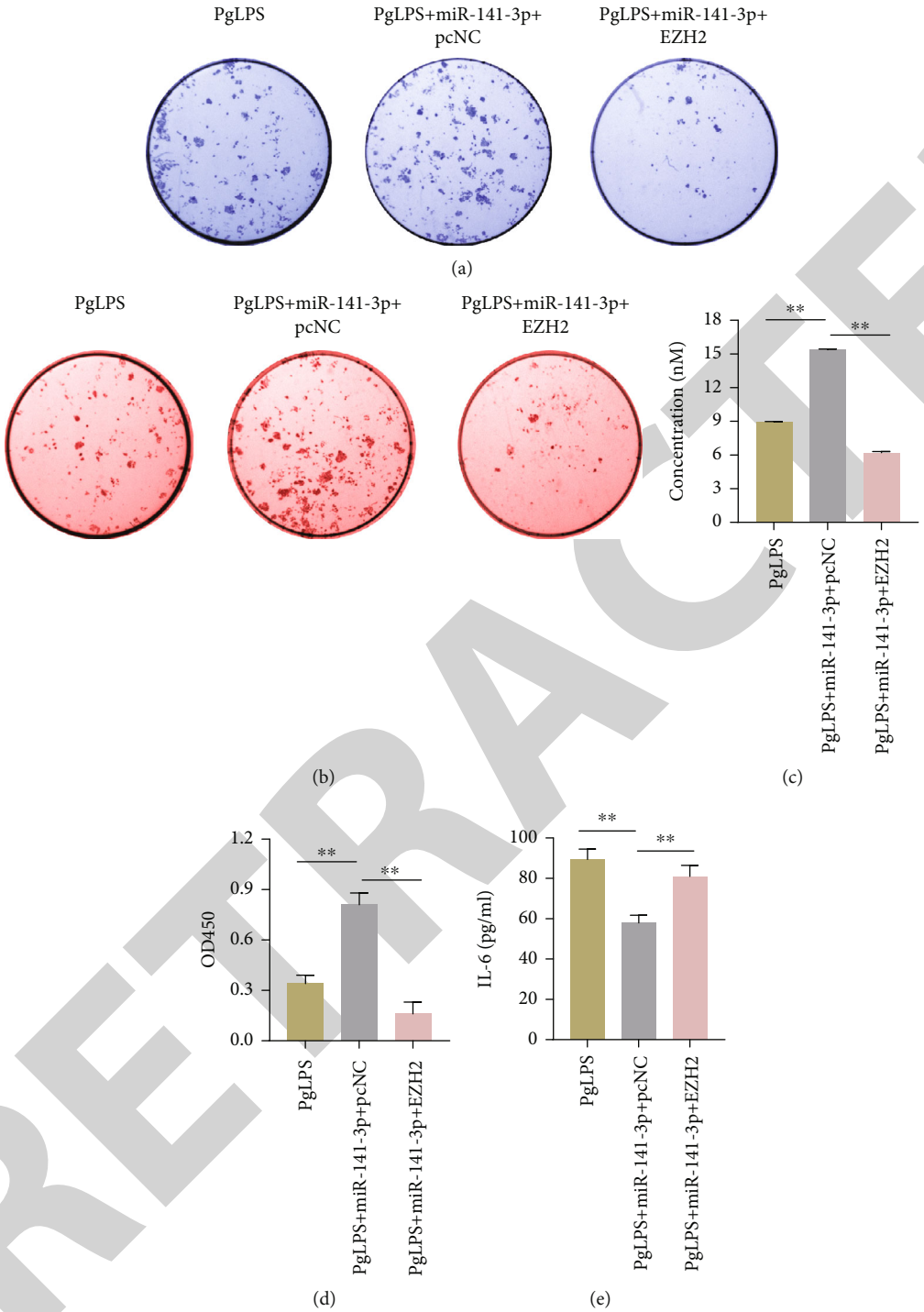

Figure 5: Continued.

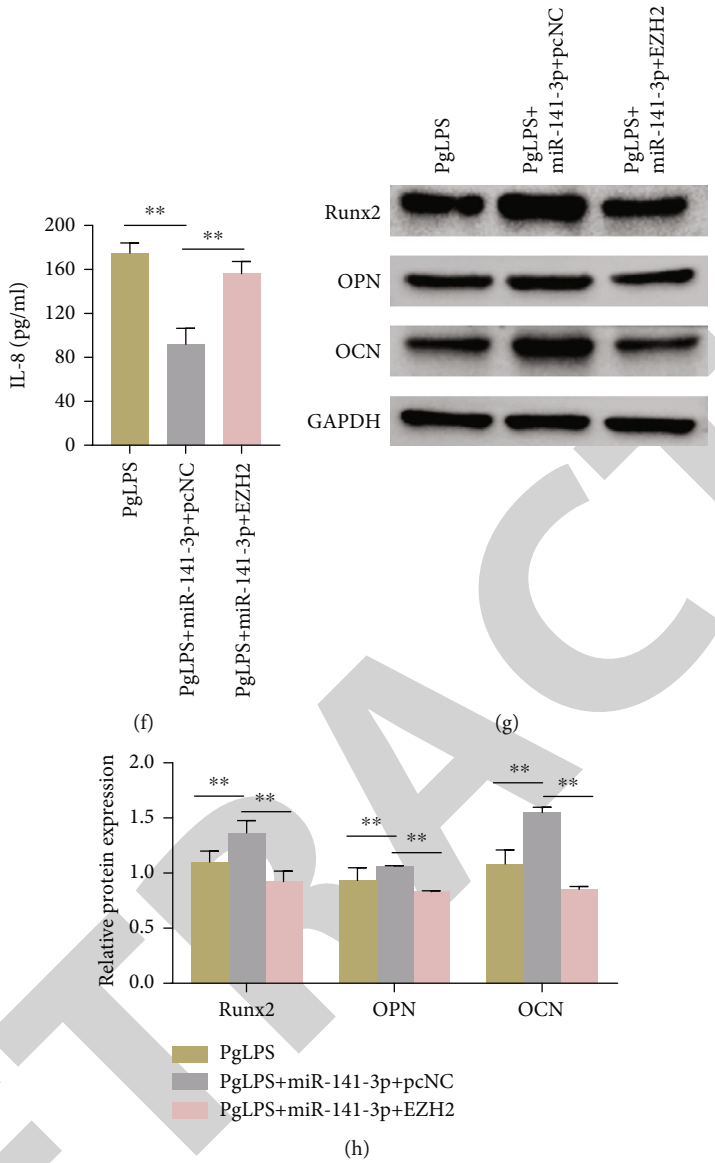

Figure 5: EZH2 reverses the therapeutic effect of miR-141-3p on PgLPS-induced PDLSCs. (a, b) ALP staining and ALP activity levels of cells in each group; (c, d) alizarin red staining and quantification of calcium level; (e, f) ELISA assay for IL-6 and IL-8 expression; (g, h) western blot detection of Runx2, OPN, and OCN protein expression. $^{*}P < 0.05$ and $^{**}P < 0.01$.

proliferation, migration, differentiation, immunoregulatory attributes, and the Wnt pathway, and the interaction and subsequent regulation may be a potential cause affecting periodontal tissue regeneration and repair [23]. A study shows that the inflammatory environment induced by PgLPS can promote the secretion of TNF-α, IL-8, and IL-18 from hPDLSCs [24], which is consistent with our findings. In addition, our study demonstrated that PgLPS induction significantly inhibited the osteogenic activity of hPDLSCs and decreased the protein levels of osteogenic markers.

An increasing body of evidence has suggested that miRNAs can regulate the differentiation potential of stem cells through posttranscriptional mechanisms [25]. At present, miRNAs have been found to be involved in the regulation of osteogenic differentiation and bone formation in a variety of cells [26, 27]. Li et al. demonstrated that miR-141-3p is important for osteogenic differentiation of stem cells from the apical papillae (SCAPs) [28]; miR-141-3p inhibits the proliferation of SCAPs and accelerates cellular senescence by downregulating the expression of YAP [28]. Recently, it has been found that knockdown of miR-141-3p can promote the proliferation level of mesenchymal stem cells by upregulating the expression of β-catenin, C-Myc, and cyclin D1 [29]. Despite these findings, the effect of miR-141-3p on the osteogenic differentiation ability of hPDLSCs under an inflammatory microenvironment has not been elucidated. Our current study found that miR-141-3p was significantly downregulated in hPDLSCs treated with PgLPS; miR-141-3p overexpression significantly increased the osteogenic differentiation activity of hPDLSCs treated with PgLPS and inhibited the secretion of proinflammatory cytokines IL-6 and IL-8. Additionally, Runx2, OPN, and OCN osteogenic marker proteins were significantly

increased in hPDLSCs with the overexpression of miR-141-3p, also demonstrating the stimulatory effect of miR-141-3p on osteogenic activity of hPDLSCs in periodontitis.

miRNAs can exert biological functions by regulating downstream target genes. EZH2 or enhancer of zeste homolog 2 is a histone methyltransferase that plays an important role in maintaining the self-renewal and proliferation ability of stem cells [30]. EZH2 has been validated to promote the migration of bone marrow stem cells by increasing the level of H3 lysine 27 trimethylation (H3K27me3) [31]. Ma et al. believed that EZH2 overexpression enhances migration and chemotaxis of SCAPs and that SCAPs enhance homing, migration, and chemotaxis of hPDLSCs through paracrine signaling [32]. Upregulation of EZH2 induced by lipopolysaccharide inhibits osteogenic activity of hPDLSCs under inflammatory conditions through the Wnt/β-catenin pathway [33]. By contrast, inhibition of EZH2 not only promotes osteogenic differentiation of progenitor cells mediated by BMP2 but also enhances osteogenesis and myogenic regeneration by regulating the expression of differentiation genes [34, 35]. In this study, the dual-luciferase reporter gene assay proved that EZH2 was a downstream target of miR-141-3p, and it found that overexpression of EZH2 reversed the stimulatory effect of miR-141-3p on osteogenic differentiation of hPDLSCs under an inflammatory microenvironment.

In conclusion, miR-141-3p can attenuate PgLPS-induced inhibition of osteogenic differentiation and inhibit secretion of IL-6 and IL-8 in hPDLSCs. These effects of miR-141-3p are achieved by negatively regulating EZH2. Therefore, the miR-141-3p/EZH2 axis can be a potential target for the treatment of periodontitis.

Data Availability

The data used to support the findings of this study are available from the corresponding author upon request.

Conflicts of Interest

The authors declare that they have no competing interests.

References

[1] F. Mesa, A. Magan-Fernandez, G. Castellino, R. Chianetta, L. Nibali, and M. Rizzo, "Periodontitis and mechanisms of cardiometabolic risk: novel insights and future perspectives," *Biochimica et Biophysica Acta (BBA)-Molecular Basis of Disease*, vol. 1865, no. 2, pp. 476–484, 2019.

[2] B. G. Loos and T. E. Van Dyke, "The role of inflammation and genetics in periodontal disease," *Periodontology 2000*, vol. 83, no. 1, pp. 26–39, 2019.

[3] F. M. Chen, H. H. Sun, H. Lu, and Q. Yu, "Stem cell-delivery therapeutics for periodontal tissue regeneration," *Biomaterials*, vol. 33, no. 27, pp. 6320–6344, 2012.

[4] G. Li, J. Hu, H. Chen et al., "Enamel matrix derivative enhances the proliferation and osteogenic differentiation of human periodontal ligament stem cells on the titanium implant surface," *Organogenesis*, vol. 13, no. 3, pp. 103–113, 2017.

[5] X. Chen, W. Ye, J. Y. Zhan et al., "Periodontal status of Chinese adolescents: findings from the 4th National Oral Health Survey," *The Chinese Journal of Dental Research*, vol. 21, no. 3, pp. 195–203, 2018.

[6] N. J. Kassebaum, E. Bernabé, M. Dahiya, B. Bhandari, C. J. L. Murray, and W. Marcenes, "Global burden of severe periodontitis in 1990-2010: a systematic review and meta-regression," *Journal of Dental Research*, vol. 93, no. 11, pp. 1045–1053, 2014.

[7] R. Bright, K. Hynes, S. Gronthos, and P. M. Bartold, "Periodontal ligament-derived cells for periodontal regeneration in animal models: a systematic review," *Journal of Periodontal Research*, vol. 50, no. 2, pp. 160–172, 2015.

[8] K. Sano, M. Usui, Y. Moritani et al., "Co-cultured spheroids of human periodontal ligament mesenchymal stem cells and vascular endothelial cells enhance periodontal tissue regeneration," *Regenerative Therapy*, vol. 14, pp. 59–71, 2020.

[9] J. Liu, J. Ruan, M. D. Weir et al., "Periodontal bone-ligament-cementum regeneration via scaffolds and stem cells," *Cells*, vol. 8, no. 6, p. 537, 2019.

[10] M. Nagata, K. Iwasaki, K. Akazawa et al., "Conditioned medium from periodontal ligament stem cells enhances periodontal regeneration," *Tissue Engineering Part A*, vol. 23, no. 9-10, pp. 367–377, 2017.

[11] J. Liu, B. Chen, J. Bao, Y. Zhang, L. Lei, and F. Yan, "Macrophage polarization in periodontal ligament stem cells enhanced periodontal regeneration," *Stem Cell Research & Therapy*, vol. 10, no. 1, pp. 1–11, 2019.

[12] P. Bartel David, "MicroRNAs: genomics, biogenesis, mechanism, and function," *Cell*, vol. 116, no. 2, pp. 281–297, 2004.

[13] B. Christina, M. Eckart, and K. Andreas, "Specific miRNA disease biomarkers in blood, serum and plasma: challenges and prospects.[J]," *Molecular Diagnosis & Therapy*, vol. 20, pp. 509–518, 2016.

[14] X. Li, Y. Zheng, Y. Zheng et al., "Circular RNA CDR1as regulates osteoblastic differentiation of periodontal ligament stem cells via the miR-7/GDF5/SMAD and p38 MAPK signaling pathway," *Stem Cell Research & Therapy*, vol. 9, no. 1, pp. 1–14, 2018.

[15] Y. Liu, C. Liu, A. Zhang et al., "Down-regulation of long noncoding RNA MEG3 suppresses osteogenic differentiation of periodontal ligament stem cells (PDLSCs) through miR-27a-3p/IGF1 axis in periodontitis," *Aging (Albany NY)*, vol. 11, no. 15, pp. 5334–5350, 2019.

[16] S. H. Jin, J. G. Zhou, X. Y. Guan, G. H. Bai, J. G. Liu, and L. W. Chen, "Development of an miRNA-array-based diagnostic signature for periodontitis," *Frontiers in Genetics*, vol. 11, p. 577585, 2020.

[17] C. Fi and W. Wo, "Periodontal disease and systemic diseases: an overview on recent progresses," *Journal of Biological Regulators and Homeostatic Agents*, vol. 35, no. 1, pp. 1–9, 2021.

[18] K. Avinash, S. Malaippan, and J. N. Dooraiswamy, "Methods of isolation and characterization of stem cells from different regions of oral cavity using markers: a systematic review," *International Journal of Stem Cells*, vol. 10, no. 1, pp. 12–20, 2017.

[19] T. Atsushi, W. Naohisa, M. Hidefumi, and P. L. S. Cells, "Periodontal ligament stem cells: regenerative potency in periodontium," *Stem Cells and Development*, vol. 28, no. 15, pp. 974–985, 2019.

[20] S. A. Tassi, N. Z. Sergio, M. Y. O. Misawa, and C. C. Villar, "Efficacy of stem cells on periodontal regeneration: systematic

Hindawi
Computational and Mathematical Methods in Medicine
Volume 2023, Article ID 9832573, 1 page
https://doi.org/10.1155/2023/9832573

Retraction

Retracted: Predicting Characteristics Associated with Breast Cancer Survival Using Multiple Machine Learning Approaches

Computational and Mathematical Methods in Medicine

Received 27 June 2023; Accepted 27 June 2023; Published 28 June 2023

This article has been retracted by Hindawi following an investigation undertaken by the publisher [1]. This investigation has uncovered evidence of one or more of the following indicators of systematic manipulation of the publication process:

(1) Discrepancies in scope

(2) Discrepancies in the description of the research reported

(3) Discrepancies between the availability of data and the research described

(4) Inappropriate citations

(5) Incoherent, meaningless and/or irrelevant content included in the article

(6) Peer-review manipulation

The presence of these indicators undermines our confidence in the integrity of the article's content and we cannot, therefore, vouch for its reliability. Please note that this notice is intended solely to alert readers that the content of this article is unreliable. We have not investigated whether authors were aware of or involved in the systematic manipulation of the publication process.

Wiley and Hindawi regrets that the usual quality checks did not identify these issues before publication and have since put additional measures in place to safeguard research integrity.

We wish to credit our own Research Integrity and Research Publishing teams and anonymous and named external researchers and research integrity experts for contributing to this investigation.

The corresponding author, as the representative of all authors, has been given the opportunity to register their agreement or disagreement to this retraction. We have kept a record of any response received.

References

[1] M. N. Haque, T. Tazin, M. M. Khan et al., "Predicting Characteristics Associated with Breast Cancer Survival Using Multiple Machine Learning Approaches," *Computational and Mathematical Methods in Medicine*, vol. 2022, Article ID 1249692, 12 pages, 2022.

Hindawi
Computational and Mathematical Methods in Medicine
Volume 2022, Article ID 1249692, 12 pages
https://doi.org/10.1155/2022/1249692

Research Article

Predicting Characteristics Associated with Breast Cancer Survival Using Multiple Machine Learning Approaches

Mohammad Nazmul Haque,[1] Tahia Tazin,[1] Mohammad Monirujjaman Khan,[1] Shahla Faisal,[2] Sobhee Md. Ibraheem,[1] Haneen Algethami,[3] and Faris A. Almalki[4]

[1]*Department of Electrical and Computer Engineering, North South University, Bashundhara, Dhaka 1229, Bangladesh*
[2]*Department of Statistics, Government College University, Faisalabad, Pakistan*
[3]*Department of Computer Science, College of Computers and Information Technology, Taif University, P.O. Box 11099, Taif 21944, Saudi Arabia*
[4]*Department of Computer Engineering, College of Computers and Information Technology, Taif University, P.O. Box 11099, Taif 21944, Saudi Arabia*

Correspondence should be addressed to Mohammad Monirujjaman Khan; monirujjaman.khan@northsouth.edu

Received 28 January 2022; Accepted 29 March 2022; Published 25 April 2022

Academic Editor: Shakeel Ahmad

Breast cancer is one of the most commonly diagnosed female disorders globally. Numerous studies have been conducted to predict survival markers, although the majority of these analyses were conducted using simple statistical techniques. In lieu of that, this research employed machine learning approaches to develop models for identifying and visualizing relevant prognostic indications of breast cancer survival rates. A comprehensive hospital-based breast cancer dataset was collected from the National Cancer Institute's SEER Program's November 2017 update, which offers population-based cancer statistics. The dataset included female patients diagnosed between 2006 and 2010 with infiltrating duct and lobular carcinoma breast cancer (SEER primary cites recode NOS histology codes 8522/3). The dataset included nine predictor factors and one predictor variable that were linked to the patients' survival status (alive or dead). To identify important prognostic markers associated with breast cancer survival rates, prediction models were constructed using *K*-nearest neighbor (K-NN), decision tree (DT), gradient boosting (GB), random forest (RF), AdaBoost, logistic regression (LR), voting classifier, and support vector machine (SVM). All methods yielded close results in terms of model accuracy and calibration measures, with the lowest achieved from logistic regression (accuracy = 80.57 percent) and the greatest acquired from the random forest (accuracy = 94.64 percent). Notably, the multiple machine learning algorithms utilized in this research achieved high accuracy, suggesting that these approaches might be used as alternative prognostic tools in breast cancer survival studies, especially in the Asian area.

1. Introduction

Breast cancer has a high mortality rate. Breast cancer affects more than 1.5 million women worldwide each year, as per the World Health Organization [1]. Breast carcinoma is one of the most well-known kinds of cancer, having been first discovered in Egypt in approximately 1600 BC [2]. Tumors may be used to screen for breast cancer. Tumors are categorized as benign or malignant. To identify malignant neoplasms, physicians must use an active detection strategy. However, even with professionals, cancers are notoriously difficult to detect [3]. As a consequence, an automated technique is required for cancer detection. Numerous studies have tried to predict the survival of carcinoma in humans using machine learning methodologies, and they have also shown that these algorithms are more successful in diagnosing carcinoma [3]. Typically, a physician's knowledge and ability are essential to ensure a patient's detection precision [4]. This capacity, however, is perfected through years of seeing the detrimental effects of

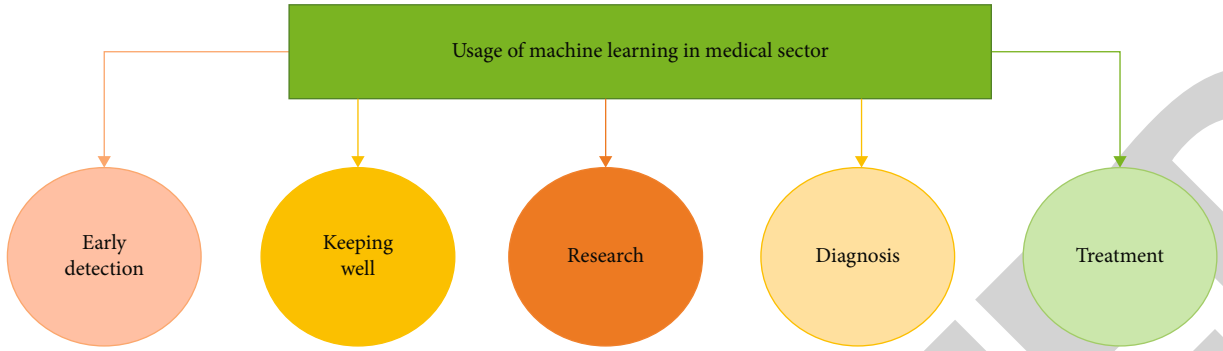

Figure 1: Application of machine learning in the medical field.

various individuals and validating diagnoses. Despite this, there is no guarantee of reliability. Due to developments in processing technology, it is now very simple to collect and maintain large amounts of data, such as specialized databases of electronic patient information [5]. Without the help of a personal computer, it would be difficult to parse these enormous datasets, considerably more so while doing broad information examination. Also, an exact replica of genuine cancer might keep individuals from getting vital therapy. As a result, precisely diagnosing and arranging bosom disease into harmless and threatening subtypes is a significant subject of study. Somewhat recently, AI calculations have been broadly utilized to distinguish bosom diseases and derive different ideas from information designs. AI is well known for its application in disease classification and demonstration. It is a strategy for finding examples of obscure consistency in a wide scope of datasets. It contains an expansive assortment of strategies for uncovering rules, ideal models, and connections inside information groupings, as well as respect to making theories about these linkages that might be used to see recently covered information. Figure 1 illustrates the primary applications of machine learning in the medical field.

As a consequence, AI's usage in healthcare contexts is quickly growing as a consequence of its predictive and classification capabilities, most notably in clinical analysis to define breast cancer, and it is now extensively utilized in biomedical research.

Breast cancer is still the most prevalent malady among Bangladeshi women. It has developed into a hidden weight, accounting for 69 percent of illness deaths in females [6]. Breast cancer has the greatest prevalence rate (19.3 per 100,000) among Bangladeshi females between the ages of 15 and 44 years [7] when compared to other types of illness. Between 2008 and 2010, cervical cancer was the second most common cancer in this group of women, with a prevalence rate of 12.4 per 100,000. The absence of infection awareness, lack of confidence in clinical decision-making, unethical screening procedures, and early metastatic misuse have all been linked to an increase in the frequency rate [8]. Additionally, patients are prevented from receiving cancer therapy due to a lack of financial resources, the infection's social stigma, and their fear of the treatment. According to findings from research conducted by Bangladesh's National Institute of Cancer Research and Hospital in 2010, breast cancer was responsible for 21% of all deaths among women aged 15 to 49. Bangladesh's National Institute of Cancer and Research Hospital urges that bosom disease become a serious public health concern for the Bangladesh government. According to a study conducted in Bangladesh's Khulna Division in 2007–2008, 87 percent of new cases of bosom illness were classified as stage III+, indicating that malignant development has spread to various body areas. Treatment options were limited and costly, even more so in low-income nations like Bangladesh. The main reason for this could be a lack of public awareness about early cancer screening, which is similar to the case in Bangladesh's rural districts.

Already, specialists have dissected factors influencing bosom malignant growth endurance rates utilizing basic programming projects like Microsoft Excel, SPSS, and STATA [9–11]. These preprogrammed measurable devices are not particularly adaptable when it comes to tracking down new factors or delivering inventive and integrative outlines [12]. Because of the shortcomings of traditional factual examinations, various AI (ML) calculations have been widely used in this domain [13–20]. The choice tree approach is a managed learning method that pictures the results in an effectively interpretable tree structure, which is the basis for breaking down tremendous measures of information [21–24]. Breiman's calculation, a subordinate of DT, is fit for working in both regulated and unaided modes and can deal with both consistent and straight-out information in order and relapse issues [25, 26]. Artificial neural networks have regularly been described as secret elements, demonstrating via preparing on information with known results and tuning loads for further developed expectations in situations with obscure results [27, 28]. Outrageous Boost is a parallelizable outfit of order and relapse trees that produces precise forecasts, is easy to utilize, and has beaten different calculations in different AI challenges [29]. Strategic relapse is based on Gaussian dispersion and is capable of dealing with various types of factors, such as nonstop, discrete, and dichotomous, without making any assumptions about their ordinariness [30, 31]. For regulated grouping, support vector machines are used. They work by defining the best choice limit for isolating main elements into specific groups and then forecasting the class of future perceptions based on this detachment limit [32]. Despite

the fact that AI strategies for bosom disease have been created and inspected before, factors like area, way of life, and open information might shift. We confirmed that it is indispensable to foster models for the Bangladeshi setting to learn the factors influencing bosom malignant growth patients' endurance rates. In addition, it is very useful to execute variable choice utilizing AI approaches in the clinical area, where experts have an inclination for old-style factual strategies. The goal of this study is to use conventional AI approaches to develop interpretable prognostic models to uncover the primary characteristics that affect persons with heart disease's survival rates in an Asian climate. The major goal of this study is to demonstrate how machine learning may be used to detect breast cancer features. The study's most significant aspect is that we used a variety of well-known machine learning algorithms to achieve the best results. In our investigation, we used many well-known machine learning algorithms. The RF, DT, K-NN, SVM, voting classifier, GB classifier, AdaBoost classifier, and LR algorithms achieved 94.64 percent, 89.22 percent, 83.87 percent, 84.67 percent, 88.26 percent, 91.78 percent, 89.0 percent, and 80.57 percent accuracy, respectively. The accuracy percentage of the models utilized in this analysis is substantially higher than in earlier investigations, indicating that these models are more reliable. Several model evaluations have demonstrated their resilience, and the strategy may be extrapolated from the study.

According to research, the situation may improve if women can detect and cure breast cancer early. They must do so by accurately forecasting the disease's development from a mild condition to breast cancer. Machine learning technology may aid in the early generation of correct forecasts. There are several machine learning systems, but unfortunately, their predictions are unreliable and inaccurate. They are also concerned about over- and underfitting. As a result, we developed a machine learning model to assist medical technicians in the early detection of cancer sickness. It will confirm and indicate whether or not an individual has breast cancer.

Our study's key contribution, as previously stated, is that we used numerous machine learning models on a publically available dataset. Previously, the majority of research used a large model to predict breast cancer. However, we tested many different machine learning algorithms to predict breast cancer features and compared the results to earlier studies. The remainder of this work is organized as follows. Section 2 discusses the Method and Experiment Methodology, Section 3 discusses the Result Analysis, and Section 4 discusses the Conclusions.

2. Method and Experiment Methodology

This part includes a description of the dataset, a block diagram, a flow diagram, assessment matrices, and information on the techniques and materials utilized.

2.1. Dataset. This breast cancer patient database was compiled from the November 2017 update of the National Cancer Institute's SEER Program, which provides population-based cancer statistics [33]. Female patients diagnosed with infiltrating duct and lobular carcinoma breast cancer (SEER primary cites recode NOS histology codes 8522/3) between 2006 and 2010 were included in the study. Patients with uncertain tumor size, patients with investigated regional LNs, patients with positive regional LNs, and patients with less than one month of survival were omitted; hence, 4024 patients were eventually included. The complete number of data in the "status" column of the dataset is shown in Figure 2.

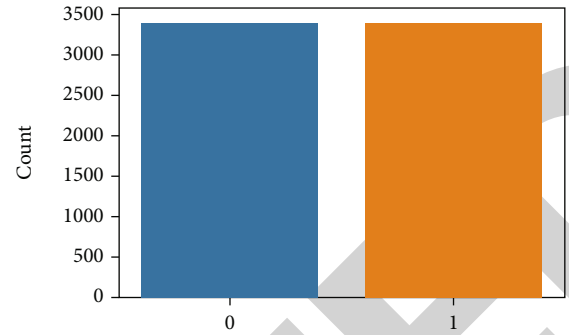

Figure 2: Total number of data in the "status" column after preprocessing.

The overall number of missing values in each column of the database is shown in Figure 3. Due to the absence of a missing value, the outcome has been displayed as zero.

2.2. Block Diagram of the System. The block diagram of the AI framework is displayed in Figure 4. The components that contribute to the expectation have been identified, and the model's objective value has been established so that it can hypothesize. After that, the dataset was divided into equal portions for preparation and testing. The split was accomplished by random examination, which results in an unequal distribution of preparation and testing time.

Following that, two examinations were conducted, with an 80 percent preparation size and a 20% testing size. Following that, the pieces were scaled using guidelines. To facilitate comprehension, several histogram and scatterplot representations of the preparation split were created. Following that, the framework's preparation begins.

2.3. Used Algorithms. Breast cancer is the most commonly detected disease in the medical field, and the incidence of diagnosis is increasing year after year. The SEER Breast Cancer Database was used to assess eight widely used machine learning algorithms for predicting breast cancer recurrence mortality rates.

(i) Random forest

(ii) Decision tree

(iii) *K*-nearest neighbor

(iv) Logistic regression

(v) Support vector machine

```
df.isna().sum()

Age                        0
T Stage                    0
N Stage                    0
Tumor Size                 0
Estrogen Status            0
Progesterone Status        0
Regional Node Examined     0
Reginol Node Positive      0
Survival Months            0
Status                     0
dtype: int64
```

Figure 3: Outcome of missing data.

(vi) Voting classifier

(vii) Gradient boosting classifier

(viii) AdaBoost classifier

2.3.1. Random Forest Flowchart. Random forest is a technique for directed machine learning [34]. It makes a "forest" out of a group of carefully chosen trees that have been largely prepped for the "bagging" technique. The bagging strategy's basic rationale is that mixing many learning models increases the final result. Random forest generates several alternative trees and combines them to get a more precise and dependable representation. It offers the benefit of tackling the arrangement and relapse problems that plague the majority of modern machine learning frameworks. One more striking component of the random forest methodology is that deciding the overall significance of everything in the estimate is so direct. Sklearn offers a remarkable mechanical assembly for assessing the meaning of a component by looking at how much pollution is decreased all throughout the backwoods by the tree communities that utilize it. Following planning, it works out this score for each brand name and changes the discoveries, fully intent on raising the outright importance. The adaptability of the random forest is one of its most charming elements. It can be used to find backslides and gather data, and the importance of good data is clear. Moreover, it is a valuable system since the default hyperparameters it utilizes frequently produce unequivocal assumptions. Because there are not many hyperparameters to begin with, understanding them is essential. Overfitting is a notable issue in AI, yet it seldom happens with the erratic arbitrary timberland classifier. The classifier will not overfit the model if there are sufficient trees in the backwoods. The random forest approach is made up of a progression of decision trees, every one of which is developed by utilizing a bootstrap test from a preparation set. The out-of-pack (OOB) test, which we will talk about later, is 33% of the preparation test that is saved for the end goal of testing. The dataset is then infused with one more case of randomization utilizing highlight packing, expanding its assortment while diminishing the relationship across choice trees. The strategy for anticipating differs as per the situation.

2.3.2. Decision Tree Flowchart. This review utilizes a decision tree classifier. This classifier [35] appears to recursively segment the model space. A prescient worldview acts as a guide between the characteristics of a thing and its qualities [36]. It routinely isolates every potential information result into bits. Each nonleaf hub relates to an element explored, each branch to the result of the trial, and each leaf hub to a judgment or order [36]. The root hub of the tree, which is at the very top, shows the most frequently utilized forecast model. A decision tree's two hubs are the decision hub and the leaf hub. While leaf hubs are the consequence of those decisions and have no additional branches, decision hubs are utilized to settle on those choices and contain a few branches. The results of the tests or decisions are dependent upon the dataset's properties. The decision tree is not difficult to grasp since it repeats the meanings that an individual goes through while settling on a certifiable choice. It could be extremely helpful in settling issues with direction. Think about all the doable answers to an issue. Cleaning information is not needed, however much it is with different strategies.

2.3.3. K-Nearest Neighbor. One of the most important AI calculations is the K-NN technique. It is dependent on the learning approach used. The K-NN method admits that the new case and previous cases are interchangeable and assigns the new case to a classification that is similar to the previous classifications. The K-NN calculation keeps up with every single accessible data point and arranges new information accordingly in view of its comparability with recently characterized information. This truly means that using the K-NN approach, new information might be quickly arranged into a distinct classification. The K-NN method can be used for relapsing and grouping, although it is most commonly employed for order difficulties. The K-NN method is nonparametric, which means it makes no assumptions about the data. It is now and then alluded to as a "sluggish student" calculation since it does not gain from the preparation set in a flash, but rather keeps up with and orders the data later. The K-NN approach only saves the information during the preparation stage, and when it gets new information, it sorts it into a class that is generally practically identical to the new information. This review uses the K-nearest neighbor classifier, which is one of the most frequently involved order calculations in AI [37]. The K-nearest neighbor procedure is a nonparametric technique for characterizing information. This classifier characterizes things as indicated by their proximity to "k" nearest neighbors. It is worried about the quick environmental elements of the thing, as opposed to the necessary information conveyance [38].

2.3.4. Logistic Regression. Logistic regression is one of the most frequently utilized AI calculations in the regulated learning approach [39]. It is an estimating approach that utilizes a gathering of free factors to expect an all-out subordinate variable. To estimate the result of a single dependent variable, a logistic regression is used. As a result, the end result should have a clear or discrete character. It very well

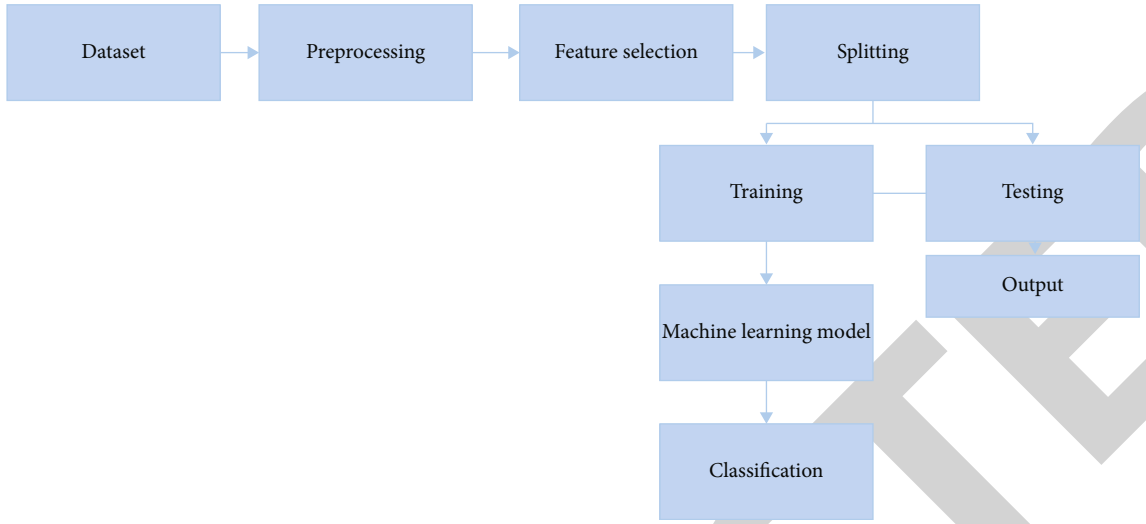

Figure 4: System block diagram.

may be Yes or No, 0 or 1, valid or bogus, etc., but probabilistic qualities somewhere in the range of 0 and 1 are presented rather than exact qualities like 0 and 1. Calculated relapse and direct relapse are moderately comparative in their application. Straight regression is utilized to tackle relapse issues, while logistic regression is utilized to address arrangement hardships. Instead of fitting a relapse line, we utilize logistic regression to fit an "S" molded calculated work that predicts two most extreme qualities (0 or 1). The calculated capacity's bend shows the likelihood of anything, for example, regardless of whether cells are harmful, or regardless of whether a mouse is fat contingent upon its weight. As a result of using both continuous and discrete datasets, calculated relapse is a common AI strategy. It can predict and group new information by using both datasets.

2.3.5. Support Vector Machine. A SVM model is a representation of events as points in space, separated by a substantial gap between examples of distinct classes [40]. Alongside direct arrangement, SVMs can achieve successful nonstraight characterization by verifiably planning their contributions to high-layered include spaces. Support vectors alone; we do not have to stress over different perceptions since the edge is determined utilizing the focuses closest to the hyperplane (support vectors), while calculated relapse characterizes the classifier across all places. Thus, SVM benefits from specific innate speedups.

2.3.6. Voting Classifier. A voting classifier is a kind of AI model that learns from a large number of models and predicts an outcome (class) based on the class that has the best chance of being chosen as the result [41]. It basically totals the consequences of every classifier that is taken care of in the democratic classifier and estimates the result class in view of the class with the biggest democratic greater part. In hard democratic, the extended outcome class is the one with the most votes, i.e., the class that had the highest likelihood of being predicted by all of the classifiers. Accept three classifiers as a starting point for predicting the result class (A, A, and B). As a result of the scenario, the majority of people predicted this. Subsequently, A will fill in as the last gauge. The resulting class in delicate democracy is the estimate in view of the normal distribution of the probabilities allotted to that class. Expect that given a contribution to three models, the forecast likelihood for class An is $(0.30, 0.47, 0.53)$ and that for class B is $(0.30, 0.47, 0.53)$ $(0.20, 0.32, 0.40)$. Hence, with a normal of 0.4333 for class An and 0.3067 for class B, class An is clearly the champ since it had the best normal likelihood of arriving at the midpoint of every classifier.

2.3.7. Gradient Boosting Classifier. Gradient boosting is an AI approach that is regularly utilized for relapse and arrangement applications [42]. It creates an expectation model utilizing an ensemble of frail forecast models, most frequently choice trees. At the point when a choice tree fills in as the frail student, the resultant technique is alluded to as "slope-supported trees." It regularly beats the arbitrary backwoods. A slope-help tree model is developed in a similar way as other supporting methodologies, but it contrasts in that it permits enhancement of any differentiable misfortune work.

2.3.8. AdaBoost Classifier. Boosting was invented in machine learning to address the issue of whether a collection of weak classifiers might be transformed into a strong classifier [43]. A poor learner or classifier is one that outperforms random guessing. Because it will be made up of a large number of weak classifiers, each of which is better than random, it will be resistant to overfitting. As a poor classifier, a simple threshold on a single feature is usually used. It is positive if the characteristic exceeds the anticipated value; otherwise, it is negative. AdaBoost is an acronym for "adaptive boosting," a technique for converting weak learners or predictors into strong predictors in order to solve classification issues.

2.4. Matrices of Evaluation. Figure 5 depicts the confusion matrix. Machine learning classification models' performance is measured using confusion matrices. To assess the performance of the models created, the confusion matrix was employed.

The confusion matrix shows how accurate our models are at forecasting and how often they predict erroneously. False positives and false negatives were attributed to values that were incorrectly predicted, whilst true positives and true negatives were assigned to values that were correctly predicted. The accuracy, precision-recall trade-off, and AUC of the model were used to assess its performance once all of the estimated parameters were entered into the matrix.

3. Result and Data Analysis

3.1. Visualization of Feature Selection. Figure 6 depicts the strategy to feature selection. The ability to understand how features are connected to one another is aided by feature selection.

As seen in Figure 6, the primary goal characteristic "status" is positively correlated with all other variables except the surviving months.

3.2. Accuracy of the Model

3.2.1. Random Forest. A random forest classifier's classification report is shown in Figure 7.

Among all the other algorithms, it had the highest accuracy (94.64 percent). The random forest model can correctly identify 95% of the characteristics that are associated with breast cancer. A random forest classifier's confusion matrix is shown in Figure 8.

There are 1291 correct guesses and 73 incorrect predictions in this example. This model predicted 642 data as 0 and 649 data as 1. So, this is its correct prediction. However, it also predicted 39 data points to be 0 and 34 data points to be 1. This is an absolutely wrong prediction.

3.2.2. Logistic Regression. Figure 9 demonstrates the classification report of the logistic regression classifier.

Here, logistic regression has achieved 81% accuracy. In this case, this model can correctly identify 81% of the characteristics that are associated with breast cancer.

Figure 10 shows the confusion matrix of the logistic regression classifier.

In this case, there are 1099 correct predictions and 265 erroneous predictions, respectively. This model predicted 572 data as 0 and 527 data as 1. So, this is its correct prediction. However, it also predicted 161 data points to be 0 and 104 data points to be 1. This is an absolutely wrong prediction. In this case, the number of wrong predictions is greater than the random forest. For this reason, the accuracy is less than that of the random forest algorithm.

3.2.3. Support Vector Machine. Figure 11 demonstrates the classification report of the support vector classifier.

Here, support vector machine has achieved 85% accuracy. In this case, this model can correctly identify 85% of the characteristics that are associated with breast cancer.

Figure 12 shows the confusion matrix of the support vector classifier.

There are 1155 correct predictions and 209 false guesses in this case. This model predicted 614 data as 0 and 541 data as 1. So, this is its correct prediction. However, it also predicted 147 data points to be 0 and 62 data points to be 1. This is an absolutely wrong prediction. In this case, the number of wrong predictions is greater than the random forest but lower than the logistic regression. For this reason, the accuracy is less than random forest but greater than logistic regression.

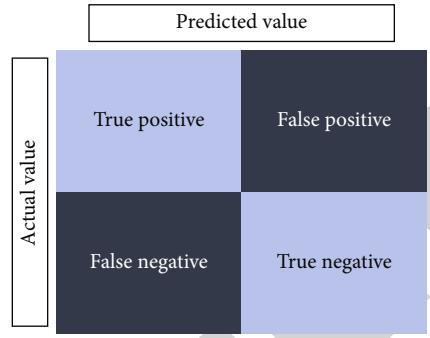

Figure 5: Block diagram of confusion matrix.

3.2.4. Voting Classifier. Figure 13 shows the classification result of the voting classifier.

The voting classifier model can correctly identify 88% of the characteristics that are associated with breast cancer. For this reason, the accuracy is 88%, which is better than logistic regression and support vector machine. A random forest classifier's confusion matrix is shown in Figure 8.

The voting classifier's confusion matrix is shown in Figure 14.

The number of correct forecasts is 1204 while the number of wrong guesses is 160. This model predicted 610 data as 0 and 594 data as 1. So, this is its correct prediction. However, it also predicted 94 data points to be 0 and 66 data points to be 1. This is an absolutely wrong prediction. In this case, the number of wrong predictions is greater than the random forest but lower than logistic regression and support vector machine. For this reason, the accuracy is less than random forest but greater than logistic regression and support vector machine.

3.2.5. Decision Tree Classifier. The classification result of the decision tree classifier is shown in Figure 15.

The decision tree classifier model can correctly identify 89% of the characteristics that are associated with breast cancer. For this reason, the accuracy is 89% which is better than LR, SVM, and voting classifier.

The decision tree classifier's confusion matrix is shown in Figure 16.

The number of correct and false predictions in this case is 1217 and 147, respectively. This model predicted 595 data as 0 and 622 data as 1. So, this is its correct prediction. However, it also predicted 66 data points to be 0 and 81 data points to be 1. This is an absolutely wrong prediction. In this case, the number of wrong predictions is greater than the random forest but lower than logistic regression and support vector machine. For this reason, the accuracy is less than random forest but greater than

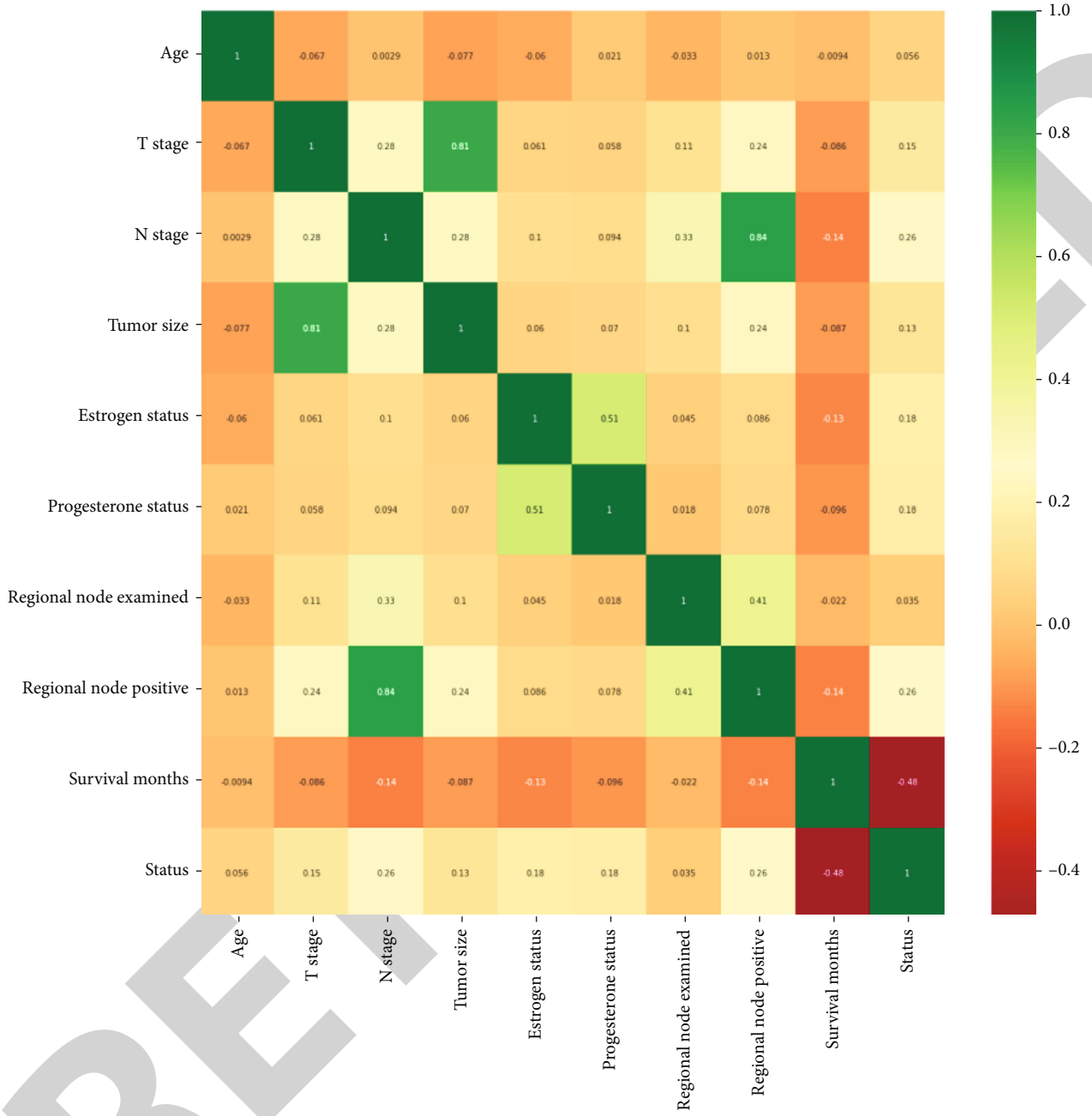

Figure 6: Visualization of feature selection.

```
print(classification_report(y_test,y_pred_rf))
```

	precision	recall	f1-score	support
0	0.94	0.95	0.95	676
1	0.95	0.94	0.95	688
accuracy			0.95	1364
macro avg	0.95	0.95	0.95	1364
weighted avg	0.95	0.95	0.95	1364

Figure 7: Random forest classifier classification report.

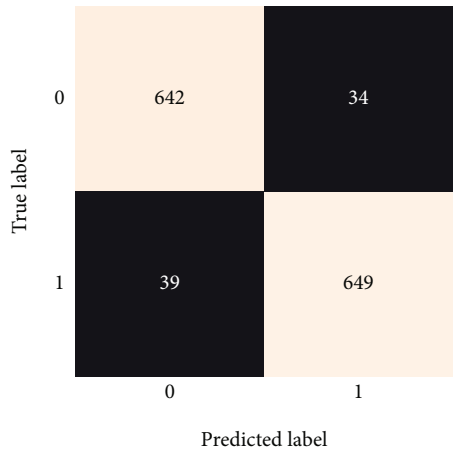

Figure 8: Confusion matrix of random forest classifier.

```
print(classification_report(y_test,y_pred_lr))
```

	precision	recall	f1-score	support
0	0.78	0.85	0.81	676
1	0.84	0.77	0.80	688
accuracy			0.81	1364
macro avg	0.81	0.81	0.81	1364
weighted avg	0.81	0.81	0.81	1364

Figure 9: Classification report of logistic regression classifier.

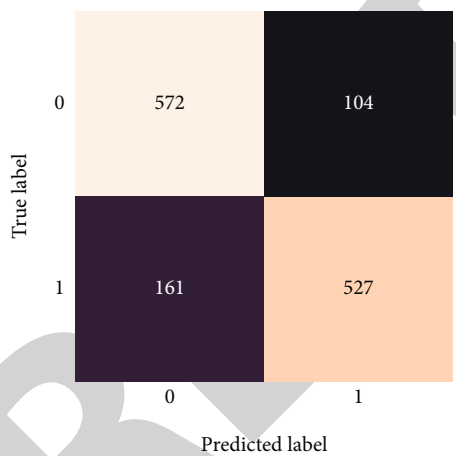

Figure 10: Confusion matrix of logistic regression classifier.

```
[ ]  print(classification_report(y_test,y_pred_svm))
```

	precision	recall	f1-score	support
0	0.81	0.91	0.85	676
1	0.90	0.79	0.84	688
accuracy			0.85	1364
macro avg	0.85	0.85	0.85	1364
weighted avg	0.85	0.85	0.85	1364

Figure 11: Support vector classifier classification report.

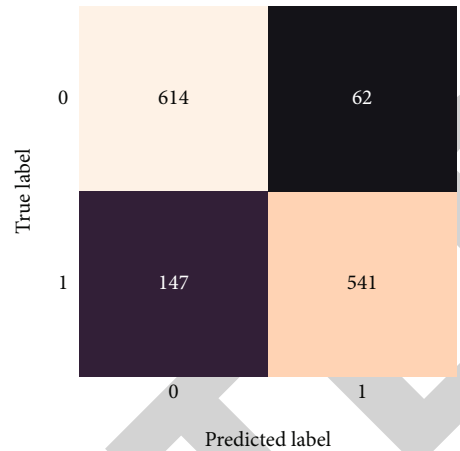

Figure 12: Confusion matrix of support vector classifier.

```
[ ]  y_pred_VC = VC.predict(X_test_s)
     print(classification_report(y_test, y_pred_VC))
```

	precision	recall	f1-score	support
0	0.87	0.90	0.88	676
1	0.90	0.86	0.88	688
accuracy			0.88	1364
macro avg	0.88	0.88	0.88	1364
weighted avg	0.88	0.88	0.88	1364

Figure 13: Voting classifier's classification report.

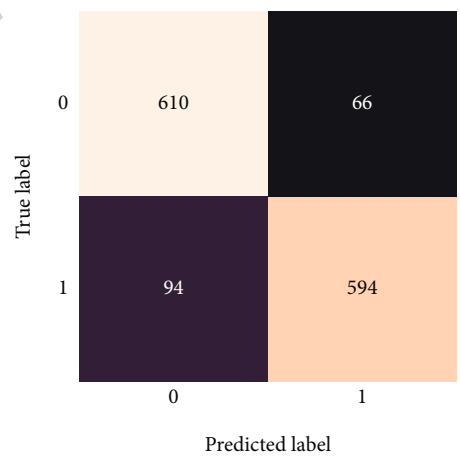

Figure 14: Confusion matrix of voting classifier.

logistic regression, support vector machine, and voting classifier.

3.2.6. Decision K-Nearest Neighbor Classifier. The *K*-nearest neighbor classifier's classification result is shown in Figure 17.

The K-NN model can correctly identify 84% of the characteristics that are associated with breast cancer. For this reason, the accuracy is 84% which is better than with logistic regression.

The K-NN classifier's confusion matrix is shown in Figure 18.

```
y_pred_Clf = Clf.predict(X_test_s)
print(classification_report(y_test, y_pred_Clf))
```

	precision	recall	f1-score	support
0	0.90	0.88	0.89	676
1	0.88	0.90	0.89	688
accuracy			0.89	1364
macro avg	0.89	0.89	0.89	1364
weighted avg	0.89	0.89	0.89	1364

Figure 15: Decision tree classifier classification report.

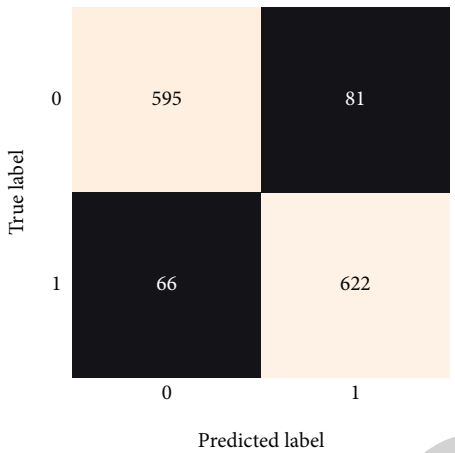

Figure 16: Confusion matrix of decision tree classifier.

```
y_pred_knn = knn.predict(X_test_s)
print(classification_report(y_test, y_pred_knn))
```

	precision	recall	f1-score	support
0	0.82	0.86	0.84	676
1	0.86	0.81	0.84	688
accuracy			0.84	1364
macro avg	0.84	0.84	0.84	1364
weighted avg	0.84	0.84	0.84	1364

Figure 17: Classification report of K-NN classifier.

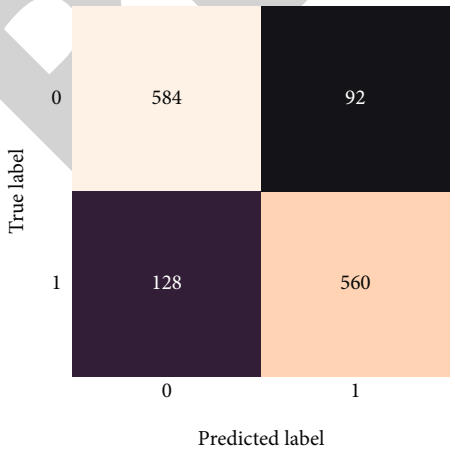

Figure 18: Confusion matrix of K-nearest neighbor classifier.

```
y_pred_grad = grad_model.predict(X_test_s)
print(classification_report(y_test, y_pred_grad))
```

	precision	recall	f1-score	support
0	0.90	0.94	0.92	676
1	0.94	0.90	0.92	688
accuracy			0.92	1364
macro avg	0.92	0.92	0.92	1364
weighted avg	0.92	0.92	0.92	1364

Figure 19: Classification report of gradient boosting classifier.

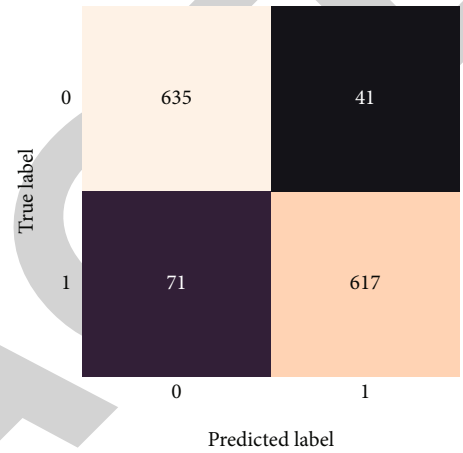

Figure 20: Gradient boosting classifier confusion matrix.

```
y_pred_ada = ada.predict(X_test_s)
print(classification_report(y_test, y_pred_ada))
```

	precision	recall	f1-score	support
0	0.87	0.92	0.89	676
1	0.92	0.86	0.89	688
accuracy			0.89	1364
macro avg	0.89	0.89	0.89	1364
weighted avg	0.89	0.89	0.89	1364

Figure 21: Classification result of AdaBoost classifier.

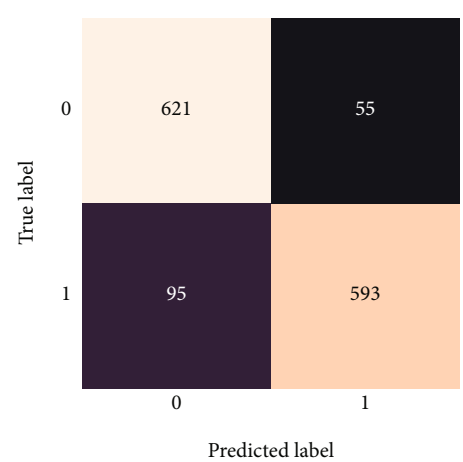

Figure 22: Confusion matrix of AdaBoost classifier.

Table 1: Model comparison.

This paper (model name)	Accuracy (%)	Reference paper (model name)	Accuracy (%)
Random forest	94.64	Ref. [20] voting classifier	87.13
Decision tree	89.22	Ref. [26] decision tree	73.2
K-nearest neighbor	83.87	Ref. [29] *K*-nearest neighbor	85.0
Logistic regression	80.57	Ref. [31] logistic regression	89.2

Here, the number of correct predictions and false predictions is 1144 and 220, respectively. This model predicted 584 data as 0 and 560 data as 1. So, this is its correct prediction. However, it also predicted 128 data points to be 0 and 92 data points to be 1. This is an absolutely wrong prediction. In this case, the number of wrong predictions is greater than the random forest but lower than logistic regression. For this reason, the accuracy is less than random forest but greater than the logistic regression.

3.2.7. Gradient Boosting Classifier. Figure 19 shows the classification result of the GB classifier.

The GB model can correctly identify 92% of the characteristics that are associated with breast cancer. As a result, the accuracy is 92 percent, which is higher than the accuracy of other techniques such as LR, SVM, voting classifier, and K-NN.

Figure 20 depicts the gradient boosting classifier's confusion matrix.

Here, the number of correct predictions and false predictions is 1252 and 112, respectively. This model predicted 635 data as 0 and 617 data as 1. So, this is its correct prediction. However, it also predicted 71 data points to be 0 and 41 data points to be 1. This is an absolutely wrong prediction. In this case, the number of wrong predictions is greater than the random forest. But it achieved the second-highest accuracy among all other algorithms.

3.2.8. AdaBoost Classifier. The classification result of the AdaBoost classifier is shown in Figure 21.

The AdaBoost model can correctly identify 89% of the characteristics that are associated with breast cancer. For this reason, the accuracy is 89% which is equal to the decision tree classifier's result.

The confusion matrix of the AdaBoost classifier is shown in Figure 22.

Here, the number of correct predictions and false predictions is 1214 and 150, respectively. This model predicted 621 data as 0 and 593 data as 1. So, this is its correct prediction. However, it also predicted 95 data points to be 0 and 55 data points to be 1. This is an absolutely wrong prediction. In this case, the number of wrong predictions is greater than the random forest.

3.3. Model Comparison. The models in Table 1 are compared to those in prior research articles. The table demonstrates unequivocally that random forest is the greatest model among the framework's several models. It has a higher *F*1 score, is more precise, has a better evaluation, and has a larger zone under the bend.

According to Table 1, all of the methods have a good level of accuracy. The random forest approach, on the other hand, is a better option because it is more accurate. In this study, the RF method was 94% accurate. The voting classifier was only 87% accurate in [20]. Using the decision tree method, this article got 89.22 percent of the time right, while the authors of [26] got 73.2 percent of the time right.

4. Conclusion

This research used machine learning methods to analyze predictive markers for breast cancer survival. When compared to other algorithms, the random forest approach produced somewhat higher accuracy when evaluating models. In this research, RF, DT, K-NN, SVM, voting classifier, GB classifier, AdaBoost classifier, and LR algorithms achieved 94.64 percent, 89.22 percent, 83.87 percent, 84.67 percent, 88.26 percent, 91.78 percent, 89.0 percent, and 80.57 percent accuracy, respectively. Nonetheless, the accuracy of all the algorithms looked to be near. In this regard, this research established the model's performance and significant factors affecting breast cancer patients' survival rates, which may be used in clinical practice, especially in the Asian scenario. The accuracy % of the models used in this study is significantly greater than in previous research, implying that the models used in this study are more accurate. The random forest technique beats other approaches when cross-validation measures are used to predict breast cancer. The framework models could be improved in the future by adding a larger dataset and machine learning models like majority voting and bagging. This increases the framework's reliability and enhances its presentation. By simply submitting MRI data, the machine learning framework may assist the general community in determining the risk of cancer in adult patients. Ideally, it will aid patients in obtaining early cancer treatment and reclaiming their lives.

Data Availability

The data used to support the findings of this study are freely available at https://http://ieee-dataport.org/open-access/seer-breast-cancer-data.

Conflicts of Interest

The authors declare that they have no conflicts of interest to report regarding the present study.

Acknowledgments

This research was funded by the Deanship of Scientific Research at Taif University, Kingdom of Saudi Arabia, through Taif University Researchers Supporting Project Number TURSP-2020/265.

References

[1] M. A. Mohammed, B. Al-Khateeb, A. N. Rashid, D. A. Ibrahim, M. K. A. Ghani, and S. A. Mostafa, "Neural network and multi-fractal dimension features for breast cancer classification from ultrasound images," *Computers & Electrical Engineering*, vol. 70, pp. 871–882, 2018.

[2] M. M. Y. Al-Hashimi and X. J. Wang, "Breast cancer in Iraq, incidence trends from 2000-2009," *Asian Pacific Journal of Cancer Prevention*, vol. 15, no. 1, pp. 281–286, 2014.

[3] B. M. Gayathri, C. P. Sumathi, and T. Santhanam, "Breast cancer diagnosis using machine learning algorithms–a survey," *International Journal of Distributed and Parallel Systems (IJDPS)*, vol. 4, no. 3, pp. 105–112, 2013.

[4] P. Meesad and G. G. Yen, "Combined numerical and linguistic knowledge representation and its application to medical diagnosis," *IEEE Transactions on Systems, Man, and Cybernetics-Part A: Systems and Humans*, vol. 33, no. 2, pp. 206–222, 2003.

[5] S. A. Pavlopoulos and A. N. Delopoulos, "Designing and implementing the transition to a fully digital hospital," *IEEE Transactions on Information Technology in Biomedicine*, vol. 3, no. 1, pp. 6–19, 1999.

[6] International Agency for Research on Cancer, "GLOBOCAN 2008: cancer incidence and mortality worldwide," 2008, http://www.iarc.fr/en/media-centre/iarcnews/2010/globocan2008.php.

[7] A. F. Uddin, Z. J. Khan, J. Islam, and A. Mahmud, "Cancer care scenario in Bangladesh," *South Asian Journal of Cancer*, vol. 2, no. 2, pp. 102–104, 2013.

[8] A. D. Shrestha, D. Neupane, P. Vedsted, and P. Kallestrup, "Cervical cancer prevalence, incidence and mortality in low and middle income countries: a systematic review," *Asian Pacific Journal of Cancer Prevention*, vol. 19, no. 2, pp. 319–324, 2018.

[9] N. B. Pathy, H. M. Verkooijen, E. Y. Tan et al., "Trends in presentation, management and survival of patients with *de novo* metastatic breast cancer in a Southeast Asian setting," *Scientific Reports*, vol. 5, no. 1, article 16252, 2015.

[10] C. H. Yip, N. B. Pathy, C. S. Uiterwaal et al., "Factors affecting estrogen receptor status in a multiracial Asian country: an analysis of 3557 cases," *Breast*, vol. 20, pp. S60–S64, 2011.

[11] C. H. Ng, N. B. Pathy, N. A. Taib, G. F. Ho, K. S. Mun, A. Rhodes et al., "Do clinical features and survival of single hormone receptor positive breast cancers differ from double hormone receptor positive breast cancers?," *Asian Pacific Journal of Cancer Prevention*, vol. 15, no. 18, pp. 7959–7964, 2014.

[12] C. B. Pearce, R. Gunn, A. Ahmed, and C. D. Johnson, "Machine learning can improve prediction of severity in acute pancreatitis using admission values of APACHE II score and C-reactive protein," *Pancreatology*, vol. 6, no. 1-2, pp. 123–131, 2006.

[13] B. Eftekhar, K. Mohammad, H. E. Ardebili, M. Ghodsi, and E. Ketabchi, "Comparison of artificial neural network and logistic regression models for prediction of mortality in head trauma based on initial clinical data," *BMC Medical Informatics and Decision Making*, vol. 5, no. 1, p. 3, 2005.

[14] T. Verplancke, S. Van Looy, D. Benoit et al., "Support vector machine versus logistic regression modeling for prediction of hospital mortality in critically ill patients with haematological malignancies," *BMC Medical Informatics and Decision Making*, vol. 8, no. 1, p. 56, 2008.

[15] M. Khalilia, S. Chakraborty, and M. Popescu, "Predicting disease risks from highly imbalanced data using random forest," *BMC Medical Informatics and Decision Making*, vol. 11, no. 1, p. 51, 2011.

[16] C. S. Son, B. K. Jang, S. T. Seo, M. S. Kim, and Y. N. Kim, "A hybrid decision support model to discover informative knowledge in diagnosing acute appendicitis," *BMC Medical Informatics and Decision Making*, vol. 12, no. 1, p. 17, 2012.

[17] P. Melillo, A. Orrico, M. Attanasio et al., "A pilot study for development of a novel tool for clinical decision making to identify fallers among ophthalmic patients," *BMC Medical Informatics and Decision Making*, vol. 15, no. S3, p. S6, 2015.

[18] Y. Chen, W. Cao, X. Gao, H. Ong, and T. Ji, "Predicting postoperative complications of head and neck squamous cell carcinoma in elderly patients using random forest algorithm model," *BMC Medical Informatics and Decision Making*, vol. 15, no. 1, p. 44, 2015.

[19] J. Wei, J. Wang, Y. Zhu, J. Sun, H. Xu, and M. Li, "Traditional Chinese medicine pharmacovigilance in signal detection : decision tree-based data classification," *BMC Medical Informatics and Decision Making*, vol. 18, no. 1, p. 19, 2018.

[20] M. Huber, C. Kurz, and R. Leidl, "Predicting patient-reported outcomes following hip and knee replacement surgery using supervised machine learning," *BMC Medical Informatics and Decision Making*, vol. 19, no. 1, p. 3, 2019.

[21] G. Sudhamathy, M. Thilagu, and G. Padmavathi, "Comparative analysis of R package classifiers using breast cancer dataset," *International Journal of Engineering & Technology*, vol. 8, pp. 2127–2136, 2016.

[22] W. Chen, X. Xie, J. Wang et al., "A comparative study of logistic model tree, random forest, and classification and regression tree models for spatial prediction of landslide susceptibility," *Catena*, vol. 151, pp. 147–160, 2017.

[23] D. Muchlinski, D. Siroky, J. He, and M. Kocher, "Comparing random forest with logistic regression for predicting class-imbalanced civil war onset data," *Political Analysis*, vol. 24, no. 1, pp. 87–103, 2016.

[24] Y. Dong, B. Du, L. Zhang, and S. Member, "Target detection based on random forest metric learning," *IEEE Journal of Selected Topics in Applied Earth Observations and Remote Sensing*, vol. 8, no. 4, pp. 1830–1838, 2015.

[25] E. Mosca, R. Alfieri, I. Merelli, F. Viti, A. Calabria, and L. Milanesi, "A multilevel data integration resource for breast cancer study,," *BMC Systematic Biology*, vol. 4, no. 1, p. 76, 2010.

[26] R. Genuer, J. M. Poggi, and C. Tuleau-Malot, "An R package for variable selection using random forests," *The R Journal*, vol. 7, no. 2, pp. 19–33, 2015.

[27] F. Amato, A. Lopez, E. M. Pena-mendez, P. Vanhara, and A. Hampl, "Artificial neural networks in medical diagnosis," *Journal of Applied Biomedicine*, vol. 11, no. 2, pp. 47–58, 2013.

[28] S. I. R. H. Atkins, J. L. Hayward, D. J. Klugman, and A. B. Wayte, "Treatment of early breast cancer: a report after ten

Hindawi
Computational and Mathematical Methods in Medicine
Volume 2023, Article ID 9785034, 1 page
https://doi.org/10.1155/2023/9785034

Retraction

Retracted: lncRNA GHET1 Promotes the Progression of Triple-Negative Breast Cancer via Regulation of miR-377-3p/GRSF1 Signaling Axis

Computational and Mathematical Methods in Medicine

Received 27 June 2023; Accepted 27 June 2023; Published 28 June 2023

This article has been retracted by Hindawi following an investigation undertaken by the publisher [1]. This investigation has uncovered evidence of one or more of the following indicators of systematic manipulation of the publication process:

(1) Discrepancies in scope

(2) Discrepancies in the description of the research reported

(3) Discrepancies between the availability of data and the research described

(4) Inappropriate citations

(5) Incoherent, meaningless and/or irrelevant content included in the article

(6) Peer-review manipulation

The presence of these indicators undermines our confidence in the integrity of the article's content and we cannot, therefore, vouch for its reliability. Please note that this notice is intended solely to alert readers that the content of this article is unreliable. We have not investigated whether authors were aware of or involved in the systematic manipulation of the publication process.

Wiley and Hindawi regrets that the usual quality checks did not identify these issues before publication and have since put additional measures in place to safeguard research integrity.

We wish to credit our own Research Integrity and Research Publishing teams and anonymous and named external researchers and research integrity experts for contributing to this investigation.

The corresponding author, as the representative of all authors, has been given the opportunity to register their agreement or disagreement to this retraction. We have kept a record of any response received.

References

[1] Y. Wang and C. Li, "lncRNA GHET1 Promotes the Progression of Triple-Negative Breast Cancer via Regulation of miR-377-3p/GRSF1 Signaling Axis," *Computational and Mathematical Methods in Medicine*, vol. 2022, Article ID 8366569, 15 pages, 2022.

Hindawi
Computational and Mathematical Methods in Medicine
Volume 2022, Article ID 8366569, 15 pages
https://doi.org/10.1155/2022/8366569

Research Article

lncRNA GHET1 Promotes the Progression of Triple-Negative Breast Cancer *via* Regulation of miR-377-3p/GRSF1 Signaling Axis

Yu Wang and Chen Li

Molecular Testing Center, The First Affiliated Hospital of Jinzhou Medical University, Jinzhou, Liaoning Province 121000, China

Correspondence should be addressed to Chen Li; lichenxuna@126.com

Received 25 January 2022; Revised 22 March 2022; Accepted 11 April 2022; Published 25 April 2022

Academic Editor: Muhammad Zubair Asghar

Objective. This study is aimed at investigating the role of lncRNA GHET1 in the progression of triple-negative breast cancer (TNBC). *Methods*. Tumor tissues and paracancerous tissues (normal) of TNBC patients were collected. Human normal breast cells (MCF10A) and TNBC cells (MDA-MB-468 and HCC1937) were employed for *in vitro* analysis. The expression of lncRNA GHET1, miR-377-3p, and GRSF1 was detected by qRT-PCR. The lncRNA GHET1 and miR-377-3p were overexpressed or knocked down in the TNBC cells, respectively. To determine the specific biological activities of the TNBC cells, MTT, flow cytometry, and wound healing assay were adopted to evaluate the cellular proliferation, apoptosis, and migration abilities, respectively. MMP-9 and MMP-2 protein expression levels were detected as well by Western blot in the cells. The relationship between miR-377-3p and lncRNA GHET1, miR-377-3p, and GRSF1 was validated using dual-luciferase reporter assay. *Results*. lncRNA GHET1 was significantly upregulated in the TNBC patients' tissues and the TNBC cell lines. Overexpression of lncRNA GHET1 significantly increased the proliferation and migration ability, but decreased apoptosis in the TNBC cells. Additionally, overexpression of lncRNA GHET1 upregulated both MMP-9 and MMP-2 protein expression levels. Correlation analysis found that miR-377-3p had a positive relationship with GRSF1, but had a negative relationship with lncRNA GHET1. miR-377-3p mimic attenuated the effects of lncRNA GHET1 on cellular proliferation, apoptosis, and migration of the TNBC cells. *Conclusion*. lncRNA GHET1 promotes TNBC progression through the miR-377-3p/GRSF1 signaling axis.

1. Introduction

Breast cancer (BC) is the most prevalent cancer, becoming the leading cause of cancer death among women worldwide. The American Cancer Society estimated that there were 42,260 BC deaths and 27, 1270 new BC cases in 2019, accounting for about 30% of all female cancer diagnoses [1]. This cancer is divided into five different subgroups based on histological features and molecular biological techniques. Among them, 15%-20% cases belong to triple-negative breast cancer (TNBC). TNBC diagnostic features are negative expression of estrogen receptor (ER), progesterone receptor (PR), and human epidermal growth factor receptor 2 (HER2) [2]. Clinically, it is characterized as high invasiveness and high rates of metastasis, recurrence, and mortality. TNBC frequently metastasizes to internal organs and brain at an early stage; however, it is usually diagnosed at a late stage [3]. The median overall survival of the metastatic TNBC is less than 1 year, whether or not accepting the intensive systemic chemotherapy [4]. Despite significant improvements in BC therapy, the clinical management of TNBC remains challenging compared to the other subtypes because of its aggression and lack of specific targeted therapies [5]. Current clinical treatment options for TNBC are restricted to surgery, radiotherapy, and chemotherapy. Although some studies have shown that TNBC patients are more sensitive to anthracycline-based chemotherapy

regimens, the overall survival rate is still low [6]. Therefore, development of specific treatments to prevent and treat BC metastasis is currently a critical aspect of BC research.

Among the new and potentially useful biomarkers, abnormal expression of noncoding RNAs (ncRNAs) has a close relation to TNBC occurrence and progression [7]. Long noncoding RNAs (lncRNAs) are a class of ncRNAs over 200 nucleotides in length, which are believed to be dysregulated in various cancers (breast, ovarian, and others) [8]. Misregulation and mutations of lncRNAs involve tumor pathogenesis. Alterations or mutations of some lncRNA levels could induce tumor growth or metastasis. lncRNAs may appear oncogenic or tumor-suppressive activity. In addition, because of the characteristics of their tissue-specific distribution, lncRNAs may be applied as novel biomarkers for cancer therapy as well [9]. Many dysregulated lncRNAs have been proved to significantly affect TNBC. For example, Zheng et al. found that lncRNA GAS5 could target miR-378a-5p/SUFU to promote TNBC cell apoptosis and regulate the sensitivity of the cancer cells to chemotherapeutic agents [10]. In a study by Wang et al., lncRNAs could regulate TNBC development through the formation of encoded small peptides, such as LINC00908-encoded polypeptide ASRPS, to reduce angiogenesis [11]. In addition, lncRNAs can also control expression levels of their target genes *in cis* or *in trans via* interacting with transcription factors or histone-modifying enzymes. For instance, binding of lncRNA DANCR and RXRA could increase RXRA serine 49/78 phosphorylation and subsequent activate PI3K/Akt signaling, ultimately affecting TNBC cell proliferation [12]. However, there are still many related lncRNAs that have not been explored. It has previously been pointed out that in a hypoxic environment, lncRNA GHET1 can promote TNBC glycolysis, proliferation, and invasion via the Hippo/YAP pathway [13]. However, the role of this lncRNA in TNBC has not been comprehensively elucidated. We therefore attempted to carry out further research.

miRNAs are also a kind of ncRNAs, containing only 20-24 nucleotides [14]. Many of them play a key role in the development and progression of cancers, such as miR-377-3p. Previous study shows that miR-337-3p serves as a tumor suppressor gene in a variety of cancers. Although it has been demonstrated that Linc00339 promotes TNBC progression through the miR-377-3p/HOXC6 signaling pathway [15], the detail mechanism is still uncovered. It is also not allowed to ignore that lncRNAs act as a sponge for miRNAs. Therefore, we try to interrogate what is the relationship between lncRNAs GHET1 and miR-377-3p and what are the effects of them on TNBC, to provide new biomarkers and therapeutic targets of TNBC.

2. Materials and Methods

2.1. Clinical Samples. 20 tumor tissue samples were collected from the patients with luminal A TNBC without any chemotherapy who received surgical section treatment in our hospital between January 2020 and March 2021. The central parts of the tissue were applied as TNBC samples, and the peripheral tissues of the mass were used as normal control tissue. The samples were identified as TNBC tissues by three independent pathologists. This study had obtained informed consent from each patient and an approval from the Ethics Committee of the First Affiliated Hospital of Jinzhou Medical University (KYLL202123).

Table 1: Primer sequences.

RNA	Sequences (5′ to 3′)
lncRNA GHET1	F: CAACAAAGCAGGTAAACATTGG
	R: GCAAAGGCAGAGTGAAAGGT
miR-377-3p	F: ATCACACAAAGGCAACTTTTGT
	R: GGTGCAGGGTCCGAGGTAT
GRSF1	F: TGGAGTCAGAGCAGGATGTGCA
	R: GGCGAAGATTTGACCTGCAAGC
GAPDH	F: GTCTCCTCTGACTTCAACAGCG
	R: ACCACCCTGTTGCTGTAGCCAA
U6	F: CTCGCTTCGGCAGCACA-3′
	F: AACGCTTCACGAATT TGCGT-3′

F: forward primer; R: reverse primer.

2.2. Cell Culture. TNBC cells (MDA-MB-468 and HCC1937) and human normal breast cells (MCF10A) were provided by the American Type Culture Collection (ATCC, Manassas, VA, USA). The cells were cultured in a complete DMEM containing 10% fetal bovine serum (FBS) (Gibco, EI Paso, Texas, USA), 100 mg/mL penicillin, and 10 mg/mL streptomycin in an incubator with 5% CO_2 at 37°C.

2.3. Cell Transfection. lncRNA GHET1 overexpression plasmid (GHET1), shRNA scramble (sh-NC), lncRNA GHET1 shRNA (sh-GHET1), mimic scramble (NC mimics), miR-377-3p overexpression plasmid (miR-377-3p mimics), miR-377-3p inhibitor (miR-377-3p inhibitor), and inhibitor NC were constructed by GenePharma (Shanghai, China). The plasmids of these constructions were transfected into MDA-MB-468 and HCC1937 cells, respectively, by using Lipofectamine 2000 transfection kit (Sigma-Aldrich, St. Louis, MO, USA). The transfection medium was replaced by complete medium 6 h later, and subsequent experiments were performed after 48 h of the transfection.

2.4. qRT-PCR. The nucleus and cytoplasm were extracted by using a Nuclear and Cytoplasmic Extraction Kit (Thermo Fisher Scientific, Waltham, MA, USA). TRizol method (Thermo Fisher Scientific) was employed for RNA extraction from the nucleus, cytoplasm, whole cells, or tissues. The concentration and purity of the extracted RNA was then analyzed by a NanoDrop-based detection. The RNA was then reverse transcribed into cDNA by using a Reverse Transcriptase Kit (Zomanbio, Beijing, China). lncRNA GHET1, miR-377-3p, or GRSF1 was amplified with the cDNA by using a SYBR GREEN kit (TaKaRa, Tokyo, Japan). The primers of the lncRNAs GHET1, miR-377-3p, and GRSF1 are listed in Table 1. Six replicates were set up for each experiment. U6 or GAPDH was applied as internal

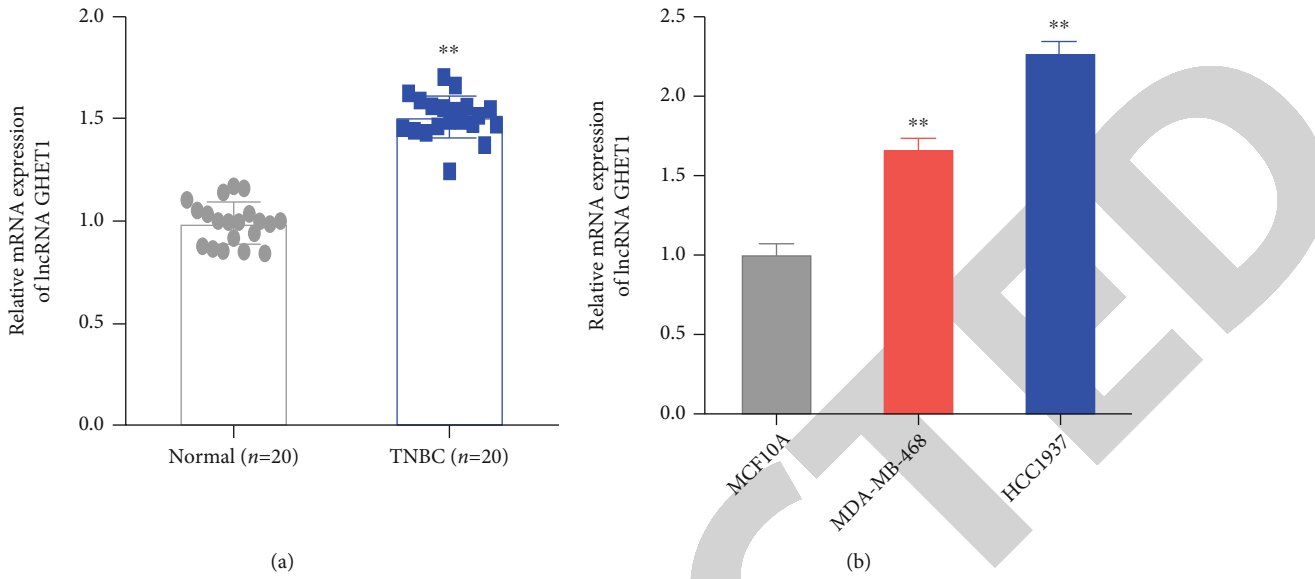

Figure 1: lncRNA GHET1 expression is increased in TNBC. qRT-PCR-based measurement of lncRNA GHET1 expression in tissues ((a) $^{**}P < 0.01$ *vs.* the normal group) and in indicated cells ((b) $^{**}P < 0.01$ *vs.* the MCF10A group).

reference controls. Quantification of the target gene relative expression was analyzed by the $2^{-\Delta\Delta Ct}$ method.

2.5. MTT Assay. MDA-MB-468 or HCC1937 cells were seeded in 96-well plates (5000 cells/well) for 24 h. The cells were stained with 20 μL of 5 mmol/L MTT for 4 h in a 37°C incubator. After that, 150 μL of DMSO was added to melt the cells for 15 min. Finally, the viability rate was detected by OD 450 nm measurement.

2.6. Apoptosis Assay. The Annexin V-FITC/PI Apoptosis Detection Kit (Yeasen, Shanghai, China) was employed to do the apoptosis assay. MDA-MB-468 cells or HCC1937 cells to be detected were collected into a centrifuge tube, twice rinsed with precooled sterile PBS, and adjusted to 5×10^5 cells/mL. Subsequently, 200 μL of the cell suspension, 10 μL of Annexin V-FITC, and 10 μL of 20 mg/L PI solution (all from the kit) were mixed and incubated at avoiding light condition at room temperature for 10 min, followed by dilution with 500 μL of the PBS. The apoptotic rate was detected by a FACSCalibur flow cytometer (BD Biosciences, CA, USA).

2.7. Wound Healing Assay. Treated cells were seeded into 6-well plates and cultured until confluence. A 10 μL sterile tip was applied to scratch the cells to create a wound field. After removing the cellular debris and detached cells by PBS, fresh serum-free medium was added for 24 h culture. The migrated cells on the scratched area were photographed under an inverted microscope. ImageJ software was used to calculate the migrated area from the original scratched wound area.

2.8. Western Blotting. The protein concentration of the cellular or tissue lysate was detected with a BCA Protein Assay Kit (Beyotime, Shanghai, China). Each 20 μg of the samples to be detected was boiled in 1x Loading Buffer (Beyotime) and cooled on an ice box, loaded and separated on a SDS-PAGE, and transferred to a PVDF membrane for 1 h. The membrane was then blocked with 5% nonfat dry milk for 1 h, incubated with corresponding primary antibody overnight at 4°C, triplicate rinsed with 1x TBS-T buffer (Beyotime), continue reacted with corresponding secondary antibody for 1 h, and triplicate washed with TBS-T again. For protein development, Chemiluminescence Reagents (Beyotime) were dropped on the membrane for 1 min. The acquisition of images was completed using a Gel Imaging System (Thermo Fisher, Waltham, MA, USA). Densitometry of the target protein bands was analyzed by the ImageJ software. GAPDH was applied as an internal reference to calculate the relative protein expression.

2.9. Dual-Luciferase Reporter Assay. 293T cells (ATCC) were transfected with NC mimics/miR-377-3p mimics and dual-luciferase reporter vectors of lncRNA GHET1 wild type (WT-GHET1)/mutant (MUT-GHET1) or GRSF1 wild type (WT-GRSF1)/mutant (MUT-GRSF1), respectively. Firefly and Renilla luciferase activities were measured 48 h later using a dual-luciferase reporter assay system (CAS: E1910, Promega, Madison, Wisconsin, USA). The luciferase activity was recorded with a GloMax 96 Microplate Fluorometer (Promega).

2.10. Statistical Analysis. SPSS 26.0 was used for statistical analysis. One-way analysis of variance and independent sample *t*-test analysis were employed for comparison among multiple groups and between two groups, respectively. The results were expressed as mean ± standard deviation (SD). Further, Pearson correlation was used to analyze the expression correlation between two parameters in tissue samples. $P < 0.05$ served as the cutoff value of a significant difference.

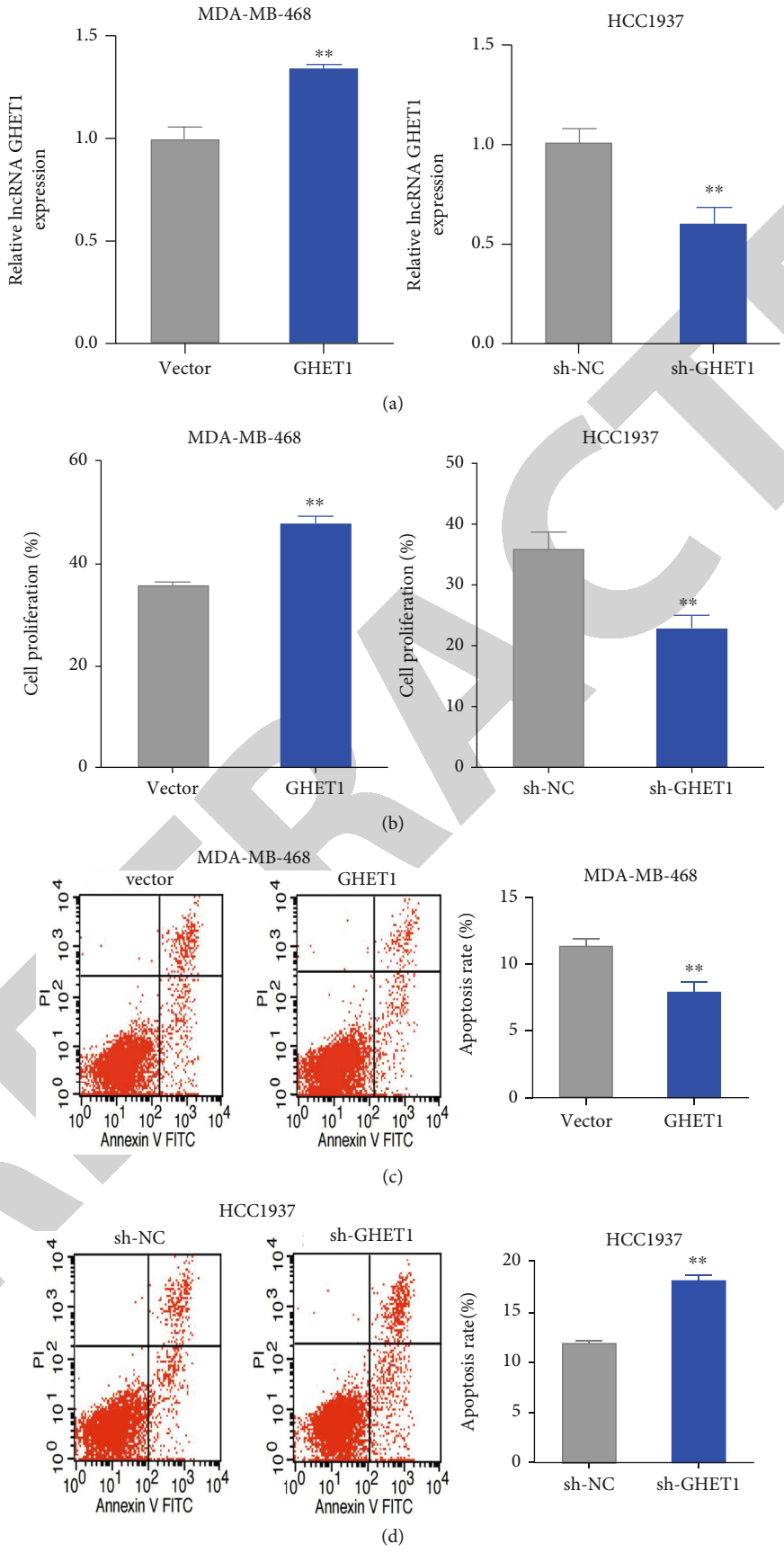

Figure 2: Continued.

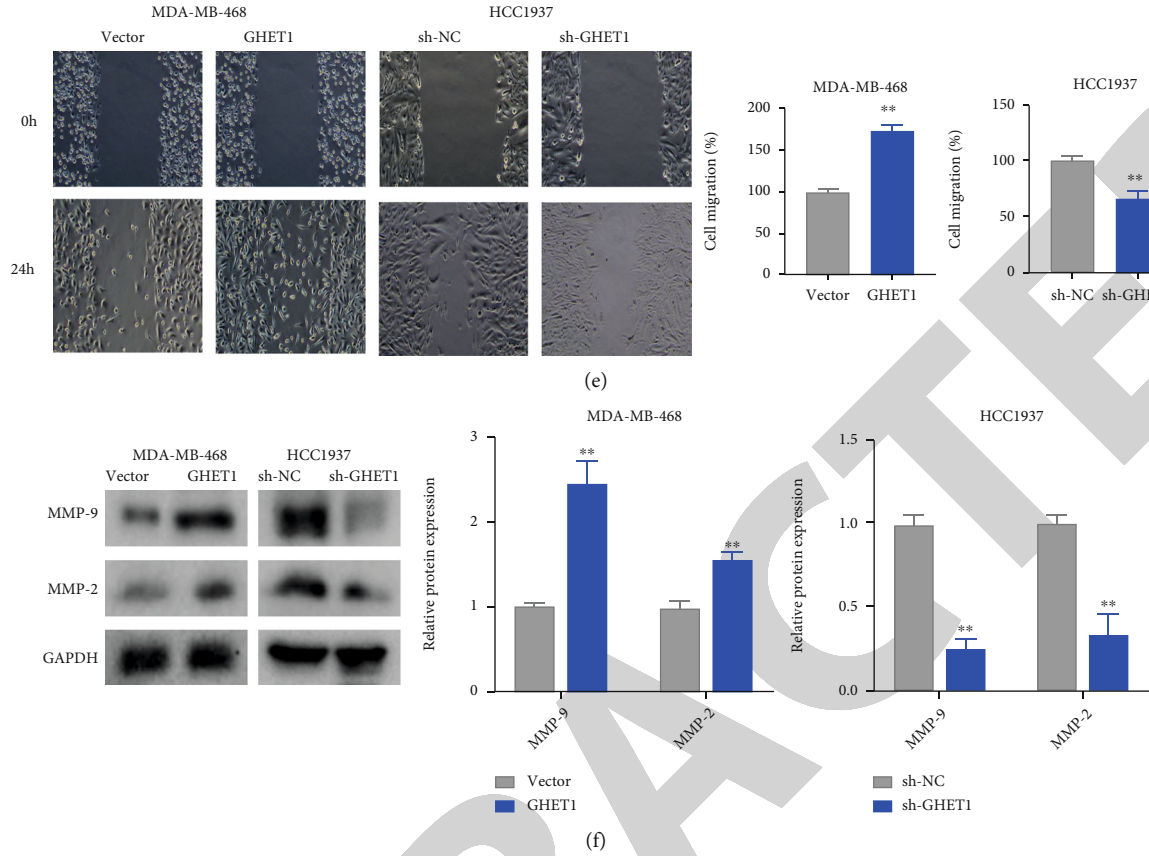

Figure 2: Oncogenic activity of lncRNA GHET1 in TNBC cells. (a) lncRNA GHET1 expression was analyzed by qRT-PCR in the lncRNA GHET1 overexpressed (GHET1) MDA-MB-168 and knocked down (sh-GHFT1) HCC1937 cells. (b) Cellular proliferation was detected by MTT assay in the indicated cells. Cellular apoptosis was analyzed by flow cytometry in the (c) MDA-MB-468 and (d) HCC1937 cells. (e) Cellular migration was evaluated by wound healing assay in the indicated cells. (f) Protein expression levels of MMP-9 and MMP-2 were detected by Western blot in the indicated cells, $^{**}P < 0.01$ vs. the vector/sh-NC group. Each data came from independent triplicate assays.

3. Results

3.1. The Expression of lncRNA GHET1 Is Significantly Upregulated in TNBC. According to qRT-PCR results regarding lncRNA GHET1 expression in TNBC, we found that the lncRNA was significantly increased in the TNBC tissue (Figure 1(a)), as well as in HCC1937 and MDA-MB-468 cells (Figure 1(b)). At the cellular level, lncRNA GHET1 showed the highest expression at TNBC cell HCC1937. These results suggested that lncRNA GHET1 might play a role in TNBC oncogenes.

3.2. lncRNA GHET1 Promotes the Malignant Process of TNBC Cells. To validate the role of lncRNA GHET1 in TNBC development, the lncRNA was overexpressed in MDA-MB-468 cells and knocked down in HCC1937. The efficacy of the overexpression and knockdown was checked by qRT-PCR (Figure 2(a)). MTT assay for cell proliferation, flow cytometry for apoptosis, and wound healing assay for migration ability found that lncRNA GHET1 overexpression has an oncogenic activity to remarkably increase the cellular proliferation and migration and obviously decrease the apoptosis, while knockdown of the lncRNA GHET1 caused the opposite changes (Figures 2(b)–2(e)). Further examination of the protein expression of matrix metalloproteinases 9 (MMP-9) and 2 (MMP-2) showed that the protein expression levels of MMP-9 and MMP-2 were significantly increased after overexpression of the lncRNA GHET1 in the cells, but decreased after its knockdown (Figure 2(f)), indicating that both MMP-9 and MMP-2 were closely related to tumor migration. The results above indicated that lncRNA GHET1 was involved in the oncogenes of TNBC.

3.3. lncRNA GHET1 Acts as a miR-377-3p Sponge in TNBC. The detailed mechanism by which lncRNA GHET1 affects TNBC progression was further investigated. Analysis of subcellular distribution of the lncRNA GHET1 showed that it was mainly distributed in the cytoplasm (Figure 3(a)). Interestingly, ENCORI (https://starbase.sysu.edu.cn/) prediction revealed a binding site of lncRNA GHET1 and miR-377-3p. It was verified by dual-luciferase assay that miR-377-3p overexpression reduced the fluorescence intensity of lncRNA WT-GHET1 without affecting that of MUT-GHET1-MUT (Figure 3(b)).

Noticeably, miR-377-3p level was significantly decreased in TNBC tissues (Figure 3(c)). Subsequent detection revealed that overexpression of lncRNA GHET1 declined the miR-377-3p level. However, knockdown of lncRNA GHET1

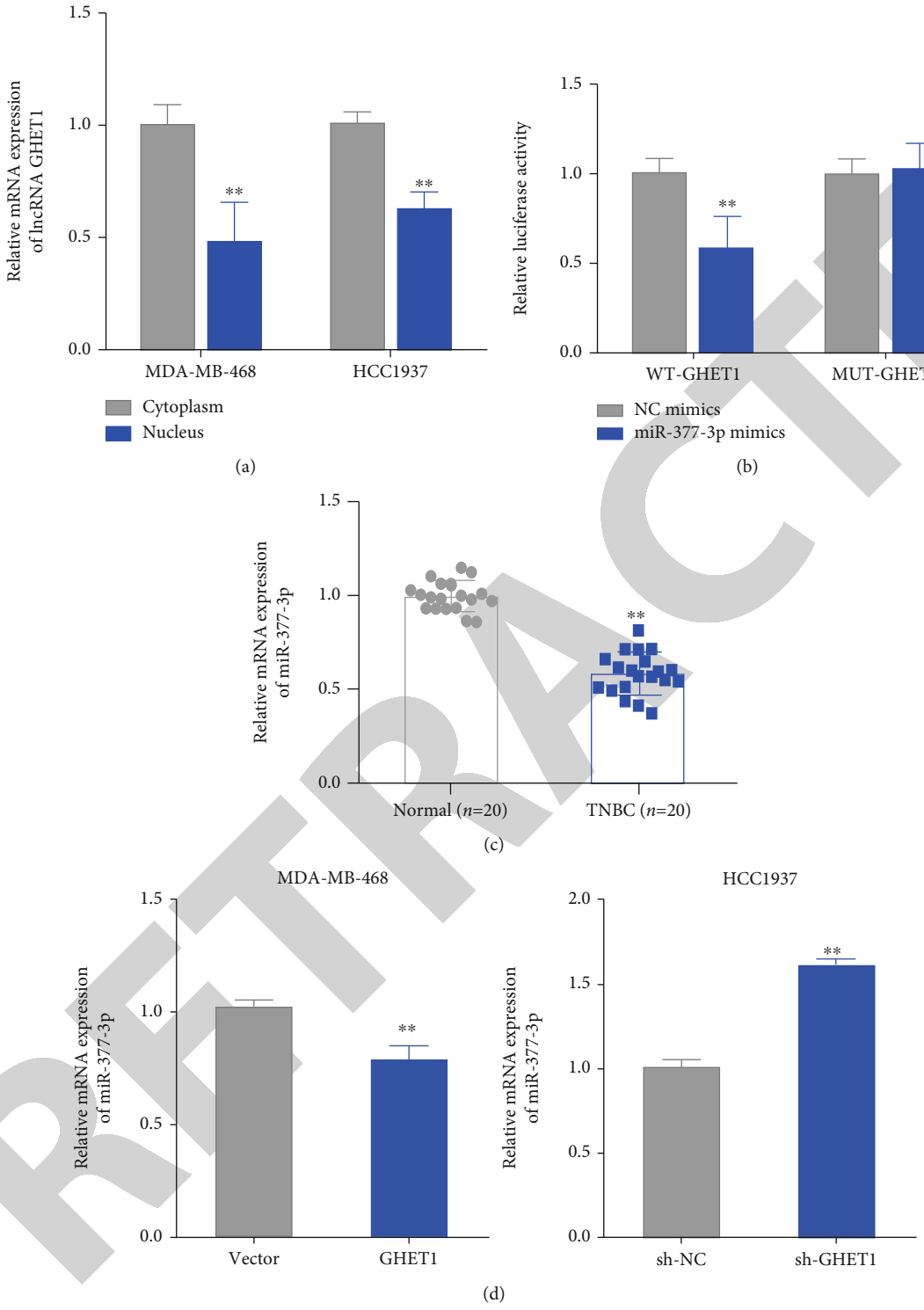

Figure 3: Continued.

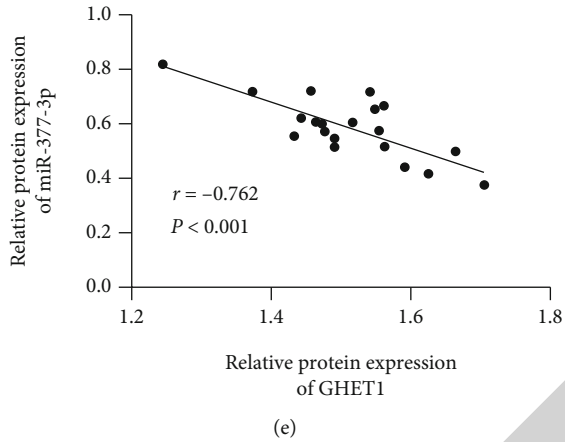

(e)

Figure 3: Relationship between lncRNA GHET1 and miR-377-3p in TNBC. (a) Cellular distribution of lncRNA GHET1 was analyzed by qRT-PCR-based measurement in the nucleus (blue) or cytoplasm (grey). $^{**}P < 0.01$ *vs.* the cytoplasm group. (b) The relationship between lncRNA GHET1 and miR-377-3p was analyzed by dual-luciferase reporter gene assay in the indicated groups. $^{**}P < 0.01$ *vs.* the NC mimic group. miR-377-3p expression was detected by qRT-PCR in the TNBE tissues; peripheral tissues of the mass were used as (c) negative control (normal) and (d) indicated TNBC cells. $^{**}P < 0.01$ *vs.* the normal group *vs.* the vector/sh-NC group. (e) The correlation between lncRNA GHET1 and miR-377-3p expression was analyzed by the Pearson correlation method in the TNBC tissues. Each data in (a–d) represented the average of three independent assays.

significantly elevated the miR-377-3p level (Figure 3(d)). Correlation analysis showed a negative correlation between the lncRNA GHET1 and miR-377-3p (Figure 3(e)). Collectively, lncRNA GHET1 targeted to miR-377-3p in TNBC.

3.4. Knockdown of miR-377-3p Reversed the Effect of lncRNA GHET1 Knockdown on TNBC Cells. To validate the role of the interaction of lncRNA GHET1 and miR-377-3p in TNBC, we performed rescue experiments. TNBC cells were treated with simultaneous overexpression or knockdown of either lncRNAs GHET1 or miR-377-3p. The biological performance of cells was then measured. According to the results, lncRNA GHET1 mimics (GHFT1) significantly upregulated GRSF1 protein expression, cellular proliferation, and migration, but decreased cellular apoptosis in the MDA-MB-468 cells. However, such alterations were obviously reversed by GHET1+miR-377-3p mimic overexpression in the HCC1937 cells. Furthermore, sh-lncRNA GHET significantly reduced GRSF1 protein expression and cellular proliferation and migration, but promoted apoptosis. Interestingly, transfection with both sh-lncRNA GHET and miR-377-3p inhibitor successfully reversed the alteration patterns induced by sh-GHFT1 (Figures 4(a)–4(d)). Collectively, knockdown of miR-377-3p restored the lncRNA GHET knockdown-induced inhibitory effect on the malignant progression of TNBC cells.

3.5. GRSF1 Was a Target Gene of miR-377-3p. To further investigate the antioncogenic mechanism of miR-377-3p, we used the TargetScan program (http://www.TargetScan.org/vert_72/) to predict the target genes of miR-377-3p, which found an interaction site between miR-377-3p and GRSF1 (Figure 5(a)). Further, miR-377-3p overexpression significantly inhibited the fluorescence intensity of WT-GRSF1. However, it did not affect MUT-GRSF1 fluorescence intensity by the dual-luciferase reporter assay (Figure 5(a)), demonstrating that there was an interaction between miR-377-3p and GRSF1.

GRSF1 expression was found to be significantly increased in TNBC tissues by qRT-PCR (Figure 5(b)). Both the mRNA and protein expression of GRSF1 was upregulated by miR-377-3p inhibitor. However, miR-377-3p mimic obviously decreased the expression levels of GRSF1 in the TNBC cells (Figures 5(c)–5(e)). Correlation analysis also showed a negative correlation between GRSF1 and miR-377-3p (Figure 5(f)).

The regulation of GRSF1 by lncRNA GHET1 was subsequently investigated as well. The results showed that lncRNA GHET1 mimic significantly increased GRSF1 expression in the TNBC cells, while knockdown of lncRNA GHET1 led to a decreased expression of GRSF1 (Figure 5(g)). Correlation analysis also indicated a positive relationship between GRSF1 and lncRNA GHET1 (Figure 5(h)). Collectively, GRSF1 was a target gene of miR-377-3p, and lncRNA GHET1 could regulate miR-377-3p/GRSF1 to affect the process of TNBC.

4. Discussion

TNBC is an aggressive subtype of BC, and its progression is attributed to a variety of oncogenes and tumor suppressor genes. A full understanding of molecular events and identification of critical biomarkers can improve the efficacy of TNBC therapy [16]. In recent years, increasing evidence strongly supports the involvement of lncRNAs in the pathogenesis and progression of human cancers [17]. In order to develop new cancer treatments, the functions and mechanisms of lncRNAs require further investigation. lncRNA GHET1 has been shown to be a key regulatory molecule in the development of many cancers. Zhu et al. found that lncRNA GHET1 also enhanced the proliferation of prostate cancer cells through activation of HIF-1α/Notch-1 signaling

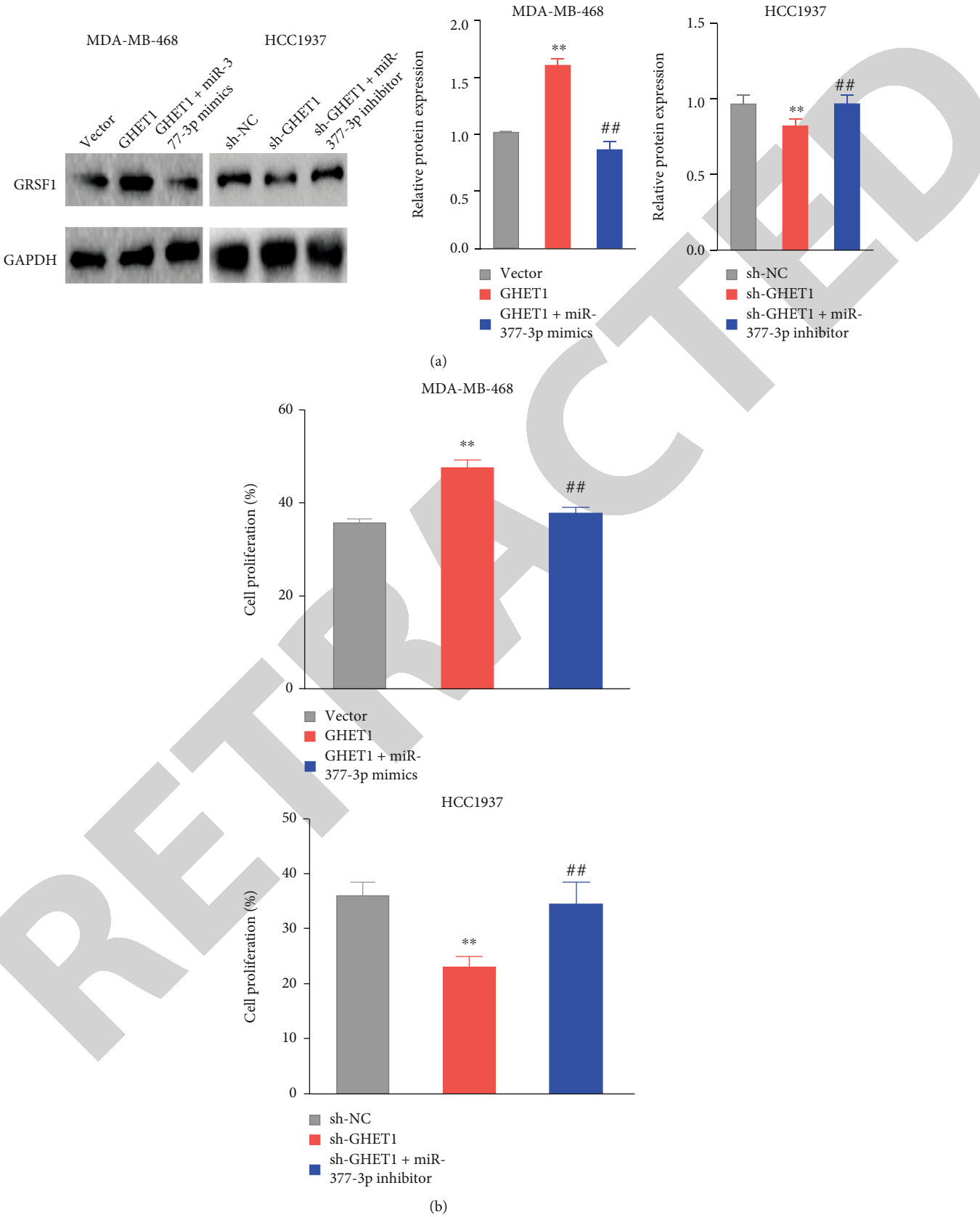

Figure 4: Continued.

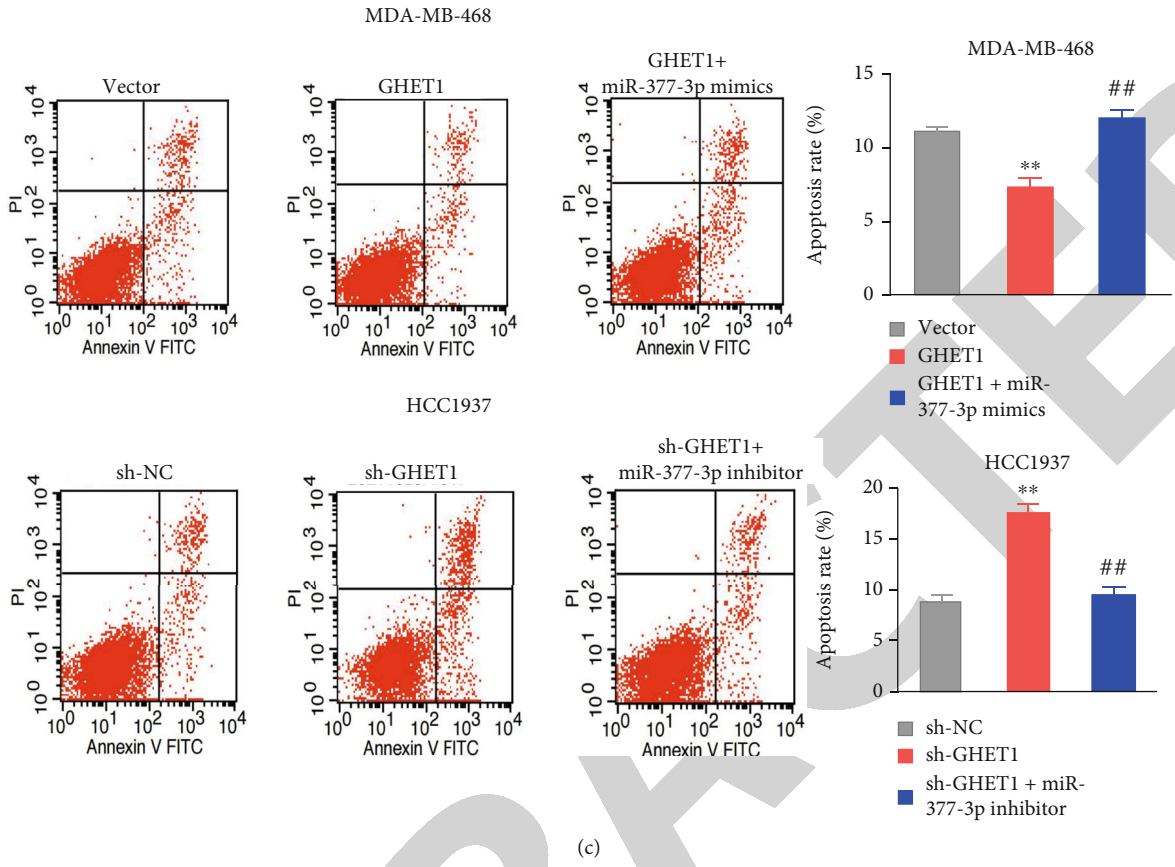

(c)

Figure 4: Continued.

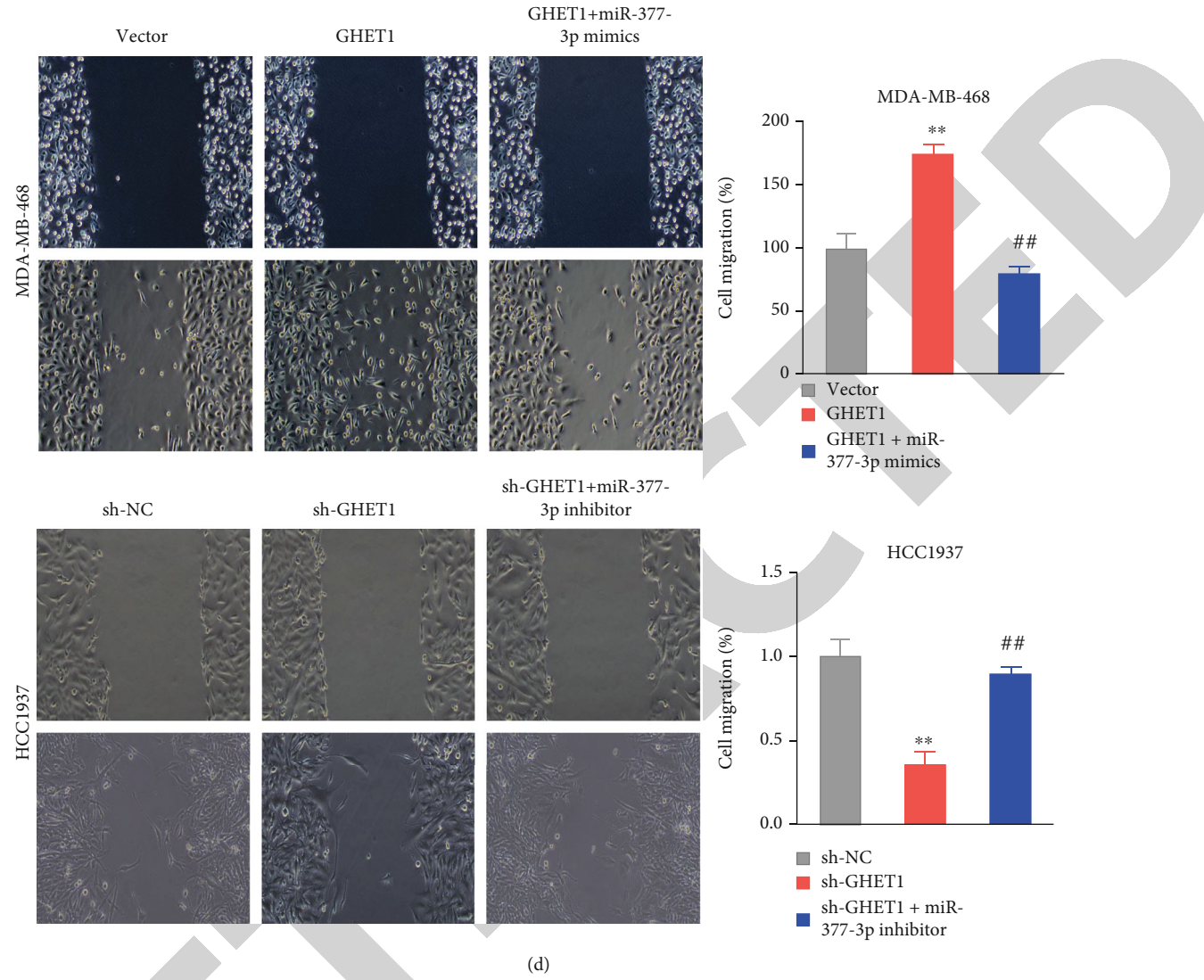

Figure 4: miR-377-3p inhibitor reversed the lncRNA GHET1 mimic-induced bioactivities in TNBC cells. GRSF1 (a) protein expression, (b) cellular proliferation, (c) cellular apoptosis, and (d) cellular migration were detected by (a) Western blot, (b) MTT assay, (c) flow cytometry, and (d) wound healing assay, respectively, in the indicated cells. $^{**}P < 0.01$ *vs.* vector/sh-NC, $^{\#\#}P < 0.01$ *vs.* GHET1/sh-GHET1. Each data was the average of three independent assays.

by binding to KLF2 [18]. It is worth noting that inhibition of lncRNA GHET1 could downregulate the expression of EGFR protein and inhibit PI3K/AKT signaling activity, thereby inhibiting the cellular activity of BC [19]. Consistent with previous studies, our study showed that lncRNA GHET1 was significantly upregulated in TNBC tissues and cells. High expression of the lncRNA GHET1 significantly promoted cell proliferation and migration and inhibited apoptosis. These findings suggest that lncRNA GHET1 plays a key role in the development of TNBC.

Similar to other cancers, the therapy for BC includes surgical resection, chemotherapy, radiotherapy, and targeted therapy. Endocrine therapy could also be applied to common BC. Although the benefits of chemotherapy are limited, TNBC is sensitive to it and still the standard treatment. Only a small partial of TNBC patients respond to targeted immunosuppressive sites or poly-ADP-ribose polymerase (PARP) inhibitors. However, they often develop drug resistance and even recurrence. There are few other options for TNBC therapy [20]. The finding of this study that lncRNA GHET1 regulates TNBC via the miR-377-3p/GRSF1 pathway undoubtedly provides a new clue for the treatment of TNBC.

It is now generally recognized that the expression of lncRNAs can be used as a signal of a specific cell state or a measure of active cellular processes. Hence, this kind of biomarkers can provide prognostic value for cancer and even provide treatment options for cancer patients [21]. Recent studies have shown that lncRNAs can regulate gene expression at different levels, including chromatin modification and transcriptional and posttranscriptional regulation [22]. They can act as miRNA and compete with miRNA-targeted mRNAs, thereby affecting miRNA-mediated gene regulation [23]. This crosstalk forms a complex posttranscriptional

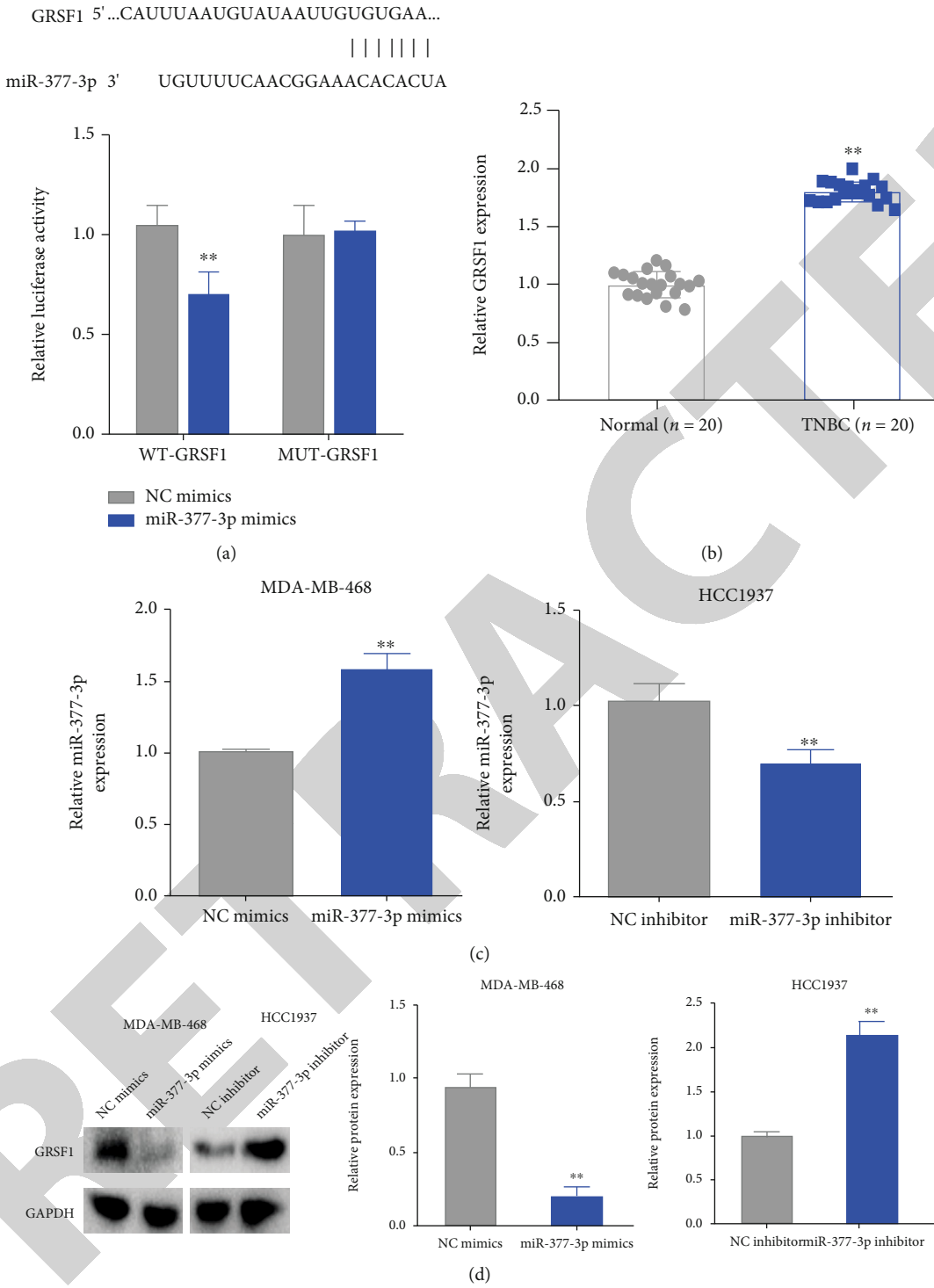

Figure 5: Continued.

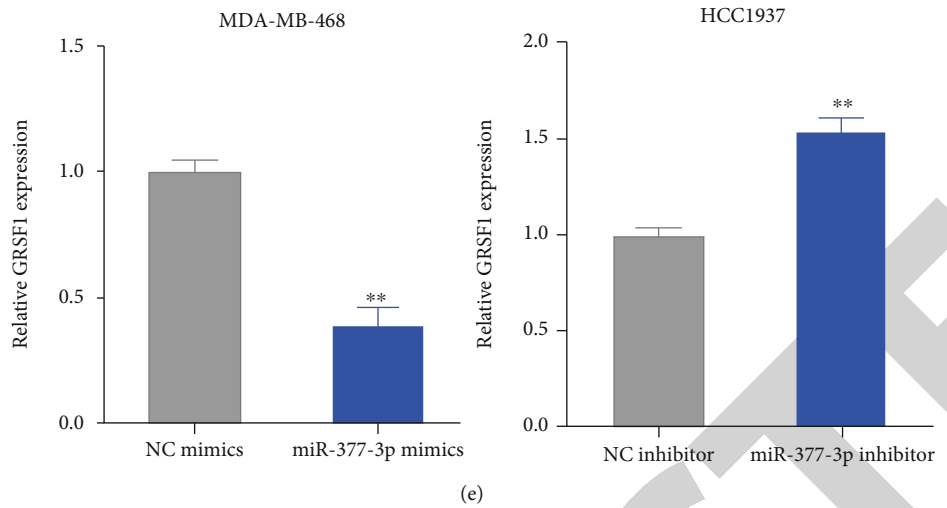

(e)

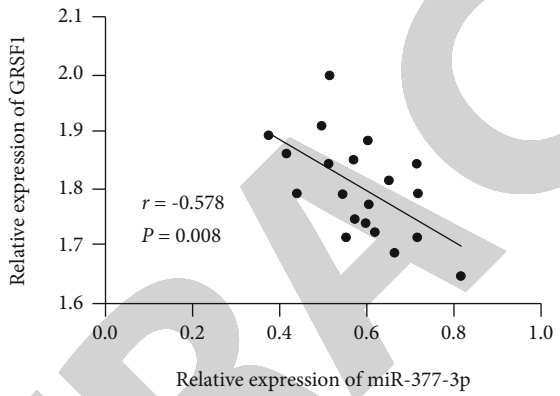

(f)

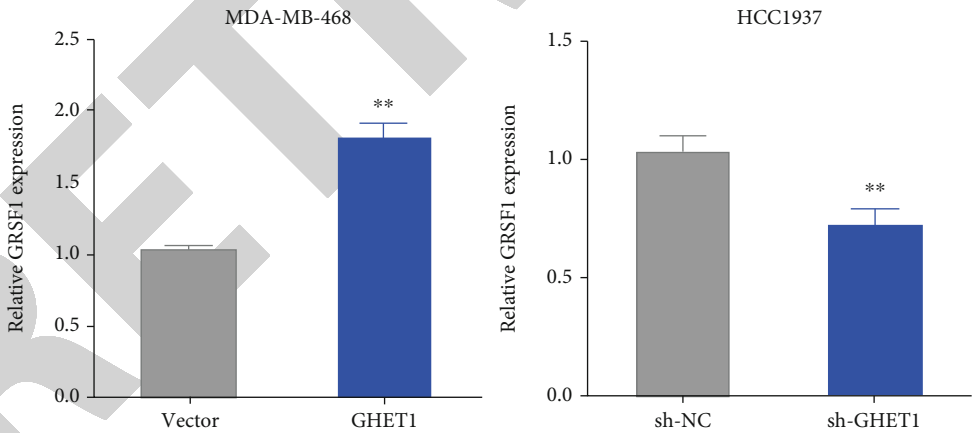

(g)

Figure 5: Continued.

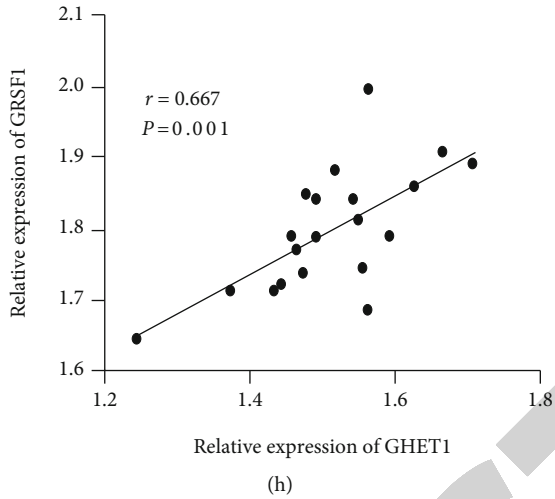

Figure 5: GRSF1 is a downstream target of miR-377-3p. (a) Target gene of miR-377-3p was predicted by the TargetScan database (up panel). Interaction between miR-377-3p and GRSF1 was analyzed by dual-luciferase reporter gene, $^{**}P < 0.01$ *vs.* NC mimics. (b) GRSF1 expression was detected by qRT-PCR in TBNC tissues, $^{**}P < 0.01$ vs. the normal group. (c) miR-377-3p expression was detected by qRT-PCR in the indicated TNBC cells. (d) GRSF1 protein expression was detected by Western blotting in the indicated TNBC cells. (e) GRSF1 mRNA expression was detected by qRT-PCR in the miR-377-3p mimic- or inhibitor-transfected TNBC cells, $^{**}P < 0.01$ *vs.* NC mimics/NC inhibitor. (f) Correlation between miR-377-3p and lncRNAGRSF1 in TNBC tissues was analyzed by Pearson correlation. (g) qRT-PCR was used to detect GRSF1 expression in the TNBC cells overexpressed or knocked down lncRNA GHET1, $^{**}P < 0.01$ vs. the vector/sh-NC group. (h) Correlation between GRSF1 and lncRNA GHET1 in TNBC tissues was analyzed by Pearson correlation analysis. Each data was the average of three independent assays.

regulatory network that includes mRNAs and lncRNAs and is called competitive endogenous RNA (ceRNA) network. The ceRNA-mediated regulatory mechanism is an important pathway for posttranscriptional regulation by lncRNAs in TNBC. The ceRNA regulatory network can help us understand the potential characteristics of biological functions and pathological roles of lncRNAs in TNBC development and progression [24]. In this study, lncRNA GHET1 was found to directly target miR-377-3p as an ecRNA. Previously, it has been shown that miR-377-3p acts as a tumor suppressor in many types of cancers. For example, it inhibited the development and progression of esophageal cancer by targeting CD133 and VEGF [25] and inhibited gastric cell proliferation and metastasis by suppressing VEGFA expression [26]. Moreover, miR-377-3p is an important component of the ceRNA network mediated by lncRNAs during cancer development. Existing studies reported that LINC00339 promoted gastric cancer progression by inhibiting miR-377-3p to increase DCP1A expression [27]. lncRNA SNHG4 promoted osteosarcoma proliferation and migration by sponging miR-377-3p [28]. In this study, we also found that miR-377-3p could reverse the effects induced by overexpression of lncRNA GHET1 on TNBC cells, demonstrating the joint involvement of lncRNA GHET1 and miR-377-3p in TNBC development.

GRSF1 is a mitochondrial RNA-binding protein, a guanine-rich sequence factor, and a component of the mitochondrial RNA particle, large ribonucleoprotein (RNP) structure [29]. Previous studies have pointed out that GRSF1 is required to maintain mitochondrial function and that loss of GRSF1 triggers DNA damage and impairs cell proliferation [30]. During the development of cancer, GRSF1 expression is significantly increased, and high expression of GRSF1 predicts a poor prognosis [31]. In this study, we found that GRSF1 was a target gene of miR-377-3p, and it was significantly elevated in TNBC tissue. To determine the role of lncRNA GHET1/miR-377-3p/GRSF1 in TNBC, we simultaneously knocked down or overexpressed lncRNAs GHET1 and miR-377-3p, and correspondingly, GRSF1 expression was affected and biological performance of TNBC cell was also influenced. Such findings suggest that the lncRNA GHET1/miR-377-3p/GRSF1 network plays a critical role in TNBC development.

MMPs belong to zinc endopeptidases which act as critical factors for extracellular matrix (ECM) degeneration [32]. MMPs play crucial roles in many pathological and physiological issues, including inflammation, embryonic development, wound healing, tumor metastasis, and invasion [33]. In cancer, elevation of MMP-2 and MMP-9 causes ECM degradation, resulting in tumor invasion and metastasis [34]. In addition, MMP-2 and MMP-9 also involve tumor growth through regulation of cellular proliferation, apoptosis, and angiogenesis [35–37]. Upregulation of MMP-2 and MMP-9 by lncRNA GHET1 clearly exhibits the oncogenic mechanism of the lncRNA GHET1 *via* MMP-2 and MMP-9 regulation.

5. Conclusions

In summary, lncRNA GHET1 enhances TNBC cell proliferation and migration ability and reduces apoptosis by regulating the miR-377-3p/GRSF1 pathway, thus playing a cancer-promoting role in TNBC. These results suggest that lncRNA GHET1/miR-377-3p/GRSF1 may be a potential prognostic marker and therapeutic target of TNBC.

Data Availability

The data used to support the findings of this study are available from the corresponding author upon request.

Conflicts of Interest

All authors declare no conflicts of interest in this paper.

Acknowledgments

This research was supported by the project supported by the Liaoning Provincial Department of Education (No. LJKZ0807) and the Horizontal Project Fund supported by Jinzhou Medical University (No. 2021005).

References

[1] C. E. DeSantis, J. Ma, M. M. Gaudet et al., "Breast cancer statistics, 2019," *CA: a Cancer Journal for Clinicians*, vol. 69, no. 6, pp. 438–451, 2019.

[2] T. Sørlie, "Molecular portraits of breast cancer: tumour subtypes as distinct disease entities," *European Journal of Cancer*, vol. 40, no. 18, pp. 2667–2675, 2004.

[3] M. Smid, Y. Wang, Y. Zhang et al., "Subtypes of breast cancer show preferential site of relapse," *Cancer Research*, vol. 68, no. 9, pp. 3108–3114, 2008.

[4] R. Chang, L. Song, Y. Xu et al., "Loss of Wwox drives metastasis in triple-negative breast cancer by JAK2/STAT3 axis," *Nature Communications*, vol. 9, no. 1, p. 3486, 2018.

[5] S. Yin, L. Xu, R. D. Bonfil et al., "Tumor-initiating cells and FZD8 play a major role in drug resistance in triple-negative breast cancer," *Molecular Cancer Therapeutics*, vol. 12, no. 4, pp. 491–498, 2013.

[6] S. Wang, Y. Shi, Z. Yuan et al., "Classical CMF regimen as adjuvant chemotherapy for triple-negative breast cancer may be more effective compared with anthracycline or taxane-based regimens," *Medical Oncology*, vol. 29, no. 2, pp. 547–553, 2012.

[7] S. R. Volovat, C. Volovat, I. Hordila et al., "MiRNA and LncRNA as potential biomarkers in triple-negative breast cancer: a review," *Frontiers in Oncology*, vol. 10, article 526850, 2020.

[8] C. V. Camacho, R. Choudhari, and S. S. Gadad, "Long noncoding RNAs and cancer, an overview," *Steroids*, vol. 133, pp. 93–95, 2018.

[9] A. Bhan, M. Soleimani, and S. S. Mandal, "Long noncoding RNA and cancer: a new paradigm," *Cancer Research*, vol. 77, no. 15, pp. 3965–3981, 2017.

[10] S. Zheng, M. Li, K. Miao, and H. Xu, "lncRNA GAS5-promoted apoptosis in triple-negative breast cancer by targeting miR-378a-5p/SUFU signaling," *Journal of Cellular Biochemistry*, vol. 121, no. 3, pp. 2225–2235, 2020.

[11] Y. Wang, S. Wu, X. Zhu et al., "LncRNA-encoded polypeptide ASRPS inhibits triple-negative breast cancer angiogenesis," *Journal of Experimental Medicine*, vol. 217, no. 3, 2020.

[12] A. Tariq, Q. Hao, Q. Sun et al., "LncRNA-mediated regulation ofSOX9expression in basal subtype breast cancer cells," *RNA*, vol. 26, no. 2, pp. 175–185, 2020.

[13] Y. Wang and S. Liu, "LncRNA GHET1 promotes hypoxia-induced glycolysis, proliferation, and invasion in triple-negative breast cancer through the hippo/YAP signaling pathway," *Frontiers in Cell and Development Biology*, vol. 9, article 643515, 2021.

[14] G. C. Shukla, J. Singh, and S. Barik, "MicroRNAs: processing, maturation, target recognition and regulatory functions," *Molecular and Cellular Pharmacology*, vol. 3, no. 3, pp. 83–92, 2011.

[15] X. Wang, T. Chen, Y. Zhang et al., "Long noncoding RNA Linc00339 promotes triple-negative breast cancer progression through miR-377-3p/HOXC6 signaling pathway," *Journal of Cellular Physiology*, vol. 234, no. 8, pp. 13303–13317, 2019.

[16] N. J. McCleary and J. A. Meyerhardt, "New developments in the adjuvant therapy of stage II colon cancer. Risk assessments in the older patient," *Oncology*, vol. 24, 1 Supplement 1, pp. 3–8, 2010.

[17] H. Zhang, D. Zhou, M. Ying et al., "Expression of long non-coding RNA (lncRNA) small nucleolar RNA host gene 1 (SNHG1) exacerbates hepatocellular carcinoma through suppressing miR-195," *Medical Science Monitor*, vol. 22, pp. 4820–4829, 2016.

[18] Y. Zhu, Y. Tong, J. Wu, Y. Liu, and M. Zhao, "Knockdown of LncRNA GHET1 suppresses prostate cancer cell proliferation by inhibiting HIF-1α/Notch-1 signaling pathway via KLF2," *BioFactors*, vol. 45, no. 3, pp. 364–373, 2019.

[19] M. Han, Y. Wang, Y. Gu et al., "lncRNA GHET1 knockdown suppresses breast cancer activity in vitro and in vivo," *American Journal of Translational Research*, vol. 11, no. 1, pp. 31–44, 2019.

[20] A. R. T. Bergin and S. Loi, "Triple-negative breast cancer: recent treatment advances," *F1000Res*, vol. 8, 2019.

[21] J. R. Prensner and A. M. Chinnaiyan, "The emergence of lncRNAs in cancer biology," *Cancer Discovery*, vol. 1, no. 5, pp. 391–407, 2011.

[22] B. K. Dey, A. C. Mueller, and A. Dutta, "Long non-coding RNAs as emerging regulators of differentiation, development, and disease," *Transcription*, vol. 5, no. 4, article e944014, 2014.

[23] L. Poliseno, L. Salmena, J. Zhang, B. Carver, W. J. Haveman, and P. P. Pandolfi, "A coding-independent function of gene and pseudogene mRNAs regulates tumour biology," *Nature*, vol. 465, no. 7301, pp. 1033–1038, 2010.

[24] X. Song, G. Cao, L. Jing et al., "Analysing the relationship between lncRNA and protein-coding gene and the role of lncRNA as ceRNA in pulmonary fibrosis," *Journal of Cellular and Molecular Medicine*, vol. 18, no. 6, pp. 991–1003, 2014.

[25] C. Q. Wang, L. Chen, C. L. Dong et al., "MiR-377 suppresses cell proliferation and metastasis in gastric cancer via repressing the expression of VEGFA," *European Review for Medical and Pharmacological Sciences*, vol. 21, no. 22, pp. 5101–5111, 2017.

[26] B. Li, W. W. Xu, L. Han et al., "MicroRNA-377 suppresses initiation and progression of esophageal cancer by inhibiting CD133 and VEGF," *Oncogene*, vol. 36, no. 28, pp. 3986–4000, 2017.

[27] C. Shi, T. Liu, J. Chi et al., "LINC00339 promotes gastric cancer progression by elevating DCP1A expression via inhibiting miR-377-3p," *Journal of Cellular Physiology*, vol. 234, no. 12, pp. 23667–23674, 2019.

[28] Y. F. Huang, L. Lu, H. L. Shen, and X. X. Lu, "LncRNA SNHG4 promotes osteosarcoma proliferation and migration by sponging miR-377-3p," *Molecular Genetics & Genomic Medicine*, vol. 8, no. 8, article e1349, 2020.

Hindawi
Computational and Mathematical Methods in Medicine
Volume 2022, Article ID 9869812, 1 page
https://doi.org/10.1155/2022/9869812

Retraction

Retracted: Prevention Methods of Fitness and Bodybuilding Exercise Injury Based on Data Mining

Computational and Mathematical Methods in Medicine

Received 4 November 2022; Accepted 4 November 2022; Published 16 November 2022

Computational and Mathematical Methods in Medicine has retracted the article titled "Prevention Methods of Fitness and Bodybuilding Exercise Injury Based on Data Mining" [1] due to concerns that the peer review process has been compromised.

Following an investigation conducted by the Hindawi Research Integrity team [2], significant concerns were identified with the peer reviewers assigned to this article; the investigation has concluded that the peer review process was compromised. We therefore can no longer trust the peer review process and the article is being retracted with the agreement of the Chief Editor.

References

[1] J. Xie, "Prevention Methods of Fitness and Bodybuilding Exercise Injury Based on Data Mining," *Computational and Mathematical Methods in Medicine*, vol. 2022, Article ID 7083991, 13 pages, 2022.

[2] L. Ferguson, "Advancing Research Integrity Collaboratively and with Vigour," 2022, https://www.hindawi.com/post/advancing-research-integrity-collaboratively-and-vigour/.

Hindawi
Computational and Mathematical Methods in Medicine
Volume 2022, Article ID 7083991, 13 pages
https://doi.org/10.1155/2022/7083991

Research Article

Prevention Methods of Fitness and Bodybuilding Exercise Injury Based on Data Mining

Jun Xie

School of Physical Education and Health, A'ba Teachers' University, Wenchuan, 623002 Sichuan, China

Correspondence should be addressed to Jun Xie; 20119639@abtu.edu.cn

Received 21 January 2022; Revised 28 February 2022; Accepted 14 March 2022; Published 14 April 2022

Academic Editor: Shakeel Ahmad

Fitness and bodybuilding are becoming the trend of the development of sports projects today, not only to bring health to the exercisers, but also to keep the body in good condition. However, due to the wrong attitudes and methods of exercisers, they often have negative effects on exercisers, such as sprains, strains, and tendon strains. This article is based on data mining technology to realize the research of exercise injury prevention methods, so firstly, it introduces the steps and applications of data mining technology and highlights the cluster analysis method in data mining technology. Then it discusses the injury factors of fitness and bodybuilding and outlines the best measures to prevent exercise injury. At the same time, the C4.5 algorithm was introduced to realize the processing of the data set, and the effectiveness of preventive measures was proved by investigating the damage of fitness and bodybuilding exercises in 15 clubs in a certain city. The results of the study show that the number of people who exercise more than 3 times a week accounts for 65.6% of the total number of people, which shows that exercisers in a city's fitness club exercise more frequently each week.

1. Introduction

The society is developing rapidly, and the nationwide fitness program is being implemented more and more. Most sports enthusiasts agree to spend money on exercise. However, from the perspective of long-term training goals, many bodybuilders are injured, which has some negative effects on bodybuilders who want to continue training during actual exercise. Therefore, it is very important to take appropriate and timely treatment measures and methods, and we must attach great importance to the prevention of sports and sports injuries. Only by strengthening the awareness of exercise injury prevention can the occurrence of injury be avoided as much as possible.

Regarding the research on data mining and fitness exercise injury prevention methods, scholars at home and abroad have provided a large number of references. Amodio uses the People-Environment-Occupation (P-E-O) framework to determine the factors that cause traumatic brain injury in male and female workers. The study found five factors: unexplained human factors, colleagues' behavior, external environment, safety measures, and equipment failures. Due to equipment failure or malfunction, male workers are more likely to experience traumatic brain injury than female workers. A statistically significant gender difference was observed in the P-E-O factor [1]. Cui researched data mining based on intelligent recommendation system. First, mathematically model the intelligent recommendation system based on association rules. Then, the fuzzy clustering algorithm is used to optimize the system. After the system is built, the performance of the system is evaluated. The evaluation indicators include accuracy, coverage, and response time. Finally, put the system into trial operation on the e-commerce platform. Comparing the click-through rate and purchase conversion rate of recommended products before and after operation, randomly launch a questionnaire survey to platform users to analyze user satisfaction [2]. Shin found that classification, text mining, and clustering are the main data mining techniques used by researchers. Compared with the field of mathematics education, the research using data mining is more likely to be carried out in the field of science education. Shin provides enlightenment for the research and teaching of science and mathematics and proposes potential research directions [3]. Bbosa compared parametric

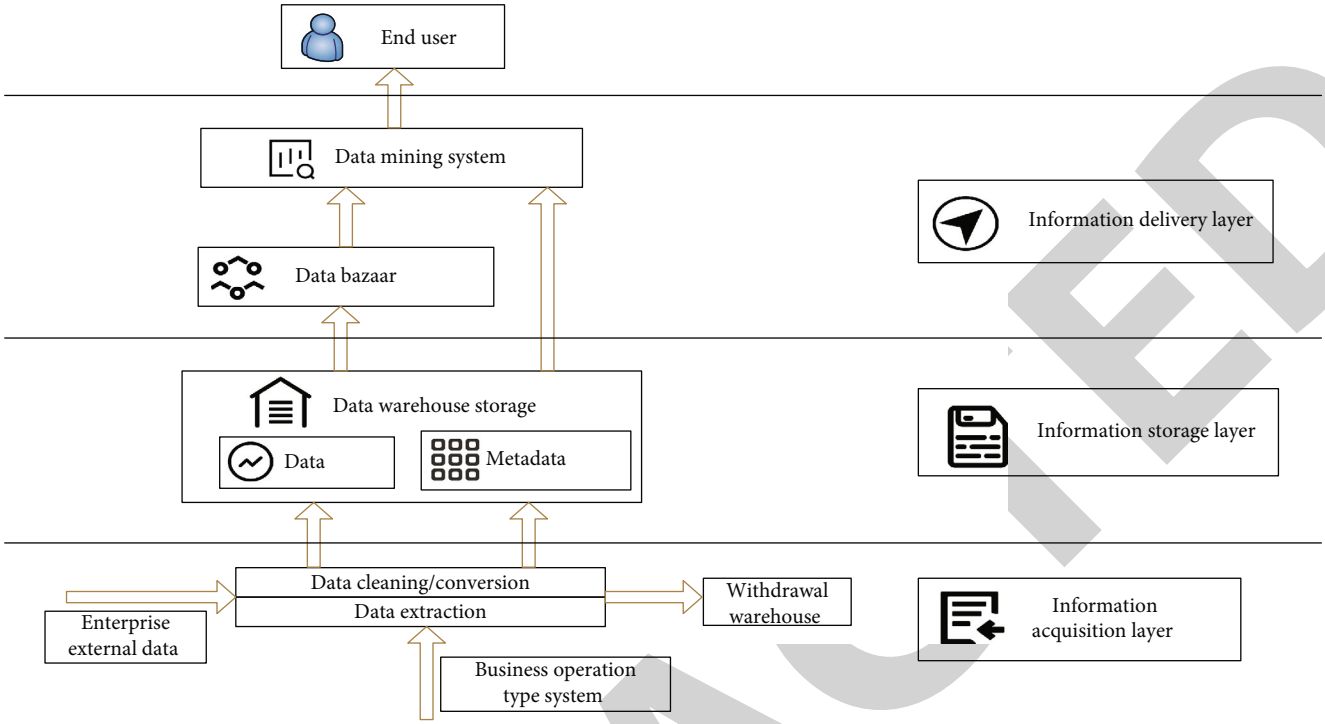

Figure 1: Data warehouse architecture.

techniques in the form of naive Bayes and logistic regression with non-parametric techniques in the form of support vector machines and artificial neural networks to determine which model is best for predicting the unbalanced malaria incidence data set [4]. Based on experimental data obtained under various environmental settings, Zhao C analyzed the probability distribution of skin reflection model parameters in RGB space. Based on this distribution, a new pulse extraction algorithm is proposed, which uses the center of the distribution as a model parameter for preliminary pulse separation and uses a cascaded minimum mean square adaptive filter to compensate the modeling error [5]. Min briefly emphasized the positive effects of exercise on promoting brain function. In general, Min provides an understanding of the importance of motor neuroscience and emphasizes recommendations for future health research [6]. The data of these studies are not comprehensive, and the experimental conclusions are yet to be discussed, so they cannot be popularized and cannot be recognized by the public.

The innovation of this research is to use the cluster analysis method of data mining technology, combined with the C4.5 algorithm to realize the research of exercise injury prevention methods. In this way, not only can the knowledge that is useful for the core of the research be extracted, but also some methods that have never appeared can be integrated and analyzed based on this knowledge. In addition, this research has collected data in the field of fitness and bodybuilding by means of investigation, which shows the effectiveness and robustness of the research. Finally, it expounds the factors of fitness and fitness exercise injury from the four aspects of physiology, psychology, technology, and clubs and comprehensively summarizes the injury prevention methods.

2. Data Mining Technology and Fitness and Bodybuilding Exercise Injury Prevention

2.1. Data Mining. Data mining is the process of extracting potentially useful information and knowledge hidden in it that people do not know beforehand from a large amount of incomplete, noisy, fuzzy, and random data.

The use of data mining technology is inseparable from the data warehouse, so here is a brief introduction to the structure of the data warehouse, as shown in Figure 1.

Data mining includes the following steps, as shown in Figure 2:

(1) It obtains data for analysis [7]. Data mining resources can take many forms, but to create a good model, it must have a high-quality information source. The data in the database system is filtered and cleaned with high-quality information. Therefore, obtaining the source from the database is a wise choice

(2) It chooses appropriate data processing tools and algorithms for data mining [8, 9].

(3) It explains the results. Since the results of data mining do not provide a direct explanation for a specific field, it is very important for relevant personnel to analyze the results to determine the success or failure of the data mining project [10]. If the data extraction

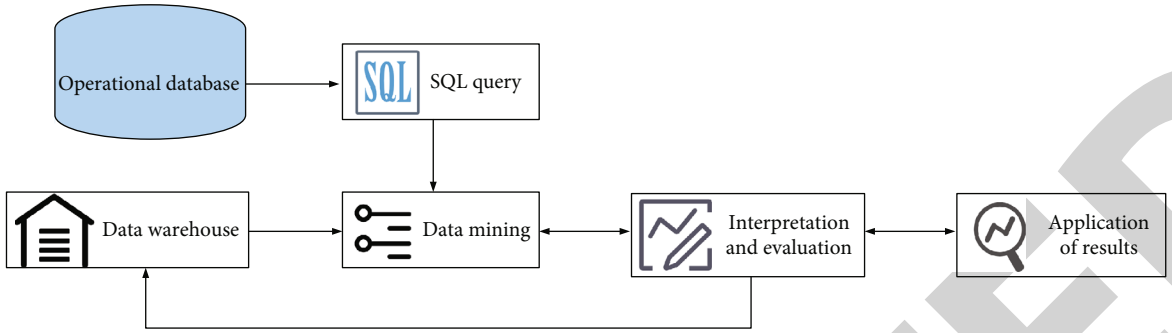

Figure 2: The process of data mining.

results are not satisfactory, the reasons should be analyzed and reused

(4) It applies the results to the problem to be solved. Data mining is a repetitive process. In the repetitive process, it tends to be more towards the essence of things [11].

The general processing flow of data mining is clear goals, data preparation, model building, evaluation and interpretation of output results, and implementation of 5 stages. The processing flow is shown in Figure 3 [12].

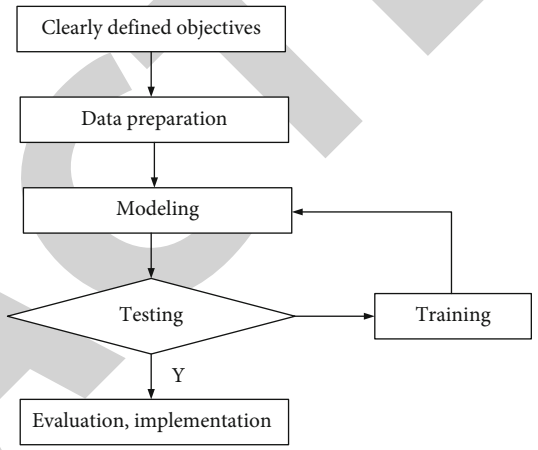

Figure 3: Data mining processing flow.

2.1.1. Clear Goals. The main task of a data mining application is to locate and explain the problems that need to be solved. In addition to choosing a suitable extraction method, the target details should also be detailed and clear in order to study the impact of data extraction and the effectiveness of the model creation [13].

2.1.2. Data Preparation. It extracts the required data according to the purpose of the data mining business. In addition to necessary checks and corrections to ensure data quality, data compatibility between different sources should also be considered. If there are multiple data fields in the data set, it should use a specific method to find the data field that has the greatest impact on the model output and reduce the input fields accordingly. Commonly used methods are "descriptive data mining" and link analysis. Combining multiple variables (addition, subtraction, ratio, etc.) may have a greater impact than these variables. If expand the scope of certain variables, then these variables are very good predictors. Therefore, it is necessary to consider whether to create some new variables during the data preparation process. Dealing with missing data is also an important part of the data preparation process, some of which are very important in themselves [14, 15].

2.1.3. Building a Model. Building a model is the most important step in the entire data mining process. It serves as the basis of data mining. Whether the model is built or not will determine whether the output results meet the requirements [16].

2.1.4. Evaluation and Interpretation of Output Results. After the model is created, its effectiveness must be evaluated and its value explained. For practical applications, the model validity criteria will vary depending on the application data. However, accuracy is not the only way to evaluate the best design. The analysis of the results should take into account the type of error and related cost factors. If the cost of each calculation error is different, the lowest cost model (not necessarily the smallest error) will be a better choice. It is important to test the model directly from actual needs and solve actual problems. First apply in a small area and then gradually expand the coverage area until sufficient test results are obtained [17].

2.1.5. Implementation. After creating and verifying the template, there are two main ways to use it. One is to allow relevant personnel to analyze and make comments and suggestions; the other is to use templates for different data sets. This model can be used to determine the type of case, or it can be used in other databases to select records that meet specific needs, so that tools can be used for further analysis. After applying the model, it need to continuously monitor the effectiveness of the model. Even if the model is used successfully, the tracking cannot be undone. This is because things are constantly evolving, and when the unit's requirements, capabilities, and conditions change over time, the model may no longer be effective. Therefore, as the time spent on the model increases, new models need to be continuously tested, and sometimes new models are created [18].

In a nutshell, the data mining process generally consists of three main stages: data preparation, mining operations, result expression, and interpretation.

(1) Data Preparation Process. This process can be divided into three subphases: data integration, data selection, and preprocessing. Data integration is to integrate data into a multi-file or multi-database operating environment to solve semantic instability, manage data instances, and clean up dirty data. The purpose of data selection is to identify the data set that needs to be analyzed, reduce processing boundaries, and improve the quality of data extraction. Data preprocessing is to overcome the limitations of current data mining tools.

(2) Data Mining Stage. In this stage, actual mining operations are carried out. The key points included are the following:

(1) First decide how to generate hypotheses, whether to let the data mining system generate hypotheses for users or whether users themselves make hypotheses about the knowledge that may be contained in the database. The former is called discovery data mining, and the latter is called verification data mining

(2) Choosing the right tool

(3) The operation of mining knowledge

(4) Confirming the discovered knowledge

(3) Result Presentation and Interpretation Stage. Analyze the extracted information according to the decision-making purpose of the end user, distinguish the most valuable information, and submit it to the decision-maker through decision support tools. Therefore, the task of this step is not only to express the results, such as the use of information visualization methods, but also to filter the information.

Cluster analysis is a commonly used method of data mining. There are various methods of cluster analysis. The more commonly used methods can be simply summarized as follows:

(1) Clustering Method Based on Partition. The total number of clusters K that is less than the number of objects in the data set is preset, and the division is performed on this condition, and finally K clusters are obtained. These K groups meet the following conditions: at least one piece of data belongs to each group, and for each piece of data, it can only belong to a specific group and cannot appear in multiple different groups at the same time. The execution of the algorithm can be seen as an iterative process. First, the data is divided into K groups according to the K value, and then after result evaluation and iterative methods, each time the attribution of the data in the group is corrected, after the process converges, a clustering result is obtained [19].

(2) Hierarchical Clustering Method. The hierarchical clustering method first initializes a clustering tree and then decomposes the data according to the hierarchical relationship between the data until the preset conditions are met. On the one hand, due to the different actual situations that need to be dealt with, and on the other hand, considering the needs of algorithm implementation, the order of hierarchical clustering can be divided into (1) top-down and (2) bottom-up [20].

(3) Density-Based Clustering Method. The clustering method based on distance measurement is largely limited by the distance definition method and can only mine simple clusters with a relatively regular shape (spherical). In response to this shortcoming, some scholars have proposed a density-based clustering method, which uses the density of data to construct clusters and can produce clustering results of arbitrary shapes. The method is specifically described as analyzing the tightness between the data and presetting a density threshold; when the density of the data is higher than this threshold, the data points in the area are gathered into clusters. At the same time, compared with the distance measurement method, this method is not affected by the noise of outliers to a greater extent and obtains better results [21].

(4) Model-Based Clustering Method. This method deeply studies the existing model and analyzes the data characteristics of the data set to be mined on the basis of it, so that the subdata set consistent with the model characteristics is regarded as a cluster. Before the clustering starts, the model is specified according to the characteristics of the data set, and the data conforming to the model is gathered into clusters to form clusters [22]. One of its underlying assumptions is that the generation of the data set to be mined conforms to a certain probability density distribution. In this type of algorithm, the clustered data is also automatically determined based on statistics, and noise and outliers are also analyzed through statistics [23].

There is also a commonly used data mining method—association rules. The core purpose of association rule analysis is to discover the interrelated and interdependent relationships that exist in the data. Association rule mining is also a data mining method derived from database theory and has a very wide range of practical applications. Specifically, in relational databases, there are often some data that appear synchronously, which is called a pattern. When this pattern appears frequently in the database, it is considered that there is a specific association relationship, which is called an association rule.

The architecture of data mining is shown in Figure 4:

An authoritative survey report pointed out that data mining technology will develop rapidly within 3-5 years and be widely used in all walks of life. The development of technology is always driven by the increase in demand. Due to the great development of the information industry, various fields and industries have begun their informatization construction, which has caused an explosive growth in the scale of data, and massive data cannot be left unused as data. Data mining methods can find relevant knowledge that is useful to humans and can improve the efficiency of

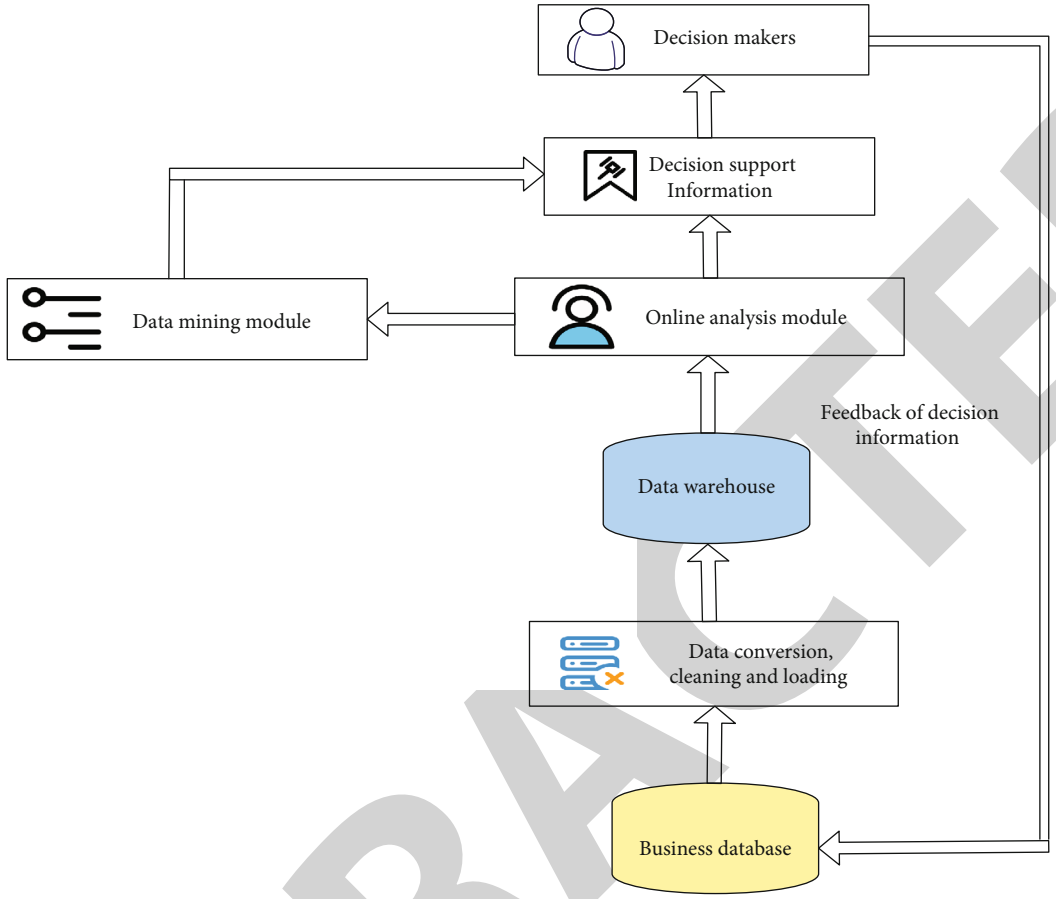

Figure 4: Architecture of data mining.

production and life from these massive data and use this knowledge to further promote the rapid and steady development of productivity. It is precisely because of this that the research of data mining technology has become the current research hotspot in the field of database, machine learning, and statistics, and various rich application examples have been completed.

The application of data mining is extremely wide. Through the combination of specific data in various industries and fields, many professional data mining basic applications have been produced, representative of which are applications in the retail industry, insurance industry, astronomical and meteorological research, food engineering, and biotechnology.

Compared with the above majors, data mining technology is used more widely in the business field, and the more typical applications are marketing and shopping basket analysis. The former conducts basic clustering of customers through the mining and analysis of user historical purchase data and distinguishes key customers from general customers. Selectively increasing marketing efforts for key customers can effectively improve marketing effects. The latter is mainly used in retail industries such as supermarkets, through massive retail data, to refine the buying habits of shoppers, in order to adjust the way the goods are placed. While providing customers with a convenient shopping environment, it has also increased the actual operating income of the supermarket. One of the representative examples is the successful case of "Beer and Diapers."

In addition, data mining has a very wide range of applications in the banking and financial industries, such as risk assessment and price prediction.

2.2. Fitness and Bodybuilding Exercise Damage Prevention. According to different analysis angles, the classification of exercise injuries can be roughly divided into the following categories:

(1) According to the damaged tissue, it can be divided into muscle injury, ligament injury, nerve injury, blood vessel injury, bursal injury, tendon sheath injury, cartilage injury, etc.

(2) According to the severity, it is divided into severe injury, moderate injury, and mild injury

Severe injury. Cannot exercise at all for more than one week after injury and needs rest and treatment

Moderate injury. The normal physical exercise cannot be carried out according to the training plan within one week after the injury, and local physical activities need to be stopped or reduced

Mild injury. After injury, normal training can be carried out in accordance with the teaching and training plan, and the injury will not be aggravated

(3) According to the integrity of the skin and mucous membrane after sports injury, it can be divided into: closed injury and open injury

Closed injury. The skin and mucous membrane of the injured area remain intact, with no cracks communicating with the body surface

Open injury. The skin or mucous membrane of the injured area is destroyed, and there are cracks communicating with the body surface

2.2.1. Injury Factors

(1) Technical Factors. (1) Incorrect Technical Action. Most of the injuries caused by incorrect technical movements are aimed at beginners. Due to the wide variety of exercises during the exercise, it is difficult to master technical activities in a short period of time. However, out of curiosity, beginners often prefer new exercises. Studies have shown that most beginners do not actively learn fitness knowledge and are seriously lacking in science. In terms of fitness equipment, most beginners imitate the movements of European and American bodybuilders through online videos and take some methods that are not suitable for beginners to complete technical movements. For exercisers, mastering the correct exercise technique is a reliable way to improve their fitness performance while avoiding injuries caused by technical exercise errors.

(2) Violation of the Principle of Gradual and Orderly Progress. The complexity of sports training should be based on the principle of combining practice from simple to heavy and from simple to visual. Under the influence of external conditions, the body gradually adapts and produces repeated stimulation. Therefore, it is impossible to change the shape, function, physical activity, and other adaptive changes of various organs and systems of the body through high-intensity training. Instead, repeated training creates a gradual process of adaptation. The health of the human body is a process of gradual accumulation. Excessive exercise not only fails to obtain the effect of exercise, but also leads to sports injuries. In the early stages of exercise, beginners may blindly perform high-intensity exercise without mastering the correct and necessary exercise skills, resulting in incorrect exercise movements and impaired physical function.

(3) Partial Load Is Too Heavy. The dynamic changes of load play an important role in the development of exercise posture, improvement of physical fitness, and load management within the range of physical endurance capabilities. It is of great significance to improve the sports ability of members and prevent sports injuries. The scientific nature of training is to know how much exercise the body can or should take, and adjust to own physical condition in time, rather than causing deformity or injury. Therefore, exercisers should consider their own physical characteristics during the training process to reduce the injury rate.

Table 1: Expert validity questionnaire survey.

Title	Number of people	*A*	*B*	*C*	*D*	*E*
Professor	6	2	2	2	0	0
Associate professor	4	2	1	1	0	0
Lecturer	2	1	1	0	0	0
Total	12	5	4	3	0	0

(4) Unreasonable Warm-Up Activities. Unreasonable warm-up activities mainly include insufficient warm-up activities, excessive warm-up activities, failure to do warm-up activities, unreasonable connection between activity content and training content, and excessive time between warm-up activities and formal training or competition.

(2) Physiological Factors. (1) Poor Physical Fitness. Physical fitness is usually a comprehensive manifestation of the functions of various organs and system muscles in the human body. Physical fitness usually includes speed, strength, endurance, agility, and flexibility. Good exercise is not only an important basis for improving the ability of exercisers, but also an important guarantee for preventing sports injuries and reducing the degree of injury.

(2) Body Fatigue. Sports fatigue is the reduction of physical strength during exercise. After a good rest, the body's functions can be restored. The principle of improving physical function through training is not only stress-fatigue-relieving fatigue-recovery. Therefore, scientifically and optimally adjusting the recovery speed of each load can make training more effective. When physical fatigue cannot be recovered in time and effectively, exercise performance is poor, such as poor exercise coordination, decreased strength, and technical dyskinesias during exercise. Exercisers after get off work should be based on their own feelings rather than training plans. Stop the training when feel tired; when full of energy, increase the training intensity accordingly.

(3) Psychological Factors. (1) Inattention. Studies have shown that it is difficult for people to maintain long-term concentration, which is also a normal phenomenon. People's attention is easily distracted by changes in the outside world and also changes due to changes in their own emotions. There are roughly several reasons for inattention: fatigue, environment, psychology, etc. When people exercise when they are inattentive, their reaction speed will slow down. Therefore, it should develop the habit of concentration during daily training or can exercise some training to exercise the problem of concentration, so as to slowly form a set of training framework for own concentration and avoid injury caused by inattention.

(2) The Training Mood Is Too Excited or Low. When a person's emotions are too excited or low during training, some physical injuries often occur. For example, lifting a barbell

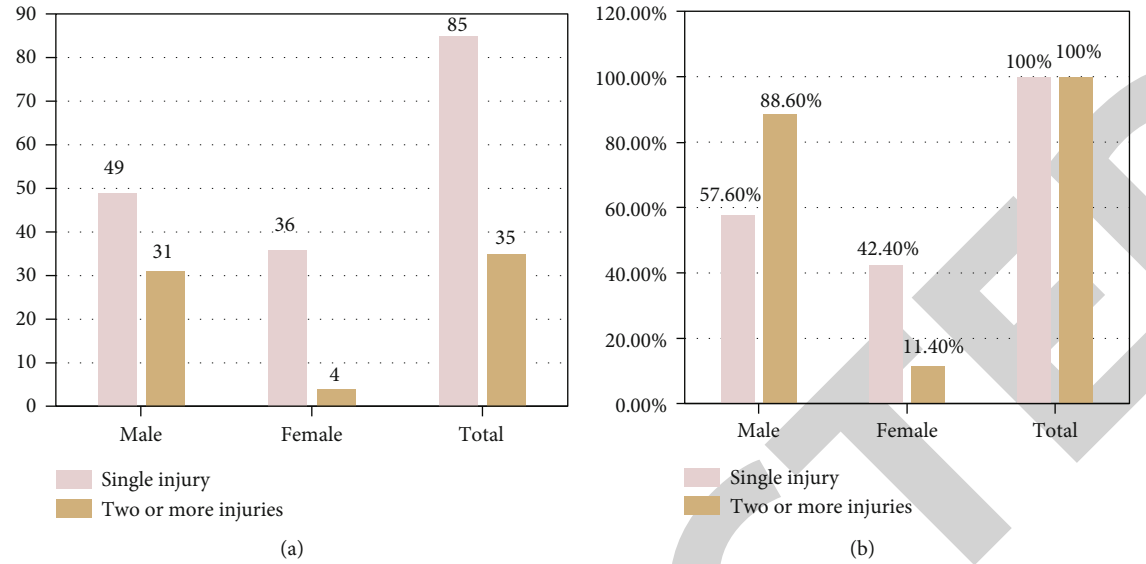

Figure 5: Statistics on the ratio of men to women and the number of injuries.

Table 2: Fitness motivation and exercise injury survey results.

	Health		Relieve work stress		Fat loss, shaping		Increase muscle mass	
	Male	Female	Male	Female	Male	Female	Male	Female
Total	49	47	20	7	10	58	65	0
Number of injuries	13	7	5	1	1	23	42	0
Aggregate injury rate	20.8%		22.2%		35.2%		64.6%	

when too excited may cause to exceed usual training volume due to emotional reasons. If the individual did not pay attention at the time, this will cause hand injuries. And in the case of too low, it is very likely that the whole body will be ignored due to one's own emotional reasons, which is also very prone to injury.

(4) Fitness Club Factors. (1) Poor Venue. There are some projects that cannot be separated from a good venue. Aerobics, for example, involves some jumping movements, so if the venue is too hard, slippery, or unequal, it will affect the progress of the training program and cause damage to the human body.

(2) Device Factors. The damage caused by equipment factors mainly includes the following situations: equipment aging, lack of maintenance, warning signs indicating defects, and unreasonable design. Some surveys show that the more serious one is the injury caused by the treadmill, which is mainly because the speed is set too fast. In addition, loose screws, high friction, and inconsistent left and right weights may cause damage. In this case, it is necessary for the club to do regular inspections and maintenance, and the exercisers themselves must carefully check the condition of the equipment before using the equipment.

2.2.2. Countermeasures to Prevent Exercise Injury. People pay more attention to the improvement of their own comprehensive quality. The number of people participating in fitness and bodybuilding exercises continues to increase. The intensity and density of exercises increase accordingly, and the chances of injury are also increasing. Preventive measures become more important.

Table 3: Nature and proportion of knee injuries.

Site and type of injury	Example	Proportion (%)
Knee sprain	5	27.2%
Knee joint strain	7	38.8%
Knee lacerations	4	22.2%
Other	2	11.1%

(1) Strengthen Ideological Education and Theoretical Guidance and Improve Exercisers' Awareness of Preventing Exercise Injuries. The core reason for the higher injury rate is the lack of awareness of self-protection of exercisers and the lack of awareness of preventing exercise injury. Therefore, it is necessary for exercisers to strengthen the study of the basic theoretical knowledge of exercise injuries and improve their awareness of prevention and the ability to deal with injuries according to the actual situation, so as to treat exercise injuries correctly.

(2) Reasonably Arrange Training Content and Load. The content and load of training should be arranged according

Figure 6: Example of knee injury.

Table 4: Nature and proportion of lumbar injuries.

Site and type of injury	Example	Proportion (%)
Back sprain	9	37.5%
Low back strain	8	33.3%
Intervertebral disc injury	4	16.6%
Other	3	8.8%

to the individual's own situation. If high-load training is carried out due to impulse or other motivations, it will cause personal injury. Therefore, it is particularly important to arrange the content and load of training reasonably. At the same time, adjust the arrangement in time according to own situation, so as to avoid physical damage as much as possible.

(3) Pay Attention to Comprehensive Training of Physical Fitness. The original intention of exercise is to have a strong physique. Therefore, in actual training, attention should be paid to the overall improvement of physical fitness, so as to prevent the occurrence of exercise injuries.

(4) Checking the Equipment. Develop the habit of checking whether the equipment is broken and firm every time you start exercising, so that it can also avoid exercise damage due to equipment problems.

When an exerciser is injured, he should first determine whether his condition is critical. If the situation is critical, he should call for help immediately; if there is no major problem, he should deal with it by himself or go to the hospital for examination.

3. C4.5 Algorithm

The classification rules generated by the C4.5 algorithm are easy to understand and have a high accuracy rate. The C4.5 algorithm uses the information gain rate to optimize the attributes of the decision tree, and the information gain rate calculation method is as follows:

Supposing a data set T, a classification set $\{C_1, C_2, C_3 \cdots C_k\}$, and the data set T is divided into multiple subsets by the attribute V. Supposing that V has n values $\{v_1, v_2, v_3 \cdots v_n\}$, and each value is not repeated. The data set T is divided into $T_1, T_2, T_3 \cdots T_n$, and the value of all instances in T_i is v_i.

Probability of category occurrence:

$$P(C_j) = |C_j|/|T| = freq(C_j, T)/|T|. \tag{1}$$

Probability of attribute:

$$P(v_i) = |T_i|/|T|. \tag{2}$$

In the attribute instance, the conditional probability of class C_j:

$$P(C_j|v_j) = |C_{jV}|/|T_i|. \tag{3}$$

Information entropy of category:

$$\begin{aligned} H(C) &= -\sum_j P(C_j)\log_2(P(C_j)) \\ &= -\sum_j \frac{freq(C_j, T)}{|T|} * \log_2\left(\frac{freq(C_j, T)}{|T|}\right) \\ &= \inf\ o(T). \end{aligned} \tag{4}$$

The conditional entropy of the category divides the set T according to the attribute V, and the conditional entropy of the category after segmentation:

$$\begin{aligned} H(C|V) &= -\sum P(v_i)\sum P(C_j|v_j)\log_2(P(C_j|v_i)) \\ &= \sum_{i=1}^{n} \frac{|T_i|}{|T|} * \inf\ o(T_i) = \inf\ ov(T). \end{aligned} \tag{5}$$

Information gain:

$$I(C, V) = H(C) - H(C|V) = \text{int}\ o(T) - \inf\ ov(T) = gain(V). \tag{6}$$

Information entropy of attribute V:

$$\begin{aligned} H(V) &= \sum_i p(v_i)\log_2(P(v_i)) = -\sum_{i=1}^{n} \frac{|T_i|}{|T|} * \log_2\left(\frac{|T_i|}{|T|}\right) \\ &= spit\_\inf\ o(V). \end{aligned} \tag{7}$$

Figure 7: Example of low back injury.

Table 5: Health club exercisers sports injury causing factors statistics.

Sort by	Injury causing factors	Number of injuries	Percentage
1	Technical movements are not standard	12	11.2%
2	Unreasonable preparation activities	10	8.62%
3	Fatigue of the organism	9	7.76%
4	Excessive local load	8	6.89%
5	Against the principle of gradual and orderly progress	8	6.89%
6	Poor physical fitness	7	6.03%
7	Inattentiveness	7	6.03%
8	Coaching factors	7	6.03%
9	Excessive exercise load	6	5.17%
10	Venue and equipment factors	6	5.17%

(a) (b)

Figure 8: Occurrence of exercise injuries in different parts of the body.

Information gain calculation formula:

$$gain\_ratio = gain(V)/spit\_\inf o(V). \tag{8}$$

Relationship coefficient:

$$\Delta \min = \min_i \min_k |y_0(k)y_i(k)|, \tag{9}$$

$$\Delta \max = \max_i \max_k |y_0(k)y_i(k)|, \tag{10}$$

$$\Delta = |y_0(k) - y_i(k)|, \tag{11}$$

$$\xi_i(k) = \frac{\Delta \min + \alpha \Delta \max}{\Delta + \alpha \Delta \max}. \tag{12}$$

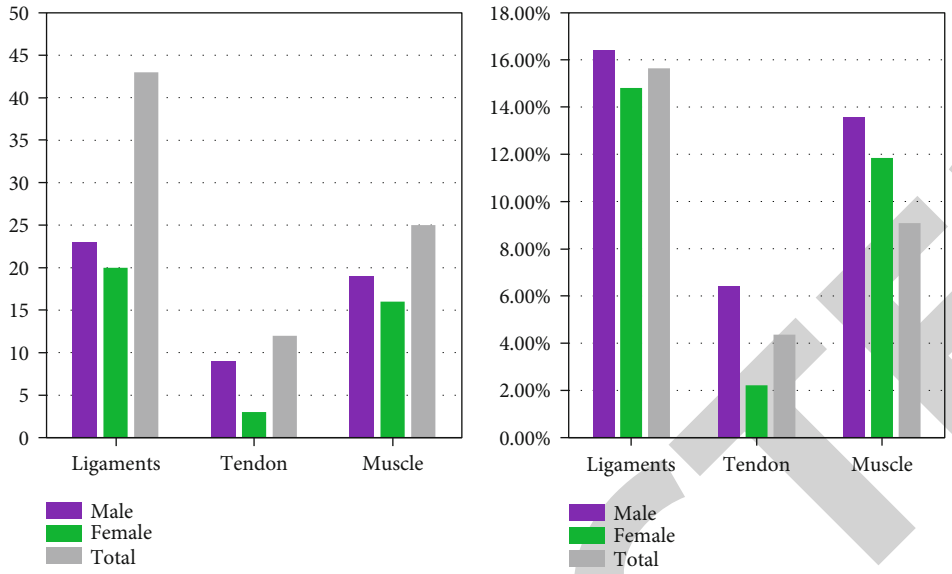

Figure 9: Occurrence of different types of exercise injuries.

Grey correlation calculation:

$$f_i = \frac{1}{m}\sum_{k=1}^{m}\xi_i(k). \tag{13}$$

Net input of unit j:

$$I_j = \sum_i w_{ij}O_i + \theta_j. \tag{14}$$

Error Err_j of output layer unit j:

$$\mathrm{Err}_j = O_j(1-O_j)(T_j - O_j). \tag{15}$$

Error of hidden layer unit j:

$$\mathrm{Err}_j = O_j(1-O_j)\sum_k Err_k w_{kj}. \tag{16}$$

Weight update:

$$\omega(k) = \omega(k-1) + \Delta\omega(k) + a\omega[(k-1)-(k-2)]. \tag{17}$$

Z-score like formula:

$$v' = \frac{v - \overline{A}}{\sigma_A}. \tag{18}$$

Min–max normalized conversion function:

$$v' = \frac{\mathrm{x} - \min}{\max - \min}. \tag{19}$$

The number of hidden layer nodes can be determined by experimental methods:

$$\mathrm{b} = \sqrt{m+n} + a. \tag{20}$$

Among them, a is a constant between 0 and 10, m is the number of nodes in the output layer, and n is the number of nodes in the input layer.

Through the method of quantitative and qualitative evaluation of the structure and content of the questionnaire, relevant experts are asked to evaluate the content indicators of the questionnaire according to five levels: A is very suitable, B is more suitable, C is general, D is general suitable, and E is not suitable. The specific evaluation results are shown in Table 1:

Taking 18-60 year-old people from 15 fitness clubs in 8 districts of a city as the research object, we randomly sampled 20 people from each club, half of them male and female. Among the 275 valid questionnaires returned, 85 people have experienced exercise injuries, with a total of 120 injuries. Figure 5 shows the statistics of the number of injured male and female ratios.

It can be seen from Figure 5 that the proportion of male injuries is 57.6%, which is slightly higher than the 42.4% of females. There is no statistically significant difference between the two. Among the secondary and above injuries, 88.6% of men were significantly higher than 11.4% of women, and there was a significant difference between the two.

Investigating the relationship between people's fitness orientation and motivation and exercise injury, it is found that fitness motivation generally includes health, relieving work pressure, reducing fat and shaping, and increasing muscle content as shown in Table 2.

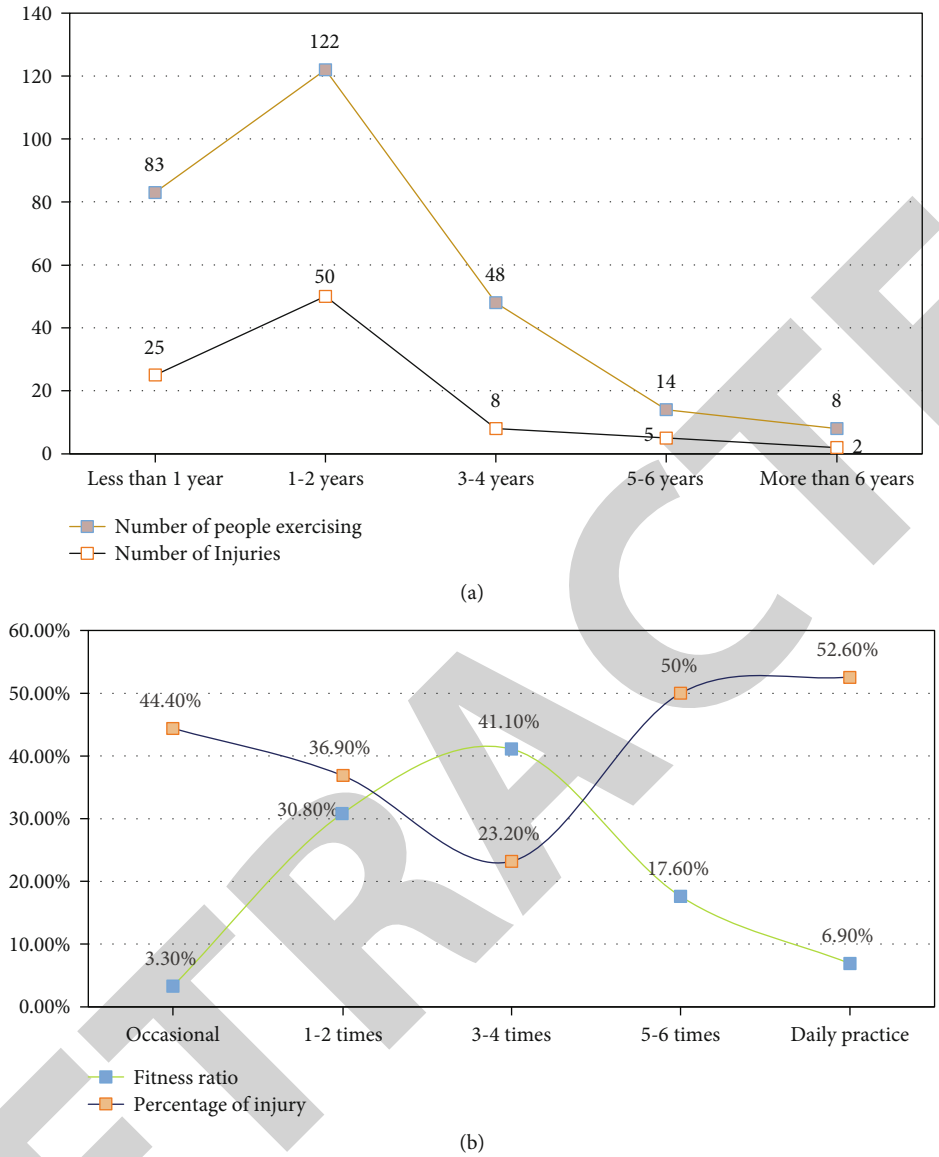

Figure 10: Exercise injury occurrence.

It can be seen from Table 2 that the proportion of different motivational injuries is different. Women's pursuit of appearance is much higher than that of men. They tend to lose fat and shape their bodies. They are keen on aerobics, yoga, and other body exercises and various jumping exercises. They have more exercises. The main motivation of men is to increase muscle content and relieve work pressure, and they are keen on fitness equipment.

The main types of knee injuries include sprains, lacerations, and strains, as shown in Table 3. An example of knee injury is shown in Figure 6.

In fitness club knee exercise injuries, the main manifestations are men, and they are mainly caused by training factors, such as heavy squats and leg lifts, followed by long-term exercises, and overloaded spinning exercises. Knee joint injuries are mostly caused by exercisers' incorrect technical movements, large movements, repeated overloading of the knee joints, and sports fatigue.

The waist sports injuries of exercisers in fitness clubs are mostly acute injuries. The nature and proportion of waist injuries are shown in Table 4. An example of waist injury is shown in Figure 7.

There are many reasons why exercisers may cause sports injuries during exercise. In order to find out the main injury factors and analyze them in detail, a questionnaire for sports injury factors for exercisers in fitness clubs is designed; 10 injury factors were determined, and after statistical analysis, the results are shown in Table 5.

According to the investigation and statistics of the injury site, it is found that the incidence of ankle joint injury is the highest, and it is mainly concentrated in women, as shown in Figure 8.

It can be seen from Figure 8 that the injured parts of male exercisers are relatively scattered, while the injured parts of females are mainly concentrated in the lower extremities.

Whether male or female, the most vulnerable tissues are ligaments, tendons, and muscles, as shown in Figure 9.

It can be seen from Figure 9 that compared with the female exercise group, the male exercise group is more prone to damage to ligaments, tendons, and muscles.

The relationship between fitness years of exercisers and sports injuries is shown in Figure 10(a). The relationship between exerciser's fitness frequency and sports injury is shown in Figure 10(b).

It can be seen from Figure 10(a) that most exercisers lack common sense of fitness, have poor physical fitness, and are prone to sports injuries. With the increase in fitness years, the injury rate gradually decreases, which has a certain relationship with the improvement of exercisers' physical fitness, the increase of fitness knowledge, and the enhancement of fitness experience. From Figure 10(b), it can be seen that the number of people who exercise more than 3 times per week accounted for 65.6% of the total number of people, which indicates that exercisers in a fitness club in a city have a higher number of exercises per week

4. Discussion

With the increasing popularity of sports and bodybuilding, many bodybuilding enthusiasts like to do simple exercises, hoping to have a strong body. The goal of exercisers is to change from simple participation to gradual improvement in body shape. However, exercise is often accompanied by injuries during exercise, which may be dangerous to the athlete's body and will significantly reduce their enthusiasm for exercise.

Sports injury is an injury that occurs in sports activities, and the injured part is closely related to sports equipment and sports equipment. Related research results show that compared with other parts of the body, limb joints are more prone to limb injuries during exercise. Due to the large number of joints, the external force is quite large, leading to various injuries during exercise. Many injuries occur during sports, such as running and swimming.

Data mining technology can analyze and learn patterns and rules useful to users from a large amount of data. Using these learned patterns and rules, when new sample data is available, the possible characteristics of the sample data can be predicted based on the existing patterns and rules.

5. Conclusion

Exercise has a positive effect on physical and mental development, but if the movement is not standard or the preparation before exercise is not sufficient, it is easy to cause injury. Therefore, we must be highly vigilant about sports safety and be fully prepared before exercise to prevent injuries. This article mainly explains the injuries that are likely to occur in fitness exercises, do a good job in the prevention of sports injuries, reduce the incidence of injuries, and do better exercises while ensuring that the body is not damaged. This article analyzes the injuries that are likely to occur in the process of fitness exercise and puts forward some reasonable suggestions.

Data Availability

The data underlying the results presented in the study are available within the manuscript.

Conflicts of Interest

The author declares no conflicts of interest.

References

[1] V. Amodio, H. Bruch, T. Mollayeva, and A. Colantonio, "Using the narratives of Ontarians with a work-related traumatic brain injury to inform injury prevention: a mixed methods approach," *Work*, vol. 56, no. 4, pp. 563–570, 2017.

[2] Y. Cui, "Intelligent recommendation system based on mathematical modeling in personalized data mining," *Mathematical Problems in Engineering*, vol. 2021, no. 3, Article ID 6672036, p. 11, 2021.

[3] D. Shin and J. Shim, "A systematic review on data mining for mathematics and science education," *International Journal of Science and Mathematics Education*, vol. 19, no. 4, pp. 639–659, 2021.

[4] B. F. F. Nabukenya, J. Nabende, P. Nabende, and R. Wesonga, "On the goodness of fit of parametric and non-parametric data mining techniques: the case of malaria incidence thresholds in Uganda," *Health and Technology*, vol. 11, no. 4, pp. 929–940, 2021.

[5] C. Zhao, C. L. Lin, W. Chen, M. K. Chen, and J. Wang, "Visual heart rate estimation and negative feedback control for fitness exercise," *Biomedical Signal Processing and Control*, vol. 56, no. 5, article 101680, 2020.

[6] M. C. Lee, K. Byun, J. S. Kim, H. Lee, and K. Kim, "Trends in exercise neuroscience: raising demand for brain fitness," *Journal of Exercise Rehabilitation*, vol. 15, no. 2, pp. 176–179, 2019.

[7] S. N. Alsubari, S. N. Deshmukh, A. A. Alqarni et al., "Data analytics for the identification of fake reviews using supervised learning," *CMC-Computers, Materials & Continua*, vol. 70, no. 2, pp. 3189–3204, 2022.

[8] K. Selvi and Z. Bozo, "The dark side of bodybuilding: the role of bodybuilding activities in compensation of frustrated basic psychological needs," *Motivation and Emotion*, vol. 44, no. 2, pp. 190–208, 2020.

[9] K. A. Ogudo, D. Muwawa Jean Nestor, O. Ibrahim Khalaf, and H. Daei Kasmaei, "A device performance and data analytics concept for smartphones' IoT services and machine-type communication in cellular networks," *Symmetry*, vol. 11, no. 4, pp. 593–609, 2019.

[10] X. Li, H. Liu, W. Wang, Y. Zheng, H. Lv, and Z. Lv, "Big data analysis of the internet of things in the digital twins of smart city based on deep learning," *Future Generation Computer Systems*, vol. 128, pp. 167–177, 2021.

[11] O. I. Khalaf and G. M. Abdulsahib, "Energy efficient routing and reliable data transmission protocol in WSN," *International Journal of Advances in Soft Computing and its Application*, vol. 12, no. 3, pp. 45–53, 2020.

[12] E. Merino García, F. J. Borrego Utiel, M. Martínez Arcos, J. Borrego Hinojosa, and M. P. Pérez del Barrio, "Kidney damage due to the use of anabolic androgenic steroids and practice of bodybuilding," *Nefrología (Madrid)*, vol. 38, no. 1, pp. 101–103, 2018.

Hindawi
Computational and Mathematical Methods in Medicine
Volume 2023, Article ID 9753817, 1 page
https://doi.org/10.1155/2023/9753817

Retraction

Retracted: Effect of Dexmedetomidine on Cardiac Output among Parturient with Severe Preeclampsia after Cesarean Section

Computational and Mathematical Methods in Medicine

Received 27 June 2023; Accepted 27 June 2023; Published 28 June 2023

This article has been retracted by Hindawi following an investigation undertaken by the publisher [1]. This investigation has uncovered evidence of one or more of the following indicators of systematic manipulation of the publication process:

(1) Discrepancies in scope

(2) Discrepancies in the description of the research reported

(3) Discrepancies between the availability of data and the research described

(4) Inappropriate citations

(5) Incoherent, meaningless and/or irrelevant content included in the article

(6) Peer-review manipulation

The presence of these indicators undermines our confidence in the integrity of the article's content and we cannot, therefore, vouch for its reliability. Please note that this notice is intended solely to alert readers that the content of this article is unreliable. We have not investigated whether authors were aware of or involved in the systematic manipulation of the publication process.

Wiley and Hindawi regrets that the usual quality checks did not identify these issues before publication and have since put additional measures in place to safeguard research integrity.

We wish to credit our own Research Integrity and Research Publishing teams and anonymous and named external researchers and research integrity experts for contributing to this investigation.

The corresponding author, as the representative of all authors, has been given the opportunity to register their agreement or disagreement to this retraction. We have kept a record of any response received.

References

[1] Y. Lv, Y. Zhou, Y. Qiao et al., "Effect of Dexmedetomidine on Cardiac Output among Parturient with Severe Preeclampsia after Cesarean Section," *Computational and Mathematical Methods in Medicine*, vol. 2022, Article ID 4742350, 7 pages, 2022.

Hindawi
Computational and Mathematical Methods in Medicine
Volume 2022, Article ID 4742350, 7 pages
https://doi.org/10.1155/2022/4742350

Research Article

Effect of Dexmedetomidine on Cardiac Output among Parturient with Severe Preeclampsia after Cesarean Section

Yanxiang Lv, Ying Zhou, Yuan Qiao, Rui Hu, Yan Liang, Yanan Lian, and Tongqiang He

Department of Obstetrics and Gynecology Intensive Care Unit, Northwest Women and Children's Hospital, Xi'an 710032, China

Correspondence should be addressed to Tongqiang He; xbfymicu@163.com

Received 26 January 2022; Revised 23 February 2022; Accepted 5 March 2022; Published 14 April 2022

Academic Editor: Shakeel Ahmad

This study was to investigate the hemodynamic effect of dexmedetomidine among parturient with severe preeclampsia after cesarean section. Parturient with severe preeclampsia were randomly allocated to receive dexmedetomidine (0.2-0.7 μg/kg/h) or equivalent volumes of 0.9% saline as control after cesarean section, respectively. A total of 36 parturient with severe preeclampsia were enrolled, including 18 in the dexmedetomidine (DEX) group and 18 in the saline group. Compared with the saline group, among those in the DEX group, CO was reduced by 1.30 L/min (95% CI: -2.36 to 0.25; $P = 0.019$). Additionally, HR (-13.79 bpm, 95% CI: -22.02 to -5.58; $P = 0.002$), SBP (-16.11 mmHg, 95% CI: -30.56 to -1.66; $P = 0.030$), DBP (-10.48 mmHg, 95% CI: -18.27 to -2.69; $P = 0.002$), and MAP (-12.36 mmHg, 95% CI: -22.05 to -2.66; $P = 0.014$) were reduced in the DEX group compared with the saline group. In contrast, there were no changes observed in SV and ICON between groups. In conclusion, dexmedetomidine reduces cardiac output by inhibiting the acceleration of heart rate without sacrificing myocardial contractility and stroke volume.

1. Introduction

Preeclampsia is the most common complication of pregnancy affects 2% to 8% of pregnancies [1, 2]. This disorder of pregnancy increases maternal and fetal morbidity as well as mortality prominently. Various complications [3–5], such as eclampsia, heart failure, and exacerbated or persistent hypertension, still occur frequently in parturient with preeclampsia postpartum, especially with pain, anxiety, and scare postoperative. Sedation and analgesia are widely recommended as an approach to control agitation, blunt the stress response, and reduce metabolism in intensive care unit (ICU) [6]. Timely sedation postpartum could minimize patient discomfort that may obtain many benefits. However, specific recommendations for patients with severe preeclampsia are lacking in postoperative sedation.

Dexmedetomidine, a highly selective α-2-receptor agonist, is a first-line sedative medication in ICU and has been increasingly used for obstetric anesthesia. Dexmedetomidine, which provides light sedation, possesses analgesic, sympatholytic, anxiolytic properties and attenuates the stress response without significant respiratory depression [7, 8]. Due to the short half-life, dexmedetomidine was undetectable in milk at 24 hours after discontinuation of the administration and conducive to the early conversion of infant feeding to exclusive breastfeeding [9], suggesting that dexmedetomidine is compatible with breastfeeding [10]. Theoretically, dexmedetomidine might make it an ideal sedative for parturient with severe preeclampsia postoperative. We designed this study to explore the hemodynamic security of dexmedetomidine in parturient with severe preeclampsia after cesarean section.

2. Methods

2.1. Inclusion Criteria and Exclusion Criteria. This prospective, randomized, and controlled study was approved by the Ethics Committee of Northwest Women and Children's Hospital (NWCH; approval number: 21-048). The inclusion

criteria were patients with severe preeclampsia over 18 years old and patients who received cesarean section in the Department of Obstetrics and Gynecology Intensive Care Unit, NWCH, from 1 January to 31 December 2019. The exclusion criteria were cardiovascular disease, sick sinus syndrome or atrioventricular block, bradycardia (heart rate < 50 beats·min^{-1}), multiple pregnancies, allergy to dexmedetomidine, currently receiving antipsychotic drugs, eclampsia, or acute heart failure before cesarean section.

2.2. Usual Management. All participants signed informed consent and were divided into two groups randomly using a computer-generated table of random numbers. Every patient equally received a usual postoperative care including administration of oxytocin, magnesium sulfate for seizure prophylaxis, analgesia, and antihypertensive agent. Antihypertensive medications were administrated when systolic blood pressure ≥ 160 mmHg and/or diastolic blood pressure ≥ 110 mmHg. All patients received analgesia protocol consisted of 100 μg sufentanil diluted into 100 mL postoperative.

2.3. Interventions. In the DEX group, patients received continuous infusion of dexmedetomidine without loading dose at a rate of 0.2-0.7 μg/kg/h to achieve RASS score in the target range on the night of surgery. The target of sedation scores on the Richmond Agitation and Sedation Scale was −2 to +1 (lightly sedated to restless), on which scores range from −5 [unresponsive] to +4 [combative], as assessed at least every 2 hours. The saline group received equivalent volumes of saline. If bradycardia occurred which was defined as heart rate < 50 beats·min^{-1}, the infusion of dexmedetomidine was terminated and the patient was excluded from the study.

2.4. Diagnostic Criteria. Severe preeclampsia met the Clinical Management Guidelines for Obstetrician-Gynecologists of ACOG criteria for preeclampsia diagnosis and fulfilled one of the severe features [11]: systolic blood pressure ≥ 160 mmHg and/or diastolic blood pressure ≥ 110 mmHg; severe persistent right upper quadrant or epigastric pain not accounted for by alternative diagnoses and abnormally elevated liver enzymes which indicated impaired liver function; renal insufficiency; thrombocytopenia; pulmonary edema; new-onset headache; and visual symptom.

2.5. Outcome Measures. The primary outcome was the change of cardiac output (CO) from baseline. Secondary outcomes included the change of other hemodynamic variables from baseline: stroke volume (SV), index of contractility (ICON), heart rate (HR), systolic blood pressure (SBP), diastolic blood pressure (DBP), and mean arterial blood pressure (MAP). Variables were obtained before dexmedetomidine or saline administration as baseline and at 10 hours after dexmedetomidine or saline administration, respectively. Adverse events such as eclampsia, heart failure, bradycardia, and nausea and vomiting (PONV) were monitored and recorded. The hemodynamic variables were obtained by the ICON™ monitor, a noninvasive hemodynamic monitoring device (Osypka Medical, Berlin, Germany).

2.6. Statistical Analysis. Study data from Lee et al. showed a decrease of CO from 3.72 ± 1.0 L/min at baseline to 2.90 ± 0.5 L/min at 20 min after administration in the DEX group with no changes (from 3.61 ± 1.1 L/min to 3.87 ± 1.4 L/min) in the saline group. A two-sided 0.05 level of significance and a sample size of 36 patients (18 per group) provided 80% statistical power to demonstrate this difference in CO. To accommodate for a 10% attrition rate, we will recruit a total of 40 patients (PASS11, independent t tests; allocation ration = 1).

The normality of the data distribution was verified by the Shapiro-Wilk tests. For continuous data, means with standard deviations (SDs) were presented. The changes of hemodynamic variables were calculated as the value after drug administration minus the value at baseline. Mean differences were expressed with their 2-sided 95% confidence intervals. Independent-samples *t* tests were performed for between-group differences. Within-group comparisons from baseline to drug administration were tested with paired-samples *t* tests. All statistical analyses were conducted with SPSS 25.0 software package, a 2-sided *P* value of <0.05 was considered statistically significant.

3. Results

From the 64 patients who met the enrollment criteria, 40 patients agreed to participate. Thirty-six parturient with severe preeclampsia completed the study, 18 in each group, respectively (Figure 1).

Demographic characteristics and baseline of hemodynamic variables were similar in the two groups (Table 1).

As Figure 2 shows, CO decreased by 0.10 ± 0.68 L/min in the DEX group and significantly increased by 1.2 ± 1.7 L/min in the saline group compared with baseline. The change in CO was significantly different between groups by -1.30 L/min (95% CI: -2.36 to 0.25; $P = 0.019$). Similarly, HR was remarkably accelerated in the saline group and significantly reduced in the DEX group compared with the saline group (-13.79 bpm; 95% CI: -22.02 to -5.58; $P = 0.002$). No changes were observed in SV and ICON in either group (-7.63 mL, 95% CI: -17.83 to 2.57; $P = 0.133$), (-8.27, 95% CI: -21.22 to 4.69; $P = 0.1.94$).

Systolic blood pressure (-16.11 mmHg, 95% CI: -30.56 to -1.66; $P = 0.030$) and diastolic blood pressure (-10.48 mmHg, 95% CI: -18.27 to -2.69; $P = 0.002$) as well as mean arterial blood pressure (-12.36 mmHg, 95% CI: -22.05 to -2.66; $P = 0.014$) were also significantly reduced in the DEX group compared with the saline group (Figure 3).

Five patients in the DEX group received antihypertensive medication and 6 in the saline group during study period (27.8% vs. 33.3%, $P > 0.05$). No major adverse events such as eclampsia and heart failure were recorded during the study. Three patients reported nausea and vomiting in both groups after intervention.

4. Discussion

The most important finding of present study is the infusion of dexmedetomidine without loading dose reduce cardiac

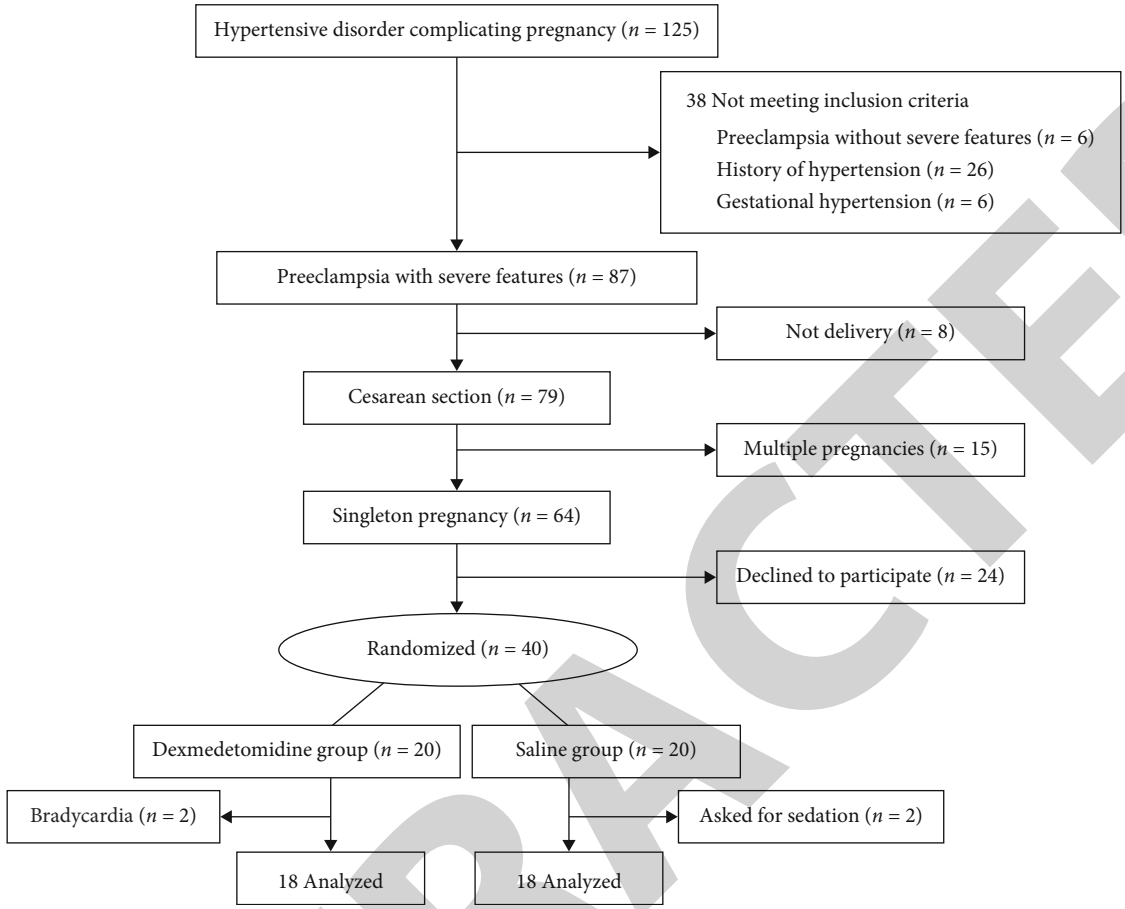

Figure 1: Flow diagram of the studied patients enrolled in the study.

output by attenuated heart rate in patients with severe preeclampsia postoperative but does not impair stroke volume and index of contractility. It is also suggested that the administration of dexmedetomidine decrease blood pressure.

Several researches reported the effects of dexmedetomidine on cardiac function. Lee et al. [12] assessed cardiac function in healthy patients during general anesthesia by the echocardiographic examinations and found that dexmedetomidine did not impair biventricular systolic and diastolic function but decreased cardiac output by reducing heart rate. Snapir et al. [13] reported that dexmedetomidine significantly reduced CO and HR of healthy male subjects in parallel with a reduction in myocardial oxygen demand and did not induce evident myocardial ischemia but caused a decrease in SV when the dosage exceed the recommended therapeutic level. Additionally, escalading dose of dexmedetomidine also led reduced CO and SV [14, 15]. However, high dose effect of dexmedetomidine on CO is contrary in animal experiment [16]. A series of animal experiments [17–21] showed that dexmedetomidine prevents myocardial dysfunction via multiple signaling pathways. A meta-analysis [22] showed that dexmedetomidine is an efficacious cardioprotective drug in adults and children undergoing cardiac surgery. Compared to previous studies, the present study was conducted in women with preeclampsia. Preeclampsia is a pathological condition, which is accompanied with reduced compensatory function associated with hypertension and myocardial ischemia. In consideration of loading dose transient hypertension reported [23], we adopted

Table 1: Baseline demographic and clinical characteristics (mean ± SD).

	DEX ($n = 18$)	Saline ($n = 18$)	P
Age (year)	30.50 ± 4.82	32.22 ± 4.13	0.259
BMI (kg/m^2)	29.03 ± 2.95	28.61 ± 3.05	0.675
Delivery week	34.90 ± 2.23	35.02 ± 2.66	0.878
CO (L/min)	4.66 ± 0.88	4.46 ± 1.15	0.560
HR (bmp)	82.94 ± 12.16	78.00 ± 11.93	0.227
SV (mL)	56.11 ± 8.08	57.28 ± 10.40	0.709
ICON	37.92 ± 7.92	38.76 ± 12.06	0.806
SBP (mmHg)	143.67 ± 11.75	138.56 ± 13.19	0.228
DBP (mmHg)	94.56 ± 9.40	92.56 ± 9.62	0.532
MAP (mmHg)	110.22 ± 9.16	107.83 ± 10.29	0.467

DEX: dexmedetomidine; BMI: Body Mass Index; CO: cardiac output; HR: heart rate; SV: stroke volume; ICON: index of contractility; SBP: systolic blood pressure; DBP: diastolic blood pressure; MAP: mean arterial blood pressure.

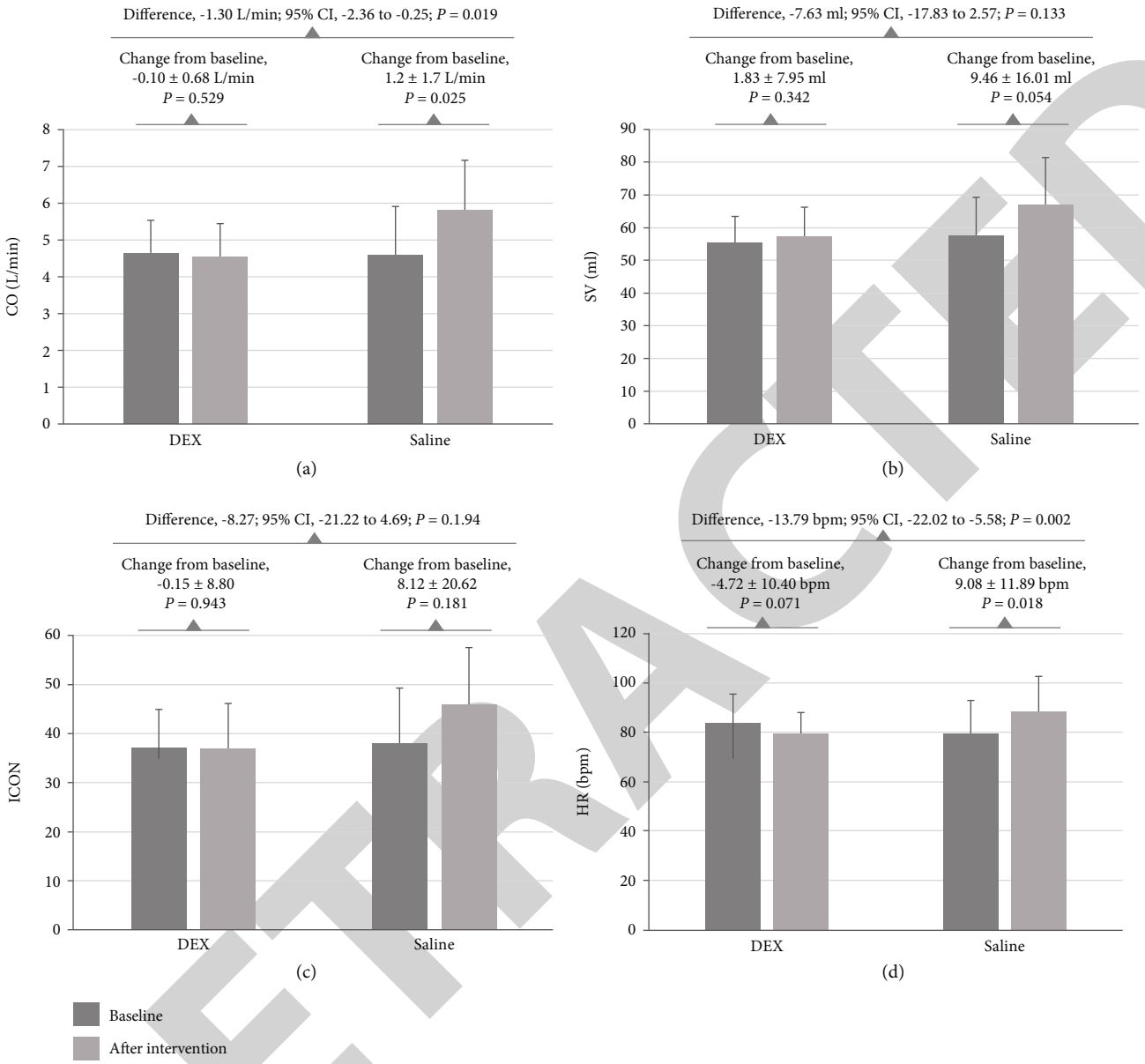

Figure 2: Changes in cardiac output. (a) Change from baseline to the end of treatment in cardiac output; (b) change from baseline to the end of treatment in stroke volume; (c) change from baseline to the end of treatment in index of contractility; (d) change from baseline to the end of treatment in heart rate. DEX: dexmedetomidine; CO: cardiac output; SV: stroke volume; ICON: index of contractility; HR: heart rate; CI: confidence interval.

a method of continuous infusion at recommended rate without loading dose [2] in patients with severe preeclampsia postoperative. Our study reveals that dexmedetomidine reduces cardiac output by inhibiting the acceleration of heart rate without sacrificing myocardial contractility and stroke volume. According to these data, we can infer that patients with severe preeclampsia may benefit from dexmedetomidine by decelerating heart rate and therefore reducing cardiac work and myocardial oxygen consumption.

Previous studies have reported that administration of dexmedetomidine provided a significant hemodynamic stability during cesarean section in patients with preeclampsia [24–28]. There is very little published research on administration of dexmedetomidine for postoperative sedation of preeclampsia patients. A few of the published studies showed that dexmedetomidine sedation in eclampsia patients were effective in reducing blood pressure [29–31]. This also accords with our research, which showed that blood pressure was significantly reduced after dexmedetomidine administration. However, all of these studies did not evaluate the effects of dexmedetomidine on cardiac function. We monitored the effects of dexmedetomidine on cardiac function in patients with severe preeclampsia by noninvasive hemodynamics technology for the first time. It is the strength of this study.

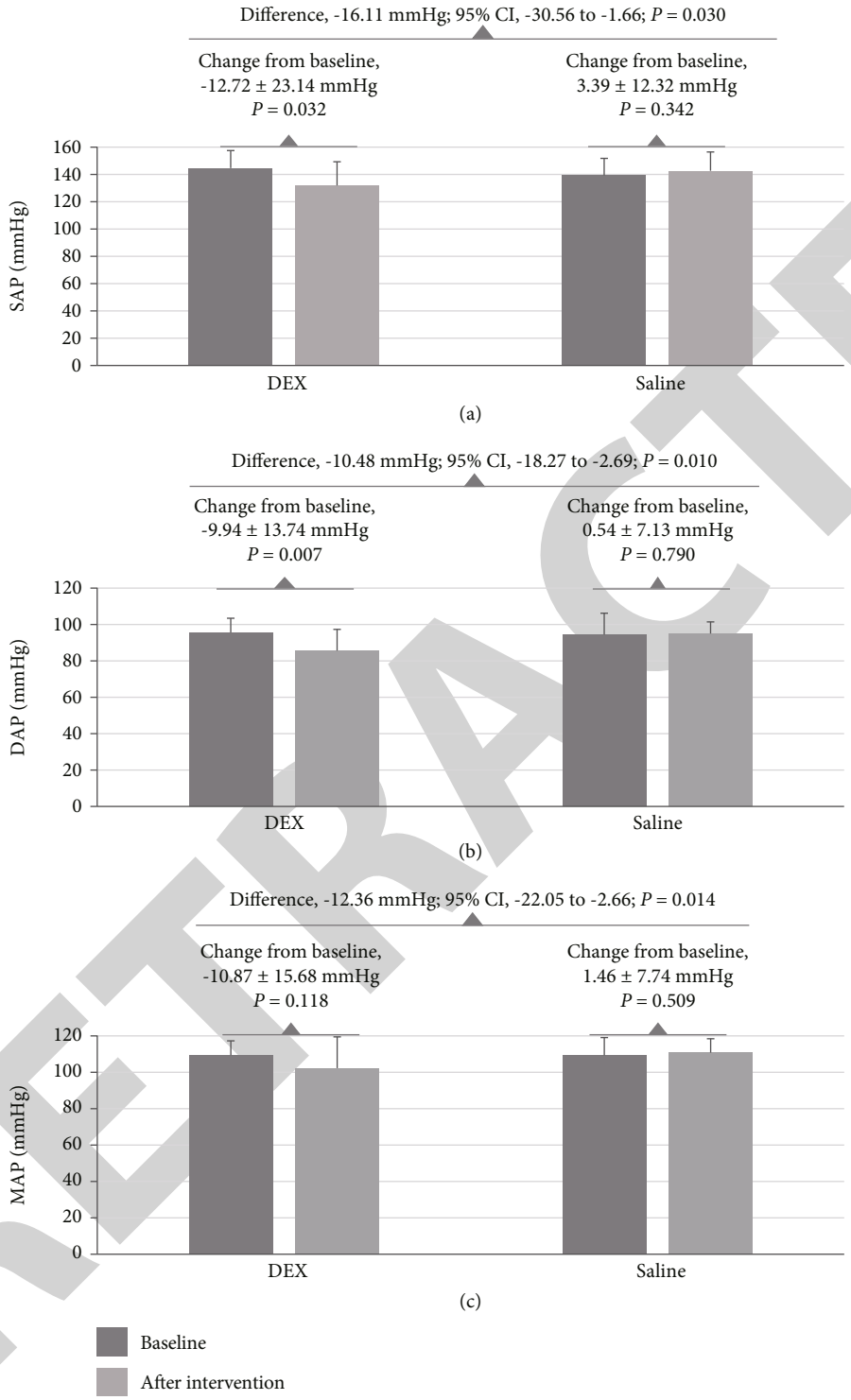

Figure 3: Changes in blood pressure. (a) Change from baseline to the end of treatment in systolic blood pressure; (b) change from baseline to the end of treatment in diastolic blood pressure; (c) change from baseline to the end of treatment in mean arterial blood pressure. DEX: dexmedetomidine; SBP: systolic blood pressure; DBP: diastolic blood pressure; MAP: mean arterial blood pressure; CI: confidence interval.

5. Limitations

The first limitation is associated with lack of blinding. The unblinded manner may have introduced subjective bias by clinicians. In addition, the plasma concentration of dexmedetomidine was not measured, which may be useful to determine whether plasma concentration varied hemodynamic effects, especially on cardiac function. Thirdly, we did not monitor the plasma level of cortisol and noradrenaline, which could improve our understanding in the potential mechanism of dexmedetomidine on hemodynamic.

6. Conclusion

In conclusion, dexmedetomidine may reduce the risk of heart failure by reducing cardiac work and cardiac afterload. Sedation should be routinely performed in parturient with severe preeclampsia after cesarean section to cope with adverse events caused by stress, pain, postoperative hypertension, and increased cardiovascular volume.

Data Availability

The data used to support the findings of this study are available from the corresponding author upon request.

Conflicts of Interest

None of authors have a conflict of interest.

Authors' Contributions

Yanxiang Lv, Ying Zhou, and Yuan Qiao contributed equally to this work.

Acknowledgments

This study was supported by Shaanxi Provincial Science and Technology Department, China (Grant number 2018SF-078), and Scientific Research Project of Northwest Women and Children's Hospital (Grant number 2018LQ03).

References

[1] K. Melchiorre, R. Sharma, and B. Thilaganathan, "Cardiovascular implications in preeclampsia," *Circulation*, vol. 130, no. 8, pp. 703–714, 2014.

[2] C. V. Ananth, K. M. Keyes, and R. J. Wapner, "Pre-eclampsia rates in the United States, 1980-2010: age-period-cohort analysis," *BMJ*, vol. 347, 2013.

[3] M. C. Chames, J. C. Livingston, T. S. Ivester, J. R. Barton, and B. M. Sibai, "Late postpartum eclampsia: a preventable disease?," *American Journal of Obstetrics and Gynecology*, vol. 186, no. 6, pp. 1174–1177, 2002.

[4] M. F. Mogos, M. R. Piano, B. L. McFarlin, J. L. Salemi, K. L. Liese, and J. E. Briller, "Heart failure in pregnant women," *Circulation. Heart Failure*, vol. 11, no. 1, article e004005, 2018.

[5] A. Goel, M. R. Maski, S. Bajracharya et al., "Epidemiology and mechanisms of de novo and persistent hypertension in the postpartum period," *Circulation*, vol. 132, no. 18, pp. 1726–1733, 2015.

[6] J. Barr, G. L. Fraser, K. Puntillo et al., "Clinical practice guidelines for the management of pain, agitation, and delirium in adult patients in the intensive care unit," *Critical Care Medicine*, vol. 41, no. 1, pp. 263–306, 2013.

[7] D. Yuan, Z. Liu, J. Kaindl et al., "Activation of the α_{2B} adrenoceptor by the sedative sympatholytic dexmedetomidine," *Nature Chemical Biology*, vol. 16, no. 5, pp. 507–512, 2020.

[8] N. Bhana, K. L. Goa, and M. C. Kj, "Dexmedetomidine," *Drugs*, vol. 59, no. 2, pp. 263–268, 2000, discussion 269-270.

[9] Y. Wang, X. Fang, C. Liu, X. Ma, Y. Song, and M. Yan, "Impact of intraoperative infusion and postoperative PCIA of dexmedetomidine on early breastfeeding after elective cesarean section: a randomized double-blind controlled trial," *Drug Design, Development and Therapy*, vol. 14, pp. 1083–1093, 2020.

[10] R. Nakanishi, M. Yoshimura, M. Suno et al., "Detection of dexmedetomidine in human breast milk using liquid chromatography- tandem mass spectrometry: application to a study of drug safety in breastfeeding after Cesarean section," *Journal of Chromatography. B, Analytical Technologies in the Biomedical and Life Sciences*, vol. 1040, pp. 208–213, 2017.

[11] ACOG Practice Bulletin No, "202: gestational hypertension and preeclampsia," *Obstetrics and Gynecology*, vol. 133, no. 1, p. 1, 2019.

[12] S. H. Lee, Y. S. Choi, G. R. Hong, and Y. J. Oh, "Echocardiographic evaluation of the effects of dexmedetomidine on cardiac function during total intravenous anaesthesia," *Anaesthesia*, vol. 70, no. 9, pp. 1052–1059, 2015.

[13] A. Snapir, J. Posti, E. Kentala et al., "Effects of low and high plasma concentrations of dexmedetomidine on myocardial perfusion and cardiac function in healthy male subjects," *Anesthesiology*, vol. 105, no. 5, pp. 902–910, 2006, quiz 1069-1070.

[14] T. J. Ebert, J. E. Hall, J. A. Barney, T. D. Uhrich, and M. D. Colinco, "The effects of increasing plasma concentrations of dexmedetomidine in humans," *Anesthesiology*, vol. 93, no. 2, pp. 382–394, 2000.

[15] H. Basar, S. Akpinar, N. Doganci et al., "The effects of preanesthetic, single-dose dexmedetomidine on induction, hemodynamic, and cardiovascular parameters," *Journal of Clinical Anesthesia*, vol. 20, no. 6, pp. 431–436, 2008.

[16] P. J. Pascoe, "The cardiopulmonary effects of dexmedetomidine infusions in dogs during isoflurane anesthesia," *Veterinary Anaesthesia and Analgesia*, vol. 42, no. 4, pp. 360–368, 2015.

[17] F. Y. Yang, L. Zhang, Y. Zheng, and H. Dong, "Dexmedetomidine attenuates ischemia and reperfusion-induced cardiomyocyte injury through p53 and forkhead box O3a (FOXO3a)/p53-upregulated modulator of apoptosis (PUMA) signaling signaling," *Bioengineered.*, vol. 13, no. 1, pp. 1377–1387, 2022.

[18] T. Sun, Q. Gong, Y. Wu et al., "Dexmedetomidine alleviates cardiomyocyte apoptosis and cardiac dysfunction may be associated with inhibition of RhoA/ROCK pathway in mice with myocardial infarction," *Naunyn-Schmiedeberg's Archives of Pharmacology*, vol. 394, no. 7, pp. 1569–1577, 2021.

[19] Y. Li, M. Qu, F. Xing et al., "The protective mechanism of dexmedetomidine in regulating Atg14L-beclin1-Vps34 complex against myocardial ischemia-reperfusion injury," *Journal of Cardiovascular Translational Research*, vol. 14, no. 6, pp. 1063–1074, 2021.

[20] Y. Deng, L. Cai, F. Wang et al., "Upregulated microRNA-381-5p strengthens the effect of dexmedetomidine preconditioning to protect against myocardial ischemia-reperfusion injury in mouse models by inhibiting CHI3L1," *International Immunopharmacology*, vol. 92, article 107326, 2021.

[21] Y. Chen, S. Cao, H. Chen, C. Yin, X. Xu, and Z. Yang, "Dexmedetomidine preconditioning reduces myocardial ischemia-reperfusion injury in rats by inhibiting the PERK pathway," *Arquivos Brasileiros de Cardiologia*, vol. 117, no. 6, pp. 1134–1144, 2021.

[22] Z. Gong, L. Ma, Y. L. Zhong, J. Li, J. Lv, and Y. B. Xie, "Myocardial protective effects of dexmedetomidine in patients undergoing cardiac surgery: a meta-analysis and systematic

Hindawi
Computational and Mathematical Methods in Medicine
Volume 2023, Article ID 9846079, 1 page
https://doi.org/10.1155/2023/9846079

Retraction

Retracted: Factors That Affect Maternal Mortality in Rwanda: A Comparative Study with India and Bangladesh

Computational and Mathematical Methods in Medicine

Received 3 October 2023; Accepted 3 October 2023; Published 4 October 2023

This article has been retracted by Hindawi following an investigation undertaken by the publisher [1]. This investigation has uncovered evidence of one or more of the following indicators of systematic manipulation of the publication process:

(1) Discrepancies in scope

(2) Discrepancies in the description of the research reported

(3) Discrepancies between the availability of data and the research described

(4) Inappropriate citations

(5) Incoherent, meaningless and/or irrelevant content included in the article

(6) Peer-review manipulation

The presence of these indicators undermines our confidence in the integrity of the article's content and we cannot, therefore, vouch for its reliability. Please note that this notice is intended solely to alert readers that the content of this article is unreliable. We have not investigated whether authors were aware of or involved in the systematic manipulation of the publication process.

In addition, our investigation has also shown that one or more of the following human-subject reporting requirements has not been met in this article: ethical approval by an Institutional Review Board (IRB) committee or equivalent, patient/participant consent to participate, and/or agreement to publish patient/participant details (where relevant).

Wiley and Hindawi regrets that the usual quality checks did not identify these issues before publication and have since put additional measures in place to safeguard research integrity.

We wish to credit our own Research Integrity and Research Publishing teams and anonymous and named external researchers and research integrity experts for contributing to this investigation.

The corresponding author, as the representative of all authors, has been given the opportunity to register their agreement or disagreement to this retraction. We have kept a record of any response received.

References

[1] M. Patrick, M. S. u. Zaman, G. Afzal, M. Mahsud, and M. N. Hanifatu, "Factors That Affect Maternal Mortality in Rwanda: A Comparative Study with India and Bangladesh," *Computational and Mathematical Methods in Medicine*, vol. 2022, Article ID 1940188, 9 pages, 2022.

Hindawi
Computational and Mathematical Methods in Medicine
Volume 2022, Article ID 1940188, 9 pages
https://doi.org/10.1155/2022/1940188

Research Article

Factors That Affect Maternal Mortality in Rwanda: A Comparative Study with India and Bangladesh

Mugenzi Patrick,[1] Muhammad Sami uz Zaman,[1] Ghazala Afzal,[2] Minhas Mahsud,[3] and Mumuni Napari Hanifatu[4]

[1]*Beijing University of Aeronautics & Astronautics (BUAA), Beijing, China*
[2]*Pak Red Crescent Teaching Hospital Dinanath, Lahore, Pakistan*
[3]*National University of Sciences and Technology Islamabad, Pakistan*
[4]*University for Development Studies, Ghana*

Correspondence should be addressed to Mumuni Napari Hanifatu; hanifatu@aims.edu.gh

Received 5 December 2021; Revised 27 January 2022; Accepted 18 February 2022; Published 9 April 2022

Academic Editor: Shakeel Ahmad

Healthcare sector is one of the most pivotal pillars of the administrative setup of a country. It addresses one of the most important dilemmas that countries have to face: provision of quality healthcare to public in affordable prices. Africa lags behind in many health indicators. One of the contemporary health issues faced by countries, especially for those in sub-Sahara countries, is maternal mortality rate (MMR). It has had a significant part to play in the social conditions of the population and needs immediate attention. In spite of many years of civil war and the terrible genocide in the mid-1990s, as of late, Rwanda is showing signs of improvement in healthcare sector. This research is aimed at studying the current state of maternal mortality rate in Rwanda and the factors behind its performance, in a comparative study with India and Bangladesh for a cross-section of time mainly between 1990 and 2015. After a literature review, pivotal indicators that affect healthcare are shortlisted and a comparative analysis of the three countries is made on the basis of these indicators. A regression is run between historical MMR data and these indicators. A directly significant relationship is found between MMR and healthcare expenditure per capita and government commitment to health, closely followed by female literacy and healthcare infrastructure.

1. Introduction

In spite of many years of civil war and the terrible genocide in the mid-1990s which crushed the nation's health framework, as of late, Rwanda has been a model of enhancing access to maternal human services. Rwanda has a big poverty problem, and the nation has an expansive rustic populace, influencing access to healthcare facilities, especially for women. Unintended pregnancies lead to prebirth complications and risky premature births, which, coupled with strained assets at the provincial and regional levels, adds to maternal dismalness and mortality.

However, the Rwandan government has made enhancing family planning services a national priority. Working with the World Health Organization, the Rwandan Ministry of Health has organized contracting and preparing health workers to give family planning instruction, family counseling, and such services to the men and women throughout the nation. Thus, Rwanda's maternal mortality rate (MMR) fell by a lot recently. The maternal mortality rate in Rwanda has seen a huge drop from 750 in 2005 (DHS) to 540 in year 2008 and under 400 as indicated by Health Management Information System (HMIS: 2010) and under 300 (RDHS) in 2015. Deliveries by Health Workers expanded from 38 percent in 2005 (DHS) to 52 percent in 2007 (DHS 2007) and 63.5 percent in 2010 (HMIS). The maternal mortality rate has fallen as of late, but is still high. Enhanced healthcare reconnaissance and responsibility have assumed a huge part in diminishing the MMR and expanding the quantity and quality of assisted deliveries in Rwanda. Enhanced surveillance has enabled Rwanda's Ministry of Health to better track the reasons for maternal deaths all through the nation, bringing about more focused approaches

and techniques to counter the issues. Some important factors comprise the high percentage of births that take place without skilled assistance (52%) and the lesser utilization of family planning and basic obstetrics care (CPR: 27%).

UNFPA is another organization that has been working in these fields in Rwanda since 1975. From that time on, it has been effective in progressing and supporting reproductive health and rights, gender, population, and development in Rwanda at both the focal and decentralized levels. According to UNFPA, roughly 800 women pass away from preventable issues during pregnancy and childbirth, 99% of all maternal deaths happen in developing nations, and they are to a great extent preventable [1]. The maternal mortality proportion in developing nations is 240 for each 100,000 births versus 16 for each 100,000 in developed nations. There are substantial incongruities between nations in MMR, with some nations having a very high maternal mortality rate of 1,000 or more per 100,000 live births; more than half of all maternal deaths happen in sub-Saharan Africa and just about 33 percent happen in South Asia [1]. The WHO classifies limited access to services, poverty, information lack, and a dearth of cultural practices in health as main causes of variances in MMR. The strategy reports on maternal mortality only from time to time demonstrate trainings as a reason, and the research has almost nothing to say with regard to the connection between maternal mortality and training. All things considered, it could be said that a positive relationship among instruction and different pointers of well-being exists. A viewpoint suggests that people who are more educated care for and look for medical care more often than those who are less literate [2–4]. This is predictable with the viability that education helps procuring and handling significant data [5, 6]. Education may likewise impact health through its effect on pay but not the same as that of income [4, 6]. However, the studies [7, 8] underscore the influential role of education in reducing maternal mortality. Generally, this study is aimed at studying the data on maternal mortality and how it is affected by some of the selected health indicators, including education, as shall be seen later.

In the Rwandan context, MMR has had a significant part to play in the social conditions of the population. The issue of MMR is not being given serious thought and that is why it needs the immediate attention for the betterment of healthcare provision to adult Rwandan females. If we look on the global scale, sustained health plans, government commitment and foreign aid for health programs have shown meaningful results all across the globe in reducing MMR. Some countries like Bangladesh, Nepal, India, and Honduras have taken concrete steps and performed really well, indicating that if the vision is correct, things shall and do get better. It is important that we learn from the past and not repeat the same mistakes. A previous research by a study [9] evidently points out a relationship between increased maternal survival and the need of education among other factors. It is of utmost importance that these factors are continually investigated especially for all developing countries, not only Rwanda, so as to pinpoint where things are going wrong and why. This research undergoes some limitations; specifically, few empirical researches have analyzed the factors behind improved maternal mortality rate.

This study intends to investigate some facets of Rwandan economy, society, social set-up, governance, and the relevant infrastructure in place and their contributions to the health of an average Rwandan woman. In this regard, this research is aimed at studying the current state of maternal mortality rate in Rwanda and the factors behind its performance, in a comparative study with India and Bangladesh which have been able to perform very well in decreasing MMR for the adult female populations. The choice of variables used in this study resulted from the review of the literature and as a result pivotal indicators or factors that affect healthcare are shortlisted, and we have identified country's economy represented by GDP per capita, health expenditure per capita, government commitment, female literacy rate, healthcare infrastructure and improvement in sanitation, sanitation facilities, and presence of nurses and midwives as commendable studies recommend these factors as building blocks contributing to maternal health [10–14].

2. Literature Review

2.1. Definition of Maternal Mortality. As per the United Nations Maternal Mortality Estimation Inter-office Group, which comprises delegates from the World Health Organization (WHO), United Nations Children's Fund (UNICEF), the United Nations Population Fund (UNFPA), United Nations Population Division, the World Bank, and widely acclaimed academicians, maternal demise is the passing of a woman while pregnant or within 42 days after delivery of a baby, regardless of the term and the site of the pregnancy, from any reason identified with or exasperated by the pregnancy or its administration, not from inadvertent or accidental causes [15]. Maternal death is measured by some indicators of MMR such as the maternal mortality rate, maternal death lifetime risk, and maternal deaths among deaths of women of age of reproduction (PM).

2.2. Factors Determining Maternal Mortality. Variables that determine maternal death can either be direct or indirect. For the most part, direct causes of maternal demise occur as the after effect of an issue of the pregnancy, delivery, or mismanagement of either of these; indirect maternal demise is a pregnancy-related death in a patient with a prior or recently created health issue not related to pregnancy. Fatalities, during but not related to pregnancy, are namely accidental, incidental, or nonobstetrical maternal deaths. As expressed by a study [16] "Make Each Mother and Child Count," the major direct reasons for maternal deaths are serious blood-loss/hemorrhage (25 percent), infections (13 percent), hazardous abortions (13 percent), eclampsia (12 percent), deterred labor (8 percent), other direct causes (8 percent), and indirect causes (20 percent). Indirect causes are malaria, anemia, HIV/AIDS, and cardiovascular sickness, all of which may confound pregnancy or be exasperated by it. Socioeconomic factors, like age, access to resources, and salary level, are noteworthy pointers of maternal demise. Young mothers confront higher dangers of complexities and demise during pregnancy than older mothers, who have higher dangers of creating postpartum hemorrhage, puerperal-endometriosis, operative vaginal delivery, episiotomy,

low birth weight, preterm delivery, and small-for-gestational-age babies, all of which can prompt demise of the mother. Basic care and family support influences results for mothers. Besides, social disservice and social seclusion unfavorably influence maternal well-being, which can prompt increments in maternal demise. Also, absence of access to skilled Medicare during labor, trouble of movement to the closest center to get appropriate care, number of earlier births, absence of prebirth therapeutic care, and poor health framework all add to maternal mortality. Another investigation [17] states that unsafe abortion is another significant reason for maternal passing. As per the World Health Organization, one mother passes from inconveniences emerging from perilous premature births every eight minutes from intricacies arising from hemorrhage, infection, sepsis, and genital trauma. Universally, preventable demise from improperly performed procedures constitutes 13% of maternal mortality, and at least 25% in a few nations where maternal mortality from different causes is moderately low, making unsafe abortion the biggest reason for maternal mortality.

Another study [18] considerably suggested that maternal mortality is significantly related to women education which is also influenced by various aspects including geographical, economic, religious, sociocultural, legal, and political issues.

2.3. Measurement of Maternal Death. The four measures of maternal demise are maternal mortality proportion (MMP), maternal mortality ratio (MMR), lifetime risk of maternal demise, and extent of maternal demise among deaths of Women of Reproductive Years (PM). Maternal mortality proportion (MMP) is the proportion of the quantity of maternal deaths amid a given time period per 100,000 live births over the same time period. Maternal mortality rate (MMR) is the quantity of maternal deaths in a populace isolated by the quantity of women of regenerative age, normally measured per 1,000 women. Lifetime risk of maternal death alludes to the likelihood that a 15-year-old female will pass on in the end from a maternal reason on the off chance that she encounters, all through her lifetime, the dangers of maternal demise, and the general levels of fertility and mortality that are watched for a given population. This rate can be determined utilizing either the maternal mortality proportion (MMP) or the maternal death rate (MMR). Finally, the extent of maternal` deaths among deaths of women of reproductive age (PM) is the quantity of maternal deaths in a given day and age partitioned by the aggregate demises among women between the ages of 15 and 49 years. This study employs and uses the MMR for countries in comparison and analysis/results. Ways to deal with estimating maternal mortality incorporate civil registration framework, household reviews, census, Reproductive Age Mortality Studies (RAMOS), and verbal autopsies.

2.4. The State of Maternal Mortality in Developing Countries. At the end of the last century, sub-Saharan Africa still had high maternal mortality and death rates, with the objectives of safe parenthood eluding numerous administrations. The Program of Action of the International Conference on Population and Development, 1994, and the Fourth World Conference on Women, 1995, were made to handle these issues. These projects drew extraordinary regard for reproductive well-being and rights and to sexual orientation value and equality. The scourge of the Human Immunodeficiency Virus (HIV) and Acquired Immune Deficiency Syndrome (AIDS) desolated the population and left in its wake untold demolition in the statistic, monetary, and social circles (UN, 2003). Statistics from the most recent decade are in sharp contrast to those in the 1980s, while diminishing infant, young, and grown-up death rates and maternal mortality proportions (MMP) were prompting expanding life expectancy and better health status for women in the locale.

Bangladesh is a great instance of a low and middle wage nation accomplishing the improbable, which numerous others neglected to do. It lessened its maternal mortality by 66 percent in the period of 1990 and 2010; the decrease was 40 percent from 2001 and 2010 alone. These were accomplished by bringing down the maternal mortality rate (the quantity of maternal deaths per 100,000 Live Births) from 574 to fewer than 200 in the period from 1990 to 2010. The diminishment was significant for eight years (1990 to 1998), as MMR diminished from 574 to 322 for each 100,000 live births. According to the 2012 WHO statistics, the normal yearly rate of this decrease was 5.9 percent in a period from 1990 to 2010, which is more than the Millennium Development Goal 5 focus of 5.5 percent or more. What is all, the more astonishing is that the diminishment in MMR (maternal deaths per 100,000 live births) was nearly the same in both the urban and provincial territories. At the present rate, Bangladesh is well on its way in achieving the MDG 5 focus of 143 for each 100,000 live births an entire year before its designated time. Another example is India which has been able to excessively lessened maternal mortality by 65 percent from 569 to 190 for each 100,000 live births from 1990 to 2013. However, with 4.5 percent annual decrease in MMR, India might just miss the MDG 5 focus of 5.5 percent or more abatement rate before 2015. Be that as it may, the execution by India has been excellent from that point onward. [19].

2.4.1. Pivotal Success Factors for MMR Decrease. A study [20] exhibited that the decline in maternal mortality was given due importance in mid-to-late 19th century in northwestern Europe (Sweden, Netherland, Denmark and Norway). The concept of MMR expanded later in Britain and USA, moving in to lesser developed countries as a pivotal factor of maternal well-being. Today, maternal health is an important measure of national health. How did Bangladesh, one of the poorest nations on the planet with the most population density and where 75 percent of the populace lives in rural areas, rapidly accomplish MMR decrease? Furthermore, how did India oversee such a change? It is a difficult inquiry to reply to. As indicated by [21], the status and value of women have definitely improved. They are more literate in ways of the world. Oppression of women has descended too.

Between 1930 and 1995, Malaysia and Sri Lanka succeeded, through similar means, in diminishing their MMRs significantly every 6-12 years down to fewer than 50 for each 100,000 live- births by 1995. In the 1930s, Malaysia, notwithstanding gloating a moderately solid economy, and Sri Lanka, a low-salary nation with extraordinarily large amounts of female education, were both tormented by MMRs of more than

500 for every 100,000 Live Births and more than 2000 for every 100,000 Live-Births, respectively. Understanding the overwhelming impact of the poor providence of maternal health on national development and advancement, the two nations actualized exhaustive national systems to diminish maternal mortality. Four key parts added to the achievement of both national projects: extensive strengthening of human development programs (i.e., education, infrastructure, sanitation, and health frameworks) particularly in poor and underserved territories; noteworthy interests in enhanced maternal well-being administrations, enhanced access to proficient nurses and midwives; and progressing political help will decrease MMR. Outstandingly, concurrent with maternal mortality decay amid this period, Sri Lanka additionally diminished its TFR from 5 to 2.2 live births per woman in age of conception and Malaysia from 6.3 to 3.4 live births per women of reproductive age. Supported by great political will and dynamic political bodies focused on decreasing Maternal Mortality in both nations, infrastructure investments, rural health facilities, and human resources empowered the administrations of Sri Lanka and Malaysia to help underprivileged masses [22]. Access to essential health centers quickly expanded. Other human advancement programs, for example, adult education activities and maternal well-being efforts, prompted enhanced information and comprehension of the significance of skilled attendance during childbirth. Surprisingly, neither one of the countries spent in excess of 3 percent of its GDP on health, uniquely lower than different nations of a comparative monetary standing. Against this background, both Sri Lanka and Malaysia set out a remarkable journey to end MMR. These projects prepared nurses and midwives to deal with essential complications in childbirth, connected them to the formal healthcare framework and empowered coordinated effort with doctor's facilities and focus on health. With the advantage of a recently expanded status inside networks, naturally prepared nurses and midwives were sent in provincial areas [23]. Family planning inputs would allow for considerable reductions in maternal deaths worldwide, with the authors estimating that the equivalent of 44% of maternal deaths in 2008 were averted due to contraceptive use and that meeting unmet demand for family planning could prevent a further 29% of maternal deaths [21].

A research study suggested that skilled attendance at childbirth is effectively linked to decrease in maternal mortality in Sweden. On the other hand, the researches that have been done in USA and Netherlands in the 1900s attributed a decline in maternal mortality to the changes in population age and parity [24].

In this study, we shall take a special look at the four human development factors (i.e., education, infrastructure, sanitation, and health frameworks) recommended in many studies [10–14], which are pivotal for success in decreasing MMR substantially. A comparison shall be made between countries of India and Bangladesh with Rwanda, and analysis shall be done, to see how Rwanda fares against these two.

3. Design and Data Analysis

A detailed cross-sectional comparative study between Rwanda and the South East Asian countries of Bangladesh and India shall be done. These are countries that have been able to effectively achieve their MDG 5 goals, especially in maternal mortality, as per the WHO guidelines. The studies shall focus on the most important points relevant to this study as mentioned in the literature and shall elaborate how; over time, these countries have fared. This study [25] defines a source of data as one of the materials the researcher utilize for collecting information during investigation. The study has incorporated data from comprehensive country reports by the UN, World Health Organization (WHO), DHS, UNICEF, World Bank, and other international and national agencies with published data. Historical data taken only from commendable sources from different cross-sections of time (mainly between 1990 and 2015) are used in the analysis. A regression shall be run on the basis of this data, and results shall be achieved.

3.1. Maternal Mortality (MMR). The indicator MMR, that measures number of annual maternal deaths as a fraction of 100,000 live births of a country in the same period, is the most important feature. An optimum value to be achieved for it is 143, which shall be used as a benchmark. The comparison is in Figure 1. Figure 1 as per SDGs shows that the MMR curves for India and Bangladesh are pretty linear, starting around the 600 mark in 1990 and decreasing somehow linearly up till the latest data line, which shows the MMR to have dropped to the 170/100,000 maternal deaths around 2015 for India and Bangladesh. According to expert forecasts, Bangladesh is being tipped to achieve the desired mark fairly soon now in 2020, whereas India is expected to miss it by a narrow margin. Rwanda, after a qualitative forecast analysis depending upon historical data, is tipped to achieve this number by 2025. The data for Rwanda has been nothing short of a revelation which saw MMR rates start from as high as 1300/100,000 in 1990 and then almost becoming half from 1020 in 2000 to 567 in 2005. It has since been decreasing at a rate faster than that of either Bangladesh or India, due to efficient government policies and a healthcare system designed for those who cannot afford it. It has been because of these efforts the MMR for Rwanda is being predicted to fall below that of India and Bangladesh, a huge result. The rates after 2020 are forecasts based upon past data.

3.2. GDP per Capita Data. To measure the rate of economic wealth per person for all three countries (gross domestic product divided by midyear population as per World Bank), following is a comparative study of GDP/capita (in USD) of the countries over a period starting from 1990, although data from commendable sources is from 2000 onwards to 2017.

Figure 2 shows how India has been able to accumulate its wealth and is fast becoming an economic power to reckon with after the turn of the century, and the economic growth has been constant, with some hiccups in the middle. A steady increase since 2003 reached a record when it was doubled in 2009, and it kept on increasing at a steady rate, reaching a peak of around 1900 USD in 2017. For Bangladesh, more than a 100 percent increase was seen between 2003 and 2011 with the amount increasing from around 950 USD/person to 1500 USD/person, a net increase on more than 50 percent, between 2013 and 2017, a sign of

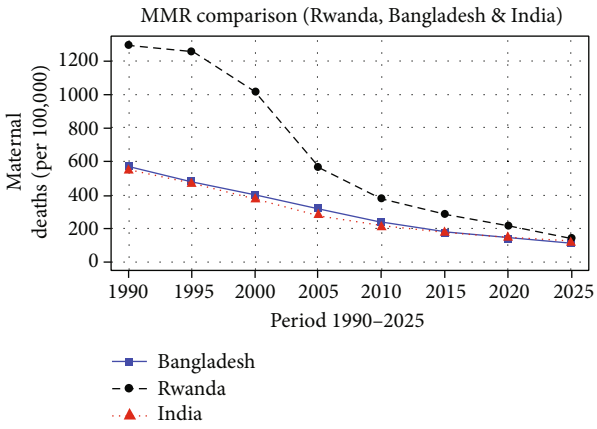

Figure 1: Maternal mortality rate.

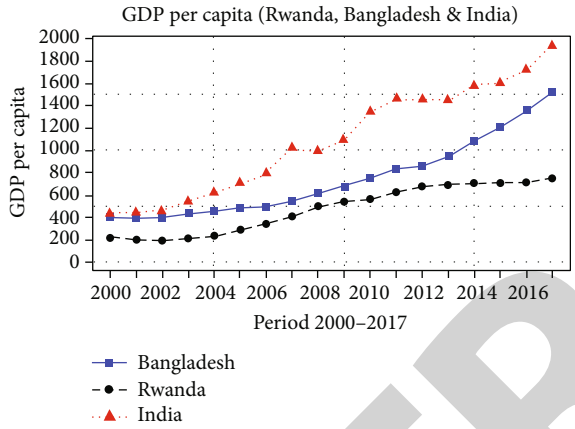

Figure 2: GDP per capita.

why things have been turning around in Bangladesh especially in the health sector. Rwanda is not a country with such big amounts of economy to boast, but with the slump in the early 2000s, the economy of the country is at a steady rise with the government investing more and more. This rate though somehow stalled as of late.

3.3. Health Expenditure per Capita. A very important factor of those mentioned before has been the government commitment to making health a priority in policy setting for country and appreciable budget allocation to improving healthcare. Figure 3 shows a trend of how the three governments have fared in health expenditure per capita in US dollars from 2000 to 2015. The results show a steady increase in the health expenditure data for all three countries, which is instrumental in improving the outlook of healthcare provision. Bangladesh has seen a steady increase in health expenditure per capita doubling the rate of 15.4 USD per capita from 2008 to around 32 USD according to data. The same for India has also been seen to rise at a fast rate, picking up in 2009 to around 34 and soaring to 63 USD per capita according to data. Rwanda has shown the most improvement, whereby the per capita spending increased exponentially after 2002 and kept on increasing. The per capita funding doubled in a single year 8.6 USD per capita in 2002 to more than 16 USD in 2003 and reaching a record high of 59 USD in 2014. A good explanation of these phenomena can be attributed to the health and Medicare aid provided to Rwanda from external sources and other countries, which currently fund 53 percent of all healthcare resources of Rwanda.

3.4. Government Commitment (Monetary). An important indicator when talking about health is the government commitment. The budget committed to the cause of health is a direct indicator of how seriously a country wants to address this issue. A comparison for the three countries is done, and Figure 4 rightly presents the results from 1995 to 2012.

Rwanda has especially surpassed both India and Bangladesh due to appreciable foreign funding for health sector, which is bringing about major changes in the way things are shaping up. Especially in the 2000s the commitment to health has been solid, with the record high of 16% for Rwanda in 2003 and then a whopping 23% in 2006. The number for Rwanda presented here is in 2012 at around 24%. The government commitment trend remains somehow linear for India and Bangladesh, standing at 9% and 8%, respectively.

3.5. Female Literacy Rate. Another important indicator especially for this specific research is the female education. It is a very relevant indicator to give us an insight into how lives can be saved through education. The following comparison shows the numbers for adult female literacy rates in these countries in Figure 5 with commendable data from 1991 to 2015.

Bangladesh has shown a very optimum improvement in the literacy rate when in 1991 it was recorded to be around 26 percent and it went up to around 70% in 2015, a figure which is commendable. The percentage for India was 63% in 2015, which is appreciable, but the rise has been steady, starting from 34 percent in 1991. Rwanda has also shown a somehow steady rise in adult female literacy rate, going up from 37% in 1991 to around 67% in 2015.

3.6. Healthcare Infrastructure and Improvement in Sanitation. A prime factor that is being measured is the investment in healthcare infrastructure by the government and improvement in access to sanitation facilities. Figure 6 presents a comparative study between the three countries in terms of healthcare infrastructure (measured primarily by the increase in hospital beds per person and number of nurses and midwives (which effects MMR directly) with data only from the most commendable sources (2005-2011)). The figure portrays the number of hospital beds per 1000 people in three countries Bangladesh, India, and Rwanda. It reveals that there is an upward slope in the number of hospital beds in both countries Rwanda and Bangladesh, while India presents a steady decrease between 2005 and 2006 and a sharp drop of hospital beds after 2006. In general, Rwanda has a high ratio of hospital beds per 1000 people, though there is no global cutoff metric.

3.7. Sanitation Facilities. Governments of the three countries Rwanda, Bangladesh, and India have endeavored to improve health through providing better sanitation facilities to the

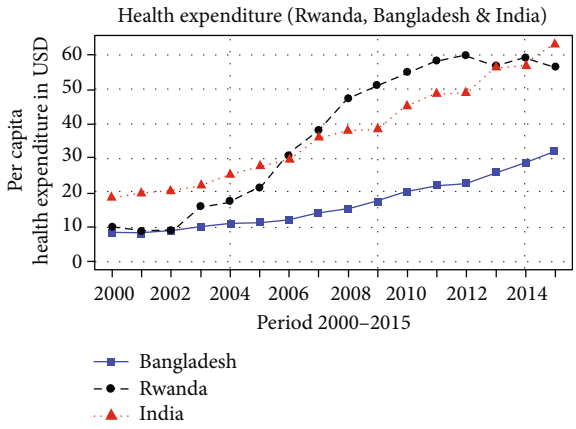

Figure 3: Health expenditure.

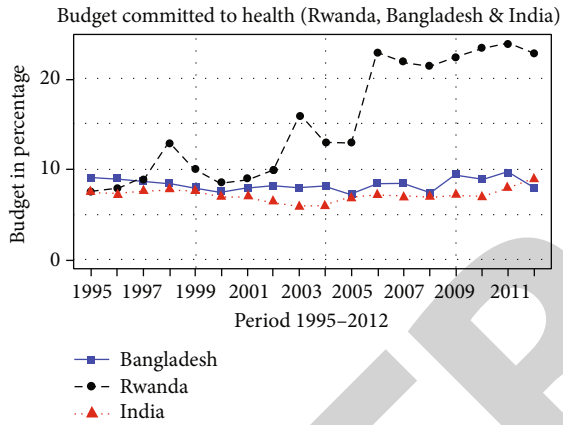

Figure 4: Government commitment (monetary).

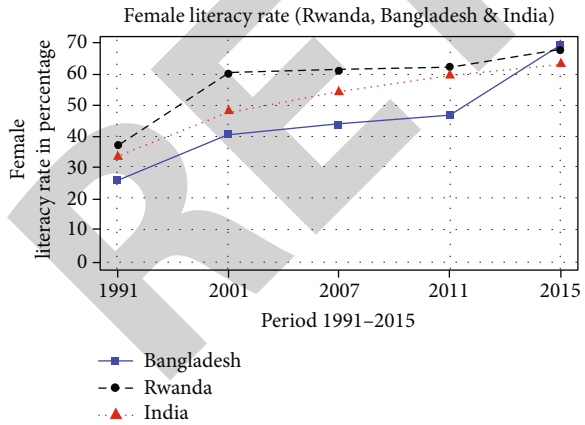

Figure 5: Female literacy rate.

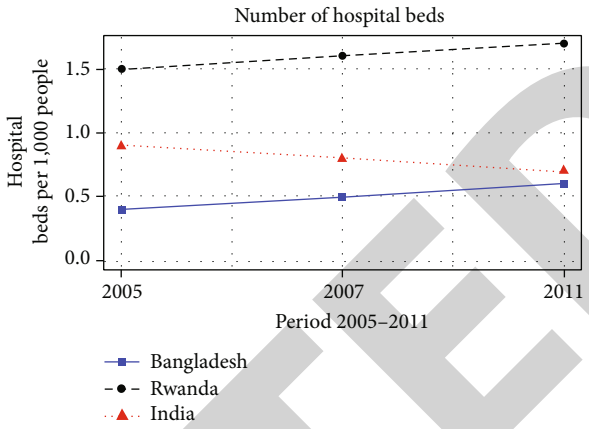

Figure 6: Number of hospital beds per 1000 people.

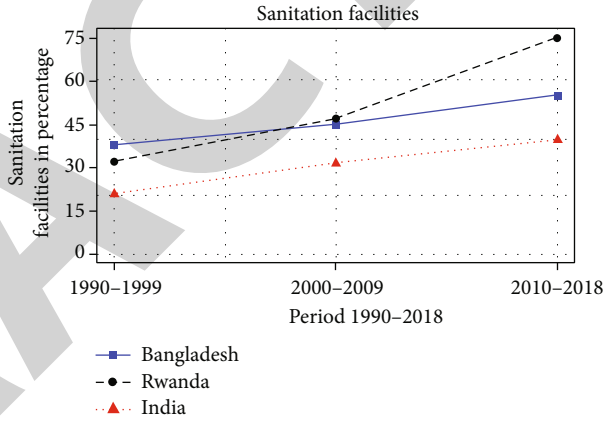

Figure 7: Sanitation facilities.

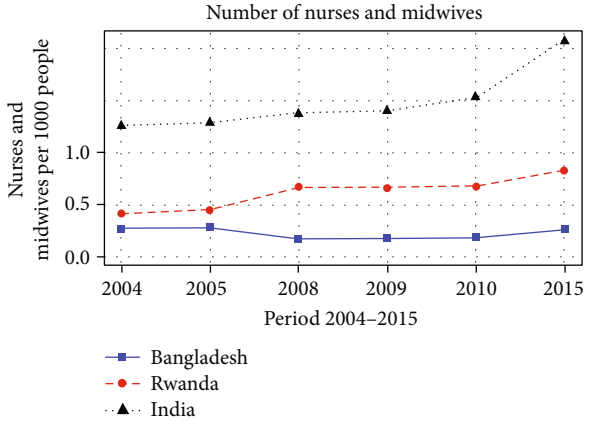

Figure 8: Number of nurses and midwives.

public. Figure 7 presents the comparison of percentage of population with improved access to sanitation facilities in those countries from 1990 to 2018. In the period between 1990 and 1999, Bangladesh had a higher percentage compared with others nearly 40%; however, from 2000 onwards, Rwanda rose sharply in numbers and hit approximately 45% of its population that have access to sanitation facilities and increased the slope thereafter. Finally, from 2010 onwards, Rwanda shows improvement with more than 75% of population who access sanitation facilities; more generally in all the period, India exhibits a small number less than 40% of population who have access to sanitation.

Table 1: Reports the results of the estimation of multiple regression model (equation (1)) using time series data. The dependent variable is the maternal mortality rate (MMR). Standard errors are reported in italics, and ∗∗∗, ∗∗, and∗ denote statistical significance at the 0.1%, 1%, and 5% levels, respectively. The values in parentheses are P values generated from statistical software (R studio).

	Dependent variable: maternal mortality rate (MMR)					
	(1)	*(2)*	*(3)*	*(4)*	*(5)*	*(6)*
GDP	*-1.6990 (0.07332)*					
FLR		−0.3497* *(0.02700)*				
BCH			−0.5035** *(0.005258)*			
Per capita Health Expenditure				−17.01** *(0.006297)*		
Nurses and midwives					−1.8085* *(0.01181)*	
Sanitation Facilities						−0.21557* *(0.031)*
Constant	1268.18** *(0.00855)*	753.93** *(0.00905)*	1303.02*** *(0.000485)*	1231.12*** *(0.000353)*	691.10** *(0.00153)*	200.69* *(0.0182)*
R Squared	*0.5928*	*0.7442*	*0.884*	*0.8733*	*0.8279*	*0.9976*

GDP: gross domestic product; FLR: female literacy rate; BCH: budget committed to health.

3.8. Nurses and Midwives. The ratio of nurses and midwives is among the factors that are highly considered in analyzing the progress of health sector. Therefore, following Figure 8 compares Rwanda, Bangladesh, and India in respect of number of nurses and midwives per 1000 people in the period between 2004 and 2015. At first glance, India clearly exhibits a high number since 2004 and increased slightly until 2010. More interestingly from 2010, the ratio increased sharply close to hit the global target of 2.3 which is presumed to be attained soon. In addition, Rwanda also shows an increase in the period of 2005 to 2008 and recently between 2010 and 2015, and we can predict that if the number continues to grow at this rate Rwanda will hit the global target by 2050 [2].

3.8.1. Model: Regression Analysis. Now that we have had a cursory look at the data, this paper utilizes simple regression model in estimating the factors that affect maternal mortality in Rwanda. The software used is R. The model is specified as follows:

$$\mathrm{MMR}_t = \beta_0 + \beta_1 X_t + \varepsilon_t. \quad (1)$$

The above general specification model is divided into six simple regression models, with each model account variables such as female literacy rate (FLR), budget committed to health (BCH), health expenditure (HE), nurses and midwives (NMd), and sanitation and facilities (SF) as grouped in one single variable X_t in equation (1). The dependent variable MMR stands for maternal mortality rate. This research uses published commendable data from international sources spanning from a cross-section of time.

From the results of regression presented in Table 1, a positively significant relationship is found between MMR and healthcare expenditure per capita. The test indicates that if there is an increase of 1 unit of percentage of healthcare expenditure per capita by the government (measured in USD), it can save as many as 17 female Rwandan lives. As an example, as the latest healthcare expenditure per capita is 67.3 USD for Rwanda for one person, a unit increase of 1% in this amount per person might be able to save 17 female lives who can conceive (Model 4). This is a very significant statistic. Budget commitment to health is also significantly related, whereby the data reveals that if 2 units of the measurement are increased in allocation of healthcare budget, it can save one female Rwandan life ($2 * 0.5035 = 1.07$ lives, model 3). Female literacy (model 2) and sanitation infrastructure (model 6) also demonstrate significant trends towards MMR (Table 1).

4. Conclusion and Recommendation

After presenting all of these results, the conclusions in a nutshell and an analysis of how Rwanda is progressing in the quest to decrease MMR shall be presented. The MMR rate for Rwanda has gone down at an appreciable extent, and it is ably competing with other countries, which have been doing well in this regard. At the present rate, Rwanda shall also be listed in countries that have successfully battled with maternal mortality, especially among those of sub-Saharan Africa where it still remains a big issue. Rwanda is on the way to a steady recovery after a slump in the early 2000s, as the government is also investing more towards health as it has now a very impressive share in the GDP per capita spending. Rwanda has shown the most improvement in Health expenditure per capita, whereby the per capita spending increased exponentially after 2002, reaching a record high of 59 USD in 2014, and it has kept on increasing. Rwanda has surpassed both India and Bangladesh in Government Commitment of Budget to health sector with the record high of 16 percent commitment in 2003 and a whopping 23 percent in 2006, currently standing at around 25 percent. Rwanda has also shown a somehow steady rise in adult female literacy rate, going up from 37 percent in 1991 to around 67 percent according to the latest data, which is appreciable but more needs to be done here. In infrastructure development, Rwandan progress has been steady, boasting good numbers for public access to healthcare facilities and sanitation facilities as compared to India and Bangladesh with a little improvement needed in the sector of training healthcare professionals and caregivers during pregnancy and childbirth. A good explanation of these phenomena can be attributed to the health and Medicare aid

provided to Rwanda from external sources and other countries, which currently fund 53 percent of all healthcare resources of Rwanda, which is bringing about major changes in the way things are shaping up. We believe that Rwanda is firmly progressing upon its path to a decreasing MMR and provision of quality healthcare, and the changes are appreciable as seen through the indicators.

The current healthcare system of Rwanda has been a revelation, whereby the populace is now getting more healthcare coverage in affordable prices. More studies need to be done in the healthcare sector to build upon this good work, which shall help fortify Rwanda reputation not only among sub-Sahara but also Africa as a good example to follow in healthcare delivery. It is believed that this study has a direct impact on the Rwandan maternal healthcare system and it was conducted so that some indicators in the Rwandan healthcare industry may be highlighted and reasons for some shortcomings are investigated. A policy recommendation could be that the Rwandan government and the healthcare sector should take relevant measures that enhance healthcare system, and this ultimately will reduce maternal mortality. This study shows how pivotal the prescribed indicators are when studying the MMR. We can conclude from this study that increase in per capita healthcare expenditure is the most effective element to diminish MMR, followed by numbers of nurses and midwives, budget committed to health, female literacy, and sanitation conditions finally. GDP was not found to have a significant relationship with MMR. More detailed studies may also be conducted to further this idea or to conduct this research in a different way. The idea of this study can be duplicated and can also act as a roadmap for other studies in healthcare provision in Africa and other continents.

Data Availability

The empirical data used to support the findings of this study is currently under embargo while the research findings are commercialized. Requests for data, 6/12 months after the publication of this article, will be considered by the corresponding author.

Conflicts of Interest

We confirm that there is no conflict of interest regarding the publication of this paper.

References

[1] WHO, U.B.2012, http://www.maternalmortalitydata.org/Definitions.html.

[2] S. Goldman, "Can patient self-management explain the health gradient," *Social Science and Medicine*, vol. 70, no. 1, pp. 813–815, 2010.

[3] M. Currie and E. Moretti, "Mother's education and the intergenerational transmission of human capital: evidence from college openings," *The Quarterly Journal of Economics*, vol. 118, no. 4, pp. 1495–1532, 2003.

[4] D. M. Cutler and A. Lleras-Muney, "Understanding differences in health behaviors by education," *Journal of Health Economics*, vol. 29, no. 1, pp. 1–28, 2010.

[5] M. Rosenzweig and T. Schultz, "Schooling, information and nonmarket productivity: contraceptive use and its effectiveness," *International Economic Review*, vol. 30, no. 2, pp. 457–477, 1989.

[6] A. Lleras-Muney, "The relationship between education and adult mortality in the United States," *Review of Economic Studies*, vol. 72, no. 1, pp. 189–221, 2005.

[7] A. Weitzman, "The effects of women's education on maternal health: evidence from Peru," *Social Science & Medicine*, vol. 180, no. 2017, pp. 1–9, 2017.

[8] E. Koch, B. Calhoun, P. Aracena, S. Gatica, and M. Bravo, "Women's education level, contraceptive use and maternal mortality estimates," *Public Health*, vol. 128, pp. 384–387, 2014.

[9] A. McCaw-Binns, "Safe motherhood in Jamaica: from slavery to self-determination," *Paediatric and Perinatal Epidemiology*, vol. 19, no. 4, pp. 254–261, 2005.

[10] J. Batist, "An intersectional analysis of maternal mortality in sub-Saharan Africa: a human rights issue," *Journal of Global Health*, vol. 9, no. 1, article 010320, 2019.

[11] B. Tlou, "Underlying determinants of maternal mortality in a rural South African population with high HIV prevalence (2000–2014): A population-based cohort analysis," *PLoS One*, vol. 13, no. 9, p. e0203830, 2018.

[12] R. Musarandega, R. Machekano, S. P. Munjanja, and R. Pattinson, "Methods used to measure maternal mortality in sub-Saharan Africa from 1980 to 2020: a systematic literature review," *International Journal of Gynecology & Obstetrics*, vol. 156, no. 2, pp. 206–215, 2022.

[13] N. Gunawardena, G. Bishwajit, and S. Yaya, "Facility-based maternal death in Western Africa: a systematic review," *Frontiers in Public Health*, vol. 6, 2018.

[14] R. Musarandega, M. Nyakura, R. Machekano, R. Pattinson, and S. P. Munjanja, "Causes of maternal mortality in sub-Saharan Africa: a systematic review of studies published from 2015 to 2020," *Journal of Global Health*, vol. 11, 2021.

[15] WHO, UNICEF, UNFPA, and World Bank Group and the United Nations Population Division, *Maternal mortality: Levels and trends - 2000 to 2017*, World Health Organization Publication, 2019, ISBN: 978-92-4-151648-8.

[16] WHO, *Make Every Mother and Child Count*, World Health Organization, Geneva, 2005.

[17] L. Haddad, "Unsafe abortion: unnecessary maternal mortality," *Obstetrics and Gynecology*, vol. 2, no. 2, p. 122, 2009.

[18] C. Brock and N. Cammish, *Factors affecting female participation in education in seven developing countries-education research paper no. 09.1993*, Cammish University of Oxford and Hull, Oxford, 1997.

[19] World Health Organization, *Trends in maternal mortality: 1990-2015: estimates from WHO, UNICEF, UNFPA, World Bank Group and the United Nations Population Division: Executive Summary*, World Health Organization Publication, 2015, WHO Ref no: WHO /RHR/15.23.

[20] I. Loundon, *Death in Childbirth: An International Study of Maternal Care and Maternal Mortality 1800-1950*, Clarendon Press, UK, 1992.

[21] L. Ahmed, Q. Li, L. Liu, and A. O. Tsui, "Maternal deaths averted by contraceptive use: an analysis of 172 countries," *The Lancet*, vol. 380, no. 9837, pp. 111–125, 2012.

[22] WHO & UNFPA and P. Hunt, 2015, https://www.unfpa.org/sites/default/files/pub-pdf/reducing_mm.pdf.

Hindawi
Computational and Mathematical Methods in Medicine
Volume 2023, Article ID 9791271, 1 page
https://doi.org/10.1155/2023/9791271

Retraction

Retracted: The Effect of Endoscopy on Patients with Malignant Esophageal Cancer after Medical Treatment and Chemotherapy

Computational and Mathematical Methods in Medicine

Received 27 June 2023; Accepted 27 June 2023; Published 28 June 2023

This article has been retracted by Hindawi following an investigation undertaken by the publisher [1]. This investigation has uncovered evidence of one or more of the following indicators of systematic manipulation of the publication process:

(1) Discrepancies in scope

(2) Discrepancies in the description of the research reported

(3) Discrepancies between the availability of data and the research described

(4) Inappropriate citations

(5) Incoherent, meaningless and/or irrelevant content included in the article

(6) Peer-review manipulation

The presence of these indicators undermines our confidence in the integrity of the article's content and we cannot, therefore, vouch for its reliability. Please note that this notice is intended solely to alert readers that the content of this article is unreliable. We have not investigated whether authors were aware of or involved in the systematic manipulation of the publication process.

Wiley and Hindawi regrets that the usual quality checks did not identify these issues before publication and have since put additional measures in place to safeguard research integrity.

We wish to credit our own Research Integrity and Research Publishing teams and anonymous and named external researchers and research integrity experts for contributing to this investigation.

The corresponding author, as the representative of all authors, has been given the opportunity to register their agreement or disagreement to this retraction. We have kept a record of any response received.

References

[1] Y. Liu, L. Zhao, X. Tan, N. Liu, and T. Long, "The Effect of Endoscopy on Patients with Malignant Esophageal Cancer after Medical Treatment and Chemotherapy," *Computational and Mathematical Methods in Medicine*, vol. 2022, Article ID 7906302, 12 pages, 2022.

Hindawi
Computational and Mathematical Methods in Medicine
Volume 2022, Article ID 7906302, 12 pages
https://doi.org/10.1155/2022/7906302

Research Article

The Effect of Endoscopy on Patients with Malignant Esophageal Cancer after Medical Treatment and Chemotherapy

Yu Liu,[1] Lingqiong Zhao,[1] Xingping Tan,[2] Nana Liu,[2] and Teng Long[3]

[1]*Department of Oncology, Chongqing General Hospital, University of Chinese Academy of Sciences, Chongqing 400014, China*
[2]*Department of Oncology, People's Hospital of Chongqing Hechuan, Chongqing 401520, China*
[3]*General Surgery, People's Hospital of Chongqing Hechuan, Chongqing 401520, China*

Correspondence should be addressed to Nana Liu; 161847179@masu.edu.cn and Teng Long; longteng1983@163.com

Received 22 January 2022; Revised 25 February 2022; Accepted 8 March 2022; Published 9 April 2022

Academic Editor: Muhammad Zubair Asghar

The esophagus is one of the most commonly used parts in a person's life, and its importance is self-evident. With the unhealthy food diet, people are more and more likely to suffer from esophageal cancer, and there is an urgent need for breakthroughs in the treatment of esophageal cancer. This article is aimed at studying the effects of medical treatment and chemotherapy for patients with malignant esophageal cancer. To this end, this article proposes a treatment method based on endoscopy and improves the image imaging of the endoscopy and the image quality of the image and the edge processing of the image. At the same time, this article designs an experiment to conduct statistical analysis of the situation during the treatment process. The experimental results in this article show that the improved treatment method has a 21% increase in success rate compared with the existing treatment method. And the optimized image quality has increased by 27%. It can very well help the attending doctor to improve the efficiency of treatment in the actual treatment process. Its most important contribution is that through the edge optimization and image enhancement processing technology, the success rate of endoscopic treatment has been better improved, and the treatment efficiency has also been improved.

1. Introduction

Endoscopic resection can objectively diagnose early esophageal cancer and precancerous lesions and classify them into the disease stage, but the resection technique is a destructive treatment. Because postoperative specimens are not available, early esophageal cancer and precancerous lesions cannot be diagnosed and classified into the disease stage. In order to treat early esophageal cancer and precancerous lesions, it is necessary to develop high-frequency cauterization techniques and research on related factors that affect the clinical prognosis of early esophageal cancer. Now that the more accurate diagnosis of early esophageal cancer and precancerous lesions is established, the prediagnosis system provides the basis for guiding the treatment options of early esophageal cancer and cancer lesions.

The general risk factors for the onset of esophageal cancer are age, smoking, drinking, the intake of pickles, and insufficient trace elements and vitamins. With the improvement of living standards, changes in dietary life, and improvements in sanitation, these are the main reasons that contribute to the suppression of the onset of esophageal cancer, which greatly improves the level of diagnosis and treatment of esophageal cancer. Therefore, the research on effective treatment methods for esophageal cancer is urgent.

With the advent of the era of healthy living, people pay more and more attention to their own bodies, and the improvement of medical standards also guarantees the realization of this demand of the people. Malignant esophageal cancer is one of the most common diseases in the modern era. More and more people are beginning to invest in his treatment research. Tiloke et al. studied the antiproliferative effect of MOE on SNO and determined the cell death mechanism by measuring PS externalization and flow cytometry [1]. In order to solve the uncertainty of whether the clinical staging group (cTNM) of esophageal cancer has the same prognostic significance as the pathological group after simple esophagectomy (pTNM), Rice et al. described the types

of cancers and their risks in clinical patients with esophageal cancer from all over the world. The statistical standard is the standard definition of 33 institutions on six continents [2]. Zeng et al. used the latest data collected from the National Central Cancer Registry to provide an estimate of the burden of esophageal cancer in China in 2011. It is based on 177 eligible population-based cancer registries [3]. Feng et al. proposed that Pterocarpus (PTE) is a natural dimethylated resveratrol analogue from blueberries, which is known to have a variety of pharmacological activities, including anticancer properties [4]. Wang et al. proposed to study the definition of planned target volume (PTV) based on four-dimensional computed tomography (4DCT) and traditional PTV definition and the definition of primary thoracic esophageal cancer using asymmetric resection margins. 43 esophageal cancer patients underwent 3DCT and 4DCT simulation scans during free breathing [5]. Otterstatter et al. obtained cancer incidence and mortality from 1986 to 2006 from the Canadian Cancer Registry, the National Cancer Incidence Reporting System, and the Canadian Vital Statistics Death Database [6]. Tan et al. believes that esophageal cancer is composed of esophageal adenocarcinoma and esophageal squamous cell carcinoma. It is one of the most common malignant tumors in the world, especially in southern Iran and China [7]. In Ugo's review of 4,930 resections reported in the Western literature, similar changes are also evident in the literature of Japan and China. The survival rate of the unscreened population has risen from 9% to 23%, and the survival rate of early cancer is as high as 90% [8]. The contents of the mentioned documents are all reasonably designed, and the descriptions of the technology-related content involved in the article are carefully elaborated. However, the experiments carried out are partly based on the experimental results in the theoretical environment, without considering the experimental error brought by the actual operation process and the reliability of the experimental results.

The innovation of this article lies in the theoretical support of the actual operability of ESD technology and the technical support of image enhancement and image edge processing to optimize the medical treatment and chemotherapy of patients with malignant esophageal cancer tumors based on endoscopy. After the improvement, the success rate of the treatment can be effectively improved, and the image quality in the actual operation process has been effectively improved. Compared with the existing system, the improved system has higher recognition sensitivity, the image recognition accuracy rate is also more accurate, and the actual recognition image quality has also been better improved.

2. Research Methods

2.1. ESD

2.1.1. Definition. ESD is the process of separating the tissue after injection into the submucosal tissue. Choose an appropriate special electrosurgical knife to completely peel off the diseased mucosa and submucosal tissue [9].

2.1.2. ESD Steps. All ESD operations are performed by experienced endoscopy doctors.

Before ESD, narrow-band light observation (NBI) and magnifying endoscopy were used to observe the lesion again to clarify the scope of the lesion. Mark about 5 mm outside the boundary of the target lesion, and after the boundary of the lesion is completely marked, inject the submucosa (glyceride, epinephrine, toluene blue, or a mixture of the solutions). Use the injection needle outside the marked point, and the sign of lifting is positive, during the marking and injection process. According to the various physiological structures of the esophagus and stomach, appropriately adjust the strength of the marking and the depth of injection. After that, incision is made with mucosa around the marking point, and the lesion is slowly peeled off. The incision knife and warm water biopsy forceps are alternately used during the operation. The exposed large blood vessels and the oozing part of the blood are alternately electrically coagulated. Until the lesion is completely peeled off, rinse the wound with water at the same time and observe repeatedly to confirm that there is no bleeding from the wound until the edge of the lesion is completely resected, and the resected lesion is taken out through the mouth [10, 11]. The specific operation steps are shown in Figure 1.

2.1.3. Specimen Processing. Flatten the excised specimen of the endoscope, fix the mucosal surface, and observe and record the relevant data of the specimen (the size and shape of the specimen, the visual field of the lesion). After shooting the film, immerse the specimen in 10 formaldehyde solution [12]. Serial sections were collected every 2 mm and wrapped in paraffin. The steps of endoscopic mucosal dissection are shown in Figure 2.

2.1.4. Pathological Evaluation. Horizontal edge (lateral edge) means that cancer cells remain on the horizontal edge or cannot be distinguished by burning or partial resection that cannot be completely reconstructed. Positive vertical resection edge (undercut edge) means that cancer cells remain on the vertical resection edge or cannot be distinguished due to burning or partial resection that cannot be completely reconstructed. Removal of residual cancer cells on the edge fix the resection specimens of the endoscope; after resection every 2 mm, the sections of the most marginal tissues contain tumor cells. That is to say, the cancer cells are less than 2 mm from the edge of the resection. The so-called total resection refers to the removal of the lesion into one during endoscopy and the collection of one specimen at the same time. Curative resection refers to complete removal of ESD resection specimens without risk of lymph node metastasis. Tumor remains are defined as additional gastrectomy or second endoscopic treatment, and the excised specimens show tumor cells [13].

2.2. Research Status of Wireless Endoscopic Image Processing Algorithms

2.2.1. Image Workstation. Various wireless endoscopy devices currently used in clinical practice have corresponding image workstation software. Let us take the software of

Figure 1: ESD operation steps.

Israel's Kiven company as an example to introduce. The software is used to support the various stages of wireless endoscopy, including patient login, recorder initialization, data downloading, viewing endoscopic video recordings, and generating inspection reports [14].

2.2.2. Image Enhancement. Image enhancement refers to the preprocessing of wireless endoscopic images to meet the needs of doctors for diagnosis or subsequent processing. It proposes a wireless endoscopic image emphasis method based on diffusion tensor [15]. Experimental results show that the enhanced bleeding image is easily recognized and diagnosed by doctors. In fact, wireless endoscopic images not only affect the uneven brightness distribution but also have disadvantages due to hardware limitations and wireless transmission noise, noise pollution, and blurred edges [16]. Therefore, the wireless endoscope image must be emphasized at the same time as contrast enhancement, image smoothing, and edge sharpening. The image enhancement effect is shown in Figure 3.

2.2.3. Anomaly Detection. Anomaly detection belongs to the highest level of image understanding technology in image processing technology. It is also a field of extensive research and application in wireless endoscope processing technology, but the current research and results in wireless endoscope image disease diagnosis cannot be said to be sufficient [17].

2.2.4. PDE Form of Histogram Equalization. The histogram equalization method is a histogram correction technique with extremely high practical performance. It is suitable for various image imaging conditions, and the direct histogram equalization technology can enhance the contrast of the entire image. However, its enhancement effect is difficult to effectively control, and the image visual effect is relatively rigid and not soft enough. And it is easy to cause the loss of image details [18]. To this end, the following energy functional is established:

$$G(I) = \frac{1}{2}\int \left(I(p,q) - \frac{1}{2}\right)^2 dpdq. \tag{1}$$

The gradient descent flow of the energy functional of the formula can be expressed as

$$\frac{\partial I(p,q,t)}{\partial t} = \left[1 - \frac{I(p,q,t)}{I_{\max}}\right] A_\Omega - A(I(p,q,t)). \tag{2}$$

Equation (2) has a unique steady-state solution:

$$I(p,q,\infty) = I_{\max} \times E(I), \tag{3}$$

where $E(I)$ represents the cumulative histogram of the input image. We generalize the histogram equalization operation to the more general arbitrary contrast enhancement operation. Equation (2) can be rewritten as follows:

$$\frac{\partial I(p,q,t)}{\partial t} = f(I(p,q,t)) - I(p,q,t). \tag{4}$$

Traditional image smoothing methods include linear smoothing filters such as mean filtering and Gaussian filtering and statistical sorting filters such as median filtering. The partial differential equation corresponding to the image Gaussian filter is a two-dimensional linear diffusion equation:

$$\frac{\partial I(p,q,t)}{\partial t} = \operatorname{div}(\nabla I), \tag{5}$$

$$\frac{\partial^2 I}{\partial x^2} + \frac{\partial^2 I}{\partial y^2} = \Delta I, \tag{6}$$

where div represents the divergence operator, through the Fourier transformation method, and the solution of the formula can be obtained:

$$I(p,q,t) = I_0(p,q) * G_t(p,q). \tag{7}$$

Add a conductivity term to Equation (5), and it becomes the following form:

$$\frac{\partial I(p,q,t)}{\partial t} = \operatorname{div}[g(|\nabla I|)\nabla I]. \tag{8}$$

Since the initial value problem of the equation may be ill-conditioned, that is, the steady-state solution of the equation does not have continuous dependence on the initial conditions. Therefore, the equation is improved, and the improved regularized diffusion equation is shown in the following equation:

$$\frac{\partial I(p,q,t)}{\partial t} = \operatorname{div}\left[g\left(|\nabla(G_\sigma * I)|^2\right)\nabla I\right], \tag{9}$$

where $E(I)$ represents the cumulative histogram of the input image, and div represents the divergence operator.

The use of total variation as the smoothness measure of the image will protect the edges of the image:

$$G(I) = \frac{1}{2}\lambda \int (I - I_0)^2 dpdq. \tag{10}$$

The gradient descent flow that minimizes the energy function is shown in the following equation:

$$\frac{\partial I(p,q,t)}{\partial t} = \operatorname{div}\left(\frac{\nabla I}{|\nabla I|}\right) - \lambda(I - I_0). \tag{11}$$

In order to alleviate the fragmentation effect of the processing result, the improved total variation denoising model

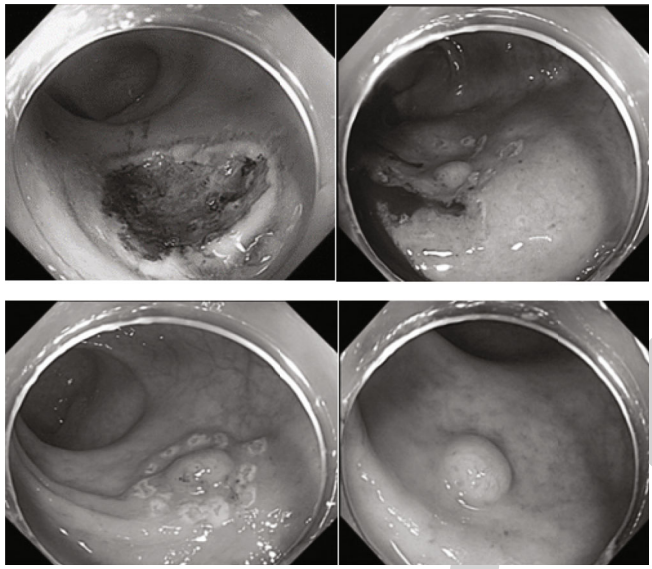

Figure 2: The process of endoscopic mucosal dissection.

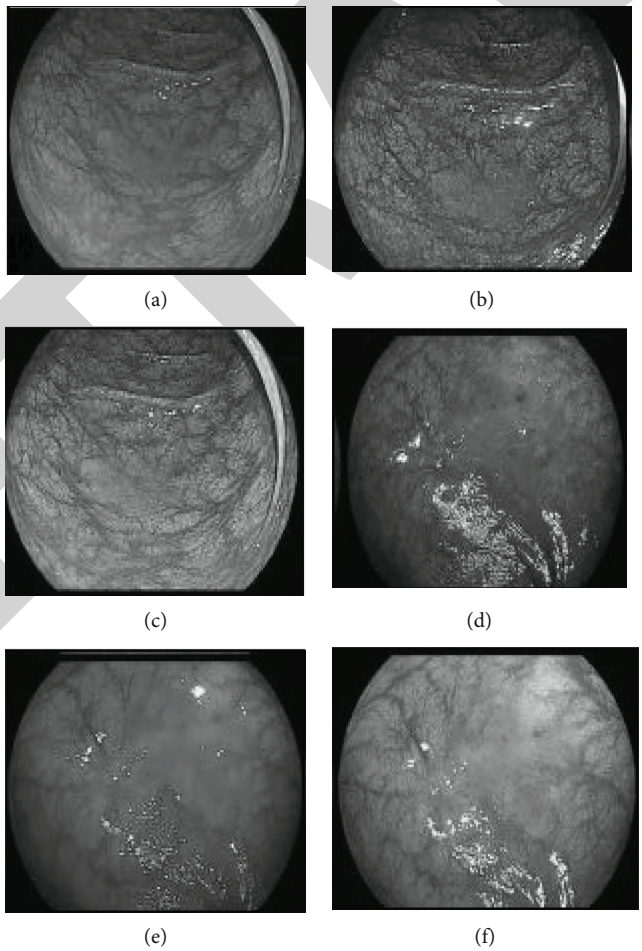

Figure 3: Image enhancement effect.

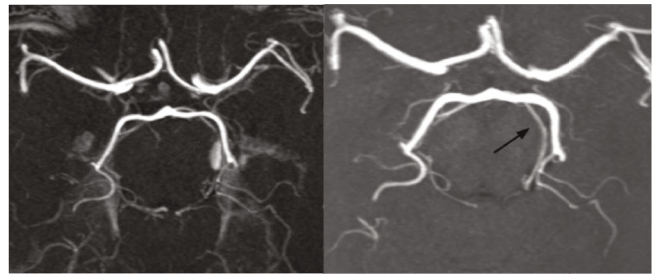

Figure 4: Comparison of edge processing effects.

is multiplied by the gradient modulus at the right end of the formula to obtain the following form:

$$\frac{\partial I(p,q,t)}{\partial t} = |\nabla I| \operatorname{div}\left(\frac{\nabla I}{|\nabla I|}\right) - |\nabla I|\lambda(I - I_0). \tag{12}$$

2.2.5. PDE Form with Sharp Edges. Edge sharpening operation and image smoothing are essentially a contradictory process. It corresponds to the reverse diffusion of the image. The most widely used in image sharpening is the Laplacian based on second-order differentiation, which is defined as

$$\nabla^2 f(p,q) = \frac{\partial^2 f}{\partial p^2} + \frac{\partial^2 f}{\partial q^2}. \tag{13}$$

For discretized two-dimensional images, the following formula can be used as an approximation of the second-order partial differential:

$$\nabla^2 f = [f(p+1,q) + f(p-1,q) + f(p,q+1) + f(p,q-1)] - 4f(p,q). \tag{14}$$

To achieve the image sharpening effect, the original image needs to be subtracted from the image processed by the sharpening operator, namely,

$$g(p,q) = f(p,q) - \Delta f(p,q). \tag{15}$$

Sharpen the edges of the image by restoring the result of the two-dimensional linear diffusion equation:

$$\frac{\partial I(p,q,t)}{\partial t} = -\Delta I. \tag{16}$$

The edge detection operator can also adopt more complex forms to enhance the effect of edge detection:

$$\frac{\partial I(p,q,t)}{\partial t} = -\operatorname{sgn}(\Delta I)|\nabla I|. \tag{17}$$

From the analysis of the two sections, it is not difficult to see that the smoothing of the image and the sharpening of the edge of the image are essentially a form of diffusion of the image: in the flat area of the image, that is, the area where the gray value does not change much. Perform positive diffusion on the image to smooth the noise points in the image and control the smoothness of the image. In the detailed areas of the image, such as edges, corners, and other shapes, the forward diffusion stops to protect the detailed areas [19, 20]. The specific effect is shown in Figure 4.

2.2.6. Image Enhancement Model. Based on the existing image enhancement methods, we propose an image enhancement scheme based on the image partial differential equation framework. As shown in Equation (18), the framework includes three parts: image contrast enhancement, edge sharpening, and image smoothing [21].

$$\frac{\partial I(p,q,t)}{\partial t} = \alpha(f_1(I)) + \beta(f_2(I)) + \gamma(f_3(I)). \tag{18}$$

Although the improved denoising model avoids the defect of constant image segmentation, the edge protection capability of total variation is also weakened accordingly. We add an edge stop function to weaken the diffusion rate near the edge, so as to achieve the effect of protecting the edge [22]. After the improvement, the fidelity item can be expressed as

$$\frac{\partial I(p,q,t)}{\partial t} = g(|\nabla I|)|\nabla I| \operatorname{div}\left(\frac{\nabla I}{|\nabla I|}\right). \tag{19}$$

Finally, we proposed the following two-way diffusion equation:

$$f_2(I) = \frac{\partial I(p,q,t)}{\partial t} = g_N I_{NN} + g_T I_{TT}. \tag{20}$$

In this article, we use the following spread function g:

$$g_N = \begin{cases} 0, & \text{if } |\nabla(G_\sigma * I)| > T \\ 1, & \text{otherwise} \end{cases}, \tag{21}$$

$$g_T = 1 - \exp\left(-3.315/(\nabla(G_\sigma * I)/m)^8\right). \tag{22}$$

Experiments have proved that this value can obtain satisfactory results. Of course, more complex forms can also be used. Adjust the value adaptively according to the size of the gradient near the edge to achieve better results [23].

Compared with images in medicine, the use of machine learning requires a lot of time and data in the early stage, and when there are some more difficult problems, machine

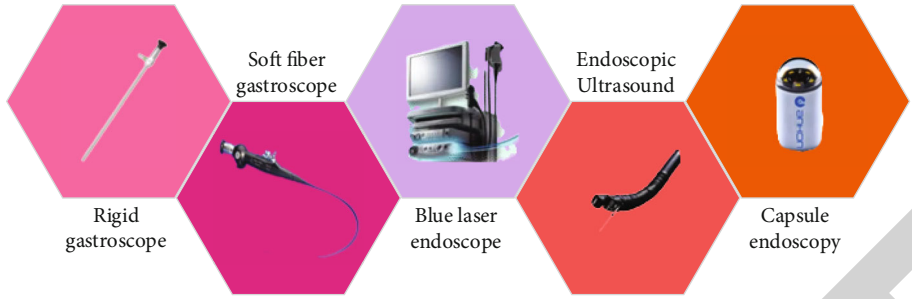

Figure 5: The development history of endoscopy.

learning cannot handle better and may even be missed; so, there is no use and learn to classify.

2.3. The Development and Clinical Application of Endoscopy Technology. After more than 100 years of development, digestive endoscopy devices started from rigid endoscopes from the first generation, have been used only for diagnosing digestive tract diseases from the initial stage, and gradually developed to the advanced minimally invasive treatment stage integrating diagnosis and treatment. Compared with surgical operation, endoscopic treatment has less damage to the patient's body, relatively simple technical requirements, faster recovery of patients, less trauma, and a more economical choice. The development process of the endoscope is shown in Figure 5.

Endoscopic resection and endoscopic dissection have been widely carried out in gastroenterology and endoscopic wards of major hospitals. Some secondary hospitals are also actively investing. This endoscopic treatment technique has been widely developed clinically and is mainly used to treat tumors and precancerous lesions that originate in the mucosa and submucosa of the digestive tract. ESD is developed from EMR technology. In addition, after EMR and ESD endoscopic treatment techniques, domestic and foreign scholars have successively proposed more difficult treatment techniques such as endoscopic excavation (ESE), endoscopic tunnel resection, and endoscopic full-thickness resection. It greatly reduces the misdiagnosis rate.

With the continuous maturity of endoscopy technology, innovation and development of endoscopic treatment technology through the natural cavity have been developed. Because it has no incision and no scar after operation, it is now being paid attention to by the majority of endoscopy doctors and patients. In 2009, China established a special NOTES treatment management committee to strictly implement the clinical supervision and application of NOTES. NOTES does not go through a surface approach, which is another milestone in minimally invasive surgery. It is the gospel for obese patients and some patients who cannot tolerate traditional surgery. And because this kind of operation has less interference to the internal environment and less damage to normal tissues and organs, the patient has a relatively fast recovery period and lower cost, and it is more and more accepted by patients. Peroral endoscopic pyloromyotomy is a kind of new NOTES, which is based on ESD technology and transendoscopic tunneling.

Acute upper gastrointestinal bleeding is often caused by acute massive bleeding that causes a sharp decrease in the peripheral blood volume, causing sudden changes in the patient's vital signs. It has become one of the common clinical diseases that threaten the lives of patients. According to global statistics, its annual prevalence and fatality rate are among the best among all acute and critical illnesses. At present, the clinical treatment of acute nonvarice upper gastrointestinal hemorrhage is often performed through endoscopic OTSC metal clip closure. This method of treatment is also considered to be a safe and effective treatment in recent years. However, acute bleeding from esophageal and gastric fundus varices can cause severe bleeding and rapid changes in the condition at the onset of the disease, which often endangers the life of the patient. Therefore, it usually requires painless gastroscopy within 24 hours to clarify the bleeding site and the bleeding situation. According to the performance under the microscope, treatment methods such as endoscopic band ligation, sclerotherapy, and tissue adhesive embolization can be adopted. In addition, a variety of complex endoscopic treatment techniques such as double-gas award enteroscopic polypectomy, hemostasis, stenosis dilation, endoscopic myotomy, acute biliary pancreatitis, combined biliary, and pancreatic drainage can also be used. These endoscopy technologies are clinically emerging in recent years and doctors, and patients are keen on endoscopy. The method of endoscopic metal clip closure is shown in Figure 6.

SMTs of the upper gastrointestinal tract are mainly leiomyomas and GIST, and it is difficult to distinguish GIST from leiomyomas in clinical practice. At present, the most commonly used method is fine needle puncture guided by ultrasound endoscopy. However, the diagnosis rate is not ideal, and the mitotic figures cannot be calculated in pathological specimens obtained by puncture. If SMI's is clinically diagnosed as stromal tumor, its follow-up treatment is controversial. The NCCN guidelines recommend surgical removal of GIST with a diameter of more than 2 cm. If the diameter is less than 2 cm, but EUS finds irregular shape, pockets, ulcers, echogenic foci, or heterogeneity, surgical removal of the lesions is also recommended. The ESMO guidelines recommend that if the histology is confirmed as GIST, surgical resection should be performed.

Endoscopic treatment is a minimally invasive method to remove SMTs in the upper gastrointestinal tract. It is less traumatic, quick to recover, and does not affect the function

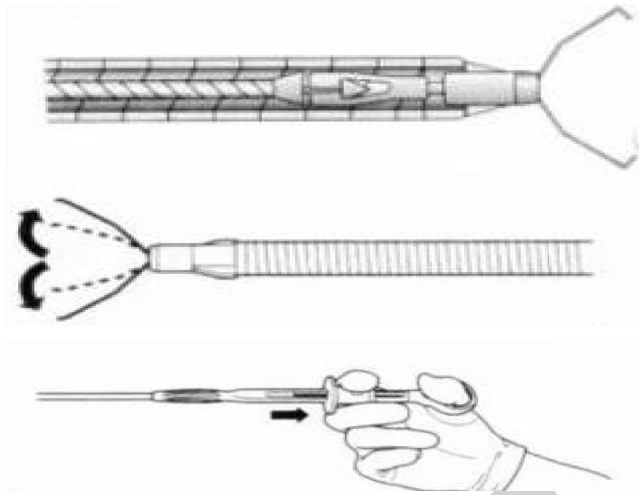

Figure 6: Endoscopic metal clip closure operation.

Table 1: Survey statistics of experimental subjects.

Basic parameters	ESD treatment group	Surgical treatment	p value
Number of cases	60	66	0.468
Age	64 ± 7	61 ± 6	0.272
Gender: male female	42/18	42/24	0.769
Upper section	4	10	0.366
Middle section	46	44	0.523
Next paragraph	10	12	0.379

Table 2: Composition ratio of different resection degrees.

Basic parameters	ESD treatment group	Surgical treatment	p value
En bloc resection rate	(60/60) 100%	(66/66) 100%	—
Complete resection rate	(58/60) 96.6%	(64/66) 96.9%	0.923
Curative resection rate	(58/60) 96.6%	(64/66) 96.9%	0.647

of the digestive tract. It can not only remove tumors but also provide complete specimens for pathological examination. At present, the main techniques for endoscopic treatment of SMTs derived from the muscularis propria are STER, ESE, and EF. STER is one of the endoscopic tunneling techniques used in clinical practice in the past 4 years. At present, it is mainly used to treat SMTs derived from the esophagus and the lamina propria of mouth. The advantage is that a submucosal tunnel is established at the normal mucosa where the endoscopic space and position are better, the tunnel is separated and extends below the tumor body, and the normal mucosal tissue above the tumor body is preserved. Because the spatial position of the opening is good for the closure of the tablet holder, and after the tunnel is closed, the integrity of the mucosal layer is ensured, and the contact between the wound surface at the tumor bed and the digestive juice and air is isolated. It is more conducive to postoperative recovery and also reduces postoperative complications. However, the tunnel technology itself has its shortcomings. In other words, not all SMTs can be removed using the STER method. Furthermore, endoscopic tunneling technology is one of the most challenging endoscopic technologies at present. It requires a long time of practice, and it takes time to establish the tunnel itself; so, the operation time is longer. Finally, due to the limited space in the tunnel cavity, when the tumor is large, the endoscope cannot be completely removed. Compared with the STE technology, the ESE technology is a direct extension of the ESD technology. It directly cuts the mucosa above the SMTs, then separates the tumor body to complete resection, and finally seals the wound. The advantage is that most upper gastrointestinal SMTs can be treated with this technique. And its operation time is relatively short. The disadvantage is that if the tumor protrudes out of the lumen or the tumor is closely related to the serosal layer, it needs the support of EF technology. In addition, when the tumor is large or the location is special, once perforation occurs, it is difficult to seal the wound with endoscopy, and it is even necessary to suture the wound with thoracoscopy. At the same time, it was found that STER technology has no significant advantages over ESE in terms of complete resection rate and complication rate of upper gastrointestinal submucosal tumors.

Especially in the cardia subgroup, when the tumor is larger (>1.5 cm), the complete resection rate of ESE technique decreases significantly, which may be related to the physiological stenosis of the cardia and the extremely difficult endoscopic operation. Furthermore, the space in the tunnel is limited, and it takes longer to separate the tumor from the tunnel than it takes to separate the tumor after directly incising the mucosa. The main complications of the STER group were subcutaneous emphysema, pneumothorax, and pneumoperitoneum caused by gas entering the interstitial space during the treatment. Due to the use of CO_2 gas, these complications are within a controllable range. In addition, if the tumor body is found to be closely related

Table 3: Relevant time of the patient's surgery.

Basic parameters	ESD treatment group	Surgical treatment	p value
Operation time (minutes)	128.14 ± 35.61	321.49 ± 98.35	<0.001
Hospitalization time (days)	15.64 ± 6.23	31.26 ± 11.36	<0.001

Table 4: Statistics of postoperative complications and recurrence of patients.

Basic parameters	ESD treatment group	Surgical treatment	p value
Relapse	(2/60) 3.33%	Without	—
Bleeding	(2/60) 3.33%	(16/66) 24.24%	<0.01
Perforation	(2/60) 3.33%	Without	—
Narrow	(4/60) 6.67%	(6/66) 9.09%	0.127
Infect	Without	(6/66) 9.09%	—

Table 5: Postoperative quality of life of patients.

Basic symptoms	ESD treatment group	Surgical treatment	p value
Digestive symptoms			
Nausea	6	24	<0.05
Vomit	2	20	<0.05
Acid reflux	10	40	<0.05
Heartburn	12	44	<0.05
Bloating	6	10	>0.05
Decreased appetite	4	16	<0.05
Weight loss	4	8	>0.05
Endoscopic performance			
Anastomotic hyperemia	2	20	<0.05
Anastomotic erosion	4	10	>0.05
Narrow	2	0	>0.05

to the serosal layer during the separation process, in order to ensure the complete resection of the tumor body, it must be removed together with the serous layer. The integrity of the tunnel is destroyed, and the gas enters the interstitial space from the tunnel inevitably occurs. In the cases where the tumor was completely resected, there was no postoperative gastrointestinal thinness and gastrointestinal infection.

From the experience of endoscopic treatment, the larger the tumor, the longer the operation time of endoscopic resection and the more difficult the operation. The risk of intraoperative perforation, postoperative infection, and delayed bleeding has also increased accordingly. We divided the tumors into subgroups for analysis based on the size of the tumors, and the lesion diameter was 15 mm as the boundary for selection into the group. The results show that the size of the disease has no significant influence on the choice of treatment technique. In other words, the size of the tumor is not a decisive factor in choosing a treatment technique. Especially when the lesions are located in the esophagus-cardia subgroup or the cardia-fundus/high gastric body subgroup, the operation time of the ESE group is shorter than that of the STER group.

Although the intraoperative complications in the STER group were higher, most of them were mild. Statistical analysis shows that we do not need to choose the treatment technique based on the diameter of the lesion but can measure the choice based on multiple factors such as the location of the lesion, the operation time, the complications, and the difficulty of the operation. For this reason, we recommend the STER method for SMTs with larger diameters (diameter > 1.5 cm) at the EGJ site, especially for lesions with irregular shapes, because of its high complete resection rate and low complication rate (except for the complications of gas entering the interstitial space). For smaller SMT (1.5 cm diameter), we recommend ESE treatment, because of its relatively short operation time, high complete resection rate, and relatively few complications.

3. Questionnaire Experiment

3.1. Lesion Characteristics. This experiment randomized investigation 126 conducted experimental investigations for patients. Before the experiment, first conduct a statistical investigation on the experimental objects. The specific information is shown in Table 1.

From the table, we can see that there are 60 cases in the ESD group, including 42 males and 18 females; the age is 57-71 years old. There were 4 cases in the upper segment, 46 cases in the middle segment, and 10 cases in the lower segment; there were 66 cases in the surgical group. Among them, there were 42 males and 18 females, aged 67-55 years, 10 cases in the upper segment, 44 cases in the middle segment, and 12 cases in the lower segment. It can be seen that in the ESD group, most of the cases are distributed in the middle section, and this is also the case in surgical operations. Therefore, we should focus on the middle section in the later experimental research. And the two groups of patients were not statistically significant in terms of age and gender ($p > 0.05$). At the same time, this experiment carried out experimental statistics on the resection rate at different degrees, and the specific conditions are shown in Table 2.

From the table, we can see that in the ESD treatment group, the en bloc resection rate is 100%. In the surgical treatment group, the en bloc resection rate was also 100%. In the ESD treatment group, the probability of complete resection rate was 96.6%. The complete resection rate in the surgical treatment group was 96.9%, which was higher than the 96.6% in the ESD treatment group. In the ESD

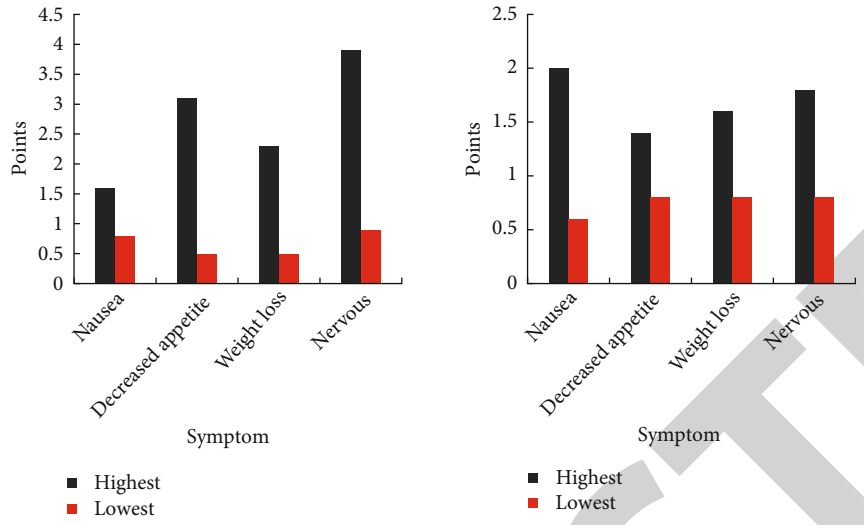

Figure 7: Comparison of follow-up results of patients with noncurable resection and endoscopic treatment.

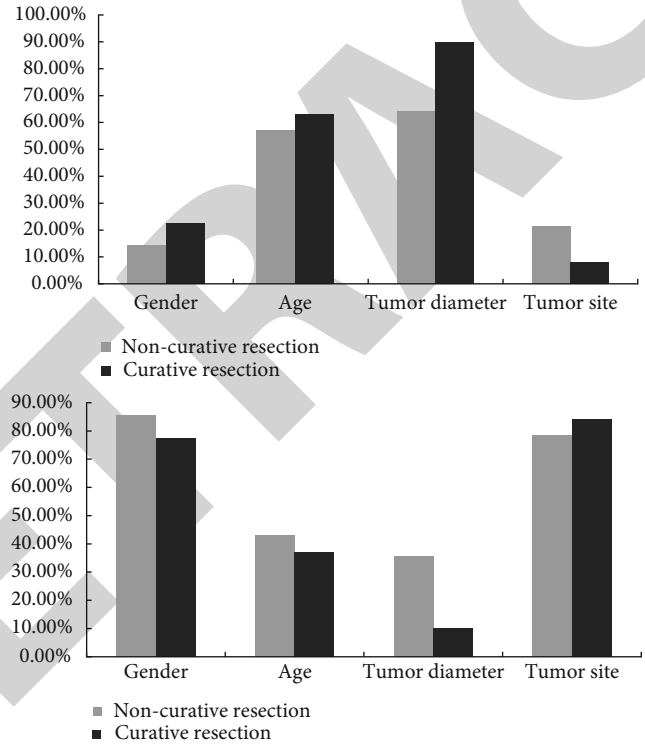

Figure 8: Comparison of clinical characteristics of early esophageal cancer patients with cured/noncurable resection.

treatment group, the curative resection rate was 96.6%. In the surgical treatment group, the curative resection rate was 96.9%. At the same time, this experiment counts the relevant time of the experiment and counts the integration of its operation time and hospitalization time. The specific data is shown in Table 3.

From the table, we can see that the operation time of the ESD treatment group was 128.14 ± 35.61 minutes, and the hospital stay was 15.64 ± 6.23 days. In the surgical treatment group, the operation time was 321.49 ± 98.35, and the hospital stay was 31.26 ± 11.36 days. In terms of time comparison, it can be seen that the time of the surgical treatment group is much longer than that of the ESD treatment group, no matter in the operation time or the number of days of hospitalization. At the same time, the operation time and hospitalization days of the two groups were statistically significant ($p < 0.05$). The operation time and hospital stay of the surgical group were longer. At the same time, in order to explore the problems of complications and recurrence after and during the operation, this article counts the complications during the operation. The statistics are shown in Table 4.

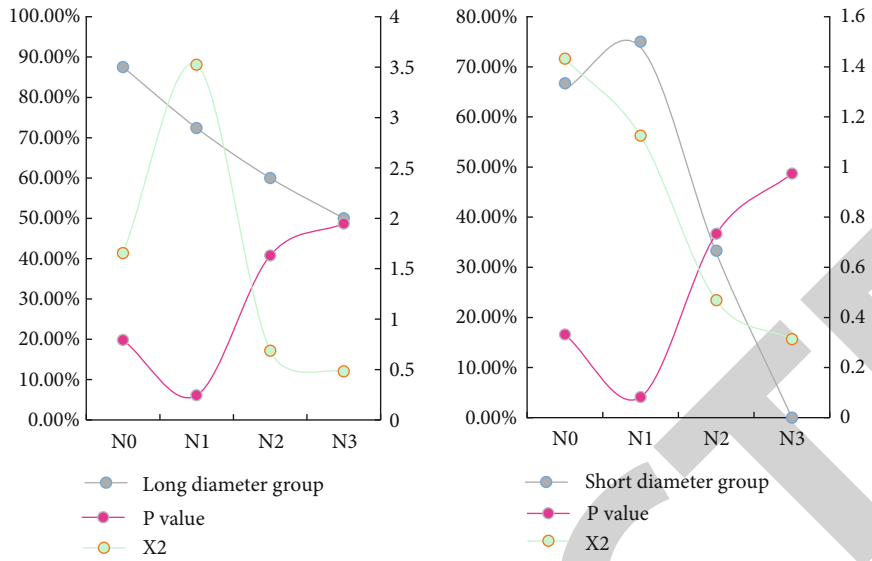

Figure 9: Comparison of survival rates of different lymph node metastases.

From the table, we can see that in the ESD treatment group, the probability of recurrence is 3.33%, the probability of bleeding is 3.33%, the probability of perforation is 3.33%, the probability of stenosis is 6.67%, and there is no infection. In the surgical treatment group, there was no recurrence, the probability of bleeding was 24.24%, there was a probability of no perforation, the probability of stenosis was 9.09%, and the probability of infection was 9.09%. At the same time, we design here to conduct statistics on the postoperative quality of life of patients through review of endoscopy, telephone follow-up, and outpatient review. The statistics are shown in Table 5.

From the data in the table, we can see that in the results of the review endoscopy and telephone follow-up, patients with gastrointestinal symptoms mainly have the following symptoms: abdominal distension, acid reflux, and heartburn. The endoscopic manifestations mainly have the following three symptoms: whether the anastomosis is healed, whether there is erosion, and whether there is stenosis. Statistical analysis showed that the chi-square value was $p < 0.001$, and the difference was statistically significant. The ESD treatment group was better than the surgical operation group.

4. Result Analysis

4.1. Analysis of Follow-Up Results and Clinical Characteristics of Patients with Noncurable Resection of Early Malignant Esophageal Cancer Tumors and Patients Treated with Endoscopy. In order to ensure the accuracy and reliability of the follow-up results, the patients surveyed in this experiment were conducted in accordance with standards. It is based on a certain degree of follow-up, investigating the quality of life, evaluating using a scoring scale for scoring, and at the same time conducting follow-up in combination with telephone to ensure the diversity of follow-up. At the same time, a questionnaire survey experiment was carried out for all early patients, and statistics were collected on the conditions and emotional problems of the patients during the investigation and follow-up. According to the statistical results, the results are shown in Figure 7:

At the same time, the clinical characteristics of early esophageal cancer patients with cured/noncured resection were compared and analyzed. The comparison result is shown in Figure 8.

From the two figures, we can see that the treatment of nausea in patients with early noncurative resection is slightly due to the low level of patients treated under endoscopy. The scores of the rest of the adverse conditions are higher than the treatment scores based on patients under endoscopy. The highest nausea score of early patients was 1.6, and the lowest was 0.8, which was lower than the highest 2.0 and lowest 0.6 based on endoscopic treatment. Among the adverse symptoms of decreased appetite, the early score is the highest 3.1 and the lowest 0.5, which is higher than the highest 1.4 and the lowest 0.8 based on endoscopic treatment. Among the adverse symptoms of weight loss, the early score is the highest 2.3 and the lowest 0.5, which is higher than the highest 1.6 and the lowest 0.8 based on endoscopic treatment. Among the adverse symptoms of nervousness, the early score is 3.9 at the highest and 0.9 at the lowest, which is higher than the highest 1.8 and the lowest 0.8 based on endoscopic treatment. In terms of clinical features, the early cure of esophageal cancer has less impact on gender. The overall age is higher than the clinical characteristics of patients with noncurable resection. In terms of tumor diameter, there is little difference between the two, but noncurative resection is more likely to be affected by the tumor site. In summary, it can be seen that nausea can occur in treatment based on endoscopic treatment, which is slightly higher than that of early treatment. Other symptoms are obviously better than early treatment.

4.2. Comparison of 3-Year Survival Rate between Two Groups of Patients with Different Lymph Node Metastases. A stratified analysis of the independent factors affecting the

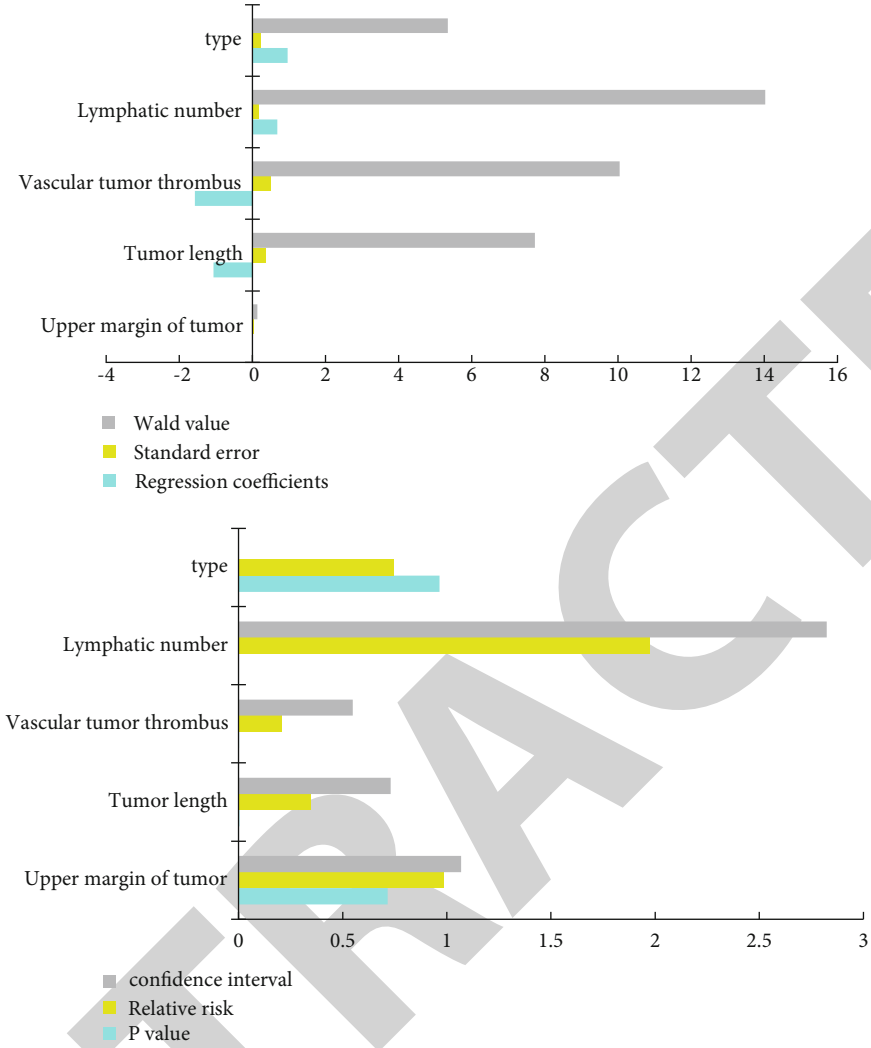

Figure 10: Analysis of prognostic factors affecting the whole group of patients.

prognosis of the entire group of patients showed that the 3-year survival rate of pN0 patients in the long-diameter group and the short-diameter group was not statistically significant ($p > 0.05$). The 3-year survival rate of pN1 patients in the long-diameter group and the short-diameter group was not statistically significant ($p > 0.05$). The specific situation is shown in Figure 9.

4.3. Factors Affecting the Prognosis of the Whole Group of Patients. According to univariate analysis, the position of the upper edge of the tumor under the endoscope, the length of the tumor under the endoscope, the vascular tumor thrombus, the number of lymph node metastases, and the pathological type were found. Further analysis based on the COX proportional hazard model showed that endoscopic tumor length, vascular tumor thrombus, and number of lymph node metastases were independent factors affecting the prognosis of the entire group of patients. The risk model analysis is shown in Figure 10.

It can be seen that the length of the tumor is a factor that cannot be ignored. It is closely related to other factors such as the depth of esophageal cancer tumor invasion and lymph node metastasis. As the length of the tumor increases, the number of lymph node metastases increases. The longer the tumor length, the deeper the invasion and the more extensive the lymph node metastasis.

5. Conclusion

The main research content of this article is based on the effects of medical treatment and chemotherapy in patients with malignant esophageal cancer tumors under endoscopy. For endoscopic treatment, this article first analyzes it in the method section. This article has a detailed understanding of its treatment methods and treatment process. There is also this article to optimize the imaging of the endoscope. This paper proposes edge optimization and methods for image enhancement processing. The experimental part also used questionnaires to understand the patient's response during the operation and after the operation. By comparing the advantages of endoscopic treatment, it is finally analyzed. The analysis results show that the success rate of

Hindawi
Computational and Mathematical Methods in Medicine
Volume 2023, Article ID 9828324, 1 page
https://doi.org/10.1155/2023/9828324

Retraction

Retracted: Influence of Health Education Based on IMB on Prognosis and Self-Management Behavior of Patients with Chronic Heart Failure

Computational and Mathematical Methods in Medicine

Received 27 June 2023; Accepted 27 June 2023; Published 28 June 2023

This article has been retracted by Hindawi following an investigation undertaken by the publisher [1]. This investigation has uncovered evidence of one or more of the following indicators of systematic manipulation of the publication process:

(1) Discrepancies in scope

(2) Discrepancies in the description of the research reported

(3) Discrepancies between the availability of data and the research described

(4) Inappropriate citations

(5) Incoherent, meaningless and/or irrelevant content included in the article

(6) Peer-review manipulation

The presence of these indicators undermines our confidence in the integrity of the article's content and we cannot, therefore, vouch for its reliability. Please note that this notice is intended solely to alert readers that the content of this article is unreliable. We have not investigated whether authors were aware of or involved in the systematic manipulation of the publication process.

In addition, our investigation has also shown that one or more of the following human-subject reporting requirements has not been met in this article: ethical approval by an Institutional Review Board (IRB) committee or equivalent, patient/participant consent to participate, and/or agreement to publish patient/participant details (where relevant).

Wiley and Hindawi regrets that the usual quality checks did not identify these issues before publication and have since put additional measures in place to safeguard research integrity.

We wish to credit our own Research Integrity and Research Publishing teams and anonymous and named external researchers and research integrity experts for contributing to this investigation.

The corresponding author, as the representative of all authors, has been given the opportunity to register their agreement or disagreement to this retraction. We have kept a record of any response received.

References

[1] W. Liu, Y. Zhang, H. Liu, T. Song, and S. Wang, "Influence of Health Education Based on IMB on Prognosis and Self-Management Behavior of Patients with Chronic Heart Failure," *Computational and Mathematical Methods in Medicine*, vol. 2022, Article ID 8517802, 13 pages, 2022.

Hindawi
Computational and Mathematical Methods in Medicine
Volume 2022, Article ID 8517802, 13 pages
https://doi.org/10.1155/2022/8517802

Research Article

Influence of Health Education Based on IMB on Prognosis and Self-Management Behavior of Patients with Chronic Heart Failure

Wei Liu,[1] Yan Zhang,[1] Hai-jing Liu,[2] Tian Song,[3] and Song Wang[4]

[1]*Nursing Department, Qiqihar Medical University, Qiqihar, 161006 Heilongjiang, China*
[2]*Cardiovascular Internal Medicine Ward 6, The Second Affiliated Hospital of Qiqihar Medical University, Qiqihar, 161006 Heilongjiang, China*
[3]*Emergency Medicine, The Third Affiliated Hospital of Qiqihar Medical University, Qiqihar, 161006 Heilongjiang, China*
[4]*Internal Medicine Ward 5, Staff Hospital of Qiqihar Machine Tool Group Co. Ltd., Qiqihar, 161006 Heilongjiang, China*

Correspondence should be addressed to Yan Zhang; zhangyan123@qmu.edu.cn

Received 18 January 2022; Revised 22 February 2022; Accepted 5 March 2022; Published 8 April 2022

Academic Editor: Shakeel Ahmad

As the contemporary society is increasingly entering an aging society, heart failure, as a common disease in the elderly population, has an increasing impact on people. The common one is mainly chronic heart failure. Coupled with the influence of various complications, such as hypostatic pneumonia and venous thrombosis, the mortality and hospital admission rates of patients are very high. Moreover, the current technology is not very effective for the prevention and treatment of chronic heart failure. The per capita consumption level of ordinary people in China is low, and it is not suitable to promote high-cost treatment programs. Based on this, this paper proposes the intervention management of mental failure patients under the intervention of health education based on IMB, in order to explore the impact of the intervention of health education on patients. The research in this paper selected 112 patients with chronic heart failure who were admitted to the cardiovascular ward of a city public hospital in 2017 and divided the patients into two groups. One group received health education intervention, which was the intervention group. The other group was the control group. The control group was given routine education and nursing. The experimental results of this paper show that the satisfaction of the intervention group is higher, accounting for 85.3%, and the satisfaction of the control group is lower than that of the intervention group, about 67.9%. Dissatisfaction with health education and the probability of short-term readmission were higher than those in the intervention group.

1. Introduction

Chronic heart failure is a common clinical circulatory system disease, which mostly occurs in middle-aged and older. It is usually the long-term abnormal function of the heart that reduces the ability of the heart muscle to contract and causes poor blood circulation. Most patients had other types of cardiovascular disease, as heart failure was often caused by exacerbations of other cardiovascular diseases and was the leading cause of death in patients. A large number of studies at home and abroad show that chronic heart failure has become a global public health problem. Chronic heart failure patients have the characteristics of repeated attacks, long course of disease, lack of effective treatment, complex pathogenesis, and many pathogenic factors. The development of the disease can lead to a series of complications, affecting a person's survival, seriously affecting family life, and creating a double burden. It is a severe clinical syndrome with poor recovery prospects and high rates of unplanned readmissions and deaths. In recent years, in addition to significant progress in the research and development of targeted drugs, no effective treatment for chronic heart failure has been found in terms of clinical symptoms. Overseas studies have shown that more than 27% of patients with

chronic heart failure return to the hospital within 3 to 6 months. The five-year survival rate for clinically diagnosed patients is only about 50%. In severe cases, the one-year mortality rate is as high as 50%. Therefore, treatment of chronic heart failure should not be limited to symptom relief, but should focus on multiple aspects of a patient's life to reduce mortality and readmission rates. Today, the medical model has entered the stage of biopsychosocial medicine. In the era of biopsychosocial medicine, health education plays an important role in the hospital system. Health education is based on the service center of medical institutions and takes people as the guiding ideology. Through daily education and communication, patients are introduced to the concept of health in a planned and purposeful manner. The goal is to change unhealthy behaviors in patients and improve their quality of life and well-being [1]. Appropriately intervene in patients' daily behavior through health education, change their concept, and thus, change their daily behavior. It can effectively improve the patient's self-care ability, reduce pain, relieve symptoms such as psychological depression, improve the quality of life of the patient, and indirectly reduce the cost of treatment.

The IMB model mainly affects the patient's self-management behavior through three elements: information, motivation, and behavioral ability. Information is a prerequisite for healthy behavior. In this study, we used three scales to identify subjects' common weaknesses in disease knowledge, daily life style, and related skills. And it adopts the method of issuing health education manuals to respond to the subjects' confusion and misunderstanding of relevant knowledge in a timely manner. Through individual guidance, let them establish correct understanding, change misconceptions, and fully understand the occurrence and development of diseases. It helps patients reduce psychological stress and pain. It can provide an effective approach to health education to improve the lives of patients with chronic heart failure.

In this study, the benefits of a doctor-nurse collaborative health education model were fully exploited. The traditional method of health education only carried out by nurses has been replaced by the method of cooperation between doctors and nurses, deepening and broadening health education from different angles and achieving better results in health education. Based on the IMB model, we can solve the confusion and misunderstanding of patients in various ways, establish a correct understanding, and reduce psychological pressure.

2. Related Work

As the current society begins to enter the aging process, heart failure, which is multiple and accompanied by other diseases, has become one of the key points of the world's attention. Scholars at home and abroad have carried out in-depth research on it. Among them, Zhang et al. evaluated the effect of conductive health education on the self-management behavior of elderly patients with hypertension and gastric ulcer. The results show that conductive health education can effectively improve the self-management behavior of elderly patients with hypertension and gastric ulcer [2]. Paying attention to the self-care skills of patients with chronic diseases, especially those with cardiovascular diseases, based on educational interventions will help them improve their conditions. The Barkhordari-Sharifabad study investigated the effects of promoting health literacy through virtual education on self-care behaviors in patients with heart failure. The intervention included four themes on self-care issues in text, photos, animations, and short films. Participants will be provided with a topic link each week. After the link is sent, through the cyberspace system, the necessary follow-up on the acquisition and understanding of the information and its application is carried out, and the correct self-care essentials results are emphasized. According to the paired t-test results, the mean scores of overall self-care in both groups increased after the intervention compared to before the intervention ($P < 0.05$) [3]. The safety and efficacy of aerobic exercise in heart failure (HF) patients with atrial fibrillation (AF) have not been well evaluated. Luo et al.'s study investigated whether the outcomes of high-frequency training differed by atrial fibrillation. In the overall population, there were no significant differences in the incidence of AF by randomization to treatment assignment or baseline AF status (all $P > 0.10$). There was no interaction between atrial fibrillation and exercise training on functional status or clinical outcome measures (all $P > 0.10$). Atrial fibrillation in patients with chronic HF was associated with older age, lower exercise capacity at baseline, and a higher overall frequency of clinical events, but did not respond differently to training-induced changes in clinical outcomes or exercise capacity [4]. The cost-effectiveness of heart failure management interventions can be further understood by combining the expected benefits and costs of future survival. The Maru et al.'s study compared long-term costs (mean intervention duration = 12 months) per quality-adjusted life-year (QALY) obtained from home (HBI) and specialist clinic intervention (CBI) in elderly patients discharged with heart failure (mean age = 71 years). Compared with CBI (outpatient specialist HF clinic-based intervention), HBI (mostly home-based, but not exclusively home-based) has a potential long-term cost-effectiveness threshold of A$50,000/QALY in elderly heart failure patients willing to pay [5]. A novel biomarker, human epididymal protein 4 (HE4), shows prognostic value in patients with acute heart failure (HF). Piek et al. measured HE4 levels in patients with chronic heart failure (CHF) and correlated it with HF severity, renal function, and biomarkers of HF to determine its predictive value [6]. Nymo et al. seek to use a systematic approach to assess whether a panel of biomarkers can improve outcomes in patients with heart failure (HF) and ischemic reduced ejection fraction, as required by recommendations for validation of new biomarkers. In conclusions, in the specific HF patient population studied, a multimarker approach using a specific biomarker panel measured has limited clinical value in determining the risk of adverse future outcomes [7]. The studies of the scholars all have the corresponding advantages of improving the diagnosis and treatment of patients with heart failure, but the research is time-consuming, and the experimental data

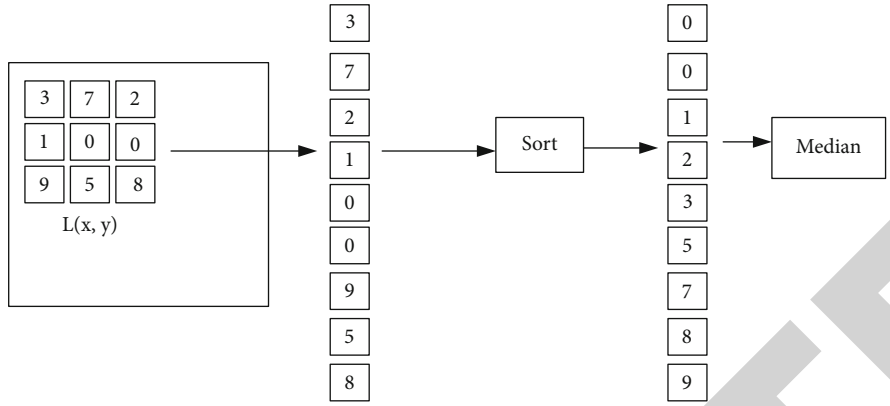

Figure 1: Schematic diagram of median filtering.

are limited, which cannot represent the whole, and suitable and sufficient samples are not easy to gather.

3. Detection of Chronic Heart Failure

3.1. Preprocessing of Medical Images Based on Chronic Heart Failure. Medical images are mostly used for medical treatment or medical research. The purpose of medical image processing is to restore images with insufficient clarity, to highlight some feature information, or to classify images, etc.

3.1.1. Image Filtering. In the process of image formation or transmission, the image will be affected by various factors, resulting in poor quality [8]. Therefore, smoothing filtering is used to remove part of the noise [9]. Smoothing filtering is mainly achieved by smoothing out high-frequency details in the image to reduce contrast and enhance the details of low-frequency parts. Use $G(x, y)$ to represent the filter, $L(x, y)$ to represent the input image sample, and the expression of the output image $T(x, y)$ at this time is:

$$T(x,y) = G(x,y) \cdot L(x,y) = \sum_{r=1}^{i-1} \sum_{s=0}^{j-1} G(r,s) * L(x-r.y-s). \tag{1}$$

Among them, $G(x, y)$ can select appropriate filters through different selection requirements, such as median or mean filter.

Median filtering is a signal processing method that, in some cases, overcomes the nonlinear problem of blurring image details caused by the previous filter. The specific implementation of median filtering is relatively simple because it reduces the dependence on the statistical properties of the image [10–12]. In contrast, median filtering mainly refers to the method of replacing the gray value of the central pixel with the median value [13]. As can be seen in Figure 1, median filtering is implemented with a sorting method for pixel gray levels in a sliding window [14].

Using $A1, A2, \cdots, Ai$ to represent the domain gray value of a point (A, B), the formula of median filtering is expressed as follows:

$$G(A,B) = \mathrm{Med}[A1, A2, \cdots, Ai]. \tag{2}$$

Median filtering has advantages in reducing noise and preserving signal compared to mean and Gaussian filtering. Therefore, by choosing median filtering for image filtering, isolated points can be eliminated.

After smoothing and denoising the image using filtering techniques, image enhancement techniques in the zero domain or frequency domain can also be used to highlight the contrast between the object and the background and to emphasize the information describing the strong features of the image [15–17].

3.1.2. Image Interpolation. When analyzing medical images, it is necessary to view a specific angle, or the area to be viewed may actually be just a section of the image. This requires the use of grayscale interpolation techniques to construct a viewing plane based on predictions of new data points from known data points [18–20]. Image comparison analysis in medical image classification requires the use of interpolation techniques, also known as resampling or resampling [21]. There are three common modes of grayscale interpolation of two-dimensional images, nearest neighbor interpolation, bilinear interpolation, and cubic polynomial interpolation. The principle of grayscale interpolation of two-dimensional images is shown in Figure 2.

3.2. Shape Feature Extraction of Medical Images. There are two main approaches to describe shape features: boundary-based and region-based [22]. Boundary-based methods use only the outer edges of the shape, while region-based methods use the entire area of the shape.

3.2.1. Boundary-Based Shape Features. The boundary of the image can be reflected by the discontinuity of grayscale. The CT image is a grayscale image. If a pixel is a boundary point, the value of its gradient vector is generally outside a certain range [23]. After decades of development, many experts and scientists have proposed edge detection operators to find edge points and describe edge features [24]. Two classical principles for finding edge points are widely

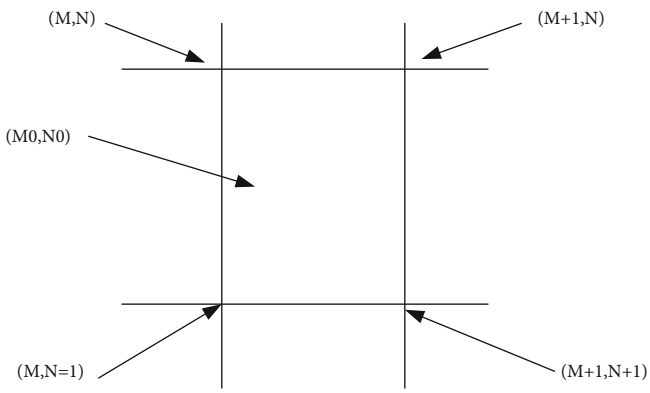

Figure 2: Schematic diagram of two-dimensional image gray difference.

used: one is the first derivative of the maxima of the derivative, and the other is that the second derivative of the point is zero [25].

(1) Edge Detection Operator with First-Order Differential. The boundary is extracted by calculating the gradient of each pixel in the image corresponding to the maximum value of the first-order differential [26]. The commonly used first-order differential detection operators include Robert and Sobel operators.

The Robert operator locates the edge by the local difference operator. The formula for the Robert operator is:

$$J(y(A,B)) = \left|[y(A,B) - y(A+1,B+1)]^2 + [y(A+1,B) - y(A,B+1)]^2\right|^{1/2}. \quad (3)$$

The calculated value of $J(y(A,B))$ can detect the point at the edge, and its size reflects the local change of the image.

Another commonly used first-order differential operator is the Sobel operator, which detects edges by computing neighborhood differences [27]. The weighting method is generally used in the calculation. Weighting the influence of the position of the pixels can reduce the degree of edge blur, so the effect is better. If the weights are different, the results of the operators will be different [28, 29]. The size of the weights is related to different distances, and small distances have a large impact on the neighborhood and the current pixel [30–33]. In the calculation, the difference value is obtained by calculating the average value of the gray level of the pixel by weighting, and the expression is:

$$Q = \sqrt{Q_A^2 + Q_B^2}, \quad (4)$$

$$Q_A = [y(A-1,B-1) + 2y(A,B-1) + y(A+1,B-1)], \quad (5)$$

$$Q_B = [y(A+1,B-1) + 2y(A+1,B) + y(A+1,B+1)]. \quad (6)$$

In the formula, A and B represent two directions, and analyzing their directions can reveal the extended edge information needed to select two spaced rows or columns for difference calculation.

(2) Second-Order Differential Detection Operator. Laplacian is a common direction-independent second-order differential detection operator, which is mainly used for 3×3 convolution of edge extraction. It is a direction-independent edge detection operator developed by selecting thresholds and finding boundary points based on the principle of zero-crossing of second-order differential derivatives [34]. Let $y(A,B)$ represent the image and $T(A,B)$ represent the Laplacian edge operator, and its expression formula is:

$$T(A,B) = y(A-1,B) + y(A+1,B) + y(A,B-1) + y(A,B+1) - 4y(A,B). \quad (7)$$

In the formula, to get edge information, it is only necessary to take the opposite sign of adjacent pixels. And $y(A,B+1)$ represents the filtered image of $y(A,B)$.

(3) Optimization Detection Operator. Compared with the first-order and second-order difference detection operators, the Canny operator is a multistage optimization operator. It measures the product of signal-to-noise ratio and localization, but since it can achieve filtering, enhancement, and detection at the same time, the actual computation is cumbersome [35]. However, the Canny operator can only detect the edge in the image once, and it will also mark the possible image noise as the edge. The specific implementation steps are as follows.

First, to define a one-dimensional Gaussian filter function $g(A)$, through which the image is smoothed:

$$g(A) = \frac{1}{\sqrt{2\pi}\alpha} ex\left(-\frac{A^2}{2\alpha^2}\right). \quad (8)$$

Secondly, it is assumed that the convolution templates of the first-order difference are $W1$ and $W2$, according to which the corresponding gradient direction and amplitude can be calculated. It is required to take the point with the largest local gradient, which needs to be obtained by suppressing the amplitude, which can better preserve the refined edge.

$W1 = \begin{vmatrix} -1, & -1 \\ 1, & 1 \end{vmatrix}$ and $W2 = \begin{vmatrix} 1, & -1 \\ 1, & -1 \end{vmatrix}$, and their corresponding directions and magnitudes are:

$$F1(i,j) = y(i,j) \cdot W1(A,B), \quad (9)$$

$$F2(i,j) = y(i,j) \cdot W2(A,B), \quad (10)$$

$$\beta(i,j) = \sqrt{F_1^2(i,j) + F_2^2(i,j)}, \quad (11)$$

$$\chi\beta = \arc\left[\frac{F2(i,j)}{F_1(i,j)}\right]. \tag{12}$$

Finally, edges are detected by thresholding.

3.2.2. Regional Shape Features. The region-based shape description is mainly described by extracting the features of the region of interest. Commonly used extraction methods include roundness, moment of inertia, and geometric moment features.

(1) Roundness [36]. Assuming that the area of a circle is P and the perimeter is S, the perimeter will change with the change of the outside world. In the case of the same area, the perimeter is the shortest, and the shape features can be expressed most densely at this time. The definition formula of roundness, that is, the density E, is:

$$E = \frac{S^2}{(4\pi P)}. \tag{13}$$

(2) Moment of Inertia [37]. In terms of physical definition, the concept based on the center of gravity can represent the center of mass (ZA, ZB) of the center of gravity of the grayscale image $y(A, B)$, and the expression is as follows:

$$ZA = \frac{\sum_{A=1}^{i}\sum_{B=1}^{j} A \cdot y(A,B)}{\sum_{A=1}^{i}\sum_{B=1}^{j} y(A,B)}, \tag{14}$$

$$ZB = \frac{\sum_{A=1}^{i}\sum_{B=1}^{j} B \cdot y(A,B)}{\sum_{A=1}^{i}\sum_{B=1}^{j} y(A,B)}. \tag{15}$$

Assuming that the moment of inertia around the center of mass (ZA, ZB) is $L(ZA, ZB)$, the definition formula is as follows:

$$L(ZA,ZB) = \sum_{A=1}^{i}\sum_{B=1}^{j} [(A,B) - (ZA,ZB)]^2 y(A,B), \tag{16}$$

$$L(ZA,ZB) = \sum_{A=1}^{i}\sum_{B=1}^{j} \left((A-ZA)^2 + (B-ZB)^2\right) Y(A,B). \tag{17}$$

The formula of moment of inertia is normalized, and the moment of inertia is expressed as NM as follows:

$$NM = \frac{\sqrt{L(ZA,ZB)}}{w}, \tag{18}$$

$$NM = \frac{\sqrt{\sum_{A=1}^{i}\sum_{B=1}^{j}\left((A-ZA)^2 + (B-ZB)^2 y(A,B)\right)}}{\sum_{A=1}^{i}\sum_{B=1}^{j} y(A,B)}. \tag{19}$$

In the formula, $w = \sum_{A=1}^{i}\sum_{B=1}^{j} y(A,B)$ is the quality of the image, which can represent the sum of all grayscale values of the image.

(3) Geometric Moment [38]. Suppose $y(A, B)$ is a piecewise continuous probability density distribution function, and $(i + j)$ represents a two-dimensional continuous random function. The unique moment sequence wij of each order of the function can be determined by the density distribution function. Therefore, the definition formula of the origin moment wij of $(i + j)$ is:

$$Wij = \int\int A^i B^j y(A,B) rArB. \tag{20}$$

The central moment is:

$$Vij = \int\int \left(A - \bar{A}\right)^i \left(B - \bar{B}\right)^j y(A,B) rArB. \tag{21}$$

In Formula (21), $\bar{A} = w10/w00$, $\bar{B} = w01/w00$, and $(\bar{A}, \bar{B})$ represent the centroid of the image $y(A, B)$.

Normalize the central moment:

$$\begin{gathered} \delta \mathrm{ij} = Vij/V00, \\ k = i + j + 2/2, i + j = 2, 3, \cdots \end{gathered} \tag{22}$$

3.3. Basic Flow of Medical Image Processing. The main modules of feature extraction and classification of medical images are image preprocessing, feature extraction, and classification. Its algorithm also focuses on feature extraction and classification. The main steps in extracting features from medical images are as follows.

(1) Extract the features of the processed medical image, select appropriate feature information, and form a feature vector

(2) According to the feature information to be classified, a category model is established between the images

(3) Develop classification algorithms, and develop classifiers through similarity measures, neural networks, support vector machines, and other methods

(4) Train the classifier by inputting the image data to be classified, called training images and test images, respectively

(5) The classification result of the output image

The main process of classifying medical images is shown in Figure 3.

3.4. The Theoretical Basis of IBM. The IMB model recognizes that there are three main factors that are important in the initiation and maintenance of healthy behaviors: accurate information, personal and social motivation (including

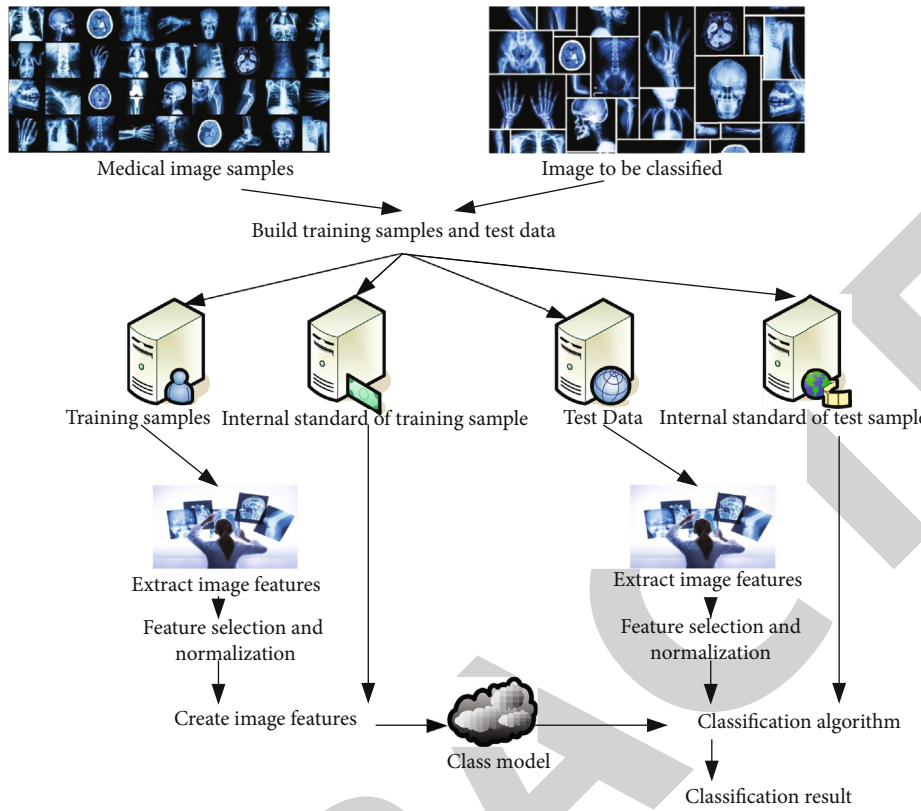

Figure 3: The basic flow of medical image extraction and classification.

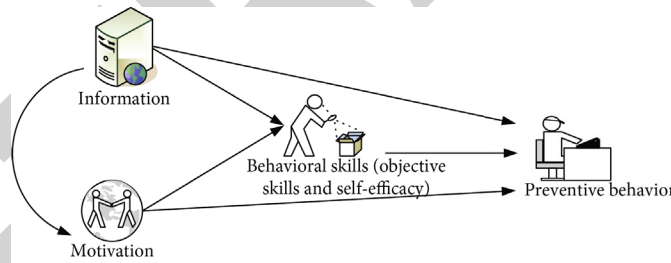

Figure 4: IMB mode process.

attitudes, intentions, and norms), and behavioral skills. This is shown in Figure 4.

Informational factors are a prerequisite in the behavior change process, including events, inspirations, or theories related to the behavior change process. However, in practice, it was found that the interaction between information and behavioral change was not significant when individuals had good knowledge. This theoretical model suggests that information and behavioral change are affected by skill complexity and that behavioral change does not have to be information-based, but when complex behavioral skills are required, information must be involved in an individual's behavioral change.

Motivational factors include personal and social motivations. Personal motivation refers to the subject's forward-looking perception of behavior change, including his attitude, willingness to change, and perception of its importance, whereas social motivation includes support from family, friends, and relatives and their perception of behavioural change; in other words, the attitudes and opinions of people outside the subject. This theoretical model suggests that only when individuals possess high levels of information and related behavioral skills should they be strongly motivated to prevent behavioral change and maintain it.

The IMB model argues that behavioral change is a continuous process where each factor is intertwined. That is, an individual acquires the appropriate level of accurate knowledge, has a positive attitude and motivation, changes behavior with the support of family members, and acquires relevant skills.

This intervention was used in this study not only because it is widely used abroad but also because it accounts for the variability in the causes of behavioral change and the interaction between various factors.

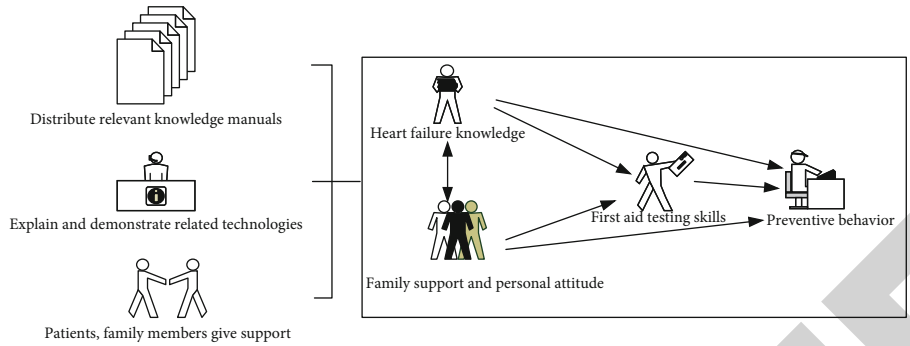

Figure 5: Improved research framework based on the original IMB.

4. Experiment of IMB-Based Health Education on Patients with Chronic Heart Failure

4.1. Improved Research Framework Based on the Original IMB. This intervention is based on the three phases of the IMB model: information transfer, motivation building, and skills transfer. The aim was to understand the impact of the IMB model on risk perception, medical coping, and self-management in patients with chronic heart failure. The flow of IBM's intervention structure is shown in Figure 5.

4.2. Health Education Based on IMB

4.2.1. Determination of the Study Population. The number of heart failure patients admitted to a public hospital in a city within one year was taken as the research object of this work. Patients who met the inclusion criteria were selected from the Department of Cardiology.

(1) Inclusion criteria

First, it meets the diagnostic criteria for heart failure.

The second is a person with a cardiac function class II to IV.

Third, people who are ≥18 years old, are conscious, can speak fluently, and can communicate by telephone.

Fourth, primary school or above.

Fifth, the course of disease ≥3 months.

Sixth, participate voluntarily and sign the informed consent.

(2) Exclusion criteria

First: people with cognitive impairment or mental illness.

Second: people with other serious systemic diseases, such as lung disease and malignant tumors.

Third: people with heart failure due to alcoholism or systemic diseases.

Fourth: people with severe hearing or visual impairment.

Fifth: people who live in nursing homes for a long time.

4.2.2. Confirmation of the Number of Samples.

$$I1 = I2 = 2\left[\frac{(V\varepsilon + V\gamma)}{\varphi/\phi}\right]^2 + \frac{1}{4}V\varepsilon^2. \quad (23)$$

Among them, I is the content of the sample, φ is the mean difference between the two samples, and ϕ is the standard deviation of the population.

4.2.3. Research Group. Control group (usual care and health education): patients received routine care and health education in cardiology during their hospital stay. It includes medication care, dietary care, symptomatic care during hospitalization, and discharge guidance. Patients receive a "Heart Failure Health Education Handbook" that contains information on medication management and self-efficacy.

Intervention group (on the basis of routine health education, implement health education in the mode of cooperation between doctors and nurses): the attending physician and the attending nurse jointly implement health education for the patients. The physician and the nurse should not only divide the labor but also cooperate, communicate with each other, learn from each other, and establish a cooperation model between the physician and the nurse. Leadership of the team rests with the senior nurse. In order to ensure the fairness and impartiality of the two health education methods, the training plan was jointly formulated by the department head and senior nurses, and the training and assessment of the health education knowledge of chronic heart failure were jointly carried out by the nurses in charge and senior doctors. The ward environment, medical equipment, treatment, nursing, and rules and regulations are the same, and the staff levels of the two wards are also the same, which ensures that the two groups of patients participate in health education with the same propaganda content in different ways.

4.3. Intervention Methods for Heart Failure Patients and the Basic Situation of the Samples. The research data were processed and analyzed with SPSS17.0 statistical software. Quantitative data are expressed as mean ± standard deviation, and t-test was used to compare the observed indicators between the two groups; qualitative data were

Table 1: Basic information of the two groups of patients.

Normal information		Control group	Intervention group	P
Gender	Male	31 (55.4%)	26 (46.4%)	0.35
	Female	25 (44.6%)	30 (53.6%)	
Average age		64.3 ± 15.5	64 ± 18.5	0.91
Education level	College degree and above	12 (21.4%)	14 (25%)	0.99
	Middle school or high school	16 (28.6%)	15 (26.8%)	
	Elementary school and below	28 (50%)	27 (48.2%)	
Family monthly income	<2000	19 (33.9%)	16 (28.6%)	0.74
	2000-4000	27 (48.2%)	32 (57.1%)	
	>4000	10 (17.9%)	8 (14.3%)	
Expense reimbursement method	Medical insurance	19 (33.9%)	21 (37.5%)	0.97
	Rural cooperative	22 (39.3%)	22 (39.3%)	
	Poor	8 (14.3%)	7 (12.5%)	
	Own expense	7 (12.5%)	6 (10.7%)	
Profession	Worker	6 (10.7%)	12 (21.4%)	0.29
	Farmer	27 (48.2%)	20 (35.7%)	
	Other	10 (17.9%)	8 (14.3%)	
	Unemployed	7 (12.5%)	12 (21.4%)	
	Retire	6 (10.7%)	4 (7.1%)	

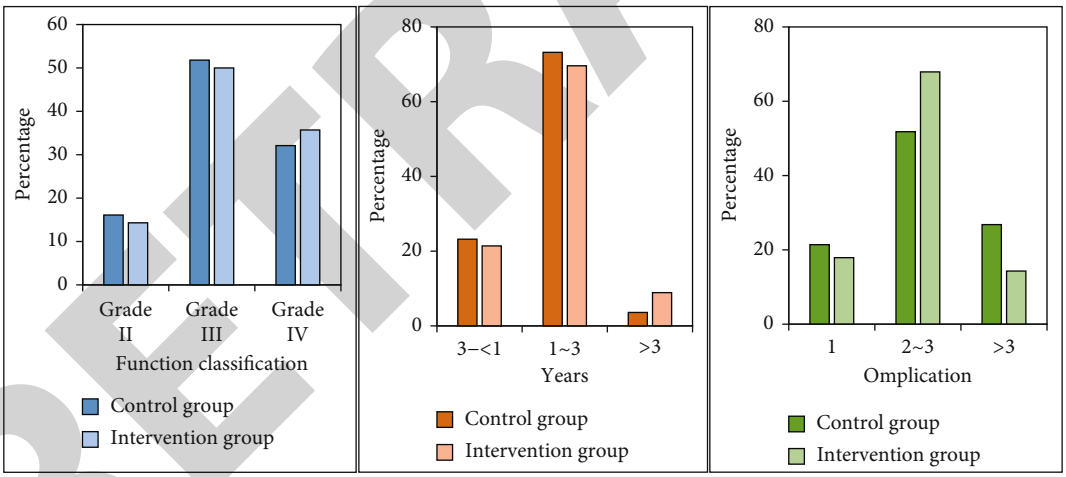

Figure 6: Comparison of the symptoms of heart failure between the two groups.

Table 2: Comparison of negative emotions between the two groups of patients on admission.

On admission Content	Control group	Intervention group
Concern	3.1 ± 0.4	3 ± 0.5
Negative emotions	3 ± 0.5	2.9 ± 0.4
t	0.6	1.15
P	0.55	0.25

Table 3: Comparison of the negative emotions of the two groups of patients at the time of discharge.

On discharge Content	Control group	Intervention group
Concern	2 ± 0.5	1.8 ± 0.5
Negative emotions	2 ± 0.4	1.7 ± 0.5
t	3.4	3.36
P	0.001	0.001

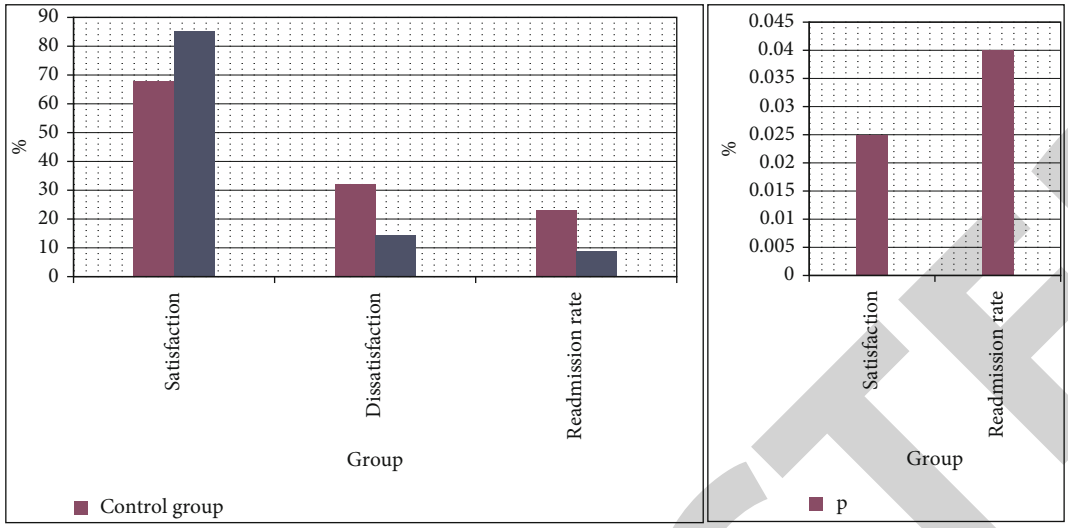

Figure 7: Satisfaction of the two groups of patients with health education and the probability of short-term readmission.

analyzed as percentages. Differences were considered statistically significant at $P < 0.05$.

According to the basic conditions of the two groups of patients in Table 1, the general information of the two groups of patients was collected. It includes the average age, gender, educational level, occupation, family monthly income, and reimbursement method of hospitalization expenses of the two groups of chronic heart failure patients. The gender comparison of the two groups of patients is relatively average. The educational background of the patients is mostly below the primary school level, the income range is 2000-4000, and the occupation is mostly concentrated in farmers. There was no significant difference between the two groups of patients ($P > 0.05$), which was comparable.

From the comparison probability map of disease data in Figure 6, we have a preliminary understanding of the basic conditions of the two groups of patients. From the overall comparison of cardiac function classification, years of illness, and the number of comorbidities, the difference between the two groups is not large, but there are individual differences. This may affect the bias of later experimental data. Second, most of the patients' disease years were concentrated in 1 to 3 years, and most of the patients who participated in the experiment had 2 to 3 combined diseases.

5. Experimental Analysis of IMB-Based Health Education on Patients with Chronic Heart Failure

5.1. Emotional Comparison of Two Groups of Chronic Heart Failure Patients Based on IMB Health Education. Table 2 and Table 3 are the negative emotion comparison data of the two groups of patients at the time of admission and discharge. In the control group, the anxiety score was 3.1 ± 0.4 and the negative emotion score was 3 ± 0.5 at admission. The anxiety score of the patients in the intervention group was 3 ± 0.5, and the negative emotion score was 2.9 ± 0.4 at admission. After the two groups received treatment and were discharged from hospital for a period of time, the quality of life questionnaire was conducted again. The anxiety score of the control group was 2 ± 0.5, and the negative emotion score was 2 ± 0.4. The anxiety score of the experimental group was 1.8 ± 0.5, and the negative emotion score was 1.7 ± 0.5, and the difference was statistically significant $P < 0.05$. Anxiety and negative emotions were significantly improved in both the control and intervention groups compared to admission, but the improvement was greater in the experimental group.

5.2. Comparison of Satisfaction Rate and Readmission Rate of Two Groups of Chronic Heart Failure Patients Based on IMB Health Education. As can be seen from Figure 7, the satisfaction of health education of heart failure patients in the two groups was compared, and the satisfaction of the intervention group was higher, accounting for about 85.3%, and the dissatisfaction only accounted for 14.3%. The short-term readmission probability was 8.9%. In contrast, the satisfaction of the control group was lower than that of the intervention group, about 67.9%, and the dissatisfaction with health education and the probability of short-term readmission were higher than those of the intervention group, 32.1% and 23.2%, respectively.

5.3. Comparison of Self-Care Behavior of Two Groups of Patients Based on IMB Health Education. From the self-care situation table in Table 4, the total and maintenance scores of self-care in the intervention group were significantly higher than those before the intervention. The total score and maintenance score of self-care in the control group were also higher than those before the intervention, but the scores of self-care management and self-care confidence were not significantly different, and $P > 0.05$, which was not statistically significant.

Figure 8 shows the comparison of risk perception between the control group and the intervention group before and after the intervention. The results showed that before the intervention, the P values of the two groups of heart

Table 4: Comparison of self-care behaviors of two groups of patients with heart failure.

Group	Project	Before intervention	After the intervention	t	P
Intervention group	Self-care total score	137.5 ± 28	186.4 ± 22	-21.7	<0.001
	Self-care maintenance	46.8 ± 10	60.4 ± 8.6	-14.3	<0.001
	Self-care management	43.8 ± 11.4	64 ± 10.6	-20.68	<0.001
	Self-confidence	47 ± 11	62 ± 9.6	-9.3	<0.001
Control group	Self-care total score	135.3 ± 18.5	138.7 ± 17.3	-3.1	0.004
	Self-care maintenance	45 ± 9.7	48.2 ± 9.2	-8.7	<0.001
	Self-care management	43.5 ± 10.4	44.4 ± 10.1	-1.14	0.26
	Self-confidence	47.2 ± 10.8	46 ± 9.7	1.3	0.2

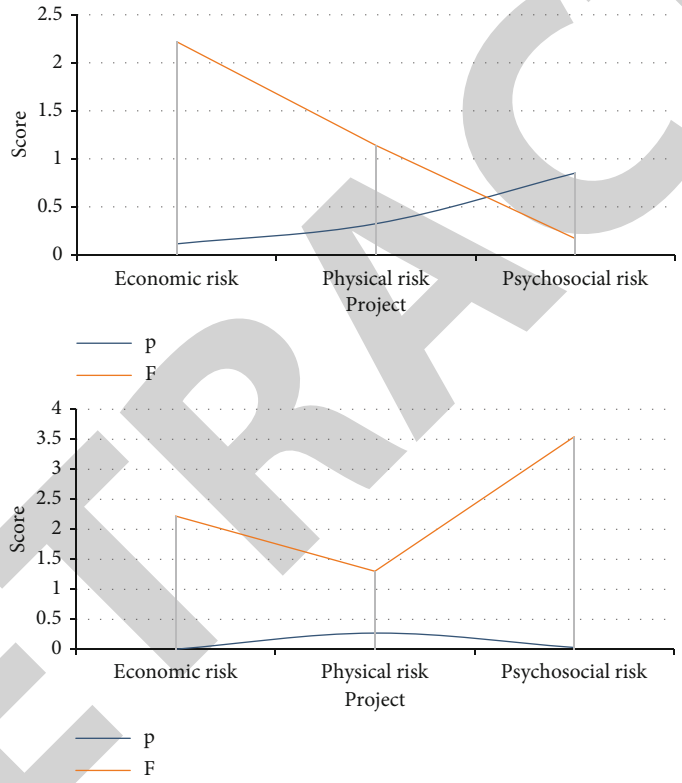

Figure 8: Comparison of risk perception between control group and intervention group before and after intervention.

failure patients in terms of economic risk, physical diagnosis and treatment risk, and psychosocial risk were >0.05, which was not statistically significant. After the intervention, the risk perception P value of the two groups of patients was >0.05, which was not statistically significant.

Paired sample t-tests were used to compare sentiment scores at baseline, six months, one year, and two years later, as well as data on readmissions between the two groups.

From the data in Figure 9(a), the emotional scores of patients in both groups showed an upward trend with time. But from a detailed point of view, the emotional score of the intervention group was the lowest in the half-year period, only 3.1, and then, although it increased, it was still lower than the baseline level. In contrast, the emotional scores of the control group gradually leveled off after increasing over time. The comparison chart in Figure 9(b) clearly shows the number of readmissions in the two groups. The number of readmissions in both groups also showed an upward trend over time, but the increase in the intervention group was significantly lower than that in the control group.

5.4. Interventions to Improve the Quality of Life of Patients with Chronic Heart Failure

(1) Psychological intervention: listen carefully to the patient's chief complaint, respect the patient, pay attention to protecting the patient's privacy, put yourself in the shoes of the patient to understand

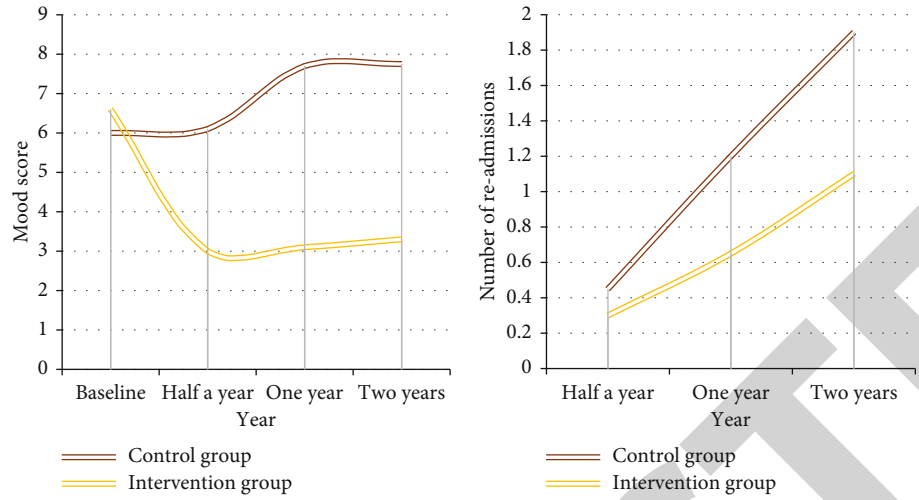

Figure 9: The emotional changes of the two groups of patients over time and the number of readmissions.

the inner thoughts that cause the patient's negative emotions, give answers and suggestions to the patient, shorten the patient's hospital stay as much as possible, and reduce their economic burden

(2) Cognitive intervention: improve patients and their families' awareness of chronic heart failure and correct misconceptions. They should also be made aware of and actively intervene in various risk factors and avoid risky behaviors and predisposing factors to improve disease and quality of life and prevent further disease progression

(3) Nutritional intervention: good nutritional self-management can effectively improve patients' compliance with medical treatment, regulate individual behavior, enhance self-confidence, delay the development of disease, and improve quality of life and survival rate

(4) Medication intervention: inform patients and their families of the names, doses, uses, effects, and adverse reactions of commonly used drugs to improve their knowledge of medication. Educate them about common adverse effects of the medications they take, and suggest family members to help monitor patients' medication and improve their compliance

(5) Exercise intervention: numerous studies have confirmed that proper exercise can improve physical function. The role of exercise rehabilitation in patient rehabilitation and treatment has been widely recognized. It can improve the patient's cardiopulmonary function, improve the patient's exercise tolerance and amount of exercise, and improve the patient's quality of life

6. Conclusions

The research model of this paper is based on IMB, the experimental samples are divided, and effective health education guidance is provided to the intervention group on the basis of group formation. There are also some innovations in the health education guidance. It has introduced the health education model of cooperation between doctors and nurses from the original nursing care of only nurses. The experimental results show that the health education model can effectively improve the quality of life of patients with chronic heart failure, improve the patient's compliance behavior, improve the negative emotions of patients with chronic heart failure, and promote the recovery of the disease. It can better meet the health education needs of patients, improve the quality of health education, and can effectively improve the satisfaction rate of patients when they are discharged from the hospital, and reduce the readmission rate in a short period of time. It is worthy of clinical promotion and application. From the research data in this paper, the impact on patients with chronic heart failure is mainly reflected in two aspects. First of all, the risk perception of patients is relatively high, and the main factors affecting the risk perception of patients are education, gender, type of expense, and work status. Second, the health education model based on the IMB medical cooperation model can reduce patients' overall risk perception, improve their self-management ability, and deal with disease stress with a more positive attitude. However, the data source for this study was a single site and resided in the same area, which may limit interpretation of the results.

Data Availability

The data that support the findings of this study are available from the corresponding author upon reasonable request.

Conflicts of Interest

The authors declared no potential conflicts of interest with respect to the research, authorship, and/or publication of this article.

Acknowledgments

This work was supported by the "Qiqihar Academy of Medical Sciences, China (grant no. QMSI2019M-14)".

References

[1] Z. Lv and H. Ko, "Introduction to the special issue on recent trends in medical data security for e-health applications," *ACM Transactions on Multimidia Computing Communications and Applications*, vol. 17, no. 2s, pp. 1–3, 2021.

[2] L. P. Zhang, J. J. Hu, and H. Wang, "Effect of conductive health education on self-management behavior of patients with hypertension complicated with peptic ulcer," *World Chinese Journal of Digestology*, vol. 26, no. 27, pp. 1612–1617, 2018.

[3] M. Barkhordari-Sharifabad, "The effect of health literacy promotion through virtual education on the self-care behaviors in patients with heart failure: a clinical trial," *Journal of Health Literacy*, vol. 6, no. 1, pp. 51–60, 2021.

[4] N. Luo, P. Merrill, K. S. Parikh et al., "Exercise training in patients with chronic heart failure and atrial fibrillation," *Journal of the American College of Cardiology*, vol. 69, no. 13, pp. 1683–1691, 2017.

[5] S. Maru, J. M. Byrnes, M. J. Carrington, S. Stewart, and P. A. Scuffham, "Long-term cost-effectiveness of home versus clinic-based management of chronic heart failure: the WHICH? study," *Journal of Medical Economics*, vol. 20, no. 4, pp. 318–327, 2017.

[6] A. Piek, W. C. Meijers, N. F. Schroten, R. T. Gansevoort, R. A. de Boer, and H. H. Silljé, "HE4 serum levels are associated with heart failure severity in patients with chronic heart failure," *Journal of Cardiac Failure*, vol. 23, no. 1, pp. 12–19, 2017.

[7] S. H. Nymo, P. Aukrust, J. Kjekshus et al., "Limited added value of circulating inflammatory biomarkers in chronic heart failure," *JACC: Heart Failure*, vol. 5, no. 4, pp. 256–264, 2017.

[8] S.-S. Claudia, "Patient education in the context of rehabilitation self-management interventions and patient coaching integral components of pulmonary rehabilitation (PR)," *Therapeutische Umschau. Revue therapeutique*, vol. 76, no. 8, pp. 442–448, 2019.

[9] R. Citro, C. Prota, A. Silverio, and E. Bossone, "Takotsubo syndrome: emerging concepts about diagnosis, prognosis and therapy," *Giornale italiano di cardiologia (2006)*, vol. 20, no. 9, pp. 512–522, 2019.

[10] S. Brown and S. Braman, "Recent advances in the management of acute exacerbations of chronic obstructive pulmonary disease," *Medical Clinics of North America*, vol. 104, no. 4, pp. 615–630, 2020.

[11] M. Elhoseny, G. Ramírez-González, O. M. Abu-Elnasr, S. A. Shawkat, N. Arunkumar, and A. Farouk, "Secure medical data transmission model for IoT-based healthcare systems," *Ieee Access*, vol. 6, pp. 20596–20608, 2018.

[12] M. Abdolmaleky, M. Naseri, J. Batle, A. Farouk, and L. H. Gong, "Red-green-blue multi-channel quantum representation of digital images," *Optik*, vol. 128, pp. 121–132, 2017.

[13] S. Roth, C. Fernando, S. Azeem, and G. W. Moe, "Is there a role for ivabradine in the contemporary management of patients with chronic heart failure in academic and community heart failure clinics in Canada?," *Advances in Therapy*, vol. 34, no. 6, pp. 1340–1348, 2017.

[14] A. A. Kotby, O. I. Youssef, M. O. Elmaraghy, and O. S. el Sharkawy, "Galectin-3 in children with chronic heart failure with normal and reduced ejection fraction: relationship to disease severity," *Pediatric Cardiology*, vol. 38, no. 1, pp. 95–102, 2017.

[15] S. Statsenko, S. V. Turkin, S. V. Fabritskaya, and N. N. Shilina, "Efficacy of short-term therapy with meldonium in patients with chronic heart failure of ischemic etiology and type 2 diabetes mellitus," *Kardiologiia*, vol. 57, no. 4, pp. 58–63, 2017.

[16] K. G. Srinivasa, B. J. Sowmya, A. Shikhar, R. Utkarsha, and A. Singh, "Data analytics assisted internet of things towards building intelligent healthcare monitoring systems: IoT for healthcare," *Journal of Organizational and End User Computing 30*, vol. 4, pp. 83–103, 2018.

[17] Y. Zhao, H. Li, S. Wan et al., "Knowledge-aided convolutional neural network for small organ segmentation," *IEEE Journal of Biomedical and Health Informatics*, vol. 23, no. 4, pp. 1363–1373, 2019.

[18] S. von Haehling, U. Gremmler, M. Krumm et al., "Prevalence and clinical impact of iron deficiency and anaemia among outpatients with chronic heart failure: the PrEP registry," *Clinical Research in Cardiology*, vol. 106, no. 6, pp. 436–443, 2017.

[19] M. Hu, Y. Zhong, S. Xie, H. Lv, and Z. Lv, "Fuzzy system based medical image processing for brain disease prediction," *Frontiers in Neuroscience*, vol. 15, 2021.

[20] Q. Wang, Y. Li, and X. Liu, "(2018) "The influence of photo elements on EEG signal recognition"," *Eurasip Journal on Image and Video Processing*, vol. 1, 2018.

[21] J. H. Traverse and T. D. Henry, "Myocardial injury as a new target for cell therapy in patients with chronic heart failure: when something bad is actually good?," *Circulation Research*, vol. 120, no. 12, pp. 1857–1859, 2017.

[22] M. V. Menzorov, A. M. Shutov, V. I. Midlenko, N. V. Larionova, I. V. Morozova, and O. V. Akulova, "Value of N-terminal pro brain natriuretic peptide in predicting acute kidney injury in patients with acute decompensated chronic heart failure," *Terapevticheskiĭ Arkhiv*, vol. 89, no. 3, pp. 78–84, 2017.

[23] T. O. Awotidebe, V. O. Adeyeye, R. A. Adedoyin et al., "Assessment of functional capacity and sleep quality of patients with chronic heart failure," *Hong Kong Physiotherapy Journal*, vol. 36, no. C, pp. 17–24, 2017.

[24] A. Cichocka-Radwan and M. Lelonek, "Annual prognostic factors in chronic heart failure in patients over 80 years old," *Kardiologia Polska*, vol. 75, no. 2, pp. 164–173, 2017.

[25] P. Sulzgruber, L. Koller, M. P. Winter et al., "The impact of CD4+CD28null T-lymphocytes on atrial fibrillation and mortality in patients with chronic heart failure," *Thrombosis & Haemostasis*, vol. 117, no. 2, pp. 349–356, 2017.

[26] T. Gombos, Z. Förhécz, Z. Pozsonyi, L. Jánoskuti, Z. Prohászka, and I. Karádi, "Long-term survival and apolipoprotein A1 level in chronic heart failure: interaction with tumor necrosis factor α −308 G/A polymorphism," *Journal of Cardiac Failure*, vol. 23, no. 2, pp. 113–120, 2017.

[27] D. Kessing, J. Denollet, J. Widdershoven, and N. Kupper, "Self-care and health-related quality of life in chronic heart failure: a longitudinal analysis," *European Journal of Cardiovascular Nursing Journal of the Working Group on Cardiovascular Nursing of the European Society of Cardiology*, vol. 16, no. 7, pp. 605–613, 2017.

Hindawi
Computational and Mathematical Methods in Medicine
Volume 2023, Article ID 9843487, 1 page
https://doi.org/10.1155/2023/9843487

Retraction

Retracted: An Inhibitor of Nuclear Factor-Kappa B Pathway Attenuates the Release of TGF-β1 and Inhibits the Fibrogenic Progress in a Model of Airway Remodeling Induced by Acrolein

Computational and Mathematical Methods in Medicine

Received 27 June 2023; Accepted 27 June 2023; Published 28 June 2023

This article has been retracted by Hindawi following an investigation undertaken by the publisher [1]. This investigation has uncovered evidence of one or more of the following indicators of systematic manipulation of the publication process:

(1) Discrepancies in scope

(2) Discrepancies in the description of the research reported

(3) Discrepancies between the availability of data and the research described

(4) Inappropriate citations

(5) Incoherent, meaningless and/or irrelevant content included in the article

(6) Peer-review manipulation

The presence of these indicators undermines our confidence in the integrity of the article's content and we cannot, therefore, vouch for its reliability. Please note that this notice is intended solely to alert readers that the content of this article is unreliable. We have not investigated whether authors were aware of or involved in the systematic manipulation of the publication process.

Wiley and Hindawi regrets that the usual quality checks did not identify these issues before publication and have since put additional measures in place to safeguard research integrity.

We wish to credit our own Research Integrity and Research Publishing teams and anonymous and named external researchers and research integrity experts for contributing to this investigation.

The corresponding author, as the representative of all authors, has been given the opportunity to register their agreement or disagreement to this retraction. We have kept a record of any response received.

References

[1] P. Chen, X. Wang, Y. Li, and H. Liu, "An Inhibitor of Nuclear Factor-Kappa B Pathway Attenuates the Release of TGF-β1 and Inhibits the Fibrogenic Progress in a Model of Airway Remodeling Induced by Acrolein," *Computational and Mathematical Methods in Medicine*, vol. 2022, Article ID 4984634, 7 pages, 2022.

Hindawi
Computational and Mathematical Methods in Medicine
Volume 2022, Article ID 4984634, 7 pages
https://doi.org/10.1155/2022/4984634

Research Article

An Inhibitor of Nuclear Factor-Kappa B Pathway Attenuates the Release of TGF-β1 and Inhibits the Fibrogenic Progress in a Model of Airway Remodeling Induced by Acrolein

Peng Chen,[1] Xiaoxia Wang,[1] Yanping Li,[1] and Hong Liu[2]

[1]*Department of Respiratory Medicine, The Third People Hospital of Chengdu, Chengdu, Sichuan 610031, China*
[2]*Department of Radiology, The Third People Hospital of Chengdu, Chengdu, Sichuan 610031, China*

Correspondence should be addressed to Hong Liu; liuhong3061380@foxmail.com

Received 18 January 2022; Revised 18 March 2022; Accepted 22 March 2022; Published 6 April 2022

Academic Editor: Muhammad Zubair Asghar

Airway inflammation, airway hypersecretion, and airway remodeling are believed to be involved in the process of lung fibrosis. Nowadays, acrolein is widely used to establish the model of airway remodeling. An active component of propolis, named caffeic acid phenethyl ester (CAPE), is recognized as an inhibitor of the NF-κB pathway and shows anti-inflammatory effect. The purpose of this study was to investigate the protective effect of CAPE on acrolein-induced airway remodeling. 24 mice were divided into 4 groups: control group; acrolein group, mice received acrolein (inhalation of acrolein for 20 days); CAPE group, mice received CAPE (30 mg/kg); and acrolein+CAPE group, mice received acrolein and CAPE. After 20 days, lung tissue was removed for histopathology and immunohistochemical evaluations. TGF-β1 and Muc5ac levels were measured at the protein and molecular levels. Additionally, the phospho-P65/P65 values in the airway smooth muscle cells treated with TGF-β1 or CAPE were detected by Western blot. The results showed that compared with the control, subepithelial collagen deposition, airway inflammation, and peribronchus fibrosis were inhibited in the group treated with CAPE. Furthermore, TGF-β1 was significantly decreased in the acrolein+CAPE group compared with the acrolein group. Additionally, we identified CAPE inhibited P65 phosphorylation. However, CAPE did not inhibit the Muc5ac overproduction and hypersecretion induced by acrolein. In conclusion, as an inhibitor of the NF-κB pathway, CAPE attenuated the release of TGF-β1, which inhibited the fibrogenic progress induced by acrolein in mice and took no effect on inhibiting airway mucus hypersecretion.

1. Introduction

Repeatedly airway inflammatory injury, imperfect tissue repair, and aberrant fibrosis are now recognized as key pathophysiological features of inflammatory diseases of the airways, including cystic fibrosis, bronchiectasis, and chronic obstructive pulmonary disease (COPD). Airway inflammation, airway hypersecretion, and airway remodeling are believed to be involved in the process of pulmonary fibrosis (PF) [1–3]. Nowadays, the underlying mechanisms involved in lung fibrosis remain obscure and conventional therapeutic strategies, including glucocorticoid and oxidation inhibitor, have limited efficacy in treating PF [4]. Therefore, we tried to find more effective drugs for the treatment of PF.

In the last decade, many studies have revealed that some particular cellular signaling pathways have been involved in such fibrogenic process [5, 6]. In animal experiments [7, 8] and in vitro [9], blocking cellular signaling pathway at different stages may inhibit the fibrogenic process to some extent at least. The nuclear factor- (NF-) kappa B (NF-κB) signaling pathway not only participates in cell growth and differentiation but also takes part in the inflammation reactions by regulating the expression of related genes, which is related to the fibrogenic progress [10, 11]. P65 is an important member of the NF-κB family. The phosphorylation of P65 initials the activation of the NF-κB pathway. Transforming growth factor beta (TGF-β) is a factor synthesized in a wide variety of tissues, which is believed to play an important role in cellular differentiation, embryonal development,

immune function, and hormone secretion [12]. TGF-β is found mostly as homodimer forms of separate gene products TGF-β1, TGF-β2, or TGF-β3. Currently, TGF-β1 has been found to induce NF-κB p65 phosphorylation and mediate collagen synthesis [13]. Verma et al. [14] also discovered that quercetin-3-rutinoside attenuates radiation-induced lung inflammation and fibrosis by modulating the NF-κB/TGF-β1 signaling pathway.

A low-molecular-weight aldehyde found in photochemical smog and tobacco smoke, named acrolein, can induce mucus hypersecretion, airway inflammation, and airway remodeling [15, 16]. Acrolein-induced mucus hypersecretion is accompanied by mucous cell differentiation and followed by fibrogenic process, which may be related to the pathogenesis of cystic fibrosis, bronchiectasis, and COPD. Recently, acrolein has been widely used to establish the model of airway remodeling [17, 18]. However, the fibrogenic phenotype and the increased level of TGF-β1 induced by acrolein have not been fully reported in the mice model.

Caffeic acid phenethyl ester (CAPE) is an active component of honeybee propolis. In recent years, CAPE has been recognized as a phenolic antioxidant and is known to have potential anticancer, anti-inflammatory, antimicrobial, and other beneficial medical properties [19, 20]. The underlying mechanisms refer to the suppression of NOX4 expression [21], inhibition of the MAPK/NF-κB signaling pathway [22], and so on. Through inhibition of NF-κB signaling, CAPE had a protective effect *in vitro* [23] or in amiodarone-induced PF rat model [19]. However, the potential property of antifibrosis of CAPE has not been observed in an airway remodeling process induced by acrolein in mice.

Mucus overproduction and hypersecretion are also involved in the process of airway remodeling [24]. Mucin 5AC (Muc5ac) is a representative mucus protein [25]. Cheng et al. showed that microRNA-145 decreased Muc5ac expression to attenuate airway remodeling [26]. Therefore, based on the above study, in the current study, we investigated the fibrogenic progress in mice treated with acrolein inhalation, evaluated the dynamic changes of TGF-β1 and Muc5ac level, and tested the interventional effect of CAPE.

2. Materials and Methods

2.1. Animals. The Animal Care and Use Committee of West China Hospital of Sichuan University approved this animal study. Specific pathogen-free (SPF) grade male C57BL/6 mice (20~30 g) (National Rodent Laboratory Animal Resources, Shanghai Branch, Shanghai, China) at the age of 4 weeks were used for experiments. The mice were housed in independent chambers (0.7 m × 0.4 m × 0.6 m, equipped with ventilation holes) and were maintained on a 12 h diurnal cycle with water and food provided ad libitum. Each chamber was at a temperature of 23 ± 3°C with a relative humidity of 50 ± 5%.

Consulting the animal model of mucus hypersecretion made by Ying et al. [27], we established an airway remodeling model induced by acrolein in mice. 24 mice were randomly divided into 4 groups ($n = 6$ for each group): control group, no treatment; acrolein group, mice received acrolein (inhalation of 0.0004% acrolein fog 6 h a day on 20 consecutive days in a chamber); CAPE group, mice received CAPE (30 mg/kg) via intraperitoneal injection every other day, and acrolein+CAPE group, mice received acrolein and CAPE.

2.2. Tissue Preparation. On the 20th day, each mouse was anesthetized by intraperitoneal injection with 2% pentobarbital sodium before tissue collection. The chests were opened, and the lungs were excised completely, which were carefully washed off the bronchoalveolar lavage fluid (BALF) and fixed by 4% paraformaldehyde subsequently. After being embedded in paraffin, tissue sections were reserved for hematoxylin-eosin (H&E) and Masson stains.

2.3. BALF Collection. BALF was collected through a tracheal cannula with physiological saline on day 20 after anesthesia. Physiological saline (1 ml) was used to inflate the lung, and the lavage fluid was recovered with 90% of the original volume, which was reserved for total cell count. The lavage fluid was centrifuged at 400 × g for 15 min at 4°C. The cell-free supernatant was kept at a temperature of -70°C, while the sediment was prepared for differential cell count under a microscope.

2.4. Histopathology. Tissue sections were reserved for H&E stain to observe the morphologic changes of airway and peribronchus including mucus hypersecretion, infiltration of inflammatory cells, and proliferation of alveolar epithelial cells. Masson stain was made to evaluate the degrees of subepithelial collagen deposition and peribronchus fibrosis. The images were analyzed with Image-Pro plus 4.5 Software (Media Cybernetics Co, USA). And based on that, each sample's Ashcroft score was recorded according to the average scores from different visual fields under a light microscope [28]. This score was operated by four observers.

Hydroxyproline concentration of lung tissue was detected by a hydroxyproline assay kit (Nanjing Jiancheng Bioengineering Institute, Nanjing, China) in accordance with the manufacturer's protocol.

2.5. Enzyme-Linked Immunosorbent Assay (ELISA). Total protein in BALF was evaluated using the Bradford method. TGF-β1 and Muc5ac protein levels in BALF were determined according to the instruction of the commercial ELISA kits (OriGene, USA). Samples were measured photometrically by an automated plate reader.

2.6. Reverse Transcription-Quantitative Polymerase Chain Reaction (RT-qPCR). Total RNA was extracted from pulmonary tissue homogenates with TRIzol (Invitrogen Co., USA) and reverse transcribed, and then, the complementary DNA was amplified by polymerase chain reaction with the PCR kit (Takara Bio Inc., Dalian, China). Primers are as follows: forward, 5′-CAGCCTATGTGAAAGATGCC-3′ reverse 5′-GTAGAGGGAAGTGGAGTTATTGC-3′ for Muc5ac and forward 5′-TGTCACCAACTGGGACGATA-3′ reverse 5′-AGGTCTTTACGGATGTCAACG-3′ for β-actin. The

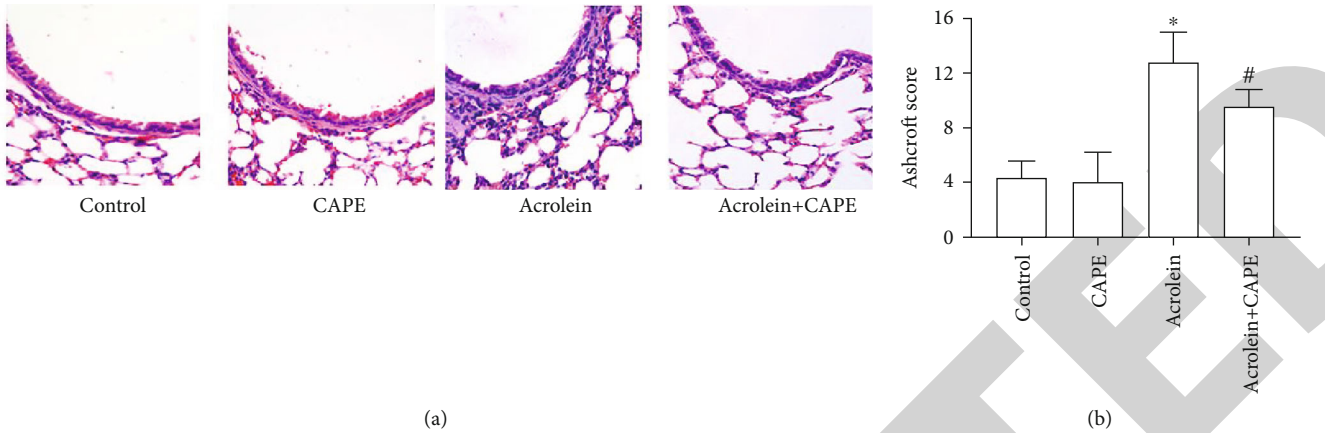

Figure 1: Histopathological examination of lung tissue section by H&E staining. (a) Representative pictures of H&E staining. Scale bars = 200 μm. Magnification: ×400. (b) Ashcroft Score for the image. CAPE: caffeic acid phenethyl ester. $^{*}P < 0.05$ vs. the control group; $^{\#}P < 0.05$ vs. the acrolein group.

products amplified were separated by agarose gel electrophoresis and visualized by Bio-Rad system. Relative quantity of Muc5ac mRNA was obtained by a comparative method using β-actin as an internal control.

2.7. Western Blot. Airway smooth muscle cells were obtained from normal airways of mice by tissue isolation. This experiment was divided into 3 groups: (a) blank control group; (b) TGF-β1 group, the smooth muscle cell was treated with 10 ng/ml TGF-β1 for 30 minutes; (c) TGF-β1+CAPE group, before stimulation with TGF-β1, the cell was pretreated with CAPE (100 nM) for 30 minutes.

After that, whole-cell lysate was extracted and antibodies against P65 and phospho-P65 (p-P65) (Cell Signaling Technology, USA) were used for immunoblot. The results were expressed by histogram which was based on the values of p-P65(p-P65)/P65 from 3 independent experiments.

2.8. Statistical Analysis. Statistical analysis was performed with SPSS 22.0 software. Data was expressed as mean ± standard deviation (SD). The comparisons between each group were analyzed by t-test. P values < 0.05 were considered significant.

3. Results

3.1. General Condition. Mice in the acrolein group and acrolein+CAPE group developed lassitude and anepithymia after inhalation of acrolein fog for 1 week. And 20 days later, the mice became languid and unresponsive as well as their furs turned matt. Moreover, the mice lost weight compared with the control and acrolein groups.

3.2. Morphological Changes. Compared with the control group, obvious mucus hypersecretion, mass infiltration of inflammatory cells, serous effusion, and proliferation of alveolar epithelial cells were observed in airway and peribronchus tissues of mice in the acrolein group (Figure 1(a)). Some alveolar epithelial cells thicken as the shock induced by acrolein progresses. What is more, we discovered fibrosis of peribronchus tissue, which was visually

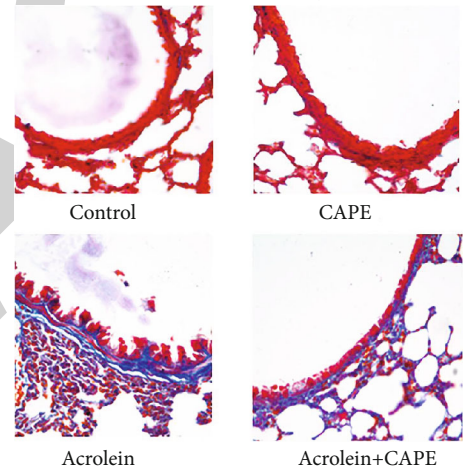

Figure 2: Fibrosis examination of lung tissue by MASSON staining. Scale bars = 200 μm. Magnification: ×400. Blue color indicates collagen deposition. CAPE: caffeic acid phenethyl ester.

hyperplastic and septus. All these results above were evaluated by Ashcroft score (Figure 1(b)). The Ashcroft score was significantly higher in the acrolein group compared to the control group. However, CAPE treatment significantly reduced the scores of rats in the acrolein group.

Further by Masson staining (Figure 2), we found that the lung tissue of mice in the acrolein group showed significant collagen deposition, airway interval thickening, and peribronchus fibrosis. However, after CAPE treatment, the collagen fibers were reduced. These results suggested a potential protective effect of CAPE on such a pathological process.

3.3. Total and Differential Cell Count. After inhalation of acrolein for 20 days, mucus overproduction and increased serous effusion as well as infiltration of inflammatory cells were noticed in the mice. Total cell count and neutrophilic granulocyte count in the acrolein group were significantly increased in BALF compared with the control group ($P < 0.05$), which were evidently reduced after the treatment with CAPE ($P < 0.05$, compared with the acrolein group) (Figure 3).

3.4. Hydroxyproline Concentration of Lung Tissues. Hydroxyproline concentration of lung tissue was an indicator of the change of the collagen fiber level. There was no statistical difference between each group ($P > 0.05$) (Figure 4).

3.5. TGF-β1 Level in BALF. After collecting BALF from each group of mice, we measured the level of TGF-β1 by ELISA. TGF-β1 level in BALF was visually increased after inhalation of acrolein for 20 days ($P < 0.05$, compared with the control group), which was significantly reduced through intraperitoneal injection with CAPE ($P < 0.05$) (Figure 5).

3.6. Muc5ac mRNA and Muc5ac Protein Levels. By RT-qPCR and ELISA, we observed visible increases of Muc5ac mRNA level in lung tissue and Muc5ac protein in BALF after treated with acrolein ($P < 0.05$, compared with the control group). However, the increased levels of Muc5ac mRNA and muc5ac protein were not affected by the administration of CAPE (Figures 6 and 7). This suggested the inhibitions of airway mucin overproduction and hypersecretion were not the roles that CAPE played.

3.7. P65 Phosphorylation. After stimulated with TGF-β1, phospho-P65 level was increased in the airway smooth muscle cells. However, the expression was reversed by pretreatment with CAPE ($P < 0.05$) (Figure 8), which suggested the inhibition effect of CAPE on P65 phosphorylation induced by TGF-β1.

4. Discussion

Airway remodeling is characterized by proliferation of smooth muscle cells and deposition of extracellular matrix, which narrows the airway and enhances the bronchial hyperresponsiveness. Together with airway inflammation and airway hypersecretion, airway remodeling is believed to be involved in the process of PF [1, 2]. Smoking inhibits the immune response of T cell in pulmonary and disorders the tissue repair, which causes complex pathological progress as above. For a long time, it has remained obscure what has been the crucial component of cigarettes to play such a role. Lambert et al. declared acrolein, a kind of aldehydes extracted from cigarettes, inhibited T cell response and was related to the NF-κB signaling pathway by alkylating cysteine and arginine residues [29].

As we know, the pathologic process of interstitial lung disease is commonly divided into two phases: inflammatory phase and fibrosis phase. Nowadays, many kinds of animal models are used to reproduce this process. Some researchers believe the "switch" between inflammation and fibrosis appears to occur around day 9 after the treatment with revulsant [3]. Therefore, to cover the complete picture of such process and pay attention to the secondary phase, we set the end time on the 20th day rather than the 9th day in the present study. After inhalation of acrolein fog for 20 days, marked mucus hypersecretion, substantial infiltration of inflammatory cells, serous effusion, and proliferation of alveolar epithelial cells were observed in airway and peribronchus tissues of mice. Additionally, total and neutrophilic cell counts in BALF were increased. Together with the hyperplasia of smooth muscle cells, all of these showed the typical pathological changes of airway remodeling, which was similar to the rat model established by Chen et al. in 2013 [30]. On the other hand, Masson stain revealed collagen deposition, airway interval thickening, and peribronchus fibrosis, which meant the fibrogenic progress and coincided with the representation of the secondary phase as expected. The expression of collagen protein was significantly increased during tissue repairing. This was in accordance with previous studies [31].

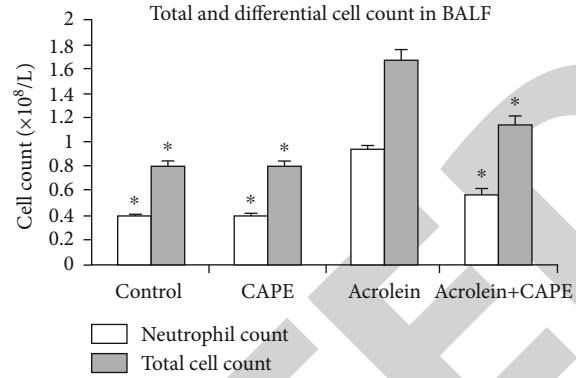

Figure 3: Total and differential cell count in bronchoalveolar lavage (BALF). After inhalation of acrolein for 20 days, total cell count and neutrophilic granulocyte count were measured in BALF compared. CAPE: caffeic acid phenethyl ester. $^*P < 0.05$ vs. the acrolein group.

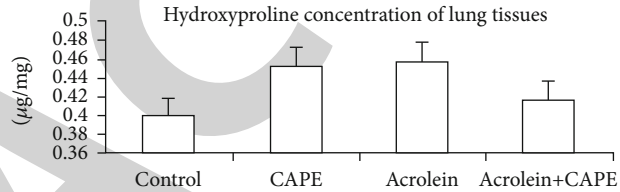

Figure 4: Hydroxyproline concentration of lung tissues. Hydroxyproline concentration of lung tissue was detected by a hydroxyproline assay kit. CAPE: caffeic acid phenethyl ester.

Hydroxyproline is a hydroxylated form of the proline, which is a kind of amino acid contained in the peptide chains forming collagen. Meanwhile, with the catalysis of collagenase, hydroxyproline is formed as a decomposition product of collagen. The process is essentially dynamic during fibrosis [32]. Therefore, we measured the hydroxyproline concentration of lung tissues to indirectly reflect the metabolic situation of collagen. Unexpected, there was no statistical difference in hydroxyproline concentration between each group on the 20th day, which was quite different from the other PF models induced by bleomycin, asbestos, or paraquat. We considered this might be due to the unique physicochemical property of acrolein. Bleomycin, asbestos, and paraquat were more likely to induce acute tissue damage and lung fibrosis, while acrolein inclined the model to chronic progress. However, we did discover the collagen deposition and peribronchus fibrosis by Masson stain. As the secondary phase continued, hydroxyproline

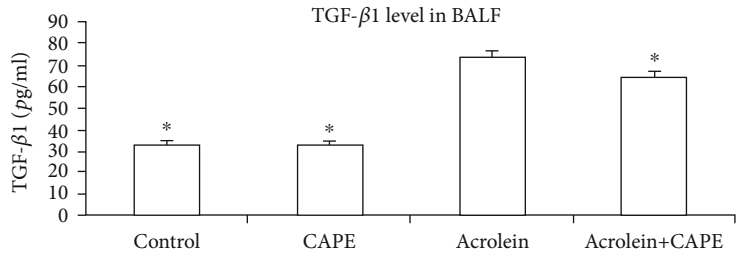

Figure 5: TGF-β1 level in bronchoalveolar lavage (BALF). TGF-β1 level in BALF was detected by ELISA assay. CAPE: caffeic acid phenethyl ester. $^*P < 0.05$ vs. the acrolein group.

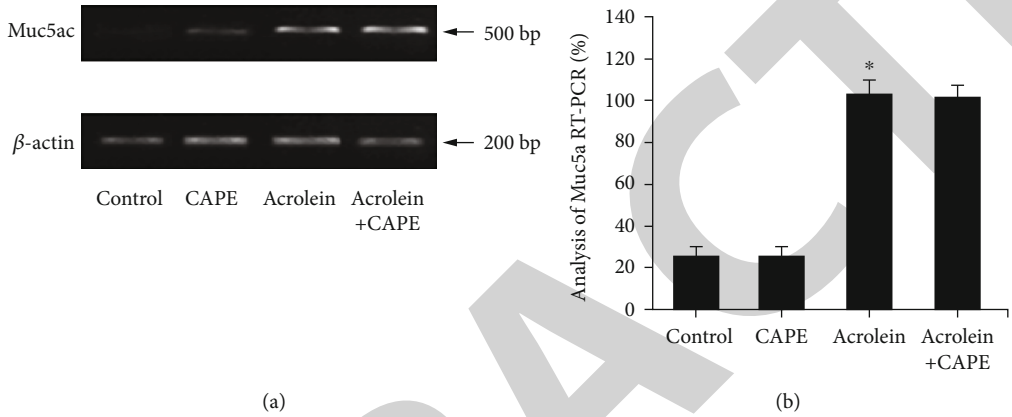

Figure 6: Muc5ac level in lung tissue. (a) The protein expression of Muc5ac in the lung tissue was detected by Western blot. (b) The mRNA expression of Muc5ac in the lung tissue was detected by RT-qPCR. CAPE: caffeic acid phenethyl ester. $^*P < 0.05$ vs. the control group.

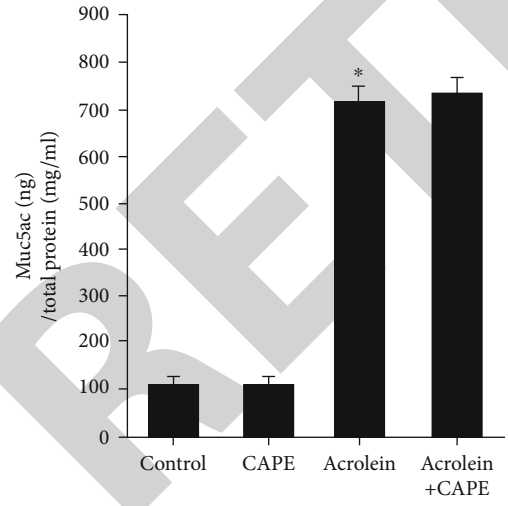

Figure 7: Muc5ac protein level in bronchoalveolar lavage (BALF). The Muc5ac protein level in BALF was measured by ELISA. CAPE: caffeic acid phenethyl ester. $^*P < 0.05$ vs. the control group.

concentration of lung tissues might be increased, which needed further experiments to confirm.

Intervention in the process of airway remodeling at an early stage may contribute to regulating tissue repairing and fibrogenic progress, which would eventually cause physiological dysfunction of airway [33]. As Selroos et al. declared, early intervention with inhaled anti-inflammatory drugs in asthma might prevent patients from developing chronic airway obstruction [34]. The problem is in which joint we can break the chain. TGF-β1 plays an important role in cell growth, differentiation, and inflammation reaction. TGF-β1 could take effect in tissue repairing via promoting collagen synthesis [35]. In the previous studies, TGF-β1 was found to be involved in the MAPK, JNK, SMAD, and PI3K signaling pathways [36]. Recently, more and more researchers have begun to pay attention to the effect of TGF-β1 in the NF-κB signaling pathway, especially in the animal models of tissue fibrosis. Chen et al. declared that through inactivation of NF-κB but not the ERK1/2 signaling pathway, proliferation and migration of rat airway smooth muscle cells induced by TGF-β1 were inhibited [37]. In the same year, Zhao et al. also discovered that through the inhibition of NF-κB signaling, proinflammatory and fibrogenic phenotypes of lipopolysaccharide-stimulated hepatic stellate cells were attenuated [23]. Researchers above used the CAPE as an inhibitor of NF-κB in their study. In this study, CAPE attenuated the release of TGF-β1 and inhibited the fibrogenic progress in a model of airway remodeling induced by acrolein. In our study, we also identified the inhibitive effect of CAPE on NK-κB pathway activation was related to the inhibition of P65 phosphorylation in mouse airway smooth muscle cell.

Muc5ac is a representative mucus protein, which is widely used as an evaluation criterion of airway secretion. The NF-κB signaling pathway possibly takes part in such

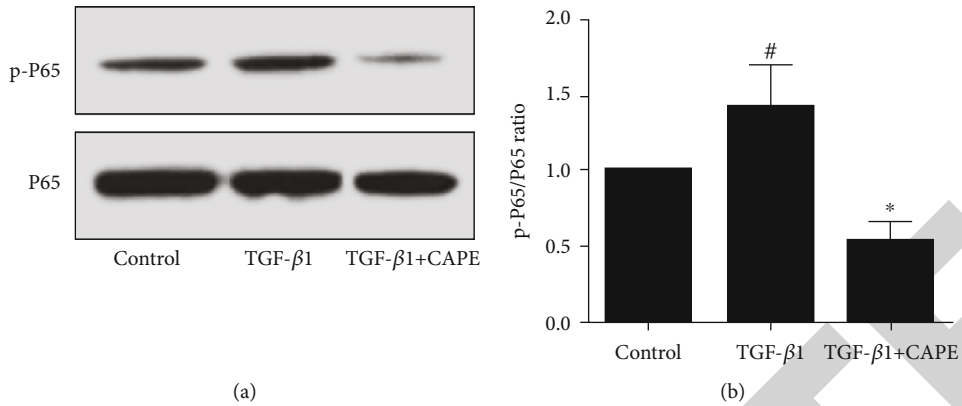

Figure 8: P65 phosphorylation level in the TGF-β1-induced smooth muscle cells. (a) The protein expressions of phospho-P65 and P65 were detected by Western blot. (b) The ratio of p-P65/P65 was quantified. TGF-β1 group: the smooth muscle cells were treated with 10 ng/ml TGF-β1 for 30 minutes; TGF-β1+CAPE group: before stimulation with TGF-β1, the cell was pretreated with CAPE (100 nM) for 30 minutes. $^{\#}P < 0.05$ vs. the control group. $^{*}P < 0.05$ vs. the TGF-β1 group.

process. Now that CAPE, as an inhibitor of the NF-κB pathway, took a protective effect on airway remodelling in our model, would it also play a role in prevention of Muc5ac overproduction and hypersecretion? Unfortunately, we observed obvious increases of Muc5ac mRNA level in lung tissue and Muc5ac protein level in BALF after being treated with acrolein. However, the increased levels of Muc5ac mRNA and muc5ac protein were not affected by the administration of CAPE. This suggested the inhibitions of airway mucin overproduction and hypersecretion were not the roles that CAPE played. This needs to be confirmed by further experimental studies.

In conclusion, CAPE, an inhibitor of the NF-κB pathway, inhibited the process of acrolein-induced lung fibrosis in mice and attenuated the release of TGF-β1. This provides a theoretical basis for CAPE to be a clinical treatment for pulmonary fibrosis.

Data Availability

The data used to support the findings of this study are available from the corresponding author upon request.

Conflicts of Interest

The authors declare that they have no conflicts of interest.

Authors' Contributions

Peng Chen and Xiaoxia Wang contributed equally to this work.

Acknowledgments

This study was supported by the National Natural Science Foundation of China (No. 30971327).

References

[1] S. S. Sohal, C. Ward, W. Danial, R. Wood-Baker, and E. H. Walters, "Recent advances in understanding inflammation and remodeling in the airways in chronic obstructive pulmonary disease," *Expert Review of Respiratory Medicine*, vol. 7, no. 3, pp. 275–288, 2013.

[2] N. Hirota and J. G. Martin, "Mechanisms of airway remodeling," *Chest*, vol. 144, no. 3, pp. 1026–1032, 2013.

[3] A. Moeller, K. Ask, D. Warburton, J. Gauldie, and M. Kolb, "The bleomycin animal model: a useful tool to investigate treatment options for idiopathic pulmonary fibrosis?," *The International Journal of Biochemistry & Cell Biology*, vol. 40, no. 3, pp. 362–382, 2008.

[4] R. Rasooli, F. Pourgholamhosein, Y. Kamali, F. Nabipour, and A. Mandegary, "Combination therapy with pirfenidone plus prednisolone ameliorates paraquat-induced pulmonary fibrosis," *Inflammation*, vol. 41, no. 1, pp. 134–142, 2018.

[5] C. Vancheri, "Common pathways in idiopathic pulmonary fibrosis and cancer," *European Respiratory Review*, vol. 22, no. 129, pp. 265–272, 2013.

[6] K. C. Flanders, "Smad3 as a mediator of the fibrotic response," *International Journal of Experimental Pathology*, vol. 85, no. 2, pp. 47–64, 2004.

[7] Y. Q. Zhang, Y. J. Liu, Y. F. Mao, W. W. Dong, X. Y. Zhu, and L. Jiang, "Resveratrol ameliorates lipopolysaccharide-induced epithelial mesenchymal transition and pulmonary fibrosis through suppression of oxidative stress and transforming growth factor-β1 signaling," *Clinical Nutrition*, vol. 34, no. 4, pp. 752–760, 2015.

[8] K. Murakami, M. Kohno, M. Kadoya et al., "Knock out of S1P3 receptor signaling attenuates inflammation and fibrosis in bleomycin-induced lung injury mice model," *PLoS One*, vol. 9, no. 9, article e106792, 2014.

[9] E. De Langhe, C. Aznar-Lopez, V. De Vooght, J. A. Vanoirbeek, F. P. Luyten, and R. J. Lories, "Secreted frizzled related proteins inhibit fibrosis in vitro but appear redundant in vivo," *Fibrogenesis & Tissue Repair*, vol. 7, no. 1, p. 14, 2014.

[10] G. Si, Z. H. Tao, W. A. Wei, X. I. Min, X. C. Wang, and Z. H. Chen, "Glucagon like peptide-1 attenuates bleomycin-induced pulmonary fibrosis, involving the inactivation of NF-κB in mice," *International Immunopharmacology*, vol. 22, no. 2, pp. 498–504, 2014.

[11] Y. Meng, C. H. Yu, W. Li et al., "Angiotensin-converting enzyme 2/angiotensin-(1-7)/Mas axis protects against lung

Hindawi
Computational and Mathematical Methods in Medicine
Volume 2023, Article ID 9814020, 1 page
https://doi.org/10.1155/2023/9814020

Retraction

Retracted: Controversy on Positive Peritoneal Cytology of Endometrial Carcinoma

Computational and Mathematical Methods in Medicine

Received 27 June 2023; Accepted 27 June 2023; Published 28 June 2023

This article has been retracted by Hindawi following an investigation undertaken by the publisher [1]. This investigation has uncovered evidence of one or more of the following indicators of systematic manipulation of the publication process:

(1) Discrepancies in scope

(2) Discrepancies in the description of the research reported

(3) Discrepancies between the availability of data and the research described

(4) Inappropriate citations

(5) Incoherent, meaningless and/or irrelevant content included in the article

(6) Peer-review manipulation

The presence of these indicators undermines our confidence in the integrity of the article's content and we cannot, therefore, vouch for its reliability. Please note that this notice is intended solely to alert readers that the content of this article is unreliable. We have not investigated whether authors were aware of or involved in the systematic manipulation of the publication process.

Wiley and Hindawi regrets that the usual quality checks did not identify these issues before publication and have since put additional measures in place to safeguard research integrity.

We wish to credit our own Research Integrity and Research Publishing teams and anonymous and named external researchers and research integrity experts for contributing to this investigation.

The corresponding author, as the representative of all authors, has been given the opportunity to register their agreement or disagreement to this retraction. We have kept a record of any response received.

References

[1] Y. Liu, H. Wang, and Y. Gao, "Controversy on Positive Peritoneal Cytology of Endometrial Carcinoma," *Computational and Mathematical Methods in Medicine*, vol. 2022, Article ID 1906769, 5 pages, 2022.

Hindawi
Computational and Mathematical Methods in Medicine
Volume 2022, Article ID 1906769, 5 pages
https://doi.org/10.1155/2022/1906769

Review Article

Controversy on Positive Peritoneal Cytology of Endometrial Carcinoma

Yi-Si Liu, Hui-Min Wang, and Yan Gao

Department of Gynecology, Cancer Hospital of China Medical University, Liaoning Cancer Hospital & Institute, Shenyang, 110042 Liaoning, China

Correspondence should be addressed to Yan Gao; lzgaoyan1777@163.com

Received 20 January 2022; Accepted 4 March 2022; Published 1 April 2022

Academic Editor: Shakeel Ahmad

Endometrial carcinoma (EC) is one of the most common gynecological malignancies. Its incidence rate has been increasing year by year. The prognostic factors and treatment strategies of EC have aroused wide concern. The effects of peritoneal cytology on the prognosis and treatment of EC remain controversial. Some factors, such as differentiation degree, muscle invasion, and tumor size, are related to positive peritoneal cytology. Hysteroscopy is commonly used in the diagnosis and treatment of endometrial cancer, but hysteroscopic surgery may cause the tumor to spread into the abdominal cavity, resulting in positive peritoneal cytology. In this review, we discuss the factors related to positive peritoneal cytology and the influence of positive peritoneal cytology on the prognosis of endometrial cancer. Suspicious positive peritoneal cytology may be an independent risk factor for endometrial cancer. The positive rate of peritoneal tumor cells in type II endometrial cancer is higher than other cells and is an independent risk factor for type II endometrial cancer. We also discuss the effects of peritoneal cytology on treatment decisions. Aggressive treatments seem to be more beneficial for patients with positive ascites cytology, but there is a lack of large-scale prospective clinical studies on their effectiveness and safety. The application of peritoneal cytology for endometrial cancer has been decreased in recent years. We believe that peritoneal cytology is necessary for this type of cancer. However, more studies on peritoneal cytology in endometrial cancer should be carried out.

1. Introduction

Endometrial carcinoma is one of the most common gynecological malignancies. There are 319 500 new cases in the world every year, and the mortality is as high as 23% [1, 2]. The main risk factors for endometrial cancer include genetic correlation [2–4] (Lynch syndrome, Cowden syndrome, etc.), continuous estrogen stimulation, and metabolic syndrome. In recent years, with changes in diet and lifestyle, the incidence of endometrial cancer has been gradually increasing [5, 6]. At present, early screening of endometrial cancer has not been widely used. The diagnosis is made mainly by diagnostic curettage or hysteroscopic endometrial biopsy, and the preliminary clinical staging is carried out [7]. The treatment of endometrial cancer is mainly surgery and comprehensive treatment according to the patient's condition [8]. Targeted therapy and immunotherapy are also widely used for endometrial cancer [9, 10]. The prognosis of endometrial carcinoma is related to the age of onset, stage, degree of tumor differentiation, and pathological type [11–15].

According to the different etiology and prognosis of endometrial cancer, Bokhman [16] divided it in 1983 into type I hormone dependent with good prognosis and type II hormone independent with poor prognosis. The common histopathological types are endometrioid carcinoma, serous carcinoma, clear cell carcinoma, and undifferentiated carcinoma [17]. Clinical staging is based on the 8th edition of the American Joint Cancer Committee (2017 edition) staging and the International Federation of Gynecology and Obstetrics (FIGO) [18] staging (2009 edition). The main treatment for endometrial cancer is surgery and chemoradiotherapy. The prognostic factors of endometrial carcinoma include pathological type, tumor stage, age, molecular typing, and vascular invasion [19]. According to the Federation International of Gynecology and Obstetrics

(FIGO) in 1988 [20], endometrial cancer with positive peritoneal cytology is classified as phase IIIA. It is suggested that positive peritoneal cytology is one of the high-risk factors affecting prognosis of endometrial cancer, although FIGO revised the staging criteria in 2009 [21], and positive peritoneal cytology was not included. National Comprehensive Cancer Network (NCCN) [22] guidelines for endometrial cancer and Japan Society of Gynecologic Oncology (JSGO) guidelines [23] still recommend that peritoneal cytology be retained. The effect of positive peritoneal cytology on prognosis is still controversial. We discuss the effect of positive peritoneal cytology on prognosis of endometrial cancer and the effect of hysteroscopy on peritoneal cytology.

2. Effect of Hysteroscopy on Peritoneal Cytology

The gold standard for the diagnosis of endometrial cancer is histopathological examination [24]. There are two main ways to obtain histopathological specimens: fractional curettage [25], a traditional diagnostic method; and the guidelines recommend hysteroscopy as the preferred diagnostic method. Diagnostic curettage is a necessary skill for gynecologists and obstetricians, and it is widely used in the diagnosis and treatment of abnormal vaginal bleeding. Diagnostic curettage [26] has the advantages of simple and easy operation and less trauma. It enables pathological examination of the uterine cavity and cervical canal, and hysteroscopy can be used to treat vaginal bleeding caused by endometrial lesions. Under the direct vision of hysteroscopy, the location of suspicious lesions can be observed closely, and the range of abnormal lesions and the degree of lesion invasion preliminarily judged. Due to its visual controllability and magnification effect, hysteroscopy is more accurate than diagnostic curettage in sampling both sides of the uterine angle and the lower uterine segment near the cervical canal. Garzetti et al. [27] and Zhu et al. [28] have proved that the pathological diagnosis rate and postoperative pathological coincidence rate of hysteroscopy are significantly higher than those of diagnostic curettage, and the pathological diagnosis rate of hysteroscopy is as high as 97%. Hysteroscopy is more advantageous for thin endometrial carcinoma (intimal thickness only 2–3 mm) [29]. Current domestic and foreign guidelines for the treatment of early endometrial cancer with fertility preservation are mainly recommend hysteroscopic evaluation and local lesion resection combined with progesterone treatment [30, 31]. However, hysteroscopy is completed by uterine dilation (normal saline, glucose, and mannitol) under pressure compared with diagnostic curettage. At present, there is a widespread controversy about whether hysteroscopy increases the positive rate of tumor cytology and has an impact on prognosis. Some studies [32] have suggested that the positive and suspicious positive rates of peritoneal cytology in endometrial carcinoma by hysteroscopy are significantly higher than that in diagnostic curettage. Cohort studies [33] have suggested that although hysteroscopy increases the risk of positive peritoneal cytology in early endometrial cancer, it has no significant effect on prognosis. Vilos et al.'s study [34] showed that the positive rate of peritoneal cytology increased by 30% in patients with serous endometrial carcinoma before hysteroscopy. However, there was no significant difference in progression-free survival (PFS) and overall survival (OS) after 66 months of follow-up. One study [35] has suggested that although tumor cells may migrate to the peritoneal cavity during hysteroscopy, this is only temporary and peritoneal cytology becomes negative after some time. Obermair et al. [36] believe that if hysteroscopy is used for too long or too many lesions are removed to obtain more pathological tissues, it can cause lung metastasis of tumor cells under high-pressure perfusion via the blood vessels. Therefore, hysteroscopy should be performed carefully in patients with suspected endometrial cancer. Some studies [37] have suggested that uterine dilatation at a pressure <70 mmHg can significantly reduce the movement of intrauterine fluid from the fallopian tube into the abdominal cavity. In summary, diagnostic curettage can be selected for patients with highly suspected endometrial cancer by imaging, especially when the lesion is clear. In the case of necessary hysteroscopy, soft mirror and fine mirror can be used. In addition, in the case of suspected malignancy, the pressure of dilatation must be controlled.

3. Factors Related to Positive Peritoneal Cytology

A meta-analysis [38] has suggested that for patients with surgical stage 1 early-stage endometrial cancer, the incidence of myometrial invasion ≥1/2 tended to be higher and 5-year progression-free survival was worse in the positive peritoneal cytology group than the negative peritoneal cytology group. A retrospective analysis of the SEER database [39] has shown that the higher the tumor stage, the higher the positive cytology and suspicious positive rates are. In stage IA endometrial cancer, if the tumor diameter is ≤2 cm, the positive rate of peritoneal cytology is only 4%; if the tumor diameter is >2 cm, the positive rate of peritoneal cytology is 10%. The positive rate of peritoneal cytology in endometrial adenocarcinoma is about 6.8%, while that of serous carcinoma is 23.4%. Therefore, positive peritoneal cytology in endometrial carcinoma is closely related to tumor pathological type, tumor size, depth of invasion, lymph node metastasis, and other poor prognostic factors. Studies in China [40] have suggested that the prognosis of early endometrial carcinoma with positive peritoneal cytology is worse, which may be related to undetected peritoneal metastasis or micrometastasis.

4. Effect of Positive Peritoneal Cytology on Prognosis of Endometrial Carcinoma

NCCN and JSGO guidelines recommend that peritoneal cytology specimens should be retained for endometrial cancer staging surgery. ESMO-ESGO-ESTRO [41] guidelines did not retain peritoneal cytology specimens for early endometrial cancer staging surgery. A retrospective study [29] of the SEER database in the USA in 2018 showed that the

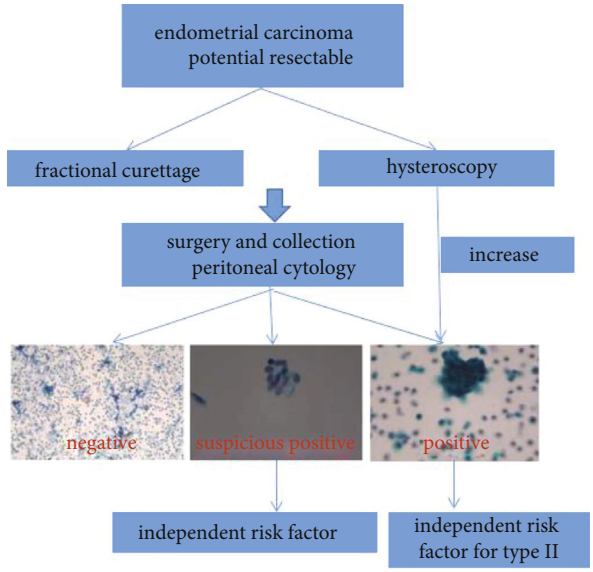

Figure 1: Peritoneal cytology results.

collection of peritoneal cytology has decreased by 44% since 2010. Daix et al. [42] suggested that the missed peritoneal cytology during hysterectomy was related to an increased risk of death in women with endometrial cancer. Peritoneal cytology results are negative, suspicious positive, or positive. The patients with stage I–III endometrial cancer who had peritoneal cytology results during hysterectomy in the USA from 2010 to 2016 were retrospectively analyzed [43]. The positive rate of cytology was 8.0%, and the suspicious positive rate was 1.7%. Compared with negative cytology, women in the suspicious peritoneal cytology group were younger. Peritoneal-cytology-negative, 5-year OS rate was 86.8%, suspicious cytology-positive rate was 77.8%, and cytology-positive rate was 66.5%. After controlling variables, suspicious positive peritoneal cytology was an independent risk factor for endometrial cancer. The 5-year PFS was 8.2% for negative peritoneal cytology, 16.8% for suspicious positive cytology, and 28.7% for positive cytology. Multivariate analysis showed [44] that suspicious positive peritoneal cytology was associated with an increased risk of endometrial cancer mortality and could predict mortality. In 2021, a retrospective study [45] for >20 years was conducted to analyze the effect of peritoneal cytology on the prognosis of type II endometrial cancer. The positive rate of peritoneal tumor cells in type II endometrial cancer was as high as 22%. The positive rate of peritoneal cytology in patients with recurrence was 27%, and the positive rate of peritoneal cytology without recurrence was 16%. Positive peritoneal tumor cells were an independent risk factor for type II endometrial cancer.

5. Effect of Peritoneal Cytology on Treatment Decisions

In 2009, FIGO revised the staging criteria for endometrial cancer. Positive peritoneal cancer cells were not included in the staging of endometrial cancer. At present, ESMO [46], NCCN, and FIGO [47] guidelines do not provide treatment guidance for patients with positive or suspected positive peritoneal cytology. However, some studies [48] have shown that for stage II/III endometrial cancer patients with positive peritoneal cytology, combined chemotherapy and radiotherapy can improve survival rate, but not in patients with negative peritoneal cytology. In addition, in type II [49] endometrioid carcinoma, patients with stage II-III and positive peritoneal cytology only received chemotherapy; and for the peritoneal cytology negative patients, the effect of combined treatment effect is better. Aggressive treatment seems to be more beneficial for patients with positive peritoneal cytology, but there is a lack of large-scale prospective clinical studies on its effectiveness and safety (Figure 1).

6. Summary

In recent years, because the available guidelines for endometrial cancer with positive peritoneal cytology did not provide clear treatment recommendations, the application of peritoneal cytology has been decreased [50]; we believe that peritoneal cytology collection is necessary. Hysteroscopy has irreplaceable advantages in the diagnosis and treatment of endometrial cancer, but it has a certain probability of positive peritoneal cytology and tumor proliferation, and a new type of safe endometrial lesion sampling should be developed. Positive peritoneal cytology is related to many adverse prognostic factors of endometrial cancer, which is consistent with the results of high recurrence rate and low survival rate of patients with positive peritoneal cytology. Especially in type II endometrial carcinoma, the peritoneal tumor cell positive rate is high, and long-term prognosis is poor. At present, the optimal treatment strategy for patients with positive and suspected peritoneal tumor cells is still uncertain, which needs to be confirmed by large sample studies or prospective multicenter controlled studies. However, the current research results show that more active treatment of patients with positive peritoneal cytology may benefit patients. More studies on peritoneal cytology in endometrial cancer should be carried out.

Data Availability

The data used to support the findings of this study are available from the corresponding author upon request.

Conflicts of Interest

The authors declare that they have no conflicts of interest.

References

[1] H. Sung, J. Ferlay, R. L. Siegel et al., "Global cancer statistics 2020: GLOBOCAN estimates of incidence and mortality worldwide for 36 cancers in 185 countries," *CA: a cancer journal for clinicians*, vol. 71, no. 3, pp. 209–249, 2021.

[2] F. Bray, J. Ferlay, I. Soerjomataram, R. L. Siegel, L. A. Torre, and A. Jemal, "Global cancer statistics 2018: GLOBOCAN estimates of incidence and mortality worldwide for 36 cancers in 185 countries," *Ca-a Cancer Journal for Clinicians*, vol. 68, no. 6, pp. 394–424, 2018.

[3] C. B. Post Cathalijne, S. Ellen, T. H. B. M. Smit Vincent et al., "Prevalence and prognosis of lynch syndrome and sporadic mismatch repair deficiency in endometrial cancer," *JNCI: Journal of the National Cancer Institute*, vol. 113, no. 9, pp. 1212–1220, 2021.

[4] G. M. Kalish, E. Barrett-Connor, G. A. Laughlin, B. I. Gulanski, and Postmenopausal Estrogen/Progestin Intervention Trial, "Association of endogenous sex hormones and insulin resistance among postmenopausal women: results from the Postmenopausal Estrogen/Progestin Intervention Trial," *The Journal of Clinical Endocrinology & Metabolism*, vol. 88, no. 4, pp. 1646–1652, 2003.

[5] P. Veena, P. Rajan, and S. Soundara Raghavan, "Cowden's Syndrome," *Indian Journal of Gynecologic Oncology*, vol. 15, no. 1, 2017.

[6] R. L. Siegel, K. D. Miller, H. E. Fuchs, and A. Jemal, "Cancer statistics, 2021," *CA: a Cancer Journal for Clinicians*, vol. 71, no. 1, pp. 7–33, 2021.

[7] A. Mullins Megan and M. L. Cote, "Beyond obesity: the rising incidence and mortality rates of uterine corpus cancer," *Journal of clinical oncology: official journal of the American Society of Clinical Oncology*, vol. 37, no. 22, pp. 1851–1853, 2019.

[8] J. D. Wright, N. I. Barrena Medel, J. Sehouli, K. Fujiwara, and T. J. Herzog, "Contemporary management of endometrial cancer," *Lancet (London, England)*, vol. 379, no. 9823, pp. 1352–1360, 2012.

[9] M. J. Quinn, "Secondary analyses from a randomized clinical trial: age as the key prognostic factor in endometrial carcinoma," *American Journal of Obstetrics and Gynecology*, vol. 210, no. 6, p. 588, 2014.

[10] E. A. Sloan, K. L. Ring, B. C. Willis, S. C. Modesitt, and A. M. Mills, "PD-L1 expression in mismatch repair-deficient endometrial carcinomas, including Lynch syndrome-associated and MLH1 promoter hypermethylated tumors," *The American Journal of Surgical Pathology*, vol. 41, no. 3, pp. 326–333, 2017.

[11] Y. Li, P. Cong, P. Wang, C. Peng, M. Liu, and G. Sun, "Risk factors for pelvic lymph node metastasis in endometrial cancer," *Archives of Gynecology and Obstetrics*, vol. 300, no. 4, pp. 1007–1013, 2019.

[12] C. Presti, C. Tian, E. Robinson et al., "The impact of age and stage on the competing risk of cancer-related and non-cancer death in low-or high-grade endometrioid endometrial carcinoma and uterine serous carcinoma," *Gynecologic Oncology*, vol. 162, Supplement 1, pp. S293–S294, 2021.

[13] K. Pan, J. Gong, K. Huynh, and M. Cristea, "Current systemic treatment landscape of advanced gynecologic malignancies," *Targeted Oncology*, vol. 14, no. 3, pp. 269–283, 2019.

[14] S. Ferrero, *Endometrial Cancer: Risk Factors, Management and Prognosis*, Nova Science Publishers, Inc., 2018.

[15] A. van der Meer, "Obesity, Endometrial Cancer and the Mirena IUS: A Cautionary Tale," *Conference Abstract Book of BIT's 5th International Congress of Gynaecology and Obstetrics-2017*, , Lewisham and Greenwich NHS Trust UKp. 152, 2017.

[16] M. E. Ahsen, T. P. Boren, N. K. Singh et al., "Sparse feature selection for classification and prediction of metastasis in endometrial cancer," *BMC Genomics*, vol. 18, no. S3, p. 233, 2017.

[17] J. Bokhman, "Two pathogenetic types of endometrial carcinoma," *Gynecologic Oncology*, vol. 15, no. 1, pp. 10–17, 1983.

[18] S. Pecorelli, "Revised FIGO staging for carcinoma of the vulva, cervix, and endometrium," *International Journal of Gynecology & Obstetrics*, vol. 105, no. 2, pp. 103-104, 2009.

[19] W. Creasman, "Revised FIGO staging for carcinoma of the endometrium," *International Journal of Gynecology & Obstetrics*, vol. 105, no. 2, p. 109, 2009.

[20] P. Morice, A. Leary, C. Creutzberg, N. Abu-Rustum, and E. Darai, "Endometrial cancer," *Lancet (London, England)*, vol. 387, no. 10023, pp. 1094–1108, 2016.

[21] H. D. Homesley, "Revised 1988 International Federation of Gynecology and Obstetrics staging systems for endometrial and vulvar cancer: an assessment," *Journal of gynecologic oncology*, vol. 35, no. 1, pp. 89–94, 1992.

[22] D. G. Mitchell, B. Snyder, F. Coakley et al., "Revised FIGO staging for carcinoma of the vulva, cervix, and endometrium," *International Journal of Gynecology & Obstetrics*, vol. 105, no. 2, pp. 103-104, 2006.

[23] National Comprehensive Cancer Network, "NCCN clinical practice guidelines in oncology: antiemesis. v. 1," 2021.

[24] S. Nagase, T. Ohta, F. Takahashi, N. Yaegashi, and Board Members of the 2020 Committee on Gynecologic Oncology of the Japan Society of Obstetrics and Gynecology, "Annual report of the committee on gynecologic oncology, the Japan Society of Obstetrics and Gynecology: annual patient report for 2017 and annual treatment report for 2012," *The journal of obstetrics and gynaecology research*, vol. 47, no. 5, pp. 1631–1642, 2021.

[25] S. Pace, A. Grassi, S. Ferrero, and M. Figliolini, "Diagnostic methods of early detection of endometrial hyperplasia and cancer," *European journal of gynaecological oncology*, vol. 5, no. 16, pp. 373–381, 1995.

[26] P. Bistoletti, A. Hjerpe, and G. Möllerström, "Cytological diagnosis of endometrial cancer and preinvasive endometrial lesions," *Acta obstetricia et gynecologica Scandinavica*, vol. 67, no. 4, pp. 343–345, 1988.

[27] G. G. Garzetti, A. Ciavattini, G. Goteri, M. De Nictolis, and C. Romanini, "Proliferating cell nuclear antigen in endometrial carcinoma: pretreatment identification of high-risk patients," *Gynecologic Oncology*, vol. 61, no. 1, pp. 16–21, 1996.

[28] H. Zhu, X. Liang, J. Wang, H. Cui, and L. Wei, "Value of hysteroscopic with biopsy or dilatation and curettage in the diagnosis of endometrial carcinoma," *Chinese Journal of Practical Gynecology and Obstetrics*, vol. 6, no. 27, pp. 439–442, 2011.

[29] R. Bedner and I. Rzepka-Górska, "Hysteroscopy with directed biopsy versus dilatation and curettage for the diagnosis of endometrial hyperplasia and cancer in perimenopausal women," *European journal of gynaecological oncology*, vol. 5, no. 28, pp. 400–402, 2007.

[30] H. Dong, Y. Wang, M. Zhang, M. Sun, and Y. Yue, "Whether preoperative hysteroscopy increases the dissemination of endometrial cancer cells: a systematic review and meta-analysis," *The journal of obstetrics and gynaecology research*, vol. 47, no. 9, pp. 2969–2977, 2021.

[31] Z. R. Xiao, Q. Lu, R. Zhou et al., "Analysis of pregnancy outcome after fertility-preserving treatment among women with

Hindawi
Computational and Mathematical Methods in Medicine
Volume 2022, Article ID 9872404, 1 page
https://doi.org/10.1155/2022/9872404

Retraction

Retracted: A Diagnostic Model of Volleyball Techniques and Tactics Based on Wireless Communication Network

Computational and Mathematical Methods in Medicine

Received 4 November 2022; Accepted 4 November 2022; Published 22 November 2022

Computational and Mathematical Methods in Medicine has retracted the article titled "A Diagnostic Model of Volleyball Techniques and Tactics Based on Wireless Communication Network" [1] due to concerns that the peer review process has been compromised.

Following an investigation conducted by the Hindawi Research Integrity team [2], significant concerns were identified with the peer reviewers assigned to this article; the investigation has concluded that the peer review process was compromised. We therefore can no longer trust the peer review process and the article is being retracted with the agreement of the Chief Editor.

The authors do not agree to the retraction.

References

[1] Z. Yuan, Y. Zhang, B. Li, and X. Jin, "A Diagnostic Model of Volleyball Techniques and Tactics Based on Wireless Communication Network," *Computational and Mathematical Methods in Medicine*, vol. 2022, Article ID 2185908, 12 pages, 2022.

[2] L. Ferguson, "Advancing Research Integrity Collaboratively and with Vigour," 2022, https://www.hindawi.com/post/advancing-research-integrity-collaboratively-and-vigour/.

Hindawi
Computational and Mathematical Methods in Medicine
Volume 2022, Article ID 2185908, 12 pages
https://doi.org/10.1155/2022/2185908

Research Article

A Diagnostic Model of Volleyball Techniques and Tactics Based on Wireless Communication Network

Zhigang Yuan,[1] **Yongkui Zhang**,[2] **Bo Li**,[1] **and Xinlong Jin**[3]

[1]*Volleyball Teaching and Research Office, Harbin Sport University, Harbin, 150000 Heilongjiang, China*
[2]*China Volleyball College, Tianjin University of Sport, Tianjin 300000, China*
[3]*Academic Affairs Office, Dalian University of Science and Technology, Dalian, 116000 Liaoning, China*

Correspondence should be addressed to Yongkui Zhang; vzyk007@tjus.edu.cn

Received 21 January 2022; Revised 16 February 2022; Accepted 23 February 2022; Published 30 March 2022

Academic Editor: Muhammad Zubair Asghar

Volleyball is a sport of teamwork competition and tactical coordination. It tests the ability of team members to cooperate with each other and personal resilience. With the development of wireless communication networks, how to use wireless communication networks in the analysis of volleyball tactics is the subject of this article. To explore how to design the volleyball tactics analysis model of the wireless communication network, this paper proposes the method of LTE system and MIMO technology and designs the tactics analysis model based on the characteristics of the wireless network, then combined volleyball tactics and game theory to design a wireless communication network volleyball tactics analysis model. Then, this paper designs the simulation experiment of scene allocation problem, the algorithm simulation experiment, and the comparative investigation and analysis of volleyball game spiking technical ability. The results of the experiment are optimized for the tactical analysis model, and finally, the improvement of the training of the volleyball tactical analysis model based on the wireless communication network is verified through comparative experiments. The experimental results show that the team fit of the volleyball tactical analysis model training based on the wireless communication network has increased by 22.12% compared with the traditional volleyball tactical training. Compared with the traditional volleyball tactical training, the personal on-the-spot adaptability of the volleyball tactical analysis model training based on the wireless communication network has increased by 9.05%.

1. Introduction

In recent years, the domestic communication industry has developed rapidly, and earth-shaking changes have occurred in both the technical field and the market field. The importance of wireless communication network planning has increased day by day. With the establishment of the L company, the old wireless communication network planning methods can no longer fully meet the requirements of the times. Discussing how to apply the wireless communication network to the analysis of volleyball tactics, to greatly improve the flexibility and technicality of volleyball tactics, will have important theoretical and practical significance.

This article will rank the technical index data of attack and defense, analyze the ranking of related teams, and have a more accurate and detailed understanding of the technical factors affecting volleyball competition. The participating teams are divided into groups, the attack and defense skills are compared and analyzed, the advantages and disadvantages of traditional volleyball tactics are found, and the disadvantages of traditional volleyball tactics duel in the game are analyzed. The volleyball tactics analysis model designed through the wireless communication network can effectively improve the volleyball team's team fit and personal resilience, which is of great significance to the training of volleyball players.

To study the improving the performance of cooperative spectrum sensing, Yao et al. consider a cluster-based cooperative spectrum sensing (CSS) scheme in the Energy Harvesting Cognitive Wireless Communication Network (EH-CWCN). Among them, the cognitive node (CN) clusters according to its received power level to improve the perception performance

[1]. Its main research is the application of wireless sensor networks in cooperative spectrum sensing, but the tactical analysis model is not comprehensive enough. To improve the performance of the sports team, it is essential to analyze the team's tactics from the game video. Athlete's trajectory is the most useful tactical analysis clue in sports videos. Chen et al. proposed a technique to reconstruct player trajectories from broadcast basketball videos [2]. He proposed to obtain tactical information from the video, but the application of the wireless communication network is not complete. To study the application of wireless communication networks, Uddin proposed a two-hop wireless communication architecture for the smart grid (SG) composed of smart meters (SM), aggregators (AG), and cellular base stations (BS) [3]. The wireless communication architecture studied can be applied to the analysis of volleyball tactics studied in this article. The advancement of smart grids and the advocacy of "green communications" have inspired wireless communication networks to obtain energy from the surrounding environment and operate in an energy-saving manner to achieve economic and ecological benefits. Hu et al. conducted a contemporary review of the latest breakthroughs in the utilization, redistribution, trading, and planning of energy collected in wireless networks that interoperate with smart grids in the future [4]. It applies the wireless network to the smart grid, but it does not involve enough tactical analysis. Jokgu is a South Korean online sport that has both volleyball and football skills in the form of challenge skills and games. Chang et al.'s main research is that Jokgu provides students with opportunities to develop physical fitness components related to health and skills, such as eye-foot coordination, flexibility, kicking, and juggling basic motor skills [5]. It mainly describes a sport similar to volleyball. If it can increase the application of volleyball tactics, it will be more in line with the purpose of this article. To study motion capture technology, Fang et al. proposed a new type of data glove, which can capture the movement of the arms and hands through inertial and magnetic sensors [6]. The motion capture technology he studied can be used in the analysis of volleyball tactics, but the application of wireless communication networks is not complete. Optical motion capture is based on estimating the three-dimensional position of the marker through triangulation from multiple cameras. Rahimian and Kearney introduced and compared two camera placement methods. The first method is based on a metric that calculates the visibility of the target point in the presence of dynamic occlusion from a camera with a "good" view. The second method is based on the view distribution of the target point [7]. Although the motion capture method he designed can capture the motion of volleyball, it is not sufficiently applied in wireless communication networks. To study the application of wireless communication networks, Bhatnagar's work mainly focuses on the design and analysis of wireless communication networks. He also explored the spectrum and energy efficiency aspects of next-generation networks such as smart grid communications [8]. Its research on wireless communication networks is very in-depth, but it would be better if it can be applied in the analysis of volleyball tactics. All above documents are mostly about wireless communication networks and motion capture, which are relatively small in the analysis of volleyball tactics. This requires an in-depth understanding of the connotations of volleyball tactics and how to combine wireless communication networks to analyze volleyball tactics.

The innovation of this paper is to use the characteristics of network management and network objects in the wireless communication network to design a tactical analysis model based on the wireless communication network based on the LTE system and MIMO technology. Then, write volleyball tactics and game analysis into the tactical analysis model, and get the wireless communication network volleyball tactics analysis model studied in this paper. The innovation in the experiment of this paper is to design the scenario assignment problem simulation experiment, the algorithm simulation experiment, and the comparative investigation and analysis of the volleyball game, spiking technical ability, and optimize the volleyball tactics analysis model through the data obtained from the experimental analysis.

2. Method of Volleyball Tactics Analysis Model Based on Wireless Communication Network

2.1. Wireless Communication Network. The application of wireless communication network [9] is shown in Figure 1.

2.1.1. Cognitive Radio. Cognitive radio (CR) [10] technology in a narrow sense refers to the detection of the user status of authorized spectrum resources by unlicensed users, without affecting the normal data communication of authorized users, opportunistic/shared/leased reuse of authorized spectrum for own data communication. Cognitive radio technology in a broad sense generally refers to nodes or subsystems in the network through sensing external environmental information, adaptively adjusting their own internal data transmission parameters (e.g., frequency band, transmit power, and beam direction) to improve the overall resource utilization efficiency of the network. The structure of the cognitive radio network is shown in Figure 2.

The classic cognitive wireless network model consists of two parts: a primary network and a secondary network. The primary network includes a primary user transmitter (PT) [11] and multiple primary user receivers (PR) [12]. For communication on the allocated authorized frequency band, the secondary network includes a secondary user transmitter (ST) and multiple secondary user receivers (SR). By detecting the use of the authorized spectrum, opportunistic/sharing/lease access to the authorized spectrum for own data communication. It can be seen from the description here that the research on cognitive wireless networks can be divided into two categories; one is the spectrum detection technology, and the other is the spectrum multiplexing technology.

(1) Spectrum Detection. The spectrum detection technology in the cognitive wireless network [9] is a signal detection technology born out of its own. Its goal is to determine the user status of the licensed frequency band by sampling and analyzing the transmission signal on the licensed frequency band. According to the different detection target nodes, cognitive network spectrum detection can be divided into main network sending node detection and main network receiving

Figure 1: Application of wireless communication network.

node detection. Since the receiving node does not send data, the commonly used receiving node detection method is to detect whether there is a corresponding receiving node in the coverage of the sending node by detecting the leakage of the local crystal oscillator (L0) at the radio frequency (RF) front end of the receiving node.

(2) Spectrum Reuse. Spectrum multiplexing technology refers to the cognitive network obtaining the access rights of the authorized spectrum through a certain method and carrying out its own data transmission under the premise of not affecting the normal communication of the main network. At present, spectrum multiplexing technology [13] can be roughly divided into spectrum sharing technology and spectrum collaboration technology. The former refers to the sharing of authorized spectrum resources by primary and secondary networks from the perspective of time division, frequency division, power division, or space division. The latter refers to the secondary network assisting the primary network in data transmission to obtain part of the spectrum resource utilization rights.

2.1.2. Network Management and Network Objects. Network management [14] is to monitor and control the network. Network planning, network configuration, and network monitoring are the main functions of network management. Network planning refers to the planning the parameters required for the normal operation of the communication network according to the communication requirements. The network configuration is to set the planning parameters for the communication network equipment by realizing the parameter configuration means of the communication network connection. Network monitoring is the process of collecting network status information and providing corresponding feedback during network operations. The main functions of network management are shown in Figure 3.

2.1.3. Overall Protection Framework. The LTE [15] access system must not only meet the security requirements of wireless network data transmission such as confidentiality, integrity, and antiforgery but also meet the security requirements related to wireless services. The LTE network needs to separately design the production control area and the management information area according to the characteristics of the different security zones of the network, focusing on protection in three parts: the main station side, the terminal side, and the boundary. The secure access scheme is mainly to provide a relatively secure communication channel between the system and the terminal and provide a safe and effective communication environment for network terminal users by using technical means such as identity authentication, data signature, and data encryption/decryption. Regardless of whether using an LTE public network or a private network, it should keep the gateway securely connected to the business network. LTE terminals should have information processing and calculation functions, two-way authentication, and encryption functions with low computational complexity.

The overall security protection architecture is divided horizontally into four parts: business layer, security access layer, LTE access layer, and terminal business layer in accordance with the principles of division, classification, and domain division. Vertically, it is divided into two major parts: production control area (I and II areas) and management information area (III, IV). Through this architecture system, it provides the required security protection requirements for LTE wireless networks. In the overall security protection architecture of the LTE wireless communication system, the service terminal layer at the bottom is composed of collection and detection terminals such as processing terminals, handheld mobile inspection terminals, sensor networks, and service terminals and is the source of service information data. The LTE access layer consists of four parts: a core network, a dedicated backhaul network, a base station, and a communication terminal, generally composed of software and hardware devices such as firewalls. The business layer is the data information control and processing center of the business layer and the main station platform of the business system.

To protect the user's true identity from being cracked during the LTE wireless transmission process, it then causes personal interest issues related to personal privacy and key information, each time the LTE network accesses the network, each user will be assigned a temporary identity GUTI corresponding to their real identity, which protects the real identity of the user in this way. Moreover, every time a user accesses the network, the network will assign an S-TMSI to the user as the identity of the user in this session. After the user accesses the network, the MME will generate a random number S-TMSI according to a preappointed random generation algorithm. The MME corresponds the generated random number S-TMSI with the real identity ID of the corresponding user. After the user access is completed, to protect the identity information from being leaked, the user uses the temporary identity assigned by the system for this session to perform data transmission with the mobility management entity. To ensure that both the user and the LTE network enjoy secure data transmission, identity authentication is required before the formal data transmission between

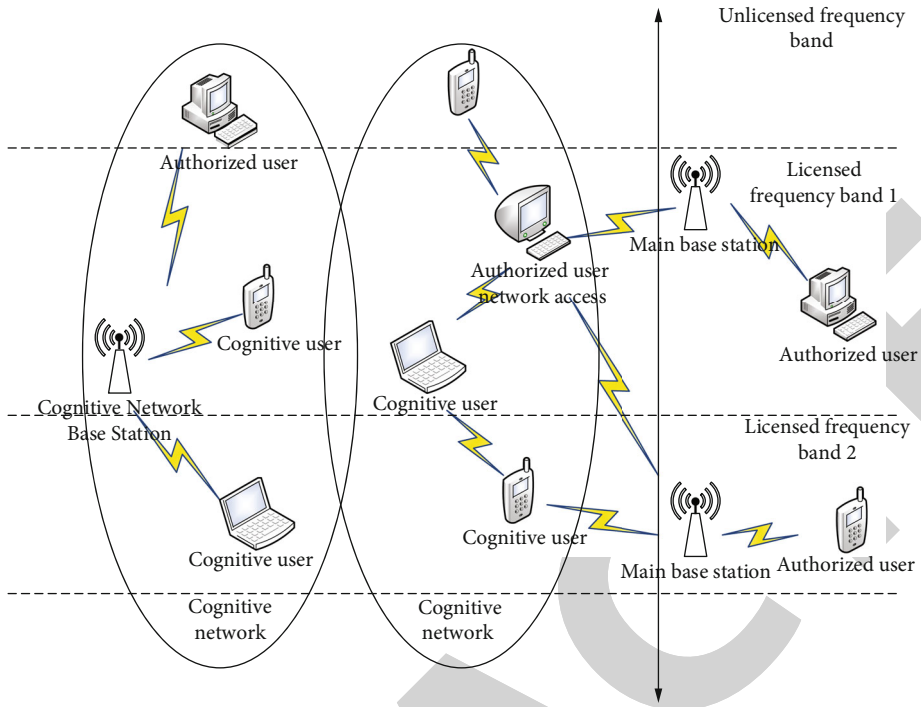

Figure 2: Cognitive radio network structure.

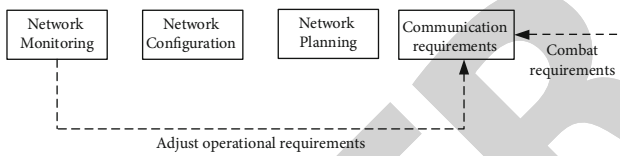

Figure 3: Main functions of network management.

the two, and the session key for this communication is negotiated during the authentication process.

2.1.4. MIMO Technology. At present, the method of improving the system capacity can be summarized as follows: first is setting up more base stations, but the increase of base stations means the increase of communication cost, and the gain is not worth the loss. The second is to broaden the frequency band, but the available wireless frequency band resources are relatively limited; the third is to improve the spectrum efficiency, which has more practical significance than the previous two schemes in terms of cost and implementation. The structure of MIMO technology [16] is shown in Figure 4.

There are generally two ways to improve spectrum utilization efficiency. One is to increase the signal-to-noise ratio. According to the channel capacity formula, the signal-to-noise ratio is increased by 3 dB, and the channel capacity can be increased by 1 bit/s/Hz. Increasing the signal-to-noise ratio needs to increase the amplification power, but the existing power amplifiers are difficult to meet the requirements because it is difficult for the amplifier to maintain high power transmission in a wide linear range. At the same time, the heat dissipation of the device needs to be considered when the power is high.

In the traditional wireless communication system, there will be multipath propagation due to the characteristics of the wireless channel during the transmission process, and the multipath propagation will cause the energy of the wireless signal to fade rapidly, which will seriously affect the transmission performance of the system. The MIMO technology uses multiple antennas at both the transmitting end and the receiving end, which can effectively utilize multipath propagation, eliminate the impact of multipath propagation on system performance, and improve system performance. At the same time, MIMO technology can provide the system with spatial multiplexing gain to increase the capacity, eliminate the influence of wireless channel multipath and time-varying fading, enhance the reliability of signal transmission, and reduce the spatial diversity gain of transmission error rate.

MIMO technology can increase the system capacity, but the premise is that the subchannels need to be independent of each other, and at the same time, the physical adjacent antenna spacing between the transmitting end and the receiving end is required to be large enough, to prevent excessive correlation between received signals. However, it is difficult to install multiple antennas for mobile terminals and electronic devices that currently require small volumes.

2.2. Volleyball Tactics

2.2.1. Tactical Analysis. Tactics [17], as an important part of the capability of sports competition itself, often appears in the field of military science, and it is also a professional term

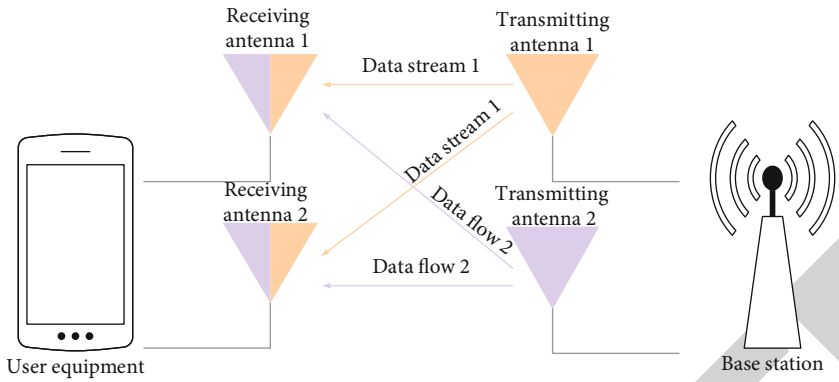

Figure 4: Structure of MIMO technology.

in this field. The objective reality of the existence of things is the basis of tactics. When a war occurs, the use of tactics is essential, and the tactics directly reflect the laws of war itself. Social productivity has progressed with the development of the times, and the material conditions determined by productivity are also gradually developing.

Based on the characteristics of volleyball games, this article believes that volleyball tactics are mainly reflected in the following aspects.

(1) The Internal Laws of Different Manifestations in the Use of Volleyball Tactics. With the continuous development and progress of society, volleyball is also constantly advancing, and the competition has become increasingly fierce. The level of all players has improved in varying degrees, which has intensified the intensity of the competition. If volleyball players want to achieve excellent sports performance, they must constantly master the tactical expressions such as the game play used in the volleyball game. According to the characteristics of one's own position, the key to master the tactical application form, in ordinary training, it is necessary to develop high-efficiency contact according to the position and focus.

The use of the above tactics requires athletes to fully master the inherent laws of these tactics, improve tactical awareness, accurately predict the opponent's intentions, and take corresponding actions in time to achieve ideal results.

(2) Familiar with the Problems That Should Be Paid Attention to in Tactical Cooperation. The expression of tactics is abstract and concise in the theory of written expression, but it is more complicated in actual application, and there are many changes in actual application. To use these tactics flexibly and accurately under these changing and complex circumstances, higher requirements are put forward for the application.

During the volleyball game, the situation on the game field changes rapidly. Due to the influence of many factors, the effects achieved by the tactics used by the athletes also change. Every sports team and athlete has its own tactical style of play, and there is a problem of mutual growth and mutual restraint. Based on the consideration of these issues, to achieve excellent sports performance in the game, defeat the opponent, and win the game, it is necessary to have a comprehensive and profound understanding and mastery of the tactical manifestations and characteristics of the team. At the same time, we must carefully study and understand the opponent's tactical play and performance characteristics and adopt threatening tactical cooperation to defeat the enemy, actively attack and defend, fight hard, gain the advantage of the game, and keep it.

(3) Keen Observation and Prediction Ability. The volleyball match is a contest between two sports teams. The victory of the match depends not only on one's own performance level but also on the overall performance of the opponent in the game. Tactics are used during the confrontation between the two teams. Without confrontation, there is no use of tactics. In the game, it is necessary to use tactical forms and tactical cooperation consciously and rationally. According to the performance of the opponent, choose one's own tactics in a targeted manner and defeat the enemy; only in this way, we can win the game. During the fierce competition, the competition was carried out with high intensity and tension, and the changes were very rapid. During the game, it is necessary to observe and predict the opponent's situation in a timely and accurate manner, accurately judge the opponent's intentions, adjust their own response measures in time, and take targeted measures to resist the opponent's attack. There will be many unexpected accidents during the game. We must have sharp observation and prediction ability for these emergencies to be able to deal with them in time and make correct and timely action measures. Therefore, keen observation and prediction ability play an important role in the application of volleyball game tactics.

2.2.2. Game Theory. Game theory [18] particularly emphasizes that the possible reactions of competitors must be considered when formulating strategies, to adjust their actions according to the reactions of competitors and to maximize the interests of individuals or collectives. Its main application areas are shown in Figure 5.

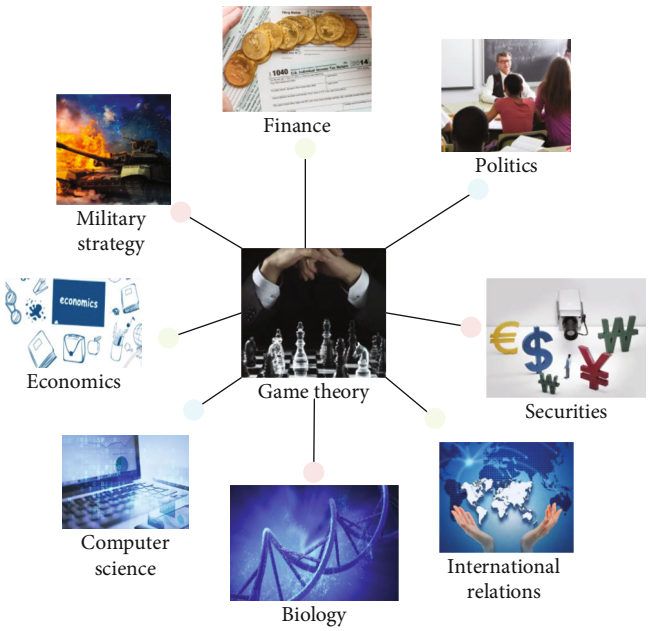

Figure 5: Application areas of game theory.

(1) The Basic Elements of the Game Model. Game theory uses mathematical analysis to express its game model. The manifestations of game theory can be divided into standard and extended forms. Although game theory can be different in form, any game theory must have its basic elements, including as follows:

(1) Players in the game. Players in the game refer to the participants who have the right to make their own decisions

(2) Strategy set, which is also called strategy space

(3) Payout function. The payout function in game theory can also be called the profit function or utility function of each player

(2) Cooperative Game. In a cooperative game [19], all game participants obey the game rules to make rational decisions, while the latter mainly studies the game participants to make game decisions without considering the impact on other participants. In the cooperative game, each participant is rational, emphasizing the overall fairness, and its Nash equilibrium is the state where the overall benefits are maximized.

In a static game, the players in the game make the game strategy at the same time or the two sides of the game make the game strategy without knowing what actions each other will take. In a dynamic game, all participants make game strategies one after the other, knowing the actions of both parties in the game. That is, in the dynamic game, the two sides of the game only act on the basis of information sharing.

The complete information game means that the players in the game can make the second round of game strategy only after they have fully grasped the game information. If the players do not have all the information of the game, or only understand part of the information, it will lead to some games with incomplete information, which is the game of incomplete information.

2.2.3. Game Analysis of Volleyball Tactics. Individuals or collectives (such as institutions, companies, governments, and countries) who can independently choose strategies and implement them in game activities and can independently bear the corresponding game results are called game parties. In the "Prisoner's Dilemma," although the police formulated the rules of the game, they themselves did not participate in the decision-making process and did not assume the corresponding game results. Therefore, the police cannot be regarded as a game player by definition. Two teams participating in a volleyball match can be regarded as two opposing players. Although the volleyball game is a collective confrontation event, once one party confirms to choose a certain tactic, it immediately needs the whole team to cooperate and complete the implementation of the tactic. That is, the selection and implementation of the strategy of the entire volleyball team are consistent. And regardless of whether the game wins or loses, the whole team jointly assumes the result of the game, which also satisfies the above description of the definition of the game party.

However, due to the dynamic nature of game activities, the process will interact and influence each other due to the different strategies chosen by different players. Therefore, the more parties participating in the game, the more difficult it is to analyze the game process, and the entire game process may therefore exhibit different attributes and characteristics. For this reason, when studying game problems, game activities are often divided into "single-player games," "two-player games," and "multiplayer games" according to the number of players participating in the game. The "person" here does not necessarily refer to a single individual person but the aforementioned game party.

Single-player game means that only one player participates in the game activity. Compared with two-player games and multiplayer games, the game process of single-player games is much simpler. Because the single-player game process in competitive volleyball is difficult to clarify, the volleyball player's choice of serve in daily training is used to establish a model to clarify the single-player game in volleyball.

The serving practice in the competitive training of volleyball players can be regarded as a single-player game played by the players themselves. For example, athletes have two options when serving the ball: one is to jump and serve vigorously, and the other is to jump and serve floating. The strong jump serve is strong and fast, which poses a greater threat to the opponent, but it also increases the risk of own mistakes accordingly. The miss rate of jump serve is low. Although the flight path of the ball is erratic, it poses relatively little threat to the opponent. It is suitable for targeted serve to find someone or find area tactics. During training, athletes will choose the way of serving practice according to their own technical characteristics, physical stamina, and

combined with tactical needs. We assume that athletes who practice serving have two strategies to choose from: vigorously jump serve and jump serve float. A straight jump serve or a straight jump serve can make one satisfied, while the diagonal line fails to achieve the training goal, which is not satisfied, and it cannot get a sense of self-identity.

2.3. System Model and Outage Probability. The system model of a full-duplex single-carrier single-antenna SG relay is shown in Figure 6. The entire relay system is composed of source node L, relay node E, and destination node S. The transmitter (or receiver) of each node has only one antenna. Among them, the relay node E works in full-duplex mode, and while receiving the signal a_L transmitted by the source node, it also uses the same frequency to transmit the signal a_E to the destination node. Due to the imperfect self-interference cancellation technology, the relay node will also receive residual self-interference. In addition, assuming that the direct link from the source node to the destination node is weak but not negligible, the signal model of the entire relay system is

$$b = Ga + k. \tag{1}$$

Among them, $b = [b_E, b_S]^T$ represents the received signal, $a = [a_L, a_E]^T$ represents the transmitted signal, $k = [k_E, k_S]^T$ is additive white Gaussian noise, and G is the channel matrix. The relay system shown in Figure 6 is a double-hop system; that is, it contains only one relay node, so the channel matrix G can be equivalent to the following 2×2 dimensional form

$$G = \begin{bmatrix} f_{LE} & f_{EE} \\ f_{LS} & f_{ES} \end{bmatrix}. \tag{2}$$

Assuming all channels

$$f_{xy}(x \in \{L, E\}, y\{E, S\}). \tag{3}$$

They are all Rayleigh fading channels; that is, the channel parameter $f_{x,y}$ obeys the cyclic symmetric complex Gaussian distribution, and the amplitude$|f_{xy}|$ of the channel parameter obeys the Rayleigh distribution, and its probability density function (PDF) is

$$f_{|g|}(a) = \frac{2a}{\Omega_{xy}} q^{-a^2/\Omega_{xy}}. \tag{4}$$

Among them, Ω_{xy} is the mean square error of $|f_{xy}|$.

Let s_i represent the transmit power of node E_i, namely

$$\varepsilon\left\{\left|a_{E_i}\right|^2\right\} = q_i. \tag{5}$$

Then, the SNR and the average SNR of the signal received by the node E_i transmitting node E_j are, respectively

$$\begin{aligned} \gamma_{xy} &= \frac{\left|f_{xy}\right|^2 q_i}{\sigma^2}, \\ \overline{\gamma_{xy}} &= \frac{\Omega, yq_i}{\sigma^2}. \end{aligned} \tag{6}$$

Among them, σ^2 is the power (variance) of the additive white Gaussian noise, γ_{xy} obeys the exponential distribution, and its probability density function is

$$f_\gamma\left(\gamma_{xy}\right) = \frac{1}{\overline{\gamma_{xy}}} e^{-\gamma_{xy}/\overline{\gamma_{xy}}}. \tag{7}$$

Its cumulative distribution function (CDF) is

$$F_\gamma\left(\theta_{xy}\right) = \int_0^{\theta_{xy}} f_\gamma\left(\gamma_{xy}\right) d\gamma_{xy} = 1 - e^{-\theta_{xy}/\overline{\gamma_{xy}}}. \tag{8}$$

In the relay system, the relay node E can receive the desired signal from the source node and the residual self-interference signal at the same time, and the destination node S can receive the desired signal from the relay node and the direct signal from the source node at the same time. Assuming that the signal from the source node to the destination node is weak, but not negligible, and the relay system does not adopt the joint coding scheme of the source node and the relay node, the SINR of the signal received by the relay node E and the destination node S, respectively

$$\begin{aligned} \gamma_E &= \frac{|f_{LE}|^2 qL}{\sigma^2 + |f_{EE}|^2 qE} = \frac{\gamma_{LE}}{1 + \gamma_{EE}}, \\ \gamma_S &= \frac{|f_{ES}|^2 qE}{\sigma^2 + |f_{LS}|^2 qL} = \frac{\gamma_{ES}}{1 + \gamma_{LS}}. \end{aligned} \tag{9}$$

At this time, the end-to-end channel capacity of the SG relay system is

$$Z = \min\{Z_{LE}, Z_{ES}\} = \min\{\log_2(1 + \gamma_E), \log_2(1 + \gamma_S)\}. \tag{10}$$

If the end-to-end capacity of the system cannot reach the given target information rate E, an outage occurs. The outage probability of the SG relay system is

$$Q_0 = U\{Z < E\}. \tag{11}$$

It is equivalent to the interruption of the source node to the relay node (the L-E link is interrupted) or the relay node to the destination node (the E-S link is interrupted), that is,

$$Q_0 = 1 - (1 - U\{Z_{LE} < E\})(1 - U\{Z_{ES} < E\}), \tag{12}$$

making

$$\gamma_{th} = 2^E - 1. \tag{13}$$

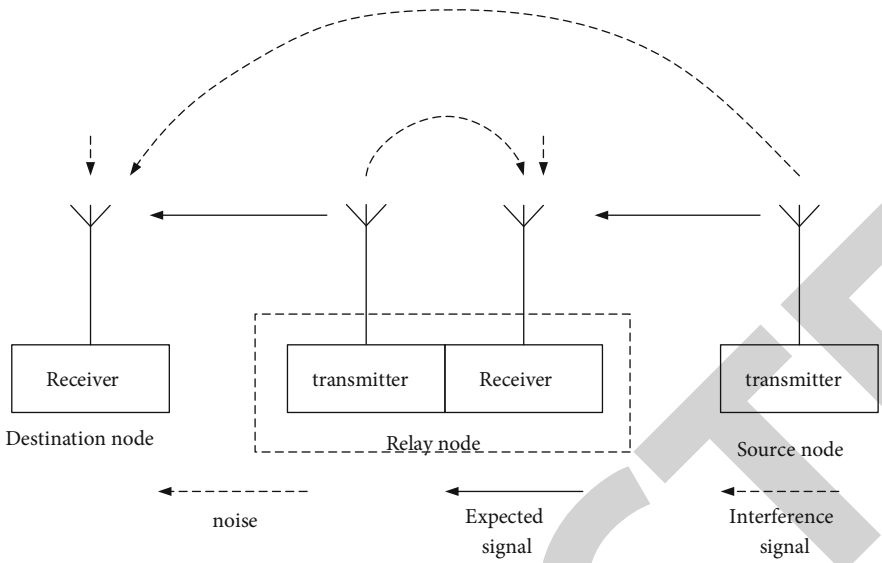

Figure 6: Full-duplex single-antenna single-carrier DF relay system model.

Table 1: China mobile TD-LTE wireless network planning index requirements.

Type	Penetration loss	RSRP		RS-SINR	Coverage	Cell edge rate
		F band	*D* band			
Main city	High	>-100	>-98	>-3	95%	1
Main city	Low	>-103	>-101	>-3	95%	1
General urban area		>-103	>-101	>-3	95%	1
County and suburbs		>-105	>-103	>-3	95%	1

Then, γ_{th}^2 is the SINR required to reach the target information rate, so the system interruption can be equivalent to the relay node's SINRγ_E not satisfying γ_{th} or the destination node's SINRγ_S not satisfying γ_{th}, so there is

$$Q_0 = 1 - (1 - U\{\gamma_E < \gamma_{th}\})(1 - U\{\gamma_S < \gamma_{th}\}). \quad (14)$$

Among

$$U\{\gamma_E < \gamma_{th}\}. \quad (15)$$

That is, the probability that the link between the source node and the relay node is interrupted, and $U\{\gamma_S < \gamma_{th}\}$ is the probability that the link between the relay node and the destination node is interrupted.

For the probability $U\{\gamma_E < \gamma_{th}\}$ that the link from the source node to the relay node is interrupted is

$$U\{\gamma_E < \gamma_{th}\} = 1 - \frac{1}{1 + (\gamma_{th}\bar{\gamma}EE/\bar{\gamma}L, E)} e^{-\gamma_{th}/\bar{\gamma}L,E}. \quad (16)$$

In the same way, the probability $D\{\gamma_S < \gamma_{th}\}$ that the link between the relay node and the destination node is interrupted is

$$U\{\gamma_S < \gamma_{th}\} = 1 - \frac{1}{1 + (\gamma_{th}\bar{\gamma}LS/\bar{\gamma}ES)} e^{-\gamma_{th}/\bar{\gamma}LES}. \quad (17)$$

Incorporating formula (16) and formula (17) into formula (14), the end-to-end outage probability of the full-duplex SG relay system is finally obtained as

$$Q_0 = 1 - \frac{1}{1 + (\gamma_{th}\bar{\gamma}EE/\bar{\gamma}L, E)} e^{-\gamma_{th}/\bar{\gamma}L,E} 1 - \frac{1}{1 + (\gamma_{th}\bar{\gamma}LS/\bar{\gamma}ES)} e^{-\gamma_{th}/\bar{\gamma}LES}. \quad (18)$$

3. Volleyball Tactics Analysis Simulation Test Experiment Based on Wireless Communication Network

3.1. Simulation Experiment of Scene Allocation Problem. China mobile's wireless network planning index requirements are shown in Table 1.

China Unicom's wireless network planning index requirements are shown in Tables 2–4.

China telecom's LTEFDD wireless network planning index requirements are shown in Table 5.

Considering the comparison of the social utility and spectrum utilization performance of each algorithm in a simplified scenario, it is assumed that the central decision-maker divides the frequency range into 144 continuous

Table 2: China Unicom LTEFDD wireless network planning index requirements.

Area type	RSRP	RS-SINR	Coverage	Cell edge rate	Average cell throughput
Dense urban area	>-100	>-5	90%	DL/UL:4/1	DL/UL:35/25
General urban area	>-100	>-5	90%	DL/UL:4/1	DL/UL:35/25
Tourist attraction	>-105	>-5	90%	DL/UL:4/1	DL/UL:30/20
Airport express, high-speed rail	>-110	>-5	90%	DL/UL:2/0.512	DL/UL:25/15

Table 3: China Unicom TD-LTE wireless network planning index requirements.

Area type	RSRP	RS-SINR	Coverage	Cell edge rate	Average cell throughput
Dense urban area	>-105	>-5	90%	DL/UL:1/0.128	DL/UL:18/10
General urban area	>-105	>-5	90%	DL/UL: 1/0.128	DL/UL: 18/10
Tourist attraction	>-110	>-5	90%	DL/UL: 1/0.128	DL/UL: 18/10

Table 4: China Unicom U900 wireless network planning index requirements.

Area type	RSCP	Ec/Io	Coverage
County town	>-90	>-12	90%
Suburban township	>-95	>-14	90%
Rural area	>-100	>-14	90%
Airport express, high-speed rail	>-90	>-12	90%
Provincial high-speed, high-speed train	>-95	>-12	90%
Other roads	>-95	>-14	90%

subintervals. The maximum number of requirements for each secondary user frequency subinterval is 36, and each secondary user randomly selects the number of requirements on [1,36] and normalizes the quotations of secondary users to a uniform distribution on [0,1]. At the same time, because the WSDP-S problem is a special case of the WSDP problem, the latter can also be used to simplify performance comparisons in scenarios. Figure 7 shows a comparison of social utility in a simplified scenario. Among them, the abscissa is the number of secondary users, the ordinate is the social utility, and the curve represents the relationship between the social utility of different algorithms and the number of secondary users.

Figure 7 shows a comparison of spectrum utilization in a simplified scenario. The spectrum utilization of each algorithm increases as n increases. Among them, the spectrum utilization rate under the optimal solution is not the highest, which can be considered as a trade-off between spectrum utilization rate and social utility.

3.2. Algorithm Simulation Experiment. This article simulates a communication system topology with 2 hotspots, and the α value of each base station is set to 0.5. That is, the zero-load power of each base station is half of its maximum operating power, and each base station has 2000 resource blocks to meet user needs. The simulated scene data is as follows: the area of the area is $2*2$ square kilometers, there are a total of 60 base stations in the area, the coverage radius of each base station is 200 to 400 meters, and the number of simulated users ranges from 1,000 to 20,000. The path loss model adopted is $l(dB) = 35.2 + 35\log_{10}(d)$, where d represents the distance from the user to the base station in meters.

The users are uniformly distributed in the area, and the user's signal-to-noise ratio (SNR) can be derived based on the distance from the base station and the path loss model, as shown in Figure 8.

As can be seen from Figure 8, the power savings of these two algorithms decrease as the number of users increases. This is because as the number of users increases, the load of the base station increases, and more base stations must be in operation to ensure the quality of service for users. The algorithm proposed in this paper saves more power. This is because the distributed access algorithm calculates the utility value of the mobile device at the same time, so it may produce a ping-pong effect, which makes the mobile station switch infinitely between the original base station and the target base station. The algorithm proposed in this paper can effectively avoid this problem. On the other hand, each base station can determine by itself whether it should be shut down. It can be seen that more base stations can be shut down using the algorithm proposed in this paper, so the energy saving is higher.

4. Improved Results of Volleyball Tactics with Wireless Communication Networks

4.1. Comparative Investigation and Analysis of Volleyball Spiking Technical Ability. Smashing is the basic technique of volleyball, and it is also the most powerful technique among the various techniques of volleyball. It is the main means of scoring in the game. The ability level of the spiking technique, which can best show the offensive ability of a team, is the key to victory in the game. Therefore, this paper investigates and analyzes the data of four groups of college volleyball matches, and the results are shown in Figure 9.

From the spiking data in Figure 9, it can be seen that the total spiking success rate of the first group of universities is 59%, and the total spiking success rate of the second group of universities is 53.27%. The third group of universities

Table 5: China telecom LTEFDD wireless network planning index requirements.

Area type	RSRP	RS-SINR	Coverage	Cell edge rate
Dense urban area	>-105	>-3	97%	DL/UL:4/0.256
General urban area	>-105	>-3	96%	DL/UL:4/0.256
Suburbs, county towns	>-105	>-3	95%	DL/UL:4/0.256

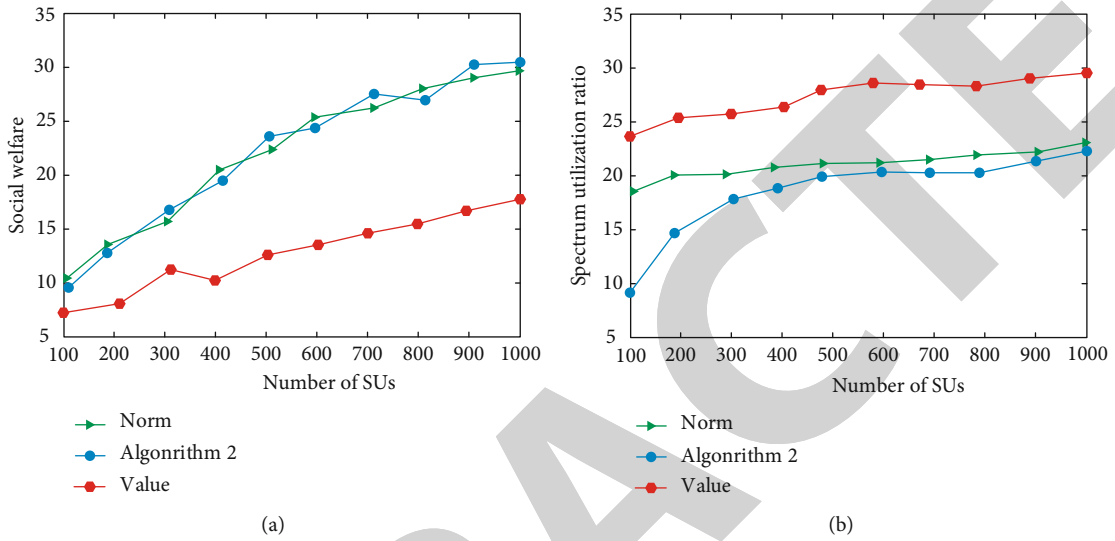

Figure 7: Comparison results of social utility and spectrum utilization in a simplified scenario: (a) comparison of social utility in simplified scenarios; (b) comparison of spectrum utilization in simplified scenarios.

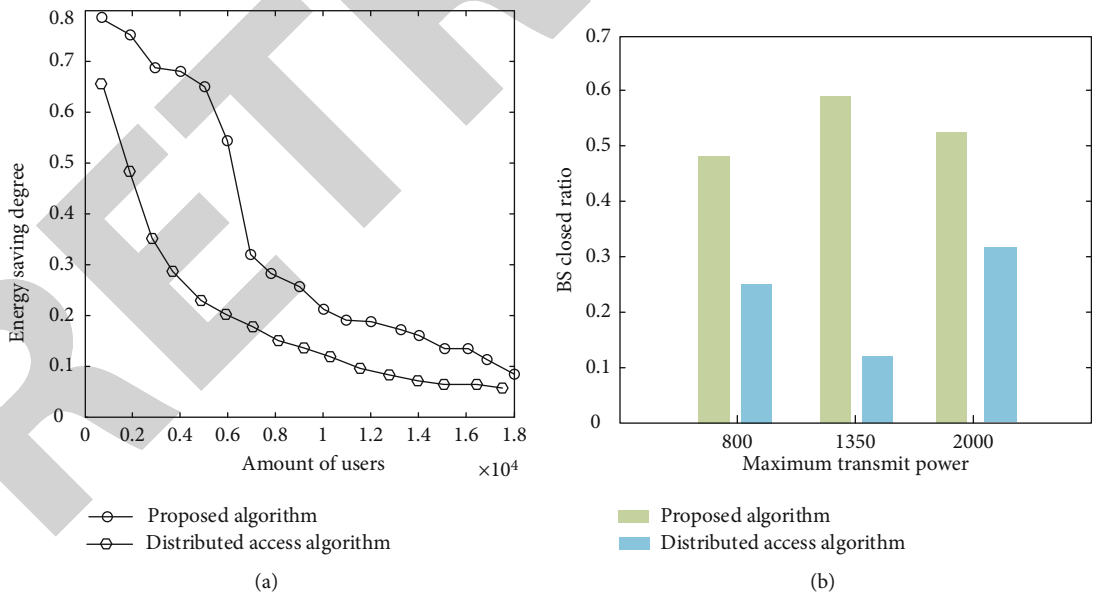

Figure 8: Simulation experiment results: (a) the impact of the number of users on power consumption; (b) proportion of base stations closed.

has a spiking success rate of 42.07%, and the fourth group of universities has a total spiking success rate of 48%.

4.2. Test Analysis of Volleyball Tactics Analysis Model Based on Wireless Communication Network. This paper optimizes the volleyball tactics analysis model of the wireless communication network through the data collected in the experiment. To explore the effect of the optimized volleyball tactics analysis model on volleyball matches, this article compares 20 volleyball teams into two groups. One group

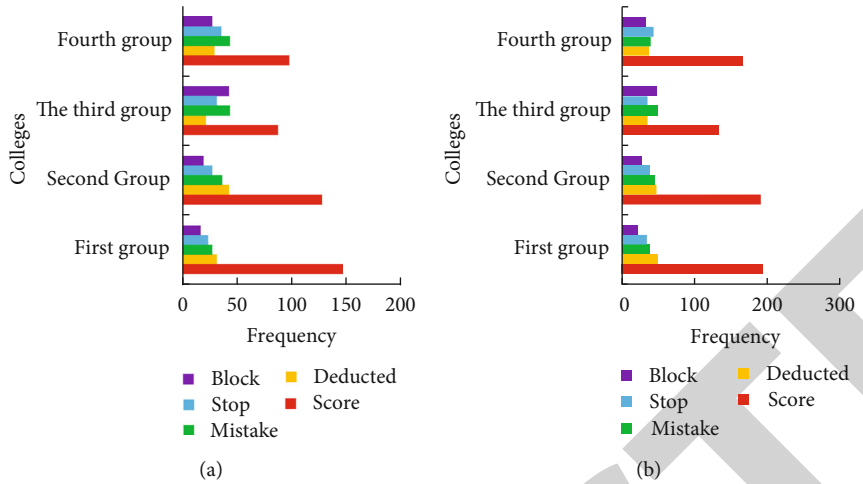

Figure 9: Comparison results of spiking techniques in colleges and universities: (a) anticounterfeiting situation comparison; (b) comparison of the first attack situation.

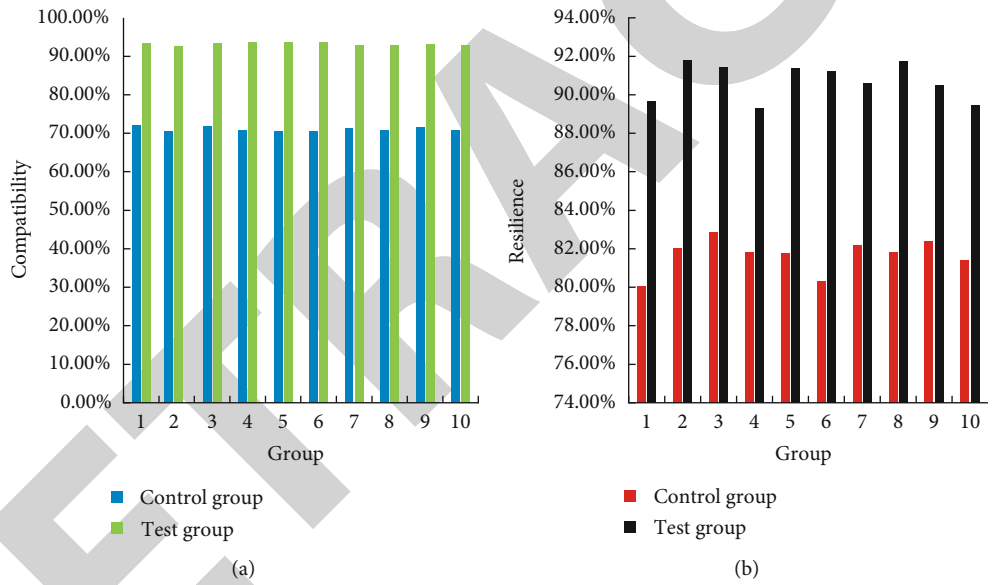

Figure 10: Experimental comparison results: (a) team fit; (b) on-the-spot adaptability.

is a control group, which only conducts ordinary training; the other group is an experimental group, which conducts volleyball tactics analysis and model training based on wireless communication network. Taking its team fit and on-the-spot adaptability as the evaluation criteria, the results of the experiment were recorded, and the results of the experiment are shown in Figure 10.

It can be seen from Figure 10 that the control group is traditional volleyball tactical training, and its team fit is only 71.02%, while the experimental group based on the wireless communication network-based volleyball tactical analysis model training has a team fit of 93.14%, an increase of 22.12%. The traditional volleyball tactics training individual on-the-spot adaptability is only 81.65%, while the experimental group based on the wireless communication network-based volleyball tactical analysis model training individual on-the-spot adaptability can reach 90.7%, an increase of 9.05%. This shows that the volleyball tactics analysis model based on the wireless communication network can very effectively improve the team fit of the volleyball team, and it can also improve the individual resilience of the team by a small amount.

5. Conclusions

This article mainly studies the establishment of the volleyball tactics analysis model based on the wireless communication network, so this article combines the characteristics of the radio network and the characteristics of the wireless communication network and accesses the LTE system. Based on the MIMO technology, the tactical analysis model of the wireless communication network is established, and

Hindawi
Computational and Mathematical Methods in Medicine
Volume 2023, Article ID 9827568, 1 page
https://doi.org/10.1155/2023/9827568

Retraction

Retracted: Left Atrial Appendage Depth and Tachycardia Bradycardia Syndrome as Important Predictors of Left Atrial Appendage Thrombus in Patients with Nonvalvular Atrial Fibrillation

Computational and Mathematical Methods in Medicine

Received 27 June 2023; Accepted 27 June 2023; Published 28 June 2023

This article has been retracted by Hindawi following an investigation undertaken by the publisher [1] This investigation has uncovered evidence of one or more of the following indicators of systematic manipulation of the publication process:

(1) Discrepancies in scope

(2) Discrepancies in the description of the research reported

(3) Discrepancies between the availability of data and the research described

(4) Inappropriate citations

(5) Incoherent, meaningless and/or irrelevant content included in the article

(6) Peer-review manipulation

The presence of these indicators undermines our confidence in the integrity of the article's content and we cannot, therefore, vouch for its reliability. Please note that this notice is intended solely to alert readers that the content of this article is unreliable. We have not investigated whether authors were aware of or nvolved in the systematic manipulation of the publication process.

In addition, our investigation has also shown that one or more of the following human-subject reporting requirements has not been met in this article: ethical approval by an Institutional Review Board (IRB) committee or equivalent, patient/participant consent to participate, and/or agreement to publish patient/participant details (where relevant).

Wiley and Hindawi regrets that the usual quality checks did not identify these issues before publication and have since put additional measures in place to safeguard research integrity.

We wish to credit our own Research Integrity and Research Publishing teams and anonymous and named external researchers and research integrity experts for contributing to this investigation.

The corresponding author, as the representative of all authors, has been given the opportunity to register their agreement or disagreement to this retraction. We have kept a record of any response received.

References

[1] Y. He, P. Chen, Z. Zhu, J. Sun, and Y. Zhao, "Left Atrial Appendage Depth and Tachycardia Bradycardia Syndrome as Important Predictors of Left Atrial Appendage Thrombus in Patients with Nonvalvular Atrial Fibrillation," *Computational and Mathematical Methods in Medicine*, vol. 2022, Article ID 4632823, 5 pages, 2022.

Hindawi
Computational and Mathematical Methods in Medicine
Volume 2022, Article ID 4632823, 5 pages
https://doi.org/10.1155/2022/4632823

Research Article

Left Atrial Appendage Depth and Tachycardia Bradycardia Syndrome as Important Predictors of Left Atrial Appendage Thrombus in Patients with Nonvalvular Atrial Fibrillation

Yinge He, Panpan Chen, Ziqiang Zhu, Junhua Sun, and Yujie Zhao

Department of Cardiology, Zhengzhou No. 7 People's Hospital, No. 17, Jingnan Fifth Road, Economy and Technical Development Zone, Zhengzhou, Henan Province, 450000, China

Correspondence should be addressed to Yujie Zhao; zhaoyujie6zy5j@163.com

Received 28 January 2022; Revised 24 February 2022; Accepted 5 March 2022; Published 30 March 2022

Academic Editor: Shakeel Ahmad

Background. Atrial fibrillation (AF) is the most common heart rhythm disorder that has been shown to be associated with a significant increase in stroke and systemic embolism risk. The left atrial appendage (LAA) is a finger-like extension originating from the left atrium; the formation of thrombus in LAA is the main reason of stroke and systemic embolism in patients with nonvalvular atrial fibrillation (NVAF). This study is aimed at finding out the risk of left atrial appendage thrombus (LAAT) in patients with nonvalvular atrial fibrillation (NVAF). *Method*. We retrospectively examined the clinic and left atrial computer tomography angiography (CTA) features of patients assessed in Zhengzhou No. 7 People's Hospital between January 2020 and January 2021 derivation. Student's *t*-test, chi-square test, receiver operating characteristics (ROC) curves, and logistic regression analysis were used to identify predictors of LAAT. *Result*. Of 480 patients included in the analysis, LAAT was found in approximately 9.2% of all patients. Univariate demographic predictors of LAAT included left atrium top and bottom diameter (LTD), left atrial appendage depth (LAAD), CHA2DS2-VASc, tachycardia bradycardia syndrome (TBS), and nonparoxysmal atrial fibrillation (PAF). In a multiple logistic regression analysis, the independent predictors of thrombus were LAAD > 23.45 mm (odds ratio: 4.216, 95% CI: 1.869-9.510, $P = 0.001$), TBS (odds ratio: 4.076, 95% CI: 1.655-10.038, $P = 0.002$), and non-PAF (odds ratio: 2.896, 95% CI: 1.183-7.094, $P = 0.02$). *Conclusion*. In NVAF patients with LAAT, evidence suggested that larger LAAD, non-PAF, and TBS present a high risk of LAAT. This is the first report demonstrating that the LAAD and TBS are associated with LAAT in patients with NVAF.

1. Introduction

Nonvalvular atrial fibrillation (NVAF) is independently associated with a four- to fivefold increased risk of ischemic stroke attributed to the thrombus from left atrium [1], and the number of AF patients is increasing annually [2]. Thrombus formation needs triad events [3, 4]: (1) endocardial damage or dysfunction and related structural abnormal changes, (2) abnormal blood stasis, and (3) abnormal haemostasis, platelets, and fibrinolysis; these variables are clearly evident in NVAF.

Left atrial appendage (LAA), a finger-like structure in the left atrium, has pectinate muscles with trabeculation leading to its uniqueness. LAA is the source of thrombus in more than 90% of the individuals with NVAF [5]. With the development of NVAF, the LAA develops mechanical dysfunction and fibroelastotic changes on the endocardial surface and this results in LAA remodeling and ultimately left atrial appendage thrombus (LAAT) [6–8]. A larger left atrial diameter, wider LAA orifice, and increased LAA depth indicate remodeling of the left atrial and LAA [9]; we measured the left atrium anteroposterior diameter (LAD), LTD, left atrial lateral diameter (LLD), maximum LAA ostium axis (max-LAAOA), minimum LAA ostium axis (min-LAAOA), and LAAD with CTA to compare the difference between the LAAT group and non-LAAT group.

TBS is characterized by prolonged sinus pause on the termination of atrial tachyarrhythmias. The association

between AF and sick sinus syndrome has been long recognized and is thought to form the basis of TBS. AF promote structural abnormalities and electrical remodeling in the form of fibrosis in atrium and sinus node; this is considered to be the important mechanism for the occurrence of TBS in AF [10–12]. Based on the evidence, we hypothesize that AF patients with TBS have worse atrial fibrosis; this can lead to more serious atrial dysfunction and LAAT. In this study, TBS was included to explore whether it was a risk factor for LAAT.

2. Methods

2.1. Patient Population. The cohort included consecutive NVAF patients referred to Zhengzhou No. 7 People's Hospital between January 2020 and January 2021. All patients were first diagnosed with NVAF and did not receive anticoagulant therapy. All LAAT were detected on CTA.

Diagnosis of TBS was made by Holter electrocardiogram (ECG). All clinical data included gender, age, and CTA data (LAD, LTD, LLD, max-LAAOA, min-LAAOA, and LAAD). The history of disease included hypertension, diabetes, coronary heart disease (CHD), PAF, non-PAF, and massive regurgitation of mitral valve (MR of MV) assessed by transthoracic echocardiography.

All clinical, laboratory, and CTA data were obtained retrospectively from medical records.

2.2. Statistical Analysis. Continuous variables were expressed as the mean ± SD. Categorical variables were expressed as numbers and frequencies. Student's *t*-test was used to compare the differences in continuous variables. The chi-square test was used to compare the difference in incidence between the two groups. Logistic regression was used to assess risk markers. The ROC analysis was used to evaluate the predictive effect of the model on LAAT. All statistical tests were performed with SPSS 23.0 (developed by International Business Machines Corporation). *P* value of <0.05 was considered a signifificant statistical difference.

3. Results

3.1. Baseline Characteristics. Of the 480 patients who underwent CTA prior to therapy, we identified 37 patients with LAAT. All 480 patients were first diagnosed with atrial fibrillation and not took anticoagulation. 37 patients have LAAT (7.7%); compared with non-LAAT, LAAT patients were older and have a higher prevalence of hypertension, non-PAF, MR of MV and TBS; the CHA2DS2-VASc scores are higher too; larger LAD, LTD, LLD, max-LAAOA, min-LAAOA, and LAAD were also found in LAAT patients. There was no difference in gender, renal insufficiency, diabetes, and CHD (Table 1).

3.2. Predictors of LAAT. Multiple candidate clinical predictors and CTA measurements were assessed as univariate independent predictors for LAAT. The statistically significant univariate predictors of events were LTD, LAAD, CHA2DS2-VASc, TBS, and non-PAF (Table 2). Furthermore, we conducted ROC curve analysis to statistically significant parameters for LAAT prediction in patients with

Table 1: Demographic and clinical data of patients.

	LAAT $N = 37$ (%)	Non-LAAT $N = 443$ (%)	*P* value
Male	18 (48.6)	280 (63.2)	0.111
Age (≧75)	13 (35.1)	71 (16)	0.006
Renal insufficiency	5 (13.5)	29 (6)	0.169
Diabetes	13 (35.1)	105 (23.7)	0.162
Hypertension	25 (67.6)	207 (46.7)	0.017
Non-PAF	30 (81)	222 (50.1)	<0.001
CHD	21 (56.8)	198 (44.7)	0.172
CHA2DS2-VASc	4.46 ± 1.71	2.86 ± 1.88	<0.001
MR of MV	15 (40.5)	109 (24.6)	0.049
TBS	9 (24.3)	28 (6.3)	0.003
LAD	55.84 ± 8.37	48.35 ± 9.63	<0.001
LTD	66.14 ± 7.88	60.23 ± 7.92	<0.001
LLD	81.86 ± 8.98	75.43 ± 10.17	<0.001
Max-LAAOA	30.12 ± 5.49	28.00 ± 5.42	0.023
Min-LAAOA	20.84 ± 5.07	24.30 ± 5.13	<0.001
LAAD	26.21 ± 4.52	22.36 ± 4.46	<0.001

LAAT: left atrial appendage thrombus; non-PAF: nonparoxysmal atrial fibrillation; CHD: coronary heart disease; MR of MV: massive regurgitation of mitral valve; TBS: tachycardia bradycardia syndrome; LAD: left atrium anteroposterior diameter; LTD: left atrium top and bottom diameter; LLD: left atrial lateral diameter; max-LAAOA: maximum left atrial appendage ostium axis; min-LAAOA: minimum left atrial appendage ostium axis; LAAD: left atrial appendage depth.

Table 2: Binary logistic regression analysis for risk markers.

	OR	95% CI	*P* value
Non-PAF	3.30	1.252-8.710	0.016
CHA2DS2-VASc	1.421	1.110-1.819	0.005
LTD	1.070	1.009-1.135	0.025
LAAD	1.155	1.048-1.272	0.004
TBS	0.165	0.062-0.442	<0.001

non-PAF: nonparoxysmal atrial fibrillation; LTD: left atrium top and bottom diameter; LAAD: left atrial appendage depth; TBS: tachycardia bradycardia syndrome.

NVAF; the area under ROC curves (AUC) for LAAD was 0.735 (sensitivity: 75.7%, specificity: 74.9%, 95% CI: 0.66-0.82, $P < 0.001$). The AUC for LTD was 0.705 (sensitivity: 75.7%, specificity: 73.7%, 95% CI: 0.63-0.73, $P < 0.001$). The AUC for CHA2DS2-VASc was 0.736 (sensitivity: 10.8%, specificity: 96.4%, 95% CI: 0.63-0.73, $P < 0.001$) (Figure 1). The statistically significant multivariable predictors of events were LAAD > 23.45 mm (odds ratio: 4.216, 95% CI: 1.869-9.510, $P = 0.001$), TBS (odds ratio: 4.076, 95% CI: 1.655-10.038, $P = 0.002$), and non-PAF (odds ratio: 2.896, 95% CI: 1.183-7.094, $P = 0.02$) (Table 3).

4. Discussion

LAA possesses high compliance and forms a good reservoir for the blood in the heart to modulating the LA pressure

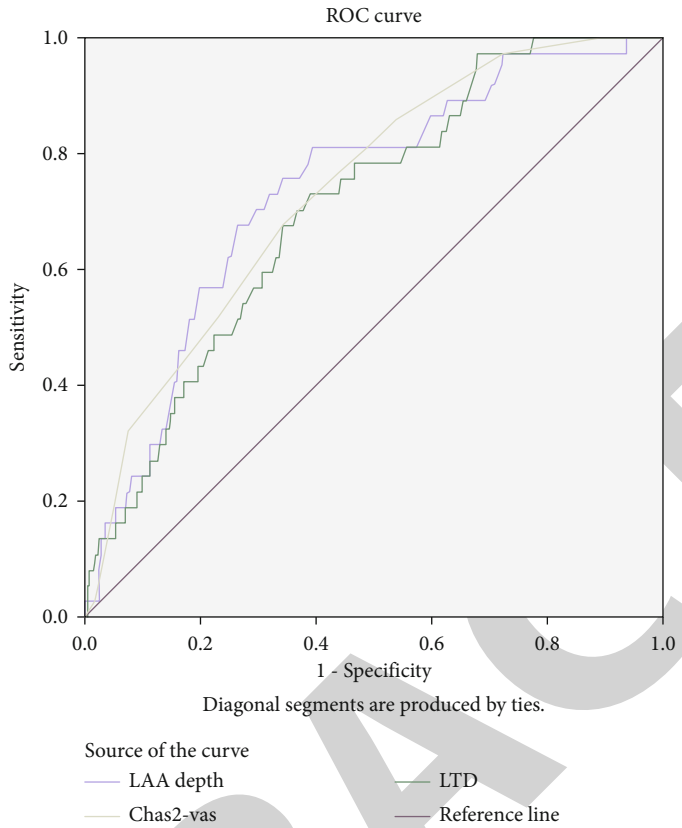

Figure 1: ROC curve for LAAD, LTD, and CHA2DS2-VASc score. LAAD: left atrial appendage depth; LTD: left atrium top and bottom diameter.

Table 3: Multivariate logistic regression analysis for risk markers.

	OR	95% CI	*P* value
LAAD > 23.45 mm	4.216	1.869-9.510	0.001
Non-PAF	2.896	1.183-7.094	0.02
TBS	4.076	1.655-10.038	0.002

LAAD: left atrial appendage depth; non-PAF: nonparoxysmal atrial fibrillation; TBS: tachycardia bradycardia syndrome.

[13]. LA strain caused by NVAF can directly measure LAA remodeling which manifests itself as enlargement of LAA orifice area and volume [14–19], and remodeling was associated with LAAT [20–25]. Remodeling means not only larger size but also greater endocardial thickening with fibrous tissue making a decreased velocity in LAA, further affecting LAA emptying; these may play a role in LAA thrombus formation in NVAF [19, 22–29]. LAA depths were also associated with increased LAAT in our study. Our findings support the notion that the remodeling of LAA depth is involved in the chain of events leading from NVAF to LAAT. Therefore, any direction of the LAA remodeling will result in LAAT.

Another attributing factor is TBS. A proportion of AF patients have TBS. Prolonged sinus pauses can be observed in AF patients; that is a condition known as TBS [30]. Sinus node (SN) dysfunction is the main reason of TBS; SN remodeling caused by atrial tachyarrhythmia, including AF, leads to reversible SN dysfunction [31, 32]. AF can lead to anatomical and electrophysiological remodeling within the SN and surrounding atrial tissue that prompts and accelerates the development of SN dysfunction [33]; fibrosis is a key aspect of remodeling which serves to slow conduction and cause atrial contractile dysfunction [34]. In AF patients, LAA remodeling occurs in both left and right atrial appendages, but more severe endocardial changes were found in the LAA than that in the right atrial appendage (RAA) [35]; TBS means serious RAA remodeling; there may also be severe remodeling in LAA that leads to LAAT. LA blood emptying benefits from active atrial contraction and passive ventricular diastolic emptying, which is also the decisive factor of LAA emptying [27], TBS occurs, and the ventricle stops contracting and diastolic, causing further blood stasis in the atria which has lost the ability to contract; those contribute to LAAT. Our results found that patients with non-PAF had a higher risk of LAAT.

Patients with non-PAF had a significant higher risk of LAAT; these findings are consistent with the study before [36–38]. The major difference between paroxysmal AF and non-PAF is whether AF is sustained. Atrial substrate is the most important factor to sustain AF that means atrial remodeling [39, 40]. Remodeling results in severe fibrosis of LA and LAA, which leads to systolic dysfunction and decreased LAA flow velocity as compared with PAF [38]. This makes non-PAF more prone to LAA. This is consistent with our findings.

5. Limitations

Our study had several limitations. First, the study was retrospect analysis. Second, we did not analyze the history of peripheral embolism because the data were incomplete. Most patients with acute cerebral infarction are treated in the department of neurology; for some of those patients, screening for atrial fibrillation was neglected. Third, LAAT measured by CTA does not have 100% sensitivity in detecting LAAT.

6. Conclusion

There are many factors that impact on thromboembolic events in NVAF patients. This study suggests that large LAAD, non-PAF, and TBS may present a high risk group of LAAT.

Data Availability

The data used to support the findings of this study are available from the corresponding author upon request.

Conflicts of Interest

The authors declare that they have no conflicts of interest.

Authors' Contributions

Yinge He and Panpan Chen contributed equally.

Acknowledgments

This study was supported by Henan Medical Key Laboratory of Arrhythmia.

References

[1] E. J. Benjamin, M. J. Blaha, S. E. Chiuve et al., "Heart Disease and Stroke Statistics-2017 Update: a report from the American Heart Association," vol. 135, Tech. Rep. 10, .

[2] A. Wang, J. B. Green, J. L. Halperin, and J. P. Piccini Sr., "Atrial fibrillation and diabetes mellitus," *Journal of the American College of Cardiology*, vol. 74, no. 8, pp. 1107–1115, 2019.

[3] A. Choudhury and G. Y. Lip, "Atrial fibrillation and the hypercoagulable state: from basic science to clinical practice," *Pathophysiology of Haemostasis and Thrombosis*, vol. 33, no. 5-6, pp. 282–289, 2003.

[4] D. A. Zateyshchikov, A. N. Brovkin, D. A. Chistiakov, and V. V. Nosikov, "Advanced age, low left atrial appendage velocity, and factor V promoter sequence variation as predictors of left atrial thrombosis in patients with nonvalvular atrial fibrillation," *Journal of Thrombosis and Thrombolysis*, vol. 30, no. 2, pp. 192–199, 2010.

[5] D. R. Holmes, V. Y. Reddy, Z. G. Turi et al., "Percutaneous closure of the left atrial appendage versus warfarin therapy for prevention of stroke in patients with atrial fibrillation: a randomised non-inferiority trial," *Lancet*, vol. 374, no. 9689, pp. 534–542, 2009.

[6] A. Kanmanthareddy, Y. M. Reddy, A. Vallakati et al., "Embryology and anatomy of the left atrial appendage: why does thrombus form?," *Interventional Cardiology Clinics*, vol. 3, no. 2, pp. 191–202, 2014.

[7] S. Miyauchi, T. Tokuyama, Y. Uotani et al., "Association between left atrial appendage fibrosis and thrombus formation: a histological approach," *Journal of Cardiovascular Electrophysiology*, vol. 23, 2022.

[8] R. Beinart, E. K. Heist, J. B. Newell, G. Holmvang, J. N. Ruskin, and M. Mansour, "Left atrial appendage dimensions predict the risk of stroke/TIA in patients with atrial fibrillation," *Journal of Cardiovascular Electrophysiology*, vol. 22, no. 1, pp. 10–15, 2011.

[9] O. Yosefy, B. Sharon, C. Yagil et al., "Diabetes induces remodeling of the left atrial appendage independently of atrial fibrillation in a rodent model of type-2 diabetes," *Cardiovascular Diabetology*, vol. 20, no. 1, p. 149, 2021.

[10] G. Tse, T. Liu, K. H. Li et al., "Tachycardia-bradycardia syndrome: electrophysiological mechanisms and future therapeutic approaches (review)," *International Journal of Molecular Medicine*, vol. 39, no. 3, pp. 519–526, 2017.

[11] F. Pathan, H. Hecht, J. Narula, and T. H. Marwick, "Roles of transesophageal echocardiography and cardiac computed tomography for evaluation of left atrial thrombus and associated pathology: a review and critical analysis," *JACC: Cardiovascular Imaging*, vol. 11, no. 4, pp. 616–627, 2018.

[12] W. Chang and G. Li, "Clinical review of sick sinus syndrome and atrial fibrillation," *Herz*, 2021.

[13] X. Lu, T. Chen, G. Liu et al., "Relations between left atrial appendage contrast retention and thromboembolic risk in patients with atrial fibrillation," *Journal of Thrombosis and Thrombolysis*, vol. 53, no. 1, pp. 191–201, 2022.

[14] S. Nedios, M. Tang, M. Roser et al., "Characteristic changes of volume and three-dimensional structure of the left atrium in different forms of atrial fibrillation: predictive value after ablative treatment," *Journal of Interventional Cardiac Electrophysiology*, vol. 32, no. 2, pp. 87–94, 2011.

[15] V. Y. Reddy, S. K. Doshi, S. Kar et al., "5-year outcomes after left atrial appendage closure," vol. 70, no. 24, pp. 2964–2975, 2017.

[16] W. Bai, Z. Chen, H. Tang, H. Wang, W. Cheng, and L. Rao, "Assessment of the left atrial appendage structure and morphology: comparison of real-time three-dimensional transesophageal echocardiography and computed tomography," *The International Journal of Cardiovascular Imaging*, vol. 33, no. 5, pp. 623–633, 2017.

[17] R. J. Hunter, Y. Liu, Y. Lu, W. Wang, and R. J. Schilling, "Left atrial wall stress distribution and its relationship to electrophysiologic remodeling in persistent atrial fibrillation," *Circulation. Arrhythmia and Electrophysiology*, vol. 5, no. 2, pp. 351–360, 2012.

[18] J. J. Park, J. H. Park, I. C. Hwang, J. B. Park, G. Y. Cho, and T. H. Marwick, "Left atrial strain as a predictor of new-onset atrial fibrillation in patients with heart failure," *JACC. Cardiovascular Imaging*, vol. 13, no. 10, pp. 2071–2081, 2020.

[19] G. Murtaza, B. Yarlagadda, K. Akella et al., "Role of the left atrial appendage in systemic homeostasis, arrhythmogenesis, and beyond," *Cardiac Electrophysiology Clinics*, vol. 12, no. 1, pp. 21–28, 2020.

[20] H. Kato, M. Nakanishi, N. Maekawa, T. Ohnishi, and M. Yamamoto, "Evaluation of left atrial appendage stasis in patients with atrial fibrillation using transesophageal echocardiography with an intravenous albumin-contrast agent," *The*

Hindawi
Computational and Mathematical Methods in Medicine
Volume 2023, Article ID 9796860, 1 page
https://doi.org/10.1155/2023/9796860

Retraction

Retracted: Rehabilitation Treatment of Muscle Strain in Athlete Training under Intelligent Intervention

Computational and Mathematical Methods in Medicine

Received 3 October 2023; Accepted 3 October 2023; Published 4 October 2023

This article has been retracted by Hindawi following an investigation undertaken by the publisher [1]. This investigation has uncovered evidence of one or more of the following indicators of systematic manipulation of the publication process:

(1) Discrepancies in scope

(2) Discrepancies in the description of the research reported

(3) Discrepancies between the availability of data and the research described

(4) Inappropriate citations

(5) Incoherent, meaningless and/or irrelevant content included in the article

(6) Peer-review manipulation

The presence of these indicators undermines our confidence in the integrity of the article's content and we cannot, therefore, vouch for its reliability. Please note that this notice is intended solely to alert readers that the content of this article is unreliable. We have not investigated whether authors were aware of or involved in the systematic manipulation of the publication process.

In addition, our investigation has also shown that one or more of the following human-subject reporting requirements has not been met in this article: ethical approval by an Institutional Review Board (IRB) committee or equivalent, patient/participant consent to participate, and/or agreement to publish patient/participant details (where relevant).

Wiley and Hindawi regrets that the usual quality checks did not identify these issues before publication and have since put additional measures in place to safeguard research integrity.

We wish to credit our own Research Integrity and Research Publishing teams and anonymous and named external researchers and research integrity experts for contributing to this investigation.

The corresponding author, as the representative of all authors, has been given the opportunity to register their agreement or disagreement to this retraction. We have kept a record of any response received.

References

[1] Y. Qiao, L. Zhang, and B. Zhang, "Rehabilitation Treatment of Muscle Strain in Athlete Training under Intelligent Intervention," *Computational and Mathematical Methods in Medicine*, vol. 2022, Article ID 5403681, 11 pages, 2022.

Hindawi
Computational and Mathematical Methods in Medicine
Volume 2022, Article ID 5403681, 11 pages
https://doi.org/10.1155/2022/5403681

Research Article

Rehabilitation Treatment of Muscle Strain in Athlete Training under Intelligent Intervention

Yu Qiao,[1] Lei Zhang,[2] and Bin Zhang[3]

[1]*Angeles University Foundation, Angeles City, Pampanga, Philippines*
[2]*Anhui Wannan Medical College, Wuhu, 241000 Anhui, China*
[3]*Wanjiang College of Anhui Normal University, Wuhu, 241000 Anhui, China*

Correspondence should be addressed to Bin Zhang; 2015286@mail.ahnu.edu.cn

Received 21 January 2022; Revised 24 February 2022; Accepted 10 March 2022; Published 29 March 2022

Academic Editor: Muhammad Zubair Asghar

With the development of artificial intelligence technology in the medical field, clinical trials using artificial intelligence as an intervention method are constantly emerging. This article mainly introduces the intervention of artificial intelligence and emotional intelligence on the rehabilitation of athletes' muscle strains. Among them, artificial intelligence and emotional intelligence are a brand-new nursing intervention method. This article compares conventional rehabilitation therapy with these two new types of intelligent interventions to explore the effects of artificial intelligence intervention and emotional intelligence intervention in the rehabilitation of athletes. The experimental results show that the average number of muscle restrains under the intervention of artificial intelligence is 4.1 times, the average restrain rate of muscles is 27.7%, and the average recovery degree of athletes is 94.7%. The average SPB score under emotional intelligence intervention was 56 points. Artificial intelligence interventions can enhance rehabilitation through advanced technology, and emotional intelligence interventions can provide emotional support to effectively improve treatment outcomes and quality of life.

1. Introduction

Artificial intelligence technology originated in the 1950s. Artificial intelligence is based on big data network resources. According to the characteristics of human intelligence, the artificial system is simulated and designed with computer information technology using it for the development of machines, software, or new technologies and finally applying them in various fields. With the rapid development of computer technology and the updating of algorithms, artificial intelligence technology has also gone from concept to practical application. It has gradually realized a variety of technologies such as speech recognition, image recognition, language recognition, and natural language processing and is gradually being widely used in education, medical, security, finance, autonomous driving, etc. With the continuous development and maturity of artificial intelligence technology, based on cloud computing, cloud storage, wireless communication, RFID, and other technologies, artificial intelligence technology has been widely used in the medical and health fields. Smart medical refers to a regional medical information platform for establishing medical and health files. It uses artificial intelligence technology to enable patients, medical staff, medical institutions, and medical equipment to communicate with each other and gradually realize information and intelligence. This promotes the development of medical services [1, 2].

In normal training and high-intensity competitions, athletes often experience sports injuries, which seriously affect athletes' daily training and life. In sports and training, muscle strain is a relatively common sports injury. If too much tension is exerted on the muscle during exercise, it will exceed its capacity. Or the muscles are suddenly stretched too much, which can cause strains. If the later injury is not handled well, or there is no timely rehabilitation treatment, it will lead to the recovery of the muscle, which will lead to the muscle strain again. Therefore, the correct diagnosis and the development of a reasonable rehabilitation treatment plan are very necessary. Based on the background of the Internet of

Things, the intelligent medical treatment can provide an intelligent intervention for the muscle strain in the training of athletes.

This article starts from artificial intelligence and emotional intelligence intervention, using intelligent magnetic resonance technology to accurately diagnose and evaluate muscle strains and to provide active psychological counseling to athletes. It explores the effects of these two interventions on the rehabilitation of muscle strains. So that researchers can better carry out such experiments in the future and promote the application of artificial intelligence and emotional intelligence intervention in medical health.

2. Related Work

In terms of theoretical research, domestic and foreign experts and scholars have discussed the application and development prospects of artificial intelligence technology in the field of medicine and have done relevant research on various links and applications of medical intelligence. Based on AmI-MS, Cicotti proposes a new hazard-driven and evidence-based V-model approach to monitor medical conditions and better inform medical decisions for physicians. The problem of unsafe medical devices and nonstandard treatment options is addressed by defining a sequential and consistent exploitation process. The novelty of the approach is the intertwining of risk management and software development activities and the use of case studies to explore quality of care issues [3]. Godinho et al. aim to solve the problem of medical data in communication and storage systems by creating a system that simulates a medical image repository in three steps: an index of sample data sets, a pattern extraction, and a modeling of data studies. The system builds up the model based on a representative time window of the medical data repository and extends it for medical data. In addition, the system has been applied in other studies for medical validation, aiming to evaluate the functionality and extensibility of the explored system [4]. Under the existing deteriorating medical safety big data ecosystem, Zhang and Wang design and construct a safe health big data ecosystem on the Hadoop big data platform. The authors use the Hadoop big data platform to realize centralized storage and analysis of the original data using data synchronization and independent data collection system, so that patients can keep themselves informed of their medical treatment and recovery, and thus provide personalized medical management services for patients [5]. Based on the informatization of medical devices and the use of single-disease medical consumables, Jianghua has built an intelligent clinical path and early warning management system based on medical devices, which ensures the rational use of medical devices. The system will improve the means of supervision so that it can better play the role of fine management. By establishing an intelligent clinical pathway management system and early warning systems for medical devices, it can play a better role in guiding the efficient use of healthcare equipment. This will allow monitoring and control of data for future cost-effective analysis of the treatment of individual diseases [6]. Based on the incremental learning method, Ali et al. have built an intelligent medical platform in the form of dialogue to provide medical guidance and recommendation services. The platform shows 90% knowledge acquisition rate, 80% user satisfaction with the system interaction, and 95% system integration accuracy rate with legacy systems [7]. To study and assess the key influencing variables (and their correlation) on consumer adherence decisions, Liu et al. use a mixed modified multiattribute decision model (MADM) for enhancing and promoting the smart medical terminal to achieve the set expected level in all dimensions and standards. MADM uses an improved VIKOR methodology that uses the INRM and DANP impact weights as a combined weight to figure out how to close the gap and offer the optimum enhancement mechanism to reach the set desired level [8]. Alexander et al. report on recent research findings from McKinsey & Company and discuss the development of artificial intelligence in clinical imaging. The article highlights the progress in its clinical application, the prospects for market adoption, and the obstacles that may be encountered. Artificial intelligence will have a significant influence on the clinical imaging market and, in turn, on the way radiosurgeons operate, enabling faster processing times, more precise resolutions, and reduced tasks [9].

3. Artificial Intelligence and Emotional Intelligence

3.1. Artificial Intelligence. Since the Dartmouth Conference in 1956, AI has experienced a history of more than 60 years, from calculative intelligence to perceptual intelligence to sensory intelligence, as shown in Table 1. Calculative intelligence is the prototype of AI and is the foundation of AI development. At present, the focus of AI development at home and abroad is still cognitive intelligence, while sensory intelligence is the superior form of AI and is an important breach in the development of AI [10].

3.1.1. Calculative Intelligence Stage. Computational intelligence is the most basic form of artificial intelligence, enabling it to compute, store, and transmit in a way that humans do [11]. Computers are far faster than humans in terms of storage and computation, and they can state and process large amounts of data quickly. In particular, the whole system has a degree of intelligence based on large deposits and megacomputing. Calculative intelligence performs some tasks through methods such as playing chess and searching the Internet. For example, "IBM's Deep Blue Chess" surpassed human beings in 2006, and Google's search engine can help users find relevant information in "tens of thousands" of pages [12]. Its applications in teaching mainly include fast storage and transmission of massive learning resources and intelligent management of students.

3.1.2. Perceptual Intelligence Stage. Perceptual intelligence is an important phase in the current advances in artificial intelligence. It enables robots to read, distinguish, perceive, and respond as humans do. Currently, the growth of perceptual intelligence has become fairly developed. It mainly uses geometrical patterns, deep learning, and other algorithms to

Table 1: The three stages of artificial intelligence development.

Development stage	Feature	Application
Computing intelligence	Can store and compute	Storage and delivery of massive learning resources and intelligent management system for student information
Perceptual intelligence	Can listen and speak, see, and recognize	Language teaching, oral assessment, and image search
Cognitive intelligence	Can understand and think	Personalized learning and independent learning

simulate human perception and help people complete their work [13]. Its research scope is very wide, including speech recognition and image recognition, such as Amazon's "Alexa" smart assistant and Google assistant. It can support human-computer interactive voice communication in multiple devices and different languages and provide users with personalized services through voice and text retrieval. Baidu image retrieval uses image recognition technology to achieve real-time retrieval, which greatly meets the needs of users. The application of perceptual intelligence in real life mainly includes intelligent transportation, medical health, modern agriculture, energy supply, logistics sales, as shown in Figure 1.

3.1.3. Sensory Intelligence Stage. Sensory intelligence is an advanced form of artificial intelligence. It imitates the human ability to think, assimilate, and organize knowledge and it has certain concepts, consciousness, and thoughts [14]. In addition to logical thinking, AI in this period also has various modes of thinking such as figurative thinking and inspired thinking that could help or replace certain human tasks in a comprehensive manner. Sensory intelligence is currently a major part of AI research. Cognitive intelligence is a current emerging area of AI research, and various technology companies are actively conducting research with certain results. For example, AlphaGO, an intelligent educational robot developed by the Hong Kong University of Science and Technology, has a "human-like mind." Its comprehension, articulation, and intelligence will improve with profound study, and it can offer visualized training and automatic learning.

3.2. Emotional Intelligence. American psychologists invented the term "emotional intelligence." It refers to the individual's ability to perceive, clearly understand, and successfully control the feelings of oneself and others. It uses emotional intelligence to intervene in nursing, fully communicate with patients, help patients improve their emotional ability, overcome negative emotions, and thereby improve their mental state [15].

3.3. Smart Technology

3.3.1. Wireless Sensing Technology. Wireless sensor technology is a wireless network composed of a large number of sensor nodes with wireless communication functions in a self-organizing and self-management mode. In the application environment, it can collect the data of the connected objects through the sensing device and then present the result obtained by the application system to the receiver at the other end of the network [16, 17].

Figure 2 shows the architecture of the WSN. The whole system generally consists of sensing units, aggregation units (Gateway), and task management units. After collecting the data from the sensors, the self-organizing network of nodes transmits the acquired data to the aggregation gateway [18, 19]. The convergence gateway then transmits this information to external networks such as UAV, satellite communication network, or the Internet. After that, the data information is transmitted to the remote task management server through the external network, so that the received data can be processed on the remote task management server. Finally, the remote task management server will present the result data after preliminary processing to the user. After the user receives the data from the remote task management node, the data will be processed according to their own needs [20].

When the WSN is working, the sensor unit is mainly responsible for target tracking, location recognition, forwarding, and storage of other sensor node information. At the same time, it can also perform simple data processing. Sensor nodes can communicate wirelessly to form a self-organizing network and transmit the sensed external information to the sink node through multiple hops. The sink node acts as a bridge to connect the wireless sensor network to the external network with a larger communication range for data conversion and transmission. The sink node receives the data from each sensor node and further analyzes and processes the data. Then, the data is transmitted to the server on the task management node [21]. The task management node is responsible for receiving and storing data in the monitored area and providing visual results to end users through the server, thereby realizing real-time monitoring of the system. A typical wireless sensor network structure means that a large number of sensor nodes are randomly distributed throughout the monitoring area, and the information collected from the monitoring target is transmitted through the neighboring nodes by each sensor node, then, the information is processed and data is fused through a predetermined information, and then sent to the terminal via satellite or wired network.

Sensor nodes usually include four modules: sensors, information processing, wireless communication, and energy supply. Figure 3 represents the configuration of a sensor node. The main task of the sensor module is to collect data from the monitored area. The A/D conversion module converts the information that cannot be directly processed into digital information that can be directly processed by the chip. As the center of the WSN node, the information processor module controls the total wireless sensor network junction as a whole system. It consists of two parts: calculation and

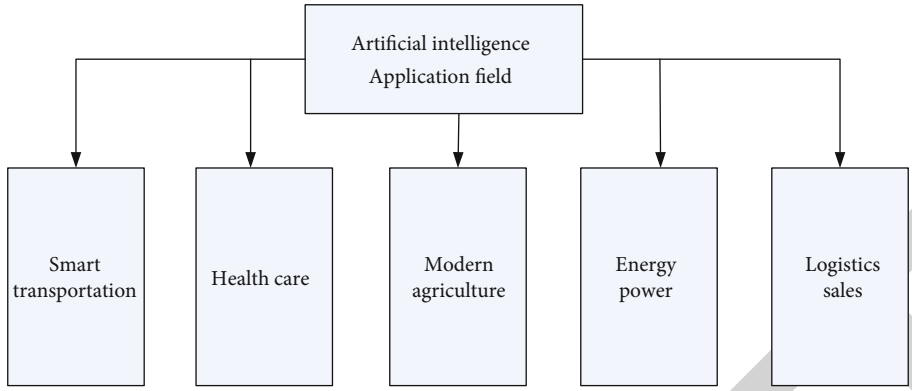

Figure 1: Artificial intelligence application field.

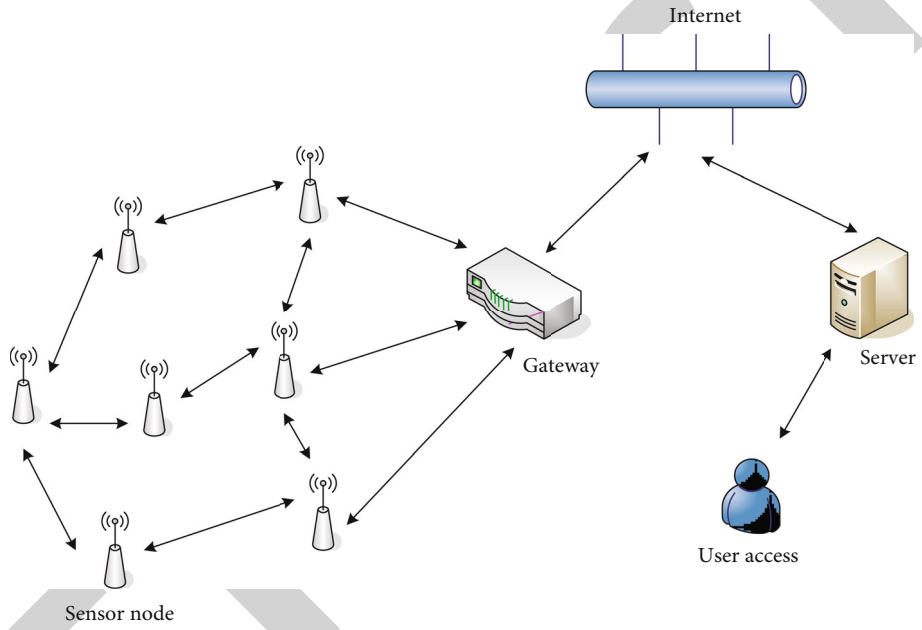

Figure 2: Network structure of wireless sensor network.

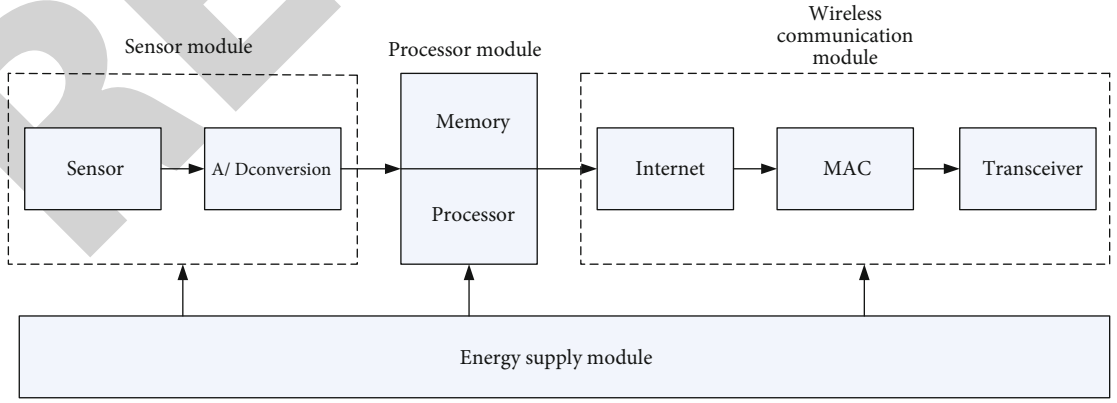

Figure 3: Sensor node structure diagram.

storage, which are responsible for storing and processing sensor data from the sensor module, and for information exchange with the wireless communication module. After the wireless communication module is enabled, communication, coordination, and monitoring can be carried out between various node devices. The main function of the

energy supply module is to provide energy for several other modules [22].

According to the nanotope architecture of the WSN, the energy consumed by the nodes for communication can be obtained:

$$E_{rt}(i,j) = E_{rx}(i,j) + E_{tx}(i,j). \quad (1)$$

Among them, $E_{\mathrm{rx}}(i,j)$ is the energy required for the node to receive a packet with a length of i bit, it is used by a node to send a packet of length i bits.

The energy $E_{\mathrm{rx}}(i,j)$ consumed by the node receiving a packet with a length of i bit can be expressed as

$$E_{\mathrm{rx}}(i,j) = E_{\mathrm{elec}} \times i. \quad (2)$$

In formula (2), E_{elec} is the energy required by the node receiving circuit to receive i bit data.

The energy $E_{\mathrm{tx}}(i,j)$ consumed by a node to send a packet with a length of i bit can be expressed as

$$E_{tx}(i,j) = E_{elec} \times i + \varepsilon_{amp} \times i \times j^{r}. \quad (3)$$

In formula (3), E_{elec} is the energy required by the node sending circuit to send i bit data, it is the amplification factor of the power amplifier circuit and related to the distance between two nodes in communication. And j is the distance between two nodes in communication.

When $j \le j_0$, there are

$$E_{\mathrm{tx}}(i,j) = E_{\mathrm{elec}} \times i + \varepsilon_{fs} \times i \times j^{2}. \quad (4)$$

When $j > j_0$, there are

$$E_{\mathrm{tx}}(i,j) = E_{\mathrm{elec}} \times i + \varepsilon_{\mathrm{mp}} \times i \times j^{4} \quad (5)$$

Incorporating formulas (4) and (5) into equation (1), the energy consumed by a node in the wireless sensor network to forward a packet of length i is

$$E_{\mathrm{rt}}(i,j) = \begin{cases} E_{\mathrm{elec}} \times i \times 2 + \varepsilon_{\mathrm{fs}} \times i \times j^{2} & j \le j_0 \\ E_{\mathrm{elec}} \times i \times 2 + \varepsilon_{\mathrm{mp}} \times i \times j^{4} & j > j_0 \end{cases}. \quad (6)$$

3.3.2. GPS Positioning. GPS is a new type of satellite-based navigation technology with all-round three-dimensional positioning and navigation on the ground, ocean, and space. As shown in Figure 4, the system has the characteristics of 24 hour, high accuracy, multifunction, fast positioning, etc. It can provide users around the world with three-dimensional navigation, speed, time, and other applications. GPS has been widely used in military and civilian fields.

GPS positioning refers to the calculation of the change in the time coordinate of the distance between the satellite in high-speed operation and the measurement point through GPS. It first obtains the position of the satellite from the navigation information, and then, the receiver calculates the distance of the carrier. The positioning principle is shown in Figure 5. There are two ranging methods: one is to calculate the time between the satellite and the receiver based on the coded information of the ranging, and the other is to measure the carrier phase based on the phase difference between the GPS satellite and the receiver. Both methods use four or more satellites for observation and then use pseudorange and phase to calculate the position of the carrier. But pseudorange positioning has better real-time performance and higher carrier phase accuracy [23, 24].

When the satellite sends a false stochastic code, the receiver will transmit the same false stochastic code. After a delay τ of propagation distance, the satellite signal reaches the receiver and is processed with the local code. The local code is moved to maximize the correlation. The GPS system uses a multisatellite high-orbit ranging system with distance-based ranging and uses four satellites for simultaneous falsely ranging to obtain the location of the receiver [25, 26].

GPS positioning has errors due to satellite timing parameters, satellite almanac parameters, refracted ambient parameters, antenna phase center deviation, and multipath effects. Positioning errors can be divided into regular systematic errors that can be corrected by humans and unexpected and uncertain random errors. The following errors are mainly analyzed.

3.3.3. Satellite Timing Parameters. The satellite timing parameter is the discrepancy that exists on the satellite ephemeris between the satellite orbit represented in the satellite ephemeris and the real orbit. The orbit error depends on the mathematical model of the orbit calculation, the software, the size of the tracking network used, the distribution of the tracking stations, and the length of the tracking station data observation time.

The following formula is usually used to estimate the influence of satellite orbit error on relative positioning:

$$\frac{1}{10}\frac{d\rho}{\rho} < \frac{dB}{\mathrm{B}} < \frac{1}{4}\frac{d\rho}{\rho}. \quad (7)$$

Among them, ρ is the radial position of the geometric distance from the satellite to the station; d is the satellite ephemeris parameter; B is the baseline vector length; dB is the baseline vector measurement error caused by the satellite ephemeris error.

3.3.4. Star Clock Error. Although a high-precision atomic clock is installed on the satellite, there are still problems such as frequency offset and frequency drift in the GPS system. The gap for the difference between the star clock and the GPS norm time difference is called the star clock error. The change of satellite clock can be simulated with a quadratic polynomial:

$$\Delta t = a_0 + a_1(t - t_0) + a_2(t - t_0)^2. \quad (8)$$

3.3.5. Ionospheric Delay. When an EMI wave travels thru the ionosphere, its path will curve and change its propagation rate. The delay of the ionosphere caused by the refraction

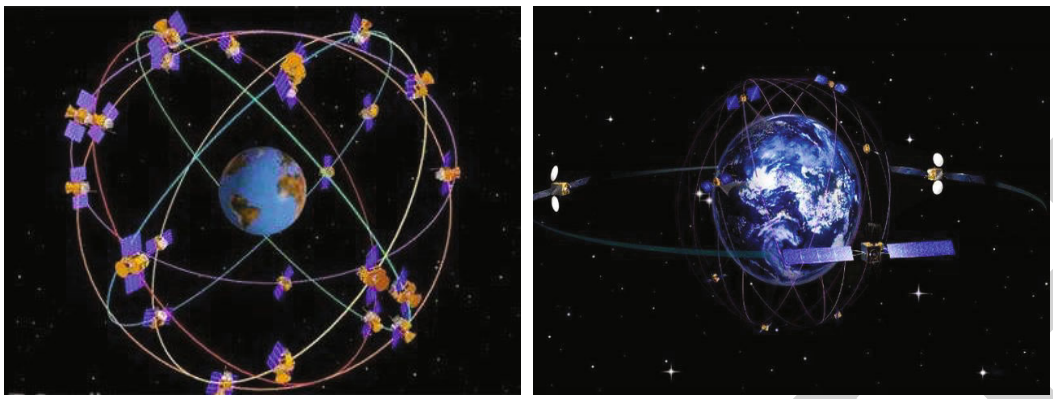

Figure 4: GPS positioning system chart.

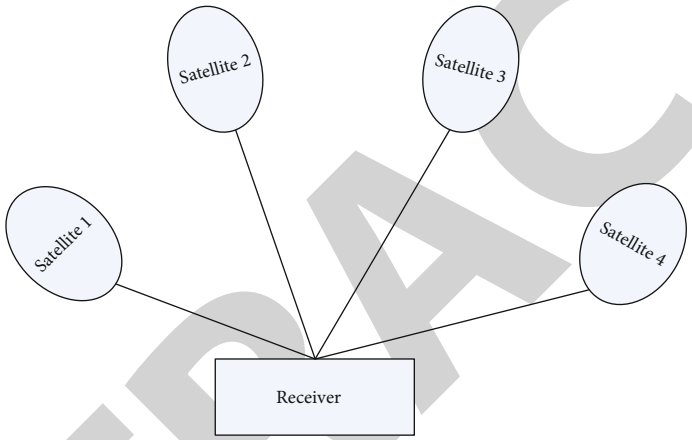

Figure 5: GPS positioning principle diagram.

Table 2: China's artificial intelligence medical market size.

Time	Market size of artificial intelligence in medical field/100 million yuan	Growth rate
2015	120	—
2016	160	0.25
2017	220	0.65
2018	415	0.7
2019	660	0.65
2020	890	0.4

of the ionosphere is the ionospheric delay, and the result can be expressed by the following equation:

$$\Delta\rho = \int (n-1)\mathrm{ds}. \tag{9}$$

Among them, n is the refractive index of the ionosphere. The phase refractive index in the atmosphere is

$$n_\rho = 1 - 40.28\frac{N_e}{f^2}. \tag{10}$$

The group refractive index is

$$n_g = 1 + 40.28\frac{N_E}{f^2}. \tag{11}$$

Therefore, the corresponding propagation path delay is

$$\Delta\rho_\rho = -40.28\frac{N_e}{f^2}, \tag{12}$$

$$\Delta\rho_g = 40.28\frac{N_\varepsilon}{f^2}. \tag{13}$$

In order to reduce the influence of the ionosphere, the following measures are usually used in GPS positioning: correction by using dual-frequency observation; correction by using the ionospheric model for single-frequency GPS user receivers; simultaneous observation of the same satellite or group of satellites by two or more receivers; and then the difference of the simultaneous observation values.

In the formula, f represents the frequency of the electromagnetic wave, and the total amount of electrons along

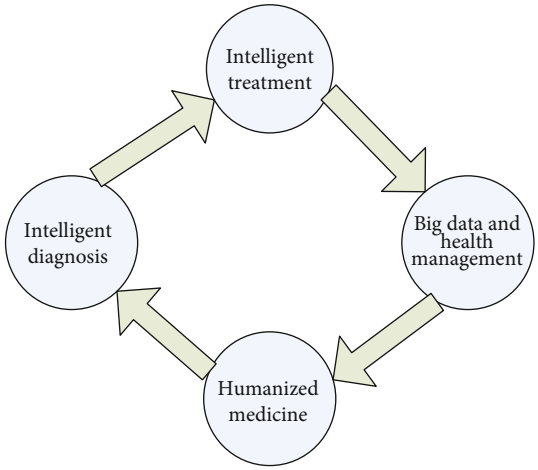

Figure 6: Intelligent medical structure diagram.

the propagation path of the electromagnetic wave N_ε is expressed as follows:

$$N_\varepsilon = \int N_e \mathrm{ds}. \tag{14}$$

3.3.6. Tropospheric Delay. Tropospheric delay generally refers to the delayed signal formed by the refraction of electromagnetic waves in the troposphere. Because the troposphere is not a dispersive medium for the propagation of electromagnetic waves. That is to say, the tropospheric delay has nothing to do with the frequency of the radio wave, and the dual-frequency correction method cannot be used to reduce its influence, and the model method can only be used [27]. The commonly used tropospheric delay model is the Hopfield model, and the model uses the following formula.

The latency of the dry Tropospheric Fraction in the Zeppo orientation is

$$\Delta D_{z,\mathrm{dry}} = 10^{-6} k_1 \frac{P_s}{T_s} \frac{H_d - h}{5}. \tag{15}$$

The latency of the wet Tropospheric Fraction in the Zeppo orientation is

$$\Delta D_{z,\mathrm{wet}} = 10^{-6} [k_3 + 273(k_2 - k_1)] \frac{e_s}{T_s^2} \frac{H_w - h}{5}. \tag{16}$$

Among them, the top heights of the dry and wet atmospheres are

$$H_d = 40136 + 148.72(T_s - 273.15)\mathrm{m}, \tag{17}$$

$$H_w = 11000\mathrm{m}. \tag{18}$$

Therefore, the total tropospheric delay of the zenith is obtained as

$$\Delta D_{z,\mathrm{trop}} = \Delta D_{z,\mathrm{dry}} + \Delta D_{z,\mathrm{wet}}. \tag{19}$$

The projection function of the wet and dry components with the following equation can be stated as

$$M_{\mathrm{dry}}(E) = \frac{1}{\sin\left[E^2 + \left(2.5^0\right)^2\right]^{1/2}}, \tag{20}$$

$$M_{\mathrm{wet}}(E) = \frac{1}{\sin\left[E^2 + \left(1.5^0\right)^2\right]^{1/2}}.. \tag{21}$$

4. System Verification

In the wave of deep learning, technologies such as visual recognition, speech processing, and natural language processing have all made huge breakthroughs. Artificial intelligence has gradually been widely used in the field of healthcare, and its focus is on medical and health management, medical services, rehabilitation, clinical scientific research, and drug development industry management. Table 2 shows the market size of artificial intelligence in the medical and health field.

In the context of the Internet of Things, the concept of smart medical treatment has emerged. Intelligent medical equipment is combined with modern artificial intelligence technology to perform intelligent diagnosis on medical data. In the field of treatment, surgical robots are used to perform intelligent treatment and to manage big data and normal health services. At the same time, it promotes humanized medical care and allows patients, hospitals, and doctors to communicate closely with each other. Finally, patients can achieve disease prevention and treatment. Figure 6 shows the smart medical structure diagram.

The wide utilization of AI technique in healthcare not only solves people's urgent needs for health but also promotes the integration and optimization of the entire medical industry. The rapid development of medical technology can intelligently analyze the patient's body data, synchronize medical, equipment, drug and other data, and process and update them in a timely manner. In this way, the core services of the medical platform can be improved and medical safety risks can be minimized. Currently, with the increasing innovation of IOT, Da Data, cloud computing, the intelligent sanitation management industry, and equipment have achieved rapid development. At home, people can use the Internet and medical equipment to seek medical treatment, check their health in a timely and convenient manner, and conduct disease prevention and early diagnosis. The intelligent medical Internet of Things solves the technical bottleneck and makes the health management model gradually enter the lives of ordinary people. With the user's health file as the core, through the integration of information technology, a medical and health service platform with the patient's health file as the core is established. Intelligent

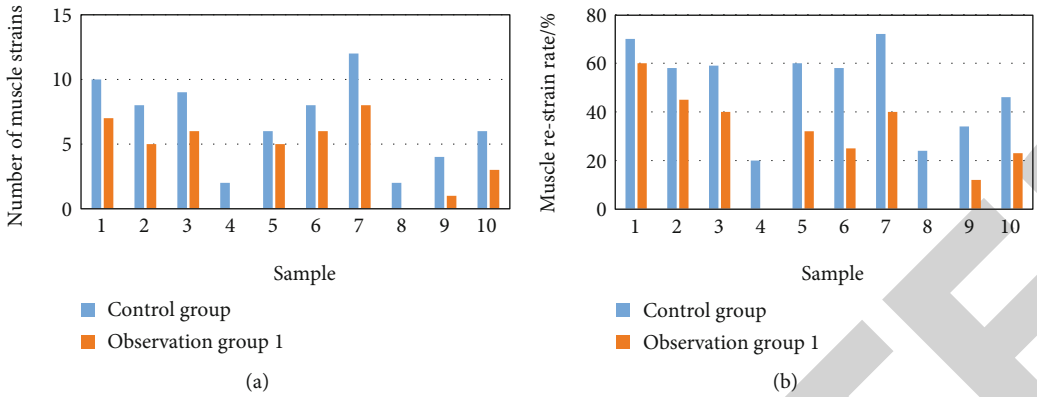

Figure 7: Diagram of muscle restrain.

Table 3: Self-feeling burden table.

	Before intervention	Control group intervention	Observation group 2 intervention
Sample 1	90	80	70
Sample 2	80	80	60
Sample 3	90	90	60
Sample 4	70	70	50
Sample 5	80	80	60
Sample 6	80	70	50
Sample 7	100	90	60
Sample 8	60	60	40
Sample 9	90	80	60
Sample 10	80	80	50

collection of patient data can enable better configuration of regional medical and health services and can also reduce risks in the medical process, allowing patients to enjoy better medical services under convenient and fast conditions.

The use of AI in the health care arena can be divided into three processes. The first process is medical informatization, that is, through various network technologies, medical data and information can be presented on multiple platforms; the second process is medical networking. Through RFID technology, Wind computing, Da Data, and other technologies, various links of network consultation, hospital visits, and postdiagnosis observation can be implemented smoothly, and medical accuracy and efficiency can be improved; the third process is intelligent medical treatment. It uses artificial intelligence machine learning and calculation methods for intelligent diagnosis, surgical robots for intelligent treatment, medical databases for tracking and analysis of cases, and electronic medical assistants to assist doctors in treatment. Realizing the intellectualization of the whole process of medical treatment and health care runs through the whole medical treatment. It includes disease prevention and health management before diagnosis, auxiliary diagnosis during diagnosis, clinical decision making, auxiliary post-diagnosis treatment and other auxiliary rehabilitation. At present, the adoption of AI in the healthcare arena in China is still in the second stage, but it is moving towards the third stage.

5. Experimental Design of Athlete Muscle Strain Rehabilitation

In order to observe the clinical effects of the middle and late rehabilitation treatment of muscle strains, three different treatment programs were performed on muscle strain patients during the muscle strain period, and the treatment effects and the incidence of restrains of the three groups of patients were observed.

Thirty cases of athletes with muscle strains, aged 18-24 years, were randomly chosen as study subjects. The athletes were split arbitrarily among reference team, experimental team 1, and experimental team 2, with 10 cases in each team. There was no apparent statistical difference in the strains among the three groups, and they were comparable.

The reference team received traditional muscle exercise rehabilitation treatment. And the specific methods were as follows: after 2 to 3 days of injury, perform restorative exercise on the injured part of the athlete. Under the protection of elastic bandages, first perform static training, then transition to dynamic training, and finally speed training. The best practice intensity is to reduce static training: Use exercises such as thigh tightening, calf tightening, and static resistance to statically contract the muscles for 5 to 10 seconds, with an interval of 10 to 20 seconds. Repeat the exercise 10 times, 1 to 2 times a day. Dynamic training: muscle contraction through exercises such as supine leg lift or prone straight leg, heel lift, and squat-up exercises. When the muscle is contracted to its maximum amplitude, keep it for $3 \sim 5$ s. Repeat the exercise 10 times, 1 to 2 times a day. Speed training: After the athlete's muscles have basically returned to normal, they can start running training and gradually complete the transition from jogging to normal running and fast running.

Experimental team 1 used intelligent magnetic resonance technology to make accurate diagnosis and assessment of muscle strain and then used acupuncture therapy to implement rehabilitation treatment. Specific method: Oblique acupuncture treatment is performed on the injured

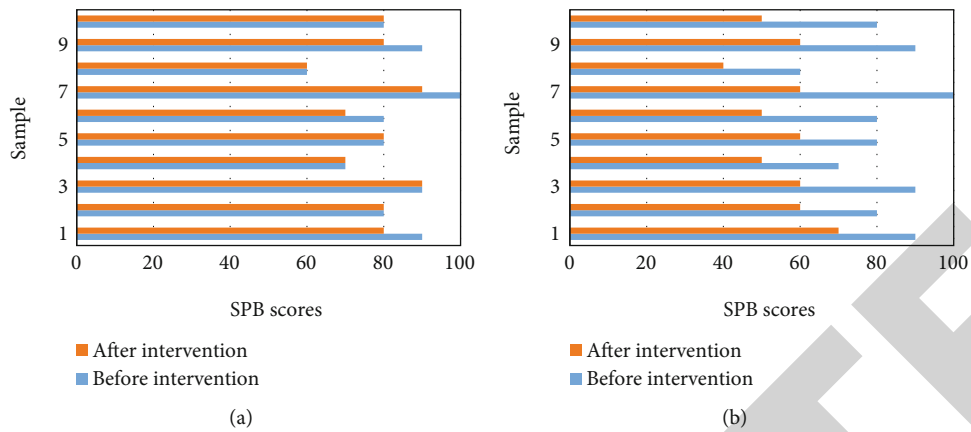

Figure 8: Self-perceived burden score chart.

Table 4: Quality of life assessment form.

Quality of life index	Marks
Feeling	25
Body movement	25
Self-care	25
Normal activity	25

area with a suitable filigree needle to find the most obvious tenderness point, and puncture the needle about 1 inch above, below, left, and right from the pain point. The needle and the skin form an angle of about 45 degrees, reaching the depth of the injured muscle bundle. The upper and lower needles are treated with an electroacupuncture instrument, with continuous wave treatment for 10 minutes, and then dense wave treatment for 10 minutes. It is once a day, the intervention time is two weeks.

Experimental team 2 added the content of cognitive and emotional intelligence intervention on the basis of conventional rehabilitation treatment. The specific measures are as follows: Adopt the method of diversion, use emotional communication, encourage patients to cultivate positive psychological cues, and enable patients to spontaneously and actively participate in sports exercises; Improve patients' cognitive execution ability and help patients formulate clear rehabilitation goals and daily plans; Enhance patients' awareness of participation, establish tripartite awareness of participation with patients and their families, communicate together, and give patients emotional support. The intervention time is two weeks.

5.1. Number and Rate of Muscle Strains. Figure 7(a) is a comparison diagram of the number of muscle strains among the reference team and experimental team 1. The abscissa is different sample cases, each group has 10 cases. The ordinate is the number of muscle strains. The average number of muscle restrains in the control group was 6.7 times, while the average number of muscle restrains in the observation group 1 was 4.1 times. Figure 7(b) is a comparison diagram of the muscle restrain rate among the reference team and experimental team 1. The abscissa is different sample cases, and the ordinate is the muscle restrain rate. The average restrain rate of muscles in the reference team was 50.1%, while the average restrain rate of muscles in experimental team 1 was 27.7%. As shown in Figure 7, both muscle tone and myotonia were remarkably less in experimental team 1 compared to the reference team. The incidence and prevalence of muscle injuries in the athletes under the artificial intelligence intervention were reduced compared to the conventional method.

5.2. Mental Health Assessment. Mental health assessment of patients. In this study, "self-perceived burden" was assessed as an indicator of "self-perceived burden." This scale is divided into 10 items with a total score of 100. The higher the score, the higher the psychological stress of the patient and the worse his or her mental state. Table 3 shows the SPB scores of the control group and the experimental team 2.

Figure 8(a) shows the SPB scores of the control group before and after the intervention, and Figure 8(b) shows the SPB scores of the observation group 2 before and after the intervention. The abscissas and ordinates are the sample and SPB scores, respectively, with an average SPB score of 82 points before intervention. The average SPB score of athletes in the control group was 78 points after the intervention, and the average SPB score of the observation group 2 after the intervention was 56 points. It can be seen from Figure 8 that the self-perceived burden after the intervention is lower and the mental health status is better. The degree of mental health under the intervention of emotional intelligence is significantly better than that of conventional treatment programs.

5.3. Life Quality Assessment. The patients' quality of life was assessed to evaluate the quality of survival both preintervention and postintervention. Four quality-of-life rating scales were used, including four items: sensory, motor, self-care, and normal activities. The higher the mark, the greater the improvement in quality of life, as shown in Table 4.

Figure 9(a) shows the evaluation scores of the athletes' quality of life in observation group 1 before and after the

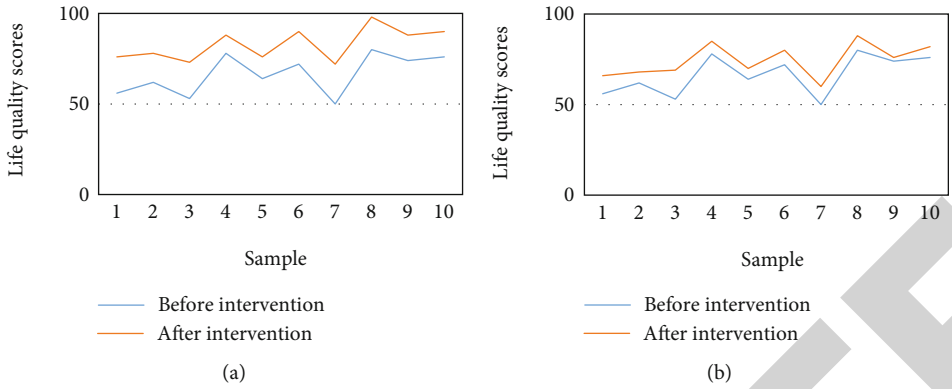

Figure 9: Quality of life score chart.

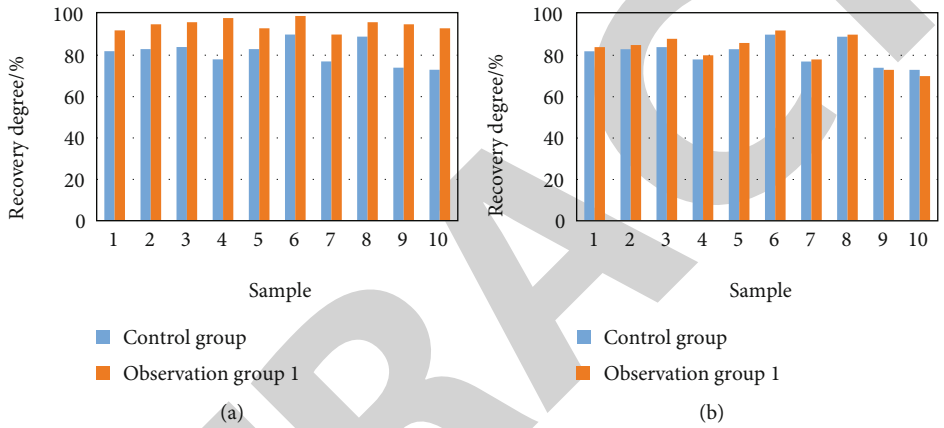

Figure 10: Rehabilitation degree comparison chart.

intervention, and Figure 9(b) shows the evaluation scores of the athletes' quality of life in observation group 2 before and after the intervention. The abscissa is the sample case, and the ordinate is the quality of life assessment score. The athletes' average quality of life score before intervention was 66.5. The mean quality of life score after the intervention was 82.9 for experimental team 1 and 74.4 for experimental team 2 after the intervention. As shown in Figure 9, the quality of life scores were higher postintervention than preintervention. After the intervention, the score of quality of life was significantly higher in experimental team 1 than in experimental team 2.The quality of life was better in the AI intervention group compared to the emotional intelligence intervention group.

5.4. Degree of Rehabilitation. Figure 10(a) shows the rehabilitation degree of athletes in the reference team and experimental team 1 after intervention, and Figure 10(b) shows the rehabilitation degree of athletes in the reference team and experimental team 2 after intervention. The average rehabilitation degree of the athletes in the reference team was 81.3%, the average rehabilitation degree of the athletes in the experimental team 1 was 94.7%, and the average rehabilitation degree of the athletes in the experimental team 2 was 82.6%. It can be seen from Figure 10 that the average rehabilitation degree of the athletes in reference team 1 is higher than that of reference team 2 and the reference team, and the effect of emotional intelligence intervention on the rehabilitation degree of athletes is not obvious. The average rehabilitation degree under artificial intelligence intervention is higher than the average rehabilitation degree under emotional intelligence intervention.

6. Conclusion

The experimental findings have shown that the mean time of muscle restrain under AI intervention was 4.1, and the average restrain rate of muscles is 27.7%, and the average recovery degree of athletes is 94.7%; In the reference team, the average number of muscle restrains was 6.7 times, the average muscle restrain rate was 50.1%, and the average recovery degree of athletes was 81.3%. In contrast to the reference team, the number of muscle strains under the intervention of artificial intelligence was significantly reduced, and the degree of recovery was higher; the mental health under the intervention of emotional intelligence was better. Moreover, under the intervention of artificial intelligence, the quality of life of athletes is better than that under the intervention of emotional intelligence. In summary, artificial intelligence intervention has a significant effect on the promotion of

Hindawi
Computational and Mathematical Methods in Medicine
Volume 2023, Article ID 9767846, 1 page
https://doi.org/10.1155/2023/9767846

Retraction

Retracted: Information Monitoring of Animal Husbandry Industry Based on the Internet of Things and Wireless Communication System

Computational and Mathematical Methods in Medicine

Received 27 June 2023; Accepted 27 June 2023; Published 28 June 2023

This article has been retracted by Hindawi following an investigation undertaken by the publisher [1]. This investigation has uncovered evidence of one or more of the following indicators of systematic manipulation of the publication process:

(1) Discrepancies in scope

(2) Discrepancies in the description of the research reported

(3) Discrepancies between the availability of data and the research described

(4) Inappropriate citations

(5) Incoherent, meaningless and/or irrelevant content included in the article

(6) Peer-review manipulation

The presence of these indicators undermines our confidence in the integrity of the article's content and we cannot, therefore, vouch for its reliability. Please note that this notice is intended solely to alert readers that the content of this article is unreliable. We have not investigated whether authors were aware of or involved in the systematic manipulation of the publication process.

Wiley and Hindawi regrets that the usual quality checks did not identify these issues before publication and have since put additional measures in place to safeguard research integrity.

We wish to credit our own Research Integrity and Research Publishing teams and anonymous and named external researchers and research integrity experts for contributing to this investigation.

The corresponding author, as the representative of all authors, has been given the opportunity to register their agreement or disagreement to this retraction. We have kept a record of any response received.

References

[1] Y. Shen, "Information Monitoring of Animal Husbandry Industry Based on the Internet of Things and Wireless Communication System," *Computational and Mathematical Methods in Medicine*, vol. 2022, Article ID 8794044, 12 pages, 2022.

Hindawi
Computational and Mathematical Methods in Medicine
Volume 2022, Article ID 8794044, 12 pages
https://doi.org/10.1155/2022/8794044

Research Article

Information Monitoring of Animal Husbandry Industry Based on the Internet of Things and Wireless Communication System

Yuhong Shen

Physics and Electronic Information College, Hulunbuir University, Hulunbuir, 021008 Inner Mongolia, China

Correspondence should be addressed to Yuhong Shen; syh2005@hlbec.edu.cn

Received 21 January 2022; Revised 24 February 2022; Accepted 8 March 2022; Published 28 March 2022

Academic Editor: Muhammad Zubair Asghar

This paper was aimed at discussing the information monitoring of animal husbandry based on the Internet of Things and wireless communication system. The breeding and health of animals in the breeding industry has always been a topic that people talk about. The advent of the wireless communication system has made monitoring and positioning technologies more and more simple. The wireless communication network technology is applied to the environmental monitoring of animal breeding farms, and a real-time reporting system is designed to pay attention to animal health in real time. This article focuses on the connection between the two. First, this article briefly describes the state of the wireless communication network and the aquaculture industry, furthermore explains the research methods, such as the livestock breeding environment monitoring system model, which needs to have the characteristics of humanization, fast and simple, easy to maintain, high reliability, compatibility, scalability, and intelligence, and designs related monitoring systems and hardware systems to integrate carbon dioxide, ammonia, and other gas sensors with temperature and humidity sensors to sense the environment. Next, this article shows the wireless communication network monitoring and positioning algorithm, namely, the TOA-based wireless communication positioning algorithm and the LTE prediction algorithm. The predicted time is used as the link weight, and the weight within the wide link cluster is defined according to the time threshold, making the link maintain stability for a short time to enhance the network topology. Then, this article conducts experiments based on ZigBee wireless communication network sensor combined with improved genetic algorithm in the temperature and humidity test of farms, designs the environmental monitoring system, improves the algorithm, and cooperates with experiments and analysis to verify the feasibility and apply it to the temperature and humidity test of the livestock farm. The results are good, and the temperature and humidity errors are reduced by 88.28% and 84.21%, respectively. It has a certain degree of guidance. Finally, it is discussed and summarized. It can be seen that the system and algorithm designed in this paper have a good prospect in the development of animal husbandry. However, this algorithm takes a long time and has a broader research space.

1. Introduction

The economic situation in the society is constantly improving, so people's requirements for living standards are also constantly improving, and the demand for fresh meat food is rising day by day. In such an environment, people's requirements for food quality will be more stringent, safe and harmless, green and pollution-free, etc., which has become one of the criteria for judging the quality of food. Therefore, the country's requirements for the breeding industry are even more stringent, especially the emergence of unfavorable infectious diseases such as avian influenza and mad cow disease, which necessitates changes and improvements in the prior breeding technology. The use of new breeds and detection and monitoring technologies can adapt to the needs of the general environment. This article focuses on the breeding situation of animals in livestock houses and conducts targeted research and exploration in terms of breeding process, breeding environment, breeding monitoring, etc., and establishes a low-cost, high-stability livestock breeding environment monitoring system suitable for the breeding

industry. Livestock breeding has gradually been industrialized, diversified, and integrated, but the breeding environment is still a major problem hindering the development of the breeding industry. Therefore, farmers should focus on calibrating the standards of the breeding environment. The breeding environment has a greater impact on the stable growth of livestock, and summer and winter are very unfavorable for livestock production, resulting in a decrease in livestock production capacity by about 10% to 20%. At the same time, high temperature and cold will also have a great impact on the health and development of livestock. Therefore, timely and effective monitoring of the quality of the breeding environment can reduce the impact of the environment on livestock to a reasonable range. The temperature and humidity in the breeding environment, gas concentration, light intensity and intensity, etc., will all have varying degrees of impact on the development and reproduction of livestock, and it is necessary to arrange corresponding sensors. It is necessary to analyze and establish the breeding environment in advance. According to the environmental characteristics, it is necessary to arrange suitable monitoring facilities and systems, so as to monitor the harmful components in the breeding environment in real time and provide powerful reference data for subsequent treatment and improvement.

ZigBee communication networking technology has been widely used in various fields, especially in the field of low speed; it has been widely used in M2M industries in the IoT industry chain, such as smart grid, smart transportation, smart home, finance, mobile POS terminals, supply chain automation, industrial automation, smart buildings, fire protection, public safety, environmental protection, meteorology, digitalization Medical, telemetry, agriculture, forestry, water, coal, petrochemical, and other fields [1, 2]. In the short-distance wireless personal local area networks, the emergence of this technology has played a vital role in the establishment of a breeding environment monitoring system. Whether it is data transmission or remote control and viewing, it needs to be developed and designed based on ZigBee technology. Through this technology, a high proportion of automatic operations can be realized, such as automatic transmission and processing of data and automatic generation of data curve graphics, and remote control and viewing functions of users can also be realized. Under the guidance of this technology, various troubles caused by complicated on-site wiring and postmaintenance are avoided. The construction cost and maintenance cost of traditional breeding environment detection technology are much higher than this technology. Not only that ZigBee technology is far superior to traditional detection technology in terms of data acquisition accuracy, sensitivity, and transmission performance. While bringing convenience to users, it also brings obvious advantages of low cost and high experience. This technology can provide stable and reliable technical support for monitoring and control and improve the current breeding management mode and has great significance in terms of breeding safety, quality, and safety.

This article uses ZigBee communication networking technology to design an environmental monitoring system that can monitor temperature, humidity, NH3 concentration, etc., combined with the proposed algorithm based on traditional genetic algorithms, mutation operators, and hybrid operators to improve the temperature in the farm, using humidity sensor test experiment. Finally, it is concluded that there are better results, small errors, stable performance, and strong guidance.

2. Related Work

Wireless network communication technology has research significance in various fields. Yuan et al. studied the approximate traversal secrecy rate of the two beamformers of the relay: (1) generalized matched forwarding (GMF) beamformer to maximize the legal channel rate and (2) general rank beamformer (GRBF). In addition, a lower limit maximization (LBM) beamformer at the relay is also discussed, which is used to maximize the lower limit of the traversal secrecy [3]. Yao et al. considers a cluster-based cooperative spectrum sensing (CSS) scheme in the Energy Harvesting Cognitive Wireless Communication Network (EH-CWCN), in which cognitive nodes (CN) are clustered according to their received power levels to improve sensing performance. In the CSS scheme, time resources are limited and shared by energy harvesting, spectrum sensing, and data transmission [4]. Jee et al. said that there are more than 300 standard blocks defined in the IEC61131-3 standard, but the existing mutation operator set does not fully cover the functional elements of the FBD program. And by comprehensively considering the functional elements that can be used in the FBD program and the types of errors that may appear in the FBD program, additional mutation operators are defined and through a case study to evaluate the impact of mutation operator expansion [5]. Zhang and Ming believes that its application is limited due to its imperfect search structure and the risk of falling into a local optimum. In order to improve the performance of the algorithm, an optimized GWO (MR-GWO) based on mutation operator and elimination reconstruction mechanism is proposed. The introduction of mutation operator facilitates better search, and the elimination-reconstruction mechanism is adopted for the search of the difference, which not only effectively expands the random search but also accelerates its convergence [6]. Friggens et al. said that as the environment for raising livestock becomes more and more variable, the robustness of animals has become an increasingly valuable attribute. Therefore, people pay more and more attention to its management and cultivation. However, robustness is a phenotype that is difficult to correctly characterize because it is a complex feature consisting of multiple components, including dynamic elements, such as response rate and recovery rate to environmental disturbances [7]. In view of the current situation of green environmental protection lighting policy and the problems of high automation, low energy efficiency, and difficult management of traditional residential lighting systems, Liang and Xu proposed a residential community street lamp monitoring and management system based on ZigBee and GPRS. This design is proposed using sensor technology, ZigBee, and GPRS wireless communication technology network. In order to realize intelligent lighting parameter adjustment, a coordinated control method of multiple sensors is adopted [8]. These studies have a certain degree of guidance, but there are insufficient arguments or insufficient precision, which can be further improved.

3. Livestock House Monitoring Model and Wireless Communication Network Algorithm

3.1. Model of Monitoring System for Livestock Breeding Environment. The design and realization of the whole system should be changed according to the actual situation. The layout of the various sensors in the entire system also needs to be adapted to local conditions and cannot cause cumbersome and interference [9, 10]. Therefore, the overall system design needs to be carried out in accordance with the following rules:

(1) Humanization of operation: the whole system highlights the intelligent mode of human-computer interaction. It is not only necessary to pay attention to the richness of system functions but also to consider whether the various functions will cause operational problems for farmers and workers. The main interface of the system should display the frequently used functions and operation buttons, which can be reached directly by one key without repeated operations. At the same time, efforts should be made to reduce the operational interference items in the software design to prevent the adverse consequences caused by misoperation [11]

(2) Fast and simple: the operation of the various sensing lines in the system can be adjusted quickly, while providing users with a higher degree of freedom of independent customization functions. The system must not only preset a certain amount of practical parameters but also provide users with space for independent adjustment. And in the interface of the data report of the sensor, the displayed data strives to be simple and direct [12]

(3) Easy to maintain and high reliability: because the user groups of the system are generally farmers and workers, all require both software and hardware to maintain good stability under long-term working conditions. At the same time, the reserved software and hardware maintenance interface should also be easy to view. The data acquisition equipment of the sensor needs to have the function of directly displaying the data in order to read and analyze the data intuitively [13]

(4) Compatible scalability: as mentioned above, when designing software and hardware, it is necessary to reserve interfaces for subsequent maintenance. These interfaces also have to undertake upgrades and extensions to reduce the user's expenditure in subsequent use. The entire system should achieve dual compatibility and stable use of software and hardware for various equipment and new equipment to be implemented in the future. In this way, the entire system can maintain a long use cycle without causing waste of resources [14]

(5) Intelligence: in the current technological environment, artificial intelligence is a big craze. In terms of software functions, it is necessary to intelligently recognize and correct errors and eliminate risks for users in a timely manner. At the same time, prompt and notify in a conspicuous position to improve work efficiency [15]

The livestock breeding environment monitoring system is designed based on a variety of existing mature technologies, such as database technology, remote communication technology, sensor technology, and computer technology. Therefore, from an overall perspective, the entire system has the characteristics of complexity and comprehensiveness. The whole system consists of three parts, namely, environmental monitoring communication networking equipment, data collection system, and remote reading system. The data collection system has functional modules such as visual report definition, audit relationship definition, report approval and release, data reporting, data preprocessing, data review, and comprehensive query statistics. The specific framework is shown in Figure 1.

The environmental monitoring communication networking equipment is composed of a variety of sensors and network equipment. Among them, the sensors include temperature and humidity detection, light intensity detection, and gas concentration detection, and the network equipment is mainly based on ZigBee networking equipment, GRPS wireless communication, and RS485-wired communication equipment [16, 17]. Therefore, the entire system has both wired communication and wireless communication functions, which can be operated on the spot, and can also be controlled remotely, which enriches the user's choice space. The remote reading system is mainly able to provide users with mobile terminal query and control functions, including sensor data query, overall data curve query, and remote control of related hardware devices [18]. The data collection system mainly provides operations such as data collection, processing, and uploading and at the same time receives remote instructions from the user's mobile terminal [19].

The normal operation of the software is based on hardware. Therefore, the hardware system is the physical basis of the entire livestock breeding environment monitoring system. When the hardware system meets the conditions, we can optimize more physical devices, such as display screens and communication antennas. The hardware system includes environmental monitoring and communication networking equipment. The responsibility of these equipment is to detect the data in the environment and transmit it to the cloud in real time [20]. Environmental monitoring and communication networking are interdependent, and the data provided by environmental monitoring equipment needs to be transmitted and stored to the data collection system through the communication networking equipment. Figure 2 shows the overall structure of the hardware system.

In the entire livestock breeding environment, the space occupied by the equipment is optimized, and the carbon dioxide, ammonia, and other gas sensors and the temperature and humidity sensors are integrated on a panel, which is called the parameter sensing concentrator in the breeding environment [21]. The device has both networking and wired interfaces, namely, RS485 and ZigBee, which is convenient for data upload. At the same time, the equipment is equipped with an LCD display screen and supports keyboard operation,

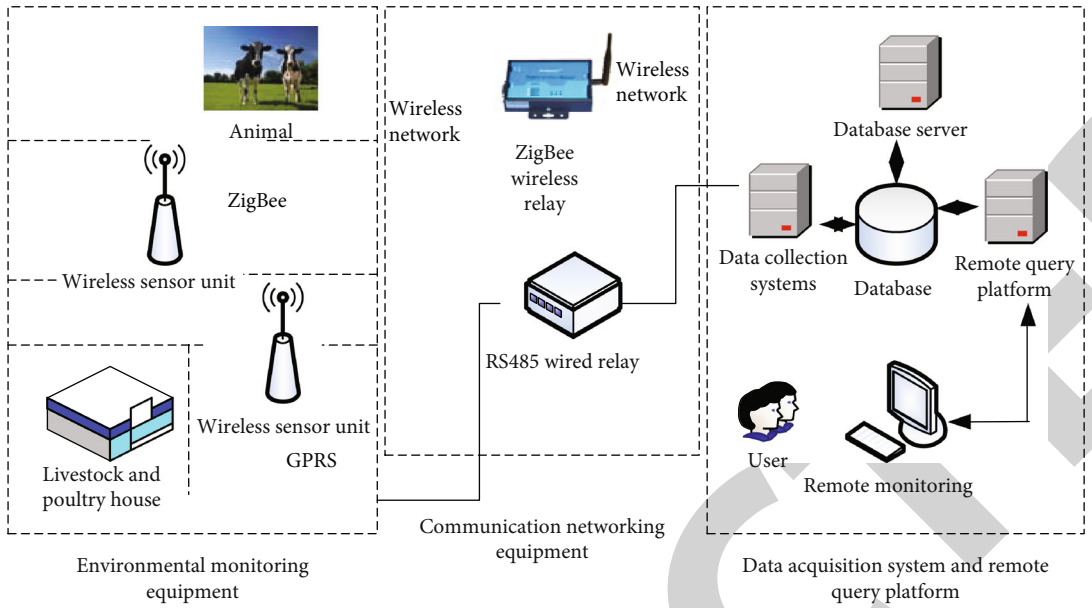

Figure 1: The structure of the monitoring system for livestock breeding environment.

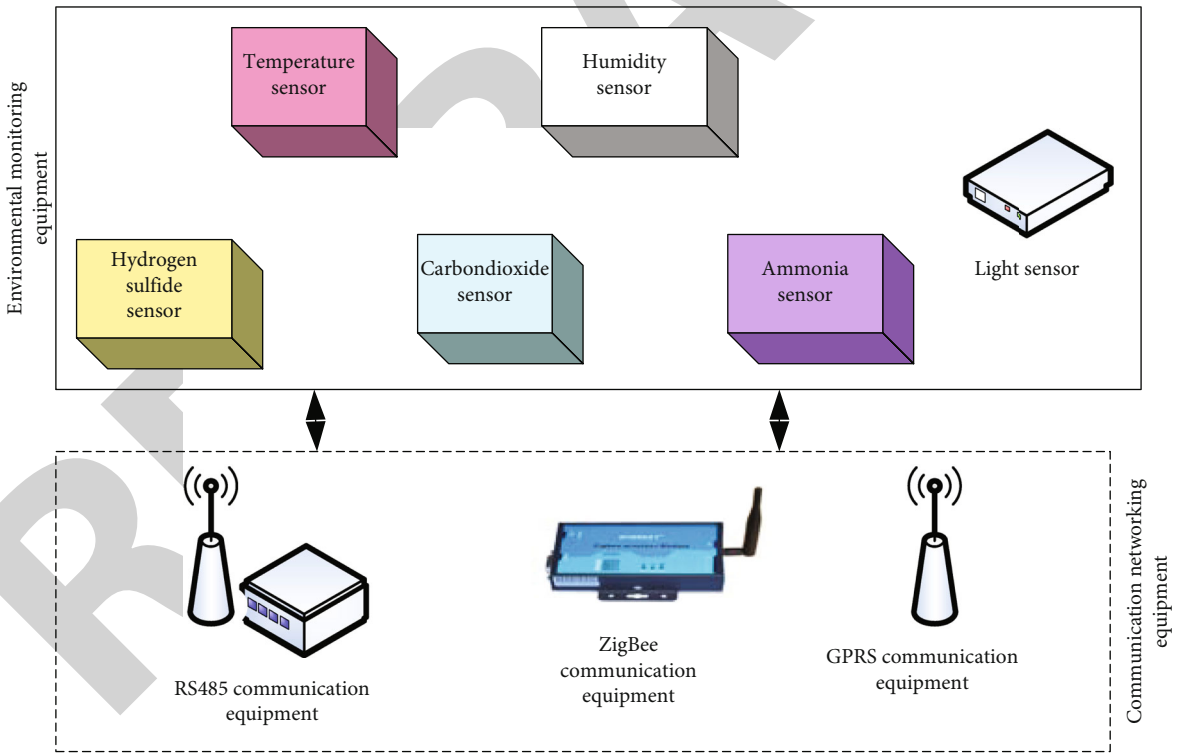

Figure 2: The overall hardware structure of the livestock breeding environment monitoring system.

which is convenient for real-time on-site query and analysis of environmental data. The concentrator effectively reduces the environmental space occupied by multisensor laying and realizes multifunctional integration under the small-sized precursor [22]. Therefore, the device cannot only be fixed in a certain environment for use, but its high degree of integration makes it easy to carry. The overall structure of the environmental parameter sensing concentrator is shown in Figure 3.

3.2. Wireless Communication Network Monitoring and Positioning Algorithm

3.2.1. TOA-Based Wireless Communication Positioning Algorithm. When there are more than 3 wireless network node distance measurement values, the corresponding two-dimensional estimation result will be obtained. At this time, a set of nonlinear equations will be formed. The solution to this equation is the exact positioning point. This equation is obtained by combining the distance equations of the node and the mobile terminal in the LOS environment. The trilateral algorithm in this problem is shown in Figure 4.

This problem can be solved by the maximum likelihood method and the least square method. In the maximum likelihood method, the optimal estimation value must satisfy the maximum condition probability density function. Letting $\widehat{\phi} = [\widehat{a}, \widehat{b}]^n$ be the estimated coordinates and $\phi = [a, b]^n$ be the real coordinates, n in the estimated coordinates is the bias factor. Letting $\widehat{w} = w + s$ be the ranging vector of the wireless communication base station and s be the zero mean Gaussian noise and be in the independent and identically distributed state, then the conditional probability p can be obtained as

$$\widehat{\phi} = \arg \max_{\phi} p(\widehat{w}|\phi),$$
$$p(\widehat{w}|\phi) = \prod_{k=1}^{M} \frac{1}{\sqrt{2\pi\sigma_k^2}} \exp\left\{-\frac{(\widehat{w}_k - w_k)^2}{2\sigma_k^2}\right\}. \quad (1)$$

In this formula, σ_k^2 is the variance of the k ranging noise. At this time, the approximate maximum likelihood algorithm is used to solve the problem that cannot be solved in the maximum likelihood method. The approximate likelihood method used is a two-step ML (TS-ML) algorithm. There are also linear least squares and nonlinear least squares based on TOA data, letting $\lambda_{ef}(\phi)$ be the prediction result and the difference measurement between Euclidean distance $\|\phi - \phi_k\|$ and distance measurement $\widehat{w}_k$ between wireless communication base stations. μ_k is one of the weighted values, which can adjust the weight of the equation. The algorithm can obtain the weight value based on the variance value of the node data and other data, and then, the positioning estimation algorithm of the nonlinear algorithm is

$$\widehat{\phi} = \arg \min_{\phi}\{\lambda_{ef}(\phi)\} = \arg \min_{\phi}\left\{\sum_{k=1}^{m} \mu_k(\widehat{w}_k - \|\phi - \phi_k\|)^2)\right\}. \quad (2)$$

The linear least squares rule is to linearize a nonlinear equation:

$$G(\phi) = \begin{bmatrix} \sqrt{(a-a_1)^2 + (b-b_1)^2}, \\ \sqrt{(a-a_2)^2 + (b-b_2)^2}, \\ \vdots \\ \sqrt{(a-a_M)^2 + (b-b_M)^2}. \end{bmatrix} \quad (3)$$

The coordinate of base station m is $[x_m, y_m]$, and it is expanded at position ϕ_0 through Taylor expansion. There is $G(\phi) \approx G(\phi_0) + Q(\phi - \phi_0)$, and $Q(\phi - \phi_0)$ are the Jacobian matrix with Q at position ϕ_0, and we can get

$$Q = \begin{bmatrix} \frac{\partial g_1}{\partial a} & \frac{\partial g_2}{\partial a} & \cdots & \frac{\partial g_m}{\partial a} \\ \frac{\partial g_1}{\partial b} & \frac{\partial g_2}{\partial b} & \cdots & \frac{\partial g_m}{\partial b} \end{bmatrix}^N_{\phi=\phi_0}. \quad (4)$$

At this time, the solution of the linear least squares can be solved as

$$\widehat{\phi} = \phi_0 + \left(Q^H Q\right)^{-1} Q^H [\widehat{w} - G(\phi_0)], \quad (5)$$

where H represents the Hermitian transposition and the lower bound of the Krameruo offline prediction variance using the LLS positioning algorithm:

$$E\left[\left(\widehat{\phi} - \phi\right)^2\right] \geq I^{-1}(\phi). \quad (6)$$

$E(\bullet)$ is the expected value, and $\mathrm{I}(\varphi)$ is the Fisher information matrix; we can get

$$I(\varphi) \triangleq E\left[\left(\frac{\partial}{\partial\varphi} \ln g(\widehat{w}|\varphi)\right)^2\right] = E\left[\frac{\partial}{\partial\varphi} \ln g(\widehat{w}|\varphi) \cdot \left(\frac{\partial}{\partial\varphi} \ln g(\widehat{w}|\varphi)\right)^N\right]. \quad (7)$$

In formula (7), $g(\widehat{w}|\phi)$ is the joint PDF of $\widehat{w}$; letting $\widehat{w} = w + s$ be the true distance between the wireless communication base station and the MS, s is the zero mean Gaussian noise, and w is a function of ϕ, because

$$\frac{\partial}{\partial\phi} \ln g(\widehat{w}|\phi) = \frac{\partial w}{\partial\phi} \cdot \frac{\partial}{\partial w} \ln g(\widehat{w}|w). \quad (8)$$

So,

$$I(\phi) = E\left[\frac{\partial}{\partial\phi} \ln g(\widehat{w}|\phi) \cdot \left(\frac{\partial}{\partial\phi} \ln g(\widehat{w}|\phi)\right)^N\right] =$$
$$\frac{\partial w}{\partial\phi} E\left[\frac{\partial}{\partial\phi} \ln g(\widehat{w}|\phi) \cdot \left(\frac{\partial}{\partial\phi} \ln g(\widehat{w}|\phi)\right)^N\right] \frac{\partial w^N}{\partial\phi}, \quad I(\phi) = QI_w Q^N, \quad (9)$$

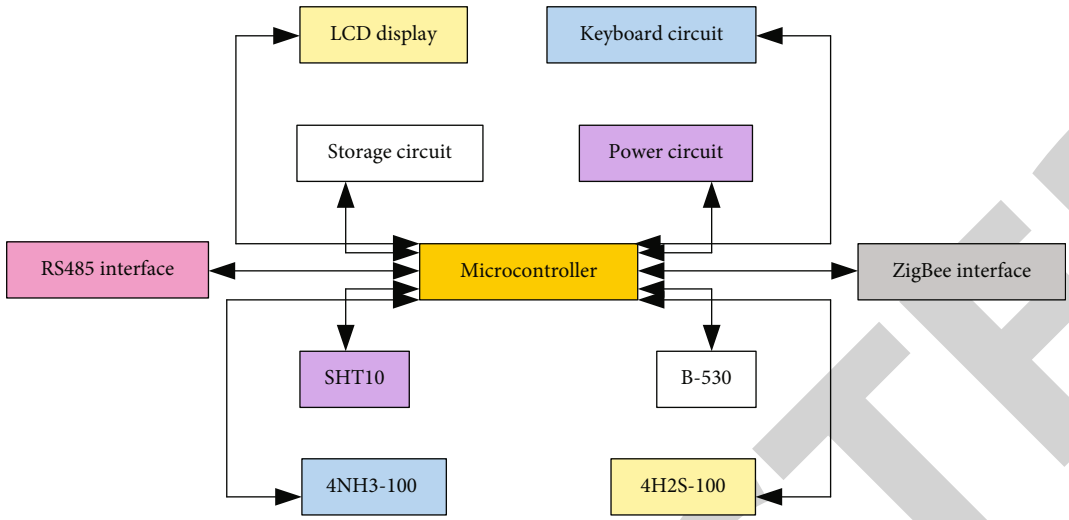

Figure 3: Equipment structure of aquaculture environment parameter sensing concentrator.

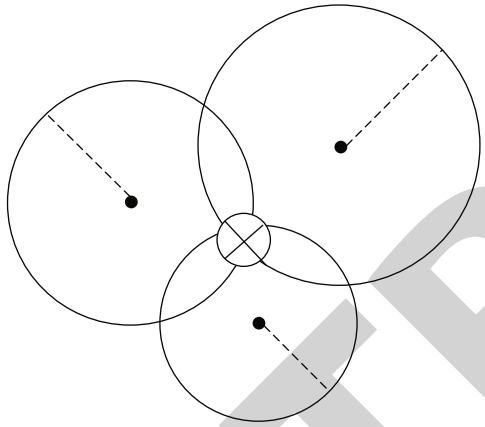

Figure 4: Concept of trilateral positioning algorithm.

where Q is

$$Q = \begin{bmatrix} \frac{a-a_1}{\sqrt{(a-a_1)^2+(b-b_1)^2}} & \cdots & \frac{a-a_M}{\sqrt{(a-a_N)^2+(b-b_M)^2}} \\ \frac{b-b_1}{\sqrt{(a-a_1)^2+(b-b_1)^2}} & \cdots & \frac{b-b_M}{\sqrt{(a-a_N)^2+(b-b_M)^2}} \end{bmatrix},$$
$$I_w = \Sigma^{-1} = \operatorname{diag}\left(\sigma_1^{-2}, \sigma_1^{-2}, \cdots, \sigma_M^{-2}\right). \tag{10}$$

It can get the CRLB of MS position estimation:

$$I(\phi)^{-1} = \left(QI_wQ^N\right)^{-1}. \tag{11}$$

3.2.2. LTE Prediction Algorithm. This algorithm uses an effective link time prediction algorithm to stabilize the network state; the actual link survival time value and the estimated time value can be estimated under the condition that the error formed is not large. Figure 5 is a simplified time estimation model to simplify the complex calculation data.

Taking the coordinates of the rectangular coordinate system as the model vector, then use the vector to get the correlation quantity. At this time, the coordinate of m is $S_m = (x_m, y_m)$, and the coordinate of n is $S_n = (x_n, y_n)$, and the initial speed is v_{mo} and, and the acceleration is a_{mo} and a_{no}. The target rates are v_{mp} and v_{np}, and the model directions are $\mu$and ω. The specific calculation process of LTE is as follows:

(i) Step 1: the initial rate and v_{no} target rate of nodes m and n are as follows:

$$\begin{aligned} v_{mo} &= (v_{mo}\sin\mu, v_{mo}\cos\mu) \\ v_{mp} &= (v_{mp}\sin\mu, v_{mp}\cos\mu) \\ v_{no} &= (v_{no}\sin\omega, v_{no}\cos\omega) \\ v_{np} &= (v_{np}\sin\omega, v_{np}\cos\omega) \end{aligned} \tag{12}$$

(ii) Step 2: the initial relative speed v_o and target relative speed $v_p$between nodes m and n are as follows:

$$\begin{aligned} v_o &= v_{mo} - v_{no} = (v_{mo}\sin\mu - v_{no}\sin\omega, v_{mo}\cos\mu - v_{no}\cos\omega) \\ v_p &= v_{mp} - v_{np} = (v_{mp}\sin\mu - v_{np}\sin\omega, v_{mp}\cos\mu - v_{np}\cos\omega) \end{aligned} \tag{13}$$

(iii) Step 3: calculating the relative position S and distance d between nodes m and n:

$$S = S_n - S_m = (x_n - x_m, y_n - y_m), d = |S| \tag{14}$$

In this formula, x_m and y_m, respectively, refer to the size of the abscissa and ordinate of the node m, and similarly, x_n and y_n, respectively, refer to the size of the abscissa and ordinate of the node n

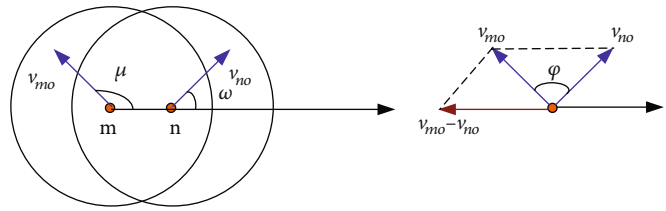

Figure 5: Link survival time estimation model.

(iv) Step 4: obtaining the required movement distance h and relative acceleration a' outside the included angle ϕ and the communication range k between nodes m and n through the above formula:

$$\begin{aligned} v_o \cdot S &= |v_o||S| \cos \phi \\ h^2 + d^2 - 2hd \cos \phi &= k^2 \\ a' &= |a_m - a_n| \end{aligned} \tag{15}$$

In this formula, a_m and a_n, respectively, represent the acceleration of each node and its neighboring nodes

(v) Step 5: solving the time required for the node from the initial relative speed to the final relative speed t_o and the travel distance of the acceleration phase l_o:

$$t_o = \frac{v_p - v_o}{\hat{a}} ; l_o = \frac{v_p^2 - v_o^2}{2\hat{a}} \tag{16}$$

(vi) Step 6: determining whether the movement distance of the acceleration stage is smaller than the movement distance, make the node perform a uniform linear movement, let t_2 be the node acceleration time, and solve the link survival time $LTE(m, n)$:

$$\begin{aligned} l_o + v_p t_1 &= h ; LET(m, n) = t_o + t_1 \\ v_o t_2 + \frac{1}{2}\hat{a}{t_2}^2 &= h ; LET(m, n) = t_2 \end{aligned} \tag{17}$$

1The link survival time is solved. The predicted time is used as the link weight, and the weight in the wide link cluster is defined according to the time threshold. Promoting the link will not be disconnected for a short time, maintain continuous stability, thereby enhancing the network topology

4. Experiments Based on ZigBee Wireless Communication Network Sensor Combined with Improved Genetic Algorithm in the Temperature and Humidity Test of Farms

4.1. Design of a Farm Information Monitoring System Based on ZigBee Wireless Communication Network Sensors. The information collection subsystem in the breeding environment is mainly composed of three nodes, which are sensor detection nodes, router nodes, and coordinator nodes. The coordinated work of the three has enabled the ZigBee wireless communication technology with CC2530 as the core to successfully collect data in the breeding environment [23]. Among the three nodes, the sensor detection node is mainly responsible for collecting real-time data of various sensors in the breeding environment, such as temperature and humidity, gas concentration, and water and electricity consumption. The layout of sensor detection nodes requires a reasonable analysis of the breeding environment. Through the data collection of all sensor detection nodes in the breeding environment, after calculation by the ZigBee sensor node, the data is converted into data frames and transmitted. The entire transmission process needs to rely on the router node, which provides the wireless forwarding function for the transportation process. The data from the ZigBee sensor node is transmitted through the router node and sent to the final coordinator node. The coordinator node has the highest authority in the entire system. It has the authority to determine the joining and leaving of each node, and it can also receive the incoming data from each node. After all the data is summarized at the coordinator node, it is finally transmitted to the corresponding monitoring system. The subsystem of the monitoring system of the entire host computer is responsible for the data collection and monitoring of the entire ZigBee network system. The host computer monitoring system is designed using Delphi technology. By combining the database of SQL Server2005 to store sensor data, it connects the coordinator node in the information collection system and collects the data, thereby displaying the corresponding data graph on the user interface. The monitoring system not only analyzes data but also plays a role in data viewing and storage. The correct execution of all systems is based on reasonable hardware, and the CPU used in the ZigBee wireless communication technology comes from the CC2530 single chip. The chip integrates SOC and supports the IEEE802.15.4 standard. The entire CPU also includes a powerful RF transceiver, programmable flash memory, and 8 KB of running memory. Its flash memory supports up to 256 KB. Because of its unique design, it also has personalized functions such as timing and customization [24]. The main structure of the sensor node is shown in Figure 6. Its components are temperature and humidity sensors, gas concentration sensors, water and electricity sensors, etc., as well as corresponding circuits and power supply devices. In the circuit of the temperature and humidity sensor, the coordinated work of CC2530 and CC2591 improves the working voltage and power of the node and further improves the stability of wireless transmission and increases the transmission range.

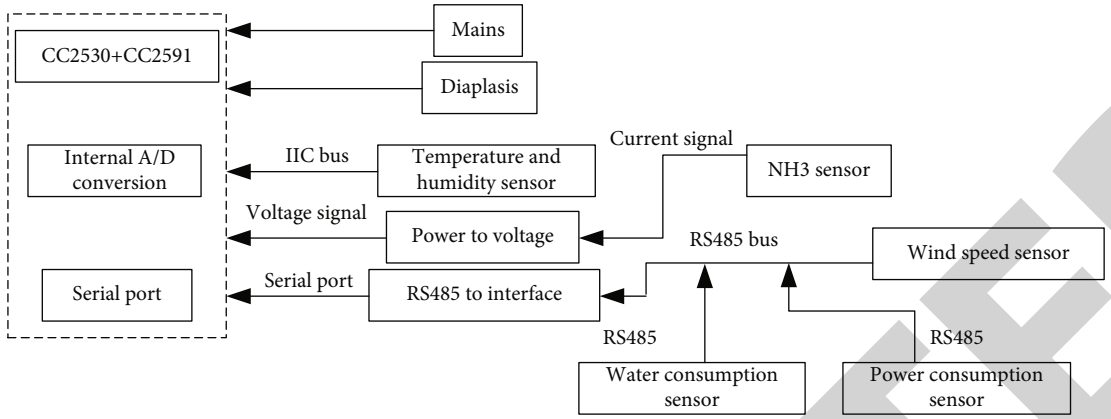

Figure 6: Sensor acquisition node structure.

Table 1: Rosenbrock function minimum optimization results.

Optimization	Average value	Standard deviation	The optimal value	Worst value	Time-consuming (seconds)
Traditional genetic algorithm	0.8301	1.1623	0.0138	5.0096	2.458
Gaussian mutation genetic algorithm	0.1427	0.1417	0.0024	0.5229	2.965
Improved genetic algorithm	4.48E-04	1.03E-03	6.19E-07	4.61E-03	3.146

Table 2: Optimization results of the minimum value of Rastrigin function.

Optimization	Average value	Standard deviation	The optimal value	Worst value	Time-consuming (seconds)
Traditional genetic algorithm	1.4122	1.2966	0.0152	5.3027	2.402
Gaussian mutation genetic algorithm	0.4198	0.4699	0.0056	1.8395	2.997
Improved genetic algorithm	2.45E-02	1.38E-01	1.34E-07	4.40E-03	3.983

Table 3: Minimum optimization results of Griewank function.

Optimization	Average value	Standard deviation	The optimal value	Worst value	Time-consuming (seconds)
Traditional genetic algorithm	0.9872	1.2853	0.0508	5.1266	2.451
Gaussian mutation genetic algorithm	0.0601	0.0499	3.86E-04	0.2012	3.697
Improved genetic algorithm	3.00E-03	4.00E-03	1.00E-06	1.11E-02	4.581

In view of the working environment of the sensor node, such as humidity and high and low temperature, the shell needs to use corrosion-resistant, waterproof, and dust-proof materials to protect the internal chips and circuits to ensure the normal operation of all nodes in the breeding environment. The detailed name of the gas concentration sensor is BGD-NH3 electrochemical sensor. The working principle of the sensor is to detect the concentration of the gas by reacting with the gas to be detected and generating a corresponding electrical signal. Its measurement accuracy is ±1%F.S, and its measurement range is 0~100 mg/L. The power consumption sensor mainly calculates the power consumption and transmits it via RS-485. Finally, the CC2530 uses the data frame command to read the relevant power consumption information. The water consumption sensor adopts a direct design, which reflects the real-time water consumption through the number of turns of the internal magnetic needle. The installation position of the magnetic needle will have a significant impact on the accuracy of the water consumption reading, so reasonable installation should be carried out according to the actual environment.

4.2. Experimental Results Based on Improved Genetic Algorithm. The genetic algorithm adopted in this article is different from the traditional genetic algorithm. The entire iterative process of the traditional genetic algorithm always uses a fixed crossover

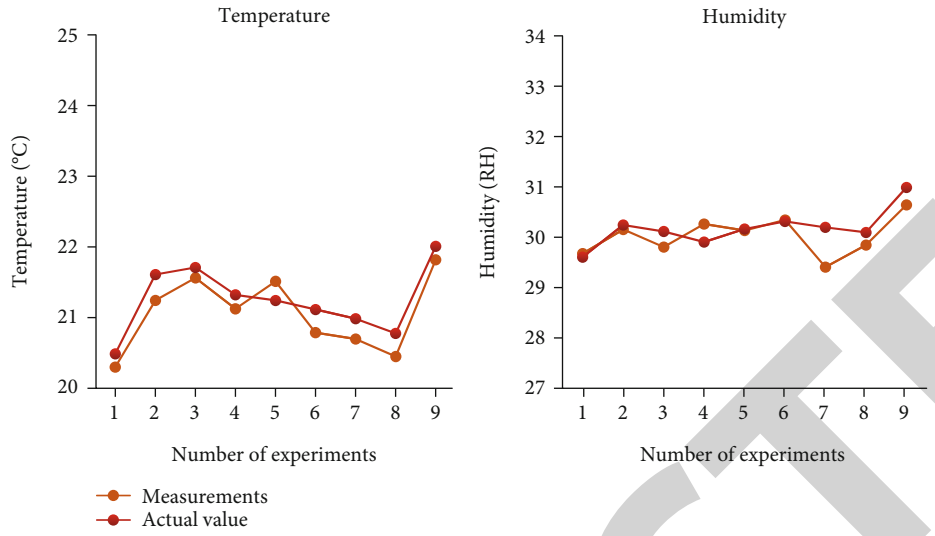

Figure 7: Indoor environment temperature and humidity comparison.

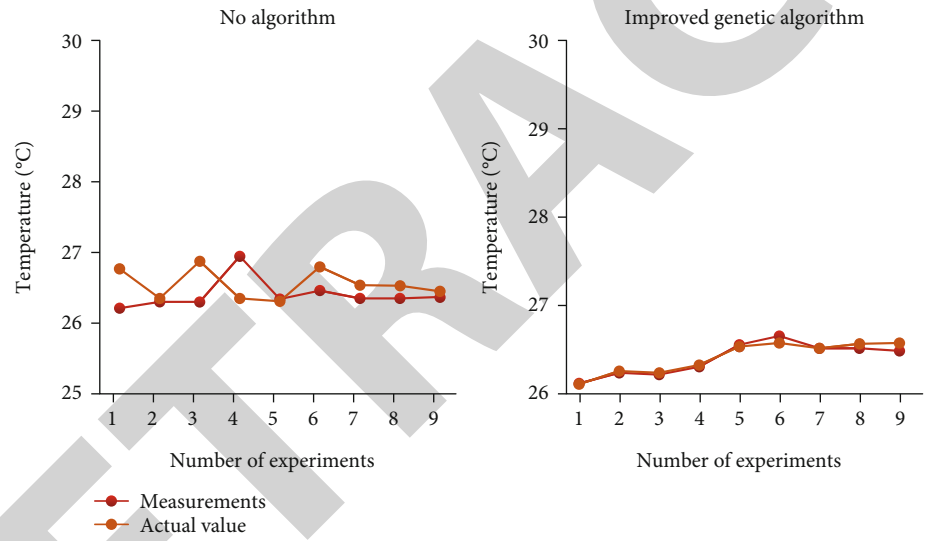

Figure 8: Comparison of temperature test results with and without this algorithm.

operator and mutation operator. The research method in the article is to combine the characteristics of a certain population in different time periods during the whole iterative process, so as to encourage the organisms in the population to make independent selection of hybridization operators and mutation operators. Through such a new genetic algorithm, we can effectively improve the accuracy of the algorithm and the reference value of the experimental structure. For a detailed analysis of the algorithm in the article, the main feature of the algorithm is the innovative introduction of two crossover operators, namely, directed crossover and random vector arithmetic crossover, which fully considers the universality and convergence in the calculation process, so as to avoid the premature occurrence of local optimal solutions in the algorithm and premature problems. Among them, the introduction of random vector arithmetic hybridization can ensure the fairness and stability of the algorithm during the entire iterative process. Therefore, at the beginning of the research, it is best to use random vector arithmetic hybridization. Because effective hybridization can improve the convergence of the overall algorithm, in the later stage of the research, the method of directional hybridization is adopted to promote the entire population to the most reasonable direction. After that, based on the three commonly used benchmark speed measurement functions, such as Rosenbrock, Rastrigin, and Griewank, we evaluate the performance of the adaptive genetic algorithm described above. When the number of iterations is set to 88 times, the results are shown in Tables 1–3.

The genetic algorithm used in the article is improved based on the multivariate continuous function. This algorithm is more stable in performance than traditional genetic algorithms, and its performance is smoother during the entire

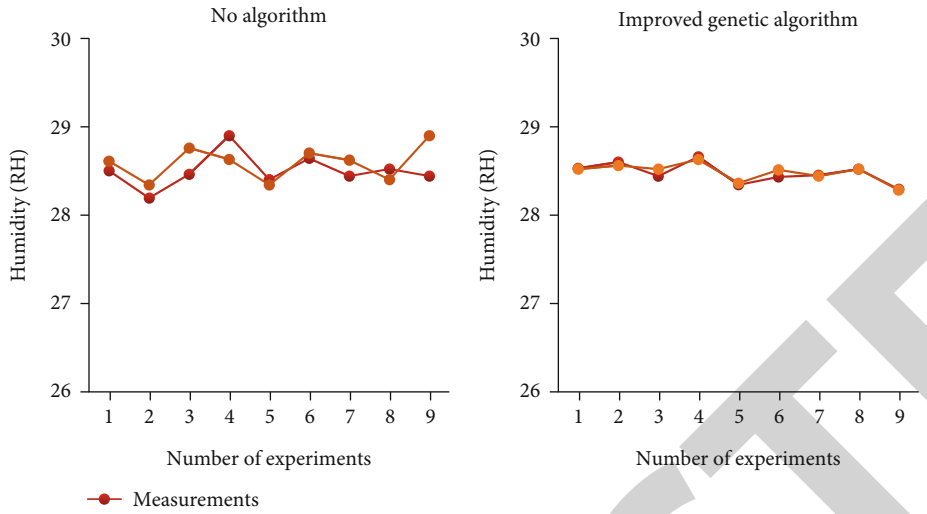

Figure 9: Comparison of humidity test results with and without this algorithm.

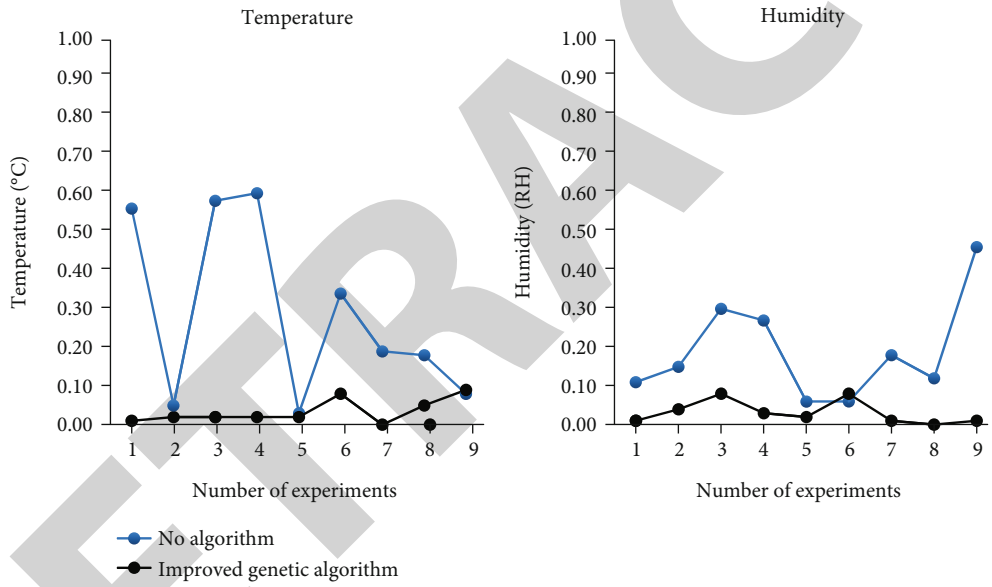

Figure 10: Comparison of the absolute value of the error of the temperature and humidity test results with and without the improved genetic algorithm.

convergence process. At the same time, in the comparison of the two algorithms, the genetic algorithm used in the article has higher global optimization accuracy on the optimal optimization of complex multivariable continuous functions, and for the optimization of various objective functions, the algorithm performs better in terms of stability.

4.3. Temperature and Humidity Test Experiment Based on the Livestock Breeding Base Based on ZigBee Wireless Communication Network Sensor and the Above-Mentioned Improved Algorithm. In a certain breeding environment with universal reference value, perform relevant tests on the performance of the sensors used in reality. By using the new HOBOUX100-011 temperature and humidity recorder, the standard data of temperature and humidity in the breeding environment is selected. The recorder has built-in corresponding temperature and humidity sensors, and its effective temperature measurement range is -20°C~+70°C, and the test accuracy is ±0.21°C. The effective humidity measurement range is 5%~95%, and the test accuracy is ±2.5%RH. Before starting the test, debug the recorder correctly, and then connect the temperature and humidity sensor mentioned in Section 4.1. The factors tested in the experiment are temperature and humidity. A total of 9 times of temperature and humidity data were extracted before and after. Through the analysis of the data, the temperature and humidity were first tested indoors, and the measured values and actual values of indoor temperature and humidity can be compared as shown in Figure 7.

With reference to Figure 7, it can be seen that the temperature value collected from the environment differs from the actual value absolute value by 0.26°C, while the humidity value collected from the environment differs from the actual

value absolute value by 0.25RH. It can be seen that the fluctuation of the value is within the normal usable range, so the results obtained by the experiment can meet the overall requirements, can ensure the normal operation of the system, and can be used in practical applications. Select a certain suburban livestock house with universal reference value to carry out the actual test of the relevant system. Through the operation of the system and the computer and the control of the relevant hardware equipment, the wireless and wired network communication and the monitoring function are correspondingly effectively tested. All sensors in the entire environment will be placed in the control cabinet. In the previous article, the stability and reliability of the system have been strictly verified. The entire system can accurately measure the effective adjustment of the accuracy of the new genetic algorithm to the sensor. During the entire experiment, the data storage and processing cycle are controlled to 12 s, which can more accurately measure the temperature and humidity changes in the environment, and the system will perform a parameter judgment and identification during this period. When the sensor is monitoring, the temperature comparison between using the improved genetic algorithm and not using it is shown in Figure 8.

It can be seen that the test data using the improved genetic algorithm has been greatly improved. When the temperature is tested, the average absolute value error without the algorithm is 0.29, but the average absolute value error of the improved genetic algorithm is only 0.034, and the error is relatively reduced by 88.28%, which is a great improvement. Figure 9 shows the comparison of humidity with and without using improved genetic algorithm.

It can be seen that the test data using the improved genetic algorithm has been greatly improved. When the humidity is tested, the average absolute value error without algorithm is 0.19, but the average absolute value error of the improved genetic algorithm is only 0.03, and the error is relatively reduced by 84.21%, which is a great improvement. Figure 10 shows the temperature and humidity absolute value error comparison with or without improved genetic algorithm.

The error of the improved genetic algorithm is extremely small, the temperature deviation is within 0.09, and the humidity deviation is within 0.08. The performance is obviously better, and it is extremely suitable for the temperature and humidity measurement and control of the livestock house.

5. Discussion

The breeding environment monitoring system developed and designed based on ZigBee wireless communication networking technology can effectively improve the problems of incomplete monitoring information of the breeding environment and low reference value. At the same time, it greatly reduces the manpower consumption and avoids errors caused by manual data recording. The monitoring system can perform multidimensional monitoring and analysis of a certain breeding environment, such as temperature and humidity, gas concentration, and water and electricity consumption in the current environment. The entire system can read, collect, summarize, process, and transmit data from each sensor completely autonomously and automatically. The relevant data is transmitted by the ZigBee wireless network to the upper computer monitoring system. This system can store, view, and analyze the received data. Through the application of the system in actual conditions, the results show that the system can indeed provide stable monitoring functions effectively, properly, and autonomously operate all kinds of information in the entire breeding environment, with low cost, less wiring, and high customization and scalability, so that it has extremely high application and promotion value. In an indoor breeding environment with universal reference value, adequate verification of the feasibility of the program is carried out. At the same time, the measurement of temperature and humidity in the outdoor breeding environment is also a complete program verification. During the entire control and monitoring process, a new genetic algorithm is used to strictly verify the control accuracy. Obtaining the corresponding data from the above experiments, visually display the data in the form of a line graph, which can reflect the performance change trend of the system during operation. Through the summary of experimental data, detailed data analysis is carried out to obtain the expected results.

6. Conclusions

In the experiment based on ZigBee wireless communication network sensor combined with improved genetic algorithm in the temperature and humidity test of the breeding farm, the data collection and monitoring system of the ZigBee network system is designed. As the temperature and humidity sensor to be used below, and use hybridization operator and mutation operator to improve the genetic algorithm, based on Rosenbrock, Rastrigin, and Griewank and other three commonly used benchmark speed measurement functions for algorithm testing, it is concluded that the algorithm is more stable in performance than the traditional genetic algorithm, and in the whole process of convergence, its performance is smoother and has higher global optimization accuracy. The temperature and humidity test experiment of the livestock breeding base is carried out again, and the average absolute value error without algorithm is 0.29 when the test temperature is tested, and the absolute value error under the improved algorithm is only 0.034, which is a relative decrease of 88.28%. In the humidity experiment, the average absolute value error without algorithm is 0.19, and the absolute value error under the improved algorithm is only 0.03, and the error is relatively reduced by 84.21%. And under the improved algorithm, the temperature deviation is within 0.09 and the humidity deviation is within 0.08, which has monitoring stability and has a good development prospect in the application of animal husbandry farms.

Data Availability

No data were used to support this study.

Hindawi
Computational and Mathematical Methods in Medicine
Volume 2023, Article ID 9842627, 1 page
https://doi.org/10.1155/2023/9842627

Retraction

Retracted: Status Quo Analysis of Physical Fitness Test Data Based on Health Monitoring

Computational and Mathematical Methods in Medicine

Received 27 June 2023; Accepted 27 June 2023; Published 28 June 2023

This article has been retracted by Hindawi following an investigation undertaken by the publisher [1]. This investigation has uncovered evidence of one or more of the following indicators of systematic manipulation of the publication process:

(1) Discrepancies in scope

(2) Discrepancies in the description of the research reported

(3) Discrepancies between the availability of data and the research described

(4) Inappropriate citations

(5) Incoherent, meaningless and/or irrelevant content included in the article

(6) Peer-review manipulation

The presence of these indicators undermines our confidence in the integrity of the article's content and we cannot, therefore, vouch for its reliability. Please note that this notice is intended solely to alert readers that the content of this article is unreliable. We have not investigated whether authors were aware of or involved in the systematic manipulation of the publication process.

In addition, our investigation has also shown that one or more of the following human-subject reporting requirements has not been met in this article: ethical approval by an Institutional Review Board (IRB) committee or equivalent, patient/participant consent to participate, and/or agreement to publish patient/participant details (where relevant).

Wiley and Hindawi regrets that the usual quality checks did not identify these issues before publication and have since put additional measures in place to safeguard research integrity.

We wish to credit our own Research Integrity and Research Publishing teams and anonymous and named external researchers and research integrity experts for contributing to this investigation.

The corresponding author, as the representative of all authors, has been given the opportunity to register their agreement or disagreement to this retraction. We have kept a record of any response received.

References

[1] W. Ye and X. Shao, "Status Quo Analysis of Physical Fitness Test Data Based on Health Monitoring," *Computational and Mathematical Methods in Medicine*, vol. 2022, Article ID 3931404, 13 pages, 2022.

Hindawi
Computational and Mathematical Methods in Medicine
Volume 2022, Article ID 3931404, 13 pages
https://doi.org/10.1155/2022/3931404

Research Article

Status Quo Analysis of Physical Fitness Test Data Based on Health Monitoring

Wenping Ye[1] and Xianfang Shao[2]

[1]*Institute of Physical Education, Huanggang Normal University, Huanggang, 438000 Hubei, China*
[2]*Institute of Physical Education, Hubei University of Science and Technology, Xianning, 437100 Hubei, China*

Correspondence should be addressed to Xianfang Shao; shaoxianfang@hbust.edu.cn

Received 20 January 2022; Revised 21 February 2022; Accepted 5 March 2022; Published 24 March 2022

Academic Editor: Muhammad Zubair Asghar

One of the important symbols of a country's level of social progress and the continuous spread of civilization throughout the world includes the level of national physique and health. People's living standards have been significantly improved, and a moderately prosperous society has been preliminarily realized. The national physique should be improved, especially the teenagers who are in the rapid and golden period of physical and psychological development. But not everything develops according to wishes. For the past 20 years, the physical health of Chinese students has been in a downward trend. Therefore, it is urgent to analyze and study the data of adolescent health monitoring and physical fitness test. Through the analysis of D-S evidence theory composition rules, SVM network protocol, and other technologies, the accuracy of adolescent physique monitoring data has been improved by 38.4%, enhanced students' willingness to exercise, 65% of students have enhanced physical health awareness, and a network data platform has been established, which can clearly reflect the physical health of students and summarize all monitoring data information. Teenagers are the future builders and successors of the country, and they play a pivotal role in the entire country. The analysis of the status quo of adolescent physical fitness test data is related to the strength of the country, the rise and fall of the nation, the happiness of the family, and the future of the individual.

1. Introduction

The educational concept of "people-oriented, health first" not only emphasizes the main position of students in the education system but also emphasizes the improvement of students' comprehensive quality and ability. A healthy physique is the premise of development, and the health of college students' physique is the key to the implementation of the national talent strategy. From the perspective of social development, the physical health of citizens is an important part of judging a country's comprehensive strength. To a certain extent, it can reflect the basic situation and future development trends of social groups or individuals in terms of body shape development, physical function, physical quality, and social adaptability in a certain period of time. Therefore, promoting the healthy development of college students' physical fitness not only provides a guarantee of human resources for national progress and social development but also reflects the development of China's social, economic, and comprehensive national strength.

This subject investigates and studies the physical health status and influencing factors of students in a university through scientific investigation and research methods. By measuring and analyzing various physical fitness monitoring indicators of students in a university, we can scientifically, objectively, and accurately grasp the physical characteristics, health status, and development and change laws of young students. Specific and targeted investigation of the current content of sports activities for young students, efforts to scientific development of physical education for young students, and the development of sunshine sports put forward reasonable suggestions and provide theoretical basis for the national and government decision-making departments to formulate relevant policies.

The innovation of this paper is that China, as a developing country, has become the world's largest economy with a "rocket" growth in its gross national economic output. However, the physical health of young people is not optimistic and faces many serious problems, such as obesity, high blood pressure, and early development, and thus, the "National Student Physical Health Monitoring Network" was established. Through the monitoring network, we can grasp the physical health status of students in China and their development trends and provide a scientific basis for formulating the development plan of school sports health work and scientifically carrying out school sports health work. The status quo of physical fitness test data based on health monitoring is analyzed.

2. Related Work

Structural health monitoring (SHM) using wireless sensor networks (WSNs) has aroused the research interest of Adam. SHM systems have been used to monitor critical infrastructure and have the potential to increase structural life and improve public safety. The high data collection rate of WSN for SHM brings unique network design challenges. Adam provides a comprehensive survey of SHM using WSN, outlining algorithms for damage detection and localization, as well as network design challenges and future research directions. Solutions to network design problems are compared and discussed, and the survey also outlines testbeds and real-world deployments of WSNs for SH [1]. Mizoue has developed a semiautomatic image analysis system CROCO for objective and low-cost assessment of tree canopy conditions in forest health monitoring. After preprocessing, the macro automatically generates contours from color images according to the between-class variance method and computes the exponential DSO as a measure of crown transparency based on two fractal dimensions. The results show that CROCO can provide consistent DSO measurements, whether it is cloudy or sunny, if the shooting conditions meet the criteria of CA less than about 45 degrees and OR less than about 50% of crown width [2]. Today, human beings are facing increasingly serious energy crisis and electromagnetic radiation pollution. An energy harvester with the function of protecting human health from electromagnetic radiation is an ideal solution to this problem. Here, a stretchable electromagnetically shielded hybrid nanogenerator (ES-HNG) is reported. Zhang reported a stretchable electromagnetically shielded hybrid nanogenerator (ES-HNG), which can not only remove thermal and mechanical energy from the living environment but also protect and monitor human health. Furthermore, ES-HNG is able to monitor human health by attaching it to the human abdomen as a self-powered sensor. This work opens up new prospects for efficient energy harvesting and protection and monitoring of human health from the electromagnetic radiation environment [3]. To monitor local critical regions of structures, impedance-based methods utilize the high-frequency impedance responses sensed by piezoelectric sensors as local dynamic features. Huynh et al. present current progress and future challenges in impedance-based structural health monitoring. First, the theoretical background of the impedance-based method is outlined. Next, the recent advances in wireless impedance sensor nodes, interface impedance sensing devices, and temperature effect compensation algorithms are summarized. Various research efforts on these topics are reviewed to share the latest information on research activities and implementation of impedance-based techniques. Finally, the future research challenges of this technology are discussed, including the applicability of wireless sensing technology, the predetermination of the effective frequency band, the sensing area of the impedance response, robust compensation of noise and temperature effects, and quantification [4]. The Internet of Things (IoT) has recently received a lot of attention due to its potential and ability to be integrated into any complex system. C introduces a structural health monitoring (SHM) framework for intelligent and reliable monitoring using IoT technology. Specifically, the techniques involved in the implementation of IoT and SHM systems and data routing strategies in an IoT environment are presented. As the volume of data generated by sensing devices is greater and faster than ever, big data solutions have been introduced to process the complex and large volumes of data collected from sensors mounted on structures [5]. Degradation is a complex and intricate process, and due to the unclear mechanism of Li-ion batteries and the sensitivity to objective factors, it is difficult to identify the degradation state of batteries and monitor the SoH of batteries. Xiong proposed a degradation state identification method for online estimation of remaining capacity. First, Xiong uses EIS measurements to detect degradation levels through the analysis of electrochemical impedance spectroscopy (EIS) test results of different SoHs. Secondly, according to fractional order theory, an online parameter identification method with fractional order impedance model is proposed for degradation analysis. Third, Xiong discusses the correlation between parameter changes and degradation levels and extracts the SEI (solid electrolyte interface) resistance to predict the remaining capacity by choosing a suitable fitting function. Finally, the effectiveness of the proposed method is verified by test data, and the residual capacity estimation error can be guaranteed to be within 3% [6]. Alamdari presents results from a large-scale structural health monitoring application for the Sydney Harbour Bridge, Australia. The bridge has many structural components concentrated on a subset of the lane's seven 800-jack arches. The goal of Alamdari was to identify which jack arches (if any) were responding differently to traffic input or instrumentation issues due to potential structural damage. Alamdari proposes a new non-model-based approach to achieve this using spectrally driven features based on spectral moments (SMs) from the measured responses of the jack arches. SM contains information from the entire frequency range, so subtle differences between normal and distorted signals can be identified. Alamdari's method applies a modified k-means clustering algorithm to these features, followed by a selection mechanism of the clustering results to identify jack arches with anomalous responses. The proposed method was extensively evaluated by Alamdari using real data from bridges [7] These studies

are relatively one-sided, the experimental methods are relatively simple, and there are relatively few related studies on the combination of health monitoring and physical fitness testing.

3. Youth Physical Health

3.1. Physical Health. The term "physique" is interpreted as the quality of the human body, which includes five dimensions: the developmental level of body shape, the level of physiological function, the developmental level of physical fitness and athletic ability, the developmental level of psychology, and the ability to adapt and resist. The strength of an individual's physique is reflected in these five dimensions. Most people think that a person is healthy as long as there is no disease; this view is very one-sided and very inaccurate. To be truly healthy, an individual must be physically, socially, intellectually, emotionally, and spiritually healthy and to come up with a marker that reflects health. Health signs include good health, no disease in major organs, well-developed body shape, strong physique, well-proportioned body shape, good physiological function of respiratory system, cardiovascular system and motor system, strong athletic ability and labor ability, healthy mental development, optimistic mood, firm will, strong anti-interference, antistimulation ability, and strong adaptability to natural and social environment.

3.2. Health Monitoring. Teenage students are the future of every country. The government has already started testing the physical health of adolescent students and has continuously issued policy documents to improve students' physical quality and guide students to participate in physical exercise. "Monitoring" means supervisory control so that the monitored person cannot move freely or go beyond the prescribed range [8]. From the perspective of physical health monitoring in junior high schools, it is mainly divided into two parts: external monitoring and internal monitoring. The external monitoring of the school is mainly that the relevant departments under the supervision of the Municipal Education Bureau need to organize the middle schools to carry out physical fitness tests in a planned way every year and check the preparation of the test instruments and venues of each middle school. The test results are evaluated, analyzed, and fed back, and necessary intervention measures are implemented for the problems that arise [9]. The internal monitoring of the school is mainly under the leadership of the main person in charge of the school, actively responding to the call of the superior department, implementing the implementation of the "New Standard," and coordinating and cooperating with all relevant departments and organizations to ensure the smooth development of the test work. It organizes, analyzes, evaluates, feedbacks, and reports the test results and formulates and adopts measures that conform to the actual situation of the school. The organizational structure of students' physical fitness monitoring is shown in Figure 1.

With students' physical health survey results, conduct in-depth research. There is an endless stream of literature research on students' physical health. Statistics on the number of literature publications on students' physical health in recent years are shown in Figure 2.

It is not difficult to find from the data that the related research on students' physical health is increasing every year, and even the number is approaching a thousand. It highlights the importance that social and academics attach to students' physical health, and therefore, many researchers provide a lot of strategies and methods for students' physical health monitoring [10].

3.3. Improvement of Students' Physical Health. People's cognition and behavior of things have a high degree of consistency. In general, what kind of cognition will lead to what kind of behavior? People's attitude to something depends on their understanding of it, so do sports cognition and sports behavior, which is highly consistent. Whether taking the physical fitness test as a means of evaluating students' comprehensive quality or an inevitable process of education reform, students' cognition of physical fitness test is of great significance [11]. Physical fitness exercise is particularly important for a person's physical and mental development. It will affect the normal growth and development of students and their physical and mental health and will make people aggressive, short-tempered, and depressed. It will also lead to low learning efficiency and memory loss and seriously affect academic performance. Investigating the attitudes of students in a certain university towards physical health exercise is shown in Table 1.

A survey on the attitudes of freshman to junior college students towards physical fitness exercise found that freshman students pay more attention to physical fitness exercise. On the other hand, only less than 20% of the sophomore and junior students believe that physical fitness exercise is very necessary, and then, less than half of the students think that physical fitness exercise is necessary; the reason for this is roughly because freshmen who have just entered the school do not have too much academic pressure, so they still have most of their spare time for exercise. But sophomore and junior students will face a lot of exams, etc., which take up their exercise time, and the students' physical health problem is not optimistic.

According to the data of college students' physical health test in colleges and universities over the years, the physical quality of young college students has not been really improved. Although after the reform and opening up the country's economy has begun to take off, people's living standards are getting better and better, and the physical development and nutritional level of young people have been improved, but at the same time, it has also led to an increase in the obesity rate of young college students and an increase in the incidence of hypertension among young people. And because of lack of exercise, bad living habits, and heavy study pressure, the physical quality of young college students has been in a downward trend for many years [12].

3.4. Status Quo of Students' Physical Health. Physical fitness and health level and the economic development of society influence each other. In today's world where the comprehensive national strength based on economy and science and technology is in fierce competition, human resources are the basic conditions for the development of national competition, and

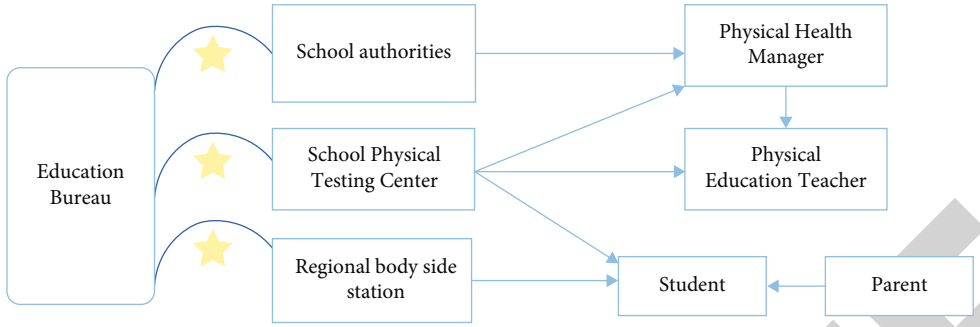

Figure 1: Organizational structure of student physique monitoring.

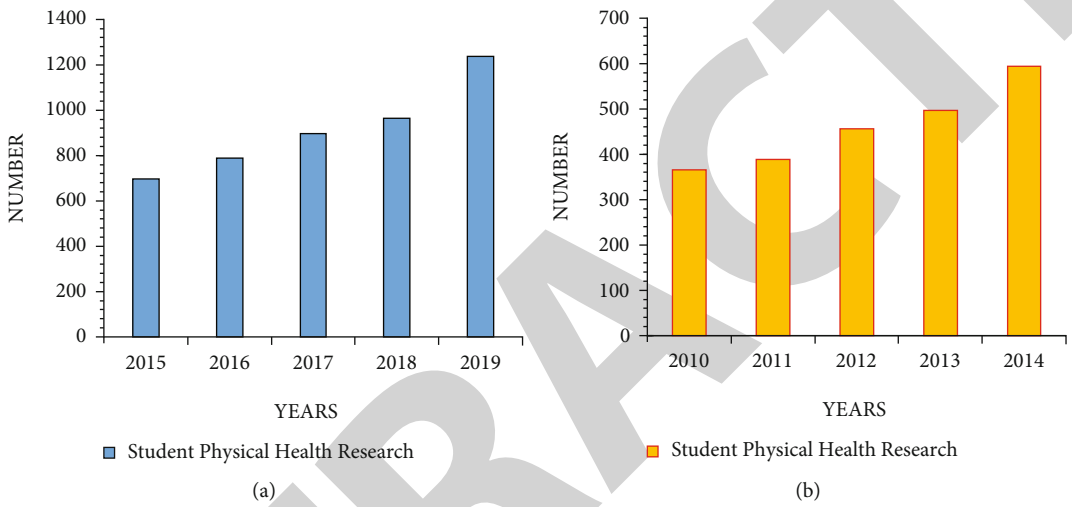

Figure 2: The number of publications about students' physical health in recent years around 2015.

Table 1: Attitudes of students in a university towards physical fitness exercise.

	No need	Generally	Necessary	Very necessary
Freshman	12%	35%	31%	22%
Sophomore	10%	44%	28%	18%
Junior	9%	44%	30%	17%

the healthy development of national quality is the prerequisite for the development of national social economy. High-level human resources are the comprehensive performance of ideological and moral, scientific and cultural, psychological quality, and other aspects on the basis of physical health. Statistics on the physical fitness monitoring of male and female students in a certain college are shown in Figure 3.

As can be seen from Figure 3, the physical fitness monitoring data of freshman to senior year students shows that the qualified situation of boys is better than that of girls. However, there are still nearly half of the boys in the second and third grades who are unqualified, and the pass rate in the senior year is less than 80%. The pass rate of girls from freshman to senior year is below 70%, and the pass rate of freshman and senior year is nearly half of the number. Obviously, this situation is not optimistic.

3.5. Monitoring of Students' Physical Health

3.5.1. Monitoring Personnel Training. Local governments should lead the overall implementation of physical health monitoring of young students [4]. And each school actively cooperates with the higher-level departments to issue the test requirements and make full use of the existing resources of the school to prepare for the training of personnel before the test, the supervision, guidance, and explanation during the test, and the evaluation and feedback after the test, as shown in Figure 4.

Judging from the data presented above, the results are delightful; each school organizes testers to participate in professional training every year and strictly implements the requirements of the higher authorities [5]. However, in the field test, it is found that most school teachers are obviously insufficient in the professionalism of the test and the normative requirements of the test items.

3.5.2. Preparation of Facilities and Equipment. The use of venue facilities and equipment in the students' physical fitness test has an objective impact on the results of the students' physical fitness test. It is necessary to increase the investment in funds; it is necessary to strengthen the construction of test sites, facilities, and equipment. Detailed

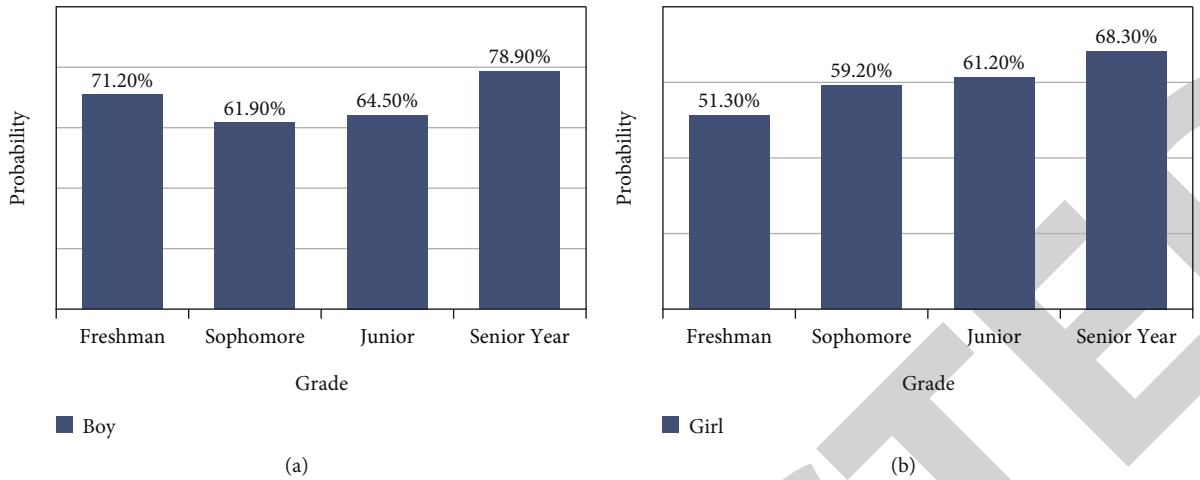

Figure 3: Eligibility of physical fitness monitoring for male and female students from freshman to senior year.

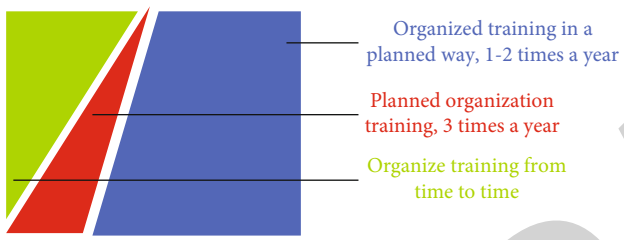

Figure 4: Training of testers.

rules must be developed for scientifically and accurately testing students' physical health data [8]. Taking the number of students in a certain university as an example, the detailed rules are formulated as shown in Table 2.

The physique of young college students continues to decline. In view of the problems that have arisen in the management and utilization of students' physique health test data in colleges and universities over the years, a college is taken as an example. Through the analysis of the college's physical health test work, we can grasp the students' physical development needs and understand the needs of school sports work. This paper analyzes the functional requirements of the current physical fitness test data monitoring platform and tries to theoretically design and construct a physical fitness test platform for colleges and universities, in order to promote the standardization and scientific use of students' physical fitness test data in China [13].

3.6. Monitoring Data Platform System. The wide application of Internet technology makes life easier and easier and improves efficiency. The college students' physical health test data platform also regards convenience and ease of use as one of its principles for serving schools, teachers, and students. In the actual physical fitness testing work, manual data collection takes up a lot of manpower and material resources on the one hand, resulting in a waste of resources and reducing work efficiency. On the other hand, the accuracy of manually collected data depends on the individual, and the error of the data is greater, which may not truly reflect the actual situation of the individual to a certain extent. At the same time, the operating interface of the existing data reporting system is simple and not comfortable and friendly, and some functions need to wait for a long time to receive the prompt, which is not very practical [14]. Therefore, based on the principle of convenience and ease of use, the design of the data platform for college students' physical health test should be based on the principle of convenience and ease of use, and design a data platform with a friendly and comfortable interface, convenient operation of functional modules, and fast server response. The design data platform system is shown in Figure 5.

The data storage and use efficiency of the network data platform has been greatly improved, and an electronic health system file has been established for each student to ensure the authenticity, objectivity, and continuity of each student's historical physical health test data. Due to the adoption of the information-based operation process, the student's health physique test data is directly backed up on the cloud platform and bound with the student's electronic student ID card, which is convenient for students to query, and the cloud platform can realize personalized statistical analysis functions. Another significant advantage is that it establishes a corresponding system feedback mechanism. After the completion of the students' physical health test, the platform uses modern and rich communication and self-media means to timely transmit the test results and the generated report to the education administrative department and students' parents through the WeChat public account and the APP client. It feeds back the students' physical fitness test results and proposes scientific exercise methods and healthy nutritional diet guidance programs for students based on the students' physical fitness test results, hoping to improve students' physical fitness [15].

4. Students' Physical Health Monitoring Technology

4.1. Data Collection and Fusion of Health Monitoring. It is the foundation of structural health monitoring technology to collect all kinds of information of the structure through

Table 2: Detailed test rules for students' physical health data.

Test items	Equipment	Equipment	Site
Height	1 height gauge	7 height measuring device	1 gym
Weight	8 weight scales	2 scales	1 gym
Vital capacity	9 electronic spirometers	2 scales	1 gym
50 m run	8 stopwatches	2 stopwatches	1 track-and-field field
Standing long jump	8 tapes	1 long jump pad	1 bunker
Sitting forward bending	9 seated forward bends	1 standing body forward bending instrument	1 gym
1000-meter run	8 stopwatches	2 stopwatches	1 track-and-field field
800-meter run	8 stopwatches	2 stopwatches	1 track-and-field field
Pull-ups	8 horizontal bars	1 tester	1 tester
1-minute sit-ups	4 cushions, 1 stopwatch	1 gymnastics mat	1 gym

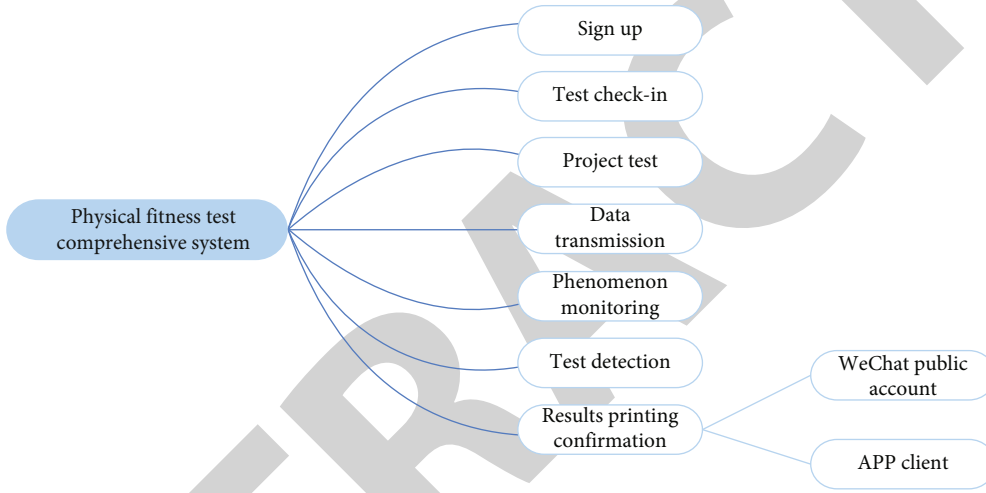

Figure 5: Monitoring data network platform system.

the sensor network and successfully transmit it to the management center. At present, the data collection of various health monitoring is mainly realized by using wired sensor network. However, the monitoring network composed of wired sensors has a large amount of wiring and high maintenance costs. Smart sensors have computing power and wireless communication capabilities. The wireless sensor network formed by them has the advantages of high flexibility, light load, low cost, convenient construction and movement, and easy maintenance. Therefore, their application in structural health monitoring systems has broad prospects. The technical structure of health monitoring is shown in Figure 6.

The data collection of various health monitoring requires information fusion. People can be compared to an information fusion system. It has two important characteristics: it is complex and highly adaptive. There are many different external physiological organs in the human body, which are equivalent to many different types of sensors, which can understand the external environment information and make correct action decisions, as shown in Figure 7.

4.2. Anomaly Detection of Multisign Parameters. For the human health monitoring system, the input data is mainly collected through the wireless sensor network, so there will be a problem; the original data collected by the sensor has abnormal data [16]. In the wireless sensor network, due to node failure, environmental anomalies, and certain time occurrences, the data we collect deviates from the actual data, and the data collected at this time can be called abnormal data. So we need to detect abnormal data.

4.2.1. Detection of Local Abnormal Factors. The LOF algorithm is what we often call the local outlier factor detection method. Among all abnormal data detection algorithms, it is a very classic algorithm, and it can be seen in many fields. Its principle is to detect whether the data is abnormal by calculating the abnormal degree of each data in a sample data. By calculating the value of LOF to determine whether it is abnormal, if the LOF is greater than 1, it is an abnormal point, and if it is close to 1, it is normal data. Performing sample data analysis of C1, C2, O1, and O2, is shown in Figure 8.

For the current problem, we are looking for a general algorithm to identify these abnormal data, and LOF is one of them [17].

As a classic algorithm, the LOF algorithm has several basic definitions: concept 1 $d(p, o)$, this symbol represents the distance between p and o, usually using Euclidean distance. Concept 2 k-distance has the same definition as concept 1, using

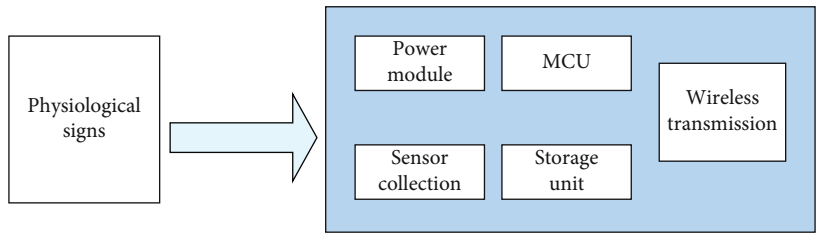

Figure 6: Health monitoring technology structure.

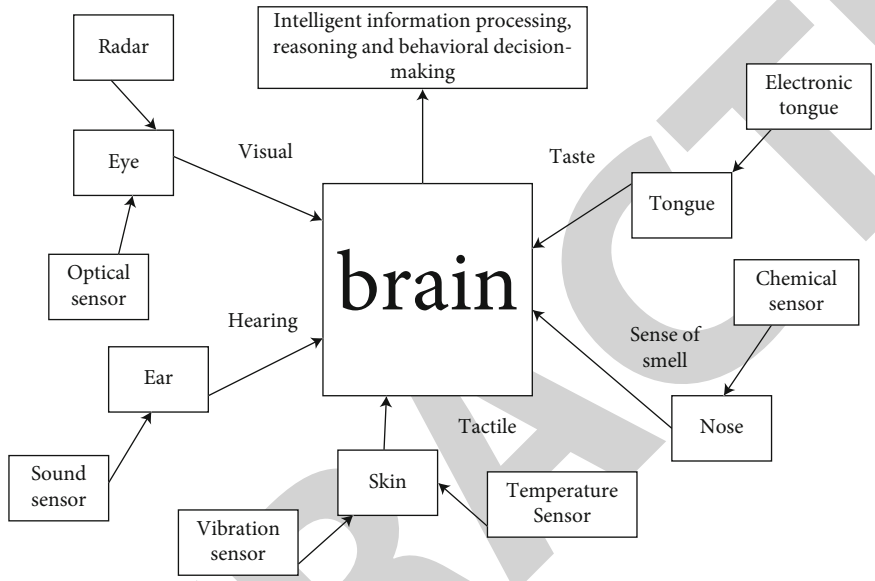

Figure 7: Information fusion process.

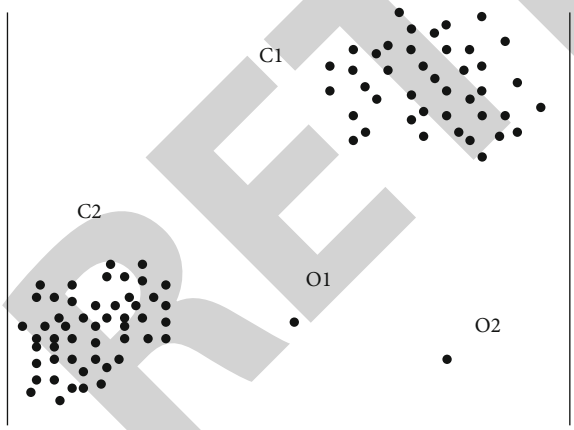

Figure 8: Schematic diagram of exceptions.

Euclidean distance.

$$d_k(p) = d(p, o). \tag{1}$$

At the same time, point o must meet the following two conditions:

(1) Set D contains at least

$$ko \in C\{x \neq p\}, d(p, o) \leq d(p, o). \tag{2}$$

(2) Set D contains at least

$$-ko \in C\{x \neq p\}, d(p, o) \leq d(p, o). \tag{3}$$

The definition diagram is shown in Figure 9:

(3) k distance neighborhood of $p-$: k distance neighborhood represents the set of all points in a dataset D whose distance is less than k distance from p:

$$N_d = (p) = \{q \in D|d\}(p, o) \leq k\text{-dist}(p). \tag{4}$$

(4) Reach distance−: in dataset D, the reachable distance between o and p is expressed as

$$\text{reach-distance}_k(p, o) = \max\{k\text{-distance}(o), d(p, o)\}. \tag{5}$$

The reachable distance of O1 can be represented by

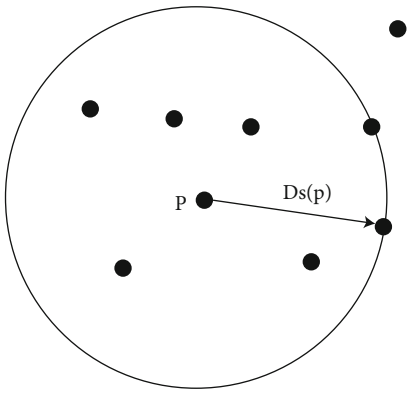

Figure 9: Schematic diagram of the kth distance.

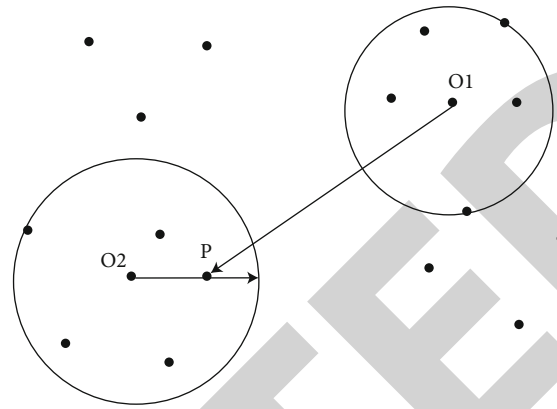

Figure 10: Diagram of reachable distance.

$d(p, o)$, and the reachable distance of O2 can be represented by $2d(p, o)$, as shown in Figure 10.

Advantages of LOF are as follows:

(1) The algorithm does not calculate a point in isolation, but comprehensively analyzes the surrounding points to make the result more accurate

(2) The algorithm adopts quantitative analysis instead of qualitative analysis, and the results are clear at a glance

(3) There are few algorithm parameter settings

The disadvantage of LOF is that the selection of parameters will affect the entire result, and different values can lead to opposite results. For datasets with unknown number of outliers, it is difficult to select the parameter k to ensure the mining number of outliers.

4.2.2. Data Anomaly Detection Based on Multicorrelation. For the wireless sensor network, its main purpose is to send the collected data to the aggregation node, and then, the aggregation node sends the data to the cloud server. However, for the human body, the changes of physical parameters are regular and easily affected by changes in the external environment. Because the LOF algorithm calculates the outlier factor based on the distance between the data, and for a single data source, it is prone to misjudgment. If it is used directly, there will be a lower recall rate and a higher false alarm rate, so this paper introduces the correlation of multimodal data into the LOF algorithm [18]. Therefore, the steps of anomaly detection in this paper are as follows:

$$\begin{gathered}\left|\left(r(t_i)-\frac{(E_a(t)+E_b(t))}{2}\right)\right|\rangle C^2,\\ r(t_i)=r(t_{i-1}),\\ Z(t_i)=Z(t_{i-1})+de^2,\\ Z_r(t_i)=\sum_{j=1}^{m}\alpha_j\cdot Z_j(t_i),\\ \sum_{j=1}^{m}\alpha\frac{((E_a(t)+E_b(t)))}{2}.\end{gathered} \tag{6}$$

Through research, the difference and robustness between different modal data is found, it is not appropriate to set the threshold to a fixed value, and the threshold setting should be combined with the correlation of different datasets to highlight different proportions. Therefore, the weighted average of the multidimensional data means is used to eliminate this effect.

4.3. D-S Evidence Theory Composition Rules. In the D-S evidence theory, the composition rule is used to reflect the combined effect of evidence. We can use a variety of composition rules to judge an uncertain proposition and obtain the degree of correlation between different evidences, synthesizing through rules in order to get the correct result.

4.3.1. The Synthesis Rule of Two Evidences Is Divided into the following Two Steps.

$$\begin{gathered}m(A)*=\sum_{\substack{A\cap B_j=A\\ A\subseteq\Omega,A\neq\varphi}} m_1(A_i)m_2(B_j),\\ k=\sum_{A_i\cap B_j=\varphi} m_1(A_i)m_2(B_j),\\ m(A)=m(A)^*+\frac{m(A)*}{1-k}k,\quad k\neq 1.\end{gathered} \tag{7}$$

It can get

$$\begin{gathered}m(A)=\frac{\sum_{A_i\cap B_j} m_1(A_i)m_2(B_j)}{1-k},\quad A\neq\varphi,\\ m(A)=0\cdot A=\varphi.\end{gathered} \tag{8}$$

4.3.2. Combining Rules for Multiple Evidences. When there are multiple evidences, the basic probability distribution function is $m_1, m_2, \cdots, m_n$, and the synthesis rule can be expressed as

$$m(A)=\frac{\sum_{\cap A_i=A}\prod_{1\le i\le N} m_i(A_i)}{1-k},\quad A\neq\varphi. \tag{9}$$

The conflict coefficient k becomes the formula

$$k = \sum_{\cap A_i = \varphi} \prod_{1 \le i \le N} m_i(A_i), \quad k \ne 1. \tag{10}$$

4.4. Basic Concepts and Definitions of SVM. For support vector machines, it is actually a machine learning algorithm. Machine learning can be explained as follows: it designs an algorithm to learn by inputting historical data samples to obtain a certain attribute relationship and then test or judge by inputting unknown data. The main process of machine learning is to generate a general model. Machine learning is to learn to construct a relationship model between input and output given sample data. The classification process is actually a machine learning process. It is a generalized linear classifier that performs a binary classification of data according to supervised learning, and its decision boundary is the maximum margin hyperplane of the sample data for a solution, as shown in Figure 11.

If a certain sample data can be correctly divided into two categories, then there must be an optimal hyperplane available formula in the middle:

$$g(x) = W^T \cdot x_i + b, \tag{11}$$

where W represents the weight coefficient vector and b is a constant term. Usually, training on sample data is actually getting an optimal hyperplane to classify it correctly. In order for a standard SVM model to classify the samples correctly, it must satisfy the formula

$$\begin{aligned} W^T x_i + b \ge 1, \quad y_i = 1, \\ W^T x_i + b \le -1, \quad y_i = 1 = -1. \end{aligned} \tag{12}$$

In summary, the specific flowchart of the computational optimization model is shown in Figure 12.

In order to directly measure the performance of the algorithm in this paper, a comparison is made in terms of accuracy, as shown in Figure 13.

5. System Design and Testing

For the human health monitoring system, the collected information is processed and analyzed by big data and fed back to individual. Through this system, we collect human physiological parameters, wirelessly transmit them to the server, process and analyze the data, and feed it back to the individual. It can realize intelligent health monitoring and assist users to manage their own health, and at the same time, it can achieve the purpose of prevention.

5.1. System Design Principles. The main function of the human health monitoring system is to develop a sensor-integrated intelligent terminal, which is easy to carry on the surface of the human body and collects and transmits the physiological parameters of the human body through wireless communication technology, and use the big data platform for processing and analysis to realize the monitoring of human health status. In response to this demand, the system has the following design principles.

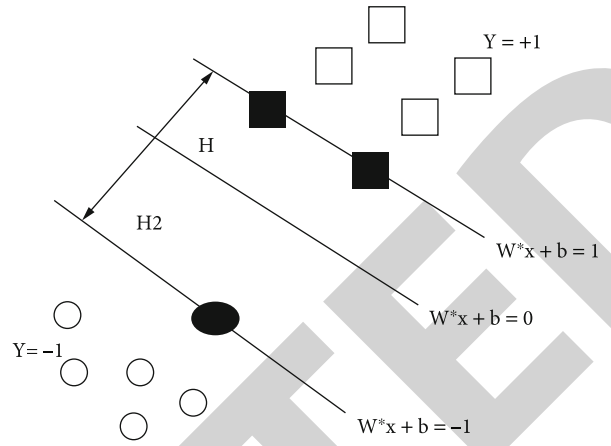

Figure 11: Schematic diagram of the optimal hyperplane.

(1) Low cost: in practical applications, each node may require a variety of sensors for data acquisition, so cost is considered in the device selection process

(2) Low energy consumption: energy consumption has always been a key issue in wireless sensor networks, because most nodes are powered by lithium batteries, so low energy consumption can make the system have a longer life. Therefore, this paper uses LoRa for wireless communication and adopts modular design to reduce energy consumption, thereby extending network life

(3) Extensible: for this system, in the subsequent practical application, it is faced with the increase of system requirements, which requires the system to have a certain expansibility, which is convenient for subsequent addition of functions. Therefore, the design of this paper adopts a modular design and reserves a certain interface to facilitate subsequent addition of functions

Since the system monitors human health, it sometimes encounters harsh environments. Therefore, the stability of the system is considered in the design of the system. The organizational structure of the system is designed for this purpose, as shown in Figure 14.

5.2. Living and Eating Habits. Parents are the direct managers of students' daily life and diet, but students have some unhealthy eating habits, like eating snacks, drinking carbonated beverages, and even eating snacks as meals. Some students prefer to play while eating and watch TV while eating, which causes students to be distracted while eating, which affects their appetite. At the same time, it also affects the chewing degree of food and nutrient absorption problems. Under the traditional concept, people are accustomed to using fat as a criterion for evaluating whether a child is healthy and mistakenly believe that fat is a sign of health.

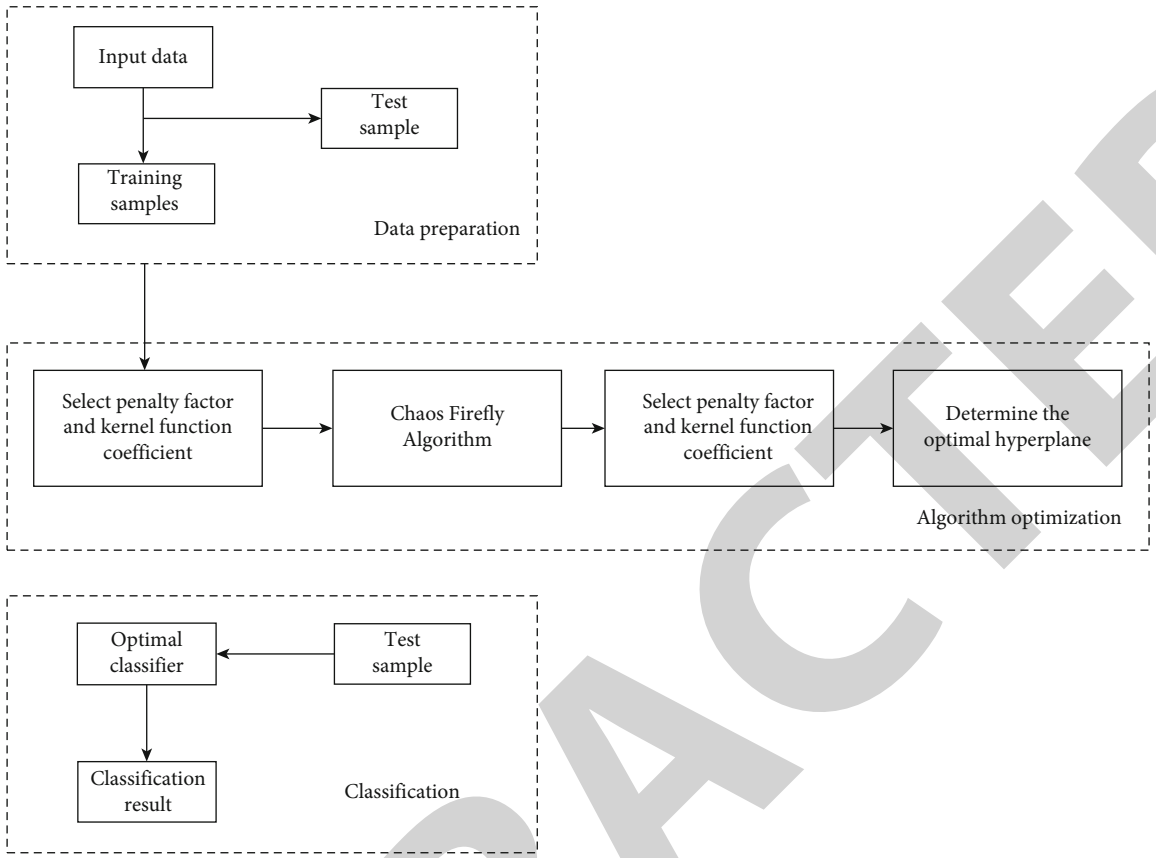

Figure 12: SVM parameter optimization flowchart.

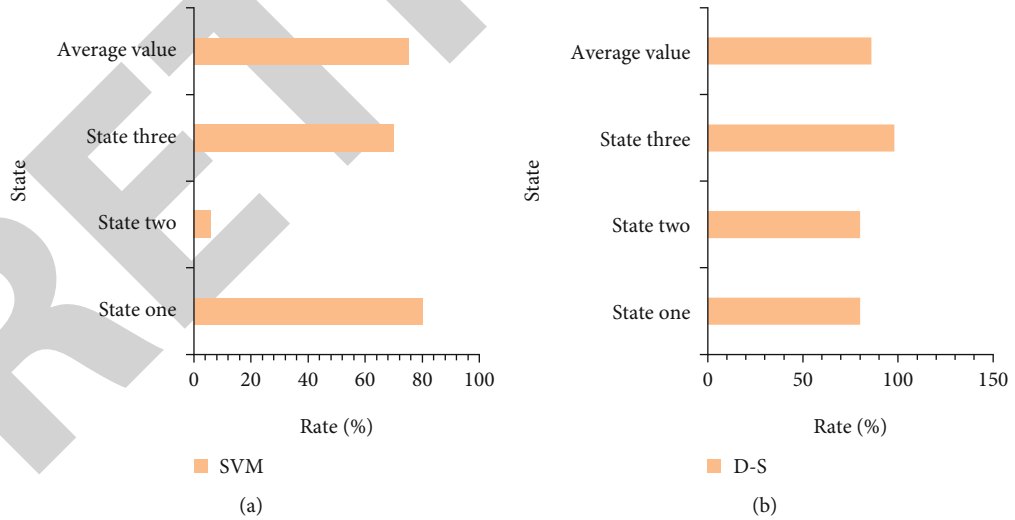

Figure 13: Comparison of recognition accuracy of different algorithms.

Some parents mistakenly believe that the more nutrition the better, they do not pay attention to the daily diet, the meat and vegetables are unreasonable, and if they think that what is nutritious, just feeding the students what they eat can lead to health problems for the students. Breakfast has an important impact on people's health and nutritional status. It is the most important meal of the day. It is an important source of energy and nutrients throughout the day. Eating breakfast every day is a healthy behavior and lifestyle. There are many hazards of skipping breakfast, such as susceptibility to gastritis, peptic ulcer, gallstones, cholecystitis, cardiovascular disease, and other adverse symptoms. It is easy to cause

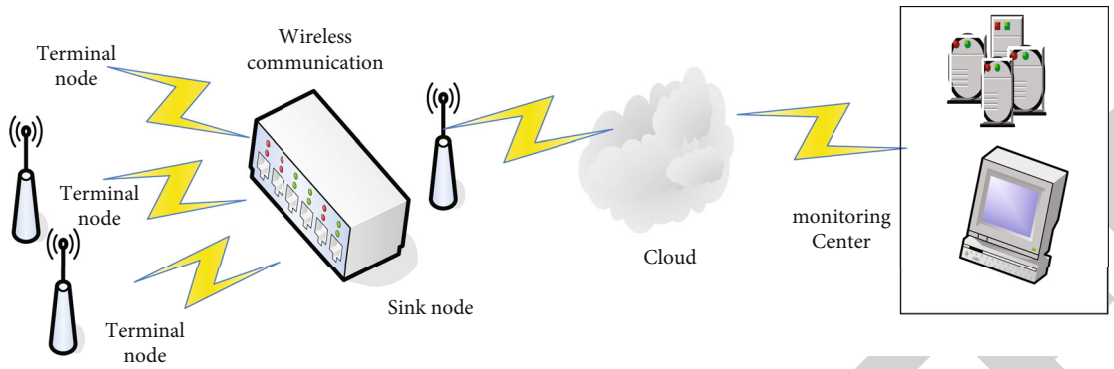

Figure 14: System overall design architecture diagram.

Table 3: Survey on breakfast every morning.

Survey object	Never eat		Eat occasionally		Eat every day	
	Number of people	%	Number of people	%	Number of people	%
Elementary school student	16	2	25	7	749	91
Junior high school student	98	11	258	29	535	60
High school student	9	1	269	31	591	68

Table 4: Survey on the time taken by students for sleep and rest.

Survey object	6 to 7 hours		7 to 8 hours		8 to 9 hours		9 to 10 hours		More than 10 hours	
	Number	%	Number	%	Number	%	Number	%	Number	%
Elementary school student	49	6	156	19	246	30	303	37	66	8
Junior high school student	205	23	383	43	214	24	27	3	0	0
High school student	495	57	156	18	9	1	0	0	9	1

hypoglycemia and diabetes, make people irritable, have memory loss, and reduce work ability. Statistics on the breakfast situation of teenagers are shown in Table 3.

Parents should start with themselves, pay attention to their children's nutrition, and maintain reasonable eating habits in the family. We should pay attention to children's breakfast, parents should not be partial eclipse, and they should help children put an end to partial eclipse and create a harmonious and relaxed dining atmosphere, etc.

5.3. Sleep Habits. With age, people's sleep time needs are different. Adults typically sleep 7 to 8 hours, newborns 18 to 20 hours, and children 12 to 14 hours. Age is a key period for the development and establishment of sleep habits. Primary school students sleep no less than 10 hours a day, and middle school students sleep no less than 9 hours. Statistical sleep status of adolescents is shown in Table 4.

There are many factors for students' long-term lack of sleep, mainly in the following aspects. (1) It is very likely that the child's study pressure is relatively large and the mental burden is relatively heavy. (2) The child's studies are heavy, so he often stays up late to do his homework, which leads to a serious lack of sleep in the child. (3) There are problems in the learning environment (school environment and family environment). (4) There is Internet addiction or TV addiction.

Students' lack of sleep time for a long time can easily lead to many problems. For example, in terms of physiology, it will affect the normal growth and development of students and their physical and mental health. With the vicious circle of bad life, the interest in learning will be seriously affected and sharply diminished, which will lead to the generation of school weariness.

5.4. Physical Exercise. From primary school to university, the daily physical exercise time of students shows a decreasing trend. Exam-oriented education is still very serious; schools do not pay enough attention to sports work and lack strict organization and management; students have heavy learning tasks, which reduce the opportunities for junior and senior students to participate in physical exercise and cause some students to lack enthusiasm and initiative for physical exercise. Due to subjective and objective factors, individual students spend all their time on study or would rather waste their extra time in vain than invest in physical exercise. In order to advance to higher education, schools or teachers increase the teaching time and the amount of homework,

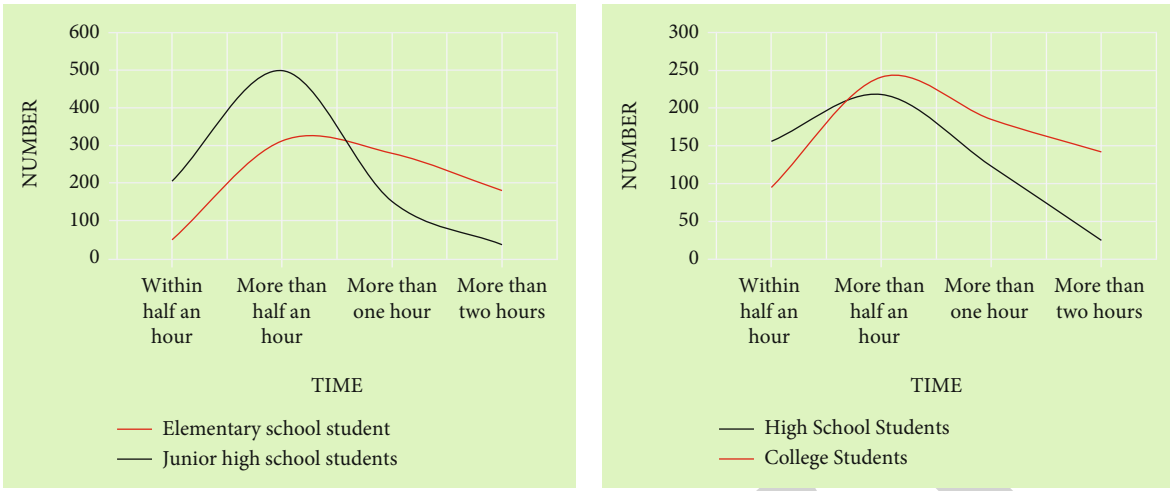

Figure 15: Number of students at different levels at different exercise times per day.

which increases the student's learning burden. The heavy schoolwork burden has crowded out the time for physical exercise. In order to successfully pass the high school and college entrance examinations, it is common to make up classes on weekends. Even if the school does not arrange make-up classes, many parents have hired tutors for their children or signed up for special classes and interest classes. Because of venues, habits, time, and other reasons, extracurricular physical exercise for teenagers has only become a slogan, and some schools have not implemented "sunshine sports" in place. This paper randomly selects 500 students from four levels of primary school, junior high school, high school, and university to conduct a questionnaire survey on physical exercise time. The recovery rate is 100%, and the questionnaire efficiency is 100%. The survey results are shown in Figure 15.

It can be seen from Figure 15 that the exercise time of primary school students and junior high school students is significantly less than that of college students. Although the number of high school students exercising is relatively large, most of them are concentrated in the period of half an hour to one hour, and the exercise time is relatively short. To a certain extent, it reflects students' contempt for system health.

6. Conclusion

With the deepening of education reform, people pay more and more attention to quality education, and quality education is a systematic education project coordinated and cooperated by families, schools, and society. Students' physical fitness test is a means of education, evaluation, and feedback to promote the healthy development of students' physical fitness and encourage students to participate in physical exercise. It focuses on monitoring students' physical shape, physical function, physical quality, and athletic ability and their changing trends. The mass media should vigorously publicize the scientific concept of health and popularize health knowledge to the general public, especially the knowledge of scientific parenting, reversing the incorrect concept of talent and education that principals, parents, and students have a life-long and incorrect view. Correcting the deviations and mistakes of family education, school education, and social education thinking and understanding, the four aspects of society, school, family, and individual students can be organically combined. Through a variety of publicity and education methods, it effectively promotes the active participation of primary and secondary school students in physical exercise, establishes the idea of "health first" and "lifelong sports," and improves the physical health of young students.

Data Availability

The data underlying the results presented in the study are available within the manuscript.

Conflicts of Interest

The authors declare that they have no conflicts of interest.

Acknowledgments

This work was supported by "Teaching Research Project of Huanggang Normal University, China (Grant No. 2018CE49)".

References

[1] A. B. Noel, A. Abdaoui, T. Elfouly, M. H. Ahmed, A. Badawy, and M. S. Shehata, "Structural health monitoring using wireless sensor networks: a comprehensive survey," *IEEE Communications Surveys & Tutorials*, vol. 19, no. 3, pp. 1403–1423, 2017.

[2] N. Mizoue, "CROCO : semi-automatic image analysis system for crown condition assessment in forest health monitoring," *Journal of Forest Planning*, vol. 8, no. 3, pp. 17–24, 2017.

[3] Q. Zhang, Q. Liang, Z. Zhang et al., "Electromagnetic shielding hybrid nanogenerator for health monitoring and protection," *Advanced Functional Materials*, vol. 28, no. 1, 2018.

[4] T. C. Huynh, N. L. Dang, and J. T. Kim, "Advances and challenges in impedance-based structural health monitoring,"

Hindawi
Computational and Mathematical Methods in Medicine
Volume 2023, Article ID 9865029, 1 page
https://doi.org/10.1155/2023/9865029

Retraction

Retracted: Recognition of Human Body Feature Changes in Sports Health Based on Deep Learning

Computational and Mathematical Methods in Medicine

Received 27 June 2023; Accepted 27 June 2023; Published 28 June 2023

This article has been retracted by Hindawi following an investigation undertaken by the publisher [1]. This investigation has uncovered evidence of one or more of the following indicators of systematic manipulation of the publication process:

(1) Discrepancies in scope

(2) Discrepancies in the description of the research reported

(3) Discrepancies between the availability of data and the research described

(4) Inappropriate citations

(5) Incoherent, meaningless and/or irrelevant content included in the article

(6) Peer-review manipulation

The presence of these indicators undermines our confidence in the integrity of the article's content and we cannot, therefore, vouch for its reliability. Please note that this notice is intended solely to alert readers that the content of this article is unreliable. We have not investigated whether authors were aware of or involved in the systematic manipulation of the publication process.

Wiley and Hindawi regrets that the usual quality checks did not identify these issues before publication and have since put additional measures in place to safeguard research integrity.

We wish to credit our own Research Integrity and Research Publishing teams and anonymous and named external researchers and research integrity experts for contributing to this investigation.

The corresponding author, as the representative of all authors, has been given the opportunity to register their agreement or disagreement to this retraction. We have kept a record of any response received.

References

[1] C. Jiao, "Recognition of Human Body Feature Changes in Sports Health Based on Deep Learning," *Computational and Mathematical Methods in Medicine*, vol. 2022, Article ID 1736350, 14 pages, 2022.

Hindawi
Computational and Mathematical Methods in Medicine
Volume 2022, Article ID 1736350, 14 pages
https://doi.org/10.1155/2022/1736350

Research Article

Recognition of Human Body Feature Changes in Sports Health Based on Deep Learning

Chendao Jiao

P.E. Scientific College, Harbin Normal University, Harbin, 150080 Heilongjiang, China

Correspondence should be addressed to Chendao Jiao; daodao_2009@hrbnu.edu.cn

Received 19 January 2022; Revised 19 February 2022; Accepted 5 March 2022; Published 24 March 2022

Academic Editor: Muhammad Zubair Asghar

With the rapid development of social economy and the extensive and in-depth development of national fitness activities, national physical fitness monitoring and research work has achieved rapid development. In recent years, the application of deep learning technology has also achieved research breakthroughs in the field of computer vision. How deep learning technology can effectively capture motion information in sample data and use it to realize the recognition and classification of human actions is currently a research hot spot. Today's popularization of various shooting devices such as mobile phones and portable action cameras has contributed to the vigorous growth of image data. Therefore, through computer vision technology, image data is widely used in practical application scenarios of human feature recognition. This paper proposes a deep learning network based on the recognition of human body feature changes in sports, improves the recognition method, and compares the recognition accuracy with the original method. The experimental results of this paper show that the result of this paper is 1.68% higher than the original recognition method, the accuracy rate of the improved motion history image is increased by 14.8%, and the overall recognition rate is higher. It can be seen from the above experimental results that this method has achieved good results in human body action recognition.

1. Introduction

With the prosperity of sports, the demand for human body recognition technology has gradually increased. Human body feature recognition technology has a good auxiliary effect on activities in the sports field. Through the three-dimensional model, the human body's movement process can be better analyzed. At the same time, with the rapid development of mobile terminals, this technology has been widely used, which has also increased the growth of image data. Therefore, image data is widely used in actual scenes of human body feature recognition through computer vision. With the emergence of deep learning and the enhancement of computing power, deep learning and artificial intelligence methods are being used for automatic feature learning in different fields such as health and image classification. Recently, they are used for extraction and classification of simple and complex human activity recognition features in mobile devices. With the active development of sports in people's lives, the demand for human body feature recognition technology is increasing. The technology can help sports professionals perform 3D human modeling to analyze human movement in images.

At present, most of the research on human behavior recognition is focused on video data, which is based on the number of videos. At the same time, due to the complexity of video image data, it is easy to invade personal privacy. The recognition of human behavior characteristics has always been the focus of computer vision and artificial intelligence research. However, the behavioral characteristics of the human body not only contain spatial information but also need to further consider the dynamic characteristics of the human body. Therefore, the research on the extraction and classification of the human body's behavioral characteristics is very challenging.

The innovation of this article lies in two points. One is to recognize human body motion characteristics with the hot deep learning technology in recent years, and its own learning advantages can more accurately classify human body characteristics. The second is that this article has improved

some of the recognition methods, and the experiment shows that the improved method has a better recognition effect than the unimproved method.

2. Relating Work

Deep learning algorithms have a wide range of applications and have played an important role in a variety of recognition and analysis fields. The prevalence of sports and health care has led many scholars to conduct in-depth research on the recognition technology of the human body in order to obtain better auxiliary effects. The continuous development of science and technology puts forward higher requirements for sports research. Hou analyzed the topic description and behavior recognition based on human motion visual features, mainly introduced the main content of feature extraction and description, and discussed the main content and research methods of human behavior recognition in the thesis. The results show that the improved algorithm proposed has a good effect on behavior recognition and provides a new idea for future research on feature extraction and recognition of sports behavior [1]. Shin and Cha propose a new system to overcome the problems existing in the two existing methods of identifying diverse and complex human behaviors. These two methods are the direct sensor measurement method and the artificial intelligence-based method. In order to realize this system, a multimodal sensor composed of acceleration, gyroscope, and height sensors was developed, and a method that combines sensor measurements and deep learning research results in real time to more accurately recognize gestures and behaviors is described. The practicability and effectiveness of the proposed system are verified by experiments in a real environment [2]. The main purpose of various methods of evaluating athletes' feature recognition is to monitor the athlete's current health status, so as to provide some feedback on the quality of individual training. Based on deep learning and convolutional neural network, Liu and Ji study the target recognition of athletes and propose a feature vector extraction method based on the zero point of curvature. In addition, on the basis of their ideas, they constructed an athlete feature recognition model and optimized the algorithm. The research results show that the proposed method has certain advantages in athlete feature extraction and can be used in subsequent sports training systems [3]. Because the existing player evaluation methods rely heavily on game statistics, they cannot capture the qualitative impact of each player in the game. By combining quantitative game statistics and qualitative analysis provided by news articles, Park et al. propose a player evaluation model in deep learning-based approach. The proposed system was applied to the Korean Professional Baseball League (KBO), and it was proven to be able to understand the sentence polarity of news articles about player performance [4]. Under the influence of COVID-19, there is a great need for research on behavior recognition. Zheng et al. proposed a recurrent neural network algorithm based on long- and short-term memory (LSTM) to realize the recognition of behavior patterns, thereby improving the accuracy of human activity behavior recognition [5]. Improving the level of sports has always been a concern of my country's sports industry. With the continuous improvement of the computer level, how to effectively identify the trajectory of the movement has become a hot spot in the research of related institutions. Based on this, Baoshan researched a motion recognition method based on depth information. First, it briefly introduces the basic knowledge of related theories, including general methods of motion recognition, and the use of depth information for motion recognition. On this basis, a motion recognition method based on depth information is proposed [6]. The above-mentioned scholars have high demand for related research, all require a solid theoretical foundation and are not easy to operate. And it is not easy to collect complete and comprehensive information in data collection.

3. Human Feature Recognition Based on Deep Learning

3.1. Human Body Recognition Based on Deep Learning

3.1.1. The Nature of the Depth Image. In 3D computer graphics, a depth map is a special image, which is different from the traditional gray-scale image where the pixel points represent the pixel intensity value. The depth image records the distance information from the camera to the surface of the scene object [7]. The reason why the depth image is also called the distance image is because the change of the pixel value in the depth map corresponds to the change of the distance in the real three-dimensional world, and the real three-dimensional scene can be reflected by the difference in the depth value [8, 9]. In the human action recognition based on the depth image, each pixel (x, y) in the depth image represents the distance of each part of the human body from the depth camera plane [10]. Normally, RGB image and depth image are obtained at the same time, so their pixels are in a completely contrasting relationship. Due to the unique properties of depth images, depth images are often not disturbed by complex backgrounds, and there is no need to design foreground extraction algorithms for them. Only using the distance information in the depth map to obtain foreground target information requires feature extraction to make the entire recognition system relatively simple.

According to the above description, two properties of depth images are obtained: Color independence and changes in pixel values correspond to changes in the Z axis of the three-dimensional world [11]. Color independence means that the depth image is not sensitive to environmental factors such as the surface color, shadow, and lighting of the object. Another feature of the depth map can be used to separate the various parts of the same object, which causes the problem of overlapping parts of the same object solved in a certain sense. And the use of depth images can be used to reconstruct a part of an object in three dimensions [12].

3.1.2. Commonly Used Human Motion Recognition Database. In view of the fact that most of the current work is mostly tested and verified in the public video database, therefore, the collection of the database plays a vital role in

the recognition of human actions. Nowadays, more and more human movement databases are made public. The early databases were all RGB color image databases, and the most widely used ones were Weizmann and KTH [13]. The actions in these two databases are relatively simple, the background is relatively simple and static, and the fixed angle of view is used when recording, so the difficulty of identification is relatively low. In recent years, some databases with complex backgrounds, rich types of actions, and interactive actions have appeared one after another, for example, Hollywood2 database, UCF sports database, UCF101 database, and HMDB51 database [14]. In addition, the IXMAS database is mainly used for human action recognition in multiview scenes.

3.2. Action Feature Extraction. In the field of computer vision, if the computer is to be able to understand the image, to realize the real "vision." This requires extracting useful data or information from the image and expressing it in a digitized form (such as numerical values or vectors). This process is feature extraction [15].These extracted digital representations are features. Then, through the training of these features, the computer has the ability to recognize images [16].

3.2.1. Depth Motion Maps. Depth Motion Map (DMM) is a projection map model designed specifically for depth images. It first projects each frame of the action video sequence onto three orthogonal Cartesian planes (xoy plane, xoz plane, and yoz plane). In this way, each frame of the depth image of the entire sequence can be viewed from the front view (mapf), the side view (maps), and the top view (mapt). After removing the areas where there is no human body motion on each projection image, the projection image is normalized by bilinear interpolation to reduce the interference caused by the difference of personal height and range of motion [17]. Then, calculate the absolute value difference between two consecutive frames before and after each view, and the difference between the absolute value difference and a certain set threshold is called the motion energy. Movement energy reflects where the action occurs during the duration of the action and provides important discriminant information for identifying the type of action. Then, the motion energy of the entire sequence is accumulated to obtain the depth motion map of the action sequence [18]. The calculation formula of the depth motion map (DMMv) in each view is as follows:

$$\mathrm{BWW}\wedge = \sum_{t=d}^{\mathrm{d}} \left(\left| MAP_{\wedge}^{t+1} - MAP_{\wedge}^{t} \right| > \alpha \right). \tag{1}$$

In the above equation, $\wedge \in \{y, h, i\}$, and y, h, and i, respectively, represent the three perspectives of front, side, and top, and d is the label of the end frame. The projection of the action of the tth frame under the view angle $\wedge$ is $\mathrm{MAP}_{\wedge}^{\mathrm{t}}$. α is the manually input threshold.

3.2.2. Histograms of Oriented Gradients. The HOG descriptor was first proposed by French researcher Dalal at the CVPR2005 conference and has achieved good results in pedestrian detection [19]. HOG can be applied to the feature extraction of RGB images and depth images. Because the edge of the image is the region with the most gradient distribution, the gradient direction histogram can well describe the shape and appearance information of the object. It calculates the weighted projection of the gradient magnitude in the gradient direction in some regions of an image and then connects each local region to form the final feature. Its calculation steps are as follows:

(1) Normalized image: since the changes in illumination and shadow have a greater impact on the texture intensity of the image, in order to reduce the influence of these factors, the commonly used method is to normalize the image [20]. Here, the image is grayed out first, and then, Gamma compression is used for the gray image obtained

(2) The calculation equation of the gradient size $W(A, B)$ and direction $S(A, B)$ of the pixel is

$$W(A,B) = \sqrt{[q(A+1,B) - q(A-1,B)]^2 + [q(A,B+1) - (A,B-1)]^2}, \tag{2}$$

$$S(A,B) = arc\frac{q(A+1,B) - q(A-1,B)}{q(A,B+1) - q(A,B-1)}, \tag{3}$$

where $W(A, B)$ is the gradient amplitude value of a certain pixel, $S(A, B)$ represents the direction of the gradient, and $q(A, B)$ represents the pixel value of a certain point

(3) Constructing the histogram of the gradient direction of the image: first, dividing an image into grids. These grids are called cells. Dividing the 360-degree circle into a number of artificially set bins and then calculating the histogram of the weighted projection of each pixel of the image in these small areas according to the gradient direction. Finally, connecting the histograms of these cell units in series, and then using L2-norm to normalize the entire gradient histogram to further reduce the interference of external environmental factors. Finally, the normalized histogram is the final feature descriptor. The L2-norm calculation formula is as follows:

$$\wedge \longrightarrow \vee / \sqrt{\|(\vee)\|_2^2 + \alpha} \tag{4}$$

3.2.3. Local Binary Patterns. Local Binary Pattern (LBP) is often used to describe the local texture information of an image in the field of computer vision and pattern recognition. Because the texture information described has a high degree of discrimination, it is fast and convenient to implement, has a small amount of data, and has gray-level invariance and rotation invariance. In the early days, it was mostly used in research directions such as target detection and face

recognition. The LBP compares the gray value of the central pixel with the relationship between the gray value of other pixels in the space and then encodes this relationship to achieve the purpose of describing texture features [21].

The most basic LBP descriptor is a 3×3 neighborhood structure, as shown in Figure 1. In the figure, 139 is the LBP value of the central pixel in this square area. However, this square field can only encode a fixed range and cannot adapt to changes in image scale. Subsequently, some scholars proposed a circular field to solve this problem, which can calculate the LBP value of any number of pixels in different radius ranges.

Assuming that $Qa(A0, B0)$ is the center of the pixel, then, there are w domain points uniformly distributed on the radius R of the circle. The coordinates are as follows:

$$(\mathrm{A0} - R \sin(2\pi t/w, B0 + \cos(2\pi t/w))). \tag{5}$$

Since sampling is performed on a circle, the coordinate values of some points may not be integers. But the pixel value of the image must be an integer, so the bisexual interpolation method is mostly used to estimate the value of the coordinate. The calculation equation of the LBP of Qa under the circular field framework is as follows:

$$\mathrm{LBP}(w, R)(Qa) = F(y(Bt)), \tag{6}$$

$$Bt = Qt - Qa, \tag{7}$$

$$F(m) = \sum_{t=0}^{m-1} mt \cdot 2^t, \tag{8}$$

$$y(Qa) = \begin{cases} 1 & Qa \geq 0 \\ 0 & Qa < 0 \end{cases}. \tag{9}$$

In the above equation, $F(m)$ represents a function that can convert the x-bit binary to the decimal system, and the difference from the tth point to the center pixel is Bt. As shown in Figure 2, the radius $R = 1$, and the number of fields is 8.

3.3. Action Classification Recognition. After feature extraction, a feature vector that can effectively describe human actions is obtained. In general, the dimensionality of the feature vector is relatively high and contains more redundant information. If it is directly sent to the classifier, not only will the calculation amount be quite large, but some invalid information may affect the accuracy of recognition. Therefore, it is necessary to reduce the dimensionality of the original feature vector. While avoiding the disaster of dimensionality, it also obtains the most important component of the feature vector and saves memory at the same time. At present, the commonly used dimensionality reduction methods mainly include linear dimensionality reduction (PCA) and nonlinear dimensionality reduction (manifold learning and local linear embedding). In this paper, principal component analysis (PCA), which is relatively simple in calculation, is mainly used for feature dimensionality reduction [22].

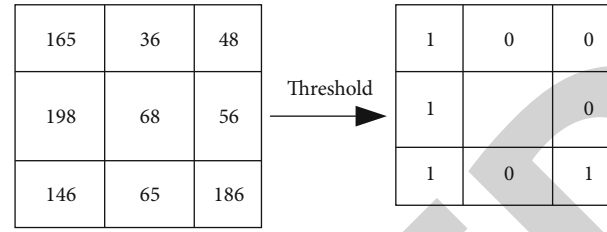

Figure 1: The calculation process of the LBP value of the central pixel in the square area.

In addition, some classifiers based on probability graph models are often used to identify classification problems. They mainly calculate the conditional probabilities of the data to be classified (observed data) under all labels. Under which label has the highest probability, it means that the current data belongs to the category represented by this label. The most representative ones are Bayesian networks and random field models [23]. There are also some commonly used classifiers, such as random forest, AdaBoost classifier, and artificial neural network, which are widely used in various fields [24]. The following is a detailed introduction to the classifier used in this article.

3.4. Support Vector Machine.

3.4.1. SVM Is Linearly Separable. There are two types of data on the two-dimensional plane as shown in Figure 3, which are represented by circles and squares. For these linearly separable data, you only need to find a cutting line that can perfectly separate the two types of data [25].

While maximizing the classification interval, it is necessary to ensure that the classification of other sample points is correct. The constraints are as follows:

$$Bt\left(m^i A + d\right) \geq 1. \tag{10}$$

So this classification problem is transformed into a problem of minimizing the following objective function under the above constraints.

$$\beta(m) = \frac{1}{2} m^i m. \tag{11}$$

The constructed Lagrange function is

$$\mathrm{La}(m, d, \chi) = \frac{1}{2} m^i m - \sum_{t=1}^{n} \chi\left[Bt\left(m^i At + d\right) - 1\right]. \tag{12}$$

Solving Equation (12), the optimal solution χ^*, m^*, and d^* of χ, m, and d is obtained, so the optimal classification function can be expressed as

$$H(b) = \mathrm{sgn}\left(m^* b + d^*\right) = \mathrm{sgn}\left[\sum_{t=1}^{n} \chi^* At(bt \cdot b) + d^*\right]. \tag{13}$$

3.4.2. SVM Is Inseparable Linearly. In the case of linear

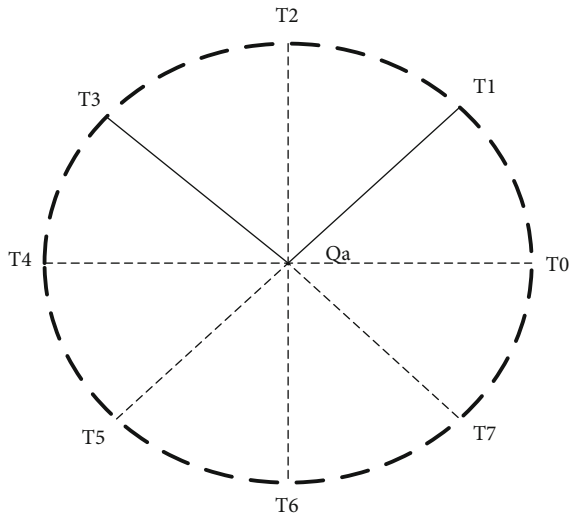

Figure 2: Schematic diagram of the LBP of a circular field with 8 fields.

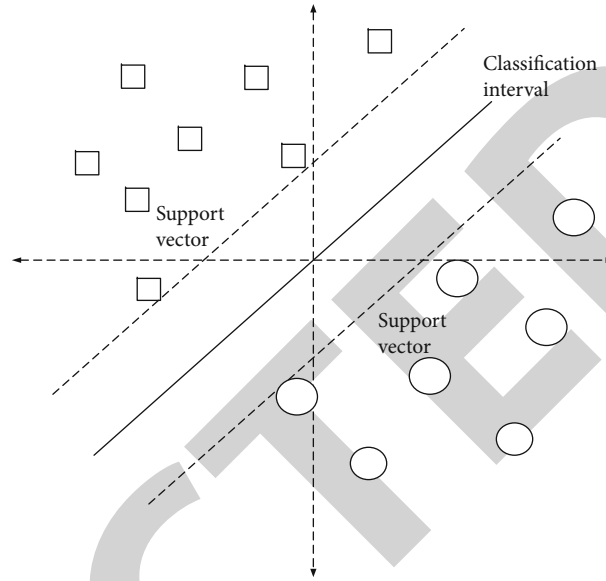

Figure 3: Linear separability diagram of support vector.

inseparability, SVM solves this problem by introducing a kernel function, which plays a crucial role in the classification of SVM, it does not carry out the calculation of the data in the high-dimensional space after the kernel function is mapped, and the main calculation amount still occurs in the low-dimensional space. Here, the kernel function only plays the role of a space transformation and dimensional space to calculate the optimal hyperplane. But it is often difficult to construct a new kernel function. So the simplest method is to directly select and use from the existing kernel functions [26]. The three commonly used kernel functions are as follows:

Polynomial:

$$\left(A^t At + 1\right)^q, \tag{14}$$

where q represents the power parameter.

Hyperbolic tangent:

$$\tan\left[\delta 0 A^t At + \delta 1\right], \tag{15}$$

where $\delta 0$ and $\delta 1$ both represent specially selected parameters.

RBF is

$$\mathrm{ex}\left[-\frac{1}{2\theta^2}\left\|A - At\right\|^2\right], \tag{16}$$

where θ^2 is an optional parameter.

For linear and inseparable problems, you need to map the data to a high-dimensional space.

$$A \longrightarrow \left\{(\varphi(\mathrm{At})\right\}_{t=1}^{w1}. \tag{17}$$

The classification hyperplane constructed in high-dimensional space is

$$\sum_{t=1}^{n} \chi tBt\varphi(At)\varphi(A) = 0. \tag{18}$$

At this time, the defined kernel product is

$$R(A, At) = \varphi^t(A)\varphi(At) = \sum_{t=1}^{n} \varphi t(A)\varphi t(At). \tag{19}$$

Based on the same idea of linear separability, the problem is transformed into:

$$\max \sum_{t=1}^{n} \chi t - \frac{1}{2}\sum_{t=1}^{n}\sum_{t=1}^{n} \chi t \chi BtR(A, At), \tag{20}$$

$$\sum_{t=1}^{n} \chi tBt = 0, \quad 0 \le \chi t \le D. \tag{21}$$

In Equation (21), D is a positive parameter selected by the user, and Equation (21) is a constraint condition. After the equation is constructed and solved, the parameters are substituted into Equation (18) to obtain the optimal decision surface.

3.5. Challenges Faced by Human Feature Recognition. Human action recognition has been developed rapidly in the last ten years. In order to make action recognition can be well applied in real life, more and more effective and robust methods have been proposed. These methods are often more inclined to be applied in real life scenarios. Although relatively ideal recognition results have been achieved, there are still many thorny problems and challenges.

3.5.1. Interference from the External Environment. The interference of the complex external environment has always been a big problem in the field of action recognition. Complicated backgrounds, including messy backgrounds, dramatic changes in illumination, and camera shake, make it extremely difficult to extract the foreground. Occlusion generally occurs in relatively complex interactive actions. For example, in multiperson interactive actions, the occlusion of actions between people makes the recognition of the overall interactive actions inaccurate. In addition, in the case of camera movement, the expression of human actions in different viewing angles is very different, so it is also a great challenge to extract robust features for recognition in a multiview environment.

3.5.2. It Is Difficult to Recognize Continuous Unsegmented Actions and Complex Actions. Since human body movements are a continuous process in time, there is no clear sign to indicate the end of the previous movement and the beginning of the next movement, which makes it often difficult to distinguish a single movement. At this stage, most of the data used in the research is segmented and marked action data. Good results have been achieved in the recognition of relatively simple single actions, simple interactions between two people, and interactions between a single person and a single object. However, the recognition effect for those continuous undivided actions, complex multiperson interaction actions, and group behaviors is not ideal.

3.5.3. The Influence on Recognition within and between Action Types. For the same action, different people will behave differently when performing the action, which results in different amplitude and duration of the same action. In this way, in the design of the feature extraction method, the spatial scale and movement speed should not be deformed. In addition, there may also be greater similarities between different actions, which brings great difficulties to the accurate recognition of actions. For example, "Draw a cross" and "Draw a circle" have a very high similarity, resulting in a high rate of misjudgment of the recognition results.

4. Convolutional Neural Network

In recent years, deep neural networks have gradually become a very popular research direction and have made breakthroughs in computer vision and other fields. Accurately detecting and extracting key regions of human motion from video is the first step in human action recognition, and its accuracy will directly affect the effect of subsequent action recognition tasks. The deep convolutional neural network is greatly affected by the dataset in the training stage, and the size of the samples in the dataset directly affects the structure and performance of the network. As an important branch of deep neural networks, convolutional neural networks are widely used in video image, speech recognition, and other fields. Its appearance also provides a new solution for the human action recognition problem that we are studying.

4.1. Common Convolutional Network. Convolutional neural networks are mostly used for image classification, detection, and recognition tasks. Structurally, in a convolutional neural network, the convolutional layer and the subsampling layer can form a feature extractor. In the convolutional layer, a mechanism called "local receptive field" is used, which means that neurons are not connected to all neurons in the adjacent layer, but are partially connected. Second, another feature of the network is shared weights. The so-called shared weights refer to the use of convolution kernels of the same size. In addition, subsampling is also a major feature. Subsampling is also called pooling, and there are two methods commonly used: mean pooling and maximum pooling. Mean pooling means that the center point coordinates take the average value of the elements covered by the pooled template, and maximum pooling means that the maximum value of the elements is taken. The different combinations of these features or mechanisms have become the cornerstones of some of our commonly used convolutional neural network structures today. Its advantage is that it can greatly reduce the number of weights and greatly reduce the complexity of the model. The main convolutional neural networks involved in this article are AlexNet and GoogleNet. Then, I will introduce these two networks.

4.1.1. AlexNet. AlexNet was published in 2012 and became an instant hit. It can be called a classic of the year [27]. The emergence of AlexNet has reversed the decline of convolutional neural networks and inspired the confidence of scholars in this field. Many more excellent networks have been proposed one after another. When participating in the ImageNet competition that year, the top5 error rate was only 19.8%. Compared with the previous machine learning classification algorithm, the network is already very impressive. The model is divided into eight layers in total, including five convolutional layers and three fully connected layers, and each convolutional layer contains a linear rectification function and a local response normalization process and then undergoes a pooling process. The specific structure distribution is shown in Figure 4.

In general, pooling is nonoverlapping, while the pooling used by AlexNet is overlapping, that is, when pooling, the step length of each move is smaller than the side length of pooling. After the pooling is completed, the network sets up a local corresponding normalization mechanism, which can increase the generalization ability, smoothly process the data, and improve the recognition rate. The calculation formula is shown in formula (22).

$$d_{a,b}^{t} = \frac{\alpha_{a,b}^{t}}{\left(R + \alpha \sum_{t=\max(0,t-1)}^{\min(n-1,t+n/2)} \left(\alpha_{a,b}^{t}\right)^{2}\right)}. \tag{22}$$

The equation shows that multiple values before and after a value are standardized, where the value of the tth convolution (a, b) coordinate is expressed as $\alpha_{a,b}^{t}$, and R, n, and α are all hyperparameters.

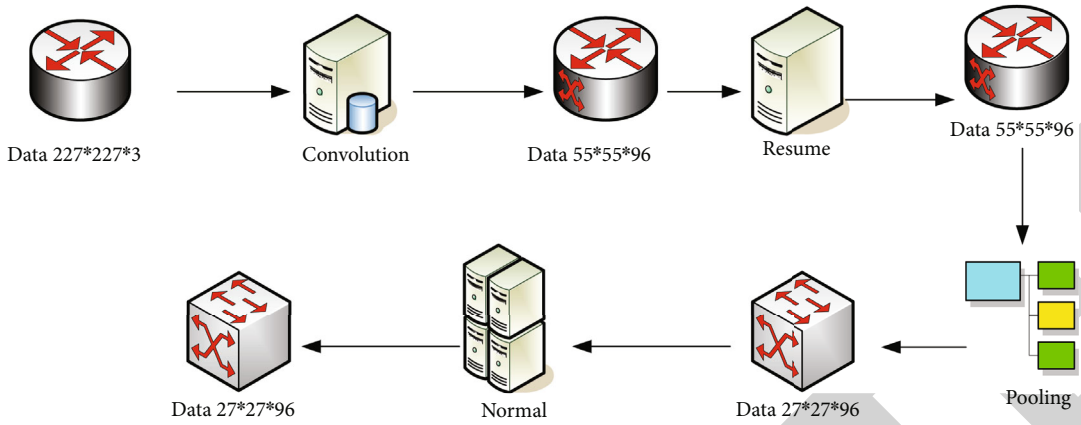

Figure 4: The first layer network structure of AlexNet.

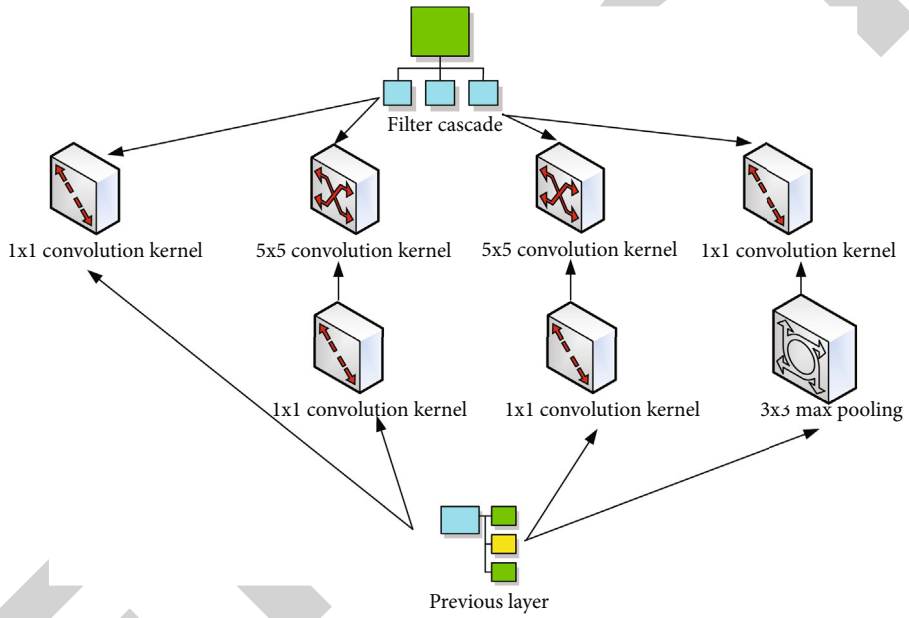

Figure 5: Inception module of GoogleNet network.

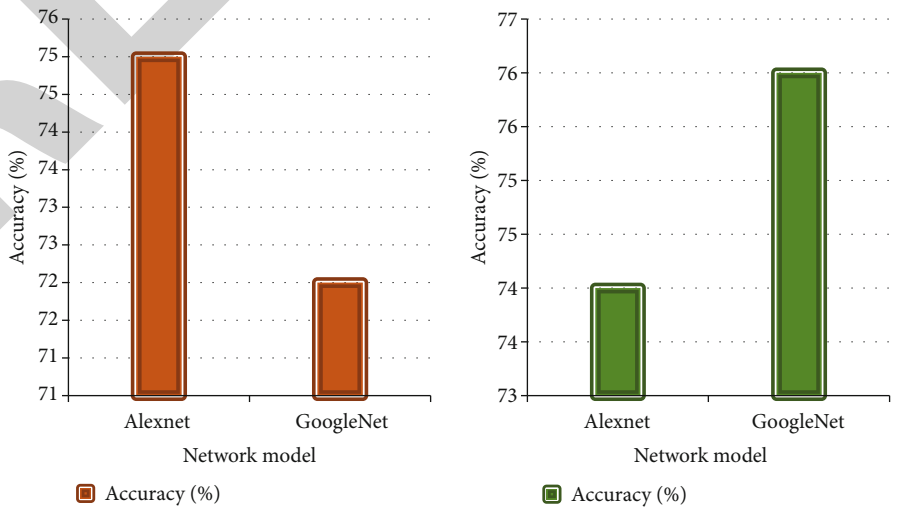

Figure 6: The recognition accuracy of different networks when the input values are different.

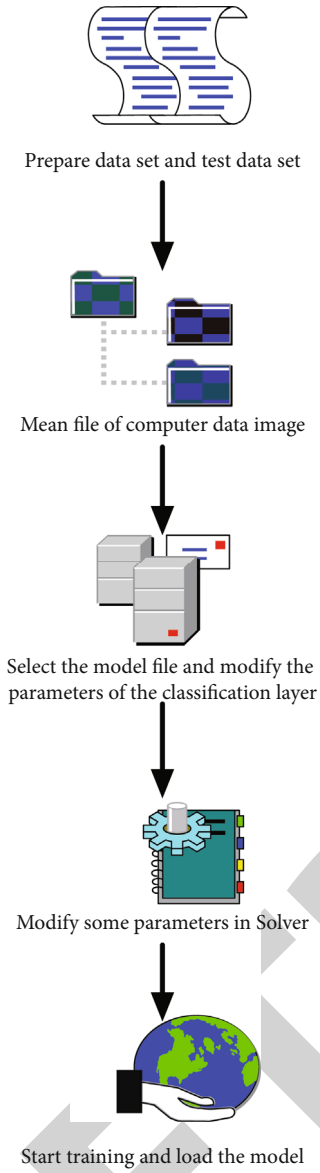

Figure 7: Basic steps for fine-tuning the network.

4.1.2. GoogleNet. One common point of the two models, GoogleNet and VGG, is that there are more layers and a deeper network structure. Structurally speaking, VGG inherits some frameworks of Lenet and alexNet. Unlike VGG, GoogleNet has made a bolder attempt on the Internet. Although this model has 22 layers, its size is much smaller than AlexNet and VGG, and it still performs well [28]. The most effective way to obtain a higher-quality model is to increase the number of layers (that is, depth) of the model or the number of convolution kernels or neurons in each layer of the model (model width).

The GoogleNet model has 22 layers, and the number of layers is deeper. At the same time, in order to avoid the gradient dispersion problem mentioned earlier, GoogleNet cleverly added two loss functions at different depths to eliminate the gradient dispersion phenomenon. Not only has the network depth increased, GoogleNet has also increased the network width, thereby reducing the complexity of the feature map and achieving the effect of dimensionality reduction, as shown in Figure 5. In addition, the use of this modular structure design can also facilitate the addition and modification of the network structure.

In addition, GoogleNet has made the following improvements:

(1) The network finally uses average pooling to replace the fully connected layer. This idea originates from NIN, the reason why NIN uses a multilayer perceptron is that the structure of MLP is compatible with CNN, both can be trained using backpropagation, and it is also a deep model, which is consistent with the concept of feature reuse. And experiments have shown that this method can increase the accuracy of TOP-1 by 0.6%

(2) In order to solve the problem of gradient disappearance caused by the deepening of the network layer, the network designed two branches and added two softmax classifiers at the end of the branches to assist in adjusting the network parameters. Some researchers have proposed to add attenuation coefficients to the two classifiers, but in the end, it is proved through experiments that the improvement is not very meaningful [29, 30]. When we actually test, these two extra softmax will be removed, only based on the output result of the main softmax. Softmax maps some inputs to real numbers between 0 and 1, and the normalization guarantees that the sum is 1, so the sum of the probabilities of multiclassification is exactly 1. It is widely used in multiclassification scenarios

4.2. Recognition Based on Deep Learning Network

4.2.1. Result Analysis. In order to compare the performance of the two networks AlexNet and GoogleNet in this article, the experiment uses the color motion history image and the front view of the depth motion map as data, trains the network from zero under the same conditions, and compares and analyzes the experimental performance of the two networks.

From the data in Figure 6, we can find that, not in all data, the deeper the network and the more layers, the higher the recognition accuracy. When the input data is motion history images, AlexNet outperforms GoogleNet, with a recognition accuracy of 75% and 72%, respectively, and the latter has a deeper and wider network structure. When the input data is a front view, the recognition accuracy of the two is 74% and 76%, respectively, and the effect of GoogleNet is relatively good. Therefore, we can conclude that when the amount of training data is small, the recognition effect of the network with fewer layers is better, and the network with a deeper structure is slightly less effective. This is because the deep structure network has more parameters that need to be optimized and adjusted, and a small amount of data cannot train the parameters well.

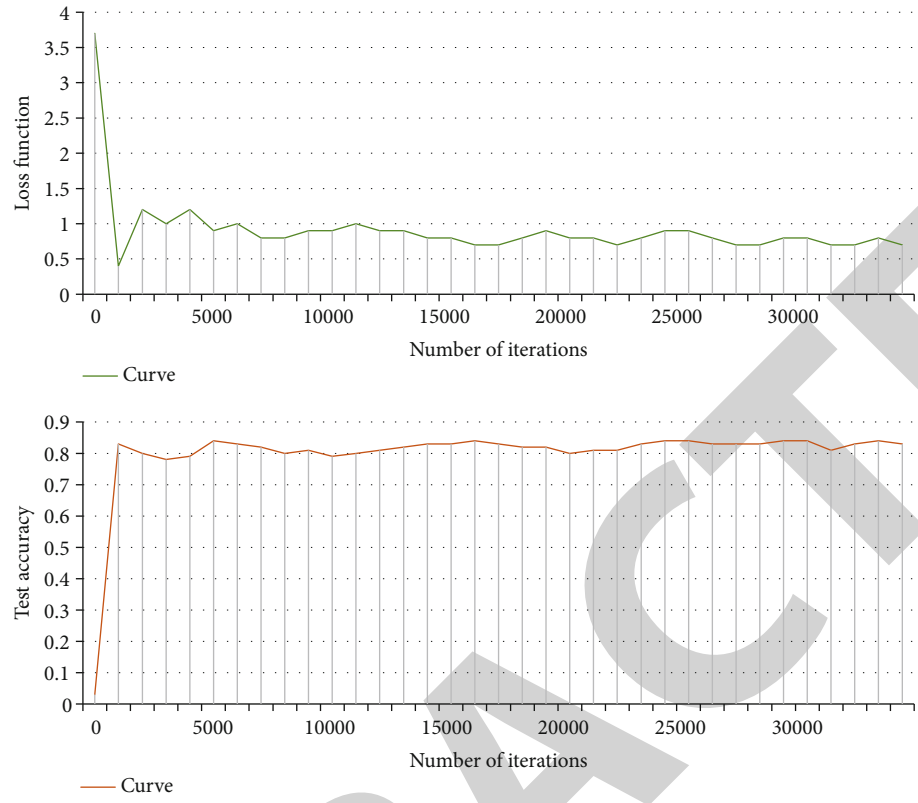

Figure 8: Test curve of exercise history graph.

Table 1: Number of training data and test data.

	MHI	Front	Side	Top
Training samples	435	3798	3798	3798
Test data	429	429	429	429
Mean	432	2113.5	2113.5	2113.5

4.2.2. Fine-Tuning the Network. Due to insufficient data volume, the parameters cannot be adjusted optimally. At this point, if there is a model with pretrained parameters, we adjust it on the basis of it to adapt it to the problem we want to solve; then, things become less tricky. This process is called fine-tuning. In this article, we choose the AlexNet and GoogleNet networks trained on the ImageNet dataset. ImageNet is an image dataset organized according to the WordNet hierarchy and is free for academic research and noncommercial use. First, we need to download the trained caffemodel. Then, the entire process of network fine-tuning is shown in Figure 7.

4.3. Drawing of Precision Curve and Loss Function Curve. In the Caffe training process, in order to better understand the convergence of the network and show your own results, you usually graph your own training data. This not only facilitates the adjustment of parameters during the training process but also facilitates the display of the final results. The graph finally obtained is shown in Figure 8.

Figure 8(b) is a graph of the test accuracy and the number of iterations. After the increase, the overall trend is stable within a range. Figure 8(a) is a graph of the loss function and the number of iterations. At the beginning of the iteration, it shows a sudden downward trend and then tends to a stable state.

5. Human Body Characteristics Based on Deep Learning

5.1. Two Deep Learning Networks Experimental Results. Because these two types of data have orders of magnitude difference. As shown in Table 1, the amount of training data and test data of the exercise history graph and the side view and top view data amount of the experiment in this article are also listed in the table. The training network structure still uses two deep learning networks, AlexNet and GoogleNet, and the training starts from the most primitive state. The experimental results are shown in Figures 9(a) and 9(b).

It can be seen from the experimental results that whether it is the motion history image as the input or the front view of the depth motion map as the input, and whether it is AlexNet or GoogleNet in the network framework, Fine-tuning on the trained model has a higher recognition accuracy than restarting the training. At the same time, it can also be found that the recognition accuracy obtained by fine-tuning the motion history image on AlexNet is higher than that on GoogleNet, while the situation of the depth motion image is just the opposite. This is why this article

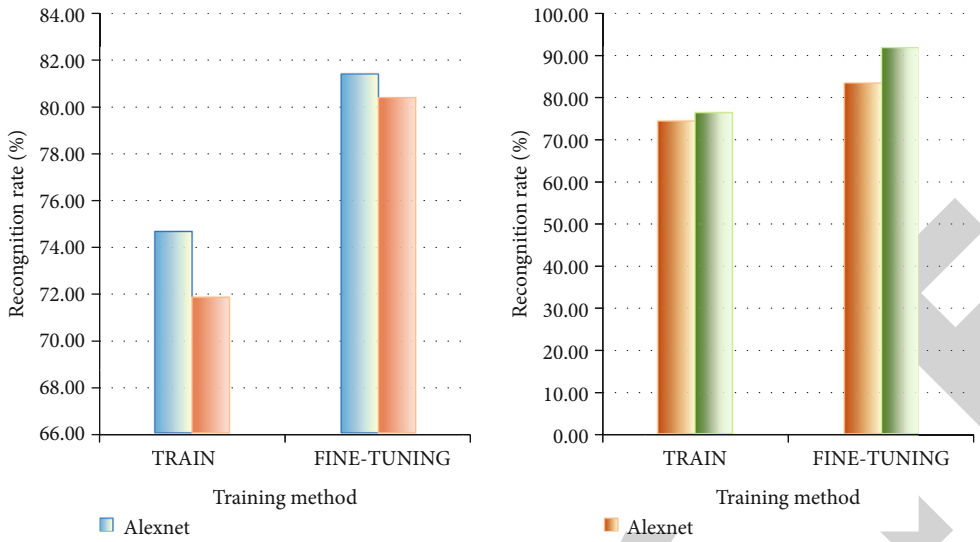

Figure 9: Comparison of the recognition rate of the two networks under the two methods of training and fine-tuning.

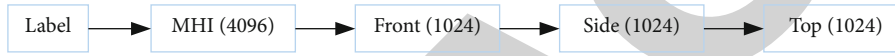

Figure 10: Schematic diagram of feature stitching.

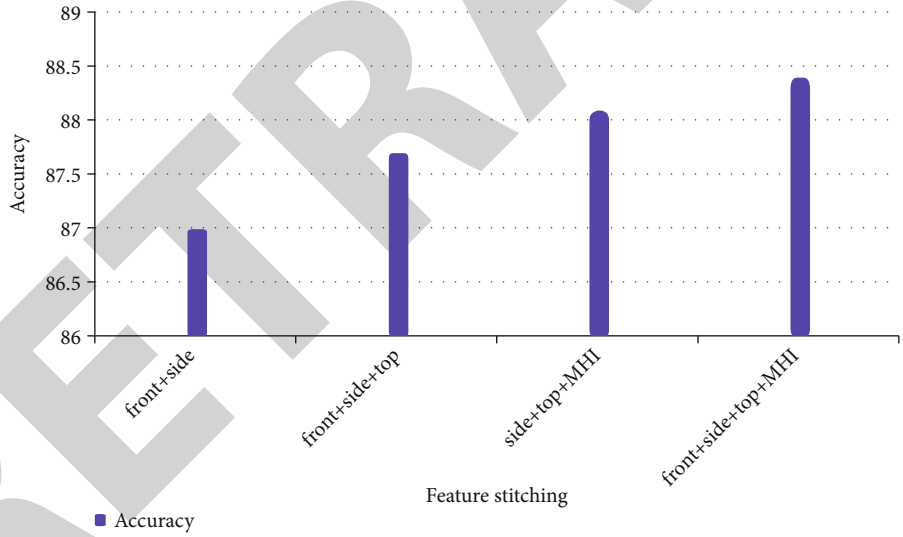

Figure 11: Recognition rate of different stitching features.

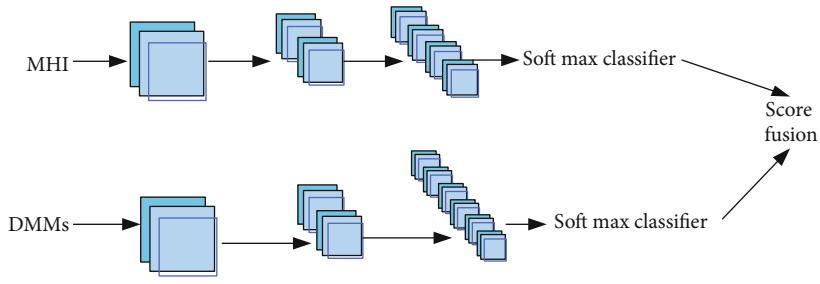

Figure 12: Flow chart of decision fusion.

Table 2: Accuracy of recognition under different fusion rules.

Law of fusion	Recognition rate%
3331Mfst	87.5
Fst	89.6
442fst	89.6
Mfst(+)	91
Mfst(∗)	91.8

Table 3: Recognition accuracy under different verification methods.

Ways of identifying Fusion decision	Multiplication rule	Law of peace	Weight rule
Same target verification	99.5	98.1	98.8
Cross-target verification	91.9	91.8	87.6
Mean	95.7	94.95	93.2

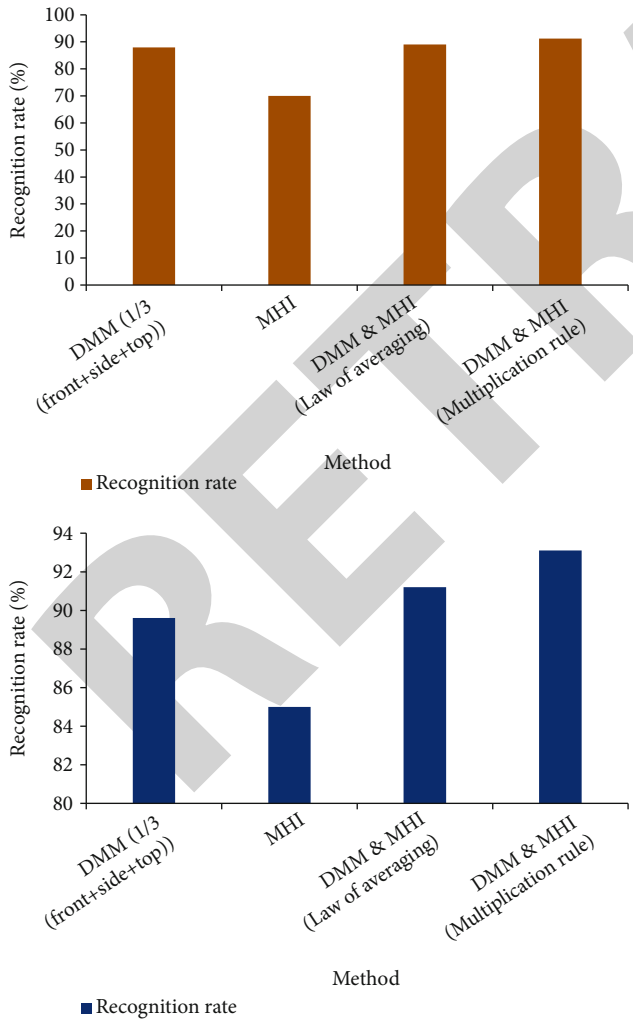

Figure 13: Comparison of the recognition effect of the original and the improved recognition effect of different methods.

finally chose to fine-tune AlexNet for motion history images and fine-tune GoogleNet for deep motion images.

5.2. Feature-Level Fusion and Decision-Level Fusion. Information fusion, also known as data fusion, refers to the integration of different information together to remove redundancy. The information obtained after fusion will benefit our subsequent analysis and processing. In the field of image processing, information fusion is divided into three types: data fusion, feature fusion, and decision fusion. The fusion of data or sample level in the data acquisition and preprocessing stages is called data fusion, the combination of features in the feature extraction stage is called feature fusion, and the fusion of recognition results in the classification decision stage is called decision fusion. This article uses feature fusion and decision fusion, so the following two parts of the content are related experiments and explanations.

5.2.1. Feature Level Fusion. This article is mainly based on the convolutional neural network to extract features, then performs feature splicing, and then uses the softmax classifier to train and classify the spliced features. The overall framework is shown in Figure 10.

The result is shown in Figure 11. From the table, we can see that the more feature samples and the higher the feature dimension, the better the classification effect of the trained classifier. When we stitch all the four features, the classification effect is the best.

5.2.2. Decision-Level Integration. Decision fusion refers to the training of multiple features to obtain multiple classifiers, and then, these classifiers are combined according to different rules, and finally a target judgment result is obtained under the common action. In this article, the front view, side view, and top view of the motion history image and the depth motion map are mainly used to train the convolutional neural network to obtain four classification results. Then, we use different rules to fuse these four classifiers, as shown in Figure 12.

5.3. Recognition of Different Fusion Rules Based on Deep Learning. This article uses the five different fusion rules listed in the table to conduct experiments.

It is not difficult to find from Table 2 that by using different fusion rules to combine the recognition results of the motion history map, the front view of the depth motion map, the side view, the top view, and different final recognition accuracy rates can be obtained. Among them, the results of the four kinds of motion characterization images are fused by the multiplication rule, and the highest recognition accuracy can be obtained in the end.

5.4. Recognition Accuracy of Different Verification Methods Based on Deep Learning. This section first conducts experiments on different verification methods and different decision fusion methods and compares their accuracy. The experimental results are shown in Table 3. It can be seen from the table that there will be big differences in the effects of different performers of the same type of action, and the same actions will also show differences. Because even if the

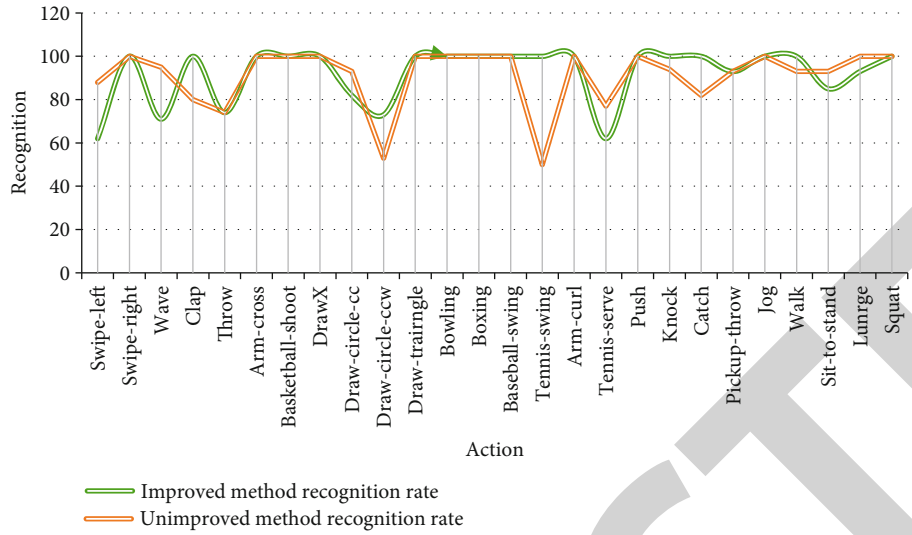

Figure 14: The recognition rate of each type of action of the method in this paper and the unimproved method.

same target verification is used, the recognition accuracy cannot reach 100%. But in comparison, same-target verification is more accurate than cross-target verification. But at the same time, cross-target verification can better explain the robust performance and generalization performance of the trained model.

As shown in Figure 13, we have done the same experiment for comparison. The results prove that the improvements made in this article on the motion history image and the depth motion map and the selection of a more appropriate network for different numbers of networks have an effect on the accuracy of recognition. The depth motion map uses the average rule for decision fusion, and the result of this paper is 1.68% higher than the original recognition method. The improved motion history image accuracy rate has increased by 14.8%, and when the depth motion map and the motion history map are fused by the average rule, it is increased by 2.4%, and when the multiplication rule is used, it is increased by 0.69%.

Figure 14 shows the comparison of the recognition rate of each type of action between the method in this paper and the unimproved method. It can be seen that there are 17 categories where the action recognition rate reaches 100% in this paper, while only 13 categories have not improved methods. Although the recognition rate of some actions is not as high as that of the unimproved method, the overall recognition rate is higher. It can be seen from the experimental results that this method has achieved good results in human action recognition. At the same time, the RGB video and depth video captured by the depth camera are used, and the motion history map and the depth motion map are used to represent and enhance the motion information. Combined with the convolutional neural network, four parallel network architectures are used, which can combine depth information with RGB video information and improve the accuracy of action recognition.

6. Conclusions

This article briefly introduces the convolutional neural network and the internal structure of the two networks selected in this article. Then, three methods of information fusion are introduced, and two fusion methods experimented in this paper are described in detail. Finally, at the end of this chapter, the experiments done at this stage and the analysis of their results are given. This paper mainly studies the recognition and classification of human actions combined with deep learning. First of all, human action contains time dimension information and spatial dimension information in the execution process, which is of great significance to the recognition of the action. How to extract and characterize the movement information is particularly important. Secondly, how to effectively use the characterization information for action recognition and classification also has a great influence on the final result. Finally, for small-scale databases, how to make full use of limited data to achieve higher accuracy is also a problem that needs to be solved. In response to the above problems, this paper has conducted some related studies. The results show that the same-target verification is more accurate than cross-target verification, but at the same time, cross-target verification can better explain the robust performance and generalization performance of the trained model. The comparison of the action recognition rate between the method in this paper and the unimproved method shows that the improved method is more excellent.

Data Availability

No data were used to support this study.

Disclosure

We confirm that the content of the manuscript has not been published or submitted for publication elsewhere.

Conflicts of Interest

There is no potential competing interests in our paper.

Authors' Contributions

The author has seen the manuscript and approved to submit to your journal.

Acknowledgments

This work was supported by the Philosophy and Social Science Research Planning Project of Heilongjiang Province in 2021: Research on the integration path of online and offline education based on OBE concept, General Project 21EDB077.

References

[1] J. Hou, "Research on the feature description and behavior recognition of sports human body based on vision," *Agro Food Industry Hi Tech*, vol. 28, no. 1, pp. 2636–2640, 2017.

[2] S. Y. Shin and J. H. Cha, "Human activity recognition system using multimodal sensor and deep learning based on LSTM," *Transactions of the Korean Society of Mechanical Engineers A*, vol. 42, no. 2, pp. 111–121, 2018.

[3] Y. Liu and Y. Ji, "Target recognition of sport athletes based on deep learning and convolutional neural network," *Journal of Intelligent and Fuzzy Systems*, vol. 40, no. 2, pp. 2253–2263, 2021.

[4] Y. J. Park, H. S. Kim, D. Kim, H. Lee, S. B. Kim, and P. Kang, "A deep learning-based sports player evaluation model based on game statistics and news articles," *Knowledge-Based Systems*, vol. 138, pp. 15–26, 2017.

[5] B. Zheng, D. Yun, and Y. Liang, "Research on behavior recognition based on feature fusion of automatic coder and recurrent neural network," *Journal of Intelligent and Fuzzy Systems*, vol. 39, no. 6, pp. 8927–8935, 2020.

[6] T. Baoshan, "Research on the recognition method of sports based on the depth information," *Agro Food Industry Hi Tech*, vol. 28, no. 1, pp. 1886–1889, 2017.

[7] M. S. Roobini, T. K. Kedar, and A. Sivasangari, "Self-intelligence with human activities recognition based in convolutional neural network," *Journal of Computational and Theoretical Nanoscience*, vol. 17, no. 8, pp. 3484–3490, 2020.

[8] M. Abdolmaleky, M. Naseri, J. Batle, A. Farouk, and L. H. Gong, "Red-green-blue multi-channel quantum representation of digital images," *Optik*, vol. 128, pp. 121–132, 2017.

[9] O. I. Khalaf, C. A. T. Romero, A. A. J. Pazhani, and G. Vinuja, "VLSI implementation of a high-performance nonlinear image scaling algorithm," *Journal of Healthcare Engineering*, vol. 2021, 10 pages, 2021.

[10] H. K. van der Burgh, R. Schmidt, H.-J. Westeneng, M. A. de Reus, L. H. van den Berg, and M. P. van den Heuvel, "Deep learning predictions of survival based on MRI in amyotrophic lateral sclerosis," *Neuro Image: Clinical*, vol. 13, pp. 361–369, 2017.

[11] P. Wang, "Research on sports training action recognition based on deep learning," *Scientific Programming*, vol. 2021, no. 7, 2021.

[12] H. Peng and Q. Li, "Research on the automatic extraction method of web data objects based on deep learning," *Intelligent Automation and Soft Computing*, vol. 26, no. 3, pp. 609–616, 2020.

[13] D. K. Vishwakarma and K. Singh, "Human activity recognition based on spatial distribution of gradients at sublevels of average energy Silhouette images," *IEEE Transactions on Cognitive & Developmental Systems*, vol. 9, no. 4, pp. 316–327, 2017.

[14] Y. Zhao, H. Di, and J. Zhang, "Region-based mixture models for human action recognition in low-resolution videos," *Neurocomputing*, vol. 247, pp. 1–15, 2017.

[15] R. San-Segundo, H. Blunck, J. Moreno-Pimentel, A. Stisen, and M. Gil-Martín, "Robust human activity recognition using smartwatches and smartphones," *Engineering Applications of Artificial Intelligence*, vol. 72, pp. 190–202, 2018.

[16] A. Kl and Y. Kaya, "A new approach for human recognition through wearable sensor signals," *Arabian Journal for Science and Engineering*, vol. 46, no. 4, pp. 4175–4189, 2021.

[17] B. Zou and A. Gofuku, "Evaluation of operation state for operators in NPP Main control room using human behavior recognition," *Multimedia Tools and Applications*, vol. 80, no. 14, pp. 21809–21821, 2021.

[18] M. Lv, C. Ling, and T. Chen, "Bi-view semi-supervised learning based semantic human activity recognition using accelerometers," *IEEE Transactions on Mobile Computing*, vol. 17, no. 9, pp. 1991–2001, 2018.

[19] D. Wu, "Online position recognition and correction method for sports athletes," *Cognitive Systems Research*, vol. 52, pp. 174–181, 2018.

[20] R. Chereshnev and A. Kertesz-Farkas, "RapidHARe: a computationally inexpensive method for real-time human activity recognition from wearable sensors," *Journal of Ambient Intelligence and Smart Environments*, vol. 10, no. 5, pp. 377–391, 2018.

[21] S. Ouellet and F. Michaud, "Enhanced automated body feature extraction from a 2D image using anthropomorphic measures for silhouette analysis," *Expert Systems with Application*, vol. 91, pp. 270–276, 2018.

[22] P. Bao, A. I. Maqueda, and C. R. Del-Blanco, "Tiny hand gesture recognition without localization via a deep convolutional network," *IEEE Transactions on Consumer Electronics*, vol. 63, no. 3, pp. 251–257, 2017.

[23] S. Zhou, J. Wu, F. Zhang, and P. Sehdev, "Depth occlusion perception feature analysis for person re-identification," *Pattern Recognition Letters*, vol. 138, no. 3, pp. 617–623, 2020.

[24] G. Litjens, T. Kooi, B. E. Bejnordi et al., "A survey on deep learning in medical image analysis," *Medical Image Analysis*, vol. 42, no. 9, pp. 60–88, 2017.

[25] Y. Chen, Z. Lin, and Z. Xing, "Deep learning-based classification of hyperspectral data," *IEEE Journal of Selected Topics in Applied Earth Observations & Remote Sensing*, vol. 7, no. 6, pp. 2094–2107, 2014.

[26] D. Shen, G. Wu, and H. I. Suk, "Deep learning in medical image analysis," *Annual Review of Biomedical Engineering*, vol. 19, no. 1, pp. 221–248, 2017.

[27] T. Oshea and J. Hoydis, "An introduction to deep learning for the physical layer," *IEEE Transactions on Cognitive Communications & Networking*, vol. 3, no. 4, pp. 563–575, 2017.

[28] D. Gharavian, M. Bejani, and M. Sheikhan, "Audio-visual emotion recognition using FCBF feature selection method

Hindawi
Computational and Mathematical Methods in Medicine
Volume 2023, Article ID 9895751, 1 page
https://doi.org/10.1155/2023/9895751

Retraction

Retracted: Analysis of Influencing Factors for Chronic Diseases: A Large Sample Epidemiological Survey from Liaoyang

Computational and Mathematical Methods in Medicine

Received 27 June 2023; Accepted 27 June 2023; Published 28 June 2023

This article has been retracted by Hindawi following an investigation undertaken by the publisher [1]. This investigation has uncovered evidence of one or more of the following indicators of systematic manipulation of the publication process:

(1) Discrepancies in scope

(2) Discrepancies in the description of the research reported

(3) Discrepancies between the availability of data and the research described

(4) Inappropriate citations

(5) Incoherent, meaningless and/or irrelevant content included in the article

(6) Peer-review manipulation

The presence of these indicators undermines our confidence in the integrity of the article's content and we cannot, therefore, vouch for its reliability. Please note that this notice is intended solely to alert readers that the content of this article is unreliable. We have not investigated whether authors were aware of or involved in the systematic manipulation of the publication process.

Wiley and Hindawi regrets that the usual quality checks did not identify these issues before publication and have since put additional measures in place to safeguard research integrity.

We wish to credit our own Research Integrity and Research Publishing teams and anonymous and named external researchers and research integrity experts for contributing to this investigation.

The corresponding author, as the representative of all authors, has been given the opportunity to register their agreement or disagreement to this retraction. We have kept a record of any response received.

References

[1] C. Jiang and Q. Wang, "Analysis of Influencing Factors for Chronic Diseases: A Large Sample Epidemiological Survey from Liaoyang," *Computational and Mathematical Methods in Medicine*, vol. 2022, Article ID 1537906, 6 pages, 2022.

Hindawi
Computational and Mathematical Methods in Medicine
Volume 2022, Article ID 1537906, 6 pages
https://doi.org/10.1155/2022/1537906

Research Article

Analysis of Influencing Factors for Chronic Diseases: A Large Sample Epidemiological Survey from Liaoyang

Cuiqin Jiang and Qian Wang

Neurology Department, Liaoyang Central Hospital, Liaoyang, 111000 Liaoning, China

Correspondence should be addressed to Cuiqin Jiang; jcq3363@163.com

Received 18 January 2022; Revised 20 February 2022; Accepted 28 February 2022; Published 9 March 2022

Academic Editor: Shakeel Ahmad

Purpose. Northeast China is a region with a serious aging population. There are fewer articles on epidemiological surveys on the prevalence of chronic diseases in aging areas of China. The study is aimed at understanding the prevalence of chronic noncommunicable diseases such as hypertension and diabetes mellitus (DM) in Liaoning Province, northeast China, and analyzing the risk factors for these chronic diseases. *Methods*. A questionnaire survey and physical examination were conducted in 5008 permanent residents in 2 streets (Henan Street and Hebei Street) covered by Liuerbao Central Health Center in Liaoyang and 4 villages (Miaogou Village, Wangjia Village, Heyan Village, and Shuiquan Village) covered by Shuiquan Health Center in Tianshui Town of Liaoyang from January 2020 to December 2020. *Results*. A total of 4990 patients were included. The prevalence rates of hypertension, DM, dyslipidemia, and obesity in residents in Liaoyang were 54.13%, 12.30%, 43.31%, and 20.52%, respectively. The prevalence of hypertension and DM was highest in both male and female patients aged 40-60 years, which was higher than that in the other age groups ($P < 0.05$). The prevalence of dyslipidemia was highest in men over 60 years old and women 18 – <40 years old. Obesity was most common in men aged over 60 and in women 40 – <60 years old. The proportion of male smokers in all age groups was significantly higher than that of female smokers. Smoking, dyslipidemia, and significant overweight or obesity are common risk factors for hypertension and DM. *Conclusion*. In Liaoyang, northeast China, the prevalence of noninfectious chronic diseases was high, and the prevalence rate in people over 40 years old was significantly higher than that in people under 40 years old. The prevalence and progression of chronic diseases were obviously related to local living and eating habits; thus, health education needs to be improved.

1. Introduction

In recent years, the average life expectancy of China's population has increased. Data from the seventh Chinese population census show that the population aged 60 years and above in China is 264.02 million, accounting for 18.70% [1]. Liaoning Province, located in northeast China, has the highest aging population in China. The elderly over 60 years old account for 25.72%, and the elderly over 65 years old account for 17.42% [2]. An increasing aging population and a marked decline in the prevalence of communicable diseases have influenced the composition and prevalence of the main chronic disease spectrum in developing countries. Chronic noninfectious metabolic disorders such as hypertension, diabetes mellitus (DM), dyslipidemia, and obesity have become the main diseases in populations, seriously threatening people's physical and mental health and causing huge economic burden to families and society due to treatment of these diseases [3]. According to a data analysis in 2015, the prevalence rates of hypertension, DM, and hypercholesterolemia were 58.3%, 19.4%, and 10.5%, respectively, in residents aged ≥60 years in China. Up to 75.8% of the residents aged ≥60 years had at least one chronic disease [4]. There are several reports on the results of epidemiological surveys of chronic diseases in northeast China [5, 6], but relatively few reports focus on areas characterized by aging. The occurrence of these chronic diseases is closely related to bad behavior, lifestyle, and eating habits. In order to understand the main occurrence and development trend of metabolism-related chronic diseases in northeast China,

understand the distribution and epidemiological characteristics of the risk factors related to chronic diseases, and formulate chronic disease prevention and treatment strategies, this study investigated and analyzed the epidemiology of some chronic diseases and provided a theoretical basis for the formulation of community-based chronic disease prevention strategies in Liaoyang of Liaoning Province in northeast China.

2. Data and Methods

2.1. Case Data. From January 2020 to December 2020, 5008 permanent residents in 2 streets (Henan Street and Hebei Street) covered by Liuerbao Central Health Center of Liaoyang County and 4 villages (Miaogou Village, Wangjia Village, Heyan Village, and Shuiquan Village) covered by Shuiquan Health Center of Tianshui Township of Liaoyang County were investigated. The survey coverage rate of the selected community or administrative village in the screening site was greater than or equal to 85% of the resident population over 30 years old (born before December 31, 1988).

2.2. Methods

2.2.1. Diagnostic Criteria. (1) According to the WHO-Asian diagnostic criteria [7], overweight was defined as body mass index (BMI) $\geq 23\,kg/m^2$. Obesity was defined as BMI $\geq 25\,kg/m^2$. (2) Hypertension: according to the 2018 Revision of Chinese Hypertension Prevention and Treatment Guidelines [8], the diagnostic criteria for hypertension are defined as systolic blood pressure (SBP) ≥ 140 mmHg and/or diastolic blood pressure (DBP) ≥ 90 mmHg, or hypertension was explicitly diagnosed previously. (3) DM: conforming to the diagnostic criteria of the China Diabetes Prevention and Treatment Guidelines in 2017 [9]: fasting blood glucose (FBG) > 7.0 mmol/L or having been clearly diagnosed with DM and are currently taking oral hypoglycemic drugs. (4) Dyslipidemia: diagnosis was made according to the Chinese Guidelines for the Prevention and Treatment of Dyslipidemia in Adults (2016 revised Edition) [10]. (5) Smoking: diagnosis was made according to the Guideline on China clinical smoking cessation (2015) [11].

2.2.2. Methods. The on-site registration personnel verified the identity of the participants undergoing physical examination according to the register of the permanent population, with emphasis on verifying whether they were the correct person, whether they belonged to the target investigation group, and had signed the informed consent after confirming the information was correct (the informed consent was collected by the registrar). General information including lifestyle, eating habits, smoking status, and family history of disease was collected through questionnaires. Height, weight, abdominal circumference, and blood pressure were measured on site. If blood pressure was higher than normal, it was repeated twice at an interval of 5 minutes and the average value was recorded. Weight and height were measured on an empty stomach, undressed, bareheaded, and with shoes off. All subjects had 5 mL of elbow venous blood drawn after 12 h fasting for blood glucose and lipid testing. The staff collected the questionnaires and test results and entered all the information of the respondents into the Big Data Platform for Cerebrovascular Disease (http://chinasdc.cn/). The study was approved by the Ethics Committee of Liaoyang Central Hospital, and the subjects were given detailed information when they were enrolled in the study and were asked to sign the informed consent.

2.3. Statistical Analysis. The SPSS 20.0 statistical software was used for data analysis. The prevalence of chronic diseases in different age groups was compared by the χ^2 test. The risk factors were screened by univariate analysis, and then, the risk factors that were significant by univariate analysis were screened by multivariate logistic regression. $P < 0.05$ was considered statistically significant.

3. Results

3.1. Basic Information. A total of 4990 patients were included, consisting of 1988 males and 3002 females, with an average age of 54.72 ± 14.46 years. 2701 patients (54.13%) had hypertension, 2161 patients (43.31%) had dyslipidemia, 614 patients (12.30%) had DM, 1024 patients (20.52%) were overweight, and 1203 patients (24.11%) were smokers.

3.2. Comparison of the Prevalence of Chronic Diseases and Risk Factors by Sex. Detailed results are shown in Table 1. A comparison of gender showed that the prevalence of hypertension, DM, and dyslipidemia in males was higher than that in females, and the smoking rate was also much higher than that in females, with statistically significant differences. There were no significant differences in the prevalence of overweight or obesity between men and women.

3.3. Comparison of the Prevalence of Chronic Diseases and Risk Factors in Different Age Groups. Detailed results are shown in Table 2. The prevalence of hypertension in men aged 18-40 years was similar to that in men aged 40 – <60 years ($P > 0.05$), which were both higher than that in men over 60 years. Trends in the prevalence of hypertension in women were similar to those in men. The prevalence of hypertension in the male ≥ 60 years old group was higher than that in the female ≥ 60 years old group ($\chi^2 = 75.03$, $P < 0.01$), and the prevalence of hypertension in males and females in other age groups was similar ($P > 0.05$). The prevalence of DM was highest in the age group 40 – <60 years, both in men and women and was higher than that in other age groups ($P < 0.05$). The prevalence of DM in women aged 40 – <60 years was higher than that in men in the same age group ($\chi^2 = 5.389$, $P < 0.05$). There was no significant difference in the prevalence of DM between men aged 18 – <40 years and ≥60 years ($\chi^2 = 0.057$, $P = 0.811$). There were statistically significant differences in the prevalence of DM among the different age groups in women ($\chi^2 = 62.42$, $P < 0.05$). There was no significant difference in the prevalence of DM between males and females aged 18-40 years and ≥60 years (18 – <40: $\chi^2 = 2.34$ and ≥60: $\chi^2 = 0.002$). The

Table 1: Comparison of the prevalence of chronic diseases among different genders and age groups (number of cases (%)).

Group	Hypertension	Diabetes mellitus	Dyslipidemia	Significantly overweight or obese	Smoking
Male (1988 cases)	1190 (59.86)	222 (11.17)	925 (46.53)	418 (21.03)	1016 (51.11)
Female (3002 cases)	1511 (50.33)	392 (13.06)	1236 (41.17)	606 (20.19)	187 (6.23)
χ^2	43.71	3.96	13.98	0.52	1316.51
P value	<0.01	0.047	<0.001	0.472	<0.001

Table 2: Comparison of the prevalence of chronic diseases among different genders and age groups (number of cases (%)).

Group	Hypertension	Diabetes mellitus	Dyslipidemia	Significantly overweight or obese	Smoking
18 – <40 male (405 cases)	264 (65.19)[1)]	35 (8.64)[3)]	172 (42.47)[1)]	66 (16.30)[1)]	215 (53.09)
40 – <60 male (854 cases)	557 (65.22)[1)]	127 (14.87)	367 (42.97)[1)]	167 (19.56)[1)]	423 (49.53)
≥60 male (729 cases)	369 (50.62)	60 (8.23)[3)]	386 (52.95)	185 (25.38)	378 (51.85)
18 – <40 female (529 cases)	338 (63.89)[2)]	62 (11.72)[4)]	294 (55.58)[4)6)]	85 (16.07)	47 (8.88)[6)]
40 – <60 female (1213 cases)	782 (64.46)[2)]	227 (18.71)[3)]	559 (46.08)	270 (22.26)[5)]	86 (7.09)[3)]
≥60 female (1260 cases)	391 (31.03)[1)]	103 (8.17)[4)5)]	383 (30.40)[1)4)5)]	251 (19.92)[1)4)5)]	54 (4.29)[1)]

[1)]Compared with ≥60 male group, $P < 0.05$. [2)]Compared with ≥60 female group, $P < 0.05$. [3)]Compared with 40 – <60 male group, $P < 0.05$. [4)]Compared with 40 – <60 female group, $P < 0.05$. [5)]Compared with 18 – <40 female group, $P < 0.05$. [6)]Compared with 18 – <40 male group, $P < 0.05$.

prevalence of dyslipidemia in men aged 18-40 years was similar to that in men aged 40 – <60 years ($\chi^2 = 0.029$, $P > 0.05$), which was lower than that in men aged over 60 years ($P < 0.05$). For women, there were statistically significant differences in the prevalence of dyslipidemia in the different age groups ($\chi^2 = 117.755$, $P < 0.05$), and the prevalence of dyslipidemia was highest in the group aged 18 – <40 years. There was no significant difference in the prevalence of dyslipidemia between males and females aged 40 – <60 years ($\chi^2 = 1.960$, $P = 0.162$). There were significant differences in the prevalence of dyslipidemia in the other age groups in both men and women. The prevalence of significant overweight or obesity in men aged 18-40 years was similar to that in men aged 40 – <60 years ($\chi^2 = 1.93$, $P = 0.164$), which was lower than that in men over 60 years ($P < 0.05$). There were significant differences in the prevalence of overweight or obesity among different age groups of women ($\chi^2 = 8.823$, $P < 0.05$). The prevalence of significant overweight or obesity in men and women was similar in the 18-40 and 40 – <60 age groups (18 – <40: $\chi^2 = 0.009$ and 40~60: $\chi^2 = 2.20$). There was a statistically significant difference in the prevalence of significant overweight or obesity in men and women over 60 years of age. The prevalence of smoking in male groups is high than that in the same age female group. There was no significant difference in the prevalence of smoking prevalence among male age groups.

3.4. Analysis of the Risk Factors Related to Chronic Diseases. Univariate analysis of hypertension, DM mellitus, and related risk factors was carried out, and then, logistic analysis was performed to determine statistically significant risk factors. The detailed results are shown in Tables 3 and 4. Smoking history, dyslipidemia, significant overweight or obesity, and hypertension were risk factors for DM, while age, dyslipidemia, DM, and significant overweight or obesity were risk factors for hypertension.

4. Discussion

In China, due to attention at the national decision-making level, people's health management has become an important national strategy [12]. Due to development of the social economy, the progress of medical and health undertakings, and the change in people's lifestyle, the spectrum of diseases in China has changed greatly, and chronic diseases closely related to environmental factors and bad lifestyle are becoming more and more serious. The World Economic Risks Report in 2011 warned that five chronic diseases, including cardiovascular diseases, cancer, DM, respiratory diseases, and psychiatric diseases, will have a profound impact on countries' healthcare and economic systems over the next 20 years [13]. The death toll due to chronic diseases accounts for 87% of the total death toll in China, and the disease burden accounts for about 70% of the total disease burden in China. The prevention and treatment of chronic diseases is a severe challenge [14].

The present survey showed that the prevalence of hypertension in Liaoyang, Liaoning Province, northeast China, was 54.13% in people aged over 30 years, which was higher than the 40.9% in middle-aged people in Liaoning from 2006 to 2015 and ranked first among the chronic diseases investigated in the survey. The prevalence of hypertension increased with age, especially in the group aged 40-60 years [15]. Evidence-based medical studies have shown that hypertension is the most important risk factor for cardiovascular and cerebrovascular diseases in the Chinese population, and more than half of the occurrences and deaths due to cardiovascular and cerebrovascular diseases are related to hypertension [16]. Therefore, the key to preventing and curing cardiovascular and cerebrovascular diseases is to control hypertension. The crude (adjusted) rates of hypertension among the population aged ≥15 years were 5.1%, 7.7%, 13.6%, 18.8%, and 25.2%, respectively, according to five national hypertension sampling surveys carried out in

Table 3: Logistic analysis of diabetes mellitus risk factors.

Risk factors	β	Wald	SE	OR	95 CI	P value
Age	-0.005	2.700	0.003	0.995	0.988-1.001	0.112
Smoking	-0.453	15.984	0.113	1.572	1.259-1.963	<0.01
Dyslipidemia	0.851	83.259	0.093	0.427	0.356-0.513	<0.01
Hypertension	0.742	51.471	0.103	2.101	1.715-2.573	<0.01
Significantly overweight or obese	0.407	16.736	0.100	0.665	0.548-0.809	<0.01

Table 4: Logistic analysis of hypertension risk factors.

Risk factors	β	Wald	SE	OR	95 CI	P value
Age	-0.033	210.228	0.002	0.968	0.963-0.972	<0.01
Dyslipidemia	0.434	46.238	0.064	0.598	0.530-0.675	<0.01
Significantly overweight or obese	0.873	113.165	0.082	0.475	0.406-0.555	<0.01
Diabetes mellitus	0.733	49.975	0.104	0.468	0.383-0.571	<0.01

1958-1959, 1979-1980, 1991, 2002, and 2012. These results showed that the prevalence of adult hypertension in China has increased significantly [17]. Data from the survey on hypertension in 450,000 people in 31 provinces, municipalities, and autonomous regions in China from 2012 to 2015 showed that [18] the crude prevalence of hypertension in residents aged 18 and above was 27.9%. The prevalence of hypertension in adult residents significantly increased with age. Nearly 1/3 of people aged 45-59 years suffered from hypertension, and more than half of the elderly suffered from hypertension [19]. The 2012-2015 National Hypertension Survey [20] showed that the awareness rate, treatment rate, and control rate of hypertension among residents over 18 years old were 46.9%, 40.7%, and 15.3%, respectively, although higher than that in 2002. However, the awareness rate and treatment rate have not yet reached 1/2, and the control rate is even lower, especially far from developed countries [21]. The results of this study show that the situation has not improved, and that the prevalence of hypertension is higher in men or women under the age of 60 than in those over 60.Therefore, improving the prevention and treatment of hypertension, which is an important public health problem in Chinese residents ,is urgently required.

DM is associated with many chronic diseases [22]. According to the monitoring of chronic diseases and their risk factors in China by the Chinese Center for Disease Control and Prevention in 2013, the prevalence of DM in people aged 18 years and above was 10.4%, and the prevalence of prediabetes was as high as 35.7% [23–25]. The present study showed that the prevalence of DM in Liaoyang, Liaoning Province, northeast China, was 12.30%, and the prevalence of DM was highest in men and women aged 40-60 years, which also indicated that with the acceleration of population aging, the prevalence of DM is increasing. In recent years, the prevalence of overweight and obesity in China has shown a rapid growth trend, which seriously harms the health of residents. Data from the China Health and Nutrition Survey (CHNS) showed that from 1997 to 2009, the rate of overweight and obesity among Chinese adults rose from 25.1% to 39.6%. The prevalence of abdominal obesity in adults increased from 18.6% to 37.4% [26]. The survey results in the present study showed that the proportion of obese and overweight patients was 20.52%, lower than the previous survey results, which may be related to the implementation of healthy diet policies in the Liaoyang area [27]. According to the Nutrition and Health Survey of Chinese Residents in 2002 [28], the prevalence of dyslipidemia in residents over 18 years old was 18.6%, and according to the 2011 China Health and Nutrition Survey [29], the prevalence of dyslipidemia in Chinese adult residents was 39.9%. These results show that the prevalence of dyslipidemia in Chinese adults has increased significantly during the past 10 years. The results of this study showed that the prevalence of dyslipidemia in Liaoyang was 43.31%, suggesting that the prevalence of dyslipidemia in Liaoyang was high and had not been effectively controlled. We have become the country with the largest number of people with diabetes in the world; what is more serious is that 63% of people with diabetes in China are undiagnosed and unable to receive early and effective treatment and education [9]. The high prevalence of diabetes in patients aged 40 – <60 years in this study indicates that young people (<40 years old) have become aware of the dangers of diabetes. Multivariate analysis showed that DM was associated with smoking history, dyslipidemia, significant overweight or obesity, and hypertension, indicating that the prevalence of DM is related to many factors. Therefore, only by actively improving the lifestyle and the treatment of chronic diseases can chronic diseases such as cardiovascular and cerebrovascular diseases and metabolic diseases be prevented. This study has several limitations: (1) the sample size needs to be increased. The results of the prevalence of high blood pressure and DM were higher in this study than in other studies, which may be related to the high prevalence of chronic diseases in Liaoyang and the climate, living habits, and long-term high-salt diet. It could also be related to the higher overall age of the sample studied. A large-scale epidemiological survey should be designed to reflect the prevalence of chronic diseases in Liaoyang. (2) The investigation requires improvement. Chronic diseases are affected by a variety of factors. At present, most

of the existing clinical epidemiological studies also include ultrasound, X-ray and other imaging examinations, and laboratory indicators including blood glucose monitoring. In addition, hypertension, DM and other common chronic diseases, chronic obstructive pulmonary disease, osteoporosis, and other diseases should also be included.

5. Conclusion

Based on this questionnaire survey and physical examination in Liaoyang, Liaoning, northeast China, it was found that the area has a high prevalence of hypertension, DM, dyslipidemia, and obesity, and the prevalence tends to increase with age. The prevalence rate in people over 40 years old was significantly higher than that in people under 40 years old. It is suggested that reducing the prevalence of risk factors (such as hyperlipidemia, hyperglycemia, and high BMI) is extremely important to prevent the development of chronic diseases. The effective control of these risk factors is significantly related to people's dietary habits, economic level, education level, and regional differences. There is a long latency period between exposure to risk factors and the appearance of obvious signs and symptoms, so the key to reducing chronic diseases is etiological prevention. Reducing or even eliminating risk factors can fundamentally reduce the prevalence and incidence of chronic diseases.

Data Availability

The data used to support the findings of this study are available from the corresponding author upon request.

Conflicts of Interest

There is no potential competitive advantage in our paper.

Authors' Contributions

All the authors have reviewed the manuscript and agreed to submit it to your journal.

References

[1] J. Z. Ning, "Main data of the seventh national population census," 2021, http://www.stats.gov.cn/english/PressRelease/202105/t20210510_1817185.html.

[2] "The age composition of the population in different regions by the seventh national census," 2021, https://www.sohu.com/a/465720508_120365037.

[3] L. M. Wang, Z. H. Chen, M. Zhang et al., "Study of the prevalence and disease burden of chronic disease in the elderly in China," *Zhonghua Liu Xing Bing Xue Za Zhi*, vol. 40, no. 3, 2019.

[4] W. Kopp, "How western diet and lifestyle drive the pandemic of obesity and civilization diseases," *Diabetes, metabolic syndrome and obesity: targets and therapy*, vol. 12, pp. 2221–2236, 2019.

[5] X. D. Shi, Q. Wei, S. M. He, Y. C. Tao, J. Sun, and J. Q. Niu, "Epidemiology and analysis on risk factors of non-infectious chronic disaseases in adults in northeast China," *Journal of Jilin University*, vol. 37, no. 2, pp. 379–383, 2011.

[6] B. Li, Y. Q. Yu, C. G. Kou et al., "Investigation and analysis of common chronic diseases among community residents in northern China," *Journal of Jilin University*, vol. 29, no. 8, pp. 844–846, 2003.

[7] WHO/NUT/NCD, *Obesity: preventing and managing the global rpidemic: teport of a WHO vonsultation on obesity*, vol. 894, no. 12, 1998, World Health Organization, Geneva, 1998.

[8] C. H. Prevention, T. G. R. Committee, Hypertension League (China) et al., "Guidelines for prevention and treatment of hypertension in China (2018 Revised edition)," *Chinese Journal of Cardiovascular Medicine*, vol. 24, pp. 24–56, 2019.

[9] Chinese Diabetes Society, "Chinese guidelines for the prevention and treatment of type 2 diabetes (2017 edition)," *Chinese Journal of Diabetes Mellitus*, vol. 10, pp. 4–67, 2018.

[10] Joint Committee on the Revision of Guidelines for the Prevention and Treatment of Dyslipidemia in Chinese Adults, "Guidelines for prevention and treatment of dyslipidemia in Chinese adults (revised 2016)," *Chinese Journal of Cardiology*, vol. 44, no. 10, pp. 833–853, 2016.

[11] National Health and Family Planning Commission of People's Republic of China, "Guideline on China clinical smoking cessation (2015)," *Chinese Journal of Health Management*, vol. 10, no. 2, pp. 88–95, 2016.

[12] J. Wang, W. H. Qiu, and J. J. Liu, "The role of comprehensive geriatric assessment in elderly people' s health management," *Chinese Journal of Clinical Healthcare*, vol. 21, no. 5, pp. 714–718, 2018.

[13] L. Z. Kong, "Healthy China - mission and responsibility," *Capital Journal of Public Health*, vol. 13, pp. 113-114, 2019.

[14] X. Zhi, "Challenges and control of chronic disease prevention in China," *Chinese Journal of Prevention and Control of Chronic Diseases*, vol. 27, no. 9, pp. 720-721, 2019.

[15] L. Zhu and S. Y. Wang, "Analysis of long-term prevalence trend of hypertension among middle-aged people in Liaoning Province from 2006 to 2015," *Chinese Remedies and Clinics*, vol. 20, pp. 1850-1851, 2020.

[16] S. Monticone, F. D'Ascenzo, C. Moretti et al., "Cardiovascular events and target organ damage in primary aldosteronism compared with essential hypertension:a systematic review. and meta-analysis," *The lancet Diabetes & endocrinology*, vol. 6, no. 1, pp. 41–50, 2018.

[17] Chinese Hypertension Prevention, Treatment Guidelines Revision Committee, Hypertension League (China), Chinese Society of Cardiology et al., "Guidelines for prevention and treatment of hypertension in China (2018 Revised edition)," *Chinese Journal of Cardiovascular Medicine*, vol. 24, no. 1, pp. 24–55, 2019.

[18] Z. Wang, Z. Chen, L. Zhang et al., "Status of hypertensionin China: results from the China hypertension survey,2012-2015," *Circulation*, vol. 137, no. 22, pp. 2344–2356, 2018.

[19] S. Oparil, M. C. Acelajado, G. L. Bakris et al., "Hypertension," *Nature Reviews Disease Primers*, vol. 4, article 18014, 2018.

[20] Z. Wang, Z. Chen, L. Zhang et al., "Statusofhypertension in China: results from the China hypertension survey, 2012-2015," *Circulation*, vol. 137, no. 22, pp. 2344–2356, 2018.

[21] B. M. Egan, J. Li, R. A. Davis et al., "Difference in primary cardiovascular disease prevention between the 2013 and 2016 cholesterol guidelines and impact of 2017 hypertension

Hindawi
Computational and Mathematical Methods in Medicine
Volume 2023, Article ID 9785636, 1 page
https://doi.org/10.1155/2023/9785636

Retraction

Retracted: Brain Decoding Using fMRI Images for Multiple Subjects through Deep Learning

Computational and Mathematical Methods in Medicine

Received 1 August 2023; Accepted 1 August 2023; Published 2 August 2023

This article has been retracted by Hindawi following an investigation undertaken by the publisher [1]. This investigation has uncovered evidence of one or more of the following indicators of systematic manipulation of the publication process:

(1) Discrepancies in scope

(2) Discrepancies in the description of the research reported

(3) Discrepancies between the availability of data and the research described

(4) Inappropriate citations

(5) Incoherent, meaningless and/or irrelevant content included in the article

(6) Peer-review manipulation

The presence of these indicators undermines our confidence in the integrity of the article's content and we cannot, therefore, vouch for its reliability. Please note that this notice is intended solely to alert readers that the content of this article is unreliable. We have not investigated whether authors were aware of or involved in the systematic manipulation of the publication process.

Wiley and Hindawi regrets that the usual quality checks did not identify these issues before publication and have since put additional measures in place to safeguard research integrity.

We wish to credit our own Research Integrity and Research Publishing teams and anonymous and named external researchers and research integrity experts for contributing to this investigation.

The corresponding author, as the representative of all authors, has been given the opportunity to register their agreement or disagreement to this retraction. We have kept a record of any response received.

References

[1] M. B. Qureshi, L. Azad, M. S. Qureshi, S. Aslam, A. Aljarbouh, and M. Fayaz, "Brain Decoding Using fMRI Images for Multiple Subjects through Deep Learning," *Computational and Mathematical Methods in Medicine*, vol. 2022, Article ID 1124927, 10 pages, 2022.

Hindawi
Computational and Mathematical Methods in Medicine
Volume 2022, Article ID 1124927, 10 pages
https://doi.org/10.1155/2022/1124927

Research Article

Brain Decoding Using fMRI Images for Multiple Subjects through Deep Learning

Muhammad Bilal Qureshi[1], **Laraib Azad**[2], **Muhammad Shuaib Qureshi**[3], **Sheraz Aslam**[4], **Ayman Aljarbouh**[3] and **Muhammad Fayaz**[3]

[1]*Department of Computer Science & IT, University of Lakki Marwat, Lakki Marwat 28420, KPK, Pakistan*
[2]*Department of Computer Science, Shaheed Zulfikar Ali Bhutto Institute of Science and Technology, Islamabad 44000, Pakistan*
[3]*Department of Computer Science, School of Arts and Sciences, University of Central Asia, Kyrgyzstan*
[4]*Department of Electrical Engineering, Computer Engineering, and Informatics, Cyprus University of Technology, Cyprus*

Correspondence should be addressed to Muhammad Shuaib Qureshi; muhammad.qureshi@ucentralasia.org

Received 8 January 2022; Revised 6 February 2022; Accepted 11 February 2022; Published 1 March 2022

Academic Editor: Muhammad Zubair Asghar

Substantial information related to human cerebral conditions can be decoded through various noninvasive evaluating techniques like fMRI. Exploration of the neuronal activity of the human brain can divulge the thoughts of a person like what the subject is perceiving, thinking, or visualizing. Furthermore, deep learning techniques can be used to decode the multifaceted patterns of the brain in response to external stimuli. Existing techniques are capable of exploring and classifying the thoughts of the human subject acquired by the fMRI imaging data. fMRI images are the volumetric imaging scans which are highly dimensional as well as require a lot of time for training when fed as an input in the deep learning network. However, the hassle for more efficient learning of highly dimensional high-level features in less training time and accurate interpretation of the brain voxels with less misclassification error is needed. In this research, we propose an improved CNN technique where features will be functionally aligned. The optimal features will be selected after dimensionality reduction. The highly dimensional feature vector will be transformed into low dimensional space for dimensionality reduction through autoadjusted weights and combination of best activation functions. Furthermore, we solve the problem of increased training time by using Swish activation function, making it denser and increasing efficiency of the model in less training time. Finally, the experimental results are evaluated and compared with other classifiers which demonstrated the supremacy of the proposed model in terms of accuracy.

1. Introduction

The most advanced imaging technique that is able to capture that functional part of the brain is fMRI [1]. However, task-based fMRI practices BOLD as opposed to maps of neural function in the brain. The deoxyhemoglobin concentration in the brain localizes the magnetic field. The BOLD functional magnetic resonance imaging (fMRI) shows changes to the concentration of deoxyhemoglobin arising from the regulation of a neuronal metabolism caused by activities or by spontaneity [2]. Since the activated brain regions require oxygenated blood in order to provide a significant amount of energy to neurons, the fMRI technique can distinguish both areas which are vigorous or nonvigorous in the brain underneath cognitive control. In task-based functional magnetic resonance imaging scans, the healthy participants perform various resting-state tasks during the scans [3].

The goal to practice analytical methods to classify the fMRI data is to develop efficient models that are able to predict the response of the brain stimuli in response to task-based fMRI experiments. These models imply the response of the brain with respect to the cognitive tasks performed by the human participants. The cognitive activity of the brain is involved in the construction of the brain pattern in

response to the external stimulus. The purpose of this study is to accomplish the brain interpretation of the multisubject by using a predictive neural network model [4].

Various machine leaning and deep learning models have been used to analyze the fMRI data and predict the cognitive states of the brain. Various statistical models are used in machine learning to extract highly dimensional features of the brain. In deep learning, highly dimensional imaging data is converted into low dimensional subspace vector to extract features. The most commonly used deep learning-based architecture to analyze the fMRI data is convolutional neural networks [5]. The design of CNN was used from scratch with the initialization of the utilized weights from the start along with an optimizer for the effectiveness with parameters.

The goal of this study is to focus on a deep learning-based model to classify fMRI data. In the literature, various CNN methodologies have been proposed to decode brain activity. From the literature, it is observed that statistical models [6], traditional machine learning models like K-NN [7], and SVM perform well for small datasets [8] and successfully extract the region of interest, but when experiments or number of fMRI scans are increased, the amount of data received from the fMRI imaging for multisubjects becomes relatively large which results in model overfitting and increased classification errors. Even existing deep learning models like VAE [9, 10], transfer learning techniques, LSTM [11], and reconstructed fc7 layers [12] take more training time which increases computational cost. So, to overcome this, we will use a denser convolutional neural network to train high-level features. In order to train the model in less amount of time, we will be using dense connectivity CNN which will extract features with very robust learning capability, increased speed, and less training time.

We studied various types of deep learning models to classify highly dimensional-based fMRI data. To address the issue identified in the literature, we proposed an improved 3D CNN-based model to classify fMRI data which includes the combination of the best activation functions called Swish [13] along with ReLu [14] in the first few layers to convert highly dimensional data into low dimensional subspace and extract high-level features from the CNN model. The proposed method [15] first feeds raw input data into the proposed CNN model for feature extraction. At the first layer, various filters are applied to the feature maps hence reducing the feature size. Various hyperparameters were used to avoid data loss in the convolutional layers. The Swish activation function is then applied for dimensionality reduction after every layer. Later, ReLu activation function is applied before transforming the feature maps into a 1D fully connected layer. Tanh activation function is applied in every fully connected layer to minimize errors. The weights are autoadjusted. The classification is performed using a Softmax classifier.

The proposed model uses a 3D image acquired from a brain imaging experiment conducted by the Human Connectome Project (HCP) [16]. The performance of the model was examined by various performance matrixes such as F1 score, accuracy, and precision. The training time, training, and validation loss were also computed in this study to examine the model's performance. Three benchmark models were compared with the proposed model to classify the imaging data.

The rest of the paper is organized as follows. Section 2 discusses related work. Section 3 details the proposed improved 3D CNN architecture, and it is evaluated experimentally in Section 4. In Section 5, the produced results are discussed, and the paper is concluded in Section 6.

2. Related Work

The main goal of machine learning is to find the optimal parameters for its functions. Two approaches are used to make feature selection of the fMRI images. The first approach is called univariate analysis, and the second approach is called multi-voxel-based feature selection or MVPA [17]. Univariate analysis is the statistical analysis technique [18] which involves only one variable whereas multi-voxel-based pattern analysis involves multiple variables or voxels in order to identify patterns among observed conditions. We have done review of papers with MVPA-based techniques as the most recent researches are following the MVPA-based approach for feature selection whereas univariate feature selection is not preferred in the most recent researches due to its limitations on doing analysis on only one voxel.

Xu et al. [19] focused on univariate-based analysis to extract features on the voxel level and ROI level of the brain. Xu et al. used two methods to extract features to find out the better feature selection approach by using different features extracted from different human participants. The two approaches used to extract features were ANOVA followed by Kendall's coefficient. A technique called SSOMs was used in [20] for the classification of fMRI data. This technique gave better results when compared to the classic machine learning model *k*-nearest neighbor. However, as the dataset increased, SSOMs were outperformed by SVM. In order to handle highly dimensional samples, various dimensionality reduction techniques have already been applied. The very basic type of dimensionality reduction technique applied on fMRI data is called "factor models" [21]. In the existing literature, we have seen various techniques like PCA [22]; ICA [23] has been applied to the fMRI images after preprocessing. Another dimensionality reduction method called sliced inverse reduction was proposed by Tu et al. [24]. The difficulty with brain imaging is that various factors are very much correlated. Another issue is that the total number of samples is very small with very little procurement time. L1 and L2 regression [25] was used at solving the issue of high covariance across different variables by the sparse regression method. The novelty is solving the issue by sparse brain imaging retrieval technique by eliminating the noninformative region. According to Yargholi and Hossein-Zadeh [26], the key concern of decoding studies is decoding classification, but there is an inadequate consideration and much effort to improve the problem of restoring (decoding) stimulus images from fMRI records, in particular natural images. Another study [27] focused on the first contribution to a

modern system of mapping connectomes based on decomposing and stitching blocks. The second contribution was to demonstrate how this structure for decomposition blocks will promote tractable link restoring with profound learning.

According to recent studies, CNN and deep learning have played an important role in the area of brain decoding. Most of the previous researches used the voxel-based classification technique and then apply the CNN model to decode the pattern [28, 29].

Preprocessing was applied to help reduce noise, SNR, head motion, and various false positive voxels which affect the accuracy score. The most frequently used classifiers for the classification of the dataset were Softmax in deep learning approaches [30] and SVM in machine learning methods. The preprocessed data for machine learning-based models was normalized using mean, cross-validation, and standard deviation whereas the deep learning-based approaches used validation and testing sets and trained the model on various epochs.

3. Improved 3D CNN Architecture

The 3D brain images are 3 anatomical planes as coronal, sagittal, and axial planes in the x, y, and z axes, respectively. The proposed model is aimed at reducing the training time with the ability to eliminate model overfitting with a reduced validation error. In the model, the fMRI data is collected from the Human Connectome Project dataset repository. The dataset is first preprocessed to remove noise caused by the human subject head movements. The HCP [31] dataset is a resting-state fMRI data where the fMRI scan is taken on healthy human subjects while the subjects are performing tasks. The spatial and temporal resolution of the HCP data is very high. The scans included the human subjects performing different tasks such as gambling, motor, language, social cognition, relational processing, working memory-related tasks, and tasks related to emotional processing. The dataset is spatially smoothed followed by temporal normalization and band pass filtering. The 3D CNN model is shown in Figure 1.

After preprocessing, the proposed convolutional neural network model is used for feature extraction. The model uses a feature map with nine different filters with stride and padding as hyperparameters to reduce feature size. The swish activation function is applied on the feature map. For dimensionality reduction, maximum pooling is applied after every convolution. To reduce training time, the dropout layer is used after every feature map followed by the batch normalization. The feature size is reduced in three feature maps followed by Swish, max pooling, and dropout layer. Finally, all feature maps are converted into a 1D fully connected layer. Deep neural networks are applied with cross-entropy to minimize the error. In the final layer, the classification model "Softmax" is applied to classify the images into correct labels. The proposed model is trained on 70% of the fMRI data. Later on, the training model is applied to validate the testing data. The classifier is evaluated in terms of accuracy, error estimation, and efficiency in the training phase. Finally, the confusion matrix is used to identify the model's classification performance and identify whether the model has correctly identified all seven classes on the fMRI HCP dataset. The comparison of Softmax is made with the SVM classifier to identify which classifier provides better accuracy. The detailed description of the proposed decoding model shown in Figure 2 is given below.

3.1. Input Layer. The convolutional layer stack is used in the CNN model. The multidimensional fMRI image is converted into a 2-dimensional image tensor with hyperparameters of batch size, rows, columns, and channels. To analyze the effect of initial representation over the brain decoding performance, three different input representations are fed into the deep architectures. The acquired 3D images are the slices of the brain stacked up and forming volume. During analysis, the X and Y voxels in each scan are equal to the total number of slices. The spatial dimensions of the images are in the format of $3 \times 3 \times 3$ mm. Some of the images are rotated along with spatial dimensions. This did not involve any distortion of the image. Each slice of the brain contains a different area of the brain as the fMRI scan takes the scan of the whole brain in the form of multiple slices.

3.2. Convolutional Layer. The first and foremost layer in the convolutional neural network is the layer where the raw input image is placed with a series of filters. This layer is responsible for applying various filters to extract the important features. The dot product is taken of the image with filter by sliding the filter on each pixel of the image. The size of the filter with respect to the input image is considered (mxm). The final output extracted by the dot product is placed in the feature map. The feature map gives information regarding the edges, corners, and important features also called voxel extracted from the images. The feature map is then fed into other layers to extract other features.

Depth scaling given in Equation (1) is the most common technique to scale a convolutional neural network. To increase the depth of the network, more layers are added, whereas to decrease the depth of the network, the layer of convolutions is removed. The reason why depth scaling is so important is because the deeper and denser the convolutional neural network is, the most complex and richer feature the model can extract. Specially in fMRI, a more complex voxel can be extracted when the model is denser, although increasing the density of the network sometimes results in the vanishing gradient problem:

$$\begin{aligned} \text{depth}: \; & d = \alpha^{\varnothing} \\ \text{s.t.} \; & \alpha \cdot \beta^2 \cdot \gamma^2 \approx 2 \\ & \alpha \geq 1, \beta \geq 1, \gamma \geq 1. \end{aligned} \tag{1}$$

The purpose behind width scaling is to train the model efficiently. Width scaling keeps the model small resulting in reduced training time. The advantage of width scaling is that it extracts fine-grained features in less time resulting in more accuracy in less training time. It is important to note that a wider network with less density will saturate the

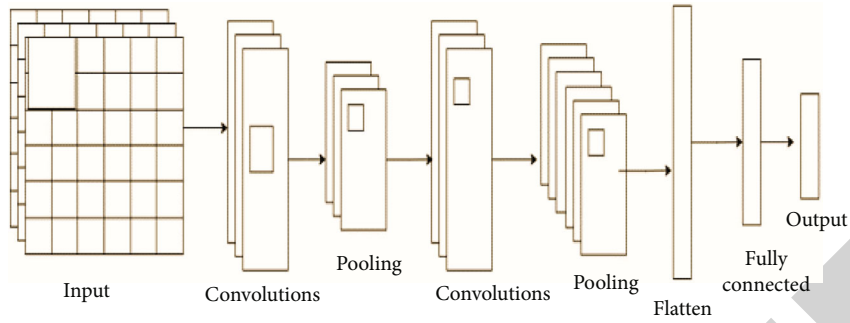

Figure 1: 3D CNN architecture model.

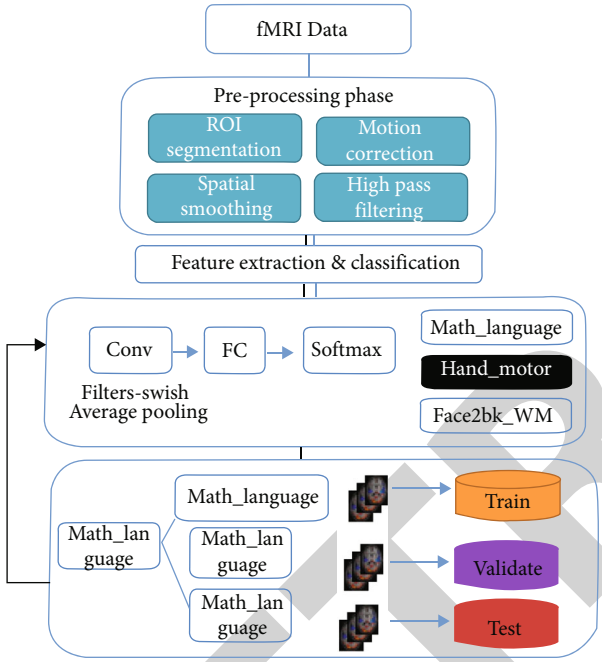

Figure 2: Proposed CNN decoding model.

accuracy more quickly, so width with density is used to stabilize the performance of the model in less training time. Width scaling is calculated using

$$\begin{aligned} &\text{width}: \ w = \beta^{\varnothing} \\ &\text{s.t.} \ \alpha \cdot \beta^2 \cdot \gamma^2 \approx 2 \\ &\alpha \geq 1, \beta \geq 1, \gamma \geq 1. \end{aligned} \tag{2}$$

3.3. Pooling Layer. It is a common practice to use a pooling layer right after the convolutional layer. The basic purpose of a pooling layer is to reduce the total size of the convolutional layer's feature maps which were convolved. This step is important in order to minimize the computational power. The step is performed by reducing the layer connections followed by each feature map's standalone operation. Pooling operations are of various types. It depends on the scenario regarding the pooling layer that is to be used. The two commonly used pooling operations are max pooling and average pooling. Max pooling involves the extraction of the highest element from the feature map whereas average pooling involves the extraction of the average value of the feature map where the average is extracted from all elements. The pooling layer is basically acting as a bridge which connects the two layers which are the convolutional layer and the fully connected layer. Swish activation function and ReLu will be used in the pooling layer. Swish mathematical representation is given in

$$\sigma(x) = x \frac{x}{1 - e^{-x}}. \tag{3}$$

Table 1: Parameters and values used in experiments.

Parameter	Value
Sequence	Gradient echo EPI
Repetition time (TR)	720 ms
Time to echo (TE)	33.1 ms
Flip angle	52 deg
Field of view (FOV)	208 × 180 mm (RO × PE)
Matrix	104∗90 (RO × PE)
Slice thickness	2.0 mm; 72 slices; 2.0 mm isotropic voxels
Multiband factor	8
Echo spacing	0.58 ms
Bandwidth (BW)	2290 Hz/Px

3.4. Fully Connected Layer. The fully connected (FC) layer is comprised of neurons and weights followed by biases. This layer is used to connect the neurons between two layers. These layers of neurons are among the last few layers of the CNN model. The FC layer basically transforms the input matrix into a 1D vector. Then, it acts as an artificial neural network where the hidden layers are responsible of performing the final computation before the classification of the input images. The term flattening is used before being fed into the FC layer. The FC layer goes through more computation error calculation and weight change before starting the classification process.

3.5. Output Layer. The output layer is the last layer of the CNN model where classification is performed. Software

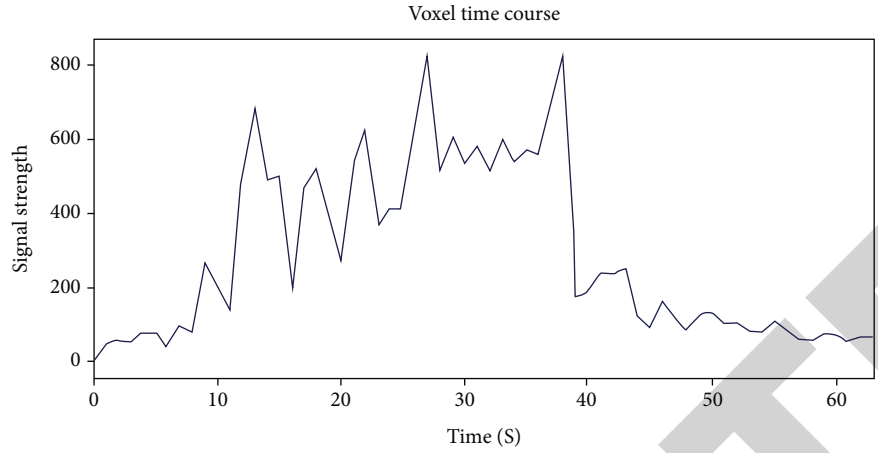

Figure 3: Single voxel time series.

Table 2: Summary of accuracy score on HCP tasks.

Task	Accuracy
Emotion	94.0 ± 1.6% (mean ± SD)
Gambling	83.7 ± 4.6% (mean ± SD)
Language	97.6 ± 1.1%(mean ± SD)
Motor	97.3 ± 1.6%(mean ± SD)
Relational	89.8 ± 3.2%(mean ± SD)
Social	96.4 ± 1.0%(mean ± SD)
WM	91.9 ± 2.3%(mean ± SD)

Table 3: Summary of HCP task run details per subject condition on volumetric images.

Task	Volume per each run	Minimum duration in seconds	Subjects	Total runs	Condition
Emotion	405	25	1085	2	8
Gambling	284	12	1083	2	5
Language	316	12	1051	2	2
WM	274	23	1051	2	2
Cognition	232	16	1043	2	2
RP	176	18	1047	2	2

activation function is mostly used to find the probability of the class which is closest to the image label.

3.6. Softmax Classifier. Softmax is the most commonly used activation function for the classification of the CNN model. It gives the probability of a class that is close to the image label. It is used to normalize the values between 0 and 1, and then, it gives the final output in the form of probability by dividing by their sum resulting in the output of a particular class. Softmax is only used for the output layer for classification. Softmax mathematical representation is mentioned in

$$\sigma(z)j = \frac{ezj}{\sum_{k=1}^{k} e^{z_k}} \text{ for } \longrightarrow j = 1 \cdots k. \quad (4)$$

4. Experiments

4.1. Experimental Setup. For HCP [31], the setup contains experiments of different human participants ranging from under 10 to 1200 participants. The dataset used in this study contained HCP experiments with total of 45 human participants with perfect health conditions both physically and mentally. Each subject had 1-hour-long session with a 6-minute resting session in between. The position of each subject was supine. The room was dark where the experiment took place. The subject's eyes were open during the experiment. Each subject performed six different physical and cognitive tasks. The fMRI experiment type is resting-state fMRI also called rsfMRI. For this experiment, we used an Intel core i7 computer with 64 GB RAM and GeForce GTX 660 2 GB GPU. The language used to implement the model is Python using Keras 1.2.2 and TensorFlow 1.15.0. The imaging data is reshaped using Nibabel's built-in functions. The experimental setup statistics is given in Table 1.

4.2. Dataset Acquisition. In this study, we used the HCP dataset to understand the efficacy of the proposed model and accuracy of the classification results on the HCP dataset. The HCP dataset includes both structural MRI and rsfMRI known as resting-state fMRI images. In this study, only resting-state fMRI data is used where the participants are performing a set of tasks. rsfMRI comprises 46 healthy human participants in the scope of this study. Due to the limited computation power, the preprocessed images are of 47 human subjects collected to train our deep learning model. The fMRI images which are passed through various steps of preprocessing are thoroughly explained in the upcoming section.

In this experiment, the human participants are in a perfectly healthy condition. Each participant is exposed to different types of stimuli. In total, seven different tasks were performed by all participants. The seven different types of stimulus/tasks are named as working memory also known

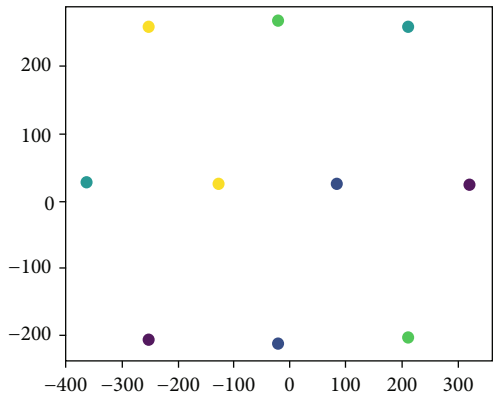

Figure 4: WM task fMRI correlation matrix.

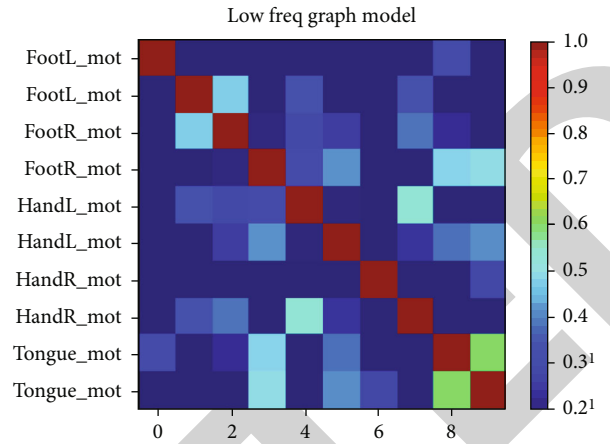

Figure 5: WM task frequency correlation matrix.

as WM, gambling also known as GB, motor task also known as MT, social cognition also known as SC, relational processing also known as RP, and emotional processing also known as EP. A total of about 1940 fMRI images were acquired from each human participant performing these seven types of tasks or stimuli. The fMRI data for each task was gathered in only one run. It is important to note that data from all subjects were collected performing all seven tasks. A total of more than 180000 plus images were acquired for this experimental study. The samples collected from the HCP dataset had 150000 voxels per sample. A voxel in the neuroimaging data is like a pixel in an image. In order to feed preprocessed input data, the region of interest based on voxels are already highlighted through the FSL software package in the preprocessed HCP dataset. A single voxel time series is portrayed in Figure 3.

4.3. Preprocessing. The acquired images were already preprocessed to remove noise and other unnecessary misalignments from the images. The first step was realignment. During the fMRI scan, it is common for the human subject to move his head. Constant head motion during the fMRI scan causes noise and sends wrong signals to the brain such that the areas of the brain get highlighted due to the increased blood flow. So, it is important to realign the images to reduce head motion. So, each fMRI 3D image is realigned to another reference image over the time of acquisition. This results in the reduced head motion effect.

4.4. Feature Extraction. The design of CNN was used from scratch with the initialization of the utilized weights from the start. Adam optimizer was used for the effectiveness with parameters $\beta_1 = 0.9$ and $\beta_2 = 0.99$. Adam optimizer [32] is a technique for gradient descent which is used for optimization in order to train deep learning models. Due to the limitations related to the memory, the size of the batch was kept 32. 0.001 learning was set as the initial learning rate. The LR was decayed by 10 every time the validation loss increased after 10 epochs. Swish activation function was used after every convolution to minimize the vanishing gradient due to backpropagation. In order to overcome the problem of overfitting data, the training of the model was stopped when the loss function was reduced to the minimum. The validation of the training set included the cross-validation approach. Five-fold cross-validation was used to validate data among the training set.

As mentioned in the previous section, the data is split into three sets [33]. The three sets are the training, validation, and testing datasets. This generalization approach will prevent the model from overfitting and also help to evaluate the model effectually. We used training data to train our CNN model, the validation set is used to choose the optimal hyperparameter, and the testing set is used to evaluate the model. The testing set (20%) is followed by the training set (70%) followed by the validation set which is 10%. Subsampling of the images was also done. The samples for all three datasets were changed for the fivefolds.

Deep learning has so many advantages; one of the most important benefits of deep learning is its reusability [34]. Traditional machine learning approaches where the features are extracted manually are outperformed by deep learning models in accuracy and efficiency. The most important advantage of this proposed CNN approach is also its reusability on similar tasks where the model is trained and tested on the validation dataset [35]. Once the model is trained in multiple epochs or iterations, the model is then tested on testing data where the images are completely different then the images where the model is trained. The transfer learning approach for the Efficient Net-based CNN model is to increase the efficiency of the model during training. The basic workflow approach is fairly similar as compared to the training time at the start. The only difference is after each convolutional layer, the activation function applied is Swish and the final output layer is left untrained.

The proposed model for brain state annotation consisted of six convolutional layers. These convolutional layers had graph filters. In total, 32 filters were used for each convolutional layer. The fully connected layers used in this model were two which were used after the flattening for the classification phase. The model takes the HCP preprocessed data in Mat format as input. The input data when fed to the convolutional neural network model propagated the information among the regions of the brain which were connected. This model generated was trained to generate graph

Table 4: Confusion matrix on HCP tasks.

Emotion	0.029	0.017	0.011	0.003	0.026	0.012	0.002
Gambling	0.025	0.829	0.003	0.001	0.115	0.022	0.005
Language	0.003	0.007	0.977	0.001	0.004	0.005	0.002
Motor	0.009	0.009	0.010	0.956	0.007	0.005	0.004
Relational	0.007	0.047	0.011	0.001	0.912	0.010	0.012
Social	0.002	0.006	0.006	0.001	0.007	0.977	0.001
WM	0.000	0.010	0.006	0.000	0.071	0.007	0.905
	Emotion	Gambling	Language	Motor	Relational	Social	WM

Table 5: Summary of F1 score on HCP tasks.

Task	F1 score
WM	0.84
Social	0.91
Emotion	0.92
Motor	0.94
Language	0.96
Relational	0.81

representation followed by the classification of the labels predicted. The model is trained on 30 epochs. The batch size of the model is set to 10 subjects. The learning rate used is 0.001. The model after gaining better accuracy results is then evaluated on the testing dataset separately. After achieving high accuracy on the training model and validating through the validation dataset, the model is then evaluated on the testing dataset. L2 regularization with dropout is also used to decrease the training time. The L2 regularization value used is 0.0005, and the rate of dropout which is 0.5 was applied on all layers. The model is trained for 1000 participants. The motor task and memory task were done on diverse time windows. The fMRI volumes were 5 which were taken as input. The motor task had 10 windows whereas the memory task had 20 windows. The wrapping method was applied for task events. The layers were fine-tuned from random initialization.

4.5. Classification. The initial layers of CNN were responsible for feature extraction. In the next phase, the extracted features are flattened to the one-dimensional matrix. The parameters of the 1D matrix are reduced through dense hidden layers. The layer of CNN is used to classify the multiclass classification on the fMRI data. The activation function "Softmax" was used as a classifier. Softmax gave the classification score of every single fMRI image in the form of probability.

4.6. Evaluation. In this phase, firstly, the models built by 70% training data perform classification of the remaining 30% testing fMRI instances. Secondly, the classification results of the testing instances are evaluated by means of evaluation measures. These performance metrics are utilized to comparatively analyze various classifiers for the proposed brain decoding model. The following subsections briefly narrate the evaluation measures of accuracy, misclassification error, precision, and F1 score. Equations (5), (6), (7), and (8) are the mathematical representations of accuracy, misclassification rate, precision, and F1 score, respectively:

$$\frac{(\mathrm{TP}+\mathrm{TN})}{\mathrm{Total}}, \tag{5}$$

$$\mathrm{Error\ Rate} = \frac{(\mathrm{FP}+\mathrm{FN})}{\mathrm{Total}}, \tag{6}$$

$$P = \frac{\mathrm{TP}}{\mathrm{Predicted}}, \tag{7}$$

$$\mathrm{F1\ Score} = \frac{2}{1/\mathrm{Recall} + 1/\mathrm{Precision}}. \tag{8}$$

5. Results and Discussion

5.1. Classification Results on HCP Dataset. The F1 score analysis showed the performance of the classifier across all the tasks. Each task's accuracy score is mentioned in Table 2.

The average test accuracy achieved across the cross-validation of 10-fold is 91% with a random chance of 20%.

The use of the activation function followed by the domain feature transfer provided the 7% gain. Fine-tuning the convolutional layers gave no additional improvements and no impact on training time. Direct accuracy on decoding tasks was achieved by using the base efficient net model. The accuracy of 97.5% was received when the decoding model was yielded. Table 3 shows the summary of the HCP task run details.

This also represents the high stability of the motor tasks. Fine-tuning was able to learn the specific features, but this approach might not work well when the size of the dataset is decreased as this may cause the problem of overfitting. Some distinct patterns were seen in the WM task.

At first, the generalizability shown on the HCP participants was very low with an accuracy of 30% followed by a low chance level of 12.5%. However, high variability was seen in WM and behavior tasks. The random initialization on the decoding model gave the results of 41%. The features when transferred gave an accuracy boost of 5%. The random initialization approach was used for the feature transfer. These results showed that the WM had a

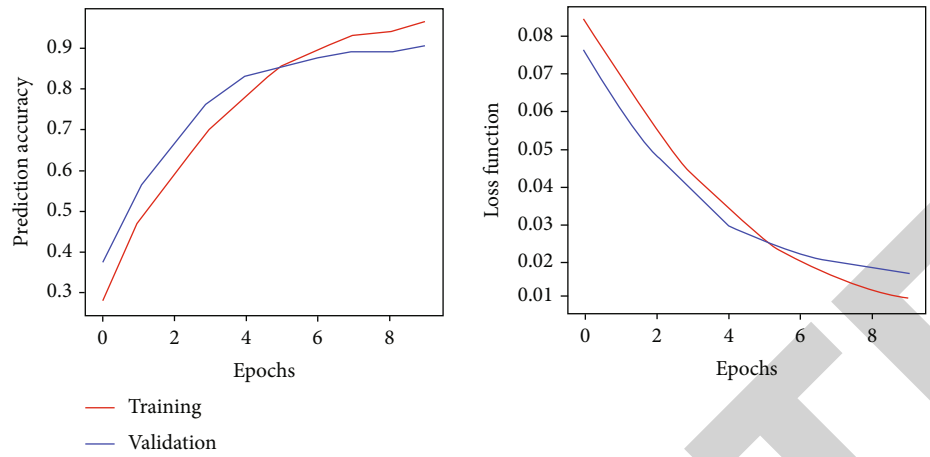

Figure 6: Prediction accuracy per 8 epochs.

strong learning representation effect. Figures 4 and 5 show WM task correlation matrices.

After the validation on the main hyperparameters with a kernel of $1 * 1 * 1$, the model recorded the high accuracy as mentioned in the previous section. $N_{ch1} = 3, 9, 27$. The model did not converge when the N channel reached the value of $N_{ch} = 1$. This channel was reduced to 10 epochs. In short, the CNN model was evaluated by mainly focusing on 6 stimuli. The 10 s time window for the fMRI series was used. The average test accuracy was 88%. The chance level was slightly different around 4.7%. The confusion matrix of six cerebral realms was summarized. The precision recall for each domain other than emotion was greater than 80%. According to the confusion matrix given in Table 4, the top confusions were caused by two tasks: gambling and WM.

As mentioned in the previous section, the motor tasks followed by the language tasks were easily identified. The language tasks included story and math tasks whereas the motor tasks included movements of the right and left hands followed by tongue and right and left feet. 95% score was achieved for the language task whereas an average of 94% was achieved for motor tasks. The lowest accuracy was achieved by the relational tasks followed by the working memory task. The relational processing task achieved an 81% F1 score while the average of 83% F1 score was gained by the working memory task. Some misclassification was also observed in WM, relational, and emotion tasks. The overall summary of the F1 score on different HCP tasks is given in Table 5.

The validation and training accuracy achieved between different tasks is pictorially shown in Figure 6. The loss function and prediction accuracy for the highest accuracy tasks followed by the loss function and prediction accuracy for the lowest accuracy tasks in eight epochs are illustrated.

6. Conclusion

The brain decoding models like CNNs and VAEs are used for feature extraction of the brain images. This is a good approach as CNNs perform better than other existing deep learning models due to high efficiency when extracting features and then classifying the images using a classifier. CNN models give better accuracy when training the images, but this includes some major limitations. The main problem with using CNN models is the issues of vanishing gradients when back propagating the images. Similarly, large datasets often cause exploding gradient problems during model training. This issue is followed by the increased computational power as CNNs-based deep learning models are trained on GPUs. Various researchers propose the technique of training the model on CPU, but this approach has its limitations. Training the model on GPU with less computational cost is another challenge. Similarly, GPU-based models take more training time but give better accuracy results. So, various researchers proposed a model where increased density can give better accuracy and increase the performance of the model. Increasing the model's density increases the accuracy, but it also increases the training time and computation. So, the proposed CNN model was implemented where the images are trained by the combination of the best activation functions. The Swish activation function overcomes the problem of vanishing gradients. Moreover, Swish activation plays an important role in reducing the computation and training time of the model. After the extraction of the features, the images were flattened to a one-dimensional matrix where the multiple hidden layers reduced the parameters and extracted the optimal features and predicted the classification results based on the extracted features using the "Softmax" classifier. Furthermore, the reliability of the proposed method was validated using the validation dataset during training followed by the testing dataset after the model training. In addition, the best-evaluated classifier followed by the existing machine learning approach was compared with the proposed model to validate the efficiency of the model. For the HCP dataset, the proposed model gave impressive results in terms of accuracy, efficiency, and specificity. The analysis of the model was also conducted in order to demonstrate the usefulness of the brain imaging analysis and feature extraction followed by classification of the model.

Data Availability

Data used in the preparation of this work were obtained from the MGH-USC Human Connectome Project (HCP) database (https://ida.loni.usc.edu).

Conflicts of Interest

The authors declare that they have no conflicts of interest.

References

[1] X. U. Gui, C. H. Chuansheng, L. U. Zhong-Lin, and D. O. Qi, "Brain imaging techniques and their applications in decision-making research," *Acta Psychologica Sinica*, vol. 42, no. 1, p. 120, 2010.

[2] G. H. Glover, "Overview of functional magnetic resonance imaging," *Neurosurgery Clinics*, vol. 22, no. 2, pp. 133–139, 2011.

[3] S. Zhang, X. Li, J. Lv, X. Jiang, L. Guo, and T. Liu, "Characterizing and differentiating task-based and resting state fMRI signals via two-stage sparse representations," *Brain Imaging and Behavior*, vol. 10, no. 1, pp. 21–32, 2016.

[4] T. Hill, L. M. Marquez, O. Connor, and W. Remus, "Artificial neural network models for forecasting and decision making," *International Journal of Forecasting*, vol. 10, no. 1, pp. 5–15, 1994.

[5] R. Yamashita, M. Nishio, and T. K. Do RK, "Convolutional neural networks: an overview and application in radiology," *Insights Into Imaging*, vol. 9, no. 4, pp. 611–629, 2018.

[6] M. Martin, "Statistical analysis of fMRI time-series: a critical review of the GLM approach," *Frontiers in Human Neuroscience*, vol. 5, p. 28, 2011.

[7] R. Gui, T. Chen, and H. Nie, "Classification of task-state fMRI data based on circle-EMD and machine learning," *Computational Intelligence and Neuroscience*, vol. 2020, Article ID 7691294, 10 pages, 2020.

[8] M. Wang, C. Li, W. Zhang et al., "Support vector machine for analyzing contributions of brain regions during task-state fMRI," *Frontiers in Neuroinformatics*, vol. 13, p. 10, 2019.

[9] J. H. Kim, Y. Zhang, K. Han, Z. Wen, M. Choi, and Z. Liu, "Representation learning of resting state fMRI with variational autoencoder," *Neuro Image*, vol. 241, article 118423, 2021.

[10] K. Han, H. Wen, J. Shi et al., "Variational autoencoder: an unsupervised model for encoding and decoding fMRI activity in visual cortex," *Neuroimage*, vol. 198, pp. 125–136, 2019.

[11] H. Li and Y. Fan, "Brain decoding from functional MRI using long short-term memory recurrent neural networks," in *International Conference on Medical Image Computing and Computer-Assisted Intervention*, Cham, 2018Springer.

[12] M. Svanera, M. Savardi, S. Benini et al., "Transfer learning of deep neural network representations for fMRI decoding," *Journal of Neuroscience Methods*, vol. 328, 2019.

[13] P. Ramachandran, B. Zoph, and Q. V. Le, "Swish: a self-gated activation function," *Neural and Evolutionary Computing*, vol. 7, no. 1, 2017https://arxiv.org/abs/1710.05941.

[14] K. Eckle and J. Schmidt-Hieber, "A comparison of deep networks with ReLU activation function and linear spline-type methods," *Neural Networks*, vol. 110, pp. 232–242, 2019.

[15] X. Wang, X. Liang, Z. Jiang et al., "Decoding and mapping task states of the human brain via deep learning," *Human Brain Mapping*, vol. 41, no. 6, pp. 1505–1519, 2020.

[16] M. F. Glasser, S. M. Smith, D. S. Marcus et al., "The Human Connectome Project's neuroimaging approach," *Nature Neuroscience*, vol. 19, no. 9, pp. 1175–1187, 2016.

[17] M. J. Chadwick, H. M. Bonnici, and E. A. Maguire, "Decoding information in the human hippocampus: a user's guide," *Neuropsychologia*, vol. 50, no. 13, pp. 3107–3121, 2012.

[18] I. Pillet, H. Op de Beeck, and H. Lee Masson, "A comparison of functional networks derived from representational similarity, functional connectivity, and univariate analyses," *Frontiers in Neuroscience*, vol. 1348, 2020.

[19] W. Xu, Q. Li, X. Liu, Z. Zhen, and X. Wu, "Comparison of feature selection methods based on discrimination and reliability for fMRI decoding analysis," *Journal of Neuroscience Methods*, vol. 335, article 108567, 2020.

[20] V. De Angelis, F. De Martino, M. Moerel, R. Santoro, L. Hausfeld, and E. Formisano, "Cortical processing of pitch: model-based encoding and decoding of auditory fMRI responses to real-life sounds," *NeuroImage*, vol. 180, no. Part A, pp. 291–300, 2018.

[21] C. M. Ting, H. Ombao, S. B. Samdin, and S. H. Salleh, "Estimating dynamic connectivity states in fMRI using regime-switching factor models," *IEEE Transactions On Medical Imaging*, vol. 37, no. 4, pp. 1011–1023, 2018.

[22] Y. Zhong, H. Wang, G. Lu, Z. Zhang, Q. Jiao, and Y. Liu, "Detecting functional connectivity in fMRI using PCA and regression analysis," *Brain Topography*, vol. 22, no. 2, pp. 134–144, 2009.

[23] Y. Du and Y. Fan, "Group information guided ICA for fMRI data analysis," *NeuroImage*, vol. 69, pp. 157–197, 2013.

[24] Y. H. Tu, Z. N. Fu, A. Tan et al., "A novel and effective fMRI decoding approach based on sliced inverse regression and its application to pain prediction," *Neurocomputing*, vol. 273, pp. 373–384, 2018.

[25] S. Ryali, K. Supekar, D. A. Abrams, and V. Menon, "Sparse logistic regression for whole-brain classification of fMRI data," *NeuroImage*, vol. 51, no. 2, pp. 752–764, 2010.

[26] E. Yargholi and G. A. Hossein-Zadeh, "Brain decoding-classification of hand written digits from fMRI data employing Bayesian networks," *Frontiers in Human Neuroscience*, vol. 10, p. 351, 2016.

[27] L. Jiang and X. N. Zuo, "Regional homogeneity: a multimodal, multiscale neuroimaging marker of the human connectome," *The Neuroscientist*, vol. 22, no. 5, pp. 486–505, 2015.

[28] J. Hu, Y. Kuang, B. Liao, L. Cao, S. Dong, and P. Li, "A multichannel 2D convolutional neural network model for task-evoked fMRI data classification," *Computational Intelligence and Neuroscience*, vol. 2019, Article ID 5065214, 9 pages, 2019.

[29] D. Wen, Z. Wei, Y. Zhou, G. Li, X. Zhang, and W. Han, "Deep learning methods to process fMRI data and their application in the diagnosis of cognitive impairment: a brief overview and our opinion," *Frontiers in Neuroinformatics*, vol. 12, p. 28, 2018.

[30] A. Riaz, M. Asad, S. M. Al Arif et al., "Deep fMRI: an end-to-end deep network for classification of fMRI data," in *2018 IEEE 15th International Symposium on Biomedical Imaging (ISBI 2018)*, Washington, DC, USA, 2018.

[31] *Humanconnectome*https://db.humanconnectome.org/.

[32] D. P. Kingma and B. J. Adam, "Adam: a method for stochastic optimization," 2017, https://arxiv.org/abs/1412.6980.

Hindawi
Computational and Mathematical Methods in Medicine
Volume 2023, Article ID 9757086, 1 page
https://doi.org/10.1155/2023/9757086

Retraction

Retracted: Internet of Things with Deep Learning-Based Face Recognition Approach for Authentication in Control Medical Systems

Computational and Mathematical Methods in Medicine

Received 10 October 2023; Accepted 10 October 2023; Published 11 October 2023

This article has been retracted by Hindawi following an investigation undertaken by the publisher [1]. This investigation has uncovered evidence of one or more of the following indicators of systematic manipulation of the publication process:

(1) Discrepancies in scope

(2) Discrepancies in the description of the research reported

(3) Discrepancies between the availability of data and the research described

(4) Inappropriate citations

(5) Incoherent, meaningless and/or irrelevant content included in the article

(6) Peer-review manipulation

The presence of these indicators undermines our confidence in the integrity of the article's content and we cannot, therefore, vouch for its reliability. Please note that this notice is intended solely to alert readers that the content of this article is unreliable. We have not investigated whether authors were aware of or involved in the systematic manipulation of the publication process.

Wiley and Hindawi regrets that the usual quality checks did not identify these issues before publication and have since put additional measures in place to safeguard research integrity.

We wish to credit our own Research Integrity and Research Publishing teams and anonymous and named external researchers and research integrity experts for contributing to this investigation.

The corresponding author, as the representative of all authors, has been given the opportunity to register their agreement or disagreement to this retraction. We have kept a record of any response received.

References

[1] T. Hussain, D. Hussain, I. Hussain et al., "Internet of Things with Deep Learning-Based Face Recognition Approach for Authentication in Control Medical Systems," *Computational and Mathematical Methods in Medicine*, vol. 2022, Article ID 5137513, 17 pages, 2022.

Hindawi
Computational and Mathematical Methods in Medicine
Volume 2022, Article ID 5137513, 17 pages
https://doi.org/10.1155/2022/5137513

Research Article

Internet of Things with Deep Learning-Based Face Recognition Approach for Authentication in Control Medical Systems

Tahir Hussain,[1] **Dostdar Hussain**,[2] **Israr Hussain**,[2] **Hussain AlSalman**,[3] **Saddam Hussain**,[4] **Syed Sajid Ullah**,[5] **and Suheer Al-Hadhrami**[6]

[1]*Department of Computer Science and Communication Engineering, National Cheng Kung University, 70101, Taiwan*
[2]*Department of Computer Sciences, Karakoram International University, Gilgit 15100, Pakistan*
[3]*Department of Computer Science, King Saud University, Riyadh 11543, Saudi Arabia*
[4]*Department of Information Technology, Hazara University, Mansehra, Pakistan*
[5]*Department of Information and Communication Technology, University of Agder, Norway*
[6]*Computer Engineering Department, Engineering College, Hadhramout University, Hadhramaut, Yemen*

Correspondence should be addressed to Saddam Hussain; saddamicup1993@outlook.com
and Suheer Al-Hadhrami; s.alhadhrami1@gmail.com

Received 4 December 2021; Accepted 15 January 2022; Published 12 February 2022

Academic Editor: Shakeel Ahmad

Internet of Things (IoT) with deep learning (DL) is drastically growing and plays a significant role in many applications, including medical and healthcare systems. It can help users in this field get an advantage in terms of enhanced touchless authentication, especially in spreading infectious diseases like coronavirus disease 2019 (COVID-19). Even though there is a number of available security systems, they suffer from one or more of issues, such as identity fraud, loss of keys and passwords, or spreading diseases through touch authentication tools. To overcome these issues, IoT-based intelligent control medical authentication systems using DL models are proposed to enhance the security factor of medical and healthcare places effectively. This work applies IoT with DL models to recognize human faces for authentication in smart control medical systems. We use Raspberry Pi (RPi) because it has low cost and acts as the main controller in this system. The installation of a smart control system using general-purpose input/output (GPIO) pins of RPi also enhanced the antitheft for smart locks, and the RPi is connected to smart doors. For user authentication, a camera module is used to capture the face image and compare them with database images for getting access. The proposed approach performs face detection using the Haar cascade techniques, while for face recognition, the system comprises the following steps. The first step is the facial feature extraction step, which is done using the pretrained CNN models (ResNet-50 and VGG-16) along with linear binary pattern histogram (LBPH) algorithm. The second step is the classification step which can be done using a support vector machine (SVM) classifier. Only classified face as genuine leads to unlock the door; otherwise, the door is locked, and the system sends a notification email to the home/medical place with detected face images and stores the detected person name and time information on the SQL database. The comparative study of this work shows that the approach achieved 99.56% accuracy compared with some different related methods.

1. Introduction

In the world of technology, security has become a necessity in everyday life. Nowadays, technology is becoming an integral part of everyone's lives, so the security of every home is not left behind [1]. With the latest development in the area of artificial intelligence and big data, there is a huge gap for advancement in the field of computer vision for face recognition systems, especially in medical and healthcare environments and places to combat the spreading of infectious diseases due to touch authentication tools. In this work, the instance of a smart door unlocks the system. We have to remove conventional features and update the system to remodel the device. The main issues of a traditional security system are that anyone can access the

door by copying or robbing the key and breaching the pattern. We can just update this conventional lock system into a smart one to remove such drawbacks. Face recognition technology is one of the hottest topics in computer vision and biometrics systems [2], since it is a challenging task to recognize faces with distinct expressions. There are many algorithms to run the face recognition model. We take the pretrained convolutional neural network (ResNet-50 and VGG-16) for feature extraction and compared with LBPH algorithm, and for classification, we used SVM algorithm. The ResNet-50 gives the best result compared to other algorithms [3] for image recognition. And Haar cascade technique is used for face detection purposes. We use Haar cascade classifier due to its high detection accuracy, speed, and low false rate. It was trained a lot of positive (face) and negative images (without face) [4].

The system's drawbacks are blindly trusting someone or in traditional security measures like a key, ID card, password, or pattern and giving permission to the system. Despite that, such types of security systems have weaknesses. For example, password forgot losing the key or being stolen from an unofficial person [5, 6]. Therefore, we need to remove the conventional security measures and update the new ones. So, the face recognition (FR) is the most desired method of biometric technology system [7, 8]. In comparison to other smart technology, like voice recognition, retina scan, and fingerprint, face recognition will be considered more natural. FR can only give privileges to certain people. Therefore, we used ResNet-50 and VGG-16 for deep feature extraction, and for classification, we used SVM algorithm and then compared the result with LBPH algorithms for FR-based door unlock system. This system contains a webcam to detect the face images of a person and then validate it with the images in database. Once the face is successfully recognized, the door lock opened and send an email to the homeowner along with the face image and save the information to the SQL database; else, the door remained locked and also notify the owner through email alert as an unknown person with detected face image. The main controller in this system is Raspberry Pi 4 and the relay circuit. The FR system authenticates the person's identification with the database system. We adopt the (open-source computer vision) OpenCV library. The flow of the FR system is equipped with the camera and relay module solenoid lock, and Haar cascade classifiers were used for the face detection process. After the face detection process, the system will compare and classify the detected face images with the database images; this classification is done with a SVM algorithm.

Furthermore, there are many academic efforts to find out the robust and reliable dataset for testing and formulating the proposed study: getting a better dataset is an important task especially for facial recognition. To find the effectiveness of the method, accurate datasets are needed which (1) contain a large number of person face images and (2) check the effectiveness of these methods. Our contributions in this study are as follows:

(1) IoT with DL can help users in this field to get an advantage in terms of enhanced touchless authentication, especially in spreading infectious diseases like coronavirus disease 2019 (COVID-19)

(2) Even though there is a number of available security systems, they suffer from one or more of issues, such as identity fraud, loss of keys and passwords, or spreading diseases through touch authentication tools. To overcome these issues, IoT-based intelligent control medical authentication systems using DL models are proposed to enhance the security factor of medical and healthcare places effectively

(3) This work applies IoT with DL models to recognize human faces for authentication in smart control medical systems. We use Raspberry Pi (RPi) because it has low cost and acts as the main controller in these systems

(4) The installation of a smart control system using general-purpose input/output (GPIO) pins of RPi also enhanced the antitheft for smart locks, and the RPi is connected to smart doors

(5) We analyze and compare several in-depth learning methods according to the architecture implemented and their performance assessment metrics

(6) In this study, we use novel approach using Raspberry Pi-based cloud-assisted framework for unauthorized person detection and recognition and send the detected person image to the owners for better safety

(7) The Viola-Jones detection classifier is used in the proposed study, which provides efficient detection results; furthermore, the Viola-Jones Haar cascade classifier is computationally inexpensive and it is suitable for Raspberry Pi-based framework

(8) The DL methods (ResNet-50 and VGG-16) are used for deep feature extraction and then used its outputs to feed the SVM classifier. The pretrained models are used as fixed feature extraction when the dataset is small

The training samples for various face poses, occlusion, and illumination are generally required. Sometimes it is difficult, if it is not possible due to restriction of time and space constraints; it is difficult to obtain sufficient facial image dataset. To address the issue of insufficient samples, effective data augmentation techniques are used in [9, 10]. The idea behind the augmentation is to generate virtual sample to increase the training datasets. In this study, geometric modification, image brightness changes, and performance using different filtering techniques are used to modify the training datasets.

This proposed system is easy to install with low operational cost. This system plays a major contribution to the field of smart medical control system.

2. Related Work

This part gives different techniques for door unlock system. The preceding work is where we deal with algorithms and used different electronic devices for door unlock system.

The author in [11] proposed a "real-time control using Arduino-based door unlocking system"; in this study, they used radio frequency identification (RFID) codes to scan card for door unlock. If a person wants to enter the room first, it is needed to scan the card then someone can able to enter the room. The drawback of this system is misplaced a card that leads to access the door. The author in [12] proposed a "secured room access module". In this work, he used a keyboard-based unlock system using a microcontroller where the user needs to enter the password to get access to the door. This method is reliable if we compared with the previous study and also better in today's era. Although this method is better, but there are some drawbacks; if someone notices your password, then someone can gain access to the door. The authors in [13] used a system that takes images through Raspberry Pi 3 model B and compared the detected images with database images, although the confinement in this model did not work properly due to poor lighting. The authors in [14] proposed an IoT-based security system using face recognition. In this system, Raspberry Pi is used along with camera module to take images and compared it with database images. It used OpenCV with Python for feature extraction. This system performs better for both known and unknown images. The authors in [15] have proposed door lock unlock system using web application. In this work, they monitor the door for locking and unlocking using web application. Someone can get access with his mobile and also check the status of door locking/unlocking. The drawback is someone hack the code and easily enter the door. The authors in [16] proposed an embedded platform. In this study, taking image in embedded system with Raspberry Pi considers the recognition and image capturing requirements. Raspberry Pi with other hardware device develops on this platform. The designed system is fast to run image recognition algorithm. The data flows in between camera module and Raspberry Pi. The authors in [17] proposed face detection along with equivalent time recognizer using OpenCV and eigenface; this proposed system has done on Raspbian operating system in Raspberry Pi model B. Pi camera is used for image capturing with the help of face recognition ability. This method assists the police tasks to recognize detected faces from captured images of a camera-based system, which can be immensely a reliable system. The authors in [18] proposed the inputs for the project are capturing the face in camera module from webcam and classifying on that image using CNN algorithm then verifying the user. The author in [19] has implemented the work based on Raspberry Pi model B, with Pi camera for capturing the images and then converting the image into grayscale. He finalized that the results are good and the system is technically advanced compared to image interface on a private PC. The authors in [20] have proposed door locking/unlocking system through different controllers. They used technology like Bluetooth that is available on gadget and consumes less power. They also added special features to enhance the security capabilities and make it easy to use. The authors in [21] proposed the global system for mobile communication (GSM) based on digital security system. This proposed system has designed built-in near-field communication (NFC) capabilities and this would become a key for door lock/unlock using the logical link control protocol that matches the password to lock/unlock the door. The authors [22] proposed a face recognition-based real-time application, by generating a MATLAB code using an image acquisition tool box, with the simple approach that is principle component analysis (PCA) and eigenfaces. The authors in [23] proposed face recognition-based real-time security system using Raspberry Pi. This work has done using LBPH, fisherfaces, and eigenface algorithms. To compare with different processors and know the accuracy and time complexity of the model, this system is secure and no one can get access without the face matching. Recently, a researcher published a number of research papers using deep neural networks in the field of facial biometrics with impressive results, and it compared with traditional algorithms [24]; for facial recognition, CNNs are trained using a data-driven network architecture. In addition, CNN combines the extracted features and classifier into a single framework [25]. A CNN model mainly includes convolutional layers, pooling layers, fully connected layers, and an input and an output layer. CNNs are better for feature extraction and play an important breakthrough for face recognition.

There are multiple door locking/unlocking systems have been designed. The comparative study of door unlocking system based on face authentication and verification is depicted in Table 1. The table comprises of different types of smart door locking/unlocking systems that have already designed in previous studies. These studies mainly require the additional device for system operation and obtain the system authentication condition using smartphone; to operate the system, user needs to input command manually through smartphone interface. The problem arises in the systems, if the person is not familiar to the smart technology and its user interface, which leads the difficulty to use. Therefore, this conducted study provides an efficient way, which is not only for safety purposes for real-time face detection and recognition technique but also easier to use, because the design of the system is more user friendly, which does not need any extra manual commands nor technical skills are needed. The entire system is embedded into a door that is automatically operatable. The innovation of smart door locking/unlocking system will also be discussed in this study which is depicted in Table 1.

3. System Architecture and Design

3.1. System Architecture. This proposed system has many modules such as image module, control module, and door locking/unlocking module shown in Figure 1. The image module takes a face image of a person and sends it to the main control system (Raspberry Pi) for further process. It is achieved through a web camera (Logitech). The door locking/unlocking module mainly contains 5 V relay circuit (RC) and electromagnetic solenoid lock (EMSL), which deal with locking/unlocking the door, are discussed in [29, 30]. The control module is heart of the system, which is realized by utilizing the Raspberry Pi 4 module B+ depicted in Figure 1.These particular system responsibilities include

Table 1: Related work.

Verification technique	Adopted device	Input	Reference no.
Password verification	Keypad	Needed	[26]
Near-field communication (NFC) verification and password comparison	Android phone	Needed	[21]
Smart phone-based network authentication	Android phone	Needed	[27]
Taking images for face recognition authentication	Android phone	Needed	[28]
Real-time face recognition	Not needed	Not needed	Proposed method

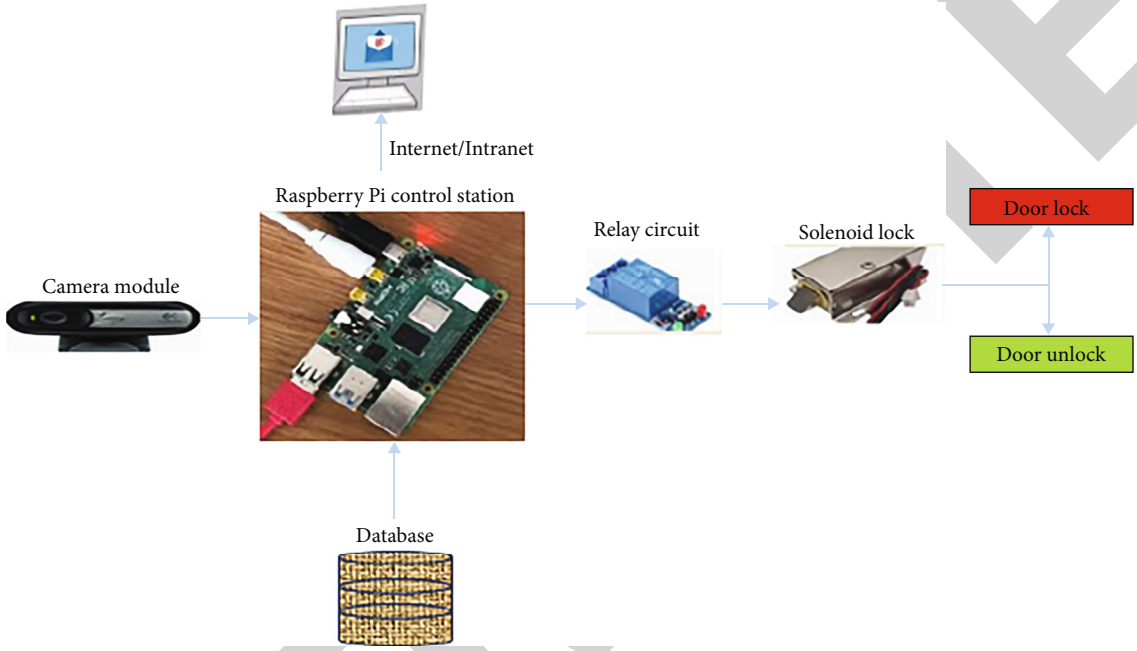

Figure 1: Block diagram architecture.

Figure 2: USB web camera.

taking face images through web camera, process the image as required, contain the facial image database, compare obtained images with stored database image, and send query to the door locking/unlocking module. The function of the control module acts as a web server for sending and receiving the emails notifications. For short message service (SMS) notifications and backend access have been studied in [31].

3.2. System Description

3.2.1. Image Module. This module utilizes a webcam (Logitech); the reason of using Logitech instead of Pi camera is due to the effectiveness of cost. The feature of Logitech is high-quality image resolution of 1080 pixels with 30 frames per second (30 fps). It is also good for low-light picture and equipped with night version footage. The interface of camera with Raspberry Pi via USB 2.0 ports that are conducted taking image is presented in Figure 2.

3.2.2. Raspberry Pi Control Module. The control module of the designed system using Raspberry Pi 4 model B+ is developed and designed by Raspberry Pi Foundation. The feature of Pi 4 contains a 64-bit ARM Cortex A72 4GB of RAM. It has video core VI graphical processing unit (GPU) for the graphical processing application (GPA). Furthermore, it consists of two USB ports and 40 GPIO pins to connect Pi with external electronic devices; the door locking/unlocking module utilized the GPIO pins. Raspberry Pi is developed to execute Linux-based operating system (LOS) having its own operating system, i.e., Raspbian operating system (ROS), and used Python as official programming language. The core module plays an effective role which is responsible for several functions (i.e., obtains image from webcam, processes and stores images, and maintains database image of authorized persons). It detects and recognizes the person which is authorized or not. The control system is responsible for sending the query to lock/unlock the door using the Python programming code through GPIO pins to the relay as shown in Figure 3.

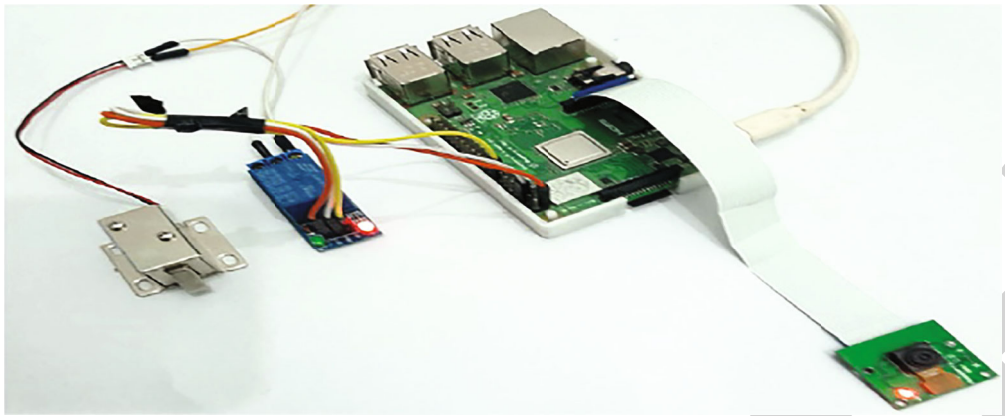

Figure 3: Raspberry Pi 4 model B+ control module.

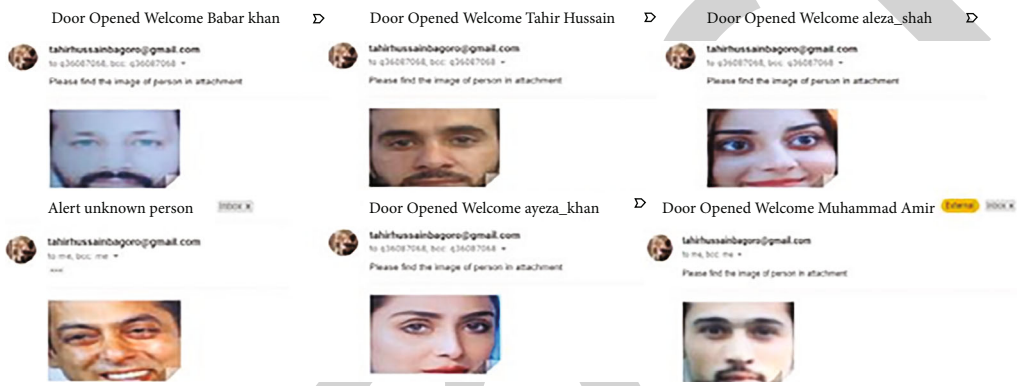

(a)

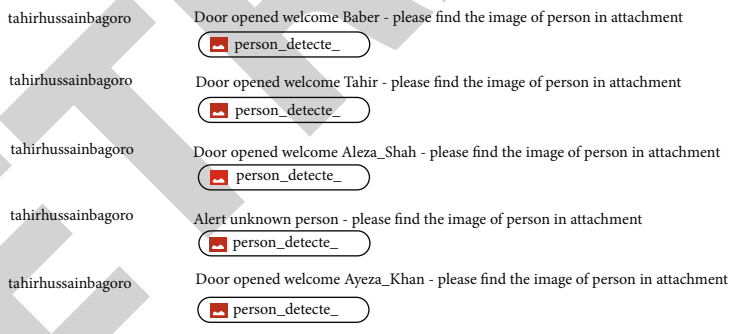

(b)

(c)

Figure 4: E-mail notification.

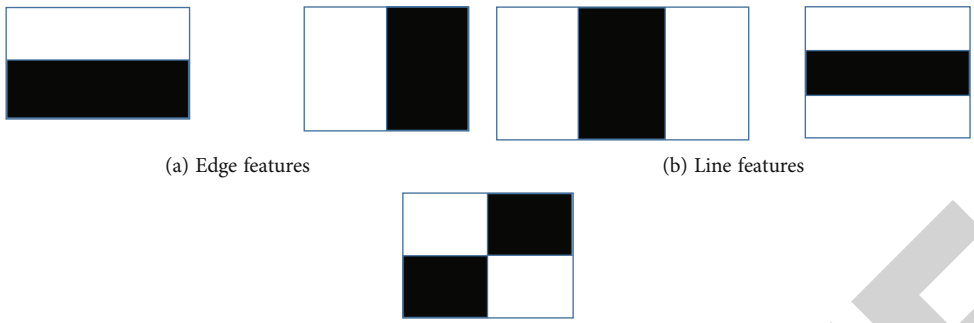

(a) Edge features (b) Line features

(c) Four-rectangle features

Figure 5: Haar features.

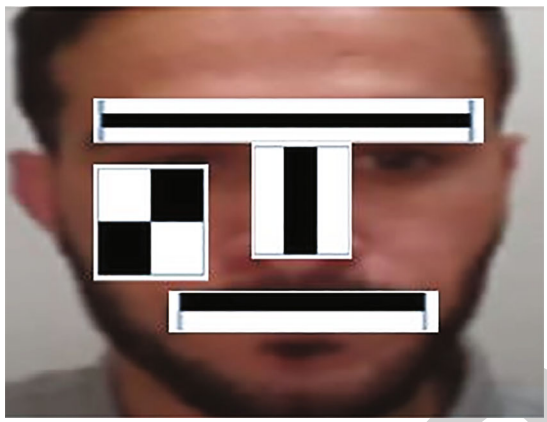

Figure 6: Feature extraction.

3.2.3. Embedded Server and IoT for E-mail Notification. The system has another core module which acts as an embedded web server. The main function of the server includes sending visitors detected face image via email to the owner. In this proposed work, the system will notify the homeowner about the detected person using simple mail transfer protocol (SMTP). By using this protocol, the system sends email along with detected face image, either it is known or unknown person to the owner which is shown in Figures 4(a) and 4(b). This system saves the time and name of detected person either recognized or not recognized person in the SQL database file shown in Figure 4(c).

3.2.4. Face Detection. There are various face detection algorithms used for different applications, like security surveillance, gaming, and human-computer interaction [32]. The face detection function detects faces from photos or videos and it differentiates from other objects. Viola and Jones developed an object detection algorithm based on Haar cascade classifier [33]. It is machine learning algorithm in which there are lots of positive and negative images used to train the classifier; the cascade classifier is trained for feature extraction and then used for face detection [34]. The use of the classifier is due to its high detection accuracy, speed, and its low false positive rate [35]. The image value of each simple feature is calculated by Paul Viola and Michael Jones methods [36] which can be calculated by using the following equation:

$$F = \text{dark} - \text{white} = \frac{1}{n}\sum_{\text{dark}}^{n} F(x) - \frac{1}{n}\sum_{white}^{n} F(x), \quad (1)$$

where n denotes the number of pixel value and $F(x)$ is the value got from the image, which is depicted in Figures 5 and 6.

There are many detection algorithms that have been developed, with various computational times and detection methods. Paul Viola and Michael Jones developed a Haar classifier which can boost rejection cascade architecture. This architecture was used for the first time in a real-time face detector with a high classification accuracy [37]. Paul Viola and Michael Jones were able to produce rapid facial detection by developing a method to quickly calculate digital image features. The Haar features are good at detecting edges and lines, and it is effective for face detection. If the edge and line features give to the network or any algorithm that detects faces, then it is only able to detect objects with clear edges and lines.

The method proposed by Viola and Joins [38] was improved later upon the work presented by Lienhart and Maydt [39]. This method has a high detection rate at the cost of low rejection [40]. With a low rejection rate, the number of false positive or wrongly detected objects can be high. By applying image processing and multiple "feature" classifiers to the area of the image detected containing an object, we can lower the false positive rate. With only a slight increase in computation time, the OpenCV can also provide a set of public domain classifiers that can be used to improve the false positive detection rate of a single classifier. Using the baseline classifier, we determine areas of the image that have a high probability containing a face. These areas are used to create regions of interest for the multiclassifier system.

3.2.5. Face Recognition (FR). The FR model basically finds out the identity of the face image by comparing the images stored in database studied in [41]. In general, the FR is divided into three main stages, i.e., face detection, feature extraction, and FR, presented in [42]. The face detection model is used to locate the occurrence of face in the image. In some libraries, face alignment is used to enhance the potency of FR models; in general, there are some difficulties in recognizing the same faces with different orientations. The feature extraction is done on the aligned face to obtain

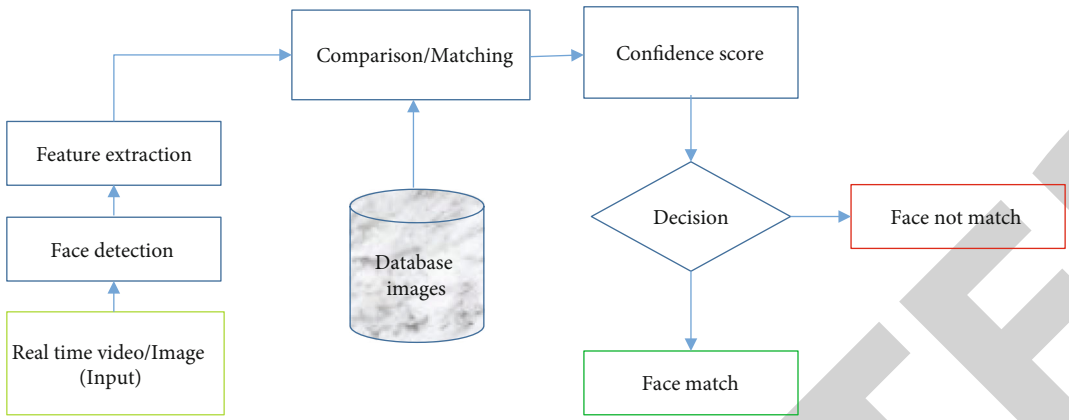

Figure 7: Face recognition work flow.

Figure 8: The detected frontal and profile faces.

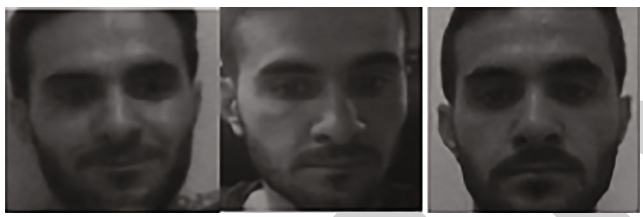

Figure 9: The illumination variation.

main features which is useful for recognition. The face patch detected is transform into vector points depending on the implemented model. Lastly, FR is carried out by feature comparison from the detected face-to-face features stored in database utilizing classification model based on confidence score. Figure 7 explains the whole work flow of FR system.

3.2.6. Pose. To address the problem of pose variation, we can use a multiview face visual approach, using both frontal face recognition and profile to capture the entire face pose. Therefore, we perform some preprocessing steps to detect the faces, like (1) setting the face image size and (2) converting the image into grayscale. (3) The illumination is normalized using a histogram equalization algorithm, which are shown in Figure 8.

3.2.7. Illumination. The illumination represents light variations. A slight change in lighting conditions creates a major challenge for automatic facial recognition and can have a profound effect on its results. If the illumination tends to vary, the same individual gets captured with the same sensor and with an almost identical facial expression and pose; the results that emerge may appear quite different. Illumination changes the appearance of the face drastically. It was found that the difference between two identical faces with different illuminations is higher than two different faces taken under the same illumination which is shown in Figure 9.

3.3. Proposed Methodology

3.3.1. Face Image Dataset. We have collected 8422 face images of 100 different people in the RGB format shown in Figure 8; these images are captured through camera, and faces are automatically cropped using face OpenCV library. The split rate is 70% training, 15% testing, and 15% validation, where each category has 5895 training images, 1263 for validation, and 1263 for testing images. Each image has different sizes and backgrounds. The images are taken in different places and different lightening conditions for better recognition accuracy. Most existing studies are exploring their method to benchmark databases accrued in a written and managed environment. It has been shown in available research that after experimenting with the face inside in the wild, the accuracy of detection decreases drastically [43, 44]. Our work right here makes use of a small dataset that proves that the proposed study is handled well with real-world applications. The samples of our database images are shown in Figure 10.

3.4. Data Preprocessing. Image preprocessing reduces the processing time and enhances the chances of the perfect matching. Face images are preprocessed to meet the requirements of feature extraction. The steps we used for preprocessing are as follows.

3.4.1. Image Cropping. The location of the image where the face can be found is cropping and can be used for face recognition.

3.4.2. Image Resize. Different image sizes give different information so the best image size needs to be considered in detail. The reason for image resizing is to produce a lower data size, which speeds up the processing time.

3.4.3. Changing the Brightness. Changing the brightness is one of the simplest preprocessing techniques. It refers to the total light or darkness of an image. To increase the

Figure 10: Database face images.

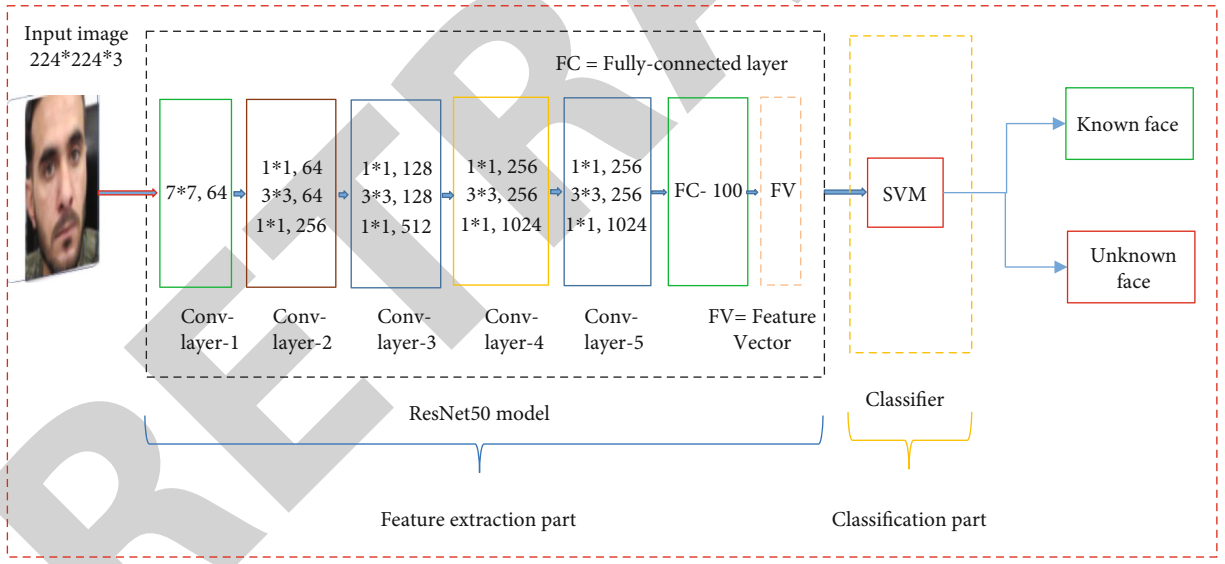

Figure 11: ResNet-50 model with SVM.

brightness, a certain fixed value must be added to each pixel. To reduce brightness, certain fixed values must be extracted from each pixel. The brightness value usually lies from -255 to +255, the negative values refer to the darker side of the image, and the positive value refers to the brighter side of the image.

3.4.4. Converting Color Image to Grayscale Image. Preprocessing of grayscale is also very fast. If we assume that processing a color image of three channels takes three times longer than processing a gray image, so we can save the processing time by removing color channels. In fact, color channel enhances the complexity of the model and often delays processing.

3.4.5. Normalization. It is an important step of data preprocessing in which we have scaled the data values in a specified range (-1.0 to 1.0 or 0.0 to 1.0).

3.5. Pretrained CNN Model. In this proposed method, we used two pretrained convolutional neural network (ResNet-50 and VGG-16) models. These models were used for feature extraction and used them in the classification part.

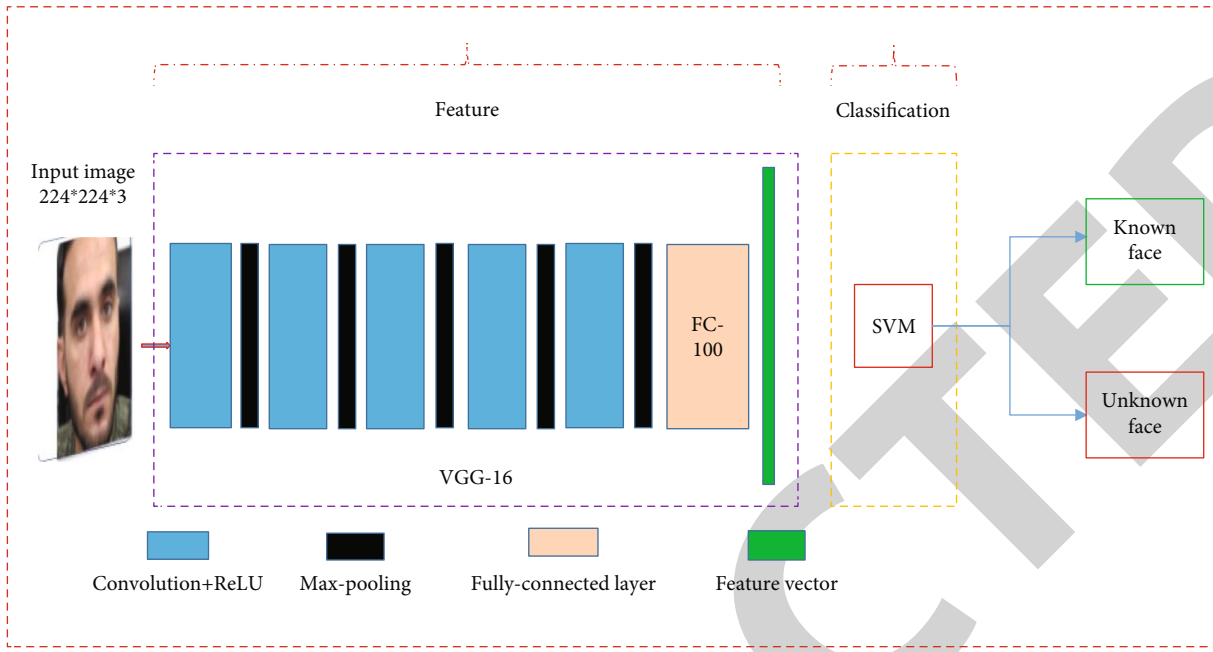

Figure 12: VGG-16 model with SVM.

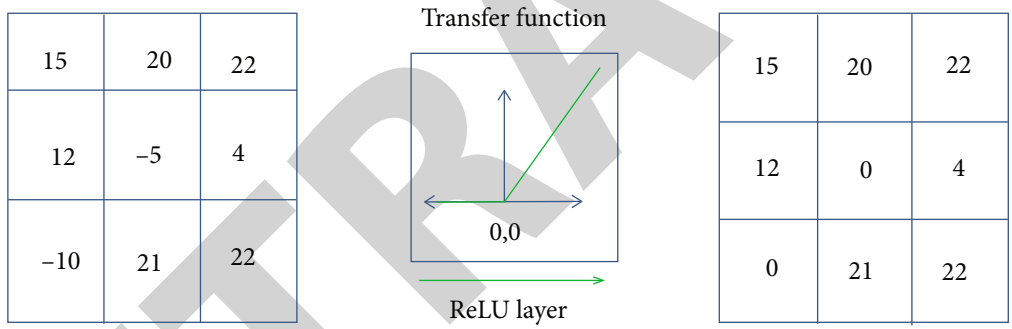

Figure 13: ReLU operation.

3.5.1. ResNet-50 Model with SVM. ResNet means deep residual network [45], developed by He et al. It is an advanced convolutional neural network in terms for image recognition. ResNet won the ImageNet competition in 2015 (ILSVRC-15). In this study, we will use ResNet-50 for feature extraction which consists of 5 convolutional layers; this model used an input image size of $224 \times 224 \times 3$ in an RGB format.

This model is comprised in two parts. The first part is for image feature extraction part and second is the classification part which is shown in Figure 11. The implementation process of ResNet model is first we divide the data into 70% for training and 30% for testing dataset. In the preprocessing step, the ResNet-50 network can only process RGB format images which are $224 \times 224 \times 3$. Deep layers were used because of higher level image feature extraction for better recognition task. Before the classification part, we use fully connected layer which is named as Fc-100 that is used for feature extraction by using the activation function. Once we get the feature, then these features are used to train and test the SVM classifier. On the base of these features, the SVM classifier classifies the images either known or unknown faces shown in Figure 9 which show that the ResNet-50 model obtained a higher recognition accuracy.

ResNet-50 and VGG-16 are the deep architectures of convolutional neural networks for images. Although ResNet is much deeper as compared to VGG-16, the model size is much smaller due to the usage of global average pooling rather than fully connected layers. This reduces the model size down to 102 MB for ResNet-50. ResNet-50 is superior due to using deep layers for higher-level features which give better distinct features for recognition tasks. Deep neural networks (DNN) improve accuracy and performance. This is because of adding more layers; for that, these layers continue to learn complex features.ResNet-50 is faster due to the bottleneck blocks. It is composed of five convolutional blocks with shortcuts added between layers. The last convolution layer is used to extract deep residual features (DRF).

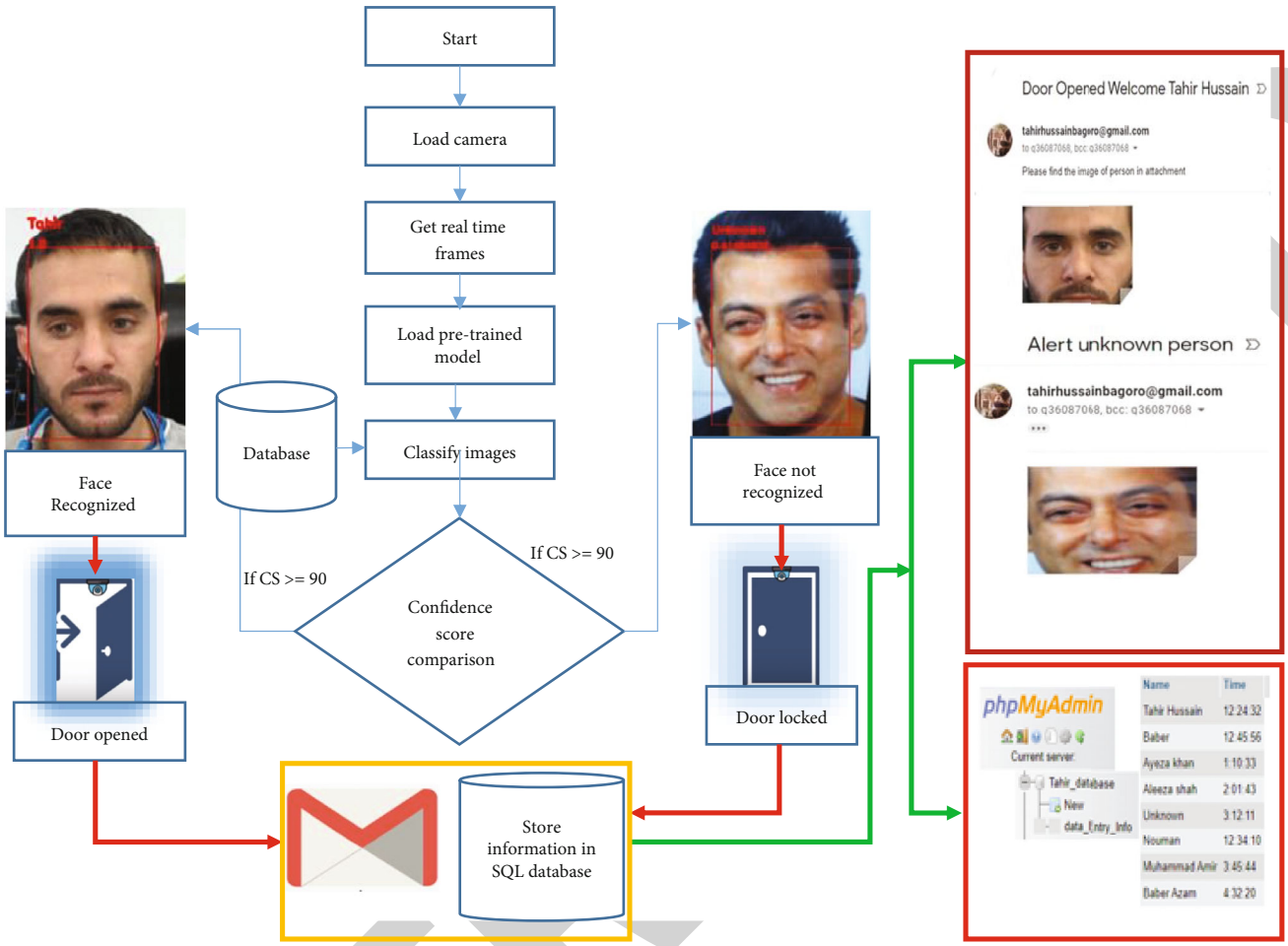

Figure 14: System work flow.

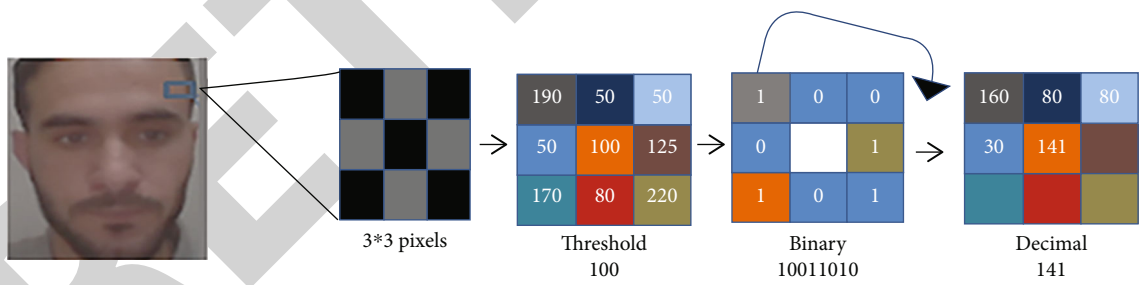

Figure 15: Converting grayscale to decimal.

3.5.2. Pretrained VGG-16 Model with SVM. VGG-16 is a pretrained convolutional neural network model, which can be used for deep feature extraction from images [46], and for the classification, we used SVM classifier. The VGG-16 used in this paper is a 16-layer deep convolutional network and the specific parameters. This network is improved on the basis of AlexNet [47], replacing the 7×7 and the 5×5 convolution kernels in AlexNet with three 3×3 convolution kernels and two 3×3 convolution kernels, respectively, whose depth is improved under the same receptive field conditions, thereby the effect of it has been improved.

VGG-16 is basically a transfer learning model and is trained on lots of face datasets, and the input image size of image is $224 * 224 * 3$. These input images are fed through different layers of convolutions and pooling and are followed by fully connected (FC) layers. Each convolutional used filter a size of $3 * 3$ and stride of 1 and used the same padding. Although the max pool layer used the $2 * 2$ filter and stride of 2 and the fully connected layers, we extract the features from the last fully connected layer named as fc-100 which is used to extract the features and passed it to SVM classifier to classify the images either known or unknown face. In addition, the hidden layers used nonlinear rectification (ReLU) to show nonlinearity in the system. We employed the generic model of VGG-16 presented in Figure 12. This network consists of 138 million parameters approximately.

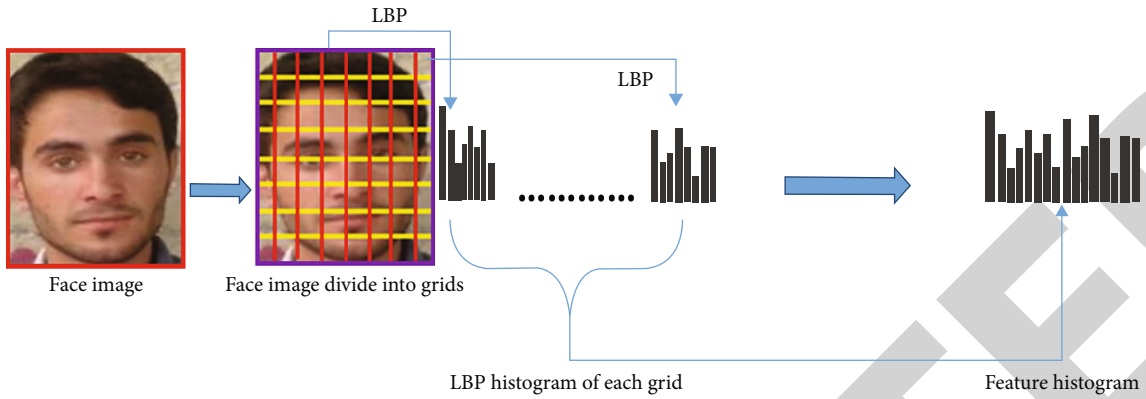

Figure 16: Local binary pattern histogram for face description.

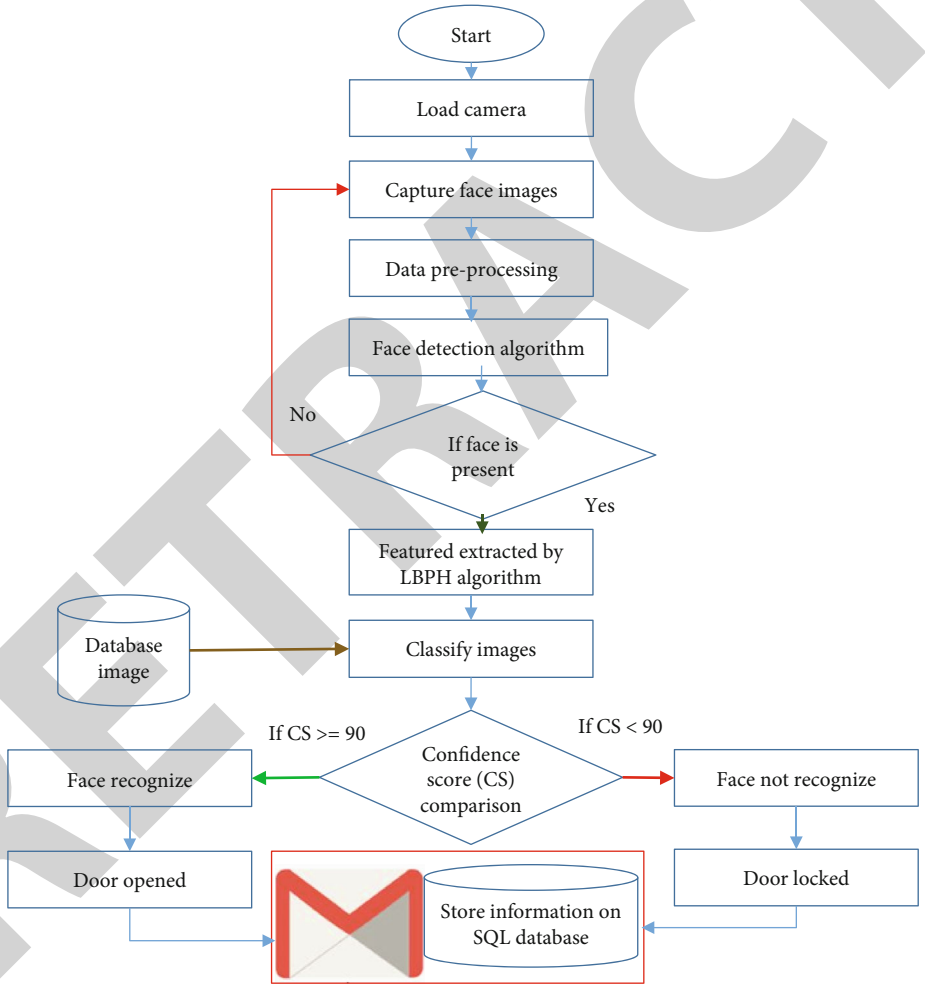

Figure 17: Flow chart of LBPH algorithm.

3.5.3. Support Vector Machines. Support vector machine (SVM) is a machine learning algorithm that is used for classification and regressing tasks. It used supervised learning to group the data into two categories. It is trained with a collection of categorized data. The purpose of SVM is to examine which category a new data point belongs to. It cannot only classify the data but also draw a boundary between two categories.

It is one of the important machine learning classifiers which can be used for classification problems. The reason for its widespread use is its simplicity and ease of use. The reason we can choose the SVM classifier is that its performance on small devices with limited resources is implacable. This classifier can be used by many researchers and proved its significance over the other classifier [48]. The other variant of SVM is like fuzzy SVM and LS-SVM, but the

Table 2: Machine for testing model.

Machine	Operation system	Processor	Main memory
Intel	Windows 10	Core i7 (6th gen)	8 GB
Raspberry Pi 4	Raspbian	ARM Cortex A72	4 GB

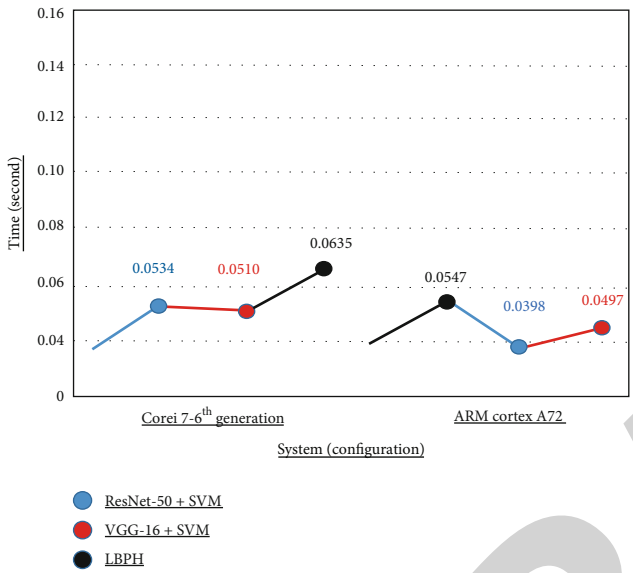

Figure 18: Testing time graph of pretrained CNN and LBPH model.

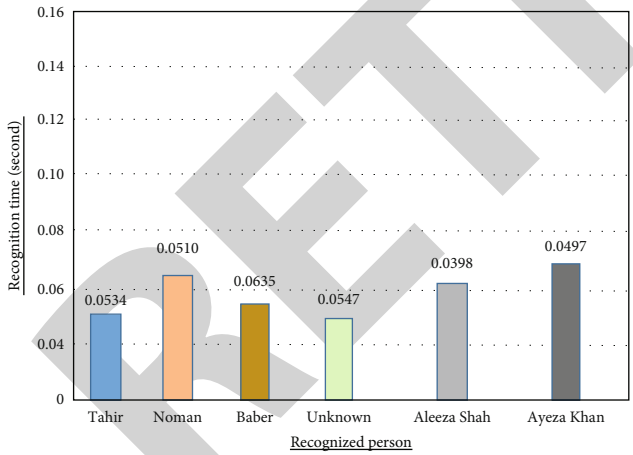

Figure 19: Response time for recognition of a person.

performance regarding the accuracy of the original SVM is very good. Many researchers used SVM as a classifier like in medical imaging classification [49–51], fruit classification [52], and face recognition [53]. We use SVM due to its simplicity to implement on Raspberry Pi. The resource available on the raspberry pi is very limited, so the classification process took much time and effective user experience; this proves that SVM is very efficient and compared the performance with a different model with SVM on Raspberry Pi.

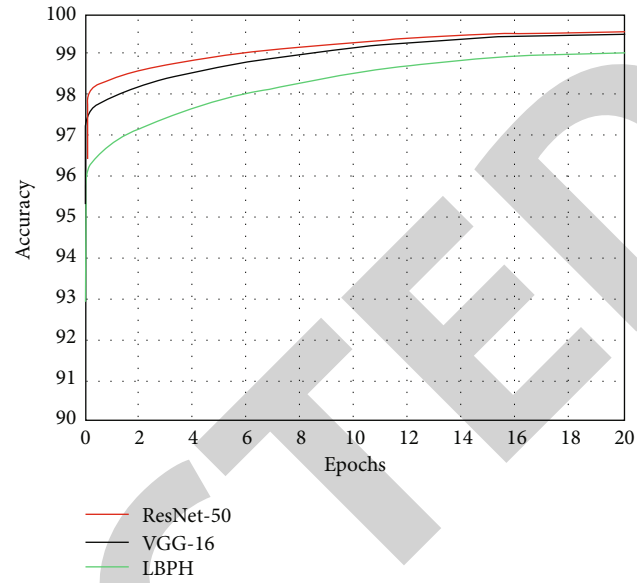

Figure 20: Model accuracy.

3.5.4. Rectified Linear Unit (ReLU). ReLU stands for rectified linear unit for a nonlinear operation. The output of function is as follows:

$$F(x) = \max\ (0, x). \tag{2}$$

ReLU purpose is to introduce nonlinearity in our ConvNet. There are many nonlinear functions such as tanh, sigmoid, and ReLU that can achieve better performance than other functions. In our ConvNet, we use ReLU function to deal with the non-linearity problem. The ReLU operation is shown in Figure 13.

3.5.5. System Work Flow. From Figure 14, first start the model, and then it loads the camera module; once the camera is loading, if the person stands in front of the camera, the camera gets the real timeframe from images or videos. Then, load the pretrained convolutional neural network models (ResNet-50 and VGG-16) for feature extraction and classify the images on the base of database images. The classification is done using SVM classifier on the base of confidence scores (CS); we set the CS as 90%. If the CS is greater than or equal to 90%, the face is recognized and door is opened; else, if CS is less than 90%, the door remained locked. Then, the system sends alert email notification to the owner along with detected face images and also saves name and time information on the SQL database which is shown in Figure 14. The system is controlled by the Raspberry Pi 4 model B+.

3.6. Linear Binary Pattern Histogram Algorithm. The open-source computer vision (OpenCV) library gives varieties of feature extraction and recognition algorithms. So, the generally used algorithms are eigenfaces, fisherfaces, and local binary pattern histogram (LBPH) [54]. The LBPH algorithm works better as compared to other two algorithms; it is because it can not only see the frontal face but also recognize the side face which is more flexible. The computational

Table 3: Model performance.

Method	Training time	Accuracy
ResNet-50	1.205 hours	99.56%
VGG-16	1.346 hours	98.49%
LBPH	0.189 hours	98.47%

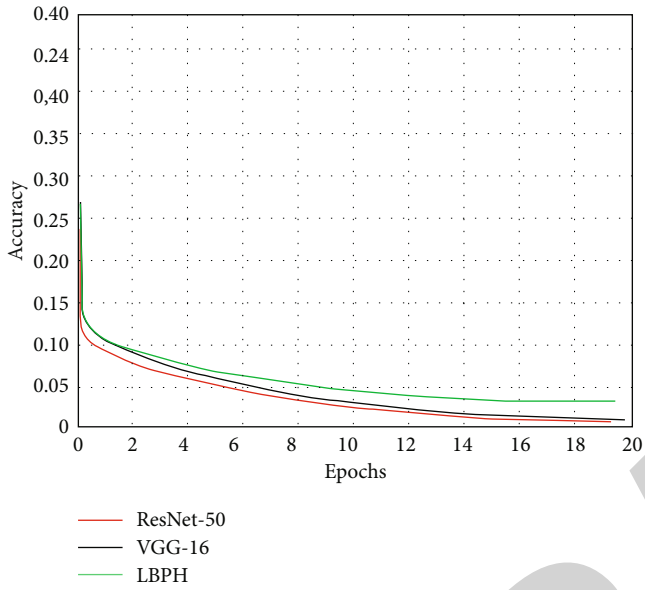

Figure 21: Model loss.

complexity of LBPH is low, but has some vulnerable features such as rotational fluctuations, grayscale variability face analysis, and recognition [55]. These features make LBPH useful for low computation platforms in Raspberry Pi. The computation of LBPH algorithm contains a set of rule that converts image into a decimal value; the conversion process is highlighted in Figure 15. The image is divided into 9-grid $(3 * 3)$ pixels; each pixel value range is from 0 to 255. The pixel value can be converted into binary value, before converting into a decimal value in which the center pixel value becomes the threshold. If the pixel value is equal or greater than threshold, the binary value is 1; else, binary value is 0. After that, the system has threshold result of linear binary pattern (LBP), though the resulted threshold value can be converted into histogram by multiplying the threshold result to binary and decimal as depicted in Figure 16, which shows the final histogram to divide the image into $8 * 8$ grid. Each histogram grid contains a decimal value from 0 to 255. After that, the final histogram is combined which gets the result from each generated histogram. The value of LBPH can represent in a histogram as shown in the following equation:

$$H(k) = \sum_{i=0}^{n} \sum_{j=1}^{m} f(\mathrm{LBP}_{s,r}(i,j),k), \quad k \in \{0,k\}, \tag{3}$$

where s represents the sampling point and r is the radius.

Once the histogram of each input image is obtained, then each histogram represents each image from the training dataset. The face recognition process is performed by feeding a new image, which is generated using a face detection algorithm from a real-time video, which creates a histogram that displays the image and calculates the distance between two histograms with a trained dataset. Hence, the LBPH algorithm used Euclidean distance (ED) presented in the following equation:

$$D = \sqrt{\sum_{i=1}^{n} (\mathrm{histogram1}i - \mathrm{histogram2}i)^2}. \tag{4}$$

The output of this formula shows the image ID with the nearest histogram. The LBPH algorithm also returns the distance that can be represented as confidence score (CS). The Euclidean calculates the gap between images; the smaller the distance has more similarity studied in [56].

3.7. LBPH Work Flow. The flow chart of our proposed method (LBPH) algorithm focuses on several factors, face detection, and recognition for person identification from real-time video source; the proposed system can be discussed using the flow chart which is shown in Figure 17. The proposed activities are explained as follows:

(i) Camera module used to take pictures from real-time source

(ii) Take a photo and save it and compare it to a database image

(iii) On the base of confidence score (CS), if the CS is greater than or equal to 90, the face is recognized and door is opened. Else, if CS is less than 90, the face is not recognized and door is remained locked

(iv) System sends email to the owner with detected face image and saves the name and time of the detected person in the SQL database which is shown in Figure 17

The interaction between the camera module and the solenoid lock is controlled by a Raspberry Pi using a relay module. The LBPH flow chart algorithm is shown in Figure 17.

4. Results and Discussion

This section describes the implementation result achieved from system development, and model successfully deployed in the container which is able to run on IoT. The system can be trained using appropriate datasets, which is able to detect the face of the visitor/visitors in real-time video frames. The success rate that was observed during the testing accuracy is 99.56% for person recognition, it can decide the authenticity of the person, and the decision made by the system can be used for multiple use cases, for instance, to open security doors based on the authenticity of the person.

Table 4: A comparative study of different methods.

Method	Face recognition accuracy
Eigenfaces [57]	36.19%
HOG [58]	66.45%
Laplacian faces [59]	65.07%
Open face [60]	75.72%
Dense U-Nets [61]	81.43%
Retina face [62]	83.87%
Hierarchical network (ResNet101+FaceNet) [63]	87.36%
ResNet-50, VGG-16, and LBPH (our model)	99.56%, 98.49%, 98.47%

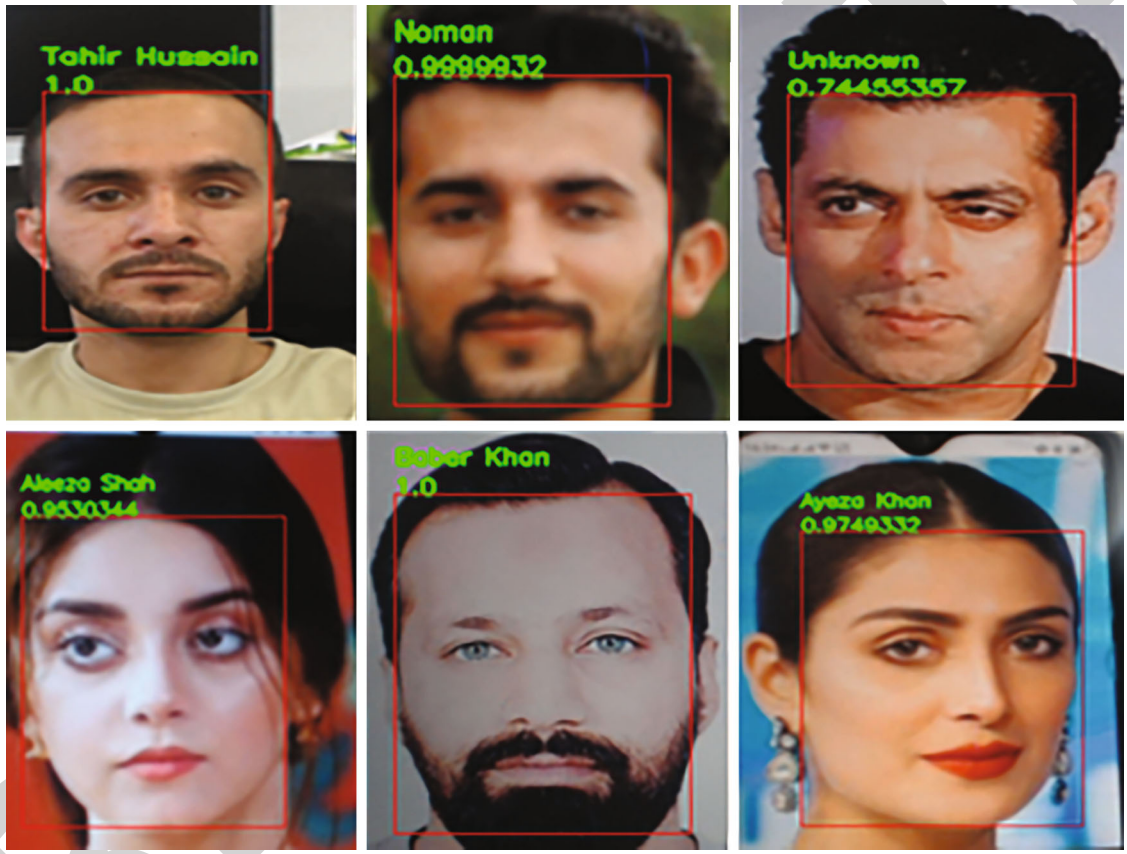

Figure 22: Model recognizing faces.

The proposed system is compared with pretrained CNN model (ResNet-50 and VGG-16) and LBPH algorithm. We use multicore system for comparing the accuracy along with the model recognition time to run this algorithm on these systems (Raspberry Pi 4 model B+ and Intel Core i7) which are shown in Table 2.

Figure 18 shows the testing time of pretrained CNN model (ResNet-50 and VGG-16) and LBPH algorithm with different system configurations. So, the LPBH takes more time as compared to ResNet-50 and VGG-16, because LBPH works on a bit-by-bit binary pattern calculation. So, the testing time graph is shown in Figure 18.

Figure 19 shows the recognition time for each recognition person with time.

5. Experimental Results

In this study, we test the model with different epochs and different batch sizes using Adam optimizer, until we get a good result which is shown in Figure 20. In this experiment, the ResNet-50 model achieves the highest accuracy which is 99.56%, VGG-16 gets 98.49%, and LBPH algorithm achieves 98.47%. The accuracy criterion was used to calculate the performance of our proposed method.

The numerical test results and training time are shown in Table 3. The network ResNet with SVM achieves better result as compared to other two algorithms which is shown in Table 3.

The main goal of all machine learning algorithms is to decrease the loss. Loss function is also called cost function which is presented in the following equation:

$$\mathrm{MSE} = \frac{1}{n}\sum_{i=1}^{n}\left(y_i^{\mathrm{true}} - y_i^{\mathrm{predicted}}\right)^2, \tag{5}$$

where n is the batch size.

A loss function defines how "good" or "bad" our model. The smaller the loss, the better the model and you need to be careful not to overfit the model.

In our proposed study, the training loss is quiet stable with ResNet-50 (ResNet − 50 = 0.012%) model as compared to other two models (VGG − 16 = 0.024% and LBPH = 0.045%) which is shown in Figure 21.

The comparative study of different face recognition methods with the proposed study is presented in Table 4.

We have successfully programmed with Raspberry Pi and get better results depicted in Figure 22, which shows that a face recognition system using the Raspberry Pi (RPi) has successfully implemented. RPi enabled a 5 V relay adapter. Raspbian was accessed remotely from PuTTY software installed on the system.

Our model is succeeded in detecting and recognizing the face of the person along with the labelled name, and a confident score of the person was displayed. The process of identifying and recognizing persons faces is performed in a real-time of capturing video frames.

6. Conclusion

In this proposed project, we have successfully implemented a security system that automatically unlocks the face system using the Raspberry Pi 3 model B+. Unlike the traditional method like keys, pattern, or password-based, we get rid of the conventional systems. The implementation of a face recognition system using Raspberry Pi can make it smaller, lighter with low-power consumption, so it is more convenient than a PC-based system. The face recognition system is able to recognize the known and unknown person based on the database images, and the system is also able to send notification emails to the owner with detected face image; this will be done through SMTP protocol. This work has a large room to improve the performance of the image processing component due to the use of the Raspberry Pi module; the processing time took longer; with the help of another method, this work may be modified in a better way.

We worked with algorithms such as Viola and Jones for face detection and for feature extraction; we used pretrained CNN models, i.e., ResNet-50 and VGG-16 with SVM classifier, for classification purpose along with LBPH algorithm for face recognition. The results of these were compared, and we found ResNet-50 worked more effectively by giving 99.56% recognition accuracy as compared to other two algorithms. So, we found that ResNet-50 performed better with the lower computation time as compared to VGG-16 and LBPH algorithms.

Data Availability

The data used to support the findings of this study are available from the corresponding authors upon request.

Conflicts of Interest

There are no conflicts of interest associated with publishing this paper.

Acknowledgments

This research was supported by the Researchers Supporting Project number (RSP-2021/244), King Saud University, Riyadh, Saudi Arabia.

References

[1] R. Nareshkumar, A. Kamat, and D. Shinde, "Smart door security control system using Raspberry Pi," *International Journal of Innovations & Advancement in Computer Science (IJIACS)*, vol. 6, pp. 499–503, 2017.

[2] A. Najmurrokhman, K. Kusnandar, A. B. Krama, E. C. Djamal, and R. Rahim, "Development of a secured room access system based on face recognition using Raspberry Pi and Android based smartphone," *EDP Sciences*, vol. 197, p. 11008, 2018.

[3] A. B. Perdana and A. Prahara, "Face recognition using light-convolutional neural networks based on modified Vgg16 model," in *2019 International Conference of Computer Science and Information Technology (ICoSNIKOM)*, pp. 1–4, Medan, Indonesia, 2019.

[4] M. K. Dabhi and B. K. Pancholi, "Face detection system based on Viola-Jones algorithm," *International Journal of Science and Research (IJSR)*, vol. 5, no. 4, pp. 62–64, 2016.

[5] M. Agarwal, H. Agrawal, N. Jain, and M. Kumar, "Face recognition using principle component analysis, eigenface and neural network," in *2010 International Conference on Signal Acquisition and Processing*, pp. 310–314, Bangalore, India, 2010.

[6] S. Liu and M. Silverman, "A practical guide to biometric security technology," *IT Professional*, vol. 3, no. 1, pp. 27–32, 2001.

[7] S. Kar, S. Hiremath, D. G. Joshi, V. K. Chadda, and A. Bajpai, "A multi-algorithmic face recognition system," in *2006 International Conference on Advanced Computing and Communications*, pp. 321–326, Mangalore, India, 2006.

[8] W. Xueguang and D. Xiaowei, "Study on algorithm of access control system based on face recognition," in *2009 ISECS International Colloquium on Computing, Communication, Control, and Management*, pp. 336–338, Sanya, China, 2009.

[9] J. Salamon and J. P. Bello, "Deep convolutional neural networks and data augmentation for environmental sound classification," *IEEE Signal Processing Letters*, vol. 24, no. 3, pp. 279–283, 2017.

[10] E. Okafor, R. Smit, L. Schomaker, and M. Wiering, "Operational data augmentation in classifying single aerial images of animals," in *2017 IEEE International Conference on*

INnovations in Intelligent SysTems and Applications (INISTA), pp. 354–360, Gdynia, Poland, 2017.

[11] S. Nath, P. Banerjee, R. N. Biswas, S. K. Mitra, and M. K. Naskar, "Arduino based door unlocking system with real time control," in *2016 2nd International Conference on Contemporary Computing and Informatics (IC3I)*, pp. 358–362, Greater Noida, India, 2016.

[12] S. Shavi, "Secured room access module," in *2017 International Conference on Smart Technologies for Smart Nation (SmartTechCon)*, pp. 1134–1138, Bengaluru, India, 2017.

[13] G. Senthilkumar, K. Gopalakrishnan, and V. S. Kumar, "Embedded image capturing system using Raspberry Pi system," *International Journal of Emerging Trends & Technology in Computer Science*, vol. 3, pp. 213–215, 2014.

[14] I. M. Sayem and M. S. Chowdhury, "Integrating face recognition security system with the Internet of Things," in *2018 International Conference on Machine Learning and Data Engineering (iCMLDE)*, pp. 14–18, Sydney, NSW, Australia, 2018.

[15] C. Vongchumyen, P. Watanachaturaporn, C. Jinjakam et al., "Door lock system via web application," in *2017 International Electrical Engineering Congress (iEECON)*, pp. 1–4, Pattaya, Thailand, 2017.

[16] S. Jogdand and M. Karanjkar, "Implementation of automated door accessing system with face design and recognition," *International Journal of Science and Research (IJSR)*, vol. 4, 2015.

[17] H. H. Lwin, A. S. Khaing, and H. M. Tun, "Automatic door access system using face recognition," *International Journal of Scientific and Technology Research*, vol. 4, pp. 294–299, 2015.

[18] Y. Taigman, M. Yang, M. A. Ranzato, and L. Wolf, "Deepface: closing the gap to human-level performance in face verification," in *Proceedings of the IEEE Conference on Computer Vision and Pattern Recognition*, pp. 1701–1708, Columbus, OH, USA, 2014.

[19] J. O. Helvig, *Implementing the Viola-Jones Face Detection Algorithm*, Diss Technical University of Denmark, DTU, DK-2800 Kgs Lyngby, Denmark, 2008.

[20] A. P. Mrudula, K. Dinesh, and P. Reethika, "Smart door unlocking system," *International Research Journal of Engineering and Technology*, vol. 7, pp. 4980–4984, 2020.

[21] C.-H. Hung, Y.-W. Bai, and J.-H. Ren, "Design and implementation of a door lock control based on a near field communication of a smartphone," in *2015 IEEE International Conference on Consumer Electronics-Taiwan*, pp. 45-46, Taipei, Taiwan, 2015.

[22] N. Dalal and B. Triggs, "Histograms of oriented gradients for human detection," in *2005 IEEE Computer Society Conference on Computer Vision and Pattern Recognition (CVPR'05)*, pp. 886–893, San Diego, CA, USA, 2005.

[23] M. A. Khan, M. K. Shaikh, S. A. bin Mazhar, and K. Mehboob, "Comparative analysis for a real time face recognition system using Raspberry Pi," in *2017 IEEE 4th International Conference on Smart Instrumentation, Measurement and Application (ICSIMA)*, pp. 1–4, Putrajaya, Malaysia, 2017.

[24] Y. Qian, M. Gong, and L. Cheng, "Stocs: an efficient self-tuning multiclass classification approach," in *Canadian Conference on Artificial Intelligence*, Springer, 2015.

[25] Z. Wu, M. Peng, and T. Chen, "Thermal face recognition using convolutional neural network," in *2016 International Conference on Optoelectronics and Image Processing (ICOIP)*, pp. 6–9, Warsaw, 2016.

[26] A. Jain, A. Shukla, and R. Rajan, "Password protected home automation system with automatic door lock," *MIT International Journal of Electrical and Instrumentation Engineering*, vol. 6, pp. 28–31, 2016.

[27] A. Kassem, S. El Murr, G. Jamous, E. Saad, and M. Geagea, "A smart lock system using Wi-Fi security," in *2016 3rd International Conference on Advances in Computational Tools for Engineering Applications (ACTEA)*, pp. 222–225, Zouk Mosbeh, Lebanon, 2016.

[28] A. Hegde, N. Prathviraj, and N. R. Shetty, "Illumination enhanced face recognition for smart access system," *International Journal of Mechanical Engineering and Technology*, vol. 10, pp. 501–510, 2019.

[29] P. Feng, *Face Recognition Based on Elastic Template*, Beijing University of Technology, China, 2004.

[30] M. H. Yang, D. J. Kriegman, and N. Ahuja, "Detecting faces in images: a survey," *IEEE Transactions on Pattern Analysis and Machine Intelligence*, vol. 24, no. 1, pp. 34–58, 2002.

[31] R. Nosaka, Y. Ohkawa, and K. Fukui, "Feature extraction based on co-occurrence of adjacent local binary patterns," in *Pacific-Rim Symposium on Image and Video Technology*, pp. 82–91, Springer, 2011.

[32] K. Dang and S. Sharma, "Review and comparison of face detection algorithms," in *2017 7th International Conference on Cloud Computing, Data Science & Engineering-Confluence*, pp. 629–633, Noida, India, 2017.

[33] P. Viola and M. Jones, "Robust real-time object detection," *International Journal of Computer Vision*, vol. 4, pp. 34–47, 2001.

[34] A. Hadid, M. Heikkilä, T. Ahonen, and M. Pietikäinen, "A novel approach to access control based on face recognition," in *Proc Workshop on Processing Sensory Information for Proactive Systems (PSIPS)*, pp. 68–74, Citeseer, 2004.

[35] P. Viola and M. J. Jones, "Robust real-time face detection," *International Journal of Computer Vision*, vol. 57, no. 2, pp. 137–154, 2004.

[36] S. Sandar and S. A. N. Oo, "Development of a secured door lock system based on face recognition using Raspberry Pi and GSM module," *Development*, vol. 3, no. 5, 2019.

[37] M. J. Saberian and N. Vasconcelos, "Boosting classifier cascades," in *NIPS*, pp. 2047–2055, Citeseer, 2010.

[38] P. Viola and M. Jones, "Rapid object detection using a boosted cascade of simple features," in *Proceedings of the 2001 IEEE Computer Society Conference on Computer Vision and Pattern Recognition CVPR*, Kauai, HI, USA, 2001.

[39] R. Lienhart and J. Maydt, "An extended set of Haar-like features for rapid object detection," in *Proceedings International Conference on Image Processing*, Rochester, NY, USA, 2002.

[40] G. Bradski and A. Kaehler, *Learning OpenCV: Computer Vision with the OpenCV Library*, O'Reilly Media, Inc., 2008.

[41] R. Jafri and H. R. Arabnia, "A survey of face recognition techniques," *Journal of Information Processing Systems*, vol. 5, no. 2, pp. 41–68, 2009.

[42] W.-L. Chao, *Face Recognition*, GICE, National Taiwan University, 2007.

[43] G. B. Huang, M. Mattar, T. Berg, and E. Learned-Miller, "Labeled faces in the wild: a database for studying face recognition in unconstrained environments," in *Workshop on Faces*

Hindawi
Computational and Mathematical Methods in Medicine
Volume 2023, Article ID 9849173, 1 page
https://doi.org/10.1155/2023/9849173

Retraction

Retracted: Machine Learning-Based Automated Diagnostic Systems Developed for Heart Failure Prediction Using Different Types of Data Modalities: A Systematic Review and Future Directions

Computational and Mathematical Methods in Medicine

Received 8 August 2023; Accepted 8 August 2023; Published 9 August 2023

This article has been retracted by Hindawi following an investigation undertaken by the publisher [1]. This investigation has uncovered evidence of one or more of the following indicators of systematic manipulation of the publication process:

(1) Discrepancies in scope

(2) Discrepancies in the description of the research reported

(3) Discrepancies between the availability of data and the research described

(4) Inappropriate citations

(5) Incoherent, meaningless and/or irrelevant content included in the article

(6) Peer-review manipulation

The presence of these indicators undermines our confidence in the integrity of the article's content and we cannot, therefore, vouch for its reliability. Please note that this notice is intended solely to alert readers that the content of this article is unreliable. We have not investigated whether authors were aware of or involved in the systematic manipulation of the publication process.

Wiley and Hindawi regrets that the usual quality checks did not identify these issues before publication and have since put additional measures in place to safeguard research integrity.

We wish to credit our own Research Integrity and Research Publishing teams and anonymous and named external researchers and research integrity experts for contributing to this investigation.

The corresponding author, as the representative of all authors, has been given the opportunity to register their agreement or disagreement to this retraction. We have kept a record of any response received.

References

[1] A. Javeed, S. U. Khan, L. Ali, S. Ali, Y. Imrana, and A. Rahman, "Machine Learning-Based Automated Diagnostic Systems Developed for Heart Failure Prediction Using Different Types of Data Modalities: A Systematic Review and Future Directions," *Computational and Mathematical Methods in Medicine*, vol. 2022, Article ID 9288452, 30 pages, 2022.

Hindawi
Computational and Mathematical Methods in Medicine
Volume 2022, Article ID 9288452, 30 pages
https://doi.org/10.1155/2022/9288452

Review Article

Machine Learning-Based Automated Diagnostic Systems Developed for Heart Failure Prediction Using Different Types of Data Modalities: A Systematic Review and Future Directions

Ashir Javeed,[1] Shafqat Ullah Khan,[2] Liaqat Ali,[3] Sardar Ali,[4] Yakubu Imrana,[5,6] and Atiqur Rahman[7]

[1]*Aging Research Center, Karolinska Institutet, Sweden*
[2]*Department of Electrical Engineering, University of Science and Technology Bannu, Pakistan*
[3]*Department of Electronics, University of Buner, Buner, Pakistan*
[4]*School of Engineering and Applied Sciences, Isra University Islamabad Campus, Pakistan*
[5]*School of Engineering, University of Development Studies, Tamale, Ghana*
[6]*School of Computer Science and Engineering, University of Electronic Science and Technology of China (UESTC), Chengdu, China*
[7]*Department of Computer Science, University of Science and Technology Bannu, Pakistan*

Correspondence should be addressed to Yakubu Imrana; yakubu.imrana@uds.edu.gh

Received 22 December 2021; Accepted 15 January 2022; Published 3 February 2022

Academic Editor: Muhammad Zubair Asghar

One of the leading causes of deaths around the globe is heart disease. Heart is an organ that is responsible for the supply of blood to each part of the body. Coronary artery disease (CAD) and chronic heart failure (CHF) often lead to heart attack. Traditional medical procedures (angiography) for the diagnosis of heart disease have higher cost as well as serious health concerns. Therefore, researchers have developed various automated diagnostic systems based on machine learning (ML) and data mining techniques. ML-based automated diagnostic systems provide an affordable, efficient, and reliable solutions for heart disease detection. Various ML, data mining methods, and data modalities have been utilized in the past. Many previous review papers have presented systematic reviews based on one type of data modality. This study, therefore, targets systematic review of automated diagnosis for heart disease prediction based on different types of modalities, i.e., clinical feature-based data modality, images, and ECG. Moreover, this paper critically evaluates the previous methods and presents the limitations in these methods. Finally, the article provides some future research directions in the domain of automated heart disease detection based on machine learning and multiple of data modalities.

1. Introduction

A variety of conditions that affect the normal working of the heart are known as heart diseases. Heart diseases are classified into heart failure (HF), CAD, vessel disease, heart rhythm problems, and many more. Heart disease, also referred to as cardio vascular disease (CVD), defines the condition where the blood vessels are narrowed or blocked leading to a heart attack (myocardial infarction) and chest pain (angina). Symptoms of heart disease include chest pressure, chest discomfort (angina), shortness of breath, abnormal heartbeats, and heart defects [1]. HF is a chronic disease that affects the heart chambers. Cardiovascular disease abrupts the normal working of the heart that pumps sufficient amount of blood in the human body, without boosting the intracardiac pressure. As the heart becomes unable to pump sufficient blood to the rest of the body, the kidney reacts by inducing the body to retain fluid which results in lung congestion and swelling in the arms and legs. CHF is an expeditious healthcare problem [2] of the modern world, and 26 million adults around the globe are suffering from congestive heart failure [3]. Approximately 17.9 million patients with cardiovascular disease die every year that is 31% of the overall deaths around the world [4].

Heart failure has many risk factors such as gender, family history, and increased age, which are classified into uncontrolled risk factors, while high cholesterol, smoking, high blood pressure, and obesity are classified into controllable risk factors [5]. To understand the HF, we explore and overview the most common types of heart failure diseases for better problem awareness. Herein, Figure 1 depicts the four chambers of the heart that are responsible for blood pumping.

In recent times, a large amount of data on patients has been generated in the healthcare sector. However, researchers and practitioners are not efficiently using this data for effective diagnosis of the disease. The healthcare sector is facing major challenges in quality of service (QoS) which ensures correct and timely diagnosis of disease that results in competent treatment of the patients. Impaired diagnosis leads to detrimental results which are not acceptable [7].

1.1. Major Types of Heart Diseases

1.1.1. Coronary Artery Disease (CAD). CAD is a heart disease which commonly occurs as result of the build of fatty deposits (plaque) inside the arteries responsible for supplying blood to the heart muscles. The obstruction in the arteries reduces blood flow to heart muscles which results in the impairment of the heart functions. This phenomenon is known as myocardial ischemia. The partial or complete blockage of arteries results in inevitable damage done to the heart also known as a heart attack. The human heart has four chambers that are divided into upper receiving chamber (right and left atria) and lower pumping chambers (right and left ventricle (LV)). The right atrium is responsible for gathering deoxygenated blood, and the right ventricle pumps the deoxygenated blood to the lungs for oxygenation process. Oxygenated blood from the lungs enters into the left atrium and is then transferred to all parts of the body through LV. The size and function of the LV chamber make it the most efficient responsible part of the heart. As such, the major reason for heart failure is due to damage of the LV chamber. Echocardiography helps in detecting CAD by examining or monitoring the heart for the evolution of CAD and wall motion abnormalities that begin to arise [8]. CAD can be diagnosed through LV measurement and wall motion scoring. Therefore, monitoring of LV is essential to avoid protracted damages that will affect size, shape, and function of the LV. Echocardiography is an imaging method that captures different cardiac views, structure, and their movement from ultrasound videos. Heart functional and morphological assessment is done to diagnose the cardiac disease through echocardiography [9]. Furthermore, echocardiography is also utilized for quantitative analysis of the LV ejection fraction and cardiac output [10].

1.1.2. Congestive Heart Failure (CHF). Congestive heart failure also known as chronic heart failure is a condition whereby the heart fails to pump a sufficient amount of blood to the body to meet oxygen demand [11]. CHF is a chronic disease that affects the heart muscles. There are various risk

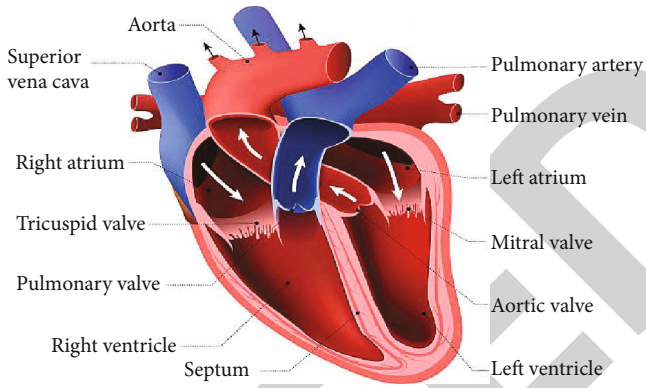

Figure 1: Anatomy of the heart [6].

factors behind CHF but the most common risk factors consist of high blood pressure, old age, obesity, and diabetes. Congestive heart failure is more common in men as compared to women. The term heart failure does not refer to the complete cease of the heart, but it actually diminishes the normal functionality of the heart as compared to a healthy person [12]. Heart failure means the body tissues are not getting enough blood and oxygen as needed for normal function. Systolic and diastolic are the two types of heart failures. In systolic heart failure, the pumping action of the heart is decreased. To test the systolic heart failure, a typical clinical test ejection fraction (EF) is done. The ejection fraction is measured as the amount of blood ejected out from the left ventricle (LV) divided by the maximum amount of blood remains in the left ventricle (LV) at the end of diastole. For a normal person, the value of ejection fraction is more than 55%, while for diastolic heart failure, the threshold value of ejection fraction is below 55%. In diastolic heart failure, the heart contracts normally but rigid and inflexible while it is relaxing and being filled with blood. Due to the stiffness of the heart, it is unable to be properly filled with blood to push back into the lungs which causes or leads to heart failure. The ejection fraction in diastolic heart failure is normal or hike.

1.1.3. Abnormal Heart Rhythms. Abnormal heart rhythms, also known as arrhythmias, are a condition whereby the heart beats too slow/too fast or irregularly due to a problem in the heart electrical system. The electrical system provides the heart with a clue of when to beat and supply blood to each part of the body [13]. Palpitations, tiredness, losing consciousness, dizziness, and breathlessness are the most common symptoms of an abnormal heart rhythm. The symptoms of heart failure are arduous to notice; therefore, it is also known as the silent killer. Doctors recommend various medical tests [14] for the diagnosis of heart failure, such as echocardiogram, where blood flow through the heart is monitored with the help of ultrasound waves. Electrocardiogram (ECG) is another way to diagnose heart problems related to the heart's rhythm. Holter monitoring is a portable device used to record continuous ECG data of the patient. Cardio computerized tomography (CT) scans provide the facility of an X-ray cross-sectional view of the

patient's heart, to detect heart failure. Cardiac magnetic resonance imaging (MRI) helps to generate an image of the heart and tissues of the heart through the use of powerful magnets and radio waves.

We have studied three major types of heart diseases for which researcher has proposed ML-based automated diagnosis systems, but Figure 2 presents the detail view of the various heart diseases.

1.2. Rationale and Aim of the Study. Previous studies that reviewed automated methods for heart diseases mainly targeted one specific type of data modality. Moreover, those studies lacked highlighting the limitations in the previously developed automated methods for heart disease prediction. Hence, we provide a systematic review of automated diagnostic systems developed for heart disease prediction based on three commonly used data modalities which are images, ECG, and clinical feature-based data modalities as shown in Figure 3. Moreover, we discuss the development of image-based, ECG-based, and data mining-based diagnostic systems that exploit deep learning and ML algorithms for the automated diagnosis of heart diseases such as CAD, HF, CHF, and CVD. All the computer-aided detection systems based on ECG, images, and clinical feature-based data techniques have four key steps: preprocessing of data, features extraction, significant feature selection, and classification. Finally, we explore the potential issues in the diagnostic systems based on the images, ECG, and clinical feature-based data modality for heart disease detection and propose solutions. To meet this objective, data is gathered from various databases and sources like ScienceDirect, PubMed, IEEE Xplore Digital Library, Springer, Hindawi, Plos, and Google Scholar based on the keywords: automated heart disease prediction or detection, ML-based detection of CHF, prediction of heart failure, coronary disease detection, data mining, and CVD. The literature used in this study was selected on the basis of a particular criteria as given:

(i) Only CAD, HF, CVD, and CHF are targeted in this study

(ii) The articles published from 1995 to 2021

(iii) Those papers were considered that employed ML techniques for the diagnosis of the heart diseases

(iv) The articles published in the English language are targeted in this study

(v) Articles that used different types of data modalities like ECG, images, and clinical features for automated detection of heart diseases were considered

(vi) The research articles that made use of publicly available datasets and electronic health records

2. Machine Learning for Heart Disease Prediction

Recently, large number of diagnostic systems have been developed for automated diagnosis of different diseases like Parkinson's disease [15–19], hepatitis [20], carcinoma [21], lung cancer [22], and mortality prediction systems [23, 24] using machine learning, deep learning [25], data mining [26], and optimization methods [27–30]. Heart disease detection through machine learning is not an exception, and recently, numerous approaches have also been successfully implemented on various datasets for automated heart disease detection [31–37]. The proposed algorithms have validated the efficient detection and prediction of heart failure. This study comprehensively reviews the ML approaches for HF prediction and detection based on three modalities (images, ECG, clinical features). This study provides the following key objects based on explicit analysis of the works that have been published in last 26 years:

(i) The proposed ML techniques on the basis of the modality used (such as images, ECG, clinical feature-based data), their benefits, and weaknesses

(ii) The dataset properties according to modalities

(iii) Performance measurement of the ML algorithms in terms of different evaluation metrics, namely, accuracy (ACC), specificity (Spec), and sensitivity (Sen)

(iv) Comparative analysis of ML techniques based on a specific data modality

The results of this study present the best modality more suitable for the prediction or detection of HF through ML approaches. It also assists researchers and physicians to improve the quality of heart disease diagnosis. The comparative analysis in this study helps to identify the effectiveness and weaknesses of previously proposed ML techniques for the diagnosis of heart disease and also suggests challenges in future works for accurate, reliable, and cost effective development of automated diagnosis system. Figure 4 provides an overview procedure for automated diagnostic system.

2.1. Article Selection. The articles selection procedure was based on the three modalities (clinical feature-based data, images, ECG) for heart disease diagnosis. We collected 105 research articles on CHF and CAD detection from various publishers such as IEEE, MDPI, Springer, Elsevier, Hindawi, and PubMed based on the keywords CAD, HF, CVD, ML, deep learning, neural networks, etc. 35 articles were selected for each modality. Researchers around the globe have been working on ML-based heart disease detection system since 1992 [38] but the number of research papers in this domain as of 2014 was very limited. In recent years, researchers have developed a lot of CAD and HF detection systems based on ML. Therefore, the number of research papers in this field has seen a tremendous increase as depicted in Figure 5.

2.2. Datasets. This section describes the datasets that are considered in the selected research articles for experiments and performance evaluation of the developed automated diagnostic systems. A total number of 56 datasets are considered from the selected research articles. These datasets are collected from various organizations all over the world.

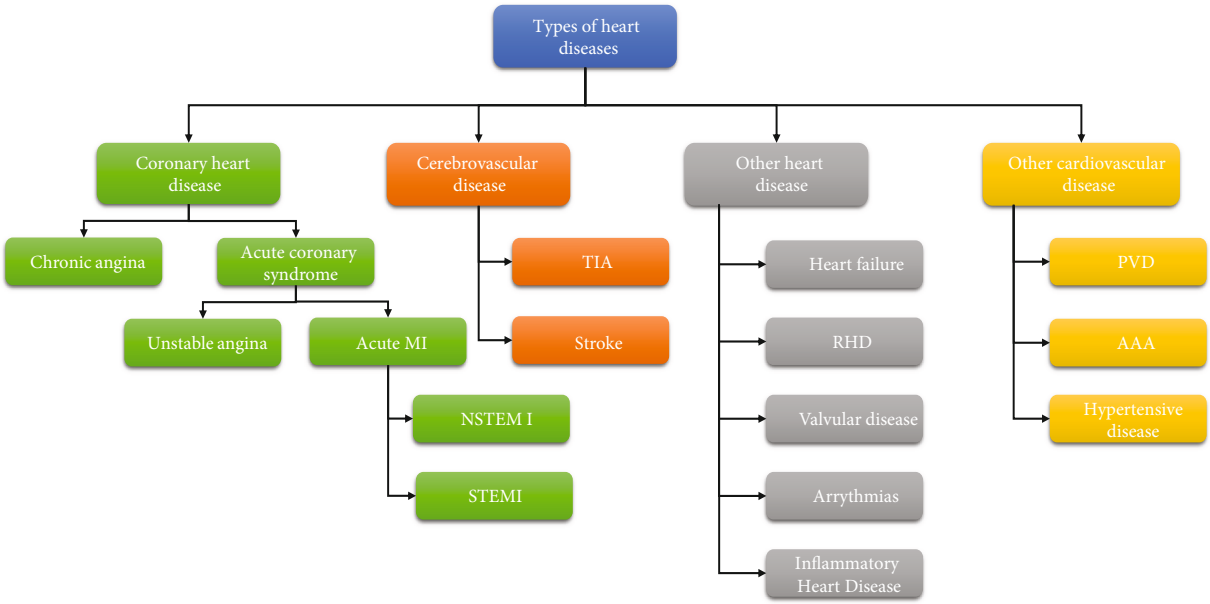

Figure 2: Types of heart diseases.

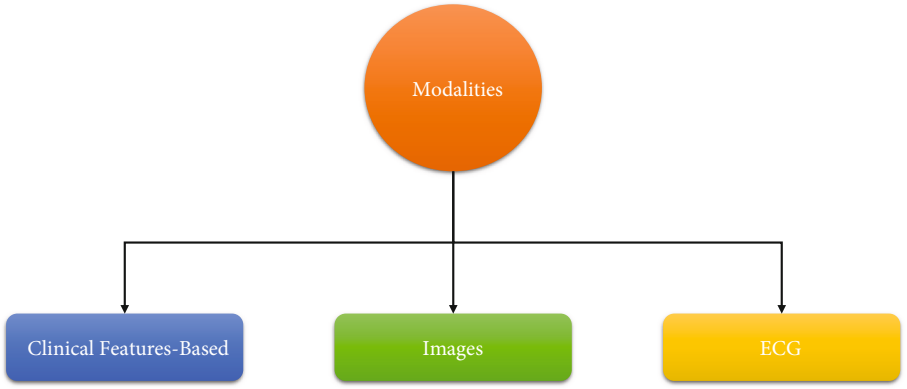

Figure 3: Different modalities used for automated heart failure diagnosis.

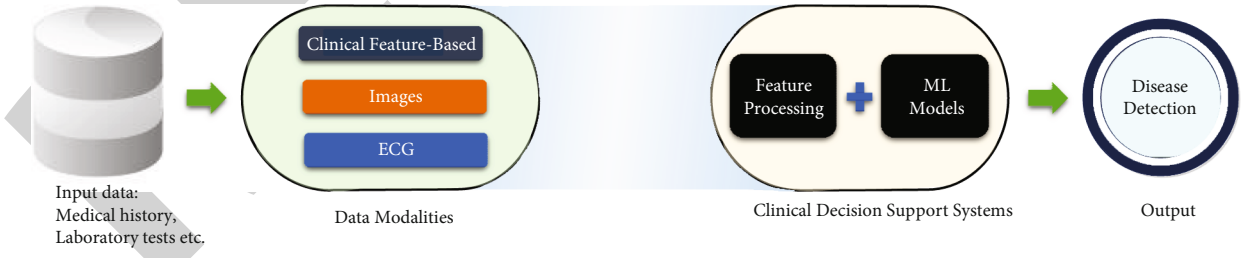

Figure 4: Overview of ML-based diagnostic system.

Few datasets are publicly available while others are collected by researchers from different hospitals and healthcare organizations. We only listed those datasets that are used for diagnosis of HF, CVD, CHF, and CAD by using ML and data mining techniques. As our study is based on the three heart disease modalities, we therefore considered datasets based on these modalities. Thus, datasets differ in terms of samples and number of features.

Table 1 depicts the properties of datasets in terms of number of subjects, dataset features, missing values, etc. Based on the modalities (clinical feature-based data, images, ECG), the nature of the datasets is diverse. For instance, dataset IDs 01, 02, and 09 are used for patients' medical reports data (age, sex, chest pain type, resting blood pressure, etc.). The most famous dataset used in clinical feature-based data modality is UCI datasets, namely,

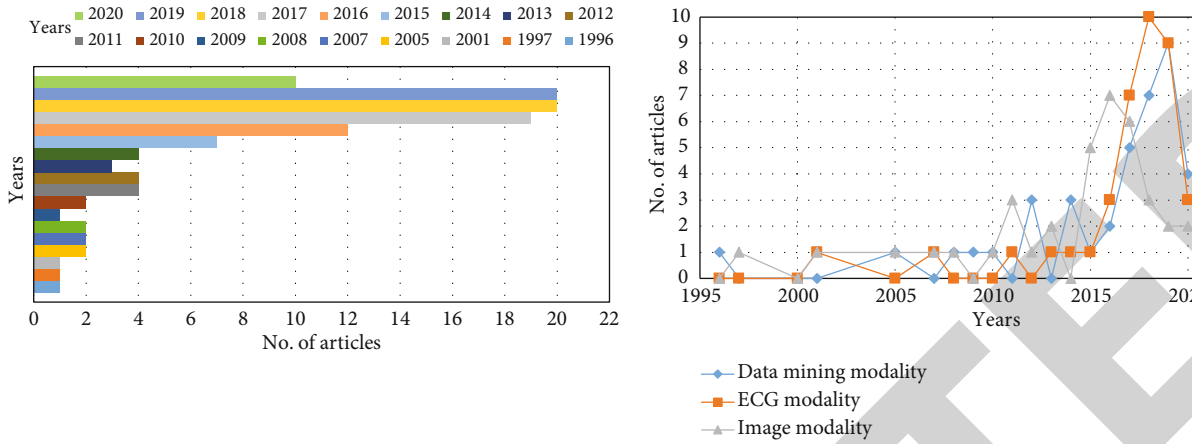

(a) Selected number of articles yearwise

(b) The comparsion of selected articles regarding modality

FIGURE 5: Selected research articles published from 1996 to 2021 as shown in Figure 5(a). The topic has gradually attracted the attention of researchers with the passage of time. In recent years, the topic got a peak attraction from researchers as a lot of articles have been published in the past few years, while Figure 5(b) depicts the comparison of published articles with respect to the modality.

Cleveland dataset, Hungarian dataset, Switzerland dataset, and Statlog dataset. UCI datasets consist of clinical features (age, serum cholesterol, exercise induced angina, etc.) that are used for automated diagnosis of HF through ML techniques. Other well-known datasets that belong to the clinical features modality are Z-Alizadeh Sani dataset and Extended Z-Alizadeh Sani dataset. Some datasets are based on ECG modality. ECG signals are used to record patients' medical data. ECG-based datasets are used by the researchers through ML and data mining approaches for the prediction and detection of the CVD and CHF disease. ECG signals are sampled to extract features from the signals. The extracted features are then used for training and testing purposes through ML models. Dataset IDs, 19, 20, 21, etc., are examples of the ECG datasets (MIT/Beth Israel Hospital (BIH), arrhythmia database, Physikalisch-Technische Bundesanstalt diagnostic ECG database). Image-based datasets consist of features that are extracted from the medical image data. ML approaches are deployed for extracting features from the images. Furthermore, models are trained and tested based on the features for automated diagnosis of the HF and CVD disease. Dataset IDs 30, 31, 32, etc., are instances of image based datasets (Cedars-Sinai Medical Center, Los Angeles CA and MCG data, Hospital Fernando Fonseca dataset). Moreover, Figure 6 depicts in detail the total number of samples in a given dataset along with total numbers of features for different datasets.

3. Automated Heart Disease Detection Based on Different Modalities

3.1. ML-Based HF Diagnosis: Clinical Feature-Based Data Modality. In recent years, data mining and ML researchers have proposed different automated methods for heart disease detection based on clinical feature-based data modality [16, 17, 39]. For example, Verma et al. [40] developed a hybrid system for the prediction of CAD using noninvasive clinical data. Their hybrid system used correlation-based subset (CFS) selection and particle swam optimization (PSO) search technique to reduce the feature space from the dataset for better performance. A number of optimized feature subset are then input into the proposed model. The model is composed of multinomial logistic regression (MLR), multilayer perceptron (MLP), C4.5, and fuzzy unordered rule induction algorithm (FURIA). The proposed model is tested on the dataset of IGMC that has 26 features and 335 subjects. MLR achieved the highest accuracy of 88.4% while for benchmark dataset such as Cleveland heart disease, it obtained an accuracy of 90.28%. Shah et al. [41] proposed a method that extracted high impact features from the feature space by using probabilistic principal component analysis (PPCA). PPCA was used to extract the new feature vectors that helped to reduce the feature space. New feature vectors were selected by parallel analysis (PA). These reduced feature vectors were supplied to the radial basis function (RBF) kernel-based support vector machine (SVM). The RBF function performed the job classification into types, i.e., normal subject and heart patient. The proposed system achieved the accuracy of 91.30%, sensitivity of 100%, and specificity of 50%. Ali et al. proposed a novel method based on optimized and stacked support vectors machine and obtained 92.22% of HF prediction accuracy [42]. In another study, Ali et al. developed a hybrid system based on χ^2 statistical model and deep neural network and further improved the HF prediction accuracy to 93.33% . In yet another study, Ali et al. highlighted the problem of overfitting to the testing data and proposed the development of mutually informed neural networks for better generalization of the decision support systems developed for HF prediction [43]. Dwivedi [44] evaluated the performance of the six ML methods on the data of StatLog heart disease dataset [6 King RD (1992) Statlog databases. Department of Statistics and Modelling Science, University of Strathclyde, Glasgow] for heart disease prediction. The

Table 1: Summary of dataset properties.

Dataset_ ID[a]	Dataset	Total samples[b]	Features[c]
01	Cleveland (UCI), heart disease dataset	303	76 raw features, 14 prominent features
02	StatLog heart disease dataset (UCI)	150, (healthy: 150, patient: 120)	13 distinct features
03	CHF database (chf2db)	136, (healthy: 46, patient: 90)	12 distinct features
04	MIT-BIH Normal Sinus Rhythm (NSR) database	54, (male: 30, female: 24)	Sampling rate: 128 samples per second
05	Congestive heart failure database (BIDMC-CHF)	15, (male: 11, female: 4)	Sampling rate: 500 samples per second
06	Fantasia database (FD)	18, (male: 5, female: 13)	Sampling rate: 128 samples per second
07	Congestive Heart Failure RR Interval Database (CHF-RR)	29	Sampling rate: 500 samples per second
08	Normal Sinus Rhythm RR Interval Database (NSR-RR)	40	Sampling rate: 500 samples per second
09	Cleaveland(UCI), Hungarian heart disease dataset	590	76 features
10	mARSupio database, Italy	14616, (patients: 347)	572 features
11	NHANES CVD dataset	4434	23-65 features
12	MIMIC-II clinical database	8059	32 features
13	Z-Alizadeh Sani dataset	303	54 features
14	Heart disease dataset, Andhra Pradesh, India	N/A	14 features
15	Physionet databases	40, (male: 20, female:20)	95300 segmented ECG
16	MITDB database, Physionet	47	22 features
17	China Kadoorie Biobank (CKB)	520000	86 features
18	MIT-BIR arrhythmia database	47	Sampling rate of 360 Hz
19	MIT/Beth Israel hospital (BIH), arrhythmia database	4,000 ambulatory ECGs	360 samples per second
20	PTB diagnostic ECG database	52 healthy, 7 HCM, 8 DCM, and 148 MI subjects	Sampled at 1,000 Hz, 250 samples per second
21	Physikalisch-Technische Bundesanstalt diagnostic, ECG database	200 (patients: 148, healthy: 52)	Sampling rate of 1000 Hz
22	1st China Physio-logical Signal Challenge	6877	Sampled at 500 Hz
23	Mayo Clinic ECG laboratory	180922, (patients: 116061, healthy: 64931)	Sampling 1500 Hz
24	Subrogated fragmented database (Sfrag-DB) + subrogated wide-fragmented database (SWfrag-DB) + fragmented database (FHCM-DB) + fibrosis database (HCM-DB)	616 records	Sampling rate: 500 Hz
25	Collected at the University of Pennsylvania	209	20 features
26	MICCAI 2017 challenge on Automated Cardiac Diagnosis	100	567 features, 13 optimal features
27	STACOM 2015 challenge	200	11 features
28	St.Francis Heart Hospital in Roslyn, New York	200	3 feature
29	Nuclear Medicine Department	288	10 features
30	Cedars-Sinai Medical Center, Los Angeles, CA	713	13 features
31	MCG data	800	2 features
32	Hospital Fernando Fonseca dataset	496	80 features
33	Siemens Somatom sensation	137	N/
34	ACS dataset (Mersin University Research and Training Hospital)	228	6 features
35	University Hospital Arnau de Vilanova, Lleida, Spain	56	Image resolution: 8.5 pixels per mm

Table 1: Continued.

Dataset_ ID[a]	Dataset	Total samples[b]	Features[c]
36	Sutter Palo Alto Medical Foundation	58652000	2 attribute
37	LIDC-IDRI public dataset	802	NoGT transformation
38	SunnyBrook Cardiac Data (SCD)	45 (male: 32 and female: 13)	Sampling: 30 frames per second
39	NSTEACS	2302 patients	N/A
40	Hospital Universiti Kebangsaan Malaysia	10	N/A
41	Department of Medicine, University of Alabama at Birmingham	109	9 features
42	UK Biobank	9135867	N/A
43	SPECT	135	30 Fourier components
44	Ham-mersmith Hospitals	1093 subjects	N/A
45	Cohn-Kanade dataset (CK+)	400	N/A
46	Sacred Heart Medical Center, Eugene	215	N/A
47	Sacred Heart Medical Center	2619	50 features
48	AGES-I Dataset	628 (male: 419, female: 209)	11 Radiodensitometric features
49	Clinical Research Centre of Medical University of Bialystok, Poland	67	63 features
50	Sugam Multispecialty Hospital, India	507 patients (35 to 90 years of age)	22 features
51	Germany	15510 observations	N/A
52	Italian Local Health Authority (ASL)	2722	06 features
53	ML repository	3000	13 features
54	USA	1000	15 echocardiographic variables
55	USA	340	15 echocardiographic variables
56	Faisalabad Institute of Cardiology and at the Allied Hospital in Faisalabad (Punjab, Pakistan)	299	13 features

[a]Dataset_ID is a reference number used for the identification of the dataset. [b]Total samples represent the total number of records in a dataset. [c]Feature represents the total number of features a dataset consist.

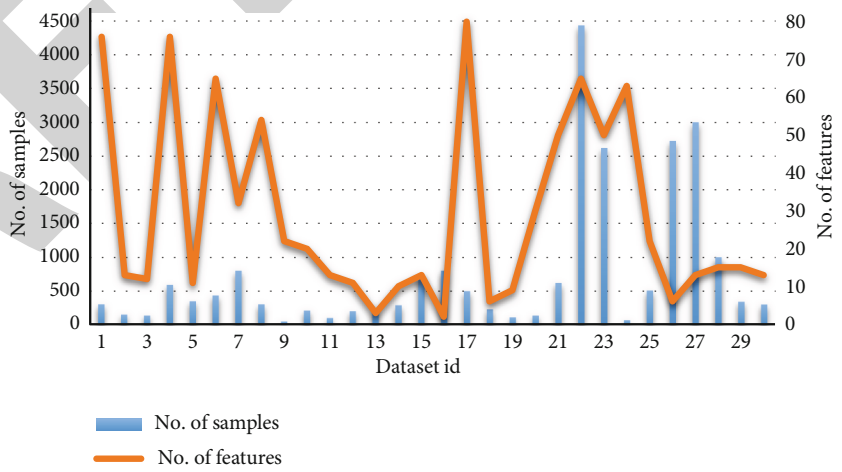

Figure 6: Demonstrates the number of samples and features in each dataset. *X*-axis of the graph represents the dataset ID while the *Y*-axis displays the number of samples and number of features. Blue bar in the figure depicts number of sample, and the orange line denotes number of features.

performance of the ML techniques was evaluated through k -fold crossvalidation test. The highest accuracy of classification was reported in this study (85%) with sensitivity of 89% and specificity of 81% through logistic regression.

An ML-based system was proposed by Guidi et al. [45] for the assistance of heart failure patient. Clinical decision support system (CDSS) has two major components for providing the assistance to heart patients. One of the component evaluates the severity of the HF while the other component predicts the HF. Additionally, CDSS also provides an interface for the comparison of various patient's follow-ups. The core of the CDSS was developed based on ML techniques such as SVM, NN, RF, and fuzzy-genetic rules. A supervised database was populated for ML techniques. The number of patients in the database was 90 with 136 records. The proposed CDSS was tested through the K -fold crossvalidation scheme. The prediction performance was reported with respect to the ML models as NN: 84.73%, SVM: 85.2%, fuzzy-genetic: 85.9%, CART: 87.6%, random forest: 85.6%, and severity performance given as NN: 77.8%, SVM: 80.3%, fuzzy-genetic: 69.9%, CART: 81.8%, and random forest: 83.3%.

Pawlovsky [46] designed an ensemble model using distance for KNN (k nearest neighbor) method for the diagnosis of heart disease. The proposed model was implemented by using three distances and five-distance configuration. A weight is also added at the base of the average accuracy that was calculated through KNN. The dataset used in this study was Cleveland, UCI dataset, and an average accuracy reported through the proposed system was 85%. Yu and Lee [47] proposed a system for CHF recognition based on heart rate variability through bispectrality analysis and genetic algorithms. Bispectrality analysis and genetic algorithm were used for the feature selection while SVM employed was a classifier. The proposed system obtained the accuracy of 98.79%.

Wang et al. [48] proposed a deep ensemble model for the detection of CHF through short-term RR intervals and deep neural network. For the experiments, they selected five open-source databases, namely, BIDMC Congestive Heart Failure Database (BIDMC-CHF), MIT-BIH Normal Sinus Rhythm (NSR) database), Congestive Heart Failure RR Interval Database (CHF-RR), Normal Sinus Rhythm RR Interval database (NSR-RR), and Fantasia database (FD). To evaluate the proposed method, three RR segment length types ($N = 500$, 1000, and 2000) were used. Deep learning features were automatically extracted from the expert feature of RR intervals, a long/short-term memory-convolutional neural network-based. The proposed method achieved the accuracy of 99.85%, 99.41%, and 99.17% on $N = 500$, 1000, and 2000 length RRIs.

Methaila et al. [49] designed a heart disease prediction system based on data mining techniques. The proposed system used ML methods, i.e., decision tree, NB, and NN for the prediction of heart disease. An online dataset from the Cleveland Heart Disease database was utilized for the experiments. To reduce the feature dimension, apriori algorithm and frequent pattern mining using MAFIA were deployed. Significance weight calculation of the features was evaluated for better feature selection. Results from the proposed research suggest that decision tree outperformed the other ML techniques with accuracy of 99.62% while using 15 features.

Jan et al. [50] proposed an ensemble model based on multiple classifiers for better prediction accuracy of the heart disease. In this study, SVM, Naive Bayesian, linear regression, ANN, and random forest were combined to improve the prediction accuracy. An open source dataset from Cleveland and Hungarian CVD had been utilized for the experiments to evaluate the performance of the proposed model. The dataset had 76 features, but for the experiments, Jan et al. focused on 13 key features of the dataset that highly contributed to obtain the highest accuracy. K-fold crossvalidation (with $k = 10$) scheme was employed to validate the results of the proposed model. The proposed model obtained the accuracies according to classifiers as given, Naive Bayesian: 93.223%, ANN: 94.915%, SVM: 98.136%, and LR: 93.22%.

Pecchia et al. [61] developed a remote health monitoring system for the detection of heart failure. Data mining technique was employed with CART method and HRV for feature extraction. The proposed system achieved the accuracy of 96.39% and precision of 100.00%, respectively, for heart failure detection. In regards to severity assessment of HF, the achieved accuracy was 79.31%, and precision was 82.35%. A public dataset of Congestive Heart Failure RR Interval Database was utilized for the experiments. The total number of subjects in the dataset was 83 of which 54 were healthy and 29 were suffering from HF. Kurnar [62] proposed a method for heart disease detection using fuzzy resolution mechanism. The proposed method was based on the combination of ANN and fuzzy logic. The method is tested on an online open source dataset of heart disease from Cleveland. The proposed ANFIS model achieved the accuracy of 91.83%. All the experiments were done through MATLAB.

Khumar et al. [82] proposed an ML-based method for the diagnosis of CVD. Dataset used in their work was collected from UCI, Cleveland, for testing the performance of the proposed model. Data cleaning techniques were employed for eliminating noise from the data. The processed data was input to the ML method for classification. The result reported from the proposed method obtained an accuracy of 86%.

Panicacci et al. [63] evaluated ML algorithms for identification of the heart failure patient. The dataset used for this study was collected from the Agenzia Regionale Sanit'a (ARS) in Florence, Tuscany, Italy. Panicacci et al. obtained the highest accuracy of 99.75% by random forest trained with SMOTE28 set. Latha et al. [64] investigated the ensemble classification method for improving the accuracy of weak algorithms through combination of multiple classifiers. The proposed method used dataset from the Cleveland heart disease dataset. The ensemble classification method of Latha et al. obtained an accuracy of 85.48%. Zikos et al. [65] conducted a Bayes study for the dynamic effect of comorbidities on hospital care for CHF patients. For this study, medical claimed data from centers for medicare and medicaid service

(CMS) was collected. Bayesian scenario-based graphs and Bayes-networks were used to visualize the results.

Das et al. [5] developed a neural network ensemble model for effective diagnosis of heart disease. Their methodology used SAS base software 9.1.3 for heart disease detection. The neural network ensemble was the key element in their proposed method that developed new models from the posterior probabilities. The proposed model obtained the accuracy of 89.01% with 80.95% and 95.91% sensitivity and specificity, respectively. Mohan et al. [66] proposed a hybrid random forest with linear model (HRFLM) for CVD prediction. Their proposed model found the key features on which ML techniques provided improved accuracy for CVD. To test the effectiveness of the proposed model, an online open source dataset for Cleveland heart disease from UCI was collected. The accuracy achieved by HRFLM model was 88.7%.

A hybrid neural network system based on ANN and FNN was proposed by Kahramanli and Allahverdi [67]. To validate the performance of the proposed model, an online line dataset from the ML repository was collected. The UCI heart disease dataset was employed for performance evaluation. The proposed system obtained an accuracy of 86.8%. Maji and Arora [68] presented a hybrid method based on ANN and decision tree for improved prediction of the heart disease. The UCI dataset is used to evaluate the effectiveness of the proposed model with WEKA tool. Tenfold crossvalidation testing is used to report the accuracy, sensitivity, and specificity of the proposed system. The system achieved the accuracy, sensitivity, and specificity of 78.14%, 78%, and 22.9%, respectively.

Polat et al. [69] proposed an artificial immune recognition system (AIRS) for heart disease diagnosis. Their proposed system used fuzzy weighted preprocessing method for extracting new features from the features space. The new features were input to the AIRS for prediction of the heart disease. The proposed system achieved an accuracy of 96.28% on an open source dataset of heart disease from UCI ML repository. To evaluate the performance of the proposed system, 10 k-fold crossvalidation testing was done. A comparative study of neural networks with traditional methods of medical diagnosis was done by Ster and Dobnikar [70]. In this study, five types of datasets were utilized for diagnosis of three kinds of diseases which were CAD, breast cancer, hepatitis, diabetes, and heart disease. The results of the study were obtained on default parameters. The highest accuracy achieved for heart disease by LDA was 84.5% and 59.7% for CVD by SNB.

Chen et al. [71] developed a CHF detection method through deep learning with RR intervals. Features from the dataset were extracted through the use of autoencoder. Extracted features were then supplied to deep neural network. The proposed system obtained an accuracy of 72.41% with sensitivity and specificity of 48.78% and 85.72%, respectively. Rajliwall et al. [73] proposed an ML-based CVD prediction model. A scalable algorithm named as the neuron network was presented which attained accurate results on fuzzy data. To evaluate the performance of the proposed model, two open source datasets were collected for the experiments. The best accuracy of 98.5% was obtained by random forest. Samuel et al. [74] proposed a model based on the fuzzy analytic hierarchy process (Fuzzy_AHP) technique that computed the global weight of the features for their individual contribution. Higher global weight features were supplied to the ANN classifier for prediction of heart failure. Cleveland dataset on heart disease from the UCI online repository was utilized for evaluating the performance of the proposed model. The proposed model obtained an accuracy of 91.10%.

Venkatalakshmi and Shivsankar [75] developed a predictive model for the heart disease diagnosis. The proposed model was based on the Naive Bayes and decision tress. The dataset used for the experiments was heart disease dataset from UCI. Wake tool was utilized for the extraction of useful features from the dataset. The proposed model achieved an accuracy of 85.03% for Naive Bayes and 84.01% for decision tree. Maio et al. [76] developed a predictive model of hospital mortality for heart failure patients through improved random survival forest. A public dataset of MIMIC II clinical database which consisted of 8059 patients with 32 features was used for the experiments. The proposed system achieved the accuracy of 82.01%.

A computer-aided decision-making system based on hybrid neural network-genetic algorithm for heart disease detection was developed by Arabasadi et al. [34]. To evaluate the performance of the hybrid system, Z-Alizadeh Sani dataset was used for the experiments. 10-fold crossvalidation was used as performance measurement metric. The proposed system achieved an accuracy, sensitivity, and specificity of 93.85%, 97%, and 92%, respectively. A normalized technique was developed for the preprocessing of the data. A genetic algorithm along with particle swarm optimization was utilized for improving the performance. For performance evaluation of the proposed method, 10-fold crossvalidation was performed. A new optimization method N2Genetic optimizer was proposed in this study. Experimental results of the proposed method N2Genetic-nuSVM demonstrated that the proposed method achieved an accuracy of 93.08% and f1-score of 91.51%.

Laskshmi and Haritha [79] proposed a ML model using SVM and Naive Bayes. In this study, an online dataset from the Cleveland heart disease dataset was collected for the experiments purpose. The result of the proposed model was validated from the ROC chart, and reported accuracy was 84.87%. Javeed et al. [81] presented an intelligent learning system based on a random search algorithm and optimized random forest model for improved heart disease detection. For feature selection, random search algorithm was used by the proposed diagnostic system while the grid search algorithm was used for optimization. Experiments were performed using an online heart failure database, namely, Cleveland dataset. The proposed system used only 7 features for the detection of heart disease. The accuracy obtained by the newly proposed system was 93.33%. Figure 7 presented the various ML models based on clinical feature-based data modality.

3.2. ML-Based HF Diagnosis: Image Modality. Apart from the automated diagnostic systems based on clinical features,

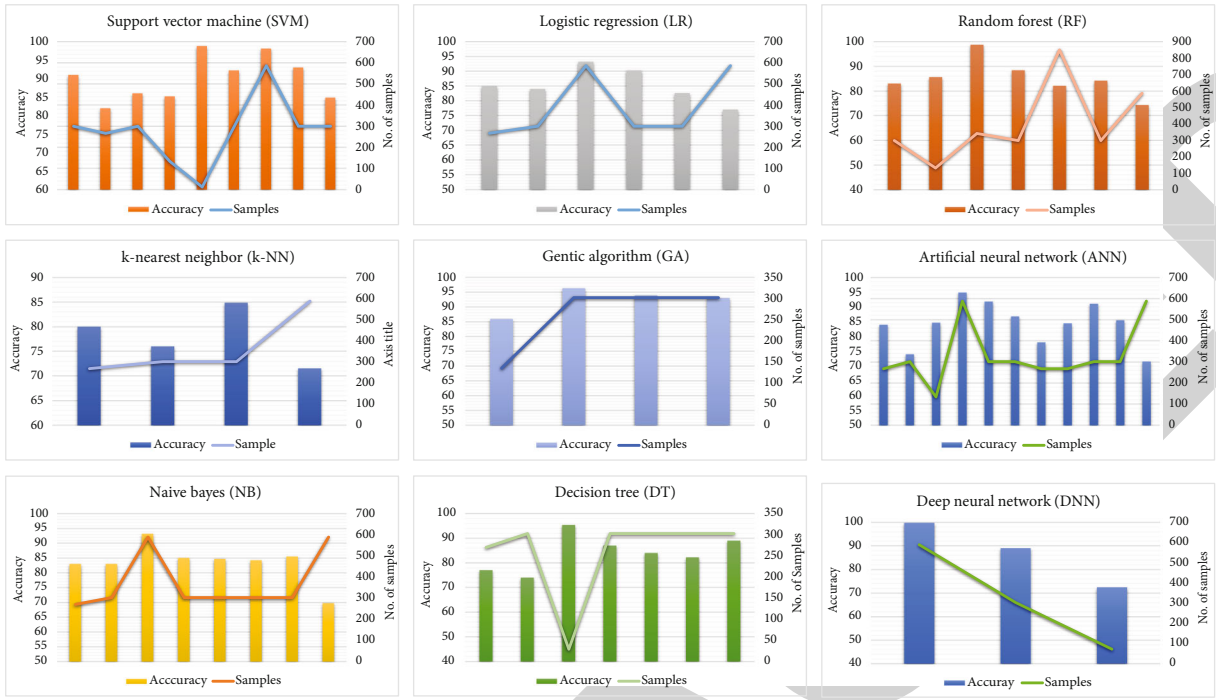

Figure 7: Performance of clinical feature-based data modality based on ML models is depicts from this figure. The performance of each ML model is measured in term of accuracy along with number of samples in the dataset.

many researchers also exploited the use of imaging data modality for the development of automated methods for heart disease detection. For example, Nirsch et al., [83] proposed a deep learning classifier for the identification of heart failure patients based on whole slide images of H&E tissue. The gold-standard for the diagnosis of heart failure is an end myocardial biopsy (EMB) when the cause of the heart failure is not identifiable. The proposed method used the CNN for the detection of heart failure from H&E stained whole-slide images from a dataset collected from the university of Pennsylvania with 209 patients. To evaluate the performance of the proposed model, a 3 k-fold crossvalidation method was deployed, and the reported accuracy with sensitivity and specificity of the proposed method was 97.4%, 99%, and 94%, respectively.

Cetin et al. [84] developed a radiomic approach of computer-aided diagnosis through cardiac cine-MRI. To reduce the feature dimensionality, sequential forward feature selection (SFFS) algorithm was selected, while for the classification purpose, SVM classifier was used in the proposed model. To evaluate the performance of the proposed model, a dataset of 100 patients was collected from the university of the Hospital of Dijon (France), and crossvalidation metric was used for performance evaluation. Bai et al. [85] proposed a method for myocardial patient classification through shape and motion features. The proposed method used principal component analysis (PCA) for features selection of the shape features, whereas motion features helped to identify the wall motion and thickness of the wall. The performance of the proposed model was evaluated on the dataset of STACOM 2015 challenge. SVM was used for the classification which achieved a maximum accuracy of 97.5%.

Qazi et al. [86] proposed a spare linear classifier for the automated detection of heart abnormality. The proposed model was developed from linear fisher's discriminant (LFD). The dataset used in this study was collected from the St. Francis Heart Hospital in Roslyn, New York. This dataset consists of a total 200 subjects amongst which 141 cases were used for the training purpose, while 59 cases were marked for testing. The performance of the proposed model was valuated with other ML methods such as SVM, RVM, and LED. The accuracy achieved by the proposed model was 89.6%, which outperformed the other ML methods. Sanj and Kukar [87] studied the image processing and ML method for medical imaging. The proposed approach suggested that significant improvement could be achieved in automated diagnostic system by improving the posttest diagnostic probabilities, using multiresolution image parameterization and feature subset selection in conjunction with ML approaches. The proposed approached achieved an accuracy of 81.3% with PCA on ArTex/Ares parameters.

Arsanjani et al. [88] proposed a method for earlier prediction of CVD through image features derived from SPECT (MPS) by a ML approach. For automatic feature selection, boosted ensemble ML algorithm (LogitBoost) was utilized for the prediction revascularization. To validate the effectiveness of the proposed model, tenfold crossvalidation scheme was adopted. The proposed model achieved an accuracy of 81% and was also tested through receiver operator characteristics (ROC) area under the curve. Udovychenko et al. [89] proposed a binary classification method for heart failure detection based on myocardial current density distribution maps. In this proposed method, KNN was utilized for the classification, while for performance validation of the

proposed method, Matthews correlation coefficient (MCC) performance evaluation metric was selected. The proposed method reported an accuracy in the range of 80-88% with 70-95% sensitivity, 78-95% specificity, and 77-93% precision, respectively.

Berikol et al. [93] proposed a method for the diagnosis of the acute coronary syndrome through SVM. Laboratory tests and ECG data were used for the experiment. Data was collected and proved by the Mersin University Research and Training Hospital Ethics Committee for this study. The dataset consists of 228 patients image records. The proposed system based on SVM classifier obtained the accuracy, sensitivity, and specificity of 99.13%, 98.22%, and 100, respectively. Leader et al. [94] developed an approach for automatic characterization of plaque composition in carotid ultrasound using convolutional neural network. CNN was used to extract information from the medical images that helped in the identification of different plaque constituents. For this study, 90000 patches extracted from the dataset of images were obtained from the University Hospital Arnau de Vilanova, Lleida, Spain. To validate the performance of the proposed model, $k-$-fold crossvalidation scheme was adopted. The proposed approach obtained the accuracy of 90%.

Sundaresan et al. [95] proposed an automated characterization approach for the fetal heart through ultrasound images based on a fully convolutional neural network (FCN). FCN was trained on 10,000 random sample frames with 10 subjects and tested on 2178 frames with 2 subjects. ROC chart was used to validate the performance of the proposed approached. The classification error reported through the proposed model was 23.48%. Choi et al. [96] designed a model for early detection of heart failure from the onset by using recurrent neural network (RNN). The proposed model used gated recurrent units (GRUs) for the detection of relationship of time-stamped events. The dataset used for the experiments was collected from the Sutter Palo Alto Medical Foundation. The performance of the proposed model was evaluated against various ML models like SVM and KNN. The proposed model achieved the highest accuracy of 83.3% as compared to the other ML models SVM (74%) and KNN (73%).

Mariachi et al. [98] proposed a framework for the detection of fetal presentation and the heartbeat through linear ultrasound video. The proposed framework classified frames into a 2D slice of the video. A conditional random field model was deployed for the regularized classification scores through temporal relationship between video frames. The kernelized linear dynamic model identified that heartbeat was detected in the frame sequence. For experiment purpose, a dataset of 323 predefined free-hand video was taken. The proposed framework reported a classification accuracy of 93.1% for the detection of a heartbeat.

Kurgan et al. [99] proposed a knowledge discovery method for automated cardiac SPECT diagnosis. A dataset of 267 patients consisting of SPECT images with 3000 2D images was used. A user friendly algorithm was designed for automated diagnosis. The proposed approach achieved an accuracy of 83.96%. Allsion et al. [104] proposed a model for detecting extensive CAD through artificial neural network for the modeling of stress single-photon emission computed on tomographic imaging. The dataset consisting of 109 patients of stress single-photon emission was collected for the experiments. The proposed model reported a sensitivity of 92%. Curiale et al. [106] proposed a method for automated myocardial segmentation through deep learning network in cardiac MRI. To evaluate the performance of the proposed method, Dice's coefficient and a mean squared error scheme are utilized. The proposed method achieved an accuracy 90%.

Moreno et al. [109] proposed a model for cardiac disease prediction through regional multiscale motion representation. The dataset was collected from the MICCAI challenge, Sunnybrook Cardiac Data (SCD) for the experiments. The SCD consist of 45 cine-MRI images. For classification of the heart disease, random forest algorithm (RAF) was employed. The performance of the proposed model was evaluated through two performance measurement metrics which are F1 score and the number of true positive from the total sample space. The proposed model obtained the average accuracy of 77.83% and F1 scored accuracy of 76.92%. Gulsun et al. [110] proposed a method for coronary centerline extraction via optimized flow paths along CNN path pruning. The proposed method automatically extracted the blood vessel centerlines. CNN is used as a classifier in the proposed method for removing extraneous paths. The proposed method was evaluated against 106 clinically annotated coronary arteries data. The proposed method achieved a specificity and sensitivity of 90% and 97%, respectively. Betancur et al. proposed a method of prognostic value of combined clinical and myocardial perfusion imaging data through ML. The predictive value of combined clinical information and myocardial perfusion single-photon emission was computed on tomography (SPECT) imaging (MPI) data based on ML for predicting the major adverse cardiac events. For the experiments, a total of 2619 patients' data were collected. The performance of the proposed model was evaluated through 10 k-fold crossvalidation. The accuracy achieved by the proposed model was 81%.

Wolterink et al. proposed an automatic coronary calcium scoring in cardiac CT angiography through convolutional neural networks. The proposed method presented a pattern recognition method that helped to identify coronary artery calcium (CAC) in coronary computed tomography angiography (CCTA). The dataset consists of 50 patients which was used for the experiments based on five cardiovascular risk categories. CNN was deployed for the identification of the coronary artery calcium (CAC), and an accuracy of 95% was achieved by the method. Figure 8 presented the performance various ML techniques based on image data modality.

3.3. ML-Based HF Diagnosis: ECG Modality. Similar to the clinical features and imaging modalities, numerous researchers also developed diagnostic systems based on ECG data modality for the detection of heart disease. For example, Zhao et al. [118] studied the simultaneous analysis of heart rate variability (HRV) and pulse transit time

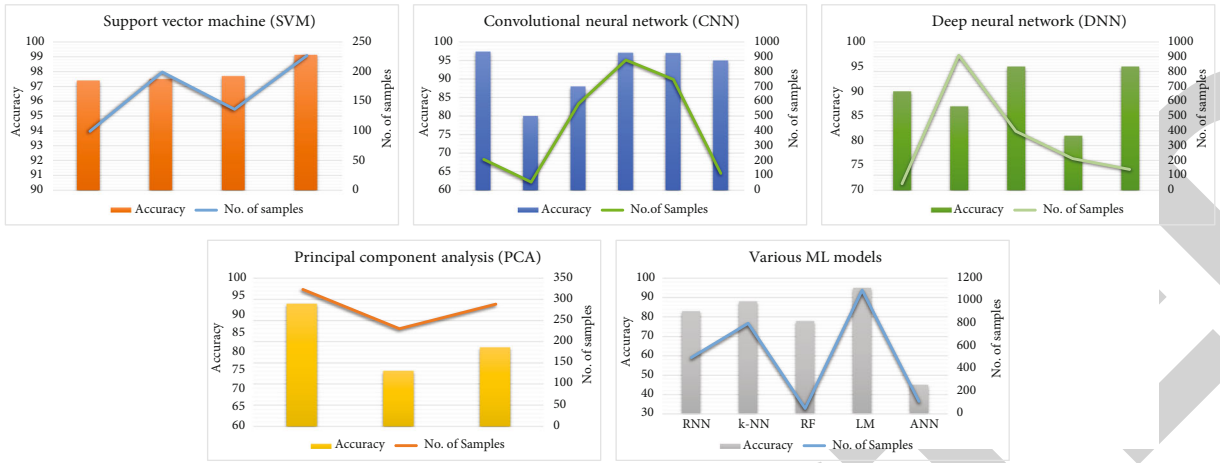

Figure 8: Performance of ML models based on image modality is depicted in this figure. The performance of each ML model is measured in term of accuracy along with number of samples in the dataset.

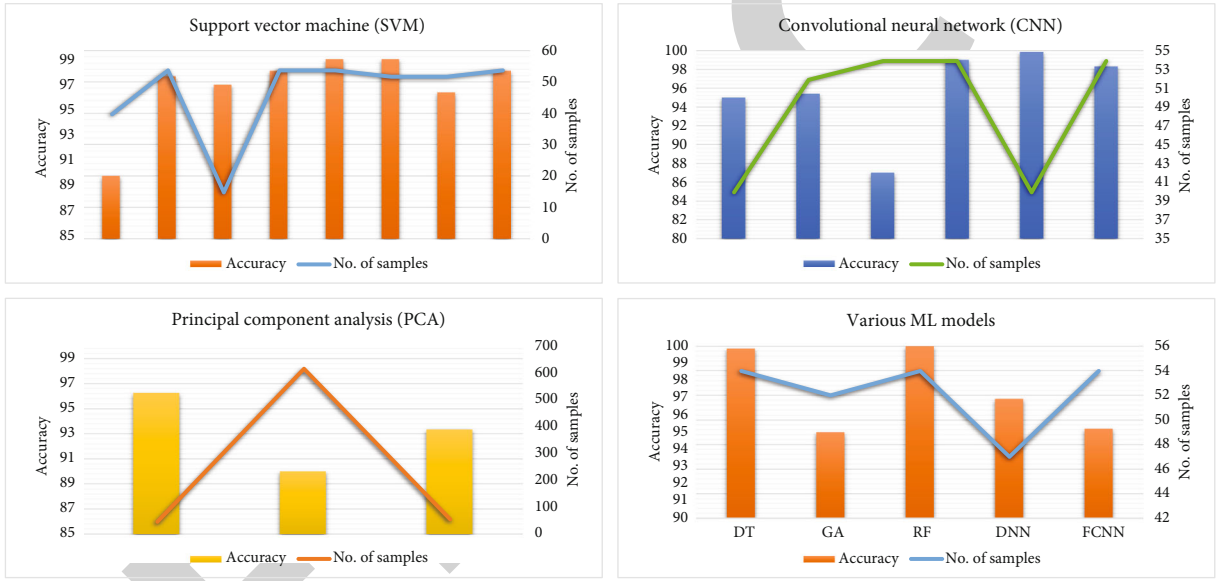

Figure 9: Performance of ECG modality-based ML models is depicted in this figure. The performance of each ML model is measured in term of accuracy along with number of samples in the dataset.

variability (PTTV) on healthy subjects and heart patients with the purpose of examining the improvement of HRV-based HF detection by using PTTV. For this objective, a data of 40 subjects through standard limb lead-II electrocardiogram (ECG) and radial artery pressure waveforms (RAPW) was collected. Moreover, SVM was deployed for the classification purpose along with probabilities generated from the distance distribution matrix- (DDM-) based CNN. The study demonstrated the accuracy, sensitivity, and specificity of 90%, 93%, and 88%, respectively. Sudarshan et al. [119] proposed a novel method for automated diagnosis of CHF based on dual tree complex wavelet transform and statistical features extraction from ECG signals. Dual tree complex wavelet transform (DTCWT) was performed on ECG segments for 2 seconds to obtain the six level coefficients. Features from the DTCWT were extracted through rank implementation using Bhattacharyya, entropy, minimum redundancy maximum relevance (mRMR), receiver-operating characteristics (ROC), Wilcoxon, t-test, and relief methods. For classification, ranked features were tested through K-nearest neighbor (KNN) and decision tress (DT). The proposed method reported the accuracy, specificity, and sensitivity of 99.86%, 99.94%, and 99.78%, respectively.

Acharya et al. [120] proposed a model that automatically detected the CAD using various durations of ECG segments with CNN. For this study, a dataset of fantasia was collected from the Physionet database to evaluate the performance of the proposed model. ECG signal (lead II) from 40 healthy subjects (20 males, 20 females) and 7 CAD patients (1 male and 6 females) data was collected. The proposed method reported the accuracy, specificity, and sensitivity of 99.86%,

Table 2: Summary of state-of-the-art research articles.

P_ID	Author	Technique	Data	Feature selection	Data sampling	Conclusion
PI_106	Ricciardi et al.,(2020) [51]	Logistic regression + tree-based ML	AGES-I dataset + AGES-II dataset	Nonlinear trimodal regression analysis (NTRA) + RF	k-fold crossvalidation $k = 12$	CVD (AUC: 91.4%) CHD (AUC: 93.6%) CHF (AUC: 99.4%)
PI_107	Butun et.al. (2020) [52]	Capsule networks (DNN)	Physionet database	Layer of CNN	Crossvalidation, 5-fold	Accuracy: 99.44%
PI_108	Ramachandran et al., (2020) [53]	Softmax discriminant classifier (SDC) and Gaussian mixture model classifier (GMM)	IEEE TMBE pulse oximeter dataset	Singular value decomposition (SVD)	F-measure	Accuracy: 97.88%
PI_109	Ghiasi et al. (2020) [54]	Decision tree	Z-Alizadeh Sani CAD dataset	Classification and regression tree (CART)	Crossvalidation,10-fold	Accuracy: 100%
PI_110	Joloudari et al. (2020) [55]	RT + SVM + C5.0	Z-Alizadeh Sani dataset	Random trees	Crossvalidation, 10-fold	Accuracy: 91.47%
PI_111	Ali et al. (2019) [42]	L_1-regularized-linear-SVM stacked with nonlinear SVM	Cleveland (UCI), heart disease dataset	L_1-regularized-linear-SVM	Matthews relation coefficient (MCC)	Accuracy: 92.22%
PI_112	Ali et al.,(2020) [43]	Mutual information based feature selection and deep neural network	Cleveland (UCI), heart disease dataset	Mutual information	Matthews relation coefficient (MCC)	Accuracy: 93.33%
PI_113	Gjoreski et al. (2020) [56]	Fully connected neural network (FCNN)	947 subjects	openSMILE feature extraction tool	Crossvalidation 10-fold	Accuracy: 93.2%
PI_114	Hussain et al. (2020) [57]	DT + SVM + KNN	Physionet databases	Multimodal features	Crossvalidation 10-fold	Accuracy: 97% (SVM)
PI_115	Aouabed et al. (2019) [58]	Nested ensemble (NE) model	Cleveland (UCI), heart disease dataset	GA	Crossvalidation 10-fold	Accuracy: 98.34%
PI_116	Liu et al. (2020) [59]	Multiscale convolutional neural networks (CNN)	1000 OCT images	Layers of CNN	Matthews relation coefficient (MCC)	Accuracy: 94.12%

99.94%, and 99.78%, respectively. Chen et al. [121] proposed an early predictor of heart problems by using predictive analysis of ECG signals. The proposed method was based on a two-step predictive framework for ECG signal processing. A global classifier factor was employed to compare the abnormalities against a universal reference model. The proposed model obtained a classification accuracy of 96.6%.

Shen et al. [122] analyzed the ECG data for the risk prediction of CVD. ML techniques were employed for the improved risk evaluation of CVD through ECG. Their work investigated the detection of heart abnormality by using 3 one-class classification, predicting probabilities of normality, ischemia, hypertrophy, and arrhythmia through multiclass approach. One-class approach obtained the accuracy of 75.6% and an area-under-curve (AUC) of 83%. With a four-class approach, a classifier accuracy of 75.1% was achieved. Acharya et al. [123] designed an automated characterization of arrhythmias through nonlinear feature from tachycardia ECG beats. For classification, KNN and decision tree (DT) were employed. Open source datasets from MIT-BIH A-Fib Database, MIT-BIR arrhythmia database, and Creighton University VT Database were collected for acquiring the ECG signals. The proposed model achieved an accuracy of 96.3% with specificity and sensitivity of 84.1% and 99.3%, respectively. Mathews et al. [124] proposed a deep learning-based method for ventricular and superventricular heartbeat detection by using single-lead ECG classification. The proposed method was evaluated with data collected from the MIT-BIH database. Restricted Boltzmann machine (RBM) and deep belief network (DBN) were utilized to obtain an average identification accuracy of 93.63% for ventricular ectopic beat and supraventricular ectopic beats (95.57%) at a low sampling rate of 114 Hz.

Adam et al. [125] proposed an automated characterization of CVD through relative wavelet nonlinear feature extraction of ECG signals. A novel discrete wavelet transform (DWT) method along with nonlinear features was used for automated characterization of CVD. Relative wavelet from four nonlinear features such as fuzzy entropy, sample entropy, signal energy, and fractal dimension was extracted

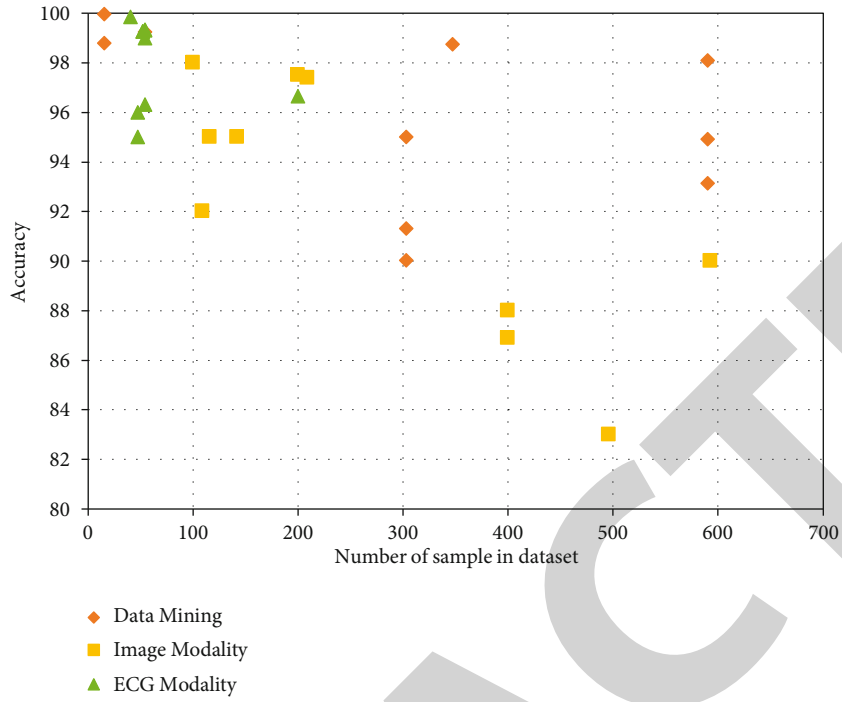

Figure 10: Performance analysis of ML techniques based on datasets for automated diagnosis of heart failure. This figure shows the highest accuracy achieved by the clinical feature-based data modality-based methods while average accuracy of ECG modality-based methods is higher. As the number of samples in dataset is increased, the performance of the clinical feature-based data modality reduces. The image modality has shown lower performance as compared to the other two modalities.

from the DWT coefficients. Features were then supplied to sequential forward selection (SFS) algorithm to rank relief method. The proposed methodology achieved an accuracy, sensitivity, and specificity of 99.27%, 99.74%, and 98.08%, respectively, with KNN classifier using 15 features ranked by relief. Tang et al. [126] developed a system for accurate identification of the CAD through stacked CNN and long short-term memory management network from ECG signals. CNN was utilized to extract features from the dataset of ECG samples. The proposed method based on a deep learning technique successfully detected CAD from the ECG signals with a diagnostic accuracy of 99.85%.

Sharma et al. [127] proposed a novel automated diagnostic system for myocardial infraction through ECG signals, based on the optimal biorthogonal filter bank for classification. Physikalisch-Technische Bundesanstalt database was used to get the raw ECG signals. An optimal biorthogonal filter bank (FB) was employed for the ECG signal analysis. The ECG signal was decomposed into six sub bands (SBs) through a newly developed wavelet FB. For features extraction, fuzzy entropy, renyi entropy, and signal-fractal-dimension (SFD) were used to compute the six SBs. KNN was used for the classification problem based on the features obtained through SBs. The proposed system obtained an accuracy of 99.62% for raw data and 99.74% for clean data.

Pucer et al. [128] proposed a topological method for delineation and arrhythmic beat detection from unprocessed long-term ECG signals. The proposed approach was based on the subject, specific adaptation of the one-dimensional discrete Morse theory (ADMT). The ADMT technique was used for noise removal and detection of the characteristic waves of the subject ECG beats. The waves were labeled with the help of ADMT technique. A decision tree algorithm was used for classification based on the input labeled beats. The proposed system used MIT-BH dataset for the performance evaluation and a classification accuracy of 92.73%, sensitivity, and specificity of 73.35% and 96.70%, respectively, were reported. Huang et al. [129] proposed a vector cardiogram-based classification system for the myocardial infarction detection. For the experiments, an open source VCG dataset of PTB database from the Physionet was collected. The dataset consists of 448 VCG recording (80 healthy controls (HCs) and 369 MIs). For the features, selection FFS and BFS were employed. The proposed method used four classifiers (MLC, k-NN, GLM, and SVM) for the classification. The proposed system obtained an overall accuracy of 96.96% with 99.89% sensitivity and 92.51% specificity. Zhou et al. [130] designed a model for premature ventricular contraction detection from ambulatory ECG using recurrent neural networks (RNN). The proposed model tested with MIT-BIH arrhythmia database and the accuracy reported in range of 96%-99%.

Sudarshan et al. [119] proposed a method for an automated diagnosis of CHF based on dual tree complex wavelet transform. From experiments, the coefficients were obtained through DTCWT implementation on ECG segments of 2 second duration to six levels. The statistical features were extracted and ranked by using Wilcoxon, t-test, relief methods, entropy, minimum redundancy maximum relevance (mRMR), receiver-operating characteristics (ROC),

Table 3: Summary of clinical features-based data modality articles.

P_ID	Author	Technique	Data	Feature selection	Data-sampling	Conclusion
PI_01	Verma et al. (2016) [40]	FURIA + MLR+ clustering + MLP	Cleveland heart disease dataset, IGMC data	CFS + PSO	*k*-fold crossvalidation k =10	Accuracy: 90.28% Accuracy: 88.4%
PI_02	Shah et al. (2017) [41]	Radial basis function (RBF) kernel-based SVM	Cleveland heart disease dataset, 303 instances	PPCA+PA	*k*-fold crossvalidation *k* =10	Accuracy: 91.30% Sensitivity: 100%
PI_03	Dwivedi (2018) [44]	LR + KNN + ANN + NB + classification tree + vector machines (SVM)	StatLog heart disease dataset	N/A	*k*-fold crossvalidation k =10	Accuracy: 85% Sensitivity: 81% Specificity: 89%
PI_04	Haq et al. (2018) [60]	Logistic regression (LR) + KNN + ANN + NB + DT + SVM	Cleveland heart disease dataset, 303 instances	Relief + mRMR + LASSO	*k*-fold crossvalidation *k* =10	Accuracy: 89% Sensitivity: 96% Specificity: 98%
PI_05	Guidi et al. (2014) [45]	NN + SVM + fuzzy-genetic + regression tree + random forest	Cardiology Department at the St. Maria Nuova Hospital in Florence, Italy Records, 90 patients	N/A	*k*-fold crossvalidation *k* =10	Prediction accuracy: NN: 84.73%, SVM: 85.2%, FG: 85.9%, CART: 87.6%, RF: 85.6%
PI_06	Pawlovsky (2018) [46]	An ensemble based on distances for a kNN (*k* nearest neighbor)	Cleveland heart disease dataset, 303 instances	Distances(Mahalanobis) + voting scheme using weights	*k*-fold crossvalidation *k* =10	Accuracy: 84.83%
PI_07	Yu and Lee (2012) [47]	SVM+ bispectral analysis	CHF database (chf2db), Physionet database (nsr2db)	Bispectrum-related features + GA	*K*-fold crossvalidation *k* =10	Accuracy: 98.79%
PI_08	Wang et al. (2019) [48]	DNN + ensemble learning method	BIDMC-CHF, NSR-RR	Time, frequency domain, nonlinear features	Blindfold validation	Accuracy: 99.96%
PI_09	Methaila et al. (2014) [49]	NN + NB + DT + apriori (algorithm + MAFIA algorithm)	Cleveland heart disease dataset, 303 instances	Significance weightage calculation	Crossvalidation	Accuracy: 99.62% (DT)
PI_10	jan et al. (2018) [50]	Ensemble model + NB + ANN + weight+ random forest + SVM	Cleveland heart disease Hungarian dataset, 590 instances	N/A	*K*-fold crossvalidation (*k* = 10)	NB: 93.22%accuracy ANN: 94.91%, accuracy SVM: 98.13%, accuracy LR: 93.22%, accuracy
PI_11	ali et al.(2019) [42]	Optimized stacked support vector machines	Cleveland heart disease dataset, 303 instances	SVM with kernels including linear + RBF.	Matthews correlation coefficient (MCC)	Accuracy: 92.22%
PI_12	Pecchia et al. (2010) [61]	CART	CHF RR interval database	Short-term HRV analysis	MCC + ROC	Accuracy: 96.39%,
PI_13	Kurnar (2012) [62]	ANN + fuzzy logic		Fuzzy resolution	Matthews correlation	Accuracy: 91.83%

Table 3: Continued.

P_ID	Author	Technique	Data	Feature selection	Data-sampling	Conclusion
			Cleveland heart disease dataset, 303 instances		coefficient (MCC)	
PI_14	Kurnar (2012) [62]	LR + RF + NB + GB + SVM	Cleveland, Hungarian, Switzerland	Data cleaning	Confusion matrix	Accuracy: 86%
PI_15	Panicacci et al. (2019) [63]	RF+ MACRO +SMOTE28 S	mARSupio database, Italy. 14616 subjects, 347 patient	N/A	F1-score, F2-score	Accuracy: 98.74%
PI_16	Beulah et al. (2019) [64]	Majority vote with NB, BN, RF, and MP	Cleveland heart disease dataset, 303 instances	Bagging, MV, stacking, boosting	F1-score, F2-score	Accuracy: 85.48%
PI_17	Zikos et al. (2019) [65]	Conditional probability +Bayesian	Medicare and Medicaid services CMS, 564,875 records	Clinical Classification Software (CSS)	N/A	Mortality rate: 2.61%
PI_18	Daset et al. (2009) [5]	Neural networks ensembles	Cleveland heart disease dataset, 303 instances	SAS base software 9.1.3 for diagnosing	MCC + ROC	Accuracy: 89.01%
PI_19	Mohan et al. (2019) [66]	Hybrid random forest with a linear model	Cleveland heart disease dataset, 303 instances	NB, GLM, LR, DL, DT, RF, GBT, and SVM	Confusion matrix	Accuracy: 88.4% Sensitivity: 90.8% Sensitivity: 82.6%
PI_20	Kahramanli and Allahverdi (2008) [67]	ANN + FNN	Cleveland heart disease dataset, 303 instances	N/A	*k*-fold crossvalidation	Accuracy: 86.8%
PI_21	Maji and Arora (2018) [68]	Decision tree +C4.5 + ANN	UCI, dataset with 13 attributes and 270 instances	Pruning	*k*-fold crossvalidation	Accuracy: 78.14%
PI_22	Polat et al. (2005) [69]	Fuzzy weighted + AI	Cleveland heart disease dataset, 303 instances	Fuzzy weighted preprocessing	*k*-fold crossvalidation	Accuracy: 96.30%
PI_23	Ster and Dobnikar (1996) [70]	Neural networks	CAD:263 subjects, UCI: 297	N/A	*k*-fold crossvalidation.	HD accuracy: 84.5% CAD accuracy: 59.7%
PI_24	Chen et al. (2017) [71]	Deep learning with RR intervals	72 healthy persons and 44 CHF patients	Autoencoder	*k*-fold crossvalidation	Accuracy: 72.41
PI_25	Purushottam and Sharma (2015) [72]	Decision trees	Cleveland heart disease dataset, 303 instances	C4.5	Confusion matrix	Accuracy: 87%
PI_26	Rajliwall et al. (2018) [73]	ML-based models for cardiovascular risk prediction	NHANES dataset + Framingham heart study dataset	C4.5	Fivefold crossvalidation	Accuracy (RF): 98.5%
PI_27	Samuel et al. (2017) [74]	ANN and Fuzzy_AHP	Cleveland heart disease dataset, 303 instances	Fuzzy_AHP	ROC	Accuracy: 91.10%
PI_28	Venkatalakshmi and Shivsankar (2014) [75]	Decision tree + naive Bayes (NB)	Cleveland heart disease dataset, 303 instances	Weka tool	Confusion matrix	NB: 85.03%accuracy
DT: 84.01%accuracy						

Table 3: Continued.

P_ID	Author	Technique	Data	Feature selection	Data-sampling	Conclusion
PI_29	Maio et al. (2017) [76]	Random survival forest	MIMIC II clinical database, 8059	N/A	OOB, C-statistics	Accuracy: 82.01%
PI_30	Arabasadi et al. (2017) [34]	Hybrid neural network-genetic algorithm	Z-Alizadeh Sani dataset	Genetic algorithm	10-fold crossvalidation	Accuracy: 93.85%
PI_31	Abdar et al. (2017) [77]	N2Genetic optimizer + N2Genetic-nuSVM	Z-Alizadeh Sani dataset	GA + PSO	Crossvalidation 10-fold + F1-score	Accuracy: 93.08% *F*-score: 91.51%
PI_32	Mezzatesta et.al. (2019) [78]	LR + KNN + CART + NB + SVM	HEMO clinical trial + IFC-CNR, Italy	Scaling techniques	Crossvalidation *K*-fold	LR: 80%, SVM: 80%
PI_33	Lakshmi et al. (2016) [79]	NB classifier + SVM	Cleveland heart dataset	Reprocessing	ROC	NB: 84.87%, accuracy SVM: 93.08%
PI_34	Bashir et al. (2019) [80]	DT + NB + LR + SVM	Cleveland heart disease dataset, 303 instances	MRMR	5-fold crossvalidation	Accuracy: 84.85%
PI_35	javeed et al. (2019) [81]	RSA + ORFA	Cleveland heart dataset	Hybrid Feature Subset	MCC	Accuracy: 93.33%

and Bhattacharyya. For automated diagnosis of the CHF, ranked features were classified through decision tree and KNN. The proposed method obtained an accuracy of 99.86%, with sensitivity and specificity of 99.78% and 99.94%, respectively. Diker et al. [132] proposed a new technique for heart disease detection through ECG signal classification, genetic algorithm, and wavelet kernel extreme learning machine. For the experiment, they utilized the Physikalisch-Technische Bundesanstalt Diagnostic ECG Dataset (PTBDB) from the Physionet Database. The critical points QRS complex, PR, QT, and ST from ECG signals were extracted through discrete wavelet transform (DWT) methods. Then, extreme learning machine (ELM) techniques were implemented on the ECG signals to find out the coefficients that were used in the wavelet kernel extreme ML. The proposed method achieved an accuracy of 95% along with sensitivity and specificity of 100% and 80%, respectively.

Acharya et al. [133] proposed a deep neural network based method for automated detection of the myocardial infraction through ECG signals. The dataset for the experiments was collected from the Physikalisch-Technische Bundesanstalt Diagnostic ECG Database (PTBDB) from Physionet. The proposed method was implemented without features extraction or feature selection method. The average accuracy of the proposed method using ECG beats with noise and without noise was 93.53% and 95.22%, respectively. Yao et al. [134] proposed a method based on the attention-based time-incremental convolutional neural network (ATI-CNN) for multiclass arrhythmia detection. The proposed model had flexible input length and halved parameter amount that reduced computation in real-time processing by 90% as compared to the conventional CNN model. The ATN-CN model achieved an accuracy of 81.2%. Vafaie et al. [135] proposed a heart disease prediction model through ECG signal classification using genetic-fuzzy system. The proposed fuzzy classifier method achieved an accuracy of 93.34%. Furthermore, with the application of genetic algorithm, the accuracy was enhanced up to 98.67%. Sahoo et al. [136] proposed a method for the detection of QRS complex features through multiresolution wavelet transform for the classification of four types of ECG beats. Features were extracted through principal component analysis (PCA). NN and SVM were used for the classification. The proposed system achieved an accuracy of 96.67% for NN and 98.39% for SVM.

Dohare et al. [137] developed a system for myocardial infraction detection in 12-lead ECG through SVM. The average beat of ECG was determined through the 12-lead ECG by using four clinical features such as ST-T complex interval, QT interval, *P* duration, and QRS duration. The principal component analysis (PCA) was used in the proposed method for the reduction of feature dimension. The dataset used for the validation of the proposed method was collected from Physikalisch-Technische Bundesanstalt (PTB) database. SVM was employed for the classification. The proposed MI detection method achieved an accuracy with specificity and sensitivity of 98.33%, 100%, and 96.66%, respectively.

An artificial intelligent- (AI-) enabled electrocardiograph (ECG) based on CNN for the detection of electrocardiography signature of atrial fibrillation was proposed by Attia et al. [138]. The patients data was collected from the Mayco Clinic ECG laboratory consisting of 180922 patient records with 649931 normal subjects. The receiver operating characteristic (ROC) curve was used to validate the results of the proposed method. The proposed model obtained an accuracy, specificity, and sensitivity of 87%, 79%, and 79.5%, respectively. Melgare et al. [139] explored ML approaches for the detection of electrocardiography fragment activity.

Table 4: Summary of image modality based research articles.

P_ID	Author	Technique	Data	Feature selection	Data sampling	Conclusion
PI_36	Nirschl et al. (2018) [83]	CNN+ whole-slide images of H&E tissue	209 patients	WND-CHARM	*k*-fold crossvalidation	Accuracy: 97.4%
PI_37	Cetin et al. (2017) [84]	Radiomic approach + cardiac cine-MRI+ SVM	MICCAI 2017 challenge on automated cardiac diagnosis	Sequential forward feature selection (SFFS)	Crossvalidation	Accuracy: 98%
PI_38	Bai et al. (2016) [85]	SVM	STACOM 2015 dataset	ED + ES phases + PCA	*k*-fold crossvalidation	Accuracy: 97.5%
PI_39	Qazi et al. (2007) [86]	SLFD	200 cases	LFD	ROC + *k*-fold crossvalidation	Accuracy: 89.1%
PI_40	Sajn and Kukar (2011) [87]	Image processing + ML	288 patients	PCA	ROC + *k*-fold crossvalidation	Accuracy: 81.3%
PI_41	R.Arsanjani et al.,(2015) [88]	Myocardial perfusion SPECT + ML	Cedars-Sinai Medical Center	LogitBoost	ROC + *k*-fold crossvalidation	Accuracy: 81%
PI_42	Arsanjani et al. (2013) [89]	SPECT for detection of CVD	Cedars-Sinai Medical Center	LogitBoost	ROC + *k*-fold crossvalidation	Accuracy: 87.2%
UPI_43	Udovychenko et al. (2015) [90]	*k*-NN binary classification of heart failures	MCG data	Variance, kurtosis, and skewness	MMC	Accuracy: 80-88%
PI_44	Carneiro and Nascimento (2013) [91]	Multiple dynamic models and deep learning architectures	Hospital Fernando Fonseca dataset, 496 images	PCA	HMD, AV, MAD, AVP	d_HMD: 83%accuracy d_AV: 91%accuracy d_MAD: 94%accuracy d_AVP: 83%accuracy.
PI_45	Zheng et al. (2008) [92]	3-D cardiac CT volumes using marginal space learning	Siemens Somatom Sensation	Steerable features	*k*-fold crossvalidation	Mean error: 2.3%
PI_46	Berikol et al. (2016) [93]	SVM	Mersin University Research	N/A	*k*-fold crossvalidation	Accuracy: 99.13%
PI_47	Lekadir et al. (2016) [94]	Plaque CNN architecture	Arnau de Vilanova	Deep learning CNN	*k*-fold crossvalidation	Accuracy: 80%
PI_48	Sundaresan et al. (2017) [95]	Fully convolutional neural networks (FCN)	C.Ioannou	Rectified linear units (ReLUs)	ROC	Classification error rate: 23.48%
PI_49	Choi et al. (2016) [96]	Recurrent neural network	Sutter Palo Alto Medical Foundation	Gated recurrent unit GRU	*k*-fold crossvalidation $k=6$	Accuracy: 88.3%
PI_50	Toth et al. (2018) [97]	Convolutional neural networks	LIDC-IDRI public dataset	(ReLU)	Qualitatively + quantitatively	Error rate: 2.92%
PI_51	Maraci et al. (2017) [98]	Analysis of linear ultrasound videos to detect fetal presentation and heartbeat	Dataset of 323 predefined free-hand videos	PCA	*k*-fold crossvalidation $k=5$	Accuracy: 93.1%
PI_52	Kurgan et al. (2001) [99]	Automated cardic SPECT diagnosis	Database of features(DF)	CLIP algorithm	Qualitative and Quantitative test	Accuracy: 83.08%
PI_53	Moreno et al. (2019) [100]	Multiscale motion for cardiac disease prediction	SPECT images dataset	RF + CLIP algorithm	F1-score + *k*-fold crossvalidation	Accuracy: 51.06% F1-score: 37.8%.
PI_54	Liu et al. (2016) [101]	ML prediction for cardiovascular	NSTEACS	PCA + MCE	*k*-fold crossvalidation	Accuracy: 75% Accuracy:95%

Table 4: Continued.

P_ID	Author	Technique	Data	Feature selection	Data sampling	Conclusion
PI_55	Shin et al. (2016) [102]	Deep convolutional neural networks for computer-aided detection	ImageNet dataset for CAD	CNN features of AlexNet pretrained + GoogleNet-RI	k-fold crossvalidation $k = 5$	
PI_56	Hisham et al. (2011) [103]	Grid independent technique	10 patients	Grid the images	Linear correlation	Accuracy:80%
PI_57	Allison et al. (2005) [104]	ANN	LAD model	Crossvalidation	Accuracy: 92%	
PI_58	Welikala et al. (2017) [105]	Automated arteriole and venule classification using deep learning	UK Biobank	RGB and HSI color spaces	Crossvalidation	Accuracy: 86.97%
PI_59	Curiale et al. (2017) [106]	Deep learning network in cardiac MRI	Sunnybrook Cardiac Dataset (SCD)	RGB and HSI color spaces.	Dice's coefficient	Accuracy: 90%
PI_60	Lindahl et al. (20197) [107]	Interpretation of myocardial SPECT perfusion images using ANN	Sunnybrook Cardiac Dataset (SCD)	Two-dimensional Fourier trans form technique	ROC + k-fold crossvalidation $k = 2$	Sensitivity: 54.4% Specificity: 70.5%
PI_61	Bai et al. (2015) [108]	Statistical parametric mapping(SPM) + linear model	Hammersmith Hospitals	PCA	Dice overlap metric + mean surface distance	LV_cavity:0.950 ± 0.024 Myocardium: 0.824 ± 0.062 RVcavity: 0.909 ± 0.03
PI_62	Moreno et al. (2019) [109]	Regional multiscale motion representation for cardiac disease prediction	Sunnybrook Cardiac Data (SCD)	Random Forest algorithm (RaF)	No. true positive over total of samples + F1-score	Accuracy: 77.83% F1-score:76.92%
PI_63	Gulsun et al. (2016) [110]	Coronary centerline extraction + CNN	CTA datasets	CNN	Up-to-first-error evaluation	Sensitivity: 97% Specificity = 90%
PI_64	Narula et al. (2016) [111]	Automate morphological and functional assessments in 2D echocardiography	77 ATH+ 62 HCM patients	Information gain (IG) algorithm	K-fold crossvalidation	Sensitivity: 96% Specificity = 77%
PI_65	Carneiro et al. (2011) [112]	Deep learning architectures and derivative-based search methods	Cohn-Kanade dataset (CK+)	PCA	ROC + HMD, HDF, MAD, MSSD	d_AVP: 95%
PI_66	Xu et al. (2012) [113]	Transient ischemic dilation for coronary artery disease in quantitative analysis	Nuclear Medicine Department, Sacred Heart Medical Center, Eugene	Mibi-Mibi TID	Standard deviation (SD)	Sensitivity: 76%
PI_67	Betancur et al. (2017) [114]	ML	Sacred Heart Medical Center	k – fold crossvalidation	Quantitative imaging analysis	Accuracy: 81%
PI_68	Coenen et al. (2018) [115]	ML + coronary computed tomographic	351 patients	ROC	ML-based CT-FFR model	Accuracy: 73%
PI_69	Wolterink et al. (2015) [116]	CNN	116 CT patients	k – -fold crossvalidation	ML-based CT-FFR model	Accuracy: 95%
PI_70	Nakazato et al. (2010) [117]	Perfusion imaging for detection of CAD	142 patients	N/A	k – -fold crossvalidation	Accuracy: 95%

For this reason, four different datasets were utilized along with three additional databases. For the classification problem, SVM, decision tree (DT), and Gaussian Naive Bayes (NB) were used for deep analysis of the selected datasets. The best results obtained for the fragmented dataset were 94% sensitivity, 88% specificity, 89% positive predictive value, 93% negative predictive value, and 91% accuracy when using SVM with Gaussian kernel.

Feng et al. [140] proposed a model for myocardial infarction classification through CNN and Recurrent_NN. A raw data was processed with the proposed algorithm to extract heart beat segments. After feature extraction, CNN

Table 5: Summary of ECG modality based research articles.

P_ID	Author	Technique	Data	Feature selection	Data sampling	Conclusion
PI_71	Zhao et al. (2019) [118]	HRV + PTTV + SVM	40 heart failure patients	RR + PTT	*k*-fold crossvalidation	Accuracy: 90%
PI_72	Sudarshan, et al. (2017) [119]	DTCWT-based methodology	BIDMC + rhythm (NSR) + fantasia	ROC + *t*-test	*k*-fold crossvalidation	Accuracy: 99.86%
PI_73	Acharya et al. (2017) [120]	CNN + ECG signal	Physionet databases	Single CNN structure	*k*-fold crossvalidation	Accuracy: 95.1%
PI_74	Chen et al. (2019) [121]	Two-step predictive framework for ECG	MITDB + Physionet	Daubechies wavelet + PCA	*k*-fold crossvalidation	Accuracy: 96.26%
PI_75	Shen et al. (2016) [122]	Generative kernel density estimator	China Kadoorie biobank (CKB)	RR interval + P wave duration	*k*-fold crossvalidation	One-class: 75.6% Acc Four-class: 75.1% Acc
PI_76	Acharya et al. (2016) [123]	Automated diagnosis of serious arrhythmias	MIT-BIH A-fib + MIT-BIR arrhythmia	Approximate entropy	Confusion matrix	Accuracy: 96.3% %
PI_77	Mathews et al. (2018) [124]	Deep learning	MIT/Beth Israel Hospital (BIH)	Heartbeat interval features + RR intervals	MCC	Accuracy: 96.94% Sensitivity: 85.22%.
PI_78	Adam et al. (2018) [125]	DWT + nonlinear features	PTB Diagnostic ECG Database	SFS	10-fold crossvalidation	Accuracy: 99.27%
PI_79	Tan et al. (2018) [126]	Stacked convolutional + long short-term memory network	Physionet database	CNN	10-fold crossvalidation	Accuracy: 99.85%
PI_80	Sharma et al. (2018) [127]	Two-band optimal biorthogonal filter bank (FB)	Physikalisch-Technische ECG database	Fuzzy entropy + signal-fractal-dimension+ Renyi entropy	10-fold crossvalidation	Noisy data:99.62%, Acc Clean data: 99.74%, Acc
PI_81	Puceret et.al. (2018) [128]	Topological approach	MIT-BIH database	ADMT	10-fold crossvalidation	Accuracy: 92.73%
PI_82	Huang et.al. (2011) [129]	Vector cardiogram-based classification	PTB database from Physionet	FFS + BFS	10-fold crossvalidation	Accuracy: 96.96% Sensitivity: 99.89% Specificity: 92.51%
PI_83	Zhou et.al. (2018) [130]	Premature ventricular contraction + RNN	MIT-BIH arrhythmia database	Long short-term memory (LSTM)	Detection indexes	Accuracy: 96-99% Sensitivity: 99-100% Specificity: 94-96%
PI_84	U.Satija et al.,(2018) [131]	ECG signal quality assessment algorithms	MIT-BIH arrhythmia database	CEEMD + temporal features	10-fold crossvalidation	Accuracy: 98.80%
PI_85	Sudarshan et al. (2017) [119]	Dual tree complex wavelet transform	PhysioBank MIT-BIH NSR + fantasia + BIDMC CHF	Statistical features extracted from 2 seconds of ECG signals	10-fold crossvalidation	Accuracy: 99.86% Sensitivity: 99.78% Specificity: 99.94%

Table 5: Continued.

P_ID	Author	Technique	Data	Feature selection	Data sampling	Conclusion
PI_86	Diker et al. (2019) [132]	Genetic algorithm wavelet kernel	Physikalisch-Technische Bundesanstalt diagnostic ECG database (PTBDB)	Discrete wavelet transform (DWT)	10-fold crossvalidation	Accuracy: 95% Sensitivity: 100% Specificity: 80%
PI_87	Acharya et al. (2017) [133]	Deep CNN	PTBDB	N/A	10-fold crossvalidation	Accuracy: 95.22% Sensitivity: 95.49%
PI_88	Yao et al. (2020) [134]	Attention-based time-incremental convolutional neural network (ATI-CNN)	1st China Physiological Signal Challenge	CNN-LSTM, 1st layer	Matthews correlation coefficient(MCC)	Accuracy: 81.2%
PI_89	Vafaie et al. (2014) [135]	Genetic-fuzzy + dynamical model of ECG signals	Physionet database	IF, THEN rules	N/A	Accuracy: 93.34%
PI_90	Sahoo et al. (2017) [136]	Multiresolution wavelet transform + ECG classification	MIT-BIH arrhythmia database	Principal component analysis (PCA)	10-fold crossvalidation	NN: 93.34% Acc SVM: 98.39% Acc
PI_91	Dohare et al. (2018) [137]	Myocardial infarction (MI) detection + SVM	Physikalisch-Technische Bundesanstalt (PTB)	Principal component analysis (PCA)	10-fold crossvalidation	Accuracy: 96.66% Sensitivity: 96.66% Specificity: 96.66%
PI_92	Attia et al. (2019) [138]	(AI)-enabled electrocardiograph (ECG) using a convolutional neural network	Mayo Clinic ECG laboratory	Non-linear ReLU	ROC	Accuracy: 87% Sensitivity: 79% Specificity: 79.5%
PI_93	Melgare et al. (2019) [139]	ML approach + electrocardiographic fragmented	Sfrag-DB + SWfrag-DB + FHCM-DB + HCM-DB	Statistics + PCA	Matthews correlation coefficient (MCC)	Accuracy: 90% Sensitivity: 94.1% Specificity: 87.5%
PI_94	Feng et al. (2019) [140]	CNN + RNN	PTB database	CNN and LSTM	10-fold crossvalidation	Accuracy: 95.4%
PI_95	Raka et.al. (2017) [141]	Time-based detection	SDDB + MIH-BIH database (NSRDB)	R-R interval duration	5-fold crossvalidation	Accuracy: 83.9%
PI_96	Kumar et al. (2017) [142]	ECG beat with flexible analytic wavelet transform (FAWT) + LS-SVM	ECG database from the Physiobank	Sample entropy (SEnt)	10-fold crossvalidation	Accuracy: 99.31%
PI_97	Yin et al. (2019) [143]	LS-SVM + multidomain electrocardiogram	MIT-BIH arrhythmia database	RR intevals, DWT, SampEn	10-fold crossvalidation	Accuracy: 99.31%
PI_98	Sahoo et al. (2017) [144]	SVM + NN	MITBIH arrhythmia database	Multiresolution wavelet transform	10-fold crossvalidation	Accuracy: 98.39%
PI_99	Masetic et al. (2016) [145]	Random forest	BIDMC CHF database (CHFDB) + NSRDB.	Autoregressive burg method	10-fold cross validation	Accuracy: 100%
PI_100	Isler and Kuntalp (2007) [146]	Classical HRV indices with wavelet entropy measures	MIT/BIH database	Genetic algorithm	Crossvalidation	Accuracy: 91.33% Sensitivity: 100%
PI_101	Bhurane et al. (2019) [147]	Frequency localized filter banks	NSRDB +BIDMC	Feature extraction	10-fold crossvalidation	Accuracy:99.66%
PI_102	Orhan (2013) [148]	Discretization method	NSRDB + BIDMC	EFiA-EWiT	10-fold crossvalidation	Accuracy: 99.33%
PI_103	Liao et al. (2015) [149]	SVM	CHFDB + MIT-BIH NSR database NSRDB	QRS wave	Ratio (ACC/SV)	Accuracy: 97.27%

Table 5: Continued.

P_ID	Author	Technique	Data	Feature selection	Data sampling	Conclusion
PI_104	Yıldırım et.al. (2018) [150]	Deep CNN	MIT-BIH arrhythmia database	PCANet algorithm	Confusion matrix of	Accuracy: 95.20%
PI_105	Yang et al. (2018) [151]	LS-SVM + PCA	MIT-BIH database	PCANet algorithm	10-fold crossvalidation	Accuracy: 97.94%

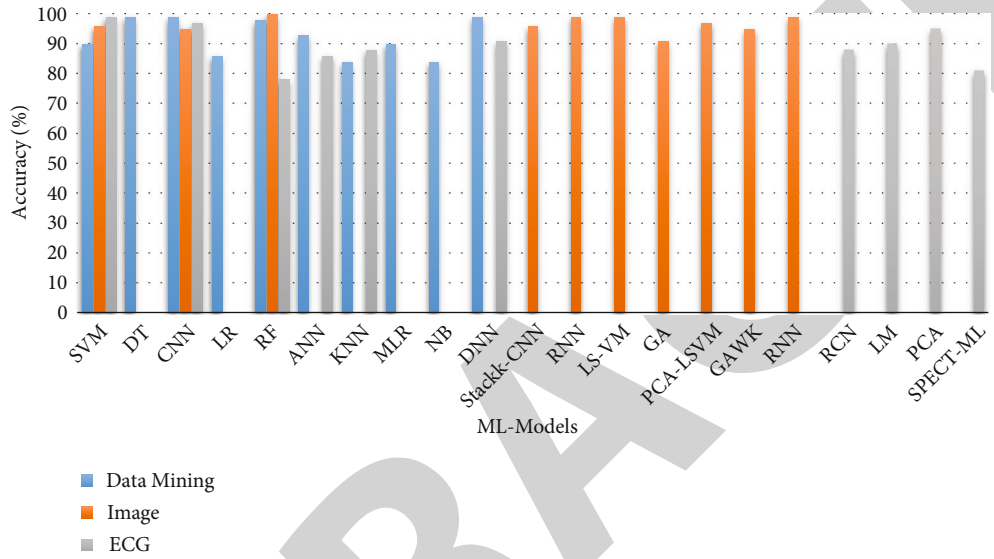

Figure 11: The performance of ML models with respect to modality can be seen in this figure. SVM, RF, and DNN models have obtained higher accuracy as compared to the other ML models. Modalities of the ML models can also be seen in this figure.

and LSTM were deployed for ECG classification. The dataset used for validating the proposed model was collected from Physikalisch-Technische Bundesanstalt (PTB). The proposed algorithm reported an accuracy, sensitivity, and specificity of 95.4%, 98.2%, and 86.5%, respectively. Kumar et al. [142] proposed a technique for automated diagnosis of myocardial infarction ECG signals based on the sample entropy in flexible analytic wavelet transform framework (FAWT). The FAWT model was implemented on every ECG beat which decomposed the ECG beats into the subband signal. Subband signals were used for computing the sample entropy (Sent) that was fed into the random forest, BRNN, and LS-SVM for classification. The highest accuracy of 99.31% was achieved through the LS-SVM.

Yin et al. [143] proposed a multidomain feature extraction method for arrhythmia classification. Dataset for the experiments was collected from the MIT-BIH arrhythmia database. 1-fold crossvalidation scheme was selected for performance evaluation of the proposed method and genetic algorithm used for the optimized selection of parameters. The average accuracy of 99.70% with sensitivity and specificity of 99.68% and 99.96%, respectively, was reported through the proposed method (SVM-RBF). Li and Zhou [152] proposed a method for ECG classification based on wavelet packet entropy and random forests. The dataset used in this study was collected from the MIT-BIH arrhythmia database. The proposed method used WPE + RR for feature extraction and random forest (RF) for classification and for which an accuracy of 94.61% was reported. Yang et al. [151] proposed a method for automatic recognition of arrhythmia using principal component analysis network and linear SVM. The principal component analysis network (PCANet) was used for the extraction of features from ECG signals while SVM was deployed for classification. For the experiment, MIT-BIH arrhythmia database was used to validate the effectiveness of the proposed model which achieved an accuracy of 97.94%. Figure 9 provide the overview of various ML techniques performance based on ECG modality.

4. State-of-the-Art Work

Ricciardi et al. [51] presented a tree-based ML method based on radiodensitometeric distribution for assessing the cardiovascular risks through mid-thigh CT image. The dataset was collected from AGES-I and AGES-II for the experimental purpose. The proposed method tested against the CHD, CVD, and CHF. The proposed method based on logistic regression and tree-based ML model achieved the accuracy for CHD (AUCROC: 0.936), CVD (AUCROC: 0.914), and CHF (AUCROC: 0.994). Butun et al. [52] developed a deep

capsule network for the detection of CAD using ECG signals. The capsule network was designed through deep learning-based methods. The proposed method was given as 1D-CADCapsNet. The dataset was obtained from Physionet databases for the experiments. The accuracy reported by the 1D-CADCapsNet was 99.44%.

Ramachandran et al. [53] proposed a computerized diagnostic system for CVD based on photoplethysmography signals. The proposed system extracted the features from photoplethysmography through singular value decomposition (SVD), statistical features, and wavelets while Softmax Discriminant Classifier (SDC) and Gaussian mixture model classifier (GMM) were used for classification. The newly proposed system obtained an accuracy of 97.88%. Dataset used for the experiments was obtained from IEEE TMBE pulse oximeter dataset to evaluate the performance of the proposed computerized diagnostic system. Ghiasi et al. [54] proposed a decision tree-based diagnosis of CAD model named as CART. The newly designed CART model obtained the accuracy of 100% on Z-Alizadeh Sani CAD dataset.

Gjoreski et al. [56] proposed a deep learning-based method for the detection of chronic heart failure using heart sound. The dataset used in this study for experiments consisted of recordings from 947 subjects from six publicly available datasets. The newly proposed system achieved an accuracy of 93.2%. Hussain et al. [57] proposed a novel CHF based on multimodal extracting features and ML approaches. The RR interval time series data was used for experiments that were obtained from the Physionet databases. The highest accuracy of 97% was achieved by SVM linear kernel. Aouabed et al. [58] developed an ensemble model for early detection of CAD. The ensemble model is based on four different kernel functions (linear, polynomial, radial basis, and sigmoid). To analyze the performance of the proposed model, an online dataset from UCI repository was obtained. Genetic algorithm was employed for feature extraction. The proposed model achieved an accuracy of 98.34%. Liu et al. [59] proposed a multiscale convolutional neural network for coronary artery fibrous plaque detection. The coronary OCT images were collected from Peking Union Medical College Hospital, China, for experiments purpose. The proposed method obtained an accuracy of 94.12%. Moreover, the summary of state-of-the-art proposed models is reported in Table 2.

5. Discussion

Herein, we scrutinized the top ten research articles from each modality based on accuracy and performance that were achieved on various datasets. Furthermore, a comparison of modality-based ML techniques is depicted in Figure 10, where modality-based ML models are ranked according to accuracy and number of samples used in the dataset. It can also be observed from Figure 10 that ML techniques based on ECG modality have better accuracy and performance as compared to clinical feature-based data modality. Furthermore, image modality has shown less accuracy in comparison to ECG and clinical feature-based data modality. Another factor that can be observed from Figure 10 is that clinical feature-based data modality and image modality-based ML techniques lose accuracy and performance when the number of samples or subjects were huge in the dataset, whereas ECG modality-based ML models performed well in case of huge or small number of samples in the datasets.

One of the key factor for an ML model to obtain the best performance is based on the nature of data that exists in the dataset. As we have observed, the three modalities used diverse datasets that means nature of data varies for each such as ECG signals, images, and medical reports data. Therefore, ECG modality-based ML models used signal data and obtained higher performance and accuracy as compared to other modalities for prediction and detection of the HF and CAD.

Feature selection/extraction is also an important part of ML-based models where we select the most appropriate feature from the feature space. The feature space is reduced by eliminating features from the feature space which helped to improve the performance and accuracy of ML models. Feature selection process differs from feature extraction in that, in the features selection process, only those features are selected from the feature vector that heavily contribute to achieving a better accuracy, while in the feature extraction process, new features are produced from the features space which increases the accuracy of the proposed ML models. Therefore, feature processing is an important part in ML models that not only does contribute to achieve higher accuracy but also reduces the model's computational cost. For example, in the ECG modality, features are extracted from the ECG signals through sampling of the signals. The most widely used methods for extracting features from the ECG signals are QR wave and R-R interval.

Performance evaluation of the ML model is another key factor of ML pipeline. Numerous types of performance metrics are utilized to measure the performance of ML models, e.g., F1 score, area under the curve (AUC), ROC, Matthews correlation coefficient (MCC), specificity, sensitivity, and accuracy [153]. Another important factor is validation methods. Different validation methods, namely, train-test holdout validation, k-fold crossvalidation, and leave-one-out (LOO) crossvalidation methods have been used by different researchers. The ML-based model for automated diagnosis of HF and CAD detection mostly used k-fold crossvalidation metric for the evaluation of the newly developed model. The modalities (Tables 3–5) also show that k-fold crossvalidation method has been widely used by the researchers, while the performance of ML models with respect to modality can be seen from Figure 11 where SVM, RF, and DNN models have obtained higher accuracy as compared to the other ML models.

5.1. Limitations in the Previously Developed Methods. ML algorithms are applied to various problems in different application domains. However, they suffer from some limitations which make them imperfect for every problem. In the area of clinical support systems, most ML methods for automated diagnosis of HF, CAD, and CHF belong to the supervised learning category. Since supervised learning has some limitations, automated diagnosis systems also suffer

from, if not all but some of these limitations. In this section, we address these limitations of ML-based methods

(i) Supervised ML models requisite training on the dataset; however, training on large amount of data is complex and time consuming task

(ii) ML models may suffer from the data overfit problem. As discussed above, *k*-fold crossvalidation method has been widely utilized by many researchers for evaluating the performance of their developed diagnostic system. However, it may result in overfitted or highly biased results due to data leakage

(iii) In recent years, deep learning technology has shown state-of-the-art performance on heart disease detection problem. However, the deep learning technology requires huge amount of data for model training which is a costly and difficult job

(iv) Time complexity is another issue in automated detection of heart disease based on ML approaches. ML model can predict only after they have been trained on the training data which requires processing time. Moreover, ML models have many parameters, which needs to be tuned manually in case of supervised learning. Therefore, a lot of time is required to fine tune the hyper parameters of the ML model for achieving better performance

(v) Another drawback in many previously proposed methods and reported results is the biased comparative study in many papers, for example, comparing results of two studies which have used different validation methods (holdout and crossvalidation) or different evaluation metrics. For an unbaised comparison, it is important to use same dataset with same validation scheme and evaluation metrics

5.2. Future Research Directions. Several ML models have been proposed for the prediction of CAD and HF in the past few years; however, there are some areas that still need to be explored by researchers and professionals. In this section, we have addressed the potential research areas and directions for further improvement in ML methods for CAD detection. Through this study, we conclude that there are three key factors that participate for efficient detection of the CAD and HF.

Firstly, data is very significant in case of ML-based automated detection of heart disease, especially, when deep learning models are brought into account. However, many of the publicly available datasets are small sized. Hence, future studies focus should be on collection of the large amount of datasets.

Secondly, as discussed above, *k*-fold crossvalidation-based model performance gives biased performance owing to data leakage. Hence, in future studies, in order to develop models that would show better generalization performance, an independent dataset should be used. After development of the model using crossvalidation, the developed model generalization capabilities should be blind tested on the independent dataset. Such type of generalized models would be of great help and could be deployed in hospitals for real time diagnosis.

Thirdly, ML is an emerging field; therefore, there are still open challenges for development of novel methods that will provide efficient performance.

Fourth, recently on many other disease detection problems, multimodal processing has provided reliable and efficient results. Hence, in future, researchers should exploit multimodal approaches for a better heart disease detection.

6. Conclusion

Unlike previous studies, in this study, we scrutinized various ML approaches for the development of automated diagnostic systems for heart disease detection based on different kinds of modalities (clinical features-based data, imaging, and ECG). Research articles were collected from various databases published between 1995 and 2021. Based on different data modalities, the previously proposed studies were critically analyzed and systematically organized. Moreover, in this study, we also pointed out the limitations and loop holes in the previously proposed methods for automated heart disease detection. Finally, to mitigate the problems present in previously developed methods and to provide better heart disease detection, some future directions were discussed for onward research in the domain of automated heart disease detection based on ML. We hope that this review will be helpful to those who intend to work in the domain of automated heart disease detection.

Data Availability

The data that support the findings of this study are available upon request from the first author.

Conflicts of Interest

The authors declare that they have no competing interests.

References

[1] M. Cotter, "A systems view of cardiovascular disease," 2019.

[2] A. P. Ambrosy, G. C. Fonarow, J. Butler et al., "The global health and economic burden of hospitalizations for heart failure: lessons learned from hospitalized heart failure registries," *Journal of the American College of Cardiology*, vol. 63, no. 12, pp. 1123–1133, 2014.

[3] A. L. Bui, T. B. Horwich, and G. C. Fonarow, "Epidemiology and risk profile of heart failure," *Nature Reviews Cardiology*, vol. 8, no. 1, pp. 30–41, 2011.

[4] E. Bathrellou, M. D. Kontogianni, E. Chrysanthopoulou et al., "Adherence to a dash-style diet and cardiovascular disease risk: the 10-year follow-up of the Attica study," *Nutrition and Health*, vol. 25, no. 3, pp. 225–230, 2019.

[5] R. Das, I. Turkoglu, and A. Sengur, "Effective diagnosis of heart disease through neural networks ensembles," *Expert Systems with Applications*, vol. 36, no. 4, pp. 7675–7680, 2009.

[6] "Heart anatomy kernel description," 2010, http://tanguay.info/learntracker/page/lectureNotesItems?idCode=heart.

[7] C. S. Dangare and S. S. Apte, "Improved study of heart disease prediction system using data mining classification techniques," *International Journal of Computer Applications*, vol. 47, no. 10, pp. 44–48, 2012.

[8] K. T. Spencer, B. J. Kimura, C. E. Korcarz, P. A. Pellikka, P. S. Rahko, and R. J. Siegel, "Focused cardiac ultrasound: recommendations from the american society of echocardiography," *Journal of the American Society of Echocardiography*, vol. 26, no. 6, pp. 567–581, 2013.

[9] D. Beymer and T. Syeda-Mahmood, "Cardiac disease recognition in echocardiograms using spatio-temporal statistical models," in *2008 30th Annual International Conference of the IEEE Engineering in Medicine and Biology Society*, pp. 4784–4788, Vancouver, BC, Canada, 2008.

[10] H. Wu, T. T. Huynh, and R. Souvenir, "Motion factorization for echocardiogram classification," in *2014 IEEE 11th International Symposium on Biomedical Imaging (ISBI)*, pp. 445–448, Beijing, China, 2014.

[11] K. Dickstein, A. Cohen-Solal, G. Filippatos et al., "Esc guidelines for the diagnosis and treatment of acute and chronic heart failure 2008: The task force for the diagnosis and treatment of acute and chronic heart failure 2008 of the european society of cardiology. developed in collaboration with the heart failure association of the esc (hfa) and endorsed by the european society of intensive care medicine (esicm)," *European Journal of Heart Failure*, vol. 10, pp. 933–989, 2008.

[12] W. S. Colucci, "Patient education: Heart failure (beyond the basics)," 2021.

[13] "AH Association," February 2014, https://www.heart.org/en/health-topics/arrhythmia.

[14] "lalpathlabs," 2017, https://www.lalpathlabs.com/blog/what-are-the-different-types-of-heart-diseases.

[15] L. Ali, S. U. Khan, M. Arshad, S. Ali, and M. Anwar, "A multi-model framework for evaluating type of speech samples having complementary information about parkinson's disease," in *2019 International Conference on Electrical, Communication, and Computer Engineering (ICECCE)*, pp. 1–5, Swat, Pakistan, 2019.

[16] L. Ali, C. Zhu, Z. Zhang, and Y. Liu, "Automated detection of parkinsons disease based on multiple types of sustained phonations using linear discriminant analysis and genetically optimized neural network," *IEEE Journal of Translational Engineering in Health and Medicine*, vol. 7, pp. 1–10, 2019.

[17] L. Ali, C. Zhu, M. Zhou, and Y. Liu, "Early diagnosis of Parkinson's disease from multiple voice recordings by simultaneous sample and feature selection," *Expert Systems with Applications*, vol. 137, pp. 22–28, 2019.

[18] L. Ali, Z. He, W. Cao, H. T. Rauf, Y. Imrana, and M. B. Bin Heyat, "Mmdd-ensemble: A multimodal data–driven ensemble approach for parkinson's disease detection," *Frontiers in Neuroscience*, vol. 15, 2021.

[19] L. Ali, C. Zhu, N. A. Golilarz, A. Javeed, M. Zhou, and Y. Liu, "Reliable Parkinson's disease detection by analyzing handwritten drawings: construction of an unbiased cascaded learning system based on feature selection and adaptive boosting Model," *IEEE Access*, vol. 7, pp. 116480–116489, 2019.

[20] W. Akbar, W. P. Wu, S. Saleem et al., "Development of hepatitis disease detection system by exploiting sparsity in linear support vector machine to improve strength of adaboost ensemble model," *Mobile Information Systems*, vol. 2020, Article ID 8870240, 9 pages, 2020.

[21] L. Ali, I. Wajahat, N. Amiri Golilarz, F. Keshtkar, and S. A. C. Bukhari, "Lda–ga–svm: improved hepatocellular carcinoma prediction through dimensionality reduction and genetically optimized support vector machine," *Neural Computing and Applications*, vol. 33, no. 7, pp. 2783–2792, 2021.

[22] T. Meraj, H. T. Rauf, S. Zahoor et al., "Lung nodules detection using semantic segmentation and classification with optimal features," *Neural Computing and Applications*, vol. 33, no. 17, pp. 10737–10750, 2021.

[23] F. S. Ahmad, L. Ali, Raza-Ul-Mustafa et al., "A hybrid machine learning framework to predict mortality in paralytic ileus patients using electronic health records (ehrs)," *Journal of Ambient Intelligence and Humanized Computing*, vol. 12, no. 3, pp. 3283–3293, 2021.

[24] F. S. Ahmed, L. Ali, B. A. Joseph, A. Ikram, R. Ul Mustafa, and S. A. C. Bukhari, "A statistically rigorous deep neural network approach to predict mortality in trauma patients admitted to the intensive care unit," *Journal of Trauma and Acute Care Surgery*, vol. 89, no. 4, pp. 736–742, 2020.

[25] Y. Imrana, Y. Xiang, L. Ali, and Z. Abdul-Rauf, "A bidirectional lstm deep learning approach for intrusion detection," *Expert Systems with Applications*, vol. 185, 2021.

[26] A. Mehbodniya, I. R. Khan, S. Chakraborty et al., "Data mining in employee healthcare detection using intelligence techniques for industry development," *Engineering*, vol. 2022, article 6462657, pp. 1–11, 2022.

[27] N. Amiri Golilarz, H. Gao, R. Kumar, L. Ali, Y. Fu, and C. Li, "Adaptive wavelet based mri brain image de-noising," *Frontiers in Neuroscience*, vol. 14, 2020.

[28] N. A. Golilarz, A. Addeh, H. Gao et al., "A new automatic method for control chart patterns recognition based on convnet and Harris hawks meta heuristic optimization Algorithm," *Access*, vol. 7, pp. 149398–149405, 2019.

[29] S. U. Khan, M. Rahim, and L. Ali, "Correction of array failure using grey wolf optimizer hybridized with an interior point algorithm," *Frontiers of Information Technology & Electronic Engineering*, vol. 19, no. 9, pp. 1191–1202, 2018.

[30] N. A. Golilarz, M. Mirmozaffari, T. A. Gashteroodkhani et al., "Optimized wavelet-based satellite image de-noising with multi-population differential evolution-assisted Harris hawks optimization Algorithm," *IEEE Access*, vol. 8, pp. 133076–133085, 2020.

[31] A. Rehman, A. Khan, M. A. Ali, M. U. Khan, S. U. Khan, and L. Ali, "Performance analysis of pca, sparse pca, kernel pca and incremental pca algorithms for heart failure prediction," in *2020 International Conference on Electrical, Communication, and Computer Engineering (ICECCE)*, pp. 1–5, Istanbul, Turkey, 2020.

[32] J. Nahar, T. Imam, K. S. Tickle, and Y.-P. P. Chen, "Computational intelligence for heart disease diagnosis: a medical knowledge driven approach," *Expert Systems with Applications*, vol. 40, no. 1, pp. 96–104, 2013.

[33] J. Nahar, T. Imam, K. S. Tickle, and Y.-P. P. Chen, "Association rule mining to detect factors which contribute to heart disease in males and females," *Expert Systems with Applications*, vol. 40, no. 4, pp. 1086–1093, 2013.

[34] Z. Arabasadi, R. Alizadehsani, M. Roshanzamir, H. Moosaei, and A. A. Yarifard, "Computer aided decision making for

heart disease detection using hybrid neural network-genetic algorithm," *Computer Methods and Programs in Biomedicine*, vol. 141, pp. 19–26, 2017.

[35] M. G. Tsipouras, T. P. Exarchos, D. I. Fotiadis et al., "Automated diagnosis of coronary artery disease based on data mining and fuzzy modeling," *IEEE Transactions on Information Technology in Biomedicine*, vol. 12, no. 4, pp. 447–458, 2008.

[36] A. K. Paul, P. C. Shill, M. R. I. Rabin, and K. Murase, "Adaptive weighted fuzzy rule-based system for the risk level assessment of heart disease," *Applied Intelligence*, vol. 48, no. 7, pp. 1739–1756, 2018.

[37] D. Pal, K. Mandana, S. Pal, D. Sarkar, and C. Chakraborty, "Fuzzy expert system approach for coronary artery disease screening using clinical parameters," *Knowledge-Based Systems*, vol. 36, pp. 162–174, 2012.

[38] J.-K. Kim, J.-S. Lee, D.-K. Park, Y.-S. Lim, Y.-H. Lee, and E.-Y. Jung, "Adaptive mining prediction model for content recommendation to coronary heart disease patients," *Cluster Computing*, vol. 17, no. 3, pp. 881–891, 2014.

[39] L. Ali, S. U. Khan, N. A. Golilarz et al., "A feature-driven decision support system for heart failure prediction based on statistical model and gaussian naive bayes," *Computational and Mathematical Methods in Medicine*, vol. 2019, Article ID 6314328, 8 pages, 2019.

[40] L. Verma, S. Srivastava, and P. Negi, "A hybrid data mining model to predict coronary artery disease cases using non-invasive clinical data," *Journal of Medical Systems*, vol. 40, no. 7, p. 178, 2016.

[41] S. M. S. Shah, S. Batool, I. Khan, M. U. Ashraf, S. H. Abbas, and S. A. Hussain, "Feature extraction through parallel probabilistic principal component analysis for heart disease diagnosis," *Physica A: Statistical Mechanics and its Applications*, vol. 482, pp. 796–807, 2017.

[42] L. Ali, A. Niamat, J. A. Khan et al., "An optimized stacked support vector machines based expert system for the effective prediction of heart failure," *IEEE Access*, vol. 7, pp. 54007–54014, 2019.

[43] L. Ali and S. Bukhari, "An approach based on mutually informed neural networks to optimize the generalization capabilities of decision support systems developed for heart failure prediction," *IRBM*, vol. 42, 2021.

[44] A. K. Dwivedi, "Performance evaluation of different machine learning techniques for prediction of heart disease," *Neural Computing and Applications*, vol. 29, no. 10, pp. 685–693, 2018.

[45] G. Guidi, M. C. Pettenati, P. Melillo, and E. Iadanza, "A machine learning system to improve heart failure patient assistance," *IEEE Journal of Biomedical and Health Informatics*, vol. 18, no. 6, pp. 1750–1756, 2014.

[46] A. P. Pawlovsky, "An ensemble based on distances for a knn method for heart disease diagnosis," in *2018 International Conference on Electronics, Information, and Communication (ICEIC)*, pp. 1–4, Honolulu, HI, USA, 2018.

[47] S.-N. Yu and M.-Y. Lee, "Bispectral analysis and genetic algorithm for congestive heart failure recognition based on heart rate variability," *Computers in Biology and Medicine*, vol. 42, no. 8, pp. 816–825, 2012.

[48] L. Wang, W. Zhou, Q. Chang, J. Chen, and X. Zhou, "Deep ensemble detection of congestive heart failure using short-term rr intervals," *IEEE Access*, vol. 7, pp. 69559–69574, 2019.

[49] A. Methaila, P. Kansal, H. Arya, and P. Kumar, "Early heart disease prediction using data mining techniques," *Computer Science & Information Technology Journal*, vol. 28, pp. 53–59, 2014.

[50] M. Jan, A. A. Awan, M. S. Khalid, and S. Nisar, "Ensemble approach for developing a smart heart disease prediction system using classification algorithms," *Research Reports in Clinical Cardiology*, vol. 9, pp. 33–45, 2018.

[51] C. Ricciardi, K. J. Edmunds, M. Recenti et al., "Assessing cardiovascular risks from a mid-thigh ct image: a tree-based machine learning approach using radiodensitometric distributions," *Scientific Reports*, vol. 10, no. 1, p. 2863, 2020.

[52] E. Butun, O. Yildirim, M. Talo, R.-S. Tan, and U. Rajendra Acharya, "1d-cadcapsnet: one dimensional deep capsule networks for coronary artery disease detection using ecg signals," *Physica Medica*, vol. 70, pp. 39–48, 2020.

[53] D. Ramachandran, V. Ponnusamy Thangapandian, and H. Rajaguru, "Computerized approach for cardiovascular risk level detection using photoplethysmography signals," *Measurement*, vol. 150, article 107048, 2020.

[54] M. M. Ghiasi, S. Zendehboudi, and A. A. Mohsenipour, "Decision tree-based diagnosis of coronary artery disease: cart model," *Computer Methods and Programs in Biomedicine*, vol. 192, article 105400, 2020.

[55] J. H. Joloudari, E. Hassannataj Joloudari, H. Saadatfar et al., "Coronary artery disease diagnosis; ranking the significant features using a random trees model," *International Journal of Environmental Research and Public Health*, vol. 17, no. 3, p. 731, 2020.

[56] M. Gjoreski, A. Gradišek, B. Budna, M. Gams, and G. Poglajen, "Machine learning and end-to-end deep learning for the detection of chronic heart failure from heart sounds," *IEEE Access*, vol. 8, pp. 20313–20324, 2020.

[57] L. Hussain, I. A. Awan, W. Aziz et al., "Detecting congestive heart failure by extracting multimodal features and employing machine learning techniques," *BioMed Research International*, vol. 2020, Article ID 4281243, 19 pages, 2020.

[58] Z. Aouabed, M. Abdar, N. Tahiri, J. C. Gareau, and V. Makarenkov, "A novel effective ensemble model for early detection of coronary artery disease," in *Innovation in Information Systems and Technologies to Support Learning Research. EMENA-ISTL 2019*, M. Serrhini, C. Silva, and S. Aljahdali, Eds., vol. 7 of Learning and Analytics in Intelligent Systems, pp. 480–489, Springer, Cham, 2020.

[59] X. Liu, J. Du, J. Yang, P. Xiong, J. Liu, and F. Lin, "Coronary artery fibrous plaque detection based on multi-scale convolutional neural networks," *Journal of Signal Processing Systems*, vol. 92, no. 3, pp. 325–333, 2020.

[60] A. U. Haq, J. P. Li, M. H. Memon, S. Nazir, and R. Sun, "A hybrid intelligent system framework for the prediction of heart disease using machine learning algorithms," *Mobile Information Systems*, vol. 2018, Article ID 3860146, 21 pages, 2018.

[61] L. Pecchia, P. Melillo, and M. Bracale, "Remote health monitoring of heart failure with data mining via cart method on hrv features," *IEEE Transactions on Biomedical Engineering*, vol. 58, no. 3, pp. 800–804, 2011.

[62] A. Kurnar, "Diagnosis of heart disease using fuzzy resolution mechanism," *Journal of Artificial Intelligence*, vol. 5, pp. 1–9, 2012.

[63] S. Panicacci, M. Donati, L. Fanucci, I. Bellini, F. Profili, and P. Francesconi, "Exploring machine learning algorithms to

identify heart failure patients: the tuscany region case study," in *2019 IEEE 32nd International Symposium on Computer-Based Medical Systems (CBMS)*, pp. 417–422, Cordoba, Spain, 2019.

[64] C. B. C. Latha and S. C. Jeeva, "Improving the accuracy of prediction of heart disease risk based on ensemble classification techniques," *Informatics in Medicine Unlocked*, vol. 16, 2019.

[65] D. Zikos, S. Zimeras, and N. Ragina, "A bayesian study of the dynamic effect of comorbidities on hospital outcomes of care for congestive heart failure patients," *Technologies*, vol. 7, no. 3, p. 66, 2019.

[66] S. Mohan, C. Thirumalai, and G. Srivastava, "Effective heart disease prediction using hybrid machine learning techniques," *IEEE Access*, vol. 7, pp. 81542–81554, 2019.

[67] H. Kahramanli and N. Allahverdi, "Design of a hybrid system for the diabetes and heart diseases," *Expert Systems with Applications*, vol. 35, no. 1-2, pp. 82–89, 2008.

[68] S. Maji and S. Arora, "Decision tree algorithms for prediction of heart disease," in *Information and Communication Technology for Competitive Strategies*, pp. 447–454, Springer, 2019.

[69] K. Polat, S. Sahan, H. Kodaz, and S. Günes, "A new classification method to diagnosis heart disease: supervised artificial immune system (airs)," in *Proceedings of the turkish symposium on artificial intelligence and neural networks (TAINN)*, 2005.

[70] B. Ŝter and A. Dobnikar, "Neural networks in medical diagnosis: comparison with other methods," in *International conference on engineering applications of neural networks*, pp. 427–430, 1996.

[71] W. Chen, G. Liu, S. Su, Q. Jiang, and H. Nguyen, "A chf detection method based on deep learning with rr intervals," in *2017 39th Annual International Conference of the IEEE Engineering in Medicine and Biology Society (EMBC)*, pp. 3369–3372, Jeju, Korea (South), 2017.

[72] K. S. Purushottam and R. Sharma, "Efficient heart disease prediction system using decision tree, in," in *International Conference on Computing, Communication & Automation*, pp. 72–77, Greater Noida, India, 2015.

[73] N. S. Rajliwall, R. Davey, and G. Chetty, "Machine learning based models for cardiovascular risk prediction," in *2018 International Conference on Machine Learning and Data Engineering (iCMLDE)*,, pp. 142–148, Sydney, NSW, Australia, 2018.

[74] O. W. Samuel, G. M. Asogbon, A. K. Sangaiah, P. Fang, and G. Li, "An integrated decision support system based on ANN and Fuzzy_AHP for heart failure risk prediction," *Expert Systems with Applications*, vol. 68, pp. 163–172, 2017.

[75] B. Venkatalakshmi and M. Shivsankar, "Heart disease diagnosis using predictive data mining, international journal of innovative research in science," *Engineering and Technology*, vol. 3, no. 3, pp. 1873–1877, 2014.

[76] F. Miao, Y.-P. Cai, Y.-X. Zhang, X.-M. Fan, and Y. Li, "Predictive modeling of hospital mortality for patients with heart failure by using an improved random survival forest," *IEEE Access*, vol. 6, pp. 7244–7253, 2018.

[77] M. Abdar, W. Ksikazek, U. R. Acharya, R.-S. Tan, V. Makarenkov, and P. Plawiak, "A new machine learning technique for an accurate diagnosis of coronary artery disease," *Computer Methods and Programs in Biomedicine*, vol. 179, 2019.

[78] S. Mezzatesta, C. Torino, P. De Meo, G. Fiumara, and A. Vilasi, "A machine learning-based approach for predicting the outbreak of cardiovascular diseases in patients on dialysis," *Computer Methods and Programs in Biomedicine*, vol. 177, pp. 9–15, 2019.

[79] M. S. Lakshmi, D. Haritha, and V. SRKIT, "Heart disease diagnosis using predictive data mining," *International Journal of Computer Science and Information Security*, 2016.

[80] S. Bashir, Z. S. Khan, F. H. Khan, A. Anjum, and K. Bashir, "Improving heart disease prediction using feature selection approaches," in *2019 16th International Bhurban Conference on Applied Sciences and Technology (IBCAST)*, pp. 619–623, Islamabad, Pakistan, 2019.

[81] A. Javeed, S. Zhou, L. Yongjian, I. Qasim, A. Noor, and R. Nour, "An intelligent learning system based on random search algorithm and optimized random forest model for improved heart disease detection," *IEEE Access*, vol. 7, pp. 180235–180243, 2019.

[82] K. G. Dinesh, K. Arumugaraj, K. D. Santhosh, and V. Mareeswari, "Prediction of cardiovascular disease using machine learning algorithms," in *2018 International Conference on Current Trends towards Converging Technologies (ICCTCT)*, pp. 1–7, Coimbatore, India, 2018.

[83] J. J. Nirschl, A. Janowczyk, E. G. Peyster et al., "A deep-learning classifier identifies patients with clinical heart failure using whole-slide images of h&e tissue," *PLoS One*, vol. 13, no. 4, article e0192726, 2018.

[84] I. Cetin, G. Sanroma, S. E. Petersen et al., "A radiomics approach to computer-aided diagnosis with cardiac cine-mri," in *International Workshop on Statistical Atlases and Computational Models of the Heart*, pp. 82–90, Springer, 2018.

[85] W. Bai, O. Oktay, and D. Rueckert, "Classification of myocardial infarcted patients by combining shape and motion features," in *Statistical Atlases and Computational Models of the Heart*, pp. 140–145, Springer, 2015.

[86] M. Qazi, G. Fung, S. Krishnan, J. Bi, R. Rao, and A. S. Katz, "Automated heart abnormality detection using sparse linear classifiers," *IEEE Engineering in Medicine and Biology Magazine*, vol. 26, no. 2, pp. 56–63, 2007.

[87] L. Ŝajn and M. Kukar, "Image processing and machine learning for fully automated probabilistic evaluation of medical images," *Computer Methods and Programs in Biomedicine*, vol. 104, no. 3, pp. e75–e86, 2011.

[88] R. Arsanjani, D. Dey, T. Khachatryan et al., "Prediction of revascularization after myocardial perfusion spect by machine learning in a large population," *Journal of Nuclear Cardiology*, vol. 22, no. 5, pp. 877–884, 2015.

[89] Y. Udovychenko, A. Popov, and I. Chaikovsky, "K-nn binary classification of heart failures using myocardial current density distribution maps,," in *2015 Signal Processing Symposium (SPSympo)*, pp. 1–5, Debe, Poland, 2015.

[90] R. Arsanjani, Y. Xu, D. Dey et al., "Improved accuracy of myocardial perfusion spect for detection of coronary artery disease by machine learning in a large population," *Journal of Nuclear Cardiology*, vol. 20, no. 4, pp. 553–562, 2013.

[91] G. Carneiro and J. C. Nascimento, "Combining multiple dynamic models and deep learning architectures for tracking the left ventricle endocardium in ultrasound data," *IEEE Transactions on Pattern Analysis and Machine Intelligence*, vol. 35, no. 11, pp. 2592–2607, 2013.

[92] Y. Zheng, A. Barbu, B. Georgescu, M. Scheuering, and D. Comaniciu, "Four-chamber heart modeling and automatic segmentation for 3-d cardiac ct volumes using marginal space learning and steerable features," *IEEE Transactions on Medical Imaging*, vol. 27, no. 11, pp. 1668–1681, 2008.

[93] G. B. Berikol, O. Yildiz, and İ. T. Özcan, "diagnosis of acute coronary syndrome with a support vector machine," *Journal of Medical Systems*, vol. 40, no. 4, p. 84, 2016.

[94] K. Lekadir, A. Galimzianova, A. Betriu et al., "A convolutional neural network for automatic characterization of plaque composition in carotid ultrasound," *IEEE Journal of Biomedical and Health Informatics*, vol. 21, no. 1, pp. 48–55, 2017.

[95] V. Sundaresan, C. P. Bridge, C. Ioannou, and J. A. Noble, "Automated characterization of the fetal heart in ultrasound images using fully convolutional neural networks," in *2017 IEEE 14th international symposium on biomedical imaging (ISBI 2017)*, pp. 671–674, Melbourne, VIC, Australia, 2017.

[96] E. Choi, A. Schuetz, W. F. Stewart, and J. Sun, "Using recurrent neural network models for early detection of heart failure onset," *Journal of the American Medical Informatics Association*, vol. 24, no. 2, pp. 361–370, 2017.

[97] D. Toth, S. Miao, T. Kurzendorfer et al., "3d/2d modeltoimage registration by imitation learning for cardiac procedures," *International Journal of Computer Assisted Radiology and Surgery*, vol. 13, no. 8, pp. 1141–1149, 2018.

[98] M. Maraci, C. Bridge, R. Napolitano, A. Papageorghiou, and J. Noble, "A framework for analysis of linear ultrasound videos to detect fetal presentation and heartbeat," *Medical Image Analysis*, vol. 37, 2017.

[99] L. A. Kurgan, K. J. Cios, R. Tadeusiewicz, M. Ogiela, and L. S. Goodenday, "Knowledge discovery approach to automated cardiac spect diagnosis," *Artificial Intelligence in Medicine*, vol. 23, no. 2, pp. 149–169, 2001.

[100] S. Mahendru and S. Agarwal, "Feature selection using metaheuristic algorithms on medical datasets," in *Harmony Search and Nature Inspired Optimization Algorithms*, Advances in Intelligent Systems and Computing, N. Yadav, A. Yadav, J. Bansal, K. Deep, and J. Kim, Eds., pp. 923–937, Springer, Singapore, 2019.

[101] Y. Liu, B. M. Scirica, C. M. Stultz, and J. V. Guttag, "Beatquency domain and machine learning improve prediction of cardiovascular death after acute coronary syndrome," *Scientific Reports*, vol. 6, no. 1, 2016.

[102] H. Shin, H. R. Roth, M. Gao et al., "Deep convolutional neural networks for computer-aided detection: Cnn architectures, dataset characteristics and transfer learning," *IEEE Transactions on Medical Imaging*, vol. 35, no. 5, pp. 1285–1298, 2016.

[103] M. A. H. M. Adib, N. H. M. Hasni, and P. O. A. Razak, "Analysis of echocardiography images using grid independent technique for patients with mitral valve problems (mvp)," in *2011 International Conference on Information Science and Applications*, pp. 1–5, Jeju, Korea (South), 2011.

[104] J. S. Allison, J. Heo, and A. E. Iskandrian, "Artificial neural network modeling of stress single-photon emission computed tomographic imaging for detecting extensive coronary artery disease," *The American Journal of Cardiology*, vol. 95, no. 2, pp. 178–181, 2005.

[105] R. Welikala, P. Foster, P. Whincup et al., "Automated arteriole and venule classification using deep learning for retinal images from the Uk biobank cohort," *Computers in Biology and Medicine*, vol. 90, pp. 23–32, 2017.

[106] A. H. Curiale, F. D. Colavecchia, P. Kaluza, R. A. Isoardi, and G. Mato, "Automatic myocardial segmentation by using a deep learning network in cardiac mri," in *2017 XLIII Latin American computer conference (CLEI)*, pp. 1–6, Cordoba, Argentina, 2017.

[107] D. Lindahl, J. Palmer, M. Ohlsson, C. Peterson, A. Lundin, and L. Edenbrandt, "Automated interpretation of myocardial spect perfusion images using artificial neural networks," *Journal of Nuclear Medicine*, vol. 38, no. 12, pp. 1870–1875, 1997.

[108] W. Bai, W. Shi, A. de Marvao et al., "A bi-ventricular cardiac atlas built from 1000+ high resolution mr images of healthy subjects and an analysis of shape and motion," *Medical Image Analysis*, vol. 26, no. 1, pp. 133–145, 2015.

[109] A. Moreno, J. Rodriguez, and F. Martínez, "Regional multiscale motion representation for cardiac disease prediction," in *2019 XXII Symposium on Image, Signal Processing and Artificial Vision (STSIVA)*, pp. 1–5, Bucaramanga, Colombia, 2019.

[110] M. A. Gülsün, G. Funka-Lea, P. Sharma, S. Rapaka, and Y. Zheng, "Coronary centerline extraction via optimal flow aths and cnn path pruning," in *International Conference on Medical Image Computing and Computer-Assisted Intervention-MICCAI 2016*, MICCAI 2016. Lecture Notes in Computer Science, S. Ourselin, L. Joskowicz, M. Sabuncu, G. Unal, and W. Wells, Eds., pp. 317–325, Springer, Cham, 2016.

[111] S. Narula, K. Shameer, A. M. Salem Omar, J. T. Dudley, and P. P. Sengupta, "Machine-learning algorithms to automate morphological and functional assessments in 2d echocardiography," *Journal of the American College of Cardiology*, vol. 68, no. 21, pp. 2287–2295, 2016.

[112] G. Carneiro, J. C. Nascimento, and A. Freitas, "The segmentation of the left ventricle of the heart from ultrasound data using deep learning architectures and derivative-based search methods," *IEEE Transactions on Image Processing*, vol. 21, no. 3, pp. 968–982, 2012.

[113] Y. Xu, R. Arsanjani, M. Clond et al., "Transient ischemic dilation for coronary artery disease in quantitative analysis of same-day sestamibi myocardial perfusion spect," *Journal of Nuclear Cardiology*, vol. 19, no. 3, pp. 465–473, 2012.

[114] J. Betancur, Y. Otaki, M. Motwani et al., "Prognostic value of combined clinical and myocardial perfusion imaging data using machine learning," *JACC: Cardiovascular Imaging*, vol. 11, no. 7, pp. 1000–1009, 2018.

[115] A. Coenen, Y.-H. Kim, M. Kruk et al., "Diagnostic accuracy of a machine-learning approach to coronary computed tomographic angiography–based fractional flow reserve: result from the machine Consortium," *Cardiovascular Imaging*, vol. 11, no. 6, article e007217, 2018.

[116] J. M. Wolterink, T. Leiner, M. A. Viergever, and I. Išgum, "Automatic coronary calcium scoring in cardiac ct angiography using convolutional neural networks-MICCAI 2015. MICCAI 2015," in vol. 9349 of Lecture Notes in Computer Science, pp. 589–596, Springer, Cham,, 2015.

[117] R. Nakazato, B. K. Tamarappoo, X. Kang et al., "Quantitative upright–supine high-speed spect myocardial perfusion imaging for detection of coronary artery disease: correlation with invasive coronary angiography," *Journal of Nuclear Medicine*, vol. 51, no. 11, pp. 1724–1731, 2010.

[118] L. Zhao, C. Liu, S. Wei, C. Liu, and J. Li, "Enhancing detection accuracy for clinical heart failure utilizing pulse transit time

variability and machine learning," *IEEE Access*, vol. 7, pp. 17716–17724, 2019.

[119] V. K. Sudarshan, U. R. Acharya, S. L. Oh et al., "Automated diagnosis of congestive heart failure using dual tree complex wavelet transform and statistical features extracted from 2 s of ecg signals," *Computers in biology and medicine*, vol. 83, pp. 48–58, 2017.

[120] U. R. Acharya, H. Fujita, O. S. Lih, M. Adam, J. H. Tan, and C. K. Chua, "Automated detection of coronary artery disease using different durations of ecg segments with convolutional neural network," *Knowledge-Based Systems*, vol. 132, pp. 62–71, 2017.

[121] J. Chen, A. Valehi, and A. Razi, "Smart heart monitoring: early prediction of heart problems through predictive analysis of ecg signals," *IEEE Access*, vol. 7, pp. 120831–120839, 2019.

[122] Y. Shen, Y. Yang, S. Parish, Z. Chen, R. Clarke, and D. A. Clifton, "Risk prediction for cardiovascular disease using ecg data in the china kadoorie biobank," in *2016 38th annual international conference of the IEEE engineering in medicine and biology society (EMBC)*, pp. 2419–2422, Orlando, FL, USA, 2016.

[123] U. R. Acharya, H. Fujita, M. Adam et al., "Automated characterization of arrhythmias using nonlinear features from tachycardia ecg beats," in *2016 IEEE International Conference on Systems, Man, and Cybernetics (SMC)*, pp. 000533–000538, Budapest, Hungary, 2016.

[124] S. M. Mathews, C. Kambhamettu, and K. E. Barner, "A novel application of deep learning for single-lead ecg classification," *Computers in Biology and Medicine*, vol. 99, pp. 53–62, 2018.

[125] M. Adam, S. L. Oh, V. K. Sudarshan et al., "Automated characterization of cardiovascular diseases using relative wavelet nonlinear features extracted from ecg signals," *Computer Methods and Programs in Biomedicine*, vol. 161, pp. 133–143, 2018.

[126] J. H. Tan, Y. Hagiwara, W. Pang et al., "Application of stacked convolutional and long short-term memory network for accurate identification of cad ecg signals," *Computers in Biology and Medicine*, vol. 94, pp. 19–26, 2018.

[127] M. Sharma, R. S. Tan, and U. R. Acharya, "A novel automated diagnostic system for classification of myocardial infarction ecg signals using an optimal biorthogonal filter bank," *Computers in Biology and Medicine*, vol. 102, pp. 341–356, 2018.

[128] J. Faganeli Pucer and M. Kukar, "A topological approach to delineation and arrhythmic beats detection in unprocessed long-term ecg signals," *Computer methods and programs in biomedicine*, vol. 164, pp. 159–168, 2018.

[129] C.-S. Huang, L.-W. Ko, S.-W. Lu, S.-A. Chen, and C.-T. Lin, "A vectorcardiogram-based classification system for the detection of myocardial infarction," in *2011 Annual International Conference of the IEEE Engineering in Medicine and Biology Society*, pp. 973–976, Boston, MA, USA, 2011.

[130] X. Zhou, X. Zhu, K. Nakamura, and N. Mahito, "Premature ventricular contraction detection from ambulatory ecg using recurrent neural networks," in *2018 40th annual international conference of the IEEE engineering in medicine and biology society (EMBC)*, pp. 2551–2554, 2018.

[131] U. Satija, B. Ramkumar, and M. S. Manikandan, "A new automated signal quality-aware ecg beat classification method for unsupervised ecg diagnosis environments," *IEEE Sensors Journal*, vol. 19, no. 1, pp. 277–286, 2019.

[132] A. Diker, D. Avci, E. Avci, and M. Gedikpinar, "A new technique for ecg signal classification genetic algorithm wavelet kernel extreme learning machine," *Optik*, vol. 180, pp. 46–55, 2019.

[133] U. R. Acharya, H. Fujita, S. L. Oh, Y. Hagiwara, J. H. Tan, and M. Adam, "Application of deep convolutional neural network for automated detection of myocardial infarction using ecg signals," *Information Sciences*, vol. 415-416, pp. 190–198, 2017.

[134] Q. Yao, R. Wang, X. Fan, J. Liu, and Y. Li, "Multi-class arrhythmia detection from 12-lead varied-length ecg using attention-based time-incremental convolutional neural network," *Information Fusion*, vol. 53, pp. 174–182, 2020.

[135] M. Vafaie, M. Ataei, and H. R. Koofigar, "Heart diseases prediction based on ECG signals' classification using a genetic-fuzzy system and dynamical model of ECG signals," *Biomedical Signal Processing and Control*, vol. 14, pp. 291–296, 2014.

[136] S. Sahoo, B. Kanungo, S. Behera, and S. Sabut, "Multiresolution wavelet transform based feature extraction and ecg classification to detect cardiac abnormalities," *Measurement*, vol. 108, pp. 55–66, 2017.

[137] A. K. Dohare, V. Kumar, and R. Kumar, "Detection of myocardial infarction in 12 lead ecg using support vector machine," *Applied Soft Computing*, vol. 64, pp. 138–147, 2018.

[138] Z. I. Attia, P. A. Noseworthy, F. Lopez-Jimenez et al., "An artificial intelligence-enabled ecg algorithm for the identification of patients with atrial fibrillation during sinus rhythm: a retrospective analysis of outcome prediction," *The Lancet*, vol. 394, no. 10201, pp. 861–867, 2019.

[139] F.-M. Melgarejo-Meseguer, F.-J. Gimeno-Blanes, M.-E. Salar-Alcaraz et al., "Electrocardiographic fragmented activity (ii): A machine learning approach to detection," *Applied Sciences*, vol. 9, no. 17, p. 3565, 2019.

[140] K. Feng, X. Pi, H. Liu, and K. Sun, "Myocardial infarction classification based on convolutional neural network and recurrent neural network," *Applied Sciences*, vol. 9, no. 9, p. 1879, 2019.

[141] A. Raka, G. Naik, and R. Chai, "Computational algorithms underlying the time-based detection of sudden cardiac arrest via electrocardiographic markers," *Applied Sciences*, vol. 7, no. 9, p. 954, 2017.

[142] M. Kumar, R. Pachori, and U. Acharya, "Automated diagnosis of myocardial infarction ecg signals using sample entropy in flexible analytic wavelet transform framework," *Entropy*, vol. 19, no. 9, p. 488, 2017.

[143] L. Yin, F. Chen, Q. Zhang, and X. Ma, "Arrhythmia classification based on multi-don feature extraction," *Journal of Physics: Conference Series*, vol. 1237, article 022062, 2019.

[144] P. Sahoo, H. Thakkar, and M.-Y. Lee, "A cardiac early warning system with multi channel scg and ecg monitoring for mobile health," *Sensors*, vol. 17, no. 4, p. 711, 2017.

[145] Z. Masetic and A. Subasi, "Congestive heart failure detection using random forest classifier," *Computer Methods and Programs in Biomedicine*, vol. 130, pp. 54–64, 2016.

[146] Y. İşler and M. Kuntalp, "Combining classical hrv indices with wavelet entropy measures improves to performance in diagnosing congestive heart failure," *Computers in Biology and Medicine*, vol. 37, no. 10, pp. 1502–1510, 2007.

[147] A. A. Bhurane, M. Sharma, R. San-Tan, and U. R. Acharya, "An efficient detection of congestive heart failure using

Hindawi
Computational and Mathematical Methods in Medicine
Volume 2023, Article ID 9840132, 1 page
https://doi.org/10.1155/2023/9840132

Retraction

Retracted: COVID-19 Detection Based on Lung Ct Scan Using Deep Learning Techniques

Computational and Mathematical Methods in Medicine

Received 10 October 2023; Accepted 10 October 2023; Published 11 October 2023

This article has been retracted by Hindawi following an investigation undertaken by the publisher [1]. This investigation has uncovered evidence of one or more of the following indicators of systematic manipulation of the publication process:

(1) Discrepancies in scope

(2) Discrepancies in the description of the research reported

(3) Discrepancies between the availability of data and the research described

(4) Inappropriate citations

(5) Incoherent, meaningless and/or irrelevant content included in the article

(6) Peer-review manipulation

The presence of these indicators undermines our confidence in the integrity of the article's content and we cannot, therefore, vouch for its reliability. Please note that this notice is intended solely to alert readers that the content of this article is unreliable. We have not investigated whether authors were aware of or involved in the systematic manipulation of the publication process.

Wiley and Hindawi regrets that the usual quality checks did not identify these issues before publication and have since put additional measures in place to safeguard research integrity.

We wish to credit our own Research Integrity and Research Publishing teams and anonymous and named external researchers and research integrity experts for contributing to this investigation.

The corresponding author, as the representative of all authors, has been given the opportunity to register their agreement or disagreement to this retraction. We have kept a record of any response received.

References

[1] S. V. Kogilavani, J. Prabhu, R. Sandhiya et al., "COVID-19 Detection Based on Lung Ct Scan Using Deep Learning Techniques," *Computational and Mathematical Methods in Medicine*, vol. 2022, Article ID 7672196, 13 pages, 2022.

Hindawi
Computational and Mathematical Methods in Medicine
Volume 2022, Article ID 7672196, 13 pages
https://doi.org/10.1155/2022/7672196

Research Article

COVID-19 Detection Based on Lung Ct Scan Using Deep Learning Techniques

S. V. Kogilavani,[1] J. Prabhu,[2] R. Sandhiya,[1] M. Sandeep Kumar,[2] UmaShankar Subramaniam,[3,4] Alagar Karthick,[5] M. Muhibbullah,[6] and Sharmila Banu Sheik Imam[7]

[1].*Department of Computer Science and Engineering, Kongu Engineering College, Perundurai, Erode 638060, Tamil Nadu, India*
[2]*School of Information Technology and Engineering, Vellore Institute of Technology, Vellore, Tamil Nadu, India*
[3]*Renewable Energy Lab, College of Engineering, Prince Sultan University, Riyadh, Saudi Arabia 11586*
[4]*Department of Energy and Environmental Engineering, Saveetha School of Engineering, Saveetha Institute of Medical and Technical Sciences, Saveetha University, Saveetha Nagar, Thandalam, Chennai-602105, Tamilnadu, India*
[5]*Renewable Energy Lab, Department of Electrical and Electronics Engineering, KPR Institute of Engineering and Technology, Coimbatore, 641407 Tamilnadu, India*
[6]*Department of Electrical and Electronic Engineering, Bangladesh University, Dhaka 1207, Bangladesh*
[7]*College of Computer Science & Information Technology (CCSIT), King Faisal University, Alahsa, Saudi Arabia 31982*

Correspondence should be addressed to S. V. Kogilavani; kogilavani@kongu.ac.in
and M. Muhibbullah; m.muhibbullah@bu.edu.bd

Received 12 October 2021; Accepted 7 January 2022; Published 1 February 2022

Academic Editor: Muhammad Zubair Asghar

SARS-CoV-2 is a novel virus, responsible for causing the COVID-19 pandemic that has emerged as a pandemic in recent years. Humans are becoming infected with the virus. In 2019, the city of Wuhan reported the first-ever incidence of COVID-19. COVID-19 infected people have symptoms that are related to pneumonia, and the virus affects the body's respiratory organs, making breathing difficult. A real-time reverse transcriptase-polymerase chain reaction (RT-PCR) kit is used to diagnose the disease. Due to a shortage of kits, suspected patients cannot be treated promptly, resulting in disease spread. To develop an alternative, radiologists looked at the changes in radiological imaging, like CT scans, that produce comprehensive pictures of the body of excellent quality. The suspected patient's computed tomography (CT) scan is used to distinguish between a healthy individual and a COVID-19 patient using deep learning algorithms. A lot of deep learning methods have been proposed for COVID-19. The proposed work utilizes CNN architectures like VGG16, DeseNet121, MobileNet, NASNet, Xception, and EfficientNet. The dataset contains 3873 total CT scan images with "COVID" and "Non-COVID." The dataset is divided into train, test, and validation. Accuracies obtained for VGG16 are 97.68%, DenseNet121 is 97.53%, MobileNet is 96.38%, NASNet is 89.51%, Xception is 92.47%, and EfficientNet is 80.19%, respectively. From the obtained analysis, the results show that the VGG16 architecture gives better accuracy compared to other architectures.

1. Introduction

COVID-19 is a disease, caused by a virus (SARS-CoV-2). Infections in the lungs can range from a simple cold to a life-threatening condition. Symptoms of the respiratory system often accompany infections caused by coronaviruses. Individuals may have minor, self-limiting illnesses with adverse effects like influenza on rare occasions. Fever, cough, and difficulty breathing are among the symptoms of respiratory issues, weariness, and a sore throat [1–3]. The use of X-rays and computed tomography scans is one of the fundamental approaches to diagnosing COVID-19. Chest imaging is a quick and efficient method suggested by medical health regulations, and it has been highlighted in several papers as the first

instrument in epidemic screening. Different computer vision approaches are used, such as segmentation and classification. When a quick and straightforward method running on limited computing devices is needed, an automated technique that can provide fragmentation and measurement of the infection region of patients every three to five days and monitor the evolution of infected patients through CT scan imaging and clinical detection is required. COVID-19 is a difficult disease to diagnose, even for expert doctors [4, 5].

Many studies have been undertaken on the use of deep learning in the interpretation of radiological images. They have been undertaken to solve the constraints of COVID-19 medical techniques based on radiological images. The CNN architecture is the most effective approach for detecting it among the most significant deep learning algorithms. Data processing of deep learning algorithms, notably CNN, has received much interest.

In early 2020, the COVID-19 outbreak became a worldwide epidemic. The World Health Organization declared a significant international public health emergency, and the condition was considered a health emergency. Automatic detection of lung infections through CT scans provides an excellent opportunity to extend traditional healthcare methods to address COVID-19. But CT has many problems [1]. CNN is used to detect lung tumors, pneumonia, tuberculosis, emphysema, or other pleural diseases. The disadvantages of the CT system are as follows: because the contrast of the soft tissues is lower than that of the MRI, it is an X-ray Radiation exposure [6].

Using deep learning algorithms, the suspected patient's X-ray and CT scan can be distinguished between a healthy person and a COVID-19 patient. Deep learning models are employed in creating diagnosis systems for COVID-19. DenseNet121, VGG16, Xception, EfficientNet, and NASNet are the architectures employed, and multiclass classification is used. Positive individuals with COVID-19, regular patients, and other patients are also considered. Chest X-ray images indicate pneumonia, flu, and other chest-related disorders that belong in another category. VGG16 achieves 79.01% accuracy, EfficientNet achieves 93.48 accuracy, Xception achieves 88.03 accuracy, NASNet achieves 85.03 accuracy, and DenseNet121 achieves 89.96% accuracy [7].

For disease diagnosis, the algorithms presented include the DNN based on imaging features of fractals and the CNN that directly uses lung imaging. The suggested architecture of CNN, with higher accuracy of 93.2% and a sensitivity of 96.1%, outperforms the DNN technique with 83.4% precision and 86% sensitivity. A CNN architecture is offered during the segmentation phase to detect contaminated tissue in the lung pictures. The results show that this method can see almost 4,444 infected areas with an accuracy rate of 83.84%. And the finding is used to monitor and control the growth of the patient's protected area [8].

Preprocessing, dictionary building, and picture classification are the three critical stages of the classification approach based on features. In the suggested method, features are manually retrieved and passed to a classifier neural network than modern methods in an experimental environment. On three data sets, the technique has an accuracy of 96.1, 99.84, and 98%. These results are superior to those obtained using modern approaches. The SURF method is utilized to extract objects in a visual word bag. Because the SURF technique is dependent on gradients and the obtained solution is noise-sensitive, the offered approaches may misclassify the image if the image quality is inadequate. In this case, picking the proper pretreatment procedure can help you get better outcomes [9].

Using chest CT images, a new multicore deep neural network method is proposed to detect the COVID-19 disease, also known as COVID-19. This paper extracted the characteristics from lung CT images using a CNN. A predefined DenseNet201 CNN architecture based on transfer learning is employed for this purpose. The ELM method classifier depends on various activation algorithms that calculate the architecture's performance. According to the data, when applying the MKsELMDNN model, the accuracy score reached was 98.36% [10].

Machine learning techniques based on X-ray imaging are utilized as a decision support mechanism to assist radiologists in speeding up the diagnosis process. A critical review of 12 conventional CNN designs was first proposed for natural image processing to assist radiologists in distinguishing COVID-19 diseases from radiographic pictures of the chest. COVID-19 X-ray pictures were used, as well as a massive dataset of non-COVID viral illnesses, bacterial infections, and routine radiographs were also used. When trained on a tiny image dataset, a simple CNN design can outperform architectures like Xception and DenseNet. Finally, therapists should not examine CNN conclusions despite their excellent classification accuracy until they can visually analyze the region of the input image acquired by the CNN [11].

For automatic COVID-19 categorization, different deep learning methods by extracting their features were compared. MobileNet, ResNetV2, VGGNet, ResNet, InceptionV3, DenseNet, Xception, Inception, and NASNet have been selected from a vast list of convolutional neural networks to produce the most accurate feature, which is an integral part of learning. The collected features are fed into a series of machine learning classifiers to determine whether the subjects were COVID-19 cases or controls. This strategy achieved task-specific data preprocessing approaches to promote a robust generalization capacity for unknown data. The method's accuracy was tested using the publicly available COVID-19 dataset of chest X-ray and CT images. DenseNet121 achieved 99.5 percent accuracy with a bagging tree classifier, while ResNet50 achieved 50% accuracy [12].

Chest X-ray images have recently emerged as a promising option for COVID-19 screening when combined with current AI techniques, particularly DL algorithms. The classification of COVID-19 from standard cases was evaluated using eight architectures like AlexNet, GoogleNet, SqueezeNet, VGG-16, ResNet 50, MobileNet V2, ResNet 34, and Inception V3, respectively. The models have been evaluated on publicly accessible chest X-ray images, with ResNet-34 getting the best results, with an accuracy of 98.33 percent [13]. A CT scan involves slides of a hundred scans, and using such scans to diagnose COVID-19 can cause hospital delays. Artificial intelligence tools could help radiologists diagnose

COVID-19 infections in these images more quickly and correctly. Using artificial intelligence, this study offers a technique for identifying COVID and non-COVID classes. The suggested AI method predicts COVID-19 in each 3D CT scan image using the ResNet-50 deep learning model. Using image-level predictions, an AI method detects COVID-19 in a 3D CT volume. With an accuracy of 96%, the suggested deep learning model detects the disease on CT images [14]. The ten possible best convolutional neural networks used to distinguish the infection are AlexNet, GoogleNet, VGG 19, ResNet 101, VGG 16, ResNet 50, MobileNet V2, ResNet 18, SqueezeNet, and xception. All of the networks performed well, except for ResNet-101 and Xception. For discriminating the disease, ResNet-101 had an accuracy of 99.4%, while Xception had an accuracy of 99.99%. ResNet-101 is a moderate model for identifying and detecting COVID-19 infections in radiology departments that may be used as a replacement [15].

DenseNet, InceptionV3, and Inception-ResNetV4 were recommended as three different models. In the investigation, chest X-ray radiographs were used to diagnose individuals with COVID-19 and pneumonia. Using 5-fold cross-validation, these three models create and evaluate ROC curve analyses and uncertainty matrices. The pretrained DenseNet architecture achieved an optimum classification efficiency of 92 percent in simulations, while the other two models, Inception V3 and Inception-ResNetV4, achieved 83.47 percent and 85.57 percent, respectively [16]. Radiological imaging using advanced artificial intelligence techniques can aid in precise disease detection and overcome the shortage of expert physicians in rural areas. This paper offers a new method for automated COVID-19 identification based on raw chest X-ray images. The suggested technique offers correct diagnostics for binary and multiclass classification in binary and multiclass environments. The model gives an accuracy of 98.08% for binary classes and 87.02% for the instance of multiclass [17]. The binary classification method was trained using 3,877 CT and X-ray images, including 1,917 COVID-19 patients. The binary classification had a 99.64% overall accuracy, 99.58% recall, 99.56% precision, 99.59% *F*1-score, and 100% ROC. Normal healthy people contain instances of 1917, normal healthy people contain instances of 1,960, and pneumonia contains 2200 instances. By using these instances, the classifier was tested on a total of 6,077 images for different classifications. The multiclass has a 99.87% ROC, 98.2% accuracy, 98.25% recall, 98.22% *F*1 -score, 98.22% precision, and 98.22% precision [18]. The VGG16 and ResNet50 models are improved and optimized using augmentation of data and fine-tuning strategies. The model's resilience and effectiveness were also tested using stratified 5-fold cross-validation. It performs exceptionally well in binary classification, with an average accuracy rate of more than 99% in the VGG16 and ResNet50 model models. Using the architectures as baselines, the model achieves an overall classification accuracy of 86.74 percent in multiclass classification and 88.52 percent in single-class classification. Experiments have shown their model exceeds the competition, which is used automatically to detect COVID-19 in CT scans [19].

The Bat algorithm (BA) is a nature-inspired metaheuristic algorithm commonly utilized to address universal management problems in the real world. While dealing with complicated real-world situations, one of the key obstacles the BA faces is its repeated entrapment in local optimization. The updated version of the Bat algorithm can also benefit medical image classification [20]. Since animal unstructured text data can be collected from Twitter, supervised machine learning algorithms such as deep neural networks can recognize online individuals suffering from depression [21]. Particle Swarm Optimization (PSO) is a swarm-based smart stochastic optimization approach inspired by the natural way bees swarm when looking for food. It is mainly used to solve multiple types of optimization issues. Particle swarm optimization methods are commonly used to diagnose diseases [22]. CNN is an effective tool for selecting the best features to improve prediction accuracy. The LSTM model conserves leading-up relevant information, which aids in extracting important context information at the beginning of a sentence. The CNN + LSTM framework for personality factor classification combines CNN and LSTM to help categorize input text into various personality qualities. The integrated framework is also used to detect psychopaths and gives the best accuracy of 91.67% for classification [23, 24].

The contribution of this research work is to

(i) Collect the COVID-19 sample dataset from Kaggle, containing 3873 CT scan images

(ii) Preprocess the dataset to make all images of literature the same size

(iii) The preprocessed dataset is split into training, validation, and test data

(iv) The training dataset is fed into different CNN architectures like Xception, MobileNet, NASNet, DenseNet121, EfficientNet, and VGG16

(v) The trained models are validated using a validation dataset with 50 epochs

(vi) Now the models are being tested by supplying test data

A real-time reverse transcriptase-polymerase chain reaction (RT-PCR) kit is used to diagnose the disease. Due to a shortage of kits, suspected patients cannot be treated promptly, resulting in disease spread. To develop an alternative, radiologists looked at the changes in radiological imaging, like CT scans, that produce comprehensive pictures of the body of excellent quality. The rest of this paper is formulated in the following way: the recent COVID-19 identification study results are presented in the literature review. The proposed system section discusses the detection of COVID-19. This section also gives a complete description of the classification models utilized in the proposed system. The steps involved in the architecture are described in the section on system architecture. The Results and Discussion section contains a complete analysis and comparison of the performance of the CNN models. Finally, a summary of the proposed work and future work is specified in the Conclusion section.

2. Materials and Method

2.1. Deep Learning Techniques. Artificial intelligence techniques that resemble how humans acquire knowledge and deep learning are similar to machine learning techniques. Data science, which covers statistics and predictive modeling, includes deep learning as a critical component. In deep understanding, a convolutional neural network is a kind of deep neural network used to analyze visual imagery. A deep learning method, CNN takes an input image and assigns weight to various objects in the picture, allowing it to differentiate between them. Because of its great accuracy, CNN is used to classify and identify images [25].

2.2. Classification. Deep learning architectures, namely, VGG16, DenseNet, MobileNet, Xception, EfficientNet, and NASNet, are used to classify the data. Transfer learning is used to train these models. Each model has been trained for a total of 50 epochs. A detailed explanation is given below.

2.3. Xception. The Xception network has replaced the Inception network. Extreme inception is often referred to as Xception. Instead of typical convolution layers, the Xception network uses depth-wise separable convolution layers. Xception includes mapping spatial and cross-channel correlations, which in CNN feature maps can be completely dissociated. The underlying Inception architecture survived longer than Xception. The 36 convolution layers in the Xception model can be separated into 14 different modules. After the first and last layers are removed, every layer has a continuous residual link around it. The input image is converted into spatial correlations within each output channel to obtain the cross-channel correlations in an input image. After that, a depth-wise 1×1 convolution method is performed. Instead of 3D maps, the relationships may be viewed as a 2D + 1D map. In Xception, the first step is to do a 2D space correlation, followed by 1D space correlations [7]. The architecture is illustrated in Figure 1.

2.4. VGG16. VGG16 is a CNN model, and the VGG created the model at Oxford University. The network's replacement, AlexNet, was founded in 2012. VGG16 has eight layers, three completely connected layers, five max-pooling layers, and one softmax layer, as illustrated in Figure 2. As part of the ImageNet competition, the architecture has been designed. The convolution blocks' width is set to a low integer. The width parameter is expanded by two after each max-pooling operation till it reaches 512. The VGG16 is given an image size of 224×224 pixels. Spatial padding was used to maintain the image's spatial resolution. The VGG16 network has been released as open-source so that similar operations can be carried out. The model may also be used for transfer learning because specific frameworks, like Keras, provide pretrained weights that can be utilized to construct custom models with minor alterations [7].

2.5. MobileNet. MobileNet uses Depthwise separable convolutions. While compared to a network with regular convolutions of the same depth in the nets, it substantially reduces the number of parameters. As a result, lightweight deep neural networks are created. Depthwise separable convolution layers are used to construct MobileNets. Each depth-wise detachable convolution layer comprises a depth-wise convolution layer and a pointwise convolution layer. A MobileNet contains 28 layers if depthwise and pointwise convolutions are counted separately, and the model is defined in Figure 3. The width multiplier hyperparameter can be adjusted to reduce the number of parameters in a conventional MobileNet to 4.2 million. The input image is 224×224 pixels in size [15].

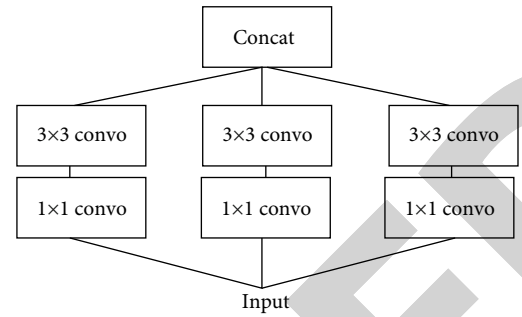

Figure 1: Xception architecture.

2.6. NASNet. The Google ML team created the NAS Network. Reinforcement learning is used to build the network architecture. The network adjustment is made based on the changes in the effectiveness of the child block. The parental block evaluates the effectiveness of the children's block. RNN and CNN are the network's components. Various changes to the architecture were made to gain the optimum performance from the web, including weights, regularisation methods, layers, and optimizer functions. Reinforced evolutionary processes select the best candidates and choose the best cells by utilizing various NASNet variants like A, B, and C algorithms [26]. The model is illustrated in Figure 4.

Using tournament selection techniques, the cells with the weakest performance are eliminated. The performance of the cell structure is enhanced by improving the child's objective functions and carrying out reinforcement mutations. A block is considered the smallest element, and a cell combines several blocks. The search space of the network is factored into cells, which are then divided into blocks. The dataset type determines the number of cells and blocks, which is not fixed. Convolutions, pooling, mapping, and other operations are executed within a block. NASNet was one of the methods used for identifying infected and not-infected patients because of its transferable learning methodology. With its minimal network design, it offers more possibilities [27].

2.7. DenseNet121. DenseNet is a densely connected neural network, a different technique to increase the extent of deep convolutional networks without experiencing problems like expanding gradients and disappearing gradients. Each layer connects directly with other layers where the maximum amount of information and gradient flow is passed. With this, the issues are solved. The objective is to focus on feature

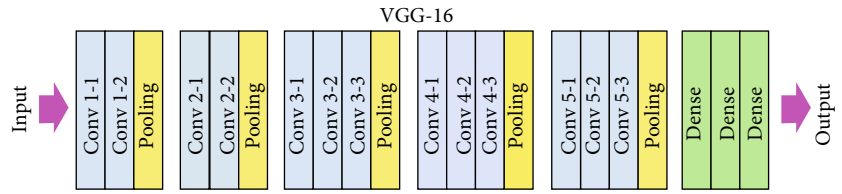

Figure 2: VGG16 architecture.

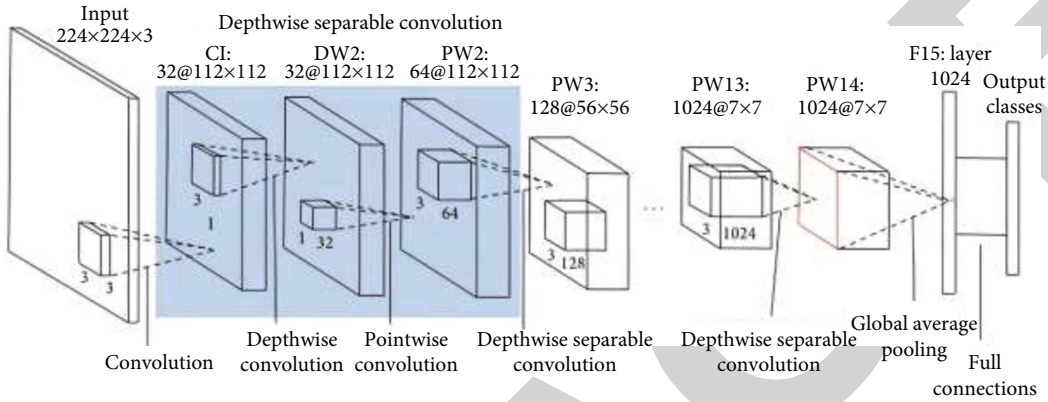

Figure 3: MobileNet architecture.

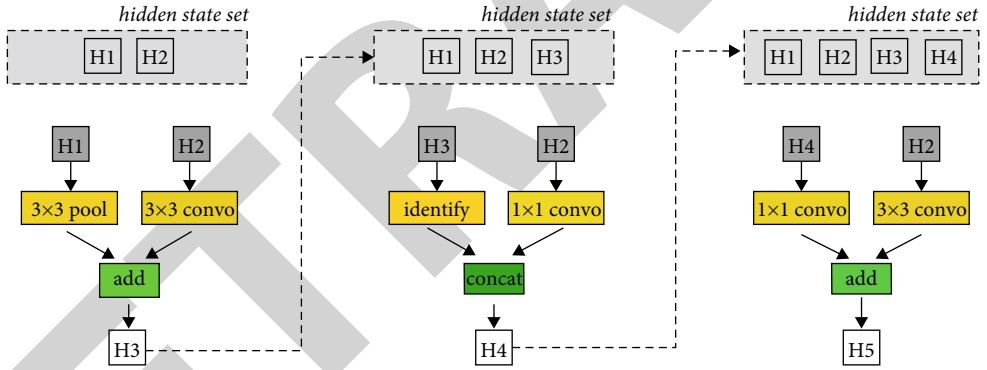

Figure 4: NASNet architecture.

reuse rather than relying on large, deep, or broad CNN architectures for symbolic power. Compared to conventional CNN, DenseNets require fewer or equal numbers of nodes. Because the feature maps are not learned in DenseNets, and the parameters are not needed. Several ResNets versions have scarcely contributed, and those layers can be removed, and the model is defined in Figure 5.

DenseNet layers add only a few significant features, and the layers are narrow with only a few other filters. The issue emerges when training the data because deep neural networks incorporate information flow and gradients. DenseNets solves these issues by directly accessing the actual input's gradients and transfer functions. Dense Net's network design gets more hierarchical as feature translation from the $(i-1)^{\text{th}}$ level becomes the intake to the p^{ith} layer. The DenseNet is a generally applicable network since the input to the width layer can originate from any level $(i-1)$, $(i-2)$, or even $(i-n)$ (where n must be less than the number of layers total). The network is normalized using a batch normalization phase, which reduces the actual error between the data and examines substantial variation [28].

2.8. EfficientNet. The scaling of the model is one of the most important considerations when utilizing CNNs. Increasing the model's depth improves the system's performance. On the other hand, selecting the model's depth is a challenging issue requiring a human hit-or-miss approach to choosing a better-performing model. MBConv is the core component of the EfficientNet models. A squeeze-and-excitation optimization block has been added to this block. The MBConv block in MobileNet V2 works similarly to the inverted residual blocks. To decrease the number of channels in the output, 3×3 depth-wise and pointwise convolutions are utilized to build a direct link between the start and finish of a convolutional block to reduce the number of channels in the output feature maps. The small layers are connected

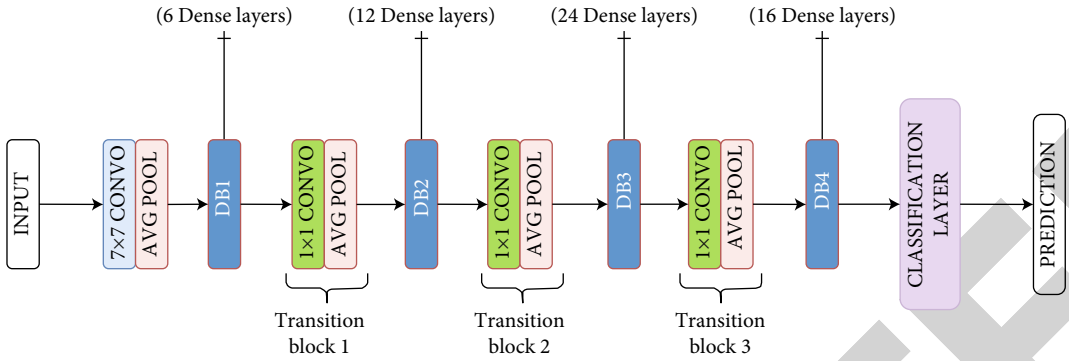

Figure 5: DenseNet121 architecture.

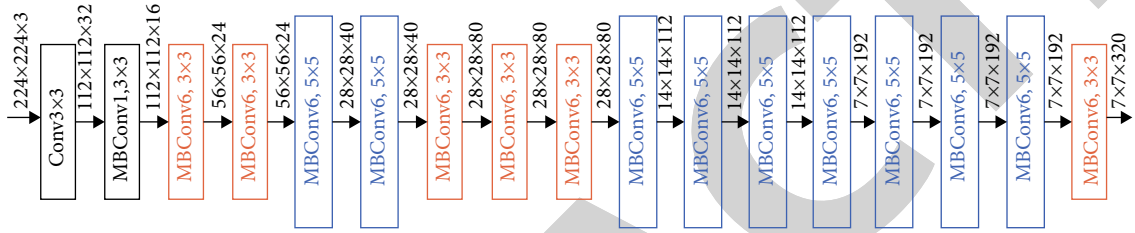

Figure 6: Efficient net architecture.

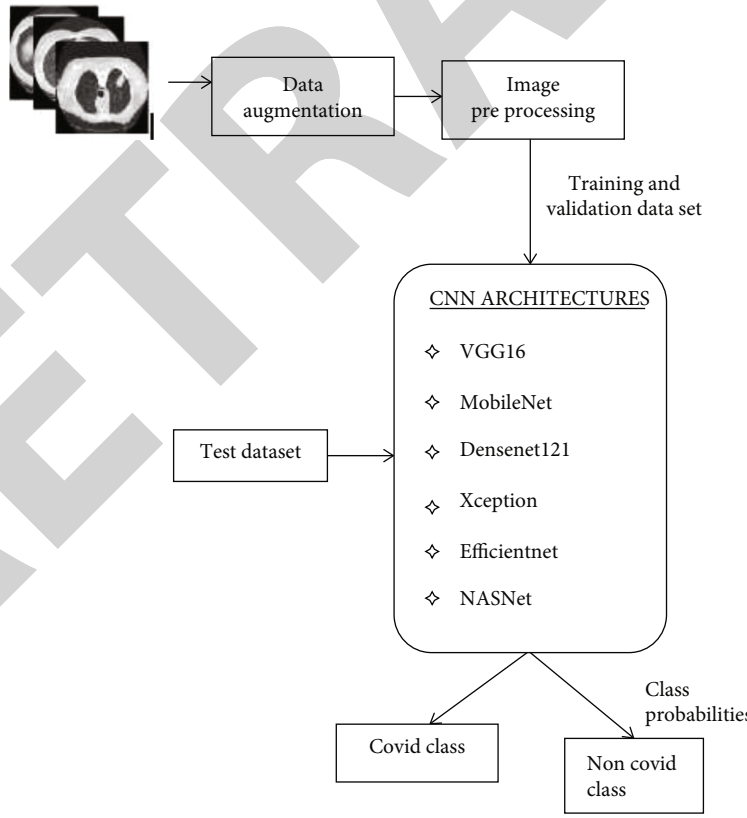

Figure 7: Proposed system architecture.

with low computational complexity, whereas the broader levels are associated with hidden neurons. The model's size and the number of functions in the structure are reduced by this architecture, which is illustrated in Figure 6. In this work, EfficientNetB6 is used to classify COVID-19 patients and healthy people.

Table 1: Parameters for training the models.

Performance measures	VGG16	DenseNet121	MobileNet	Xception	NASNet	EfficientNet
Batch size	16	16	16	16	16	16
Image dimension	224 × 224	224 × 224	224 × 224	224 × 224	224 × 224	224 × 224
Optimizer	Adam	Adam	Adam	Adam	Adam	Adam
Activation function	Softmax	Softmax	Softmax	Softmax	Softmax	Softmax
Loss function	Binary cross-entropy	Binary cross-entropy	Binary cross-entropy	Binary cross-entropy	Binary cross-entropy	Binary cross-entropy

Table 2: Kaggle dataset description.

Dataset	COVID	Non-COVID
Training	930	915
Validation	156	164
Test	166	150
Total	1252	1229

Table 3: Data augmentation dataset description.

Dataset	COVID	Non-COVID	Total
Training	1257	1234	2491
Validation	345	346	691
Test	356	335	691
Total	1958	1915	3873

Table 4: Confusion matrix representation.

	Predicted	
Actual	Yes	No
Yes	TP	TN
No	FN	FP

Where TP denotes "True Positive," TN denotes "True Negative," FN represents "False Negative," and FP represents "False Positive".

2.9. Proposed System Architecture. Chest tomography CT scan images are given as the input. The process is illustrated in Figure 7. CT images are preprocessed. The image must fit the network's input size to train it and generate predictions on the data. The data is rescaled to check the network's input size. In the proposed system, the input image size is 224 × 224. So, the data is rescaled according to the input size.

CNN architectures like VGG16, MobileNet, DenseNet121, Xception, EfficientNet, and NASNet are performed to detect COVID-19. Data augmentation such as cropping and horizontal flipping generally produces new images by zooming in and out based on the input parameters given in Table 1. The number of training examples used in one iteration is referred to as the "batch size." For all models, a batch size of 16 is chosen. Optimizers are algorithms used to change attributes of neural networks, such as weight and learning rate, to reduce losses. The Adam optimizer is used for optimization.

To reduce the nonlinearity in the output of a neuron, certain activation functions are used. The output layer's activation function determines the kind of predictions the model can make. In the proposed system, the softmax function is used as the activation function for all the models. Softmax is used in the last layer, the output layer, to predict a multinomial probability distribution. "Loss" is the network's prediction error, and the "loss function" is the method used to calculate the error. And the loss function also calculates gradients. Gradients are used to update the weights of the neural network. In binary classification tasks, binary cross-entropy compares predicted probability to actual class output, which might be either 0 or 1.

Image augmentation is expanding the available dataset for training the model. The dataset is divided into training, validation, and testing. The collection of samples used to learn how to suit the parameters is referred to as training. Validation is a collection of examples used to fine-tune a classifier's parameters. The data is trained and validated for 50 epochs, and the class probability of the images is then generated. The results were calculated by evaluating the performance measures such as accuracy, precision, recall, and F-score.

3. Performance Evaluation Measures

3.1. Dataset. The dataset collection includes lung CT scan images. A CT scan utilizes advanced X-ray technology to diagnose sensitive internal organs carefully. The dataset was taken from Kaggle and consisted of 3873 images. COVID and non-COVID are the two categories into which the data is divided. The COVID class includes CT scan images of COVID patients, while the non-COVID class includes healthy individuals. There are 1958 CT scan images in the COVID class and 1915 CT scan images in the non-COVID class. The model is trained on 70% of lung CT scans, validated on 15% of lung CT scans, and tested on 15%. These are illustrated in Table 2.

3.2. Preprocessing. A squared image with a predetermined aspect ratio is scaled to have roughly the same height and width. The image filtering preprocessing technique is used to filter the size of all input samples. In the proposed system, the images are rescaled to 224 × 224.

3.3. Image Augmentation. It is the process of expanding the existing dataset for training the model. Existing data is

Table 5: Comparison of various evaluation measures for COVID class.

Performance measure	VGG16	DenseNet121	MobileNet	Xception	NASNet	EfficientNet
Precision	1.00	0.96	0.99	0.90	0.96	0.91
Recall	0.96	0.99	0.94	0.96	0.83	0.46
*F*1-score	0.98	0.98	0.96	0.93	0.89	0.61
Support	357	357	357	357	357	315

Table 6: Comparison of various evaluation measures for non-COVID class.

Performance measure	VGG16	DenseNet121	MobileNet	Xception	NASNet	EfficientNet
Precision	0.96	0.99	0.94	0.95	0.84	0.63
Recall	1.00	0.96	0.99	0.89	0.96	0.95
*F*1-score	0.98	0.97	0.96	0.92	0.90	0.76
Support	334	334	334	334	334	307

altered using generative adversarial networks (GAN) augmentation techniques to generate new images. GAN consists of two neural models, and the goal of the method is to learn from the training data and develop new data with the same characteristics as the training data. The description of the augmented dataset is illustrated in Table 3.

3.4. Performance Measures. There are several methods to evaluate a model's performance. Accuracy, precision, recall, and *F*-score are the measures considered to estimate chest CT scan images. In the general confusion, a matrix is represented as in Table 4.

Precision—precision is defined as the ratio of correctly predicted positive cases, given in the following equation.

$$\text{Precision} = \frac{\text{TP}}{\text{TP} + \text{FP}}. \tag{1}$$

Recall—the ratio of accurately detected positive cases is the recall given in the following equation.

$$\text{Recall} = \frac{\text{TP}}{\text{TP} + \text{FN}}. \tag{2}$$

*F*1-score—the *F*1-score is the harmonic mean of precision and recall given in the following equation.

$$F1\ \text{score} = 2\,\text{x}\frac{\text{Precision x Recall}}{\text{Precision} + \text{Recall}}. \tag{3}$$

Accuracy: the percentage of correct predictions among the total number of predictions is called accuracy, specified in equation 4.

$$\text{Accuracy} = \frac{\text{TP} + \text{TN}}{\text{TP} + \text{FP} + \text{TN} + \text{FN}}. \tag{4}$$

Precision, recall, *F*1-score, and support for the COVID class are illustrated in Table 5, and the non-COVID class is represented in Table 6.

From Table 5 and Table 6, it is clear that VGG16, with fewer convolution layers, could achieve the highest precision and *F*1-score than other models.

In practical implementation, the CNN models like Xception, MobileNet, DenseNet, NASNet, and EfficientNet have many more hyperparameters than the VGG16 model. Instead of having many hyperparameters, the VGG16 model supports 16 layers and focuses on the convolution layers of 3×3 filters in stride one and padding along with Max-pooling layers of 2x2 filters in stride 2. So the *F*1 score of VGG 16 performs better for both COVID and non-COVID classes compared to other CNN models[29 - 32].

4. Results and Discussion

The confusion matrix that lists the number of correct and wrong classification model predictions was also calculated. The confusion matrix obtained for all CNN models is illustrated in Figure 8.

By the analysis, VGG16 gives better results as the number of parameters trained in VGG16 is less, and it takes less time to train the samples. So, it is better than other CNN models.

The examination of the epoch versus loss and epoch versus accuracy in the suggested model is shown by graphs. The loss gained after each epoch is represented in the epoch versus loss graph. As the number of epochs increases, the loss values are reduced, as shown in Figure 9.

The epoch is the number of times the data has been cycled over. The error over the training set, usually in terms of regression or classification, is called loss. Increasing the number of epochs, on the other hand, improves the model's accuracy, which is shown in Figure 10. This shows that the model is effectively learning the provided input with each epoch.

Table 7 shows the difference between the accuracy obtained from the existing system and the proposed system. The results show that the deep learning CNN models give better accuracies for lung CT scan images when compared to the accuracies of lung X-ray images as specified in [7].

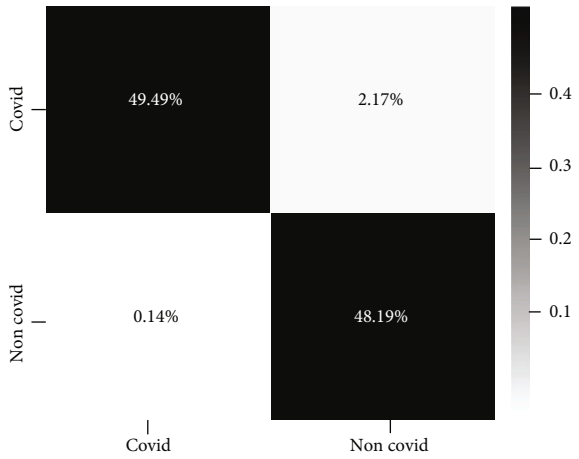

(a) VGG16 outperforms other models, predicting 342 correctly identified COVID images and 333 correctly identified non-COVID images out of 691 samples

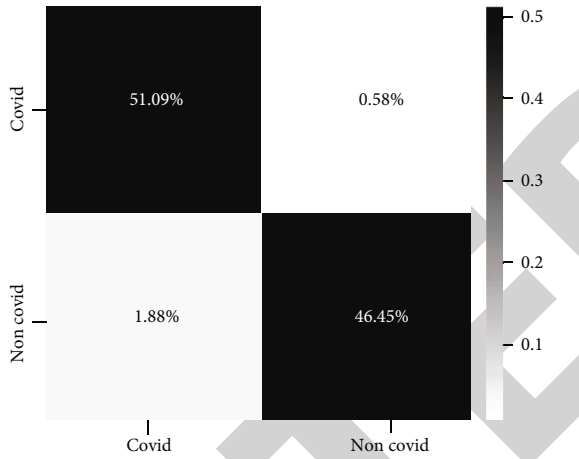

(b) DenseNet121 has more layers, which reduces parameter efficiency and makes it more prone to overfitting. This model predicts 353 correctly identified COVID images and 321 correctly identified non-COVID images out of 691 samples

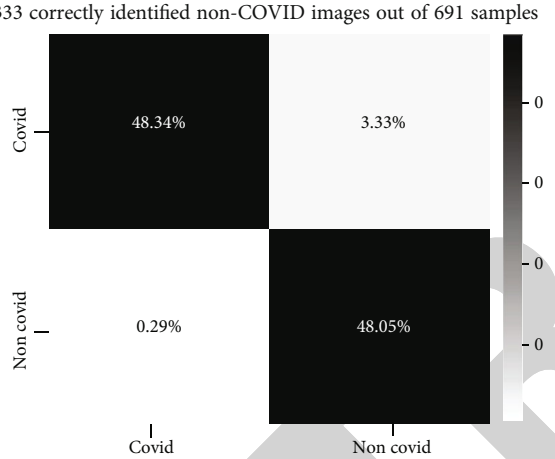

(c) Even though MobileNet is faster in performance, it gives less accuracy compared to the VGG16 model. The MobileNet model predicts 334 correctly identified COVID images and 332 correctly identified non-COVID images

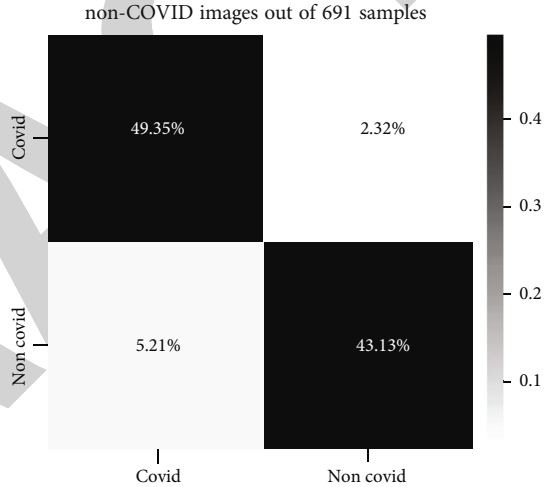

(d) The number of parameters trained is larger compared to other models. Xception model predicts 341 correctly identified COVID images and 298 correctly identified non-COVID images

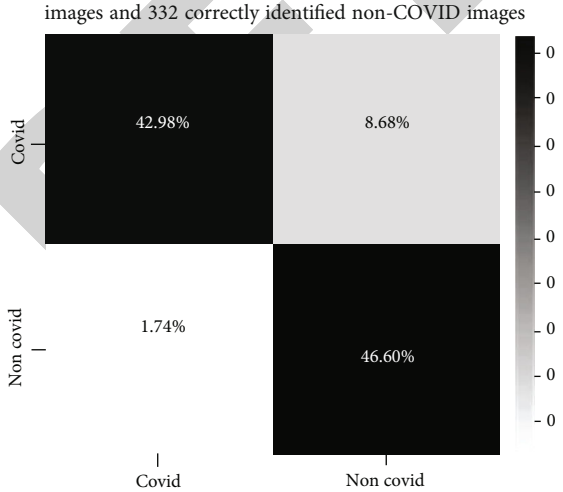

(e) The NASNet architecture predicts 297 correct COVID images and 322 correct non-COVID images

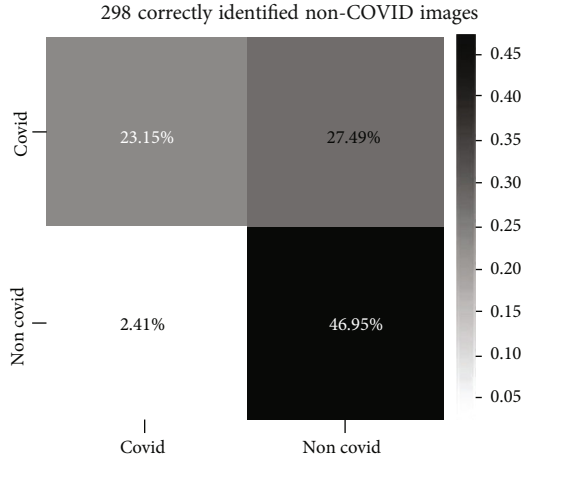

(f) EfficientNet predicts 144 correctly identified COVID images and 292 correctly identified non-COVID images with lower accuracy

Figure 8: Confusion matrix of CNN models.

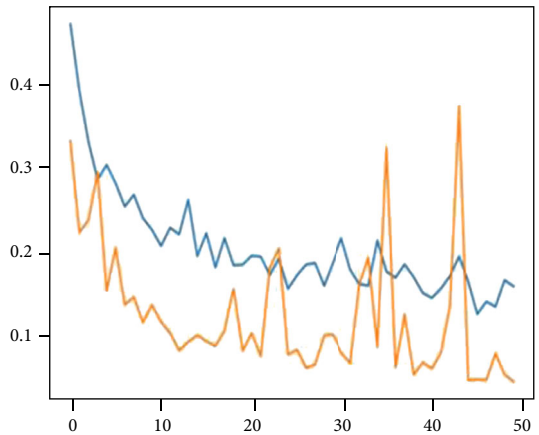

(a) A loss results in a bad prediction. Both the training loss and validation loss curves decrease to zero. So the VGG16 model is more perfectly predicted than other models

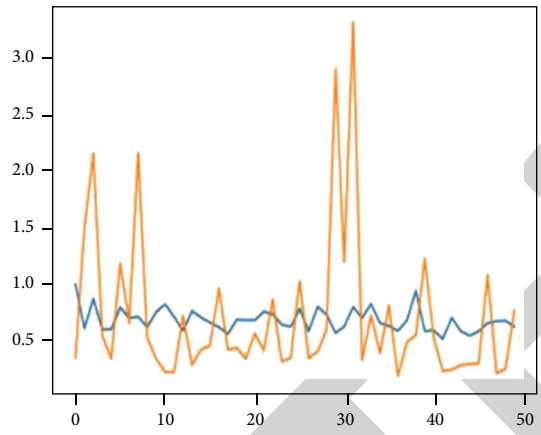

(b) In the DenseNet121 architecture, the training curve is stable with a lower rate, while the validation curve simultaneously increases and decreases

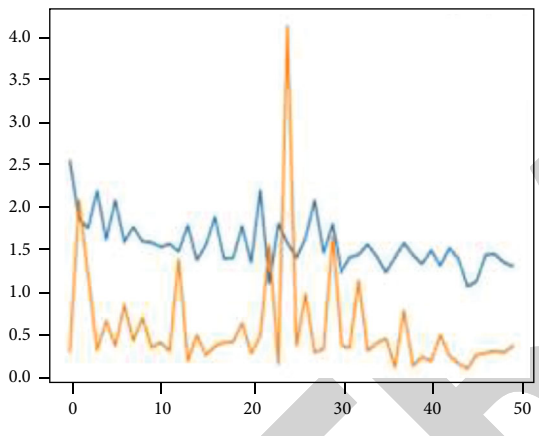

(c) The training and validation curves both decrease in the MobileNet architecture. The loss is at zero, so the model predicted it correctly

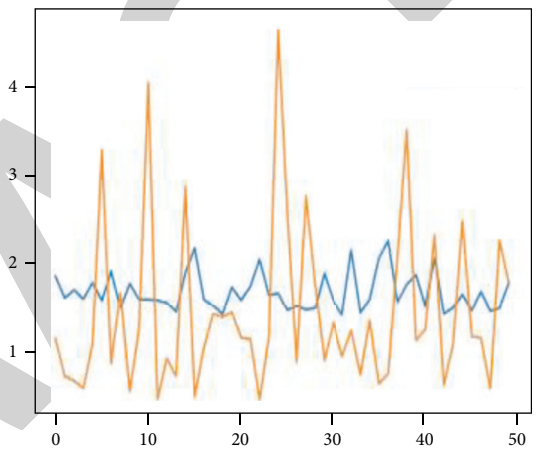

(d) In the Xception architecture, the training curve is stable with a lower rate, and the validation curve increases and decreases simultaneously, until finally the loss is decreased to zero

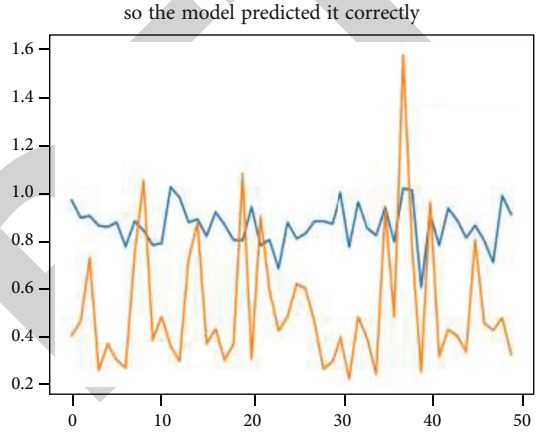

(e) In the NASNet architecture, the training curve is stable, with a lower rate, and the validation curve increases and decreases simultaneously. Finally, the loss is decreased to zero, and the model is predicted correctly

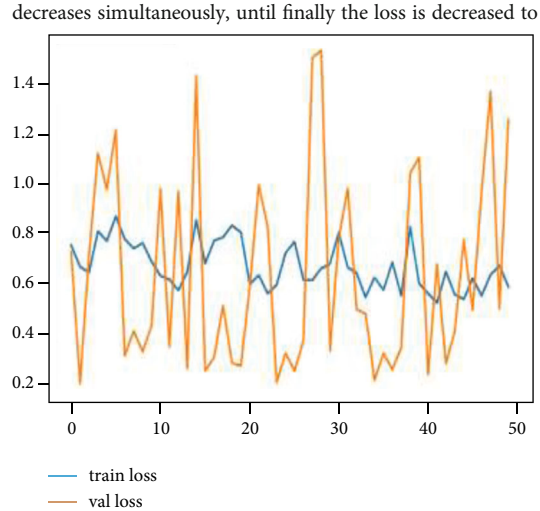

(f) In the EfficientNet architecture, the training curve is stable with a lower rate, and the validation curve increases and decreases simultaneously. Finally, the model predicts the correct outcome

Figure 9: Epochs versus loss graph for all CNN models.

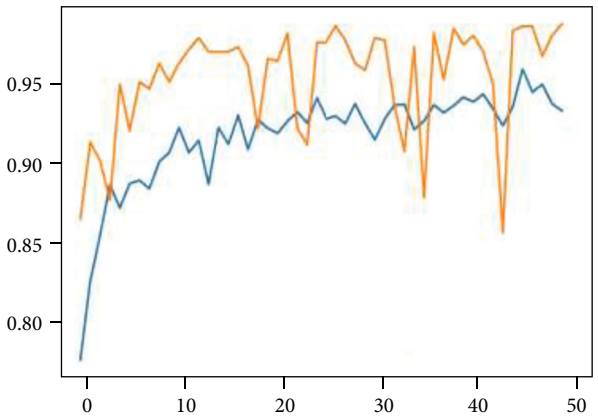

(a) The VGG16 architecture improves both training and validation accuracy. So the VGG16 model performed well. The validation accuracy is greater than the training accuracy, so the model is overfit

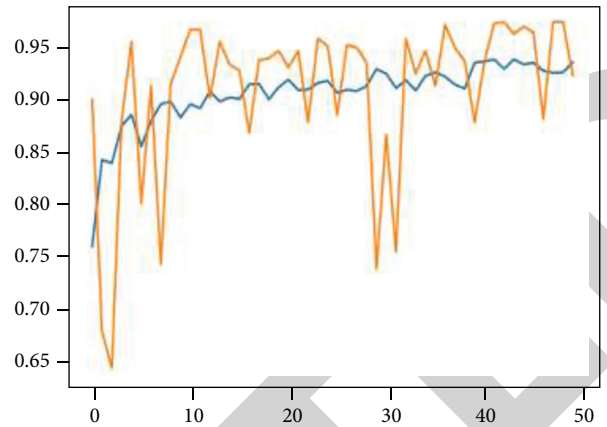

(b) In the DenseNet121 architecture, the training accuracy is stable while the validation accuracy increases and decreases at the same time, resulting in a well-performing model

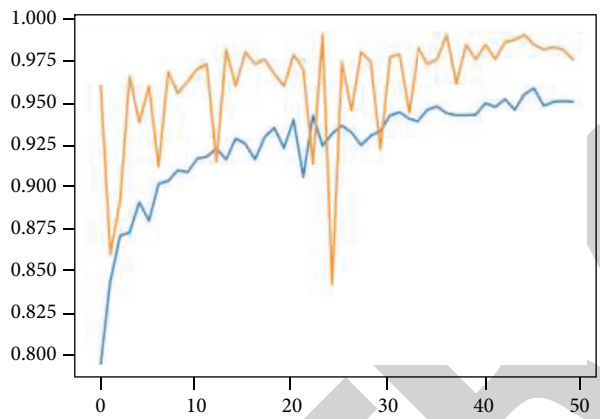

(c) The MobileNet architecture improves both training and validation accuracy. The validation accuracy is greater than the training accuracy, so the model is overfitted

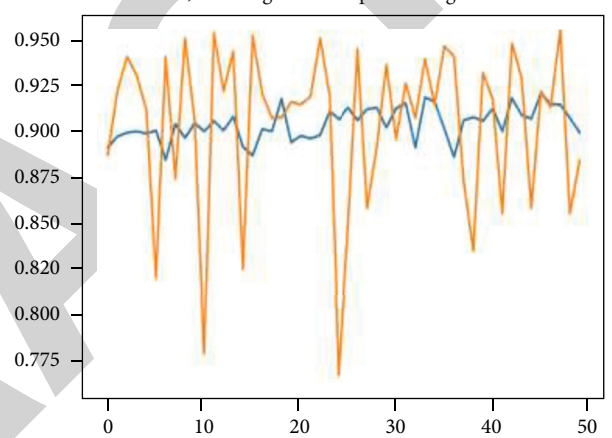

(d) In the Xception architecture, the training accuracy is stable, and the validation accuracy increases and decreases simultaneously

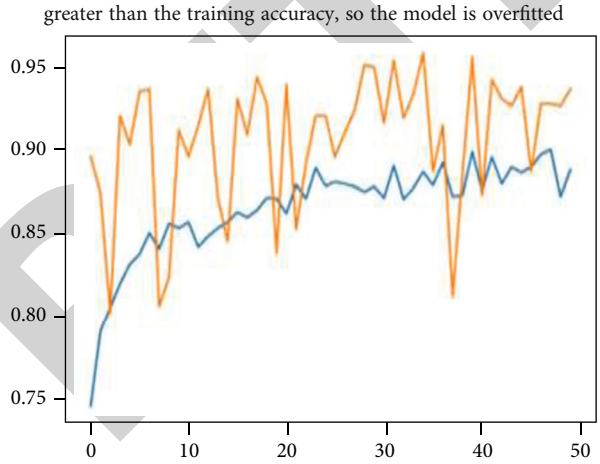

(e) The NASNet architecture improves both training and validation accuracy. The validation accuracy is greater than the training accuracy, so the model is overfitted

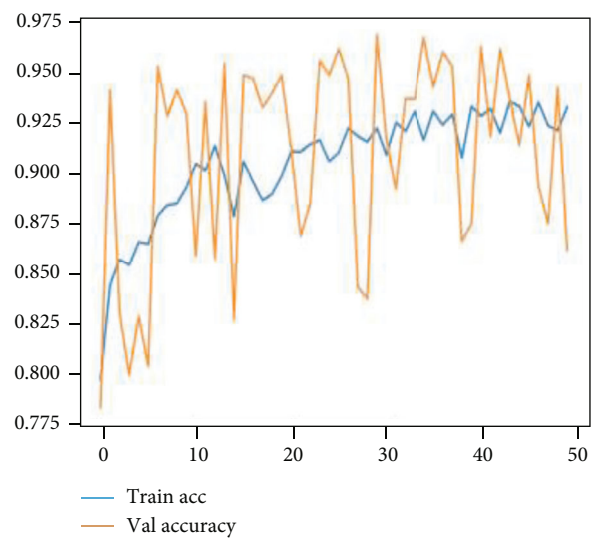

(f) In the EfficientNet architecture, training and validation accuracy increase and decrease at the same time

Figure 10: Epochs versus accuracy graph for all CNN models.

Table 7: Comparison of existing system and proposed system.

Models	Existing system	Proposed system
VGG16	79.01%	97.68%
Xception	88.03%	92.47%
DenseNet21	89.96%	97.53%
NASNet	85.05%	89.51%
EfficientNet	93.48%	80.19%

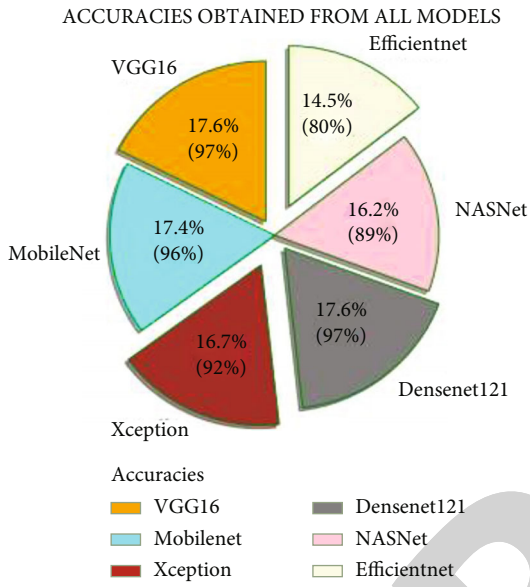

Figure 11: Accuracies obtained for all CNN models.

The accuracies attained for all CNN models are shown in Figure 11. The VGG16 model has been trained with 138 million parameters, which performs better than other CNN models. The 138 billion parameters available in VGG16 make this model a slower one, but this model is the best one to produce better accuracy. The VGG16 model gives an accuracy of 97%, the MobileNet model gives an accuracy of 96%, the Xception model gives an accuracy of 92%, the DenseNet121 model gives an accuracy of 97%, NASNet gives an accuracy of 89%, and EfficientNet gives an accuracy of 89%.

5. Conclusion

By analyzing CT scan images, the paper identifies widespread and best deep learning architectures to identify COVID-19 in suspected patients. Deep learning methods have been proposed to provide efficient results by evaluating ideas to detect the existence of COVID in an individual. High-performance deep learning architectures like VGG16, DenseNet, MobileNet, Xception, NASNet, and EfficientNet are used in this proposed work. Since the CT scan images collected by Kaggle contain fewer images, data augmentation is performed to get more pictures. The models performed well by applying preprocessing to the samples and performing CNN architectures on the training and validation datasets. The models classify COVID and non-COVID images, and their accuracy is tested using a test dataset and gives expected accuracy for all models. The model's performance is evaluated using performance measures like precision, recall, and $F1$-score. The highest accuracy acquired among all the models is VGG16, at 97.68%. Hence, the proposed system identifies the VGG16 model as the best model to classify the given CT scan images into COVID and non-COVID. But the limitation of the proposed work is that it does not identify COVID-affected areas in the lungs. A further enhancement is required to detect the affected areas in the lungs by considering a large dataset and applying other preprocessing techniques and pretrained models in transfer learning to improve the accuracy of the proposed CNN models. Future work may also investigate yolo architecture to achieve better accuracy.

Data Availability

The data used to support the findings of this study are included in the article.

Conflicts of Interest

The authors declare that there is no conflict of interest regarding the publication of this article.

References

[1] S. Kumar, V. Maheshwari, J. Prabhu et al., "Social economic impact of COVID-19 outbreak in India," *International Journal of Pervasive Computing and Communications*, vol. 16, no. 4, pp. 309–319, 2020.

[2] M. Venkatasen, S. K. Mathivanan, P. Jayagopal et al., "Forecasting of the SARS-CoV-2 epidemic in India using SIR model, flatten curve and herd immunity," *Journal of Ambient Intelligence and Humanized Computing*, pp. 1–9, 2020.

[3] K. B. Priya, P. Rajendran, S. Kumar et al., "Pediatric and geriatric immunity network mobile computational model for COVID-19," *International Journal of Pervasive Computing and Communications*, vol. 16, no. 4, pp. 321–330, 2020.

[4] S. K. Mathivanan, P. Jayagopal, S. Ahmed et al., "Adoption of e-learning during lockdown in India," *International Journal of System Assurance Engineering and Management*, pp. 1–10, 2021.

[5] S. Rajendran and P. Jayagopal, "Accessing COVID19 epidemic outbreak in Tamilnadu and the impact of lockdown through epidemiological models and dynamic systems," *Measurement*, vol. 169, article 108432, 2021.

[6] A. Oulefki, S. Agaian, T. Trongtirakul, and A. Kassah Laouar, "Automatic COVID-19 lung infected region segmentation and measurement using CT- scans images," *Pattern Recognition*, vol. 114, article 107747, 2021.

[7] B. Nigam, A. Nigam, R. Jain, S. Dodia, N. Arora, and B. Annappa, "COVID-19: automatic detection from X-ray images by utilizing deep learning methods," *Expert Systems with Applications*, vol. 176, article 114883, 2021.

[8] S. Hassantabar, M. Ahmadi, and A. Sharifi, "Diagnosis and detection of infected tissue of COVID-19 patients based on lung X-ray image using convolutional neural network approaches," *Chaos, Solitons & Fractals*, vol. 140, article 110170, 2020.

Hindawi
Computational and Mathematical Methods in Medicine
Volume 2023, Article ID 9875676, 1 page
https://doi.org/10.1155/2023/9875676

Retraction

Retracted: An Improved Strategy for Task Scheduling in the Parallel Computational Alignment of Multiple Sequences

Computational and Mathematical Methods in Medicine

Received 27 June 2023; Accepted 27 June 2023; Published 28 June 2023

This article has been retracted by Hindawi following an investigation undertaken by the publisher [1]. This investigation has uncovered evidence of one or more of the following indicators of systematic manipulation of the publication process:

(1) Discrepancies in scope

(2) Discrepancies in the description of the research reported

(3) Discrepancies between the availability of data and the research described

(4) Inappropriate citations

(5) Incoherent, meaningless and/or irrelevant content included in the article

(6) Peer-review manipulation

The presence of these indicators undermines our confidence in the integrity of the article's content and we cannot, therefore, vouch for its reliability. Please note that this notice is intended solely to alert readers that the content of this article is unreliable. We have not investigated whether authors were aware of or involved in the systematic manipulation of the publication process.

Wiley and Hindawi regrets that the usual quality checks did not identify these issues before publication and have since put additional measures in place to safeguard research integrity.

We wish to credit our own Research Integrity and Research Publishing teams and anonymous and named external researchers and research integrity experts for contributing to this investigation.

The corresponding author, as the representative of all authors, has been given the opportunity to register their agreement or disagreement to this retraction. We have kept a record of any response received.

References

[1] M. Ishaq, A. Khan, M. M. Su'ud, M. M. Alam, J. I. Bangash, and A. Khan, "An Improved Strategy for Task Scheduling in the Parallel Computational Alignment of Multiple Sequences," *Computational and Mathematical Methods in Medicine*, vol. 2022, Article ID 8691646, 11 pages, 2022.

Hindawi
Computational and Mathematical Methods in Medicine
Volume 2022, Article ID 8691646, 11 pages
https://doi.org/10.1155/2022/8691646

Research Article

An Improved Strategy for Task Scheduling in the Parallel Computational Alignment of Multiple Sequences

Muhammad Ishaq,[1] **Asfandyar Khan**,[1] **Mazliham Mohd Su'ud**,[2] **Muhammad Mansoor Alam**,[3] **Javed Iqbal Bangash**,[1] **and Abdullah Khan**[1]

[1]*Department of Computer Science and IT, Agriculture University Peshawar, Pakistan*
[2]*Faculty of Computing and Informatics Multimedia University Malaysia, Malaysia*
[3]*Faculty of Computing, Riphah International University, Islamabad, Pakistan*

Correspondence should be addressed to Muhammad Ishaq; drmishaq@aup.edu.pk

Received 20 September 2021; Accepted 17 December 2021; Published 28 January 2022

Academic Editor: Muhammad Zubair Asghar

Task scheduling in parallel multiple sequence alignment (MSA) through improved dynamic programming optimization speeds up alignment processing. The increased importance of multiple matching sequences also needs the utilization of parallel processor systems. This dynamic algorithm proposes improved task scheduling in case of parallel MSA. Specifically, the alignment of several tertiary structured proteins is computationally complex than simple word-based MSA. Parallel task processing is computationally more efficient for protein-structured based superposition. The basic condition for the application of dynamic programming is also fulfilled, because the task scheduling problem has multiple possible solutions or options. Search space reduction for speedy processing of this algorithm is carried out through greedy strategy. Performance in terms of better results is ensured through computationally expensive recursive and iterative greedy approaches. Any optimal scheduling schemes show better performance in heterogeneous resources using CPU or GPU.

1. Introduction

This research paper proposes a novel dynamic programming-based task scheduling for parallel multiple sequence alignment (MSA). Further modifications in the proposed algorithms, like iterative, recursive, and greedy strategies, enhance the performance of scheduling in any parallel system. The application of dynamic programming optimization for task scheduling in case of parallelized multiple sequence alignment is preferred over other dynamic task scheduling approaches.

The complex issue of task scheduling in any parallel processor system has multiple possible solutions. The structure of a problem like task scheduling can be characterized, then, the application of dynamic programming is the best solution. Multiple alignment operation is divided into pairwise alignments or subparts. Pairwise alignments are interrelated, and the solution of one section can be used in another part of the same problem. The same problems here mean the complete multiple alignment. In this recursion, the intermediate results are stored in a matrix where they can be recalled later in the same program.

The storage of profile alignment or intermediate results is different in each individual computational multiple sequence alignment. In dynamic programming, the structure of an optimal solution is characterized, then, the value of an optimal solution is defined recursively, and then an optimal solution is constructed from the computed information. In any array of parallel workers, a master node collects the profile scores. Similarity of sequences is determined from the alignment score or computed information. In dynamic algorithm, the exponential cost is reduced to polynomial type, so more efficient than the ordinary divide and conquer algorithm in terms of time complexity. Dynamic programming application for any stated problem is diagrammatically shown in Figure 1.

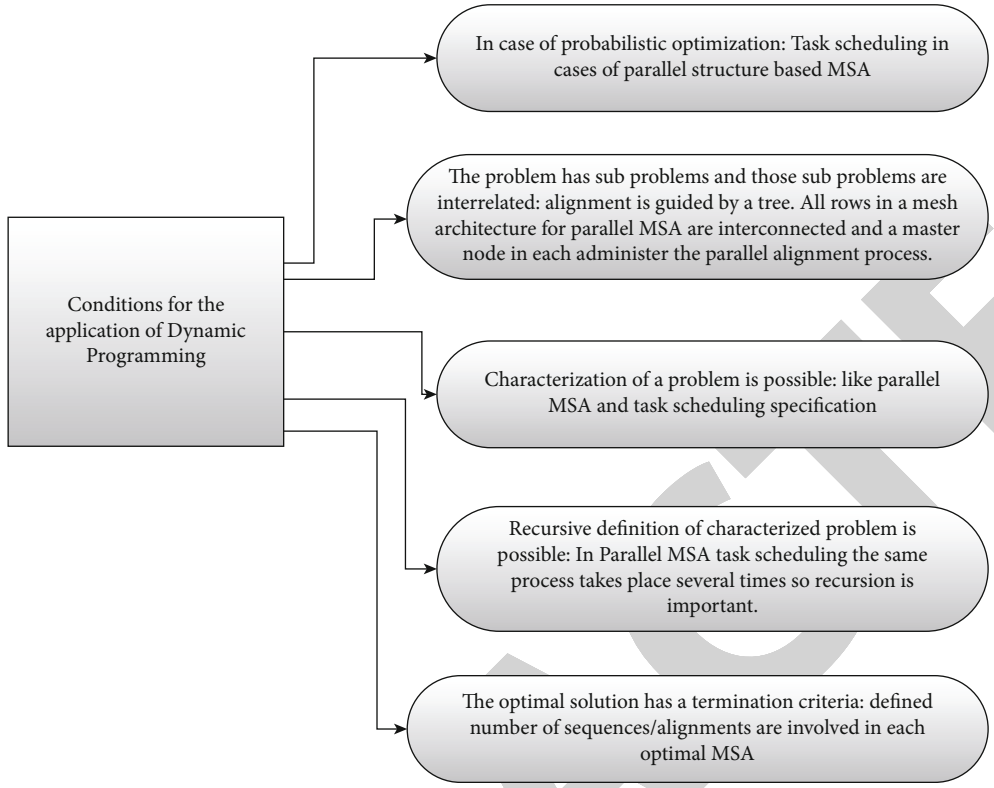

Figure 1: Diagrammatic illustration of the conditions for the application of dynamic programming optimization.

Homology modelling or potential orthologues and paralog description is also possible on the basis of protein structure comparison [1].

In a given protein structure, if the amino acid shows the interaction or association with other subunits and different atoms, then, it is called as quaternary protein structure.

Primary structure of proteins as visible in Jalview with PDB ID 4HHB. This structure is retrieved from Protein Data Bank (PDB). The primary structure is shown in Figure 2. The figure shows sample word-based sequences. Three dimensional protein structure matching is more accurate and comprehensive in terms of structure and function prediction but requires a lot of processing time.

There are many need-based word-based sequence alignment visualization tools. Figure 3 is the visualization of sample dataset. In Bioinformatics, the notion of tertiary structure is usually used for proteins rather than nucleic acids.

Greedy approach improves the efficiency of the dynamic algorithm by reducing the local maxima or the number of possible choices. Computationally complex recursive and iterative greedy techniques further enhance the application of this hybrid methodology.

2. Related Research Work in Parallel Processing of MSA

Remote homologue proteins improve sequence alignment by retrieving structural specifications from multiple structure alignment profiles. Sequences that share the same ancestry are called as homologs, and there are two kinds of homologs, orthologs and paralogs. In one approach, the score functions were combined with a systematic search algorithm. The score functions were based upon the sequence and structural information [2]. Sleater et al. proposed the MSA algorithm to be run in a parallelized fashion with the sequencing data distributed over a computer cluster or cloud-based server farm. The cloud computing technology improves the speed, quality, and capability of MSA. They introduce the next generation of cloud-based MSA algorithm [3]. Some researchers utilize BlueGene/Q or JUQUEEN supercomputing capability to evaluate the performance of parallel multiple sequence alignment. A parallel I/O interface for simultaneous and independent access to a single files collectively has been designed and verified [4]. Diaz and his coresearchers developed MC64-ClustalWP2 as a new implementation of ClustalW algorithm. They integrate a novel parallelized strategy that significantly increases the performance of alignment. The proposed method is useful when aligning long global sequences by using multicore architecture or with many processor cores [5]. Their hardware and software feature analysis were carried out for the exploitation and optimization of full potential in case of a parallelized system. To test the performance of their proposed algorithm, they use a hybrid computing system. The researchers counted manifold benefits of MC64-Clustal WP2 [6]. To improve the scalability of global sequence alignment, an MPI-based parallelization technique is proposed. In this method, a parallel waveform algorithm based on a chunk size transformation to handle large datasets with message passing model exposes high speed up and scales linearly with the increasing number of

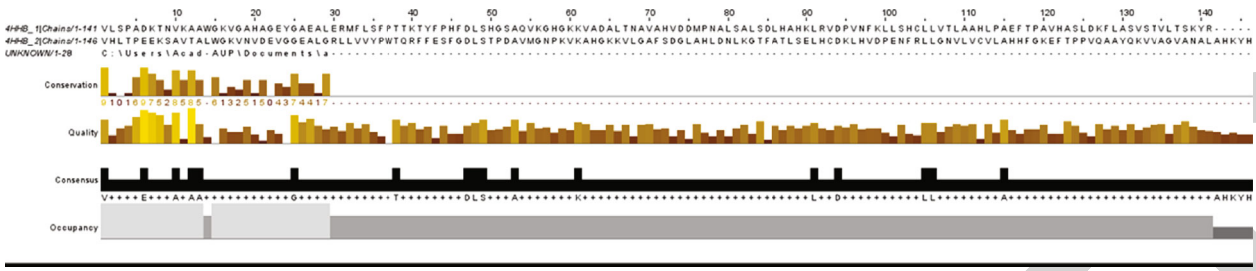

Figure 2: Primary structure of human deoxyhemoglobin (4HHB, PDB ID).

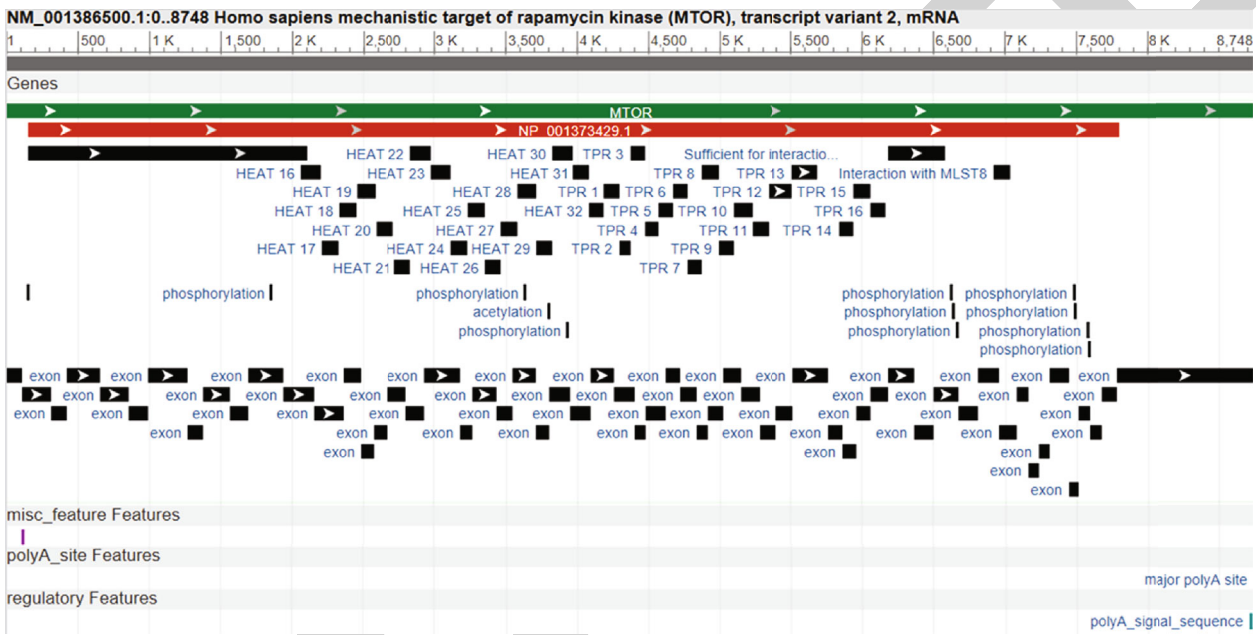

Figure 3: Dataset from GenBank: the linear nucleotide chain constitutes the primary structure of nucleic acid. Here, nucleotides are represented by their respective word-based symbols.

processes [7]. Some researchers examine different multicore machines by running a variety of MSA software [8]. In recent years, we observe various kinds of novel techniques for parallel MSA like artificial bee colony optimization [9]. R is extensively used for computational sequence alignment [10].

3. Problem Statement regarding Multiprocessor Task Scheduling through Dynamic Programming

In parallel MSA, we deal with the multiprocessor scheduling system. Assume that a set of tasks is to be executed by a parallel system with identical processors. For example, task *Xi* requires time *Ti* for execution.

Task here means a single pairwise word-based or structure-based alignment. In this case, the precedence of task execution is achieved by a tree or forest of tree data structure. Dynamic programming like genetic algorithm takes in to account all possible candidate solutions, which is not an efficient approach. Figure 4 shows the parallel processing of MSA, and each worker is responsible for one PWA at a time.

4. Application of Dynamic Programming for Task Scheduling Problem in MSA

In case of sequential or parallel processing of each pairwise alignment in MSA, a single task (pairwise alignment) is selected by each processor. Thus, an algorithm based upon dynamic programming can solve the task selection problem. If we have a set $S = \{x_1, x_2, x_3 \cdots .x_n\}$ of n tasks. Each pairwise alignment (x_i) has a starting time S_i and a finishing time F_i where $0 \leq S_i < F_i < \infty$. The tasks are sorted with respect to increasing finish time $F_1 < F_2 < F_n$. For scheduling tasks during MSA, the profile makes require the maximum size subset of closely related sequences. The aligned sequences make a profile. Pairwise alignments (tasks) cannot use a given processor at a time. Each task has a corresponding time interval $T_j = S_j, F_j$ during which the processor is busy in executing the task. For a given two tasks x_i and x_j, the interval T_i and T_j do not overlap, i.e., $S_i \geq F_j \text{or} S_j < F_i$.

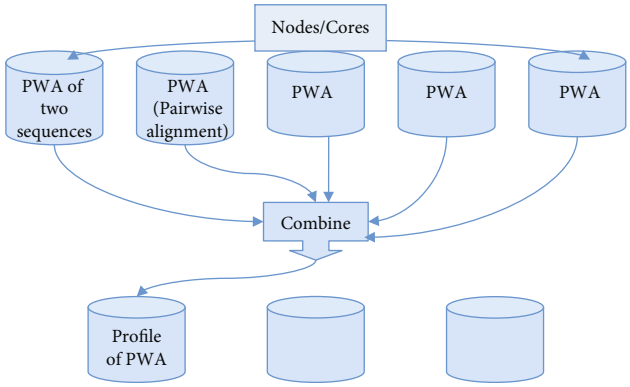

Figure 4: Parallel processing of multiple sequence alignment.

So all tasks for a given processor must be compatible in terms of their ordered time interval.

If X_{ij} is the set of all tasks a_k in X which is started when a_i finishes and finish before task a_j starts. $X_{ij} = \{a_k \forall X : F_i \leq S_k < F_k \leq S_j\}$ here $F_i$and F_k denote finish time of a_i and a_k.

$S_k$and S_j represent start time of tasks a_k and a_j. If $i = 1$ and $j = n$ then X_{ij} exclude task a_1 and a_n.

For this purpose, we can define fictitious tasks $a_0$and a_{n+1} such that the finish time of a_0 is $f_0 = 0$ and the start time of a_{n+1} is $S_{n+1} = \infty$. So $0 \leq i, j \leq n + 1$ and $X_{0\,n+1}$ include all tasks including a_1 and a_n.

Based upon a_k task X_{ij} can be divided into X_{ik} and X_{kj}. All X_{ik} tasks start after a_i finishes and finish execution before a_k starts execution. Similarly, all X_{kj} tasks start execution after a_k finishes and finish before a_j starts. X_{ik} and X_{kj} are subsets of X_{ij}, but $X_{ij} \neq X_{ik} \cup X_{kj}$ or $X_{ij} = X_{ik} \cup X_{kj} \cup a_k$ because a_k does not exist in both subsets.

A sample parallel web-based reference tree generation of 38 RefSeq Proteins is shown in Figure 5.

Also, the solution of X_{ij} can also be demonstrated as

$$Sol(X_{ij}) = Sol(X_{ik}) \cup Sol(X_{kj}) \cup (a_k). \quad (1)$$

If $Sol(X_{ij})$ is an optimal multiple sequence alignment, then, $Sol(X_{ik})$ and $Sol(X_{kj})$ are also optimal. If we have another solution $Sol(X_{ik})'$ for X_{ik}, and we replace $Sol(X_{ik})$ in $Sol(X_{ij})$ with $Sol(X_{ik})'$ then $Sol(X_{ij})'$ has more tasks than $Sol(X_{ij})$.So $Sol(X_{ij})$ is not optimal, and we encounter a contradiction so it is proved that $Sol(X_{ik})$ and $Sol(X_{kj})$ are also optimal set of tasks.

5. Recursive Solution of the above Strategy

Recursion is computationally expensive. Assume that $L[i, j]$ is the number of tasks in a maximum size subset of mutually compatible tasks in X_{ij}. If $X_{ij} = \varnothing$; then, $L[i, j] = 0$. We know that $Sol(X_{ij}) = Sol(X_{ik}) \cup Sol(X_{kj}) \cup (a_k)$ so the recurrence relation for the problem is $L[i, j] = L[i, k] + L[k, j] + 1$. The recursive definition of $L[i, j]$ becomes

$$L[i,j] = \begin{cases} 0, & \text{if } X_{ij} = \varnothing, \\ \max \text{of} \{L[i,k] + L[k,j] + 1\}, & \text{if } X_{ij} \neq \varnothing, \\ i < k < j. & \end{cases} \quad (2)$$

There is no restriction of using sequence data sets. Sequences of any specific organism are not mandatory. Figure 6 shows the chloroplast protein sequences, and chloroplast is a green pigment in many plants, responsible for photosynthesis.

6. Greedy Approach and Its Implications for the Abovementioned Problem

Greedy approach increases the efficiency of the algorithm by reducing the search space and reduces the computational complexity. If we have nonempty subproblem Y_{ij} and c_m is any task in Y_{ij} with earliest finishing time. The optimal task or the task with the earliest finishing time (quick execution) is called c_m.

The following steps should be proved for the application of greedy solution in the abovementioned task scheduling algorithm. Greedy strategy takes into account the most optimal sequences to be aligned with a given MSA profile.

In the first step, the determination of the suboptimal structure of the problem is carried out. We have to prove that the task c_m can be used in some maximum size subset of mutually compatible tasks of Y_{ij}. And the subproblem Y_{im} is empty, so that choosing c_m leaves the subproblem Y_{mj} as the only one that may be nonempty.

First of all, we have to prove the second simple problem that Y_{im} is empty. Lets Y_{im} is nonempty, it means that there is some task a_k such that $f_i \leq S_k < f_k \leq s_m < f_m \Longrightarrow f_k < f_m$. So a_k is also in Y_{ij} but its finishing time is less than c_m which contradicts with our assumption that c_m has the earliest finishing time. We show that there is another task in Y_{ij} that has less finishing time than c_m, and it proves that Y_{im} is empty.

In any approach, the power of computational techniques in case of translation as shown in Figure 7 cannot be ignored.

For a greedy approach to be applied in this case, we have also to prove that c_m can be used in some maximum size subset of mutually compatible tasks of Y_{ij} or c_m is a member of one of the optimal solutions. Suppose that A_{ij} is a maximum size subset of mutually compatible tasks of Y_{ij}. Order A_{ij} is the monotonic increasing order of finishing time. Let a_k be the first activity in A_{ij} with respect to the finishing time. If $a_k = c_m$ then we already know that and prove it before that c_m is used in some maximal subset of mutually compatible tasks of Y_{ij}. Therefore, there is nothing to prove, and we show it that there must exist at least one of the optimal solutions which contain the task c_m. So c_m belongs to A_{ij} optimal solution.

If $a_k \neq c_m$; then, there must be some other optimal solution where task c_m exists. Lets suppose A'_{ij} is another optimal

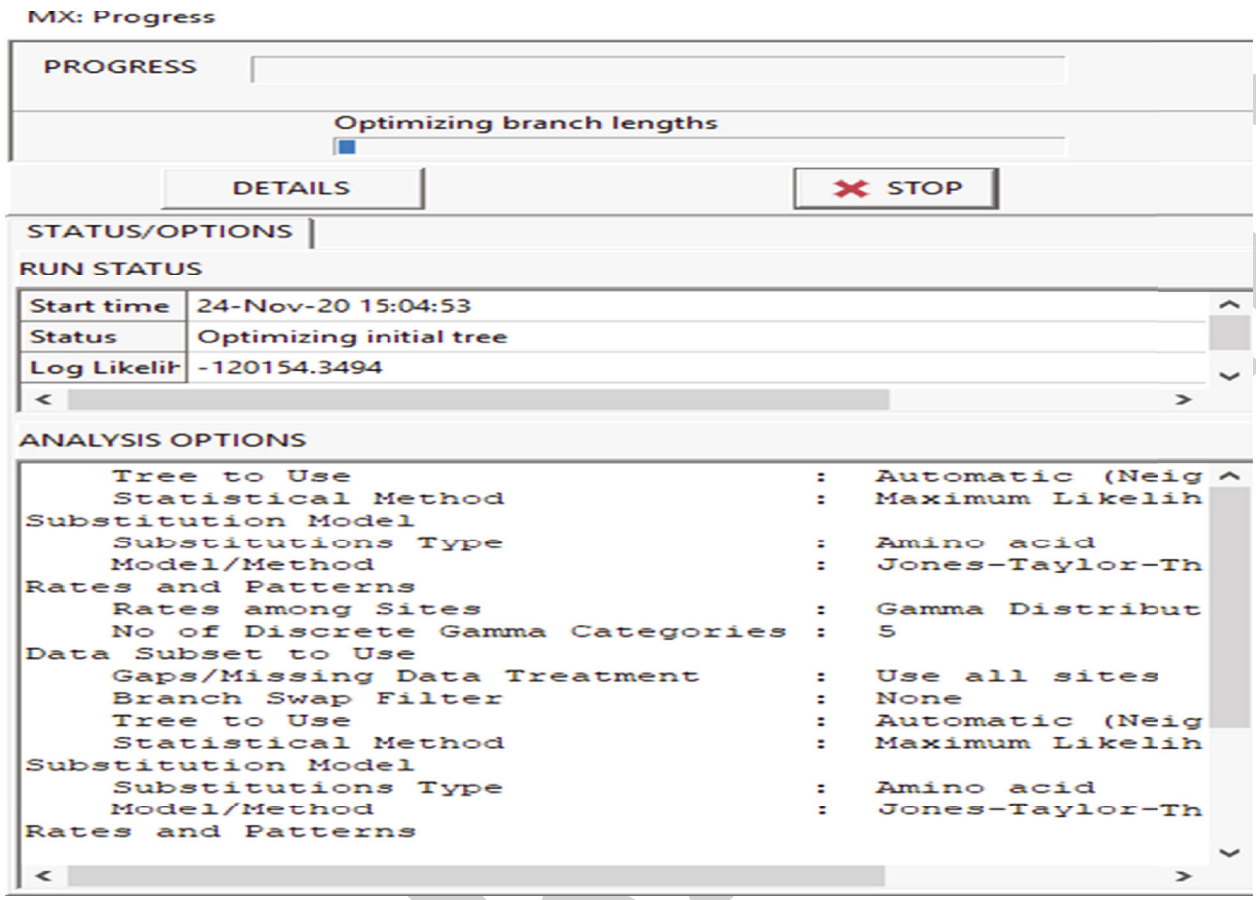

Figure 5: Sample parallel tree generation using estimated Gamma parameters for local aligned site rates.

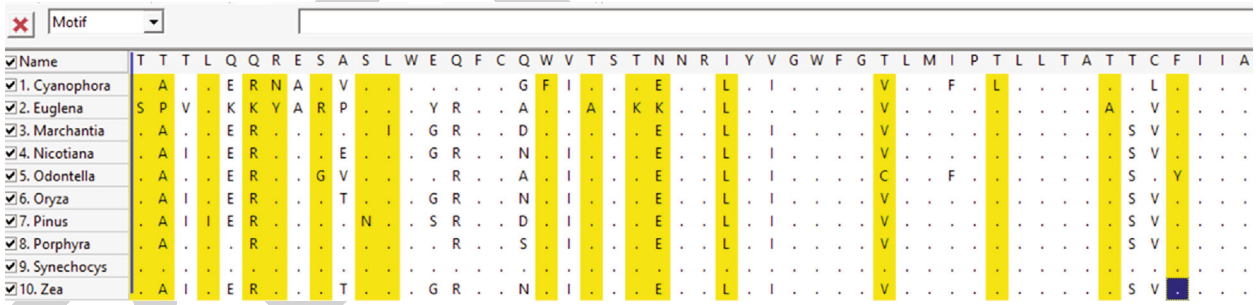

Figure 6: Chloroplast protein sequences of the given plant species.

solution and $A'_{ij} = A_{ij} \setminus \{a_k\} \cup \{c_m\}$. A_{ij} tasks are disjoint, and it is true for A'_{ij}. This statement means that c_m belongs to A'_{ij} because we negate c_m from A'_{ij}. As a_k is the first task in A_{ij} to finish and the finishing time of a_k is greater than the finishing time of $c_m f_m \leq f_k$. Here, f_m or f_k denotes finishing time of a_k or c_m. So it means that task c_m is included in optimal solution set A'_{ij} and A'_{ij} is the maximal subset of mutually compatible tasks of Y_{ij}. The number of tasks in A_{ij} and A'_{ij} is the same, and both have the same cardinality. We have proved that A'_{ij} is a maximal set of mutually compatible tasks. All tasks in A'_{ij} must be mutually compatible.

The conclusion of the above greedy approach is that task c_m belongs to Y_{mj} and $Y_{im} = \varnothing$. Therefore, it improves the efficiency of greedy approach in case of multitask scheduling algorithm compared to dynamic programming. In dynamic programming, there were two subproblems which were reduced to one by the greedy approach. The number of choices is $j - i - 1$ in dynamic programming, and there is only one choice in the greedy theorem.

Greedy algorithms do not work in some cases, i.e., in the cases of longest monotonically increasing subsequences. Suppose that we have a given sequence of <2, 3, 4, 13, 5, 6, 7>, and its longest common subsequence (LCS) is <2, 3, 4, 5, 6, 7>. If we solve this problem with greedy approach then

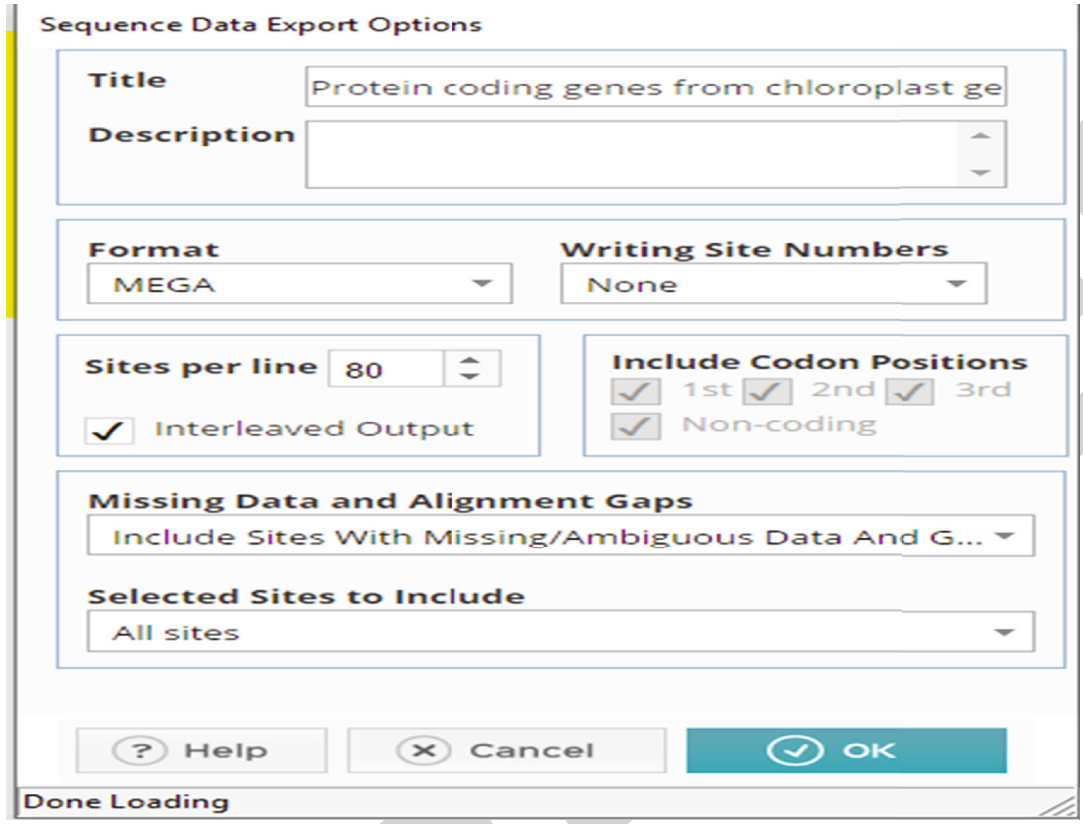

Figure 7: Other sequence data export formats available in the majority of web-based implementation tools.

its LCS is <2, 3, 4, 13> which is suboptimal. In greedy approach, the rest of three elements 13 cannot be chosen. Therefore <2, 3, 4, 13> is a monotonically increasing sequence, but it is not the longest monotonically increasing sequence. Figure 5 shows the export ability of candidate local optimal (sequences).

7. Structure of Recursive Greedy Algorithm for Task Scheduling

At each processor, the algorithm for task scheduling can be defined recursively. Recursive task selector $(s, f, i.j)$ where s is the set of tasks and f is the finishing time. The initial value of $i = 0$ and $j = n + 1$. We want to determine a task that belongs to the optimal solution. In the process of recursion, there will always be an optimal or greedy choice.

Recursive task selector$(s, f, i.j.)$.

Some computational alignment tools have unique ability to show translated proteins of given set of nucleic acid sequences as shown in Figure 8. Correct similarity index calculation of a given pairwise or multiple sequence alignment is principally related with gap and gap extension penalty as shown in Figure 9.

8. Structure of Iterative Greedy Algorithms for Task Scheduling in Parallel MSA

Iterative algorithms are more efficient than recursive algorithms. Recursive algorithms are computationally more expensive. The above recursive greedy algorithm can be expressed in an iterative manner. In task scheduling, we repeat the same process again and again, so iteration of the same process is computationally efficient. In this case, we have two tasks, s is set of all the tasks, and f is the set of the finishing time of all tasks.

Iterative task selector (s, f).

return $Sol(s)$ //The set of all tasks that are mutually compatible is retrieved. Irrespective of whether recursive, iterative or any other hybrid modification to this approach, gap penalties of PWA or MSA are also essential as shown in Figure 7.

9. Implementation Details and Results

Multiple sequence alignment is a tightly coupled processing task, so the application of map-reduce model is not valid in the parallelization of MSA. The task scheduling during parallelization of MSA is based upon a single program and multiple data (SPMD) style. Imagine that the mesh cluster as discussed above is a global matrix of $m * n$ dimensions, and individual processors own a different collection of rows in the matrix. In this case, all processors are local, so each dimension receives a general block distribution object. Figures 8 and 9 can explain the strategy.

MPI I/O over a subset of MPI cores can also be used to foster file reading in any parallel MSA data set [11].

Figure 10 shows the famous machine learning approach for estimated diversion time calculation. The proposed

1. $m \longleftarrow i+1$ //m to be the first task in X_{ij}
2. while $m < j$ and $s_m < f_i$ //find the first task (m) in X_{ij}. Here, s_m is the starting time of m.
3. do $m \longleftarrow m+1$ And f_i is the finishing time of i
4. if m < j
5. then
6. return$\{a_m\}$
7. U recursive task selector$(s, f, m.j)$ //repeat the same process from step 1 to
8. else retun ∅

Code 1

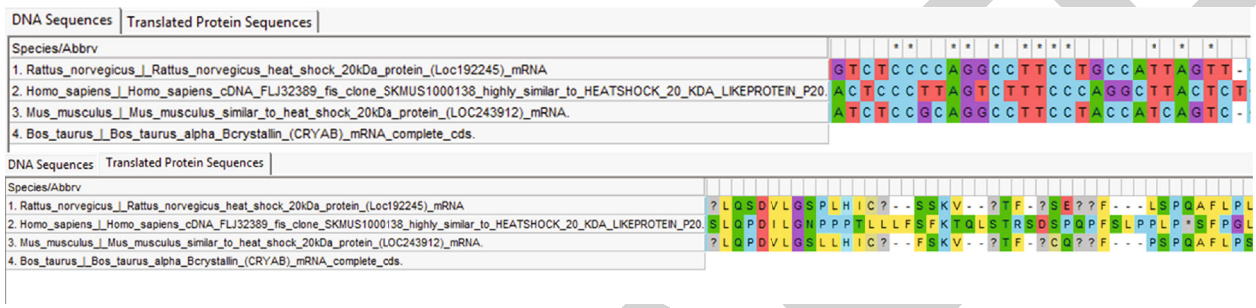

Figure 8: MSA of DNA sequences and the relevant translated proteins.

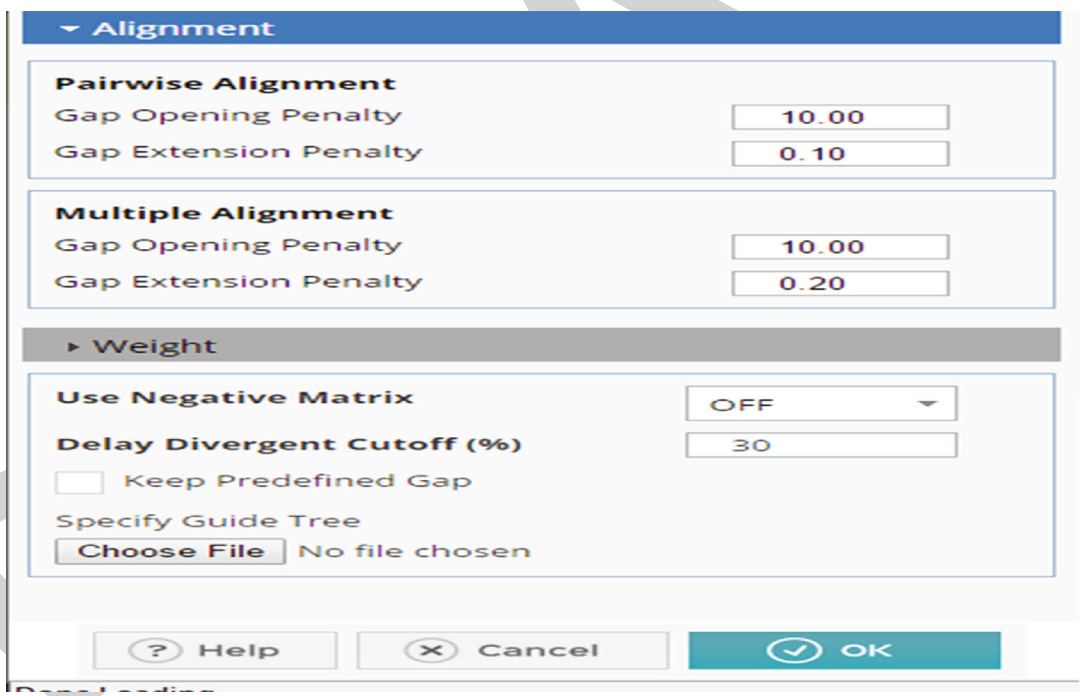

Figure 9: Pairwise and multiple alignment gap and gap extension penalty features.

scheduling algorithm using dynamic programming has O (nlogn) complexity. Each task or pairwise alignment (PWA) in the profile formation has a start and finish time. During the scheduling of MSA with multiple workers (processors), the goal is to overcome the overlap of any task (PWA) in any subset of the cluster mesh. The algorithm will also calculate the overall multiple alignment score.

In Python as a first step, a class task defines the start finish time with the calculated alignment score of each PWA. An iterative binary search is carried out to find the midpoint of any defined task with low and high indexes.

Substitution matrices are available in many libraries.

A variety of gap penalties can be opted. Some of the gap penalty functions available in Pymsa and other prominent matching libraries are as under.

Figure 11 is the conceptual design of mesh topology for parallel processing system. Some schedulers like the in-process use periodic jobs that use the builder pattern for

$n \longleftarrow$ length$[s]$ //compute the total number of tasks
$Sol(s) \longleftarrow \{a_1\}$ //sorting of all tasks according to their finishing time. The first task must be a $i \longleftarrow 1$ //initialize a variable i (ai is the part of solution) //part of our optimal solution.
for $m \longleftarrow 2$ to n
do if $s_m \geq f_i$ //here s_m is the starting time of m and f_i is the finishing time of i
then
Sol$(s) \longleftarrow$ Sol$(s) \cup \{a_m\}$
$i \longleftarrow m$ //we again select activity a_m

Code 2

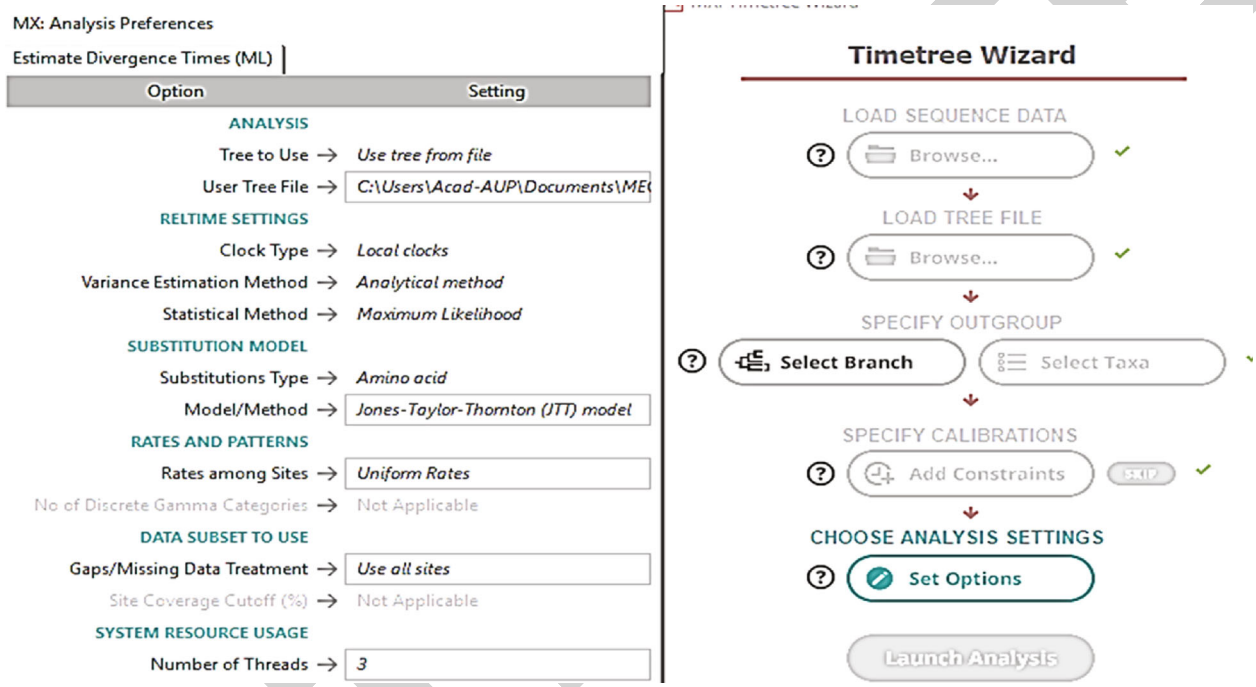

Figure 10: Estimated diversion time calculation for parallel nucleic acid and protein computational sequence alignment.

from pymsa.core.substitution_matrix import SubstitutionMatrix, FileMatrix, PAM250, Blosum62. Specific PAM and BLOSUM are also available for import from pyMSA.

Code 3

configuration. These schedulers let you run the respective Python library functions periodically. The periodic time intervals are predetermined using a simple, human-friendly syntax.

In any parallel processing system, the following libraries need to be imported for task scheduling in your work space. These libraries include collections, datetime, functions, logging, random, re, and time.

Using Python object-oriented paradigm capability, the ScheduledTask in this case has eight user-defined functions for different operations. The job class has the default scheduler. Typical operations in process scheduling are time interval definition, excuse or run operation, clear cancel job, and the definition of next run. The scheduler also manages free time.

The main features of any scheduler should be (but not limited to) an efficient and effective execution of operations. It means fail load distribution and reduction in time complexity. There are simple to use API for scheduling jobs for simulated and real test bids. These API are very lightweight having no external dependencies, excellent test coverage, and tested on all latest Python 3 versions.

Tasks are scheduled based upon their finish time. As a convention of dynamic programming, the solutions of subproblems are stored in a matrix. The matrix stores the score of PWA or task till all elements in the array. The store results are used again and again in the profile building process of MSA. The entries in the matrix are filled recursively. At each step of parallel MSA, the alignment score is stored in a matrix. Large alignment scores replace the previous low scoring matrix. Table 1 is only for three chloroplast protein sequences that can be extended to other species. Beside unique differences, the table shows identical and divergent sites.

```
gap_penalty_be_minus(),modify_the_gap_penalty(),gap_penalty_if_a_char_is_a_gap(),if_the_two_chars_are_gaps(),if_there_are_
no_gaps()
```

Code 4

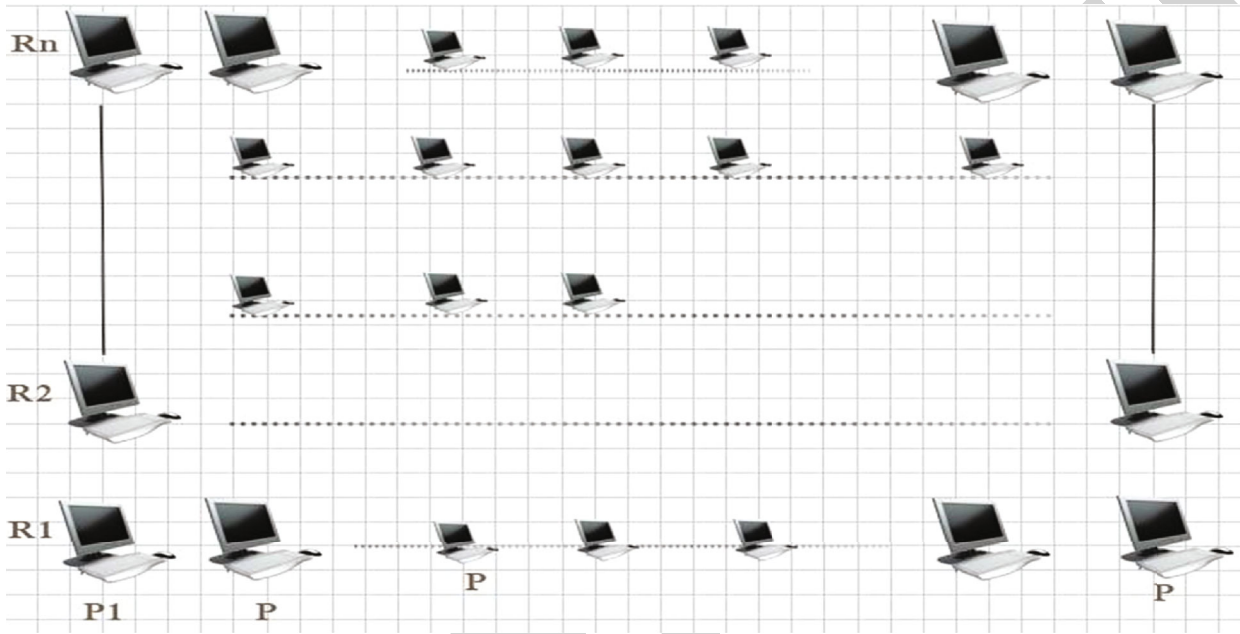

Figure 11: Mesh type topology in case of cluster for protein structure MSA. One node in each row is a master node [12].

Table 1: Similarity parameters in the computational alignment of three chloroplast protein sequences.

Results from the Tajima's test for 3 sequences	
Configuration	Count
Identical sites in all three sequences	6261
Divergent sites in all three sequences	1284
Unique differences in sequence A	1043
Unique differences in sequence B	1282
Unique differences in sequence C	603

In the first experiment, four tasks or workers get values. The time complexities remain less than many available optimal dynamic methods for this purpose.

Maximum likelihood estimate of Gamma parameter for site rates in case of protein sequences. The estimated value of the shape parameter for the discrete Gamma distribution is 0.5435.

Substitution pattern and rates were estimated under the Jones-Taylor-Thornton (1992) model (+G) [2]. A discrete Gamma distribution was used to model evolutionary differences among sites (5 categories, [+*G*]). Mean evolutionary rates in these categories were 0.03, 0.18, 0.50, 1.13, and 3.16 substitutions per site.

The amino acid frequencies are 7.69% (A), 5.11% (R), 4.25% (N), 5.13% (D), 2.03% (C), 4.11% (Q), 6.18% (E), 7.47% (G), 2.30% (H), 5.26% (I), 9.11% (L), 5.95% (K), 2.34% (M), 4.05% (F), 5.05% (P), 6.82% (S), 5.85% (T), 1.43% (W), 3.23% (Y), and 6.64% (V). For estimating ML values, a tree topology was automatically computed. The maximum Log likelihood for this computation was -119906.071. This analysis involved 10 amino acid sequences.

The number of amino acid substitutions per site from mean diversity calculations for the entire population is shown below. Analyses were conducted using the Poisson correction model. This analysis involved 2 amino acid sequences of the original chloroplast proteins. All ambiguous positions were removed for each sequence pair (pairwise deletion option). There were a total of 11039 positions in the final dataset.

Pseudomonas keratins multiple sequence alignment is shown in Figure 12. Optimal regions matching in any MSA depict the quality of algorithm.

Disorder comparison at each node of individual pairwise alignment is shown in Figure 13.

10. Discussion

Three dimensional comparisons of biological sequences involve the calculation of root mean square deviation, and parallelization of multiple protein 3D structure alignment reduces computational. This paper concludes a new technique for parallel MSA task scheduling using dynamic programming optimization in heterogeneous environments.

```
Analysis ====================
    Analysis= ====================
  Scope = Average of the overall population of sequences
    Estimate Variance = ====================
    Variance Estimation Method = None(Can be customized)
    Substitution Model= ====================
    Substitution Type = Amino acid
    Model/Method = Poisson model
    Rates and Patterns = ====================
    Rates among Sites = Uniform Rates
    Pattern among Lineages = Same (Homogeneous)
    Data Subset to Use= ====================
    Gaps/Missing Data Treatment = Pairwise deletion
    No. of Sites:11039 d:Estimate
```

Code 5

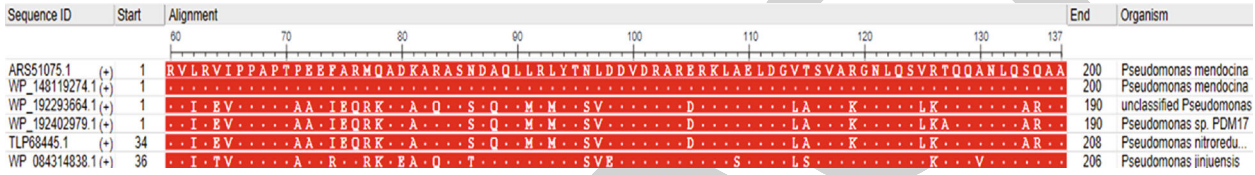

Figure 12: Graph showing results of six selected (NCBI GenBank) keratins (proteins) for MSA (word based).

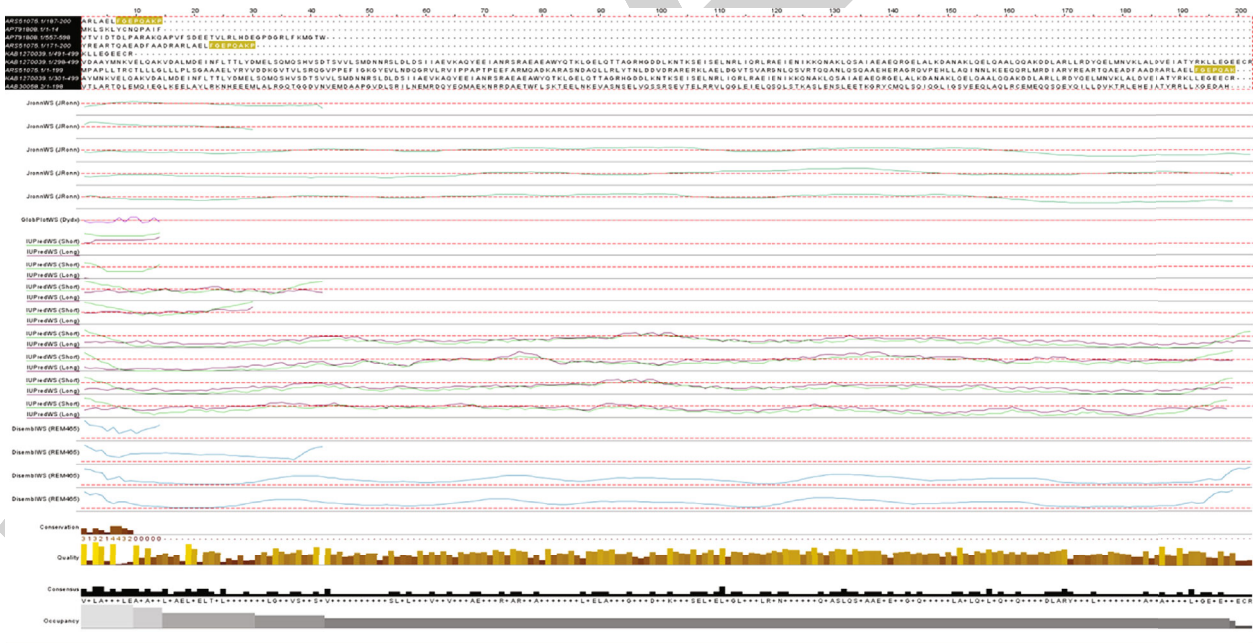

Figure 13: Graphs show pairwise aligned protein sequences from each node in parallel system with disorder comparison at the middle of image.

There are multiple choices during the scheduling of sequence matching tasks, so the application of dynamic programming (DP) is justified. DP is also used as a base method for computational sequence alignment. To further reduce the computational cost and to limit the number of candidate solutions, a greedy strategy is applied. Greedy approach does not take into account all candidate solutions in a single run.

Recursion and iteration solve the issue of optimal alignment score, but computationally expensive. In the era of fast processing machines, the greedy technique is not an efficient selection. Iteration is an efficient approach for optimal alignment and fair load distribution during parallel MSA task scheduling.

Data Availability

The data used to support the findings of this study are included within the article. Computational MSA for the

Hindawi
Computational and Mathematical Methods in Medicine
Volume 2023, Article ID 9897817, 1 page
https://doi.org/10.1155/2023/9897817

Retraction

Retracted: Energy Efficiency and Reliability Considerations in Wireless Body Area Networks: A Survey

Computational and Mathematical Methods in Medicine

Received 1 August 2023; Accepted 1 August 2023; Published 2 August 2023

This article has been retracted by Hindawi following an investigation undertaken by the publisher [1]. This investigation has uncovered evidence of one or more of the following indicators of systematic manipulation of the publication process:

(1) Discrepancies in scope

(2) Discrepancies in the description of the research reported

(3) Discrepancies between the availability of data and the research described

(4) Inappropriate citations

(5) Incoherent, meaningless and/or irrelevant content included in the article

(6) Peer-review manipulation

The presence of these indicators undermines our confidence in the integrity of the article's content and we cannot, therefore, vouch for its reliability. Please note that this notice is intended solely to alert readers that the content of this article is unreliable. We have not investigated whether authors were aware of or involved in the systematic manipulation of the publication process.

Wiley and Hindawi regrets that the usual quality checks did not identify these issues before publication and have since put additional measures in place to safeguard research integrity.

We wish to credit our own Research Integrity and Research Publishing teams and anonymous and named external researchers and research integrity experts for contributing to this investigation.

The corresponding author, as the representative of all authors, has been given the opportunity to register their agreement or disagreement to this retraction. We have kept a record of any response received.

References

[1] F. Ullah, M. Z. Khan, G. Mehmood, M. S. Qureshi, and M. Fayaz, "Energy Efficiency and Reliability Considerations in Wireless Body Area Networks: A Survey," *Computational and Mathematical Methods in Medicine*, vol. 2022, Article ID 1090131, 15 pages, 2022.

Hindawi
Computational and Mathematical Methods in Medicine
Volume 2022, Article ID 1090131, 15 pages
https://doi.org/10.1155/2022/1090131

Review Article

Energy Efficiency and Reliability Considerations in Wireless Body Area Networks: A Survey

Farman Ullah,[1] **M. Zahid Khan**,[1] **Gulzar Mehmood**,[1] **Muhammad Shuaib Qureshi**,[2] **and Muhammad Fayaz**[2]

[1]*Network Systems & Security Research Group (NSSRG), Department of Computer Science & Information Technology, University of Malakand, Chakdara, Dir (L), Khyber Pakhtunkhwa, Pakistan*
[2]*Department of Computer Science, School of Arts & Sciences, University of Central Asia, Kyrgyzstan*

Correspondence should be addressed to Muhammad Shuaib Qureshi; muhammad.qureshi@ucentralasia.org

Received 27 October 2021; Accepted 13 December 2021; Published 17 January 2022

Academic Editor: Shakeel Ahmad

In this paper, we have reviewed and presented a critical overview of "energy-efficient and reliable routing solutions" in the field of wireless body area networks (WBANs). In addition, we have theoretically analysed the importance of energy efficiency and reliability and how it affects the stability and lifetime of WBANs. WBAN is a type of wireless sensor network (WSN) that is unique, wherever energy-efficient operations are one of the prime challenges, because each sensor node operates on battery, and where an excessive amount of communication consumes more energy than perceiving. Moreover, timely and reliable data delivery is essential in all WBAN applications. Moreover, the most frequent types of energy-efficient routing protocols include crosslayer, thermal-aware, cluster-based, quality-of-service, and postural movement-based routing protocols. According to the literature review, clustering-based routing algorithms are the best choice for WBAhinwidth, and low memory WBAN, in terms of more computational overhead and complexity. Thus, the routing techniques used in WBAN should be capable of energy-efficient communication at desired reliability to ensure the improved stability period and network lifetime. Therefore, we have highlighted and critically analysed various performance issues of the existing "energy-efficient and reliable routing solutions" for WBANs. Furthermore, we identified and compiled a tabular representation of the reviewed solutions based on the most appropriate strategy and performance parameters for WBAN. Finally, concerning to reliability and energy efficiency in WBANs, we outlined a number of issues and challenges that needs further consideration while devising new solutions for clustered-based WBANs.

1. Introduction

In contemporary years, interest in uses of WBAN (wireless body area networks) and wearable technology has been remarkably boosted [1]. The number of patients, who need medical care by doctors/specialists are also increased as the increased of aging populations [2]. WBANs have been found to be the best and most cost-effective solutions for healthcare monitoring and related applications.

WBAN is a network of low-power, nonhostile, smart, and compact sensor devices that can exchange their data over wireless media and operate in, on, or around a human's body [2]. It was once used to assess physical characteristics and maintain a record of any abnormal or critical circumstances in the entity body [3]. Among other characteristics electrocardiography (ECG) measures heart electrical activity, electroencephalography (EEG) measures brain electrical activity, and electromyography (EMG) is a type of sensor for determining the electrical activity of muscles. The data is subsequently transferred to a control device, such as a sink or gateway/PDA, where it is aggregated and nonaggregated (personal-digital assistant), and the acquired data can subsequently be communicated to remote monitoring destinations for diagnostic purposes [4, 5]. "WBAN is a subset of wireless sensor network (WSN)" [6]. In terms of employment, WBAN is divided into two types: *implanted WBAN* and *wearable WBAN* [7]. In "*implanted WBAN*," the data from the implanted sensor nodes and the base station (BS)

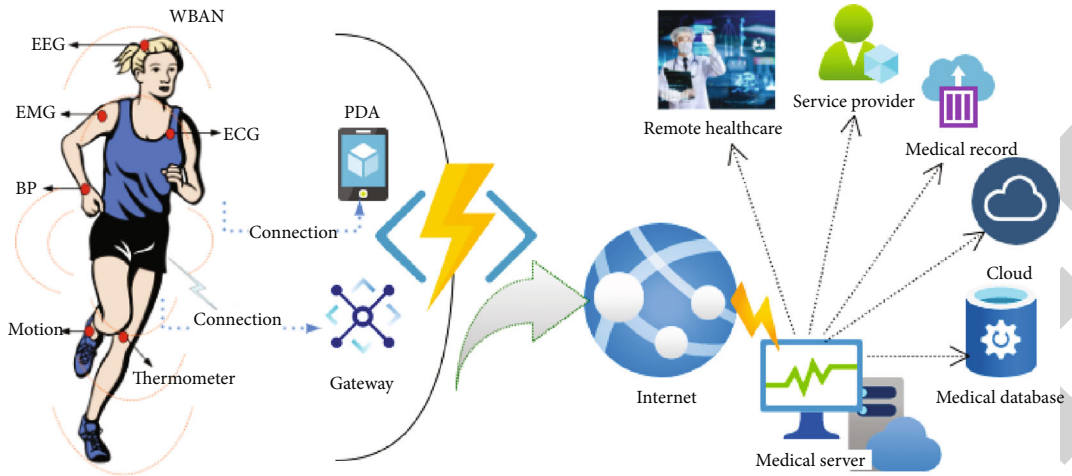

Figure 1: Generic structure of WBAN.

Table 1: Commonly used abbreviations.

WBAN	Wireless body area network
BS	Base station
ECG	Electrocardiography
WSN	Wireless sensor network
BER	Bit error rate
EMG	Electromyography
SAR	Specific absorption ratio
QoS	Quality of service

can be exchanged, while wearable devices and base stations (BS) can communicate their data with each other in "*wearable WBAN*" [8–10]. WBAN classifies each sensor into one of three categories: physiological, biokinetic, or environmental sensors [8]. Physiological sensors in WBANs, as depicted in Figure 1, are sensors that can assess corporeal phenomena/attributes such as temperature, blood pressure, and glucose monitoring. Biokinetic sensors are used to monitor and quantify human motion, such as calculating rotational angular rate and acceleration. Ambient sensors are any sensor that can measure environmental conditions, such as vibration, light, and pressure level. Environmental data is sometimes referred to as conservation data [11, 12].

Energy, processing, memory, and bandwidth are all limiting resources for WBAN. Instead of perceiving, sensor nodes waste a lot of energy while transferring data to each other. Furthermore, in most WBAN applications, changing or recharging batteries is not the best answer [13]. Because sensor nodes must be able to see and measure crucial active signs of human health, therefore, reliability is a critical concern. The key contribution of the proposed work is given as below:

(i) The proposed work effectively provides a critical analysis of energy efficiency and reliable solutions for WBANs

(ii) This paper identifies various design and performance parameters that need careful consideration while devising any solution for WBAN applications

(iii) Furthermore, research gaps are identified, and future directions are given to address these gaps in detail

(iv) Finally, this research will help researchers to advance their understanding of the area of WBAN and the related challenges and current solutions of energy efficiency and reliability in WBANs

A set of most commonly used abbreviations and notations is given in Table 1.

Section 2 explains the applications and architecture of WBAN. Section 3 shows details about various unique characteristics and features of WBAN, while Section 4 shows the motivations towards the concepts of WBAN. Section 5 explains the significance and importance of WBANs, while Section 6 explains the research issues and challenges in WBAN. Section 7 describes the related work of the proposed solutions in the area of WBAN, and Section 8 discusses the limitations in the existing work. Section 9 presents the conclusion.

2. Applications and Architecture of WBAN

WBANs have a wide range of uses, including medical and nonmedical applications. The basic purpose of all of these applications is to improve people's quality of life [14–16].

WBAN is a network that may be used to track personal health data such as heart rate and glucose levels, with the data being collected and stored on secure servers. Wearable and implantable medical applications are the two types of WBAN medical applications [2]. The following are some of the most well-known wearable medical applications of WBANs:

(i) Sleep staging: sleep is a regular physiological function and behaviour in our daily lives [17]. WBAN

Table 2: Key consideration of WBAN applications.

Application type	Sensor node	Type of sensor	Bandwidth (Hz)	Accuracy (bits)	Data rate	Duty cycle % per time	Power consumption	QoS	Privacy
In-body application	Glucose sensor	Strip-base	0-50	16	Few kbps	<1%	Very Low	Yes	High
	Pacemaker	Accelerometer	0-500	12	Few kbps	<1%	Low	Yes	High
	Endoscope capsule	A pill and contains a tiny camera	..	..	>2 mbps	<50%	Low	Yes	Medium
On-body medical application	ECG	Skin/chest electrodes	100-1000	12	192 kbps	<10%	Low	Yes	High
	EMG	Skin electrodes	0-10000	16	1.536 mbps	..	Low	..	..
	Temperature	Temperature probes or skin patch	0-1	8	56 kbps	..	Low	..	..
	SpO2	Pulse oximeter	..	..	32 kbps	<1%	Low	Yes	High
	Blood pressure	Arm cuff-based monitor	0-1	8	<10 bps	<1%	High	Yes	Medium
	Music for headsets	Sound	..	..	1.4 mbps	High	Very high	Yes	Low
On-body nonmedical application	Forgotten things monitor	Monitor	..	..	256 kbps	Medium	Low	No	Low
	Social networking	Mixed sensor	..	..	<200 kbps	<1%	Low	No	High

was used to track sleep disorders. Sleep deprivation has been linked to an increased risk of heart disease. Drowsiness at work and drowsy driving are also monitored because a big percentage of the population suffers from sleep disorders

(ii) Asthma: WBANs are utilised to monitor asthmatic patients since they can provide a real-time reaction to a surgeon by screening for sensitising substances in the air

(iii) In sports: WBAN analyses player's performance by measuring fatigue levels using glucose, temperature, and heart rate sensors. In fact, WBAN is utilised to scrutinise a player's training regimen, including motion capture and rehabilitation [18]

(iv) In a battlefield: soldiers are equipped with WBAN-based sensors that alert commanders to their motions, such as running, digging, and shooting

The phrase "implanted WBAN" refers to nodes that have been implanted into the human body and are most typically used in diabetes and cardiovascular monitoring. Similarly, WBAN sensors can sense cancer cells throughout the body and send a real-time reaction to healthcare user for diagnostic purposes [2].

WBAN is utilized in the following industries for nonmedical purposes.

(i) In the entertainment sector: in computer games and gesture detection, body sensors are used. These networks are used for real-time streaming, such as audio and video [2]. WBAN is used for amusement and social networking, as it includes an MP3 player, camera, and microphone

(ii) In a consumer electronics sector: body sensors are sensors that are affixed to a person's body and are used to send and communicate information to devices, i.e., a music player, headphones, a cell phone, and hearing aids [2]

(iii) Off-body: sensors are used to monitor and identify nonmedical situations in the home, such as fire and toxic gas, and then transfer this information to sensors linked to the body [2]

(iv) "In lifestyle sector": WBAN is a technology that can be used to recognise a person, recognise their individual data, and pinpoint their particular position [2]. It has been used to detect emotions such as fright, respiration rate, and pulse rate. It aids in the detection of posture and ambient intelligence

(v) In aerospace: WBAN used to employ a flying system to warn the pilot in the event of an emergency or other urgent circumstance by gathering data from many sensors [2]

The data requirements vary according to the different sorts of applications. When it comes to bit error rate (BER), the reliability of the conveyed data is based on the corrected data to be given to healthcare experts (BER). Applications with a low data rate have a high BER, while those with a high data rate have a lower BER [13]. The most

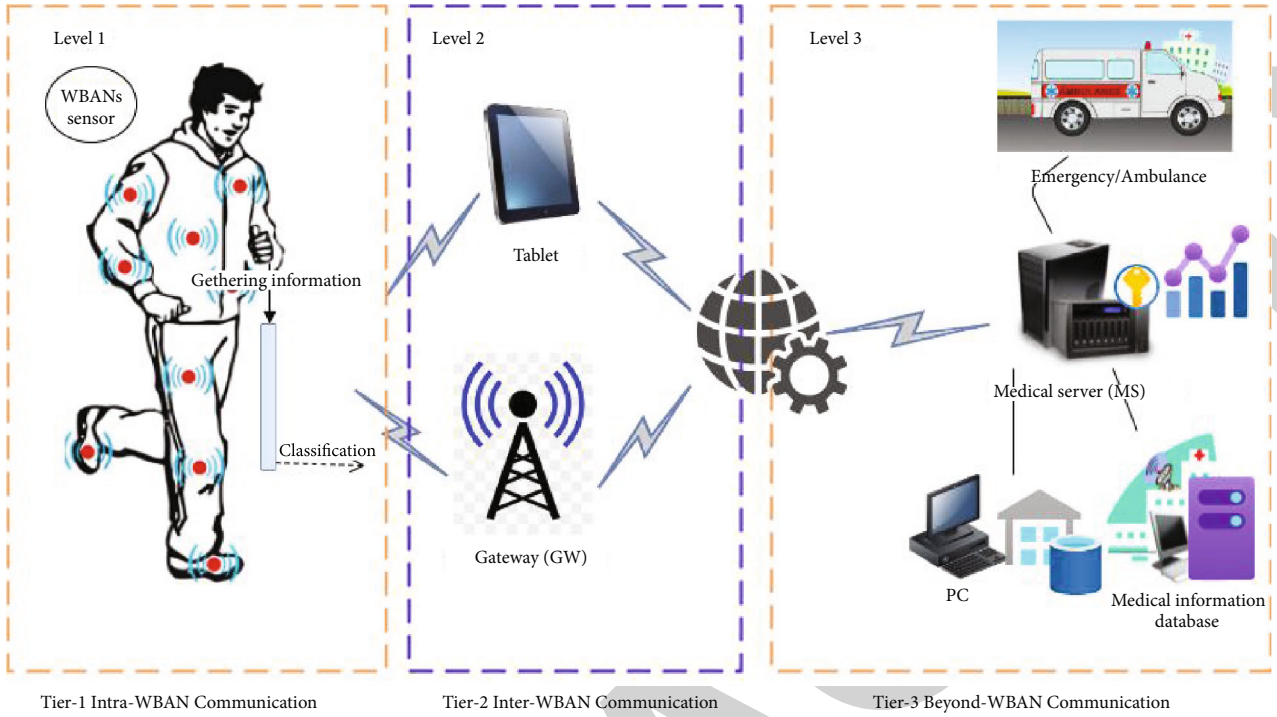

Figure 2: Communication architecture of WBAN.

important design concern, as discussed in the following sections, is reducing energy use. During sensing, processing, and communication, energy is consumed. Depending on utility, shape, and location, different applications and their basic requirements require different amounts of energy. Furthermore, providing QoS needs in medical healthcare apps is critical [19]. All these requirements associated with different categories of applications are tabulated in Table 2.

Architecture of WBAN: WBAN, from an architectural aspect, comprises of low-power sensing devices that are positioned inside or externally but are not confined to the body; in fact, WBAN has been employed in a wide range of applications, including entertainment, consumer electronics, and lifestyle. Almost every WBAN application has a three-tier architecture system as shown in Figure 2 [20].

Different sensors are utilised to analyse physiological parameters and their activities in, on, or around the human body. The data then communicated to the personal server (PS) in tier 1—also branded as intra-WBAN communication (PDA). Tier 2 communication is also recognized as inter-WBAN communication and occurs between a PS and access points. The goal of tier 2 communication is to join WBAN to a variety of systems that may be accessed easily in our daily lives, such as the Internet and cellphone networks. PDA or gateway was used as a link between layer 2 and this tier; i.e., in some applications from the Internet to the medical server in tier 3, known as beyond-WBAN communication (MS). One of the most important components is a database in tier 3 communication that stores user's profile and medical history. As a result, the emergency can be communicated to the patient or physicians via SMS (short message service) or the Internet. In WBAN communication, there are several different operational scenarios:

(i) Implant to implant

(ii) Implant to body surface

(iii) Body surface to body surface

(iv) Body surface to external

Requirements of WBANs: WBAN creation, however, is a difficult process due to the wide range of needs. The most essential IEEE TG6 requirements are discussed in this part, and some are discussed in the following sections [21]. We will go through some of the general criteria for various types of WBAN applications in this section. As indicated in Table 2, we examine bit rate, BER, and latency requirements in particular. Depending on the application and the type of data, different bit rates are necessary. BER is also discussed for a variety of applications in Table 3. Another crucial component is the end-to-end delay. Varied types of traffic have different priority levels, for example, emergency traffic requires a minimum wait.

3. Unique Characteristics of WBAN

WBANs, unlike WSNs and ad hoc networks, are a specific breed of WSN with their own set of characteristics. WBAN is typically placed in or on a human body and is utilised for healthcare purposes. As a result, design issues such as compactness, compatibility, and inconspicuous deployment are critical. The following are some of the distinctive qualities that present WBAN researchers with new technical challenges:

(i) Architecture of node: based on its functionality, implementation, and role, each device/node in the

WBAN can be classified into three groups [8]. Nodes are classified as personal devices (PDs), sensors, or actuators based on their functionality [2]. Nodes can be categorised as implant devices, body surface devices, or external devices depending on how they are implemented. Each node in the WBAN is classified as a coordinator/controller, end node, or relay node, depending on their function. Maintaining battery power at the sensor node is crucial since each sensor device used in WBAN must be noninvasive, compact, and pleasant, as well as invisible [22]

(ii) Node temperature increase: because of communication radiations and circuitry power loss, the temperature of sensor nodes in WBAN may rise [23]. As a result, SAR (specific absorption ratio) must be considered when developing any WBAN application [24]

(iii) Node density: the total number of devices in WBAN might range from a few sensors or actuators to tens of thousands of sensors or actuators. Unlike WSN, WBAN has a low density, sparsely placed nodes, and decreased node redundancy [25]

(iv) Reliability and security: in WBAN, each sensor-device may sense and monitor a patient's personal and important data [10]. As a result, it is necessary for monitoring data to be provided in a fast, accurate, and secure manner

(v) Mobility: the same pattern of mobility will be share by WBAN nodes as the user may move around [25]. Design consideration contains the packaging and placement of sensor nodes

(vi) Cost-efficient: sensors and equipment utilised in WBAN are inexpensive and readily available in consumer electronics applications [26]

(vii) Topology of the network: there are two types of network topologies utilised in resource-constrained WBAN: star and hybrid mesh topology [27]. However, it is extremely desirable to create or build a reduced topology in all WBAN applications in order to save energy while maintaining crucial network characteristics such as connection and coverage

4. Motivations towards the Concepts of WBAN

In the medical area, WBAN is a critical tool for patients who do not have access to doctors or who are experiencing difficulties owing to age, time, distance, hospitalisation costs, injuries, or disability. The majority of hospitals are also experiencing difficulties due to a lack of doctors. The following are some of them:

(i) For distance doctors who are unable to keep track of their patients

Table 3: Requirement of WBANs.

Applications	Bit rate	BER	Delay
Drug delivery	<16 kbps	$<10^{-10}$	<250 ms
ECG	3 kbps	$<10^{-10}$	<250 ms
EMG	120 kbps	$<10^{-10}$	<250 ms
Glucose level monitoring	<1 mbps	$<10^{-10}$	<250 ms
Temperature	120 bps 56 kbps	$<10^{-10}$	<100 ms
SpO2	150 kbps	$<10^{-10}$	<100 ms
Audio streaming	1 mbps	$<10^{-10}$	<20 ms
Video streaming	<10 mbps	$<10^{-10}$	<100 ms
Voice	50-100 kbps	$<10^{-10}$	<100 ms

(ii) Physical visits to the doctor for patient monitoring take time

(iii) Elders are unable to make timely visits to doctor's clinic

(iv) It is tough for doctors to keep track of patients during casualties (e.g., wars, Earth Quick)

(v) Disabled persons have a difficult time going to the doctor

Other issues include a lack of doctors and suitable equipment due to limited or nonexistent funding, as well as a scarcity of educated professionals to diagnose patients' illnesses in hospitals.

5. Significance and Importance of WBAN

The concept of WBAN is one of the solutions to all of these issues. The WBAN is beneficial since patients may require assistance at times.

(i) Continuous patient monitoring

(ii) Lowering hospitalisation costs

(iii) Lowering the rate of untimely deaths

(iv) Improving health-care efficiency through communication technology

(v) Emerging medical care

(vi) Addressing transportation issues

(vii) Patient mobility issues

(viii) Emergency care for injuries sustained in traffic accidents

In hospitals, patient monitoring is the most important responsibility for doctors to conduct. The WBAN is a new technology that is being utilised to monitor patients. Doctors are sometimes unable to supervise patients because to a variety of factors, including casualties (wars, earth rapid assaults), patient's age, disability, and hospitalisation costs. The WBAN has been shown to be a good substitute for or precursor to patient monitoring at home. It has significant

advantages, particularly for the disabled and elderly patients who can be monitored remotely from anywhere at any time. The WBAN provides assistance to patients at no cost and without causing any mishaps. As a result, the usage of WBAN in the medical area for patient facilitation and monitoring has become popular.

6. Research Issues and Challenges in WBAN

WBAN's rapid growth has posed considerable hurdles for the research community despite the fact that it has a wide range of applications and benefits. Some of the most important WBAN research issues and difficulties are listed below.

6.1. Network Topology and Energy Holes. WBANs' overall performance and energy consumption are influenced by their network topology [6]. A good network architecture is critical in WBAN due to body postural movements, poor transmission range, energy restrictions, and the different type of sensor nodes. The majority of research placed important data monitoring sensor nodes near the BS (base station), which employs single-hop communication, whereas normal data monitoring nodes further away used multiple hop communication [28]. When the demand on a sensor node is spread unevenly, node's energy is quickly depleted, resulting in an energy hole [29]. In order to prevent energy and coverage gaps, the deployment of nodes is a vital step in the WBAN process. When there is a coverage hole, the area under that node's observations is unsensed. The problem of energy holes can be addressed by establishing efficient criteria for selecting forwarder/leader nodes and communication protocols.

6.2. Energy Efficiency and Network Lifetime. Each sensor in the WBAN system has its own energy, memory, computation, and bandwidth constraints [30]. When sensor nodes exchange their data with each other rather than sensing, a large amount of energy is consumed, and due to the nature and operational limits of the application, recharging or replacing batteries is neither practicable nor desirable [31, 32]. A forwarder (FWD) node's transmission energy can be computed as:

$$E_{\mathrm{Tx}}^{\mathrm{FWD}} = N.£.E_{\mathrm{Tx}}\left(P^{\backprime}, đ\right) + N.P^{\backprime}.£.E_{\mathrm{Tx\text{-}proc}}, \quad (1)$$

where "£" is the data aggregation factor, "N" denotes the total number of nodes,"P" indicates the size of the packet, and "$đ$" is the distance between forwarder nodes, and sink is denoted by this value. ETx and ERx indicate the transmitter and receiver's per-packet energy consumption expenses. ETx-proc and ERx-proc are the energy necessary to run the electrical circuits of the transmitter and receiver, respectively. So, in terms of total network lifespan, a forwarder node's total transmit energy may simply be calculated as:

$$E_{\mathrm{Tx}}^{\mathrm{NLT}} = \int^{t.} E_{\mathrm{Tx}}^{\mathrm{FWD}} dt. \quad (2)$$

As a result, in WBAN, energy-efficient solutions are required to increase network's stability period, and, as a result, its enhance network lifetime [33].

The total duration of network activities until an end node is depleted is referred to as the network lifetime [1, 28, 29]. The network lifetime is an essential feature that directly affects network's throughput. The total number of successfully received packets is referred to as network throughput. With a longer network lifetime, throughput is maximised [1, 28, 29].

6.3. Stability Period and Reliability of Network. The time between the start of operations and the expiry of the first sensor node is known as network's stability period [1, 29]. Network's stability period is critical since we require uninterrupted functioning for days, if not weeks, without operator intervention; thus, we must reduce communication. As a result, a load balancing strategy must be proposed in which the load is spread uniformly or evenly among sensor nodes.

The term "reliability" refers to the fact that health-care practitioners receive monitoring data in a timely and accurate manner [28, 34]. WBAN sensors must be capable of viewing and detecting essential active signs of human health; therefore, reliability is critical [35]. WBAN sensors must be capable of viewing and detecting essential active signs of human health; therefore, reliability is critical [2, 36].

6.4. Fault Tolerance. In WBAN, fault tolerance is also an important issue, which means that how to maintain network operations without faults and failures, and recover failed nodes. In a resource constrained WBANs, fault-tolerance is highly important because the deployed sensors are battery operated and have a limited battery lifetime [37]. Faults can be divided into three categories: i.e., faults were caused by nodes, sinks, or network issues [38]. The main causes of node failure are hardware (sensing, processing, memory, transceiver, and battery) and software (MAC, application, and routing) [39]. Network faults can arise because WBAN applications are responsible for the delivery of collecting information from sensor nodes towards the sink. Routes or link failures can occur due to the interference in the link or collision of packets. Fault tolerance in WBAN can be performed in a variety of ways; cooperative communication and network coding, on the other hand, are two effective strategies for improving network fault tolerance and reliability [40]. Similarly, fault tolerance techniques are necessary to overcome sink failure, because the sink is a critical component of WBAN, and its failure will result in the entire network failing.

6.5. Compatibility Issue and Unobtrusive Deployment. To provide plug and play collaboration among sensors and to promote a reliable exchange of information, WBAN system ensures tights or smooth data transmission across different standards [2] such as Bluetooth and ZigBee. Therefore, the challenge is to design a WBAN that requires an unassuming placement of sensors. Such solutions must be lightweight and nondisturbing, which would not change or disturb daily routine of the user [41].

6.6. Usability and Interoperability. WBANs must have the capability of self-configuration and self-maintenance because medical staff will set up WBAN instead of ICT (Information and Communication Technology) engineer. When a sensor is placed on the body and turned on, it must be able to connect a network and determine the structure of routes without interference from the outside world [36]. When new services are added to a network, it should be capable of reconfiguring itself [6]. Moreover, an alternate path should be set up, when one path fails.

Relying on the kinds of application, WBAN applications can be wearable on the surface of the body and also can be implanted inside the body [8]. These devices, hence, can operate in dissimilar frequency bands and PHYSICAL layers (PHYs). Thus, the WBAN applications must be interoperable at multiple frequency bands and support multiple PHYs.

6.7. Security. WBAN sensor nodes collect sensitive personal information, making it subject to active and passive attacks including eavesdropping, spoofing, and snooping. Because the WBAN network allows several users to transmit and receive data, it is vital that the data be allowed to be exchanged. Information/messages must also be nonrepudiated, as repudiation happens when the sender and receiver deny that messages were transmitted and received. As a result, multiple sorts of security criteria are required to tackle security concerns, authentication, privacy, data consistency, data freshness, availability, and secure localization are just a few examples [2]. Moreover, established cryptography security techniques are employed to satisfy WBAN's basic security needs. However, due to the resource limits imposed by WBANs, such solutions should be computationally processing light [42–44].

6.8. Scalability. In the design of routing protocols for WBAN, scalability is also an important element to be considered in the application development. Scalability refers to a network's ability to add or remove devices without causing significant changes to network's structure or operations [31]. To put it another way, the protocol should be scalable and flexible to numerous alterations that may occur in WBAN owing to the addition of additional sensor devices from time to time [45].

7. Literature Review

We have covered several research issues and challenges related to the field of WBAN in the previous section, which shows that energy efficiency, reliability, and network stability period are the most vital issues in WBAN. Although much study has been done on these topics, it is still required to propose more stringent energy-efficient and reliable approaches to extend the lifetime of WBANs while keeping in mind their resource constraints. In this section, we review the most notable WBAN activities in the domain of energy efficiency and reliability, as well as the most relevant-related work.

We analysed the existing procedures and schemes critically and summarised their strengths and weaknesses. Because each sensor is battery powered, and a lot of energy is spent on communication rather than sensing, recharging or replacing batteries is a major difficulty in WBAN [41, 46, 47]. To reduce energy, WBAN routing algorithms include single-hop and multihop strategies. In a single-hop approach, a sensor node transfers sensitive data directly to the PS. Single-hop communication is ideal for sensors situated close to the sink; however, because nodes located further away from the sink use more energy while transmitting packets to the sink, this method is ineffective. A forwarder node in multihop communication transfers data from other nodes while saving energy consumption of the network [48]. In a multihop strategy, however, nodes closer to a sink become a hotspot as a result of relaying data from other nodes [41, 49].

Furthermore, the most common types of routing protocols comprise cluster-based, crosslayer, thermal-aware, quality-of-service, and postural movement-based routing protocols [16, 50]. In this study, we have focused on the first three techniques, which serve as a foundation for the other two approaches as depicted in Figure 3. These are main category of routing protocols in WBANs.

7.1. Crosslayer Routing. The crosslayer routing is a protocol stack used in WBANs that incorporates two or more levels to improve efficiency and interoperability between techniques/protocols. This category includes Braem et al. [51] proposed a Wireless Autonomous Spanning Tree Protocol (WASP) which is built on a spanning tree structure in which a time axis is separated into slots. Sensor nodes establish a link by telling their offspring nodes, and each node is assigned an isolated WASP-scheme message. However, poor link quality and routing overhead are protocol's principal drawbacks, as WASP lacks a data concatenation method for reducing the amount of transfers. To improve the WASP, Braem et al. [52] suggested a Cascading Information of Controlling Access and Distributed Slot Assignment (CICADA) protocol for WBAN that uses Time Division Multiple Access (TDMA) with two-way communication capability. It uses a data-gathering tree to manage data transfer. For data transfer to its parent node, each CICADA node calculates two parameters. To begin, figure out how many slots the parent node needs to receive all data from its child node. Second, before delivering data to the parent node, the child node determines how many slots are available. Unlike WASP, CICADA is a low-energy, high-reliability protocol that maximises throughput while reducing data loss. The authors, on the other hand, do not address the issues of poor link quality, mobility, load balancing, and routing overhead. Furthermore, the performance of the CICADA protocol declines dramatically throughout the sink to sensor-node transmission. In [53], it is intended to use the Time-Zone Coordinated Sleeping Scheme (TICOSS). By defining the shortest travel route to the WBAN coordinator, TICOSS improves the IEEE 802.15.4 standard by controlling all sensor nodes as Full Functional Devices (FDD). As a result of the V-scheduling, the sensor node's energy is preserved while concealed terminal collisions are minimised. Moreover, this method allows IEEE 802.15.4 to support mobility while also

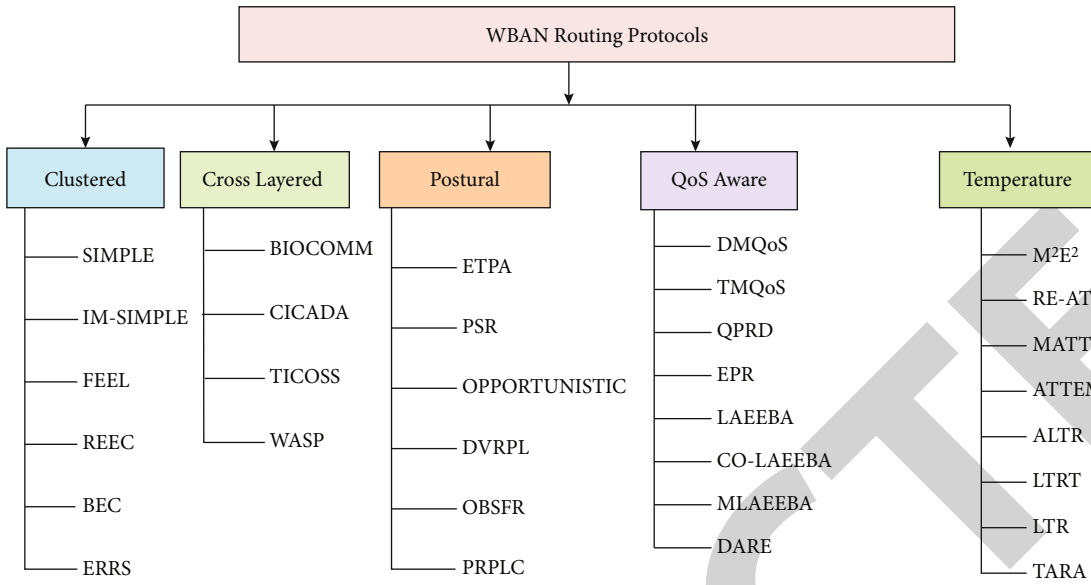

Figure 3: Classification of energy efficient routing protocols in WBAN.

doubling its operational lifetime in high-traffic environments. BIOCOMM [54] is a crosslayer routing protocol for WBANs that combines the network and MAC layers to improve overall network performance. In [55], Adaptive Multihop Tree-Based Routing (AMR) is a distributed spanning-tree system that considers battery level, Received Signal Strength Indicator (RSSI), and hop count. AMR distributes energy consumption evenly among sensor nodes, resulting in a longer network lifetime and more transmissions per packet delivered. However, extrapacket switching between sensor nodes is necessary.

7.2. Thermal-Aware Routing. In vivo sensors can be implanted inside the body, and WBANs with hot-spot monitoring are a major feature. The temperature of sensor nodes rises and thus heats up in multihop methods due to processing, communication radiation, and circuitry power consumptions, which might damage human tissues and compress blood flow. As a result, a thermally aware procedure is required, which can reduce energy usage while extending the stability period.

Tang et al. [56] TARA is a thermally aware method that was proposed (Thermal-Aware Routing Algorithm). When all which surrounds adjacent nodes are hot spot excluding the sender node, the sender node will select other paths in TARA. TARA receives these hotspot nodes as a fresh candidate for later routing after their temperatures drop below a certain threshold. However, greater packet transmission latency (latency), bandwidth waste, and energy consumption are all disadvantages of this method, making it unsuitable for WBANs. Bag et al. [57] introduced LTR (less-temperature rise), a thermally aware routing protocol based entirely on a greedy approach. It delivers data to nearby sensors with the lowest temperature for its rating, unlike TARA. Although because packets are travelling via paths that may or may not lead to the destination, this approach has disadvantages such as greater packet transmission delay (latency), bandwidth waste, and energy usage. However, to enhance LTR, Bag et al. [57] developed ALTR (adaptive less-temperature rise), a thermally aware routing protocol analogous to LTR. Disparate of LTR, when the number of hops surpasses a base threshold, Max Hop Adaptive can employ shortest hop routing (SHR) as a backup means of sending data as quickly as possible. The disadvantages of this method, like LTR, are increased energy consumption and a higher rate of packet loss.

Takahashi et al. [58] introduced the LTRT (least total route temperature) thermal conscious routing approach, which addresses the shortcomings of TARA, LTR, and ALTR. LTRT is a hybrid protocol that combines the LTR and SHR protocols (shortest hop routing). Among all possible packet delivery routes, it chooses a lower-temperature path from the source to the destination. By lowering the amount of hop counts, LTRT prevents wasting network capacity. The main disadvantage of this strategy is operational overhead, since it requires relaying a sensor's temperature state across sensor-nodes, which raises temperature and hence increases battery consumption. Javaid et al. [23] suggested M-ATTEMPT (Mobility Supporting Adaptive Threshold-Based Thermal-Aware Energy-Efficient Multihop Protocol), a well-known thermally aware routing protocol. Data must be directed away from sensor nodes capable of tracing/sensing connection hotspots in this fashion. Among the numerous accessible options, the shortest path is chosen. When there are multiple routes with the same number of hops, the one with the least amount of energy depletion is chosen. A joint-invitation request is sent if a sensor node moves during a data collection cycle, and a joint-request is allowed if the number of subnodes is less than three when checking the child nodes list of a parent. When sensor nodes detect a connection hotspot, packets are forwarded via a long alternate path, resulting in higher energy usage. Despite its benefits, when a sensor fails in M-ATTEMPT, there is no other option. Furthermore, instead of being situated based

on their energy level, the location of these sensor nodes is determined by their data rate. To handle the drawbacks of "M-ATTEMPT", Ahmad et al. [59] developed the notion of "RE-ATTEMPT," a thermally unaware routing strategy "Reliability-Enhanced Adaptive Threshold-Based Thermal Unaware Energy-Efficient Multihop Protocol (RE-ATTEMPT)." RE-ATTEMPT employs a multihop communication paradigm in which the shortest route between sensors and sink nodes is selected. In this approach, sensor nodes exchange HELLO messages to discover all accessible routes. When a current path is unavailable, it chooses a less-than-ideal alternative to ensure reliable transmission. Because of limited number of forwarder nodes, this strategy can avoid relaying of unnecessary traffic. On the other hand, direct communication with the sink is not the best solution for attaining low latency at the expense of energy and reliability since it increases the risk of packet loss due to long-distance communication [60].

Multimode Energy-Efficient Multihop Protocol was proposed (M^2E^2) by Rafatkhah and Lighvan [61]. For WBANs, M^2E^2 is a high-throughput, energy-efficient, and reliable routing system. It solves flaws in the M-ATTEMPT protocol, such as when the parent node refuses to accept a request from a moving node that is also a parent node. However, no effective method for mobility support has been provided, and there is still no alternate mechanism for sending packets to destinations after a node dies.

7.3. Cluster-Based Routing. These solutions are the best way for WBANs to address the issues in the above-mentioned schemes. In a cluster-based routing system, data is transferred to the base station through cluster heads in their respective time slots, which decreases energy drinking and hence enhances stability period. In addition, cluster-based strategies are used to extend the life of the network by decreasing energy consumption. So, Braem et al. [62] presented "relaying and cooperation techniques," a dedicated relay sensor nodes collaborate in the network. This technique extends the life of the network by balancing energy usage across sensor nodes to maximise throughput. However, on the other hand, this paper did not go into great depth regarding where to put the relay node or how to choose it. In addition, the delay and packet loss ratio must be considered.

In WBANs, Ehyaie et al. [63] suggested a relay network concept, which is a set of multiple relay nodes scattered throughout the human body that works as a WBAN transport network. With the use of a dynamic routing algorithm, the suggested approach increases reliability by providing many paths for communication from each sensor to the sink. When the sensor node and sink are not in range of one other, a relay network is the ideal option for NLOS ("Non-Line of Sight) communication"). In terms of mobility assistance, this system is effective. However, employing a relay network to analyse latency and packet loss ratio is critical.

"SIMPLE (Stable Increased Throughput Multihop Protocol for Link Efficiency)" is an energy-efficient routing protocol suggested by Nadeem et al. [28]. In SIMPLE, the minimum function is utilised to select a forwarder node. In each round, the forwarder nodes with the highest residual energy and the shortest distance to the sink node are selected. In SIMPLE, the energy depletion across sensor nodes is balanced by residual energy parameter while the distance value provides maximum throughput. This technique has a longer network lifetime, a longer stability period, and a higher throughput than the M-ATTEMPT protocol. The criterion for selecting a forwarder node, however, is unsuccessful since traffic load is not properly spread among sensor nodes. Furthermore, due to frequent data transfer, the SIMPLE protocol's performance worsens in crucial data reporting-based applications because it does not compare current sensed value to previously detected value. To address the shortcomings in the SIMPLE protocol, Javaid et al. [1] suggested the "IM-SIMPLE (Improved Stable Increased Throughput Multihop Protocol for Link Efficiency)" for WBAN. The IM-SIMPLE scheme major purpose was to handle mobility. In addition, to maximise throughput, a linear programming approach is implemented. For standard sensor nodes, IM-SIMPLE employs a multihop communication mechanism to save energy. A sink node can also choose a forwarder node with the lowest cost function using the TDMA scheduling technique, and all other nodes can send data to the forwarder node in their allowed time slot. One of scheme's significant drawbacks is the forwarder node's poor selection criterion. Because, a forwarder node closer to the sink is frequently picked, therefore, the energy of such nodes reduces quickly, and they expire quickly. In addition, given that the link quality and the path loss are not much considered in IM-SIMPLE protocol, therefore, the number or percentage of dropped packets in a given period is greater than that for SIMPLE [64]. To increase energy efficiency and reliability in WBANs, Sandhu et al. [65] have designed the "FEEL (Forwarding Energy-Efficient Data with Load Balancing) protocol" to improve energy efficiency and reliability in WBANs. FEEL is an energy-efficient protocol because it efficiently uses the battery power to provide network stability for a longer period of time, because effective criteria for the forwarder node selection is determined as compared with protocols such as SIMPLE and IM-SIMPLE. Throughput and network longevity are increased as a result of this excellent forwarder node selection. However, in the event of a path failure, the retransmission of data packets receives less attention [66]. Ullah et al. [67] present a novel "Energy-Efficient and Reliable Routing Scheme (ERRS)" to improve WBAN resource-controlled network stability and reliability. Selection of forwarder node and rotation of forwarder node are two unique ERRS solutions. The suggested ERRS uses adaptive static clustering technology to improve network life and stability, leading to greater reliability. The proposed ERRS proved to be a WBAN routing solution that is effective and reliable. But the basic problem of scalability and mobility will also be tackled in our future research work in order to deal with the wide range of prospective WBAN applications. For instance, it is fascinating to examine the impact of different human body components, on the overall stability and the network lifetime of WBANs.

7.4. QoS-Aware Routing. Quality of service (QoS) is the essential factor of all applications within WBAN. QoS

provisioning for WBAN is a key issue due to considerable challenges and the critical nature of data in many applications. Various types of traffic in WBANs have different QoS needs [68–71]. The following paragraph discusses some of the most important approaches for QoS-aware routing.

The "Data-Centric Multiobjective QoS-based Routing protocol" is introduced by Razzaque et al. [72] which is known as (DMQoS). The proposed protocol's goal is to use a modular architecture to enable different channels for packet delivery based on data priority. It is made up of five modules, one of which is dynamic packet classifier dividing data into four categories (ordinary, delay sensitive, critical, and reliability sensitive packets). In terms of energy economy, average latency, and reliability, the proposed approach improves performance. However, the suggested protocol increases traffic load, causing network congestion and compromising end-to-end latency and reliability.

Khan et al. [73, 74] suggested a delay-sensitive data QoS-aware routing technique termed as (QPRD). This protocol is an evolution of the energy-aware peering routing (EPR) protocol, which divides receiving packets into two groups: conventional packets and delay-sensitive packets. The proposed protocol devises a technique for determining the optimum route for both types of packets while taking into account QoS requirements. This protocol is made up of seven modules: the QoS-aware queuing module receives and sends incoming packets into two queues based on their kinds, which operate on a first-in-first-out basis. QPRD performs admirably with regard to the packet delivery and network load.

Monowar et al. [75] presented a WBAN-specific "thermal-aware multiconstrained intrabody QoS routing protocol" called "TMQoS." The main aim of the suggested approach is for the QoS requirements of various applications to be fulfilled while the sensor node temperature is taken into account. For routing table building, the proposed protocol makes use of the crosslayer routing architecture. There are ten modules in this technique. The arriving packets are divided into four types by a QoS-aware packet classifier. TMQoS meets the QoS standards with lower latency and improved reliability. On the other hand, the TMQoS strategy fails to balance energy utilisation between sensor nodes. In addition, the single-hop approach cannot always ensure the necessary delay and reliability in such a setting. Bangash et al. [76] proposed a "Critical Data Routing (CDR)" for WBAN in a similar way. The suggested protocol's goal is to discover the optimum path for essential data. To improve reliability, essential data must be transmitted in a short amount of time. The paper addresses difficulties caused by postural movement within the human body and by path loss and an increase in the temperature. The proposed CDR protocol met its goal of reliably delivering essential packets within a specified time limit. The recommended strategy, on the other hand, performs poorly in terms of average temperature rise.

In Tauqir et al. [14], "Distance-Aware Relaying Energy-Efficient System (DARE) was presented as an energy-efficient and high-throughput clustered-based routing protocol for WBANs." Eight patients in a medical unit were observed using DARE by evaluating several sink placement scenarios. Seven sensor nodes with infinite energy resources, including one relay node on the chest and one main sensor on the bed, were deployed/attached to every patient. The propagation latency in DARE is found to be comparatively high. Furthermore, the link quality, path loss, and cost of the network were not adequately addressed [77].

"Linked-Aware Energy-Efficient Routing Protocol (LAEEBA)" is an "energy-efficient link aware routing system for WBAN" presented in [78]. LAEEBA has proven to be a reliable scheme with low path loss and a high total network performance. Furthermore, employing both single-hop and multihop communications, the network lifetime is increased, reducing the consequences of path-loss. Furthermore, LAEEBA uses the same forwarder node selection criteria as the SIMPLE protocol, which has been shown to be effective in terms of energy efficiency and network stability. However, the fundamental disadvantage of this protocol is that data packets have a higher overhead during data exchange [64].

To address the shortcomings of LAEEBA, Ahmed et al. [79] suggested "CO-LAEEBA (Cooperative Linked-Aware Energy-Efficient Routing Protocol for WBAN)," based on a cooperative multicasting technique. Two or more pathways exist in CO-LAEEBA, and critical data is transmitted through single-hop communication while normal data is transmitted through relay nodes (a node which acted as a cooperative node). When a sensor node's remaining energy exceeds that of a relay node, packets are routed directly to the sink. When a sensor node's remaining energy is less than that of a relay node, it uses multihop communication. The CO-LAEEBA simulation results show that it enhance the existing protocols in terms of maximum throughput and network lifetime. However, as the CO-LAEEBA protocol uses only a small number of forwarder nodes, too many links for data packet transmission from source to destination are also required [64].

7.5. Postural Movement-Based Routing. The topology of the network is affected by body movements, link failure, and environmental impediments, causing linkages to disconnect. Many researchers have addressed this issue, and a cost function has been created to identify the best method to forward packets to the sink on a periodic basis. A few of the protocols that fall within this category are listed below.

In Quwaider and Biswas [80], on-body store and flood routing (OBSFR) is proposed on-body packet routing technique for wireless body area networks (WBANs) that provides improved routing time and hop count. The proposed protocol employs an opportunistic forwarding strategy depending on node distance from the on-body sink node. Furthermore, the end-to-end packet delay, number of packets per transmission, and packet delivery ratio are checked and compared to existing routing protocols. Quwaider and Biswas [81] proposed DTN routing in a wireless body area network (WBAN), taking into account a dynamic postural splitting technique called as distance vector with postural link cost (DVRPLC). A prototype WBAN has been built in the proposed work to test body topology disconnections in the presence of short-range radio links and human

postural mobility. This protocol's major purpose is to reduce end-to-end delay. The average latency, packet delivery ratio, and packet hop count are all measured. In comparison to existing probabilistic, opportunistic, and utility-based DTN routing protocols, the output results suggest that the proposed approach can deliver better outcomes. Maskooki et al. [82] In WBAN, an opportunistic routing scheme was developed to improve the network lifetime by using the movement of body components. The proposed approach's major goal is to reduce end-to-end delay. The proposed strategy outperforms the other single-hop and multihop strategies in terms of performance. The average energy usage per bit is kept as low as possible. While in Movassaghi et al. [83], ETPA (energy-efficient, thermal, and power-aware routing) protocol was designed to lower node temperature and prevent hotspot development. For the cost function calculation, ETPA took into account the node temperature, energy level, and power gain. The proposed protocol effectively exploited the available resources in WBAN routing protocols, according to the performance study. Many energy-efficient and reliable routing algorithms advise boosting network stability and reducing delay; however, during the network implementation, network organisation, and internode communication stages, less attention has been paid to energy saving and higher reliability. The load is not spread evenly among sensor nodes because the forwarder node selection criteria and the appropriate number of relay nodes are inefficient [84]. As a result, in order to improve WBAN's stability period, an energy-efficient and reliable routing approach is necessary.

8. Discussion

The previous section described and critically analysed existing energy-efficient and reliable routing protocols, such as crosslayer, temperature-aware, and clustered-based techniques. Crosslayer routing approaches are inadequate for WBAN because loads are not equally distributed among sensor nodes. This increases the odds of an energy hole. Because of the high computational cost and complexity, it is not suited for energy-constrained, low-processing, low-bandwidth, and low-memory sensor-nodes. For implanted WBAN, thermal-based techniques are required. However, in wearable WBAN, detecting hotspot nodes has a higher overhead and consumes a lot of energy. We have identified and stated the following most relevant design and performance parameters for WBANs, keeping in mind the resource-constrained nature of WBANs and based on a rigorous examination of state-of-the-art systems. When creating and testing new energy-efficient and reliable WBAN systems, these crucial parameters should be taken into account.

8.1. No. of Dead Nodes. This metric shows the total number of nodes whose remaining energy has been completely exhausted. The number of dead nodes is reduced when load is distributed consistently or evenly among sensor nodes, and vice versa, resulting in increased network lifetime.

8.2. Packets Sent to Sink. The total number of packets sent to the base station or sink is indicated by this parameter. The number of packets sent to the sink is proportional to the total number of nodes that are alive. The total number of packets transferred also depends on whether the WBAN application is time-driven or event-driven.

8.3. Packet Dropped Ratio. This indicator represents the total number of dropped packets as a proportion of the total number of sent packets. The number of transmissions is proportional to the number of packets discarded. The random uniform model is used to calculate packet dropped ratio. A communication link's status can be excellent or bad depending on the likelihood, with 0.7 being a favourable link status probability.

8.4. Packets Received at Sink. This metric represents the total number of packets successfully received at the sink. WBANs are designed to receive as much data as feasible while discarding as few packets as possible at the sink. As a result, because WBANs can monitor any type of abnormal state in the patient, the sensing data must be collected precisely at the sink.

8.5. Stability Period. Stability Period refers to the period of network activities from the start of the established network until the expiry of the first node.

8.6. Delay. The overall time it takes for packets to arrive at their destination is referred to as delay. WBAN may track any critical human body parameter, such as the electrical activity of the heart. As a result, in time-critical applications, delay must be investigated to ensure that data arrives at the sink on time.

Table 4 shows a comparison of the solutions discussed in the literature review section based on the performance factors holding above.

Clustering-based routing techniques have shown to be more suitable for WBAN applications than crosslayer and thermal-aware routing techniques since then. In a clustered-based system, data is sent to the base station through cluster heads in their designated time slots, reducing energy consumption and increasing the stability period.

(i) Further challenges: different cluster-based, energy-efficient, and reliable routing algorithms have been developed to improve the maximise throughput, network stability and achieve longevity in WBAN network operations. Still, a number of issues and concerns must be addressed by the research community, including several solutions ignore energy conservation throughout the network deployment, network organisation, and internode communication phases [29]

(ii) The forwarder node selection criteria and the optimal amount of relay nodes are ineffective, and the load is not evenly distributed among sensor nodes [28]

Table 4: Performance analysis of existing schemes.

Schemes/ solutions	Characteristics						
	No. of dead nodes	Packets sent to sink	Packet dropped ratio	Packet received at sink	Thermal aware approach	Network stability period	Delay
IM-SIMPLE [1]	Medium	High	Medium	Medium	No	Medium	Medium
DARE [14]	Medium	High	Medium	Medium	No	Medium	High
M-ATTEMPT [23]	High	Medium	Medium	Medium	Yes	Low	Medium
SIMPLE [28]	Medium	Medium	Medium	Medium	No	Medium	Medium
FEEL [29]	Medium	High	Low	High	No	High	Medium
TARA [56]	High	Low	High	Low	Yes	Low	High
LTR [57]	High	Low	High	Low	Yes	Low	High
ALTR [57]	High	Medium	Medium	Medium	Yes	Low	Medium
LTRT [58]	Medium	High	Low	High	Yes	Medium	Medium
RE-ATTEMPT [59]	Medium	High	Medium	Medium	No	Medium	Low
M^2E^2 [61]	Medium	High	High	Medium	Yes	Medium	Medium
CO-LAEEBA [79]	Low	High	Low	High	No	High	Low
WASP [85]	High	Medium	Medium	Medium	No	Low	Low
CICADA [86]	Medium	High	Low	High	No	Medium	Medium
ERRS	Medium	High	Low	High	No	High	Low

(iii) In terms of reliability, energy consumption, routing overhead, and scalability, selecting a forwarder node in round by round is inefficient. As a result, a static adaptive clustering strategy must be devised

(iv) When packets are dropped by a node to retain more residual energy for desiring a forwarder node, this is known as a selfish node assault. As a result, a trust-based provision is required to improve network reliability [87]

(v) The expected transmission count (ETX) and routing link metrics are significant elements that are not examined in existing clustering-based techniques [88]

(vi) Throughput is another important factor to consider, and the location of the sink can have a big impact on it [89]

As a result of the explanation above, it is evident that reliability and energy efficiency are major issues in resource-constrained WBANs. As a result, it is necessary to develop reliable and energy-efficient routing approaches that may improve the reliability and network stability while taking into account the particular features and requirements of resource-constraint WBANs in critical applications.

9. Conclusion

WBAN (wireless body area network) is a subset of wireless sensor networks (WSNs) with its own set of characteristics due to resource constraints and application scope. We presented an overview of WBAN applications and architecture in this post, highlighting current research topics and challenges. Because sensor nodes in WBANs have limited resources, energy efficiency and reliability are critical considerations. We assessed the present state-of-the-art solutions in WBANs for energy efficiency and reliability, identifying their strengths and drawbacks. We also identified several performance characteristics that must be considered when creating and evaluating WBAN solutions. Finally, we identified a number of issues and obstacles in terms of energy efficiency and reliability in WBANs that need to be addressed further in the development of new WBAN solutions. As part of our ongoing study, we have presented a novel energy-efficient and reliable routing strategy to improve the stability period and network lifetime in WBAN. In this research work, the emerging technology like edge computing, Fog computing, and AI techniques is not discussed. We aim to work on these limitations in our future research findings with the research community via future publications.

Data Availability

No data were used to support this study.

Conflicts of Interest

The authors declare that they have no conflicts of interest.

References

[1] N. Javaid, A. Ahmad, Q. Nadeem, M. Imran, and N. Haider, "iM-SIMPLE: iMproved stable increased-throughput multi-

hop link efficient routing protocol for wireless body area networks," *Computers in Human Behavior*, vol. 51, pp. 1003–1011, 2015.

[2] S. Movassaghi, M. Abolhasan, J. Lipman, D. Smith, and A. Jamalipour, "Wireless body area networks: a survey," *IEEE Communications surveys & tutorials*, vol. 16, pp. 1658–1686, 2014.

[3] A. Rahim and N. C. Karmakar, "Sensor cooperation in wireless body area network using network coding for sleep apnoea monitoring system," in *2013 IEEE Eighth International Conference on Intelligent Sensors, Sensor Networks and Information Processing*, pp. 432–436, Melbourne, VIC, Australia, 2013.

[4] V. M. Birari, J. Helonde, and V. M. Wadhai, "Algorithmic approach for reliable communication in wireless body area network for patient monitoring system," *International Journal of Engineering, Economics and Management*, vol. 2, p. 5, 2014.

[5] B. Abidi, A. Jilbab, and E. H. Mohamed, "Wireless body area network for health monitoring," *Journal of Medical Engineering & Technology*, vol. 43, pp. 124–132, 2019.

[6] X. Lai, Q. Liu, X. Wei, W. Wang, G. Zhou, and G. Han, "A survey of body sensor networks," *Sensors*, vol. 13, pp. 5406–5447, 2013.

[7] K. Deepak and A. Babu, "Packet size optimization for energy efficient cooperative wireless body area networks," in *2012 Annual IEEE India Conference (INDICON)*, pp. 736–741, Kochi, India, 2012.

[8] W. Kurschl, S. Mitsch, and J. Schoenboeck, "Modeling distributed signal processing applications," in *2009 Sixth International Workshop on Wearable and Implantable Body Sensor Networks*, pp. 103–108, Berkeley, CA, USA, 2009.

[9] R. Cavallari, F. Martelli, R. Rosini, C. Buratti, and R. Verdone, "A survey on wireless body area networks: technologies and design challenges," *IEEE Communications Surveys & Tutorials*, vol. 16, pp. 1635–1657, 2014.

[10] M. Chen, S. Gonzalez, A. Vasilakos, H. Cao, and V. C. Leung, "Body area networks: a survey," *Mobile networks and applications*, vol. 16, pp. 171–193, 2011.

[11] P. M. P. Dharshini and M. Tamilarasi, "Adaptive reliable cooperative data transmission technique for wireless body area network," in *International Conference on Information Communication and Embedded Systems (ICICES2014)*, pp. 1–4, Chennai, India, 2014.

[12] G. Yang, X.-W. Wu, Y. Li, and Q. Ye, "Energy efficient protocol for routing and scheduling in wireless body area networks," *Wireless Networks*, vol. 26, pp. 1265–1273, 2020.

[13] B. Latré, B. Braem, I. Moerman, C. Blondia, and P. Demeester, "A survey on wireless body area networks," *Wireless Networks*, vol. 17, pp. 1–18, 2011.

[14] A. Tauqir, N. Javaid, S. Akram, A. Rao, and S. Mohammad, "Distance aware relaying energy-efficient: dare to monitor patients in multi-hop body area sensor networks," in *2013 Eighth International Conference on Broadband and Wireless Computing, Communication and Applications*, pp. 206–213, Compiegne, France, 2013.

[15] V. M. Birari, J. Helonde, and V. Wadhai, "Seamless mobility with interference free reliable communication in WBAN," in *2015 International Conference on Computing Communication Control and Automation*, pp. 251–255, Pune, India, 2015.

[16] M. Effatparvar, M. Dehghan, and A. M. Rahmani, "A comprehensive survey of energy-aware routing protocols in wireless body area sensor networks," *Journal of Medical Systems*, vol. 40, p. 201, 2016.

[17] J. Penders, C. Van Hoof, and B. Gyselinckx, "Bio-medical application of WBAN: trends and examples," in *Bio-Medical CMOS ICs*, pp. 279–302, Springer, 2011.

[18] L. Conroy, C. O'Conaire, S. Coyle et al., "TennisSense: a multisensory approach to performance analysis in tennis," in *Proceedings of the 27th International Society of Biomechanics in Sports Conference*, pp. 1–10, Limerick, Ireland, 2009.

[19] F. R. Yazdi, M. Hosseinzadeh, and S. Jabbehdari, "A review of state-of-the-art on wireless body area networks," *International Journal of Advanced Computer Science and Applications*, vol. 11, pp. 443–455, 2017.

[20] J. I. Bangash, A. H. Abdullah, M. A. Razzaque, and A. W. Khan, "Reliability aware routing for intra-wireless body sensor networks," *International Journal of Distributed Sensor Networks*, vol. 10, Article ID 786537, 2014.

[21] B. Zhen, M. Patel, S. Lee, E. Won, and A. Astrin, "TG6 technical requirements document (TRD) ID: 802.15-08-0644," *IEEE submission*, 2008.

[22] M. Zhang and A. A. Sawchuk, "A customizable framework of body area sensor network for rehabilitation," in *2009 2nd International Symposium on Applied Sciences in Biomedical and Communication Technologies*, pp. 1–6, Bratislava, Slovakia, 2009.

[23] N. Javaid, Z. Abbas, M. Fareed, Z. Khan, and N. Alrajeh, "M-ATTEMPT: a new energy-efficient routing protocol for wireless body area sensor networks," *Procedia Computer Science*, vol. 19, pp. 224–231, 2013.

[24] C. H. W. Oey and S. Moh, "A survey on temperature-aware routing protocols in wireless body sensor networks," *Sensors*, vol. 13, pp. 9860–9877, 2013.

[25] V. Tickoo and S. Gambhir, "A comparison study of congestion control protocols in WBAN," *International Journal of Innovations & Advancement in Computer Science*, vol. 4, pp. 121–127, 2015.

[26] D. Larsen-Freeman and M. Anderson, *Techniques and Principles in Language Teaching*, vol. 3Oxford university press, 3rd edition, 2013.

[27] K. M. Mohan, R. Sudha, K. Shalini, and T. Poongothai, "A power efficient Mac protocol and fault-tolerant event boundary detection in wireless sensor networks," *International Journal of Engineering Trends and Applications (IJETA)*, vol. 2, 2015.

[28] Q. Nadeem, N. Javaid, S. Mohammad, M. Khan, S. Sarfraz, and M. Gull, "Simple: stable increased-throughput multi-hop protocol for link efficiency in wireless body area networks," in *2013 Eighth International Conference on Broadband and Wireless Computing, Communication and Applications*, pp. 221–226, Compiegne, France, 2013.

[29] M. M. M. Sandhu, *Mobility Modeling for Efficient Data Routing in Wireless Body Area Networks*, COMSATS Institute of Information Technology, 2014.

[30] J. Ding, E. Dutkiewicz, X. Huang, and G. Fang, "Energy efficient cooperative transmission in single-relay UWB based body area networks," in *2015 IEEE International Conference on Communications (ICC)*, pp. 1559–1564, London, UK, 2015.

[31] S. Nepal, S. Dahal, and S. Shin, "Does the IEEE 802.15. 4 MAC protocol work well in wireless body area networks?," *Journal of Advances in Computer Networks*, vol. 4, pp. 52–58, 2016.

[32] Y. S. Aldeen and K. N. Qureshi, "Solutions and recent challenges related to energy in wireless body area networks with integrated technologies: applications and perspectives," *Baghdad Science Journal*, vol. 17, no. 1, Supplement, pp. 0378–0384, 2020.

[33] A. Afridi, N. Javaid, S. Jamil, M. Akbar, Z. A. Khan, and U. Qasim, "HEAT: horizontal moveable energy-efficient adaptive threshold-based routing protocol for wireless body area networks," in *2014 28th International Conference on Advanced Information Networking and Applications Workshops*, pp. 474–478, Victoria, BC, Canada, 2014.

[34] R. V. Sampangi, S. R. Urs, and S. Sampalli, "A novel reliability scheme employing multiple sink nodes for wireless body area networks," in *2011 IEEE Symposium on Wireless Technology and Applications (ISWTA*, pp. 162–167, Langkawi, Malaysia, 2011.

[35] G. Wu, J. Ren, F. Xia, and Z. Xu, "An adaptive fault-tolerant communication scheme for body sensor networks," *Sensors*, vol. 10, pp. 9590–9608, 2010.

[36] H. Kaur and N. Bilandi, "Topological mechanism for sensor placement in wireless body area network," in *International Conference on Information Technology and Computer Science*, Jalandhar, India, 2015.

[37] M. Yu, H. Mokhtar, and M. Merabti, "Fault management in wireless sensor networks," *IEEE Wireless Communications*, vol. 14, pp. 13–19, 2007.

[38] M. Z. Khan, "Fault management in wireless sensor networks," *Computer Science & Telecommunications*, vol. 37, 2013.

[39] S. Pașca and M. Roșu, "A new approach for healthcare monitoring," in *E-Health and Bioengineering Conference (EHB), 2013*, pp. 1–6, Jalandhar, India, 2013.

[40] G. Mehmood, M. Z. Khan, S. Abbas, M. Faisal, and H. U. Rahman, "An energy-efficient and cooperative fault-tolerant communication approach for wireless body area network," *IEEE Access*, vol. 8, pp. 69134–69147, 2020.

[41] A. Ghani, H. A. Naqvi, M. Sher, Z. S. Khan, I. Khan, and M. Saqlain, "Energy efficient communication in body area networks using collaborative communication in Rayleigh fading channel," *Telecommunication Systems*, pp. 1–14, 2016.

[42] G. Mehmood, M. Z. Khan, H. U. Rahman, and S. Abbas, "An efficient and secure session key establishment scheme for health-care applications in wireless body area networks," *Journal Of Engineering And Applied Sciences*, vol. 63, 2018.

[43] M. A. Ferrag, L. Maglaras, A. Derhab, and H. Janicke, "Authentication schemes for smart mobile devices: threat models, countermeasures, and open research issues," *Telecommunication Systems*, vol. 73, pp. 317–348, 2020.

[44] G. Mehmood, M. S. Khan, A. Waheed et al., "An efficient and secure session key management scheme in wireless sensor network," *Complexity*, vol. 2021, Article ID 6577492, 10 pages, 2021.

[45] D. B. Smith, D. Miniutti, T. A. Lamahewa, and L. W. Hanlen, "Propagation models for body-area networks: a survey and new outlook," *IEEE Antennas and Propagation Magazine*, vol. 55, pp. 97–117, 2013.

[46] H. Wei, H. Li, and J. Tan, "Body sensor network based context-aware QRS detection," *Journal of Signal Processing Systems*, vol. 67, pp. 93–103, 2012.

[47] M. ShariatmadariSerkani, J. Mohammadzadeh, and M. Motalebi, "A reliable routing algorithm for delay sensitive data in body area networks," *Journal of Advances in Computer Engineering and Technology*, vol. 4, pp. 229–236, 2018.

[48] J. Elias, "Optimal design of energy-efficient and cost-effective wireless body area networks," *Ad Hoc Networks*, vol. 13, pp. 560–574, 2014.

[49] Z. Ullah, I. Ahmed, F. A. Khan et al., "Energy-efficient harvested-aware clustering and cooperative routing protocol for WBAN (E-HARP)," *IEEE Access*, vol. 7, pp. 100036–100050, 2019.

[50] H. Ben Elhadj, L. Chaari, and L. Kamoun, "A survey of routing protocols in wireless body area networks for healthcare applications," *International Journal of E-Health and Medical Communications*, vol. 3, pp. 1–18, 2012.

[51] B. Braem, B. Latre, I. Moerman, C. Blondia, and P. Demeester, "The wireless autonomous spanning tree protocol for multihop wireless body area networks," in *2006 Third Annual International Conference on Mobile and Ubiquitous Systems: Networking & Services*, pp. 1–8, San Jose, CA, USA, 2006.

[52] B. Braem, B. Latré, C. Blondia, I. Moerman, and P. Demeester, "Improving reliability in multi-hop body sensor networks," in *2008 Second International Conference on Sensor Technologies and Applications (sensorcomm 2008)*, pp. 342–347, Cap Esterel, France, 2008.

[53] A. G. Ruzzelli, R. Jurdak, G. M. O'Hare, and P. Van Der Stok, "Energy-efficient multi-hop medical sensor networking," in *Proceedings of the 1st ACM SIGMOBILE international workshop on Systems and networking support for healthcare and assisted living environments*, pp. 37–42, San Juan, Puerto Rico, USA, 2007.

[54] A. Bag and M. A. Bassiouni, "Biocomm – a cross-layer medium access control (MAC) and routing protocol co-design for biomedical sensor networks," *International Journal of Parallel, Emergent and Distributed Systems*, vol. 24, no. 1, pp. 85–103, 2009.

[55] A. M. Ortiz, N. Ababneh, N. Timmons, and J. Morrison, "Adaptive routing for multihop IEEE 802.15. 6 wireless body area networks," in *SoftCOM 2012, 20th International Conference on Software, Telecommunications and Computer Networks*, pp. 1–5, Split, Croatia, 2012.

[56] Q. Tang, N. Tummala, S. K. Gupta, and L. Schwiebert, "TARA: thermal-aware routing algorithm for implanted sensor networks," in *International Conference on Distributed Computing in Sensor Systems*, pp. 206–217, Marina del Rey, CA, USA, 2005.

[57] A. Bag and M. A. Bassiouni, "Energy efficient thermal aware routing algorithms for embedded biomedical sensor networks," in *2006 IEEE International Conference on Mobile Ad Hoc and Sensor Systems*, pp. 604–609, Vancouver, BC, Canada, 2006.

[58] D. Takahashi, Y. Xiao, and F. Hu, "LTRT: least total-route temperature routing for embedded biomedical sensor networks," in *IEEE GLOBECOM 2007-IEEE Global Telecommunications Conference*, pp. 641–645, Washington, DC, USA, 2007.

[59] A. Ahmad, N. Javaid, U. Qasim, M. Ishfaq, Z. A. Khan, and T. A. Alghamdi, "RE-ATTEMPT: a new energy-efficient routing protocol for wireless body area sensor networks," *International Journal of Distributed Sensor Networks*, vol. 10, no. 4, Article ID 464010, 2014.

[60] Y. Qu, G. Zheng, H. Ma, X. Wang, B. Ji, and H. Wu, "A survey of routing protocols in WBAN for healthcare applications," *Sensors*, vol. 19, no. 7, p. 1638, 2019.

Hindawi
Computational and Mathematical Methods in Medicine
Volume 2023, Article ID 9846497, 1 page
https://doi.org/10.1155/2023/9846497

Retraction

Retracted: Social Media Analytics for Pharmacovigilance of Antiepileptic Drugs

Computational and Mathematical Methods in Medicine

Received 10 October 2023; Accepted 10 October 2023; Published 11 October 2023

This article has been retracted by Hindawi following an investigation undertaken by the publisher [1]. This investigation has uncovered evidence of one or more of the following indicators of systematic manipulation of the publication process:

(1) Discrepancies in scope

(2) Discrepancies in the description of the research reported

(3) Discrepancies between the availability of data and the research described

(4) Inappropriate citations

(5) Incoherent, meaningless and/or irrelevant content included in the article

(6) Peer-review manipulation

The presence of these indicators undermines our confidence in the integrity of the article's content and we cannot, therefore, vouch for its reliability. Please note that this notice is intended solely to alert readers that the content of this article is unreliable. We have not investigated whether authors were aware of or involved in the systematic manipulation of the publication process.

Wiley and Hindawi regrets that the usual quality checks did not identify these issues before publication and have since put additional measures in place to safeguard research integrity.

We wish to credit our own Research Integrity and Research Publishing teams and anonymous and named external researchers and research integrity experts for contributing to this investigation.

The corresponding author, as the representative of all authors, has been given the opportunity to register their agreement or disagreement to this retraction. We have kept a record of any response received.

References

[1] A. A. Yahya, Y. Asiri, and I. Alyami, "Social Media Analytics for Pharmacovigilance of Antiepileptic Drugs," *Computational and Mathematical Methods in Medicine*, vol. 2022, Article ID 8965280, 24 pages, 2022.

Hindawi
Computational and Mathematical Methods in Medicine
Volume 2022, Article ID 8965280, 24 pages
https://doi.org/10.1155/2022/8965280

Research Article

Social Media Analytics for Pharmacovigilance of Antiepileptic Drugs

Anwar Ali Yahya, Yousef Asiri, and Ibrahim Alyami

Department of Computer Science, Najran University, Najran, Saudi Arabia

Correspondence should be addressed to Yousef Asiri; yasiri@nu.edu.sa

Received 7 September 2021; Accepted 4 December 2021; Published 4 January 2022

Academic Editor: Muhammad Zubair Asghar

Epilepsy is a common neurological disorder worldwide and antiepileptic drug (AED) therapy is the cornerstone of its treatment. It has a laudable aim of achieving seizure freedom with minimal, if any, adverse drug reactions (ADRs). Too often, AED treatment is a long-lasting journey, in which ADRs have a crucial role in its administration. Therefore, from a pharmacovigilance perspective, detecting the ADRs of AEDs is a task of utmost importance. Typically, this task is accomplished by analyzing relevant data from spontaneous reporting systems. Despite their wide adoption for pharmacovigilance activities, the passiveness and high underreporting ratio associated with spontaneous reporting systems have encouraged the consideration of other data sources such as electronic health databases and pharmaceutical databases. Social media is the most recent alternative data source with many promising potentials to overcome the shortcomings of traditional data sources. Although in the literature some attempts have investigated the validity and utility of social media for ADR detection of different groups of drugs, none of them was dedicated to the ADRs of AEDs. Hence, this paper presents a novel investigation of the validity and utility of social media as an alternative data source for the detection of AED ADRs. To this end, a dataset of consumer reviews from two online health communities has been collected. The dataset is preprocessed; the unigram, bigram, and trigram are generated; and the ADRs of each AED are extracted with the aid of consumer health vocabulary and ADR lexicon. Three widely used measures, namely, proportional reporting ratio, reporting odds ratio, and information component, are used to measure the association between each ADR and AED. The resulting list of signaled ADRs for each AED is validated against a widely used ADR database, called Side Effect Resource, in terms of the precision of ADR detection. The validation results indicate the validity of online health community data for the detection of AED ADRs. Furthermore, the lists of signaled AED ADRs are analyzed to answer questions related to the common ADRs of AEDs and the similarities between AEDs in terms of their signaled ADRs. The consistency of the drawn answers with the existing pharmaceutical knowledge suggests the utility of the data from online health communities for AED-related knowledge discovery tasks.

1. Introduction

With an estimated 65 million people having epilepsy worldwide [1] and an annual rate ranging from 30 to 50 per 100,000 individuals [2], epilepsy is considered the most common serious neurological disorder after stroke. It is a multifactorial disorder that involves many seizure types and syndromes with different prognoses and sensitivities to treatment. With a laudable aim of achieving seizure freedom with minimal, if any, side effects, AEDs are the mainstay of epilepsy treatment [3]. Currently, there are ample AEDs available, offering more options for the treatment of many types of seizures. Despite different mechanisms of actions of AEDs [4], none of them treat the etiology of the disorder. They instead act to symptomatically suppress seizures once they occur. Therefore, the current AEDs still fail to control seizures in 20–30% of all epilepsy patients [5, 6]. Besides their use for epilepsy treatment, AEDs are extensively used to treat other conditions, including migraine, neuropathic pain, bipolar disorder, anxiety, and many other disorders

[7]. With this wide prevalence and a reported yearly growth of AED usage, particularly of new ones [7–9], their safety in use has become a major concern.

Usually, the treatment of epilepsy using AEDs is a long-lasting journey, and hence, their safety for long-term administration is of paramount importance. According to the World Health Organization (WHO), drug safety or pharmacovigilance involves activities relating to the detection, assessment, understanding, and prevention of adverse effects or any other possible drug-related problems. Moreover, the WHO terms the adverse effects or problems of a drug as a signal and defines it as "reported information on a possible causal relationship between an adverse event and a drug, the relationship being unknown or incompletely documented previously." Among different drug signals, the ADR is the primary type, which is defined as "an appreciably harmful or unpleasant reaction, resulting from an intervention related to the use of a medicinal product, which predicts a hazard from future administration and warrants prevention or specific treatment, or alteration of the dosage regimen, or withdrawal of the product" [10].

Although the ADRs of all in-use drugs are of crucial importance, it gains even more significance in AEDs for the following distinctive peculiarities. First, the treatment of epilepsy is usually maintained for many years and can be lifelong. Besides the early occurrence of ADRs developed in this long-term treatment, several ADRs are developed insidiously over several years after the introduction of the AED. Second, while the initial choice of an AED is primarily guided by its efficacy (ability to control seizures), its retention (long-term use) depends on its ADR profile (tolerability) [7]. In this respect, it has been reported that the ADRs of AEDs represent a leading cause of treatment failure in nearly 25% of patients. Furthermore, they are a major source of disability and mortality in patients with epilepsy and substantially contribute to the use and costs of healthcare systems [1]. Third, patients are different in their response to AEDs and willingness to accept their ADRs. For example, a patient may refuse *Valproate*, though it is most likely AED to control primary generalized seizures, because of weight gain or teratogenic risk for a female patient of child-bearing age. Fourth, for a significant portion of epileptic patients, approximately 30-50%, the seizures are poorly controlled or refractory. These patients are usually on polytherapy, where multiple AEDs are used in combination, leading to potential pharmacokinetic or pharmacodynamic interactions and causing more ADRs that might occur when the AED is taken as monotherapy [11]. Fifth, despite the wide variety of existing AEDs, new ones are continuously developed. More precisely, over the past 25 years, more than 15 new AEDs with modified mechanisms of action or side effect profiles have become available for epilepsy treatment. These new AEDs create a major challenge for health professionals and postmarketing surveillance in regard to their tolerability and drug interaction [12]. Sixth, although AEDs are essentially used for epilepsy treatment, in recent years, there is an increase in their clinical use for treating other neurological and psychiatric disorders such as migraine, neuropathic pain, bipolar disorder, mania, schizophrenia, anxiety, and essential tremor. This adds new patients who are exposed to the AEDs, and thus, a new dimension of their ADRs is introduced [13].

Given the peculiarities of ADRs in AEDs, their detection has become of paramount importance to the concerned parties (patients, health professionals, pharmaceutical companies, and regulatory authorities) [1]. In general, there are two main approaches of ADR detection: premarketing review and postmarketing surveillance. The premarketing review process is required before any pharmaceutical new drugs are approved for marketing by regulatory authorities such as the Food and Drug Administration (FDA). This process focuses on identifying the risk associated with drugs, which must be established and clearly communicated to prescribers and consumers. Nonetheless, the premarketing review process is not sufficient to uncover all ADRs, because it is usually limited by the size and duration and is often incapable of detecting rare ADRs [14]. Therefore, systems for postmarketing surveillance, or pharmacovigilance, become necessary. Typically, the postmarketing surveillance is conducted by the regulatory authority and heavily relies on applying data analytics methods to analyze spontaneous reporting system (SRS) data [15]. Despite their wide adoption, SRSs have many limitations and the most frequently mentioned one is being the subject of underreporting. The reasons for this limitation are manifold and include lack of time, large effort, fear of being prosecuted, and an unawareness of the importance of reporting. Additionally, while monitoring of all undesirable reactions is necessary, it is often thought that SRSs are designed solely for detecting rare and serious ADRs [12].Given the SRS limitations, several data sources have been utilized for pharmacovigilance. In the case of AEDs, sources such as routine clinical data [12], prescription data [16], and electronic health records [17] have been considered. Despite their merits, they suffer limitations related to their accessibility and privacy [14].

In recent years, social media has emerged as a valuable data source for health informatics [18]. Data from online social media networks, such as Google, YouTube, Facebook, and Twitter, permits people to generate a massive amount of health textual content which can be utilized to tackle various medical tasks such as psychopathic class detection [19, 20], depression classification [21], disease detection [22], and adverse drug reaction detection [23]. It is the development of Web 2.0 and Health 2.0 that makes a great deal of health-related informative contents available. As for pharmacovigilance in particular, social media offers large amounts of useful data that are internet-based, patient-generated, unsolicited, and up to date. Thus, the FDA in the United States and the European medicine agency have recognized social media as a new data source to strengthen their pharmacovigilance activities [24]. Despite all this, the use of social media data for pharmacovigilance activities is not without difficulties. Issues with the credibility, recency, uniqueness, frequency, and salience of social media data always arise. In addition, difficulties and challenges in using Natural Language Processing (NLP) techniques to process and extract relevant information from social media are frequently encountered [25]. This is due to the tendency of

social media users to use nonmedical and descriptive terms to discuss health issues [26]. Nonetheless, the utilization of social media data for pharmacovigilance continues to gain increasing attention, particularly for ADR detection. In this respect, the survey of the relevant literature reveals a number of works that leverage social media data for the detection of ADRs of certain drugs such as of methylphenidate [24], statin drugs [27], breast cancer drugs [28], cancer drugs [29], diabetes drugs [30], psychiatric drugs [31], malaria drugs [32], heart disease drugs [33], and opioid drugs [34]. It also reveals the lack of work dedicated to investigating the potentiality of social media for the detection of AED ADRs.

Given the peculiarities of ADRs in AEDs, the inherent limitations of traditional data sources, the growing interest in leveraging social media for ADRs detection, and finally the lack of research efforts dedicated to investigating the potentiality of social media for AED pharmacovigilance [35], this research is proposed to investigate the validation and utilization of leveraging social media data, particularly online health communities (OHCs), for detecting the ADRs of AEDs. It does so by applying data analytics methods to data collected from two OHCs. As the collected data is of textual form, NLP techniques are employed to prepare it for ADR extraction with the aid of two medical resources, consumer health vocabulary (CHV) and ADR lexicon, to bridge the language and terminology gap between health professionals and consumers. Then, disproportionality analysis measures are applied to identify the set of ADRs for each AED. The results are then analyzed to answer two main research questions given as follows:

(i) Given the growing interest in leveraging social media data for pharmacovigilance, to what extent is OHC data valid for the task of detecting ADRs of AEDs?

(ii) Given the growing interest in leveraging social media data for pharmacovigilance, can OHC data be utilized in knowledge discovery tasks related to AEDs? More specifically, this question can be answered through the following specific knowledge discovery tasks:

  (1) Given the common characteristics of the AEDs, what does the OHC data disclose about the common ADRs of AEDs?

  (2) Given the common characteristics, mechanism of actions, and chemical structure of AEDs, what does OHC data disclose about their similarities in terms of ADRs?

The remainder of this paper is organized as follows. In Section 2, a review of the related literature on ADRs of AEDs is presented. Section 3 describes the detailed methodology of detecting ADRs from OHC data. In Section 4, the results of the conducted experiments are demonstrated and analyzed to answer the research questions. Section 5 concludes the paper and discusses the future research directions.

2. Literature Review

Over the last three decades, a remarkable increase in the AEDs available to treat patients with epilepsy has been reported [36]. Their aim is to achieve the highest efficacy with minimal ADRs. Like other types of drugs, AEDs are associated with various types of ADRs. However, since the common mechanism of AEDs is to suppress the pathological neuronal hyperexcitability that constitutes the final substrate in many seizure disorders, the ADRs that affect the Central Nerve System (CNS) are the most common type of ADRs [37]. In the literature, the ADRs of AEDs have been a matter of concern in many studies from different perspectives. In [11], three categories of AED ADRs (CNS, behavioral, and general medical issues) have been identified. The long-term ADRs of AEDs, particularly new ones, are studied in [7]. A comprehensive summary of AED ADRs affecting the CNS is reviewed in [37]. A classification and identification of psychiatric ADRs of individual AEDs and general guidelines for their prevention and management are studied in [38]. Furthermore, an assessment of the psychiatric and behavioral ADRs of AEDs is conducted in [39]. An evaluation of the ADRs of the new AEDs against the conventional AEDs in terms of their ADRs is conducted in [40], which shows that newer AEDs are associated with a similar trend of ADRs.

Owing to the cruciality of ADRs for AEDs, the safety of AEDs, particularly ADR detection, has become a major concern [13]. For this purpose, data analytics has played a vital role for analyzing AED usage data collected from different sources. In this regard, four types of data sources [14] can be identified: SRSs, electronic health records, pharmaceutical databases, and biomedical literature. Despite their merits, they suffer several limitations. The passiveness of spontaneous reporting systems leads to the extremely high underreporting ratio and makes it difficult to detect new and emerging signals. The privacy issues often make it difficult to access electronic health records. The accessibility of pharmaceutical databases is also a problem, because not all of them are free and public to everyone. In addition, the data of pharmaceutical databases focuses on the chemical aspect such as drug structure rather than textual aspect [14, 41]. Recently, in response to these limitations, social media as an alternative data source for pharmacovigilance has been receiving increasing attention. The research efforts in this area have been reviewed in several surveys [23, 25, 26, 42, 43]. According to these surveys, the following aspects characterize the current state of the art of utilizing social media for pharmacovigilance.

(i) Social media has potentials that are understudied, and its value has not yet been realized in practice [23]

(ii) Social media may add value for specific niche areas such drug abuse and pregnancy-related outcomes [43]

(iii) With the enhancement of algorithms and techniques, the scope and utility of social media may broaden over time [43]

(iv) Additional research is required to explore the value of social media for pharmacovigilance [23, 43]

In general, these surveys share a concordant view on the infancy of utilizing social media data for pharmacovigilance and the dire need for more research efforts in this regard.

Concerning the utilization of social media for the detection of ADRs, the research efforts have been reviewed and summarized, as shown in Table 1, across four dimensions: data source, target drug set, number of drugs, ADR extraction approach, and ADR signaling method. A closer look at Table 1 reveals several interesting aspects of these research efforts that inspired the design choices of this research. First, dedicated OHCs such as Askapatient and WebMD have been used as a source of data more than public social networks such as Twitter and Facebook. Second, none of the previous research in Table 1 was dedicated to detecting the ADRs of AEDs, though most of them, 14 out of 19, studied the ADRs of a specific set of drugs. Third, the lexicon-based method is widely used for extracting drugs and ADRs from social media data. Fourth, disproportionality analysis, a widely used method detecting ADRs from SRSs data is also used for the detection of ADRs from social media data.

On the other hand, a review of the previous research in Table 1, from a methodological point of view, reveals several interesting aspects of the general methodology of detecting ADRs from social media. As characterized in [25] and demonstrated in Figure 1, the general methodology involves five main steps: raw data collection, preprocessing, information extraction (drugs and ADRs), measuring drug-ADR correlations, and evaluation. The raw data can be collected from a big public platform social network site such as Facebook, Twitter, Flicker, and Tumblr or specialized healthcare social networks and forums. The specialized healthcare social network forums can be further classified into generic health-centered social network sites where users discuss their health-related experiences, including use of prescription drugs, side effects, and treatments, such as PatientsLikeMe (http://www.patientslikeme.com), DailyStrength (http://www.dailystrength.org), MedHelp (http://www.medhelp.org), WebMD (https://exchanges.webmd.com), and CureTogether (http://curetogether.com), medicine-focused sharing platforms, which allow patients to share and compare medication experiences like Askapatient (http://www.askapatient.com) and Medications.com (http://www.medications.com), or disease-specific online health forums focused on specific diseases, e.g., the TalkStroke forum (https://www.stroke.org.uk/forum) [23]. Depending on the nature of the source, different methods can be utilized to collect the raw data. For a big public platform social network site, specific application programming interfaces are utilized to extract data; however, for specialized healthcare social networks and forums, an adapted web crawler to collect web pages and web scraper to extract the messages from web pages can be used [25].

Since content and language of medical social media differ from those of general social media and of clinical documents, a preprocessing of the raw data is a crucial step. For this purpose, specific text mining methods or techniques based on NLP are employed to identify medical concepts (drugs, ADRs, symptoms, etc.) and relationships among them. In this respect, it is worth mentioning that the performance of the text mining methods plays a vital role [49]. Typically, in the preprocessing step, the following transformations can be performed.

(i) Anonymization: to remove patients' personal data to comply with medical confidentiality

(ii) Spelling correction: to maximize the detection of information in the corpus, spelling mistakes and typing errors must be corrected, because texts extracted from social networks include many abbreviations and typing errors

(iii) Cleaning web pages: to remove tags that are invisible to users

(iv) Stemming: to reduce inflected words to their stem, base, or root forms

(v) Tokenization: breaking the text up into segments of words, sentences, and paragraphs to ease analyzing the sentences and locutions in the corpus

(vi) N-gram generation: to optimize the extraction of medical concepts, the unigrams, bigrams, and trigrams are generated

After preprocessing the collected data, the information extraction step extracts medical concepts, particularly the drug names and ADRs from the cleaned data. For this purpose, the employed approach can be generally classified as machine learning- (ML-) based approaches and lexicon-based approaches. The use of ML-based approaches is motived by the fact that most drug-related posts on social media are not associated with ADRs, and therefore, irrelevant posts must be filtered out to identify ADRs. In their works, ML-based approaches require a large amount of manually annotated data to make reliable evaluations. Supervised text classification techniques such as support vector machine and naïve Bayes are the most common ML-based approaches employed to classify user posts to determine if ADRs are mentioned in the posts [26]. Besides supervised ML approaches, unsupervised ML approaches such as topic modeling and named entity recognition can be utilized [24]. Lexicon-based ADR extraction, on the other hand, is a widely adopted approach, as over 50% of the previous studies adopted it [26]. The wide use of lexicon-based ADR extraction is attributed to the wide availability of medical lexicons and knowledge bases in the healthcare domain. The Unified Medical Language System (UMLS), the FDA's Adverse Event Reporting System (FAERS), and the adverse drug event reporting system in Canada (MedEffect) are the most medical lexicons used in the previous studies. Meanwhile, the CHV, a lexicon linking UMLS standard medical terms to patients' colloquial language, has been adopted in many studies to interpret medical terms in online patient discussions [45].

Table 1: Summary of previous research on utilizing social media for ADRs detection.

Reference	Data source	Target drug set	No. of drugs	ADR extraction approach	ADR signaling method
[44]	DailyStrength	NA	6	Lexicon-based	Association rule mining
[45]	Various OHC forums	Breast cancer	4	Lexicon-based	Association rule mining
[46]	Various parenting forums	Pediatric drugs (fever, pain, influenza, viruses)	9	Lexicon-based	Disproportionality analysis
[29]	Twitter	Cancer	5	ML-based (SVM)	NA
[47]	American Diabetes Association	Diabetes	NA	Lexicon-based	Shortest dependency path-based ML algorithm
[28]	Askapatient, Drugs.com, DrugRatingZ	Breast cancer	5	Pattern-based	NA
[48]	Twitter	NA	23	Lexicon-based	Aggregated frequencies
[33]	MedHelp	Heart disease	NA	Lexicon-based	Rule-based approach for relation classification
[49]	DailyStrength	NA	38	ML-based (SVM)	Probabilities of all comments associated with each drug combined to predict if drug should be categorized as normal or blackbox
[50]	Twitter, DailyStrength	NA	81	Supervised learning via conditional random fields (CRF)	NA
[24]	Five popular and open French forums	Methylphenidate	4	Lexicon-based	Disproportionality analysis
[27]	Askapatient.com Medications.com WebMD.com	Cholesterol-lowering drugs		Lexicon-based	Log-likelihood ratio
[51]	Twitter	Attention deficit hyperactivity. Disorder drugs	44	ML-based (RNN)	NA
[14]	PatientsLikeMe MedHelp	NA	20	Lexicon-based	Association rule mining Disproportionality analysis
[52]	Five forums in France	Oral antineoplastic drugs	8 (ATC subgroup)	Lexicon-based manual	Frequency
[30]	Askapatient.com	Diabetes drug Glucophage/ metformin	1	ML-based	NA
[31]	Askapatient.com	Psychiatric drugs	4	ML-based	NA
[32]	Twitter	Malaria drugs	19	ML-based and rule-based (cTake)	Disproportionality analysis
[34]	Twitter and PubMed	Opioid drugs	3	ML-based (convolutional recurrent neural network (CRNN))	NA

As for measuring the correlation between the drugs and the extracted ADRs, different approaches can be employed. These approaches can be grouped into three categories: disproportionality analysis approaches, association rule mining approaches, and machine learning-based approaches. The disproportionality analysis approaches [53] are based on the calculation of a two-by-two contingency table that relates the observed count for an ADR and a drug of interest with all other ADRs and drugs in the dataset that together constitute a background from which an expected count is derived. The principal difference being the method by which the expected value is calculated [53]. There are primarily four different measures of disproportionality used in spontaneous reports: proportional reporting ratio (PRR) [54], reporting odds ratio (ROR) [55], information component (IC) [55], and Empirical Bayes Geometrical Mean (EBGM)

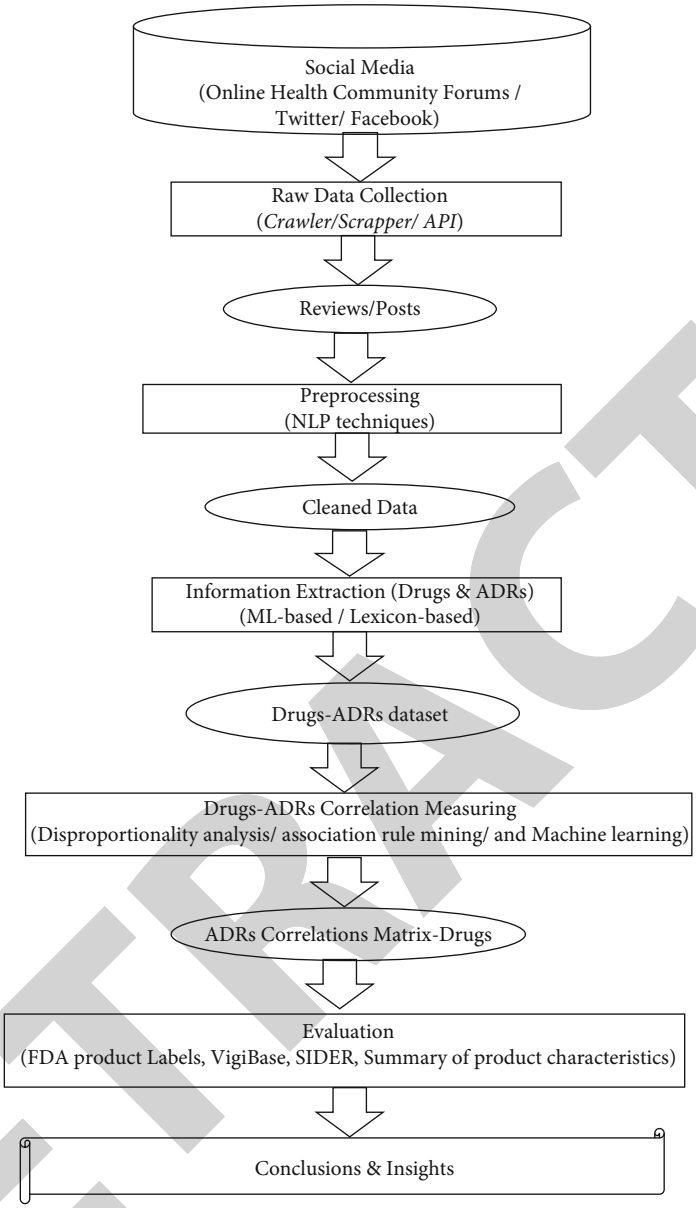

Figure 1: General methodology of detecting ADRs from social media.

[56]. Association rule mining approaches are aimed at mining the association rule of the form drug ⇒ ADR. Common measures used in association rule mining are support, confidence, and lift [14]. They are intuitive and easy to implement and computationally less intensive. However, the simple operation does not make statistical soundness in many cases because it does not adjust for the popularity of individual drug or correlation [57]. Finally, machine learning-based approaches have the merit of dealing with a common problem in the previous approaches, that is, the lake of automatic evaluation of interactions between drugs unless clearly stated in the model. Two examples of ML-based approaches that have been employed are random forests and Monte Carlo logic regression [57].

In the evaluation step, the performance of the ADR detection approach is evaluated. The common evaluation method is to use existing metrics such as recall, precision, F-score, and accuracy. Applying these metrics requires manually annotated data; however, in the absence of annotated data, these metrics can be computed using gold standards. The gold standard can be known ADRs from product labels or databases such as VigiBase, summary of product characteristics, FDA labels, and Side Effect Resource (SIDER) database [26].

3. Detecting ADRs of AEDs from OHC Data

As mentioned above, the objective of this research is to detect the ADRs of AEDs from drug consumers' reviews in OHCs. Accordingly, the methodology of achieving this objective is a customized variant of the general methodology of detecting ADRs from social media. It involves steps of

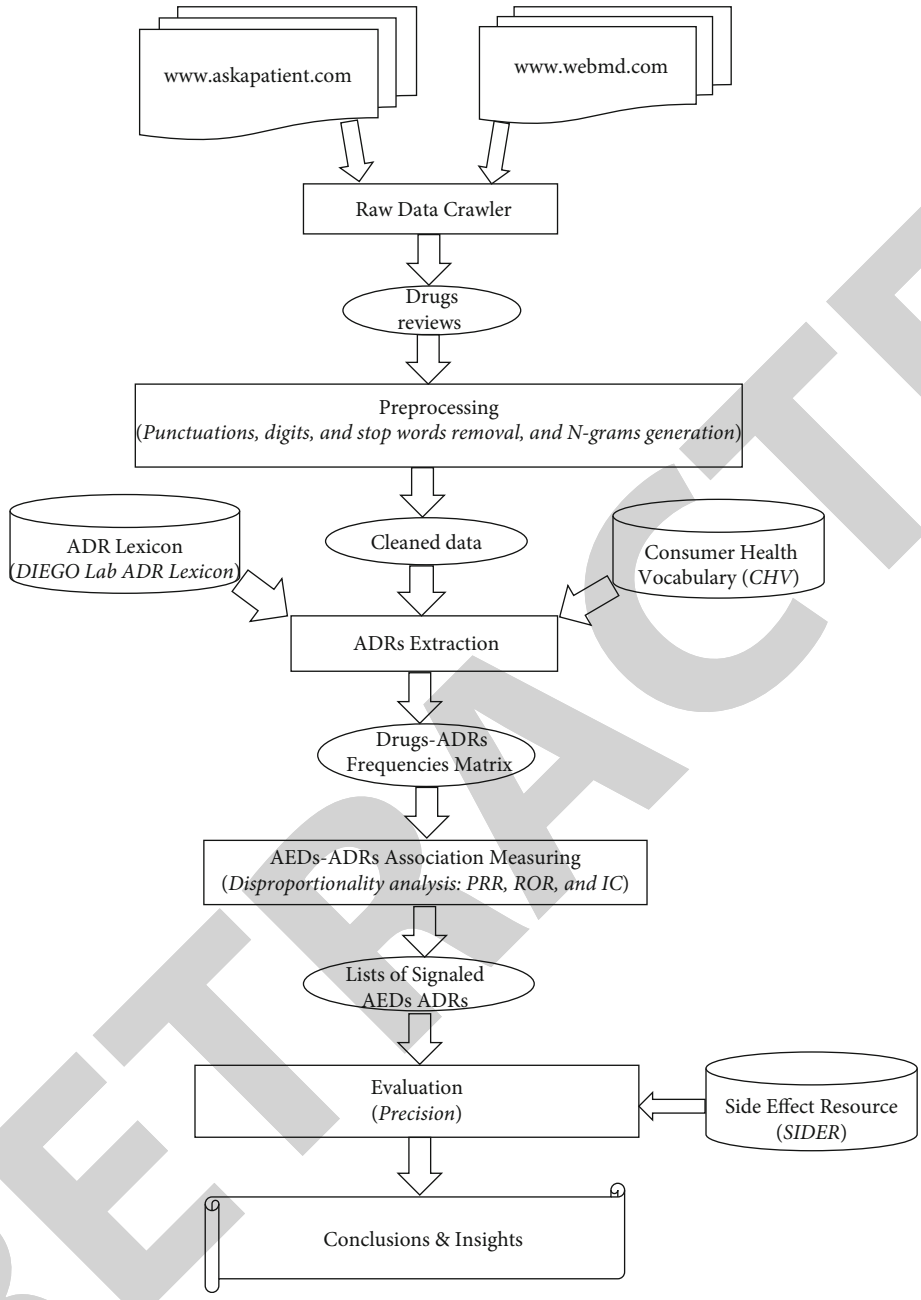

Figure 2: Methodology of AEDs' ADR detection.

collecting drug consumers' reviews from OHCs, applying NLP techniques to prepare the data, extracting ADRs for each drug, measuring the correlation between each drug and the extracted ADRs, and finally evaluating the validity and utility of the detected ADRs. Figure 2 depicts the steps of the proposed methodology, and the following subsections describe them in more detail.

3.1. AED Raw Data Collection. The raw data on AED reviews are captured from Askapatient and WebMD websites using a web crawler. The collected data from Askapatient includes ratings, reasons, side effects, comments from patients, gender, age, duration/dosage, and posting dates, whereas the collected data from the WebMD include age, sex, duration of treatment, and comments from patients. At the time of data collection, the number of patients' reviews on AEDs in Askapatient varies from 1860 for *lamotrigine* to only one review for several AEDs like *Aptiom*, whereas in WebMD, the number of patients' reviews ranges from 1818 for *Gabapentin* to 51 for *Dilantin*. For this research, the AEDs with number of reviews less than 170 are excluded from the data collection. Table 2 shows the AEDs that are considered in this research.

Additionally, to make the data more representative sample of drug population, data on non-AEDs must be collected to represent the background of the AED dataset. The

Table 2: List of considered AEDs.

No.	Generic name	Brand name	No. of reviews from Askapatient	No. of reviews from WebMD	Total No. of reviews
1	Gabapentin	Neurontin	914	1818	2732
2	Lamotrigine	Lamictal	1845	365	2210
3	Topiramate	Topamax	1764	237	2001
4	Pregabalin	Lyrica	1392	106	1498
5	Clonazepam	Clonazepam	324	1112	1436
6	Divalproex sodium	Depakote	566	133	699
7	Diazepam	Valium	393	261	654
8	Oxcarbazepine	Trileptal	357	119	476
9	Carbamazepine	Tegretol	283	150	433
10	Levetiracetam	Keppra	190	117	307
11	Phenytoin	Dilantin	183	51	234
12	Acetazolamide	Diamox	155	95	250
Total			8366	4564	12930

background data plays an essential role in the validity and reliability of ADR detection [58, 59]. For this purpose, a set of reviews on non-AEDs have been collected from Askapatient. Table 3 shows the details of 31 non-AEDs that have been considered in background data collection. They fall into five groups with a total of 43085 reviews.

Moreover, Tables 4 and 5 are snapshots of the raw data collected from the two OHCs, Askapatient and WebMD, for Lamictal (lamotrigine). The variation in the structure of the raw data among the two OHCs is notable; however, only the relevant raw data from the two OHCs are selected and complied into a unified dataset.

3.2. Data Preprocessing. The first step in the preprocessing step is the selection of the relevant data for each drug from the collected raw data. This includes side effects and comments from Askapatient and comment from WebMD. Then, the selected data are compiled into a unified dataset for each drug. Since these reviews are composed of free text, some NLP techniques are required to preprocess them. This involves the following:

(i) Text cleaning: all punctuations and digits are removed

(ii) Text normalization: convert text into lowercase

(iii) Stop word removal: the set of stop words is removed as they do not contribute to the detection of ADRs

(iv) N-gram generation: the unigrams, bigrams, and trigrams are generated from all the terms in each review. The maximum number of n-gram is set to three as the longest term of ADR in the ADR lexicon consisted of three words

3.3. ADR Extraction. In this step, the ADRs of each drug in the dataset are extracted and their frequency of occurrence is computed. The main idea of this process is to match every unigram, bigram, and trigram generated in the previous step with an ADR lexicon. However, in the casual and open environment of internet, patients tend to use very different vocabularies from professionals to express health concepts [60]. Therefore, the straightforward matching of the standard medical lexicon used by professionals cannot be used. To deal with this problem, CHV Wiki is employed to convert each term into the equivalent medical term. CHV is a collection of forms used in health-oriented communication for a particular task or need [60]. It reflects the difference between patients and professionals in expressing health concepts and helps to bridge this vocabulary gap.

After mapping every unigram, bigram, and trigram term to their equivalent CHV terms, they are mapped into ADR lexicon to identify the ADRs. For this purpose, the ADR lexicon, an exhaustive list of ADRs and their corresponding UMLS IDs compiled by the DIEGO lab, is used [50]. It includes concepts from thesaurus of Adverse Reaction Terms (COSTART), SIDER, and a subset of CHV that represents ADRs not listed in COSTART or SIDER. The final DIEGO LAB lexicon contains 13799 phrases with 7432 unique UMLS IDs. It has been made publicly available at http://diego.asu.edu/downloads/publications/ADRMine/ADR_lexicon.tsv. The result of the ADR extraction step is a list of ADRs for each AED along with its frequency in the corpus. Table 6 shows a snapshot of the extracted ADRs for lamotrigine AED represented in their UMLS ID, CHV term, lexicon ADR, and their corresponding count.

3.4. Measuring AED-ADR Association. In this step, the extracted ADRs of all AEDs are compiled into a matrix containing AEDs (columns) and ADRs (rows). Each cell in the matrix represents the frequency of an ADR in a particular AED. To measure the correlation between each AED and ADR in the AED-ADR matrix, the disproportionality analysis methods are used because they are the primary class of signal detection methods in pharmacovigilance research. In addition, they are currently applied in various national spontaneous reporting centers as well as in the Uppsala Monitoring Centre [61]. The calculations of the disproportionality analysis measures are based upon a two-by-two contingency table shown in Table 7.

Table 3: List of considered non-AEDs.

No	Drug group	Generic name	Brand name	No. of reviews from Askapatient
1	Depression drugs (19415 reviews)	Cymbalta	Duloxetine	1472
2		Effexor	Venlafaxine Hydrochloride	3907
3		Lexapro	Escitalopram Oxalate	3713
4		Zoloft	Sertraline Hydrochloride	2821
5		Wellbutrin Xl	Bupropion	2626
6		Wellbutrin	Bupropion Hydrochloride	2023
7		Celexa	Citalopram Hydrobromide	1081
8		Paxil	Paroxetine Hydrochloride	1772
9	Diabetes drugs (2336 reviews)	Actos	Pioglitazone Hydrochloride	613
10		Byetta	Exenatide Synthetic	333
11		Glucophage	Metformin Hydrochloride	1012
12		Victoza	Liraglutide Recombinant	378
13	High blood pressure (1891 reviews)	Lisinopril	Lisinopril	653
14		Coreg	Carvedilol	538
15		Inderal	Propranolol Hydrochloride	376
16		Micardis	Telmisartan	324
17	Allergy drugs (8845 reviews)	Zyrtec	Cetirizine Hydrochloride	3085
18		Claritin	Loratadine	1590
19		Allegra	Fexofenadine Hydrochloride	1346
20		Benadryl	Diphenhydramine Hydrochloride	948
21		Claritin-D 24 hour	Loratadine; Pseudoephedrine Sulfate	643
22		Astelin	Azelastine Hydrochloride	530
23		Vistaril	Hydroxyzine Hydrochloride	374
24		Xyzal	Levocetirizine Dihydrochloride	329
25	Digestive disorder (10598 reviews)	Prilosec	Omeprazole	2846
26		Nexium	Esomeprazole Magnesium	1871
27		Prevacid	Lansoprazole	434
28		Protonix	Pantoprazole Sodium	908
29		Aciphex	Rabeprazole Sodium	815
30		Zantac 150	Ranitidine Hydrochloride	376
31		Pepcid	Famotidine	364
Total				43085

a, b, c, and d are defined as follows:

(i) a: the number of ADR occurrences in the AED of interest

(ii) b: the number of other ADR occurrences in the AED of interest

(iii) c: the number of ADR occurrences in other AEDs

(iv) d: the number of other ADR occurrences in other AEDs

Table 8 contains the details of the disproportionality measures applied to measure the correlation between AEDs and ADRs. It is worth noting that each measure has its conditions that must be met to indicate a positive signal.

3.5. Evaluation. The evaluation of ADR detection is performed by comparing the proposed method with a chosen gold standard. The chosen gold standard is SIDER [63, 64]. It is a publicly available database containing ADR text mined from several public sources including the structured product labels. It has been used in numerous studies as a reference set to evaluate signal detection methods [65–67]. In SIDER 4.1 released from Oct. 2015, there are 5868 ADRs for 1430 drugs. Since the objective of this research is to investigate the validity of OHCs as a data source for ADR detection, the precision measure is used for evaluation because it is more indicative than recall. This is due to the differences in the methods of constructing the ADR lists from the OHCs and SIDER. In the case of the OHCs, the ADRs are extracted first and disproportionality analysis measures are then

Table 4: Snapshot of Askapatient raw data for Lamictal (lamotrigine).

Rating	Reason	Side effects for Lamictal	Comments	Sex	Age	Duration/ dosage	Date added
4	Anxiety, OCD, and BPD	Vivid, disturbing dreams and nightmares, increase in acne, weight loss	I really liked Lamictal. It helped with my severe anxiety and panic attacks and obsessive thoughts, and agitation. I'm not sure if it was the placebo effect because it was only a week in and it was such a small dose, but I definitely noticed an improvement. I had to stop it only 10 days in because I noticed it was making my acne worse. It wasn't anywhere as bad as Lithium, but it was still enough to make me feel more insecure. Another side effect was the vivid dreams. I was having extremely vivid, detailed, disturbing nightmares every night. I also experienced weight loss and lack of appetite but this wasn't a dealbreaker for me. The acne and nightmares were however. I really wish I could've kept taking it.	F	20	10 days/ 25 mg 1X D	3/30/ 2020
2	Personality disorder. Bipolar, co	It's hard to say that I can describe anything as being the fault of Lamictal. I also take Seroquel, propranolol, and 8 other meds for myriad of problems. Sex drive is there but no desire to pursue it. Fatigued, spaced out, thoughts scattered and unfocused. Hard to stay awake and have "blackouts". My memory was good but not now. It is non existent.		F	60	4 years/ 100 mg × 3	3/22/ 2020
3	Depression	Headaches, initial euphoria, lethargy		F	31	5 years/ 200 mg 1X D	1/30/ 2020
5	Bipolar 2	None	Before I started taking Lamictal I was being treated with Effexor alone. It helped some, but never made me feel "well". When I started taking Lamictal, everything changed. I wanted to live again, I am no longer thinking the worst about my life situations. For the first time in as long as I can remember, I am truly content. This drug saved my life.	F	52	1 month/ 75 mg	1/28/ 2020
1	Central pain syndrome	Save yourself! Terrible drug! It caused severe damage to my intestines. I have severe intestional spasms!!! There are not words to describe the amount of pain! Excruciating doesn't come close!! My suffering is caused by Lamotrigene!!!! I ubered to the is hospital because of this drug! I had no intestinal issues ever until this drug Now i have inflamation in my intestines and silent reflux, from Lamotrigine i can not eat anything acidic or spicy. I am praying this damage is NOT permanent. Or IT HAS DESTROYED MY LIFE!	Other side effects I experienced were a very dry parched mouth no matter how much you drank your mouth is dry that's awful then I started losing my balance.	F	58	3 months/ 25 mg	1/12/ 2020

applied where strict threshold values are used to determine the signaled ADRs, whereas in the case of SIDER, the ADRs are extracted from different sources, including FDA drug labels, in different frequency ranges (frequent, infrequent, rare, etc.). This makes the list of signaled ADRs from OHCs for a particular drug very short as compared to the

Table 5: Snapshot of webMD raw data for Lamictal (lamotrigine).

Condition	Review date	Reviewer info.	Comment
Condition: bipolar depression	6/7/2020 3:32:50 PM	Reviewer: Heatcap111, 35-44 on treatment for 5 to less than 10 years (patient)	I am on it for years and I feel like it makes me tired could that be
Condition: epileptic seizure	6/3/2020 1:21:23 AM	Reviewer: Girl sick of pill pushing doctors, 25-34 on treatment for 2 to less than 5 years (patient)	I've been taking this medication for a few years now and the side effects have become so unbearable that I'm getting off this medication. This is a mood suppressor for people with bipolar disorder so since given to me for seizures I feel numb, no sex drive, no motivation, and no energy. I'm lethargic and fatigued at some point every day and have trouble falling asleep at night. This med also causes constipation. The longer you take this med the more you'll have to increase the dose (more side effects) because this med is known for your body building a tolerance fast.
Condition: bipolar depression	2/8/2020 3:37:30 PM	Reviewer: K33vin, 55-64 on treatment for less than 1 month (patient)	I took 25 mg daily for a week. I think I was allergic. No sleep at all for five days. I had a headache that would not go away. I had body aches. Like the flu without fever. Nausea, vomiting, diarrhea. Chills. Stomach pain. I developed 52 cherry angiomas in one week. I lost 11 pounds. Stopped med at one week
Condition: bipolar depression	2/5/2020 8:37:33 PM	Reviewer: 19-24 on treatment for 2 to less than 5 years (patient)	
Condition: bipolar depression	1/14/2020 11:37:47 AM	Reviewer: j, 45-54 female on treatment for 1 to 6 months (patient)	I sleep just fine, I started at 25 mg and slowly went up to 100 mg currently. I'm tired and sleep great. No rash, no unbearable side effects.
Condition: bipolar depression	12/11/ 2019 3:03:57 PM	Reviewer: PekoeGirl1985, 25-34 female on treatment for 1 to less than 2 years (patient)	I did not get much sleep while on this medicine. The insomnia side effect is horrendous. Even with adding Ambien to the mix, I still would watch the sun rise. Also, the depersonalization side effect is pretty bad. I just didn't care about anything, and my passion for art was completely gone. I won't ever take this medicine again.

Table 6: Snapshot of extracted ADRs for Lamictal (lamotrigine).

CUI-CUI	CHV term	Lexicon ADR	Count
C0015230	Exanthema	Rash	358
C0003467	Anxiety	Anxiety	384
C0030193	Pain	Pain	335
C0043094	Weight gain	Weight problem	315
C0002622	Amnesia	Amnesia	301
C0344315	Depressed mood	Sadness	266
C0917801	Insomnia	Insomnia	258
C0002170	Alopecia	Alopecia	256
C0001144	Acne vulgaris	Acne vulgaris	235
C0085633	Mood swings	Mood altered	229
C0012833	Dizziness	Dizziness	198
C0015672	Fatigue	Lack of energy	195
C0226896	Oral cavity	Oral cavity	183
C0027497	Nausea	Nausea	180
C0033774	Pruritus	Pruritic disorder	171
C0026914	Mycobacterium avium complex	Mycobacterium avium intracellulare	160
C0338831	Manic	Mania	159
C0002957	Anger	Anger	146

Table 7: Two-by-two contingency table.

	ADR of interest	Other ADRs	
AED of interest	a	b	$a+b$
Other AEDs	c	d	$c+d$
	$a+c$	$b+d$	$n=a+b+c+d$

corresponding list of ADRs from SIDER. Consequently, when comparing the two lists of ADRs, the value of false negative (FN) (the number of ADRs occurred in SIDER but not in the signaled list of ADRs from OHCs) is extremely high and that makes the recall measure nonindicative to the validity of the OHCs. Formally, the precision measure is expressed as follows:

$$\text{Precision} = \frac{\text{TP}}{\text{TP} + \text{FP}} \quad (1)$$

where TP (true positive) is the number of ADRs that cooccurred in the signaled list of ADRs and SIDER and FP (false positive) is the number of ADRs that occurred in the signaled list of ADRs but not in the SIDER.

4. Results and Discussions

In this section, the results of applying the methodology described above to detect the ADRs of AEDs are presented, validated, and analyzed to answer the research questions on the validity and utility of OHC data source. Prior to this, however, useful details on the implementation settings are worth mentioning. The methodology of detecting ADRs of AEDs from OHCs is implemented using the Python programming language and a Microsoft Excel spreadsheet. More specifically, Python equipped with a powerful natural language toolkit, NLTK, is used to develop a data crawler that captures patients' reviews from Askapatient and WebMD, preprocesses the collected data, and extracts ADRs from the processed data. Moreover, MS Excel spreadsheet with a powerful data analysis package, XLSTAT, that allows users to analyze data within the Excel spreadsheet is used to perform the computation of disproportionality analysis. The size of the collected dataset is 56015 reviews, where 23.08% of the dataset is pertaining AEDs and 76.92% is for non-AEDs. In the implementation of the disproportionality analysis methods, the thresholds are set as given in Table 8 and the ADRs with frequency less than 3 are excluded from the disproportionality analysis computation.

4.1. Signaled AED ADRs. The results of applying the three dispropotionality measures to detect the ADRs are lists of signaled ADRs for each AED. In other words, three lists of signaled ADRs for each AED from the three measures are generated. It should be mentioned that for a given AED, the generated ADRs lists are different in size. Table 9 shows the size of the ADR lists signaled by the PRR, ROR, and IC for each AED. Obviously, the difference in the size of the generated ADR lists is most notable between PRR and ROR from one side and IC from the other side. This reflects the differences between the adopted computation and thresholding values among the three measures. Moreover, the size of the raw data (number of reviews) among AEDs could be used to highlight the differences in the size of the signaled ADRs. For instance, Gabapentin has the highest number of signaled ADRs and also the highest number of reviews. *Phenytoin*, on the other hand, has the lowest numbers of signaled ADRs and the lowest number of reviews as well.

Concerning the generated lists of ADRs for each AED, they are of different types: immunologic, hypersensitivity, nervous system, psychiatric, ocular, gastrointestinal, respiratory, and dermatologic. Moreover, some of them require immediate medical attention such as lymph node enlargement and renal calculi, while others such as loss of weight and weakness do not, as they may disappear during treatment as the body adjusts to the drug. In each list, each ADR is associated with a unique value that represents its correlation with a particular AED. Tables 10, 11, and 12 show the top 10 signaled ADRs for each AED.

A comparative look at the top 10 ADR lists within and across the three tables reveals a variation in the ADRs among AEDs within each table and a notable agreement between the top-10 ADR lists across the three tables. These observations suggest the need for further analysis to answer the research questions.

4.2. Validity of the Signaled AED ADRs. Since the validity of social media as a data source for pharmacovigilance is still under investigation [23] and the objective of this research is to investigate the validity of the OHC data for the detection of AEDs' ADRs, the signaled AEDs' ADR lists are compared with the counterpart lists in SIDER [63] in terms of precision as given in Equation (1). The results of precision for the signaled ADRs by the three measures (PRR, ROR, and IC) are shown in Table 13. In addition, the precision of the unified list of signaled ADRs (PRR $\cup$ ROR $\cup$ IC) as well as the common list of ADRs (PRR $\cap$ ROR $\cap$ IC) signaled by the three measures is presented.

From the above table, it is obvious that the validation results with SIDER vary notably among AEDs. It is the lowest in the case of Levetiracetam and the highest in the case of Carbamazepine. Realizing that both sides of the validation process, AED ADR detection from the OHCs reviews and the SIDER ADR collection from drug labels, depend on the quality and quantity of data sources available for each AED, which vary among AEDs, the variation of the validation results among AEDs is meaningful.

On the other hand, the limited variation among PRR, ROR, IC, and their unified and common lists of signaled ADRs is also notable. More precisely, the comparison between the validation results of the three measures indicates that the validation results of PRR and ROR are comparable and identical in 4 AED cases. As for the IC, the validation results are lower as compared to the validation results of PRR and ROR. This indicates that both PRR and ROR perform slightly better than IC, which contradicts with the previously drawn conclusion on the better performance of IC as compared to PRR and ROR. The specific

Table 8: Details of the disproportionality analysis methods.

#	Metric	Computations	Threshold	95% confidence interval
1	Proportional reporting ratio (PRR) [54]	$\mathrm{PRR} = \frac{a/(a+c)}{b/(b+d)}$ $\mathrm{SE} = \sqrt{\frac{1}{a} - \frac{1}{a+b} + \frac{1}{c} - \frac{1}{c+d}}$ $\chi^2 = \frac{(a+b+c+d)(ad-bc)^2}{(a+c)(a+b)(b+d)(c+d)}$	$\mathrm{PRR} \geq 2$ $\chi^2 > 4$ ≥3 cases reported	$\mathrm{CI} = e^{\ln \mathrm{PRR} \pm 1.96\mathrm{SE}}$
2	Reporting odds ratio (ROR) [55]	$\mathrm{ROR} = \frac{a/c}{b/d} = \frac{ad}{bc}$ $\mathrm{SE} = \sqrt{\frac{1}{a} + \frac{1}{b} + \frac{1}{c} + \frac{1}{d}}$	$\mathrm{ROR} - 1.96\mathrm{SE} > 1$ ≥2 cases reported	$\mathrm{CI} = e^{\ln \mathrm{ROR} \pm 1.96\mathrm{SE}}$
3	Information component [62]	$\mathrm{IC} = \log_2 \frac{a(a+b+c+d)}{(a+c)(a+b)}$ $\mathrm{SD} = \sqrt{\frac{b}{a(a+b)} + \frac{(b+d)}{(a+c)(a+b+c+d)}}$	$\mathrm{IC} - 2\mathrm{SD} > 0$	$\mathrm{CI} = e^{\ln \mathrm{IC} \pm 1.96\mathrm{SD}}$

Table 9: Number of signaled ADRs for each AED using PRR, ROR, and IC.

No	Generic name	No. of signaled ADRs (PRR)	No. of signaled ADRs (ROR)	No. of signaled ADRs (IC)
1	Acetazolamide	99	99	99
2	Carbamazepine	107	107	104
3	Clonazepam	151	149	139
4	Diazepam	123	123	112
5	Divalproex sodium	105	104	97
6	Gabapentin	222	214	189
7	Lamotrigine	213	200	197
8	Levetiracetam	115	115	114
9	Oxcarbazepine	139	138	132
10	Pregabalin	195	184	199
11	Phenytoin	83	83	85
12	Topiramate	184	174	174

characteristics of the two data sources, SRS and OHCs, and their associated techniques could interpret this contradiction. Despite the reported limitations of existing evaluation methods [26], the validation results shown in Table 13 indicate the validity of the OHCs as a source of data for ADR detection.

With regard to the comparison of the obtained results with the previously reported ones, the difficulty of conducting this assessment in this manner has been pointed out in [26], since in each research, a different dataset is used. Moreover, the absence of annotated benchmark dataset makes the use of the gold standard such as FDA label or SIDER, despite its reported shortcomings, the sole possible option. Nonetheless, the comparison of the obtained precision values with the precision values reported in previous research, regardless of the contextual differences, can position this research methodology within the previously proposed ones. As reported in [26], the precision values reported in eleven previous research range between 0.54 and 0.87, whereas the precision values obtained in this research range between 0.62 and 0.84. The consistency between the precision values of this research methodology and the previous research is obvious.

4.3. Common ADRs of AED Analysis. The common AEDs' ADRs are those ADRs that are shared by most, if not all, AEDs. To answer the research question on the common AEDs' ADRs that are detected from OHC data, three lists of the common ADRs signaled by PRR, ROR, and IC along with their probabilities of occurrence are generated as shown in Table 14. The high degree of agreement between the lists of common AEDs' ADR generated by the three measures is notable, though the IC generates a shorter list. Nonetheless, most of the ADRs in the three lists are common. A closer look at these lists reveals that they are dominated by the CNS ADRs, which is consistent with what is reported in the literature of AEDs' ADRs. Since AEDs act to suppress the pathological neuronal hyperexcitability that constitutes the final substrate in many seizure disorders, it is not surprising that they are prone to causing adverse reactions that affect the CNS [37]. Moreover, according to [68], the CNS ADRs are the most frequently reported type of AEDs' ADRs and this typically includes fatigue, drowsiness, concentration difficulties, memory problems, and irritability.

4.4. AED ADR Similarity Analysis. The similarity between drugs in terms of their ADRs reflects their structural composition and mechanism of action [68]. To answer the research question on the potential similarities between AEDs in terms of their signaled ADRs, a similarity measure is developed and applied to quantify the similarity between each pair of AEDs as computed from the lists of signaled ADRs

Table 10: Top 10 PRR ranked ADRs of AEDs.

Acetazolamide (Diamox)		Carbamazepine (Tegretol)		Clonazepam (clonazepam)		Diazepam (Valium)		Divalproex sodium (Depakote)		Gabapentin (Neurontin)	
ADRs	PRR	ADRs	PRR	ADRs	PRR	ADRs	PRR	ADRs	PRR	Radiculopathy	103.20
Cloudy urine	1295.13	Trigeminal neuralgia	79.19	Adiposis dolorosa	28.29	Heart septal defects, atrial	210.28	Neurosis	153.39	Chiari malformation	61.92
Diuretic effect	555.05	Lump in neck	65.99	Aortic valve incompetence	28.29	Diseases of the inner ear	210.28	Ovarian disorder	153.39	Intractable pain	61.92
Cerebrospinal fluid	333.03	Strabismus	52.80	Hemorrhage intracerebral	28.29	Ear diseases	105.14	Polycystic ovary disease	85.21	Mastocytosis	41.28
Metabolic acidosis	277.53	Hyponatremia	47.14	Delusional disorder	28.29	Fibroid tumor	105.14	Vasospasm	76.69	Multiple organ failure	41.28
Intracranial hypertension	185.02	Neuralgia	45.31	Dissociative reaction	28.29	Meniere's disease	90.12	Abnormal menstrual cycle	76.69	Rhabdomyolysis	41.28
Spinal headache	185.02	Speech disorder	44.00	Parasomnia	28.29	Muscle spasticity	63.08	Psychotic state	76.69	Mobility decreased	41.28
Glaucoma	66.61	Deja vu	33.00	Thrombosis	28.29	Premenstrual tension	63.08	Lung problem	51.13	Compression injury of nerve	39.69
Acidosis	61.67	Meningitis	33.00	Thrombosis venous	28.29	Claustrophobia	52.57	Paranoid delusions	38.35	Postherpetic neuralgia	30.96
Sarcoidosis	61.67	Dyslexia	28.69	Alanine aminotransferase increased	28.29	Cholecystectomy	35.05	Hyperthyroidism	30.68	Feet burning	25.80
Gum blister	61.67	Necrosis	26.40	Hyperpyrexia	28.29	Torticollis	35.05	Paralysis agitans	27.89	Radiculopathy	103.20
Lamotrigine (Lamictal)		Levetiracetam (Keppra)		Oxcarbazepine (Trileptal)		Pregabalin (Lyrica)		Phenytoin (Dilantin)		Topiramate (Topamax)	
ADRs	PRR	ADRs	PRR	ADRs	PRR	ADRs	PRR	ADRs	PRR	ADR	PRR
Wrinkling	50.01	Meningiomas	315.71	Coagulation disorder	112.54	Astigmatism	45.66	Eclampsia	313.32	Sulfa allergy	116.39
Tanning	24.25	Cerebral lesions	315.71	Drug eruption	112.54	Joint disorders	45.66	Facial paralysis	313.32	Narrow angle glaucoma	49.88
Stevens-Johnson syndrome	21.82	Necrotic debris	157.85	Gonorrhea	112.54	Decreased platelet	34.24	Heat stroke	156.66	Renal calculi	42.75
Lymph node enlargement	19.84	Vascular disease	157.85	Colitis microscopic	112.54	Pernicious anemia	22.83	Gum disorder	104.44	Mental blocking	33.25
Bronchopulmonary dysplasia	18.18	Attitude changed	157.85	Negative pregnancy test	112.54	Contracture	22.83	Para	104.44	Myopia	27.71
Hair disorder	18.18	Hematoma	105.24	Increased sodium	112.54	Facial nerve palsies	22.83	Mental status changes	104.44	Migraine	17.49
Hypermetropia	18.18	Pharyngitis streptococcal	78.93	Persistent dry cough	112.54	Optic neuritis	22.83	Swollen gums	104.44	Aphasia	16.63
Melancholia	18.18	Liver failure	63.14	Sodium decreased	98.48	Peripheral nervous system	22.83	Hodgkin lymphoma	78.33	Coagulation disorder	16.63
Necrotic debris	18.18	Pruritus ani	52.62	Vaginal infection	75.03	Skin fissures	22.83	Amyotrophy	78.33	Facial nerve palsies	16.63
Pregnancy complication	18.18	Pain exacerbated	52.62	Hyponatremia	65.65	Attitude changed	22.83	Verruca	78.33	Facial paralysis	16.63

Table 11: Top 10 ROR ranked ADRs of AEDs.

Acetazolamide (Diamox)		Carbamazepine (Tegretol)		Clonazepam (clonazepam)		Diazepam (Valium)		Divalproex sodium (Depakote)		Gabapentin (Neurontin)	
ADRs	ROR	ADRs	ROR	ADRs	ROR	ADRs	ROR	ADRs	ROR	ADRs	ROR
Cloudy urine	1302.31	Trigeminal neuralgia	79.99	Adiposis dolorosa	28.30	Heart septal defects, atrial	210.47	Neurosis	153.49	Radiculopathy	103.25
Diuretic effect	556.37	Lump in neck	66.03	Aortic valve incompetence	28.30	Diseases of the inner ear	210.47	Ovarian disorder	153.49	Chiari malformation	61.94
Cerebrospinal fluid	337.81	Strabismus	52.85	Hemorrhage intracerebral	28.30	Ear diseases	105.19	Polycystic ovary disease	85.49	Intractable pain	61.94
Metabolic acidosis	278.18	Hyponatremia	47.27	Delusional disorder	28.30	Fibroid tumor	105.19	Vasospasm	76.79	Mastocytosis	41.29
Spinal headache	185.31	Neuralgia	45.89	Dissociative reaction	28.30	Meniere's disease	90.36	Abnormal menstrual cycle	76.74	Multiple organ failure	41.29
Intracranial hypertension	185.16	Speech disorder	44.02	Parasomnia	28.30	Muscle spasticity	63.17	Psychotic state	76.74	Rhabdomyolysis	41.29
Glaucoma	67.08	Deja vu	33.02	Thrombosis	28.30	Premenstrual tension	63.17	Lung problem	51.16	Mobility decreased	41.29
Acidosis	61.86	Meningitis	33.02	Thrombosis venous	28.30	Claustrophobia	52.62	Paranoid delusions	38.37	Compression injury of nerve	39.78
Sarcoidosis	61.72	Dyslexia	28.77	Alanine aminotransferase increased	28.30	Cholecystectomy	35.06	Hyperthyroidism	30.70	Postherpetic neuralgia	30.99
Gum blister	61.72	Necrosis	26.41	Adiposis dolorosa	28.30	Torticollis	35.06	Paralysis agitans	27.92	Feet burning	25.84
Lamotrigine (Lamictal)		Levetiracetam (Keppra)		Oxcarbazepine (Trileptal)		Pregabalin (Lyrica)		Phenytoin (Dilantin)		Topiramate (Topamax)	
ADRs	ROR	ADRs	ROR	ADRs	ROR	ADRs	ROR	ADRs	ROR	ADRs	ROR
Wrinkling	50.05	Meningiomas	316.13	Drug eruption	112.65	Astigmatism	45.67	Eclampsia	313.74	Sulfa allergy	116.45
Tanning	24.25	Cerebral lesions	316.13	Coagulation disorder	112.60	Joint disorders	45.67	Facial paralysis	313.74	Narrow angle glaucoma	49.89
Stevens Johnson syndrome	21.83	Necrotic debris	157.96	Gonorrhea	112.60	Decreased platelet	34.26	Heat stroke	157.08	Renal calculi	42.98
Lymph node enlargement	19.87	Vascular disease	157.96	Colitis microscopic	112.60	Peripheral nervous system	22.85	Swollen gums	105.13	Mental blocking	33.26
Bronchopulmonary dysplasia	18.20	Attitude changed	157.96	Negative pregnancy test	112.60	Skin fissures	22.83	Gum disorder	104.58	Myopia	27.72
Weight fluctuation	18.19	Hematoma	105.38	Increased sodium	112.60	Intoxication	22.83	Para	104.58	Migraine	19.53
Unrest	18.19	Pharyngitis streptococcal	78.98	Persistent dry cough	112.60	Pernicious anemia	22.83	Mental status changes	104.58	Aphasia	16.64
Hair disorder	18.19	Liver failure	63.23	Sodium decreased	98.80	Contracture	22.83	Hodgkin lymphoma	78.43	Altered taste	16.64
Hypermetropia	18.19	Pruritus ani	52.65	Vaginal infection	75.10	Facial nerve palsies	22.83	Amyotrophy	78.43	Aversion	16.63
Melancholia	18.19	Pain exacerbated	52.65	Hyponatremia	65.87	Optic neuritis	22.83	Verruca	78.43	Sudden infant death	16.63

Table 12: Top 10 IC ranked ADRs of AEDs.

Acetazolamide (Diamox)		Carbamazepine (Tegretol)		Clonazepam (clonazepam)		Diazepam (VALIUM)		Divalproex sodium (Depakote)		Gabapentin (Neurontin)	
ADRs	IC	ADRs	IC	ADRs	IC	ADRs	IC	ADRs	IC	ADRs	IC
Papilledema	7.54	Aplastic anemia	7.06	Coronary bypass	5.85	Hyperplasia	6.73	Glioma	7.27	Herpes zoster	4.44
Rectal pain	7.54	Blepharospasm	7.06	Anterograde amnesia	5.85	Neck injuries	6.73	Erythropoietic protoporphyria	7.27	Myeloma	4.44
Dehiscence	7.54	Syndrome of inappropriate antidiuretic hormone	7.06	Adiposis dolorosa	4.26	Fracture of pelvis nos (disorder)	6.73	St segment depression	7.27	Otitis media	4.44
Cloudy urine	7.35	Enlarged breasts	7.06	Aortic valve incompetence	4.26	Temporomandibular joint dislocation	6.73	Neurosis	6.27	Spondylitis	4.44
Diuretic effect	7.12	Chemical meningitis	7.06	Hemorrhage intracerebral	4.26	Weal (disorder)	6.73	Ovarian disorder	6.27	Ankylosing spondylitis	4.44
Metabolic acidosis	6.80	Trigeminal neuralgia	5.64	Delusional disorder	4.26	Splinter	6.73	Polycystic ovary disease	5.78	Staphylococcal infection	4.44
Intracranial hypertension	6.54	Lump in neck	5.47	Dissociative reaction	4.26	Heart septal defects, atrial	6.14	Vasospasm	5.69	Tachyphylaxis	4.44
Spinal headache	6.54	Strabismus	5.25	Parasomnia	4.26	Diseases of the inner ear	6.14	Abnormal menstrual cycle	5.69	Total knee replacement	4.44
Glaucoma	5.62	Hyponatremia	5.13	Thrombosis	4.26	Ear diseases	5.73	Psychotic state	5.69	Neurotoxicity syndromes	4.44
Acidosis	5.54	Neuralgia	5.09	Thrombosis venous	4.26	Fibroid tumor	5.73	Lung problem	5.27	Stenosis of cervix	4.44
Lamotrigine (Lamictal)		Levetiracetam (Keppra)		Oxcarbazepine (Trileptal)		Pregabalin (Lyrica)		Phenytoin (Dilantin)		Topiramate (Topamax)	
ADRs	IC	ADRs	IC	ADRs	IC	ADRs	IC	ADRs	IC	ADRs	IC
Gouty arthritis	4.26	Dermatitis exfoliative	7.31	Reduced hearing	6.83	Anomia	4.57	Cleft lip	1.41	Anisocoria	4.14
Cognitive disorder nos	4.26	Hematoma subdural	7.31	Myasthenia gravis	6.83	Bunion	4.57	Febrile seizures	1.41	Eyelid ptosis	4.14
Diabetes insipidus	4.26	Subarachnoid hemorrhage	7.31	Genital rash	6.83	Cushing's syndrome	4.57	Lymphomas	1.41	Cysto	4.14
Dilatation and curettage	4.26	Increased bun	7.31	Myasthenia	6.83	Scleroderma	4.57	Methemoglobinemia	1.41	Emaciation	4.14
Encephalitis	4.26	Hair ingrown	7.31	Coagulation disorder	5.83	Dry eye syndrome	4.57	Loss of affect	1.41	Ocular infections	4.14
Toxic epidermal necrolysis	4.26	Normal platelet count	7.31	Drug eruption	5.83	Dwarfism	4.57	Eclampsia	1.22	Depilation	4.14
Folate deficiency	4.26	Family stress	7.31	Gonorrhea	5.83	Epicondylitis	4.57	Facial paralysis	1.22	Hepatomegaly	4.14
Herpes simplex	4.26	Lip blister	7.31	Colitis microscopic	5.83	Episcleritis	4.57	Gum disorder	1.12	Meningitis viral	4.14
External ear infection	4.26	Meningiomas	6.73	Negative pregnancy test	5.83	Cardiospasm	4.57	Para	1.12	Menstrual disorder	4.14
Head lice	4.26	Cerebral lesions	6.73	Increased sodium	5.83	Failure to thrive	4.57	Mental status changes	1.12	Mental retardation	4.14

Table 13: Precision of the generated lists of signaled ADRs.

	PRR ∪ ROR ∪ IC	PRR	ROR	IC	PRR ∩ ROR ∩ IC
Acetazolamide	0.63	0.64	0.64	0.63	0.64
Carbamazepine	0.80	0.82	0.82	0.81	0.83
Clonazepam	0.70	0.70	0.69	0.69	0.68
Diazepam	0.73	0.73	0.73	0.74	0.74
Divalproex sodium	0.73	0.74	0.74	0.73	0.74
Gabapentin	0.68	0.72	0.69	0.68	0.70
Lamotrigine	0.75	0.77	0.77	0.75	0.72
Levetiracetam	0.61	0.63	0.63	0.62	0.64
Oxcarbazepine	0.76	0.78	0.78	0.78	0.77
Pregabalin	0.76	0.77	0.81	0.77	0.80
Phenytoin	0.69	0.75	0.74	0.71	0.68
Topiramate	0.75	0.79	0.80	0.77	0.84
Average	0.71	0.74	0.74	0.72	0.73

Table 14: Common ADRs among AEDs.

PRR		ROR		IC	
ADR	Pr(ADR)	ADR	Pr(ADR)	ADR	Pr(ADR)
Amnesia	0.75	Amnesia	0.75	Amnesia	0.75
Slurred	0.75	Slurred	0.75	Slurred	0.75
Forgetfulness	0.67	Forgetfulness	0.75	Forgetfulness	0.67
Epileptic seizure	0.67	Epileptic seizure	0.67	Epileptic seizure	0.67
Mental confusion	0.58	Mental confusion	0.67	Convulsion	0.67
Somnolence	0.58	Somnolence	0.58	Mental confusion	0.58
Convulsion	0.58	Convulsion	0.58	Aura	0.58
Aura	0.58	Aura	0.58	Convulsions local	0.58
Convulsions local	0.58	Convulsions local	0.58	Somnolence	0.58
Cerebrovascular stroke	0.58	Cerebrovascular stroke	0.58	Cerebrovascular stroke	0.58
Deafness	0.50	Deafness	0.58	Vision double	0.50
Vision double	0.50	Vision double	0.50	Blurring of visual image	0.50
Blurring of visual image	0.50	Convulsion grand mal	0.50	Convulsion grand mal	0.50
Convulsion grand mal	0.50	Convulsion petit mal	0.50	Seizure grand mal	0.50
Convulsion petit mal	0.50	Seizure grand mal	0.50	Traumatic injury	0.50
Gain weight	0.50	Gain weight	0.50	Gain weight	0.50
Seizure grand mal	0.50				
Clumsiness	0.50				

generated by PRR, ROR, and IC. In this measure, the similarity between a pair of AEDs, e.g., AED_x and AED_y, is computed as follows:

$$\mathrm{Similarity}\left(\mathrm{AED}_x, \mathrm{AED}_y\right) = \frac{\mathrm{count}\left(\mathrm{ADR}_{\mathrm{AED}_x} \cap \mathrm{ADR}_{\mathrm{AED}_y}\right)}{\mathrm{count}\left(\mathrm{ADR}_{\mathrm{AED}_x}\right)}. \tag{2}$$

Since the ADR lists of AED_x and AED_y are different in size, the computed $\mathrm{Similarity}(\mathrm{AED}_x, \mathrm{AED}_y)$ and $\mathrm{Similarity}(\mathrm{AED}_y, \mathrm{AED}_x)$ are expected to be different as well. Table 15, 16, and 17 show the similarity between each AED pairs in terms of the signaled ADR lists generated by PRR, ROR, and IC, respectively.

The consistency between the ADR similarity of AED pairs across the three tables is notable. However, to obtain an overall summary of the similarity of AED pairs, the overall average similarity for each AED pair, AED_x and AED_y, is computed as the mean of the three similarity averages obtained from each table. Table 18 shows the overall average similarity for each AED pair.

From Table 18, it is obvious that the overall average similarity of a number of AED pairs is relatively remarkable such as (Pregabalin, Gabapentin), (Diazepam, Clonazepam),

Table 15: Similarity between AED pairs—PRR.

	Acetazolamide	Carbamazepine	Clonazepam	Diazepam	Divalproex sodium	Gabapentin	Lamotrigine	Levetiracetam	Oxcarbazepine	Pregabalin	Phenytoin	Topiramate
Acetazolamide	1	0.17	0.12	0.05	0.09	0.13	0.21	0.15	0.20	0.18	0.06	0.36
Carbamazepine	0.16	1	0.15	0.07	0.22	0.24	0.35	0.24	0.32	0.33	0.21	0.27
Clonazepam	0.08	0.11	1	0.28	0.09	0.19	0.13	0.11	0.09	0.16	0.09	0.10
Diazepam	0.04	0.07	0.35	1	0.10	0.20	0.13	0.10	0.11	0.17	0.11	0.08
Divalproex sodium	0.07	0.20	0.11	0.10	1	0.10	0.28	0.16	0.17	0.11	0.15	0.18
Gabapentin	0.06	0.12	0.13	0.11	0.05	1	0.13	0.10	0.14	0.34	0.09	0.12
Lamotrigine	0.10	0.18	0.09	0.08	0.16	0.14	1	0.22	0.23	0.15	0.16	0.22
Levetiracetam	0.13	0.23	0.15	0.10	0.17	0.20	0.39	1	0.26	0.18	0.21	0.24
Oxcarbazepine	0.14	0.24	0.10	0.10	0.15	0.22	0.34	0.22	1	0.20	0.15	0.20
Pregabalin	0.09	0.18	0.12	0.11	0.07	0.38	0.15	0.11	0.13	1	0.07	0.17
Phenytoin	0.04	0.12	0.08	0.07	0.10	0.11	0.17	0.13	0.11	0.08	1	0.12
Topiramate	0.20	0.16	0.08	0.05	0.12	0.14	0.24	0.15	0.14	0.18	0.12	1

Table 16: Similarity between AED pairs—ROR.

	Acetazolamide	Carbamazepine	Clonazepam	Diazepam	Divalproex sodium	Gabapentin	Lamotrigine	Levetiracetam	Oxcarbazepine	Pregabalin	Phenytoin	Topiramate
Acetazolamide	1	0.17	0.11	0.05	0.09	0.12	0.20	0.15	0.20	0.17	0.06	0.33
Carbamazepine	0.16	1	0.15	0.07	0.21	0.22	0.35	0.24	0.32	0.32	0.21	0.25
Clonazepam	0.07	0.11	1	0.28	0.09	0.19	0.13	0.11	0.09	0.15	0.09	0.08
Diazepam	0.04	0.07	0.34	1	0.10	0.20	0.12	0.10	0.11	0.17	0.11	0.07
Divalproex sodium	0.09	0.22	0.13	0.12	1	0.12	0.33	0.19	0.20	0.13	0.17	0.18
Gabapentin	0.06	0.11	0.13	0.11	0.06	1	0.12	0.11	0.14	0.33	0.09	0.10
Lamotrigine	0.10	0.19	0.10	0.08	0.17	0.13	1	0.22	0.21	0.14	0.17	0.21
Levetiracetam	0.13	0.23	0.15	0.10	0.17	0.20	0.38	1	0.26	0.17	0.21	0.24
Oxcarbazepine	0.14	0.25	0.10	0.10	0.15	0.22	0.30	0.22	1	0.19	0.15	0.17
Pregabalin	0.10	0.19	0.13	0.12	0.08	0.39	0.15	0.11	0.15	1	0.08	0.16
Phenytoin	0.07	0.28	0.17	0.16	0.22	0.23	0.40	0.29	0.25	0.16	1	0.27
Topiramate	0.19	0.16	0.07	0.05	0.11	0.12	0.24	0.16	0.13	0.17	0.13	1

Table 17: Similarity between AED pairs—IC.

	Acetazolamide	Carbamazepine	Clonazepam	Diazepam	Divalproex sodium	Gabapentin	Lamotrigine	Levetiracetam	Oxcarbazepine	Pregabalin	Phenytoin	Topiramate
Acetazolamide	1.00	0.14	0.09	0.05	0.06	0.12	0.20	0.13	0.20	0.15	0.05	0.34
Carbamazepine	0.13	1.00	0.12	0.07	0.16	0.19	0.33	0.22	0.30	0.28	0.21	0.21
Clonazepam	0.06	0.09	1.00	0.25	0.09	0.15	0.13	0.12	0.10	0.12	0.10	0.06
Diazepam	0.05	0.07	0.32	1.00	0.09	0.18	0.08	0.06	0.09	0.14	0.12	0.07
Divalproex sodium	0.06	0.18	0.13	0.09	1.00	0.10	0.33	0.18	0.20	0.11	0.15	0.19
Gabapentin	0.06	0.11	0.11	0.10	0.05	1.00	0.11	0.10	0.15	0.34	0.10	0.09
Lamotrigine	0.10	0.17	0.09	0.04	0.16	0.11	1.00	0.21	0.20	0.10	0.16	0.15
Levetiracetam	0.11	0.20	0.14	0.05	0.15	0.17	0.36	1.00	0.25	0.16	0.18	0.20
Oxcarbazepine	0.15	0.23	0.11	0.07	0.14	0.21	0.30	0.21	1.00	0.20	0.16	0.17
Pregabalin	0.08	0.15	0.09	0.08	0.06	0.32	0.10	0.09	0.13	1.00	0.07	0.11
Phenytoin	0.06	0.26	0.16	0.15	0.18	0.22	0.36	0.24	0.25	0.15	1.00	0.21
Topiramate	0.20	0.13	0.05	0.04	0.10	0.10	0.17	0.13	0.13	0.13	0.10	1.00

Table 18: Overall average ADR similarity between AED pairs using ADRs signaled by PRR, ROR, and IC.

	Acetazolamide	Carbamazepine	Clonazepam	Diazepam	Divalproex sodium	Gabapentin	Lamotrigine	Levetiracetam	Oxcarbazepine	Pregabalin	Phenytoin	Topiramate
Acetazolamide												
Carbamazepine	0.16											
Clonazepam	0.09	0.12										
Diazepam	0.05	0.07	0.30									
Divalproex sodium	0.08	0.20	0.11	0.10								
Gabapentin	0.09	0.17	0.15	0.15	0.08							
Lamotrigine	0.15	0.26	0.11	0.09	0.24	0.12						
Levetiracetam	0.13	0.23	0.13	0.09	0.17	0.15	0.30					
Oxcarbazepine	0.17	0.28	0.10	0.10	0.17	0.18	0.26	0.24				
Pregabalin	0.13	0.24	0.13	0.13	0.09	0.35	0.13	0.14	0.17			
Phenytoin	0.06	0.22	0.12	0.12	0.16	0.14	0.24	0.21	0.18	0.10		
Topiramate	0.27	0.20	0.07	0.06	0.15	0.11	0.20	0.19	0.16	0.15	0.16	

(Lamotrigine, Levetiracetam), (Oxcarbazepine, Carbamazepine), (Topiramate, Acetazolamide), and (Lamotrigine, Carbamazepine). This can be interpreted by similarity of the mechanisms of action of these AED pairs [1]. For example, both Pregabalin and Gabapentin have a common mechanism of blockade of $\alpha 2\delta$ subunit of Ca^{2+}, Oxcarbazepine and Carbamazepine are Na^{+} channel blockers, and Lamotrigine and Carbamazepine are also Na^{+} channel blockers. With regard to Diazepam and Clonazepam, they belong to the same group of drugs benzodiazepines, which have the ability to inhibit the epileptic electrical activity efficiently. They are structurally similar and composed of a Benzene ring connected to a seven-membered Diazepine ring [69]. As for Topiramate and Acetazolamide, since they share carbonic anhydrase inhibition and not serotonin activity, it seems plausible that they a common ADR [70]. Finally, with regard to Lamotrigine and Levetiracetam, despite the fact that they have different mechanisms of action (Lamotrigine blocks voltage-gated sodium channels and stabilizes their inactive state, while Levetiracetam inhibits the release of the excitatory neurotransmitter by binding to synaptic vesicle protein SV2A), evidence on their common effect has been recently reported [71].

5. Conclusion

In this paper, the validity and utility of social media as a data source for detecting the ADRs of AEDs have been investigated. To this end, patients' reviews from two OHCs have been collected and a lexicon-based method with disproportionality analysis measures has been applied to generate lists of ADRs for each AED. The generated lists of signaled ADRs have been analyzed in different manners to answer research questions on the validity of the signaled AEDs' ADRs, common AEDs' ADRs, and the similarity between AEDs in terms of ADRs. In answering the first question, the lists of signaled AEDs' ADRs are compared with the corresponding sets of AEDs' ADRs in the SIDER database. Regardless of the variations in the validation results of AEDs, the average validation results indicate the validity of the ADR detection from the OHC data. Moreover, the validation results indicate a comparable performance of PRR and ROR and slightly lower performance of IC. As for the second question, the analysis of the generated ADR lists indicates that most AED ADRs are of CNS type which is concordant with the extant pharmaceutical AED literature. Finally, the analysis of the similarity between AEDs in terms of their ADRs shows a remarkable similarity between several pairs of AEDs. Overall, the answer of the first question is evidence of the validity of using OHCs for the detection of AEDs' ADRs. Moreover, the answers of the second and third questions are evidence on the utility of the OHC data for the knowledge discovery tasks related to AEDs.

A final remark worth mentioning in this research context is concerning the heavy role of NLP techniques for the detection of ADRs from social media and the extraction of ADRs from drug labels to construct ADR database such as SIDER. Certainly, the continuous improvement of the NLP techniques would improve the detection and validation of ADRs from social media. On the other hand, an alternative computational paradigm that could be investigated for the detection of AEDs' ADRs is ML-based approaches. In this context, a comparison between the lexicon-based approaches and ML-based approaches would be interesting.

Data Availability

The raw data used to support the findings of this study are available from the following online health consumer's forums: (1) Askapatient (http://www.askapatient.com) and (2) WebMD (http://www.webmd.com), and the processed data are available on request from the corresponding author.

Conflicts of Interest

The authors declare that they have no conflicts of interest.

Acknowledgments

The authors would like to express their gratitude to the Ministry of Education and the Deanship of Scientific Research, Najran University, Kingdom of Saudi Arabia, for their financial and technical support under code number (NU/-/SERC/10/576).

References

[1] H. Kubova, "Side effects of antiepileptic drugs," in *Antiepileptic Drug Discovery. Methods in Pharmacology and Toxicology*, pp. 329–350, Humana Press, New York, NY, 2016.

[2] M. L. Iorio, U. Moretti, S. Colcera et al., "Use and safety profile of antiepileptic drugs in Italy," *European Journal of Clinical Pharmacology*, vol. 63, pp. 409–415, 2007.

[3] J. S. Duncan, J. W. Sander, S. M. Sisodiya, and M. C. Walker, "Adult epilepsy," *The Lancet*, vol. 367, no. 9516, pp. 1087–1100, 2006.

[4] G. J. Sills and M. A. Rogawski, "Mechanisms of action of currently used antiseizure drugs," *Neuropharmacology*, vol. 168, p. 107966, 2020.

[5] P. Kwan and M. J. Brodie, "Early identification of refractory epilepsy," *The New England Journal of Medicine*, vol. 342, no. 5, pp. 314–319, 2000.

[6] W. Löscher, H. Klitgaard, R. E. Twyman, and D. Schmidt, "New avenues for anti-epileptic drug discovery and development," *Nature Reviews. Drug Discovery*, vol. 12, no. 10, pp. 757–776, 2013.

[7] A. Gaitatzis and J. W. Sander, "The long-term safety of antiepileptic drugs," *CNS Drugs*, vol. 27, pp. 435–455, 2013.

[8] R. Savica, E. Beghi, G. Mazzaglia et al., "Prescribing patterns of antiepileptic drugs in Italy: a nationwide population-based study in the years 2000–2005," *European Journal of Neurology*, vol. 14, no. 12, pp. 1317–1321, 2007.

[9] I. Tsiropoulos, A. Gichangi, M. Andersen, L. Bjerrum, D. Gaist, and J. Hallas, "Trends in utilization of antiepileptic drugs in Denmark," *Acta Neurologica Scand*, vol. 113, no. 6, pp. 405–411, 2006.

[10] I. R. Edwards and J. K. Aronson, "Adverse drug reactions: definitions, diagnosis, and management," *The Lancet*, vol. 356, pp. 1255–1259, 2000.

[11] J. A. Cramer, S. Mintzer, J. Wheless, and R. H. Mattson, "Adverse effects of antiepileptic drugs: a brief overview of important issues," *Expert Review of Neurotherapeutics*, vol. 10, no. 6, pp. 885–891, 2010.

[12] A. Hilgers and M. Schaefer, "Systematic adverse drug reaction monitoring of patients under newer antiepileptic drugs using routine clinical data of inpatients," *Drugs - Real World Outcomes*, vol. 3, no. 2, pp. 209–221, 2016.

[13] C. J. Landmark and S. Johannessen, "Safety aspects of antiepileptic drugs—focus on pharmacovigilance," *Pharmacoepidemiology and Drug Safety*, vol. 21, no. 1, pp. 11–20, 2012.

[14] C. C. Yang, H. Yang, and L. Jiang, "Postmarketing drug safety surveillance using publicly available health consumer contributed content in social media," *ACM Transactions on Management Information Systems*, vol. 5, no. 1, pp. 1–21, 2014.

[15] E. Poluzzi, E. Raschi, C. Piccinni, and F. De, "Data mining techniques in pharmacovigilance: analysis of the publicly accessible FDA adverse event reporting system," in *data mining applications in engineering and medicine*, pp. 255–302, INTECH, 2012.

[16] C. Zhan, E. Roughead, L. Liu, N. Pratt, and J. Li, "Detecting potential signals of adverse drug events from prescription data," *Artificial intelligence in medicine*, vol. 104, p. 101839, 2020.

[17] S. A. Choi, H. Kim, S. Kim et al., "Analysis of antiseizure drug-related adverse reactions from the electronic health record using the common data model," *Epilepsia*, vol. 61, no. 4, pp. 610–616, 2020.

[18] M. S. Nawaz, R. U. Mustafa, and M. I. Lali, "Role of online data from search engine and social media in healthcare informatics," in *applying big data analytics in bioinformatics and medicine*, pp. 272–293, IGI Global, 2018.

[19] F. M. Alotaibi, M. Z. Asghar, and S. Ahmad, "A hybrid CNN-LSTM model for psychopathic class detection from tweeter users," *Cognitive Computation*, vol. 13, no. 3, pp. 709–723, 2021.

[20] J. Asghar, S. Akbar, M. Z. Asghar, B. Ahmad, M. S. Al-Rakhami, and A. Gumaei, "Detection and classification of psychopathic personality trait from social media text using deep learning model," *Computational and Mathematical Methods in Medicine*, vol. 2021, Article ID 5512241, 10 pages, 2021.

[21] H. Ahmad, M. Z. Asghar, F. M. Alotaibi, and I. A. Hameed, "Applying deep learning technique for depression classification in social media text," *Journal of Medical Imaging and Health Informatics*, vol. 10, no. 10, pp. 2446–2451, 2020.

[22] S. Pervaiz, Z. Ul-Qayyum, W. H. Bangyal, L. Gao, and J. Ahmad, "A systematic literature review on particle swarm optimization techniques for medical diseases detection," *Computational and Mathematical Methods in Medicine*, vol. 2021, Article ID 5990999, 10 pages, 2021.

[23] D. Pappa and L. K. Stergioulas, "Harnessing socialmedia data for pharmacovigilance: a review of current state of the art, challenges and future directions," *International Journal of Data Science and Analytics*, vol. 8, pp. 113–1335, 2019.

[24] X. Chen, C. Faviez, S. Schuck et al., "Mining patients' narratives in social media for pharmacovigilance: adverse effects and misuse of methylphenidate," *Frontiers in pharmacology*, vol. 9, 2018.

[25] J. Lardon, R. Abdellaoui, F. Bellet et al., "Adverse drug reaction identification and extraction in social media: a scoping review," *Journal of Medical Internet Research*, vol. 17, no. 7, p. e171, 2015.

[26] A. Sarker, R. E. Ginn, A. Nikfarjam et al., "Utilizing social media data for pharmacovigilance: a review," *Journal of Biomedical Informatics*, vol. 54, pp. 202–212, 2015.

[27] J. Liu, A. Li, and S. Seneff, "Automatic drug side effect discovery from online patient-submitted reviews: focus on statin drugs," in *Proceedings of First International Conference on Advances in Information Mining and Management (IMMM)*, Barcelona, Spain, 2011.

[28] A. Yates and N. Goharian, "ADRTrace: detecting expected and unexpected adverse drug reactions from user reviews on social media sites," in *35th European conference on Advances in Information Retrieval*, 2013.

[29] J. Bian, U. Topaloglu, and F. Yu, "Towards large-scale Twitter mining for drug-related adverse events," in *2012 ACM International Workshop on Smart Health and Wellbeing*, Maui, Hawaii, USA, 2012.

[30] S. Li, C. H. Yu, Y. Wang, and Y. Babu, "Exploring adverse drug reactions of diabetes medicine using social media analytics and interactive visualizations," *International Journal of Information Management*, vol. 48, pp. 228–237, 2019.

[31] M. Zolnoori, K. W. Fung, T. B. Patrick et al., "A systematic approach for developing a corpus of patient reported adverse drug events: a case study for SSRI and SNRI medications," *Journal of biomedical informatics*, vol. 90, p. 103091, 2019.

[32] F. V. Duval and F. Silva, "Mining in Twitter for adverse events from malaria drugs: the case of doxycycline," *Cadernos de saude publica*, vol. 35, no. 5, 2019.

[33] X. Liu, J. Liu, and H. Chen, "Identifying adverse drug events from health social media: a case study on heart disease discussion forums," in *Smart Health. ICSH 2014. Lecture Notes in Computer Science*, vol. 8549, Springer, Cham, 2014.

[34] M. R. Hasan, M. J. R. Rifat, and S. R. H. Noori, "Pharmacovigilance study of opioid drugs on Twitter and PubMed using artificial intelligence," in *2019 10th International Conference on Computing, Communication and Networking Technologies (ICCCNT)*, Kanpur, India, 2019.

[35] A. A. Yahya, Y. Asiri, and I. Alyami, "Mining Patients' reviews in online health communities for adverse drug reaction detection of antiepileptic drugs," in *21st International Arab Conference on Information Technology (ACIT)*, 2020.

[36] S. Alick and A. Doyle, *Choosing Antiepileptic Drugs*, 2018, Accessed 2 February 2021, https://practicalneurology.com/articles/2018-oct/choosing-antiepileptic-drugs?c4src=top5.

[37] G. M. Kennedy and S. D. Lhatoo, "CNS adverse events associated with antiepileptic drugs," *CNS Drugs*, vol. 22, no. 9, pp. 739–760, 2008.

[38] B. Chen, H. Choi, L. J. Hirsch et al., "Psychiatric and behavioral side effects of antiepileptic drugs in adults with epilepsy," *Epilepsy & behavior : E&B*, vol. 76, pp. 24–31, 2017.

[39] S. C. Sarangi, N. Kaur, and M. Tripathi, "Assessment of psychiatric and behavioral adverse effects of antiepileptic drugs monotherapy: Could they have a neuroendocrine correlation in persons with epilepsy?," *Epilepsy & behavior : E&B*, vol. 100, p. 106439, 2019.

[40] S. Kumar, S. C. Sarangi, M. Tripathi, and Y. K. Gupta, "Evaluation of adverse drug reaction profile of antiepileptic drugs in persons with epilepsy: a cross-sectional study," *Epilepsy & Behavior*, vol. 105, p. 106947, 2020.

[41] H. Yang and C. C. Yang, "Harnessing social media for drug-drug interactions detection," in *IEEE International Conference on Healthcare Informatics (ICHI'13)*, 2013.

Hindawi
Computational and Mathematical Methods in Medicine
Volume 2023, Article ID 9837528, 1 page
https://doi.org/10.1155/2023/9837528

Retraction

Retracted: Breast Tumor Detection and Classification in Mammogram Images Using Modified YOLOv5 Network

Computational and Mathematical Methods in Medicine

Received 27 June 2023; Accepted 27 June 2023; Published 28 June 2023

This article has been retracted by Hindawi following an investigation undertaken by the publisher [1]. This investigation has uncovered evidence of one or more of the following indicators of systematic manipulation of the publication process:

(1) Discrepancies in scope

(2) Discrepancies in the description of the research reported

(3) Discrepancies between the availability of data and the research described

(4) Inappropriate citations

(5) Incoherent, meaningless and/or irrelevant content included in the article

(6) Peer-review manipulation

The presence of these indicators undermines our confidence in the integrity of the article's content and we cannot, therefore, vouch for its reliability. Please note that this notice is intended solely to alert readers that the content of this article is unreliable. We have not investigated whether authors were aware of or involved in the systematic manipulation of the publication process.

Wiley and Hindawi regrets that the usual quality checks did not identify these issues before publication and have since put additional measures in place to safeguard research integrity.

We wish to credit our own Research Integrity and Research Publishing teams and anonymous and named external researchers and research integrity experts for contributing to this investigation.

The corresponding author, as the representative of all authors, has been given the opportunity to register their agreement or disagreement to this retraction. We have kept a record of any response received.

References

[1] A. Mohiyuddin, A. Basharat, U. Ghani et al., "Breast Tumor Detection and Classification in Mammogram Images Using Modified YOLOv5 Network," *Computational and Mathematical Methods in Medicine*, vol. 2022, Article ID 1359019, 16 pages, 2022.

Hindawi
Computational and Mathematical Methods in Medicine
Volume 2022, Article ID 1359019, 16 pages
https://doi.org/10.1155/2022/1359019

Research Article

Breast Tumor Detection and Classification in Mammogram Images Using Modified YOLOv5 Network

Aqsa Mohiyuddin,[1] Asma Basharat,[1] Usman Ghani,[2] Veselý Peter,[3] Sidra Abbas,[4] Osama Bin Naeem,[5] and Muhammad Rizwan[1]

[1]*Department of Computer Science, Kinnaird College for Women Lahore, Pakistan*
[2]*University of Engineering and Technology Lahore, Pakistan*
[3]*Information Systems Department, Faculty of Management, Comenius University in Bratislava, Odbojárov 10 82005 Bratislava 25, Slovakia*
[4]*Department of Computer Science, COMSATS University, Sahiwal, Pakistan*
[5]*University of Engineering and Technology Narowal, Pakistan*

Correspondence should be addressed to Veselý Peter; peter.vesely@fm.uniba.sk and Sidra Abbas; sidra.abbas708@gmail.com

Received 30 October 2021; Accepted 1 December 2021; Published 3 January 2022

Academic Editor: Muhammad Zubair Asghar

Breast cancer incidence has been rising steadily during the past few decades. It is the second leading cause of death in women. If it is diagnosed early, there is a good possibility of recovery. Mammography is proven to be an excellent screening technique for breast tumor diagnosis, but its detection and classification in mammograms remain a significant challenge. Previous studies' major limitation is an increase in false positive ratio (FPR) and false negative ratio (FNR), as well as a drop in Matthews correlation coefficient (MCC) value. A model that can lower FPR and FNR while increasing MCC value is required. To overcome prior research limitations, a modified network of YOLOv5 is used in this study to detect and classify breast tumors. Our research is conducted using publicly available datasets Curated Breast Imaging Subset of DDSM (CBIS-DDSM). The first step is to perform preprocessing, which includes image enhancing techniques and the removal of pectoral muscles and labels. The dataset is then annotated, augmented, and divided into 60% for training, 30% for validation, and 10% for testing. The experiment is then performed using a batch size of 8, a learning rate of 0.01, a momentum of 0.843, and an epoch value of 300. To evaluate the performance of our proposed model, our proposed model is compared with YOLOv3 and faster RCNN. The results show that our proposed model performs better than YOLOv3 and faster RCNN with 96% mAP, 93.50% MCC value, 96.50% accuracy, 0.04 FPR, and 0.03 FNR value. The results show that our suggested model successfully identifies and classifies breast tumors while also overcoming previous research limitations by lowering the FPR and FNR and boosting the MCC value.

1. Introduction

People nowadays are concerned about their health [1–4]. Today's society faces several challenges related to chronic condition health care issues [5–7]. There is a huge surge see recently in various diseases such as breast cancer, brain tumor, COVID, Dementia, physical inactivity, and lung cancer [8–11]. Machine learning (ML) and deep learning (DL) are being utilized for brain tumor detection, cervical cancer detection, breast cancer detection, COVID detection, thermal sensation detection, and cognitive health assessment of dementia individuals [12–17]. Breast cancer is defined as the uncontrolled growth of cells in a specific area of the body [1, 18]. Breast cancer is the leading cause of cancer mortality among women worldwide. Among all cancers, breast cancer has the most significant incidence and fatality rate, and it is the world's second most common cancer. Every year, around 14.1 million individuals worldwide are diagnosed with breast cancer, with 8.2 million dying as a result. 70% of newly reported cancer cases occur in developing nations,

and it is anticipated that by 2025; there will be around 19.3 million newly reported cancer cases yearly [19].

Benign and malignant are two types of breast tumors: benign tumor, in which cancerous cells remain in place and have not extended to surroundings [20]. There is a possibility that that cancerous spread and grow to become malignant. A benign tumor can be easily treated and is not that serious compared to a malignant tumor: a malignant tumor in which cancerous cells spread throughout the body through the circulatory system and cause death. This is the most dangerous type of breast cancer, and most females suffer from this type of tumor. Most breast cancers are malignant.

Breast cancer can be treatable if taken precautions at the proper time. One of the ways of preventing the rapid growth of cells (benign tumor) from becoming full-blown cancer (malignant tumor) and preventing the more spread of cells (malignant tumor) to other organs of the body is early detection. There are effective techniques available to find out the presence of cancer.

Mammography is one of the most commonly used techniques for breast cancer screening which has made a significant contribution to reducing mortality rates through early cancer detection. Mammography [21] is like an X-ray of the breast in which breast compressed between 2 plates and two views of each breast are taken, bilateral craniocaudal (CC) and mediolateral oblique (MLO) [22]. However, the complexity of mammography and the vast amount of tests per radiologist can result in a false diagnosis.

Many researchers have worked hard to create a network that can precisely detect breast tumors with good results, but there is still a significant research gap related to false positive rate, false negative rate, and MCC value. MCC only gives a high score if the prediction performed well in all four categories of the confusion matrix. Because MCC is a more reliable performance metric than accuracy in binary classification, it should be enhanced by decreasing FPR and FNR rates.

The main contributions of this study are as follows:

(1) Propose a model that can precisely detect and classify breast tumors into benign and malignant on mammograms

(2) Reduce false positive rate (FPR) and false negative rate (FNR) without reducing the degree of accuracy and precision

(3) To boost the value of the Matthews correlation coefficient (MCC)

(4) Implement all four variants of the YOLOv5 model to determine the most suitable model for detecting and classifying breast tumors

(5) Compare our proposed model with state-of-the-art networks to evaluate performance

The rest of the paper is organized as follows: literature review in Section 2. Section 3 introduces our proposed methodology. Section 4 provides the outcomes of experimental analysis and results. Finally, conclusions and future work are discussed in Section 5.

2. Related Work

In this paper [23], the author suggested a model for the classification of breast masses using the CAD method. MIAS, self-collected datasets, and DDSM datasets are used in this study. Preprocessing, segmentation, collection, and grouping of functions are used in this system. The CAD system includes a CNN model consisting of eight coevolutionary, four max-pooling, and two fully connected layers. The results obtained are then compared to the pretrained nets, Alex Net and VGG16, demonstrating that the proposed CNN achieved higher accuracy and AUC than these two models. The proposed model achieved accuracies of 92.54%, 96.47%, and 95% and AUC scores of 0.85, 0.96, and 0.94 for MIAS, DDSM, and the self-collected dataset, respectively. An extreme learning strategy was used to map the feature fusion and extract the CNN features for breast cancer detection and classification.

In this paper [23], an author has suggested a method to detect breast cancer from mammograms. Preprocessing, segmentation, extraction of features, and classification are used in this research. Next, the image is analyzed, and then the segmentation is added. Second, characteristics are derived, and, thirdly, classification is carried out. Once the findings have been achieved, a distinction is made between various classification methods. Support vector machine (SVM), AdaBoost, decision tree, logistic regression, K nearest neighbor, and random forest classifiers are used to classify breast cancer. The accuracy obtained is 90%, 57%, 54%, 85%, 76%, and 61% for support vector machine (SVM), AdaBoost, decision tree, logistic regression, K nearest neighbor, and random forest classifiers, respectively, which means that SVM achieves the highest accuracy of all.

In this paper [24], an author proposed a method to classify breast cancer tumors using AGAN for data augmentation and CNN for classification of the tumor. Pattern detection and machine learning techniques such as deep convolutional networks have overtaken state of the art in many visual recognition tasks. This method got 89.17% accurate results but 19.41% false positive rate of classification. In this paper [25], an author proposed a method to detect breast cancer tumors using faster RCNN on OMI-H, OMI-GE, and INbreast datasets. The results achieved using this method are 93% sensitivity for OMI-H, 91% sensitivity for OMI-GE, and 99% sensitivity for INbreast but FPR and FNR rates for OMI-GE dataset increases to 12% and 20%, for INbreast dataset increases to 20% and 29%, and FNR rate for OMI-H increases to 13%, respectively. In this paper [26], an author proposed a method to classify breast cancer tumors using the VGG-16 network on the CBIS-DDSM dataset. This method achieved 82% accuracy, but the drawback is that their MCC value is 63%, FPR is high, 22%, and FNR is 15%.

In this paper [27], an author has suggested a method for identifying breast cancer in mammograms. Noise reduction, segmentation, and grouping are the steps of the proposed model. Gaussian filter is used to eliminate noise from mammogram images. Then, fuzzy C means that the clustering algorithm is used for the segmentation of the breast tumor.

The Bi-Directional Long-Term Memory Network (Bi-LSTM) classifier is used to diagnose breast cancer with optimized parameters using elephant herding optimization (EHO). MIAS dataset is used in this research. Results are then compared with CNN, DCNN, and Bi-LSTM, from which EHOBi-LSTM got good results, but FPR and FNR rates need to decrease.

In this paper [28], an author proposed a method to detect breast cancer tumors using Dense-Net-169 and Efficient-Net-B5 on a private dataset. This method achieved good accuracy 95.2% for Dense-Net-169 and 95.4% for Efficient-Net-B5, but the drawback is that their FPR and FNR for Dense-Net-169 are high, which is 12% and 13%, respectively. MCC value for both the networks also drops to 66.5% for Dense-Net-169 and 76% for Efficient-Net-B5. In this paper [29], an author suggested a model for identifying, classifying, and segmenting the cancerous area of mammograms. For this study, MIAS and CBIS-DDSM datasets are used. The dataset of images in this research is small. Preprocessing includes the removal of noise, artifacts, and muscle regions that can create a high false-positive rate. A median filter is used to eliminate noise from mammograms. Muscles are separated from the images to clear the tumor, and the images are translated to 512×512 patches. To improve system efficiency, the preprocessed image is transformed into 512Ã-512 patches. DL models MASK-RCNN and Deep Lab are then used to identify the tumor. The findings of this study are AUC 0.98 for MASK-RCNN and 0.95 for Deep Lab. The mean average accuracy for the segmentation task is 0.80 and 0.75. The accuracy of the radiologist ranged from 0.80 to 0.88. So, this research is helpful for radiologists in the case of breast tumor classification, but still, results need to improve.

In this paper [30], an author proposed a method to detect breast cancer tumors using a YOLO detector on DDSM and in breast datasets. This method achieved good results that are 99.28% F-score for DDSM and 98.02% F-score for INbreast dataset, but the drawback is that its FPR is high, which is 14%. A method was also proposed to classify a tumor further using feedforward CNN, ResNet-50, and Inception ResNet-V2. All these three methods got 90+ accuracies for both datasets, but the limitation is that for the breast dataset, FPR increased to 28.57% for CNN, 14.28% for Res-Net50, and 16.66% for Inception ResNet V2. In this paper [2], an author proposed a method to segment and classified breast cancer tumors using Firefly updated chicken-based CSO (FC-CSO) and RCNN on the MIAS dataset. This method achieved good accuracy 93%, sensitivity 97%, specificity 92%, FPR 7%, and FNR 3%, but the drawback is that its MCC value drops to 85%. In this paper [31], an author proposed a method to extract features and classify breast cancer tumors using the CNN model on the MIAS dataset. This method achieved good results: accuracy 95%, sensitivity 98%, specificity 90%, and FNR 2%, but the drawback is that its MCC value drops to 89% and FPR drops to 10%.

In this paper [32], an author proposed a method for the detection of breast cancer tumors using Mobile Net on DDSM and CBIS-DDSM datasets. This method achieved 74.5% accuracy, 76% sensitivity, and 70% precision for CBIS-DDSM dataset and 86.8% accuracy, 95% sensitivity for DDSM dataset but FNR value for CBIS-DDSM dataset increased to 24%.

In this paper [33], an author proposed a method for detection and classification of breast cancer tumors using faster R-CNN and CNN on a private dataset. This method achieved 91.86% accuracy and 94.67% sensitivity. However, the drawback is that their specificity value drops to 89.69%, FPR value increases to 10.3%, and precision value drops to 87.65%. So, results need to improve here. In this paper [34], an author proposed a method for classification of breast cancer tumors using VGG for feature extraction and multiview feature fusion- (MVFF-) based CADx for further classification on MIAS and CBIS-DDSM datasets. The results achieved from this method are accuracy 77.66%, sensitivity 81.82%, and specificity 72.02%. Its FPR and FNR values also increased to 27.9% and 18.18%, respectively. So, the overall result needs to improve here. In this paper [35], an author proposed a method for the classification of breast cancer tumors using CNN on a private dataset. The model achieved sensitivity 91.3% and accuracy 82.4%. Its specificity and MCC value decreased to 56.9% and 51.8%, respectively, and its FPR increased to 43.1%. So, results need to improve here.

In this paper [36], an author proposed a method for segmentation and classification of breast cancer tumors using the multithreshold technique and PNN on MIAS and BCDR datasets. The model achieved sensitivity 98.30%, FNR 1.7%, and accuracy 97.08%. Its specificity decreased to 89.8%, and its FPR increased to 10.2%. So, results need to improve here. In this paper [37], an author proposed a method for the classification of breast cancer tumors using VGG and ResNet-50 on the IRMA dataset. The models achieved accuracies and sensitivities are 94% for VGG-16, 91.7% for ResNet-50% and 99% for VGG-16, and 94% for ResNet-50%, respectively. Its precision for VGG and ResNet-50 decreased to 89% and 88%, respectively. So, results need to improve here. In this paper [38], an author proposed a method for preprocessing and classification of breast cancer tumors using the LBP algorithm and CNN model on the DDSM dataset. The model achieved sensitivity 96.81%, specificity 95.83%, accuracy 96.32%, FPR 4%, and FNR 3%. However, its MCC value drops to 88.48%. So, this is the gap in their research that needs to be improved.

Several researchers have implemented different networks to detect breast tumors and classified them as benign or malignant. Detection and classification accuracies ranging from 90% to 99% were achieved. However, focus on one essential factor is still missing: the false classification ratio and MCC value. In most studies, the false classification ratio is high, and the MCC value is low. Many difficulties arise as a result of fluctuations in these values. If a patient has a benign tumor and the system diagnoses it as a malignant tumor, the patient will be subjected to all of the painful procedures (biopsies, surgeries, and chemotherapies) required to remove the malignant tumor—the same as with a malignant patient. If the machine misidentifies a malignant tumor as benign, the patient will be in danger. This is due to an

increase in the false classification ratio and a decrease in the more trustworthy MCC value. As a result, it is essential to build a system that can accurately detect and categorize breast tumors with low FPR and FNR values and high MCC values to more authenticate our research.

3. Proposed Methodology

The primary goal of this study is to create a model that can effectively detect and classify breast tumors while also minimizing FPR and FNR rates and increasing MCC values. The CBIS-DDSM [26] dataset is utilized for this. As seen in Figure 1, the initial stage is to remove the rough white borders, followed by the removal of artifacts and pectoral muscles. CLAHE is useful for image enhancement. The images are then subjected to erosion, a morphological procedure. Annotation is completed with augmentation after images have been cleaned and enhanced. The prepared data is then fed into our proposed YOLOv5 model. In this study, all four versions of YOLOv5 are utilized. The original version of YOLOv5 is then compared to modified variants of YOLOv5. After a comparison of the original and modified versions, a comparison with a state-of-the-art network is performed.

3.1. Dataset Description. The Curated Breast Imaging Subset of DDSM (CBIS-DDSM) dataset comprises 10239 images, including whole mammograms, cropped images, and ROI mask images with mass and calcification are utilized in this study. This study utilized 2424 complete mammograms of benign and malignant masses (as showing in Figure 2 to implement our proposed model, leaving microcalcification for future research). Data augmentation is a technique used in image processing to produce extra training data from current data. Augmentation is done in this study by flipping pictures horizontally, rotating them at 90 and 180 degrees, and making various copies. A total of 4865 pictures were created after augmentation. 60% of data is used for training, 30% is used for validation, and 10% is used for testing. Because of the Graphics Processing Unit, we chose to build our model, which cannot handle huge pictures, and the size of the images has been decreased from 3000×4500 pixels to 1000×2000 pixels.

3.2. Preprocessing. Before implementing our proposed model, preprocessing is performed with the following few steps.

3.2.1. Removal of White Borders. To begin, images are thoroughly cleaned using several approaches. Images have a rough outside border with white lines, indicated with red lines, as shown in Figure 3. Because the white color in mammograms also represents tumors, it can lead to misdiagnosis of benign and malignant tumors.

White lines are eliminated to avoid misclassification by cropping the image area somewhat using the cropping function. Images are shown in Figure 4 after removing harsh white lines.

3.2.2. Removal of Artifacts and Pectoral Muscles. Because pectoral muscles and artifacts have the same intensity as the tumor region, removing them from mammograms is the most challenging task [39]. To locate the actual tumor area, pectoral muscles and artifacts must be removed. After cropping white lines, artifacts and pectoral muscles are removed using intensity value on specific columns in mammograms as shown in Figure 5.In Matrix Laboratory (MATLAB), the left pectoral muscles and labels are removed individually, as are the right pectoral muscles and labels.

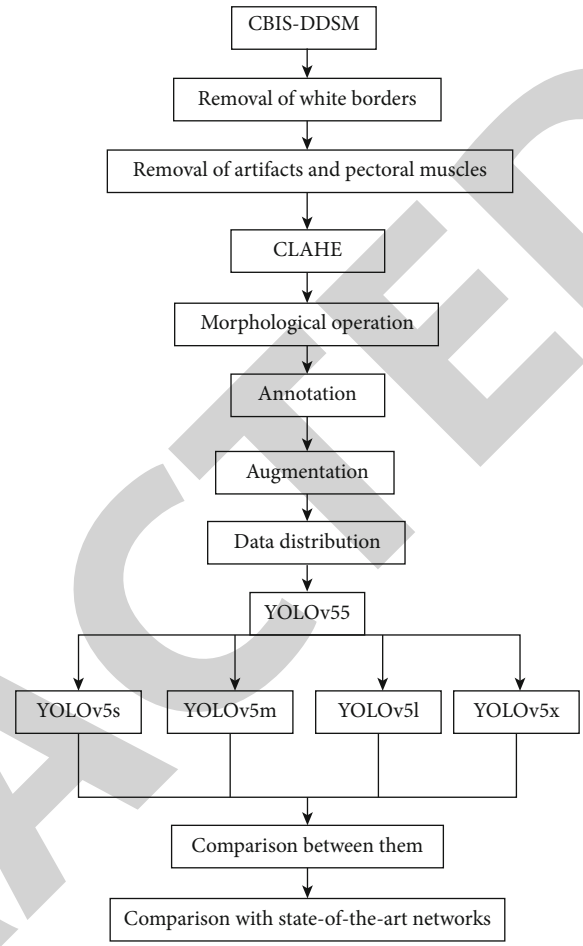

Figure 1: Proposed flow.

3.2.3. Contrast Limited Adaptive Histogram Equalization (CLAHE). After the pectoral muscles and labels have been removed, Contrast Limited Adaptive Histogram Equalization (CLAHE) [40] is utilized to improve the mammography. Image enhancement plays an essential role in medical imaging since it allows us to see hidden features in an image. So, in this study, CLAHE is utilized to enhance mammograms and provides the best results in viewing the tumor part. CLAHE works using tiles, which are small sections of a larger image rather than the entire image. The adjacent tiles are blended using bilinear interpolation to remove the false boundaries. When utilizing CLAHE, there are two factors to keep in mind. The first is clip limit, which sets the contrast threshold value to 40 by default. The second one is tile grid size, which sets the number of tiles in the row and column, and 8×8 is its default value. Figure 6 shows an image before and after applying CLAHE.

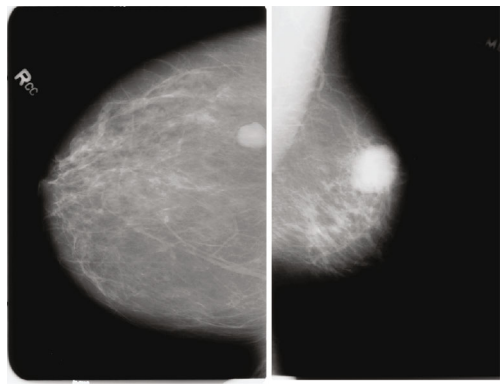

Benign Malignant

Figure 2: Benign and malignant images from CBIS-DDSM dataset.

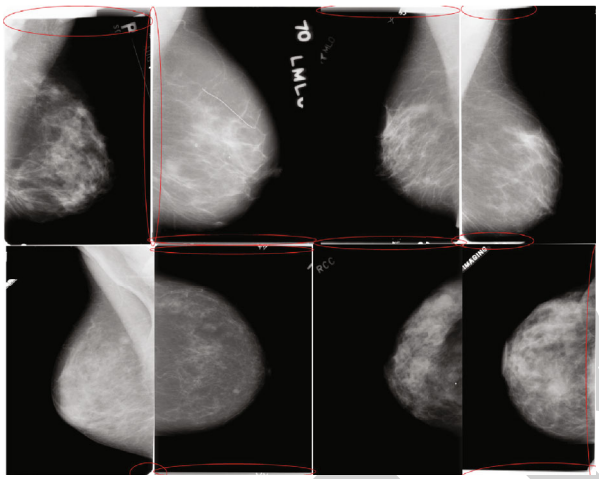

Figure 3: Rough images with white lines.

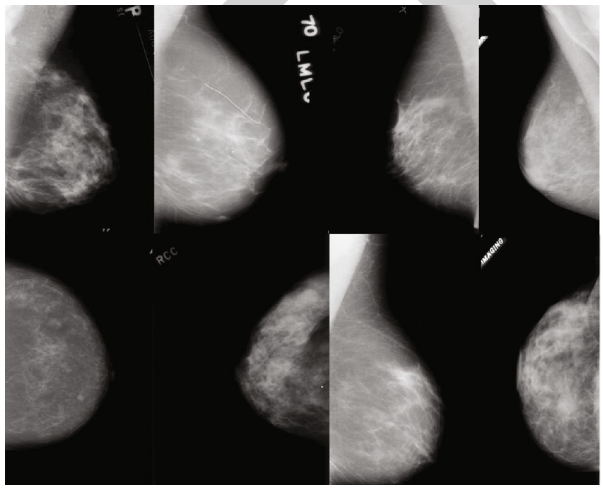

Figure 4: Images after removing white lines.

3.2.4. Morphological Operation. Morphological image processing [41] is a set of nonlinear procedures that deal with the structure or morphology of image features. Morphological operations are often used to remove minor features from

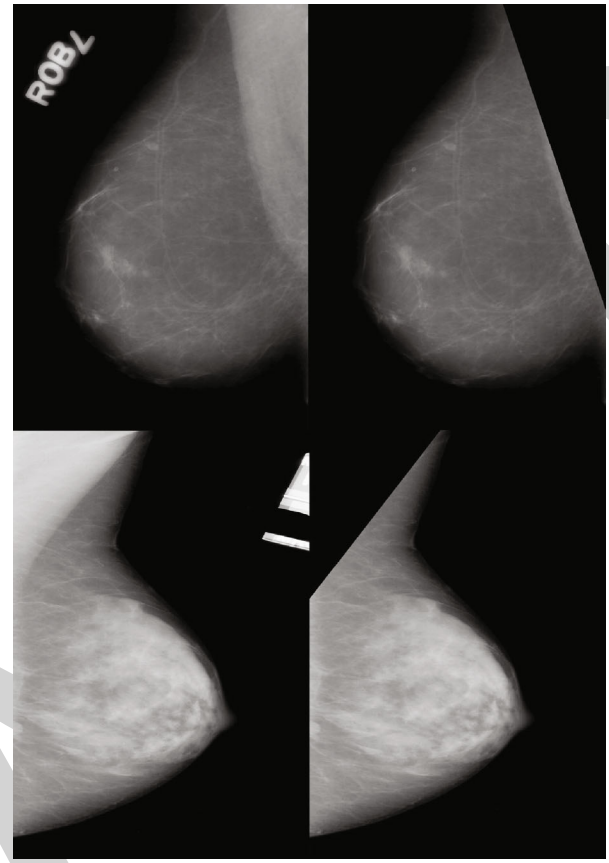

Figure 5: Images with pectoral muscles and labels are on left side and images with removal of pectoral muscles and labels are on the right side.

a picture while retaining more extensive details. There are a variety of morphological operations. In this study, morphological operations are required to remove surrounding tissues to make the tumor part apparent; so, erosion is utilized in this research to make the tumor part prominent while removing the unnecessary tiny tissue elements. Figure 7 shows an image before and after applying morphological erosion operation.

$$X!Y = \{c \in \mathscr{W} \mid Y_c \subseteq X\}. \tag{1}$$

Equation (1) shows erosion of binary image X by the structuring element Y. W is a Euclidean space, and X is a binary image in W where Y_c is the translation of Y by the vector c showing in equation (2).

$$Y_c = \{y + c \mid y \in Y\}, \forall c \in W. \tag{2}$$

3.3. Annotation. After morphological operations, the dataset is prepared for use in tumor detection and classification. The Yolov5 model is utilized in this study to detect and classify breast tumors, and we need annotated data to utilize this model. As a result, data is being annotated utilizing an online source called Roboflow. Square boxes are used to annotate images. The annotated data is shown in Figure 8. Annotated data has two types of files. One is an image file,

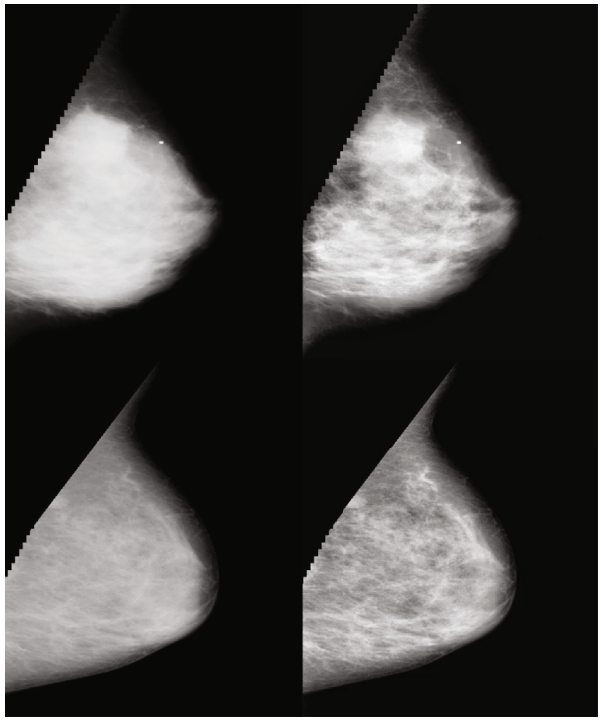

Figure 6: Before and after applying CLAHE, respectively.

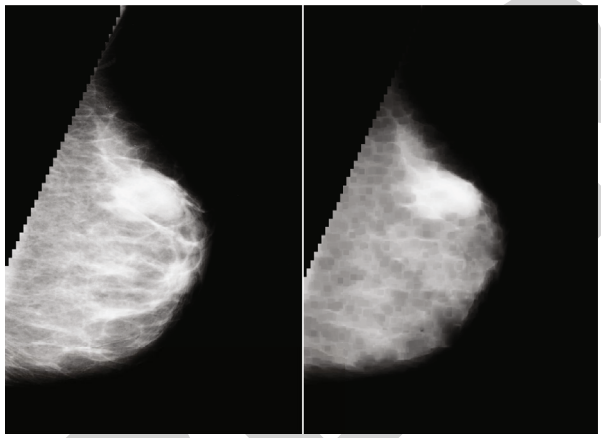

Figure 7: Before and after applying erosion morphological operation, respectively.

and the second one is a text (.txt) file. The text file contains the dimensions of the square on a tumor. The sample is shown in Figure 9.

3.4. YOLOv5. The YOLO neural network design predicts a collection of bounding boxes and class probabilities. First, it splits the entire image into many grids of varying sizes, and anchor boxes are produced in each grid of the input image using a predefined scale and size. Compared to a two-stage detector, each anchor box predicts the objectness score and box center offset x, box center offset y, box width, box height, and class scores all at once. Thus, YOLO is a one-stage object detector that is a rapid end-to-end technique for detecting objects. There are many versions of

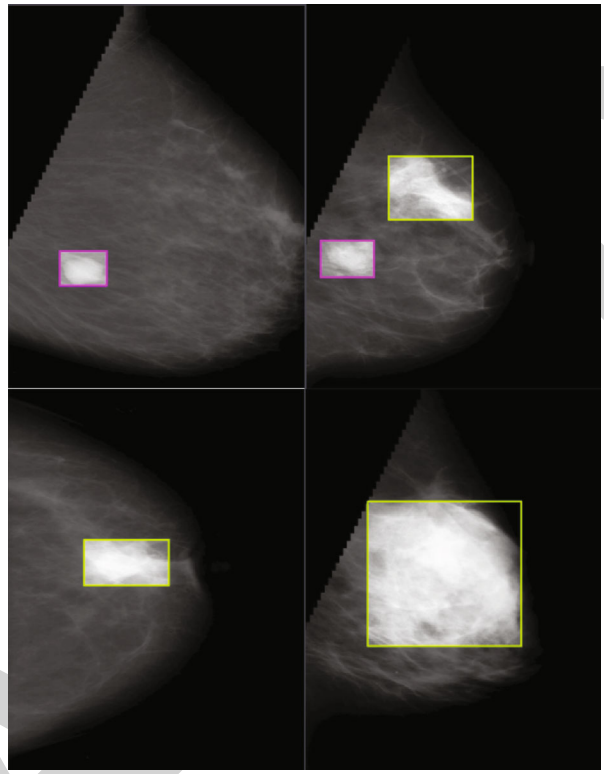

Figure 8: Annotated images.

YOLO. In this paper, YOLOv5 is used for the detection and classification of breast tumors. The YOLOv5 architecture contains four architectures, specifically named YOLOv5s, YOLOv5m, YOLOv5l, and YOLOv5x, respectively. The main difference among them is that the amount of feature extraction modules and convolution kernel in the specific location of the network is different. The size of models and the number of model parameters in the four architectures increase in turn as showing in Table 1. The basic structure of YOLOv5 (YOLOv5s) is shown in Figure 10.

In this research, all 4 versions of YOLOv5 are used for the detection and classification of breast tumors and to make a comparison between these 4 versions. Let us start with yolov5s.

$$A = \text{Min}\left(\frac{C_1}{C_0}, \frac{B_1}{B_0}\right), \tag{3}$$

$$R = \text{np.mod}\left(\frac{C_1}{A}, \frac{B_1}{A}\right), \tag{4}$$

$$C_1 \times (B_1 + R). \tag{5}$$

Equations (3)–(5) are showing the method of mosaic data enhancement. C_0 and B_0 is the original image size. C_1 and B_1 are the original image scale size, A is the scale factor, and R is the gray filled value.

It has three important parts like any other single-stage object detector as showing in Figure 10.

```
1 0.453125 0.5336538461538461 0.2439903846153846 0.14423076923076922
1 0.21875 0.5793269230769231 0.17427884615384615 0.10576923076923077
1 0.2704326923076923 0.4831730769230769 0.171875 0.10576923076923077
1 0.36778846153846156 0.5913461538461539 0.14423076923076922 0.07451923076923077
1 0.1658653846153846 0.5949519230769231 0.18629807692307693 0.07932692307692307
1 0.3425480769230769 0.5360576923076923 0.22716346153846154 0.17668269230769232
1 0.2956730769230769 0.7427884615384616 0.23798076923076922 0.14423076923076922
1 0.453125 0.5336538461538461 0.2439903846153846 0.14423076923076922
1 0.21875 0.5793269230769231 0.17427884615384615 0.10576923076923077
1 0.4110576923076923 0.47115384615384615 0.17427884615384615 0.1310096153846154
```

Figure 9: Text file details.

Table 1: Difference between four versions of YOLOv5.

	YOLOv5s	YOLOv5m	YOLOv5l	YOLOv5x
CSP1	CSP1-1	CSP1-2	CSP1-3	CSP1-4
CSP1	CSP1-3	CSP1-6	CSP1-9	CSP1-12
CSP1	CSP1-3	CSP1-6	CSP1-9	CSP1-12
CSP2	CSP2-1	CSP2-2	CSP2-3	CSP2-4
CSP2	CSP2-1	CSP2-2	CSP2-3	CSP2-4
CSP2	CSP2-1	CSP2-2	CSP2-3	CSP2-4
CSP2	CSP2-1	CSP2-2	CSP2-3	CSP2-4
CSP2	CSP2-1	CSP2-2	CSP2-3	CSP2-4

(i) Model backbone

(ii) Model neck

(iii) Model head

Model backbone is mainly used to extract key features from an input image. The focusing layer is the initial layer of the backbone network, and it is used to simplify the model calculation and boost training speed. It serves the following purposes: using a slicing technique, the three-channel image is first split into four slices of $3 \times 320 \times 320$ each. Second, concatenation is used to connect the four sections indepth, with the output feature map having a size of $12 \times 320 \times 320$, and then the output feature map with a size of $32 \times 320 \times 320$ was formed via the convolutional layer made of 32 convolution kernels. Finally, the findings are output into the next layer via the BN layer (batch normalization) and the Hardswish activation functions. The BottleneckCSP [42] module is the third layer of the backbone network, and it is designed to extract the image's indepth information more effectively. The BottleneckCSP module is primarily formed of a Bottleneck module, as shown in Figure 11, which is a residual network architecture that joins a convolutional layer (Conv2d + BN + ReLu activation function) with a convolution kernel size of 1×1 with a convolution kernel size of 3×3. The final output of the Bottleneck module is the sum of this part's output and the initial input via the residual structure.

$$A_1 = B_1 \times A_0, \tag{6}$$

$$A_2 = B_2 \times [A_0, A_1], \tag{7}$$

$$A_k = B_k \times [A_0, A_1, \cdots, A_k - 1]. \tag{8}$$

Equations (6)–(8) are showing the working of CSP network from 1st layer to the last layer. Asterisk sign shows the operator, and $[A\_0, A\_1, \cdots]$ means concatenating $[A\_0, A\_1, \cdots]$, and B_i and A_i are the weights and output of the i-th dense layer, respectively. The first input of the BottleneckCSP module is split into two branches, and the number of feature map channels is halved using convolution in two branches as shown in Figure 12. The output feature map of branches one and two is then connected in depth using concat through the Bottleneck module and Conv2d layer inbranch two. Finally, the module's output feature map is created after progressively passing through the BN layer and Conv2d layer, and the size of this feature map is the same as the size of the BottleneckCSP module's input.

The SPP module (spatial pyramid pooling) [43] is the ninth layer of the Backbone network, and it is designed to increase the network's receptive field by transforming any size of the feature map into a fixed-size feature vector. Following a cycle through the convolutional layer, the feature map with a size of $256 \times 20 \times 20$ is output; the convolution kernel size is 1×1. Then, this feature map and the output feature map are connected indepth after being subsampled through three concurrent maxpooling layers, and the size of the output feature map is $1024 \times 20 \times 20$.

The model neck is mainly used to create feature pyramids. Feature pyramids assist models in successfully generalizing when it comes to object scaling, and it facilitates the identification of the same object in various sizes and scales.

$$A = A_0 + \log_2\left(\frac{\sqrt{xy}}{224}\right). \tag{9}$$

Equation (9) is used to select the feature map. Feature pyramids are pretty beneficial in assisting models to perform well on unknown data. The model head is primarily responsible for the final detection step, and it uses anchor boxes to construct final output vectors with class probabilities, objectness scores, and bounding boxes. The detection network of the YOLOv5s structure comprises three detect layers, each with an input of a feature map with dimensions of 80×80, 40×40, and 20×20 utilized to detect image objects of various sizes. Each detects layer outputs a 21-channel vector with two classes, 1 class probability, four surrounding box position coordinates, and three anchor boxes. Then, the predicted bounding boxes and categories of the targets in the original image were generated and labeled, allowing the detection of the images' targets to be implemented.

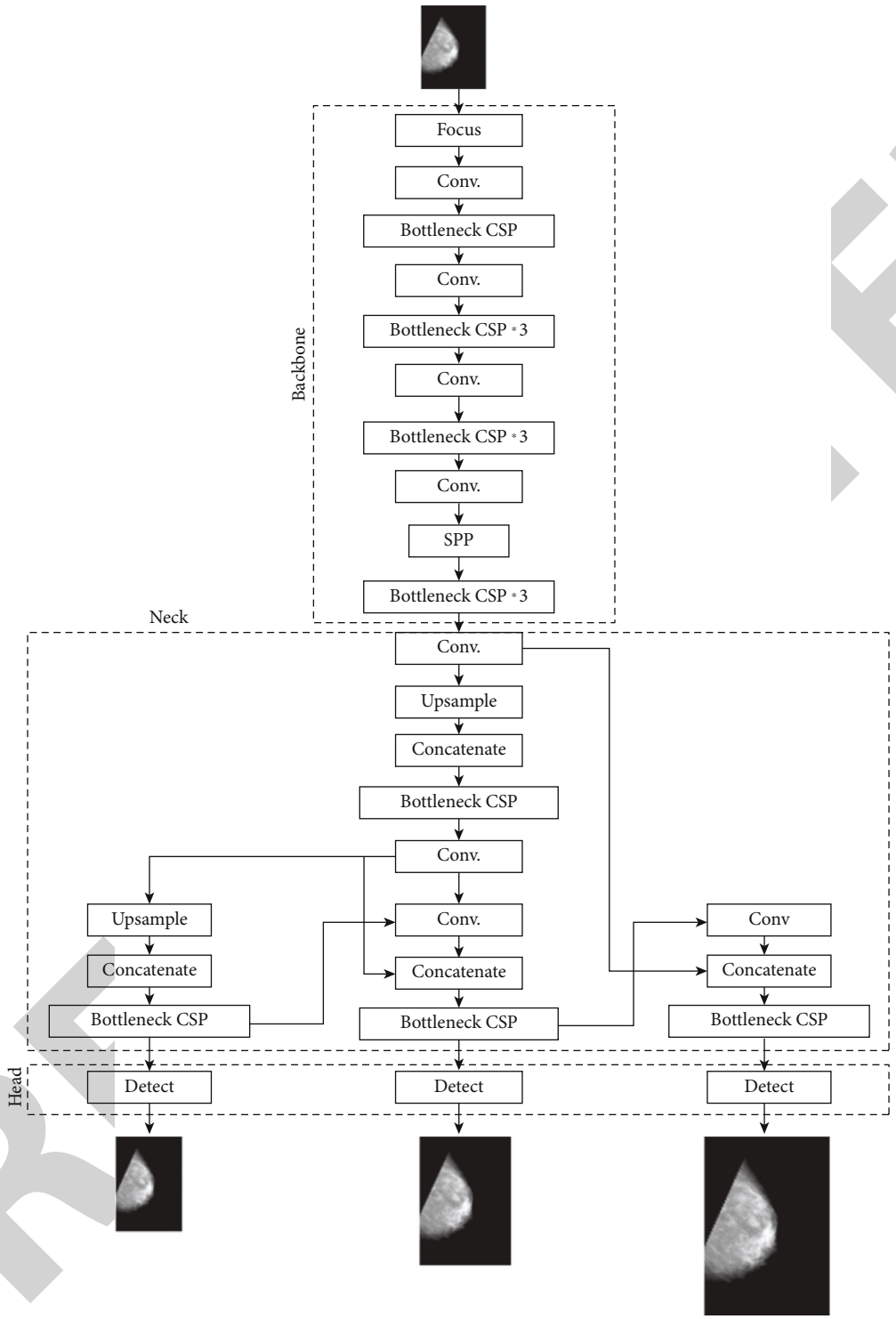

Figure 10: Architecture of original Yolov5s.

3.5. Improvement in the YOLOv5 Model. The YOLOv5 Model does not produce the desired results in its original form. Even on complex surfaces, the model should detect and categorize tumors correctly. The model's size must also be reduced as much as possible in order for it to be deployed in hardware devices. As a result, we make some changes to the model's backbone. The YOLOv5s architecture's backbone network comprises four BottleneckCSP modules, each with numerous convolutional layers. Although the convolution procedure can extract image features, the convolution kernel has many parameters, resulting in many parameters in the recognition model. As a result, the convolutional layer on the original CSP module's different branch is deleted. The BottleneckCSP module's input feature map is directly

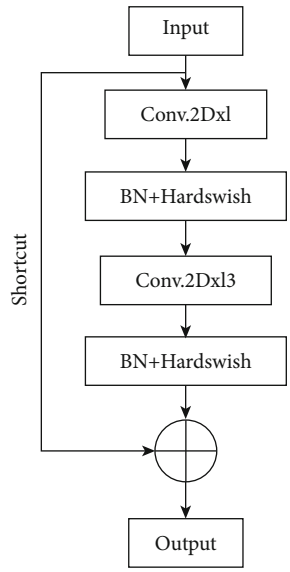

Figure 11: Bottleneck module.

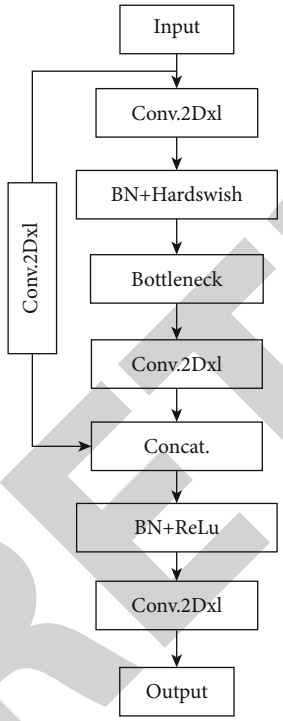

Figure 12: BottleneckCSP module.

connected with the output feature map with another branch indepth, significantly reducing the number of parameters in the module. The architecture of the improved BottleneckCSP module is shown in Figure 13.

In the study, four stages of the original backbone network where the BottleneckCSP module is used are replaced with four BottleneckCSP-new modules, as shown in Figure 14, to justify the limitation of BottleneckCSP-new, which may end up causing deficiency in the extraction of deep features in the image due to its lightweight attributes.

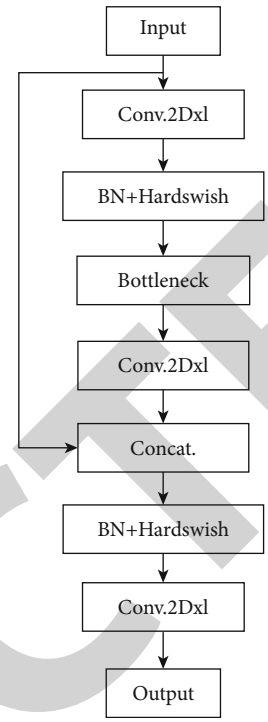

Figure 13: Improved BottleneckCSP module.

$$\text{Con.} = P(\text{Tumor}) \times \text{Loss}_p. \tag{10}$$

Equation (10) shows the function of calculation of loss. Con. denotes confidence, while P (Tumor) denotes the likelihood that the grid cell has a tumor. When the model is trained, the value is one if the target's center lies in a grid cell. Otherwise, it is 0. The loss value computes the change between the anticipated bounding box and the grid cell's ground truth box.

$$\text{IoU} = \frac{A \cap B}{A \cup B}, \tag{11}$$

$$L_{\text{GIOU}} = 1 - \text{IoU} + \frac{\left|A - B \cup B^f\right|}{|X|}. \tag{12}$$

IoU is the junction and unity of two boxes, and this is a standard statistic for describing the degree of coincidence between two boxes. The calculation method is shown in equation (11). GIoU loss function is used in this study, and the calculation method is shown in equation (12).

4. Experimental Analysis and Results

In our experiment, we begin by annotating data. Annotating the data involves highlighting a particular object (tumor) on the dataset's images. We split the data into three sections. 60% of the data is used for training, 30% for validation, and 10% for testing. In YOLOv5, there are four models: YOLOv5s, YOLOv5m, YOLOv5l, and YOLOv5x. The upgraded version of the YOLOv5 model is trained on Nvidia GPU using PyCharm frame 2020 of version 1.4.0 and

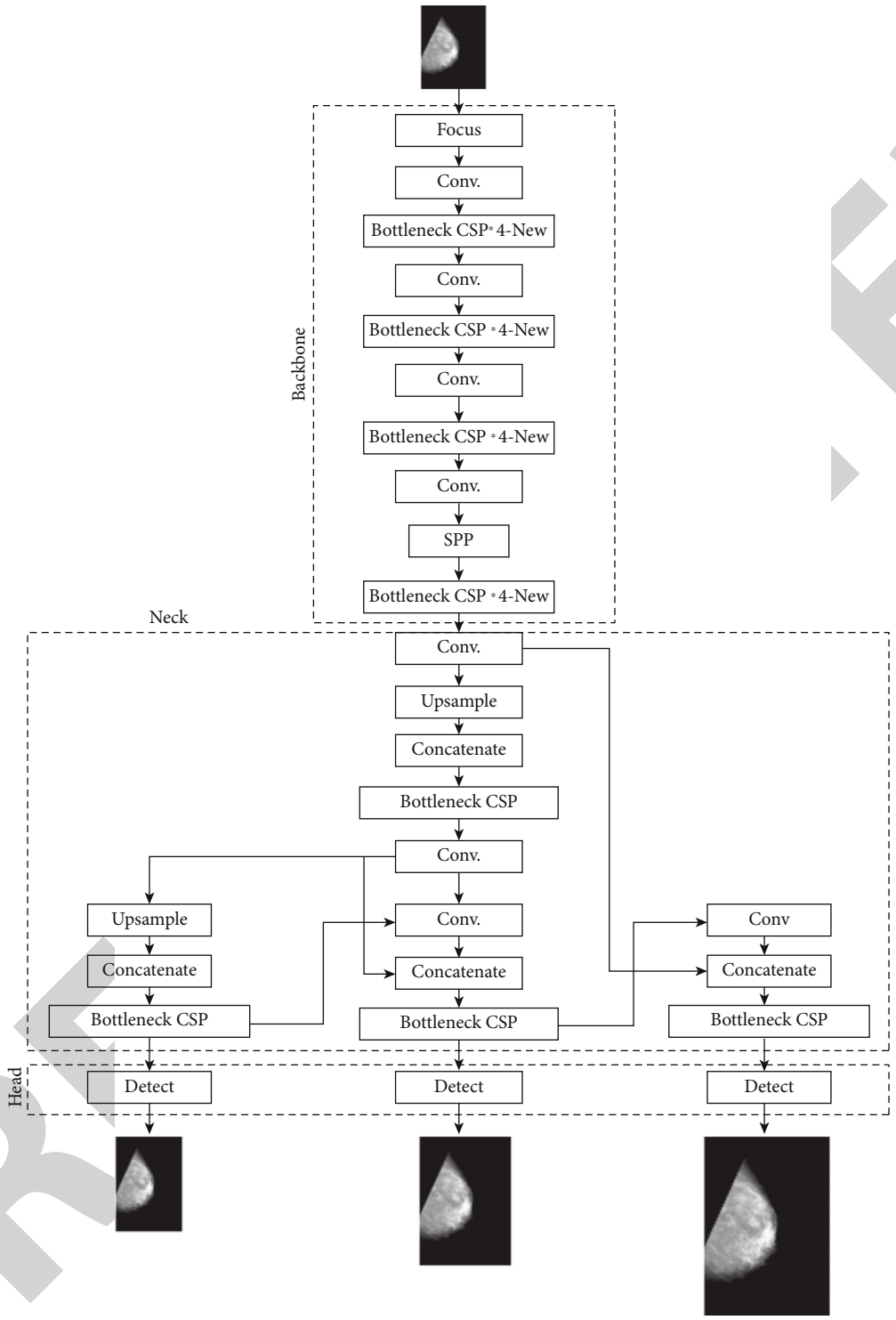

Figure 14: Modified version of YOLOv5.

Python 3.6 to train and test the breast tumor detection and classification model as calling CUDA, Cudnn, OpenCV, and other needed libraries. The experimental setup is Linux Ubuntu 16.04, with a GeForce GTX 1080Ti 11GB graphics card. The software used the Windows 10 operating system, the Keras deep learning framework, and the TensorFlow deep learning framework. The YOLOv5 model, a pretrained checkpoint on the COCO dataset, was fine-tuned. Stochastic Gradient Descent [44] is the optimizer utilized for this model (SGD). The model training batch size is set to 8, the learning rate is set to 0.01, the momentum is set to 0.843, and the decay rate is set to 0.00036. The IOU (intersection over union) value is set at 0.2. The training epoch value is set to 300. The model is trained consistently and performed well. After training, the weight file for this model is saved, and the test set is used to evaluate the model's performance.

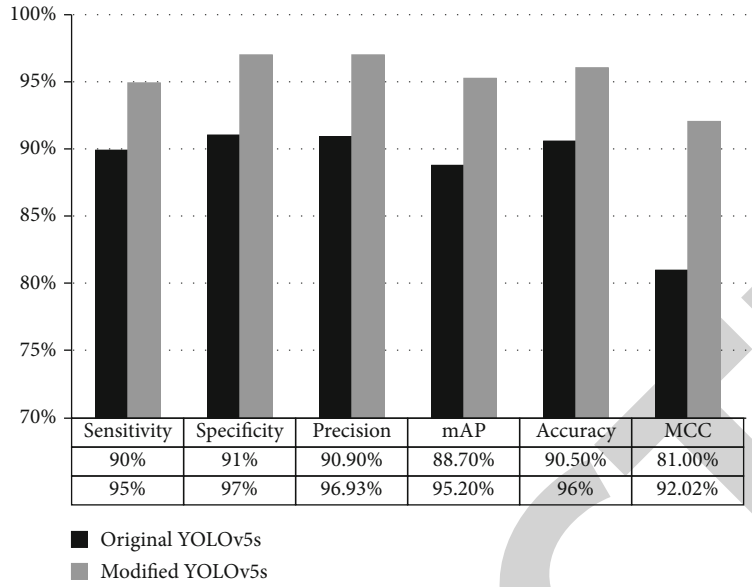

Sensitivity	Specificity	Precision	mAP	Accuracy	MCC
90%	91%	90.90%	88.70%	90.50%	81.00%
95%	97%	96.93%	95.20%	96%	92.02%

Figure 15: Comparison of modified YOLOv5s with original YOLOv5s on the basis of sensitivity, specificity, accuracy, mAP, precision, and MCC.

The network's final output is the position boxes of the two types of breast tumors (benign and malignant), as well as the likelihood of belonging to a given category.

4.1. Performance Measure. Different measures are used to evaluate the performance of the model. Accuracy [45], mAP, sensitivity 13, specificity, *F*-measure [46], MCC [47] measurements are taken using TP (true positive), TN (true negative), FP (false positive), and FN (false negative).

TP (true positive): the number of cases accurately defined in this section.

TN (true negative): the number of examples correctly refused in this section.

FP (false positive): the number of cases unfairly denied in that class.

FN (false negative): the number of instances wrongly listed in that class.

FPR (false positive rate): the results say you have the disease, but you do not.

FNR (false negative rate): the results say you do not have a disease, but you really do.

$$\text{Sensitivity} = \frac{\text{TP}}{\text{TP} + \text{FN}}, \tag{13}$$

$$\text{Specificity} = \frac{\text{TN}}{\text{FP} + \text{TN}}, \tag{14}$$

$$\text{Precision} = \frac{\text{TP}}{\text{FP} + \text{TP}}, \tag{15}$$

$$m\text{AP} = \frac{1}{N}\sum_{i=1}^{N} \text{AP}_i, \tag{16}$$

$$\text{Accuracy} = \frac{\text{TN} + \text{TP}}{\text{FP} + \text{TN} + \text{FN} + \text{TP}}, \tag{17}$$

$$F - measure = \frac{2(Sensitivity)(Precision)}{Sensitivity + Precision}, \tag{18}$$

$$\text{MCC} = \frac{(\text{TP})(\text{TN}) - (\text{FP})(\text{FN})}{\sqrt{(\text{TP} + \text{FP})(\text{TP} + \text{FN})(\text{TN} + \text{FP})(\text{TN} + \text{FN})}}, \tag{19}$$

$$\text{FPR} = 1 - \text{Specificity} = \frac{\text{FP}}{\text{FP} + \text{TN}}, \tag{20}$$

$$\text{FNR} = 1 - \text{Sensitivity} = \frac{\text{FN}}{\text{TP} + \text{FN}}. \tag{21}$$

Equations (13)–(21), represent sensitivity, specificity, precision, mAP, accuracy, *F*-measure, MCC, FPR, and FNR, respectively.

MCC value is the primary and most essential performance metric. Instead, the Matthews correlation coefficient (MCC) is a more reliable statistical rate in binary classification that yields a high score only if the prediction performed well in all four confusion matrix categories.

The mAP is an essential parameter for measuring network model training, and it is the average mean precision of each AP category. AP denotes the region contained by precision and recall as two-axis mapping, the average is denoted by *M*, and the number after @ is the threshold for evaluating IoU as positive and negative samples.

4.2. Comparison of Original YOLOv5s and Modified YOLOv5s. Modified YOLOv5s performs better than original YOLOv5s. As seen in Figure 15, modified YOLOv5s achieve 95% sensitivity, 97% specificity, 96.93% precision, 95.20% mAP, 96% accuracy, and 92.02% MCC value. Original YOLOv5s achieve 90% sensitivity, 91% specificity, 90.90% precision, 88.70% mAP, 90.50% accuracy, and 81% MCC value.

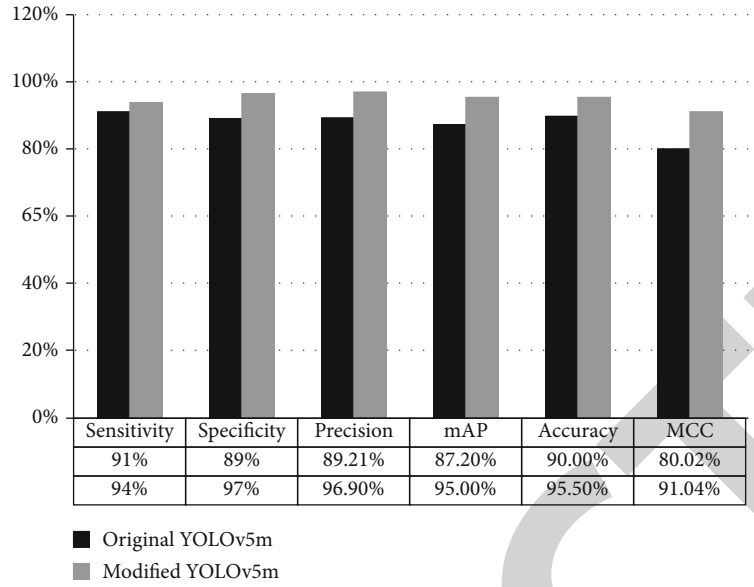

Sensitivity	Specificity	Precision	mAP	Accuracy	MCC
91%	89%	89.21%	87.20%	90.00%	80.02%
94%	97%	96.90%	95.00%	95.50%	91.04%

Figure 16: Comparison of modified YOLOv5m with original YOLOv5m on the basis of sensitivity, specificity, accuracy, mAP, precision, and MCC.

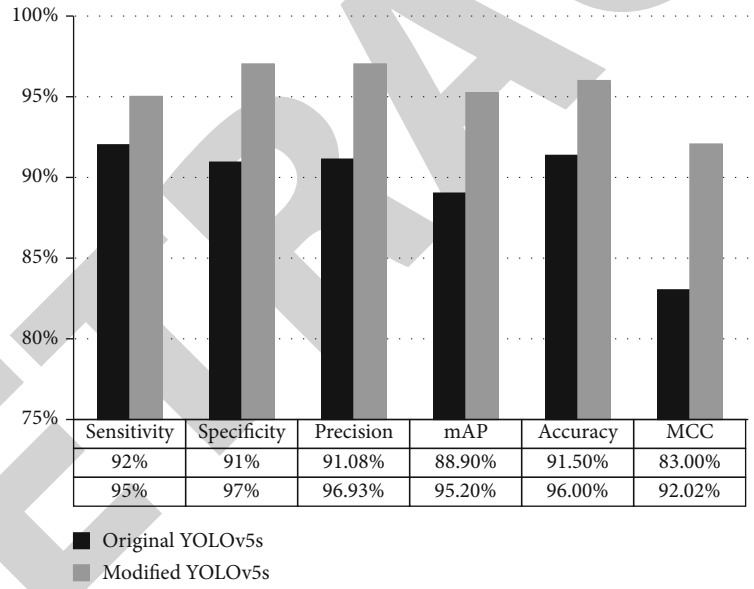

Sensitivity	Specificity	Precision	mAP	Accuracy	MCC
92%	91%	91.08%	88.90%	91.50%	83.00%
95%	97%	96.93%	95.20%	96.00%	92.02%

Figure 17: Comparison of modified YOLOv5l with original YOLOv5l on the basis of sensitivity, specificity, accuracy, mAP, precision, and MCC.

4.3. Comparison of Original YOLOv5m and Modified YOLOv5m. As seen in Figure 16, modified YOLOv5m achieves 94% sensitivity, 97% specificity, 96.90% precision, 95% mAP, 95.50% accuracy, and 91.04% MCC value. Original YOLOv5m achieves 91% sensitivity, 89% specificity, 89.21% precision, 87.20% mAP, 90% accuracy, and 80.02% MCC value. Modified YOLOv5m performs well as compared to original YOLOv5m.

4.4. Comparison of Original YOLOv5l and Modified YOLOv5l. As seen in Figure 17, modified YOLOv5l achieves 95% sensitivity, 97% secificity, 96.93% precision, 95.20% mAP, 96% accuracy, and 92.02% MCC value. Original YOLOv5l achieves 92% sensitivity, 91% specificity, 91.08% precision, 88.90% mAP, 91.5% accuracy, and 83% MCC value. Modified YOLOv5l performs well as compared to the original YOLOv5l.

4.5. Comparison of Original YOLOv5x and Modified YOLOv5x. As seen in Figure 18, modified YOLOv5x achieves 96% sensitivity, 97% specificity, 97% precision, 96% mAP, 96.50% accuracy, and 93.60% MCC value. Original YOLOv5x achieves 93% sensitivity, 92% specificity, 92.07% precision, 89.20% mAP, 92.5% accuracy, and 85% MCC value. Modified YOLOv5x performs well as compared to original YOLOv5x.

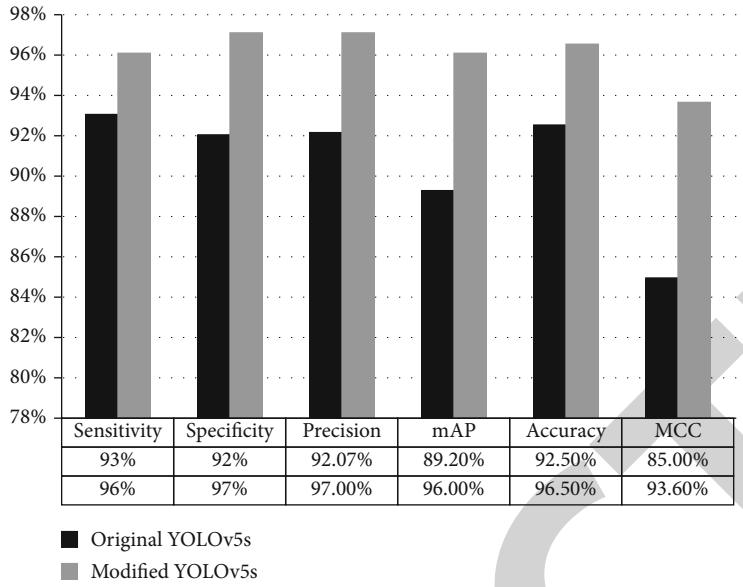

Sensitivity	Specificity	Precision	mAP	Accuracy	MCC
93%	92%	92.07%	89.20%	92.50%	85.00%
96%	97%	97.00%	96.00%	96.50%	93.60%

Figure 18: Comparison of modified YOLOv5x with original YOLOv5x on the basis of sensitivity, specificity, accuracy, mAP, precision, and MCC.

Table 2: Comparison of all four versions of modified YOLOv5 with original YOLOv5 on the basis of false positive rate (FPR) and false negative rate (FNR).

Models	FPR	FNR
Original YOLOv5s	0.09	0.10
Modified YOLOv5s	0.05	0.03
Original YOLOv5m	0.11	0.09
Modified YOLOv5m	0.06	0.03
Original YOLOv5l	0.09	0.08
Modified YOLOv5l	0.05	0.03
Original YOLOv5x	0.08	0.07
Modified YOLOv5x	0.04	0.03

The next performance measure is FPR and FNR rates, and these two rates should be low to authenticate our results. Here in this study, FPR and FNR rates for all four versions of modified YOLOv5 and original YOLOv5 are mentioned in Table 2.

4.6. Comparison of Modified YOLOv5x, YOLOv3, and Faster RCNN. We use three detection models for breast tumor detection and compare their performance: YOLOv5, faster R-CNN, and Yolov3. First, we compared all variants of the original YOLOv5 and modified YOLOv5. Then, we compare all four versions of modified YOLOv5, and we find that modified YOLOv5x outperformed all other versions. As a result, for further comparisons with faster RCNN and YoloV3, we utilize modified YOLOvx. Table 3 shows that modified YOLOv5x has the lowest FPR and FNR rates than YOLOv3 and faster RCNN. MCC, accuracy, and mAP that we achieve for modified YOLOv5x are 93.50%, 96.50%, and 96%, respectively, higher than the other two detection models. So, it is clear that modified YOLOvx performs better than faster RCNN and YOLOv3 to detect and classify breast tumors.

Table 3: Comparison of all four versions of modified YOLOv5 with original YOLOv5 on the basis of false positive rate (FPR) and false negative rate (FNR).

Models	FPR	FNR	mAP	MCC	Acc.
Modified YOLOv5x	0.04	0.03	96%	93.50%	96.50%
YOLOv3	0.15	0.19	85%	82.5%	86%
Faster RCNN	0.20	0.15	84.2%	81.7%	85.3%

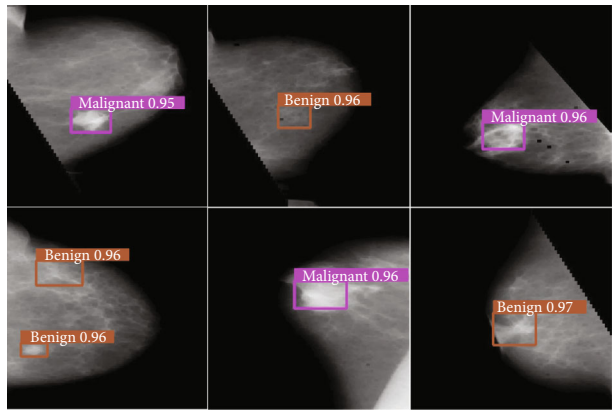

Figure 19: Results of breast tumor detection and classification using improved YOLOv5x network.

The YOLOv5 model detects and categorizes breast tumors into two classes. There are two types of tumors: benign and malignant. All four YOLOv5 variants are used to detect and classify breast tumors. The results obtained are not satisfactory, which is why all four versions of YOLOv5 have been updated. It is discovered that modified versions outperform the originals, and YOLOv5x performs well among modified

versions compared to other modified versions. Figure 19 depicts the results of breast tumor detection and classification using an enhanced YOLOv5x network.

5. Conclusion

Early detection and classification of breast tumors are increasingly required to reduce the risk of death among cancer patients. Many researchers have conducted extensive research and proposed models for detecting and classifying benign and malignant breast tumors, but something is still missing. In many studies, the model reached a performance accuracy of 90% or higher, but even though the MCC value decreased, the FPR and FNR were increased. Rates of FPR and FNR should be as low as possible. Because the MCC value is a more accurate measure for binary classification than accuracy, it should be enhanced to validate our findings further. This paper proposes a lightweight detection and classification method based on improved YOLOv5 to detect and classify breast tumors. All four versions (YOLOv5s, YOLOv5m, YOLOv5l, YOLOv5x) of modified YOLOv5 are used in this study. BottleneckCSP module is updated to BottleneckCSP-new module, which is utilized to replace the BottleneckCSP module in the backbone architecture of the original YOLOv5s network to improve results and make the network lighter. To evaluate performance, the original YOLOv5 and the modified YOLOv5 are compared.

The results show that modified versions of YOLOv5 perform better than original YOLOv5. Modified YOLOv5s, YOLOv5m, YOLOv5l, and YOLOv5x achieve (92.02%, 91.04%, 92.02%, 93.60%) MCC value, (0.05, 0.06, 0.05, 0.04) FPR value, and (0.03, 0.03, 0.03, 0.03) FNR value better than the original YOLOv5 model. Among all four modified YOLOv5 versions, YOLOv5x outperforms the other three. So, modified YOLOv5x is compared to faster RCNN and YOLOv3. It has been observed that modified YOLOv5x outperforms faster RCNN and YOLOv3 with 0.04 FPR, 0.03 FNR, 93.60% MCC, 96.50% accuracy, 96% mAP, 97% precision, 96% sensitivity, and 97% specificity. The results conclude that our suggested model successfully identifies and classifies breast tumors while also overcoming previous research limitations by lowering the false positive and false negative ratio and boosting the MCC value.

5.1. Future Work. In this work, a modified YOLOv5 model is used to detect and classify breast tumors as benign or malignant, with promising results. Our suggested model can detect tumors that are in shape or those that are lightly shaped. However, our proposed model cannot detect poorly shaped tumors in abnormal images, which is a limitation. We will improve this network in the future to recognize all shapes and sizes of tumors, making it more convenient. We have also just focused on breast mass abnormalities so far. So, the study can be expanded in the future to cover macro calcification anomalies that are not currently evaluated.

Data Availability

The dataset used to support the findings of this study are included within the article.

Conflicts of Interest

The authors declare that they have no conflicts of interest.

References

[1] S. Abbas, Z. Jalil, A. R. Javed et al., "Bcd-wert: a novel approach for breast cancer detection using whale optimization based efficient features and extremely randomized tree algorithm," *PeerJ Computer Science*, vol. 7, article e390, 2021.

[2] R. S. Patil and N. Biradar, "Automated mammogram breast cancer detection using the optimized combination of convolutional and recurrent neural network," *Evolutionary Intelligence*, 2020.

[3] A. R. Javed, M. U. Sarwar, M. O. Beg, M. Asim, T. Baker, and H. Tawfik, "A collaborative healthcare framework for shared healthcare plan with ambient intelligence," *Human-centric Computing and Information Sciences*, vol. 10, no. 1, pp. 1–21, 2020.

[4] S. Pandya, M. Mistry, K. Kotecha et al., "Smart aging wellness sensor networks: a near real-time daily activity health monitoring, anomaly detection and alert system," in *Proceedings of Second International Conference on Computing, Communications, and Cyber-Security*, P. K. Singh, S. T. Wierzchoń, S. Tanwar, M. Ganzha, and J. J. P. C. Rodrigues, Eds., pp. 3–21, Springer, Singapore, 2021.

[5] M. Awais, H. Ghayvat, A. K. Pandarathodiyil et al., "Healthcare professional in the loop (hpil): classification of standard and oral cancer-causing anomalous regions of oral cavity using textural analysis technique in autofluorescence imaging," *Sensors*, vol. 20, no. 20, article 5780, 2020.

[6] H. Ghayvat, S. N. Pandya, P. Bhattacharya et al., "Cp-bdhca: Blockchain-based confidentiality-privacy preserving big data scheme for healthcare clouds and applications," *IEEE Journal of Biomedical and Health Informatics*, p. 1, 2021.

[7] A. R. Javed, M. U. Sarwar, S. ur Rehman, H. U. Khan, Y. D. al-Otaibi, and W. S. Alnumay, "Pp-spa: privacy preserved smartphone-based personal assistant to improve routine life functioning of cognitive impaired individuals," *Neural Processing Letters*, 2021.

[8] M. U. Sarwar, A. R. Javed, F. Kulsoom, S. Khan, U. Tariq, and A. K. Bashir, "Parciv: recognizing physical activities having complex interclass variations using semantic data of smartphone," *Software: Practice and Experience*, vol. 51, no. 3, pp. 532–549, 2021.

[9] A. R. Javed, R. Faheem, M. Asim, T. Baker, and M. O. Beg, "A smartphone sensors-based personalized human activity recognition system for sustainable smart cities," *Sustainable Cities and Society*, vol. 71, article 102970, 2021.

[10] A. R. Javed, L. G. Fahad, A. A. Farhan et al., "Automated cognitive health assessment in smart homes using machine learning," *Sustainable Cities and Society*, vol. 65, article 102572, 2021.

[11] A. R. Javed, M. U. Sarwar, S. Khan, C. Iwendi, M. Mittal, and N. Kumar, "Analyzing the effectiveness and contribution of each axis of tri-axial accelerometer sensor for accurate activity recognition," *Sensors*, vol. 20, no. 8, article 2216, 2020.

[12] A. Ayoub, K. Mahboob, A. Rehman Javed et al., "Classification and categorization of covid-19 outbreak in Pakistan," *Computers, Materials and Continua*, vol. 69, no. 1, pp. 1253–1269, 2021.

[13] M. U. Sarwar and A. R. Javed, "Collaborative health care plan through crowdsource data using ambient application," in *2019 22nd International Multitopic Conference (INMIC)*, pp. 1–6, Islamabad, Pakistan, 2019.

[14] C. Iwendi, A. K. Bashir, A. Peshkar et al., "Covid-19 patient health prediction using boosted random forest algorithm," *Frontiers in public health*, vol. 8, 2020.

[15] S. U. Rehman, A. R. Javed, M. U. Khan, M. Nazar Awan, A. Farukh, and A. Hussien, "Personalisedcomfort: a personalised thermal comfort model to predict thermal sensation votes for smart building residents," *Enterprise Information Systems*, pp. 1–23, 2020.

[16] B. Aslam, A. R. Javed, C. Chakraborty, J. Nebhen, S. Raqib, and M. Rizwan, "Blockchain and anfis empowered iomt application for privacy preserved contact tracing in covid-19 pandemic," *Personal and Ubiquitous Computing*, pp. 1–17, 2021.

[17] C. Iwendi, K. Mahboob, Z. Khalid, A. R. Javed, M. Rizwan, and U. Ghosh, "Classification of covid-19 individuals using adaptive neuro-fuzzy inference system," *Multimedia Systems*, pp. 1–15, 2021.

[18] K. Shaikh, S. Krishnan, and R. Thanki, *Artificial intelligence in breast cancer early detection and diagnosis*, Springer, 2021.

[19] E. Jedy-Agba, M. P. Curado, O. Ogunbiyi et al., "Cancer incidence in Nigeria: a report from population-based cancer registries," *Cancer Epidemiology*, vol. 36, no. 5, pp. e271–e278, 2012.

[20] A.-K. Vranso West, L. Wullkopf, A. Christensen et al., "Division induced dynamics in non-invasive and invasive breast cancer," *Biophysical Journal*, vol. 112, no. 3, p. 123a, 2017.

[21] National Institute of Biomedical Imaging and Bioengineering (NIBIB), "Mammography," 2020, https://www.nibib.nih.gov/scienceeducation/sciencetopics/mammography.

[22] D. Rinella, "Mammography positioning: The cc and mlo," *Seminars in Breast Disease*, vol. 8, no. 4, pp. 206–210, 2005.

[23] V. S. Gnanasekaran, S. Joypaul, P. Meenakshi Sundaram, and D. D. Chairman, "Deep learning algorithm for breast masses classification in mammograms," *IET Image Processing*, vol. 14, no. 12, pp. 2860–2868, 2020.

[24] B. Swiderski, P. O. Gielata, P. Olszewski, S. Osowski, and M. Kołodziej, "Deep neural system for supporting tumor recognition of mammograms using modified GAN," *Expert Systems with Applications*, vol. 164, article 113968, 2021.

[25] R. Agarwal, O. Díaz, M. H. Yap, X. Llado, and R. Marti, "Deep learning for mass detection in full field digital mammograms," *Computers in biology and medicine*, vol. 121, article 103774, 2020.

[26] L. G. Falconi, M. Perez, W. G. Aguila, and A. Conci, "Transfer learning and fine tuning in breast mammogram abnormalities classification on cbis-ddsm database," *Advances in Science, Technology and Engineering Systems*, vol. 5, no. 2, pp. 154–165, 2020.

[27] M. Amalmary and A. Prakash, *Elephant herding optimization with bi-directional long shortterm memory network (ehobi-lstm) for breast cancer detection in digital mammograms*.

[28] Y. J. Suh, J. Jung, and B.-J. Cho, "Automated breast cancer detection in digital mammograms of various densities via deep learning," *Journal of Personalized Medicine*, vol. 10, no. 4, p. 211, 2020.

[29] L. Ahmed, M. M. Iqbal, H. Aldabbas, S. Khalid, Y. Saleem, and S. Saeed, "Images data practices for semantic segmentation of breast cancer using deep neural network," *Journal of Ambient Intelligence and Humanized Computing*, pp. 1–17, 2020.

[30] M. A. Al-Antari, S.-M. Han, and T.-S. Kim, "Evaluation of deep learning detection and classification towards computer-aided diagnosis of breast lesions in digital X-ray mammograms," *Computer methods and programs in biomedicine*, vol. 196, article 105584, 2020.

[31] M. Alfifi, M. Shady, S. Bataineh, and M. Mezher, "Enhanced artificial intelligence system for diagnosing and predicting breast cancer using deep learning," *International Journal of Advanced Computer Science and Applications*, vol. 11, no. 7, 2020.

[32] W. Ansar, A. R. Shahid, B. Raza, and A. H. Dar, "Breast cancer detection and localization using mobilenet based transfer learning for mammograms," in *International Symposium on Intelligent Computing Systems*, pp. 11–21, Springer, Cham, 2020.

[33] S. Hadush, Y. Girmay, A. Sinamo, and G. Hagos, "Breast cancer detection using convolutional neural networks," 2020, https://arxiv.org/abs/2003.07911.

[34] H. Nasir Khan, A. R. Shahid, B. Raza, A. H. Dar, and H. Alquhayz, "Multi-view feature fusion based four views model for mammogram classification using convolutional neural network," *IEEE Access*, vol. 7, pp. 165724–165733, 2019.

[35] L. Hao-Chun, E.-W. Loh, and S.-C. Huang, "The classification of mammogram using convolutional neural network with specific image preprocessing for breast cancer detection," in *2019 2nd International Conference on Artificial Intelligence and Big Data (ICAIBD)*, pp. 9–12, Chengdu, China, 2019.

[36] A. M. Alqudah, H. M. S. Algharib, A. M. S. Algharib, and H. M. S. Algharib, "Computer aided diagnosis system for automatic two stages classification of breast mass in digital mammogram images," *Biomedical Engineering: Applications, Basis and Communications*, vol. 31, no. 1, article 1950007, 2019.

[37] N. S. Ismail and C. Sovuthy, "Breast cancer detection based on deep learning technique," in *2019 International UNIMAS STEM 12th Engineering Conference (EnCon)*, pp. 89–92, Kuching, Malaysia, 2019.

[38] R. Touahri, N. AzizI, N. E. Hammami, M. Aldwairi, and F. Benaida, "Automated breast tumor diagnosis using local binary patterns (lbp) based on deep learning classification," in *2019 International Conference on Computer and Information Sciences (ICCIS)*, pp. 1–5, Sakaka, Saudi Arabia, 2019.

[39] M. Mehmood, E. Ayub, F. Ahmad et al., "Machine learning enabled early detection of breast cancer by structural analysis of mammograms," *Computers, Materials and Continua*, vol. 67, no. 1, pp. 641–657, 2021.

[40] M. Ravikumar, P. G. Rachana, B. J. Shivaprasad, and D. S. Guru, "Enhancement of mammogram images using clahe and bilateral filter approaches," in *Cybernetics, Cognition and Machine Learning Applications*, pp. 261–271, Springer, 2021.

[41] C. Lupaşcu, C. Pleşca, and M. Togan, "Privacy preserving morphological operations for digital images," in *2020 13th International Conference on Communications (COMM)*, pp. 183–188, Bucharest, Romania, 2020.

[42] Y. Fang, X. Guo, K. Chen, Z. Zhou, and Q. Ye, "Accurate and automated detection of surface knots on sawn timbers using

Hindawi
Computational and Mathematical Methods in Medicine
Volume 2023, Article ID 9823571, 1 page
https://doi.org/10.1155/2023/9823571

Retraction

Retracted: MKA: A Scalable Medical Knowledge-Assisted Mechanism for Generative Models on Medical Conversation Tasks

Computational and Mathematical Methods in Medicine

Received 10 October 2023; Accepted 10 October 2023; Published 11 October 2023

This article has been retracted by Hindawi following an investigation undertaken by the publisher [1]. This investigation has uncovered evidence of one or more of the following indicators of systematic manipulation of the publication process:

(1) Discrepancies in scope

(2) Discrepancies in the description of the research reported

(3) Discrepancies between the availability of data and the research described

(4) Inappropriate citations

(5) Incoherent, meaningless and/or irrelevant content included in the article

(6) Peer-review manipulation

The presence of these indicators undermines our confidence in the integrity of the article's content and we cannot, therefore, vouch for its reliability. Please note that this notice is intended solely to alert readers that the content of this article is unreliable. We have not investigated whether authors were aware of or involved in the systematic manipulation of the publication process.

Wiley and Hindawi regrets that the usual quality checks did not identify these issues before publication and have since put additional measures in place to safeguard research integrity.

We wish to credit our own Research Integrity and Research Publishing teams and anonymous and named external researchers and research integrity experts for contributing to this investigation.

The corresponding author, as the representative of all authors, has been given the opportunity to register their agreement or disagreement to this retraction. We have kept a record of any response received.

References

[1] K. Liang, S. Wu, and J. Gu, "MKA: A Scalable Medical Knowledge-Assisted Mechanism for Generative Models on Medical Conversation Tasks," *Computational and Mathematical Methods in Medicine*, vol. 2021, Article ID 5294627, 10 pages, 2021.

Hindawi
Computational and Mathematical Methods in Medicine
Volume 2021, Article ID 5294627, 10 pages
https://doi.org/10.1155/2021/5294627

Research Article

MKA: A Scalable Medical Knowledge-Assisted Mechanism for Generative Models on Medical Conversation Tasks

Ke Liang[1,2], **Sifan Wu**[3] and **Jiayi Gu**[4]

[1]*Pennsylvania State University, PA 16801, USA*
[2]*National University of Defense Technology, 410073, China*
[3]*Nvidia, Shanghai 201210, China*
[4]*TMiRob, Shanghai 201203, China*

Correspondence should be addressed to Ke Liang; kul660@psu.edu

Received 16 September 2021; Accepted 7 December 2021; Published 23 December 2021

Academic Editor: Shakeel Ahmad

Using natural language processing (NLP) technologies to develop medical chatbots makes the diagnosis of the patient more convenient and efficient, which is a typical application in healthcare AI. Because of its importance, lots of researches have come out. Recently, the neural generative models have shown their impressive ability as the core of chatbot, while it cannot scale well when directly applied to medical conversation due to the lack of medical-specific knowledge. To address the limitation, a scalable medical knowledge-assisted mechanism (*MKA*) is proposed in this paper. The mechanism is aimed at assisting general neural generative models to achieve better performance on the medical conversation task. The medical-specific knowledge graph is designed within the mechanism, which contains 6 types of medical-related information, including department, drug, check, symptom, disease, and food. Besides, the specific token concatenation policy is defined to effectively inject medical information into the input data. Evaluation of our method is carried out on two typical medical datasets, MedDG and MedDialog-CN. The evaluation results demonstrate that models combined with our mechanism outperform original methods in multiple automatic evaluation metrics. Besides, MKA-BERT-GPT achieves state-of-the-art performance.

1. Introduction

Difficulty in seeing a doctor, long queuing time, and inconvenience of making appointments have long been hurdles facing patients when they try to access primary care services. To solve these challenges, many advanced artificial intelligence (*AI*) technologies [1–3] have been combined with healthcare to boost the availability of medical resources, such as applying pattern recognition methods on medical images [4, 5] and leveraging natural language processing (*NLP*) technologies to design medical chatbots [6, 7]. The medical chatbot is mainly aimed to offer the medical assistants including disease identification, self-reports based medical suggestions for drugs, foods and checks, and medical front desk service guiding the patient to suitable healthcare service department, etc [8, 9]. It has a significant potential to simplify the diagnostic process and relieve the cost of collecting information from patients. Besides, the preliminary diagnosis results generated by the model may assist doctors to make a diagnosis more efficiently.

As the core of the medical chatbot, different methods have been investigated recently. In general, typical methods can be divided into two types [10], including information retrieval-based methods and neural generative methods. As for the first type, the methods usually match the response from the user-built question and answer (Q&A) pool based on the dialogue context, which means it can only provide the response that occurred in the existing pool. In another word, the poor-quality pool will influence a lot on the response. The second type of methods usually takes the dialogue context history as input and generates the suitable response word by word. Compared to retrieval-based methods, neural generative methods are more intelligent and flexible, which is what we focus on in this paper.

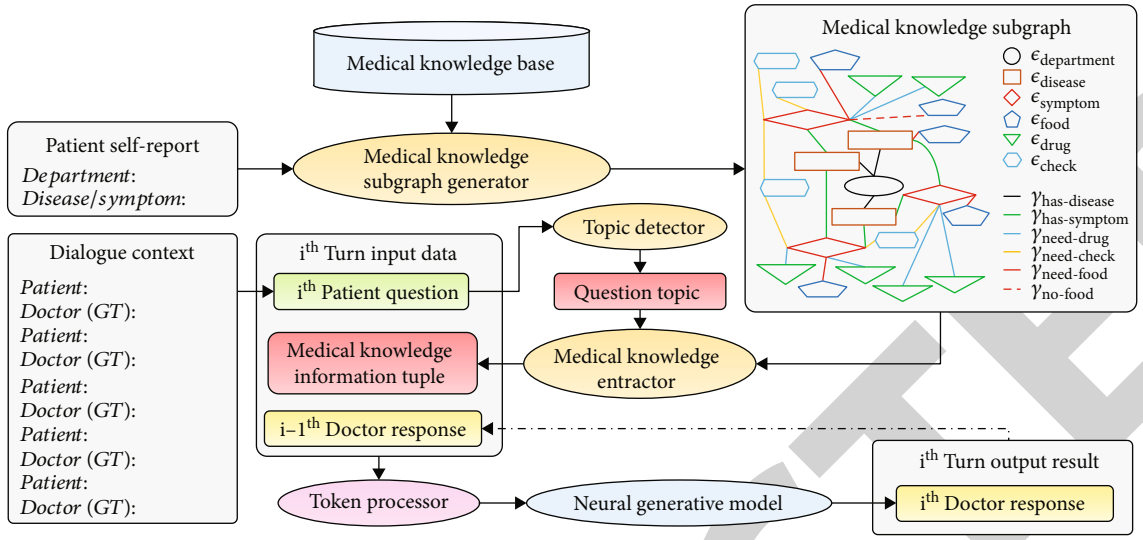

Figure 1: Framework of our scalable medical knowledge-assisted generative model, *MKA*. In the figure, the ellipsoids represent the modules inside of our method. The orange ellipsoids show the automatic and scalable medical knowledge generation module. The figure legend inside of medical knowledge subgraph is corresponding to the entity types and relation types shown in Tables 1 and 2.

Table 1: Definition of entity types in medical knowledge graphs.

Entity type	Description
$\epsilon_{department}$	Entities for the clinical departments
$\epsilon_{disease}$	Entities for the diseases
$\epsilon_{symptom}$	Entities for the symptoms
ϵ_{food}	Entities for the food
ϵ_{check}	Entities for the drugs
ϵ_{drug}	Entities for the checks

Currently, different neural generative models are applied to medical domain, including *LSTM-based* models, *Transformer*, *GPT*, and *BERT-GPT*. However, none of them performs well on the medical domain, which is reasonable. Here is the fact that the doctor makes diagnosis not only based on their experiences but also on the medical knowledge learned from professional books, especially when they meet rarely seen symptoms or diseases. The training procedure of the models only imitates the learning procedure of the experiences but leaves out the learning procedure from books. However, few works are about how to effectively integrate the medical knowledge with the neural generative models. Besides, patients are usually asked to fill in the patient self-report before the conversation starts with the doctor in real-world scenario. There are two common questions in the patient self-report, including "which department do you want to go?" and "what kind of the disease or symptom do you have?" Previous medical neural generative models will either leave out the information or roughly concatenate the original context in the patient self-report with the conversation history. It may cause either information loss or redundancy problem for the methods.

To address the limitations, the objective of the paper is to propose a medical knowledge-assisted mechanism (*MKA*) to assist common neural generative models to achieve better performance for the medical conversation task. *MKA* is an effective and lightweight method to integrate the medical knowledge with neural generative models. The mechanism first introduces a medical knowledge generation module to generate the related medical knowledge, which generates the medical knowledge subgraph (MKG_{sub}) generated from the patients' self-report. The designed knowledge graphs contain related medical knowledge for each patient, including 6 types of entities (i.e., $\epsilon_{department}$, $\epsilon_{disease}$, $\epsilon_{symptom}$, ϵ_{food}, ϵ_{check}, and ϵ_{drug}) and 6 types of relations (i.e., $\gamma_{has-disease}$, $\gamma_{has-symptom}$, $\gamma_{need-drug}$, $\gamma_{need-check}$, $\gamma_{need-food}$, and $\gamma_{no-food}$). Then, the medical knowledge information is fed into the token processor together with the dialogue contexts. Within the token processor, all the tokens will be reorganized based on the specific token concatenation policy. Finally, the processed data will be taken by selected generative models for training. In summary, we make the following contributions:

(1) The paper proposes an effective and lightweight mechanism to integrate the medical knowledge into different neural generative models, *MKA*. Besides, the specific medical knowledge graph is designed to store the medical knowledge. To the best of our knowledge, *MKA* is the first scalable work that can integrate the medical knowledge into all kinds of neural generative models, especially for large-scale pretrained model, such as *BERT-GPT*

(2) To verify our method, we implement two models based on our mechanism, *MKA-Transformer* and *MKA-BERT-GPT*. The evaluation is carried out on 2 typical medical conversation benchmarks: MedDialog [11] and MedDG [12]. Our experiments

Table 2: Definition of relation types in medical knowledge graphs.

Relation type	Description
$\gamma_{\text{has–disease}}$	Relations between $\epsilon_{\text{department}}$ entity and $\epsilon_{\text{disease}}$ entity
$\gamma_{\text{has–symptom}}$	Relations between $\epsilon_{\text{disease}}$ entity and $\epsilon_{\text{symptom}}$ entity
$\gamma_{\text{need–drug}}$	Relations between $\epsilon_{\text{disease}}/\epsilon_{\text{symptom}}$ entity and ϵ_{drug} entity
$\gamma_{\text{need–check}}$	Relations between $\epsilon_{\text{disease}}/\epsilon_{\text{symptom}}$ entity and ϵ_{check} entity
$\gamma_{\text{need–food}}$	Relations between $\epsilon_{\text{disease}}/\epsilon_{\text{symptom}}$ entity and recommended ϵ_{food} entity
$\gamma_{\text{no–food}}$	Relations between $\epsilon_{\text{disease}}/\epsilon_{\text{symptom}}$ entity and not recommended ϵ_{food} entity

show that the model combined with our method outperforms previous methods in multiple automatic evaluation metrics. Besides, the *MKA-BERT-GPT* achieves the best performance on the task

The paper will be separated into 5 parts. Section 2 will present the existing works related to medical dialogue generation tasks. Section 3 will explain the details of the proposed mechanism. Section 4 shows the experiment results and the analysis of the results. Section 5 concludes the advantages and disadvantages of our work and its potential future works.

2. Related Works

Recent research on medical chatbots focuses on natural language understanding which leverages different advanced natural language processing (*NLP*) techniques. In general, the medical dialogue methods can be divided into information retrieval-based methods and neural generative methods according to the types of the applied *NLP* techniques. The retrieval-based methods can be further classified into different subtypes, such as the entity inference [12, 13], relation prediction [14, 15], symptom matching and extraction [16, 17], and slot filling [18–20]. However, the retrieval-based methods are not so intelligent and flexible that they required a well-defined user-built question and answer (Q&A) pool, which can offer different potential response to different kinds of answer. In another word, the retrieval-based methods only predict the link between question and answers in the pool, instead of learning how to respond to different questions like the doctors. Therefore, the neural generative methods have drawn more and more attention.

Nowadays, there is merely research on developing neural generative methods on medical domain. As an emerging research direction, most of the existing researches focus on testing different neural generative models on the benchmark domain-specific datasets. To figure out well the generative tasks in *NLP*, Hochreiter and Schmidhuber first proposed long short-term memory (*LSTM)* [21], which inspires multiple *LSTM-based* models [22–24]. Later, with the proposal of *Transformer* [25], researchers start to leverage *Transformer* units into novel dialogue generation models [26, 27]. Then, a more accurate and faster mechanism *GPT* is proposed [28]; different large-scale dialogue generative models are developed based on it [29, 30]. Meanwhile, some of the works also attempt to combine the different units to develop novel methods, where the state-of-the-art model is *BERT-GPT* model [31, 32]. However, the existing generative models for medical domain only learn the experience knowledge from the training procedure; few works effectively integrate the medical knowledge with the generative models.

3. Methodology

In this section, we discuss the methodology of *MKA*, which is a scalable, effective, and lightweight mechanism to integrate the medical knowledge into neural generative models, especially for large-scale pretrained model, such as *BERT-GPT*.

As shown in Figure 1, our *MKA* consists of 3 parts, including the medical knowledge generation module, token processor, and neural generative model. The medical knowledge generation module is constituted by medical knowledge subgraph generator, topic detector, and medical knowledge extractor. It is aimed at generating related medical knowledge information tuple. The token processor is proposed to concatenate the medical knowledge information tuple with the dialogue context for each conversation turn. Besides, the neural generative model is leveraged for training and prediction. The details of each module will be illustrated in Sections 3.1, 3.2, and 3.3.

3.1. Medical Knowledge Generation Module. The medical knowledge generation module is proposed to generate the related medical knowledge information when the doctor handles a case. Within the module, there exist three parts, including medical knowledge subgraph generator, topic detector, and medical knowledge extractor. The medical knowledge subgraph generator first takes the patient self-report which contains the department and disease/symptom information described in Section 1 as input and generates the medical knowledge subgraph (MKG_{sub}) based on a global medical knowledge base (MKG_{base}). MKG_{base} can be treated as a container which contains all the required medical professional books, while MKG_{sub} stores the potential useful medical knowledge related to the specific case. Different questions will be asked in different turns for the multi-turn conversation task. To reduce the redundant information, the topic detector inputs the patient question at i^{th} turn and infers what question topic it related to. With the question topic and MKG_{sub}, the medical knowledge

Algorithm 1: the generation of the medical knowledge subgraph
Input:
Medical knowledge base $\mathrm{MKG}_{\mathrm{base}} = (\mathscr{E}_b, \mathscr{R}_b, \mathscr{G}_b)$.
Patient self-report PSR. (PSR ⟶ Department represents the blank for the patient's ideal clinical department, and PSR ⟶ Disease/Symptom represents the blank for the description of the patient's disease or symptom.)
Output:
Medical knowledge subgraph $\mathrm{MKG}_{\mathrm{sub}} = (\mathscr{E}_s, \mathscr{R}_s, \mathscr{G}_s)$
Main:
1: **if**PSR ⟶ Department exists **then**
2: Extract the Info_1 from PSR ⟶ Department.
3: $\epsilon_1^* = \arg\min_{\epsilon}(\mathrm{dist}(\mathrm{Info}_1, \epsilon))$, where $\epsilon \in \epsilon_{\mathrm{department}}$ and $\epsilon \in \mathscr{E}_b$.
4: $G_1 = (\mathscr{E}_1, \mathscr{R}_1, \mathscr{G}_1)$, where $\forall\{\epsilon_{11}, \epsilon_{12}\} \subset \mathscr{E}_b, \forall\{g_{11}, g_{12}\} \subset \mathscr{G}_b, \gamma_{11} = \gamma_{\mathrm{has-disease}}, \gamma_{12} = \gamma_{has-symptom}, \exists g_{11} = (\epsilon_1^*, \gamma_{11}, \epsilon_{11}) \in \mathscr{G}_1, g_{12} = (\epsilon_{11}, \gamma_{12}, \epsilon_{12}) \in \mathscr{G}_1$.
5: **end if**
6: **if**PSR ⟶ Disease/Symptom exists **then**
7: Extract the Info_2 from PSR ⟶ Department/Symptom
8: $\epsilon_2^* = \arg\min_{\epsilon}(\mathrm{dist}(\mathrm{Info}_1, \epsilon))$, where $\epsilon \in (\epsilon_{disease} \mid \epsilon_{symptom})$ and $\epsilon \in \mathscr{E}_b$.
9: $G_2 = (\mathscr{E}_2, \mathscr{R}_2, \mathscr{G}_2)$, where $\forall\{\epsilon_{21}, \epsilon_{22}, \epsilon_{23}, \epsilon_{24}\} \subset \mathscr{E}_b, \forall\{g_{21}, g_{22}, g_{23}, g_{24}\} \subset \mathscr{G}_b, \gamma_{21} = \gamma_{\mathrm{has-disease}}, \gamma_{22} = \gamma_{\mathrm{has-symptom}}, \forall\gamma_{23} \subset \{\gamma_{\mathrm{need-drug}}, \gamma_{\mathrm{need-check}}, \gamma_{\mathrm{need-food}}, \gamma_{\mathrm{no-food}}\}$, (1) if $\epsilon_2^* \in \epsilon_{\mathrm{disease}}$, $\exists g_{22} = (\epsilon_2^*, \gamma_{22}, \epsilon_{22}) \in \mathscr{G}_2, g_{23} = (\epsilon_2^*, \gamma_{23}, \epsilon_{23}) \in \mathscr{G}_2, g_{24} = (\epsilon_{22}, \gamma_{23}, \epsilon_{24}) \in \mathscr{G}_2$; (2) if $\epsilon_2^* \in \epsilon_{\mathrm{symptom}}$, $\exists g_{21} = (\epsilon_{21}, \gamma_{21}, \epsilon_2^*) \in \mathscr{G}_2, g_{22} = (\epsilon_{21}, \gamma_{22}, \epsilon_{22}) \in \mathscr{G}_2, g_{23} = (\epsilon_{21}, \gamma_{23}, \epsilon_{23}) \in \mathscr{G}_2, g_{24} = (\epsilon_2^*, \gamma_{23}, \epsilon_{24}) \in \mathscr{G}_2$.
10: **end if**
11: $\mathrm{MKG}_{\mathrm{sub}} = (\mathscr{E}_s, \mathscr{R}_s, \mathscr{G}_s) = (\mathscr{E}_1 \cup \mathscr{E}_2, \mathscr{R}_1 \cup \mathscr{R}_2, \mathscr{G}_1 \cup \mathscr{G}_2) = G_1 \cup G_2$

Algorithm 1: Pseudocode of the medical knowledge subgraph generator.

Algorithm 2: the detection of the question topic
Input:
Key phrase set $\mathrm{KPS} = [\mathrm{KPS}_{\mathrm{di}}, \mathrm{KPS}_{\mathrm{s}}, \mathrm{KPS}_{\mathrm{dr}}, \mathrm{KPS}_{\mathrm{c}}, \mathrm{KPS}_{\mathrm{rf}}, \mathrm{KPS}_{\mathrm{nrf}}]$. ($\mathrm{KPS}_{\mathrm{di}}$ is the set for disease topic, $\mathrm{KPS}_{\mathrm{s}}$ is the set for symptom topic, $\mathrm{KPS}_{\mathrm{dr}}$ is the set for drug topic, $\mathrm{KPS}_{\mathrm{c}}$ is the set for check topic, $\mathrm{KPS}_{\mathrm{rf}}$ is the set for the positive food topic, and $\mathrm{KPS}_{\mathrm{nrf}}$ is the set for the negative food topic.)
The patient question in i^{th} conversation turn PQ_i.
Similarity coefficient δ for checking whether the phrase is inside of the patient question
Output:
Question topic tuple in i^{th} conversation turn QT_i
Main:
1: QT_i={}
2: **for**kps in KPS**do**
3: **for**kp in kps**do**
4: **if**(kp in PQ_i) | ($\mathrm{dist}(\mathrm{PQ}_i, \mathrm{kp}) > \delta$)**then**
5: **if**kps = $\mathrm{KPS}_{\mathrm{di}}$**then**
6: Append the "disease" topic in QT_i
7: **else if**kps = $\mathrm{KPS}_{\mathrm{s}}$**then**
8: Append the "symptom" topic in QT_i
9: **else if**kps = $\mathrm{KPS}_{\mathrm{dr}}$**then**
10: Append the "drug" topic in QT_i
11: **else if**kps = $\mathrm{KPS}_{\mathrm{c}}$**then**
12: Append the "check" topic in QT_i
13: **else if**kps = $\mathrm{KPS}_{\mathrm{rf}}$**then**
14: Append the "recommended food" topic in QT_i
15: **else if**kps = $\mathrm{KPS}_{\mathrm{nrf}}$**then**
16: Append the "not recommended food" topic in QT_i
17: **end if**
18: **end for**
19: **end for**

Algorithm 2: Pseudocode of the topic detector.

Algorithm 3: the extraction of medical knowledge information tuple
Input:
Medical knowledge base $\mathrm{MKG}_{\mathrm{sub}} = (\mathscr{E}_s, \mathscr{R}_s, \mathscr{G}_s)$.
Question topic tuple in i^{th} conversation turn QT_i
Corresponding $\epsilon_{\mathrm{department}}$ and $\epsilon_{\mathrm{disease}}/\epsilon_{\mathrm{symptom}}$entities in patient self-report $\epsilon_1^*, \epsilon_2^* \longrightarrow$ Table 3
Output:
Medical knowledge information tuple in i^{th} conversation turn MKI_i
Main:
1: $\mathrm{MKI}_i = \{\epsilon_1^*, \epsilon_2^*\}$
2: **for**qt in QT_i**do**
3: **if**QT_i = "disease"**then**
4: Append all $\epsilon_{\mathrm{disease}}$ entities except ϵ_2^* in $\mathrm{MKG}_{\mathrm{sub}}$ to MKI_i
5: **else if**QT_i = "symptom"**then**
6: Append all $\epsilon_{\mathrm{symptom}}$ entities except ϵ_2^* in $\mathrm{MKG}_{\mathrm{sub}}$ to MKI_i
7: **else if**QT_i = "drug"**then**
8: Append all ϵ_{drug} entities in $\mathrm{MKG}_{\mathrm{sub}}$ to MKI_i
9: **else if**QT_i = "check"**then**
10: Append all $\epsilon_{\mathrm{check}}$ entities in $\mathrm{MKG}_{\mathrm{sub}}$ to MKI_i
11: **else if**QT_i = "recommended food"**then**
12: Append all ϵ_{food} entities connected with $\gamma_{\mathrm{need-food}}$ relation in $\mathrm{MKG}_{\mathrm{sub}}$ to MKI_i
13: **else if** QT_i = "not recommended food"**then**
14: Append all ϵ_{food} entities connected with $\gamma_{\mathrm{no-food}}$ relation in $\mathrm{MKG}_{\mathrm{sub}}$ to MKI_i
15: **end if**
16: **end for**

Algorithm 3: Pseudocode of the medical knowledge extractor.

Table 3: Comparison of the models on MedDialog-CN, where the best results are in bold.

Model	Dialog-GPT	Transformer	BERT-GPT	MKA-Transformer	MKA-BERT-GPT
Perplexity	9.71	9.52	8.23	8.81	**8.04**
BLEU-2	5.21%	4.92%	4.88%	5.02%	**5.71%**
BLEU-4	1.83%	0.90%	0.97%	0.99%	**1.35%**
NIST-2	0.36	0.42	0.40	0.43	**0.44**
NIST-4	0.32	0.40	0.39	0.40	**0.43**
METEOR	12.32%	13.11%	12.83%	13.4%	**13.94%**
Entropy-4	13.73	13.51	13.8	13.72	**14.1**
Dist-1	0.02%	0.03%	0.03%	0.03%	**0.04%**
Dist-2	2.01%	2.02%	2.14%	2.11%	**2.22%**

extractor will extract the related medical knowledge information tuple. The details of each part will be shown as follows.

3.1.1. Medical Knowledge Subgraph Generator. Within the medical knowledge subgraph generator, the medical knowledge subbase can be generated from the medical knowledge base based on the medical-related information extracted from patient self-report. In this paper, the knowledge base is represented the knowledge graph (KG), which is constituted by entities and relations. Besides, it is formally defined as below:

$$\mathrm{KG} = (\mathscr{E}, \mathscr{R}, \mathscr{G} = \mathscr{E} \times \mathscr{R} \times \mathscr{E}), \quad (1)$$

where $\mathscr{E}$ represents the set of entities (e.g., persons), $\mathscr{R}$ represents the considered types of relations between entities (e.g., friendship between persons), and $\mathscr{G}$ is a set of 3-element fact tuples where each tuple represents a factual relation between two entities.

Therefore, two kinds of the medical knowledge graph (MKG) are proposed, including the medical knowledge base ($\mathrm{MKG}_{\mathrm{base}}$) generated based on [33] by removing the redundant information and medical knowledge subgraph ($\mathrm{MKG}_{\mathrm{sub}}$). Both $\mathrm{MKG}_{\mathrm{base}}$ and $\mathrm{MKG}_{\mathrm{sub}}$ contain 6 types of entities and 6 types of relations as shown in Tables 1 and 2. The entity and relation types are decided based on the working experiences of the author for the common medical conversation topics.

Table 4: Comparison of the models on MedDG, where the best results are in bold.

Model	Dialog-GPT	Transformer	BERT-GPT	MKA-Transformer	MKA-BERT-GPT
Perplexity	8.53	8.52	5.98	8.41	**5.95**
BLEU-2	6.41%	6.30%	7.62%	6.62%	**8.09%**
BLEU-4	2.12%	2.08%	2.57%	2.40%	**2.87%**
NIST-2	0.38	0.37	0.42	0.39	**0.43**
NIST-4	0.35	0.35	0.39	0.38	**0.41**
METEOR	13.78%	14.32%	16.25%	14.88%	**16.63%**
Entropy-4	10.56	10.17	**13.38**	10.28	13.37
Dist-1	0.01%	0.01%	**0.02%**	0.01%	**0.02%**
Dist-2	1.72%	1.67%	**2.00%**	1.69%	**2.00%**

Table 5: Improvements of the models with MKA compared to the baseline model on MedDialog-CN and MedDG test sets.

Dataset	Model	Perplexity	BLEU-2,4	NIST-2,4	METEOR	Entropy-4	Dist-1,2
MedDialog-CN	MKA-Transformer	-0.71	0.10%, 0.09%	0.01, 0	0.29%	0.21	0.00%, 0.09%
	MKA-BERT-GPT	-0.19	0.83%, 0.38%	0.04, 0.04	1.11%	0.3	0.01%, 0.08%
MedDG	MKA-Transformer	-0.11	0.32%, 0.32%	0.02, 0.03	0.56%	0.11	0.00%, 0.02%
	MKA-BERT-GPT	-0.03	0.47%, 0.30%	0.01, 0.02	0.38%	-0.01	0.00%, 0.00%

According to the definition of the entity and relation types, $\mathrm{MKG}_{\mathrm{base}}$ contains 26910 entities (i.e., 54 $\epsilon_{\mathrm{department}}$, 8807 $\epsilon_{\mathrm{disease}}$, 5998 $\epsilon_{\mathrm{symptom}}$, 4870 ϵ_{food}, 3353 $\epsilon_{\mathrm{check}}$, and 3828 ϵ_{drug}) and 158216 fact tuples regarding the different relations (i.e., 8844 $\gamma_{\mathrm{has-disease}}$, 5998 $\gamma_{\mathrm{has-symptom}}$, 59467 $\gamma_{\mathrm{need-drug}}$, 39422 $\gamma_{\mathrm{need-check}}$, 22238 $\gamma_{\mathrm{need-food}}$, and 22247 $\gamma_{\mathrm{no-food}}$).

As for $\mathrm{MKG}_{\mathrm{sub}}$, it is specific for each case, which is generated based on Algorithm 1. Within the algorithm, two subgraphs, G_1 and G_2, are extracted from $\mathrm{MKG}_{\mathrm{base}}$ to constitute $\mathrm{MKG}_{\mathrm{sub}}$. G_1 is the graph with the $\epsilon_{\mathrm{department}}$ type entity ϵ_1^* as the root. Besides, it only contains $\gamma_{\mathrm{has-disease}}$ and $\gamma_{\mathrm{has-symptom}}$ two types of relations. G_2 is the graph with the $\epsilon_{disease}$/ $\epsilon_{symptom}$ type entity ϵ_2^* as the root. Besides, it may contain all kinds of types of relations except $\gamma_{\mathrm{has-disease}}$. For more details, see Algorithm 1.

Meanwhile, it is worth noting that we propose a way to calculate the distance for entity matching as shown in

$$\mathrm{dist}(u, v) = [\alpha\ \beta] \times \begin{bmatrix} \mathrm{dist}_{\mathrm{Levenshtein}}(u, v) \\ \mathrm{dist}_{\mathrm{Hamming}}(u, v) \end{bmatrix}, \tag{2}$$

where α and β are two hyperparameters. The distance takes advantage of both the Hamming distance [34] and Levenshtein distance [35]. It can not only care about the meaning of the tokens like the Hamming distance but also the position of the tokens like Levenshtein distance.

3.1.2. Topic Detector. The medical knowledge is related to what medical topic the patient asks. As a preparation for medical knowledge extractor, the question topic should be determined first. The content in the topic set matches with the relation set (i.e., disease, symptom, drug, check, positive food, and negative food). Besides, the six key phrase sets (KPS) are built corresponding to six topics based on the users' experiences. It consists of some specific phrases related to the question topic. Based on it, the question detector is proposed as shown in Algorithm 2.

3.1.3. Medical Knowledge Extractor. The medical knowledge extractor is aimed at extracting the related medical knowledge information tuples based on question topic and medical knowledge subgraph from the previous two parts. It extracts all entities with the specific entity type and connected with specific relation type in the subgraph. Besides, $\epsilon_1^*, \epsilon_2^*$ extracted from patient self-report will be directly appended into the tuple, since they are also useful medical knowledge extracted from the source. The details are shown in Algorithm 3.

3.2. Token Processor. Compared to general neural generative models just taking dialogue contexts as inputs, our model generates the related medical knowledge information tuple which will be also fed into the models. To achieve this goal, a token processor is proposed to reorganize the tokens based on the policy shown in

$$\begin{aligned} X &= \mathrm{MKI}_i \oplus \mathrm{DR}_{i-1} \oplus \mathrm{PQ}_i = [\mathrm{MKG}_{\mathrm{sub}}\ \mathrm{Unseen\ Features}] \\ &\quad \oplus [\mathrm{PSR\ Seen\ Features}] \oplus \mathrm{DR}_{i-1} \oplus \mathrm{PQ}_i \\ &= [\mathrm{All\ the\ elements\ in\ MKI}_i \text{ except } \varepsilon_1^* \text{ and } \varepsilon_2^*] \oplus [\varepsilon_1^* \oplus \varepsilon_2^*] \\ &\quad \oplus \mathrm{DR}_{i-1} \oplus \mathrm{PQ}_i, \end{aligned} \tag{3}$$

where X represents the sequence for neural generative models and PSR represents patient self-report. MKI_i, DR_{i-1}, and PQ_i

Table 6: An example of generated responses on the MedDialog-CN test set.

Patient self-report		科室 department: 男科 andrology 疾病/症状 disease/symptom: 静索静脉曲张 varicose veins
Patient question 1		我很怕是高位结扎手术引起的附睾炎, 希望大夫能给我说说是怎么回事, 该怎么处理? I am very afraid that it is the epididymitis associated with the high ligation operation. I hope the doctor can tell me how to deal with it quickly.
Doctor response 1	Ground truth	中医药调理。 You can recuperate yourself with Chinese medicine.
	Dialog-GPT	手术部位不会引发附睾炎。 The surgical part does not cause epididymitis.
	Transformer	可能是近期没有充分休息, 免疫力下降。建议早点休息。 It may be that you do not have enough rest and cause the decrease on the immunity. It is recommended to sleep early.
	BERT-GPT	不要趴着睡觉, 影响伤口恢复。建议多休息。 Do not sleep on your stomach, which will affect the recovery of the wound. It is recommended to rest more.
	MKA-Transformer	可以吃营养的健康食品, 比如西兰花, 鸡蛋等, 同时注重卫生清洁, 每晚可以热敷缓解疼痛。 You can eat nutritious and healthy foods, such as broccoli and eggs; meanwhile, pay attention to your hygiene and cleanliness. You can heat the area around your wound every night to relieve yourself.
	MKA-BERT-GPT	不可以吃冷饮, 少吃辛辣刺激的食物, 影响伤口恢复。建议多吃蔬果类, 比如苹果。不要久坐不动, 少穿紧身裤。 Do not drink cold drinks, and eat less spicy food, which will affect the recovery of the wound. It is recommended to eat more fruits and vegetables, such as apples. Do not sit for a long time and do not wear tight pants.
Patient question 2		请问我这是附睾炎吗?或是什么?恳请大夫您为我指点!感谢。 Is this epididymitis? Or what? I hope you, the doctor, to give me some advice! Thanks!
Doctor response 2	Ground truth	局部气血不畅。 The flow of the blood and qi in the local area is not that smooth.
	Dialog-GPT	放宽心, 只是心理作用。 Relax, it is just a psychological effect.
	Transformer	只是术后伤口疼痛。 It is just that the wound is painful after the operation.
	BERT-GPT	常见血流不通问题。 It is the common problem about the blood.
	MKA-Transformer	可能是运动过量导致提睾肌过度收缩, 导致疼痛。 Excessive exercise may cause excessive contraction of the cremaster muscle. It will make you feel painful.
	MKA-BERT-GPT	血流不通, 建议过几天复查伤口恢复情况, 减轻心理负担。 The blood flow is not smooth. It is recommended to review the situation of the recovery of the wound after a few days. Besides, you need to reduce the psychological burden.

represent the medical knowledge information tuple in i^{th} conversation turn, the doctor response in $i-1^{\text{th}}$ conversation turn, and the patient question in i^{th} conversation turn separately. Besides, ϵ_1^* and ϵ_2^* are corresponding $\epsilon_{\text{department}}$ and $\epsilon_{\text{disease}}/\epsilon_{\text{symptom}}$ entities generated in Algorithm 1.

3.3. Neural Generative Model. In this paper, the neural generative model takes a source sequence $X = (x_1, x_2, x_3, \cdots, x_T)$ consisting of T tokens generated from Section 3.2 and generates the response $Y = (y_1, y_2, y_3, \cdots, y_{T'})$ of length T' tokens. In general, the model maximizes the generation probability of Y conditioned on X : $p(y_1, y_2, y_3, \cdots, y_{T'} \mid x_1, x_2, x_3, \cdots, x_T)$ [8], and the objective function of the sequence-to-sequence generative models is defined as below. Besides, as for the multiturn conversation tasks, the doctor response at i^{th} turn will be fed into the model as the existing dialogue context for next turn.

$$p\left(y_1, \cdots, y_T{}' \mid x_1, \cdots, x_T\right) = p(y_1 \mid x_1, \cdots, x_T) \cdot \prod_{t=2}^{T'} p(y_t \mid x_1, \cdots, x_T, y_1, \cdots, y_{t-1}). \tag{4}$$

4. Experiments

4.1. Experiment Settings. Our approach is implemented in Python 3.7 and PyTorch 1.4.0. We implement two MKA-Diagen models, including MKA-Transformer and MKA-

Table 7: An example of generated responses on the MedDG test set.

Patient self-report		科室 department: 肛肠科 anorectal branch 疾病/症状 disease/symptom: 便秘,便血 constipation, blood in the stool
Patient question 1		医生你好, 最近我大便总是很干燥, 而且有好几次大便之后, 发现有血, 我这个是什么情况? Hello, doctor. Recently, I have found my stools were very dry. Besides, there is blood inside of them if I poop for several times. What is wrong with me?
Doctor response 1	Ground truth	你好, 可能存在痔疮出血!但还是建议您做个肠镜! Hello, there may be bleeding from hemorrhoids! But it is still recommended that you have a colonoscopy!
	Dialog-GPT	你好, 这种情况容易出现内痔 Hello, this situation is prone to internal hemorrhoids.
	Transformer	你好, 考虑是痔疮。 Hello, it is considered as hemorrhoids.
	BERT-GPT	你好, 可能存在痔疮, 大便干结多久了? Hello, there may be hemorrhoids, and how long have the stools been dry and clumpy?
	MKA-Transformer	你好, 可能是痔疮, 建议您做个肠镜。 Hello, it may be hemorrhoids. It is recommended that you have a colonoscopy.
	MKA-BERT-GPT	你好, 可能是痔疮出血。此外, 建议您做个肠镜。 Hello, it may be bleeding from hemorrhoids. In addition, it is recommended that you have a colonoscopy.
Patient question 2		为什么我的大便是一粒一粒的, 很干燥, 像羊屎那样的? Why do my stools come in pieces, very dry, like sheep feces?
Doctor response 2	Ground truth	大便干结是功能性问题, 建议您多吃水果蔬菜, 养成排便习惯! The dry stool is a functional problem. It is recommended that you eat more fruits and vegetables to develop a bowel habit!
	Dialog-GPT	你好, 可能存在痔疮。 Hello, there may be hemorrhoids.
	Transformer	注意饮食, 多吃蔬菜水果。 Pay attention to your diet and eat more fruits and vegetables.
	BERT-GPT	建议您多吃蔬菜水果。 It is recommended that you eat more fruits and vegetables.
	MKA-Transformer	考虑是肠胃功能性紊乱, 建议您多吃水果蔬菜。 It is considered as a gastrointestinal dysfunction. It is recommended that you eat more fruits and vegetables, like apples.
	MKA-BERT-GPT	考虑是肠胃功能问题, 建议您多吃水果蔬菜, 比如梨, 香蕉。若还是这样的话建议您做个肠镜。 It is considered as the gastrointestinal functional problem. It is recommended that you eat more fruits and vegetables, such as pears and bananas. If this is still the case, it is recommended that you have a colonoscopy.

BERT-GPT. The neural generative models within them are trained with the default parameters in [11, 25]. The hyperparameters α and β in Equation (2) are set as 0.1 and -1, and the hyperparameter δ is set as 0.7. We perform all the experiments on the Matpool server with 11 GB NVIDIA GeForce RTX 2080 Ti. Our experiments were performed on Chinese MedDialog dataset [11] and MedDG [12] with the ratio 0.8 : 0.1 : 0.1 of training set : validation set : test set.

The MKA-Transformer and MKA-BERT-GPT were compared with the baseline models (i.e., Transformer and BERT-GPT) and another typical nonsequence to sequence GPT-based model [11]. We followed the automatic evaluation metrics on the datasets to evaluate the performance of our method, including perplexity, NIST-2,4 [36], BLEU-2,4 [37], METEOR [38], Entropy-4 [39], and Dist-1,2 [40]. The perplexity shows the language quality of the generated responses. NIST-n, BLEU-n, and METEOR measure the similarity between the generated responses and ground truth and Entropy-n and Dist-n measure the lexical diversity of generated responses based on n-gram matching. The model with better performance will have the lower value of perplexity, the higher value of the other metrics.

4.2. Experiment Results and Analysis. In this part, the experiment results are shown together with the in-depth analysis of the results. Tables 3 and 4 show the performance on the MedDialog-CN test set and MedDG test set separately. From the tables, we make the following observations.

4.2.1. Ablation Analysis. Focusing on the comparison between MKA-Transformer and Transformer and the performance comparison between MKA-BERT-GPT and BERT-GPT, it is easy to extract Table 5. It is easy to observe that our mechanism improves the performance from all aspects on both two datasets. It means that our method is

effective and scalable to be applied to different neural generative models and different datasets.

4.2.2. Performance Comparison Analysis. Compared to the current state-of-the-art models, our MKA-BERT-GPT outperforms all the other methods. It achieves the lowest perplexity. It is because its baseline generative model, BERT-GPT, is pretrained on a large collection of corpora before training on the medical specific datasets. The pertaining procedure helps it to better understand the linguistic structure among words; meanwhile, the medical knowledge-assisted mechanism enables the model more learnable for medical conversation task. Meanwhile, as for the machine translation metrics (i.e., NIST-4, BLEU-2, BLEU-4, and METEOR), the performance of the MKA-BERT-GPT also is the best. It even overturns the performance comparison between BERT-GPT and Transformer. It indicates that our method highly improves the overlap between the generated response and the ground truth. Besides, although the MKA-BERT-GPT improves the value on diversity metrics (i.e., Entropy and Dist), the improvement is still minor. It indicates that our model cannot make a big breakthrough on the capability in generating diverse responses.

4.2.3. Case Study Analysis. Tables 6 and 7 represent the generated response of the models on two examples in the MedDialog-CN and MedDG test set. Since the dataset contains some Chinese medical dialogues, the translation is provided as well as the raw contents. The response generated by *MKA-BERT-GPT* is clinically informative and accurate. It prescribes "gastrointestinal functional problem." Meanwhile, it can offer the detailed suggestions with rich medical knowledge information such as what kind of vegetables and fruits is recommended. Besides, the language quality of all the models is great, since all the responses are readable. Besides, there are still some spaces for the further improvement. For example, the responses generated from the models are not that overlap with the ground truth. It is because the ground truth is a Chinese medical response, which contains the concept of "qi," which is not that easy for a general model to understand and provide the response. However, the responses of *MKA-BERT-GPT* are still relatively reasonable and also mention the conclusion of "the blood flow is not smooth."

5. Conclusions

In this paper, we propose a scalable medical knowledge-assisted mechanism (*MKA*) to assist general neural generative models, especially the large-scale pretrained model, such as BERT-GPT, to achieve better performance on the medical conversation task. The mechanism introduces a medical specific knowledge graph, which contains 6 types of medical-related information, including department, drug, check, symptom, disease, and food. Besides, it also leverages the specific designed token concatenation policy and neural generative models. The promising experiment results have proven our mechanism is effective and scalable to different generative models on different medical conversation datasets. Besides, it also shows that *MKA-BERT-GPT* has achieved the state-of-the-art performance based on multiple automatic evaluation metrics compared to other existing models. In the future, we plan to apply the graph neural networks to extract and predict the related medical knowledge based on the medical knowledge base. Besides, it is also worthwhile to carry out the research on leveraging the advantages of both information retrieve methods and the neural generative methods to build a powerful dialogue generation system.

Data Availability

The data used to support the findings of this study are included in the article.

Conflicts of Interest

The authors declare that they have no competing interest.

References

[1] A. Khan, M. Z. Asghar, H. Ahmad, F. M. Kundi, and S. Ismail, "A rule-based sentiment classification framework for health reviews on mobile social media," *Journal of Medical Imaging and Health Informatics*, vol. 7, no. 6, pp. 1445–1453, 2017.

[2] N. Deepa, B. Prabadevi, P. K. Maddikunta et al., "An AI-based intelligent system for healthcare analysis using Ridge-Adaline Stochastic Gradient Descent Classifier," *The Journal of Supercomputing*, vol. 77, no. 2, pp. 1998–2017, 2021.

[3] A. R. Javed, M. U. Sarwar, M. O. Beg, M. Asim, T. Baker, and H. Tawfik, "A collaborative healthcare framework for shared healthcare plan with ambient intelligence," *Human-centric Computing and Information Sciences*, vol. 10, no. 1, pp. 1–21, 2020.

[4] M. Z. Asghar, A. Khan, K. Khan, H. Ahmad, and I. A. Khan, "COGEMO: Cognitive-Based Emotion Detection from patient generated health reviews," *Journal of Medical Imaging and Health Informatics*, vol. 7, no. 6, pp. 1436–1444, 2017.

[5] C. Dhanamjayulu, U. N. Nizhal, P. K. R. Maddikunta et al., "Identification of malnutrition and prediction of BMI from facial images using real-time image processing and machine learning," *IET Image Processing*, 2021.

[6] D. Lee and S. N. Yoon, "Application of artificial intelligence-based technologies in the healthcare industry: opportunities and challenges," *International Journal of Environmental Research and Public Health*, vol. 18, no. 1, p. 271, 2021.

[7] A. Palanica, P. Flaschner, A. Thommandram, M. Li, and Y. Fossat, "Physicians' perceptions of chatbots in health care: cross-sectional web-based survey," *Journal of Medical Internet Research*, vol. 21, no. 4, article e12887, 2019.

[8] F. A. Habib, G. S. Shakil, S. S. Iqbal, S. Mohd, and S. T. Abdul, Eds., "Survey on medical self-diagnosis chatbot for accurate analysis using artificial intelligence," in *Proceedings of Second International Conference on Smart Energy and Communication*, pp. 587–593, Singapore, 2021.

[9] A. Mohiyuddin, A. R. Javed, C. Chakraborty, M. Rizwan, M. Shabbir, and J. Nebhen, "Secure cloud storage for medical IoT data using adaptive neuro-fuzzy inference system," *International Journal of Fuzzy Systems*, no. article 5352108, pp. 1–13, 2021.

Hindawi
Computational and Mathematical Methods in Medicine
Volume 2023, Article ID 9845962, 1 page
https://doi.org/10.1155/2023/9845962

Retraction

Retracted: An Improved Brain MRI Classification Methodology Based on Statistical Features and Machine Learning Algorithms

Computational and Mathematical Methods in Medicine

Received 27 June 2023; Accepted 27 June 2023; Published 28 June 2023

This article has been retracted by Hindawi following an investigation undertaken by the publisher [1]. This investigation has uncovered evidence of one or more of the following indicators of systematic manipulation of the publication process:

(1) Discrepancies in scope

(2) Discrepancies in the description of the research reported

(3) Discrepancies between the availability of data and the research described

(4) Inappropriate citations

(5) Incoherent, meaningless and/or irrelevant content included in the article

(6) Peer-review manipulation

The presence of these indicators undermines our confidence in the integrity of the article's content and we cannot, therefore, vouch for its reliability. Please note that this notice is intended solely to alert readers that the content of this article is unreliable. We have not investigated whether authors were aware of or involved in the systematic manipulation of the publication process.

Wiley and Hindawi regrets that the usual quality checks did not identify these issues before publication and have since put additional measures in place to safeguard research integrity.

We wish to credit our own Research Integrity and Research Publishing teams and anonymous and named external researchers and research integrity experts for contributing to this investigation.

The corresponding author, as the representative of all authors, has been given the opportunity to register their agreement or disagreement to this retraction. We have kept a record of any response received.

References

[1] M. Fayaz, M. S. Qureshi, K. Kussainova, B. Burkanova, A. Aljarbouh, and M. B. Qureshi, "An Improved Brain MRI Classification Methodology Based on Statistical Features and Machine Learning Algorithms," *Computational and Mathematical Methods in Medicine*, vol. 2021, Article ID 8608305, 14 pages, 2021.

Hindawi
Computational and Mathematical Methods in Medicine
Volume 2021, Article ID 8608305, 14 pages
https://doi.org/10.1155/2021/8608305

Research Article

An Improved Brain MRI Classification Methodology Based on Statistical Features and Machine Learning Algorithms

Muhammad Fayaz,[1] **Muhammad Shuaib Qureshi**,[1] **Karlygash Kussainova**,[1] **Bermet Burkanova**,[1] **Ayman Aljarbouh**,[1] **and Muhammad Bilal Qureshi**[2]

[1]*Department of Computer Science, University of Central Asia, Naryn 722918, Kyrgyzstan*
[2]*Department of Computer Science and IT, University of Lakki Marwat, Lakki Marwat 28420, KPK, Pakistan*

Correspondence should be addressed to Muhammad Shuaib Qureshi; muhammad.qureshi@ucentralasia.org

Received 20 October 2021; Accepted 19 November 2021; Published 7 December 2021

Academic Editor: Muhammad Zubair Asghar

In this paper, we have proposed a novel methodology based on statistical features and different machine learning algorithms. The proposed model can be divided into three main stages, namely, preprocessing, feature extraction, and classification. In the preprocessing stage, the median filter has been used in order to remove salt-and-pepper noise because MRI images are normally affected by this type of noise, the grayscale images are also converted to RGB images in this stage. In the preprocessing stage, the histogram equalization has also been used to enhance the quality of each RGB channel. In the feature extraction stage, the three channels, namely, red, green, and blue, are extracted from the RGB images and statistical measures, namely, mean, variance, skewness, kurtosis, entropy, energy, contrast, homogeneity, and correlation, are calculated for each channel; hence, a total of 27 features, 9 for each channel, are extracted from an RGB image. After the feature extraction stage, different machine learning algorithms, such as artificial neural network, *k*-nearest neighbors' algorithm, decision tree, and Naïve Bayes classifiers, have been applied in the classification stage on the features extracted in the feature extraction stage. We recorded the results with all these algorithms and found that the decision tree results are better as compared to the other classification algorithms which are applied on these features. Hence, we have considered decision tree for further processing. We have also compared the results of the proposed method with some well-known algorithms in terms of simplicity and accuracy; it was noted that the proposed method outshines the existing methods.

1. Introduction

The human brain is one of the unsolved mysteries of science. Its complexity has perplexed and vexed scientists till today. It contains over 85 ± 8 billion neurons with an equal number of nonneuronal cells. Brian controls and coordinates our body movements, homeostasis–body temperature, heart rate, blood pressure, and fluid balance. It is responsible for our emotions, fight or flight mood, memory, cognition, motor learning, and learning, remembering, and communicating processes [1]. The brain is a network of nerve cells that grow, build new synapsis, and die continuously, but the abnormal and uncontrolled growth of nerve cells leads to the formation of tumors. Brain tumors can be also caused by abnormal activity of other body parts like the lungs, breast, and skin [2]. Brain tumor is one of the most fatal causes of cancer-related deaths in the world. According to the most recent report by the Central Brain Tumor Registry of the United States, there were 81,246 deaths attributed to primary malignant brain and other central nervous system (CNS) tumors for the period of 2013-2017. On average, there are 16,249 deaths per year, and the survival rate after diagnosis of a primary malignant brain and other CNS was 36%, lowest in 40+ age groups (90.2%), while in age group 0-14 years, survival rates were 97.3% [3].

Classification of normal and abnormal brain images obtained from MRI is the first step towards tackling the staggering deaths caused by brain tumors. However, the large amount of data from MRI makes their manual classification tedious, error-prone, and time-consuming and requires an

expert. The observer faces a great difficulty in analyzing and interpreting the images and detecting the tumor [4]. Hence, it is necessary to develop and implement an automatic image analyzing system. It should be faster and accurate in its inferences of the MRI images, and it should be easy to use. Research has been done in this area and in literature; we have a wide variety of automatic and accurate medical diagnostic techniques introduced by applying complex signal/image processing methods which use the computational intelligent techniques of machine learning algorithms. MRI image processing methods are categorized into two types. One is supervised classification, which exploits the algorithms like artificial neural network (ANN), k-nearest neighbor (kNN), and support vector machine (SVM). The other is unsupervised classification where methods of Self-Organization Map (SOM) and fuzzy c-means are employed. The supervised classification gives more accurate results as compared to unsupervised classification methods [5]. These techniques help doctors with diagnosis during presurgical and postsurgical procedures [4].

The information from MRI images can be analyzed and processed using supervised or unsupervised algorithms and can be categorized into normal or abnormal classes. But the accuracy of the categorization depends on how we extract the features from the images and how relevant the features are to determine the disorder. Some widely used methods include the Fourier transform-based techniques, independent component analysis (ICA), wavelet transform-based techniques [6, 7], and statistical feature extraction methods like kurtosis, skewness, quartiles, mode, median, mean, and standard deviation [8]. It is important to extract the meaningful features, but it also increases the computational burden of the classifier, so to balance the drawbacks, the best option is to choose a feature extraction method, which can determine the fewer most relevant features as possible to get the complete characteristic anatomy of the tumor hence, reducing the extra computational complications for unnecessary feature extraction. Keeping the constraints under view, one of the suitable methods is wavelet transform, which is a nonstatistical method. It provides the local frequency information and detailed coefficients of the image at various levels. Employing principal component analysis (PCA) with wavelet transform reduces the dimensions and overcomes the computational complexity [9]. Moreover, wavelet transform is good for getting frequency space information from nonstationary images; it is also amenable to computer-based analysis—the analysis can be monitored and controlled by changing the wavelets in the selected sequence [5]. In our work, we applied the methodology as image processing, feature extraction, feature reduction, and finally classification of the brain tumor.

As more useful, the feature extraction is, similarly, the challenging task it gets. Several studies have used different methods for feature extraction. For instance, Gabor feature, discrete wavelet transform, spectral mixture analysis, texture feature, principal component analysis, minimum noise fraction transform. By dimensionality reduction, we can have our focus on only few key features. The widely implemented algorithms for feature reduction are independent component analysis, principal component analysis, linear discriminant analysis, and genetic algorithms [4].

After features extraction stage, classification of the images is done. In classification stage—classification of the images into normal/abnormal or tumor/not tumor classes. The classifier takes the purified images with selected features for training and testing. Various classifiers—each having pros and cons—have been used as discussed above like k-nearest neighbor (kNN), support vector machine (SVM), artificial neural network (ANN), Hidden Markov Model (HMM), and the Probabilistic Neural Network (PNN). The common application of these algorithms can be found in handwritten digit identification, text classification, face identification, object detection and recognition, and speaker identification for medical purposes [4]. Classification has two parts—training and testing. Firstly, for training, the already labeled and known data is given to the algorithm. The algorithm gets trained on these data and builds the model to predict/classify the unknown data. Secondly, the test data which is the unknown data is given to the classifier algorithm after training has been done. After this part, the performance of the algorithm is evaluated. The error in classification or the precision of the classifier depends on the efficient training. Usually, more training data helps the classifier to get tuned and build a more feasible or general model. As analyzing human MR images of the brain manually is slow, expensive, labor-intense, and error-prone, we are proposing the accurate, automatic analyzing, and robust classification of human MR images of the brain.

Many researchers have proposed different types of approaches for brain MRI classification. A study by Chaplot et al. [6] compared the self-organizing maps and support vector machine for the classification of MR images of brain tumor into normal and abnormal. Using wavelets as inputs to neural network SOM and SVM, they concluded that SVM has a better classification rate (98%) than SOM (94%). Feature extraction was done using a two-dimensional discrete wavelet transform and Daubechies filters were used for the decomposition. Maitra and Chatterjee [10] used a unique and improved version of an orthogonal discrete wavelet transform for feature extraction—the Slantlet transform; this transform gave an improved time localized space information for nonstationary MRI images. Applying an improved feature extraction method provided a better feature vector to be used for the training of the backpropagation neural network-based binary classifier they employed—it classified normal brain images and images of patients with Alzheimer with 100% accuracy. El-Dahshan et al. [11] introduced a hybrid technique with three stages—feature extraction, dimensionality reduction, and classification—to classify MRI brain tumor images. Discrete wavelet transformation (DWT) was used in the feature extraction stage; principal component analysis (PCA) was used in dimensionality reduction stage to focus on more essential features of MRI images. Then, two classifiers, namely, feed-forward back-propagation artificial neural network (FA-ANN) and kNN, have applied for the classification of the subject MRI images into normal and abnormal images. The results for FA-ANN were 97% accurate while for kNN, the accuracy was

calculated to 98%. Furthermore, Zhang et al. [12] also proposed a three-stage classification of brain images. Zhang et al. followed the same methods as El-Dahshan, but they used the Scaled Conjugate Gradient (SCG) in Backpropagation Neural Networks to get the optimal weights. The accuracies for training and testing images were 100% (66 images), while the computational time for each image was only 0.0451 s. A similar approach was adopted by Fayaz et al. [13] with the preprocessing stage, feature extraction stage, and finally classification stage. Using median filter, the noise from MRI grayscale images was removed in the preprocessing stage and converted into RGB colored images. During feature extraction stage, the red, green, and blue channels were extracted from RGB images; for each channel, the mean, variance, and skewness are also calculated. Then, using kNN, the final classification was carried out. An accuracy of 98% training and 95% test data was obtained for normal images while 100% training and 90% test accuracy for abnormal images was obtained.

Different methodologies have been proposed by different authors for classification in different areas, such as Alotaibi et al. [14] who proposed a hybrid method based on convolutional neural network (CNN) and long short-term memory (LSTM) recurrent neural network for classification of text into psychopath or nonpsychopath classes. The results indicate that this method provides good results. Similarly, another method has been proposed by Hussain et al. [15] for depression classification in social media by using deep learning method.

In this paper, a novel method based on machine learning algorithms and statistical features has been proposed. The main aim of this paper is twofold, first to reduce the computation time and second to increase the accuracy for brain MRI classification. The main contributions of this paper are below:

(i) The grayscale images are converted to RGB images, and red, green, and blue channels are then extracted from RGB images. The histogram equalization has been applied on each channel of RGB images in order to enhance the quality of these channels

(ii) A novel method has been proposed to extract statistical features, namely, mean, variance, skewness, kurtosis, entropy, energy, contrast, homogeneity, and correlation from red, green, and blue channels of RGB images and concatenated to feed to the machine learning algorithms to classify the brain MRI images into normal and abnormal

(iii) In the proposed method, we have applied different classification algorithms, such as k-nearest neighbor, decision tree, random forest, and Naïve Bayes to select an algorithm with the highest accuracy on the extracted features

The structure of the remaining paper is organized as follows: in Section 2, the proposed methodology is explained in detail; Section 3 is about implementation, results, and discussion. The conclusion is given in the last stage.

2. Proposed Methodology

In this work, we have proposed a novel method for brain MRI classification. The proposed model consists of four stages, namely, preprocessing, feature extraction, classification, and performance evaluation. The conceptual model of the proposed model is depicted in Figure 1.

The detailed schematic diagram of the proposed methodology is shown in Figure 2. In the preprocessing stage of the proposed model, the median filter has been used to remove salt-and-pepper noise from MRI images. Usually, the MRI images are affected by salt-and-pepper noise and median filter is the most common filter used for removing such type of noise from MRI images [13, 16].

In the preprocessing stage, the original grayscale brain images have been converted to RGB images, and red, green, and blue channels are extracted from the RGB images. The next operation that is deployed on the images in the preprocessing module is histogram equalization. The histogram equalization is applied on each channel of the RGB images to improve the quality of these images and make them able to be used for further processing. In next feature extraction module of the proposed model, the statistical features have been calculated for red, green, and blue channels with the purpose to handle the curse of dimensionality.

These features are stored and combined in a file and labeled to train the machine learning algorithms. In the classification module, we have applied different machine learning algorithms, such as artificial neural network, k-nearest neighbor algorithm, naïve Bayes classifier, random forest, and decision tree classifier for classification, and the extracted features are given as inputs to these classifiers. In the classification module, we have used the percentage split method to divide the data into training and testing. In the performance evaluation module first, we have the classification algorithms by using different metrics, such as precession, recall, and F_1-score.

2.1. Preprocessing. There are three stages that make up the proposed methodology: preprocessing, feature extraction, and classification and performance evaluation as illustrated in Figure 2. Each stage consists of several steps, where preprocessing includes noise removal, grayscale to RGB conversion, and histogram equalization.

In the preprocessing stage, the images from a dataset of 140 samples are first issued for noise removal. Different types of noises exist in different image modalities, such as spackle noise, Gaussian noise, and salt-and-pepper noise. To remove these noises from images, different types of filters are used, such as Wiener filter, mean filter, and median filter. The MRI images are normally affected by salt-and-pepper noise, and the most effective and commonly used filter for this type of noise is median filter [16, 17].

A median filter can sharpen the images without disturbing the edges. In the proposed work, we have used the median with a window size 3×3 to remove salt-and-pepper noise from the images and smooth the images. Consequently, the grayscale images are converted to RGB for further processing, as illustrated in Figure 3. The necessity

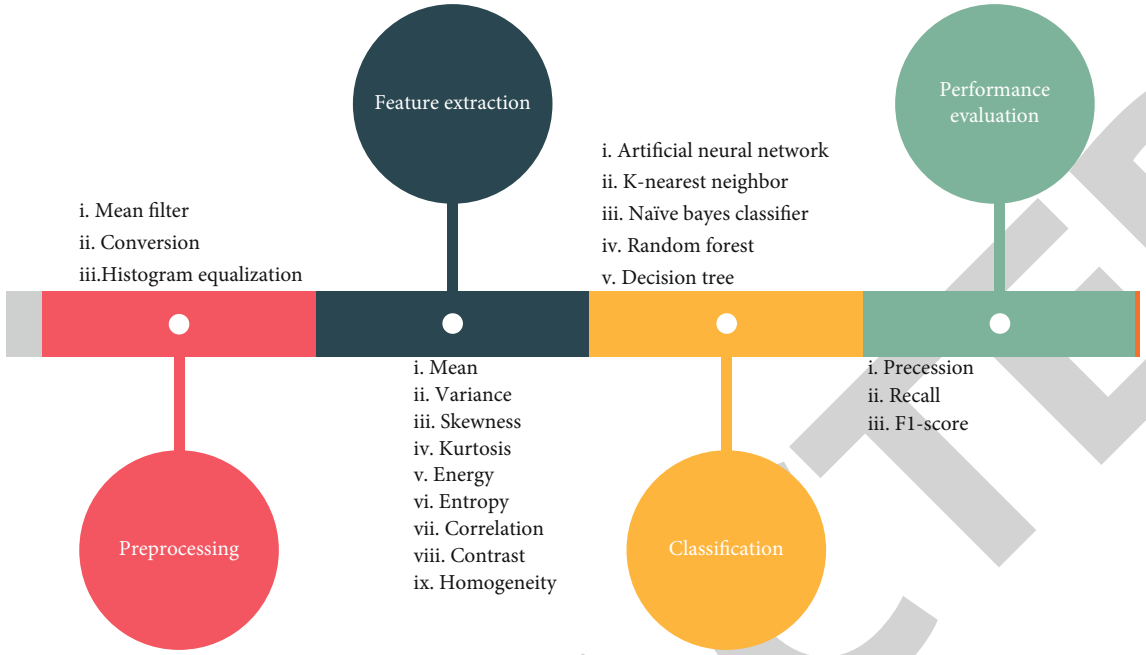

Figure 1: Abstract diagram of the proposed model.

of conversion of the grayscale image into a color image is in its detailed representation of pixels. After converting the grayscale image into RGB, it is possible to represent it in red, blue, and green channels. This allows us to extract features from different points of view and then see a more detailed analysis of the anomalies in the brain. Figure 4 illustrates the way a simple RGB image is converted into three channels (red, green, and blue).

In the proposed work, we have also used histogram equalization, which is the last step in the preprocessing stage, where it is used as a technique to adjust the image intensity for contrast enhancement [18]. In this work, we have used the histogram equalization to enhance the quality of red, green, and blue channels of an RGG image. The theoretical background of the histogram equalization is given in detail here. Assume there is a matrix of integer pixels that has a range from 0 to L − 1, and f is an image that is represented as a m(r) by m(c) matrix. In this case, L is the value/number of all possible values of the intensities (usually, L is equal to 256). And p is denoted as a normalized histogram of f as defined in equation (1), with a particular bin for each intensity. So, g, which is an equalized histogram image, is defined as in equation (2).

$$P(n) = \frac{\text{Number of pixels with intensity } n}{\text{Total number of pixels}}, \tag{1}$$

$$g(i,j) = \text{floor}\left((L-1) \sum_{n=0}^{f(i,j)} p(n) \right). \tag{2}$$

Here, floor () function is used to round down to the nearest integer value. This is the same as transforming pixel intensities k, by the f function defined in equation (3). A given transformation appears from an idea of the intensities of the f and g functions as continuous random variables X and Y on the range from 0 to $L-1$, where Y is defined as in equation (4).

$$Y = T(X) = (L-1)\int_0^x p(x)dx, \tag{3}$$

$$g(i,j) = \text{floor}\left((L-1) \sum_{n=0}^{f(i,j)} p(n) \right), \tag{4}$$

where $p(x)$ is the probability density function (PDF) and T is the cumulative distributive function. We also assume here that T is differentiable and is an invertible function. Consequently, Y, which is defined by $T(X)$ in this context, is distributed uniformly, namely, that $p(y) = 1/(L-1)$. These are defined in equation (5) and equation (6).

$$\frac{d}{dY} T\left(T^{-1}(y)\right) = \frac{d}{dy} y = 1, \tag{5}$$

$$py(y) = \frac{1}{L-1}. \tag{6}$$

2.2. Feature Extraction. An original image ($512 \times 512 = 134{,}217{,}728$) has an excessive number of pixels, and if these numbers of features are directly fed to machine learning algorithms, then it is impossible to compute in polynomial time. In the feature extraction stage, the features obtained in the proposed work, we have extracted some informative features from each channel of the RGB image. The first four statistical moments, namely, mean, variance, skewness, and kurtosis, and cooccurrence matrix features, namely, entropy,

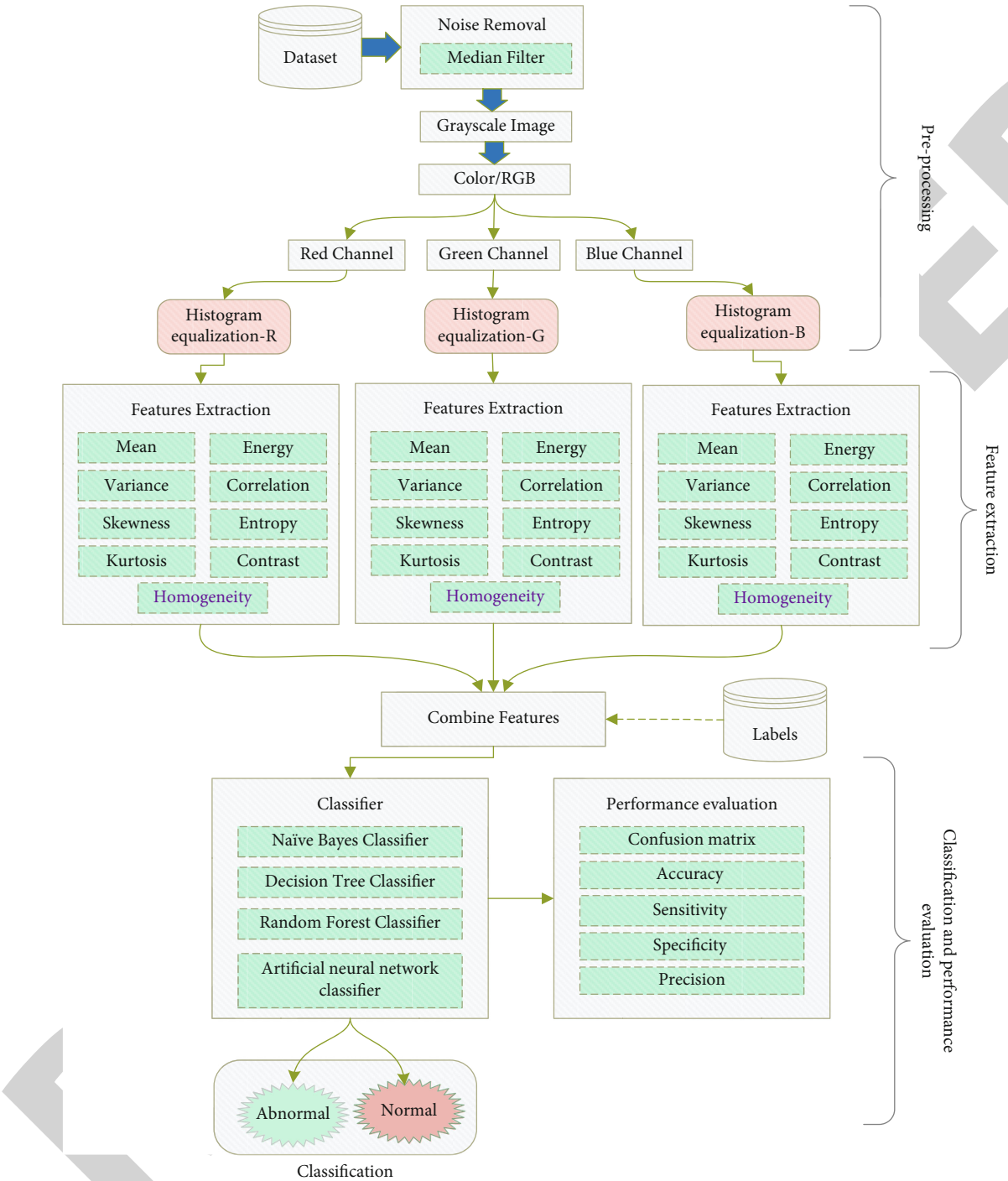

Figure 2: Detailed schematic diagram of the proposed methodology for brain MRI classification.

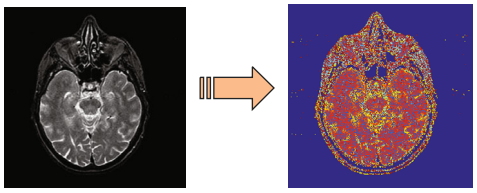

Figure 3: (a) Grayscale image and (b) RGB image.

energy, inverse difference, and correlation, have been calculated of the approximate images obtained in the feature extraction stage [19]. In equations (7)–(10), mean, variance, skewness, and kurtosis have been represented, respectively. Mean is used to describe the bright mean and dark mean in an image. Variance is used to describe the contrast of the image. Skewness is a measure of symmetry, and kurtosis is used to measure the peak and flatness relative to a normal distribution.

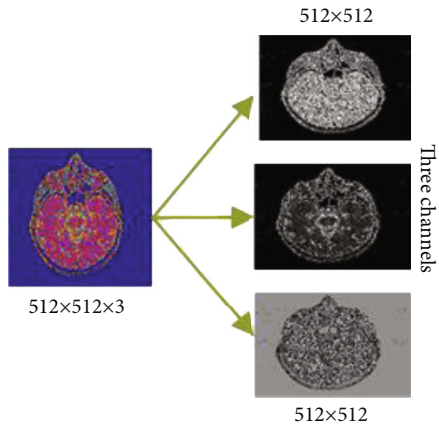

Figure 4: An RGB image and its three channels (red, green, and blue).

$$\text{Mean} = \frac{\sum_{i=1}^{N} p_i}{N}, \tag{7}$$

$$\text{Variance} = \frac{\sum_{i=1}^{N} (p_i - \bar{p})^2}{n}, \tag{8}$$

$$\text{Skewness} = \frac{\sum_{i=1}^{N} (p_i - \bar{p})^3}{n}, \tag{9}$$

$$\text{Kurtosis} = \frac{\sum_{i=1}^{N} (p_i - \bar{p})^4}{N}, \tag{10}$$

where N represents the number of pixels in total in an image; the mean of an image pixel values is represented by $\bar{p}$. The calculation of energy, correlation, entropy, contrast, and homogeneity has been done in equations (11)–(15), respectively.

$$\text{Eng} = \sum_i \sum_j \left(\Omega_{i,j}\right)^2, \tag{11}$$

$$\text{Corr} = \frac{1}{\sigma_\alpha \sigma_\beta} \sum_m \sum_n (p - \bar{p}_\alpha)\left(\left(p - \bar{p}_\beta\right)\Omega_{i,j}\right), \tag{12}$$

$$\text{Ent} = -\sum_m \sum_n \Omega_{i,j} \log_2 \Omega_{i,j}, \tag{13}$$

$$\text{Cont} = \sum_i \sum_j \left(\Omega_{i,j}\right)^2 (i-j)^2, \tag{14}$$

$$\text{Homog} = \sum_i \sum_j \frac{\Omega_{i,j}}{|i-j|}, \tag{15}$$

where Eng, Corr, Ent, Cont, and Homog represent energy correlation, entropy, contrast, and homogeneity, respectively.

In the proposed work, we have calculated nine features, namely, mean, variance, skewness, kurtosis, entropy, correlation, entropy, energy, contrast, and energy for red, green, and blue channels, respectively, in the feature extraction stage. The graphical representation of the feature extraction stage is illustrated in Figure 5. We have then combined these features in a file and have been fed to a classifier to classify the brain MRI images into normal or abnormal.

In the classification stage, two cases have been considered: the percentage split method has been used in which the whole data is divided into two datasets, namely, training and testing as visualized in Figure 6.

2.3. Classification. Artificial neural network performance is better as compared to counterpart algorithms for complex data [4, 19, 20]. The explanation of MLP is given below. The sum of products of weights and neuron values and bias is done using the below equation:

$$\varnothing_m = \sum_{n=1}^{r} P_{mn} l_m + \beta_m, \tag{16}$$

where r indicates number of inputs, input variables is presented by l_m, β_m represents the bias, and P_{mn} indicates weights. A set of activation functions are available that we can apply to hidden layer neurons.

Sigmoid, tangent hyperbolic sigmoid, and ReLU activation functions are donated in equations (17), (18), and (19) correspondingly.

$$\text{Sigmoid} = \frac{1}{1 + e^{\varnothing_m}}, \tag{17}$$

$$\tan h = \frac{e^{-\varnothing_m} - e^{-\varnothing_m}}{e^{-\varnothing_m} + e^{-\varnothing_m}}, \tag{18}$$

$$\text{ReLU} = \max\left(0, \varnothing_m\right). \tag{19}$$

The mean, variance, skewness, kurtosis, entropy, correlation, energy, contrast, and homogeneity features calculated in the feature extraction stage for each channel of the RGB image and combined are fed to the artificial neural network. By applying an activation ψ_q function on $\varnothing_m$, the output of a partial neuron can be obtained as in the following equation:

$$\psi_q = \psi_q \left[\sum_{p=1}^{k} p_{mn} l_m + \beta_m\right]. \tag{20}$$

The structure diagram of the proposed artificial neural network used in the proposed model is given in Figure 7.

The second algorithm that we have used in the proposed work for brain MRI classification based on the features extracted in feature extraction stage is decision tree classifier. Decision tree classifier is known as one of the most widespread methods in mining data used for classification purposes. It is based on varieties of classes for developing prediction models. This algorithm is used to classify a dataset into subtrees that make up a global inverted tree (consisting of the root, internal, and leaf nodes). An algorithm is efficient for huge and complicated datasets. In case the dataset is sizable, training data is divided into validation states [21]. Decision trees are basically illustrated graphically as a hierarchically represented graph. This diagram includes branches and a starting node (root node) [22]. Branches

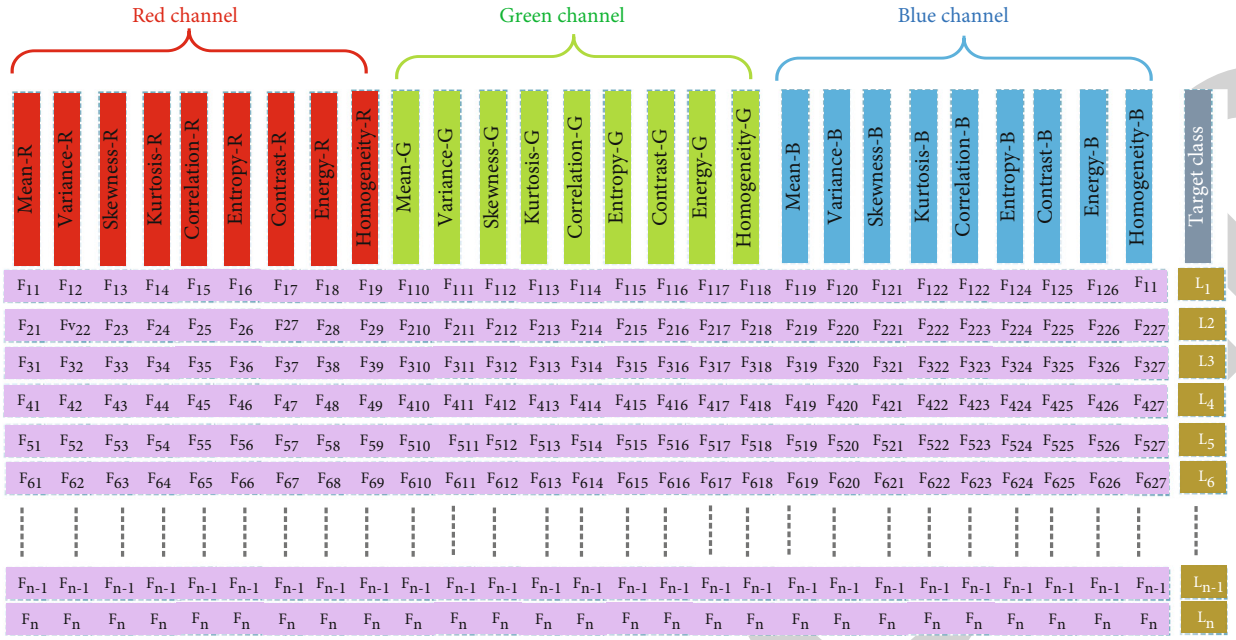

Figure 5: Visualization of feature extraction mechanism in the feature extraction stage.

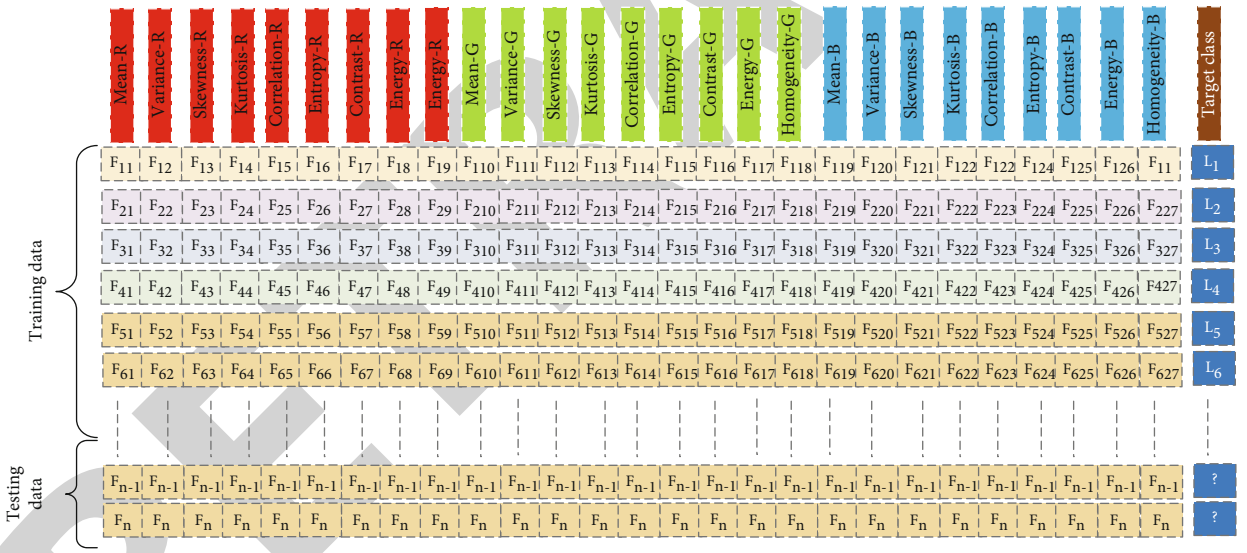

Figure 6: Visualization of the division of data into training and testing by using the percentage split method.

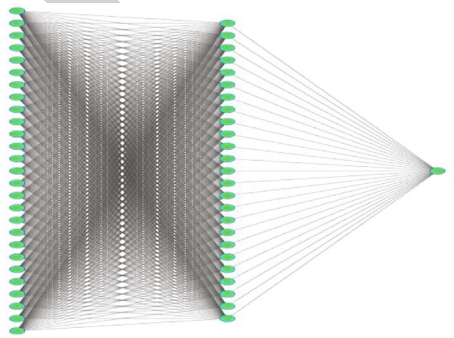

Figure 7: Structure diagram of the ANN used in the proposed work.

(conditions) are known to be a group of nodes interconnected and inherited some properties from one another that should lead to a final decision (classification class) [22]. To build branches that are based on conditions, a variety of splitting criteria are used. The most used are Gain Ratio and Gini Index [23]. When it comes to Gain Ratio, decreasing the irregularity of every node leads to the tree height reduction which is an aim of the algorithm. Irregularity is defined as in the following equation:

$$I = -\sum_{c} p(c)\ \log_2 p(c). \tag{21}$$

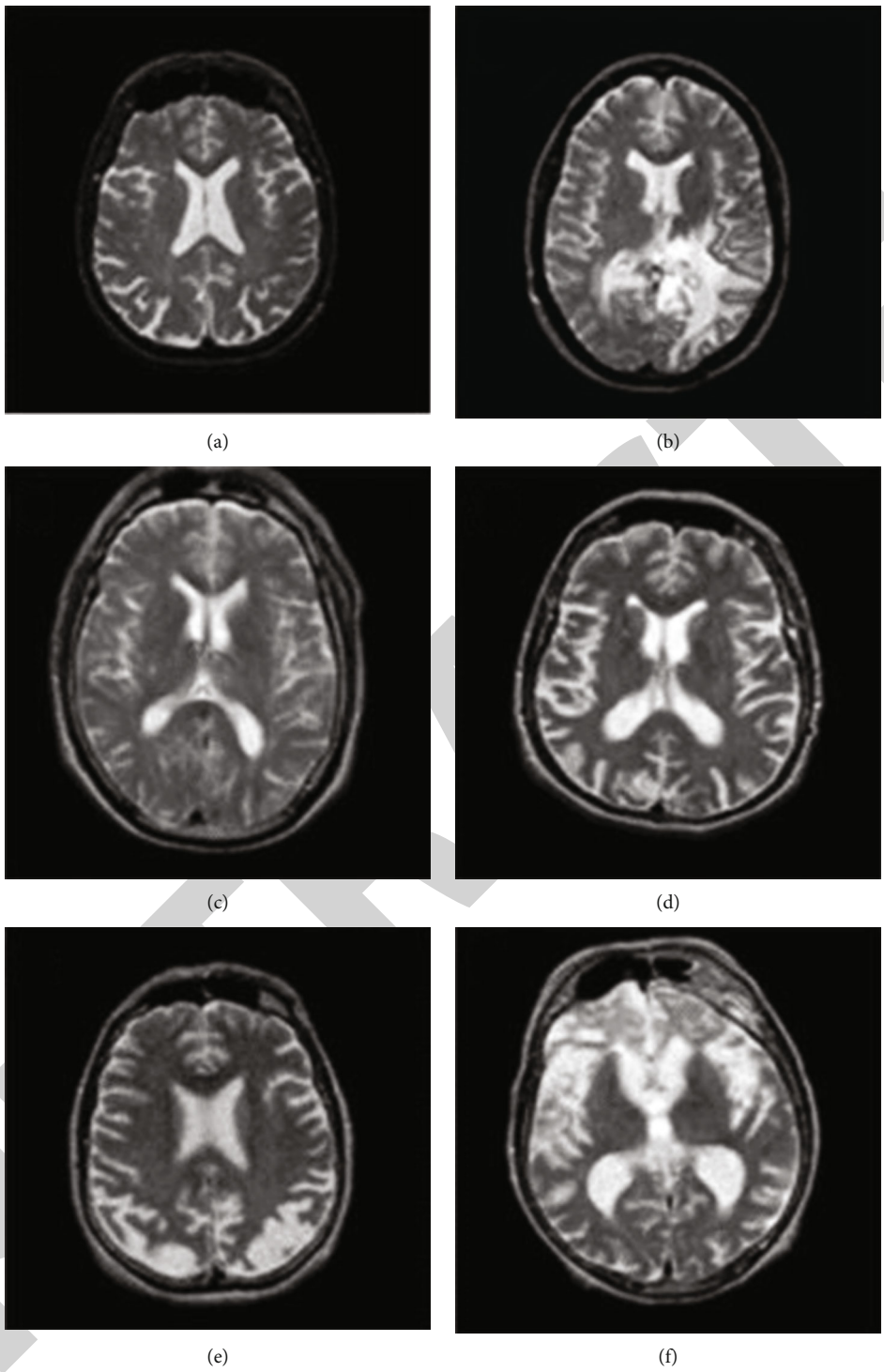

(a) (b) (c) (d) (e) (f)

Figure 8: Continued.

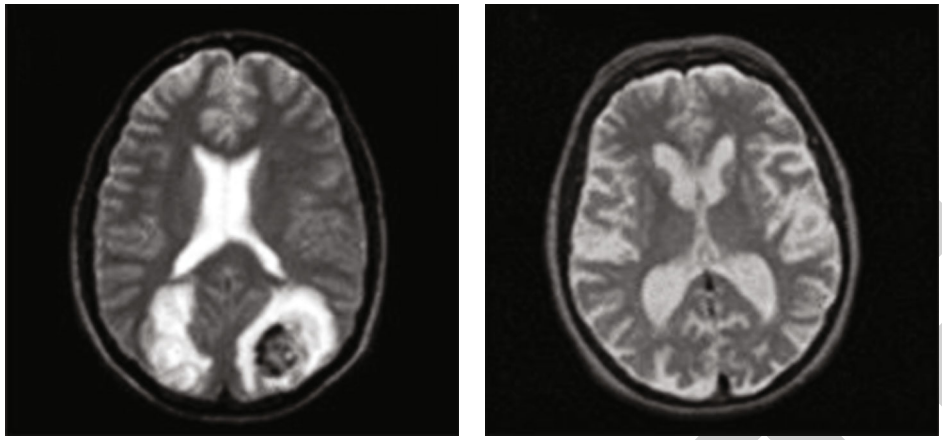

(g) (h)

Figure 8: (a) Normal brain MRI, (b) glioma, (c) meningioma, (d) Alzheimer, (e) Alzheimer plus, (f) visual agnosia and pick's disease, (g) sarcoma, and (h) Huntington's disease.

Here, $p(c)$ is a portion of the data belonging to the c class. This way, the feature with the maximum Gain Ratio is defined as a tree root (see the following equation).

$$\text{Gain}(A) = I - I(\text{res}). \tag{22}$$

Here, $I(\text{res})$ is known as irregularity at all of the classes at the moment when a particular feature was used. It is computed as in the following equation:

$$I(\text{res}) = -\sum_{v} p(v) \sum_{c} p(\text{c} \mid v) \log_2 p(c \mid v). \tag{23}$$

Gini Index is basically defined as the split measure and computed as in the following equation:

$$\mathbf{I}(\text{Gini}) = 1 - \sum_{j} p(cj)^2 \tag{24}$$

Here, $p(c)$ represents the relative frequency of cases that belong to the cj class. Then, the information gain is computed as in the following equation:

$$G = I - \sum \frac{cj}{c} I(c). \tag{25}$$

A splitting feature is then chosen to maximize the Gini Index.

The third algorithm that we have used in the proposed work for brain MRI classification based on the features extracted in feature extraction is random forest (RF). Random forest classification implies decision tree (DT) algorithm as its base. In the case of random forest, we assume that the system is already familiar with the single tree classifier and consists of a large number of them. Therefore, to examine where the input value belongs, it should go through each of the single trees made from the DTAs. After the processing is finished, each of the trees gives an output, which scientists call "votes," and the class that had the most votes is shown as a result. The mandatory rules to follow while constructing each of the trees [24] are as follows:

(i) If the number of the features of the training set is N, each tree must have a smaller number of features that are chosen randomly from the set. The subsets which construct the tree are gathered with replacement from the main features

(ii) During tree growth, it is important not to overburden the depth of the tree to conclude accurate results

(iii) The largest extent should be achieved in each tree; there is no place for pruning

In RF, the correlation between the trees defines the error rate, which means that the increase of the correlation between the feature trees grows the error rate as well. Therefore, to avoid it, an individual tree should be a strong classifier and should have its feature strength. This algorithm does not require any cross-validation or any separated tests to estimate if the result is biased or unbiased [25].

The fourth algorithm that we have used in the proposed work for brain MRI classification based on the features extracted in feature extraction is Naïve Bayes classifier. Based on strong assumptions of the independence of varieties in Bayes theorem, Naïve Bayes is an algorithm for classification purposes. The algorithm assumes that the variables are independent of each other, Gaussian distribution of numeric predictors with mean and standard deviation computed from the training dataset. The given algorithm is normally used as an alternative for decision trees, though compared to those, it skips any instance of the dataset with null (N/A) values [26].

In probabilities, Naïve Bayes is known to be a probabilistic classifier. In other words, in the dataset d, all classes $c \in C$, the class of c that has the maximum posterior probability in

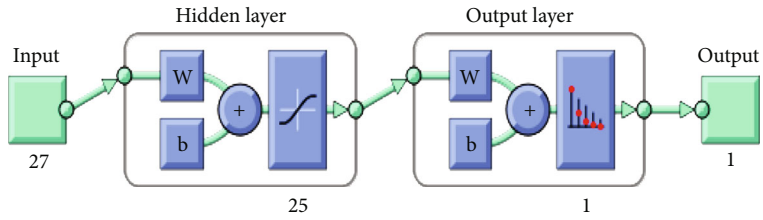

Figure 9: Implemented neural network.

the abovementioned dataset ($\hat{c}$ is the estimate of the correct class) (see the following equation).

$$\hat{c} = \operatorname{argmax} P(c \mid d). \tag{26}$$

The major idea of the Bayesian classification is to change equation (26) to other probabilities.

$$P(x \mid y) = \frac{P(y \mid x)\, P(x)}{P(y)} \tag{27}$$

might be transformed to the following equation:

$$\hat{c} = \operatorname{argmax} P(c \mid d) = \operatorname{argmax}\left(\frac{P(d \mid c)P(c)}{P(d)}\right). \tag{28}$$

If we drop the denominator $P(d)$, equation (28) might be easily simplified. Since $P(d \mid c)P(c)/P(d)$ is computed for every possible class, the formula can be simplified conveniently. However, $P(d)$ is not changed for every class; we concentrate on the class that is most probable for the same d that must present an identical $P(d)$ of probability [39, 40]. Therefore, the class that maximizes equation (29) can be chosen:

$$\hat{c} = \operatorname{argmax} P(c \mid d)p(d) = \operatorname{argmax} P(d \mid c)\, P(c). \tag{29}$$

The fourth algorithm that we have used in the proposed work for brain MRI classification based on the features extracted in feature extraction is KNN classifier.

k-nearest neighbor (KNN) is a widely spread machine learning algorithm that is used for classification purposes. It is commonly used for pattern recognition where data samples are classified based on the nearest neighbor of the class; they might belong to [27, 28]. k-nearest neighbor (KNN) is a simple algorithm, which stores all cases and classify new cases based on similarity measure KNN algorithm also called as (1) case-based reasoning, (2) k-nearest neighbor, (3) example-based reasoning, (4) instance-based learning, (5) memory-based reasoning, and (6) lazy learning [29].

For performance measurements, we have used different performance evaluators such as precession, recall, and F_1 -score [13, 19] to measure the performance of the proposed approach.

Table 1: Specified parameters of ANN in the proposed work.

Algorithm	Parameter	Value
ANN	Input layer neurons	29
	Hidden layer neurons	15
	Output layer neurons	1
	Activation function on hidden layer	Sigmoid
	Activation function on output layer	Sigmoid
	Number of epochs	1000

3. Implementation, Results, and Comparative Analysis

3.1. Implementation Setup. In this section, we have briefly discussed the implementation details. The entire implementation of the proposed work is done in Python installed on Intel(R) Core (TM) i7-7500U having NVIDIA GeForce 940MX GPU, 15 GB DDR2 RAM. In the proposed work, some libraries of Python like NumPy, Keras, SciPy, and Sklearn are used for model building and classification purposes.

In this study, we have considered T2-weighted MRI of 512×512 size images taken from the Harvard University medical website [30]. A sample image from each disease is shown in Figure 8, along with a normal brain MRI.

In the proposed work, we have applied different algorithms, such as artificial neural network, decision tree, naïve Bayes, and KNN and have applied on the data collected in the feature extraction stage. The performance evaluation results for each algorithm are given in detail in terms of confusion matrix, precision, recall, and F_1-score.

3.2. Results. A structure diagram of the implemented neural network is exhibited in Figure 9 and the corresponding specifications are listed in Table 1. The confusion matrix for classification results obtained through ANN is illustrated in Figure 10. The confusion shows that out of 42 abnormal images, the ANN accuracy classified 29 images and inaccurately classified 2 images. Similarly, out of 42 normal images, the ANN classified 8 images correctly. The precision, recall, and F_1-score are calculated for ANN classification results and are listed in Table 2. Also, you can see the visualization of the performance evaluation in Figure 11.

The confusion matrix for classification results obtained through random forest is illustrated in Figure 12. The confusion shows that out of 42 abnormal images, the random

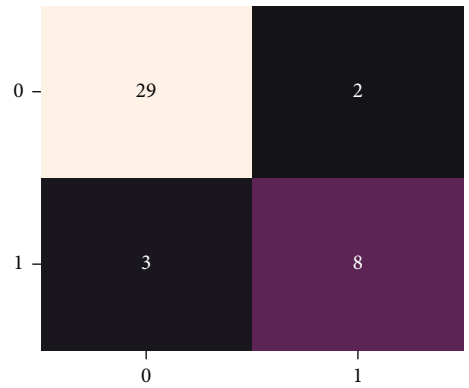

Figure 10: Confusion matrix for ANN classifier.

Table 2: Performance matrices for ANN.

	Precision	Recall	F_1-score
0	0.91	0.94	0.92
1	0.80	0.73	0.76
Overall	0.85	0.83	0.83

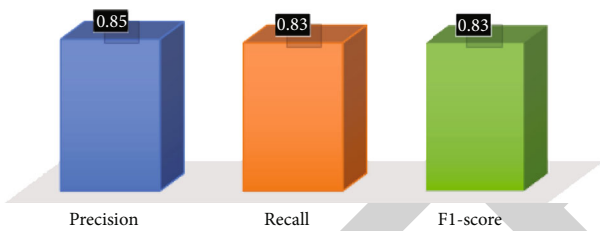

Figure 11: Graphical representation of Table 2.

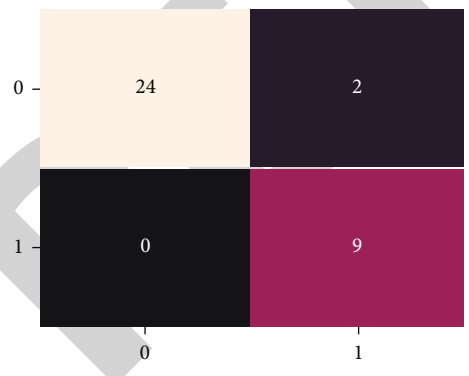

Figure 12: Confusion matrix for random forest classifier.

forest accuracy classified 24 images and inaccurately classified 2 images. Similarly, out of 42 normal images, the random forest classified 9 images correctly. The precision, recall, and F_1-score are calculated for random forest classification results and are listed in Table 3. Also, you can see the visualization of the performance evaluation in Figure 13.

The confusion matrix for classification results obtained through Naïve Bayes is illustrated in Figure 14. The confusion shows that out of 42 abnormal images, the Naïve Bayes accuracy classified 20 images and inaccurately classified 2 images. Similarly, out of 42 normal images, the Naïve Bayes classified 9 images correctly. The precision, recall, and F_1-score are calculated for Naïve Bayes classification results and are listed in Table 4. Also, you can see the visualization of the performance evaluation in Figure 15.

The confusion matrix for classification results obtained through the k-nearest neighbor algorithm is illustrated in Figure 16. The confusion shows that out of 31 abnormal images, the KNN accuracy classified 24 images and inaccurately classified 7 images. Similarly, out of 11 normal images, the KNN classified 11 images correctly. The precision, recall, and F_1-score are calculated for KNN classification results and are listed in Table 5. Also, you can see the visualization of the performance evaluation in Figure 17.

The confusion matrix for classification results obtained through decision tree classifier is illustrated in Figure 18. The confusion matrix shows that out of 42 abnormal images, the decision tree classifier accurately classified 39 images and inaccurately classified 0 images. Similarly, out of 42 normal images, the decision tree classifier classified 17 images correctly. The precision, recall, and F_1-score are calculated for

Table 3: Performance evaluations of random forest classifier.

	Precision	Recall	F_1-score
0	1.00	0.92	0.96
1	0.82	1.00	0.9
Overall	0.91	0.96	0.93

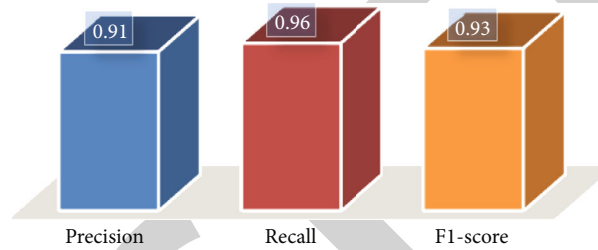

Figure 13: Graphical representation of Table 3.

Figure 14: Confusion matrix for Naïve Bayes classifier.

Table 4: Performance evaluation of Naïve Bayes classifier.

	Precision	Recall	F_1-score
0	0.65	0.91	0.75
1	0.82	0.45	0.58
Overall	0.81	0.89	0.82

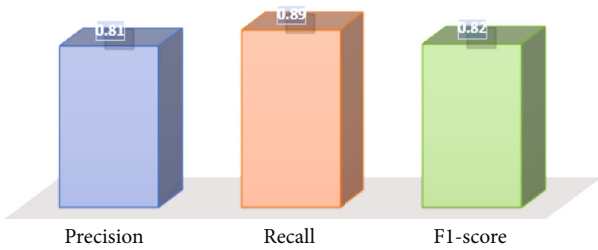

Figure 15: Graphical representation of Table 4.

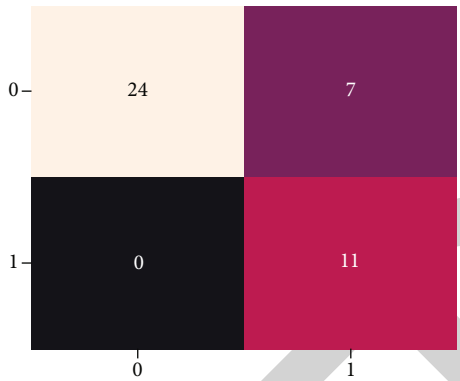

Figure 16: Confusion matrix for KNN classifier.

Table 5: Performance Metrics for KNN classifier.

	Precision	Recall	F_1-score
0	1.00	0.77	0.87
1	0.61	1.00	0.76
Overall	0.81	0.89	0.82

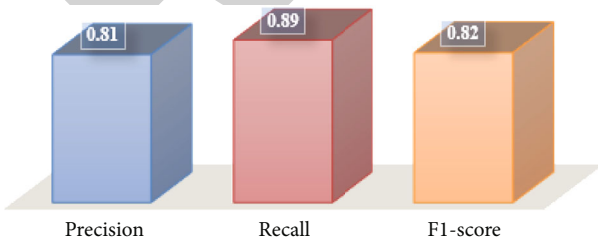

Figure 17: Graphical representation of Table 5.

decision tree classifier classification results and are listed in Table 6. Also, you can see the visualization of the performance evaluation in Figure 19.

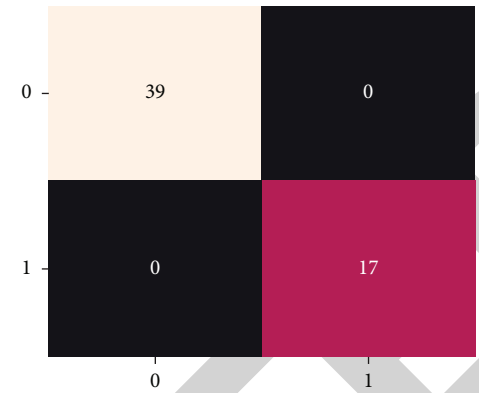

Figure 18: Confusion matrix for decision tree classifier.

Table 6: Performance metrics for decision tree classifier.

	Precision	Recall	F_1-score
0	1.00	1.00	1.00
1	1.00	1.00	1.00
Overall	1	1	1

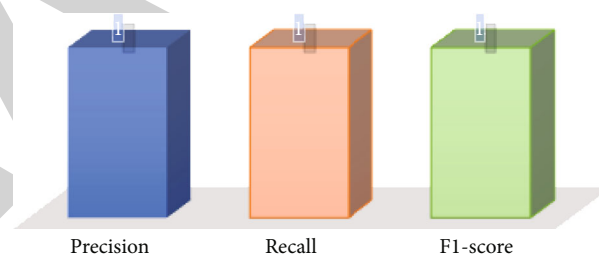

Figure 19: Graphical representation of Table 6.

Table 7: Classification accuracy of proposed method along with other well-known classification methods.

S. No.	Methodology	Classification accuracy
1	SF and ANN [31]	92%
2	DWT and ANN [32]	90%
3	SF, DWT, and ANN [4]	95%
4	SF and KNN [13]	96%
5	Proposed methodology	100%

SF: statistical features; DWT: discrete wavelet transforms; ANN: artificial neural network; KNN: *k*-nearest neighbors' algorithm.

3.3. Comparative Analysis. We have applied different machine learning algorithms in the classification stage on the features obtained in the feature extraction stage. The results indicate that classification and regression tree performance is better when we apply it to the extracted features; hence, we have considered this classification and recorded the results and compared with some well-known classification methods as listed in Table 7. We have compared the proposed method with some other methods in order to

measure the performance of the proposed method. The selection norms of the qualified algorithms are simplicity, computation complexity, and accuracy. The results exhibit that the proposed method has outshined the other algorithms.

4. Conclusion

Accurate classification of brain MRI images with a small dataset is challenging. Normally, two types of strategies are used to classify the brain MRI images, firstly to apply deep learning algorithms, such as convolutional neural network to classify the brain MRI image, but the problem with deep learning is that it requires an immense number of images to train the model. In the case of convolutional neural network, the whole image is given as input to the algorithm. Secondly, if we have a small set of images then usage of convolution of neural network is not a wise choice because convolutional neural network performs worst on a small dataset. Hence, the next choice is to apply a simple machine learning algorithm, such as an artificial neural network with one or two hidden layers, *k*-nearest neighbor algorithm, decision tree, etc., but the problem with these algorithms is that we cannot feed complete image to these algorithms because it requires a lot of computation time. Hence, proper feature engineering is required to reduce the curse of dimensionality and to extract some features of interest from images. For this purpose, in the proposed work, a novel method has been applied for extracting features of interest from images. First, the grayscale images are converted to RGB images and red, green, and blue channels are then extracted from RGB images. The histogram equalization has been applied on each channel of RGB images in order enhance the quality of these channels. Then, statistical parameters have been calculated for red, green, and blue channels of RGB images. A total of 27 (9 + 9 + 9) features are extracted for each image, and features for all images are then stored in a file and labeled accordingly to train the machine learning algorithms. We have applied different machine learning algorithms, random forest, ANN, KNN, naïve Bayes, and decision tree, on the features extracted in the feature extraction stage. The performance measures indicate that the performance of the decision tree is far better as compared to the counterpart algorithms. The proposed model is also compared with some state-of-the-art algorithms, and the results exhibit that the performance of the proposed method is far better as compared to other counterpart algorithms.

The limitation of the proposed method is that we have applied this method only on a small dataset that has 140 images and have not applied it on a large dataset.

Data Availability

The dataset is archived from the Harvard University medical website http://www.med.harvard.edu/AANLIB/home.html.

Conflicts of Interest

The authors declare that they have no conflicts of interest to report regarding the present study.

References

[1] J. D. Power, A. L. Cohen, S. M. Nelson et al., "Functional network organization of the human brain," *Neuron*, vol. 72, no. 4, pp. 665–678, 2011.

[2] A. Rehman, S. Naz, M. Razzak, F. Akram, and M. Imran, "A deep learning-based framework for automatic brain tumors classification using transfer learning," *Circuits, Systems and Signal Processing*, vol. 39, no. 2, pp. 757–775, 2020.

[3] N. P. Q. T. Ostrom, G. Cioffi, K. Waite, C. Kruchko, and J. S. Barnholtz-Sloan, "CBTRUS statistical report: primary brain and other central nervous system tumors diagnosed in the United States in 2013–2017," *Neuro-Oncology*, vol. 22, Supplement_1, pp. iv1–i96, 2020.

[4] Z. Ullah, S.-H. Lee, and M. Fayaz, "Enhanced feature extraction technique for brain MRI classification based on Haar wavelet and statistical moments," *International Journal of Advanced and Applied Sciences*, vol. 6, no. 7, pp. 89–98, 2019.

[5] M. Saritha, K. P. Joseph, and A. Mathew, "Classification of MRI brain images using combined wavelet entropy based spider web plots and probabilistic neural network," *Pattern Recognition Letters*, vol. 34, no. 16, pp. 2151–2156, 2013.

[6] S. Chaplot, L. M. Patnaik, and N. Jagannathan, "Classification of magnetic resonance brain images using wavelets as input to support vector machine and neural network," *Biomedical Signal Processing and Control*, vol. 1, no. 1, pp. 86–92, 2006.

[7] S. G. Mallat, *A theory for multiresolution signal decomposition: the wavelet representation, Fundamental Papers in Wavelet Theory*, Princeton University Press, 2009.

[8] R. K. Begg, M. Palaniswami, and B. Owen, "Support vector machines for automated gait classification," *IEEE Transactions on Biomedical Engineering*, vol. 52, no. 5, pp. 828–838, 2005.

[9] M. Ahmad, M. Hassan, I. Shafi, and A. Osman, "Classification of tumors in human brain MRI using wavelet and support vector machine," *IOSR Journal of Computer Engineering*, vol. 8, no. 2, pp. 25–31, 2012.

[10] M. Maitra and A. Chatterjee, "A Slantlet transform based intelligent system for magnetic resonance brain image classification," *Biomedical Signal Processing and Control*, vol. 1, no. 4, pp. 299–306, 2006.

[11] E. Dahshan, T. Hosny, and A. Salem, "Hybrid intelligent techniques for MRI brain images classification," *Digital Signal Processing*, vol. 20, no. 2, pp. 433–441, 2010.

[12] Y. Zhang, Z. Dong, L. Wu, and S. Wang, "A hybrid method for MRI brain image classification," *Expert Systems with Applications*, vol. 38, no. 8, pp. 10049–10053, 2011.

[13] M. Fayaz, A. S. Shah, F. Wahid, and A. Shah, "A robust technique of brain MRI classification using color features and K-nearest neighbors algorithm," *International Journal of Signal Processing, Image Processing and Pattern Recognition*, vol. 9, no. 10, pp. 11–20, 2016.

[14] F. M. Alotaibi, M. Z. Asghar, and S. Ahmad, "A hybrid CNN-LSTM model for psychopathic class detection from tweeter users," *Cognitive Computation*, vol. 13, no. 3, pp. 709–723, 2021.

[15] H. Ahmad, M. Z. Asghar, F. M. Alotaibi, and I. A. Hameed, "Applying deep learning technique for depression classification in social media text," *Journal of Medical Imaging and Health Informatics*, vol. 10, no. 10, pp. 2446–2451, 2020.

[16] F. Wahid, R. Ghazali, M. Fayaz, and A. S. Shah, "Using probabilistic classification technique and statistical features for

Hindawi
Computational and Mathematical Methods in Medicine
Volume 2023, Article ID 9795312, 1 page
https://doi.org/10.1155/2023/9795312

Retraction

Retracted: Efficient Prediction of Missed Clinical Appointment Using Machine Learning

Computational and Mathematical Methods in Medicine

Received 1 August 2023; Accepted 1 August 2023; Published 2 August 2023

This article has been retracted by Hindawi following an investigation undertaken by the publisher [1]. This investigation has uncovered evidence of one or more of the following indicators of systematic manipulation of the publication process:

(1) Discrepancies in scope

(2) Discrepancies in the description of the research reported

(3) Discrepancies between the availability of data and the research described

(4) Inappropriate citations

(5) Incoherent, meaningless and/or irrelevant content included in the article

(6) Peer-review manipulation

The presence of these indicators undermines our confidence in the integrity of the article's content and we cannot, therefore, vouch for its reliability. Please note that this notice is intended solely to alert readers that the content of this article is unreliable. We have not investigated whether authors were aware of or involved in the systematic manipulation of the publication process.

Wiley and Hindawi regrets that the usual quality checks did not identify these issues before publication and have since put additional measures in place to safeguard research integrity.

We wish to credit our own Research Integrity and Research Publishing teams and anonymous and named external researchers and research integrity experts for contributing to this investigation.

The corresponding author, as the representative of all authors, has been given the opportunity to register their agreement or disagreement to this retraction. We have kept a record of any response received.

References

[1] Z. Qureshi, A. Maqbool, A. Mirza et al., "Efficient Prediction of Missed Clinical Appointment Using Machine Learning," *Computational and Mathematical Methods in Medicine*, vol. 2021, Article ID 2376391, 10 pages, 2021.

Hindawi
Computational and Mathematical Methods in Medicine
Volume 2021, Article ID 2376391, 10 pages
https://doi.org/10.1155/2021/2376391

Research Article

Efficient Prediction of Missed Clinical Appointment Using Machine Learning

Zeeshan Qureshi,[1] **Ayesha Maqbool**,[2] **Alina Mirza**,[3] **Muhammad Zubair Iqbal**,[4] **Farkhanda Afzal**,[5] **Deborah Dormah Kanubala**,[6] **Tauseef Rana**,[1] **Mir Yasir Umair**,[3] **Abdul Wakeel**,[3] **and Said Khalid Shah**[7]

[1]*CSE, MCS, National University of Sciences and Technology, Islamabad, Pakistan*
[2]*DCS, NBC, National University of Sciences and Technology, Islamabad, Pakistan*
[3]*DEE, MCS, National University of Sciences and Technology, Islamabad, Pakistan*
[4]*ORIC, National University of Modern Languages, Islamabad, Pakistan*
[5]*H&BS, MCS, National University of Sciences and Technology, Islamabad, Pakistan*
[6]*Academic City University, Accra, Ghana*
[7]*CS, University of Science and Technology, Bannu, Pakistan*

Correspondence should be addressed to Deborah Dormah Kanubala; dkanubala@aimsammi.org

Received 17 July 2021; Accepted 25 September 2021; Published 22 October 2021

Academic Editor: Muhammad Zubair Asghar

Public health and its related facilities are crucial for thriving cities and societies. The optimum utilization of health resources saves money and time, but above all, it saves precious lives. It has become even more evident in the present as the pandemic has overstretched the existing medical resources. Specific to patient appointment scheduling, the casual attitude of missing medical appointments (no-show-ups) may cause severe damage to a patient's health. In this paper, with the help of machine learning, we analyze six million plus patient appointment records to predict a patient's behaviors/characteristics by using ten different machine learning algorithms. For this purpose, we first extracted meaningful features from raw data using data cleaning. We applied Synthetic Minority Oversampling Technique (SMOTE), Adaptive Synthetic Sampling Method (Adasyn), and random undersampling (RUS) to balance our data. After balancing, we applied ten different machine learning algorithms, namely, random forest classifier, decision tree, logistic regression, XG Boost, gradient boosting, Adaboost Classifier, Naive Bayes, stochastic gradient descent, multilayer perceptron, and Support Vector Machine. We analyzed these results with the help of six different metrics, i.e., recall, accuracy, precision, F1-score, area under the curve, and mean square error. Our study has achieved 94% recall, 86% accuracy, 83% precision, 87% F1-score, 92% area under the curve, and 0.106 minimum mean square error. Effectiveness of presented data cleaning and feature selection is confirmed by better results in all training algorithms. Notably, recall is greater than 75%, accuracy is greater than 73%, F1-score is more significant than 75%, MSE is lesser than 0.26, and AUC is greater than 74%. The research shows that instead of individual features, combining different features helps make better predictions of a patient's appointment status.

1. Introduction

During the COVID-19 pandemic, the world has experienced that the care of critical patients is most strenuous for the health system. Governments have opted for full long-term lockdowns as preventive measures to keep the numbers of urgent care patients low. There are many reasons due to which a patient may reach such a critical state. One of which is not following up with the Primary Care Provider (PCP). The complete treatment of any disease or health issue requires proper treatment and multiple patient visits to PCP. So, PCP needs to plan policies that will provide appropriate alerts/notifications to the patients in a difficult situation and failing to follow up. Mostly, socio and financial

challenges lead the patient to miss appointments. Based on the medical specialist review [1], missing appointments cause much more damage than just revenue generation. It affects the care of a patient, patient satisfaction, staff, and overall medical resource utilization. The resource includes valuable time, arrangement of environment for surgery, or any special care suggested to the patient.

Research shows that lowering the rate of missed appointments can improve clinical efficiency and utilization, reduce waste, improve provider satisfaction, and lead to better health outcomes for patients [2]. In this research, we worked on over 6 million records of data. We performed different analyses over it to extract previously unknown and hidden causes and relationships between unique attributes of the patient that lead them not to show up in follow-up appointments. We analyzed unique attributes of patients and applied different algorithms to extract useful features for our analysis. Data we receive at first was not in analyzable form. Using data stored in Electronic Healthcare Record (EHR) systems, we got over six million records that we used in our research to predict which type of patient will miss follow-up appointments (termed as no-show-up appointment in the rest of the article).

Data used for analysis is obtained from thirty-five PCP systems. As per ethics and privacy issues, we have followed guidelines set out under the Health Insurance Portability and Accountability Act (HIPAA), amended by the Health Information Technology for Economic and Clinical Health (HITECH) and Omnibus Final Rule. Therefore, we will only discuss aggregated statistics in the rest of the paper. Protected Health Information (PHI) attributes that create any privacy issue are discarded from feature lists like medical record numbers, patient names, addresses, contact details, and language. The investigated algorithms will take some PHI as inputs to create a useful feature like date of birth to age and then to age range. But outputs and metrics used to optimize and score the algorithms do not use any PHI directly that can cause privacy protection issues.

The motivation of this research is to help healthcare providers make policies so they can find outpatients having a higher risk of chronic disease and having a higher probability of missing their appointments. With the help of this analysis, hospital administration can formulate ways and policies to support the patient in the follow-up of their appointments. Using knowledge of this analysis, the hospital can optimize the utilization of resources, including highly qualified doctors and hospital rooms. Another focus of our research is finding the seasonality/trends of appointments. With the help of this information, hospitals and other healthcare centers can make a necessary plan for seasons having a large number of appointments. Thus, resource utilization can be improved by utilizing our analysis.

In this paper, Section 2 refers to the related work in the field of machine learning, in particular, to no-show-up appointment analysis. In Section 3, we have discussed our technique and process of preparing data for analysis. Then, we discussed methods we applied for predicting missed appointments. In Section 4, we presented the results that we obtain by using the mentioned algorithms. Section 5 discusses our results by comparing them with existing studies and explaining how our analysis adds value to the field. Section 6 is the conclusion of our work.

The construction of a good ML model is more of an art than a science. Each model has its features, strengths, and applications. It is essential to distinguish the performance of each model on some standard criteria. In ML, we have four different types of metrics to evaluate the performance of a model: (1) threshold type of discriminator metrics, (2) mean square error (MSE) [3], (3) area under ROC curve (AUC) [4], and (4) hybrid discriminator metric. Davis et al. well drawn detailed comparison of evaluation metrics [5]. It is found that the most commonly used metrics are threshold-type discriminator metrics. Among these, accuracy is considered the most critical measure. But one of the main limitations of accuracy is that it produces less distinctive and less discriminable values [6, 7]. If data classes are imbalanced, an attempt made to analyze data may achieve better accuracy. But that accuracy is not helpful as other metrics like recall, precision, and F1-score values are very low due to poor discrimination of data as mentioned in papers [6, 7]. Therefore, we need the help of different techniques to balance data classes so all metrics give a better result.

Furthermore, it is also powerless in terms of informativeness [8] and less favorable toward minority class instances [8–12]. Informativeness is a characteristic that helps to discriminate how good or bad (informative and noninformative) a solution is. Being less favorable to the minority is a big flaw of accuracy. Solely based on accuracy, one cannot infer that a solution is good or bad. A combination of accuracy with other metrics can give a better understanding of the efficiency of the solution. Other useful features are precision, recall, F1-score, sensitivity (sn), and specificity (sp). While accuracy and recall have a relationship between them [13], by improving one metric, the other is also affected. MSE is used in Supervised Learning Vector Quantization (LVQ) to measure classification performance [14]. AUC is one of the most popular ranking type metrics. The most beneficial characteristic of these metrics is the overall ranking of the performance of the classifier in the multiclass problem [15]. A hybrid discriminator metric is a combination of different threshold type discriminator metrics. Optimized precision [11] and optimized accuracy with recall and precision [16] fall under hybrid metrics. These are evaluation metric criteria based on which solution will be evaluated later in this paper.

While dealing with data, one of the crucial tasks is to deal with imbalance classes of data. Data balancing techniques are used to manipulate data, to have an equal number of records in each class for analysis. For this purpose, the Synthetic Minority Oversampling Technique (SMOTE) algorithm generates excellent results. Using the SMOTE algorithm, the minority class is oversampled by taking each minority class sample and introducing synthetic examples along the line segments joining any/all of the K-nearest neighbors [17]. In the case of the imbalance class, improved accuracy can be obtained. But recall and other metrics will show very low values. This indicates poor discrimination

in data. The SMOTE algorithm improves results by balancing minority classes. But relying on balanced data using one technique may also lead us toward biased analysis due to the inherent nature of the algorithm. For instance, SMOTE does not handle datasets with all nominal features but handle mixed datasets of continuous and nominal features. [18]. Therefore, its different variations are proposed. To cope up with these issues, we choose two other techniques Adasyn and RUS. So that we can compare differently balanced data rather than relying on a single technique dataset.

2. Related Work

At present, there is a scarcity of studies addressing the prediction of no-show-up appointments. Most papers describe the use of one parametric model, for instance, the use of ordinary least square to predict on a given day how many no-show-up appointments will occur. Logistic regression for binary classification is used to predict appointment misses of the patient [19]. Most studies use very few features and apply limited analysis. Few studies developed regression models to predict appointment nonadherence [20, 21]. Some retrospective studies also worked on predicting no-show-up appointments [22]. But that applies to a small dataset of few thousand records.

The most relevant analysis can be seen in the paper of Denney et al. [23]. In this paper, the authors predicted no-show appointments using machine learning algorithms, as the article focused on the effects of missed appointments on revenue, which is a practical application of missed appointment analysis. For this purpose, they focused on the income class category for analysis, which is a significant concern in no-show-up. In this analysis, they used data in millions. They applied analysis of 10 algorithms Adaboost, logistic regression [24], Support Vector Machine (SVM) [25], Naive Bayes [26], stochastic gradient descent [27], extra trees, decision tree, XG Boost, and random forest [28]. Table 1 shows the critical contributions of our work in comparison to other existing studies.

Another paper by AlMuhaideb et al. [29] shows an analysis of no-show appointments through artificial intelligence. In this paper, the authors use a dataset of over a million records. They build predictive models with machine learning algorithm JRip [32] and Hoeffding tree algorithm [33]. In [31], data used is provided by their national health center of authors' country. Five algorithms, random forest, gradient boosting, logistic regression, SVM, and multilayer perceptron, were used [34]. We have adopted the same algorithms as [34]. We further analyzed our results on five different metrics for better evaluation. Mentioned research helps us to identify some of the essential factors to predict the no-show appointments. Mohammadi et al. [30] collected electronic health record (EHR) data and appointment data, including patient, provider, and clinical visit characteristics, over three years. It applied logistic regression, artificial neural network, and Naive Bayes' classifier models to predict missed appointments.

Our work has analyzed similar models with extended five different metrics for better evaluation of the performance model. We have identified important factors to predict the no-show appointments. To get any ML model to work well, good feature selection and better algorithm parameters to create a model are vital tasks. The following are the contributions of our research work:

(i) Extraction of meaningful attributes based upon entropy and information gain of features

(ii) Analysis and comparison of the performance of three different balancing techniques: SMOTE, Adasyn, and RUS

(iii) Application of ten ML models, namely, random forest classifier, decision tree, logistic regression, XG Boost, gradient boosting, Adaboost Classifier, Naive Bayes, stochastic gradient descent, multilayer perceptron, and Support Vector Machine

(iv) Evaluation of results based on six metrics, i.e., recall, accuracy, precision, F1-score, area under the curve, and minimum mean square error

By considering only recall, the random forest classifier gives us a maximum score. By considering other metrics, the decision tree algorithm gives better results by comparing all balancing techniques.

3. Technique and Method Used

In this paper, the data contains about six million records. In raw format, these records are straightforward entries by EHR. From this dataset, features are extracted for analysis using recommended approaches to machine learning. Steps used for analysis are mentioned in the following subsections.

3.1. Data Acquisition and Feature Generation. Data obtained for this research is in the transactional form of the SQL Database. Required data is present in different SQL tables. It is separated and dumped into csv file for further analysis. There are two types of appointments that are present in available data. The first one is the closed type, which means the patient appeared in front of PCP and the appointment has been completed by providing any prescription or treatment. The second type is the canceled one, either appointment has been canceled by proper informing to PCPs or it may contain no-show-up data. The difference between canceled and no-show-up is made upon the canceled reason feature. Appointments having a reason for no performance up are considered for our analysis, while the other is kept in the category of show-up even if canceled.

As mentioned earlier, only aggregated PHI data is used for analysis. Initial data is not directly useful for analysis; however, meaningful features are generated from this raw data using feature generations, like the feature of age range which is created with the help of date of birth. Similarly, the appointment season feature is obtained with the help of the appointment date characteristic. Individual features like appointment creation date are relevant for analysis.

Table 1: Comparison to existing research.

Studies	Data	Algorithm	Evaluation method	Performance	
Denney et al. [23]	7 million	Ada, LR, SVM, NB, SGD, ET, DT, XG, RF	Average recall	68% recall	Existing model with results
AlMuhaideb et al. [29]	1.1 million	JRip, Hoeffding trees, LR, MP, NB	Accuracy, AUC	77.13% accuracy, 0.86 AUC	
Mohammadi et al. [30]	74 thousand	LR, MP, NB	Accuracy, AUC	82% accuracy, 0.86 AUC	
Daghistani et al. [31]	201 million	RF, GB, LR, SVM, MP	Accuracy, precision, recall, F1 measure, AUC	79% accuracy, 77% precision, 79% recall, 76% F score, 0.81 AUC	
Our model	6 million	Ada, LR, SVM, NB, SGD, XG, DT, GB, RF, MP	Accuracy, precision, recall, F1 measure, AUC, MSE	86.5% accuracy, 83% precision, 94% recall, 87% F score, 0.92 AUC, 0.1069 MSE	Proposed model with result

But by combining these, a better feature is obtained like the difference between the date of appointment and creation date giving us an appointment to create the difference. This information helps us to predict that if a difference of appointment is that more than 2 months, the patient is less likely to show up for an appointment. These are just examples; numerous features can be generated using the synthetic generation of features [35]. In Table 2, we provided a list of all useful features that are either individual or formed by a combination of attributes.

By generating many features, there is a need to select the most relevant features useful for predicting no-show-up predictions. For this purpose, we used information gain [36]. It is a useful technique to predict the relevancy of data as it is adopted by many researchers [37–39]. Based upon the information, the characteristic sequence of relevant features is given in Table 3. Table 3 depicts the procedure type feature, which tells us the type of procedure, e.g., angiogram fistula and clinic office visit. There are about 30 plus different types of races available in our data, which contribute better to analysis. Civil status tells about the marital status of the patient. Attribute appointment creating a difference (number of days between the creation of appointment and the actual date of appointment) has a significant influence on predictions. But that attribute was given in the number of days which our models do not readily support. We divided description categories: 1 week, 2 weeks, 3 weeks, 1 month, 2 months, 3 months, 4 months, 5 months, 6 months, 7 months, 8 months, 9 months, 10 months, 11 months, 1 year, 2 years, 3 years, 4 years, and 5 years. The age range feature is also formed by seven categories of patients, which are below 17, 18 to 29, 30 to 39, 40 to 49, 50 to 59, 60 to 69, and 70 onward. The feature appointment season is created by finding months in which appointment has been made. In the current scenario, it is kept from January to December. Sex attribute tells whether the patient is male, female, or unknown. But by checking information gain, it is observed that this feature contributes to prediction at a very low level. In the dataset, the oldest appointment date is 10/10/2007, and the latest appointment is of date 02/28/2022. Future appointments are also present in the system whose appointment status is pending. For the current analysis, pending status appointments are ignored.

3.2. Data Cleaning. The original data had many empty values and required filtering. Empty values in each feature are analyzed carefully. Available data have some empty values in canceled appointments. But data had an additional modified date feature. The modified date is change in appointment date, which also indicates no-show-up. Once an appointment has been canceled, no further changes can be made to that appointment. So, those empty values are filled with the modified date.

Data used for analysis is obtained by a different source of software. Some of them explicitly store cancel date along with the reason. Some of them just store cancel reason. For the second case, the last modified date is the one for which the modified date is considered a canceled date, because once an appointment is canceled, no further action is performed on that one. So in these cases, the cancel date was extracted from reason and modified date. Some features have no entries and lack reference to any other attribute. Therefore, these entries were discarded. The civil status attribute also has almost five to six different types of values which are not on large counts. These are converted into three different kinds of categories alone, couple, and unknown. In the alone category, single people, divorced, or widowed are kept. While in the couple category, married people are held for analysis. The third category is maintained for those whose civil status is unknown or not mentioned in the record. Table 3 depicts the useful features acquired after proper cleaning. These features helped us to predict better results for the no-show-up final result.

3.3. Data Exploration. Before applying models to data for analysis, it is required to explore data in detail to evaluate better results obtained by analysis. Data exploration's first task is to determine how many records we have for show or no-show-up appointments from our data. A clear comparison of the show and no-show-up data can be observed in Figure 1, which shows show and no-show appointments on the x-axis and appointment count on the y-axis.

Figure 2 illustrates the comparison of patients' appointments with respect to age. Similarly, Figure 3 shows the gender-wise distribution of show and no-show-up appointments. Table 2 depicts the most relevant feature, procedure type, other than age and gender. The pie chart in Figure 4

Table 2: Useful features.

Name	Type	Range	Description
Date of birth	Input	mm/dd/yyyy	Date of birth of patient
Race	Input	Like Asian, African, white	Race of patient
Sex	Input	Male/female/other	Sex of patient
Civil status	Input	Single, married, divorced, separated, widowed	Civil status
Admit	Input	Textual format	Reason of admission
Date of appointment	Input	mm/dd/yyyy date	Date of appointment
Status of appointment	Input	Pending, closed, canceled	Status of appointment
Cancel date	Input	mm/dd/yyyy date	Canceling appointment date
Cancel reason	Input	No-show-up, death, rescheduled, out of city	Canceling appointment reason
Create time	Input	Time stamp format	Time at which database entry record was inserted
Modified time	Input	Time stamp format	Time at which database entry record was modified
Procedure type	Input	Like ultrasound, office visit see table	In which procedure patient booked appointment
Patient age	Generated	Numeric	Created by date of birth
Age range	Generated	From age category	Created by patient age feature
Create Appt difference	Generated	No of days	Created by taking difference of appointment date and create time
Appointment season	Generated	Month of year	Created with the help of appointment date
Cancel difference	Generated	No. of days	Created by taking difference of cancel date and appointment date

Table 3: List of relevant features to predict appointment status.

Relevance	Feature name	Information gain values
1	Procedure type	0.0736
2	Race category	0.04305
3	Civil status	0.019836
4	Create difference category	0.019534
5	Age range	0.000890
6	Appointment season	0.000375
7	Sex	0.0001323

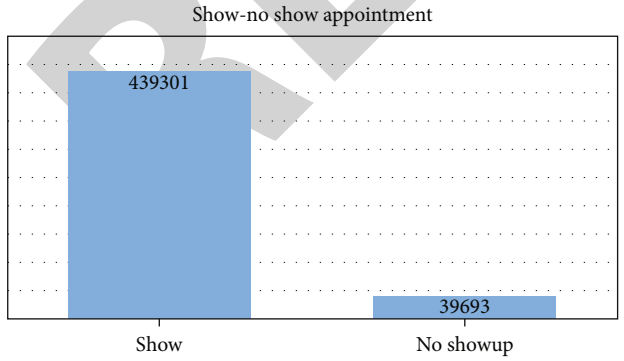

Figure 1: Comparison of show and no-show appointments.

reveals the different types of procedures in terms of percentage. In this figure, procedure type 0 shows records having an unknown value. But as mentioned in Section 3.2, values that lack valuable reference are ignored for analysis. So, procedure type 0 is discarded for further analysis in this paper.

3.4. Balancing Data. Data was cleaned and prepared for use in the analysis. Figures 1–3 depict that data have an imbalance class in nature. In such case, algorithms will tend to predict show-up appointments with greater accuracy. But this prediction is not very good as other metric scores less with such data. To address imbalance data, various techniques were used in literature [23, 40, 41]. In our work, we have adopted the following three techniques to balance classes.

3.4.1. Synthetic Minority Oversampling Technique (SMOTE). Introduced by Chawla et al. [17] and used by Denney et al. [23] for balancing medical data, SMOTE is proved to be a good approach to balance the classes. The core idea of this technique is to use the undersample of the majority class and the oversample of the minority class. Oversampling is done by introducing synthetic examples along the segment joining any/all of k minority class nearest neighbors. These new features are added in feature space, which is then considered again in the next iterations. This process keeps on repeating until a balanced dataset having equal distributed samples is formed.

3.4.2. Adaptive Synthetic Sampling Method (Adasyn). The core of this technique is similar to SMOTE for the generation of minority class elements. But here, density distribution is considered for synthetic samples, while in SMOTE, uniform weight for minority points is used. Haibo et al. [40] suggest two benefits of using Adasyn:

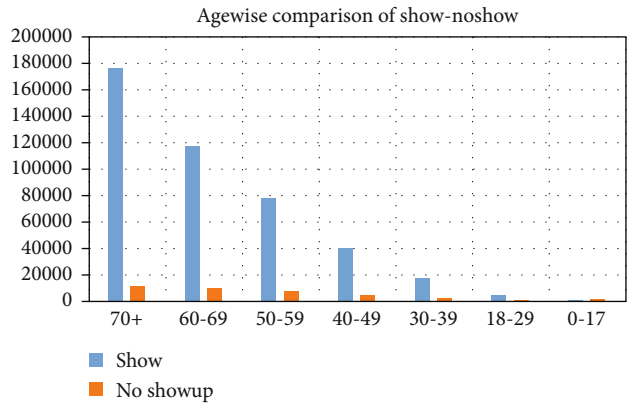

Figure 2: Age-wise comparison of show and no-show appointments.

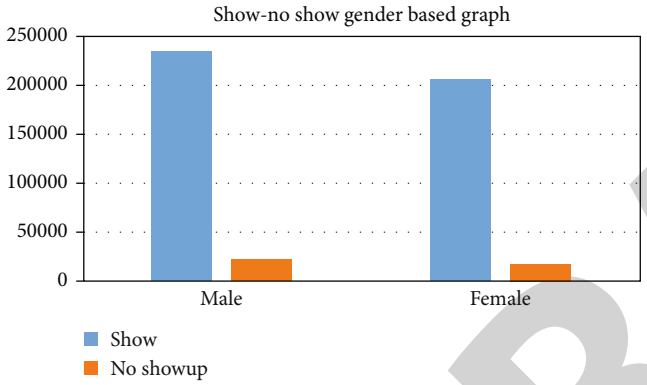

Figure 3: Gender-wise comparison of show and no-show appointments.

(1) It reduces bias introduced by the class imbalance

(2) It adaptively shifts the classification decision boundary toward the complex examples

3.4.3. Random Undersampling (RUS). We have two approaches to address oversampling of the majority class and the undersampling of the minority class. Drummond et al. [41] analyzed the benefits of random undersampling in different scenarios. Random undersampling is a simple technique that has proven beneficial in balancing data [42]. Samples of majority classes are reduced to equate minority class samples. In this way, equal samples are considered for analysis. Keeping in view the advantages of its simplicity, for analyzing our data, we considered the random undersampling technique.

Figure 5 shows the actual distribution of data, whereas Figure 6 illustrates the distribution after applying these techniques.

3.5. Methods Used. In this paper, ten different algorithms are used to no-show.

(1) Decision tree

(2) Logistic regression

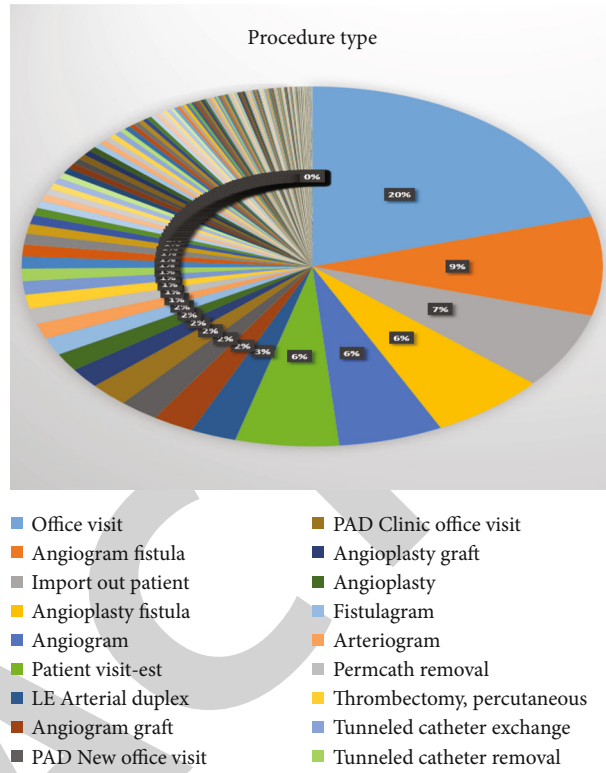

Figure 4: Procedure-wise distribution of data.

(3) Naive Bayes

(4) Random forest classifier

(5) Adaboost Classifier

(6) Support Vector Machine (SVM)

(7) XG Boost

(8) Gradient boosting

(9) Stochastic gradient descent (SGD)

(10) Multilayer perceptron

Different parameters are required to be prearranged for these algorithms to perform better. In our study, we ran a different variation and combination of parameters to achieve improved results. We established that not all parameters work best even after cleaning data. It is well known that the appropriate selection of parameters and input data plays an essential role in improved results [43, 44]. In random forest classifier and stochastic gradient descent (which gives results in continuous form), results obtained are in decimal based on their probability to be a show or no-show-up. A threshold is set to be 0.6. The values greater than 0.6 were considered 1, and below 0.6 were referred to as 0.

4. Evaluation of Results

Algorithms mentioned in Section 3.5 are applied to the dataset, and models are generated using the holdout technique

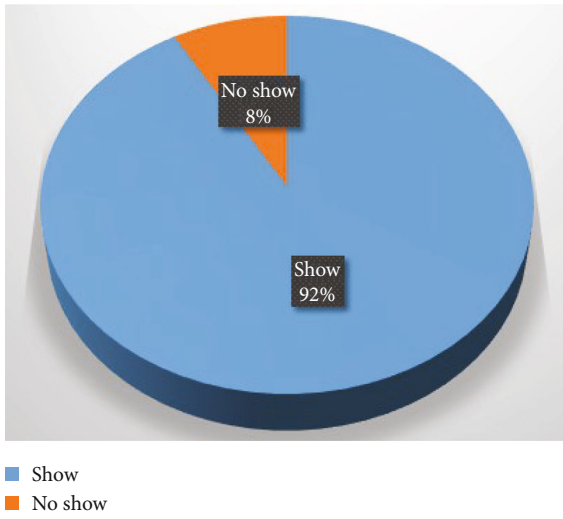

Figure 5: Percentage-wise show and no-show distribution of data.

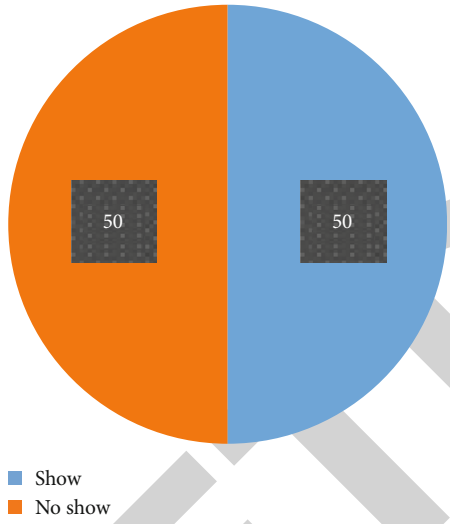

Figure 6: Percentage-wise show and no-show distribution after applying SMOTE.

[45]. Holdout is a useful machine learning technique used to analyze a large dataset. Using this technique, a small chunk of data with random record selection is considered in measuring efficiency of the algorithm while remaining data is used to train the algorithm.

In our case, the data has over 6 million entries. Thus, holdout is used to evaluate models generated using selected algorithms. The best practice of 70-30 is utilized for generating a model where 70% data is preserved for training on which model is developed, and 30% data is kept for testing performance of the algorithm. There are different types of techniques that can be applied to distribute data in training and testing parts like cross-validation and 10-fold cross-validation technique. But the holdout technique is the simplest and most useful.

Data analyzed in Table 4 is based on SMOTE. Threshold type discriminator metrics and evaluation of algorithm analysis data are presented in Figure 3. On threshold type discriminator evaluation, the best results in terms of accuracy alone are obtained by the logistic regression. But by keeping in view other attributes, improved results are obtained, i.e., accuracy, 74% precision, 82.26% F1-score, and best of all recall 91%. Recall is considered the best criteria to evaluate the performance of any algorithm. The random forest classifier gives the best recall of no-show predictions. The evaluation of proposed models based on mean square errors and the area under the curve is shown in Table 5. It can be seen that minimum mean square error, i.e., 0.1069, and better area under the curve, i.e., 92.09%, are obtained by the random forest classifier. So based on statistics, we can conclude that random forest performed better on data balanced by SMOTE. Hybrid discriminator metric values are dependent on a combination of threshold discriminator values. The good discriminator values give better metrics of hybrid discriminators [5].

Evaluations shown in Table 6 are based on data balanced by Adasyn. Threshold type discriminator metric results are presented in Table 6. Based on these values, the best result bases upon recall alone is obtained by random forest. But keeping in view other attributes, the decision tree shows better results having 85.03% accuracy, 81% precision, 86% F1-score, and 90% recall. Considering only recall, the random forest gives better results while the decision tree outperforms

Table 4: Threshold discriminative metric evaluation for show and no-show appointment prediction.

Algorithm	Accuracy	Precision	Recall	F1-score
Random forest	84.96%	80%	93%	86.25%
Decision tree	85.18%	82%	90%	86.42%
Logistic regression	85.35%	83%	89%	86.18%
XG Boost	76.69%	80%	83%	81.44%
Gradient boosting	73.53%	76%	77%	77.32%
Adaboost	70.46%	74%	72%	73.17%
SVM	67.09%	69%	74%	72.15%
Naive Bayes	63.98%	66%	70%	68.44%
SGD	67.14%	60%	84%	70.18%
Multilayer perceptron	80.93%	64%	77%	70.52%

Table 5: Show and no-show appointment prediction result by mean square error and AUC.

Algorithm	MSE	AUC
Random forest	0.1069	92.09%
Decision tree	0.1285	87.13%
Logistic regression	0.1273	87.25%
XG Boost	0.1906	80.92%
Gradient boosting	0.2330	76.69%
Adaboost	0.2646	73.53%
SVM	0.2953	70.45%
Naive Bayes	0.3277	67.21%
SGD	17.71	55.47%
Multilayer perceptron	0.3282	67.14%

Table 6: Show and no-show Adasyn appointment prediction result evaluation by threshold discriminative metrics.

Algorithm	Accuracy	Precision	Recall	F1-score
Random forest	85.26%	78%	93%	85%
Decision tree	86.50%	81%	90%	86%
Logistic regression	64.77%	66%	66%	66%
XG Boost	79.12%	77%	81%	79%
Gradient boosting	75.69%	74%	75%	75%
Adaboost	71.90%	72%	70%	71%
Naive Bayes	65.37%	65%	68%	67%
SGD	60.96%	59%	83%	69%
Multilayer perceptron	63.61%	65%	69%	67%
SVM	68.58%	67%	72%	70%

Table 7: Show and no-show Adasyn appointment prediction result by mean square error and AUC.

Algorithm	MSE	AUC
Random forest	0.16	83.26%
Decision tree	0.15	85.03%
Logistic regression	0.334	66.51%
XG Boost	0.21	78.43%
Gradient boosting	0.255	74.46%
Adaboost	0.279	71.98%
Naive Bayes	0.338	66.20%
SGD	0.339	63.49%
Multilayer perceptron	0.3408	65.94%
SVM	0.28	68.90%

in other metrics. The evaluation analysis of proposed models based on mean square errors and area under the curve is shown in Table 7. According to that, the decision tree algorithm obtains minimum mean square error, i.e., 0.15, and better area under the curve, i.e., 85.03%. Moreover, in Table 6 and the show-no-show Adasyn appointment prediction evaluation by MSE and AUC statistics, it can be concluded that the decision tree classifier performed better on data balanced by the Adasyn technique.

Data analyzed in Table 8 is based on data balanced by technique RUS. Based on threshold type discriminator metrics, the best results in terms of recall are obtained by random forest, i.e., 94%. But keeping in view other attributes, better results are obtained by the decision tree having 86.5% accuracy, 83% precision, 87% F1-score, and 92% recall. Considering only the recall attribute, the random forest outperforms, while the decision tree performs in other metrics. The evaluation results of proposed models based on mean square errors and the area under the curve are shown in Table 9. According to that, minimum mean square error, i.e., 0.135, and better area under the curve, i.e., 86.5%, are obtained by the decision tree. It can conclude by considering statistics that the decision tree classifier performed better on data balanced by RUS technique.

Table 8: Show-no-show RUS appointment prediction result evaluation by threshold discriminative metrics.

Algorithm	Accuracy	Precision	Recall	F1-score
Random forest	85.26%	80%	94%	86%
Decision tree	86.50%	83%	92%	87%
Logistic regression	64.77%	65%	65%	65%
XG Boost	79.12%	78%	81%	79%
Gradient boosting	75.69%	76%	76%	76%
Adaboost	71.90%	74%	67%	70%
Naive Bayes	65.37%	65%	68%	66%
SGD	60.96%	58%	83%	68.18%
Multilayer perceptron	63.61%	59%	88%	71%
SVM	68.58%	68%	71%	69%

Table 9: Show-no-show RUS appointment prediction result evaluation by mean square error and AUC.

Algorithm	MSE	AUC
Random forest	0.1473	85.26%
Decision tree	0.135	86.50%
Logistic regression	0.352	64.77%
XG Boost	0.208	79.12%
Gradient boosting	0.243	75.68%
Adaboost	0.281	71.9%
Naive Bayes	0.346.	65.37%
SGD	0.3546	60.96%
Multilayer perceptron	0.3648	63.62%
SVM	0.26.	68.58%

5. Discussion

Based on the result mentioned in Section 3, the following key findings are presented. By referring to research [3, 46], it can be observed that the smaller mean square error (MSE) gives a better prediction. Similarly, study [4] says that the more the value of AUC, the more improved the result. Keeping in view the results given in Table 5, it is concluded that the random forest classifier performs better on the given dataset with the lowest MSE value of 0.1069 and 92.09% AUC value. Show-no-show RUS appointment prediction results evaluated by MSE and AUC are often used to measure the performance of models. Random forest and decision tree performed better in all metrics. From the summarized results of Table 10, 85.26% accuracy from the random forest using SMOTE, Adasyn, and RUS is achieved. The recall is 94% provided by RUS in random forests. F1-score is 86.25% provided by SMOTE under random forest. Mean square error is minimum in SMOTE, i.e., 0.1069 under random forest, while the area under the curve is maximum given by SMOTE 92.09% under random forest. So, out of six metrics, three indicate that RUS balancing technique gives better results, while four indicate that SMOTE is better for the random forest. Similarly, the decision tree's statistics against SMOTE, Adasyn, and RUS are also

Table 10: Comparison of all balanced analyzed data against random forest and decision tree.

Measures	Algorithms	Random forest (%)	Decision tree
Accuracy (%)	SM-AD-RUS	84.96-83.17-85.26	85.18-85.03-86.50
Precision (%)	SM-AD-RUS	80-78-80	82-81-83
Recall (%)	SM-AD-RUS	93-93-94	90-90-92
F1-score (%)	SM-AD-RUS	86.25-85-86	86.42-86-87
MSE	SM-AD-RUS	0.1069-0.16-0.1473	0.1285-0.15-0.135
AUC (%)	SM-AD-RUS	92.09-83.26-85.26	87.13-85.03-86.50

analyzed. We attained the best accuracy under RUS, i.e., 85.5%; best precision under RUS, i.e., 83%; best recall 92% under RUS; best F1-score 87% under RUS; minimum MSE 0.1285 under SMOTE; and best AUC 87.13% under SMOTE. So, based on that, four out of six metrics indicate that the RUS technique is better, while two out of six metrics favor SMOTE balancing technique. Based on these discussions, we can say that RUS technique for balancing data performs better.

By considering only recall, the random forest classifier gives us a maximum score of 94% with RUS balancing technique. By considering other metrics, the decision tree algorithm gives better results by comparing all balancing techniques. Furthermore, different models also performed well on the given data as their value also improved to more than 55% under all balancing techniques. While referring to these results with other research [23, 29, 31], it can be observed that a better available dataset, better cleaning of data, and good feature selection improve the prediction result of no-show. Another critical factor is that only one metric cannot help categorize the model as good or bad. All values of metrics confirm this argument, that this work adds value to research.

6. Conclusion

This study has used 3 different balancing techniques to balance the dataset. The paper presents in detail an explanation of data along with an analysis of useful features for analysis. We have analyzed ten different algorithms with the help of six different types of metrics. Furthermore, we achieve better metric values with our data balancing and feature inclusion technique. Based on the results of this paper, it is validated that only one metric is not enough to tell about model performance. There is a need to evaluate models' performance from multiple metrics. Moreover, balancing techniques can also make a difference in results. The RUS balancing technique and decision tree algorithm are the best options for analyzing whether a patient will show or miss an appointment. Feature selection is a key to get better results like information gain. We have found that features, title, procedure type, races, civil status, create difference, and age range are more effective in getting better predictions. Six different types of metrics achieve improved results than mentioned in the literature. Furthermore, it is verified that the random forest classifier, decision tree, logistic regression, XG Boost, and gradient boosting performed very well, having recall greater than 75%, an accuracy greater than 73%, and F1-score greater than 75%.

Data Availability

There is no data available to support the study.

Conflicts of Interest

The authors declare that there is no conflict of interest regarding the publication of this paper.

References

[1] D. Marbouh, I. Khaleel, K. al Shanqiti et al., "Evaluating the impact of patient no-shows on service quality," *Risk Management and Healthcare Policy*, vol. 13, pp. 509–517, 2020.

[2] T. Molfenter, "Reducing appointment no-shows: going from theory to practice," *Substance Use & Misuse*, vol. 48, no. 9, pp. 743–749, 2013.

[3] D. M. Allen, "Mean square error of prediction as a criterion for selecting variables," *Techno Metrics*, vol. 13, no. 3, pp. 469–475, 1971.

[4] J. Myerson, L. Green, and M. Warusawitharana, "Area under the curve as a measure of discounting," *Journal of the Experimental Analysis of Behavior*, vol. 76, no. 2, pp. 235–243, 2001.

[5] J. V. Davis, B. Kulis, P. Jain, S. Sra, and I. S. Dhillon, "Information-theoretic metric learning," in *Proceedings of the 24th international conference on Machine learning*, pp. 209–216, Corvalis, Oregon, USA, 2007.

[6] J. Huang and C. X. Ling, *Constructing New and Better Evaluation Measures for Machine Learning*, IJCAI, 2007.

[7] A. Rakotomamonjy, *Optimizing Area under Roc Curve with SVMs*, ROCAI, 2004.

[8] D. J. Mac Kay and D. J. Mac Kay, *Information Theory, Inference and Learning Algorithms*, Cambridge University Press, 2003.

[9] S. García and F. Herrera, "Evolutionary training set selection to optimize c4. 5 in imbalanced problems," in *2008 Eighth International Conference on Hybrid Intelligent Systems*, pp. 567–572, Barcelona, Spain, 2008.

[10] M. Hossin, M. Sulaiman, A. Mustapha, N. Mustapha, and R. Rahmat, "A hybrid evaluation metric for optimizing classifier," in *2011 3rd Conference on Data Mining and Optimization (DMO)*, pp. 165–170, 2011.

[11] R. Ranawana and V. Palade, "Optimized precision-a new measure for classifier performance evaluation," in *2006 IEEE International Conference on Evolutionary Computation*, pp. 2254–2261, Vancouver, BC, Canada, 2006.

[12] S. W. Wilson, "Mining oblique data with XCS," in *International Workshop on Learning Classifier Systems*, pp. 158–174, Springer, 2000.

Hindawi
Computational and Mathematical Methods in Medicine
Volume 2023, Article ID 9825640, 1 page
https://doi.org/10.1155/2023/9825640

Retraction

Retracted: A Systematic Literature Review on Particle Swarm Optimization Techniques for Medical Diseases Detection

Computational and Mathematical Methods in Medicine

Received 1 August 2023; Accepted 1 August 2023; Published 2 August 2023

This article has been retracted by Hindawi following an investigation undertaken by the publisher [1]. This investigation has uncovered evidence of one or more of the following indicators of systematic manipulation of the publication process:

(1) Discrepancies in scope

(2) Discrepancies in the description of the research reported

(3) Discrepancies between the availability of data and the research described

(4) Inappropriate citations

(5) Incoherent, meaningless and/or irrelevant content included in the article

(6) Peer-review manipulation

The presence of these indicators undermines our confidence in the integrity of the article's content and we cannot, therefore, vouch for its reliability. Please note that this notice is intended solely to alert readers that the content of this article is unreliable. We have not investigated whether authors were aware of or involved in the systematic manipulation of the publication process.

Wiley and Hindawi regrets that the usual quality checks did not identify these issues before publication and have since put additional measures in place to safeguard research integrity.

We wish to credit our own Research Integrity and Research Publishing teams and anonymous and named external researchers and research integrity experts for contributing to this investigation.

The corresponding author, as the representative of all authors, has been given the opportunity to register their agreement or disagreement to this retraction. We have kept a record of any response received.

References

[1] S. Pervaiz, Z. Ul-Qayyum, W. H. Bangyal, L. Gao, and J. Ahmad, "A Systematic Literature Review on Particle Swarm Optimization Techniques for Medical Diseases Detection," *Computational and Mathematical Methods in Medicine*, vol. 2021, Article ID 5990999, 10 pages, 2021.

Hindawi
Computational and Mathematical Methods in Medicine
Volume 2021, Article ID 5990999, 10 pages
https://doi.org/10.1155/2021/5990999

Review Article

A Systematic Literature Review on Particle Swarm Optimization Techniques for Medical Diseases Detection

Sobia Pervaiz,[1] **Zia Ul-Qayyum**,[2] **Waqas Haider Bangyal**,[3] **Liang Gao**,[4] **and Jamil Ahmad**[5]

[1]*Department of Computer Science, Abasyn University Islamabad Campus, Islamabad, Pakistan*
[2]*Allama Iqbal Open University, Islamabad, Pakistan*
[3]*Department of Computer Science, University of Gujrat, Pakistan*
[4]*Huazhong University of Science and Technology (HUST), Wuhan, China*
[5]*Hazara University, Mansehra, KPK, Pakistan*

Correspondence should be addressed to Waqas Haider Bangyal; waqas.haider@uog.edu.pk

Received 30 June 2021; Accepted 19 July 2021; Published 14 September 2021

Academic Editor: Shakeel Ahmad

Artificial Intelligence (AI) is the domain of computer science that focuses on the development of machines that operate like humans. In the field of AI, medical disease detection is an instantly growing domain of research. In the past years, numerous endeavours have been made for the improvements of medical disease detection, because the errors and problems in medical disease detection cause serious wrong medical treatment. Meta-heuristic techniques have been frequently utilized for the detection of medical diseases and promise better accuracy of perception and prediction of diseases in the domain of biomedical. Particle Swarm Optimization (PSO) is a swarm-based intelligent stochastic search technique encouraged from the intrinsic manner of bee swarm during the searching of their food source. Consequently, for the versatility of numerical experimentation, PSO has been mostly applied to address the diverse kinds of optimization problems. However, the PSO techniques are frequently adopted for the detection of diseases but there is still a gap in the comparative survey. This paper presents an insight into the diagnosis of medical diseases in health care using various PSO approaches. This study presents to deliver a systematic literature review of current PSO approaches for knowledge discovery in the field of disease detection. The systematic analysis discloses the potential research areas of PSO strategies as well as the research gaps, although, the main goal is to provide the directions for future enhancement and development in this area. This paper gives a systematic survey of this conceptual model for the advanced research, which has been explored in the specified literature to date. This review comprehends the fundamental concepts, theoretical foundations, and conventional application fields. It is predicted that our study will be beneficial for the researchers to review the PSO algorithms in-depth for disease detection. Several challenges that can be undertaken to move the field forward are discussed according to the current state of the PSO strategies in health care.

1. Introduction

The application of computational intelligence for diagnosis of medical diseases has become a new trend in recent years. Numerous methods of medical disease diagnosis can be grouped as intelligent data classification tasks. In terms of the total number of groups that are continuously distributed, the classification techniques may are divided into two categories. The first classification distribution is Binary Classification (Two-class task), which differentiates the data solely between two classes. The second classification is Multi-Classification (multi-class task), which distinguishes data from more than two classes [1, 2]. Several scientists and researchers in the medical domain have experimented with

different techniques to improve the authenticity (accuracy) of data classification. Recently, State-of-the-Art algorithms such as Tabu Search, Genetic algorithm (GA), Bat Algorithm (BA) [3] and PSO, as well as, data mining tools like, Decision Tree and Neural Networks have been utilized in this domain, where these approaches have produced remarkable results [4].

Excluding the other standard classification complexities, the classifications of medical datasets furthermore are employed in disease detection. Consequently, doctors or patients must not only observe the classification findings that have been evaluated but also be familiar with the symptoms that have been used for the classification purpose. Linear programming [5] models and Neural Networks (NN) [6, 7] have been presented for the solution of such kinds of problems. However, the decision methods of such classification models are a black box, which had not provided any explanation related to the attainment of results. Similarly, the hybrid approaches like NN or GA that contain fuzzy rules have handled the issues resulting from black box techniques, although, they were still unable to recognize the input factors that are more suitable than others.

Many researchers in the literature have used PSO state-of-the-art algorithm to solve this problem by embedding various other approaches such as a random forest with PSO [8] and K-nearest neighbour with PSO [9, 10] etc. Our contribution in this study is to provide a comprehensive Systematic Literature Review (SLR) on the PSO and its variants for the detection of medical diseases. This study is being conducted on the basis of a particular time duration, in which the articles are collected from 2010 to 2020. The primary objective of this research is to give a baseline for the researchers who are intended to research the detection of medical diseases with the help of PSO and its improved approaches. Similarly, our work presents a detailed discussion on the past literature, as well as, describes the future directions for the scientist of this field.

The structure of this SLR is organized in the following way: A primary study related to the utilization of PSO for medical disease detection is presented in Section 2. The Systematic Review methodology for this SLR is explained in Section 3. Section 4 is illustrating the Research Planning of our study. In Section 5, the detailed discussion on the Execution Plan of this study is demonstrated. However, Section 6 is representing the Results of our work, while Section 7 provides the conclusion of this SLR.

2. Primary Studies

For diagnosis the Alzheimer's disease (AD), a novel method is introduced in [11] that is based on magnetic resonance imaging (MRI) images pre-processing, principal component analysis, feature extraction, and support vector machine (SVM) model. To optimize the parameters of SVM a novel switching delayed particle swarm optimization (SDPSO) is introduced. The introduced SDPSO-SVM method is successfully tested on the ADNI dataset for the classification of AD. The introduced algorithm achieved higher classification accuracy on 6 standard cases. Moreover, the test results conclude that the introduced method is serving as the most effective approach for diagnosis the AD.

A novel PSO and Artificial Neural Network (PSO-ANN) based model is developed for diagnosing dengue fever at an early stage [12]. In the introduced model, the PSO approach is incorporated to optimize the bias and weight factors of the ANN approach. The performance of the introduced model is examined through the sensitivity, error rate, accuracy, specificity, and area under the curve (AUC) parameters. The results of the proposed model are compared with other traditional approaches such as Decision Tree (DT), PSO, Naive Bayes (NB), and ANN. It is monitored that the proposed model is powerful and proficient for the detection of dengue fever at an early stage.

A novel machine learning model is developed for the detection of AD from brain MRI [13]. At first, the image was processed. Second, the texture features were extracted. Third, for the classification, a single-layer neural network was selected. At last, a novel approach predator-prey PSO is proposed for adjusting the biases and weights of ANN. In terms of efficiency, the proposed method outperforms 10 state-of-the-art approaches, as well as, better than the human observers to diagnose AD.

An extended ANN approach termed Optimized Artificial Neural Network (OANN) is proposed and implemented on medical datasets to diagnose heart disease [14]. For reducing the disease dimension, an Optimized PSO technique is applied. Furthermore, the filter-based ANN is used for binary classification (as positive or negative) of disease according to the disease feature. The proficiency of the proposed approach is measured by comparing with the traditional methods' performance plot, ROC values, confusion matrix, and Regression. It is observed that after embedding the proposed PSO with ANN for feature reduction, the effectiveness of the introduced model is optimized.

Two novel modified Boolean PSO are introduced named Improved Velocity Bounded BoPSO (IVbBoPSO) and Velocity Bounded BoPSO (IVbBoPSO) to figure out the feature selection challenges, while diagnosing kidney and liver cancer [15]. In modified versions, the parameter Vmin is introduced for the feature selection problem. The accuracy of modified versions is evaluated on twenty-eight classical functions selected from CEC 2013, as well as, tested for feature selection through a disease diagnostic system. The statistical results conclude that the modified versions outperform to achieve the maximum classification accuracy.

In [8], a Random Forest (RF) approach is used with PSO (RF + PSO) for the detection of lymph diseases. The approach is split into two phases: the initial phase is for feature selection, where PSO and other feature selection methods are applied for selecting discriminative features; the second phase is for classification, where RF ensemble is utilized to carry out the classification for detection of lymph diseases. In the process of feature selection, the initial and resampled partitions of datasets are used to train the RF classifier. The simulation results illustrate that the proposed approach is superior based on the accuracy rate.

A novel approach Block-Based Neural Network (BBNN) using PSO is introduced for the classification of

Electrocardiogram signals (ECG) [16]. The PSO algorithm is incorporated for optimizing the network structure and weights. The parameters of BBNN are optimized with the help of a PSO algorithm that can reduce the probable alterations of ECG signals with the variation of time and/or person. The performance of the introduced approach is measured by using the database of MIT-BIH arrhythmia, where the results show 97% classification accuracy.

3. Systematic Review Methodology

This research applied the systematic review methodology of Brereton et al. [17], which provides a reliable and precise analysis of research that is conducted through a particular topic. This sort of inspection provides the overview of evidence with the help of coherent systematic search techniques and the synthesis of elected records [18]. Furthermore, this method has been extensively used in [17–20]. However, our work is established on the ground of earlier literature, which describes that the process should be classified into three phases: First is planning, second is conducting and third is an analysis of results. Thus, the later sections explain that how we addressed these three phases.

4. Research Planning

The planning phase discussed the scientific research questions definition, identification of databases, definition of keywords, searching techniques, standards for include & exclude, and quality of article [17–20]. Thus, the following research questions (RQn) were identified on the basis of challenges:

4.1. Research Questions. RQ1: What is the brief overview of current research?

RQ2: What are the extensively applied approaches?

RQ3: How the work is distributed according to time division?

RQ4: Which research papers are frequently cited?

RQ5: What are the diseases and algorithms are used?

RQ6: What are the research possibilities?

Generally, include, exclude and quality standards are defined next to the explanation of research questions [21]. Therefore, Table 1 describes the requirements that are used in this research.

The goal of this process may be to examine the judgments related to the type of reconsiderations that should be studied in this research, which are applied to the subcategories of primary studies for directing the selection criteria [18, 22]. As a consequence, each searched article will be examined with respect to title, abstract, keywords, proposed techniques, results, and conclusions in order to verify the worth of this review. Similarly, the following digital databases are utilized for searching the papers in this article.

(i) Digital Library of IEEE

(ii) Electronic Library ACM

(iii) Google Scholars

(iv) Springer Link

(v) Elsevier Science Direct

(vi) Semantic Scholars

(vii) Emerald

Finally, the Boolean recovery approach was used to search literature from the aforementioned databases. Fundamentally, it splits the search space and defines the subcategory of the document, as stated in the criteria of consultation [23]. In our work, the following combination of strings provide us the solution: *((“Particle Swam Optimization”* OR*“PSO”* OR *“Swarm Intelligence”* OR *“Bio-inspired PSO Algorithm”* OR *“Meta-Heuristic Algorithm PSO”* OR *“Nature-inspired Algorithm PSO”* OR *“Evolutionary Computing Algorithm PSO”) AND (“Medical Disease Diagnosis”* OR *“Medical Diseases Diagnosis”* OR *“Medical Disease Detection”* OR *“Medical Diseases Detection”* OR *“Medical Disorder Diagnosis”* OR *“Medical Disorder Detection”* OR *“Health-Care”)).*

5. Execution Plan

This phase implies five steps: (1) implements the search in the preferred database; (2) correlate the search results for excluding the duplicated articles; (3) apply the include, exclude, and quality standards; (4) assessment of all articles that accepted in the preliminary study; (5) data formation [17, 18].

Figure 1 illustrates the sequence of our systematic literature review. Initially, the first step was established to run the search queries in all elected databases that identified an extensive set of 1490 articles. Subsequently, the literature issued before 2010 was discarded, which returned 970 papers.

However, to purify the search and discard the papers that were irreverent according to the scope of this review, a precise investigation was employed on the titles, keywords, and abstracts with respect to the exclude standards (Table 1). It excluded 916 articles and returned a prescreening collection of 54 papers for quality inspection. It is crucial to highlight that the queries which returned numerous papers using keywords, were inappropriate for the scope of this research; this defends the total numbers of excluded papers.

Finally, a formation (synthesis) was performed to research under the aforementioned quality criteria. As a result, 11 of the 54 publications were eliminated due to quality issues, leaving a final collection of 43 publications with important information on Particle Swarm Optimization for medical disease diagnosis.

6. Result

The results of SLR are discussed in this section. Thereby, each sub-section will demonstrate the challenges, which are addressed at the start of this research.

Table 1: Include, Exclude and Quality Standards.

	Requirements
Include	Literature in English. Methodology papers, journal articles or conferences. Literature relevant to the medical diseases diagnosis by using PSO techniques.
Exclude	Studies that are not proficient according to quality standards. Papers that are irrelevant from the road map. Literature published in another language rather than English. Literature issued before 2010.
Quality	Research with various proposals.

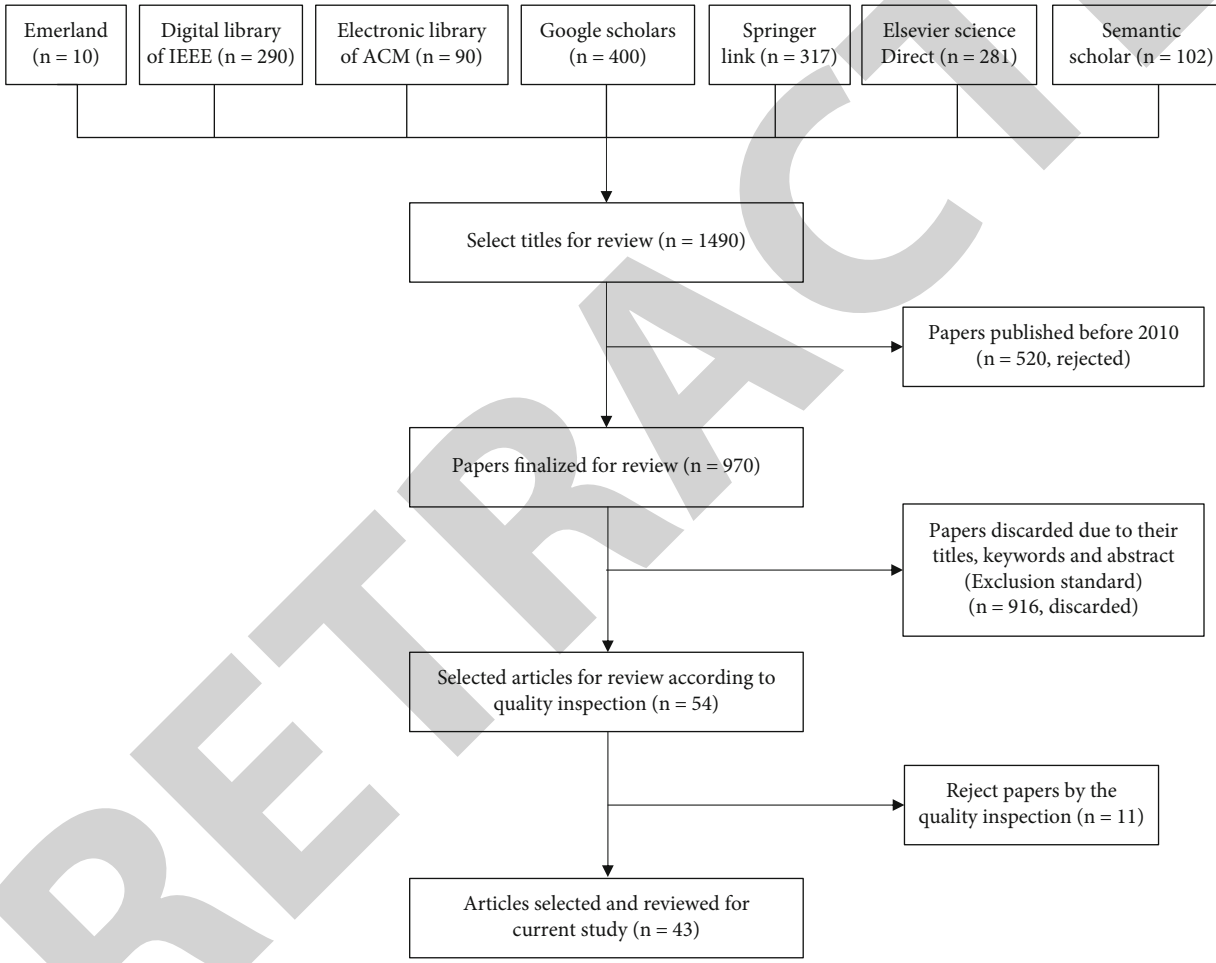

Figure 1: Research Flow of Systematic Literature Review.

6.1. RQ1: Brief Overview of Ongoing Research. The selected literature for this SLR is illustrated in Table 2. By analyzing the selected literature, we will reveal the present review (overview) of the meta-heuristic PSO algorithm for medical disease detection. Accordingly, to present an overview of the various issues that have been presented in selected literature, they were grouped into ten categories.

(i) Heart Disease

(ii) Dental Disease

(iii) Lymphatic Diseases

(iv) Celiac Disease (CD)

(v) Liver Disease

(vi) Cancer Disease

(vii) Brain Disease

(viii) Hepatitis Disease

(ix) Diabetes

Table 2: Selected Literature (ID and References).

ID	Reference
1	[24]
2	[25]
3	[26]
4	[8]
5	[16]
6	[27]
7	[28]
8	[29]
9	[30]
10	[31]
11	[32]
12	[33]
13	[34]
14	[35]
15	[36]
16	[37]
17	[38]
18	[2]
19	[39]
20	[40]
21	[41]
22	[9]
23	[24]
24	[42]
25	[43]
26	[44]
27	[45]
28	[11]
29	[12]
30	[13]
31	[14]
32	[15]
33	[46]
34	[47]
35	[48]
36	[49]
37	[50]
38	[51]
39	[52]
40	[53]
41	[54]
42	[55]
43	[56]

(x) Others

The objective of this study is to find out the PSO techniques that are used to detect the below-mentioned categorized diseases. The concerned topic of diseases and the research papers which are used in the particular diseases are displayed in Table 3.

6.2. RQ2: Extensively Used Approaches. A cloud of words is illustrated in Figure 2, in which the size of each term demonstrates the number of their occurrence. This word cloud is generated on the basis of terms enclosed in the titles of selected research articles. The supremacy of terms indicates that these are the frequently adopted techniques of PSO and medical diseases, which are applied to develop computational intelligent models for disease detection. According to the size of terms in Figure 2, it can be observed that Particle Swarm Optimization, Medical Disease Detection, and PSO algorithm are the predominant words that frequently appear in the targeted research articles.

6.3. RQ3: Literature Distribution with Time Division. The evaluation related to the Distribution of selected literature with respect to the time division is presented in Figure 3. The distribution can be analyzed through Figure 3, which shows that the years 2012 and 2016 recorded the topmost portion/quantity of research articles, with 18 articles (9 in each year), representing 41.86% of the published literature. Similarly, the years 2014 and 2015 published the same counts of articles, 5 in each that covers 23.25% portion of selected literature. The same is the situation with years 2013 and 2017, these years published a total of 8 papers, 4 every year that fills 18.60% section of the literature. However, the year 2011 released 3 (6.97%) papers, besides this, the years 2010 and 2018 issued only 4 articles (2 in each year) that satisfy an 18.60% segment of the selected literature. Hence, there is zero publications in the year 2019 and 2020 related to our study.

6.4. RQ4: Frequently Cited Research Papers. The total citations of elected top 12 papers from literature are identified as 1193 on the topic of PSO techniques and medical diseases, which can be review in Table 4. Abdulhamit Subasi [37] published his research in the Journal of Computer in Biology and Medicine that was the highest cited (343 citations) research article. The rest of the articles are issued in the following Journals: Applied Soft Computing ([56], 139 citations), Expert Systems with Applications ([39], 136 citations), International Journal of neural systems ([44], 110 citations), Neurocomputing ([11], 76 citations), Biomedical Signal Processing and Control ([16], 70), Neural Computing and Applications ([24], 60 citations), Computer methods and programs in biomedicine ([2], 58 citations), Expert Systems with Applications ([15], 55), Journal of Alzheimer's Disease ([13], 51 citations), Soft Computing ([51], 48 citations) and ISRN Artificial Intelligence ([40], 47 citations).

6.5. RQ5: Utilized Medical Diseases and Algorithms. In this question, we describe a concise explanation of medical diseases and the variants of PSO that are utilized for disease detection in the selected articles for this SLR. The comparative description of medical diseases and variants of PSO can be seen in Table 5. In Table 5, each tuple is representing the papers that used the particular variant of PSO for a specific

Table 3: Concerned Topic of Diseases.

Sr. no	Concerned topic	Reference
1	Heart disease	[9, 16, 24, 25, 28, 30, 32, 33, 37, 39, 42, 43, 46, 48, 50, 51, 53, 54, 57]
2	Dental disease	[26]
3	Lymphatic diseases	[8, 55]
4	Celiac disease (CD)	[27]
5	Liver disease	[2, 15, 24, 29, 34, 51, 52, 55]
6	Cancer disease	[2, 15, 24, 30–32, 34, 44, 51, 53, 55, 56]
7	Brain disease	[11, 13, 24, 34–36, 38, 41, 44, 45, 47, 51, 55]
8	Hepatitis disease	[30, 40, 51, 56]
9	Diabetes	[24, 30, 48, 49, 51, 53, 55, 56]
10	Others	[12, 51, 53]

Figure 2: Frequently Occurred Words in Selected Literature.

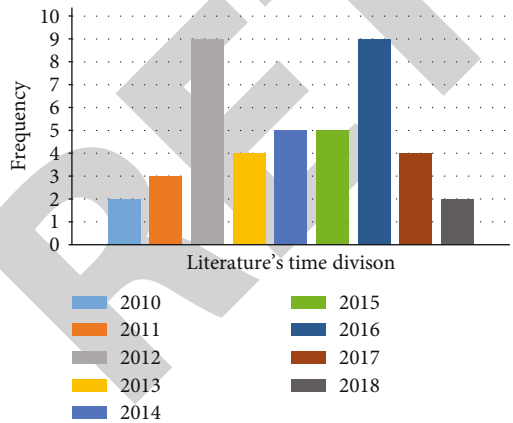

Figure 3: Temporal Distribution of Literature.

type of disease detection. It can be analyzed from Table 5 that the majority of researchers applied Standard PSO and Improved versions of PSO that are as follows: Switching delayed PSO [11], Predator-prey PSO [13], Velocity Bounded BoPSO (VbBoPSO) & Improved Velocity Bounded BoPSO (IVbBoPSO) [15], Modified PSO [49], Dynamic multi-swarm particle swarm optimizer DMS-PSO [50], Centripetal accelerated PSO (CAPSO) [51], Binary PSO (BPSO) [52, 53] and Time variant multi-objective PSO (TVMOPSO) [56]. Similarly, it can be examined from Table 5 that the researchers in the literature focused on the following diseases: Heart (detection of Coronary Heart Disease (CHD), ECG heartbeats, cardiovascular, HeartStatlog, Cleveland Heart Disease, SPECT heart, SPECTF heart, cardiac arrhythmia, and Diabetic Cardiomyopathy), Brain (Alzheimer's disease (AD), Parkinson's disease, Mild Cognitive Impairment (MCI) and Brain Abnormalities), Caner (breast cancer, Liver Cancer and Kidney Cancer), Liver, Diabetes, and Hepatitis, etc. Other than this, the hybridization of PSO and PSO with NN are very few that were incorporated for the detection of medical diseases. Additionally, Celiac and Lymphatic diseases are also miner in numbers that were used in the past study for the objective of disease detection by using PSO's techniques.

6.6. RQ6: Research Possibilities. This domain further has numerous branches that need to be investigated. Hence, in Table 6, we outlined the improved variants of PSO that could be utilized for disease detection in the medical field. In addition to this, we attached the hot topics of diseases that need to get the focus of researchers, while applying PSO's techniques for the field of disease detection can be observed in Table 7. The fundamental objective of these tables is to reveal the feasible gaps (holes) and forthcoming works that should be considered. There are well-defined gaps to be examined since, reviewing the high qualified works published from 2010 to 2010. A small number of areas have been investigated in literature while multiple medical domains could contribute from the improved variants of PSO like Gastric, Lungs, Ankle, Eye, Prostitute, SARS, Covid-19, etc. Furthermore, due to the trend of medical disease detection, there is a quite large number of fields to be reviewed. For this reason, a group of open hypotheses is given that could be investigated in future works for the researchers who are intended to contribute to the society of these thematic areas. Concluding this, it is essential to highlight the purpose of this section, which was to declare the themes and to underline certain hypotheses on the basis of SLR for future research.

Table 4: Top 12 Cited Research Articles.

Reference	Paper title	Year of publication	Citations
[37]	Classification of EMG signals using PSO optimized SVM for diagnosis of neuromuscular disorders	2013	343
[56]	Radial basis function network based on time variant multi-objective particle swarm optimization for medical diseases diagnosis	2011	139
[39]	A hybrid particle swarm optimization based fuzzy expert system for the diagnosis of coronary artery disease	2012	136
[44]	Prediction of Parkinson's disease tremor onset using a radial basis function neural network based on particle swarm optimization	2010	110
[11]	A new switching-delayed-PSO-based optimized SVM algorithm for diagnosis of Alzheimer's disease	2018	76
[16]	A new personalized ECG signal classification algorithm using block-based neural network and particle swarm optimization	2016	70
[24]	Particle swarm optimization for feature selection with application in obstructive sleep apnea diagnosis	2012	60
[2]	An attribute weight assignment and particle swarm optimization algorithm for medical database classifications	2012	58
[15]	Velocity bounded Boolean particle swarm optimization for improved feature selection in liver and kidney disease diagnosis	2016	55
[13]	Multivariate approach for Alzheimer's disease detection using stationary wavelet entropy and predator-prey particle swarm optimization	2018	51
[51]	Enhancement of artificial neural network learning using centripetal accelerated particle swarm optimization for medical diseases diagnosis	2014	48
[40]	Hepatitis disease diagnosis using hybrid case based reasoning and particle swarm optimization	2012	47

Table 5: Classification of Concerned Topics regarding PSO's Technique.

Theme/variants of PSO	Standard PSO	PSO with neural network	Improved/extended PSO	Hybridized PSO
Heart disease	[9, 16, 24, 25, 30, 32, 33, 37, 39, 42, 43, 57]	[14, 28]	[50, 51, 53, 54]	[46, 48]
Dental disease	[26]	—	—	—
Lymphatic disease	[8]	—	[55]	—
Celiac disease	[27]	—	—	—
Liver disease	[2, 24, 29, 34]	—	[51, 52, 55]	—
Cancer disease	[2, 24, 30–32, 34]	—	[15, 51, 53, 55, 56]	—
Brain disease	[24, 34–36, 38, 41, 44, 45]	—	[11, 13, 51, 55]	[47]
Hepatitis disease	[30, 40]	—	[51, 56]	—
Diabetes	[24, 30]	—	[49, 51, 53, 55, 56]	—
Others	—	[12]	[53]	—

Table 6: Improved Variants of PSO for Future work.

Sr no.	Title	Year	Reference
1	Particle swarm optimization using Sobol mutation	2008	[58]
2	A new hybrid MGBPSO-GSA variant for improving Function optimization solution in search space	2017	[59]
3	Multi-leader PSO (MLPSO): A new PSO variant for Solving global optimization problems	2017	[60]
4	Phasor particle swarm optimization: a simple and efficient variant of PSO	2019	[61]
5	An improved particle swarm optimization Algorithm with Chi-Square mutation strategy	2019	[62]

Table 7: List of Diseases need to apply in Future works.

Sr no.	Title	Year	Reference
1	Severe acute respiratory syndrome coronavirus 2 (SARS-CoV-2) and corona virus disease-2019 (COVID-19): The epidemic and the challenges	2020	[63]
2	A mouse-adapted SARS-coronavirus causes disease and mortality in BALB/c mice	2007	[64]
3	The definition \& classification of dry eye disease	2008	[65]
4	Ankle disease in juvenile idiopathic arthritis: Ultrasound findings in clinically swollen ankles	2009	[66]
5	Hydatid disease of the lungs	1992	[67]

7. Conclusion

PSO has been widely adopted to solve real-world nonlinear complex optimization problems in various areas. This study is shown a systematic review of existing studies on the standard PSO and its variants to diagnose the medical diseases for health care. Researchers have been suggested various PSO variants for medical disease diagnosis in health care, although, PSO still requires an extreme inspection to enhance its performance. The paper is giving detail on different medical diseases that have been utilized in numerous PSO approaches for solving medical disease detection in health care. We tried to give a systematic survey of various medical diseases and analyzed each PSO technique separately. In order to perform the systematic survey, the gaps in the literature are figured out and converted into six research questions. For the next stage, the research questions are taken into account for analysis, where the following points are briefly explained: the utilization of PSO and its variants in diseases detection, the worth of selected articles, the time division of published articles, generally encountered medical diseases, maximum applied PSO variants for disease detection. With the proper rate of growth in the research area, it is expected that additional work should be achieved in the future. The findings of this systematic survey depict that many researchers incorporated PSO and its variants to detect Heart disease, Cancer disease, Brain disease, Hepatitis disease, and Diabetes. Furthermore, the analytical results of the systematic survey illustrate that various scientists and researchers frequently targeted the Standard PSO and Improved versions of PSO for disease diagnosis. As the future direction, the researchers can utilize the improved versions of Neural Networks with PSO, as well as, can use the diverse hybridized versions of PSO for disease diagnosis. We anticipated that this survey will draw more attention to these problems and the substantial research will provide basic insight into how PSO mutation strategies enhance the performance of standard PSO in the health care domain. We are confident that such knowledge will encourage the PSO researchers to gain better awareness about a particular PSO, to enhance it, or to devise a new one.

Conflicts of Interest

The authors declare that they have no conflicts of interest.

References

[1] C. C. Bojarczuk, H. S. Lopes, and A. A. Freitas, "Genetic programming for knowledge discovery in chest-pain diagnosis," *IEEE Engineering in Medicine and Biology Magazine*, vol. 19, no. 4, pp. 38–44, 2000.

[2] P.-C. Chang, J.-J. Lin, and C.-H. Liu, "An attribute weight assignment and particle swarm optimization algorithm for medical database classifications," *Computer Methods and Programs in Biomedicine*, vol. 107, no. 3, pp. 382–392, 2012.

[3] M. Junaid, W. H. Bangyal, and J. Ahmad, "A novel bat algorithm using sobol sequence for the initialization of population," in *2020 IEEE 23rd International Multitopic Conference (INMIC)*, pp. 1–6, Bahawalpur, Pakistan, 2020.

[4] C. A. Pena-Reyesy and M. Sippery, "Evolving Fuzzy Rules for Breast cancer Diagnosis," in *Proceedings of 1998 International Symposium on Nonlinear Theory and Applications (NOLTA'98)*, pp. 1–4, Switzerland, 1998.

[5] K. P. Bennett and O. L. Mangasarian, *Neural Network Training Via Linear Programming*, University of Wisconsin-Madison Department of Computer Sciences, 1990.

[6] R. Setiono, "Extracting rules from pruned neural networks for breast cancer diagnosis," *Artificial Intelligence in Medicine*, vol. 8, no. 1, pp. 37–51, 1996.

[7] R. Setiono and Huan Liu, "Symbolic representation of neural networks," *Computer*, vol. 29, no. 3, pp. 71–77, 1996.

[8] W. A. O. Almayyan, "Lymph diseases prediction using random forest and particle swarm optimization," *Journal of Intelligent Learning Systems and Applications*, vol. 3, pp. 51–62, 2016.

[9] I. Babaoglu, O. Findik, E. Ulker, and N. Aygul, "A novel hybrid classification method with particle swarm optimization and k-nearest neighbor algorithm for diagnosis of coronary artery disease using exercise stress test data," *International Journal of Innovative Computing, Information and Control*, vol. 8, no. 5, pp. 3467–3475, 2012.

[10] W. H. Bangyal, A. Hameed, W. Alosaimi, and H. Alyami, "A new initialization approach in particle swarm optimization for global optimization problems," *Computational Intelligence and Neuroscience*, vol. 2021, Article ID 6628889, 17 pages, 2021.

[11] N. Zeng, H. Qiu, Z. Wang, W. Liu, H. Zhang, and Y. Li, "A new switching-delayed-PSO-based optimized SVM algorithm for diagnosis of Alzheimer's disease," *Neurocomputing*, vol. 320, pp. 195–202, 2018.

[12] S. Gambhir, S. K. Malik, and Y. Kumar, "PSO-ANN based diagnostic model for the early detection of dengue disease,"

New Horizons in Translational Medicine, vol. 4, no. 1-4, pp. 1–8, 2017.

[13] Y. Zhang, S. Wang, Y. Sui et al., "Multivariate approach for Alzheimer's disease detection using stationary wavelet entropy and predator-prey particle swarm optimization," *Journal of Alzheimer's Disease*, vol. 65, no. 3, pp. 855–869, 2018.

[14] G. K. Kumar, "An optimized particle swarm optimization based ANN model for clinical disease prediction," *Indian Journal of Science and Technology*, vol. 9, no. 21, 2016.

[15] S. Gunasundari, S. Janakiraman, and S. Meenambal, "Velocity bounded boolean particle swarm optimization for improved feature selection in liver and kidney disease diagnosis," *Expert Systems with Applications*, vol. 56, pp. 28–47, 2016.

[16] S. Shadmand and B. Mashoufi, "A new personalized ECG signal classification algorithm using block-based neural network and particle swarm optimization," *Biomedical Signal Processing and Control*, vol. 25, pp. 12–23, 2016.

[17] P. Brereton, B. A. Kitchenham, D. Budgen, M. Turner, and M. Khalil, "Lessons from applying the systematic literature review process within the software engineering domain," *Journal of Systems and Software*, vol. 80, no. 4, pp. 571–583, 2007.

[18] B. Kitchenham, ""procedures for performing systematic reviews," Keele, UK," *Keele University*, vol. 33, pp. 1–26, 2004.

[19] W. K. Bong, W. Chen, and A. Bergland, "Tangible user interface for social interactions for the elderly: a review of literature," *Advances in Human-Computer Interaction*, vol. 2018, Article ID 7249378, 15 pages, 2018.

[20] R. Parmezan Bonidia, J. Duilio Brancher, and R. Marques Busto, "Data mining in sports: a systematic review," *IEEE Latin America Transactions*, vol. 16, no. 1, pp. 232–239, 2018.

[21] V. Smith, D. Devane, C. M. Begley, and M. Clarke, "Methodology in conducting a systematic review of systematic reviews of healthcare interventions," *BMC Medical Research Methodology*, vol. 11, no. 1, p. 15, 2011.

[22] S. L. Menezes, R. S. Freitas, and R. S. Parpinelli, "Mining of massive data using hadoop mapreduce and bio-inspired algorithms: A systematic review," *Revista de Inform'atica Te'orica*, vol. 23, pp. 69–101, 2016.

[23] S. Karimi, S. Pohl, F. Scholer, L. Cavedon, and J. Zobel, "Boolean versus ranked querying for biomedical systematic reviews," *BMC Medical Informatics and Decision Making*, vol. 10, no. 1, p. 58, 2010.

[24] L.-F. Chen, C.-T. Su, K.-H. Chen, and P.-C. Wang, "Particle swarm optimization for feature selection with application in obstructive sleep apnea diagnosis," *Neural Computing and Applications*, vol. 21, no. 8, pp. 2087–2096, 2012.

[25] I. Yekkala, S. Dixit, and M. Jabbar, "Prediction of heart disease using ensemble learning and Particle Swarm Optimization," in *2017 International Conference On Smart Technologies For Smart Nation (SmartTechCon)*, pp. 691–698, Bengaluru, India, 2017.

[26] D. M. N. Fajri, W. F. Mahmudy, and Y. P. Anggodo, "Optimization of FIS Tsukamoto using particle swarm optimization for dental disease identification," in *2017 International Conference on Advanced Computer Science and Information Systems (ICACSIS)*, pp. 261–268, Bali, 2017.

[27] H. Nasiriyan-Rad, A. Amirkhani, A. Naimi, and K. Mohammadi, "Learning fuzzy cognitive map with PSO algorithm for grading celiac disease," in *2016 23rd Iranian Conference on Biomedical Engineering and 2016 1st International Iranian Conference on Biomedical Engineering (ICBME)*, pp. 341–346, Tehran, Iran, 2016.

[28] M. G. Feshki and O. S. Shijani, "Improving the heart disease diagnosis by evolutionary algorithm of PSO and Feed Forward Neural Network," in *2016 Artificial Intelligence and Robotics (IRANOPEN)*, pp. 48–53, Qazvin, Iran, 2016.

[29] P. Thangaraju and R. Mehala, "Performance analysis of PSO-KStar classifier over liver diseases," *International Journal of Advanced Research in Computer Engineering \& Technology*, vol. 4, no. 7, pp. 3132–3137, 2015.

[30] C. Subbulakshmi and S. Deepa, "Medical dataset classification: a machine learning paradigm integrating particle swarm optimization with extreme learning machine classifier," *The Scientific World Journal*, vol. 2015, 12 pages, 2015.

[31] A. Chinnaswamy and R. Srinivasan, "Hybrid feature selection using correlation coefficient and particle swarm optimization on microarray gene expression data," in *Advances in Intelligent Systems and Computing*, pp. 229–239, Springer, 2016.

[32] X. Liu and H. Fu, "PSO-based support vector machine with cuckoo search technique for clinical disease diagnoses," *The Scientific World Journal*, vol. 2014, Article ID 548483, 7 pages, 2014.

[33] N. Ghadiri Hedeshi and M. Saniee Abadeh, "Coronary artery disease detection using a fuzzy-boosting PSO approach," *Computational Intelligence and Neuroscience*, vol. 2014, Article ID 783734, 12 pages, 2014.

[34] Y.-Z. Hsieh, M.-C. Su, and P.-C. Wang, "A PSO-based rule extractor for medical diagnosis," *Journal of Biomedical Informatics*, vol. 49, pp. 53–60, 2014.

[35] M. E. Sweety and G. W. Jiji, "Detection of Alzheimer disease in brain images using PSO and Decision Tree Approach," in *2014 IEEE International Conference on Advanced Communications, Control and Computing Technologies*, pp. 1305–1309, Ramanathapuram, India, 2014.

[36] S.-T. Yang, J.-D. Lee, T.-C. Chang et al., "Discrimination between Alzheimer's disease and mild cognitive impairment using SOM and PSO-SVM," *Computational and Mathematical Methods in Medicine*, vol. 2013, Article ID 253670, 10 pages, 2013.

[37] A. Subasi, "Classification of EMG signals using PSO optimized SVM for diagnosis of neuromuscular disorders," *Computers in Biology and Medicine*, vol. 43, no. 5, pp. 576–586, 2013.

[38] S. Saraswathi, B. Mahanand, A. Kloczkowski, S. Suresh, and N. Sundararajan, "Detection of onset of Alzheimer's disease from MRI images using a GA-ELM-PSO classifier," in *2013 Fourth International Workshop on Computational Intelligence in Medical Imaging (CIMI)*, pp. 42–48, Singapore, 2013.

[39] S. Muthukaruppan and M. J. Er, "A hybrid particle swarm optimization based fuzzy expert system for the diagnosis of coronary artery disease," *Expert Systems with Applications*, vol. 39, no. 14, pp. 11657–11665, 2012.

[40] M. Neshat, M. Sargolzaei, A. Nadjaran Toosi, and A. Masoumi, "Hepatitis disease diagnosis using hybrid case based reasoning and particle swarm optimization," *ISRN Artificial Intelligence*, vol. 2012, Article ID 609718, 6 pages, 2012.

[41] C.-K. Huang, W. Wang, K.-Y. Tzen, W.-L. Lin, and C.-Y. Chou, "FDOPA kinetics analysis in PET images for Parkinson's disease diagnosis by use of particle swarm optimization," in *2012 9th IEEE International Symposium on Biomedical Imaging (ISBI)*, pp. 586–589, Barcelona, Spain, 2012.

Hindawi
Computational and Mathematical Methods in Medicine
Volume 2023, Article ID 9858237, 1 page
https://doi.org/10.1155/2023/9858237

Retraction

Retracted: Evaluating Deep Neural Network Architectures with Transfer Learning for Pneumonitis Diagnosis

Computational and Mathematical Methods in Medicine

Received 8 August 2023; Accepted 8 August 2023; Published 9 August 2023

This article has been retracted by Hindawi following an investigation undertaken by the publisher [1]. This investigation has uncovered evidence of one or more of the following indicators of systematic manipulation of the publication process:

(1) Discrepancies in scope

(2) Discrepancies in the description of the research reported

(3) Discrepancies between the availability of data and the research described

(4) Inappropriate citations

(5) Incoherent, meaningless and/or irrelevant content included in the article

(6) Peer-review manipulation

The presence of these indicators undermines our confidence in the integrity of the article's content and we cannot, therefore, vouch for its reliability. Please note that this notice is intended solely to alert readers that the content of this article is unreliable. We have not investigated whether authors were aware of or involved in the systematic manipulation of the publication process.

Wiley and Hindawi regrets that the usual quality checks did not identify these issues before publication and have since put additional measures in place to safeguard research integrity.

We wish to credit our own Research Integrity and Research Publishing teams and anonymous and named external researchers and research integrity experts for contributing to this investigation.

The corresponding author, as the representative of all authors, has been given the opportunity to register their agreement or disagreement to this retraction. We have kept a record of any response received.

References

[1] S. Krishnamurthy, K. Srinivasan, S. M. Qaisar, P. M. D. R. Vincent, and C. Chang, "Evaluating Deep Neural Network Architectures with Transfer Learning for Pneumonitis Diagnosis," *Computational and Mathematical Methods in Medicine*, vol. 2021, Article ID 8036304, 12 pages, 2021.

Hindawi
Computational and Mathematical Methods in Medicine
Volume 2021, Article ID 8036304, 12 pages
https://doi.org/10.1155/2021/8036304

Research Article

Evaluating Deep Neural Network Architectures with Transfer Learning for Pneumonitis Diagnosis

Surya Krishnamurthy,[1] **Kathiravan Srinivasan**,[2] **Saeed Mian Qaisar**,[3] **P. M. Durai Raj Vincent**,[4] **and Chuan-Yu Chang**[5]

[1]*iQGateway, Bangalore, India*
[2]*School of Computer Science and Engineering, Vellore Institute of Technology (VIT), Vellore, India*
[3]*Electrical and Computer Engineering Department, Effat University, Jeddah, Saudi Arabia*
[4]*School of Information Technology and Engineering, Vellore Institute of Technology (VIT), Vellore, India*
[5]*Department of Computer Science and Information Engineering, National Yunlin University of Science and Technology, Yunlin 64002, Taiwan*

Correspondence should be addressed to Chuan-Yu Chang; chuanyu@yuntech.edu.tw

Received 3 August 2021; Accepted 30 August 2021; Published 13 September 2021

Academic Editor: Muhammad Zubair Asghar

Pneumonitis is an infectious disease that causes the inflammation of the air sac. It can be life-threatening to the very young and elderly. Detection of pneumonitis from X-ray images is a significant challenge. Early detection and assistance with diagnosis can be crucial. Recent developments in the field of deep learning have significantly improved their performance in medical image analysis. The superior predictive performance of the deep learning methods makes them ideal for pneumonitis classification from chest X-ray images. However, training deep learning models can be cumbersome and resource-intensive. Reusing knowledge representations of public models trained on large-scale datasets through transfer learning can help alleviate these challenges. In this paper, we compare various image classification models based on transfer learning with well-known deep learning architectures. The Kaggle chest X-ray dataset was used to evaluate and compare our models. We apply basic data augmentation and fine-tune our feed-forward classification head on the models pretrained on the ImageNet dataset. We observed that the DenseNet201 model outperforms other models with an AUROC score of 0.966 and a recall score of 0.99. We also visualize the class activation maps from the DenseNet201 model to interpret the patterns recognized by the model for prediction.

1. Introduction

Pneumonitis is an acute infection of the lungs characterized by inflammation in the alveoli. The filling of alveoli with pus and fluids results in breathing difficulty, painful breathing, and a lack of oxygen intake. Pneumonitis infections can be caused by viral, bacterial, and fungal agents where bacterial is the most common and viral infection the most dangerous. They are the leading infectious cause of death in children under the age of 5. They are also one of the leading causes of death in developing countries and the chronically ill. Early detection of pneumonitis is essential to avoid serious complications and fatal consequences. They are commonly detected by examining the chest X-rays of the patient to locate the infected regions. Chest X-rays are also inexpensive and can be acquired in a short period. Distinguishing features like air-space opacities in the X-ray images often suggest pneumonitis. Not only is examining chest X-rays to detect pneumonitis a tedious task, but finding radiological examiners in some remote parts of the world is challenging [1]. Therefore, machine learning approaches on medical images like X-rays are a viable alternative. They can aid radiologists in rapid and efficient pneumonitis detection. Highly accurate models can even perform an independent diagnosis of pneumonitis.

With efficient deep learning approaches replacing the tedious traditional approaches of handcrafting useful features, neural network-based medical diagnosis systems are very accurate [2–5]. Particularly, models like convolutional neural networks (CNNs) are capable of capturing and exposing relevant and informative features from images, making them a powerful approach to feature extraction of medical images. Recently, transformers, which are self-attention-based neural network architectures that were originally designed for Natural Language Processing (NLP), show promising performance in computer vision (CV). One can build custom architectures or use tested popular architectures from the literature that are readily available and abstracted away in several deep learning programming frameworks like TensorFlow. However, with several available components to choose from to build a deep neural network (DNN), building and tuning DNN models can be cumbersome and time-consuming. Furthermore, the best performing models are often deep networks with a large number of parameters which place constraints on the space and time complexity in regard to training these models. These deep networks also require large datasets to learn the underlying feature representations and generalize to unseen data. Acquiring such large datasets is often not practical in the medical domain. Most of these limitations can be addressed by using a popular technique called transfer learning. In this technique, we use models trained on large-scale datasets and fine-tune them to our target dataset for a few iterations. Despite the variation in the distribution of the source dataset from the target dataset, the approach is surprisingly effective in medical image classification tasks. They can also be trained in a significantly shorter time as opposed to the several hours required to train an entire DNN model. In this work, we investigate transfer learning for pneumonitis classification from X-ray images with several neural network architectures.

The key contributions of the paper are as follows:

(1) We demonstrate that transfer learning using pretrained ImageNet models can achieve excellent performance in the pneumonitis classification task

(2) We apply data augmentation to improve the model performance and generalization

(3) We conduct a performance evaluation and comparison of popular DNN-based approaches for pneumonitis detection from chest X-ray images

(4) We fine-tune the feed-forward classification head on various pretrained models and evaluate the models on a test set. Our best performing DenseNet201 model achieves an AUROC of 96.6%

(5) Visual interpretation of the predictions of the best performing DenseNet201 model through Grad-CAM

The rest of the paper is organized as follows. We review various works on pneumonitis detection in Related Work. Materials and Methods provides an introduction to the DNN architectures investigated in this work and discusses the implementation details. We present the results of our experiment in Results and Discussion. Finally, we conclude the study and discuss the limitations and future work.

2. Related Work

Due to their high predictive power, neural networks are extensively used in biomedical image classification tasks. Sarvamangala surveys CNNs for medical image understanding [6]. Litjens et al. summarize 300 papers on deep learning for medical image analysis [7]. Ma et al. survey several works on various tasks for deep learning in the analysis of pulmonary medical images [8]. Liu et al. perform a comparison of deep learning models in detecting diseases from medical images [9]. Esteva et al. summarize the progress of deep learning-based medical computer vision over the past decade [10].

Varela-Santos et al. derive texture features Gray Level Cooccurrence matrix and feed it to a feed-forward neural network [11]. Sirazitdinov et al. use an ensemble of RetinaNet and Mask R-CNN for pneumonitis detection and localization [12]. Yue et al. use the Kaggle chest X-ray dataset to perform pneumonitis classification using MobileNet along with other architectures by training for 20 epochs [13]. Elshennawy and Ibrahim also report a good accuracy with MobileNet and ResNet models when the entire network was retrained [14]. Jain et al. compare their CNN models against pretrained VGG, ResNet, and Inception models [15]. Ayan et al. use transfer learning with VGG16 and Xception models and report 87% and 82% accuracy, respectively [16]. Salvatore et al. use the ensemble of ResNet50 architecture from 10-fold cross-validation using the TRACE4 platform on a chest X-ray dataset for COVID-19 predicting COVID-19 pneumonia [17]. They show promising results on two independent test sets along with their cross-validation dataset. The InstaCovNet-19 model by Gupta et al. uses stacking of pretrained InceptionV3, MobileNetV2, ResNet101, NASNet, and Xception models to achieve an accuracy of 99% in detecting COVID-19 and pneumonia [18].

High predictive performance can be obtained by developing architectures specific to our domain task and utilizing datasets from multiple sources. Karthik et al. used chest X-ray images for pneumonitis compiled from multiple sources and achieved a high accuracy of 99.8% using a custom architecture called shuffled residual CNN [19]. Rajasenbagam et al. used a DCGAN-based augmentation technique coupled with a VGG19 network on the Chest X-ray8 dataset [20]. Stephen et al. explore the performance of a custom CNN model [21]. Walia et al. developed a depthwise convolutional neural network that outperforms inception and VGG networks on the Kaggle chest X-ray dataset [22]. CheXNet by Rajpurkar et al. achieves remarkable accuracy on the ChestX-ray14 dataset in classifying 14 diseases [23]. Harmon et al. train deep learning algorithms on a multinational dataset containing chest CT scan to localize lung regions and use the crop to classify COVID-19 pneumonia [24]. They achieve an AUROC score of 95% on the testing set. Hussain et al. developed a CNN architecture called

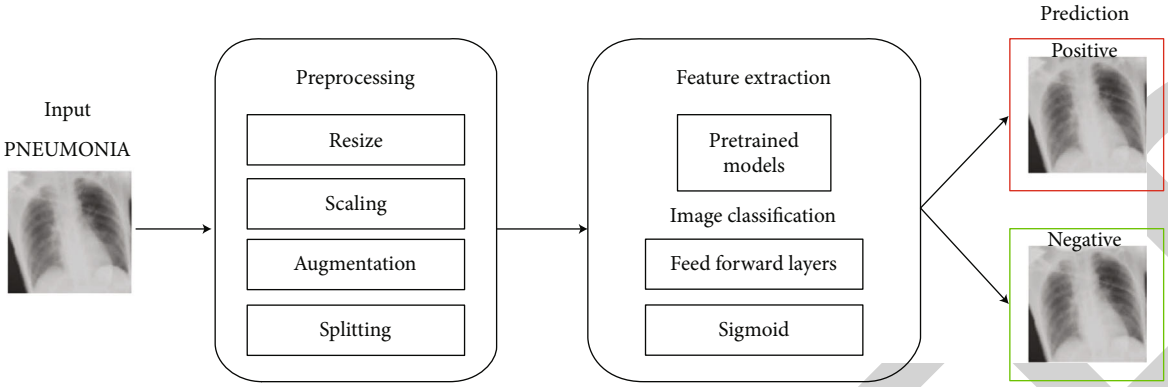

Figure 1: Pneumonitis diagnosis pipeline using DNN models.

CoroDet that achieves 99% accuracy in detecting COVID-19 pneumonia with 99% accuracy on chest X-ray and CT images containing the labels normal, non-COVID pneumonia, and COVID pneumonia [25].

3. Materials and Methods

3.1. Convolutional Neural Network. Convolutional neural networks are constructed by using several convolution layers which use learnable filters or kernels to identify patterns in images such as edges, texture, color, and shapes. CNN models possess several desirable properties that enable the extraction of complex features in images that would otherwise be hard to distill [26]. Since the success of AlexNet in the ImageNet large-scale image classification competition, several variants of CNNs have been invented that explore a variety of approaches to overcome the limitations of the standard CNN models [27].

By learning the appropriate filters using gradient descent-based optimizers, CNN can capture spatial and temporal connections in an image. They hierarchically construct high-level features from low-level features that help CNNs to effectively discriminate between the various objects present in an image. Another desirable characteristic of the CNN algorithm is parameter sharing. Since the same parameters (filters) are reused to compute specific features in different spatial positions of an input image, the number of parameters used is dramatically reduced.

Convolution layers are commonly used in tandem with other components in the network. An activation layer introduces nonlinearity between layers, which allows the network to capture the complicated relationship present in the input features. While the Rectified Linear Unit Layer is a commonly used activation function, more such functions are also available. To reduce the size of feature representations as we propagate deeper into the network, downsampling layers like max-pooling and average pooling are also used. For classification, output layers like softmax or sigmoid convert the output values into probability densities.

3.2. Image Transformers. These are architectures inspired by the success of the transformer in NLP. These models apply self-attention to the input (patches or pixels of an image, for example) to capture dependencies in the patterns on the input image. They generally involve pretraining the network on large-scale datasets through self-supervised or supervised approaches followed by fine-tuning on downstream tasks.

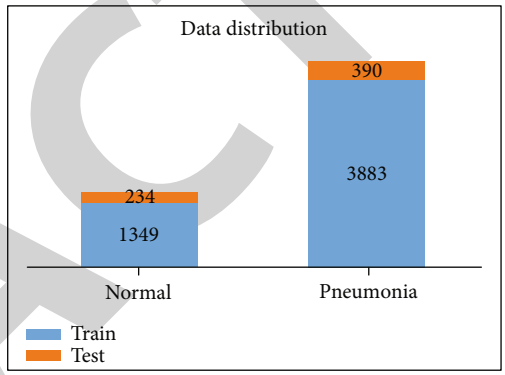

Figure 2: Distribution of the chest X-ray dataset.

3.3. Transfer Learning. DNNs can be extremely hard and expensive to train, especially when deep networks with a large number of parameters and FLOPS are required. However, several popular DNN models are built using powerful infrastructure on large-scale datasets with diverse classes (ImageNet, JFT, etc.). As such, they can capture patterns from a wide range of image inputs and are excellent feature extractors. This concept of reusing knowledge representations learnt from one task to another task is called transfer learning. One can use these estimated weights as initial weights to warm start their neural network optimization process. A more economical alternative is to freeze the weights in all layers except the penultimate layer of the network and fine-tune them for the target task. In this work, we examine the latter approach. In this section, we present the detailed approach and techniques used in the study. We leverage the pretrained models, utilities, and model training tools available in the TensorFlow framework. The overall pipeline of this study is described in Figure 1.

3.3.1. ResNet101V2. Residual networks use the concept of skip or shortcut connections to effectively retain information

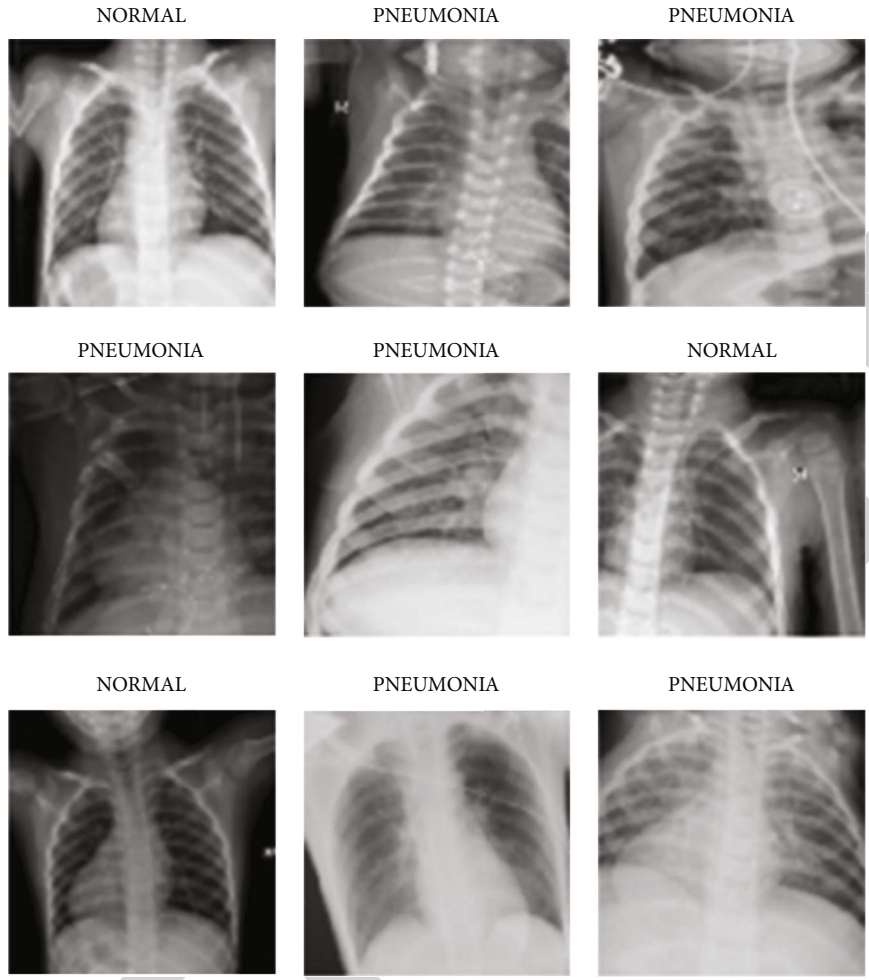

Figure 3: Sample images from the dataset.

through the layers of DNN by mitigating the vanishing gradient problem. We use the ResNet101V2 variant in this work. Unlike the NN layers, residual networks help learn features effectively at the lower and higher levels while training the network.

3.3.2. DenseNet201. Unlike standard CNN models in which each convolutional layer is connected only to the previous layer, DenseNet layers use the feature maps of all preceding layers as the input in a feed-forward fashion. We use the DenseNet201 model for our analysis. It addresses various issues like vanishing gradient issues and provides advantages like improved feature propagation and a reduced number of parameters.

3.3.3. InceptionV3 and InceptionResNetV2. These are "wide" CNN models that stack the output of convolution kernels with varying sizes on an input. The Inception-ResNet model integrates the residual connections from ResNet to Inception. Instead of making the network deep, it makes it wide to help resolve vanishing gradient issues. The architecture also introduces two auxiliary classifiers that improve convergence. We use the InceptionV3 and InceptionResNetV2 models in this work.

Table 1: Augmentations applied along with their parameters.

Method	Parameter (range)
Rotation	30°
Zoom	0.85 to 1.15
Width and height shift	0.2
Shear	0.15
Horizontal flip	True

3.3.4. Xception. The model extends inception model by incorporating depthwise separable convolution layers. These layers apply a depthwise convolution followed by a pointwise convolution to efficiently utilize the model parameters. It is an improved version of Inception using the depthwise separable convolution built by researchers of Google. Here, the order of operation is different from the original one since 1×1 convolution is applied first and then the channel-wise spatial convolution. Another difference is that here there is no intermediate ReLU nonlinearity.

3.3.5. MobileNetV2. These are lightweight models that were originally intended for low-resource environments like mobile and embedded devices [28]. They introduce several

advanced techniques to develop light neural network models. The most important of them is the use of depthwise separable convolutions. The models are optimized to efficiently trade off between various factors like accuracy, latency, width, and resolution. We use the MobileNetV2 model in this work for our analysis.

3.3.6. NASNetMobile. These are models designed using Neural Architecture Search (NAS) on small-scale datasets like CIFAR-10 and transferred to large-scale datasets like ImageNet. NASNetMobile is a convolutional neural network that is trained on more than a million images from the ImageNet database. As a result, the network has learned rich feature representations for a wide range of images. We use the NASNetMobile model for our analysis. In NASNet, although the overall architecture is predefined, the blocks or cells are searched by a reinforcement learning method. Only the structures of (or within) the Normal and Reduction Cells are searched by the controller RNN (Recurrent Neural Network).

3.3.7. ViT. The Vision Transformer (ViT) architecture uses linear projections of patches of an image as inputs for the multihead self-attention component of the transformer [29]. We use the ViT-B/16 variant of the ImageNet weights. ViT splits an image into patches, then flattens the patches, and produces lower-dimensional linear embeddings from these flattened patches. Furthermore, ViT includes positional embeddings in the sequence of image patches which it then feeds as an input to a standard transformer encoder. The transformers are pretrained on large datasets like ImageNet or JFT-300M. Unlike the transformers in language models that use self-supervised pretraining, we report a better performance with a supervised pretraining approach.

3.4. Dataset. We use chest X-ray images for pneumonitis classification by Kermany et al. [30] for developing neural network-based pneumonitis diagnosis model. The dataset contains high-quality, expert-graded images of chest X-ray images with labels indicating normal and pneumonitis-infected lungs. The pneumonitis category includes images for both bacterial and viral infections. The dataset includes 5248 images for training and 624 images for evaluation. The dataset distribution is shown in Figure 2, and some sample images are shown in Figure 3.

3.5. Data Preprocessing. We retain 10% of the training data as our validation split for early stopping. Images are resized to 224×224 and scaled to -1 to $+1$ range. Data augmentation techniques are randomly applied to artificially increase the size of the datasets and make the models robust to variations in the data. Data augmentation can help increase the generalizability of the model to unseen data. The various augmentations applied and their respective parameters are shown in Table 1. When performing augmentation, the pixels outside the boundary of the image are extrapolated using a nearest neighbor approach.

3.6. Setup, Training, and Evaluation. We perform transfer learning on various mainstream CNN architectures, retaining the convolution layer and modifying the feed-forward layer for our dataset. The models chosen were selected for experimentation. We use the pretrained ImageNet weights available in the Keras application module. Models are built with TensorFlow 2.4.1 on a Tesla P100 GPU.

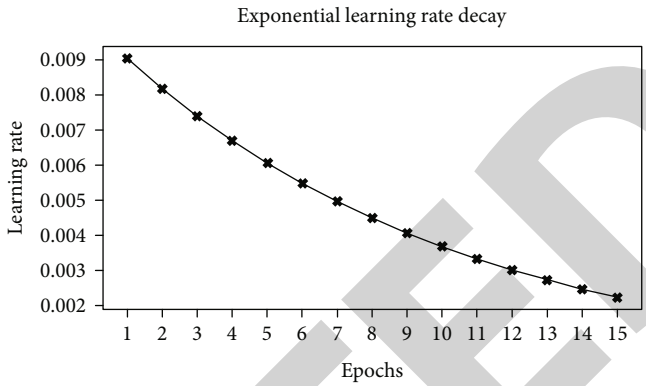

Figure 4: Epoch vs. learning rate.

Table 2: Hyperparameters and its associated values.

Hyperparameter	Value
Optimizer	Stochastic gradient descent
Initial learning rate	0.01
Learning rate decay	Exponential, decay rate 0.1
Epochs	15
Batch size	32
Feed-forward classification head	128, 128 (ReLU activated)

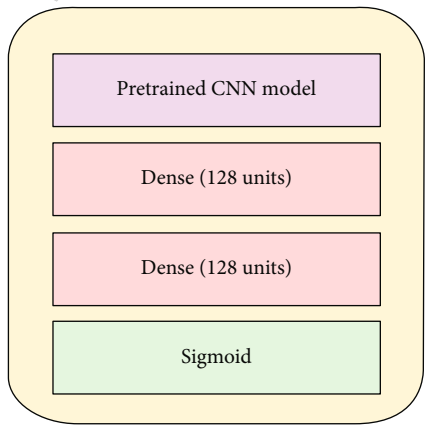

Figure 5: Transfer learning architecture.

During training, the convolution layers are frozen and only the custom feed-forward layers are trained. This allows the reuse of the filters that are already learned from the ImageNet dataset and avoids expensive retraining of the entire network. We use an exponential learning rate decay defined as follows where k is the decay rate and t is the current epoch. The epoch vs. learning rate curve is shown for the scheduler in Figure 4.

$$\mathrm{lr}_t = \mathrm{lr}_{t-1} \exp(-k). \quad (1)$$

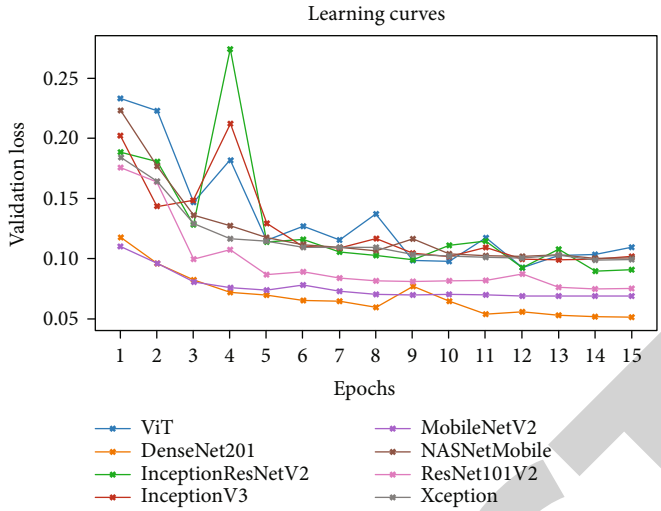

Figure 6: The learning curves of the different DNN models.

We repeat the approach for different DNN architectures and record the different performance metrics and the number of parameters in the network. We use a single validation/development split for monitoring the model training and identifying optimal hyperparameters. Hyperparameters were manually tuned to optimize the loss and the AUROC score. The test set is used for evaluating the performance of the tuned model and calculating the performance metrics and is not used in the model development process. Table 2 shows the different hyperparameters and its associated values.

Furthermore, we plot the class activation maps of the DenseNet201 model to visualize the regions of the inputs that were considered important by the model. We use the Gradient-weighted Class Activation Mapping (Grad-CAM) approach to provide visual explanations of predictions through coarse localization maps [31]. The generic architecture for our transfer learning approach is shown in Figure 5.

4. Results and Discussion

Figure 6 represents the learning curves of the different DNN models. Figures 7–10 show the testing AUROC, precision scores, recall scores, and accuracy scores of the different DNN models used in the analysis. The primary metrics in clinical diagnosis systems are recall, which is defined as the model's ability to correctly diagnose a condition and the false positive rate (FPR) [32–37]. The area under the receiver operator characteristic curve (AUROC) allows us to identify the model that best maximizes recall and minimizes FPR. We use AUROC as our primary metric of evaluation. The ROC curve is a diagnostic graphical illustration of the recall and FPR scores of a model at different cut-off points. A model's curve close to the 45-degree line is considered random. A model with high discriminating ability will have more area under its curve. We also present the specificity score (1—FPR) of our models.

The best performing model is the DenseNet201 model with an AUROC of 96.7%. Figures 11–18 illustrates the normalized confusion matrix of the various DNN models. The confusion matrix of the DenseNet201 model in Figure 11 shows a high true positive rate, which is optimal for medical

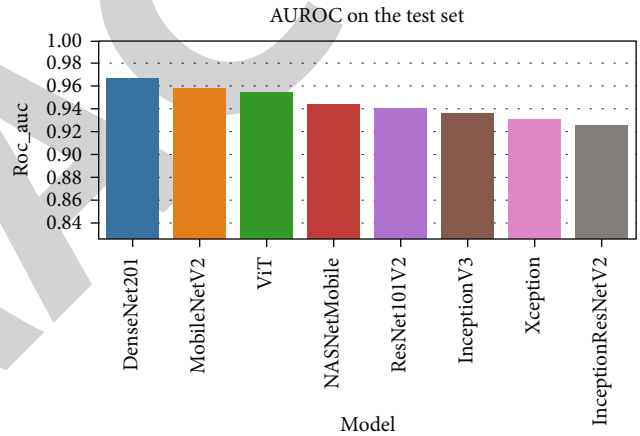

Figure 7: The comparison of the AUROC for various DNN models.

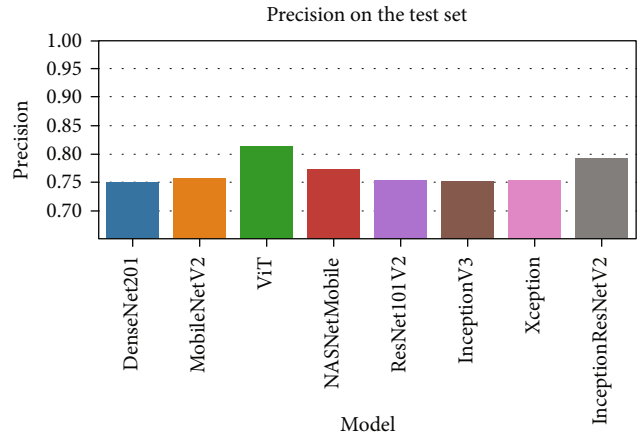

Figure 8: The comparison of the precision scores for various DNN models.

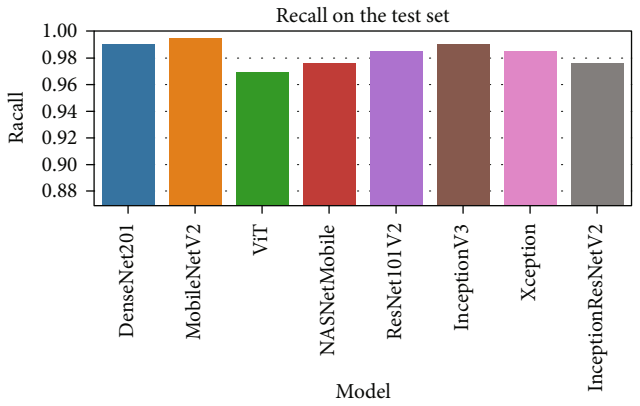

Figure 9: The comparison of the recall scores for various DNN models.

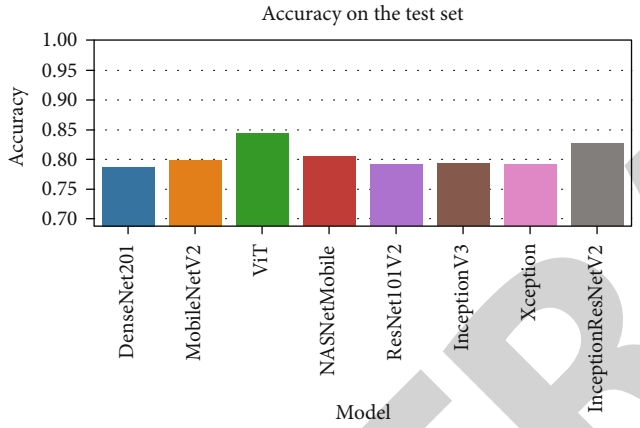

Figure 10: The comparison of the accuracy scores for various DNN models.

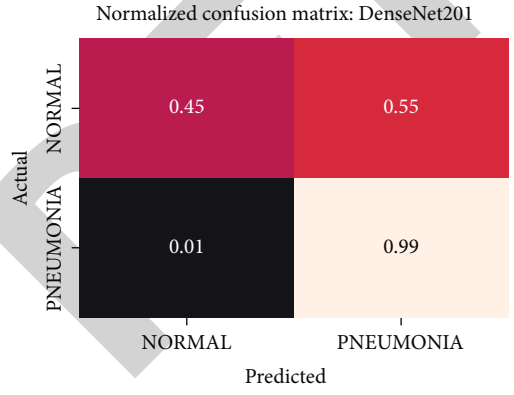

Figure 11: Normalized confusion matrix of the DenseNet201 model.

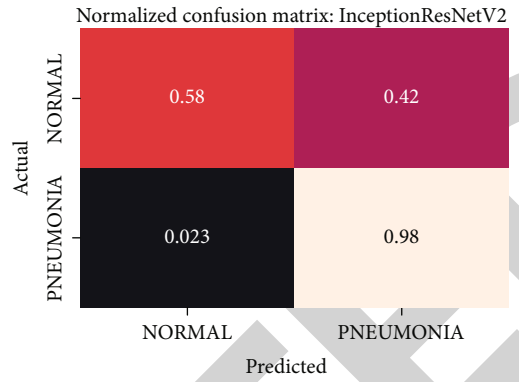

Figure 12: Normalized confusion matrix of the InceptionResNetV2 model.

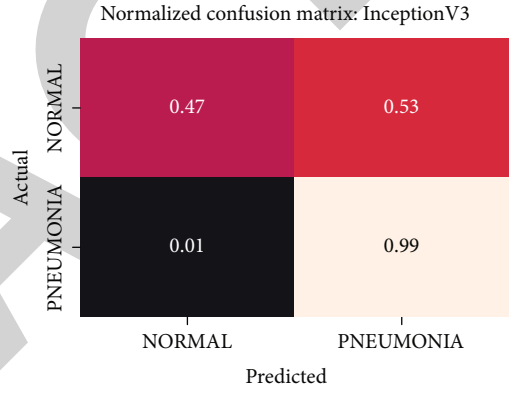

Figure 13: Normalized confusion matrix of the InceptionV3 model.

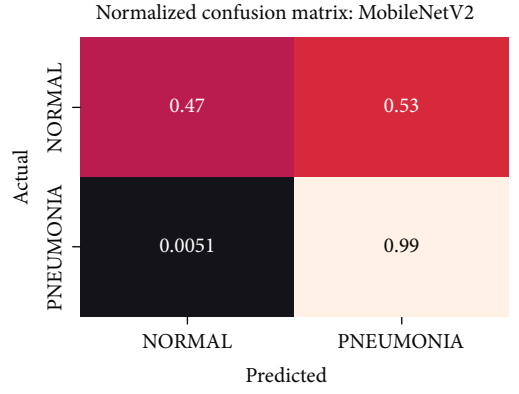

Figure 14: Normalized confusion matrix of the MobileNetV2 model.

diagnosis. Figure 6 shows that DenseNet201 model converges faster compared to the other methods. Further, the MobileNetV2 model shows the best balance between model size and predictive performance.

Figures 19–26 depict the ROC curves of the DenseNet201, ViT, MobileNetV2, NASNetMobile, ResNet101V2, Xception, InceptionV3, and InceptionResNetV2 models, respectively. The curves show how the TPR and FPR vary as the threshold values are varied. Generally, we see the FPR quickly increases as the TPR increases. Furthermore, the Grad-CAM heatmaps of DenseNet201 in Figure 27 reveal that the model, for the most part, does an excellent

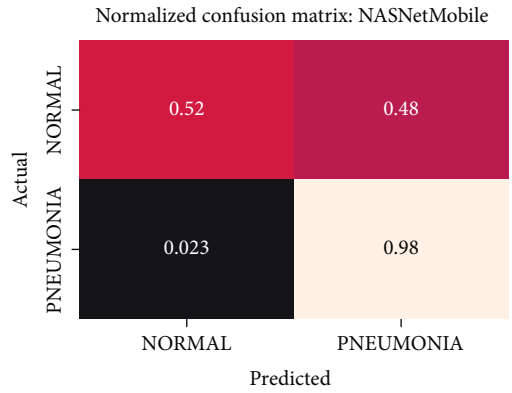

Figure 15: Normalized confusion matrix of the NASNetMobile model.

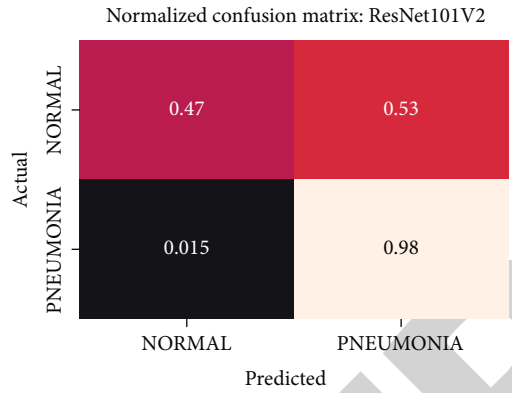

Figure 16: Normalized confusion matrix of the ResNet101V2 model.

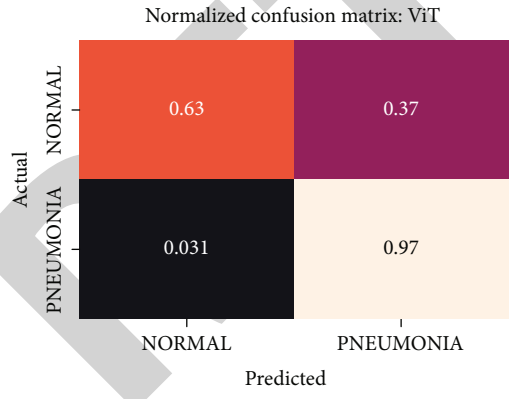

Figure 17: Normalized confusion matrix of the ViT model.

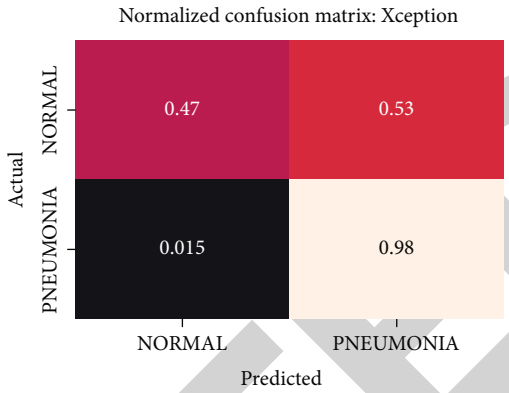

Figure 18: Normalized confusion matrix of the Xception model.

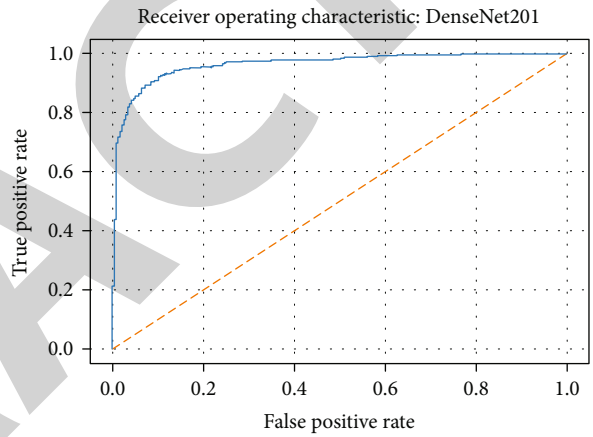

Figure 19: ROC curve of the DenseNet201 model.

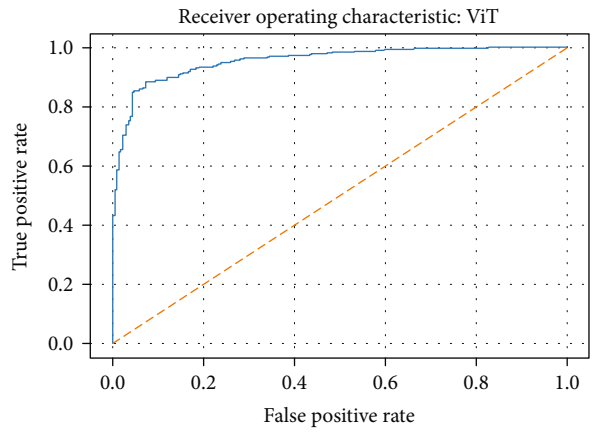

Figure 20: ROC curve of the ViT model.

job of attending to the regions of increased opacity which are often indicative of pneumonitis. The ViT model is well balanced for different performance metrics compared to the other models. Some models show a higher recall score than the DenseNet201 model but underperform with respect to the other metrics. This model bias is a consequence of the skewed distribution of the labels, where the positive labels are roughly three times the negative labels.

From our experiments, we observed that models with feature reusing techniques (DenseNet201, ResNet101V2, and MobileNetV2) and wider networks (Xception and NASNetMobile) perform significantly better. One possible explanation for this could be that with pretrained networks, not all learned feature maps could be relevant to downstream domains (X-ray lung images in this case). In wider networks, we alleviate the performance bottleneck

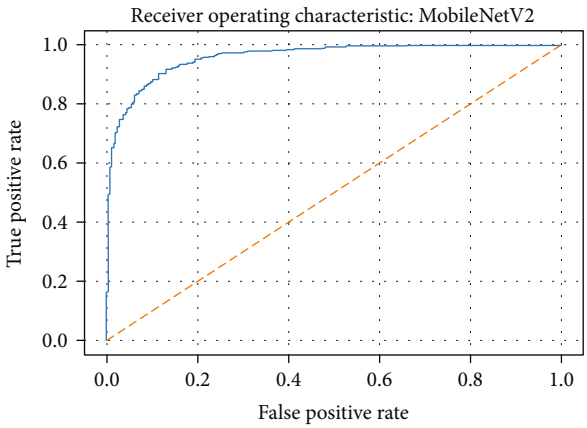

Figure 21: ROC curve of the MobileNetV2 model.

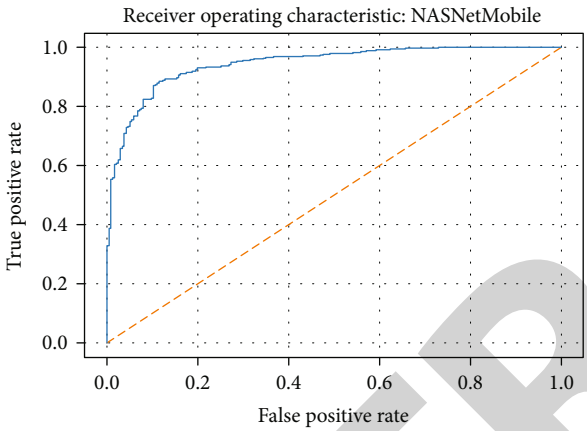

Figure 22: ROC curve of the NASNetMobile model.

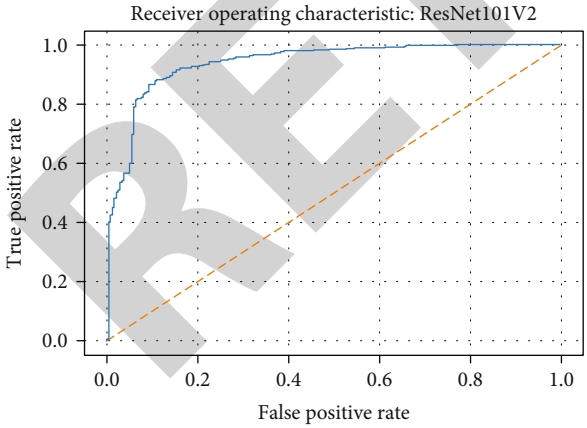

Figure 23: ROC curve of the ResNet101V2 model.

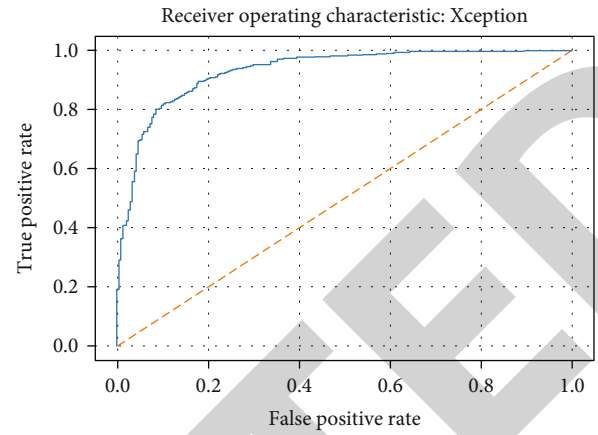

Figure 24: ROC curve of the Xception model.

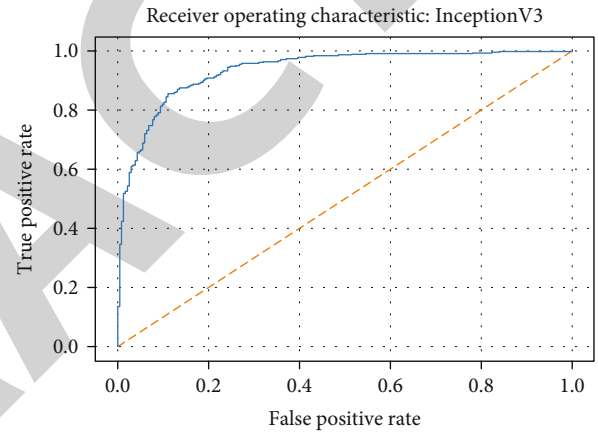

Figure 25: ROC curve of the InceptionV3 model.

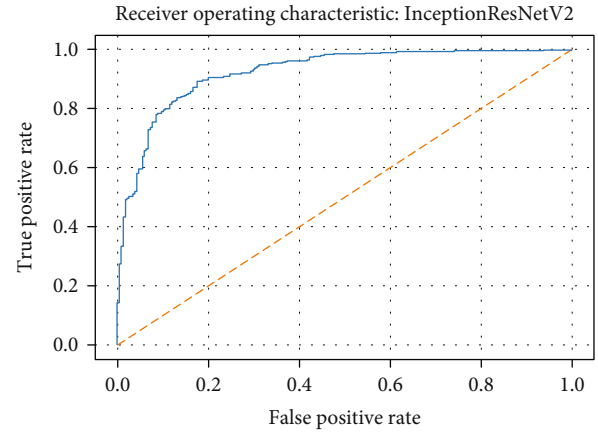

Figure 26: ROC curve of the InceptionResNetV2 model.

from compounding "irrelevancy" in the feature maps as we go deeper in the network that could cause an eventual loss of information. We also see a general improvement of performance with the size of the models as expected. The models also train remarkably fast, with most models completing an epoch in around a minute. Table 3 lists the performance metrics of the compared DNN models. Table 4 shows the number of parameters in each model. Note that while the training configuration is similar, to make the comparison fair, we can obtain higher accuracy by tuning the individual models with more trainable layers, different optimizers, etc.

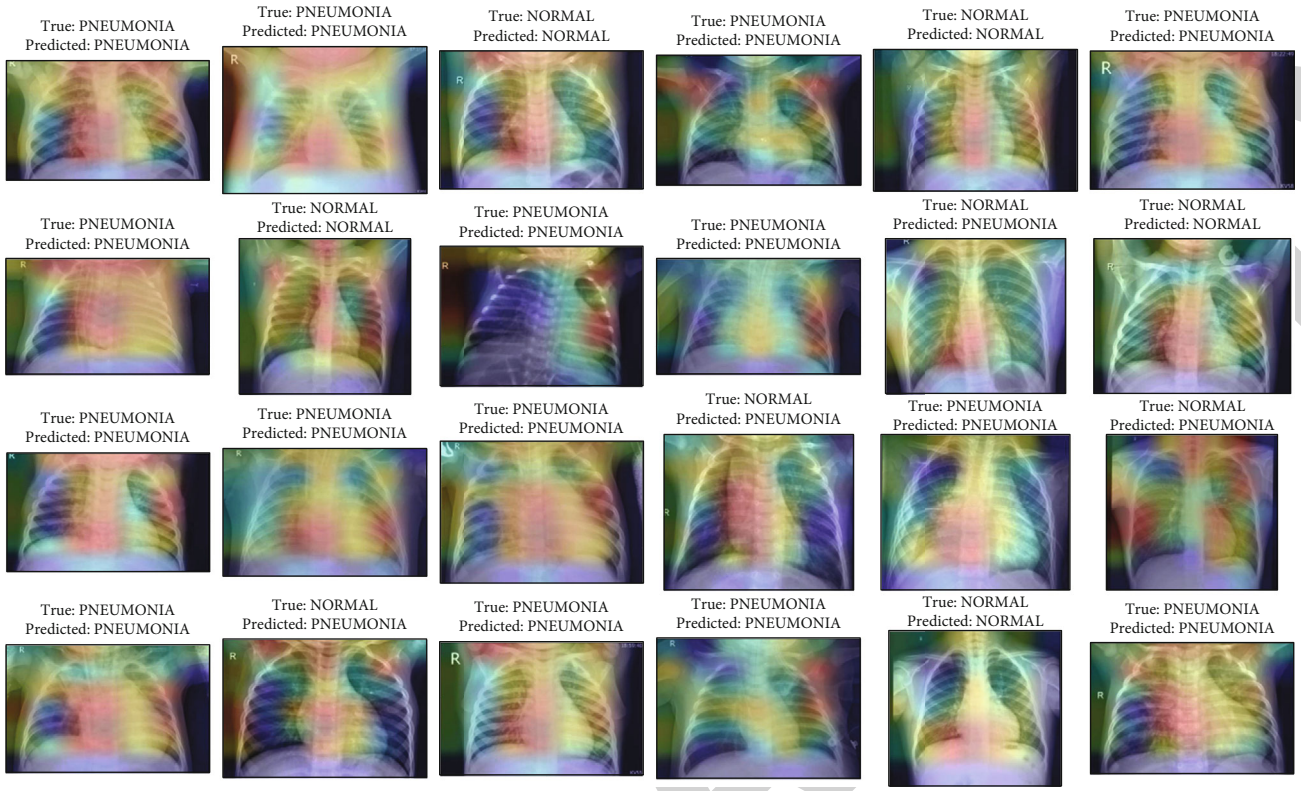

Figure 27: Activation maps from Grad-CAM on DenseNet201 along with the predictions on some sample images from the test set.

Table 3: Performance metrics of the compared DNN models.

Model	Accuracy	Precision	Recall	AUROC
DenseNet201	0.788	0.751	0.99	0.967
ViT	0.8	0.759	0.995	0.959
MobileNetV2	0.843	0.815	0.969	0.955
NASNetMobile	0.806	0.773	0.977	0.945
ResNet101V2	0.792	0.756	0.985	0.94
Xception	0.793	0.755	0.99	0.936
InceptionV3	0.792	0.756	0.985	0.931
InceptionResNetV2	0.827	0.794	0.977	0.926

Table 4: Number of parameters in the models compared.

Model	Number of parameters (in millions)
MobileNetV2	2.44
NASNetMobile	4.42
DenseNet201	18.58
Xception	21.14
InceptionV3	22.08
ResNet101V2	42.91
InceptionResNetV2	54.55
ViT	85.91

5. Conclusion

In this study, we perform a comparative analysis of transfer learning with various deep neural network models for pneumonitis detection from chest X-ray images. With some minimal preprocessing and hyperparameter tuning, our best performing DenseNet achieved an AUROC score of 96.7% on the test set. The Grad-CAM activations indicate the reliability of the predictions of the model. The high accuracy of the models indicates the efficacy of these models in the task. The models were also easier to implement using deep learning frameworks like TensorFlow. They also trained considerably faster compared to training the entire network.

Due to limitations in computational resources, we limit our experiments to Kermany et al.'s chest X-ray images and fine-tuning with frozen layers. In the future, we can expand our experiments to include transfer learning with warm-start and retraining. We can also report the performance metrics on multiple dataset sources to assess the generalization. To adopt these models to practice, additional experiments like probability calibration, threshold, and bias identification need to be performed and are outside the scope of our current work, which focuses on the general efficiency of different DNN architectures with transfer learning. Further, the future investigations could be devised for addressing the queries that are clinically relevant, and the effectiveness of advanced deep learning approaches would aid the radiologists and physicians for precisely accomplishing the pneumonitis detection from the chest X-ray images.

Nevertheless, the results presented in this work can help specialists make the best choices for their models, eliminating the need for an exhaustive search. Transfer learning with deep neural networks alleviates several issues associated with model training and allows us to build accurate models for pneumonitis detection, which helps in the early detection and management of pneumonitis.

Data Availability

The dataset used in this study is available at https://data.mendeley.com/datasets/rscbjbr9sj/3.

Conflicts of Interest

The authors declare that there is no conflict of interest regarding the publication of this paper.

Acknowledgments

This work was supported by the Ministry of Science and Technology, Taiwan (Grant no. MOST109-2221-E-224-048-MY2). This research was partially funded by the "Intelligent Recognition Industry Service Research Center" from the Featured Areas Research Center Program within the framework of the Higher Education Sprout Project by the Ministry of Education (MOE) in Taiwan.

References

[1] R. B. George, *Chest Medicine: Essentials of Pulmonary and Critical Care Medicine*, Lippincott Williams & Wilkins, 2005.

[2] S. Rajasegarar, C. Leckie, M. Palaniswami, and J. C. Bezdek, "Quarter sphere based distributed anomaly detection in wireless sensor networks," in *2007 IEEE International Conference on Communications*, pp. 3864–3869, Glasgow, UK, 2007.

[3] T. R. Gadekallu, M. Alazab, R. Kaluri et al., "Hand gesture classification using a novel CNN-crow search algorithm," *Complex & Intelligent Systems*, vol. 7, no. 4, pp. 1855–1868, 2021.

[4] T. R. Gadekallu, D. S. Rajput, M. P. Reddy et al., "A novel PCA–whale optimization-based deep neural network model for classification of tomato plant diseases using GPU," *Journal of Real-Time Image Processing*, vol. 18, no. 4, pp. 1383–1396, 2021.

[5] L. Lan, W. Sun, D. Xu et al., "Artificial intelligence-based approaches for COVID-19 patient management," *Intelligent Medicine*, vol. 1, no. 1, pp. 10–15, 2021.

[6] D. R. Sarvamangala, "Convolutional neural networks in medical image understanding: a survey," *Evolutionary intelligence*, pp. 1–22, 2021.

[7] G. Litjens, T. Kooi, B. E. Bejnordi et al., "A survey on deep learning in medical image analysis," *Medical Image Analysis*, vol. 42, pp. 60–88, 2017.

[8] J. Ma, Y. Song, X. Tian, Y. Hua, R. Zhang, and J. Wu, "Survey on deep learning for pulmonary medical imaging," *Frontiers in Medicine*, vol. 14, no. 4, pp. 450–469, 2020.

[9] X. Liu, L. Faes, A. U. Kale et al., "A comparison of deep learning performance against health-care professionals in detecting diseases from medical imaging: a systematic review and meta-analysis," *The lancet digital health*, vol. 1, no. 6, pp. e271–e297, 2019.

[10] A. Esteva, K. Chou, S. Yeung et al., "Deep learning-enabled medical computer vision," *NPJ digital medicine*, vol. 4, no. 1, pp. 1–9, 2021.

[11] S. Varela-Santos and P. Melin, "Classification of X-Ray Images for Pneumonia Detection Using Texture Features and Neural Networks," in *Intuitionistic and Type-2 Fuzzy Logic Enhancements in Neural and Optimization Algorithms: Theory and Applications. Studies in Computational Intelligence*, O. Castillo, P. Melin, and J. Kacprzyk, Eds., vol. 862, Springer, Cham, 2020.

[12] I. Sirazitdinov, M. Kholiavchenko, T. Mustafaev, Y. Yixuan, R. Kuleev, and B. Ibragimov, "Deep neural network ensemble for pneumonia localization from a large-scale chest X-ray database," *Computers and Electrical Engineering*, vol. 78, pp. 388–399, 2019.

[13] Z. Yue, L. Ma, and R. Zhang, "Comparison and validation of deep learning models for the diagnosis of pneumonia," *Computational Intelligence and Neuroscience*, vol. 2020, 8 pages, 2020.

[14] N. M. Elshennawy and D. M. Ibrahim, "Deep-pneumonia framework using deep learning models based on chest X-ray images," *Diagnostics*, vol. 10, no. 9, p. 649, 2020.

[15] R. Jain, P. Nagrath, G. Kataria, V. S. Kaushik, and D. J. Hemanth, "Pneumonia detection in chest X-ray images using convolutional neural networks and transfer learning," *Measurement*, vol. 165, p. 108046, 2020.

[16] E. Ayan and H. M. Ünver, "Diagnosis of Pneumonia from Chest -Ray Images Using Deep Learning," *2019 Scientific Meeting on Electrical-Electronics & Biomedical Engineering and Computer Science (EBBT)*, pp. 1–5, 2019.

[17] C. Salvatore, M. Interlenghi, C. B. Monti et al., "Artificial intelligence applied to chest X-ray for differential diagnosis of COVID-19 pneumonia," *Diagnostics*, vol. 11, no. 3, p. 530, 2021.

[18] A. Gupta, S. Gupta, and R. Katarya, "Insta Cov Net-19: a deep learning classification model for the detection of COVID-19 patients using chest X-ray," *Applied Soft Computing*, vol. 99, article 106859, 2021.

[19] R. Karthik, R. Menaka, and M. Hariharan, "Learning distinctive filters for COVID-19 detection from chest X-ray using shuffled residual CNN," *Applied Soft Computing*, vol. 99, article 106744, 2021.

[20] T. Rajasenbagam, S. Jeyanthi, and J. A. Pandian, "Detection of pneumonia infection in lungs from chest X-ray images using deep convolutional neural network and content-based image retrieval techniques," *Journal of Ambient Intelligence and Humanized Computing*, vol. 2021, 2021.

[21] O. Stephen, M. Sain, U. J. Maduh, and D. U. Jeong, "An efficient deep learning approach to pneumonia classification in healthcare," *Journal of healthcare engineering*, vol. 2019, 7 pages, 2019.

[22] I. S. Walia, M. Srivastava, D. Kumar, M. Rani, P. Muthreja, and G. Mohadikar, "Pneumonia detection using depth-wise convolutional neural network (DW-CNN)," *EAI Endorsed Transactions on Pervasive Health and Technology*, vol. 6, no. 23, pp. 1–10, 2020.

[23] P. Rajpurkar, J. Irvin, K. Zhu et al., "Chexnet: radiologist-level pneumonia detection on chest X-rays with deep learning," 2017, https://arxiv.org/abs/1711.05225.

[24] S. A. Harmon, T. H. Sanford, S. Xu et al., "Artificial intelligence for the detection of COVID-19 pneumonia on chest CT using

Hindawi
Computational and Mathematical Methods in Medicine
Volume 2023, Article ID 9854236, 1 page
https://doi.org/10.1155/2023/9854236

Retraction

Retracted: Influential Usage of Big Data and Artificial Intelligence in Healthcare

Computational and Mathematical Methods in Medicine

Received 10 October 2023; Accepted 10 October 2023; Published 11 October 2023

This article has been retracted by Hindawi following an investigation undertaken by the publisher [1]. This investigation has uncovered evidence of one or more of the following indicators of systematic manipulation of the publication process:

(1) Discrepancies in scope

(2) Discrepancies in the description of the research reported

(3) Discrepancies between the availability of data and the research described

(4) Inappropriate citations

(5) Incoherent, meaningless and/or irrelevant content included in the article

(6) Peer-review manipulation

The presence of these indicators undermines our confidence in the integrity of the article's content and we cannot, therefore, vouch for its reliability. Please note that this notice is intended solely to alert readers that the content of this article is unreliable. We have not investigated whether authors were aware of or involved in the systematic manipulation of the publication process.

Wiley and Hindawi regrets that the usual quality checks did not identify these issues before publication and have since put additional measures in place to safeguard research integrity.

We wish to credit our own Research Integrity and Research Publishing teams and anonymous and named external researchers and research integrity experts for contributing to this investigation.

The corresponding author, as the representative of all authors, has been given the opportunity to register their agreement or disagreement to this retraction. We have kept a record of any response received.

References

[1] Y. C. Yang, S. U. Islam, A. Noor, S. Khan, W. Afsar, and S. Nazir, "Influential Usage of Big Data and Artificial Intelligence in Healthcare," *Computational and Mathematical Methods in Medicine*, vol. 2021, Article ID 5812499, 13 pages, 2021.

Hindawi
Computational and Mathematical Methods in Medicine
Volume 2021, Article ID 5812499, 13 pages
https://doi.org/10.1155/2021/5812499

Review Article

Influential Usage of Big Data and Artificial Intelligence in Healthcare

Yan Cheng Yang,[1,2] **Saad Ul Islam**,[3] **Asra Noor**,[3] **Sadia Khan**,[3] **Waseem Afsar**,[3] **and Shah Nazir**[3]

[1]*Foreign Language Department, Luoyang Institute of Science and Technology, Luoyang, Henan, China*
[2]*Foreign Language Department/Language and Cognition Center, Hunan University, Changsha, Hunan, China*
[3]*Department of Computer Science, University of Swabi, Swabi, Pakistan*

Correspondence should be addressed to Yan Cheng Yang; 185342350@qq.com and Shah Nazir; shahnazir@uoswabi.edu.pk

Received 8 July 2021; Accepted 9 August 2021; Published 6 September 2021

Academic Editor: Muhammad Zubair Asghar

Artificial intelligence (AI) is making computer systems capable of executing human brain tasks in many fields in all aspects of daily life. The enhancement in information and communications technology (ICT) has indisputably improved the quality of people's lives around the globe. Especially, ICT has led to a very needy and tremendous improvement in the health sector which is commonly known as electronic health (eHealth) and medical health (mHealth). Deep machine learning and AI approaches are commonly presented in many applications using big data, which consists of all relevant data about the medical health and diseases which a model can access at the time of execution or diagnosis of diseases. For example, cardiovascular imaging has now accurate imaging combined with big data from the eHealth record and pathology to better characterize the disease and personalized therapy. In clinical work and imaging, cancer care is getting improved by knowing the tumor biology and helping in the implementation of precision medicine. The Markov model is used to extract new approaches for leveraging cancer. In this paper, we have reviewed existing research relevant to eHealth and mHealth where various models are discussed which uses big data for the diagnosis and healthcare system. This paper summarizes the recent promising applications of AI and big data in medical health and electronic health, which have potentially added value to diagnosis and patient care.

1. Introduction

AI is a field of computer science, which is capable of copying human characteristics, capacity of learning, and storage of knowledge. It executes human brain tasks in most of the fields in all aspects of our daily life using big data applications. Super computers are analyzing big data using the algorithms of advanced deep learning machines, which has allowed the improvement of output in the field. This field has led very needy and tremendous enhancement in every field of life, especially in healthcare. Big data analysis is entered in biomedical sciences; the foremost source of big data has been discussed and explained, especially in oncology, cardiovascular disease, allergic diseases, clinical work, ear diseases, and so on. Along with this, it also touches some aspects of need to combine several pathological and clinical sources and quality of life data [1] as well as the unprecedented and quantitative datasets of neuroscience [2]. Medical care and treatment are getting enhanced day by day. Researchers are collecting data to make human care and diagnosis disease efficiently and operationally. Medical doctors are skeptical about the help that artificial intelligence can deliver to them in their medical practices. Studies have explored an understandable experience which includes all challenges, risks, and comfort since the implementation of AI programmed with the help of big data in healthcare within a contagious disease setting. The aim of the program was at designing a set of tools which can support an accurate, objective, and clinical decision-making process efficiently [3]. In biomedicine, there are many ways to collect data from observation and experiments. Scientists are often struggling to collect data about the disease and on how data are being

generated for the treatment of disease. This biomedical information is to create thinking, managing, and analyzing and the way they can transform into further scientific perception for enhancing patient care. This is the major challenge for the National Institutes of Healthcare (NIH) to lead the big data to knowledge representation. The agencies are making efforts to collect increasingly data with increasing research productivity. Leading centers are developing to handle this type of cases with large-scale data. They are going to research how much accurate equipment is required for the new generation of biomedical data scientists. In today's world, NIH and Big Data to Knowledge (BD2K) seek the position of data sciences in biomedical research [4].

Health information technology is designed due to the solution of complex problems such as health disparities. Mix results can be obtained by demonstrating a direct impact on health outcomes. For all these, we must know about collective intelligence, big data, informatics capacities, corresponding terms of smart health, knowledge exchange knowledge, ecosystem, and situational awareness. Standards, guidelines, and objections are established by public health informatics for health equity and health disparities, which will increase health literacy and access to care [5]. Fodeh and Zeng [6] have presented the notation of big data which is used for three words: volume, variety, and velocity. This is the foremost concept which is associated with the dimension's volume, and the variety is very relevant to the biomedical data gained by patients, including tabulated and structured data. The biomedical research communities are struggling to escalate in the clustering and analysis of big data. Mining big data probably holds plenty of information and has a possible way and source for giving knowledge; data mining and machine learning methods are useful for such data series in a challenging task. Kavakiotis et al. [7] have discussed a lot of data on advance technologies which are feasible for medical persons. Researchers have led a lot of research on diseases like diabetes mellitus, concerning the different types of datasets that are mainly used. These hypotheses will lead us about the various knowledge of technologies and diseases in the world. One should have sufficient data and knowledge about machines and technology before using it, as most of the machines used in medical and healthcare emit radiation which is quite harmful and dangerous for humans and buildings. The proof of principle has been provided for lung cancers which has been collected from five locations. The euroCAT infrastructure has successfully implemented as a radiation clinic. Radiation oncology is facilitated as a euroCAT network and will facilitate the machine [8]. In daily clinical work, imaging data usage has the ability to improve cancer care by knowing tumor biology and helping in the implementation of precision medicine. For accession of the tumor and its microenvironment, radiomics helps in monitoring and evaluating the tumor features such as temporal and spatial heterogeneity.

Limkin et al. [9] have provided a study case which assists in ensuring the actual development and enhancement of radiomics as a biomarker and facilitating its implementation in clinical practice. Gebremeskel et al. have proposed a data mining technique of optimization for envisioning of knowledge extraction by examining clinical datasets to define the decisive features using modeling techniques, capable of handling and analyzing large-scale data in its context [10]. In the analysis, guidelines for using AI to speed up the drug's recovery, so that AI's vision is not strong but important, were used. The rapid development, power, and problem of AI and network medicine technology have speed up the development of treatment in healthcare. The study is a strong proof for the use of AI-assisted tools for drugs and repayment for human diseases, including COVID-19 in times of fatal disease [11]. Various studies have been considered for the qualitative analysis of the COVID-19 [12–14]. These studies have mainly considered corona virus from different perspectives.

The exposure of corona virus disease 2019 puts an increasing burden on the healthcare system. While infected patients have nonserious signs, which can be handled at home, some people develop serious symptoms and need to be hospitalized. That is why it is important to effectively evaluate the severity of COVID-19 and identify the hospital's priorities. COVID-19 has been published in a number of countries in the short term. By choosing a session as a time of patient discharge, including rescue techniques and statistical analysis, it is time to seriously prepare it for decision makers to be prepared for more hospital burden. A cube model was proposed to validate and verify the actual and confirmed cases and deaths, which was then accepted by the World Health Organization. Often during the cholera disease, this research-assisted pairing can be learned. Four diagnostic models, including lymphocytes, lactate dehydrogenase, C-reactive proteins, and neutrophils, have been developed and validated using the XGBoost algorithm [15–17].

The contribution of the proposed research is to review the existing research associated to eHealth and mHealth where various models are discussed. The approaches along with the uses of big data for diagnosis of disease in healthcare system are elaborated. The study summarizes the recent promising applications of AI and big data in medical health and electronic health. The study will possibly add value to the research in diagnosis and patient care.

This paper is structured as follows: Section 2 shows the related work to the planned research. Details regarding the applications of big data and AI are given briefly in Section 3. Challenges and barriers faced by healthcare are shown in Section 4. The conclusion of the paper is given in Section 5.

2. Literature Review

Miller et al. [18] have presented an overview of biomedical data for the derivation of new knowledge on how clinical decision support tools can be developed from the wealth of available data to modernize clinical care and scientific research of diseases related to neurodegeneration in the precision medicine era. Garcia-Ceja et al. [19] have surveyed sensor data and machine learning about mental health monitoring systems. The main focus of the study is about mental disorders or conditions like stress, anxiety, depression, and bipolar disorder. It is suggested to guide the review of the related categorization taxonomy study and present the

overall phase of MHMS. Digital health technologies allow access to optimize clinical care delivery and clinical research to access the information about age of healthcare. Despite the usage of such technologies in research and clinical care faces issues such as data quality, privacy, and regulatory, etc. Sharma et al. [20] summarizes think tank meeting proceedings with goals to delineate a framework for appropriately using digital health technologies in research and healthcare delivery. In Alzheimer's disease (AD), clinical development programs have failed to modify new diseases and to establish quality work instrument for the treatment of new and advanced diseases. The report is based on computer modeling and simulation, which plays a role of being powerful and observational in AD research [21]. Super computers are analyzing big data using algorithms of advanced deep learning machines which have allowed the improvement of output like visual image interpretation to formerly imperceptible levels and promised to change the practice of medicine. AI is a well-known field about what everyone is aware of; it is bringing a tremendous progress in such fields like automation of clinical decisions, disease detectors, imaging analysis in medical diagnosis classifiers, an interventional procedures, and it has the strength to significantly affect the practice interventional cardiology. This distinctive nature of interventional cardiology has made it a supreme target for the evolution of artificial intelligence-based approaches which are delineated to enhance real-time clinical decision making, the elegant flow of work in laboratories, and standardized catheter-based procedures using advance robotics. This study highlights the scope of artificial intelligence, its potential applications, and limitations in interventional cardiology [22].

The healthcare domain has obtained its effect by the influence of big data since the sources elaborated in the institutions of healthcare are familiar for their dimensions, heterogenous complication, and excessive spirit. Big data's analytical techniques, tools, and platforms are perceived among numerous fields; their effect on healthcare institutions for fulfilling novel use cases for possible healthcare applications shows promising research directions. In this circumstance, the success of these applications is completely dependent on the fundamental architecture and optimization of suitable and proper tools as signified by introducing research attempts. Palanisamy and Thirunavukarasu [23] have discussed many analytical areas that endure in the patient care system from stockholders' perspectives and appraise big data structure with respect to fundamental data sources, systematic capabilities, and application fields, while the intimation of big data that aids in the development of healthcare ecosystem is also discussed. The modern technique, hidden Markov model (HMM), can be used to manage massive data; the inference of the reproducible and interpretable dynamic brain network can be made possible in different dataset ranges including various other tasks [24]. The previous enhancements in ICT have indisputably improved the quality of people's lives around the globe. Computer technology has led to very needy and tremendous enhancement in the health sector which is commonly known as eHealth (electronic health). For optimizing the full and admirable benefits of this development, it is important to implement it in a cloud-based environment. Beside numerous and elegant benefits of eHealth in cloud computing, its full optimization is still obstructed by facing some challenges like privacy and security. The study mainly focuses on contemporary literatures of many techniques, and the mechanism is used to control privacy and security-related matters in eHealth. The robustness and fragility of these approaches were vocalized. 110 articles were reviewed, and several models were figured out in which solutions were adopted in it. These models were compared, and the articles were reviewed in which a standard and acceptable definition of eHealth was given as it was recommended. Privacy and security requirements were also discussed and provided as per the recommendation of the Health Insurance Portability and Accountability Act (HIPAA). Finally, a dependable and secured architecture for eHealth was proposed that could guarantee the effective, regulated, and dependable access framework to health information [25]. It has also applications in speech and language therapy. However, these therapies are often less willingly available for a few months after stroke. Palmer et al. [26] have assessed a self-managed computerized speech and language therapy (CSLT) aiming to deliver more therapy to patients than they can access through usual care alone. CSLT plus usual care significantly improved in individually relevant word findings, but they did not improve in conversation. Schoettler et al. [27] have presented a review of genome-wide association studies (GWASs) of asthma and those related to allergies, in which he concluded that childhood asthma is correlated to the most independent locus compared with other specified groups of allergic and asthma cases, while adult asthma is correlated to fewer genes which can be considered as a subset of those similar with childhood asthma.

3. Applications of Big Data and AI

A lot of data in the world is available in different hospitals and healthcare centers, which are collected from disease-affected humans. The amount of this data is increasing day by day [28]. Researchers are trying to analyze the data and extract the diseases that affect the human body. Pobiruchin et al. [29] have extracted new approaches for leveraging cancer in the development of Markov Models, from which the researchers easily extract the clinical patient of breast cancer, which can be easily used for freshly affected bodies in the real world. The study has mainly focused on publishing research on breast cancer, which is concerned with the clinical study of data. In this registry, normally, the patient is covered for 8 years from the clinical registry report. Using the Markov model is very good for creating a good opportunity to make a future planning in the existence of data in healthcare and clinical centers. This is useful to get an easy way to identify the patients and their affections in the future. A deep rule-based fuzzy system is used for accurate mortality rate prediction in hospital intensive care units (ICU'S). In pursuant to this approach, in each base building unit of DRBFS, the same system of input has to be kept. In first 48 hours in ICU, with heterogeneous featuring a set of

admissions were extracted for mortality rate in hospital [30]. With data concerned to the health records, recurrent neural networks were used for disease risk prediction. The model results were better for small datasets, whereas for large-scale ones, the concerned model and its application to different patients across the population throughout hospitals were not evaluated [31]. Epidemiologist is using electronic health records which assist evidence provision for interval guidelines and screening intervals while censoring interval and undiagnosed sickness make a path to issues like substantial analytic risk estimation which cannot be addressed by using Kaplan-Meier methods [32]. Zhao et al. [33] have determined the illustration of temporal data in electronic health record (EHR); there were several methods based on symbolic sequence representation of time series data, which can be used in several ways, while several evidence relies on the standard of symbolic sequence representation by comparing it to particular orders initiated by clinical experts with the use of domain knowledge. In various other applications of big data based on trajectory data, the regular behavior of private cars is extracted [34–36].

3.1. Disease Prediction and Big Data. Big data and artificial intelligence approaches are commonly presented in mHealth and eHealth applications for self-management and home care of many long-term health conditions. Adaptation of these applications for self-management in asthma multifactorial persistent diseases needs validation and evaluation in real-life setups along with the enhancement of the patient level to personalize predictions concerning the control status of asthma and increasing pitfalls. The study presents a short-term prophecy technique for controlling the asthma status, where multiple categorization models are considered trains for each observed framework along with obligatory preprocessing techniques to improve strength and effectiveness. The support vector machine, random forests, Bayesian network, and AdaBoost are considered machine learning algorithms used in this review [37]. Xin-Di et al. [38] have composed 252 formulae from the synopsis of prescriptions of the Golden Chamber and a treatise on exogenous febrile disease, looking to identify the basic rules dominating the choosing of herbal mixtures by probability models and big data technology. Pashazadeh and Navimipour [39] have provided a detailed and systematic review of the modern mechanisms related to healthcare applications in big data fields. Five of the discussed categories are heuristic based, hybrid mechanism, machine learning, cloud based, and agent based. Harous et al. [40] have enlightened the applications of big data for obesity management using sensory and social data in mobile health architecture, which are mainly proposed for assessing, detecting, and controlling obesity, which depend on a mobile phone to be used for complex operations and processing of the data collected. Using this newly developed mobile architecture, one can tackle the challenges of obesity control, monitoring, and prevention. Different algorithms have been used to generate featured suggestions, recommendations, and warnings to control obesity and its related diseases. In the context of large datasets of physical growth measurements which are regularly used by health professionals, this paper is aimed at regenerating a new growth chart for French children. 32 random primary care pediatricians and 10 volunteer general practitioners were selected across the French main regions where the electronic medical record software was used. All data of physical growth was extracted for pediatric patients with anonymization. A new growth chart was derived which was then compared with the WHO chart and found it correct and error free [41].

Mechanical therapies are primarily prescribed for motor, duodenal, endocrine, urinary, respiratory, digestive, neural, and cardiovascular diseases. The speedy evolution of healthcare is driven by the enhancement of technologies related to the Olympics, biomedical, and scientific sciences. Appropriate medicine has been designed to implement specific and more specific treatments for specific diseases and patients [42]. The healthcare industry was booming in the pharmaceutical industry. Once again, like the confirmations, text, numbers, photos, and catalogs, any information that lists the large and irregular discovery of various health service management systems lists patient information. At the same time, hospitals were part of several geographical departments in different locations. In different ways, fact provide patient health information from time to time. In response to these problems, Damien is a one-sided solution to healthcare interventions for a marine, vegan-based healthcare management system [43]. The incidence of pediatric and pediatric diseases such as pneumonia and diarrhea are globally challenging. The Patient Demographic and Health Survey (DHS) deportation post from India once again created cesarean section (CBNs) of the day and explored the location factors of childhood diarrhea. Location of freeware tools for DHS data, graphic structure learning with world score-based limitation, and hybrid structure learning algorithms are described. The study identified the outcome of missing values, sample size, and constraints of knowledge based on each of the structure learning algorithms and evaluates their accuracy with multiple scoring functions. [44]. Waring et al. [45] have helped healthcare specialists in the knowledge literature review in the Greater East using automated machine learning (AutoML) with the latest experience of machine learning models "O-Shelf" with limited information data specialization. The possible opportunities and risk of using AutoML in healthcare in the field are also located in the foreground, as well as the demands of AutoML in healthcare in response to the attack. The use of ML techniques has the possibility to improve outcomes of health, reduce costs of healthcare, and demonstrate clinical research. The Greatest Conventions Nowadays, using AI, previously discovered that knowledge can be found in large collections. Clinical oncology data is a start to clinical practice and research with a wealth of multithreaded documents and metadata. Most of our clients include companies and employees. Inadequate interventions, short-term stay, and vision can improve patient care. Incorporating powerful AI algorithms has been instrumental in changing the presentation and common sense of high-intensity radiation oncology. However, this is possible by establishing a clinical scientific community with radiation oncology [46].

3.2. Technological Innovations in Healthcare. Blockchain technology, such as the vascularization of inherited traits, router transparency, and identification information, was introduced in 2008 in the Bitcoin cryptocurrency. A wide range of domain-level domains engaged in the health domain. The purpose of this study is to systematically acquire startup publications and evaluate the Turkish position of the use/offer of blockchain to improve processes and services in healthcare, health sciences, and services sanitary [47]. There are some biological processes in which cell regulation and signaling are involved through the assembly of protein complexes. When there is any change occurring through protein-protein interfaces, it will affect the formation of multiprotein complexes. Due to this, sudden change occurs in the cell functions and the development of genetic diseases occurs like cancer and develops drug resistance. These proteins are essential and lead to the formation of many resources for predicting their effects. It should prepare for how mutations affect the structure and body of multiprotein complexes [48]. There are some models under development for the solution of two different problems computationally, to allocate the fund for infectious diseases in the deserts and forests of Africa. Guidance about empirical data collection and theory development for the development in the future is provided [49]. Biomedical research is getting completely changed with big data. The extraordinary advances of automatic data collection of large-scale clinical and molecular data have caused prime challenges to data simplification and analysis, summarized for the evolution of new computational techniques. The development of the system with the efficient use of biomedical big data in particular medicine will need noble scientific and technical creation in which engineering, infrastructure, financial management, and projects will be included. In this study, how the transformation of data-driven techniques provides the probability to address many of these problems has been reviewed, directing the elaboration of the theory on system functions and the generation of technical models and assisting the design of clinical procedures in precision medicine [50].

Ear disease and mastoid diseases can be easily handled if early detected with appropriate medical care. However, sometimes, we do not have specialists or we may have comparatively low diagnostic precision if a new way of diagnostic policy is needed, in which deep machine learning can play a noble role. Cha et al. [51] have presented a machine learning model for automatically diagnosing ear disease with the help of datasets having a total of 10544 images which were trained using CNN to categorize internal eardrum and external auditory canal features into 6 categories of ear diseases, which has covered most of the ear diseases.. Inception-V3 and ResNet101 are the learning models which have been chosen for the time training and accuracy, which has an average accuracy of 93.67%. This classifier is trained in various conditions and environments and gives better results of diagnosis, so it is more compatible for the use in a practical environment. For various countries, EQ-5D-3L (three-level EuroQol five-dimensional questionnaire) value sets are entrenched to evaluate the utility of the health state. Before generating these values, analysts gather values for a prechosen health state from a console who represents the public and then use a mathematical algorithm to produce values for 243 states. To estimate the rationality and correctness of both the newer criteria and, earlier, in terms of forecasting of values for all health states and of the values of common health states in specific, preexisting dataset has been used that accommodates VAS (visual analogue scale) values from 126 students while each student has valued all 243 states. A sequence of representations was produced, and eventually, data were designed according to each model. Few of them were used in the past [52]. Related to scientific activity, this study shows a large data depository, containing epidemiology, clinical, and molecular data, which offers research opportunities and is essential to assist scientific activity. The advantages of massive data may contain low-cost collection. Restrictions may contain the cost and difficulty of data storage and processing, which is essential for modern approaches like formatting, analysis, and concerns about security, accuracy, and reliability. It is explained that the source of big data and tools for its analysis can be used to help and diagnose the treatment and management of dermatologic diseases [53]. Diabetes is a condition in which glucose levels are lowered into the bloodstream with a slight delay, causing the inability to metabolize it. When the insulin in the body does not respond properly or if the body does not produce it, this results in diabetes. Serious and long-term health issues are reported. The administration does not really treat electives that include heart pain, lung disorders, skin and liver disorders, nerve damage, and noise damage; quick findings are rare. Thakkar et al. [54] has discussed some valued techniques to excavate in the future and for the diagnosis of diabetes.

Tandon et al. [55] present current issues and opportunities to use blockchain technology to improve health performance. The SLR (systematic literature review) results show that blockchain is being used to create new jobs to improve the standards for the management, distribution, and processing of personal medical records. Implementing the blockchain technology is part of the healthcare system, at verity in the healthcare industry, where the significant value has been added by improving the performance, nearness, advancement of technology, protection, security, and privacy of information management systems. The collection and elaboration of information on public technology has been incorporated by the government and by the real estate companies of the whole world as a strategic solution to alleviate the information of COVID-19 that prevents information. However, the law regarding the end-of-life monitoring system to monitor those who are unable to read the following documents for the help in using the documents of power of the public in the world. EHRs contain valuable information on the progression of Rangatahi's disease and the tragedy of treatment. In the heart failure study, Esther and her colleagues proposed a scheme for extracting short-term sequential samples from CCE data that grading improves phenotype and prediction and is also professional. Brief information on EHR on disease progression and treatment outcomes are given. This article presents a method for

representing transient transitional CCE observations up to machine learning. Using clinical data from patients with heart disease, EHR drug transfer and provisional representation from diagnostic and class records for prescribing activities are given [56]. Virtualization (AI) and machine learning are having a real impact in many areas of the healthcare industry. The cancer site is a global phenomenon. Efforts to reduce the chances of accidents should be timely. However, metastatic development, serotonin frequency, and drug inhibition are observed. It is important to find new biomarkers that stimulate group resistance and improve drug delivery to improve carriers to improve carriers [57]. Timeline risk assessment tools for heart failure use a database designed with realistic, one-time clinical document scans and low accuracy. The purpose of this study was to create a comprehensive 30-day plan for unannounced announcements and accurate forecasts for all. All-cause mortality (ACM) connects clinical and clinical information available on the electronic medical record system. There are three predictive indicators for a 30-day unstructured reading or ACM created using a step-by-step method: (a) index admission model, (b) feature-aggregated model, and (c) index discharge model [58]. The study has talked about artificial intelligence that it has the ability to mimic human characteristics, knowledge storage, learning capacity, and so on. There are a majority of techniques which have been already applied in medicine and healthcare, such as the C-statistic model, which was used in North Carolina hospitals as the finest model for the prediction and enhancement of the efficiency of preventive medicine [59]. Table 1 represents some of the existing research work available in the literature.

3.3. Cardiovascular. Cardiovascular imaging is getting changed with the rise of data science. There are many techniques which have been applied in cardiovascular medicine for exploring different types of diseases, as well as to improve patient care quality and mortality rate. The potential of AI in cardiovascular medicine is tremendous, although ignorance of the challenges may overshadow its potential clinical impact [60]. There are some complexities like efficiency, timing, and missing diagnoses which occur in all stages of the imaging chain. The dependency of AI's applications falls on vigorous data, suitable computational techniques, and tools. While in some areas, it depends on the validation of its clinical application to image sectionalization, automated measurements, and diagnosis. Cardiovascular disease has now accurate imaging combined with big data from the eHealth record and pathology to better characterize the disease and personalized therapy [61]. Research has explored the area and presented studies on the available literature in the area [62, 63].

3.4. Big Data and Disease Identification. In daily clinical work, imaging data usage has the ability to improve cancer care by knowing tumor biology and helping in the implementation of precision medicine. For accession of tumor and its microenvironment, radiomics helps in monitoring and evaluating tumor features such as temporal and spatial heterogeneity [64]. Asthma is inconsistent in clinical associations and poor replication of genetic associations. Asthma is not a single disease but a group of similar diseases with some clinical manifestations. Big data for the disease is not providing a solution, just giving information about the disease. Bayesian and frequent approaches make us understand about the ethnology of diseases commonly used in statistical machine learning and can be applied to both big and small data in healthcare research. We need to know about the reality of asthma and not to just give predictions only. We have to get awareness from methodological polemics on data science. The Bayesian and frequent paradigms of the present artificial dichotomies are given. Big data are required to divide the asthma into subtypes to get the solution. Exploiting disaggregated phenotypes and genomic research and the exploration of lung function as an intermediate phenotype. Cohering inductive and deductive statistical approaches to epidemiology pragmatic bayes and unifying graphs are presented [65]. There are techniques and methods by which patients can be classified effectively as those who have asthma and those who do not have those in long-term remission [66]. VA-PODR (Veterinary Affairs Accurate Oncology Data Collection) is a worldwide large repository of well-known data concerned with diagnosed patients of cancer in VA's (Veterans Affairs) department. This data consists of long-term clinical data from the nationwide Veterans Affairs eHealth record, medical photography data, tumor sequencing targets, pathology slides, and the Veterans Affairs central cancer registry as well as CT (computer tomography) scans. A subset of this data storage is available in GDC (genomic data commune) and the TCIA (The Cancer Imaging Archive) [67].

The allergic conjunctivitis population has a frequency of 15–20%. However, due to the lack of understanding, the multicause of chronic obstructive pulmonary disease is that the environment, residence, and direct distribution have complex relationships. The benefits of medicine for chronic kidney disease patients and the type of treatment for dementia, as well as the possibilities for other diseases that need to be known by patients that will help patients according to the symptoms and risk factors of the intervention's social empowerment and rehabilitation of people with chronic obstructive pulmonary disease to reduce the body helping to create permanent solutions and prevent the escalation of social ills [68].

In biomedical repositories, the size of somatic genomes is getting increase. So predicting documents related to cancer sets using mathematical algorithms are described. Mining models of conventional gene-based somatic cancer are unhampered by somatic gene ranking and feature extraction due to high computational cost and memory of large datasets. A wide range of characteristics, preferences, and feature squeezing procedures is available, and they are normally deployed in many areas. Each of these procedures tries to extract and squeeze some new irrelevant characteristic features from the trained datasets, having a goal of increasingly accurate results for the newly arranged documented data. Extraction or squeezing of data is an activity of delivering required and related data from a large collection of datasets according to the given information. There are criteria for

Table 1: Existing research in the area.

S. no.	Title	Year
1	Modeling future price and diffusion in health technology assessments of medical devices	2016
2	Big data effort in radiation oncology	2016
3	Processing and analyzing healthcare big data on cloud computing	2016
4	Decision rules for health system strengthening	2016
5	Use and analysis of big data in dermatology	2017
6	AI in precision cardiovascular medicine	2017
7	Disaggregating asthma	2017
8	Predicting the risk of acute care readmissions among rehabilitation inpatients	2018
9	Selecting health states for EQ-5D-3L valuation studies	2018
10	Modeling asynchronous event sequences with RNNs	2018
11	Map reduce-based hybrid NBC-TFIDF algorithm to mine the public sentiment on diabetes mellitus	2018
12	The trifecta of precision care in heart failure	2018
13	Roadmap for innovation-ACC health policy statement on healthcare transformation in the era of digital health, big data, and precision health	2018
14	Authenticating health activity data using distributed ledger technologies	2018
15	Spread of health-related misinformation on social media	2019
16	Big data analytics for personalized medicine	2019
17	Diagnosis of ear disease	2019
18	AI in cardiovascular imaging	2019
19	Big data visualization in cardiology	2019
20	Big data features, applications, and analytics in cardiology	2019
21	Transitive sequencing medical records for mining predictive and interpretable temporal	2020
22	AI and big data in cancer and precision oncology	2020
23	Electronic health data and machine learning for the prediction of 30-day unplanned readmission or all-cause mortality in heart failure	2020
24	The veteran affair precision oncology data repository	2020
25	Medical big data for P4 medicine on allergic conjunctivitis	2020
26	Somatic cancer gene-based biomedical document feature ranking and clustering	2019
27	Anatomization of data mining and fuzzy logic used in diabetes prognosis	2020
28	Blockchain in healthcare	2020

ranking the information which is sorted as the best results will have the top priority so it will be on the top of the provided list. Experimental results have different cluster sizes with different gene features for clustering of somatic documents. And their generated results prove that the existing model has a high quality of computational clustering [69].

4. Challenges and Barriers Faced by Healthcare

The healthcare organizations are facing many challenges like analyzing large-scale data. With the rapid increase in healthcare applications, many devices are used to generate verities of data and many of them are used for better analyzing data and for better decision making [70]. The following are the challenges which todays healthcare organizations are facing.

4.1. Social Media. Analysts of today's era are giving name to the period that we are living in "an era of fake news" based on the spread of misinformation produced, which may be spread intentionally or unintentionally. As it is affecting all areas and fields of life, it also creates problems and issues in fields related to health, where it may cause to detain or stop effective care, while in some cases, it is menacing the lives of individuals. Wang et al. [71] have exposed the present proof and made it clear in an understandable way; the mechanism of misinformation spreads. The most substantial and considerable topics include misinformation related to vaccination, Zika virus, and Ebola, even though others, such as fluoridation of water, nutrition, cancer, and smoking are also highlighted. Most studies employed content analysis, social network analysis, or experiments, drawing on disparate disciplinary paradigms. Respective systems are used to classify this data based on the result and condition of each sentence [72]. Future research should examine the susceptibility of different sociodemographic groups for misinformation and to understand the role of belief systems on the intention to spread misinformation.

4.2. Knowledge about Machines and Technology. Most of the technicians or users of the machines do not have enough knowledge on using the technologies/machines [73]. To overcome this problem, technicians and operators should

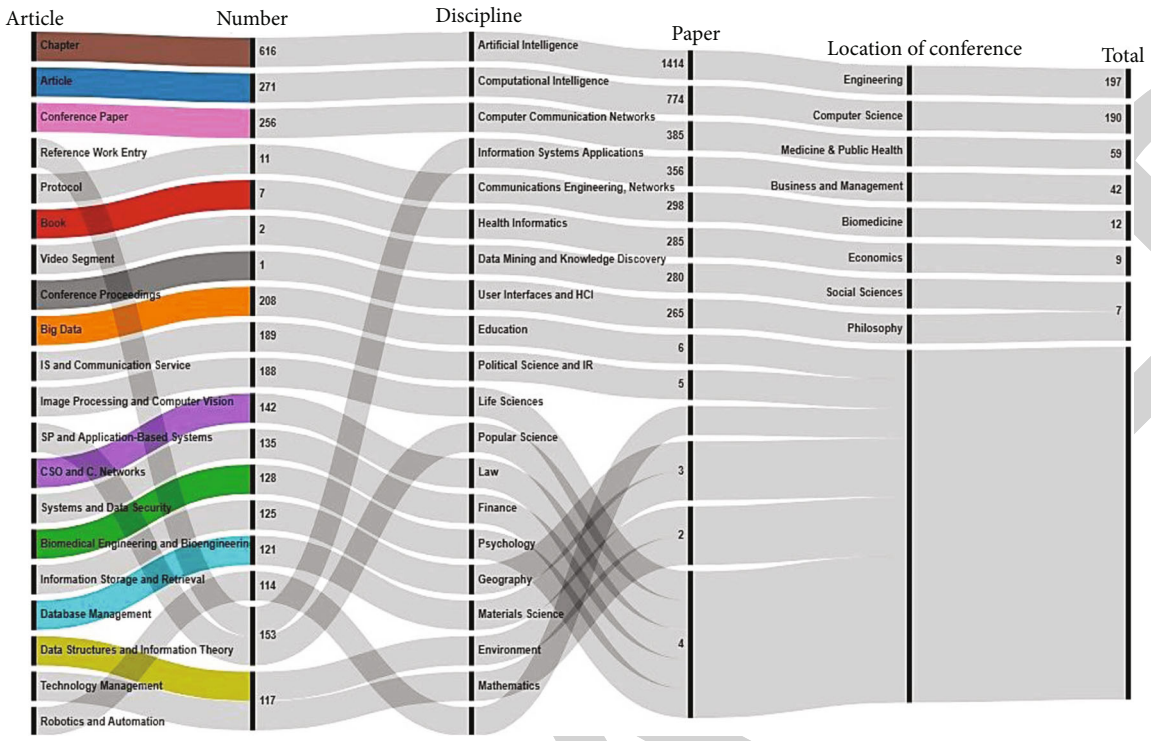

Figure 1: Details of the search process in the Springer library from various perspectives.

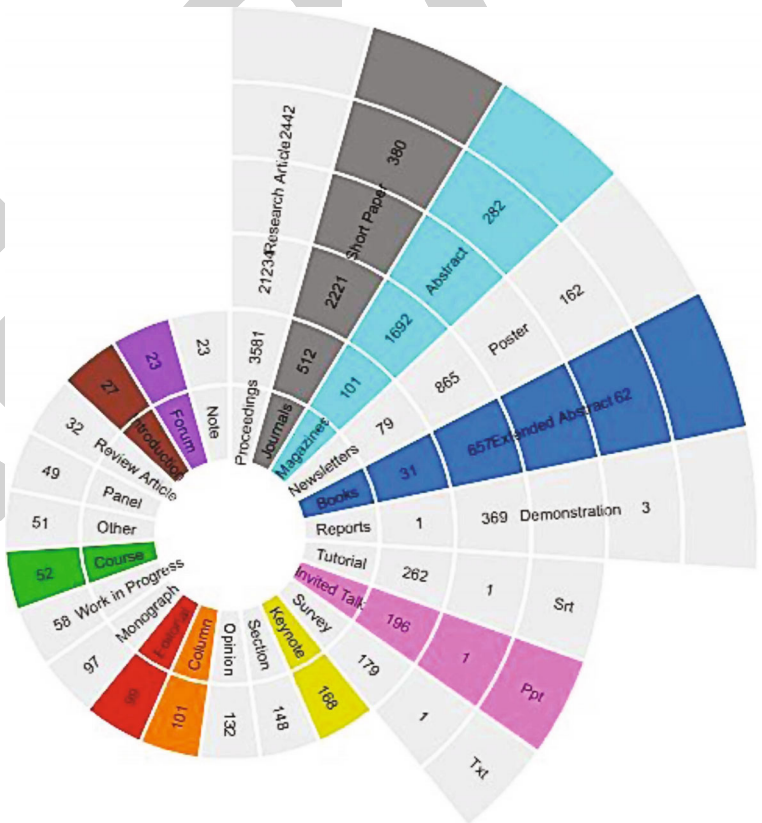

Figure 2: Details of the search process in the ACM library.

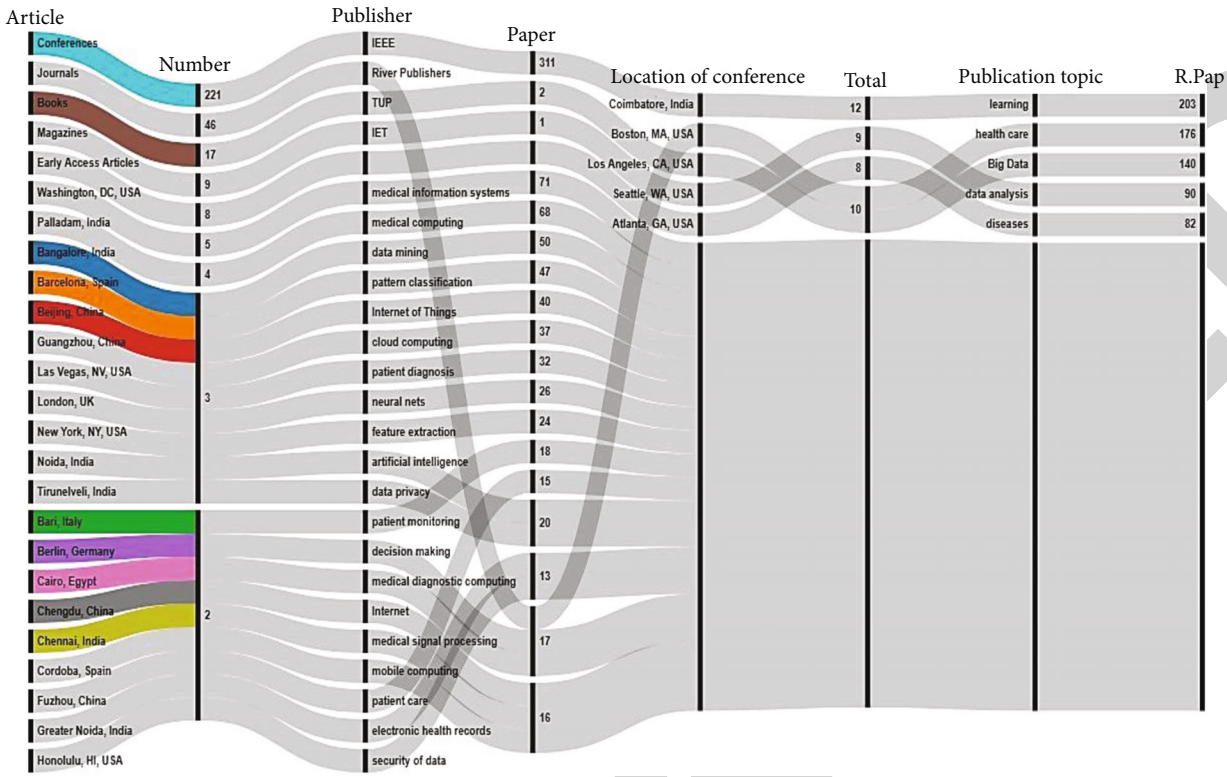

Figure 3: Details of the IEEE library from various perspectives.

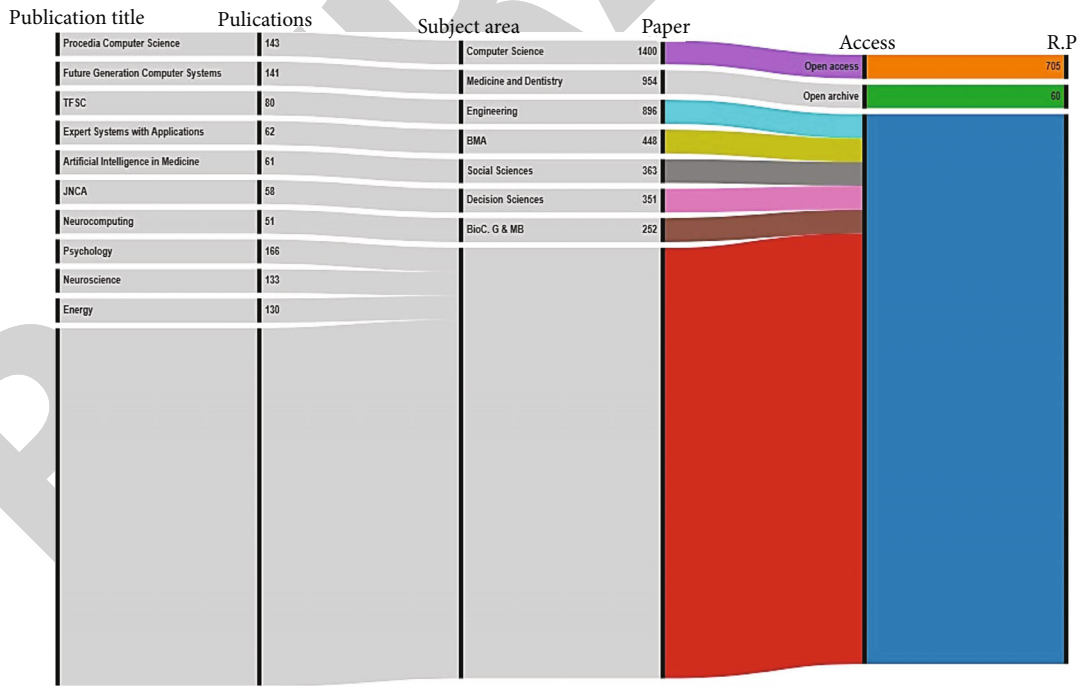

Figure 4: Details of the search process from various perspectives in the ScienceDirect library.

have sufficient data and knowledge about machines and technology before using it, as most of the machines used in medical and healthcare emit radiation which is quite harmful and dangerous for humans and buildings. The euroCAT infrastructure needs to be implemented as a radiation clinic [8].

Figure 5: Details of the ScienceDirect library.

4.3. High-Power Consuming Technologies. As these artificial machines can perform a complex tasks; many of the technologies operate on large scale in large areas for a long time, which consumes much electric power while there is a big issue of power in most of the developing countries which needs to be solved and adjusted to give plenty of facilities in healthcare.

4.4. Expensive. This is the generation of robotics and artificial intelligence which has large significance in the field of healthcare. However, technologies, machines, and data storages, either cloud database or our own database, are mostly not affordable by the organizations because of high prices. By using single-cohort model parameters, we can obtuse the price issues which we are facing and we will face in the future [74]; this will add a significant value to the medical organizations as well as patients in rural areas who cannot afford and do not have access to these technologies.

4.5. Transformation. A healthcare transformation is a method of sharing thoughts of a company to work on that. It has the importance as the old technology is transforming to a newly developed and evolving technology based on innovation, which may include digital health, eHealth, mHealth, and sensor-based technologies. Such enhancement in health may be significant in identifying diseases on the next level. There are some things which need to be observed before transforming shifting from traditional healthcare to virtual and real-time diagnoses which remains lacking in true evaluation whether these inventions are really improving and overcoming the healthcare quality or not. If any of the new technology is adopted which is not based on evidenced care may risk unintended outcomes like privacy breach, increase in care cost, etc [75]. Distributed ledger technology needs to be implemented to ensure the integrity and authenticity of data produced by embedded systems [76].

The existing literature was studied to know about the details of research available in the area of healthcare based on AI and big data. Figure 1 represents the details of the literature in the Springer library from various perspectives as given in the figure.

Figure 2 elaborates the details of the search process in the library of ACM.

The library of IEEE was also searched for getting the associated details. Figure 3 describes the details of the search process for the IEEE library.

Lastly, the ScienceDirect library was tried and the details of the library from various perspectives are shown in Figure 4.

This library was further elaborated and some of the details are shown in Figure 5.

5. Conclusion

Big data and AI have revolutionized everything that has brought comfort to people's life in all aspects of daily life. Especially, it is bringing innovative technologies in healthcare systems. It has transformed the conventional and traditional health system to a technological systems in the form of cardiovascular, oncology, ear, asthmatic, allergic, cancer, and or any other diseases. Big data has made it easy to diagnose disease through virtual and real-time systems. The contribution of this paper is to review the present research applicable to mHealth and eHealth where various approaches and models are discussed which use big data for diagnosis and healthcare system. This paper has summarized the current encouraging applications of AI and big data in medical health and electronic health, which have potentially added value to the diagnosis of disease and patient care. The proposed research will help researchers to devise new solutions in the area of healthcare.

Conflicts of Interest

The authors declare no conflict of interest.

Acknowledgments

This research was financially supported by the Humanities and Social Science Fund of the Education Department of Henan Province in 2020 (Grant number: 2021-ZZJH-233), Luoyang Humanities and Social Science Fund in 2021 (YB-153), provincial and ministerial preresearch projects in Luoyang Institute of Technology and Science of 2019, and the general grant project of the Provincial Social Science Achievements Review Committee in 2021 (Grant number: XSP21YBZ077).

References

[1] S. M. Willems, S. Abeln, K. A. Feenstra et al., "The potential use of big data in oncology," *Oral Oncology*, vol. 98, pp. 8–12, 2019.

[2] D. Bzdok and B. T. T. Yeo, "Inference in the age of big data: future perspectives on neuroscience," *Neuroimage*, vol. 155, pp. 549–564, 2017.

[3] C. Garcia-Vidal, G. Sanjuan, P. Puerta-Alcalde, E. Moreno-Garcia, and A. Soriano, "Artificial intelligence to support clinical decision-making processes," *EBioMedicine*, vol. 46, pp. 27–29, 2019.

[4] A. A. T. Bui, J. van Horn, and NIH BD2K Centers Consortium, "Envisioning the future of 'big data' biomedicine," *Journal of Biomedical Informatics*, vol. 69, pp. 115–117, 2017.

[5] T. J. Carney and A. Y. Kong, "Leveraging health informatics to foster a smart systems response to health disparities and health equity challenges," *Journal of Biomedical Informatics*, vol. 68, pp. 184–189, 2017.

[6] S. Fodeh and Q. Zeng, "Mining Big Data in biomedicine and health care," *Journal of Biomedical Informatics*, vol. 63, pp. 400–403, 2016.

[7] I. Kavakiotis, O. Tsave, A. Salifoglou, N. Maglaveras, I. Vlahavas, and I. Chouvarda, "Machine learning and data mining methods in diabetes research," *Computational and Structural Biotechnology Journal*, vol. 15, pp. 104–116, 2017.

[8] T. M. Deist, A. Jochems, J. van Soest et al., "Infrastructure and distributed learning methodology for privacy-preserving multi-centric rapid learning health care: euroCAT," *Clinical and Translational Radiation Oncology*, vol. 4, pp. 24–31, 2017.

[9] E. J. Limkin, R. Sun, L. Dercle et al., "Promises and challenges for the implementation of computational medical imaging (radiomics) in oncology," *Annals of Oncology*, vol. 28, no. 6, pp. 1191–1206, 2017.

[10] G. Belay Gebremeskel, B. Hailu, and B. Biazen, "Architecture and optimization of data mining modeling for visualization of knowledge extraction: patient safety care," *Journal of King Saud University-Computer and Information Sciences*, 2019.

[11] Y. Zhou, F. Wang, J. Tang, R. Nussinov, and F. Cheng, "Artificial intelligence in COVID-19 drug repurposing," *The Lancet Digital Health*, vol. 2, no. 12, pp. e667–e676, 2020.

[12] K. Shah, T. Abdeljawad, I. Mahariq, and F. Jarad, "Qualitative analysis of a mathematical model in the time of COVID-19," *BioMed Research International*, vol. 2020, Article ID 5098598, 11 pages, 2020.

[13] I. Arpaci, S. Alshehabi, M. al-Emran et al., "Analysis of Twitter data using evolutionary clustering during the COVID-19 pandemic," *Computers, Materials & Continua*, vol. 65, no. 1, pp. 193–204, 2020.

[14] H. Alrabaiah, M. Arfan, K. Shah, I. Mahariq, and A. Ullah, "A comparative study of spreading of novel corona virus disease by ussing fractional order modified SEIR model," *Alexandria Engineering Journal*, vol. 60, no. 1, pp. 573–585, 2021.

[15] Y. Zheng, Y. Zhu, M. Ji et al., "A learning-based model to evaluate hospitalization priority in COVID-19 pandemics," *Patterns*, vol. 1, no. 6, article 100092, 2020.

[16] M. Nemati, J. Ansary, and N. Nemati, "Machine-learning approaches in COVID-19 survival analysis and discharge-time likelihood prediction using clinical data," *Patterns*, vol. 1, no. 5, article 100074, 2020.

[17] H. T. Likassa, W. Xain, X. Tang, and G. Gobebo, "Predictive models on COVID 19: what Africans should do?," *Infectious Disease Modelling*, vol. 6, pp. 302–312, 2021.

[18] J. B. Miller, G. Shan, J. Lombardo, and G. Jimenez-Maggoria, "Biomedical informatics applications for precision management of neurodegenerative diseases," *Alzheimer's & Dementia: Translational Research & Clinical Interventions*, vol. 4, no. 1, pp. 357–365, 2018.

[19] E. Garcia-Ceja, M. Riegler, T. Nordgreen, P. Jakobsen, K. J. Oedegaard, and J. Tørresen, "Mental health monitoring with multimodal sensing and machine learning: a survey," *Pervasive and Mobile Computing*, vol. 51, pp. 1–26, 2018.

[20] A. Sharma, R. A. Harrington, M. B. McClellan et al., "Using digital health technology to better generate evidence and deliver evidence-based care," *Journal of the American College of Cardiology*, vol. 71, no. 23, pp. 2680–2690, 2018.

[21] H. Geerts, P. A. Dacks, V. Devanarayan et al., "Big data to smart data in Alzheimer's disease: the brain health modeling initiative to foster actionable knowledge," *Alzheimer's & Dementia*, vol. 12, no. 9, pp. 1014–1021, 2016.

[22] P. Sardar, J. D. Abbott, A. Kundu, H. D. Aronow, J. F. Granada, and J. Giri, "Impact of artificial intelligence on interventional cardiology: from decision- making aid to advanced interventional procedure assistance," *JACC: Cardiovascular Interventions*, vol. 12, no. 14, pp. 1293–1303, 2019.

[23] V. Palanisamy and R. Thirunavukarasu, "Implications of big data analytics in developing healthcare frameworks - a review," *Journal of King Saud University-Computer and Information Sciences*, vol. 31, no. 4, pp. 415–425, 2019.

[24] D. Vidaurre, R. Abeysuriya, R. Becker et al., "Discovering dynamic brain networks from big data in rest and task," *Neuroimage*, vol. 180, no. Part B, pp. 646–656, 2018.

[25] N. A. Azeez and C. V. der Vyver, "Security and privacy issues in e-health cloud-based system: a comprehensive content analysis," *Egyptian Informatics Journal*, vol. 20, no. 2, pp. 97–108, 2019.

[26] R. Palmer, M. Dimairo, C. Cooper et al., "Self-managed, computerised speech and language therapy for patients with chronic aphasia post-stroke compared with usual care or attention control (Big CACTUS): a multicentre, single-blinded, randomised controlled trial," *The Lancet Neurology*, vol. 18, no. 9, pp. 821–833, 2019.

[27] N. Schoettler, E. Rodriguez, S. Weidinger, and C. Ober, "Advances in asthma and allergic disease genetics: is bigger always better?," *Journal of Allergy and Clinical Immunology*, vol. 144, no. 6, pp. 1495–1506, 2019.

[28] T. Li, Z. Xiao, H. M. Georges, Z. Luo, and D. Wang, "Performance analysis of co-and cross-tier device-to-device communication underlaying macro-small cell wireless networks," *J KSII Transactions on Internet Information Systems*, vol. 10, no. 4, pp. 1481–1500, 2016.

[29] M. Pobiruchin, S. Bochum, U. M. Martens, M. Kieser, and W. Schramm, "A method for using real world data in breast cancer modeling," *Journal of Biomedical Informatics*, vol. 60, pp. 385–394, 2016.

[30] R. Davoodi and M. H. Moradi, "Mortality prediction in intensive care units (ICUs) using a deep rule-based fuzzy classifier," *Journal of Biomedical Informatics*, vol. 79, pp. 48–59, 2018.

[31] L. Rasmy, Y. Wu, N. Wang et al., "A study of generalizability of recurrent neural network-based predictive models for heart failure onset risk using a large and heterogeneous EHR data set," *Journal of Biomedical Informatics*, vol. 84, pp. 11–16, 2018.

[32] R. Landy, L. C. Cheung, M. Schiffman et al., "Challenges in risk estimation using routinely collected clinical data: the example of estimating cervical cancer risks from electronic health-records," *Preventive Medicine*, vol. 111, pp. 429–435, 2018.

[33] J. Zhao, P. Papapetrou, L. Asker, and H. Bostrom, "Learning from heterogeneous temporal data in electronic health records," *Journal of Biomedical Informatics*, vol. 65, pp. 105–119, 2017.

[34] Z. Xiao, S. Xu, T. Li et al., "On extracting regular travel behavior of private cars based on trajectory data analysis," *IEEE Transactions on Vehicular Technology*, vol. 69, no. 12, pp. 14537–14549, 2020.

[35] Y. Huang, Z. Xiao, D. Wang, H. Jiang, and D. Wu, "Exploring individual travel patterns across private car trajectory data," *IEEE Transactions on Intelligent Transportation Systems*, vol. 21, no. 12, pp. 5036–5050, 2020.

[36] Y. Huang, Z. Xiao, X. Yu, D. Wang, V. Havyarimana, and J. Bai, "Road network construction with complex intersections based on sparsely sampled private car trajectory data," *ACM Transactions on Knowledge Discovery from Data (TKDD)*, vol. 13, no. 3, pp. 1–28, 2019.

[37] O. Kocsis, A. Lalos, G. Arvanitis, and K. Moustakas, "Multi-model short-term prediction schema for mHealth empowering asthma self- management," *Electronic Notes in Theoretical Computer Science*, vol. 343, pp. 3–17, 2019.

[38] H. Xin-Di, D. Chang-Song, L. Hao, X. Shi-Wei, and L. Li-Song, "Research on herb pairs of classical formulae of ZHANG Zhong-Jing using big data technology," *Digital Chinese Medicine*, vol. 2, no. 4, pp. 195–206, 2019.

[39] A. Pashazadeh and N. J. Navimipour, "Big data handling mechanisms in the healthcare applications: a comprehensive and systematic literature review," *Journal of Biomedical Informatics*, vol. 82, pp. 47–62, 2018.

[40] S. Harous, M. El Menshawy, M. A. Serhani, and A. Benharref, "Mobile health architecture for obesity management using sensory and social data," *Informatics in Medicine Unlocked*, vol. 10, pp. 27–44, 2018.

[41] B. Heude, P. Scherdel, A. Werner et al., "A big-data approach to producing descriptive anthropometric references: a feasibility and validation study of paediatric growth charts," *The Lancet Digital Health*, vol. 1, no. 8, pp. e413–e423, 2019.

[42] C. Song, Y. Kong, L. Huang, H. Luo, and X. Zhu, "Big data-driven precision medicine: Starting the custom-made era of iatrology," *Biomedicine & Pharmacotherapy*, vol. 129, article 110445, 2020.

[43] K. A. Shakil, F. J. Zareen, M. Alam, and S. Jabin, "BAMHealthCloud: a biometric authentication and data management system for healthcare data in cloud," *Journal of King Saud University-Computer and Information Sciences*, vol. 32, no. 1, pp. 57–64, 2020.

[44] N. K. Kitson and A. C. Constantinou, "Learning Bayesian networks from demographic and health survey data," *Journal of Biomedical Informatics*, vol. 113, article 103588, 2021.

[45] J. Waring, C. Lindvall, and R. Umeton, "Automated machine learning: review of the state-of-the-art and opportunities for healthcare," *Artificial Intelligence in Medicine*, vol. 104, article 101822, 2020.

[46] J. Kazmierska, A. Hope, E. Spezi et al., "From multisource data to clinical decision aids in radiation oncology: the need for a clinical data science community," *Radiotherapy and Oncology*, vol. 153, pp. 43–54, 2020.

[47] A. Hasselgren, K. Kralevska, D. Gligoroski, S. A. Pedersen, and A. Faxvaag, "Blockchain in healthcare and health sciences-a scoping review," *International Journal of Medical Informatics*, vol. 134, article 104040, 2020.

[48] H. C. Jubb, A. P. Pandurangan, M. A. Turner, B. Ochoa-Montano, T. L. Blundell, and D. B. Ascher, "Mutations at protein-protein interfaces: small changes over big surfaces have large impacts on human health," *Progress in Biophysics and Molecular Biology*, vol. 128, pp. 3–13, 2017.

[49] A. Morton, R. Thomas, and P. C. Smith, "Decision rules for allocation of finances to health systems strengthening," *Journal of Health Economics*, vol. 49, pp. 97–108, 2016.

[50] D. Cirillo and A. Valencia, "Big data analytics for personalized medicine," *Current Opinion in Biotechnology*, vol. 58, pp. 161–167, 2019.

[51] D. Cha, C. Pae, S. B. Seong, J. Y. Choi, and H. J. Park, "Automated diagnosis of ear disease using ensemble deep learning with a big otoendoscopy image database," *EBioMedicine*, vol. 45, pp. 606–614, 2019.

[52] Z. Yang, N. Luo, G. Bonsel, J. Busschbach, and E. Stolk, "Selecting health states for EQ-5D-3L valuation studies: statistical considerations matter," *Value Health*, vol. 21, no. 4, pp. 456–461, 2018.